THE MULTIDIRECTIONAL DIRECT SIMPLE SHEAR APPARATUS WITH APPLICATION TO DESIGN OF OFFSHORE ARCTIC STRUCTURES

by

Don J. DeGroot

B. Eng., Concordia University
Montreal, Canada
(1983)

S.M. Civil Engineering
Massachusetts Institute of Technology
(1985)

Submitted to the Department of
Civil Engineering in partial fulfillment
of requirements for the degree of

Doctor of Science in Civil Engineering

at the

MASSACHUSETTS INSTITUTE OF TECHNOLOGY

August 1989

Signature of Author: Dan DeGroot
Dept. of Civil Engineering, August 16, 1989

Certified by: Charles C Ladd
Prof. Charles C. Ladd, Thesis Co–Supervisor

Certified by: John T Germaine
Dr. John T. Germaine, Thesis Co–Supervisor

Accepted by: Ole S Madsen
Prof. Ole S. Madsen
Chairman, Departmental Committee on Graduate Students

Vol. 1

THE MULTIDIRECTIONAL DIRECT SIMPLE SHEAR APPARATUS WITH APPLICATION TO DESIGN OF OFFSHORE ARCTIC STRUCTURES

by

Don J. DeGroot

Submitted to the Department of Civil Engineering on
August 16, 1989, in partial fulfillment of the requirements
for the Degree of Doctor of Science in Civil Engineering.

ABSTRACT

Foundations of offshore Arctic gravity structures, which often consist of relatively weak Arctic silts overlying relict permafrost, are subjected to complex loading conditions. The foundation soil may undergo severe lateral squeezing during set–down of a structure and will be subjected to large horizontal shear forces due to ice loads. These ice forces can produce large rotations and even reversal in the direction of shear stresses acting at soil elements within the foundation soil. This research describes a new simple shear testing device, the Multidirectional Direct Simple Shear (MDSS) apparatus, for testing soil samples under conditions which simulate, at the element level, the state of stress acting within the foundation soil of an offshore Arctic gravity structure.

The research program consists of five major components: (1) design and construction of the MDSS; (2) development of software for automated testing and data acquisition via a personal computer; (3) extensive proof testing of the new device's capabilities; (4) analysis and synthesis of results from an experimental program using the MDSS to test Boston Blue Clay (BBC) specimens under stress conditions covering a wide range of representative elements within the foundation of an offshore Arctic structure; and (5) detailed comparison of experimental results with numerical predictions from the MIT–E3 constitutive soil model.

The MDSS uses a circular sample which is consolidated under both a vertical stress (σ'_{vc}) and a horizontal shear stress ($\tau_{hc}=\tau_1$; set–down conditions). The sample is subsequently sheared undrained by applying a second independent horizontal shear stress (τ_2; ice loading) at an angle θ relative to the horizontal consolidation shear stress τ_1. Evaluation of the MDSS first compared conventional CK_0UDSS test data ($\tau_1=0$) on normally consolidated BBC with results obtained in the Geonor DSS device. The MDSS gave lower secant Young's modulus values and on average 7% lower strengths, but produced remarkably less scatter in the test results than the Geonor DSS. Kinematic proof tests with an elastic material gave excellent results, confirming that the set–up procedure, application of forces and strain measurement systems in the MDSS work properly and produce repeatable results. The overall evaluation process also included a comprehensive study of soil behavior in undrained direct simple shear. This study indicates that the pronounced strain softening always observed at large strains is at least partially due to the nonuniform state of stress caused by the DSS device.

Results from a MDSS test program on BBC wherein specimens were first normally consolidated with $\tau_{hc}=\tau_1=0.2\sigma'_{vc}$ and then sheared undrained at θ varying in 30° increments from zero (shear in same direction) to 180° (shear in opposite direction) show dramatic differences in the response of the soil as a function of θ. The peak undrained strength varied almost twofold from θ=0° to 120°, while the deformation behavior varied from very brittle at low θ angles to becoming ductile at

higher angles. Predictions of the test program results using the MIT–E3 soil model compare remarkably well with the experimental data, especially for two of the more important design parameters: peak shear resistance and undrained secant Young's modulus. Additional predictions of the ice loading response of BBC at varying consolidation stress ratios τ_{hc}/σ'_{vc} and OCR and for an Arctic silt (Harrison Bay, Alaska) show the same basic trends as measured and predicted for normally consolidated BBC with $\tau_{hc}/\sigma'_{vc}=0.2$. The experimental results and MIT–E3 predictions indicate that dramatic changes in foundation response at different θ angles will be an important design issue. The very good performance of the MIT–E3 model suggests that the MDSS and a finite element code with MIT–E3 as its constitutive model can together be used as a reliable design tool for offshore Arctic gravity structures.

Thesis Co–Supervisor: **Dr. Charles C. Ladd**
Title: Professor of Civil Engineering

Thesis Co–Supervisor: **Dr. John T. Germaine**
Title: Lecturer in Civil Engineering

to
Yukwon
and
Kemsheen

ACKNOWLEDGEMENTS

The author would like to acknowledge the following people and organizations for helping make the completion of this work possible:

Professor Charles C. Ladd and Dr. John T. Germaine, my thesis co–supervisors, whose dedication to education and research at MIT is truly remarkable. Their guidance in my research and career as well as giving me ample freedom to tackle the research objectives presented in this thesis are greatly appreciated. These two gentlemen have taught me a great deal and I am delighted that our relationship has evolved from that of supervisor–student to one of being friends and colleagues.

Professor Robert V. Whitman for serving as a member of my thesis committee and Professor Andrew J. Whittle for his help with the MIT–E3 soil model.

Professor Hormoz Poorooshasb for his continued support of my career and particularly for his friendship.

Arthur and Stephen Rudolph for their expertise as machinists and Richard Gedney for his help in sorting out some of the servo control problems.

The Natural Sciences and Engineering Research Council of Canada, MIT's Center for Scientific Excellence in Offshore Engineering and MIT's Consortium Cooperative Research in Arctic Offshore Engineering and Construction whose financial support has been greatly appreciated.

My "family–in–law" for their continued support and particularly for having faith that I would one day be able to provide for my wife!

My parents, brother and sisters who, over the past few years, have made me appreciate how fortunate I am to be part of a caring family.

My daughter Carolina who has helped me in ways she is still too young to understand.

My lovely wife Virginia without whose help this work would never have been completed. She was always there to provide all the moral support and affection to keep me going when it all seemed hopeless. I am truly proud that she is not only my wife but also my best friend.

Table of Contents

List of Tables

List of Figures

LIST OF SYMBOLS

Note:

1. Prefix Δ indicates a change.
2. Suffix f indicates a final or failure condition.
3. Suffix $_{max}$ indicates a maximum value.
4. A superscript prime on a stress indicates an effective stress.
5. A superscript prime on a property indicates value in terms of effective stress.

GENERAL

BBC	Boston Blue Clay
COV	Coefficient of variation = SD/Mean
DCDT	Direct current displacement transducer
LR	Linear regression
n,r	Linear regression parameters; n = number of observations; r = correlation coefficient
NC	Normally consolidated
SZA	"Soft Zone Area" of Harrison Bay, Beaufort Sea
OC	Overconsolidated
SD	Standard deviation

INDEX AND CLASSIFICATION PROPERTIES

e	Void ratio
e_o	Initial void ratio
G	Specific Gravity
I_l	Liquidity index
I_p	Plasticity index
S	Degree of saturation
w	Water content
w_l	Liquid limit
w_p	Plastic limit

STRESSES, STRAINS, MODULI AND STRENGTH PARAMETERS

b	$(\sigma_2 - \sigma_3)/(\sigma_1 - \sigma_3)$
c_u	Undrained shear strength
c_u(DSS)	c_u from direct simple shear test
c_u(TC)	c_u from triaxial compression test
c_u(TE)	c_u from triaxial extension test
E	Young's modulus
E_u	Undrained secant E
E_u(50)	E_u fifty percent to failure
G	Shear modulus
K_o	Coefficient of earth pressure at rest
m,n	OCR exponents
OCR	Overconsolidation ratio = σ'_p/σ'_{vo}, σ'_p/σ'_{vc}
p'	$0.5(\sigma'_v + \sigma'_h)$
q	$0.5(\sigma_v - \sigma_h)$ or $(\sigma_1 - \sigma_2)$
q_f	q at failure
S	Normally consolidated undrained strength ratio
SHANSEP	Stress History and Normalized Soil Engineering Properties
t_c	Consolidation time under last increment
t_f	Time to failure
t_s	Storage time
u	Pore water pressure
ϵ_{vol}	Volumetric strain
$\epsilon_1, \epsilon_2, \epsilon_3$	Principal strains
δ	Angle between σ_{1f} and vertical direction
γ	Shear strain
σ, σ'	Normal total stress, normal effective stress

$\sigma_1,\sigma_2,\sigma_3$	Principal stresses
σ_{ff},σ'_{ff}	Normal stress on failure plane at failure
σ_v	Vertical normal stress
σ_h	Horizontal normal stress
σ_r	Radial normal stress
τ	Shear stress
τ_{ff}	τ on failure plane at failure
τ_h	τ on horizontal plane in direct simple shear test
τ_{hc}	Horizontal consolidation shear stress in direct simple shear test
ϕ,ϕ'	Slope of Mohr–Coulomb failure envelope
θ_f	Orientation of the failure plane relative to the horizontal
θ_p	Orientation of the major principal stress relative to the horizontal
ψ	Arctan τ_h/σ'_v for direct simple shear tests.
ν	Poisson's ratio

CONSOLIDATION PARAMETERS

a_v	Coefficient of Compressibility = $\Delta e/\Delta\sigma_v$
c_v	Coefficient of consolidation for vertical flow
C_c	Virgin compression index
C_r	Recompression index
C_s	Swelling index
$C\alpha$	Rate of secondary compression = $\Delta\epsilon_v/\Delta$logt
CR	Virgin compression ratio = $\Delta\epsilon_v/\Delta\log\sigma'_{vc}$
k	Permeability
m_v	Coefficient of volume change = $\Delta\epsilon_v/\Delta\sigma_v$
RR	Recompression Ratio
SR	Swelling Ratio
T	Temperature

t	Time
t_p, t_{100}	t required for primary consolidation
ϵ_v	Vertical Strain
γ_c	Consolidation shear strain
σ'_{vc}	Vertical consolidation stress
σ'_{vo}	Initial vertical effective stress
σ'_p	Preconsolidation pressure

CONSOLIDATION AND STRENGTH TESTS

CAU	Anisotropically consolidated–undrained shear test
CAUDSS	CAU direct simple shear test
CAUMDSS	CAU Multidirectional Direct Simple Shear test
CD	Consolidated Drained test
CIUC	Isotropically consolidated–undrained triaxial compression test
CK_oU	K_o consolidated–undrained shear test
CK_oUC	CK_oU triaxial compression test
CK_oUDSS	CK_oU direct simple shear test
CK_oUMDSS	CK_oU multidirectional direct simple shear test
CRSC	Constant rate of strain consolidation test
CU	Consolidated Undrained test
DSC	Directional shear cell
DSS	Direct simple shear
LV	Laboratory vane test
MDSS	Multidirectional Direct Simple Shear
MV	Miniature vane test
PCE	Plane strain compression test
PSE	Plane strain extension test
PP	Pocket penetrometer test

TC	Triaxial compression
TE	Triaxial extension
TSHC	Torsional shear hollow cylinder
TTA	True triaxial apparatus
TV	Torvane test
UU	Unconsolidated–undrained shear test
UUC	UU triaxial compression test

MULTIDIRECTIONAL DIRECT SIMPLE SHEAR APPARATUS

x,y,z	Coordinate axis system
τ_x, τ_y	Components of τ in x,y orientation
τ_t	$(\tau_x^2 + \tau_y^2)^{0.5}$
γ_x, γ_y	Components of γ in x,y orientation
γ_t	$(\gamma_x^2 + \gamma_y^2)^{0.5}$
τ_1	First horizontal shear stress applied at an orientation θ relative to the X axis
τ_2	Second horizontal shear stress applied parallel to the X axis
θ	Horizontal angle between τ_1 and τ_2
Z DCDT	Constant height DCDT
Z1 DCDT	Vertical displacement DCDT number 1
Z2 DCDT	Vertical displacement DCDT number 2
X DCDT	Horizontal DCDT along the x axis
Y DCDT	Horizontal DCDT along the y axis

CHAPTER 1
INTRODUCTION

1.1 BACKGROUND

The United States and Canada have identified the Beaufort Sea (Figure 1.1) as a potential source of petroleum reserves. Offshore oil exploration activity in the region began in the mid 1970's and increased dramatically during the early 1980's. Although the region may not contain as large petroleum reserves as originally believed, it is still considered to be a viable source (OTA, 1985). However, development of the reserves is costly and difficult. The Arctic region is very remote and contains many hazards including cold temperatures and difficult ice conditions.

Originally, oil exploration in the Beaufort Sea was performed from drilling ships. However, the region is ice–free for only about two months a year thus severely limiting the use of ships. As a result, man–made gravel islands, up to several hundred feet in diameter, were introduced to enable year–round drilling. The gravel islands can withstand large lateral ice forces but are only economically feasible in shallow waters. As exploration moved to deeper waters mobile gravity structures that can withstand the large ice loads were introduced. Their mobility also enables them to be used repeatedly, therefore reducing the cost of explorations (AOGA, 1986).

The subsea profile within the offshore Alaskan continental shelf of the Beaufort Sea often consists of relatively weak Arctic silts overlying relict permafrost. Some regions contain particularly weak soil such as that found in the "Soft Zone Area" of Harrison Bay (Figure 1.2). Here the foundation soil consists of 20–30 feet of very soft soil overlying relict permafrost thus making foundation design a critical factor in successfully utilizing a gravity structure for exploration and production.

The foundation design of exploration and production gravity structures for the Arctic is very complicated and requires consideration of the following (Ladd, 1984):

1. The short term (undrained) behavior of the soil under gravity loads from the structure;
2. The possibility of severe lateral squeezing and large radial deformations resulting from the large width of the structure in relation to the thickness of the weak soil layer;
3. The magnitude and rate of strength gain due to consolidation of the foundation soils under the weight of the structure, possibly accelerated by prior installation of vertical drains;
4. A reliable estimate of the foundation resistance available during ice loading wherein the applied horizontal force may produce large rotations and possible reversals in the direction of the shear stresses acting within the foundation soils;
5. A foundation design for mobile exploration drilling structures that must have the capability to break away from the sea floor for relocation and also contend with a range of seafloor conditions.

The complex nature of the loading conditions to which the foundation soil of a gravity structure is subjected requires, for design purposes, detailed strength–deformation properties of the soil. Until recently, geotechnical programs in the Arctic relied upon the same exploration and testing techniques as used for the empirical designs of pile–supported platforms in the Gulf of Mexico (Ladd, 1984). Such procedures cannot adequately provide the strength–deformation properties of the soil required for design of Arctic gravity structures. New techniques need to be developed which provide the necessary soil information required to enable arctic gravity structures to be designed reliably and economically.

1.2 MIT CENTER FOR SCIENTIFIC EXCELLENCE IN OFFSHORE ENGINEERING.

The Center for Scientific Excellence in Offshore Engineering was established at MIT in September, 1983 by a five–year Grant of $2 million from the Standard Oil Company (now BP America, Inc.) with three principal objectives: 1) to conduct

coordinated interdisciplinary research on Arctic offshore engineering in partnership with industry; 2) to support students engaged in offshore engineering research; and 3) to develop a scientific interchange program. The Grant was one of five awarded by The Standard Oil Co. to universities as a result of a nationwide competition for programs which would involve university–based collaborative research on problems of national significance. The Center at MIT has involved faculty and graduate students from the Department of Civil Engineering and Ocean Engineering. They conducted research encompassing ice and structural, geotechnical, risk and reliability and hydrodynamic aspects of Arctic offshore engineering with funds from the Center and other sponsors in collaboration with Technical Representatives from the Standard Oil Production Company (SOPC). An Advisory Committee, with members from MIT and SOPC, annually reviewed research results and budgets and recommended changes in program emphasis or direction. The Center has established an international reputation for its contributions to both applied and basic technology and for providing professional leadership via participation in conferences, workshops and technical committees.

In 1987, BP reduced the Grant to $1.7 million due to the drastic drop in oil prices and concurrently opened the Center to other oil companies that led to a proposal for Consortium Cooperative Research in Arctic Offshore Engineering and Construction starting in 1988. The proposal was accepted by seven companies (Amoco Production Company; ARCO Alaska, Inc.; BP Exploration, Inc.; Chevron Oil Field Research Company; Conoco, Inc.; Exxon Production Research Company and Mobil Research and Development Corp; .) to support interdisciplinary research in the areas of ice mechanics, ice–structure interaction, geotechnical engineering and hydrodynamic modeling.

The Center's program in geotechnical engineering initially sponsored research in two main areas: 1) engineering properties of Arctic silts, and 2) theoretical

procedures for assessing the foundation stability of Arctic gravity structures. Research on the first topic started at the time of the Center's inception, and studies in the second topic commenced in September of 1984.

Funding from the MIT Sea Grant Program and from industry sponsors was initiated in July of 1984 to further support the research on geotechnical properties of Arctic silts. The industry sponsors have included: Bedford Institute of Oceanography, Nova Scotia; Brian Watt Associates, Houston; Fugro International, Inc., Houston; Golder Associates, Canada; McClelland–EBA, Inc., Alaska; Norwegian Geotechnical Institute, Oslo; Stone and Webester Engineering Corp., Boston; and The Earth Technology Corporation, Long Beach. Bi–annual meetings were held with SOPC and annually with the industry sponsors both to present results from the cooperative research and to take advantage of the practical expertise these organizations have in dealing with geotechnical exploration and design of offshore structures.

1.3 GENERAL RESEARCH OBJECTIVES

Ultimately the aim of the Center's research in experimental geotechnical engineering is to develop recommended procedures for measuring the engineering properties of Arctic silts which are necessary for the safe and economical foundation design of offshore structures. Specifically the program addresses the following issues (Sauls, et al., 1984):

1. Why Arctic silts exhibit unique behavior compared to other offshore sediments, which negates reliance on past empirical correlations;
2. What types of in situ and laboratory test programs should be used to develop reliable estimates of the initial strength–deformation properties needed to predict the performance of gravity structures during and after set down;
3. What types of laboratory shear tests should be used to obtain strength–deformation properties needed to evaluate foundation stability against massive horizontal forces due to ice loading;

Evaluation of these experimental results (together with available field performance) and input from the industry co–sponsors will provide the basis for developing guidelines for recommended practice. The research program initiated to achieve these objectives was divided into three phases of investigation:

1. Geology and composition of the deposits;
2. Basic strength–deformation properties as a function of temperature, stress history, and failure mode;
3. Foundation stability against ice loading.

1.4 PRIOR RESEARCH ACTIVITIES

The Standard Oil Production Company (SOPC), through the initiative of Dr. Jeff Weaver, furnished MIT in January 1984 with 15 undisturbed silt samples taken from one boring beneath Mukluk Island and from three others several miles to the north. These were all located within or near the "soft zone area" of Harrison Bay (Figure 1.2). The experimental program conducted on these samples included: radiography, preliminary compositional analysis, consolidation tests to determine the influence of test temperature on the estimated preconsolidation pressure, and a preliminary series of consolidated–undrained triaxial compression and extension and direct simple shear tests to investigate stress–strain–strength anisotropy and behavior under ice loading and whether or not normally consolidated silt exhibits reasonable "normalized" behavior. These results, plus a summary of research by MIT on the geology of Harrison Bay, are contained in the Center's first Research Report entitled "Strength–Deformation Properties of Harrison Bay Arctic Silts," by D. P. Sauls, J.T. Germaine and C.C. Ladd (1984). A paper (Ladd, et al., 1985) co–authored by Dr. Weaver and the same three MIT staff, presented at the ARCTIC '85 ACSE Specialty Conference, highlights the principal findings.

In April 1984, a special program of undisturbed sampling and in situ testing was conducted off the ice near the edge of Mukluk Island. SOPC funded the program, which was executed under the supervision of Dr. Germaine acting as Standard Oil's field representative and in coordination with Dr. Weaver. In situ testing included a series of piezocone testing boreholes. The program also provided the project with a vital supply of 20 high quality samples for research during the second year, and demonstrated the definitive advantage of using fixed piston rather than the conventional (for the Arctic) push sampling technique. The amount of suitable soil was increased by a factor of two to three with little increase in sampling cost.

Extensive consolidation tests run on these samples, plus radiography, show that this 25–ft thick deposit actually has two distinct layers. The Upper Layer is characterized by: highly stratified macrofabric; low natural water content; small clay size fraction; and a fairly high and relatively uniform preconsolidation pressure. In contrast, the Lower Layer is characterized by: generally uniform macrofabric; significantly higher water content and clay size fraction; and much lower preconsolidation pressures. Although the geological mechanisms responsible for this unusual condition are still unresolved, results of carbon dating, pollen analysis and review of historic sea levels suggest that the deposit is less than 5,000 years old.

Strength testing on these samples focused on undrained stress–strain–strength anisotropy via K_o consolidated–undrained triaxial compression–extension and direct simple shear modes of failure. Most of these tests were run on normally consolidated samples in order to investigate the relative influence of macrofabric, water content, clay content and consolidation stress level on undrained shear behavior. Sufficient Recompression and SHANSEP (Jamiolkowski, et al., 1985) type data are also available to reasonably predict the initial in situ response of this overconsolidated Arctic silt deposit. These results are contained in MIT Master's theses by Ayan (1985) and Yin (1985).

SOPC sponsored further geotechnical exploration programs at four sites in Smith Bay (Figure 1.2) in early 1985, that were executed by The Earth Technology Corporation (TETC). The field testing program at each site included several borings with fixed piston undisturbed sampling and piezocone penetration and one with field vane and pressuremeter tests. Laboratory testing by TETC at each site included classification and index properties, UU triaxial tests, a series of oedometer tests and several CU direct simple shear and triaxial tests. The Center worked with SOPC to evaluate the results of the geotechnical program and assist SOPC and its design consultant (EBA Engineering Consultants Ltd., Canada) in development of a site specific design. MIT also performed some additional special laboratory testing. The Center thereby obtained access to extensive data from other offshore sites for comparison with results obtained at Harrison Bay in order to determine differences in basic behavioral trends. This collaboration also allowed MIT's research results to be applied to a real life design problem with benefits to both groups.

Samples from Smith Bay were sent to MIT for a special test program at one site to supplement data obtained by TETC, plus additional testing at a second site to further MIT's research objectives. The MIT test program included consolidation tests to resolve discrepancies and fill in gaps in data for the development of stress history profiles. CU triaxial tests were run at the request of EBA to provide data for calibration on its soil model to predict foundation deformation. Also, a comprehensive series of CK_oU direct simple shear tests were run in order to better assess the resistance of the mobile platform to horizontal sliding.

One objective of this program was to compare the basic strength–deformation behavior of Smith Bay and Harrison Bay Arctic silts. The Smith Bay deposits consist of silty clay, in contrast to the clayey silts tested at Harrison Bay. Also, the effects of ice gouging have significantly affected the stress history and strength profiles at one site in Smith Bay. The test programs have allowed SHANSEP strength profiles to be

compared with each other, as well as with results from conventional strength testing. The results of this investigation are contained in an MIT Master's thesis by Young (1986).

Both the Mukluk Proximal in Harrison Bay and the Smith Bay geotechnical exploration programs included piezocone penetration tests. The piezocone penetrometer has been recognized as the most important development in penetrometer testing in recent years (Baligh, et al., 1981; De Ruiter, 1981) and one of the major tools for offshore soil investigation (De Ruiter and Richards, 1983). A number of theoretically and empirically based methods have been proposed to correlate piezocone penetration data with important soil and site characteristic parameters. However, most of the methods for interpreting penetration data in cohesive soils are based on past experience in soil deposits which exhibit characteristics that are different from those found at the investigated Beaufort Sea sites.

For these reasons, the piezocone penetration test (PCPT) data collected during the previously summarized investigations at the Beaufort Sea provided a unique opportunity to:

1. Assess the performance of the piezocone under unusual environmental conditions in a variety of soil deposits having different grain size distributions and macrofabric, different degrees of overconsolidation and remolding due to ice gouging;
2. Evaluate the applicability of existing methods of piezocone data interpretation to the conditions described above.

The state of knowledge of the soil conditions at the investigation sites, based mostly on previous research at MIT, provided the necessary framework within which PCPT data were analyzed. The results of this last investigation are contained in an MIT Master's thesis by de la Huerta (1987).

1.5 THESIS SCOPE AND OBJECTIVES

The loading conditions to which the foundation of an offshore Arctic gravity structure is subjected are complex. The foundation soil may not only undergo severe lateral squeezing during set–down of a structure but may also be subjected to large horizontal shear forces due to ice loading. The ice forces can produce large rotations and even reversal in the direction of shear stress acting within the foundation soil. In order to experimentally simulate these conditions at the element level, it is necessary to have a shear device which is capable of consolidating a sample under both a vertical stress and horizontal shear stress (set–down condition). In addition, it must be able to subsequently shear the sample undrained (ice loading) by applying a second independent horizontal shear stress at an angle relative to the horizontal consolidation shear stress. There is no laboratory testing device which is capable of applying this unique set of stresses to a soil sample. The primary objective of this research is to design and develop a shear testing device with these capabilities and to conduct an experimental program with the device on resedimented Boston Blue Clay (BBC).

In fulfilling these objectives, this research includes the following:

1. Design and construction of a new multidirectional direct simple shear apparatus;
2. Development of software for automated testing and data acquisition via a personal computer;
3. Extensive proof testing of the new device's capabilities;
4. Analysis and synthesis of the results of an experimental test program with the device on BBC tested under stress conditions which simulate that of key elements within the foundation of an offshore Arctic structure;
5. Detailed comparison of experimental results with numerical predictions from a constitutive soil model (e.g., MIT–E3);
6. Assessment of experimental and numerical results for application to foundation design of offshore Arctic gravity structures.

1.6 ORGANIZATION

Chapter 2 describes the Beaufort Sea environment and the general properties of Harrison Bay and Smith Bay Arctic silts. Issues affecting the foundation performance of offshore Arctic gravity structures are reviewed including a summary of previous research on theoretical and numerical (finite element method) analyses of the problem. The experimental requirements for simulating the stress conditions within the foundation soil are discussed including a review of the limitations of existing laboratory shear devices with respect to these requirements.

Chapter 3 presents a description of the main features of the Multidirectional Direct Simple Shear (MDSS) apparatus developed for this research. It includes application and measurement of forces, measurement of strains and computer control and data acquisition equipment (a detailed description of the MDSS is given in Appendix B). It also covers the computer control and data acquisition software and testing procedures for cohesive soils. Because the MDSS is a direct simple shear type of device, a detailed review of direct simple shear testing of cohesive soils is presented in Appendix A.

Chapter 4 covers the proof testing program performed to evaluate the capabilities of the MDSS. It includes a comparison of results from K_o consolidated and anisotropically consolidated direct simple shear tests on normally consolidated BBC in the MDSS and the Geonor Direct Simple Shear apparatus. Results from tests on an elastic material to check the kinematics of the apparatus are also presented.

The results from an experimental program on normally consolidated BBC conducted with the MDSS are presented in Chapter 5. The experimental program was conducted to provide information on the behavior of BBC under stress conditions representative of several key elements within the foundation of an offshore Arctic gravity structure. Detailed information from the tests are located in appendices.

Chapter 6 presents an evaluation and synthesis of numerical predictions of the test results given in Chapter 5 using the MIT–E3 constitutive soil model. Additional MIT–E3 predictions for tests not conducted in the MDSS are given for overconsolidated BBC and normally consolidated Harrison Bay Arctic silt. The chapter concludes with a suggested procedure for assessing the foundation stability and deformation of an offshore Arctic gravity structure using the MDSS and the finite element method with MIT–E3 as its constitutive model.

Chapter 7 provides a summary, conclusions and recommendations based on research completed to date.

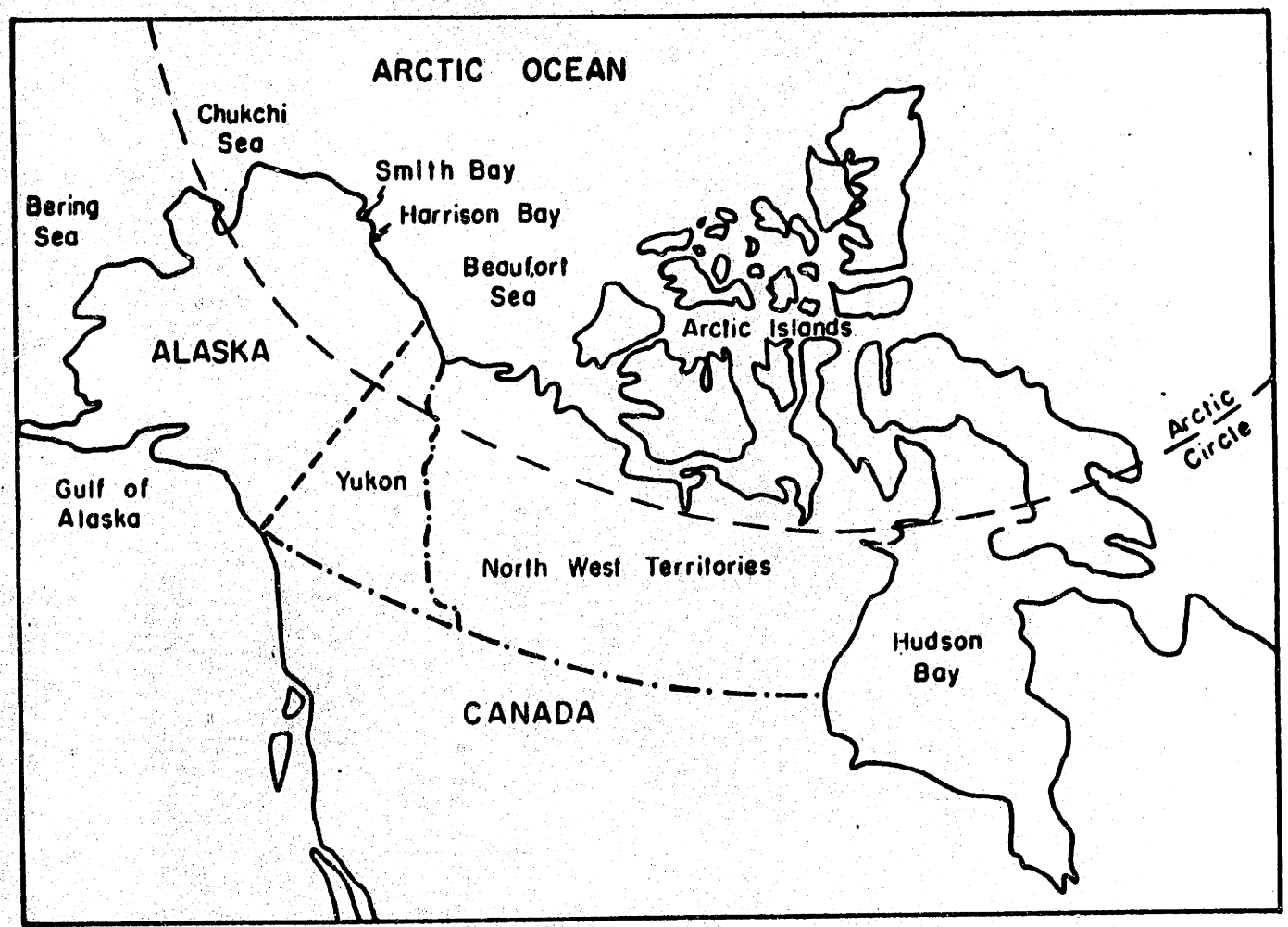

Figure 1.1: Areas of Interest to Offshore Arctic Exploration (from Young, 1986).

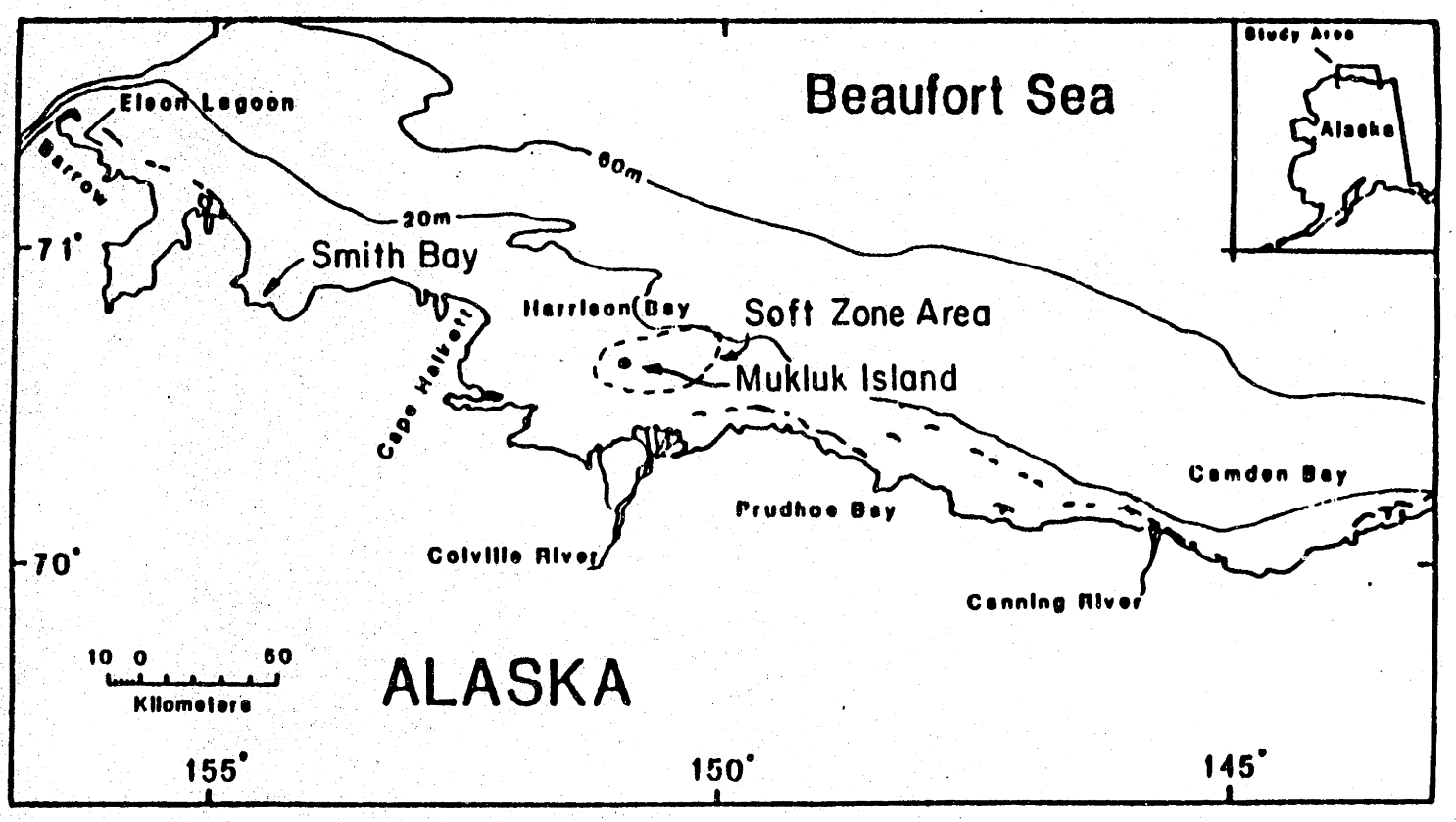

Figure 1.2: Location of Smith Bay and Harrison Bay in the Beaufort Sea (from Young, 1986).

CHAPTER 2
BACKGROUND

2.1 OVERVIEW OF OFFSHORE ARCTIC ENVIRONMENT

2.1.1 Ice Conditions

Sea ice is the most important environmental factor affecting the design of gravity platforms in the offshore Arctic region. The characteristics of sea ice and its movement are the main items of concern for design. Depending on a structure's location and configuration lateral ice forces may reach 50,000 to 200,000 tons (Gerwick, 1983).

Sea ice is identified as being either first–year ice or multi–year ice. Multi–year ice is more than one year old and may grow to about 12 to 16 feet thick whereas first–year ice may grow to 6 to 7 feet thick. In general, multi–year ice is stronger than first–year ice (OTA, 1985; Watt, 1982)

Sea ice in the Arctic is made up of three separate zones (Figure 2.1):

- Fast Ice Zone – includes landfast ice and grounded ridges;
- Transition Ice Zone – exists between the relatively motionless fast ice zone and the polar pack;
- Polar Pack Ice – Multi–year ice that covers the central Arctic Ocean.

In the Beaufort Sea, landfast ice is attached to the shoreline or sea bottom and can extend out to the 60 ft isobath and reach a thickness of approximately 6 to 7 feet (Dingle, 1982). It generally forms in the early fall and melts in early June. Near the coast the melting process is accelerated by rivers flooding over the ice surface. Once the landfast ice is detached from the shoreline or sea bottom it is moved by wind and water currents further breaking the ice into smaller floes. The length of the open water

season varies depending on the prevailing winds and water currents and generally lasts during the months of July, August and September.

The fast ice zone also contains grounded ridges which are pressure ridges that are formed and subsequently grounded to the sea bottom. The pressure ridges are formed when ice floes are driven together by wind and wave currents causing the ice to upheave and thrust downward. The grounded ridge zone is not continuous and the location and extent of the ridges vary considerably from year to year (OTA, 1985).

Between the fast ice zone and the polar pack lies the transition, or stamuki zone. This is a shear zone of considerable energy. Ridges are formed as a result of floes being driven against one another and from the shearing action between the various ice masses. The surface height of ridges may be as high as 25 ft while the depth of ridge keels may reach 100 ft. (OTA, 1985). In Harrison Bay the transition zone tends to form around the 30 ft isobath in early winter and extends beyond the 60 ft isobath by January or February (Bea, et al., 1985).

The keels that are formed beneath the pressure ridges can be driven into the sea bottom by wind, water currents and ice pressure. As a result the ice keels gouge into the sea bottom up to depths from 3 to 15 feet. Repeated gouging of the sea bottom is very common, particularly in water depths less than 45 feet. However, local shore currents and storms tend to refill the gouges with sediments. At larger depths the gouges tend not to be filled and remain until altered by later ice gouging. (OTA, 1985). The highest gouge densities generally occur in water between 30 and 130 ft deep and average more than 250 per square mile. Lowest gouge densities occur in water less than 15 ft deep or more than 150 ft deep. In water depths greater than 30 ft deep the gouges tend to be oriented within 20° of being parallel with the coastline orientation.

The polar pack region is composed primarily of multi–year ice and generally lies seaward of water depths ranging from 120 ft to 150 ft. The polar pack is approximately 1500 square miles and drifts in a clockwise direction under the influence

of the Beaufort Sea Gyre. Occasionally changes in the regional weather patterns may bring the polar pack in contact with the shoreline sometimes leaving large ice islands grounded in the coastal waters of the Beaufort Sea.

Ice islands are large enough to cause major damage if they collide with an offshore structure. However, the probability of such an occurrence is relatively low because of the scarcity of ice islands (OTA, 1985). Collision of pressure ridges with structures and ride–up of ice onto structures are events more likely to occur. The frequency of such events would be highest in the transition zone thus making it the most hazardous ice region in which to locate exploration and production structures. However, the transition zone also contains some of the most promising areas for oil exploration and production (Gerwick, 1983).

2.1.2 Geology and Depositional Environment

The subsea profile within the offshore Alaskan continental shelf of the Beaufort Sea often consists of Arctic silts overlying relict permafrost[1]. The sea level in the area reached its lowest level of 280 ft below present approximately 20,000 years ago when glaciation was at its maximum (Wang, et al., 1984). As the glacial ice retreated, the sea level continuously rose in a series of minor transgressions and regressions[2] to its present level. As a result of sea level fluctuations the continental shelf within the 100 foot isobath was exposed to the Wisconsin (30,000 – 50,000 BP) cold climate for more than 15,000 years forming permafrost (now termed relict as described above).

The Quaternary deposits in the coastal area consists of the Gubik formation and Holocene sediments. The Gubik formation developed during the Pleistocene and is predominantly a glacially derived marine deposit with evidence of lacustrine, fluvial

---

[1]Permafrost formed in the past during a colder climate and not in thermal equilibrium with the present ground temperature.

[2]Eustatic water level increases and decreases related to glaciation.

and lagoonal deposits in the upper layer. Holocene marine deposits were deposited during the most recent transgression. They form a wedge that thickens offshore to a maximum thickness of 150 feet near the continental shelf break. The wedge is thinner on the western half of the shelf than in the east. Holocene sediments exhibit a maximum thickness of 15 to 30 feet over the inner shelf and are thin or absent along the coast (Weeks, et al., 1983; Grantz and Dinter, 1980).

Ice and water are the dominant forces influencing sedimentary processes on the continental shelf of the Beaufort Sea. The bottom sediments inshore from the 65 foot isobath are dominated by wave and current related processes. Hence, sedimentary activity in this area peaks during the open water season in the summer. Ice gouging also plays a significant role by continuously reworking the surficial deposits.

Near the ice transition zone the influence of ice scour on the sea bottom dominates the sedimentary environment. Repeated ice gouging reworks the sediment mixing relic gravel material with more recent silt and clay deposits to form a heterogeneous sequence of gravelly silts and clays. The development of pressure ridges in the transition zone occurs primarily during the winter months and as a result reworking of the sediment by ice gouging peaks at this time. The effect of ice gouging decreases with increasing water depth as the ice keels become too small to interact with the sea floor. In this region hydraulic processes dominate the sedimentary environment (Barnes and Reimnitz, 1974).

2.2 GENERAL SOIL PROPERTIES

This section describes the results of experiments conducted by MIT on Arctic soils from Harrison Bay and Smith Bay (Figure 1.2). The intent of this section is to provide an overview of the soil conditions that exist at several offshore sites in the Arctic. The results presented focus on classification and index properties, stress history and undrained shear strength of the soils tested. The section begins with a

critique of the geotechnical investigations conducted in 1982 and 1983 in Harrison Bay prior to commencement of the Center's experimental work on Arctic soils. This is followed by a description of MIT's experimental approach for strength testing of the Arctic soils.

2.2.1 Previous Geotechnical Investigations in Harrison Bay (abstracted and modified from Young, 1986)

Prior to commencement of MIT's experimental work on the engineering properties of Harrison Bay soils, several proprietary studies of the region were made available to MIT. The reports, based on geotechnical investigations conducted in 1982 and 1983, identify a "Soft Zone Area" (SZA, Figure 1.2) where the undrained shear strength is very low just above the partially frozen zone overlying relict permafrost as illustrated schematically in Figure 2.2 The Soft Zone Area is distinguished from the rest of Harrison Bay by both engineering and index properties. The data obtained from both inside and outside the soft zone area show considerable scatter in index and engineering properties.

The geotechnical investigations carried out in Harrison Bay in 1982 and 1983 developed soil properties using procedures that closely parallel those developed for the empirical design of pile supported platforms in the Gulf of Mexico. In particular, undrained strengths were generally estimated from results of the following types of tests (Sauls, et al., 1984):

1. In situ tests such as the field vane and the Dutch cone penetrometer;
2. Strength index tests (Torvane, Pilcon vane, miniature lab vane, pocket penetrometer) performed on "undisturbed" push samples;
3. Other laboratory shear tests on tube samples such as unconsolidated–undrained triaxial compression (UUC) and isotropically consolidated–undrained triaxial compression (CIUC) tests.

The in situ tests require empirical correlations to obtain values appropriate for

design. The correction factor versus plasticity index recommended by Bjerrum (1972) is commonly used to adjust measured field vane strengths. However, the case histories from which the recommended correction curve was developed did not include Arctic silt type soils. The validity of the field vane test as an undrained shearing process within Arctic silts is also questionable. The permeability of some Arctic silts may be so high as to allow partially drained conditions to develop during the test. Measurement of strength using the Dutch cone poses similar problems.

In situ tests are usually the most reliable and cost effective tool for measuring spatial variability of deposits, but only for well–defined drainage conditions, i.e., either undrained or fully drained. Laboratory strength index tests are generally less efficient for this purpose due to the high cost of obtaining samples and are often unreliable due to problems caused by varying degrees of sample disturbance.

Use of UUC tests to obtain design strengths depends on uncontrollable compensating errors: the strength increase due to rapid shearing and neglect of the effect of anisotropy offsetting the effect of sample disturbance (e.g., Koutsoftas and Ladd, 1985). CIUC tests, although more sophisticated than UUC tests, are also inadequate. In CIUC tests the sample is isotropically consolidated and sheared with the major principal stress acting vertically. This type of failure mode greatly overpredicts design strengths for horizontal shearing under ice loads.

Results from CIUC tests on presumably normally consolidated samples from Harrison Bay showed that the soil exhibits dilative behavior during undrained shear (1982 and 1983 proprietary reports). Figure 2.3a illustrates that a unique value of the undrained strength cannot be chosen in the case of a dilative soil. The data also shows that there is a significant decrease in c_u/σ'_c versus σ'_c/σ'_p as shown in Figure 2.3b Such behavior is unusual compared to other marine deposits and indicates that the soil does not exhibit normalized behavior. Results from $\underline{K_o \text{ consolidated}}$ undrained shear tests (e.g., DSS and TC) conducted at MIT (Section 2.2.3) on normally consolidated

samples from the Soft Zone Area of Harrison Bay show that the soil does not exhibit significant dilative behavior and also gives reasonable normalized behavior.

A further measure of the uncertainty associated with the measurements of undrained strength in Arctic silts is illustrated by the following examples. At the SZA of Harrison Bay, Ladd, et al. (1985) reported $c_u(UUC)/\sigma'_p = 0.185 \pm 0.065$ SD where σ'_p is the preconsolidation pressure. The field vane strength was usually several times higher. In contrast, UUC strengths equaled the field vane values at Smith Bay, but both values are considered much too high for design (Young, 1986).

Issues relevant to the behavior of Arctic silts are explicitly ignored by the above strength test procedures. Specifically, the effects of anisotropy, changes in stress history, sample disturbance, strain rate, and environmental factors are not considered. These factors are discussed in the following paragraphs.

Strength–deformation properties of sedimentary soils vary with the direction (δ angle) of the applied major principal stress relative to the vertical direction of deposition (Ladd, et al., 1977). This property, anisotropy, usually causes a substantial decrease in undrained strength and increase in strain at failure as δ varies from 0° to 90°. Thus triaxial compression type tests, when considered alone, overestimate design strengths.

In considering foundation stability, anisotropy is coupled with the phenomenon of progressive failure – all elements within the zone of shearing will not reach their peak strength simultaneously. Soils exhibiting strain softening will create a situation in which some soil elements lose resistance before the strength in other elements are fully mobilized (assuming a constant value of shear strain along the potential rupture surface). The net result of averaging shear strength values at different strain levels is a decrease in the average strength. An approach which considers this "strain compatibility" is important when selecting design strengths (Koutsoftas and Ladd, 1985).

For offshore structures in the Arctic, ice loading will probably make anisotropy and progressive failure effects even more important because of the potential reversal in the direction of the major principal stress during shear. Upon initial set down of a structure, the foundation soils will first be subjected to significant radial shear stresses (possibly accompanied by large radial shear deformations due to lateral squeezing), followed by consolidation and strengthening. During this complex process the direction (given by the angle δ) of the major principal consolidation stress σ'_{1c}, will undergo rotations, the magnitude of which will depend on the depth of the soil element in the silt layer and the distance from the centerline of the structure. Application of an ice load further complicates the analyses by producing large rotations in the direction of the major principal stress within most of the foundation soils. An assessment of the limiting equilibrium condition against horizontal sliding requires knowledge of the available strength for σ'_{1f} acting at $\delta = 45 \pm \phi'/2$ degrees to the vertical direction (Sauls, et al., 1984). The inadequacy of using CIUC tests to replicate the behavior of soil under this complex loading condition is obvious. In fact, it is the major objective of this thesis to build an apparatus to test soil samples under these complex loading conditions as will be discussed further in Section 2.4.

Other considerations in evaluating design strengths from laboratory tests are strain rate effects, test temperature, and procedures to minimize the adverse effects of sample disturbance. UUC tests usually shear specimens at strains of 60% per hour. Such rapid rates will often increase the measured strength by 20 ± 10% over values from tests conducted at strain rates of 1% per hour (Ladd, et al., 1977). Standard practice is also to test specimens at room temperature whereas field conditions in the Arctic involve in–situ temperatures around 0° C, a difference which could also affect the measured strength. It is generally accepted that samples must be reconsolidated in the laboratory, both to obtain proper initial state of stress and to minimize sample disturbance effects.

Consideration of the above issues suggests the existence of considerable uncertainty in foundation designs developed based on past test procedures. The Center's objective is to provide practical ways to take these factors into account. Two design techniques, SHANSEP and Recompression, specifically address some of the difficulties associated with stress–strain–strength measurements in soils. The study of the behavior of Arctic silts at MIT was developed based on the test procedures advocated by these two approaches. The philosophy and techniques underlying both methods are described in the following section.

2.2.2 Experimental Approach for Strength Testing (abstracted and modified from Ayan, 1985)

The SHANSEP[3] procedure is a design methodology for evaluating the in situ stress–strain–strength properties of cohesive soils (Ladd and Foott, 1974). The basic steps used in applying this technique are outlined in Table 2.1. For overconsolidated deposits, soil specimens are K_o consolidated into the virgin compression range and then unloaded prior to shear to obtain data as a function of overconsolidation ratio (OCR). The procedure is based on the assumption that mechanical overconsolidation produced in the laboratory will simulate in situ behavior even though the deposit may be overconsolidated due to other mechanisms. This laboratory reconsolidation technique is specifically aimed at minimizing the adverse affects of sample disturbance. (Note: the method is not considered applicable to deposits of cemented and highly structured clays.) By conducting different types of tests (triaxial compression, triaxial extension, and direct simple shear), this method can also be used to provide measurements of soil anisotropy. Fundamental to SHANSEP is the assumption that the soil exhibits reasonable normalized behavior. This requires that, for a particular value of OCR, identical stress–strain–strength characteristics result when normalized with respect to

---

[3]SHANSEP is an acronym for Stress History And Normalized Soil Engineering Properties.

consolidation stress.

Figure 2.4 shows results obtained from applying the SHANSEP procedure to direct simple shear testing on six soils. The resulting relationships can be approximated by the expression:

$$\frac{c_u}{\sigma'_{vc}} = S \cdot (OCR)^m \qquad (2.1)$$

where:

$S = \frac{c_u}{\sigma'_{vc}}$ for normally consolidated soil

OCR = overconsolidation ratio

$m = 0.8 \pm 0.05$

c_u = undrained shear strength

σ'_{vc} = vertical consolidation stress

Once this relationship is established for a deposit, the in situ c_u profile can be computed based on knowledge of the in situ overburden stress and preconsolidation pressure. The normalized parameters thus provide a powerful design tool.

Similar in philosophy to SHANSEP is the Recompression technique (Bjerrum, 1973). This method also recognizes the problems associated with sample disturbance and attempts to mitigate these effects by K_o reconsolidating specimens to the in situ effective overburden pressure. It is not known to what degree the resulting volume decrease may affect the measured strength, particularly for low overconsolidated clays. The method is better suited for testing naturally cemented soils and for highly structured clays with high liquidity index and sensitivity (Jamiolkowski, et al., 1985). For these types of deposits, consolidating into the normally consolidated range, as would be done in the SHANSEP technique, would destroy the soil structure and seriously alter the normalized soil properties. The Recompression technique is also recommended for highly overconsolidated stiff clays and within weathered crusts where sample disturbance is likely to be less of a problem and where it may be difficult to

perform SHANSEP tests at very high OCR values.

Initial efforts during each of the Center's experimental programs were aimed at developing a detailed stress history profile for each deposit studied. This information provides basic consolidation parameters, gives perspective on the magnitude of reasonable undrained strength values, and is one of the steps in applying the SHANSEP technique. Additional tests at MIT for each deposit first concentrated on evaluating the stress–strain–strength behavior of normally consolidated Arctic silts. The laboratory consolidation of specimens into the virgin compression range was done to allow comparison of the behavior of Arctic silts with that of other sedimentary clays. The tests were run at different values of consolidation stress to check if the soil exhibited normalized behavior. SHANSEP type tests in which samples were mechanically overconsolidated were then completed to measure the effect of OCR. Recompression tests also have been performed to provide a basis for comparison with the SHANSEP tests. The testing programs generally included three types of strength tests (triaxial compression, triaxial extension, and direct simple shear) to measure anisotropy.

The SHANSEP technique has been successfully applied to major projects both on land and offshore (e.g., Ladd and Azzouz, 1983). The method is relatively expensive and time–consuming. The benefit is that the Normalized Soil Parameters, once determined, can be reused in analyzing different types of stability problems and at other sites having similar Arctic silt deposits. Little reliable Normalized Soil Parameter data were available from earlier test programs in the Arctic. In such a situation, development of a comprehensive method for evaluating soil strength as achieved through a SHANSEP type program should prove particularly useful and cost–effective, if the technique is found to apply in a reasonable fashion.

2.2.3 Harrison Bay (Soft Zone Area)

As outlined in Section 1.4, the Center's first experimental program consisted of a series of tests on samples within or near the Soft Zone Area of Harrison Bay. The program included: radiography, preliminary compositional analysis, consolidation tests, and a preliminary series of consolidated–undrained triaxial compression and extension and direct simple shear tests (Ladd, et al., 1985).

The mostly ML–MH overconsolidated Harrison Bay silts tested have widely varying grain size distributions and macrofabrics varying from uniform to highly stratified. The CK_oU triaxial compression and extension and direct simple shear tests run on normally consolidated samples show that:

- the DSS mode of shearing gives reasonable normalized behavior;
- these silts exhibit pronounced undrained strength anisotropy similar to low plasticity marine clays.

Research during the first year also led to the conclusion that CIUC tests would seriously overestimate the in situ strength appropriate for stability analysis.

The preliminary results from this test program led to a more extensive series of consolidation and strength tests on additional samples taken adjacent to Mukluk Island in the Soft Zone Area of Harrison Bay (Figure 1.2; Ayan, 1985; Yin, 1985). The samples were taken from an area where the water depth is 50 feet and the subsea profile consists of approximately 25 feet of sandy and clayey silt overlying relict permafrost. Each sample was radiographed, and classification and strength index tests were run on most samples. In addition, the following consolidation and shear strength tests were performed:

- 12 conventional incremental oedometers;
- 5 special oedometer tests consisting of: 2 constant rate of strain consolidation (CRSC) tests, 2 lateral stress oedometers, and 1 temperature controlled oedometer;

- 13 K_o consolidated–undrained direct simple shear tests (CK_oUDSS);
- 3 sets of K_o consolidated–undrained triaxial compression (CK_oUC) and triaxial extension (CK_oUE) tests on normally consolidated samples;
- 2 isotropically consolidated triaxial compression (CIUC) tests on normally consolidated samples;
- Several Recompression CK_oU triaxial compression and extension tests.

The Atterberg limits of the samples tested and plotted in Figure 2.5 generally lie slightly below and parallel to the A–line and classifies the soil as an ML–MH clayey silt. Grain size analyses indicate that the deposit consists of essentially two layers. This is clearly seen in Figure 2.6b which plots percent clay fraction (% $< 2\mu$m) versus depth below mudline. Samples above 14 ft have mostly silt size particles and less than 15% clay size while the lower layer has a finer grained silt fraction and significantly more clay size ($25 - 35\%$). The plasticity index versus depth below mudline, plotted in Figure 2.6a, is strongly related to the clay fraction. The upper layer has a lower clay content and is less plastic than the lower layer. The salt concentration data, plotted in Figure 2.6c, generally decreases with depth and is higher than seawater ($\cong$ 30 g/ℓ) in the upper material. There is a good correlation between the plasticity index and clay fraction as shown in Figure 2.7. This plot also clearly shows the differences in the index properties of the upper and lower layer soils.

Results from the oedometer and consolidation phase of DSS tests[4] show that the soil deposit is overconsolidated as shown in the Figure 2.8. It can be seen from this plot that the sediments are highly overconsolidated near the surface but that preconsolidation pressure decreases with depth. Preconsolidated sediment is commonly observed in the Beaufort Shelf (1982 & 1983 Proprietary reports; Young, 1986;

---

[4]Most of the Center's oedometer and DSS tests were performed at room temperature. Several special temperature controlled oedometers run at MIT (Sauls, et al., 1984; Yin, 1985; Young, 1986) indicate that the σ'_p measured at room temperature should be increased by 10% to represent the in situ σ'_p for the deposit at 0° to 1°C. Hence stress history profiles presented in this Chapter are corrected to 0° or 1°C.

Reimnitz, et al., 1980). Erosion of overburden would result in a constant difference between the preconsolidation pressure and the in situ vertical effective stress, which is not what is observed. Several mechanisms have been proposed which, acting alone or in combination, could be responsible for overconsolidating the deposit (Sauls, et al., 1984):

1. Ice loading and gouging could cause a highly variable pattern of overconsolidation;
2. Desiccation has been found to be significant in many offshore deposits;
3. Freezing and thawing cycles have been suggested as a possible cause of overconsolidation in the Beaufort Sea (Chamberlain, et al., 1978);
4. Wave action induces repeated shear stresses in ocean sediments (Madsen, 1978) which could result in preconsolidation;
5. Natural cementation between soil particles results in an increase in the measured preconsolidation pressure;
6. Secondary compression (aging) has been shown to cause preconsolidation (Leonards and Altschaeffl, 1964; Bjerrum, 1967) although not of the magnitude exhibited by Arctic silts.

The results from the consolidation, triaxial and direct simple shear test programs were collectively evaluated to present recommended normalized undrained strength parameters for design (Table 2.2) and to develop a SHANSEP strength profile for the deposit. The "strain compatibility" technique was applied using data from the triaxial compression, triaxial extension and direct simple shear modes of failure to get the final SHANSEP undrained strength profile shown in Figure 2.9. Conventional strength measurements based on mean UUC values (although scattered) agree with the SHANSEP design profile, while the field vane strengths were two times greater.

2.2.4 Smith Bay

As outlined in Section 1.4 the Center conducted an experimental test program on samples from two sites in Smith Bay (Young, 1986). Both sites consist of about

15–20 ft of silty clay overlying relict permafrost. The site nearer land (Site W) has a very thin layer of Holocene material over much stronger Pleistocene cohesive soils. The stratigraphy of the other site (Site T) is much more complex due to extensive ice gouging. Samples remaining from the original geotechnical investigation conducted by TETC were sent to MIT, where radiography, index tests and consolidation and strength tests were performed to supplement the TETC data. The CU strength tests included:

- 20 SHANSEP type CK_0UDSS tests on normally consolidated and overconsolidated material (11 at Site T and 9 at Site W) and 2 Recompression DSS tests;
- SHANSEP normally consolidated CIUC and CK_0UC tests at Site T;
- 2 overconsolidated SHANSEP CIUC tests at Site T;
- 8 Recompression CK_0U Triaxial Compression tests (4 at Site T and 4 at Site W).

The Atterberg limits of samples tested from both sites (Figure 2.10) lie above and parallel to the A–line. These deposits are therefore CL–CH silty clays rather than the ML–MH clayey silts found within the Soft Zone Area of Harrison Bay (Figure 2.5). The plasticity index at Site T decreases with depth whereas at Site W it is more uniform (Figure 2.11a). The liquidity index data, plotted in Figure 2.12, displays much more scatter in part due to the effects of ice gouging. At Site T, the liquidity index data is scattered in the upper region of the deposit and decreases in value and scatter at greater depths. At Site W, the liquidity index decreases less rapidly with depth. Figure 2.11 also shows convergence of liquidity index values for the portion of Site T (less gouged) with those for Site W (nongouged). At both sites the percent clay fraction is relatively uniform with depth and indicates a slightly higher clay content for Site W samples (Figure 2.11b). Figure 2.13 plots plasticity index versus clay fraction for the Smith Bay and Harrison Bay SZA samples. The Smith Bay values plot well

below the correlation established for the Harrison Bay samples and span a much smaller range of plasticity index. The pore fluid salt concentration is uniform with depth at both sites (Figure 2.11c). The percentage salt concentrations in the pore water of the soil at Smith Bay and Harrison Bay SZA allow the soil to exist unfrozen in–situ in spite of pore fluid temperatures reaching below freezing (29.5° to 34° F at Smith Bay and 28° to 31° F at Harrison Bay).

Estimates of preconsolidation pressure from oedometer tests and the consolidation phase of DSS tests were used to construct stress history profiles for both sites. At Site T, preconsolidation pressure increases gradually over the upper 8 ft of the deposit, with a large increase at greater depths (Figure 2.14). The progressive reduction in and scattered nature of the preconsolidation pressure approaching the mudline resulted from ice gouging effects. The stress history profile at Site W is much more uniform with a nearly constant preconsolidation pressure with depth (except for the upper Holocene layer; Figure 2.15). The two sites are presumed to have shared a common initial stress history, as values of preconsolidation pressure are compatible for Site W and the lower part of Site T (Figure 2.16).

The results from the consolidation, triaxial and DSS programs conducted by MIT and TETC were collectively evaluated in order to develop recommended undrained strength parameters for design. The final recommended SHANSEP undrained strength profiles for resistance to base sliding were developed for both sites using the SHANSEP parameters from the DSS program (Table 2.3). These results along with conventional strength test (UUC, Field Vane and Miniature Vane) results are plotted in Figures 2.17 and 2.18 for Sites T and W respectively. For Site T conventional strength test results are about 1.6 times greater than the SHANSEP c_u(DSS) values in the upper highly gouged zone. At Site W the conventional strength

test results are about 5 times greater than the SHANSEP c_u(DSS) values at relative elevation of 1 ft, and two times greater at relative elevation of 20 ft.

2.2.5 Summary

The results presented in this section clearly show that there are substantial differences in the nature of Arctic silts. The soil can vary from Holocene ML–MH clayey silt (Harrison Bay SZA) to Pleistocene CL–CH silty clay (Smith Bay). The preconsolidation pressure σ'_p and undrained shear strength c_u can decrease with depth as in the SZA of Harrison Bay or increase with depth as is the case in Smith Bay.

Research conducted at MIT also found that strengths from conventional c_u tests varies from reasonable to several times to high. In addition, CK_oU testing was found to give reasonable normalized behavior and also indicated that the Arctic silts exhibit significant anisotropy.

2.3 ISSUES AFFECTING THE FOUNDATION PERFORMANCE OF OFFSHORE ARCTIC GRAVITY STRUCTURES

2.3.1 Introduction

Oil exploration in the Alaskan Beaufort Sea was first performed from conventional drilling ships that are commonly used in more temperate waters (Figure 2.19a). However, the open water season only lasts about two months in the Beaufort Sea and therefore companies started to construct sand/gravel islands (Figure 2.19b). These islands can withstand large lateral ice forces and enable year–round drilling. The islands, however, are only economically feasible in shallow water (less than 50 ft) and can only be used once per exploration site.

As exploration moved to deeper water, caisson islands and mobile gravity structures were developed. The caisson islands are gravel or sand islands with reinforced caissons made of steel or concrete. The caissons are built on land and towed

to the drilling site where they are filled with dredged material such as sand and gravel (Figure 2.19c and d). Mobile gravity structures developed for the Beaufort sea can withstand large lateral ice forces and can also be reused at different exploration sites. These structures are usually towed to a site and then ballasted onto the seafloor or onto an underwater berm. Some of the typical structures used include hollow steel caissons filled with sand and reinforced tankers such as the SSDC (Figure 2.19e, f and g). Many of these structures, such as the CIDS and SSDC (Figure 2.19), spray sea water around them to create an ice barrier for additional protection against sea ice.

Production gravity platforms for the Arctic are still in the development stage. These structures will have to withstand the same lateral ice forces as exploration structures, but will have to be able to do it over a much longer period of loading and hence may require special design features and higher factors of safety. Some of the critical design issues with respect to the foundation soil include: stability of the foundation soil under gravity loads from the structure; transfer of the shear force due to ice loading to the foundation soil; ultimate resistance to large lateral ice forces and accumulated displacement under ice loading over a period of many years.

For both exploration and production gravity platforms the soil foundation problem will often consist of a large rigid gravity structure overlying a relatively thin layer of Arctic silt which is underlain by permafrost. This is shown schematically in Figure 2.12

2.3.2 Set Down Conditions (Gravity Loading)

The foundation conditions for Arctic gravity structures are unique because of the horizontal ice loads and also because the foundation's soil layer is thin compared to the width of a typical structure. In the case of vertical gravity loads, the large ratio of the structure width to the depth of soil layer (B/H > 15, see Figure 2.20) makes traditional bearing capacity analysis inappropriate for design. For Arctic gravity

structures the mechanism of failure consists of soil squeezing between the rigid structure and permafrost underlying the foundation soil layer.

Figure 2.21a illustrates the stress conditions that will exist within the foundation soil upon initial set–down of an Arctic gravity structure. The foundation soil will be subjected to significant radial shear stresses which may be accompanied by large radial deformations due to lateral squeezing. During this process the direction (given by the angle δ) of the major principal consolidation stress σ'_{1c} will rotate. The magnitude of rotation will depend on the location of a soil element relative to the centerline of the structure and its depth within the foundation layer. The magnitude and direction of the horizontal shear stress at a soil element will also depend on the element's location within the soil layer. As shown in Figure 2.21a, the horizontal shear stress changes in magnitude and orientation from the top of the soil layer to the bottom.

As part of the Center's effort in geotechnical engineering, a research project was initiated at MIT with the objective of developing reliable theoretical procedures for assessing the stability of Arctic gravity structures. Both analytical and numerical solutions were investigated for the initial set–down conditions and are presented in the paper, "Stability of Rigid Gravity Arctic Structures," by Baligh, et al., 1987. The following paragraphs present a brief summary of their findings.

A comprehensive review of available analytical solutions (Baligh, et al., 1987; Vivatrat and Watt, 1983) proved useful in providing basic information on the important mechanisms controlling the stability of rigid Arctic gravity structures. Some of the important results included:

1. Traditional bearing capacity analysis is frequently inappropriate because of the large B/H ratio of the problem;
2. A significant increase in bearing capacity can be realized if the structure is rigid and has a rough base;

3. If the soil–structure and soil–permafrost interface are sufficiently rough, the bearing capacity of thin layers increases significantly as the B/H ratio increases.

The analytic solutions are only applicable under idealized conditions (e.g., soil must be uniform, isotropic, rigid–perfectly plastic, etc.) that are generally very different from the actual situations encountered. However, they do provide a basis for conducting a rational numerical analysis of the problem. Such an analysis was performed by Baligh, et al., 1987 using the finite element program ADINA[5] (Bathe, K. J., 1976) which is a general purpose linear and nonlinear, static and dynamic finite element analysis code.

The problem geometry and boundary conditions used in their analysis is shown in Figure 2.22. It consists of a soil layer, of thickness H, supporting a rigid rough circular surface footing with a diameter, B = 400 ft. The finite element mesh consisted of 6 noded isoparametric two–dimensional solid elements. The response of the soil layer to applied loading was represented by a bilinear elasto–plastic model based on the Von Mises yield criterion (Figure 2.22). The model is described by four material properties: elastic Young's modulus E, post peak Young's modulus E_t, yield strength k and Poisson's ratio ν. The analysis consisted of a parametric study which led to the following conclusions:

1. Soil yielding develops at early stages of loading (i.e. at high values of the factor of safety) and progresses from the edge zone to the soil under the centerline of the structure;

2. Depending on the factor of safety, compressibility (ν) of the soil and the B/H ratio the foundation soil can undergo very large shear strains, particularly near the edge of the structure;

3. The strain hardening characteristic of the soil has a major effect on the stability of gravity structures. Bearing capacity can be seriously overpredicted if a small degree of strain hardening is assumed. This is primarily due to the very large shearing strains in the squeezed soil close to its contact with the footing and with the underlying permafrost;

---

[5]ADINA is an acronym for Automatic Dynamic Incremental Nonlinear Analysis.

4. For a strain hardening soil, soil compressibility has a major effect on predictions. Increasing Poisson's ratio from 0.45 to 0.499 resulted in a seven–fold increase in the average vertical stress calculated at a specified value of the settlement of the rigid structure;

5. For non–homogeneous soil deposits the mode of soil squeezing can be quite complicated and depends on the undrained shear strength profile of the deposit. If the soil layer contains a zone of weak soil (as is typical in the Soft Zone Area of Harrison Bay) the bearing capacity of the structure is primarily controlled by the undrained shear strength and post peak behavior of the weaker soil. If this soil strain softens at larger strain levels the bearing capacity can be significantly reduced.

2.3.3 Ice loading

Ice loads will impose an inclined and eccentric load on the foundation of an Arctic gravity structure. However, the sliding mode of failure becomes predominant when the horizontal ice load is a large fraction of the horizontal sliding resistance of the foundation soil (Vivatrat and Watt, 1983). In this case, application of the ice load causes incremental horizontal shear stresses within the foundation soil all acting essentially in the same direction. These can produce large rotations in the direction of the major principal stress within most of the foundation soil. An assessment of the limiting equilibrium condition against horizontal sliding requires knowledge of the available strength for σ'_{1f} acting at $\delta = 45 + \phi'/2$ degrees to the vertical direction (Figure 2.21b). As shown schematically in Figure 2.21b the failure surface may occur within the foundation soil and not necessarily at the soil–structure interface. This is particularly true if the soil profile is nonhomogeneous where a weak soil layer exists at some depth below the mudline (as is the case in the Soft Zone Area of Harrison Bay).

Figure 2.23 provides an additional illustration of the complicated nature of the shear stresses acting within the foundation soil under the combination of gravity and ice loads. This figure shows the distribution of the shear stresses acting at the soil structure interface due to application of the gravity and ice loads. Due to gravity load, W, radial shear stresses τ_1, symmetric with respect to the center line of the structure, are created due to radial deformations of the soil. Incremental horizontal shear stresses

of a magnitude τ_2 result from the application of the horizontal ice force, H. The magnitude of the final shear traction vector τ_f at the base of the structure will thus vary depending on the location along the circumference as described by the angle θ and the radius r.

The incremental shear stress τ_2 required to resist the horizontal force H also varies along the base depending on r and θ (although assumed constant for the diagram in Figure 2.23). Reliable estimates of τ_2 are complicated by the following factors (Baligh, et al., 1985b):

1. The nonlinear, stress (or strain) history dependence of soil behavior at or near the interface resulting in a lack of symmetry in the solution;
2. Possible time dependent changes in soil behavior due to consolidation under vertical loading;
3. Shear stresses acting in the radial direction are necessary for vertical equilibrium and changes in the radial shear stresses due to horizontal loading will affect vertical equilibrium. Therefore, horizontal ice loading cannot be treated without consideration of vertical equilibrium.

Clearly the stress conditions within the foundation soil due to gravity and ice loading are very complicated. A comprehensive stability investigation requires a three–dimensional analysis which takes into consideration how the soil behaves under the stress conditions described above. In addition, the time dependent change in soil behavior due to consolidation under the gravity load requires reliable estimates of the consolidation properties of the soil and the time between initial set–down and application of the design ice loads.

2.4 EXPERIMENTAL REQUIREMENTS

One of the Center's geotechnical research objectives is to develop a special laboratory shear testing device to simulate stress–strain–strength behavior of soil under very complex stress conditions imposed during ice loading of an Arctic gravity structure. From the discussion on these stress conditions in the previous section, it is

clear that such a device requires special capabilities. The device's primary requirement is to be able to allow the principal stresses to rotate during shear. Specifically, it must be able to apply a vertical stress and two independent horizontal shear stresses to a soil specimen. The vertical stress and the first shear stress represent the stresses imposed on an element within the foundation soil under gravity loading. The second shear stress represents the ice loading force.

The device will require the capability of consolidating a soil sample under both the vertical stress and the first horizontal shear stress. In addition, it must be able to subsequently shear the sample undrained by applying a second horizontal shear stress at an angle θ relative to the horizontal consolidation shear stress between 0 and 180 degrees (Figure 2.24). The second shear force is applied under undrained conditions because this represents the critical case for stability of the structures during application of the ice loads. With these capabilities the device will be able to simulate a variety of conditions under which soil elements within the foundation of an offshore Arctic gravity structure are subjected[6]. This includes conditions where (see Figure 2.23 for reference):

1. The horizontal shear force applied during consolidation and the subsequent shear force due to ice loading act in the same direction ($\theta = 0°$ case);
2. The horizontal consolidation and subsequent ice loading shear forces act in opposite directions thereby resulting in a reversal in the direction of shear stress acting on the sample ($\theta = 180°$ case);
3. The angle, θ, between the two horizontal shear forces during a test is between 0 and 180 degrees.

It is important that no restrictions be imposed on a specimen's ability to undergo shear strains during application of the two horizontal shear forces. When the

[6]From the plan view of the soil–structure interface shown in Figure 2.23, it is clear that the problem has an axis of symmetry through the center of the interface. Therefore, only those soil elements within one–half of the interface ($0° \leq \theta \leq 180°$) need to be considered for laboratory testing.

second shear force is applied to the specimen at some angle θ relative to the first shear force, the sample should be free to strain in any direction. In other words, the sample should not be constrained to undergo shear strains that are coincident with application of the second shear force.

In general the foundation soil will consolidate under the gravity loading stresses. However, the time between initial set–down of an Arctic gravity structure and application of the design ice forces may not be sufficient to allow full consolidation. The time required to reach a reasonable degree of consolidation in the field depends on the consolidation properties of the soil, the thickness of the soil layer and whether artificial drainage is used within the foundation soil. Hence, the special shear device should also have the ability to apply the second shear force before a soil specimen fully consolidates under the gravity loading stresses.

Finally, it is important that the device test specimens that are of a reasonable size and relatively easy to prepare. The specimen size to be tested is an important issue in the case of testing Arctic soils because it is more expensive to obtain these samples than those taken in more hospitable climates. Therefore, the less soil used per test, the more cost efficient the testing program becomes. It should also be fairly easy to trim the specimens and place them in the apparatus with a minimum amount of disturbance.

The remainder of this section discusses the issues related to the experimental requirements of a shear testing device to simulate the stress conditions within the foundation soil of an Arctic gravity structure. Existing laboratory shear devices will be reviewed, with a discussion of their limitations with respect to the requirements presented in the previous paragraphs. The need for development of a special direct simple shear device is also presented.

2.4.1 Review of Existing Experimental Capabilities

Most soils are inherently anisotropic and therefore their response to loading will in part depend on the orientation of the principal stresses during shear. In addition, further anisotropy may be induced by stress changes. Definitions for the various components of anisotropy have been changing over the past decades (e.g. Casagrande and Carillo, 1944; Hansen and Gibson, 1949; Ladd, et al., 1977; Jamiolkowski, et al., 1985; Ladd, 1988). The definitions presented here are based on those given by Ladd (1988). Initial anisotropy denotes differences in the stress–strain–strength response of a K_o consolidated soil with variations in the applied principal stress direction (δ) during shear. Evolving anisotropy describes how the initial cross anisotropic properties of the K_o consolidated soil change due to subsequent stressing and straining.

Initial anisotropy of a cross anisotropic natural soil (i.e., one–dimensional (K_o) strain history) has two components: 1) inherent and 2) initial shear stress anisotropy. Inherent anisotropy arises from a preferred soil structure developed during one–dimensional (K_o) deposition. This can be observed at the micro level where preferred particle orientations and interparticle forces develop in soils and at the macro level for certain soils like stiff fissured clays and varved clays. Initial shear stress anisotropy describes the directionally dependent undrained response of soils whenever shearing starts from an anisotropic initial state of stress (i.e., $K_o \neq 1$). It arises from the fact that different increments of shear stress are required to produce failure as the major principal stress at failure varies between the vertical ($\delta = 0°$) to the horizontal direction ($\delta = 90°$).

In practice we are interested in measuring the combined initial anisotropy resulting from the inherent and initial shear stress components. Evolving anisotropy cannot be realistically simulated by common laboratory shear devices because of the complexity of the principal stress rotations, as illustrated in Figure 2.25.

When comparing laboratory shear devices available for testing, two variables are commonly used to describe basic differences in the applied stress system (applied state of stress): 1) direction of the applied major principal stress relative to the vertical (depositional) direction denoted by the δ angle; and 2) the relative magnitude of the intermediate principal stress defined by $b = (\sigma_2 - \sigma_3)/(\sigma_1 - \sigma_3)$. Figure 2.26 illustrates the combinations of δ and b that can be achieved by laboratory shear devices (this figure was orginally developed by Germaine, 1982). Changes in the values of δ and b lead to different stress–strain–strength responses due to anisotropy and the σ_2 effect, respectively.

The stress conditions acting on soil elements within the foundation soil of an Arctic gravity structure cannot be completely represented on the b–δ plot of Figure 2.26. During gravity loading the major principal stress will rotate from the vertical ($\delta = 0^\circ$) to some angle δ depending on a soil element's location. The b value will be for plane strain shearing and its exact value will depend on the behavior of the soil being tested. The various combinations of b and δ for the different soil elements during gravity loading will plot along the plane strain line in Figure 2.26 (i.e., the line from symbol PSC to PSE).

During ice loading the stress conditions for most of the soil elements cannot be shown in Figure 2.26. Two exceptions include those elements where: 1) the gravity loading and ice loading shear stresses act in the same direction ($\theta = 0^\circ$), for which the δ angle will increase; and 2) the gravity loading and ice loading shear stresses act in opposite directions ($\theta = 180^\circ$), hence the δ angle will decrease and may even change direction. For all other elements, the gravity loading and ice loading shear stresses act at an angle θ ranging from 0 to 180 degrees between them. This changes the orientation of the principal stress with respect to not only the δ angle, but also changes in its orientation in the plane perpendicular to the δ plane (i.e., σ_1–σ_2 plane).

The following paragraphs describe the capabilities of several laboratory devices and their limitations with respect to simulating the stress conditions within the foundation soil of an Arctic gravity structure.

2.4.1.1 Triaxial Device

One of the most commonly used shear devices to evaluate the stress–strain–strength behavior of soils is the triaxial cell. The device is used to test solid circular cylinders and can (with some difficulty or use of special triaxial devices) achieve one–dimensional consolidation with measurements of K_o. However, the major principal stress can act only either in the vertical direction ($\delta = 0°$) or the horizontal direction ($\delta = 90°$). Furthermore, with $\delta = 0°$ the resulting test is triaxial compression (TC, b = 1) and with $\delta = 90°$, the test is triaxial extension (TE, b = 90). Hence the triaxial device cannot provide definitive data on anisotropy even in the vertical and horizontal directions let alone intermediate δ angles (see Figure 2.26).

2.4.1.2 True Triaxial Apparatus (TTA)

The true triaxial apparatus was developed to independently control the three principal stresses acting on prismatic or cubical specimens. The device is ideally suited to study σ_2 effects, but has very limited capability to study anisotropy since σ_1 must act along one of the three reference axes x, y or z (i.e. it is restricted to $\delta = 0°$ and $\delta = 90°$, see Figure 2.26). In addition relatively few devices have been developed to test cohesive soils as they are usually more complex than for sand testing (Jamiolkowski, et al., 1985).

2.4.1.3 Plane Strain Devices

Plane Strain devices have been constructed to conduct K_o consolidated tests on soils for plane strain shearing at $\delta = 0°$ (PSC) and $\delta = 90°$ (PSE). But these devices, like the triaxial cell, cannot perform tests at intermediate δ angles. For plane strain tests the b value is a function of the soil behavior during shear and cannot be determined before conducting a test.

2.4.1.4 Torsional Shear Hollow Cylinder (TSHC).

Figure 2.27 shows the idealized stress conditions that can be achieved by the torsional shear hollow cylinder (TSHC) device ($\alpha \equiv \delta$). Application of an axial load W, torque M_t, and internal and external pressure P_i and P_o generates stresses σ_z, σ_r, σ_θ and $\tau_{\theta z}$ in the wall of the specimen. By controlling these stresses the magnitude of the three principal stress σ_1, σ_2 and σ_3 can be independently controlled (an hence the value of b), together with the orientation of the major principal stress direction (δ angle). Therefore, the device has the theoretical ability to cover the entire b–δ space shown in Figure 2.26. Practically, however, the device cannot be used for testing all combinations of b and δ due to nonuniformities of stress across the specimen wall which arise from the specimen's curvature as well as to end restraints at the top and base of the sample. The problem becomes more serious as the difference in the magnitude of the internal and external pressures increase. Hight, et al., (1983) discuss these problems in more detail and present information on selecting an optimal sample geometry to partially reduce the nonuniform stress conditions.

If the external and internal pressures are held equal, then a unique relationship exists between b and δ. In this case $\sigma_r = \sigma_\theta = P_o = P_i$ and $b = \sin^2\delta$. Consequently, changes in the δ angle must be accompanied by changes in the intermediate principal stress condition, which complicate interpretation of the data. Saada and Townsend (1981) discuss the influence of device geometry on nonuniformities for testing with equal internal and external pressures and indicate that this type of TSHC can test conventional tube samples of cohesive soils.

Imperial College has developed a TSHC (Hight, et al., 1983; Symes, 1983) that has been used to investigate anisotropy and the effects of principal stress rotation (i.e. vary δ with constant b). To date, however, the device has been restricted to drained and undrained tests on medium–loose sand.

In spite of its apparent diverse capabilities the TSHC cannot be used to simulate the stress conditions within the foundation soil of an Arctic gravity structure. In theory it could be used to simulate the simple shear straining of soil elements under gravity loading (i.e., allowing rotation of the major principal stress during shear). However, only tests on loose sand have been attempted and were not completely successful (Shibuya and Hight, 1987). Since the device is restricted to allow only rotations of the major principal stress (i.e., the angle δ in the σ_1–σ_3 plane), it cannot even in theory be used to test specimens under the combined gravity and ice loading conditions. In principle, the device can be used to simulate elements where $\theta = 0^\circ$ and $\theta = 180^\circ$ but again, to date, it is not capable of conducting undrained tests on undisturbed natural clays with rotation of the major principal stress .

2.4.1.5 Directional Shear Cell (DSC)

The Directional Shear Cell was specifically developed to measure anisotropy in sands (Arthur, et al., 1977) and later in clays (Germaine, 1982). It is a flexible boundary plane strain device which has the unique capability of controlling the major principal stress direction by varying the normal stress and shear stress acting on four faces of a cubical sample contained between two rigid end platens (Figure 2.28). The device employs shear sheets for applying τ_a and τ_b, pressure bags for applying the normal stresses σ_a and σ_b and radiographic–photographic technique for measuring the distribution of strain magnitudes and directions. Although the device is fairly complex to operate, it represents a unique research tool for studying anisotropy (i.e., tests with different δ angles and b equal to the plane strain value, see Figure 2.26; Ladd, 1981).

The DSC cannot simulate the stress conditions within the foundation soil of an Arctic gravity structure. It is limited to studies where the δ angle varies between 0 and 90 degrees but cannot handle situations where two horizontal shear stresses are applied to a soil element at an angle θ between them. In addition, the DSC like the

TSHC is a very complex device that is not yet ready for routine testing of natural cohesive soils.

2.4.1.6 Geonor Direct Simple Shear

The Geonor Direct Simple Shear (DSS) apparatus has been used extensively for direct simple shear research and testing at MIT and the Norwegian Geotechnical Institute (NGI). The apparatus uses a circular wire–reinforced rubber membrane which allows specimens to be consolidated under K_o conditions. Specimens are sheared either drained or undrained by increasing the horizontal shear stress τ_h (Figure 2.29a). For K_o consolidated–undrained tests the vertical effective stress (σ'_v) is varied to maintain constant volume. The state of stress cannot be defined solely from knowing the values of τ_h and σ'_v. In addition, the device cannot apply complementary shear stresses on the specimen sides, resulting in a nonuniform state of stress. In spite of these problems the Geonor DSS offers important practical advantages compared with other shear devices for design problems involving sedimentary clays. Experience obtained over 20 years of DSS testing performed in conjunction with design problems involving construction of embankments, tanks, etc., suggest that DSS testing offers the following advantages:

1. During consolidation prior to shear, one easily obtains the same compression curve and coefficient of consolidation data as gained from conventional incremental oedometer tests (Ladd, 1981);

2. The measured values of maximum horizontal shear stress (τ_h max.) give a fairly reliable estimate of the undrained shear strength (c_u) appropriate for undrained stability and bearing capacity analysis, for example, Ladd and Foott (1974) and Ladd, et al. (1977);

3. The measured values of undrained Young's modulus (E_u) give a good indication of potential displacements due to in situ undrained shear deformations (Ladd, et al., 1977);

4. Tests are easy to run, less liable to experimental problems and, most important for testing Arctic soils, uses little soil compared to triaxial testing and other shear devices.

The Geonor DSS used at MIT is described in Appendix E. Appendix A presents a detailed literature review of direct simple shear testing with particular emphasis on monotonic testing of normally consolidated cohesive soils. The remainder of this section will focus on the device's capabilities with respect to simulating the stress conditions within the foundation of an arctic gravity structure.

The horizontal failure mode of shearing in the Geonor DSS is especially relevant to the ice loading condition and can be used to simulate the stress conditions due to the combined gravity and ice loading for two sets of soil elements. The device is capable of applying an independent horizontal shear stress to specimens during consolidation. The specimens can subsequently be sheared undrained by increasing τ_h at a constant rate of strain either in the same direction in which the horizontal consolidation shear stress acts or in the opposite direction (Figure 2.29b). These two types of tests simulate the conditions for those soil elements within the foundation where $\theta = 0^\circ$ and $\theta = 180^\circ$ respectively (see Appendix E for details on this testing procedure). But it cannot be used to simulate the conditions for all those elements where θ is in between 0 and 180 degrees.

In summary, the Geonor DSS offers many appealing features that are useful for conducting an experimental program on Arctic soils. Its testing capabilities are limited with respect to simulating the stress conditions within the foundation soil of an Arctic gravity structure. However, it provides several features that can be used for the basis of designing a special shear apparatus with the full capabilities to test soil elements with θ ranging from 0 to 180 degrees.

2.4.1.7 Gyratory Shear Apparatus

Casagrande and Rendon (1978) designed and constructed a gyratory simple shear apparatus in which cycle shear stresses could be applied in multidirectional loading conditions. The purpose of the device, built at Harvard University, was for studying the liquefaction behavior of sands. It is capable of conducting reciprocating

cyclic direct shear tests and gyratory shear tests. Figure 2.30 shows the basic mechanisms of these two types of tests. In reciprocating shear tests the top of a circular specimen is subjected to a unidirectional cyclic shear force, whereas in the gyratory shear test the shear force acting on the top of the sample rotates through 360 degrees. Figure 2.31 shows a schematic of the apparatus illustrating how the sample is confined and how the gyratory and reciprocating forces are applied to the sample.

The gyratory simple shear apparatus has the unique ability of applying a multidirectional horizontal shear stress to a specimen. Yet the device is not suitable for testing specimens under the stress conditions acting within the foundation soil of an Arctic gravity structure. The device can apply only one horizontal shear force and not two independent horizontal shear forces as required for the Arctic problem. Furthermore, it appears that the horizontal shear force cannot be varied during a test, thus it cannot even be used to conduct undrained shear to failure at a constant rate of strain.

2.4.1.8 Two–Directional Simple Shear Apparatus

Following Casagrande and Rendon's (1978) work, Ishihara and Yamazaki (1980) at the University of Tokyo built a two–directional simple shear apparatus to conduct multidirectional shaking of sands for liquefaction studies. This device, shown in Figures 2.32 and 2.33, is capable of applying two horizontal cyclic shear forces to the top of a circular specimen in two mutually perpendicular directions. As shown in Figure 2.33 the load is transmitted to the specimen by way of a specially designed load carriage fitted to the top cap of the cell. The motion of the load carriage is restrained to a movement in the horizontal plane by guide ball bearings.

A variety of shearing motions can be obtained by combining the two horizontal shear forces acting on the specimen. Two types of tests that can be

conducted include (Ishihara and Yamazaki, 1980):

1. Rotational Simple Shear Test.
   This type of test employs a resultant motion in the horizontal plane tracing circular or elliptic patterns as illustrated in Figure 2.34a. To produce the circular pattern, sinusoidal simple shear motions in two mutually perpendicular directions are programmed to have equal amplitude. In the elliptic pattern, different amplitudes are employed to execute sinusoidal simple shear motion in two mutually perpendicular directions. In both cases, one component of motion is programmed to start one quarter of a cycle later than the other so that two motions were 90 degrees out of phase with each other. As an extreme case, one component can be reduced to zero thereby reverting to unidirectional simple shear.

2. Alternate Simple Shear Test.
   This type of test merely employs alternate excursions of sinusoidal simple shear motion in two mutually perpendicular directions. One component of motion is programmed to start one full cycle later than the other. Different amplitudes are also employed between the two components of cyclic simple shear. These patterns of motion are illustrated in Figure 2.34b.

Like the gyratory shear apparatus this device has unique capabilities but it cannot be used to simulate the stress conditions within the foundation soil of an Arctic gravity structure. It has the added flexibility of applying the multidirectional shear force through two independent horizontal forces, but these forces are fixed to act in mutually perpendicular directions. At best the device may be able to conduct tests where $\theta = 0$, 90 and 180 degrees but it cannot be used to conduct tests for θ between 0° to 90° and 90° to 180°. In addition, like the gyratory shear apparatus, this device was built for the specific purpose of conducting liquefaction tests on sands and it is not clear how simple it would be to conduct consolidated–undrained tests on cohesive soils.

2.4.2 Need for Development of a New Apparatus

It is clear from the review of existing experimental apparatuses in the previous section that a new laboratory shear device needs to be developed in order to conduct tests which simulate the stress conditions within the foundation soil of an Arctic gravity structure. The Geonor DSS offers the best capabilities upon which to base the

design of a new apparatus. As outlined in Section 2.4.1.6, its horizontal failure mode of shearing is especially relevant to the ice loading condition and its many practical advantages over other devices make it a very cost effective apparatus. However, it is not feasible to make modifications to the Geonor DSS so that it can be used to conduct the tests necessary for the Arctic gravity structure problem.

In order to conduct experiments at θ angles between 0 and 180 degrees, it is necessary to have either the top of the sample displace freely in a horizontal plane relative to the bottom or vice–versa. During shear in the Geonor DSS the bottom of the sample is held fixed and the top is constrained to displace relative to the bottom in one direction (Figure 2.29). This is where the problem in trying to modify the Geonor DSS lies. It would be very difficult to change the top loading platens in the Geonor so that the additional degree of freedom is made available. An entire loading system would have to be built so that the first shear force could be applied to the sample at various angles θ relative to the direction of application of the second shear force. Also the load yoke on the Geonor would have to be changed so that the second shear force could be applied while allowing the sample to displace freely in a horizontal plane (no restrictions should be placed upon the specimen's ability to undergo shear strains during application of the two horizontal shear forces). Finally, a new instrumentation system would have to be designed to keep track of the sample displacements in the horizontal plane.

It is evident that it would require major modifications and additions to the Geonor DSS to obtain a device suitable for the Arctic gravity structure problem. Furthermore, it is not clear if changing the top loading platen to allow the extra degree of freedom in the horizontal plane is even feasible. Taking all this into consideration it was decided that a new apparatus should be built using the basic principles of the Geonor DSS shearing mode as a guide for designing the new device. The new device, called the Multidirectional Direct Simple Shear (MDSS) apparatus, is described in

detail in Chapter 3 and Appendix B. Section 2.4.1.6 gives only a brief review of direct simple shear testing and since the new apparatus is based in principle on the Geonor DSS, a detailed literature review of direct simple shear testing, with particular emphasis on monotonic testing of normally consolidated cohesive soils, is presented in Appendix A.

TABLE 2.1: Basic Steps in Application of the SHANSEP Design Procedure for Estimating the Initial In Situ Undrained Strength Profile (from Ladd, 1984)

1. Subdivide the soil deposit into representative layers based on boring logs, in situ testing, index properties, etc.

2. Develop the "best estimate" and range in the stress history profile using a combination of lab consolidation tests to measure σ'_p, results from the in situ tests (e.g., field vane and/or piezo–cone penetrometer) and knowledge of the local geology.

3. Decide what types of laboratory CK_oU shear tests best model the field stress conditions and the range of OCR values for which normalized soil properties are required. (Note: MIT includes direct simple shear tests in all offshore programs since they require the least amount of soil and yield average strengths appropriate for stability analysis.

4. Perform the CK_oU test program, first checking that normalized behavior applies by varying the ratio σ'_{vc}/σ'_p and then determining the influence of overconsolidation ratio.

5. Compare the results of step 4 to data for other deposits of similar geological composition and then select the best estimate and range in the NSP versus OCR relationship.

6. Apply the NSP relationships to the in situ stress history. For example at any given depth $c_u = \sigma'_{vo} \cdot c_u/\sigma'_{vc}$ corresponding to the OCR $= \sigma'_p/\sigma'_{vo}$ at that depth.

Table 2.2: Selected SHANSEP Undrained Strength Parameters for Mukluk Proximal, Harrison Bay (from Yin, 1985).

z (ft)	σ'^{*}_{p} (kg/cm^2)	S	m
0-6	4.0 ± 0.4SD	0.30	0.77
6-11		0.24	
11-14	2.58 ± 0.3SD at ≈ 13 ft		
14-25	1.14+0.022z		

*z in ft

Table 2.3: Selected SHANSEP Undrained Strength Parameters for Sites T and W, Smith Bay (from Young, 1986).

Site	RE (ft.)	Mode of Shear	S	m	Remarks
T	2-14	TC q_f	0.32	0.76	From CIUC @ OCR=1, 2, 5
	<8 (gouged)	DSS τ_h	0.28	0.73	From DSS @ OCR=1, 8, 16
			0.24	0.73	Minimum values
	>8 (nongouged)	DSS τ_h	0.24	0.71	Best estimate
			0.28	0.73	Max. value
W	1-20	TC q_f	0.32	0.76	From Site T test program
		DSS τ_h	0.24	0.71	From DSS @ OCR=1, 5, 10, 20

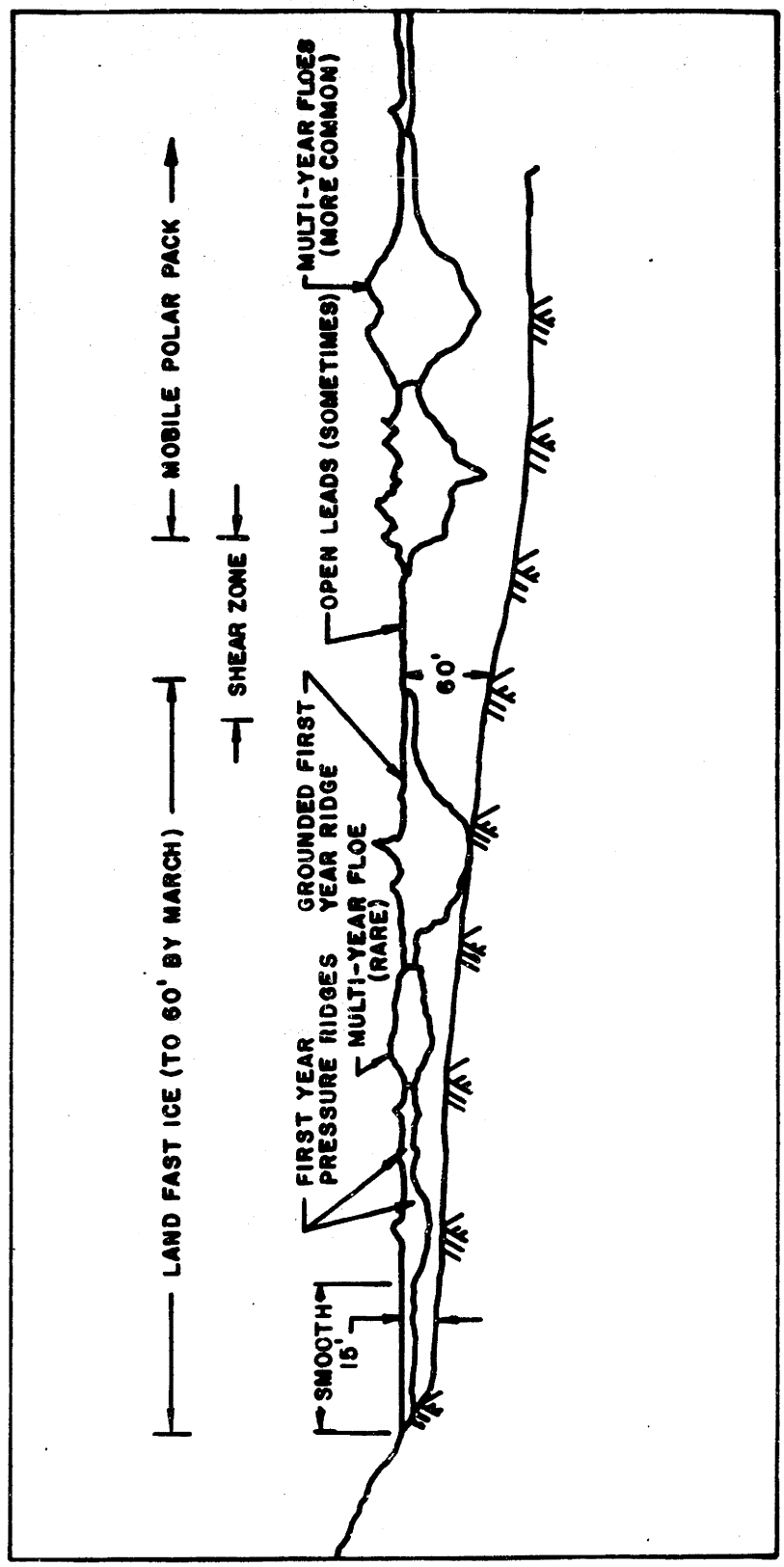

Figure 2.1: Typical Ice Features in the Beaufort Sea (after Croasdale and Marcellus, 1978).

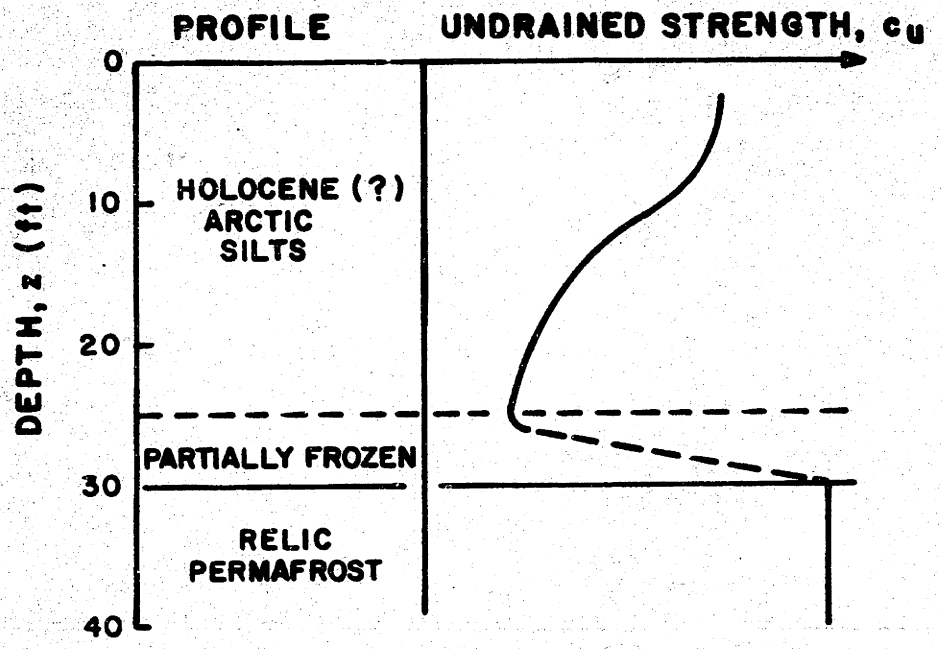

Figure 2.2: Harrison Bay "Soft Zone Area" Soil Profile (after Ladd, 1984).

(a) Effective Stress Paths During Undrained Shear

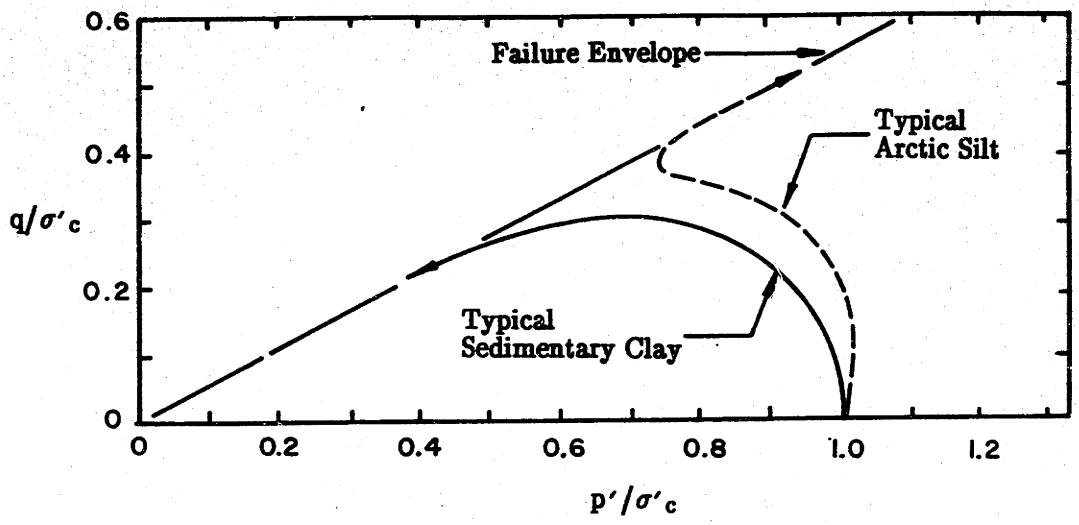

(b) Results from CIUC Tests on Arctic Silts from Harrison Bay Soft Zone Area.

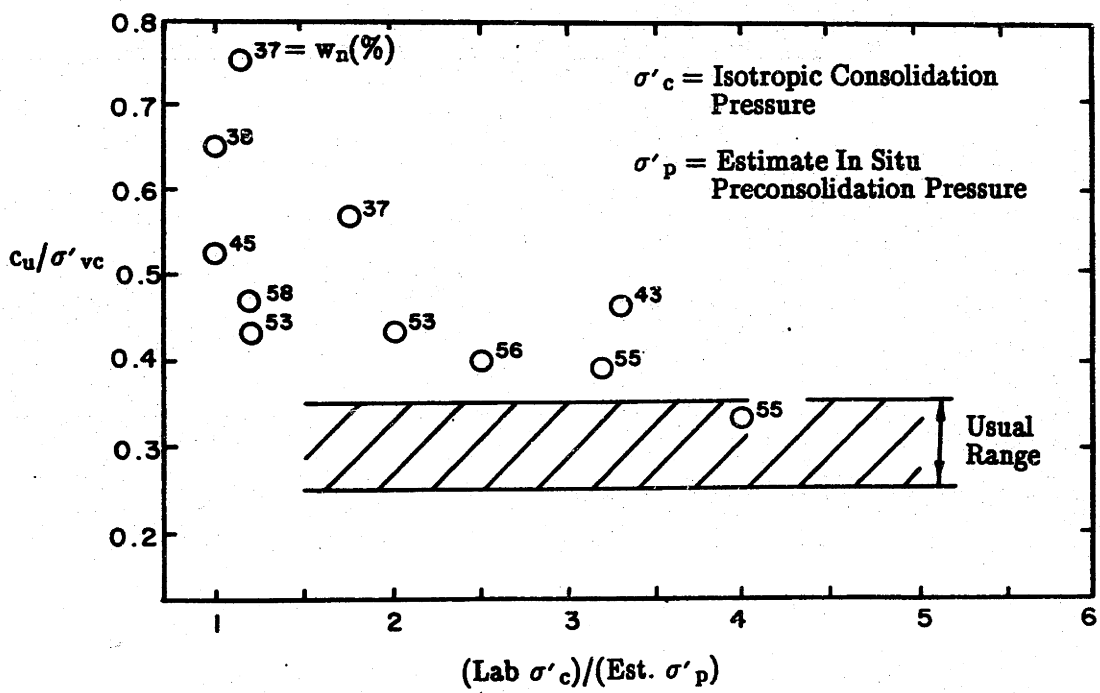

Figure 2.3: Undrained Shear Behavior of Normally Consolidated Sedimentary Deposits from CIUC Tests (after Ladd, et al., 1984).

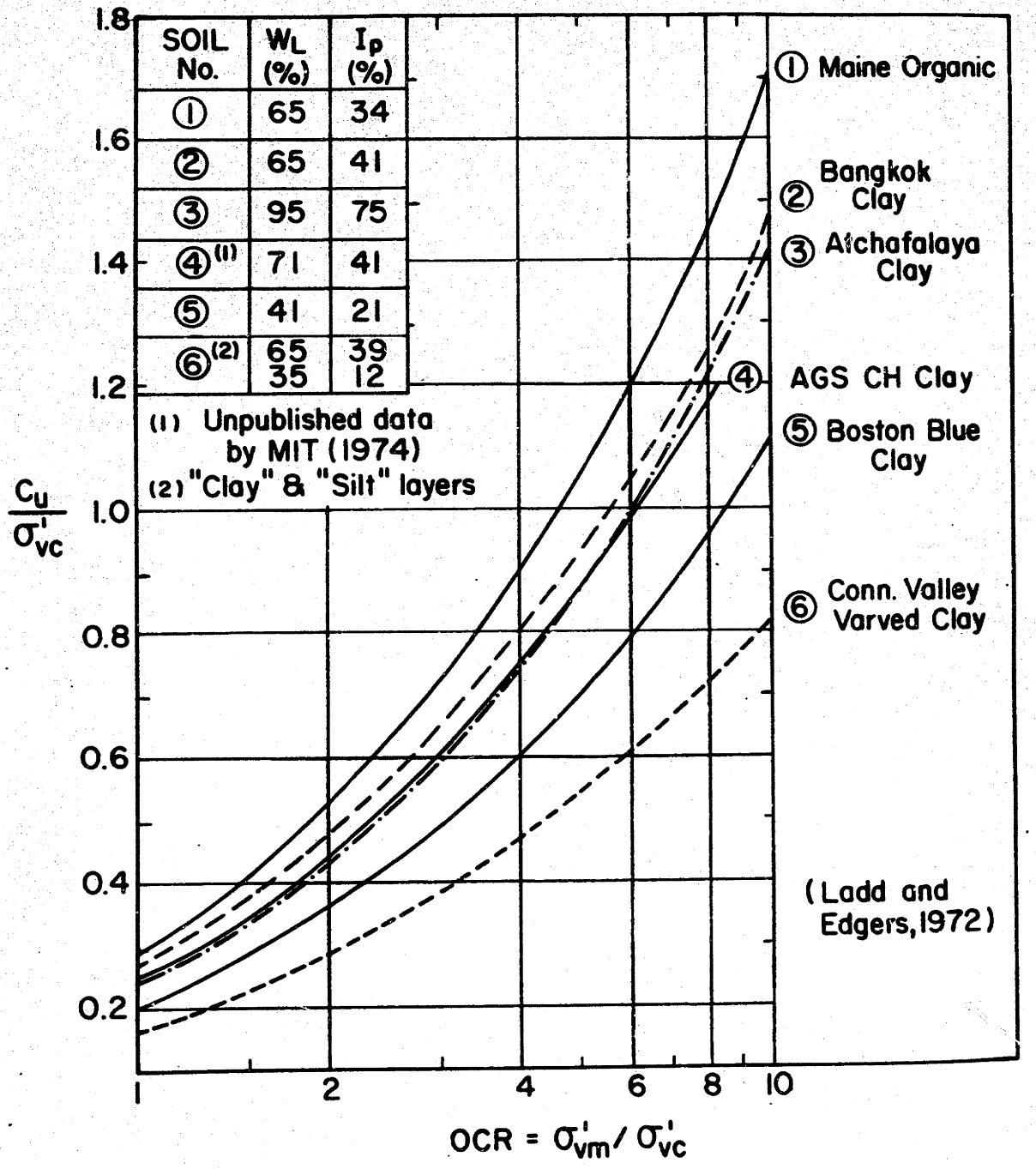

Figure 2.4: Undrained Strength Ratios versus OCR from CK_oUDSS Tests on Six Clays (from Ladd, et al., 1977).

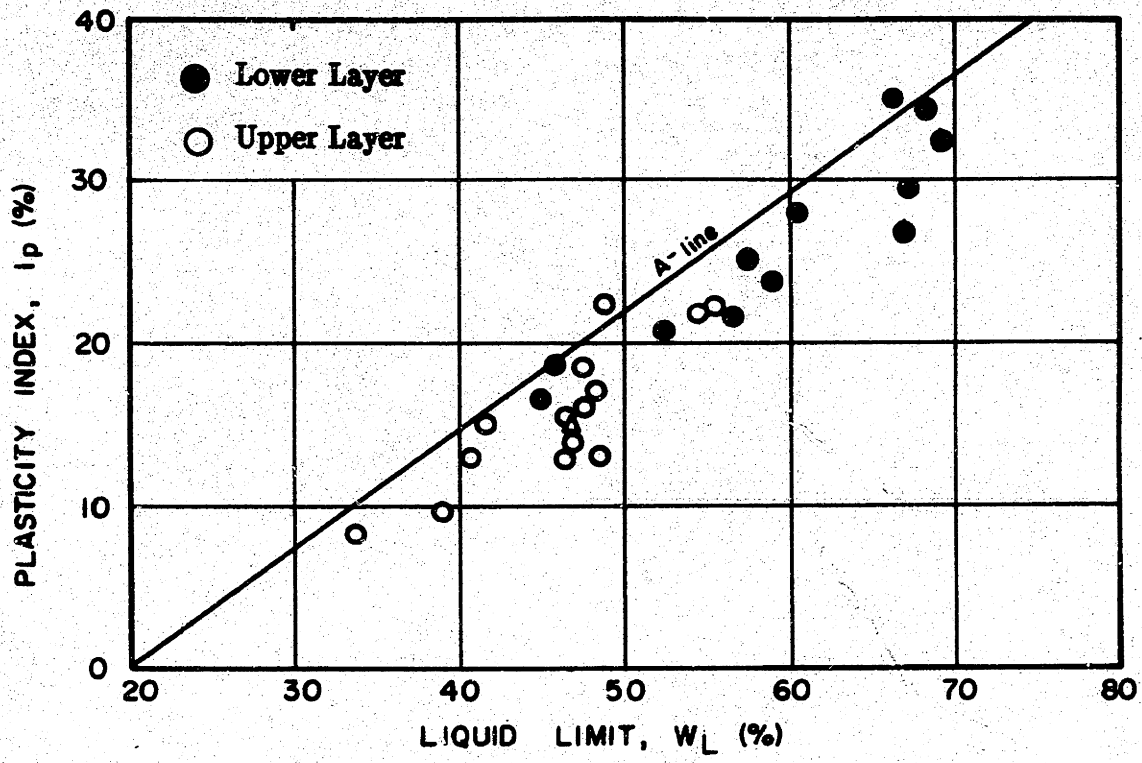

Figure 2.5: Plasticity Chart for Mukluk Proximal Samples, Harrison Bay (from Ayan, 1985).

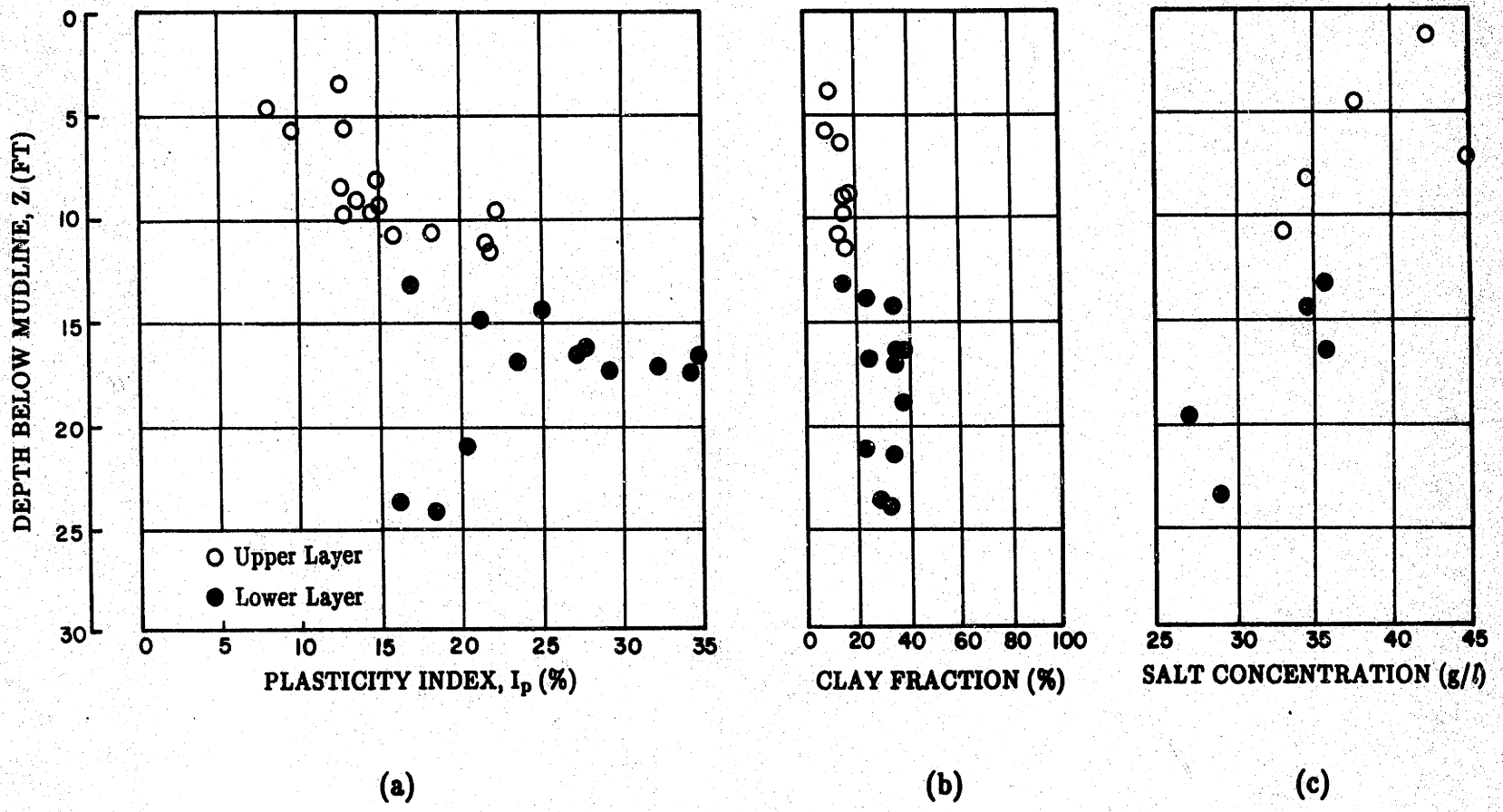

Figure 2.6: Profiles of Plasticity Index, Clay Fraction and Salt Concentration for Mukluk Proximal, Harrison Bay (after Ayan, 1985).

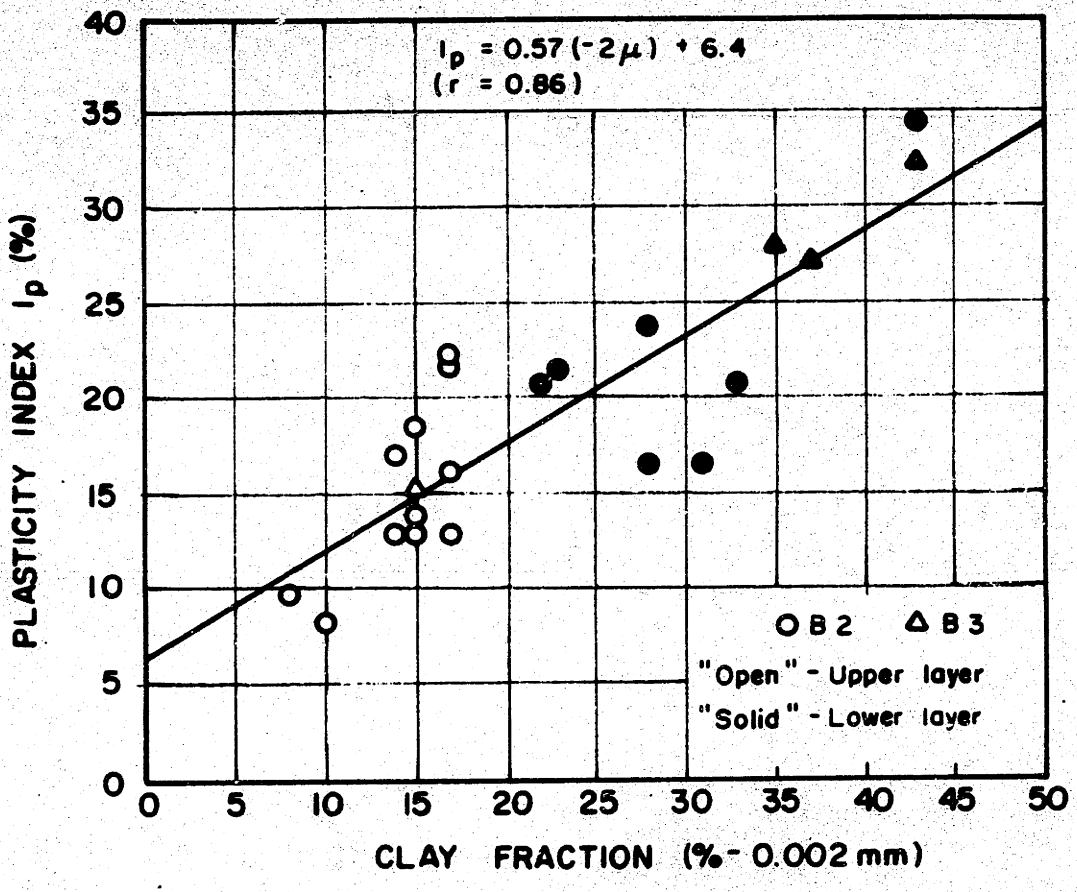

Figure 2.7: Plasticity Index versus Clay Fraction for Mukluk Proximal Samples, Harrison Bay (from Ayan, 1985).

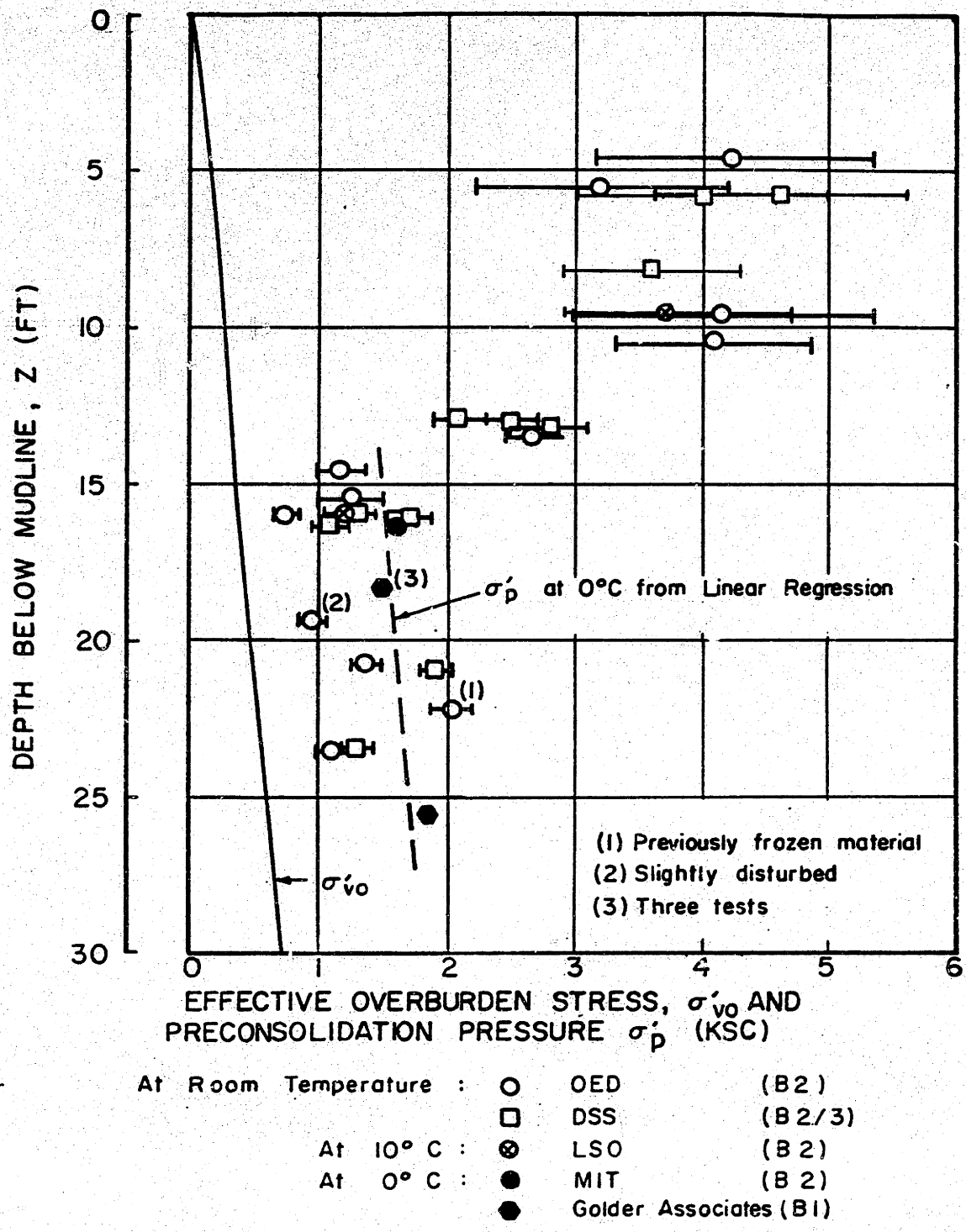

Figure 2.8: Stress History for Mukluk Proximal, Harrison Bay (after Yin, 1985).

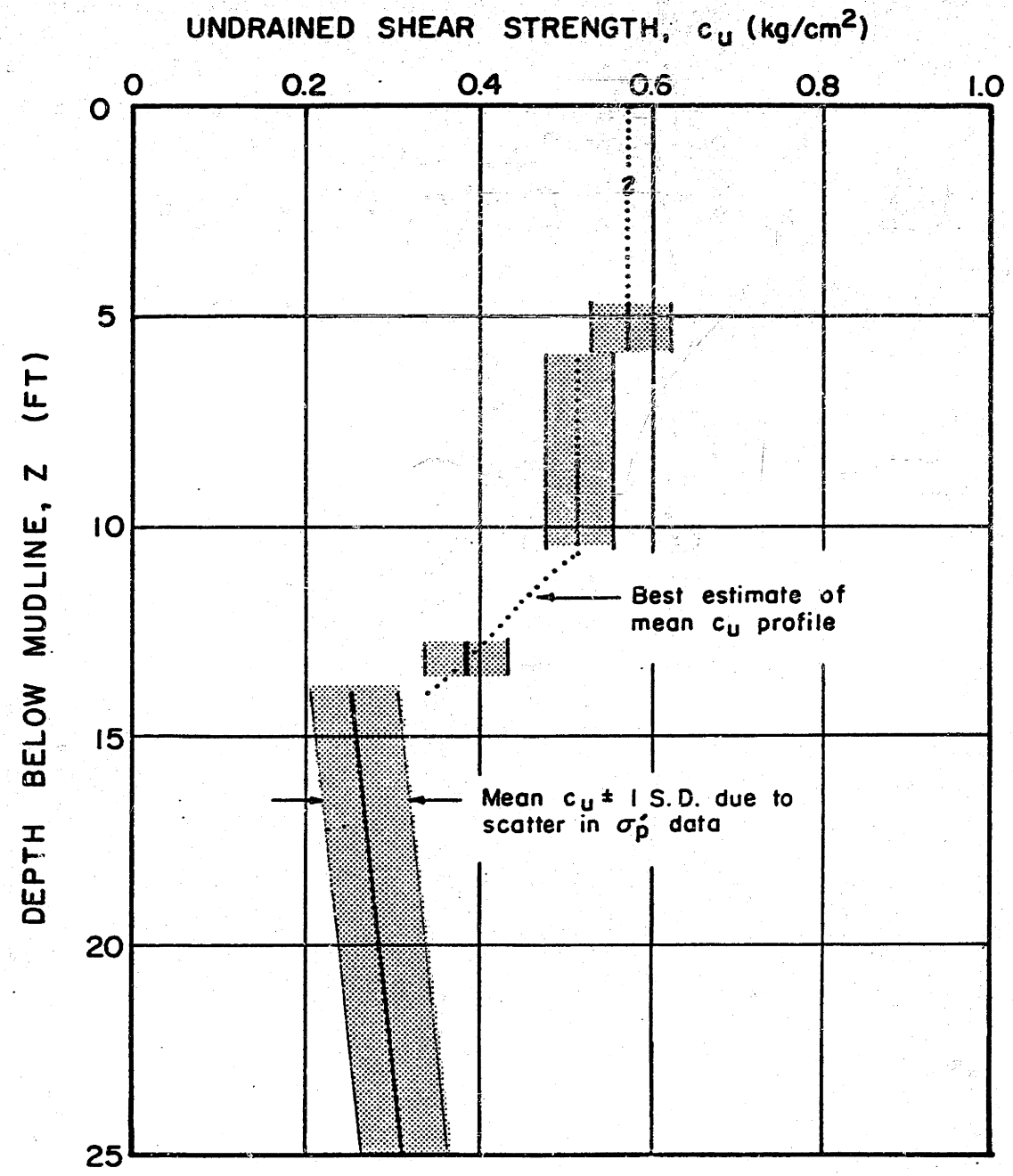

Figure 2.9: Undrained Shear Strength Profile for Mukluk Proximal, Harrison Bay (from Yin, 1985).

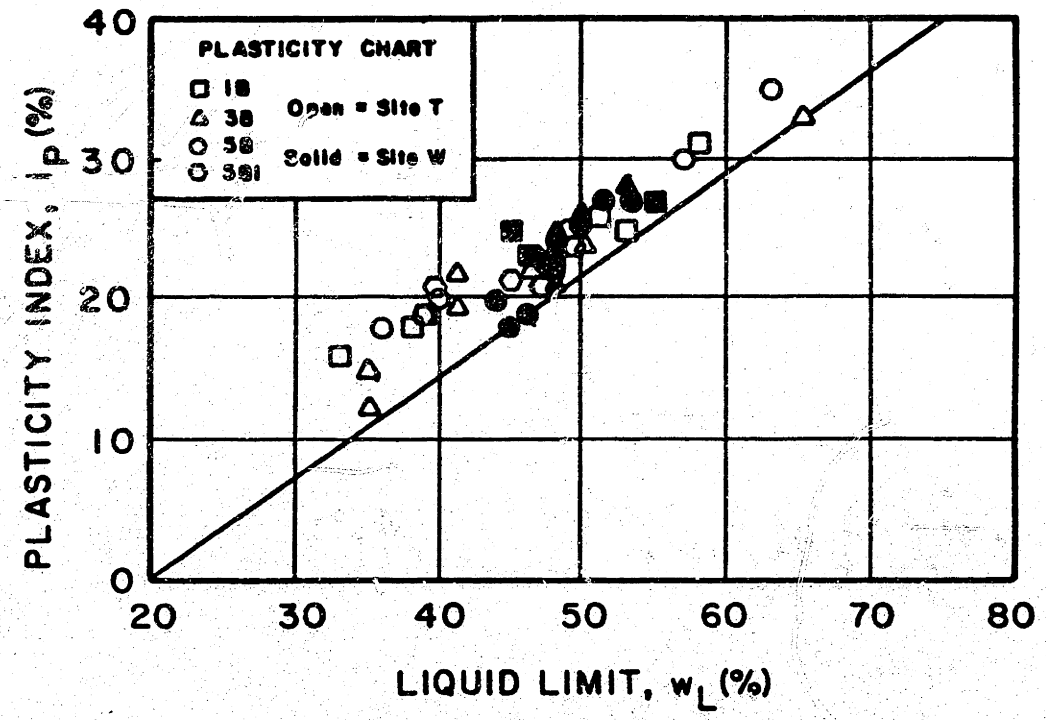

Figure 2.10: Plasticity Chart for Smith Bay Samples (from Young, 1986).

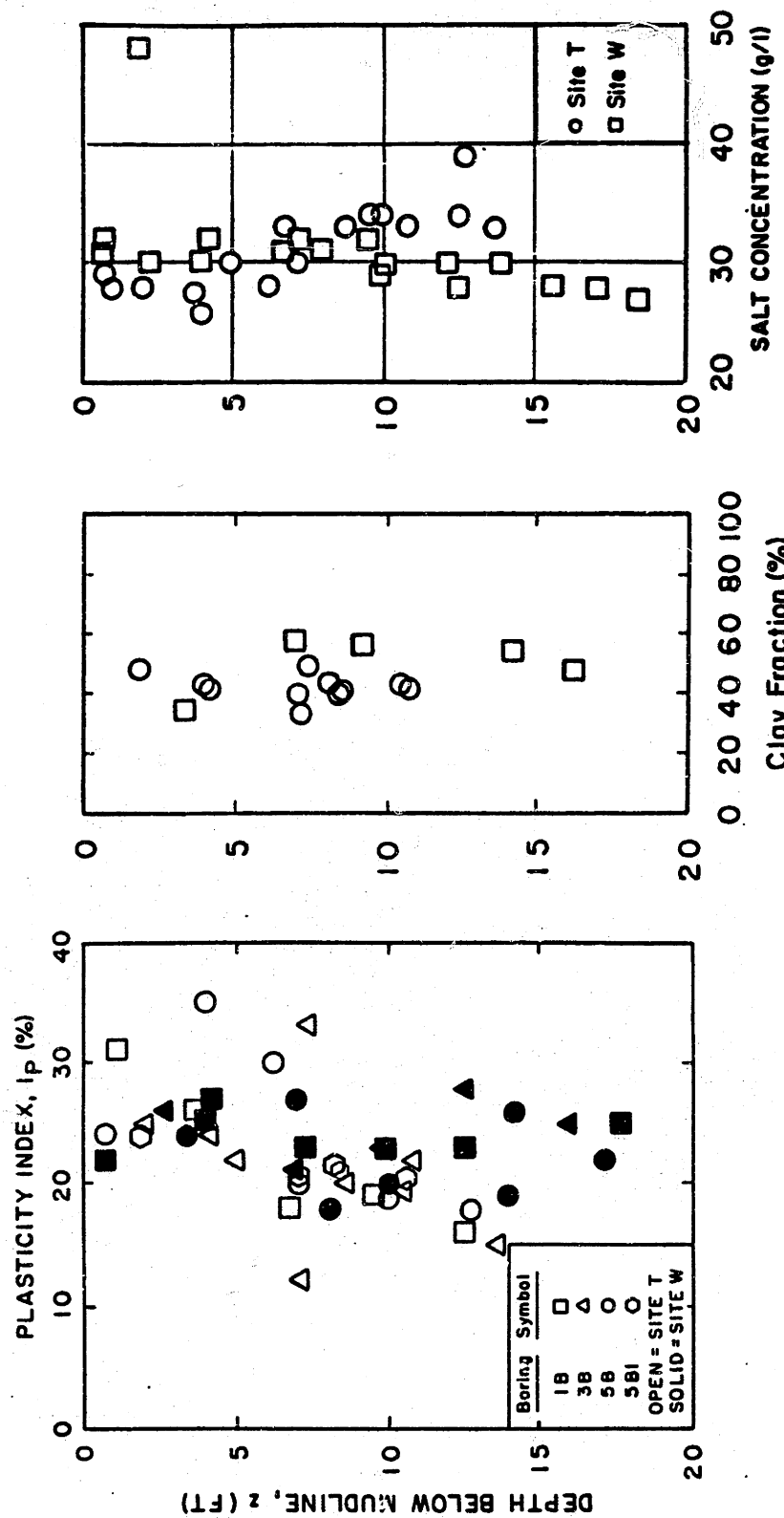

Figure 2.11: Profiles of Plasticity Index, Clay Fraction and Salt Concentration for Smith Bay (from Young, 1986).

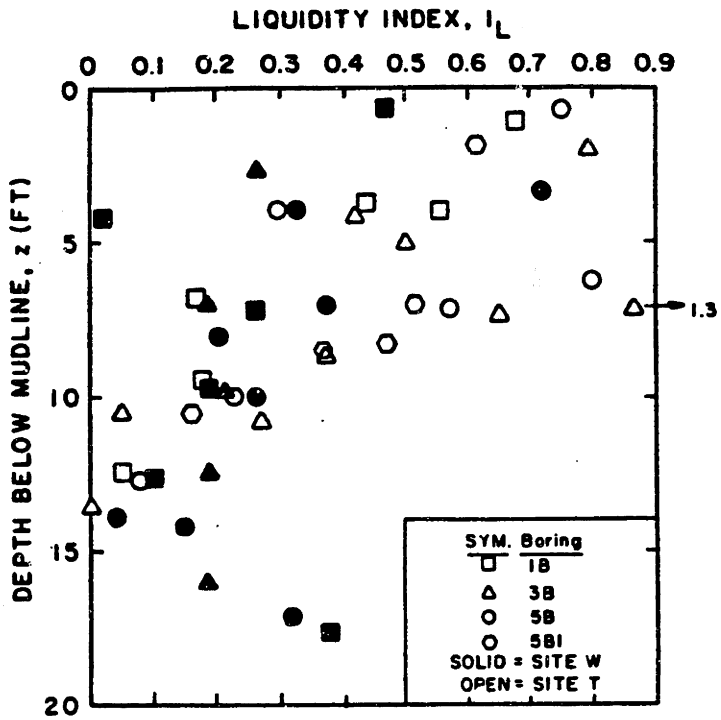

Figure 2.12: Profile of Liquidity Index for Smith Bay (from Young, 1986).

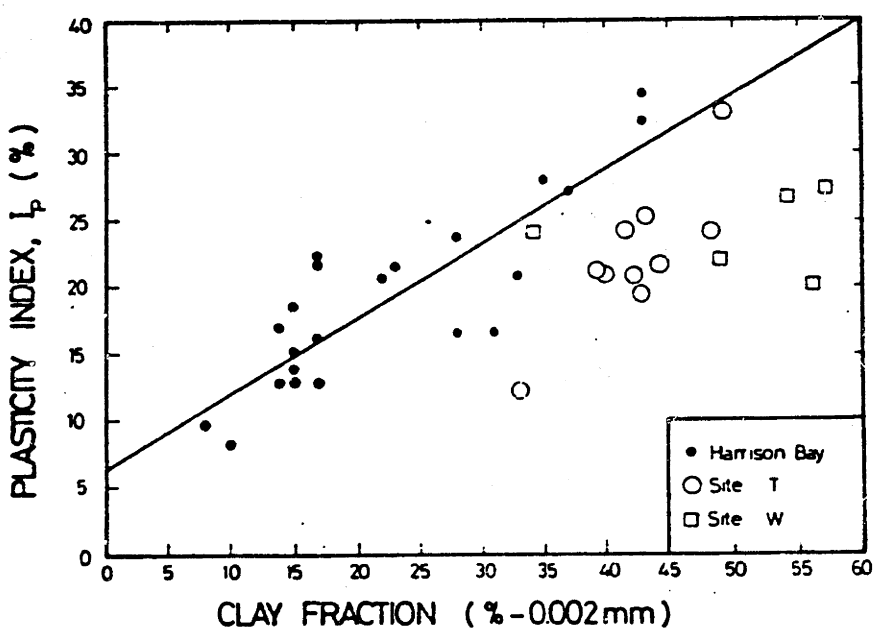

Figure 2.13: Plasticity Index versus Clay Fraction for Smith Bay Samples (from Young, 1986).

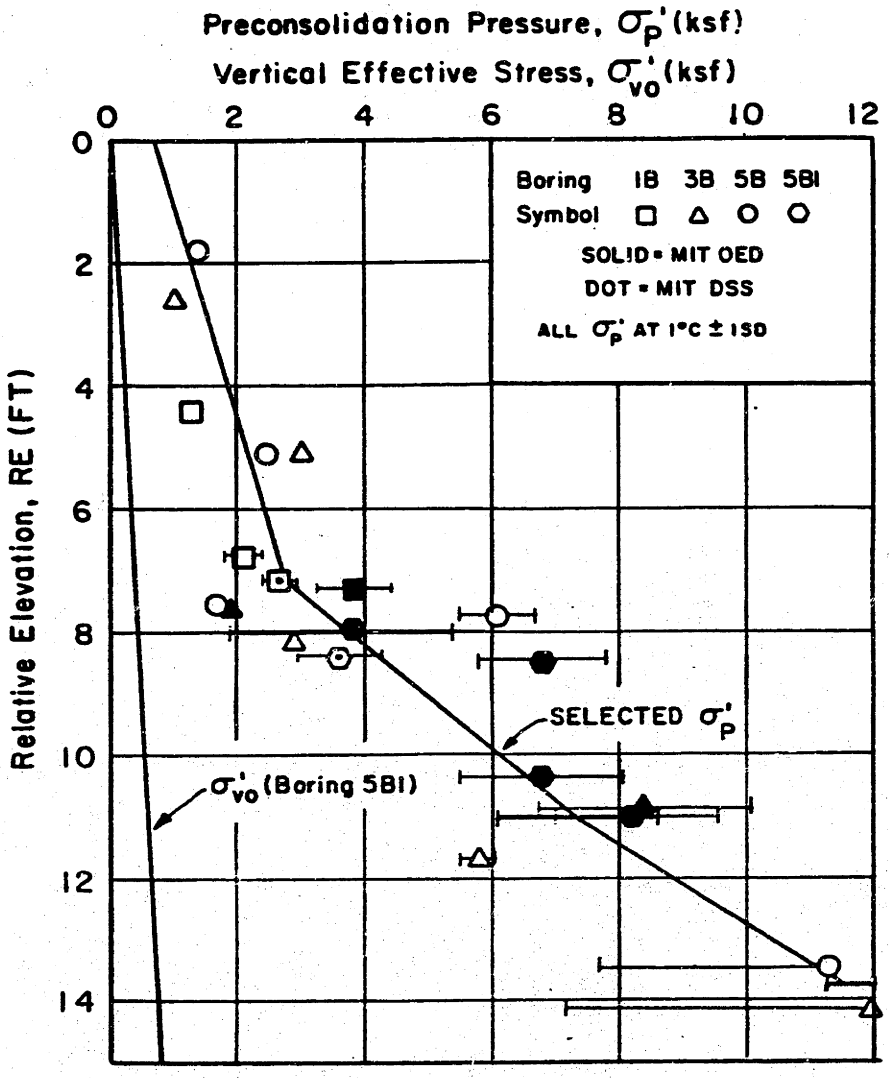

Figure 2.14: Stress History Profile for Site T, Smith Bay (from Young, 1986).

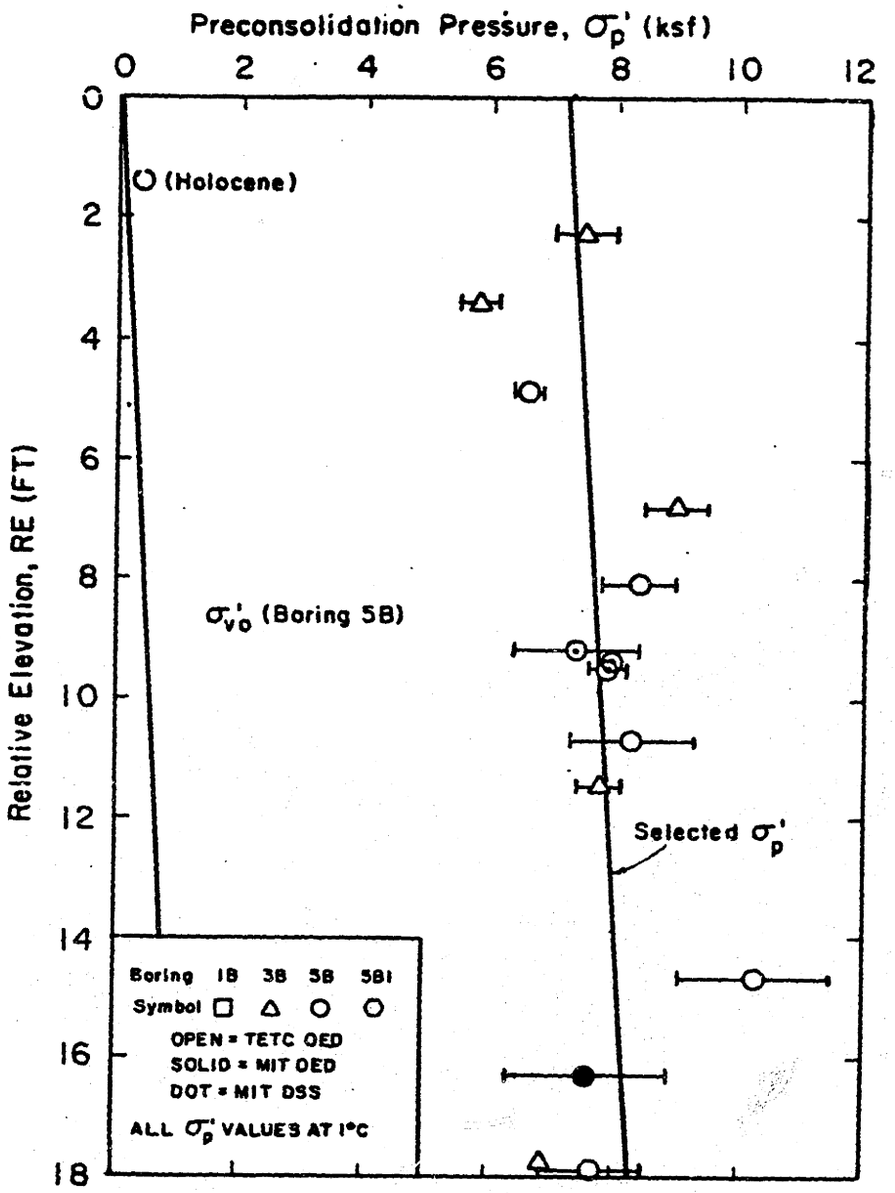

Figure 2.15: Stress History Profile for Site W, Smith Bay (from Young, 1986).

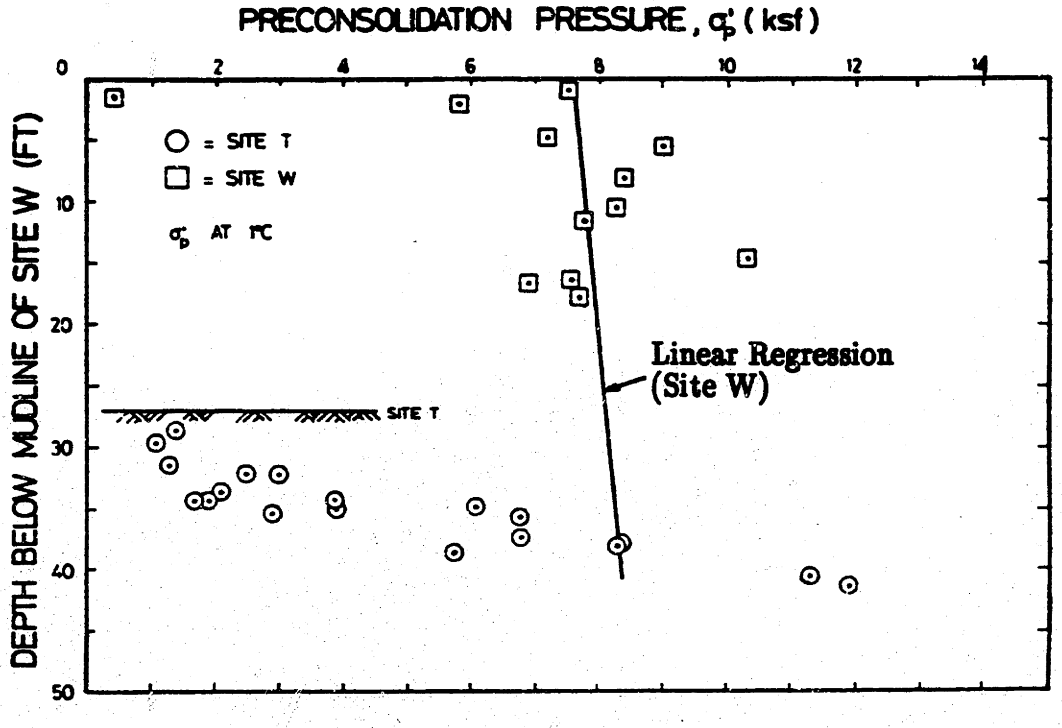

Figure 2.16: Comparison of Stress History Profiles at Sites T and W, Smith Bay (from Young, 1986).

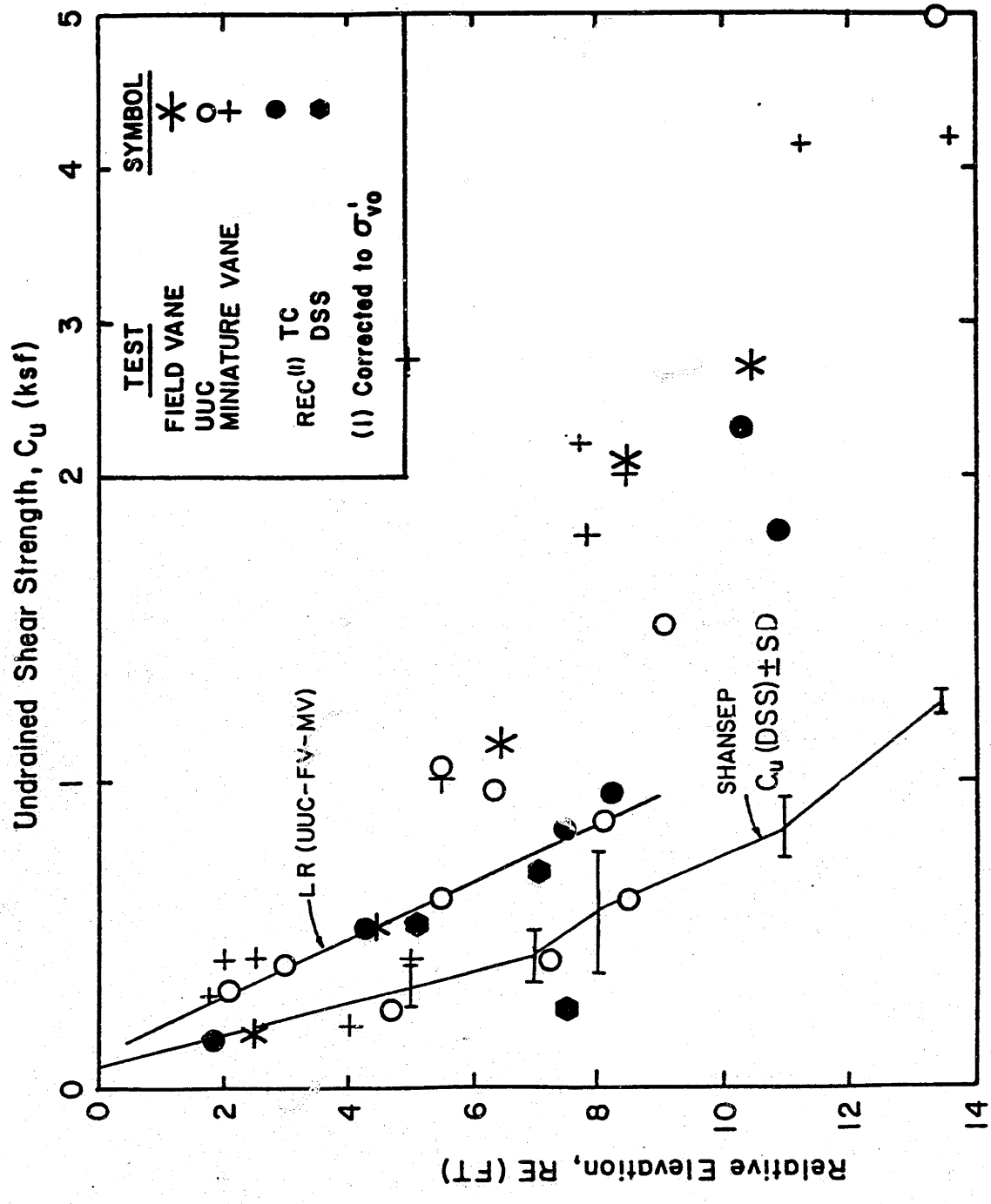

Figure 2.17: Undrained Shear Strength Profile, Site T, Smith Bay (from Young, 1986).

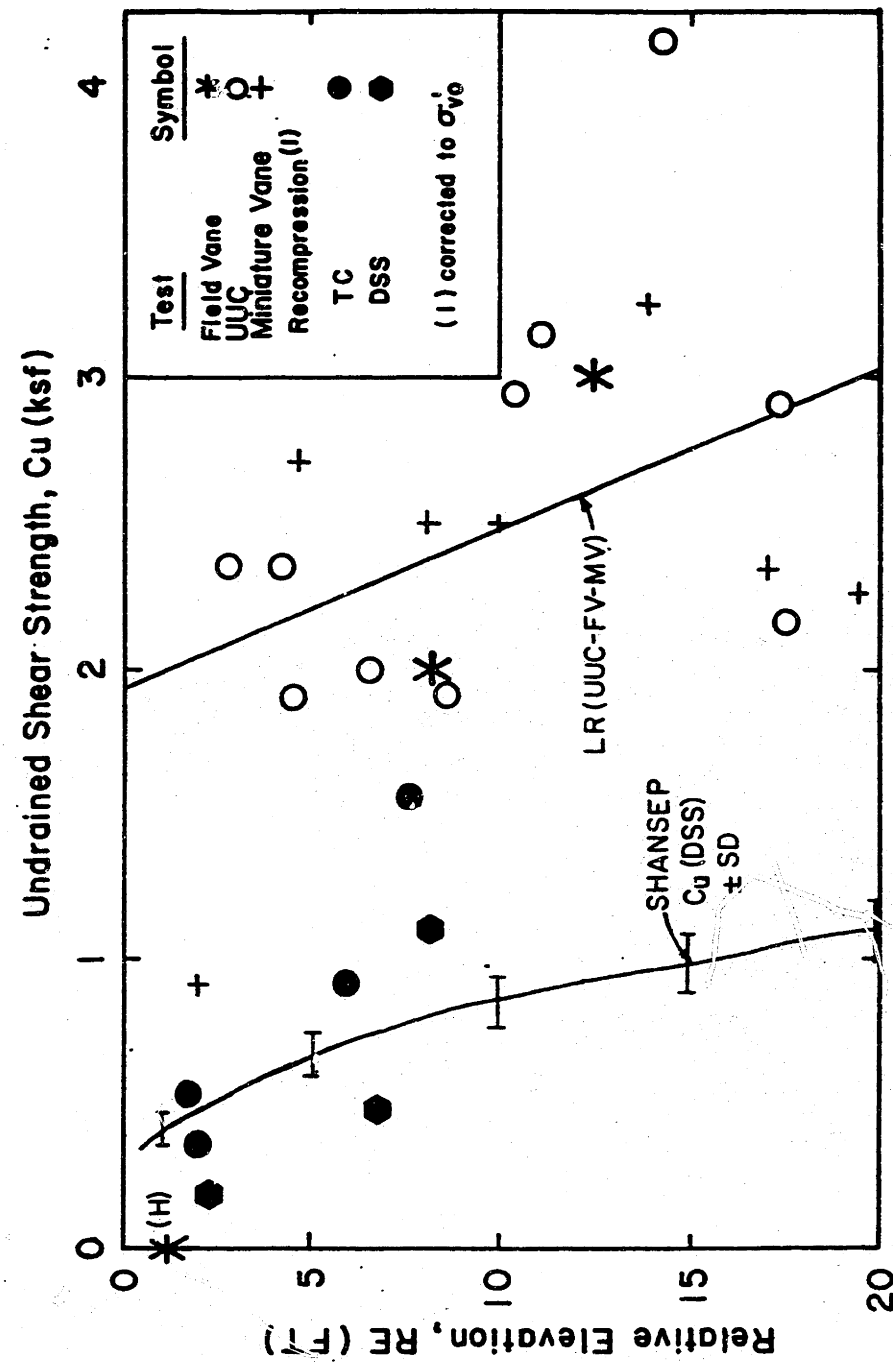

Figure 2.18: Undrained Shear Strength Profile, Site W, Smith Bay (from Young, 1986).

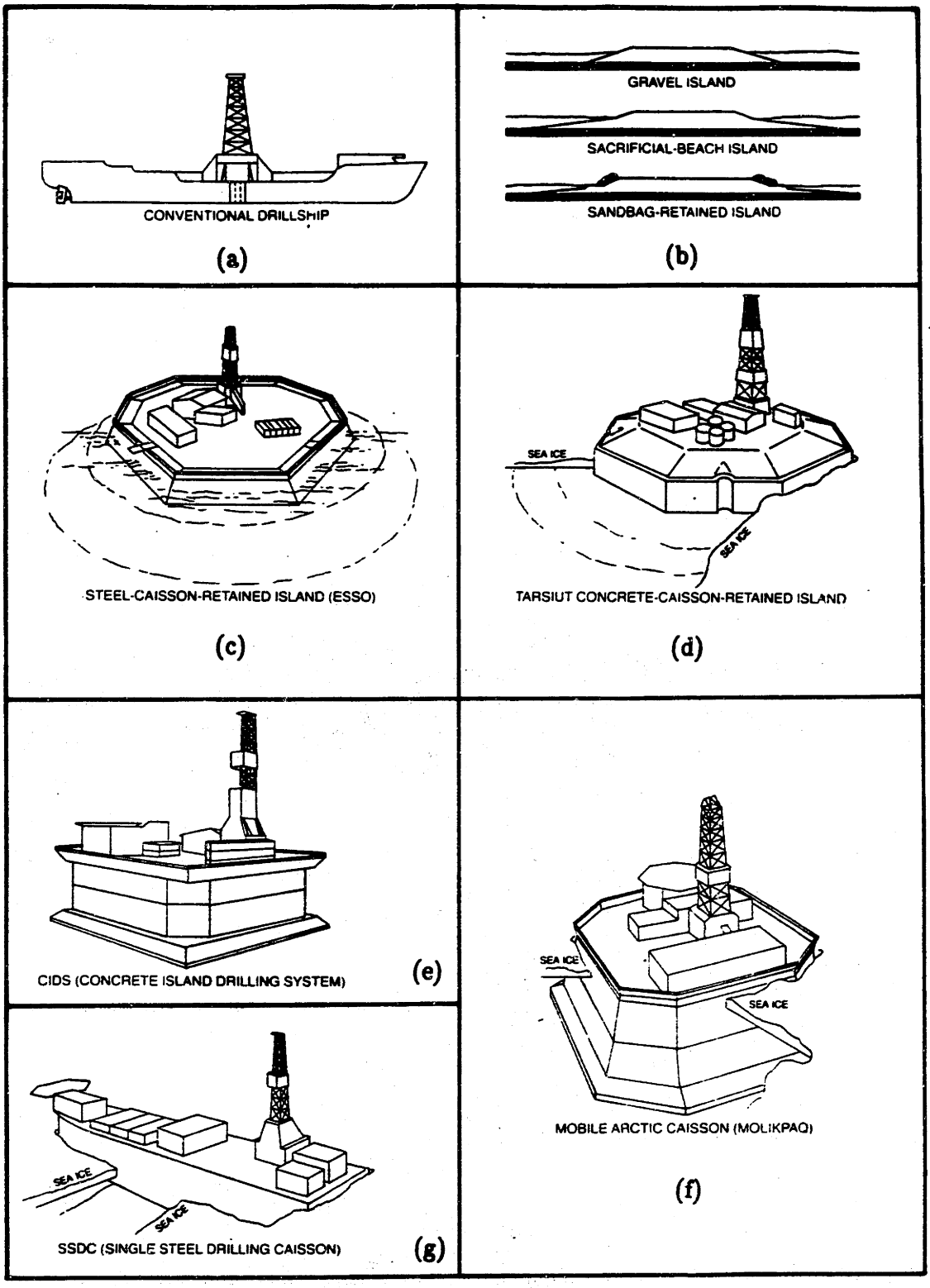

Figure 2.19: Offshore Exploratory Drilling Structures used in the Arctic (after AOGA, 1986).

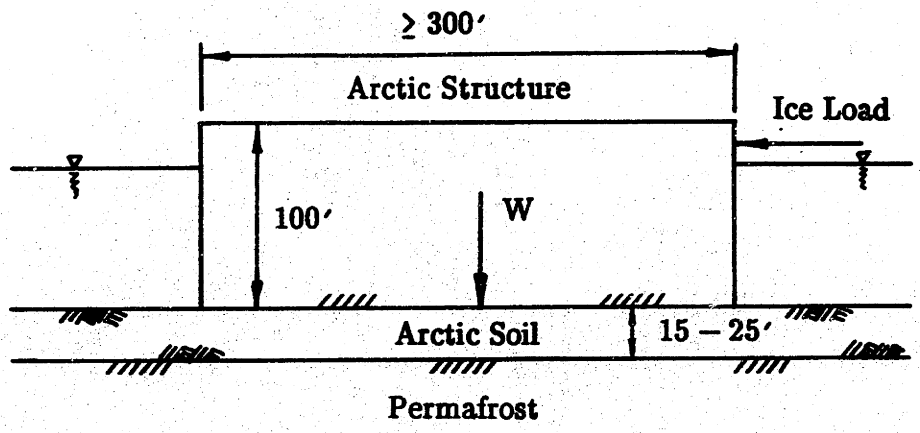

Figure 2.20: Schematic of Rigid Offshore Arctic Gravity Structure Overlying Relatively Thin Layer of Arctic Soil.

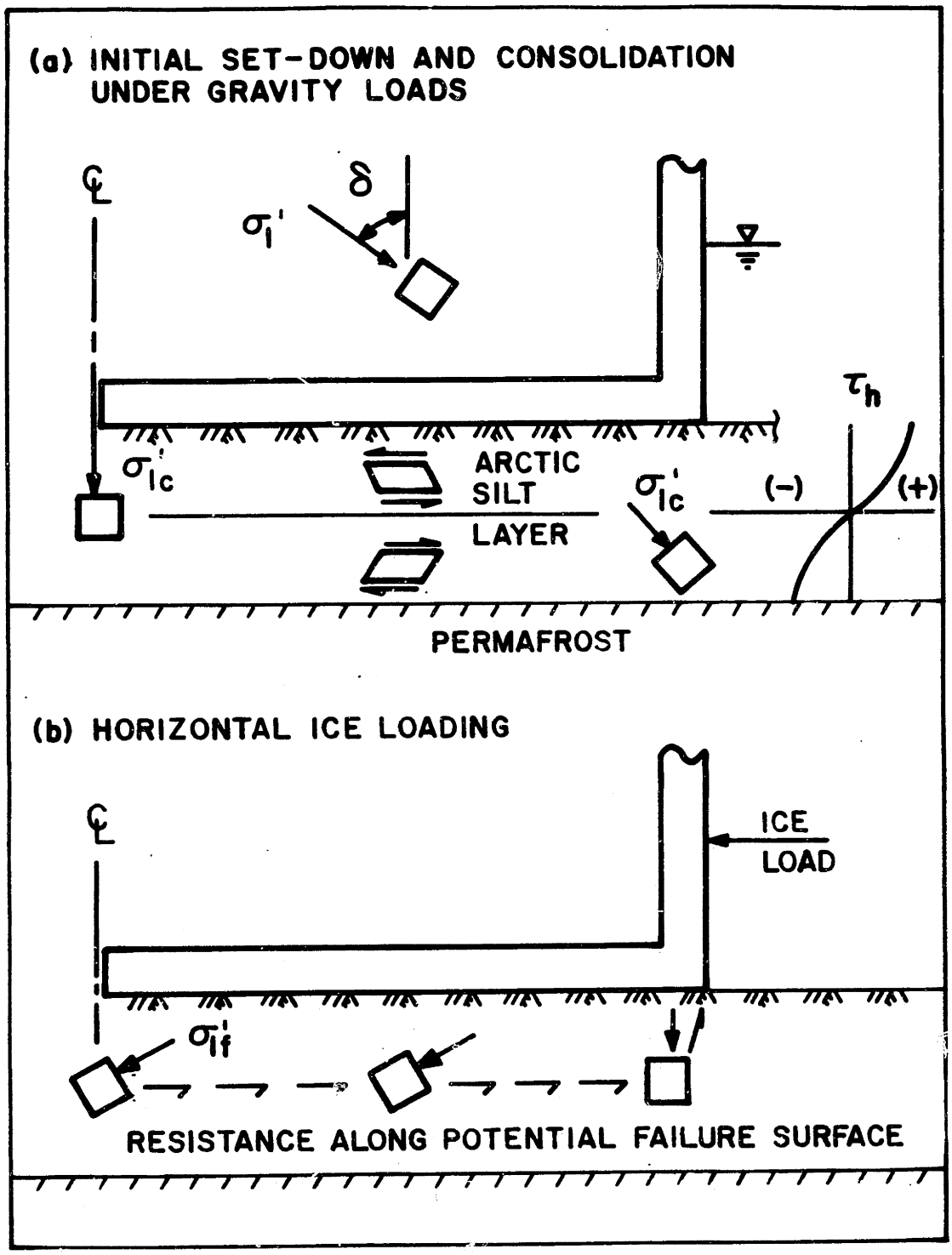

Figure 2.21: Simplified Illustration of Complex Stress Conditions Within Foundation Soils for Arctic Offshore Gravity Structures (after Ladd, 1984).

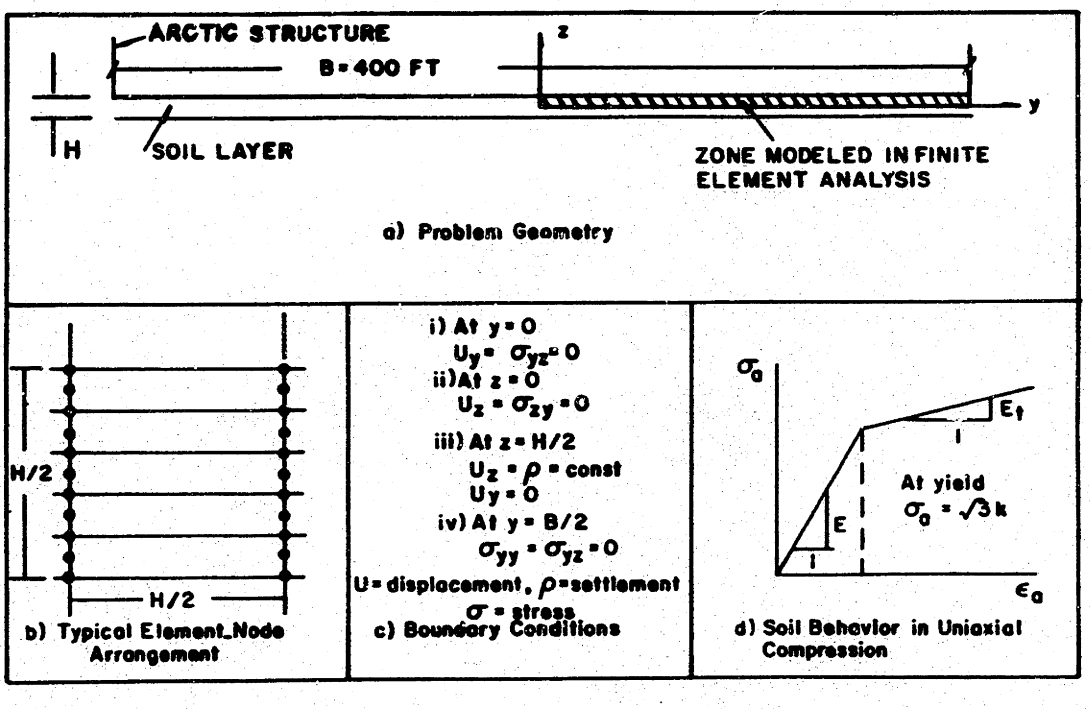

Figure 2.22: Description of Problem Considered in Finite Element Analysis by Baligh, et al., (1987).

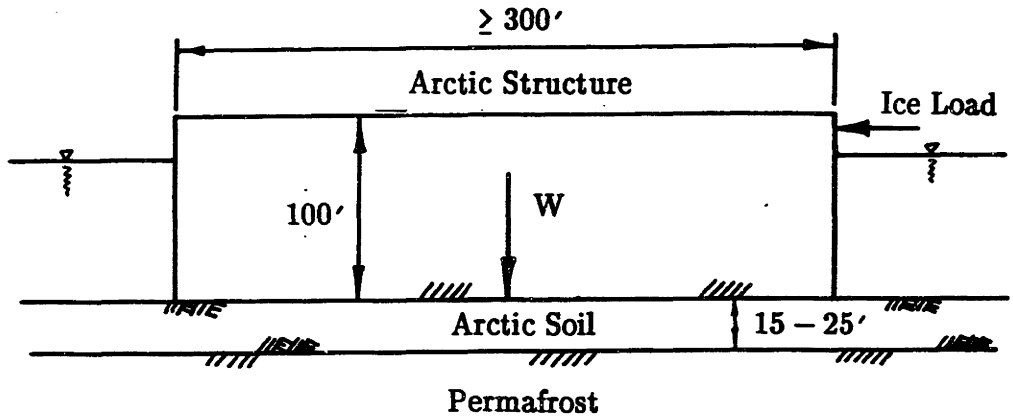

Shear Stresses on Soil at Structure Interface:

τ_1 : Weight of Structure
τ_2 : Ice Load
τ_f : Final = f(r,θ)

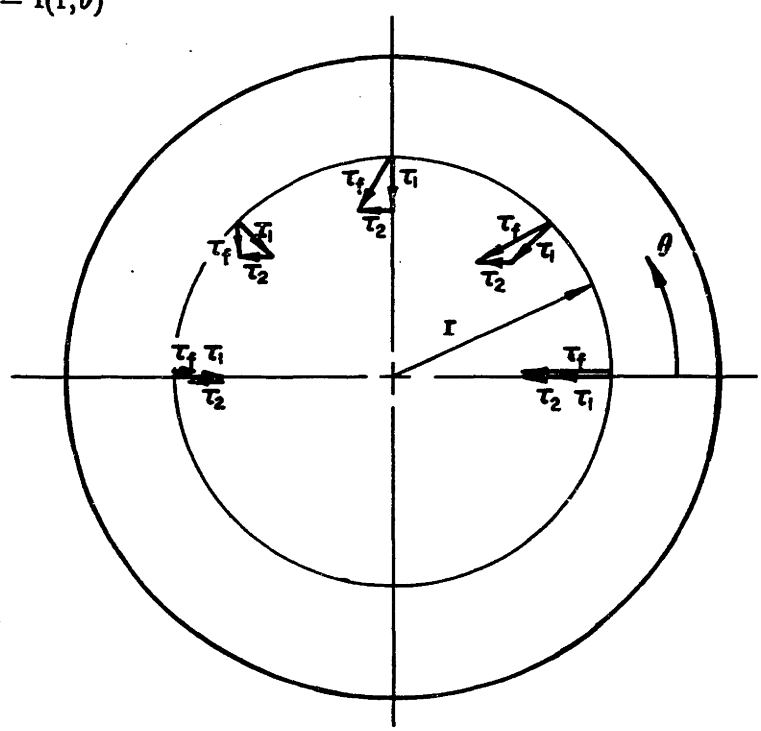

Figure 2.23: Shear Stresses on Soil at Structure Interface due to Gravity and Ice Loading (after Baligh and Azzouz, 1985b).

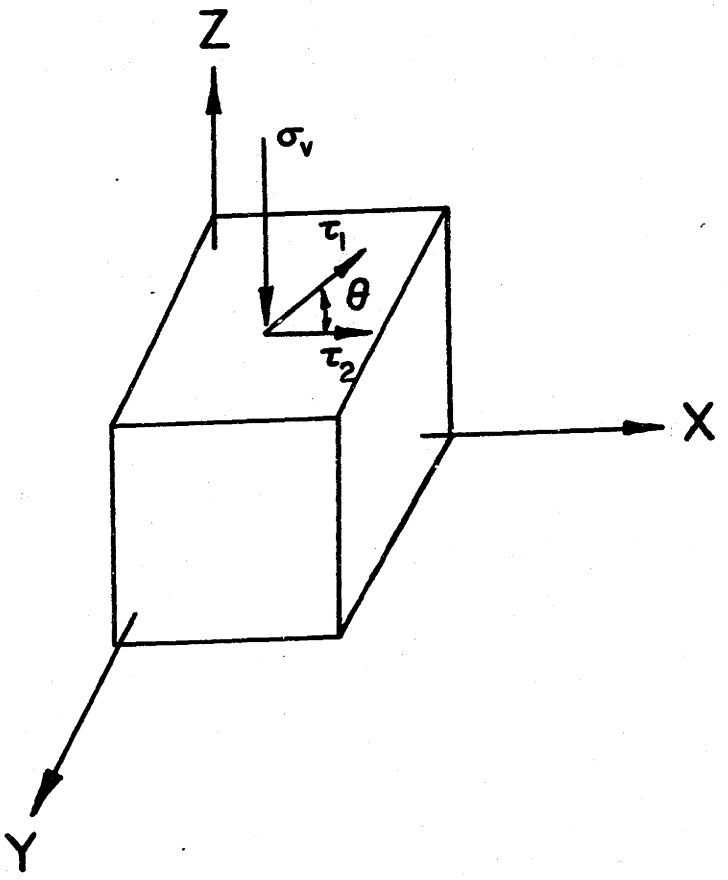

Figure 2.24: Schematic of Applied Stresses on an Infinitesimal Soil Element Required to Experimentally Simulate Stress Conditions Within the Foundation of a Rigid Arctic Gravity Structure.

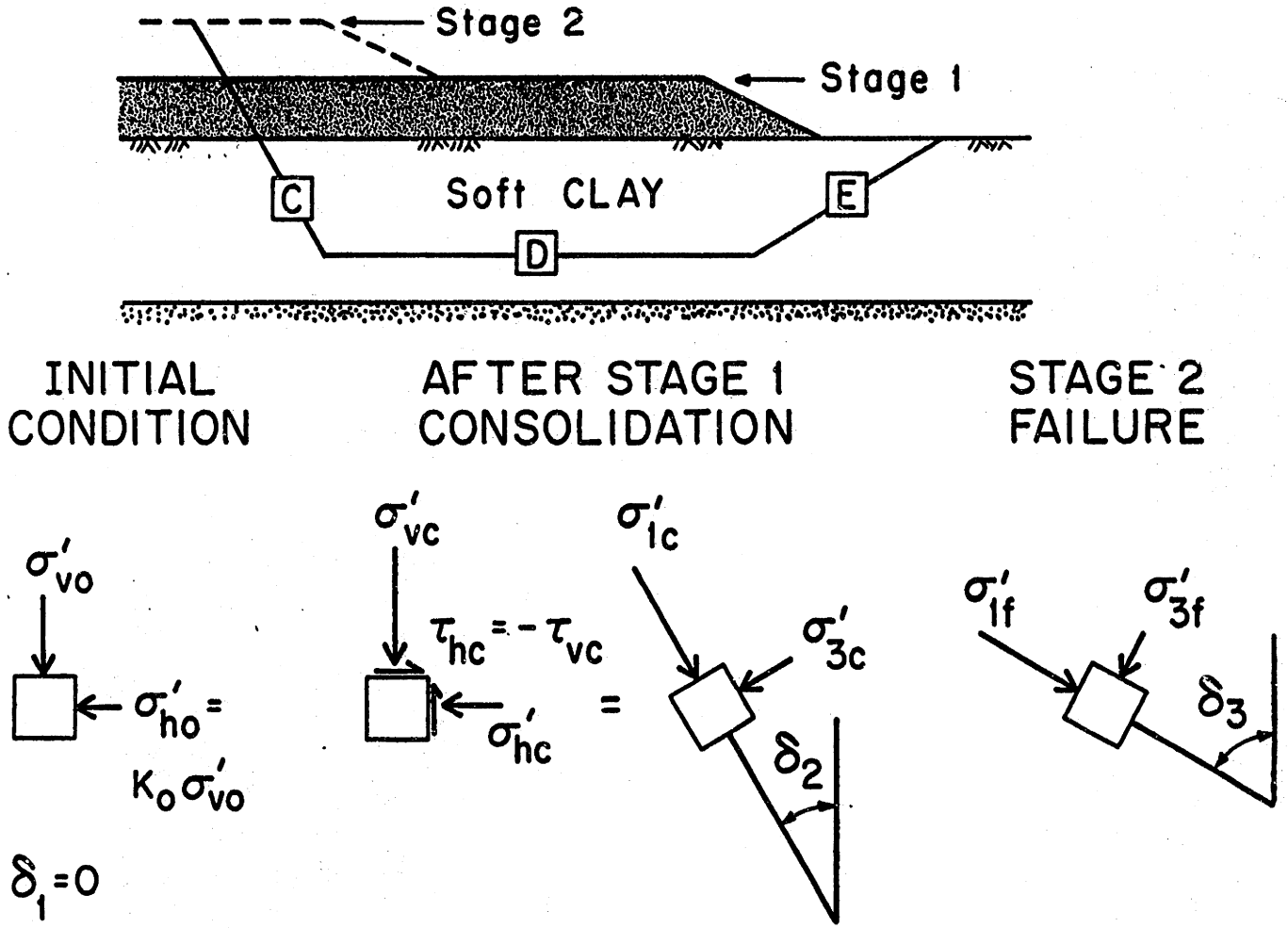

Figure 2.25: Example of Complex States of Stress During Staged Construction for Element D (from Ladd, 1988).

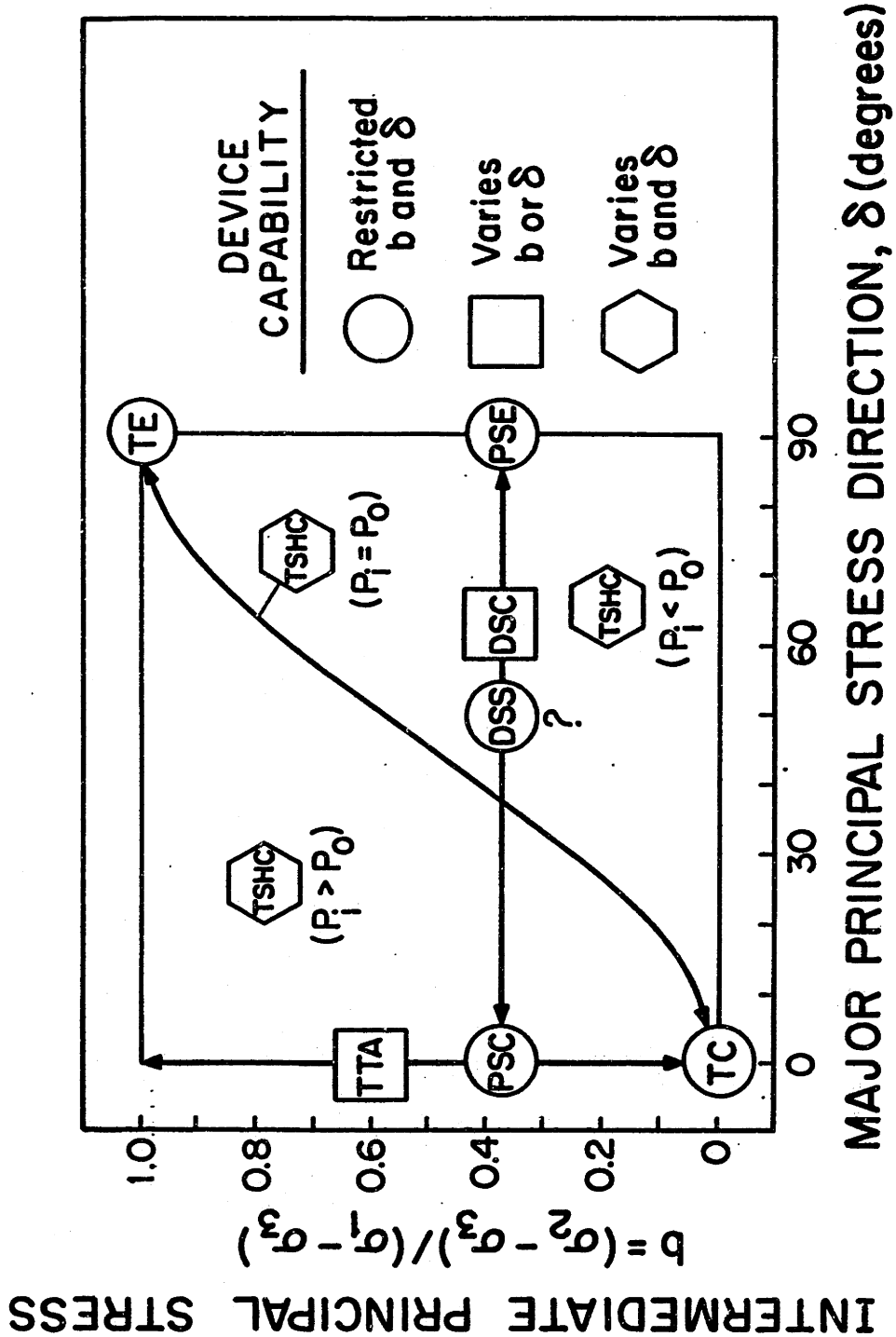

Figure 2.26: Stress Systems Achievable by Shear Devices for CK_oU Testing (from Ladd, 1988).

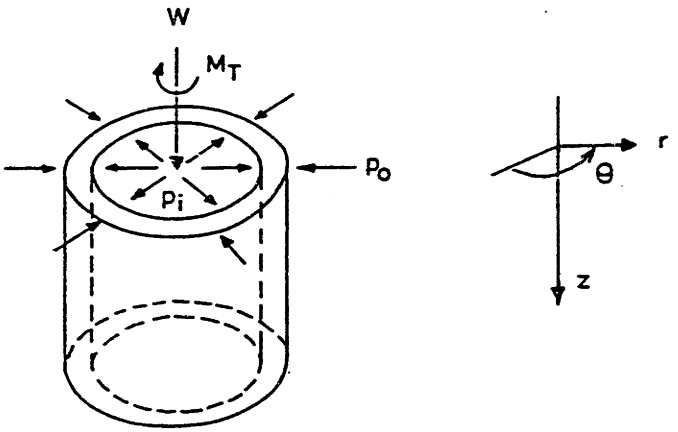

(a) Hollow cylinder sample under axial load, W, torque, M_T, internal pressure, p_i, external pressure, p_o

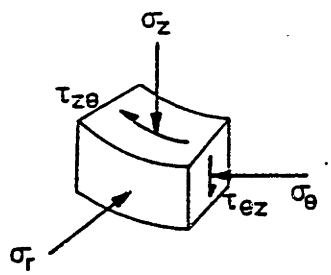

(b) Stresses on an element in the wall of a hollow cylinder sample

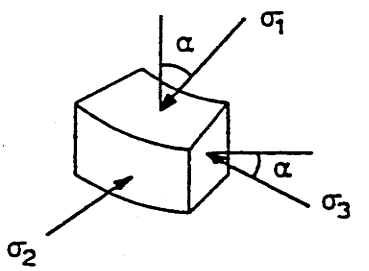

(c) Principal stresses on an element in the wall

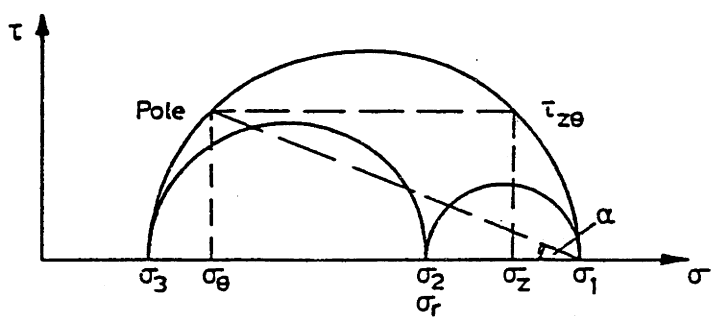

(d) Mohr circle representation of stress in the wall

Figure 2.27: Idealized Stress Conditions in a Hollow Cylindrical Element Subject to Axial Load, Torque and Internal and External Pressure (from Symes, 1983).

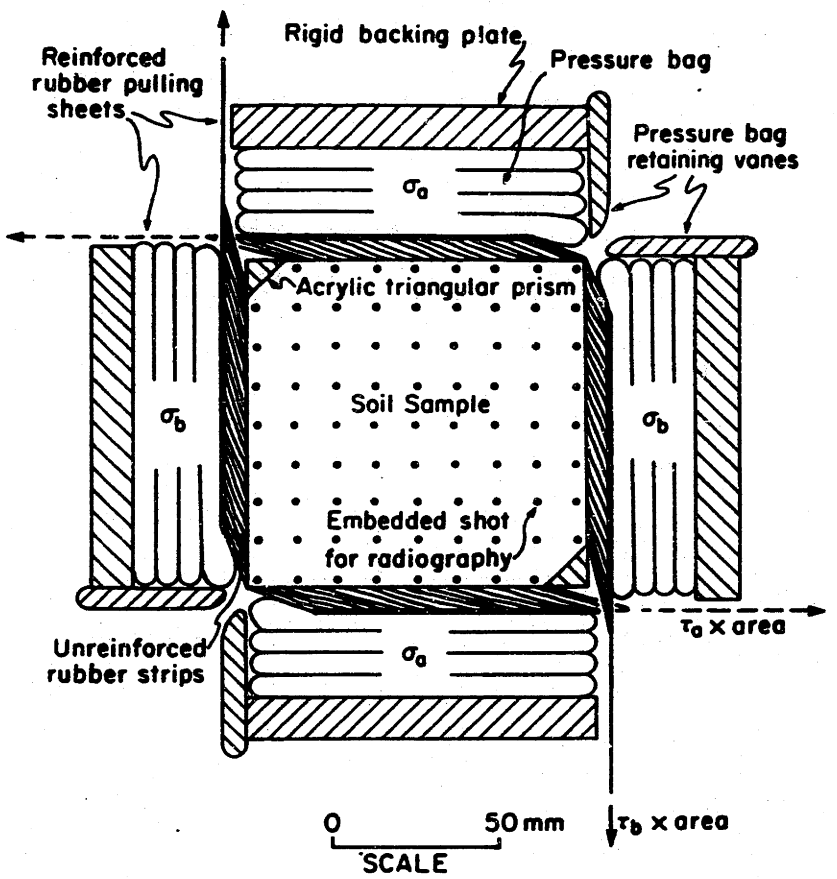

Figure 2.28: Method Used to Apply Normal and Shear Stresses in the Directional Shear Cell (from Arthur, et al., 1981).

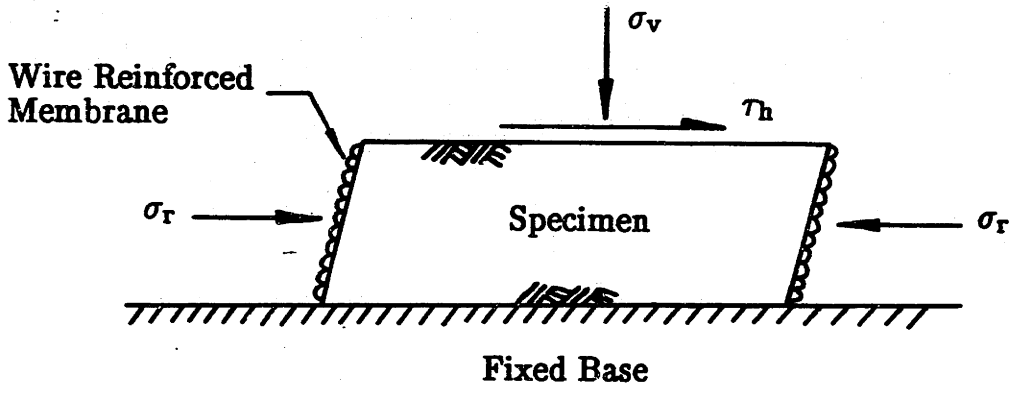

(a)

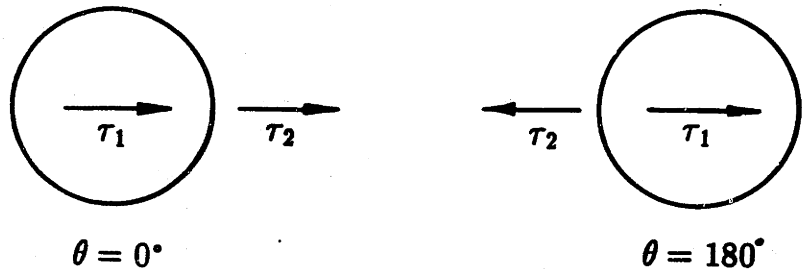

(b)

Figure 2.29: Geonor Direct Simple Shear Apparatus; (a) Schematic of Stresses Acting on a Circular Test Specimen; (b) CAUDSS Tests Possible Using the Geonor DSS.

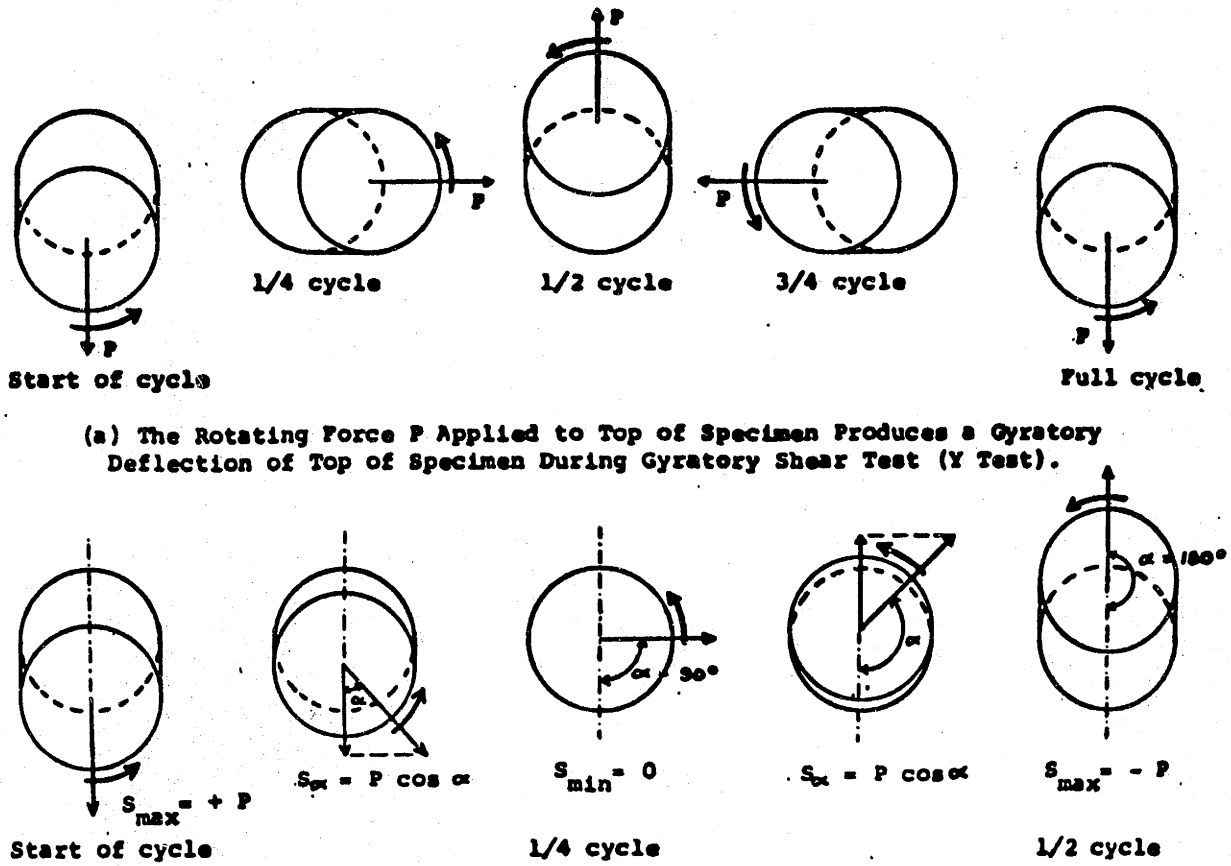

Figure 2.30: Diagrams Illustrating Mechanics of (a) Gyratory Shear and (b) Reciprocating Shear Produced by Rotating Arm of Gyratory Shear Apparatus (from Casagrande, 1979).

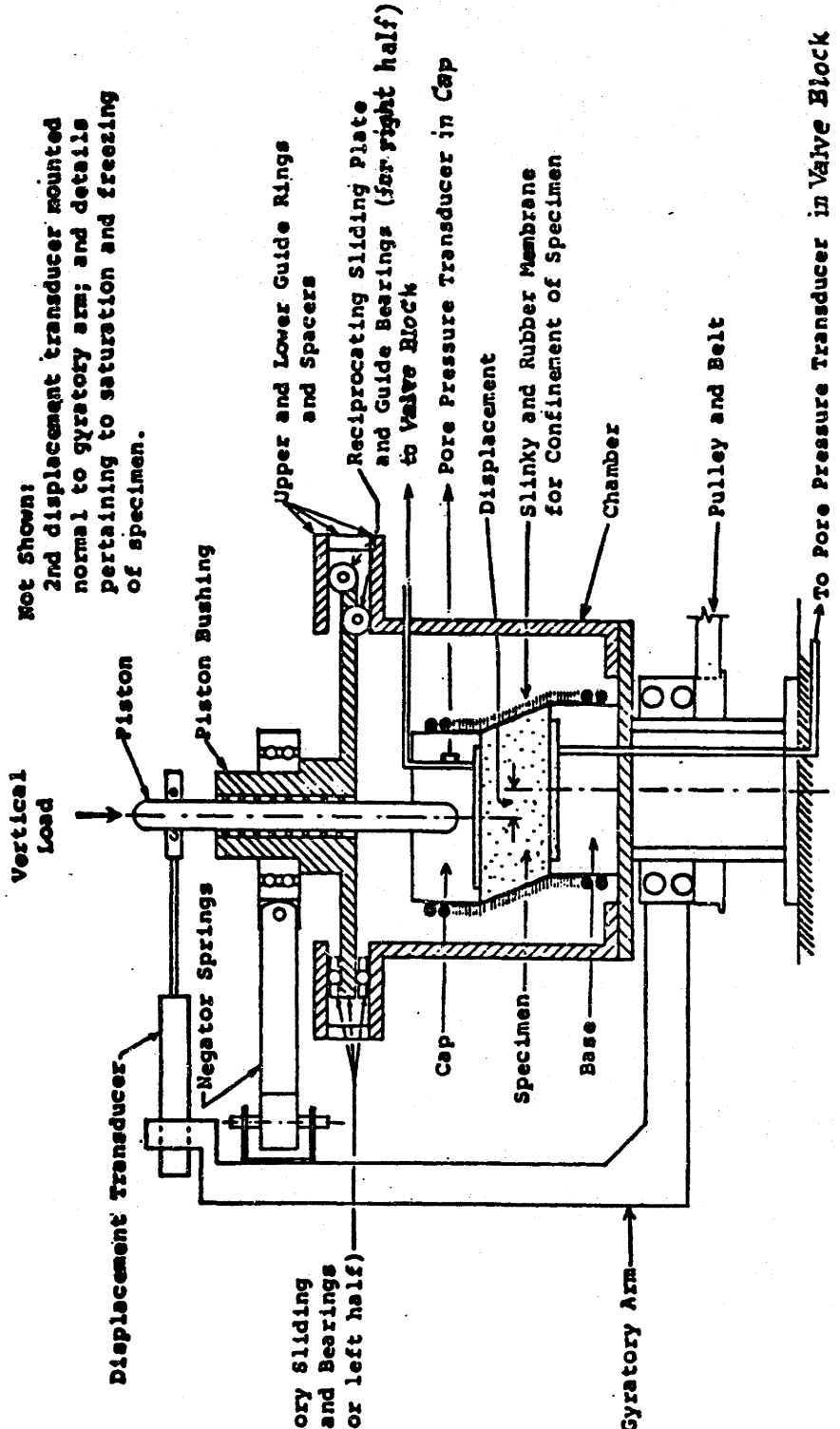

Figure 2.31: Schematic Section of Gyratory Apparatus — Left Half Sliding Plate for Gyratory Tests; Right Half for Reciprocating Tests (from Casagrande, 1979).

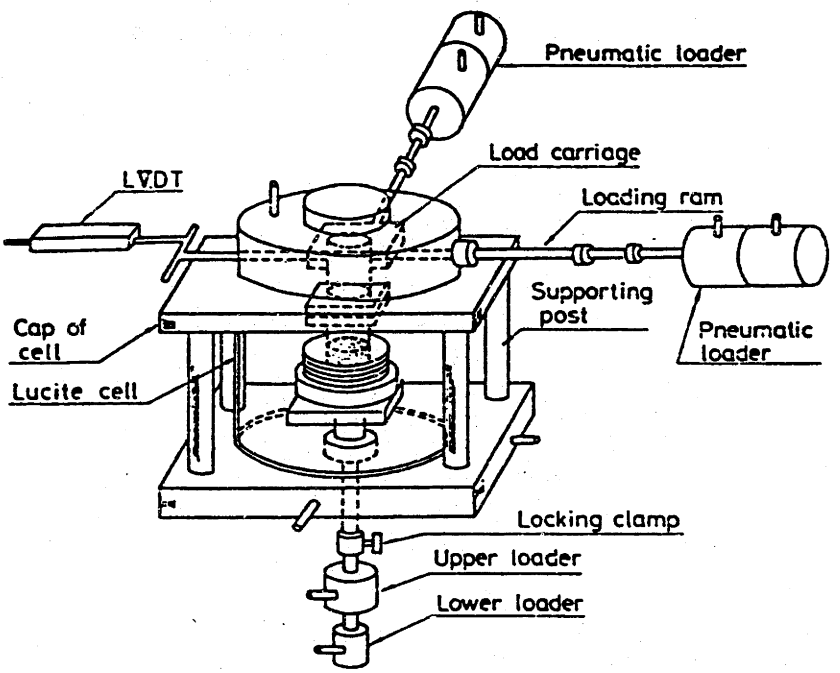

Figure 2.32: Schematic of the Two–Directional Simple Shear Apparatus (from Ishihara and Yamazaki, 1980).

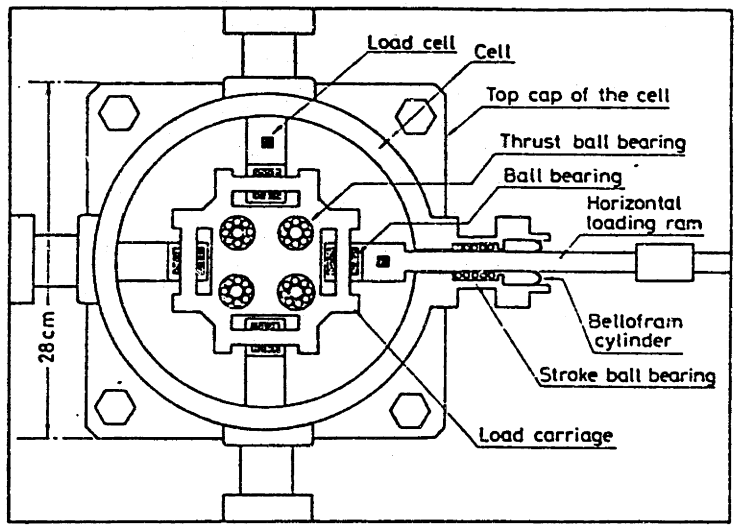

Schematic plan picture of the load carriage

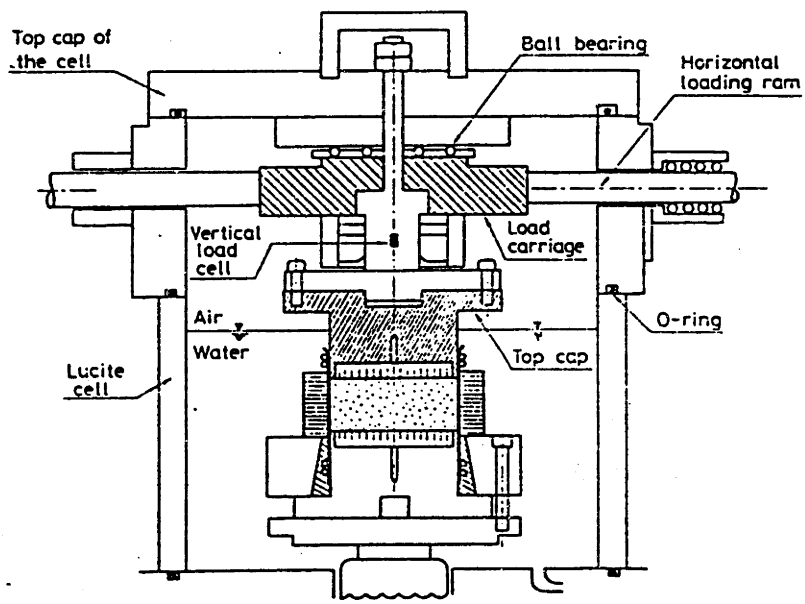

Setup of the simple shear test apparatus

Figure 2.33: Schematics of Sample Location and Load Carriage in the Two–Directional Simple Shear Apparatus (after Ishihara and Yamazaki, 1980).

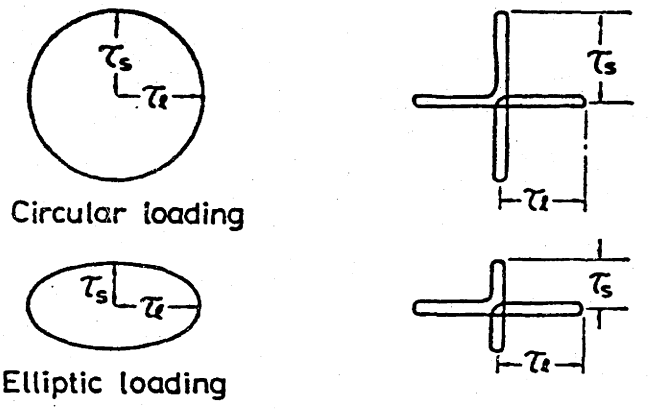

Figure 2.34: Patterns of Loading Paths Available in the Two–Directional Simple Shear Apparatus (from Ishihara and Yamazaki, 1980).

CHAPTER 3

DESCRIPTION OF THE MDSS AND TESTING PROCEDURES

3.1 INTRODUCTION

The Multidirectional Direct Simple Shear (MDSS) apparatus was developed as part of this research at MIT to experimentally simulate, at the element level, the stress conditions within the foundation soil of an offshore Arctic gravity structure. The device is a simple shear apparatus and incorporates some of the characteristics of the Geonor Direct Simple Shear (DSS) device which has been in use at MIT for over twenty years. It also uses the original variable speed drive system from the direct shear box apparatus built at MIT in 1970 (Lucks, 1970). This system provides a horizontal thrust force at a preselected constant rate of strain and is used for the shear phase in the MDSS.

Development of the MDSS also benefited from a corporate donation of computer and data acquisition equipment from the Hewlett Packard Corporation. The device is an automated soil testing apparatus and uses a Hewlett Packard (HP) Vectra personal computer and an HP PC Instruments system. The computer and instrumentation equipment are used for data acquisition and to automate the application of forces to a specimen during testing. All of the servo control software for automated testing and data acquisition for the MDSS was developed at MIT.

The MDSS is capable of applying a vertical stress and two independent horizontal shear stresses to a circular soil sample. The vertical stress and first horizontal shear stress represent the stresses acting on a foundation soil element due to initial set down of an Arctic structure (i.e., gravity loading). The second horizontal shear stress represents the shear stress due to the horizontal ice forces acting on an

Arctic structure.[1] The MDSS tests soil samples under simple shear strain conditions and is capable of applying the first shear stress at an angle relative to the second shear stress ranging from 0 to 150 degrees.

This chapter gives an overview of the MDSS and describes how tests are run in the device. It covers both hardware and software developed for the apparatus and also reviews testing procedures used for cohesive soils. A more detailed description of the device and the software can be found in Appendices B and C.

3.2 OVERVIEW OF THE MDSS APPARATUS

The MDSS uses the same size 35 cm^2 circular samples as used by MIT in the Geonor DSS apparatus. The samples are trimmed to an approximate height of 2.3 cm into a Geonor wire reinforced rubber membrane. The membrane is assumed to have negligible lateral deformation and therefore samples are consolidated under K_o conditions. The trimming apparatus is the same one used for the Geonor DSS which is specially designed to trim samples with a minimum of disturbance.

The MDSS has a set of coordinate axes, as shown in Figure 3.1, for reference in describing the direction of displacements and applied forces. The central (vertical) axis of a circular sample is referred to as the Z axis while the X and Y axes lie in a horizontal plane through the sample perpendicular to the Z axis.

3.2.1 Application and Measurement of Forces

Three independent stresses can be applied to samples in the MDSS; a vertical stress along the Z axis and two horizontal shear stresses acting in the X–Y plane. Figure 3.2 is a simplified schematic of the MDSS showing the sample location and how

---

[1]Hereafter, the horizontal shear stress due to gravity loading will be referred to as the *first* shear stress (τ_1) and the horizontal shear stress due to subsequent ice loading will be referred to as the *second* shear stress (τ_2). If τ_1 is applied under fully drained conditions (i.e., full consolidation) then τ_1 is referred to as the horizontal consolidation shear stress, τ_{hc}.

forces are applied to the sample. The first shear stress and vertical stress are applied to the sample using pneumatic cylinders. These stresses represent the gravity loading of the structure on the foundation soil and are usually applied to the sample under drained conditions (i.e., anisotropic consolidation). The second shear stress is applied by a variable speed gear drive system at a constant rate of strain. This represents the ice loading stresses on the foundation soil and is applied under undrained conditions. For a given test, the first shear stress can be applied at a fixed angle theta (θ) relative to the second shear stress ranging from 0 to 150 degrees.

The second shear stress is always applied to the sample from the same direction which is parallel to the X axis. That is, this system is fixed on the apparatus and cannot have its orientation changed. However, the direction of the application of the first shear stress can be changed from test to test thus enabling the special anisotropically consolidated tests to be run at various theta angles.

For a typical anisotropically consolidated test a sample will be consolidated under a combined vertical stress and first shear stress until the desired final state of consolidation stress is reached. Subsequently the sample is sheared undrained by application of the second shear stress at a constant rate of strain while the first shear stress is held constant. For a conventional K_0 consolidated–undrained test the sample is simply consolidated under the vertical stress and then sheared undrained by application of the second shear. In other words, by maintaining the first shear stress equal to zero, the MDSS can also perform conventional K_0 consolidated direct simple shear tests.

In the MDSS, the sample pedestal rests on a set of bearing plates (Figure 3.2) which allow the bottom of the sample to deform freely in the X–Y plane. The top cap is free to displace vertically along the Z axis as is required during consolidation. However, it is fixed against movement in the X–Y plane by a pair of precision linear bearings retained in a pillow block thus providing the fixed boundary for simple shear

straining of the sample (i.e., the bottom displaces horizontally relative to the top). The base bearing plates is one of the key components of the device enabling special anisotropically consolidated tests with a angle theta between the first and second shear stresses to be performed.

The vertical stress and first shear stress are applied by pneumatic cylinders which are controlled by Fairchild voltage to pneumatic transducers. These transducers act as computer controlled pressure regulators by regulating an air pressure in proportion to electrical signals from the computer. The forces produced by the vertical stress pneumatic cylinder and the second shear stress gear drive system are measured with Data Instruments load cells. The horizontal force acting on a sample due to the first shear stress is measured indirectly with a pressure transducer. The cylinder was calibrated so that the force it produces is known as a function of the pressure transducer reading. The vertical stress σ_v and the resultant horizontal shear stress τ_t ($\tau_t = (\tau_x^2 + \tau_y^2)^{0.5}$) acting on the sample can be computed from these measurements.

3.2.2 Measurement of Strains

In the MDSS, the sample can deform vertically and in any horizontal direction. The horizontal deformation takes place with the bottom of the sample moving relative to the top (i.e., the top cap is held fixed against horizontal displacement). To properly calculate strains of a sample, three displacement measurements are made: vertical along the Z direction, horizontal in the X direction, and horizontal in the Y direction. With these measurements the vertical strain ϵ_v and the resultant shear strain of the sample γ_t ($\gamma_t = (\gamma_x^2 + \gamma_y^2)^{0.5}$) can be computed.

All displacement measurements are made with direct current displacement transducers (DCDT). As shown in Figure 3.3, two DCDT's, Z1 and Z2 are used to measure the vertical displacement. The transducers are attached to the top cap by plexiglas retainers and measure displacements between the top cap and the circular

brass disc which is attached to the bottom pedestal. The DCDT's are located at diametrically opposite sides of the top cap to account for top cap rotation upon application of a horizontal shear stress to the sample. Therefore, the two measurements are taken and a linear interpolation is made to get the measured vertical deformation of the sample center.

The X and Y displacements are measured by two transducers that are held by plexiglas retainers on the circular brass disc. The transducers are mounted perpendicular to each other and make their measurements relative to two perpendicular flats on the top cap. With this set–up the shear strain of the sample in any direction is a vectorial sum of the X and Y measurements. For example, during undrained shear of a K_o consolidated sample the bottom of the sample will move horizontally relative to the top only in the X direction. Hence, the displacements will be recorded by the X transducer and the Y transducer will ideally show no change in its value.

The X and Y measurements are reliable only if the sample is properly setup in the device. As described in Appendix B, the sample must be trimmed and placed in the device following a special procedure so that the displacement measuring system is properly aligned with the reference (x,y) axes of the device. The results of a series of successful tests conducted to proof check the alignment system and set–up procedures are presented in Chapter 4.

3.2.3 Computer Control and Data Acquisition Equipment

The MDSS uses a Hewlett Packard (HP) Vectra Personal Computer[2] and a PC Instruments system for automated testing and data acquisition(Figure 3.4). The computer has 640 kilobytes(kb) of memory, a 20 megabyte(Mb) hard disk, and two floppy disk drives (1.2 Mb and 360 kb). The computer has several accessory card slots

[2]The Vectra is an IBM PC/AT compatible.

of which three are used for the MDSS. These include a serial/parallel interface, an HPIB interface, and a PC Instruments interface. The serial/parallel interface is used for an HP ThinkJet printer and the HPIB interface is used for an HP plotter.

The PC Instruments system consists of several instrumentation modules that are connected to the Vectra through the PC Instruments interface. Each module is a separate unit and is controlled by software commands from the computer. The modules operate outside of the Vectra hence avoiding the problem of locating data acquisition equipment inside the electronically noisy environment of a personal computer.

The MDSS uses four PC Instruments modules for data acquisition and computer control, including: (1) DC Power Supply, (2) Dual Voltage DAC, (3) Digital Multimeter, and (4) Relay Multiplexer. Each module is briefly described in the following paragraphs and Figure 3.4 schematically shows how they are used in the MDSS. Figure 3.4 also shows that all of the instrumentation transducers are connected to an instrumentation box. This box is used to distribute input voltage to the transducers, return the transducer signals to the data acquisition system and also has external connections for each transducer to allow direct visual readings to be made with a voltmeter or to connect to an X–Y plotter.

3.2.3.1 DC Power Supply

The HP PC Instruments DC Power Supply is a general purpose programmable dc power supply. Its output voltage can be programmed to vary from 0–20 volts dc and is used in the MDSS as a power supply for the instrumentation transducers (load cells, DCDT's and pressure transducer). It is connected to the MDSS's instrumentation box which in turn distributes the input voltage to the transducers.

3.2.3.2 Dual Voltage DAC

The HP PC Instruments Dual Voltage DAC is an instrument that converts digital values into analog output voltages. It supplies two independently controllable

DC voltage sources in three selectable ranges (±1v, ±5v, and ±10v). In the MDSS the Dual Voltage DAC is used to control the two Fairchild voltage to pneumatic pressure regulators. These regulators control the air pressure in the vertical stress and first shear stress cylinders. Hence, operating the regulators with the Dual Voltage DAC enables these two stresses acting on the sample to be controlled by software commands from the computer. The digital signal created by programmable statements in the Vectra is converted by the Dual Voltage DAC to a dc voltage which is then sent to the Fairchild regulator.

3.2.3.3 Digital Multimeter

The HP PC Instruments Digital Multimeter measures ± dc voltages, ac voltages and ohms (resistance). The multimeter uses an analog to digital converter so that analog signals can be recorded and stored by the computer. The instrument has programmable reading rates of 2.5 and 12.5 readings/sec and DC voltage ranges of 200mV, 2V, 20V, and 200V. The instrument can also be used in autorange where the optional range is selected. The multimeter is used in the MDSS to convert the instrumentation transducers' analog signals to digital form for recording readings on the computer and for obtaining transducer readings for the computer control system. The measurements can be taken continuously or they may be triggered one at a time.

3.2.3.4 Relay Multiplexer

The HP PC Instruments Relay Multiplexer consists of an eight channel multiplexer with a temperature reference for thermocouple applications. The multiplexer is used as an input source for all the transducers in the MDSS. A cable from the instrumentation box carries all the signal wires for the transducers and connects them to the multiplexer. The multiplexer is connected to the PC Instruments Digital Multimeter and individual transducers are read when the multiplexer is switched to the appropriate channel for a transducer. The switching among different transducer channels is controlled by programmable statements from the computer.

The maximum switching rate is 65ms but it has been found that using this periodically results in inaccurate reading because the voltage has not had enough time to stabilize, therefore, slightly slower switching times were used for the MDSS.

3.3 COMPUTER CONTROL SOFTWARE

3.3.1 Main Program Overview

Data acquisition and servo control of sample forces are performed in the MDSS with a software program written in BASIC. All of the PC Instruments modules are operated by programmable BASIC statements. The main program, MDSSTEST, used to run tests in the MDSS consists of three separate sections:

- Program Shell
- Consolidation Software
- Undrained Shear Software

The program shell is generated by an operator for a specific task using software which comes with the PC Instruments system. The program shell consists of BASIC statements that initialize the PC Instruments system at start–up so that user–written software can communicate with the system. It contains labels, interface numbers, bus addresses and other communication requirements of the modules used in a specific system. It also contains the subroutines which can be called by the user–written software to operate the PC Instruments modules.

The consolidation software section contains subroutines for applying consolidation increments and recording transducer readings. The undrained shear software section contains subroutines for the undrained shear servo control loop. The user interacts with both of these sections of the main program through keyboard function keys. These function keys represent specific tasks that can be initialized or changed during testing of a sample. When a specific key is engaged the program will prompt the user for input data (entered via the keyboard) pertinent to the task

engaged. For example, one function key allows the user to change the time interval of data readings. When this key is engaged the user will be requested to enter a new time interval. Other examples include: application of a new consolidation increment, print out of measured strains during consolidation and start of undrained shear section. The program also includes several safeguards to prevent problems from occurring during a test. For example, all data input from the keyboard is echoed on the screen so that its accuracy can be verified. When corrections are necessary, the program allows for such changes to be made before the statements are executed. The program checks if requested stress levels for consolidation increments are reasonable with respect to magnitude of stress, load increment ratio and ratio of the first shear stress to the vertical effective stress. It also does error trapping to catch accidental input errors, thus preventing the whole program from crashing and having to be restarted.

The main program MDSSTEST used for testing samples in the MDSS is listed in Appendix C. Figure 3.5 is a schematic of the software written for the main program. Each box in the figure represents a subroutine or group of subroutines for performing specific tasks. The program is generally used in the following sequence (as shown in the Figure 3.5):

1. Start up
    - setup sample, apply seating load and take initial readings.
2. Consolidation (for each increment of σ'_{vc} and τ_{hc})
    - input incremental stresses σ'_{vc} and τ_{hc} required;
    - apply stresses to the sample;
    - take readings and monitor stress levels;
    - at end of each increment, print out results and store on hard disk.
3. Undrained Shear (application of the second shear stress τ_2)
    - pre–shear set–up;

- take readings and monitor constant height servo control loop;
- store data readings on the hard disk.

Some of the steps outlined above are also described in more detail in Section 3.4 which reviews sample preparation and testing procedures for the MDSS.

There are two servo control loops used in the MDSS program; one is used to control stresses during consolidation and the other is used to control the sample height during undrained shear. These systems are described in the following two sections.

3.3.2 Constant Stress Servo Control

As outlined in Section 3.2, application of the vertical stress and first shear stress to a sample is done using the computer, PC Instruments modules, two Fairchild pressure regulators, and two air cylinders. The application of loads is automated using a stress controlled servo control loop as shown schematically in Figure 3.6 for the vertical stress system. Once the stress level for a consolidation increment is entered into the computer (using a function key) the program sends a digital signal to the Dual Voltage DAC which converts it to an analog dc signal. This signal is sent to the Fairchild voltage to pneumatic regulator which changes the air pressure in the air cylinder and hence the stress acting on the sample.

The Fairchild regulators have been calibrated so that the voltage sent by the computer (via the Dual Voltage DAC) will result in approximately the correct stress applied to the sample at the beginning of an increment. However, the stress is brought more closely to the exact value using the vertical load cell in the servo control loop. At the beginning of an increment, the stress is first applied using the voltage computed from the Fairchild regulator calibration. Immediately after, the vertical load cell is monitored to compare its current value with the value corresponding to the stress level requested (the load cell zero reading and calibration factor are stored in the computer). Any difference between the current load cell reading and that corresponding to the

stress level requested is used to adjust the voltage applied by the Dual Voltage DAC to the pressure regulator and hence changing the sample stress. This process is called the "power–up" stage where the incremental consolidation stress is quickly brought up to the desired level. For most increments this procedure takes 1 to 3 seconds and automatically brings the stress to within 0.02 ksc of the required value.

The value that is sent to the Dual Voltage DAC during "power–up" is computed using the following equation:

$$IN_i = IN_{i-1} + (DV)_i(VALPHA) \qquad (3.1)$$

where:

IN = voltage sent by the computer to the Fairchild regulator via the Dual voltage DAC

DV = voltage difference ("error") in load cell reading

VALPHA = gain factor

The gain factor is used to speed up the power–up routine and was found by trial and error to work well when equal to 120. Using higher values will cause the servo loop to become unstable and send it into oscillation because of overcorrecting.

The consolidation data readings are started once the sample stress is powered–up to the requested level. In addition the computer will also monitor the vertical stress acting on the sample at a user selected time interval. Any errors will be corrected using equation 3.1 but with a higher tolerance of 0.007 ksc, which for a sample consolidated to 3 ksc represents 0.2% of the sample stress. Experience with testing in the MDSS has shown that the electric and pneumatic components used to apply the vertical stress to the sample are very stable, and that once the stress is powered–up to the correct level the computer rarely has to make adjustments to the stress level, even over a 24 hour period. Both the time interval between consolidation data readings and servo checks of the stress acting on the sample can be changed at

any time during an increment using a function key.

The same type of servo control loop is used to apply consolidation shear stress increments for the first shear stress. The only difference is that the horizontal shear stress acting on the sample is indirectly monitored via a pressure transducer instead of a load cell. The air cylinder used to apply the first shear stress is calibrated so that the shear stress it produces is a known function of the air pressure reading on the pressure transducer. This system also takes from 1 to 3 seconds to power–up the stress to the requested level using a gain factor equal to 40 and maintains the stress during an increment to within 0.001 ksc. For a sample consolidated with a shear stress ratio τ_1/σ'_{vc} of 0.2 and $\sigma'_{vc} = 3$ ksc, this tolerance represents 0.2% of the horizontal shear stress.

3.3.3 Constant Height Servo Control

Undrained shear is conducted in the MDSS by maintaining the volume of the sample constant during shear. The sample is assumed to be confined laterally by the wire–reinforced rubber membrane and, therefore, only the height needs to be kept constant to run a constant volume test. The sample height is kept constant by varying the vertical stress acting on it during shear. Changes in vertical stress required to keep the height constant are assumed to be equal to the pore pressure that would develop if the test was truly undrained with pore pressure measurement. Dyvik, et al. (1987) showed that for normally consolidated clay this assumption is valid.

The constant height servo control system uses the Z DCDT (see Figure D.4 for its location) to monitor the height of the sample during undrained shear. The computer monitors the constant height DCDT; when a change in the sample height is detected, the computer will adjust the vertical stress by changing the voltage being sent to the Fairchild regulator. With one exception, the system components used to change the stress are the same as that used for the constant vertical stress servo

control system shown in Figure 3.6 (i.e., Dual Voltage DAC, Fairchild regulator, and the air cylinder). The difference between the two systems is that the constant height system monitors the constant height DCDT instead of the vertical stress load cell.

Initially, the software used to make adjustments to the vertical stress for maintaining the sample height constant was similar to that used for the constant stress servo control. Voltage changes detected in the constant height DCDT were used to change the voltage applied to the vertical stress pressure regulator using an equation similar to 3.1. Unfortunately, this system proved to be unsatisfactory in maintaining the sample height constant during undrained shear. The main problem with the system was that it went into an unrecoverable oscillation of vertical stress soon after the beginning of a test.

This oscillation problem is clearly shown is Figure 3.7 which is a plot of the normalized vertical stress (σ'_v/σ'_{vc}) versus shear strain for an undrained K_o consolidated MDSS test on normally consolidated resedimented Boston Blue Clay (BBC). A normally consolidated sample will tend to contract during undrained shear and, therefore, develop positive pore pressure. Hence, when running a constant volume test the vertical stress must be decreased to maintain the sample height constant as the soil contracts. In general, the plot in Figure 3.7 follows the results expected for a DSS test on normally consolidated BBC. However, it is clearly evident that the servo control system was unable to maintain the sample height constant without causing the large oscillations in vertical stress. The oscillations have a remarkably large period of approximately 8 to 10 minutes. There were also sections during the beginning of the test when the vertical stress did not change as it should have. These "no–action" phases during the test were caused by the servo control system and represent another undesirable aspect of the original system.

The constant height servo control problem was eventually solved by making the following hardware and software changes:

1. Increased precision of the constant height DCDT readings by two orders of magnitude;
2. Increased rate of the constant height DCDT readings by one order of magnitude;
3. Changed the constant height DCDT setup to a single DCDT connected directly to the vertical stress piston as shown in Figure D.4;
4. Changed the servo control algorithm to a Proportional plus Integral plus Derivative (PID) controller.

The first three changes are discussed in more detail in Appendix D while the following paragraphs describe the PID controller. The failure of the constant stress servo controller to operate the constant height servo system indicates that the latter system is more difficult to control. The constant vertical stress system only has to monitor and maintain the vertical load cell at a constant target value. The constant height system differs in that the soil sample plays a role in the response of the system. The response of the soil sample to changes in vertical stress made to maintain its height constant has to be inherently taken care of by the servo controller. This evidently is a more difficult task and hence Mr. Rich Gedney[3] recommended that a PID controller be used.

The main function of the PID controller algorithm is to determine how to produce the control signal which is used to keep the sample height constant during shear. The PID controller equation used to perform this task in the MDSS is as follows:

$$IN_i = (1-c)IN_{i-1} + (c)IN_{i-2} + K(a+ac)R$$
$$-K[(1+b)P_i + (c-1+a-2b)P_{i-1} + (ac-c+b)P_{i-2}] \qquad (3.2)$$

[3]Former graduate student, MIT Department of Mechanical Engineering.

where:

IN = voltage sent to Dual Voltage DAC to control the vertical stress

R = reference voltage value of constant height DCDT

P = current constant height DCDT voltage reading

K,a,b,c = gain factors

This equation operates by calculating what voltage to send to the vertical stress pressure regulator based on the target value for the sample height (R), the most recent readings of the constant height DCDT (P_i, P_{i-1}, P_{i-2}), and the most recent values of the voltage sent (IN_{i-1} and IN_{i-2}). In other words, the whole objective is to vary the vertical stress so as to keep the constant height DCDT reading as close as possible to the target value R. In the MDSS, the PID controller updates itself every 0.15 seconds. This includes executing the software commands to read the DCDT, calculate Equation 3.2, and sending an updated voltage to the Dual Voltage DAC.

The appropriate values to use for the four gain factors K, a, b, and c are generally found by trial and error. The trial and error procedure involves balancing the controller's response time with its stability. That is, one wants the controller to be able to response quickly to height changes but to also response in a stable manner. For the MDSS the best gain factors were found by trial and error using a rubber sample and are: K=25, a=0.01, b=0.1 and c=0.001. The most important factor is K for which changes in its value will cause the most difference in the behavior of the controller. These factors were used for all tests performed on soil and also worked very well.

The PID controller also corrects for the apparatus compressibility during shear. For an undrained test on a normally consolidated soil, the vertical stress must be decreased to maintain the sample height constant. Hence there will be an expansion of the top and bottom caps (mainly due to the porous stones), which will compress into the sample if not corrected for. The compliance of the system was measured without a sample and the load deflection curve stored in the computer program. This allows the

PID controller to make appropriate changes in the reference or target value of the constant height DCDT (the value R in Equation 3.2) depending on the changes in vertical stress during a test. Several CK_oUMDSS tests were run on normally consolidated BBC with and without correcting for the apparatus compressibility during shear. The difference in measured strength turned out to be very small and for the particular conditions under which the tests were conducted (normally consolidated BBC with $\sigma'_{vc} = 3$ ksc), making the correction was not necessary. These results and the accuracy of the PID controller in maintaining the sample height constant during shear are described in more detail in Appendix D.

Equation 3.2 and the theory behind PID controllers are described in more detail in Gedney (1988) and other references such as Ogata (1970). The objective of the description given in this section is to contrast the type of controllers needed for the constant height system and the constant stress system without having to go into detail about control theory. The main point is that controlling the sample height required a more sophisticated algorithm which was derived from fundamental control theory principles.

3.3.4 Data Reduction and Processing

All instrumentation readings taken by the computer during a test in the MDSS are stored on the computer's hard disk. During consolidation, the sample strains can be printed out at any time during an increment so that the time deflection curves can be plotted while the sample is consolidating. The calculated strains correspond to the reference axes of the device which include: vertical strain ϵ_v, shear strain component in the X direction γ_x, and shear strain component in the Y direction γ_y. The software for this is included in the main program MDSSTEST.

Reduction of the undrained shear data is done using a separate program and is performed when a test is completed. The program MDSSCKO reduces the data for K_o

consolidated tests while MDSSCAU is used to reduce the data for the anisotropically consolidated tests run with an angle theta between the first and second shear stresses. Both programs are written in BASIC and are listed with the main testing program MDSSTEST in Appendix B. Additional corrections are made for the resistance of the rubber membrane when reducing the data. Appendix B shows this correction. Once all the data are reduced, the results are plotted using the HP plotter.

3.4 TESTING PROCEDURES FOR COHESIVE SOILS

This section describes the testing procedures used for cohesive soils in the MDSS. All samples tested for this thesis came from batches of resedimented Boston Blue Clay (BBC). The procedure for preparation of the batches of BBC is given in Germaine (1982). Section 4.2 and Appendix F summarize the batching procedure and describe the test soil in more detail.

3.4.1 Sample Preparation and Setup

Each specimen of BBC is unwrapped from its protective wax and aluminum coating and trimmed in MIT's humid room. Three or four water contents of approximately 15 g each are cut from the corners of the specimen. The sample is then placed on the bottom pedestal and into the Geonor trimming jig. The edges of the sample are trimmed using the Geonor cutting shoe which cuts the sample into a circular shape of 35 cm^2. The cutting shoe also allows the top and bottom of the sample to be smoothly trimmed with a wire saw to an approximate height of 2.3 cm. The sample is then transferred to the testing laboratory where a vacuum pump is used to place the wire–reinforced rubber membrane around it. Before the vacuum is released, the top cap is placed on the sample. Once this is complete the sample height is measured with a micrometer.

The bottom pedestal with the sample and top cap is placed in the sample

enclosure circular cage along with the water bath and the X and Y DCDT holders (Figures 3.2 and 3.3). The sample enclosure is then placed in the MDSS on the main bearing plates and aligned in place with two alignment pins. This entire procedure has to be performed in such a way that the sample enclosure ends up in the MDSS with the correct orientation. The top cap must be placed on the sample so that the "flats" on it are exactly aligned with the X–Y axes of the MDSS (Figure 3.3a); otherwise the X and Y displacement measurements will be incorrect. Details of the required procedure are described in Appendix B, Section B.6 Alignment.

Once the sample enclosure is properly placed in the MDSS loading frame, the computer and PC Instruments are turned on. The vertical loading system is slowly lowered until it touches the top cap of the sample with a slight seating load ($\cong$ 0.02 ksc). This procedure is performed using the computer which allows the user to slowly increase the voltage acting on the Fairchild regulator and hence changing the stress in the vertical stress air cylinder. Once this is complete the vertical stress piston is temporary locked in place and the top cap is secured to it with four screws. In addition, the four DCDT's (Z1, Z2, X and Y) are set up securing them with their plexiglas holders and in the correct voltage range. Once this is complete the vertical piston lock is released and a slight additional seating load is applied. Now the sample is ready for testing and the computer takes the zero readings for all the instrumentation transducers.

3.4.2 Consolidation

The steps necessary to consolidate a sample in the MDSS depend on whether the sample is to be consolidated with or without application of the first horizontal shear stress.

K_o Consolidation:

When a new increment of vertical stress is to be applied to the sample, the

user initializes this action by pressing the "new increment" function key on the computer. The program will then request what stress level is to be applied, what gain level the Fairchild pressure regulator is at[4], time interval for the data readings, and finally, time interval for the constant stress servo system to check the stress level. Once all this information is entered and confirmed, the computer will start the increment and powerup the stress to its new level and then start taking data readings. At any time during an increment the data reading and servo control time intervals can be changed and the sample time–deflection–strain results can be printed out.

Water is generally added to the sample water bath when the sample has consolidated beyond its potential for swelling. For K_o consolidated samples, the two alignment pins are left in until just before applying the last increment of vertical stress.

Anisotropic Consolidation at θ:

Tests which are consolidated anisotropically with the first shear stress (for consolidation $\tau_1 \equiv \tau_{hc}$) acting at some angle θ must have the first shear piston setup (Figure 3.2a) before consolidation starts. The air cylinder that applies the first shear force is connected to its supporting frame (as described in Appendix B) at the angle θ selected for the test. Then the loading bracket which transfers the force to the sample is attached to the sample enclosure and a seating load is applied to overcome setup friction of the loading piston and bracket. Once completed, the system is ready to apply an horizontal shear stress through commands from the computer. The stress level and constant stress servo time interval are entered in the same manner as for the vertical stress system. The vertical alignment pins are removed just before application of the first increment of first shear stress (thus allowing the bottom of the sample to displace relative to its top). Typically the first few vertical stress consolidation

[4]The Fairchild pressure regulators have booster units which are manually adjusted to obtain higher air pressures as the stress level of a test increases.

increments are applied with the consolidation shear stress equal to zero. Only after the sample consolidates under these increments are increments of both vertical stress and horizontal shear stress applied.

With this setup a preselected combination of vertical stress and first shear stress increments can be applied to the sample. Once the loading schedule is selected it is entered in the computer and the results can be conveniently printed out for each loading increment for plotting and analysis.

3.4.3 Undrained Shear

After the sample is consolidated to its final state of stress (including one cycle of secondary compression) it is then ready to be sheared undrained. The undrained shear force is applied with the gear drive system that strains the sample at a constant rate of strain of approximately 5%/hr.

The undrained shear or second shear setup involves installing the constant height DCDT and setting it within the appropriate voltage range (± 200 mv) for the precision required for the servo control system. The next step is to bring the special load applicator which transfers the second shear horizontal force to the sample cage while still allowing the cage to move freely in a perpendicular direction. This is performed by manually adjusting the length of the horizontal loading system (the τ_2 thrust shaft om Figure 3.2b) to bring the applicator within contact with the circular cage. Once completed, the program takes the final pre–shear transducer readings. The gear drive motor is turned on and then the constant height PID controller starts to continuously monitor the sample height. Data readings (Input voltage, X, Y, Z1 and Z2 DCDT's and vertical and horizontal load cells) are taken at a requested time interval which normally ranges from one to four minutes.

Throughout the τ_2 shearing phase, the vertical stress is changed to maintain the sample height constant while the first shear stress is kept constant at its τ_{hc} value.

If the sample had been K_o consolidated, then the first shear stress was obviously always equal to zero. Once the sample reaches its peak shear resistance the sample is allowed to continue shear until catastrophic failure is eminent (due to τ_{hc} remaining constant). At this point (which is detected by monitoring the shear strain rate) the test is stopped .

3.4.4 End of Test

At the end of undrained shear the sample is manually brought back to its preshear configuration (i.e., X and Y coordinates $\cong$ 0) and allowed to sit overnight under just a vertical stress seating load. The following day the sample is removed from the device and a final water content is taken.

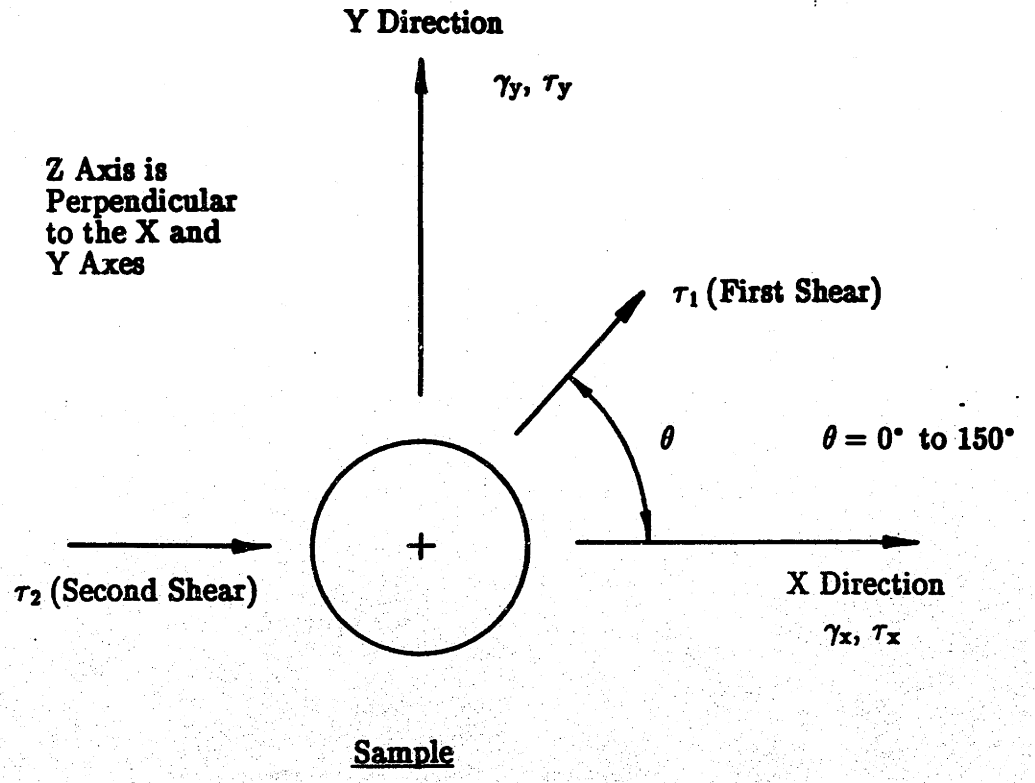

Figure 3.1: Plan View Showing MDSS Coordinate Axes for Describing Direction of Displacements and Applied Forces.

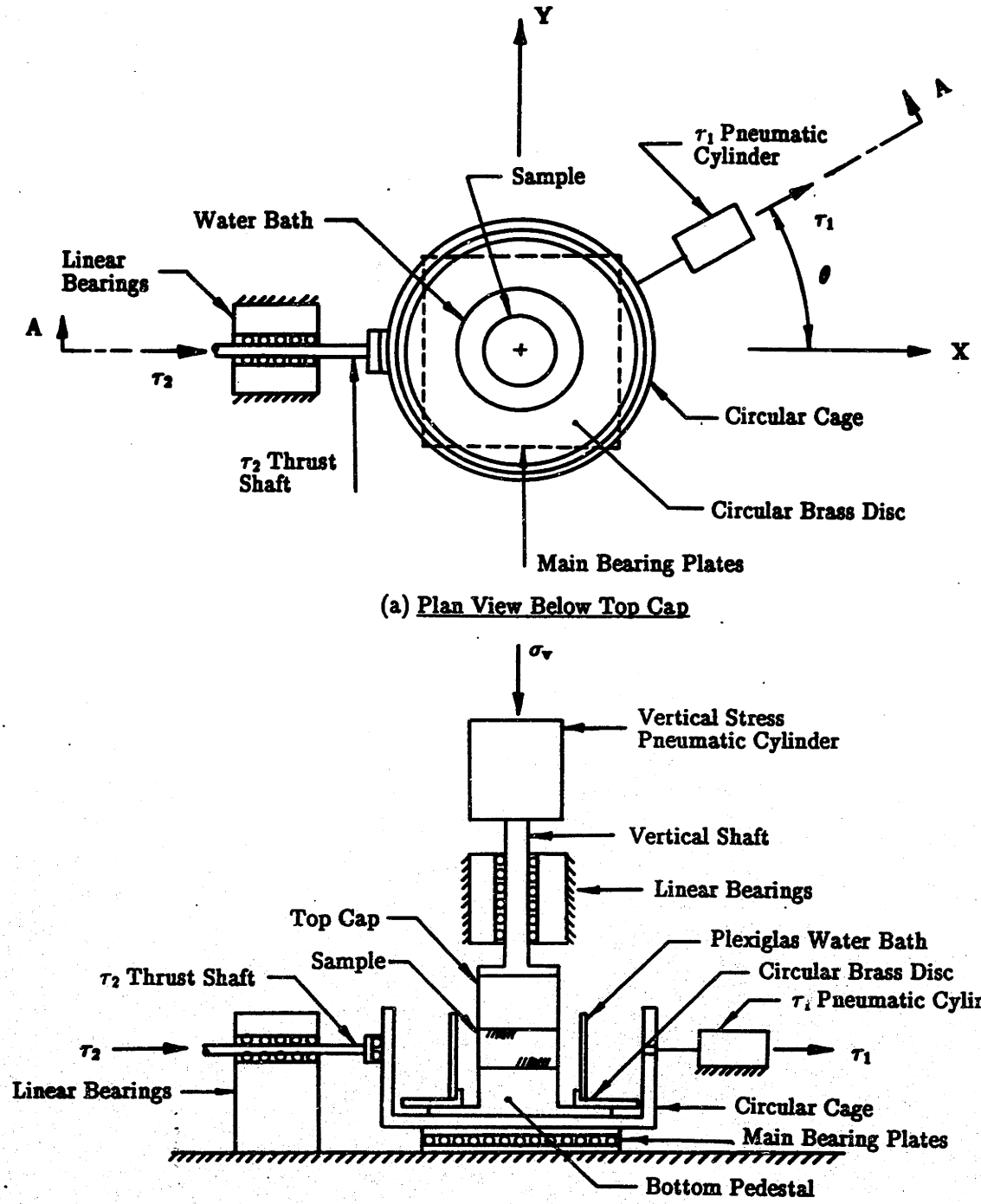

Figure 3.2: Schematic of MDSS Showing Sample Location and Application of Forces.

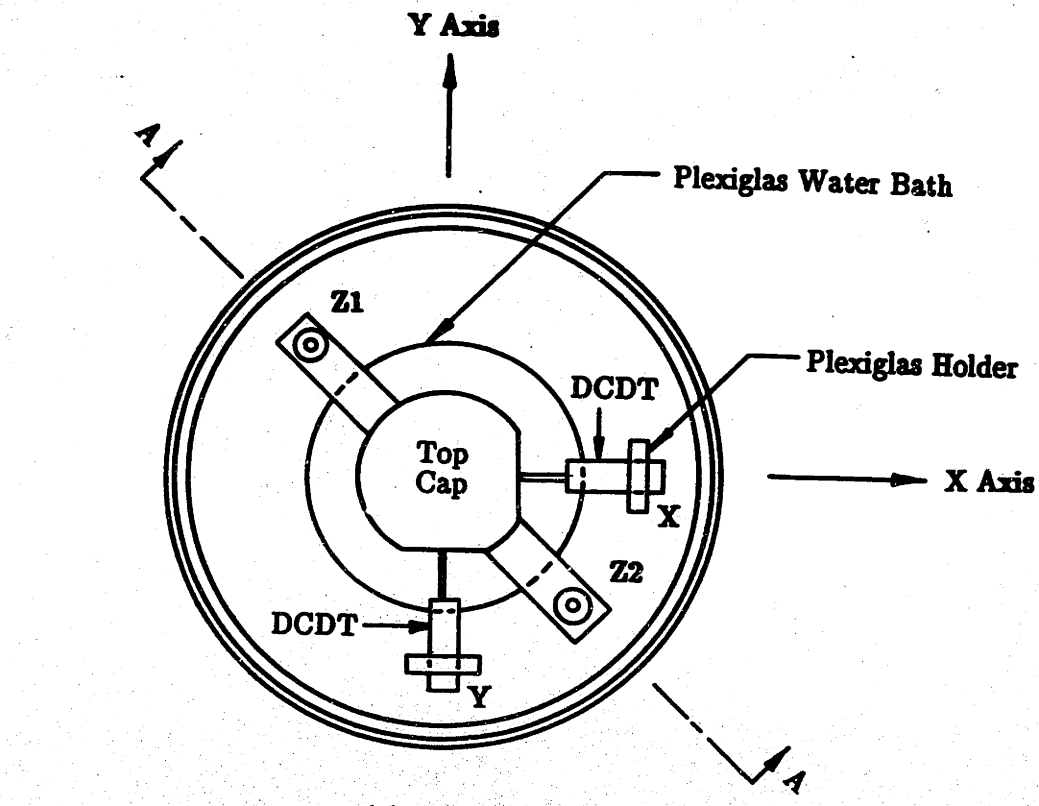

(a) Plan View

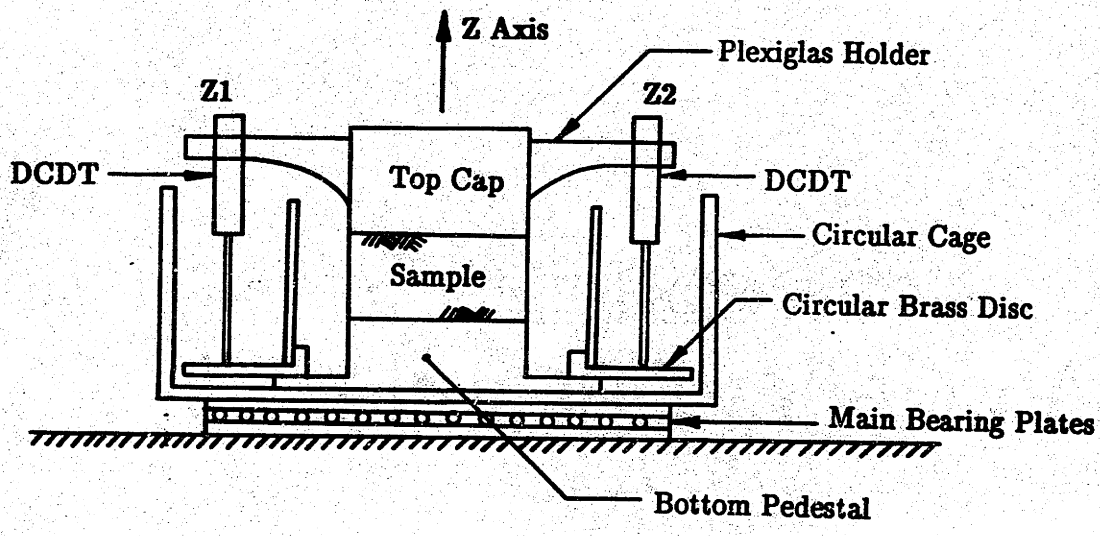

(b) Cross Section A–A

Figure 3.3: Location of X, Y, Z1, and Z2 Direct Current Displacement Transducers (DCDT) in the MDSS.

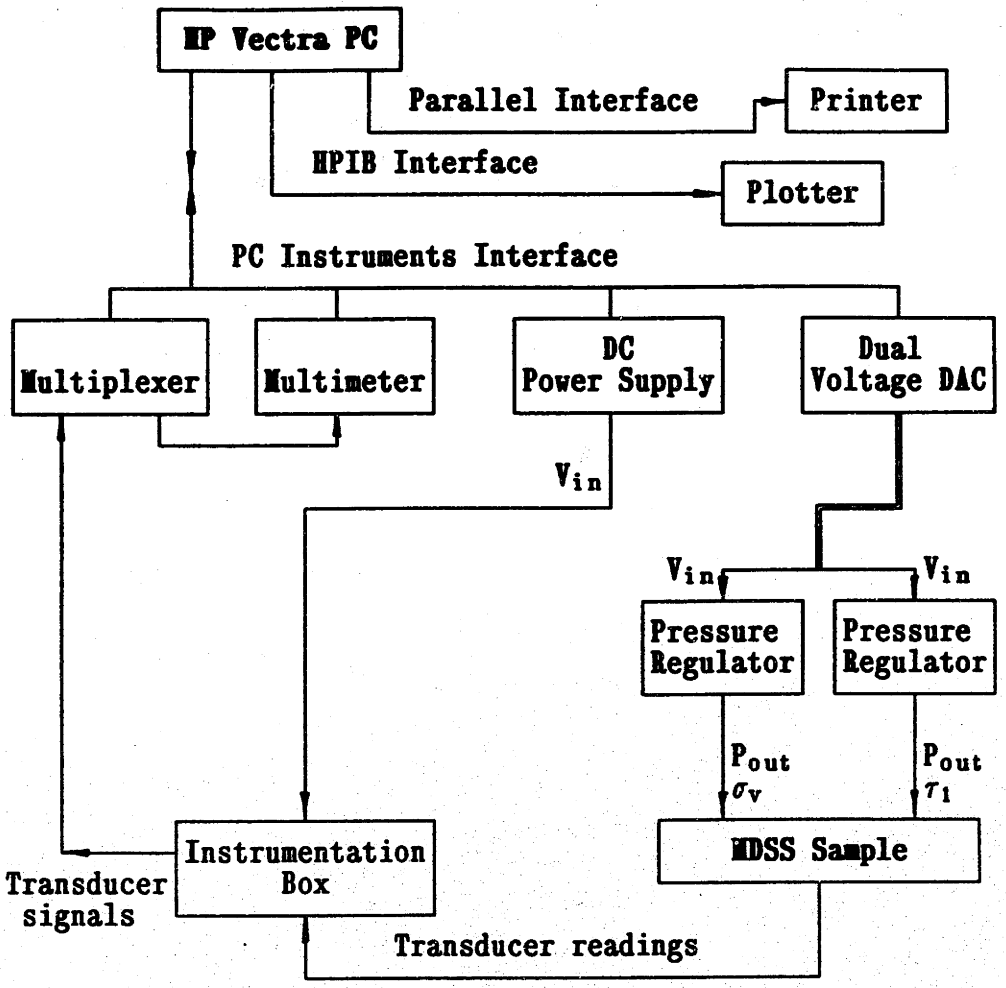

Notes:

V_{in} ≡ Input voltage
P_{out} ≡ Output air pressure
σ_v ≡ Vertical stress
τ_1 ≡ First shear stress

Figure 3.4: Schematic of Computer Control and Data Acquisition Equipment.

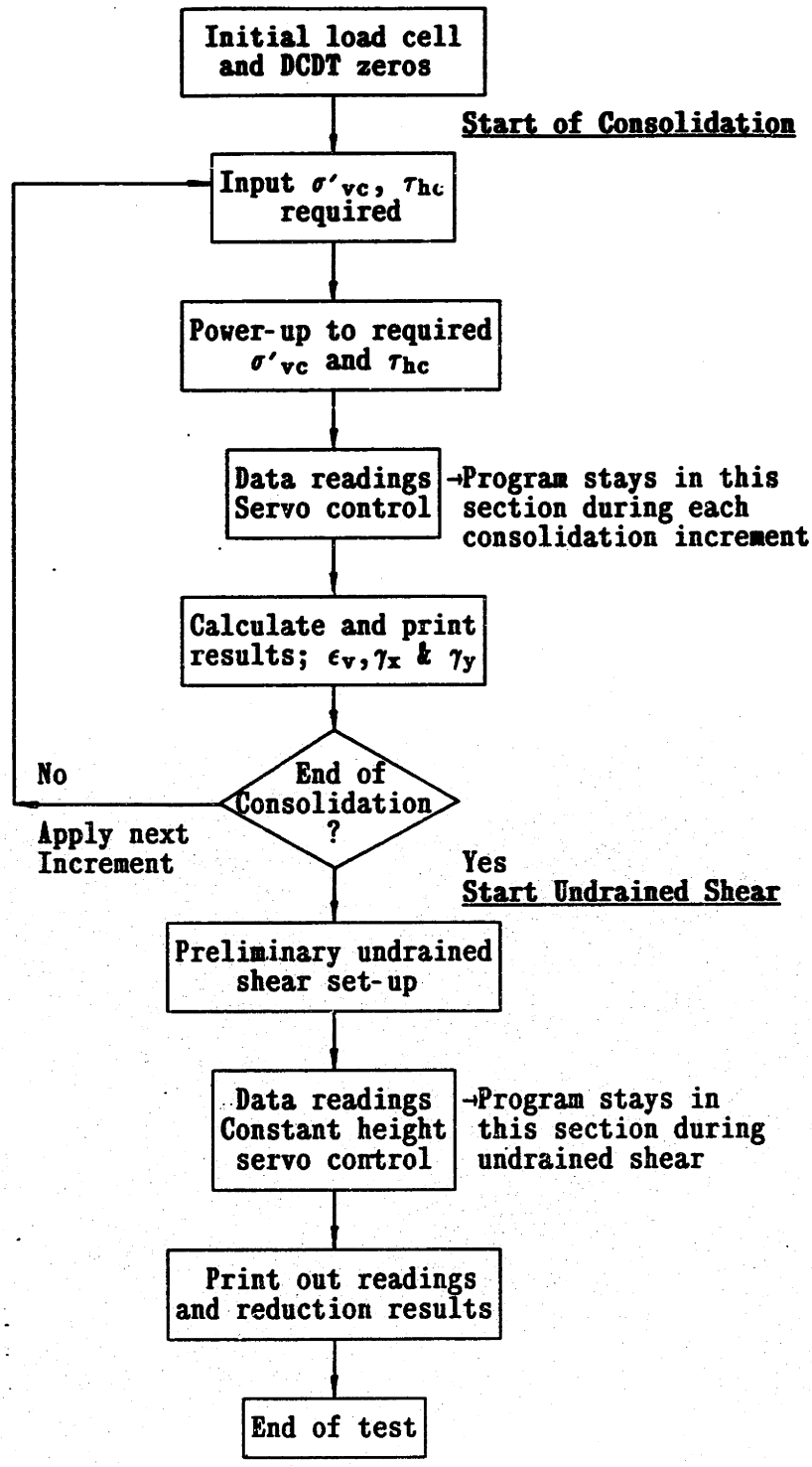

Figure 3.5: Computer Control and Data Acquisition Program.

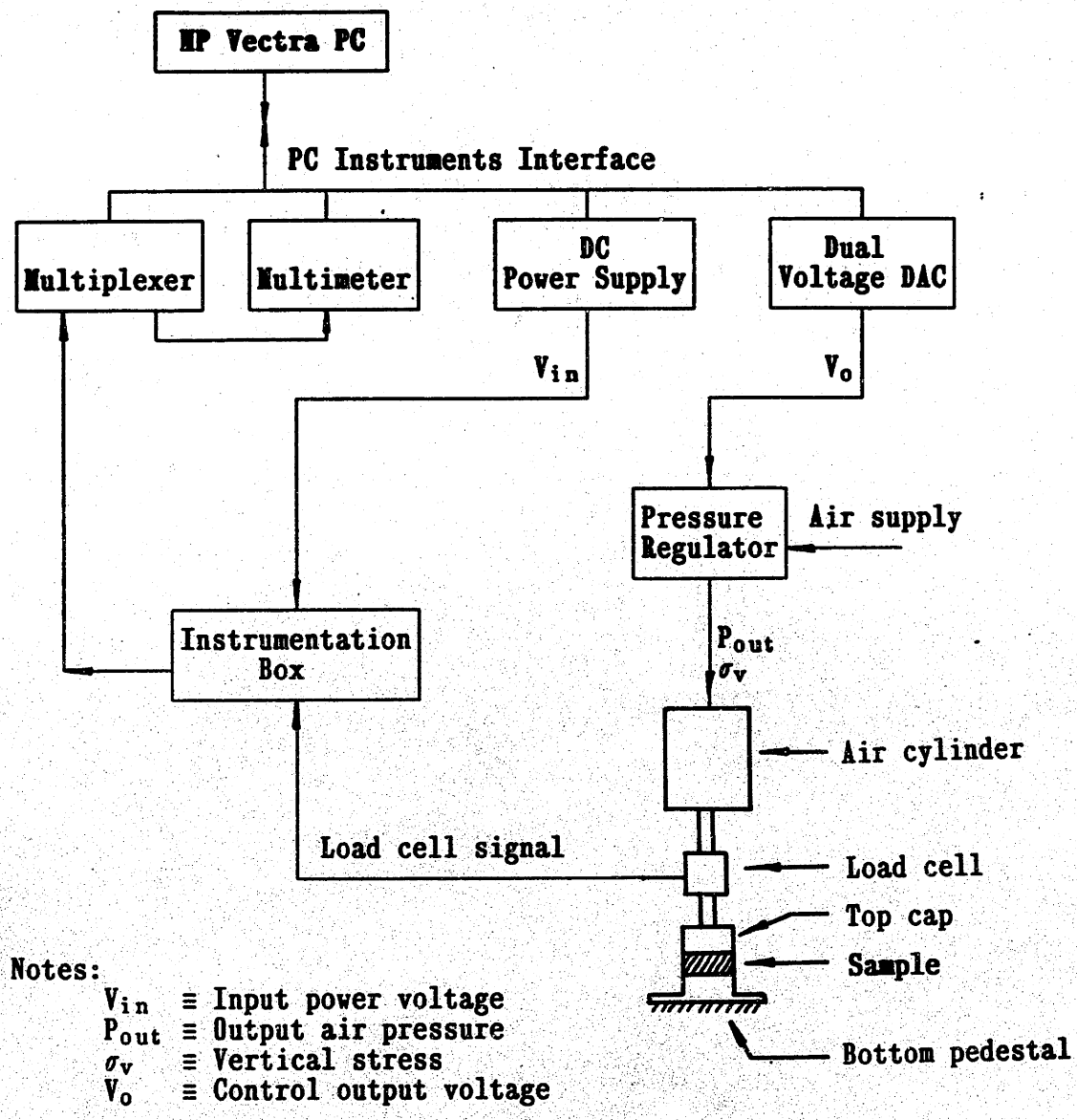

Figure 3.6: Schematic of Stress Controlled Vertical Stress Servo Control System.

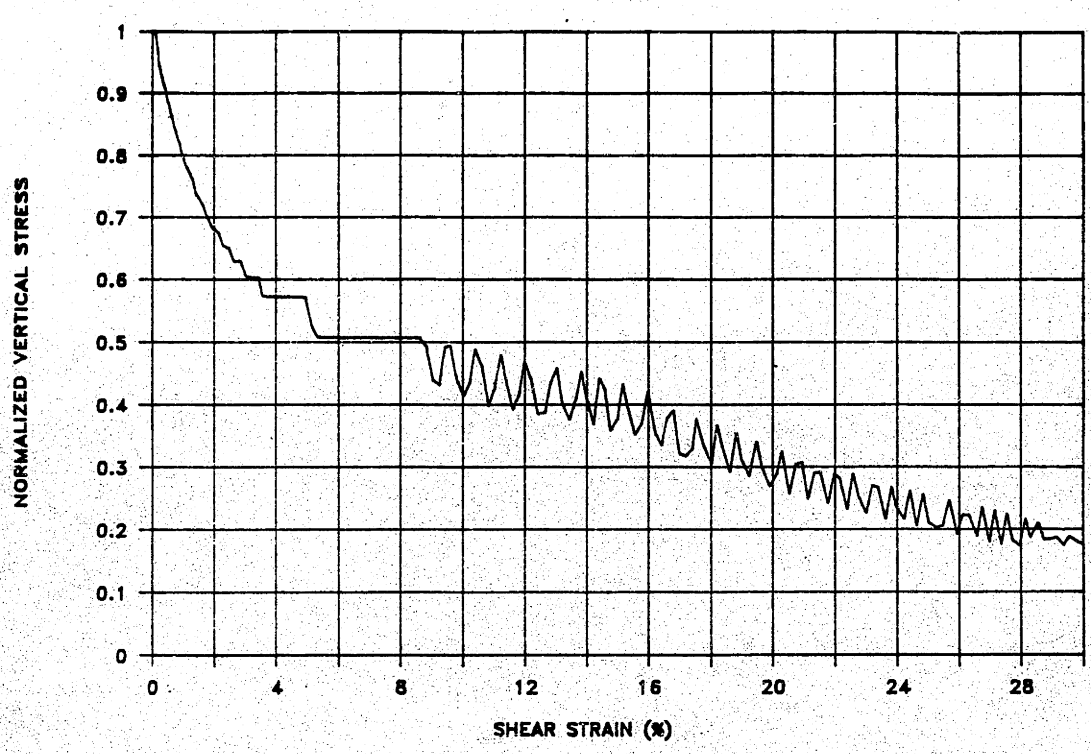

Figure 3.7: Oscillation of Vertical Stress During Undrained Shear of Test MDSS–C1.

CHAPTER 4

EXPERIMENTAL EVALUATION OF THE MDSS DEVICE AND TESTING PROCEDURES

4.1 INTRODUCTION

An experimental evaluation of the MDSS and testing procedures was conducted with the following objectives:

1. Determine if the same types of shear test run on soil specimens in the MDSS and an existing DSS apparatus produce comparable results;
2. Verify the kinematics of the new testing device.

The first objective of the evaluation program was to conduct tests on clay specimens in the MDSS which could also be performed in another apparatus so that direct comparison of the results could be made. Specifically, the Geonor DSS is capable of performing two types of tests that can also be run in the MDSS. This includes standard CK_0UDSS tests, which are routinely performed in the Geonor DSS, and CAUDSS tests with $\theta = 0°$. The second type of test provides a very important comparison because it represents the specific type of test for which the MDSS was designed. Given MIT's extensive experience with Geonor DSS testing, these test comparisons provide valuable information on the capabilities of the MDSS.

The second objective of the evaluation program was to check the kinematics of the MDSS. This evaluation is particularly important for two reasons: (1) it is necessary to determine if the first shear stress (τ_1) is applied at the correct orientation for each of the different θ angles, and (2) verify that the sample set–up procedure and strain measurement system are working properly and produce repeatable results. This phase of the evaluation program was performed with an elastic material (rubber).

The remainder of this chapter begins with a review of the test soil,

resedimented Boston Blue Clay (BBC), which was used for all the soil tests in this thesis. The consolidation and shear results for the same types of tests on BBC in the Geonor and MDSS are presented and compared. This is followed by an evaluation of the kinematic proof tests conducted in the MDSS with rubber. This chapter concludes with a summary of the experimental evaluation of the MDSS and testing procedures.

4.2 TEST SOIL – RESEDIMENTED BOSTON BLUE CLAY

Boston Blue Clay (BBC) is an illitic glacio–marine CL clay deposited in the Boston Basin approximately 12,000 to 14,000 years ago (Kenny, 1964). Resedimented BBC has been studied and tested extensively at MIT, making it an excellent reference material for research purposes. For this reason it was chosen as the test soil for conducting the experimental evaluation of the MDSS and also for conducting the first series of MDSSCAU tests (i.e., CAU tests at different θ angles – Chapter 5).

The particular clay used for this research project was acquired by MIT in 1986 during construction of a parking garage in East Cambridge. The soil came from a depth of approximately 75 feet and was described as a "medium stiff, grey–green silty clay with occasional partings" (Walbaum, 1988). Prior to laboratory testing the natural soil is resedimented using the procedure developed by Germaine (1982) which is described in the following section.

4.2.1 Resedimentation Procedure

Batches of BBC used at MIT are basically prepared by consolidating a dilute slurry of soil in a cylindrical container. At the end of consolidation the cake of clay is trimmed, sealed and stored in a humid room. This procedure was initiated in the early 1960's and has gradually been improved upon since. The most significant improvement was made by Germaine (1982) who refined the resedimentation technique

to produce saturated, uniform samples of BBC with a salt concentration of 16 grams per liter.

The process begins by wet sieving the natural soil on a U.S. Standard No. 40 sieve to remove coarser material and undesirable objects such as wood, shells, etc. The material is then oven dried and subsequently ground to a fine powder using an impact mill.

The sedimentary process uses three chambers (Figure 4.1). An upper chamber is used to mix the batch ingredients while the lower chamber consists of a 30 cm diameter stainless steel shell which receives and consolidates the soil slurry. A third chamber is used as a connection between the upper and lower chambers. The batch material consists of oven dry clay powder, distilled water, salt (NaCl) to act as a flocculant and phenol to inhibit the growth of organics. The clay powder and distilled water are de–aired and mixed under vacuum in the upper chamber using a rotary shaft with propellers attached to it. Once the slurry reaches 100% water content, it is subjected to high speed agitation for an additional 30 minutes. The slurry is then sprayed through the free fall chamber into the consolidation chamber.

The soil slurry is incrementally consolidated to a maximum vertical stress of one ksc using a load increment ratio of one. Each increment is maintained on the sample until the end of primary consolidation as determined by Casagrande's log time method. The maximum stress of one ksc is left on the sample for one cycle of secondary compression after which the sample is incrementally unloaded to 0.25 ksc (OCR = 4). O'Neill (1985) found, using MIT's Lateral Stress Oedometer and results from triaxial tests, that $K_o = 0.9$ for BBC at OCR = 4 during unloading. Therefore, the sample in the consolidation chamber is almost at an isotropic state of stress and hence "disturbance" (undrained shear deformations) due to release of shear stresses when the sample is removed from the chamber is minimized.

The cake is removed from the consolidation chamber by carefully trimming an approximate $^1/_8$ in. wide trench around its perimeter from top to bottom. This allows the chamber to be removed without any drag forces between it and the soil. Once the chamber is removed, the cake (approximately 30 cm diameter by 12 to 14 cm high) is carefully trimmed into individual specimens for Directional Shear Cell (DSC), DSS, oedometer and triaxial testing.[1] The trimming is performed using a special mitre box and all specimens are always handled and supported with glass plates to minimize disturbance. Individual specimens are coated with a 50–50 mixture of beeswax and paraffin (beeswax for moisture retention and paraffin for strength), cellophane, another coating of wax mixture, aluminum foil (for additional strength) and a final layer of wax mixture. The specimens are stored in MIT's humid room which is maintained at 95 to 100% relative humidity.

Germaine (1982) evaluated the quality of resedimented samples of BBC prepared using the procedure described above by checking for uniformity, degree of saturation, and disturbance. Uniformity was confirmed within individual batches by measuring the variation of water content with depth, using x–ray diffraction and air drying of vertical slices to check for stratification. Results from all three procedures verified that the batches were indeed uniform. Uniformity among batches was confirmed by comparing water content and consolidation characteristics (compressibility and rate of consolidation). Both procedures showed little variation among the batches. Full saturation was confirmed from measurements of Skempton's pore pressure parameter B in triaxial tests and from measurements of phase quantities (i.e., measurement of water volume, soil volume and total volume of specimens). The amount of disturbance in the test specimens, based on reconsolidation strain data and measured sampling pore pressures, was found to be minimal.

---

[1]For example, a typical batch can produce: 2 DSC specimens (5.5 in. cubes), 12 to 16 DSS/oedometer specimens and 4 standard triaxial specimens.

O'Neill (1985) found from extensive laboratory testing that resedimented BBC II (so called 100 series source material) changes in strength and compressibility as the time of storage between batch preparation and testing varied. This phenomenon is suspected to be caused by thixotropy which is defined by Mitchell (1976) as "an isothermal, reversible, time–dependent process occurring under conditions of constant composition and volume, whereby a material stiffens while at rest and softens or liquefies upon remolding." O'Neill found that the material exhibits an increasing preconsolidation pressure, decreasing recompression ratio and increasing undrained shear strength and initial stiffness as the elapsed storage time lengthens. The most remarkable change is in the measured preconsolidation pressure (via oedometer testing) which shows an approximately 100% increase over a two–year storage period. The reason why the resedimented BBC II exhibited this thixotropic nature is still unclear. And to add to this unusual behavior, all laboratory evidence indicates that the new source of clay, BBC III, used for this thesis (the 200 series versus O'Neill's 100 series batches) does not exhibit thixotropic hardening (Seah, 1989).

In summary, the batching procedure is labor intensive and takes about 3–4 weeks to produce each batch. MIT has two consolidation chambers so that, at maximum production, two batches can be made every 4–5 weeks. In spite of the effort involved, this procedure for resedimenting BBC is extremely valuable for research purposes because it produces high quality, uniform and saturated samples.

4.2.2 Index and Consolidation Properties

The samples of resedimented BBC used in this thesis came from four of the 200 series batches (200, 201, 202, and 203). Table 4.1 summarizes the results of specific gravity, water content, Atterberg limits, clay fraction, and salt concentration tests performed on the soil. The table includes results for the natural soil (before and after processing) and three of the batches.

Table 4.2 summarizes the results of five oedometer tests performed on samples from batches 200, 201 and 202. As described in Section 4.2.1, these tests provide an important check on the uniformity among batches. The results show very little variation among the three batches for preconsolidation pressure (σ'_p), virgin compression ratio (CR), coefficient of consolidation (c_v), and rate of secondary compression ($C\alpha\epsilon$). Figure 4.2 is a plot of the compression curves up to 8 ksc for each of the five tests and shows consistent results among the three batches.

It is interesting to note that the ratio of $C\alpha\epsilon$/CR for these tests averaged 0.015 ±0.002SD. Mesri and Choi (1985) report that for a majority of inorganic soft clays this ratio ranges from 0.03 to 0.05. O'Neill (1985) found for 100 series BBC that $C\alpha\epsilon$/CR averaged 0.035. The difference between the 100 and 200 series batches is a result of the fact that the 200 series soil has a significantly lower rate of secondary compression ($C\alpha\epsilon$ = 0.0024 versus 0.0060 for 100 series soil). Thus the 200 series BBC not only lacks thixotropic hardening, but it also exhibits a lower rate of secondary compression and does not fall in the range of $C\alpha\epsilon$/CR found for many inorganic soft clays.

Several UU triaxial tests with pore pressure measurements were performed on soil from the 200 series batches to check for saturation. Unfortunately, initial problems with the pore pressure transducer made results for the 200, 201 and 202 batches unreliable. However, tests performed on soil from batches 203, 204 and 205 showed the soil to be saturated (Seah, 1989).

4.3 NORMALLY CONSOLIDATED GEONOR CK_oU DIRECT SIMPLE SHEAR RESULTS

Three CK_oUDSS tests were performed in the Geonor DSS to obtain reference consolidation and shear properties for the new 200 series BBC and for comparison with

similar proof tests conducted in the MDSS. Appendix E gives a review of the Geonor DSS testing procedures used at MIT.

4.3.1 Consolidation Behavior

The Geonor DSS has been shown to give the same K_o consolidation response as measured in a conventional oedometer test (e.g., see Germaine, 1982). Three Geonor CK_oUDSS tests were performed to verify this for the new 200 series BBC and also to provide data for comparison with results from the consolidation phase of CK_oUMDSS tests.

Unfortunately, all three Geonor tests (G1, G2, and G4) showed considerably more consolidation strain than measured in the oedometer tests summarized in Table 4.2. For example, at the final $\sigma'_{vc} = 3$ ksc the Geonor samples had an average vertical strain of $\epsilon_v = 14.5\%$ compared with an average of 10.3% for the oedometer tests (plotted in Figure 4.2). Four possible reasons for this unexpected behavior were identified and evaluated:

1. Sample disturbance;
2. Membrane stretching;
3. Bent porous stones;
4. Rough porous stones.

Sample disturbance is known to result in an increase in consolidation strains at a given stress level, but was not considered to be a significant factor in this case because of the procedure MIT uses to prepare specimens for testing. Lateral deformation of the membrane was measured in test G4 by using two displacement transducers to measure the external diameter of the membrane during consolidation (the membrane is made with constantan wire). At $\sigma'_{vc} = 3$ ksc the radial strain of the membrane was found to be 0.07%, which is insignificant compared to the discrepancy

in the vertical strains (i.e., this radial strain corresponds to an increase in $\epsilon_v = 0.15\%$). For comparison, Vucetic (1984) measured the radial strain of Geonor DSS constantan membranes using a π tape and found that, for a very soft silty clay, the radial strain averaged 0.16% for $\sigma'_{vc} = 1.02$ ksc.

Given that these two factors did not appear to be the source of the large vertical strains, the focus shifted to the porous stones used in the Geonor DSS. The stones, which are made of cintered bronze, were periodically found to be bent. This undoubtedly influenced (to some undetermined degree) the measured vertical strains. As a result, the stones were subsequently inspected and flattened before each test. However, the most significant discovery was that the stones were too rough and the soil was penetrating into them during consolidation. Hence the stones were simply flipped over with their smoother side facing the soil. This change, and flattening of the stones before each test, solved the problem as will be shown in Section 4.4.1 on the consolidation results of the CK_oUMDSS tests.

4.3.2 Undrained Shear Behavior

Table 4.4 gives a summary of the undrained shear results for the three Geonor CK_oUDSS tests. Figures 4.3a, 4.4a, 4.5a, and 4.6a are plots of the normalized stress–strain curve, pore pressure versus shear strain, stress path and normalized Young's modulus respectively for the three tests. Table 4.4 also includes test No. 5 run by Walbaum (1988) on batch 202 soil.

The results show a fairly large scatter in the normalized peak shear resistance. However, this scatter is no larger than that measured in the previous test programs on BBC which were conducted at the same stress level (σ'_{vc} = 3 to 4 ksc) as shown in Figure 4.7 and summarized in Tables 4.6 and 4.7. The data in Tables 4.6 and 4.7 show that in general the average values of γ, τ_h/σ'_{vc}, σ'_v/σ'_{vc} and ψ (= arctan τ_h/σ'_v) at maximum τ_h compare very well with previous CK_oUDSS tests on BBC. The only

property which does not compare well is the normalized Young's modulus, $E_u(50)/c_u$, as shown in Figure 4.8.[2] The new tests (G1, G2 and G4) have much higher values of E_u/c_u with remarkably little scatter among the tests (Figure 4.6a). Furthermore, Seah(1989) also found the 200 series soil to be stiffer based on comparison of DSC tests on this soil and those conducted previously on the 100 series soil.

The tests conducted for this thesis were performed in MIT's new Geonor DSS which was acquired in 1984. The new Geonor uses a displacement transducer which measures horizontal displacement directly against the top loading platen (this modification was made by MIT). The original MIT Geonor DSS, used for all of the other test programs summarized in Tables 4.6 and 4.7, also measures horizontal displacement at the same location with a displacement transducer but it is connected through a dial gauge. The dial gauge is used for visual readings and was removed from the new DSS. Replacing the dial gauge with a DCDT eliminates mechanical "stick–slip" problems that periodically occur with dial gauges. Although this does represent a difference between the two measuring systems, it is not yet clear if it is one of the reasons for the difference in the modulus results cited above.

4.4 MDSS CK_oU DIRECT SIMPLE SHEAR TESTS AND EVALUATION OF RESULTS

Six CK_oU tests were performed on normally consolidated BBC in the MDSS to evaluate the device and testing procedures. Conducting this type of test in the MDSS provided an opportunity to evaluate several aspects of the device including: performance of the constant stress and constant height servo control hardware and software, trimming and set–up procedures for cohesive soils, K_o consolidation results and undrained direct simple shear results. Table 4.5 gives a summary of the six tests

[2]Figure 4.8 also shows the dependency of $E_u(50)/c_u$ on the consolidation stress (σ'_{vc}).

run in the MDSS. Consolidation and undrained shear results are discussed separately in the following two sections.

4.4.1 Consolidation Results

Tests C1, C4, C5 and C6 were run in the MDSS before the consolidation problem with the porous stones was discovered as discussed in Section 4.3.1. Table 4.3 summarizes the consolidation results for tests C11 and C14 and includes a summary of the oedometer tests listed in Table 4.2. Figure 4.9 is a plot of the compression curve for tests C11 and C14 and the range of results for the oedometer tests. Table 4.3 and Figure 4.9 show that the consolidation data obtained in the MDSS compare very well with those of the oedometers (the oedometer tests give a slightly lower virgin compression ratio). Similar to the oedometer tests, the MDSS results give a low rate of secondary compression compared to the 100 series BBC and as a result the $C\alpha\epsilon/CR$ ratio (0.011) does not fall in the range of 0.03 – 0.05 for most inorganic soft clays as suggested by Mesri and Choi (1985).

4.4.2 Undrained Shear Results

Table 4.5 gives a summary of the undrained shear results for the six CK_oUMDSS tests. Figure 4.3b, 4.4b, 4.5b, and 4.6b are plots of the normalized stress–strain curve, pore pressure versus shear strain, stress path and normalized Young's modulus respectively for tests C5, C6, C11 and C14. Tests C1 and C4 were run on BBC II clay before improvements were made to the constant height servo control system as discussed in Chapter 3 and Appendix D, and are not included in the Figures and the averages listed in Tables 4.5 and 4.7. Appendix D presents an evaluation of the constant height servo control system and discusses sample deformation during undrained shear for the Geonor and MDSS tests.

The normalized stress–strain data plotted in Figure 4.3b shows remarkably little scatter among the four MDSS tests. In fact, the lack of scatter in these test

results is unprecedented for simple shear testing of BBC at similar stress levels. Figure 4.3a shows the scatter in the Geonor DSS tests run as part of this research and Tables 4.6 and 4.7 present data for other DSS tests programs on BBC. The average normalized shear strength from the four MDSS tests equals 0.186 ±0.002SD which is 7% lower than the average from the four Geonor tests (0.201 ±0.010SD, Table 4.4). The coefficient of variation in c_u/σ'_{vc} for the MDSS tests is 1.1% compared to a range of 4.6% to 5.4% for Geonor DSS test programs on BBC conducted at similar stress levels (Table 4.7). The average strain at failure for the two devices is almost identical; 4.8 ±0.8SD for the MDSS and 5.1 ±0.4SD for the Geonor. In general, the MDSS shear stress–shear strain curves are identical in shape to the Geonor curves, except that they are shifted slightly lower.

MDSS Tests C5 and C14 were run without correcting for the apparatus compressibility during shear, whereas for tests C6 and C11 the correction was made. However, the average normalized shear strength for tests C5 and C14 is only 0.004 higher than the average for tests C6 and C11 (0.188 vs 0.184). This indicates that for BBC and the stress level used for these tests (σ'_{vc} = 3 ksc), correcting for the apparatus compressibility during undrained shear results in an insignificant change in the measured shear strength ($\cong$ 2%; these results are discussed in more detail in Appendix D).

The normalized pore pressure data for the two devices, plotted in Figure 4.4, compare very well. MDSS test C11 developed an oscillation problem with σ'_v during shear at γ = 10%. This problem was solved during the test by stopping the constant height servo control program and immediately restarting it. This indicated that some sort of electrical noise or build up of static electricity may have caused the servo system to become unstable.

Figure 4.5 compares the stress paths for the MDSS and Geonor test results. The paths are nearly identical in shape with the MDSS curves plotting slightly lower.

The average values of normalized vertical effective stress (σ'_v/σ'_{vc}) and obliquity at peak shear resistance compare very well (Tables 4.4 and 4.5). The stress paths for tests C11 and C14 display some irregularity at the very beginning of the test which is probably due to a problem with the constant height DCDT. Any physical or electrical disturbance to this transducer can cause it to deviate from its reference value. This in turn will result in a change in the vertical stress acting on the sample as the constant height servo control system reacts to the change in the constant height DCDT reading. However, in spite of this irregularity at the very beginning of shear, the remaining portion of the effective stress paths were not affected (Figure 4.5).

Figure 4.6b shows the normalized Young's modulus versus applied stress ratio for the MDSS tests. The modulus values are very consistent, except for test C6. Overall, however, the results are not very satisfactory because E_u/c_u is significantly less than measured in the Geonor DSS (Figure 4.6a). Furthermore, the initial portion of the curves for tests C5, C11 and C14 are very flat. This means that the stress–strain curve is linear during the early stages of loading. However, almost all tests performed in the Geonor DSS at MIT on cohesive soils display a continuous decrease in the modulus with increasing shear stress. The average values of $E_u(50)/c_u$ are 710 ±160 and 950 ±99 for the MDSS and Geonor DSS respectively. This represents a difference of approximately 25%. The MDSS modulus values compare reasonably well with previous test programs on BBC at the same stress level, as shown in Figure 4.8. However, as discussed in the previous section, the new 200 series BBC used for this thesis appears to be stiffer than earlier batches of BBC.

Figure 4.10 shows an expanded version of the shear stress–strain curves for the MDSS and Geonor tests. The Figure clearly shows the more rapid increase in shear stress with shear strain in the Geonor tests and the parabolic shape of the Geonor curves. On the other hand, tests C5, C11 and C14 in the MDSS have a reverse curvature at the beginning of shear. This is not the case for test C6 which has a shear

stress–strain curve that is almost bilinear with a very rapid increase in shear stress at the beginning of the test. The shape of the shear stress–strain curves for Tests C5, C11 and C14 suggest that a seating problem may be the source of the low modulus results. Why the same did not occur for Test C6 is unclear.

The modulus results for the MDSS tests are somewhat disappointing. When the device was originally designed it was felt than the modulus data would be very good because the horizontal displacement measure is made more directly in contact with the sample (Figure 3.3) than in the Geonor DSS. In the Geonor DSS the horizontal displacement is measured at the top loading platen which is further away from the sample. Moreover, computed modulus values at the beginning of shear are very sensitive to small variations in the measured horizontal displacement. At higher shear strains the MDSS and Geonor modulus results compare quite well (beyond $\tau/\tau_{max} = 0.7$, see Figure 4.6). The magnitude of the measured horizontal displacement used for calculation of modulus values at low shear strains can be appreciated from the following example. At $\tau/\tau_{max} = 0.3$ in the Geonor DSS tests, $E_u/c_u \cong 1800$ and $\gamma = 0.05\%$, which for a typical preshear sample height of 2 cm represents a horizontal displacement of 0.0010 cm (0.0004 in). In the MDSS tests at $\tau/\tau_{max} = 0.3$, $E_u/c_u \cong 700$ and $\gamma = 0.13\%$; this represents a horizontal displacement of 0.0026 cm (0.0010 in). The difference in modulus values is approximately 60% (assuming 1800 to be the correct value) and the measured horizontal displacement differs by 0.0016 cm (0.0006 in). At $\tau/\tau_{max} = 0.7$ in the Geonor tests, the horizontal displacement is equal to 0.008 cm (0.0031 in) resulting in $\gamma = 0.40\%$ and $E_u/c_u \cong 550$. Adding the difference in the Geonor and MDSS horizontal displacements found at $\tau/\tau_{max} = 0.3$ to 0.008 cm gives a normalized modulus value $\cong$ 450 or 18% less than 550. Thus, an "error" in the horizontal displacement reading of 0.0016 cm (0.0006 in) results in a 60% difference in the computed modulus values at $\tau/\tau_{max} = 0.3$ compared to a difference of 18% at

$\tau/\tau_{max} = 0.7$.[3] The purpose of this example is to show that: (1) the magnitude of the horizontal displacement used to calculate modulus values at low shear strains is very small and (2) a small "error" in the horizontal displacement reading has a very large effect on the computed modulus value at small τ/τ_{max} ratios but relatively little effect near failure.

In the MDSS, the top cap and/or lower portion of the circular cage, containing the displacement transducers, may deform during the initial stage of a test (i.e., when all parts of the equipment establish full contact) in a manner which detrimentally influences the horizontal displacement measurements. This "seating" problem may be the cause for obtaining lower modulus values in the MDSS at the beginning of shear. In addition, it is also possible that the rotational stiffness (with respect to the Y axis) of the MDSS is less than the Geonor DSS and may also detrimentally influence the measured horizontal displacements and hence the computed modulus values.

In summary, tests performed in the MDSS may experience a seating problem, as exhibited by the shear stress–strain curves plotted in Figure 4.10, resulting in lower computed modulus values. There may also be an additional factor, the rotational stiffness of the device, which influences the computed modulus values. As the measured shear strain becomes larger the potential "error" in the horizontal displacement reading due to these causes begins to have relatively little effect on the magnitude of the modulus values.

In addition to its potential influence on the computed modulus values, a difference in the relative rotational stiffness of the MDSS and Geonor DSS may also account for the difference in the measured peak shear resistance. This issue is discussed in more detail in the following section.

---

[3]The horizontal displacement transducer in the MDSS is read with a resolution of 0.1 mV which equals 0.00003 cm. Thus resolution of the horizontal displacement readings is not a problem.

4.4.3 Evaluation of the Relative Stiffness of the MDSS and Geonor DSS

When the MDSS was developed it was hoped that tests performed in it would compare well with similar tests in the Geonor DSS. Data presented in the previous section showed that in general the results compare very well, with the exception that the MDSS measures a lower undrained shear strength and much more scattered normalized Young's modulus values. An exact match of the results would have been pleasing, but the fact remains that the two devices are constructed very differently. Although they are both simple shear apparatuses and both use the Geonor type membrane, it should not be surprising that two devices which are mechanically very different would have some differences in the results they produce. Further evidence of this is found in the results of three CK_oUDSS tests performed in the Marshall Silva DSS on 100 series BBC (BBC II) by R.S. Ladd of Woodward Clyde Consultants. These test data are summarized in Table 4.8 and Figures 4.11 and 4.12 present plots of the stress–strain curve, pore pressure versus normalized shear strain, stress path and normalized modulus versus stress ratio. Compared with the Geonor data (Table 4.7) the Marshall Silva results show a larger strain at failure, higher undrained shear strength and slightly lower vertical stress ratio at peak shear resistance. Like the Geonor results, the stress–strain curves show considerable scatter, with an average normalized undrained shear strength of 0.218 ±0.019SD which is approximately 8.5% higher than the Geonor average (0.201 ±0.010SD). In general, the shape of the stress–strain curves and stress paths compare very well except that the Marshall Silva curves plot higher than those for the Geonor DSS. The pore pressure plots are almost identical and the Marshall Silva $E_u(50)/c_u$ values are slightly lower than that measured in the Geonor DSS on the same Batch II material (e.g., Malek (1987); Table 4.7).

These additional simple shear data on BBC provide a rare opportunity to compare results from devices which have the ability to perform the same type of test.

In the case of the Geonor DSS test programs on BBC, results from four different research projects have remarkably little scatter in the mean c_u/σ'_{vc} (0.200 ± 0.003SD; Table 4.7). Whereas, tests on the same soil in three different devices have a large scatter in the mean value of c_u/σ'_{vc} among the different apparatuses (7% lower and 9% higher than the Geonor average for the MDSS and the Marshall Silva devices respectively). For routine geotechnical engineering projects this difference may not be significant, however, for projects with a low factor of safety the difference can be significant. In any event, the fact remains that for the same soil three different direct simple shear devices give three different values of the peak shear resistance.

The obvious question remains: which apparatus is giving the correct value? Unfortunately, the only appropriate reply to such a question is that it cannot be answered because we do not know what the "correct" value is. For direct simple shear testing, like other shear devices, we can only gain confidence in the values a device gives through research into how well the device functions (e.g., analysis of state of stress, failure condition, etc.) and most importantly through years of experience in successfully using it for design purposes. In the case of the Geonor DSS this has been possible because of the popularity of the device at several prominent geotechnical institutions (e.g., MIT and NGI) thus providing years of experience with the device. Some of the findings based on this experience are summarized in the conclusions of Appendix A. Although the Geonor device may not necessarily produce the "correct" undrained simple shear strength, it does provide c_u values which designers have used with confidence.

Given the opportunity to work with both the Geonor DSS and the MDSS at MIT, it was decided to try and determine what may be the source of the difference in the measured undrained shear strength. One way of trying to distinguish between the devices is to measure their relative stiffness. This can be done for different deformation modes but the most appropriate measurement is the rotational stiffness.

The rotational stiffness is defined here as the moment–rotation relationship of a device as shown schematically in Figure 4.13. Unfortunately, this is not a very easy measurement to make.

The idea was not necessarily to measure the absolute rotational stiffness of the devices, but to devise a technique which could be performed in both devices so that an estimate of their relative rotational stiffness could be made. This was done using two steel disks and a $^1/_8$ in. diameter steel ball. The discs were machined to fit snugly inside the top cap and bottom pedestal where the porous stones are usually placed (Figure 4.14). Placing the steel ball in one of the off–center locations (such as positions 2, 3 or 4 in Figure 4.14) and applying a vertical force sets up a moment which causes the loading system of the device to rotate. The rotation was measured using two extensometers and the rotation angle was calculated using these measurements as shown in Figure 4.14

The measurements using this procedure were judged correct if the deformation of the devices rotated through the location of the steel ball. This allowed the rotation angle (α) to be accurately computed using the equation in Figure 4.14. An example of this is shown in Figure 4.15 which plots the measured deflection of the right and left hand sides of the loading frame for different levels of vertical force (hence moment) in the two devices. As shown in the figure, the rotation of both devices, based on extensometer measurements, was essentially through the location of the steel ball. This was found to be the case for all of the trials conducted in both devices. Given the sensitive nature of the measurements being made, each trial was conducted several times to check for repeatability.

Figure 4.16 is a summary plot of the measurements made for the two devices with the steel ball in locations 2, 3 and 4 and for different values of the vertical force. The results show that the MDSS has a lower rotational stiffness than the Geonor DSS.

This may be one reason why the MDSS measures a lower undrained shear strength than the Geonor.

It should also be kept in mind that the MDSS was designed to allow the bottom of the sample to deform freely in a horizontal plane so that CAU tests could be conducted at different θ angles. This is not the case for the Geonor DSS and hence the MDSS has an additional degree of freedom which also may be a source of the difference in the measured undrained shear strengths.

The results do not prove why the MDSS measures a lower undrained shear strength than the Geonor DSS. However, based on the technique used here, the Geonor DSS has a higher rotational stiffness than the MDSS which shows that it is a more rigid device. This and/or the additional degree of freedom in the MDSS may be the reason(s) why the undrained shear strength is lower in the MDSS than that measured in the Geonor DSS.

4.5 MDSS AND GEONOR CAU DIRECT SIMPLE SHEAR TESTS AT $\theta = 0^\circ$

Table 4.9 presents the results of CAU tests at $\theta = 0^\circ$ and $\tau_{hc}/\sigma'_{vc} = 0.2$ performed both in the Geonor DSS and the MDSS. In this type of test the sample is consolidated with a horizontal shear stress equal to 20% of the vertical consolidation stress and subsequently sheared undrained by application of an additional horizontal shear stress acting in the same direction as the consolidation shear stress (i.e., $\theta = 0^\circ$).[4] The Table also includes the results of the same type of test conducted in the Geonor DSS by Ladd and Edgers (1972). Figures 4.17 and 4.18 plot the normalized stress–strain curve, pore pressure versus shear strain, stress path and normalized Young's modulus versus applied stress ratio for the MDSS test and Geonor test G5.[5]

---

[4]The test results and procedure used during anisotropic consolidation are discussed in more detail in Chapter 5.

[5]The modulus values and applied shear stress ratio are computed based on the incremental shear stress applied after consolidation. Hence, $E_u/c_u = (3(\Delta\tau_h)/\gamma)/c_u$

This type of comparison provides an important check of the MDSS because it represents the type of test for which the MDSS was specifically designed.

The tabulated data show that the two tests conducted in the Geonor DSS compare very well. They have the same undrained strength ratio, with a higher shear strain and slightly lower vertical stress ratio at peak shear resistance in the test reported by Ladd and Edgers. Like the CK_oUDSS results in the Geonor apparatus, the modulus values for test G5 on series 200 BBC (BBC III) are higher than those for the tests run by Ladd and Edgers on an older series BBC sample (BBC I).

The results in Table 4.9 and Figures 4.17 and 4.18 show that the MDSS and Geonor DSS results are very similar. Like the CK_oU tests, the MDSS has a slightly lower undrained strength ratio (3.5% difference). The stress strain curves and stress paths are nearly identical in shape, with the MDSS curves plotting slightly lower. The shear strain and vertical stress ratio at peak shear resistance are nearly identical. Like most of the CK_oU results, the modulus values are significantly lower in the MDSS and only compare well with the Geonor DSS results at higher applied stress ratios. Strains during consolidation should not be compared because the Geonor test was performed before the problem with the porous stones was discovered as discussed in Section 4.3.1.

With the exception of the modulus values these test results are very pleasing. The MDSS, in a test for which it was specifically designed, produced results nearly identical to those measured for the same soil and type of test in the Geonor DSS.

4.6 KINEMATIC PROOF TESTS OF THE MDSS

A series of proof tests were conducted in the MDSS with an elastic material to evaluate the kinematics of the device. This evaluation program enabled two important checks on the MDSS to be performed: (1) determine if the first shear stress (τ_1) is

---

where $\Delta\tau_h = \tau_h - \tau_{hc}$ and $c_u = (\tau_h)_{max}$. The applied stress ratio is computed as $\Delta\tau_h/(\tau_h)_{max}$.

applied at the correct orientation for each of the different θ angles and (2) verify if the sample set–up procedure and strain measurement system are working properly and produce repeatable results.

In the MDSS, an elastic material should deform in the direction of any applied incremental horizontal shear stress. If the material is loaded in one direction and then subjected to a second horizontal shear stress acting in another direction, the sample should incrementally deform in the direction of application of the second shear stress. This provides an important check on the kinematics of the MDSS because the orientation of the applied horizontal shear stress is known and hence the expected orientation of the shear strain path of a specimen is also known and can be compared with measurements made in the MDSS.

An additional kinematic proof check on the MDSS is given by the results of the CK_oUMDSS tests on BBC performed in the device. In these tests the sample should deform only in the X direction (see Figure 3.1 for reference) and the horizontal displacement transducer reading in the Y direction should not change. These results and those of the tests on rubber are described in the following two sections.

4.6.1 Kinematic Proof Tests With Rubber

Table 4.10 gives a summary of the tests conducted in the MDSS on a specimen of rubber which has the same dimensions as a typical MDSS soil sample. In all of these tests the rubber specimen was loaded to a vertical stress, $\sigma_v = 3$ ksc and for the various θ tests the first horizontal shear stress (τ_1) was set equal to 20% of σ_v (i.e. $\tau_1/\sigma_v = 0.2$). These stresses were selected because they represent the same magnitude of stresses used during consolidation for the CAU tests conducted on BBC as described in Chapter 5. In the θ tests, the rubber specimen was first subjected to σ_v and τ_1 at some angle θ. The specimen was subsequently subjected to a second horizontal shear stress (τ_2) acting parallel to the X axis. Ideally, the specimen should first deform in

the direction of θ and then deform parallel to the X axis during application of τ_2. The final vertical strain (ϵ_v) and total shear strain (γ_t) during application of σ_v and τ_1 should be independent of θ (i.e., the same for all tests). In addition, the incremental stress–strain behavior in the X direction during application of τ_2 should also be independent of θ.

The data summarized in Table 4.10 show that the vertical strain and total horizontal shear strain during application of σ_v and τ_1 are nearly identical for all of the θ tests (11 tests). In addition, the results also indicate that the specimen deformed in the direction of the applied horizontal shear force τ_1 ($\arctan(\gamma_y/\gamma_x)$) with a mean value of Δ (=$\text{Arctan}(\gamma_y/\gamma_x) - \theta$) equal to 0.0° ±1.6SD (n = 10, excluded Test R22). Figure 4.19 plots γ_x and γ_y at the end of application of σ_v and τ_1 for the 11 θ tests. The results plotted in Figure 4.19 are excellent, showing that for all θ angles the specimen deformed in the correct orientation and experienced the same γ_t independent of θ. The data also show that the results are repeatable (more than one test was conducted at θ = 30°, 120° and 150°).

Figure 4.20 is a plot of the horizontal shear strain path for the 11 θ tests. The Figure shows the specimen deformation in the direction of θ during application of σ_v and τ_1 and also the subsequent deformation of the specimen during application of τ_2. In most cases the specimen deformed perfectly parallel to the X axis during application of τ_2, confirming that the rubber is indeed elastic but more importantly that kinematically the device produces excellent and repeatable results. Table 4.11 summarizes the data in Figure 4.20 listing the $\Delta\gamma_y$ for $\Delta\gamma_x$ equal to 5, 10 and 15%. ($\Delta\gamma_x$ = 0% at start of application of τ_2). The average value of $\Delta\gamma_y$ for the rubber tests at $\Delta\gamma_x$ = 5, 10 and 15% equals 0.11% ±0.20SD, 0.21% ±0.22SD and 0.37% ±0.32SD respectively.

Figure 4.21 is a plot of the incremental X shear resistance of the rubber during application of τ_2. Again, the results show the elastic nature of the rubber specimen (all

the stress–strain curves are nearly parallel) and that the MDSS clearly captures this behavior with repeatability. Computed modulus values during application of τ_2 are presented in Table 4.11. For $\Delta\gamma_x$ = 5, 10 and 15% the average value of E_u equals 11.9ksc ±0.5SD, 11.3ksc ±0.8SD and 10.5ksc ±1.0SD respectively.

4.6.2 Kinematic Proof Tests With Resedimented BBC

Figure 4.22 shows the shear strain path for four of the CK_oUMDSS tests summarized in Table 4.5 (C5, C6, C11 and C14). In the MDSS, the sample is free to deform in any direction in a horizontal plane, but for CK_oU tests it should ideally deform parallel to the X axis at $\gamma_y = 0$. With the exception of test C5 the shear strain paths are nearly parallel to the X axis with very little measured deformation in the Y direction. Test C5 was one of the first tests conducted on clay and lack of experience in properly orienting the sample during trimming and set–up may have resulted in the nonparallel strain path. However, even for this test, the magnitude of error is quite small; at γ_x equal to 30%, γ_y was –0.67%. From Table 4.11 the average value of $\Delta\gamma_y$ at $\Delta\gamma_x$ = 5, 10 and 15% equals 0.03% ±0.14SD, 0.04% ±0.30SD and 0.37% ±0.32SD respectively. The results for tests C6, C11 and C14 clearly show that the set–up procedure and strain measuring system work properly and produce repeatable results.

4.7 SUMMARY

An experimental evaluation of the MDSS was conducted using resedimented BBC and rubber. The BBC samples came from the new 200 series batches (BBC III) which were made in 1987 using the procedure developed by Germaine (1982). This procedure results in high quality, uniform saturated samples as has been confirmed for the 200 series batches from water content data, oedometer tests, and UU triaxial tests with pore pressure measurements. Several CK_oUDSS tests were conducted on OCR =1 BBC in the Geonor DSS to verify the DSS response of the new

BBC and to evaluate the results of similar tests performed in the MDSS. The Geonor DSS results compare well with previous Geonor tests conducted on BBC at MIT, except for modulus values (E_u) which are higher for the new soil (Figure 4.6a) as also measured in other types of undrained shear tests (Seah, 1989). The stress–strain curves display considerable scatter (Figure 4.3a) which was also found to be the case for previous direct simple shear tests on BBC (Figure 4.7).

Results from the consolidation phase of CK_oU direct simple shear tests performed on normally consolidated BBC in the MDSS compare very well with those obtained from oedometer tests (Figure 4.9). The undrained shear results display the same basic behavioral trends as the Geonor DSS test results (Figures 4.3 to 4.8). The shear stress–strain curves from the MDSS tests have remarkably little scatter ($COV[c_u/\sigma'_{vc}] = 1.1\%$ compared to 5.4% for the Geonor tests; Table 4.7). However, the average undrained strength ratio for the MDSS tests is 7% less than that measured in the Geonor DSS. Results from a procedure developed to evaluate the relative rotational stiffness of the two devices indicate that the Geonor DSS is slightly more rigid than the MDSS (Figure 4.16). This and/or the additional degree of freedom in the MDSS (necessary to conduct tests at different θ angles) may be the reason(s) why the measured undrained strength ratio is lower in the MDSS. The computed modulus values are considerably less than that measured in the Geonor tests comparing well only near the peak shear resistance. The initial portion of the shear stress–strain curves for three of the MDSS tests (Figure 4.10) indicate that there may have been a seating problem during these tests resulting in the lower modulus values. The lower rotational stiffness of the MDSS may also contribute to the measurement of lower modulus values compared to the Geonor DSS..

Results from CAU direct simple shear tests with $\theta = 0°$ and $\tau_{hc}/\sigma'_{vc} = 0.2$ conducted in the Geonor DSS and the MDSS compare very well except for modulus values (Figures 4.17 and 4.18). Like the CK_oU tests, the MDSS undrained strength

ratio was lower (3.5%) than that measured in the Geonor DSS and the modulus values were considerably less, except near the peak shear resistance. With the exception of the modulus values, the CAU test results are very satisfactory because the MDSS, in a test for which the device was specifically designed, produced results nearly identical to those measured for the same type of test run in the Geonor DSS.

The kinematic proof tests with an elastic material proved to be very successful. The test results showed that the rubber specimen deformed in the direction of the applied τ_1 for different θ angles. In fact, the average deviation Δ from the applied test angle θ for 11 rubber tests was 0.0° ±1.6SD (Table 4.10). Also γ_t and ϵ_v at the end of application of τ_1 and σ_v were found to be independent of θ (Table 4.10 and Figure 4.19). Furthermore, during subsequent application of the second horizontal shear stress τ_2, the specimen deformed parallel to the intended X axis showing the elastic nature of the rubber which the MDSS clearly captured with repeatability (Figure 4.20). The shear strain paths for the CK_oUMDSS tests on BBC were also parallel to the X axis during undrained shear with an average $\Delta\gamma_y = 0.03\%$ ±0.14SD at approximately the peak shear resistance ($\Delta\gamma_x = 5\%$; Table 4.11). These kinematic proof tests gave excellent results, confirming that the set–up procedure and strain measurement system in the MDSS are working properly and produce repeatable results.

TABLE 4.1: Index Properties of Resedimented Boston Blue Clay III (from Walbaum, 1988)

Source or Batch No.	G_s	w (%)	w_l (%)	w_p (%)	I_p (%)	I_l	Clay Fraction < 2μ (%)	Salt Conc. (g/L)
Natural	2.789 ±0.036	--	47.4 ±3.0	23.9 ±1.6	23.5 ±3.4	--	48.1 ±2.9	---
Oven-Dried	2.797 ±0.015	--	45.1 ±3.4	24.8 ±1.2	20.3 ±3.6	--	48.5 ±2.6	---
Screened & Ground	2.782/ 2.787	--	44.8/ 45.0	22.4/ 22.5	22.4/ 22.5	--	--	1.98 ±0.10
200	---	41.1 ±0.8	46.5	21.9	24.6	0.78	--	19.8/23.3
201	---	39.4 ±1.9	41.4†	22.9	18.5†	--	57.6 ±1.1	14.3/16.1
202	---	40.7 ±0.4	45.6	22.3	23.3	0.79	--	Nom. 16

Notes:

1. ± designates standard deviation.
2. values without ± disignates result of one test.
3. † designates questionable test.

TABLE 4.2: Results of Oedometer Tests on Samples from Batches of Resedimented Boston Blue Clay III

Test No. Batch	σ'_p (ksc)	CR	c_v x10^3 cm^2/s	$C\alpha\epsilon$	$C\alpha\epsilon$/CR	Remarks
200-1 200	1.13	0.175	1.30	0.0021	0.012	t_s = 23 days
200-2 200	1.20	0.163	1.40	0.0021	0.013	t_s = 24 days
200-3 200	0.99	0.168	1.20	0.0027	0.016	t_s = 79 days
201 201	0.97	0.166	1.30	0.0025	0.015	t_s = 1 day
202-T 202	0.98	0.162	1.50	0.0028	0.017	t_s = 9 days
Average ±1 S.D.	1.05 ±0.10	0.167 ±0.005	1.34 ±0.11	0.0024 ±0.0003	0.015 ±0.002	

Notes:
1. All data from MIT files prepared by T.H. Seah and C. P. Aubeny.
2. c_v based on log time construction for σ'_{vc} = 3 ksc.
3. $C\alpha\epsilon$ from σ'_{vc} = 2 ksc increment.
4. CR for σ'_{vc} from 1$^+$ to 4 ksc.
5. t_s = storage time between sampling of batch and test.

TABLE 4.3: Results of Consolidation Phase of CK_oUMDSS Tests on Samples from Batches of Resedimented Boston Blue Clay III

Test No. Batch	σ'_p (ksc)	CR	c_v x10^3 cm^2/s	$C\alpha\epsilon$	$C\alpha\epsilon$/CR	Remarks
C-11 202	1.00	0.189	1.08	0.0020	0.011	t_s = 106days
C-14 203	1.05	0.183	1.01	0.0020	0.011	t_s = 64 days
Average	1.03	0.186	1.05	0.0020	0.011	
Oedometer Average ±1 S.D.	1.05 ±0.10	0.167 ±0.005	1.34 ±0.11	0.0024 ±0.0003	0.015 ±0.002	Results in Table 4.2

Notes:

1. c_v based on log time contruction for σ'_{vc} = 3 ksc.
2. $C\alpha\epsilon$ from σ'_{vc} = 3 ksc increment.
3. CR for σ'_{vc} from 1.5 to 3 ksc.
4. t_s = time between sampling of batch and test.

TABLE 4.4: Summary of Geonor CK_oUDSS Tests on OCR = 1 Boston Blue Clay III

Test No.	Batch No. w_c(%)	σ'_{vc} (ksc)	ϵ_v (%) t_c (days)	At Peak τ_h				At $\gamma \cong 25\%$				$\frac{E_u(50)}{c_u}$	Remarks
				γ (%)	$\frac{\tau_h}{\sigma'_{vc}}$	$\frac{\sigma'_v}{\sigma'_{vc}}$	τ_h/σ'_v ϕ'°	γ (%)	$\frac{\tau_h}{\sigma'_{vc}}$	$\frac{\sigma'_v}{\sigma'_{vc}}$	τ_h/σ'_v ϕ'°		
G1	200 41.1	3.0	14.6 0.96	4.7	0.191	0.561	0.340 18.8	24.9	0.133	0.252	0.516 27.8	930	inaccurate ϵ_v data
G2	200 40.8	3.0	15.3 0.98	5.4	0.213	0.528	0.403 22.0	25.0	0.132	0.214	0.627 31.7	970	inaccurate ϵ_v data
G4	200 41.0	3.0	15.2 0.95	5.5	0.205	0.542	0.379 20.7	24.4	0.134	0.237	0.593 29.5	1070	inaccurate ϵ_v data
5	202 36.3	3.0	11.7 1.10	4.9	0.195	0.600	0.325 18.0	25.1	0.129	0.229	0.561 29.3	830	Test by Valbaum (1988) Excellent ϵ_v data
Average ± 1 S.D.				5.1 ±0.4	0.201 ±0.010	0.558 ±0.031	0.362 ±0.036 19.9 ±1.8		0.132 ±0.002	0.233 ±0.016	0.574 ±0.047 29.6 ±1.6	950 ±99	

Notes:

1. ϵ_v = strain at end of consolidation.
2. $\dot{\gamma}$ = 5%/hour.

TABLE 4.5: Summary of MDSS CK_oUDSS Tests on OCR = 1 Boston Blue Clay III

Test No.	Batch No. / w_c(%)	σ'_{vc} (ksc)	ϵ_v (%) / t_c (days)	At Peak τ_h: γ (%)	$\frac{\tau_h}{\sigma'_{vc}}$	$\frac{\sigma'_v}{\sigma'_{vc}}$	τ_h/σ'_v / ϕ'°	At $\gamma \cong 25\%$: γ (%)	$\frac{\tau_h}{\sigma'_{vc}}$	$\frac{\sigma'_v}{\sigma'_{vc}}$	τ_h/σ'_v / ϕ'°	$\frac{E_u(50)}{c_u}$	Remarks
C1	B108 41.8	4.0	12.9 0.86	8.2	0.207	0.507	0.408 22.2	25.0	0.133	0.211	0.631 32.2	485	-poor servo control -sample 3.5 yrs old
C4	B108 41.3	4.0	13.1 0.94	5.3	0.233	0.569	0.409 22.2	25.1	0.152	0.260	0.582 28.0	-	-servo control system too slow -sample 3.5 yrs old
C5	B201 41.6	3.0	14.5 0.92	4.2	0.188	0.617	0.306 17.0	25.0	0.109	0.205	0.529 29.3	630	-inaccurate ϵ_v data -app. comp. not used during shear
C6	B201 41.2	3.0	13.5 0.95	5.8	0.185	0.512	0.361 19.8	25.1	0.121	0.216	0.560 29.3	950	-inaccurate ϵ_v data -app. comp. used during shear
C11	B202 40.7	3.0	11.5 1.19	4.1	0.183	0.572	0.320 17.7	25.0	0.116	0.212	0.549 28.7	630	-excellent ϵ_v data -app. comp. used during shear
C14	B203 40.9	3.0	11.2 0.98	5.2	0.188	0.558	0.320 18.6	25.0	0.117	0.223	0.523 27.7	630	-excellent ϵ_v data -app. comp. not used during shear
Average ± 1 S.D.				4.8 ±0.8	0.186 ±0.002	0.565 ±0.043	0.331 ±0.024 18.3 ±1.2		0.116 ±0.005	0.214 ±0.008	0.540 ±0.017 28.4 ±0.7	710 ±160	excluding tests C1 and C4

Notes:

1. app. comp. ≡ apparatus compressibility
2. ϵ_v = strain at end of consolidation.
3. $\dot{\gamma}$ = 5%/hour.

TABLE 4.6: Results of Geonor CK_oUDSS Tests on OCR = 1 BBC from Previous MIT Research Projects

Reference Batch	Test No.	Batch w_c (%)	σ'_{vc} (ksc) ϵ_v (%)	At Peak τ_h γ (%)	τ_h/σ'_{vc}	σ'_v/σ'_{vc}	ϕ (°)	$\frac{E_u(50)}{c_u}$
Ladd and Edgers (1972) I	202	200* 37.4	4.0 15.5	6.0	0.211	0.566	20.4	470
	301	300 37.2	3.0 13.7	4.5	0.199	0.575	19.1	750
	303	300 35.6	8.0 17.0	6.2	0.194	0.565	18.9	400
	1301	1300 35.2	4.0 9.9	5.4	0.187	0.567	18.3	685
	1303	1300 35.6	8.0 -	9.0	0.196	0.531	20.3	465
Malek (1987) II	S1	111 39.8	3.1 10.1	2.4	0.201	0.592	18.8	850
	S2	111 39.7	3.1 8.1	10.7	0.192	0.447	23.2	530
	S3	111 39.2	4.0 10.8	6.8	0.214	0.515	22.6	700
	S4	111 39.5	4.0 10.0	6.8	0.195	0.505	21.1	550
	S5	112 39.2	6.0 16.4	3.5	0.222†	0.678	18.1	680
Valbaum (1988) III	1	200 39.9	12.2 -	8.1	0.202	0.538	20.6	590
	2	201 40.6	11.4 -	8.2	0.184†	0.462	21.7	515
	3	201 41.5	11.6 -	6.0	0.195	0.543	19.8	420
	4	201 40.9	11.4 -	6.8	0.194	0.545	19.6	370
	5	202 41.1	3.0 11.7	4.9	0.195	0.600	18.0	830

Notes:

1. All tests have nominal $\dot{\gamma}$ = 5%/hr.
2. Data in this Table are summarized in Table 4.7.
3. ϵ_v = end of primary strain at σ'_{vc}.
4. † denotes questionable value.
5. * Ladd and Edgers test 202 is from an old batch 200 and is not part of the new 200 series BBC.

TABLE 4.7: Summary of MIT Geonor, MDSS and Marshall Silva CK_oU Direct Simple Shear Tests on OCR = 1 BBC

Reference	Num. of Tests Batch	At Peak τ_h					$\frac{E_u(50)}{c_u}$
		γ (%)	τ_h/σ'_{vc}	COV[†]	σ'_v/σ'_{vc}	ϕ (°)	
Ladd & Edgers (1972)	5 I	6.2 ±1.7	0.197 ±0.009	4.6	0.561 ±0.017	19.4 ±0.9	554 ±154
R.S. Ladd (1985) M. Silva	3 II	8.1 ±1.3	0.218 ±0.019	8.7	0.496 ±0.032	23.7 ±1.9	612 ±163
Malek (1987)	4 II	6.7 ±3.4	0.201 ±0.010	5.0	0.515 ±0.060	21.4 ±2.0	662 ±129
Valbaum (1988)	4 III	6.4 ±1.3	0.197 ±0.004	2.0	0.557 ±0.029	19.5 ±1.1	552 ±208
DeGroot (1989) Geonor	3 III	5.2 ±0.4	0.203 ±0.011	5.4	0.544 ±0.017	20.5 ±1.6	990 ±72
DeGroot (1989) MDSS	4 III	4.8 ±0.8	0.186 ±0.002	1.1	0.565 ±0.043	18.3 ±1.2	710 ±160

Notes:

1. All values are average ± one standard deviation (SD).
2. COV[†] = coefficent of variation $(\tau_h/\sigma'_{vc})_{max}$ = SD/Mean (%).
3. Individual test data summarized in this Table can be found in Tables 4.4, 4.5, 4.6 and 4.8.
4. Averages for Malek and Valbaum exclude Tests S5 and 2 respectively (Table 4.6).
5. DeGroot MDSS averages exclude Tests C1 and C4 (Table 4.5).
6. Four of Valbaum's tests were conducted at high stress levels (Table 4.6).

TABLE 4.8: Summary of Marshall Silva CK_oUDSS Tests on OCR = 1 Boston Blue Clay II

Test No.	Batch No. w_c(%)	σ'_{vc} (ksc)	ϵ_v (%) t_c (days)	At Peak τ_h				At $\gamma \cong 25\%$				$\frac{E_u(50)}{c_u}$
				γ (%)	$\frac{\tau_h}{\sigma'_{vc}}$	$\frac{\sigma'_v}{\sigma'_{vc}}$	τ_h/σ'_v ϕ'	γ (%)	$\frac{\tau_h}{\sigma'_{vc}}$	$\frac{\sigma'_v}{\sigma'_{vc}}$	τ_h/σ'_v ϕ'	
WC1-1	112 42.8	2.0	8.6 1.0	9.4	0.215	0.460	0.467 25.1	24.2	0.144	0.232	0.621 31.8	790
WC2-1	111 41.9	4.0	9.2 1.0	6.8	0.200	0.508	0.394 21.5	25.9	0.120	0.208	0.577 30.0	470
WC2-2	111 41.6	4.0	9.2 1.0	8.0	0.238	0.520	0.458 24.6	25.6	0.164	0.276	0.594 30.7	575
Average ± 1 S.D.				8.1 ±1.3	0.218 ±0.019	0.496 ±0.032	0.440 ±0.040 23.7 ±1.9		0.143 ±0.022	0.239 ±0.034	0.597 ±0.022 30.8 ±0.9	612 ±163

Notes:

1. Tests conducted in April 1985 by R.S. Ladd of Woodward Clyde Consultants, Clifton, N.J.
2. ϵ_v = strain at end of consolidation.
3. $\dot{\gamma}$ = 4.2%/hour.

TABLE 4.9: Results of Geonor DSS and MDSS CAU Tests on OCR = 1 Boston Blue Clay at $\theta = 0°$

Device	Test No.	Batch w_c (%)	ϵ_v (%) γ_c (%) t_c (d)	At Peak τ_h			$\frac{E_u(50)}{c_u}$	Remarks
				γ (%)	τ_h/σ'_{vc}	σ'_v/σ'_{vc}		
MDSS	C7	202 42.0	13.9 19.6 0.97	0.55	0.273	0.948	545	
Geonor	G5	201 42.1	15.8 18.4 0.92	0.57	0.283	0.933	1015	inaccurate ϵ_v data
Geonor	501	- 38.8	14.2 14.8 0.85	1.10	0.283	0.870	795	Ladd and Edgers (1972)

Notes:

1. All tests have σ'_{vc} = 3.0 ksc and τ_{hc}/σ'_{vc} = 0.20.
2. ϵ_v and γ_c = strains at end of consolidation.

TABLE 4.10: Summary of MDSS Kinematic Proof Tests With Rubber

Test No.	θ (°)	ϵ_v (%)	γ_x (%)	γ_y (%)	γ_t (%)	Arctan (γ_y/γ_x)	Δ (°)	Remarks
R15	K_o	10.0	-	-	-	-	-	
R28	K_o	9.8	-	-	-	-	-	
R18	0	9.6	16.8	-0.1	16.8	-0.3	-0.3	
R29	30	9.8	13.5	7.9	15.6	30.3	0.3	
R30	30	9.9	13.5	8.7	16.1	32.8	2.8	
R19	60	10.0	7.8	14.4	16.4	61.6	1.6	
R21	90	10.1	-0.4	15.8	15.8	91.6	1.6	
R20	120	10.1	-7.7	13.8	15.8	119.1	-0.9	
R24	120	10.1	-7.5	14.2	16.1	117.8	-2.2	
R26	120	10.1	-8.1	13.8	16.0	120.4	0.4	did not apply τ_2
R22	150	10.3	-13.2	8.8	15.9	146.2†	-	
R23	150	9.8	-13.7	8.2	16.0	149.2	-0.8	
R27	150	9.9	-13.4	8.4	15.8	147.9	-2.1	did not apply τ_2
R25	180	10.9*	-15.0	-	15.0	-	-	Test run in Geonor
Ave. ±1SD		10.0 ±0.2			16.0 ±0.3		0.0 ±1.6	excluding R15,R25,R28

Notes:

1. See Figure 3.1 for definitions of θ, γ_x and γ_y.
2. $\gamma_t = (\gamma_x^2 + \gamma_y^2)^{1/2}$.
3. All tests have $\sigma_v = 3.0$ ksc.
2. All θ tests have $\tau_1/\sigma_v = 0.20$.
3. $\Delta = \text{Arctan}(\gamma_y/\gamma_x) - \theta$.
4. † initial set-up problems, final incremental strains resulted in $\theta = 148.8°$.
5. * initial set-up problems resulted in large ϵ_v for first increment. Subsequent ϵ_v same as MDSS tests.

TABLE 4.11: Summary of Strain Path Results During Application of τ_2 for MDSS Tests on Rubber and CK_oUMDSS Tests on OCR=1 BBC

Test No.	θ (°)	$\Delta\gamma_x$					
		5 (%)		10 (%)		15 (%)	
		$\Delta\gamma_y$ (%)	E_u (ksc)	$\Delta\gamma_y$ (%)	E_u (ksc)	$\Delta\gamma_y$ (%)	E_u (ksc)
R18	0	-0.04	11.5	-0.04	12.8	-	-
R29	30	0.05	11.4	0.41	10.5	0.99	9.0
R30	30	0.07	11.4	0.12	9.9	0.38	8.4
R19	60	-0.25	12.0	-0.03	11.0	0.07	10.4
R21	90	0.15	11.9	0.16	11.2	0.17	10.8
R20	120	0.51	12.8	0.68	11.6	0.73	11.1
R24	120	0.15	11.7	0.16	11.4	0.16	11.1
R22	150	0.19	12.4	0.23	11.5	0.26	11.2
R23	150	0.17	12.0	0.18	11.7	0.23	11.1
Average ±1SD Rubber Tests		0.11 ±0.20	11.9 ±0.5	0.21 ±0.22	11.3 ±0.8	0.37 ±0.32	10.5 ±1.0
C5	CK_oU	-0.16	-	-0.39	-	-0.57	-
C6	CK_oU	0.16	-	0.29	-	0.43	-
C11	CK_oU	0.02	-	0.09	-	0.17	-
C14	CK_oU	0.10	-	0.18	-	0.28	-
Average ±1SD BBC Tests		0.03 ±0.14		0.04 ±0.30		0.06 ±0.35	

Notes:

1. See Figure 3.1 for definitions of θ, γ_x and γ_y.
2. $E_u = 3\Delta\tau_h/\gamma$, $\Delta\tau_h = \tau_h - \tau_1$.
3. Strain Paths plotted in Figures 4.20 and 4.22.

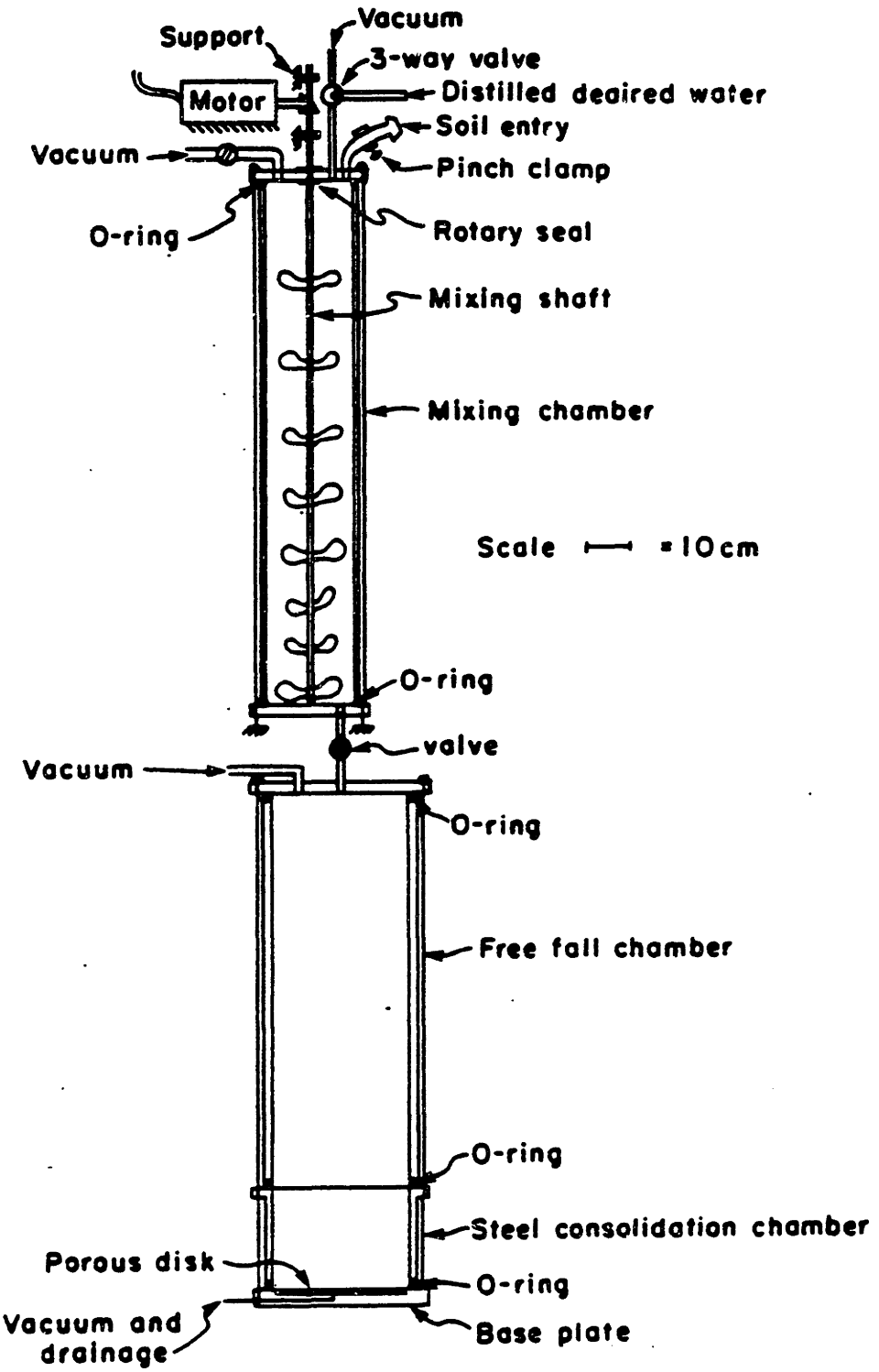

Figure 4.1: Schematic of Equipment Used to Saturate Resedimented Boston Blue Clay (from Germaine, 1982).

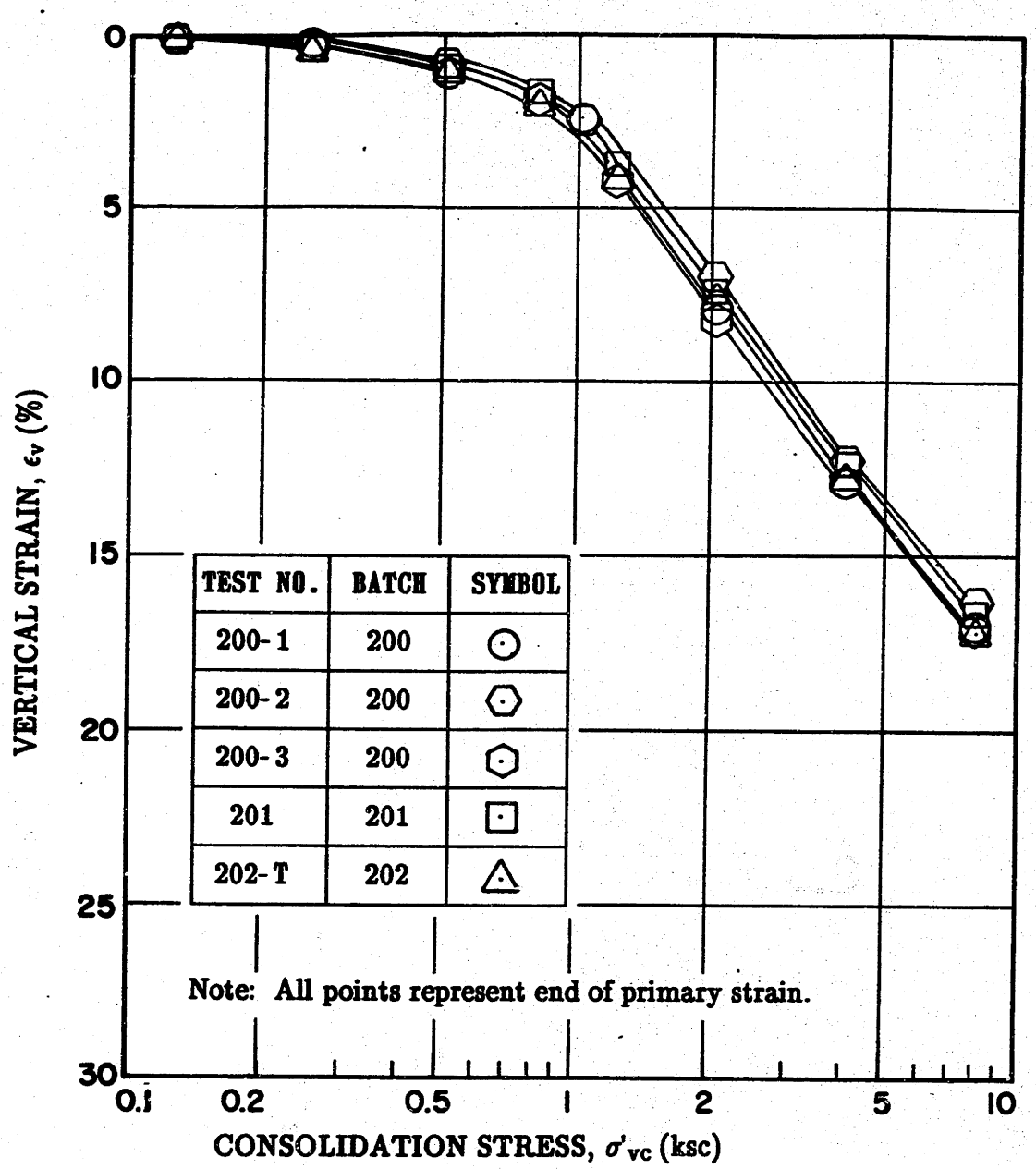

Figure 4.2: Compression Curves from Oedometer Tests on Series 200 BBC.

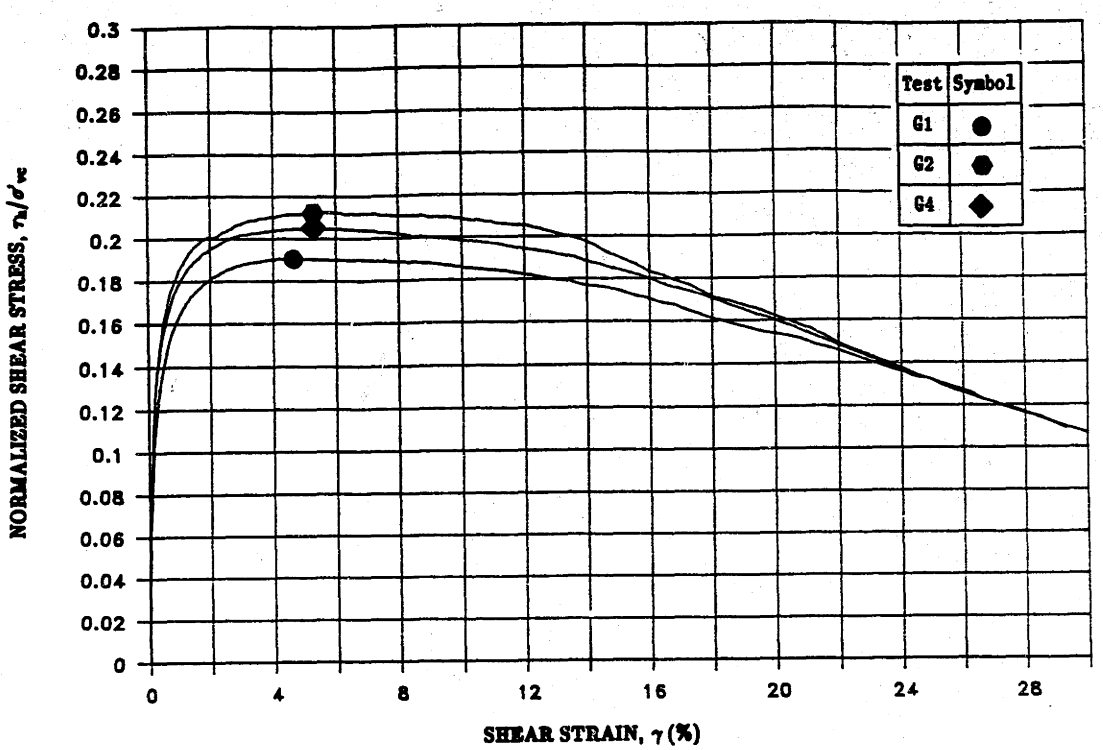

(a)

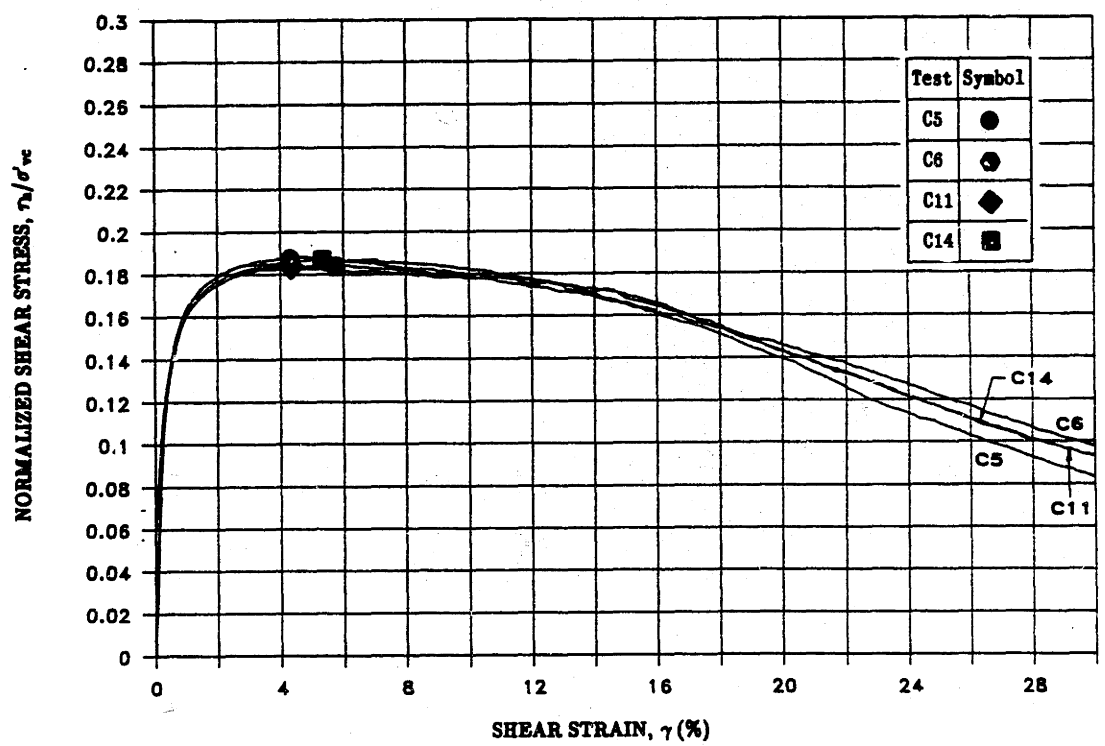

(b)

Figure 4.3: Shear Stress–Strain Curves for CK_oU Direct Simple Shear Tests on BBC: (a) Geonor DSS; (b) MDSS.

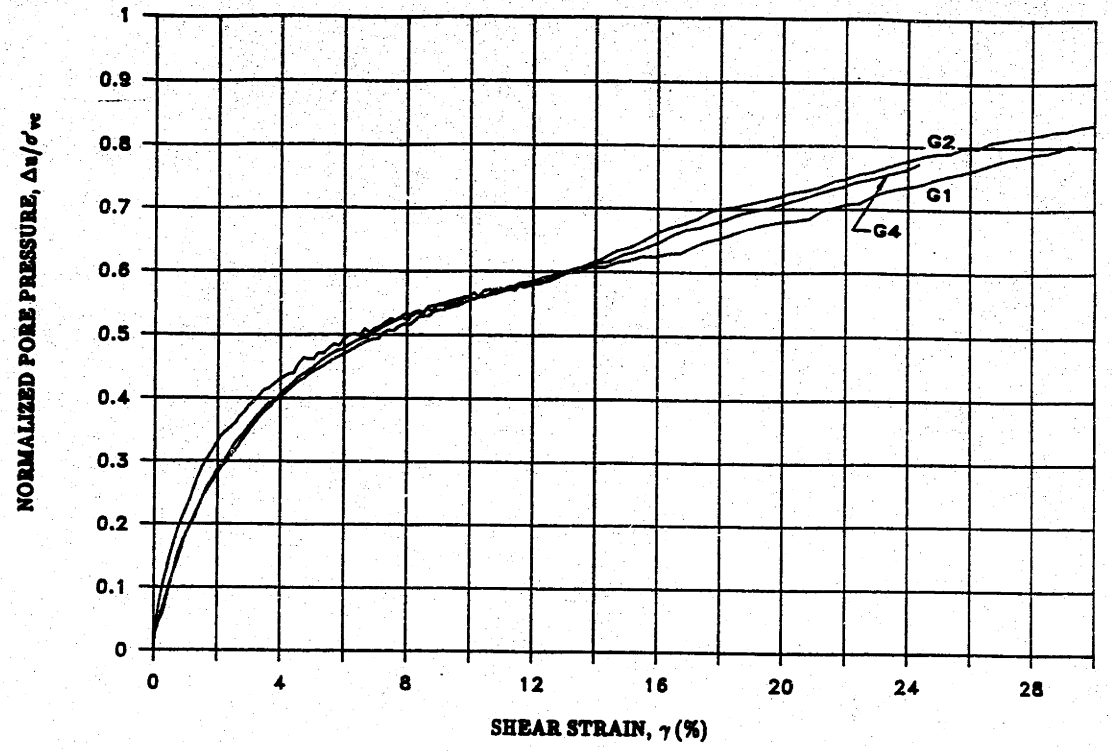

(a)

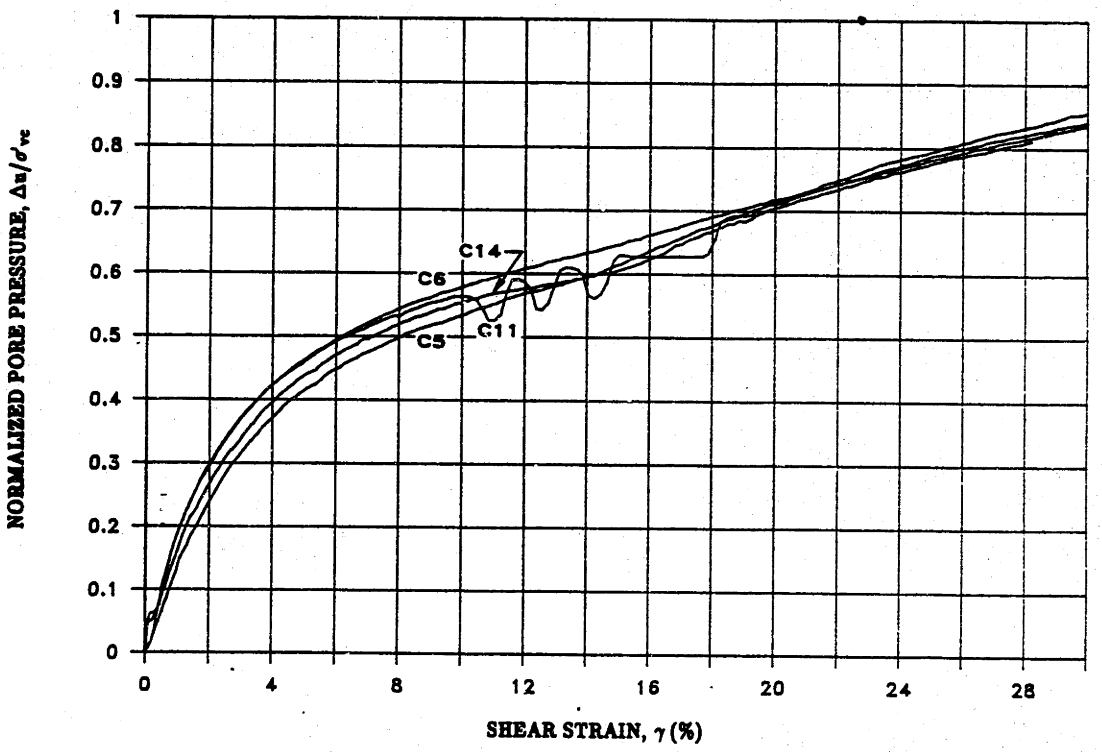

(b)

Figure 4.4: Pore Pressure versus Shear Strain for CK_oU Direct Simple Shear Tests on BBC: (a) Geonor DSS; (b) MDSS.

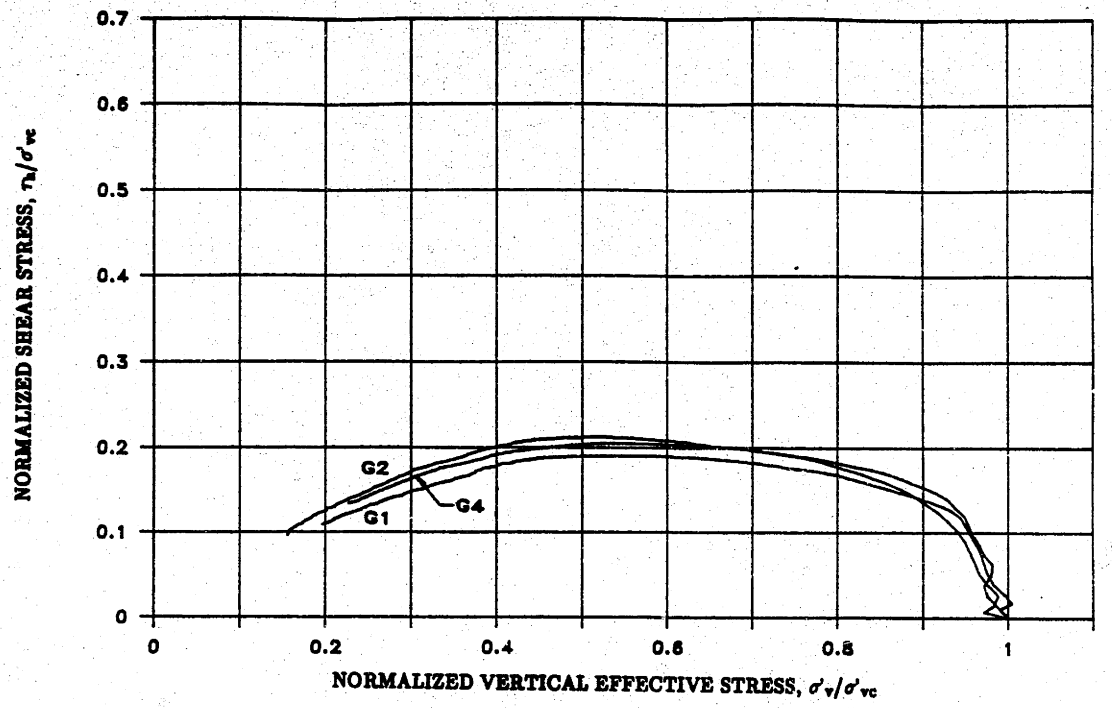

(a)

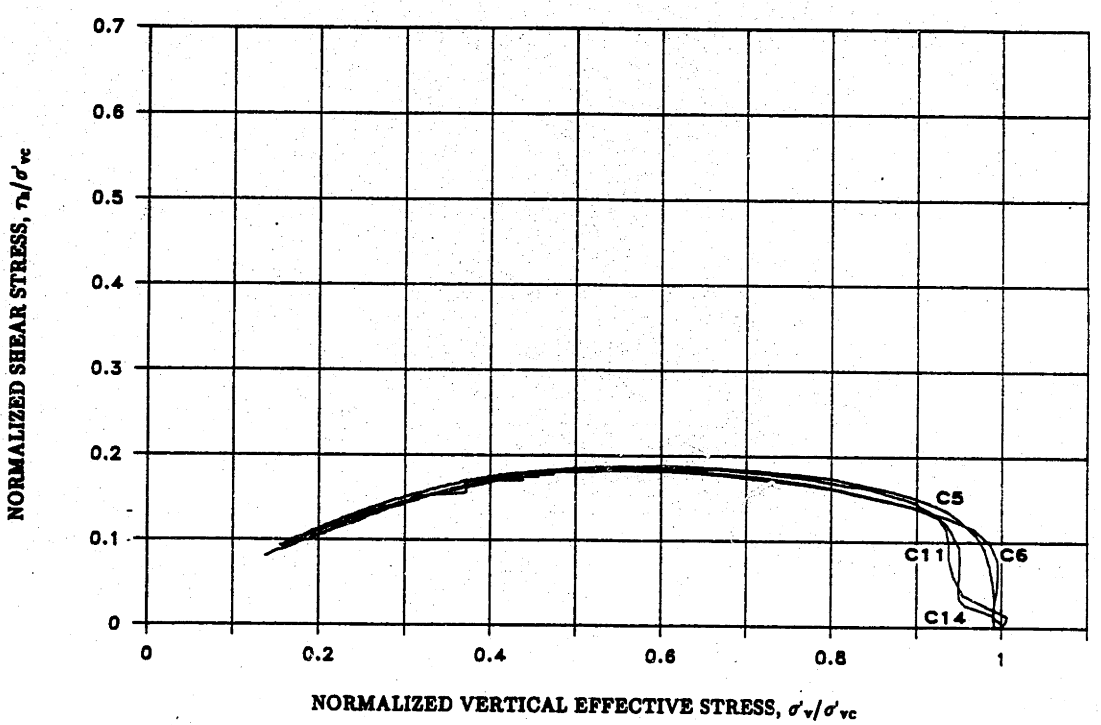

(b)

Figure 4.5: Stress Paths for CK_oU Direct Simple Shear Tests on BBC: (a) Geonor DSS; (b) MDSS.

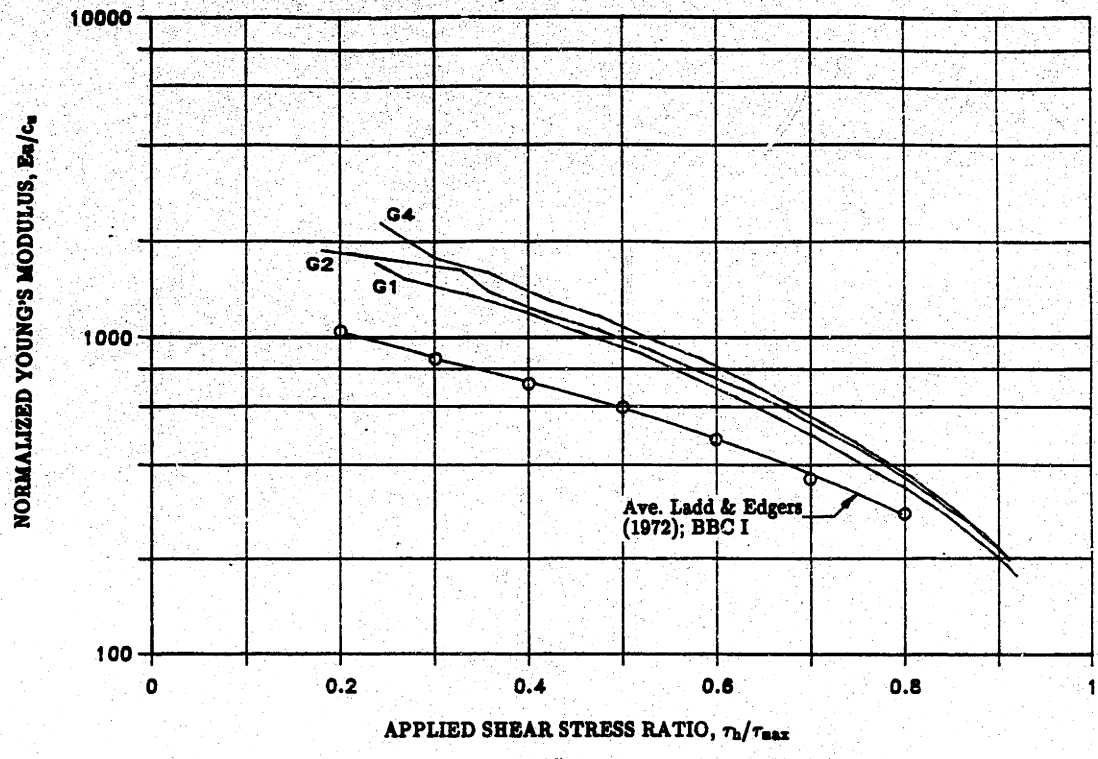

(a)

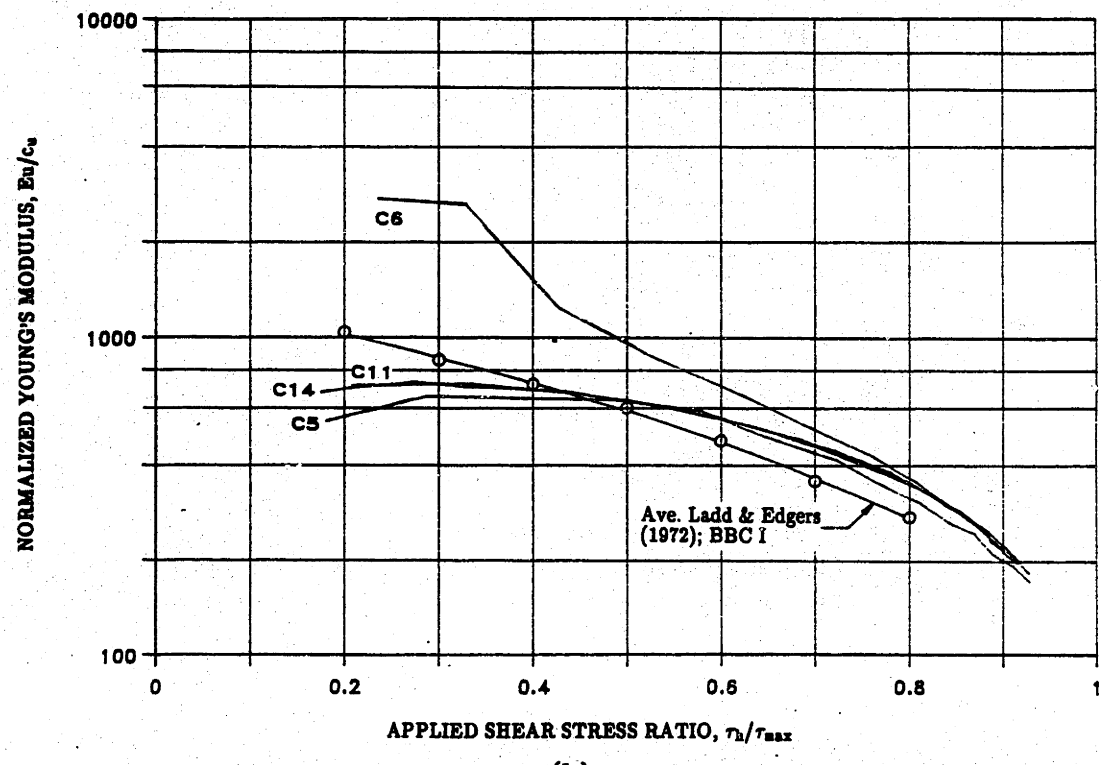

(b)

Figure 4.6: Young's Modulus versus Applied Shear Stress Ratio for CK_0U Direct Simple Shear Tests on BBC: (a) Geonor DSS; (b) MDSS.

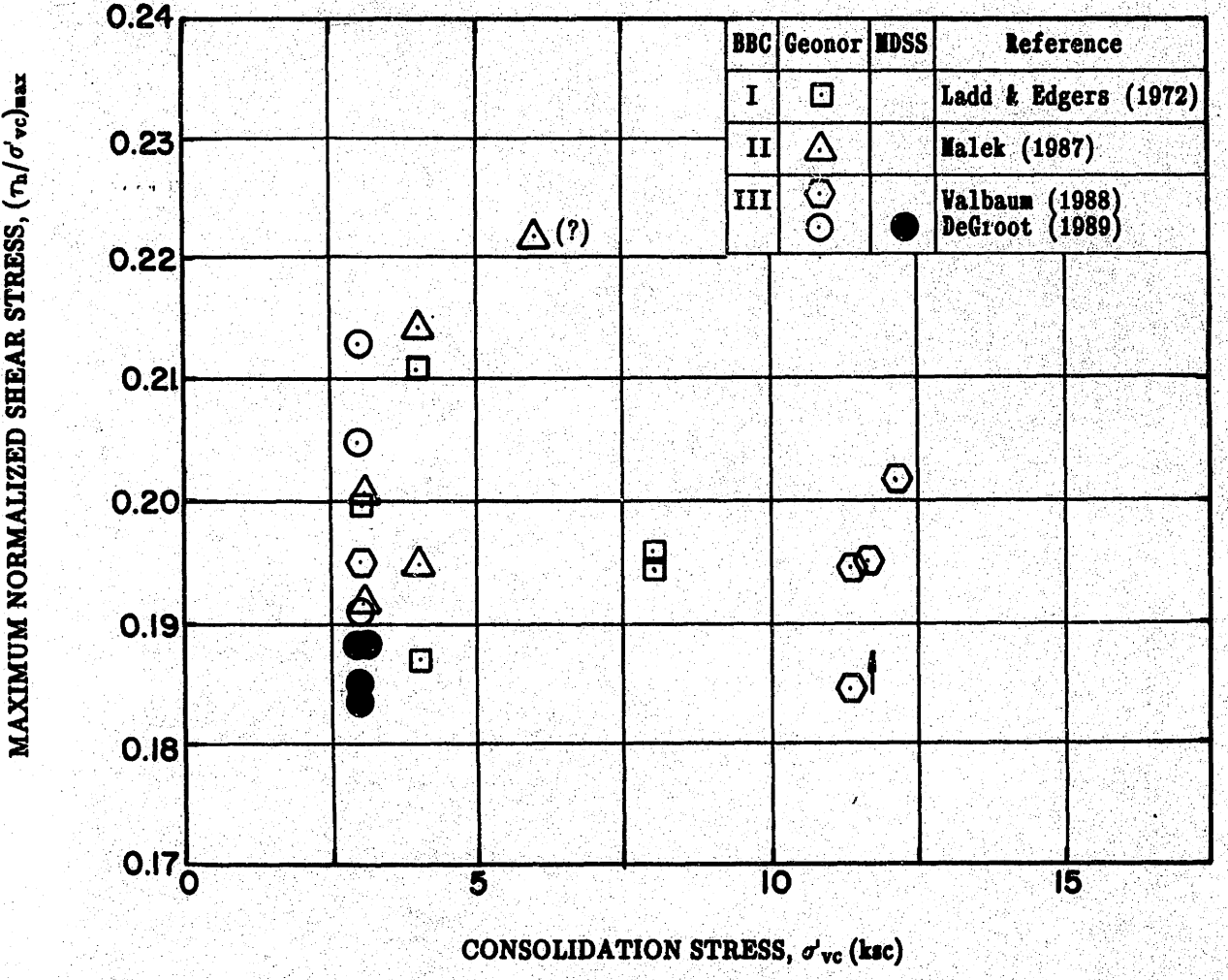

Figure 4.7: Maximum Normalized Shear Stress versus Vertical Consolidation Stress for CK_oU Direct Simple Shear Tests Conducted at MIT on Boston Blue Clay.

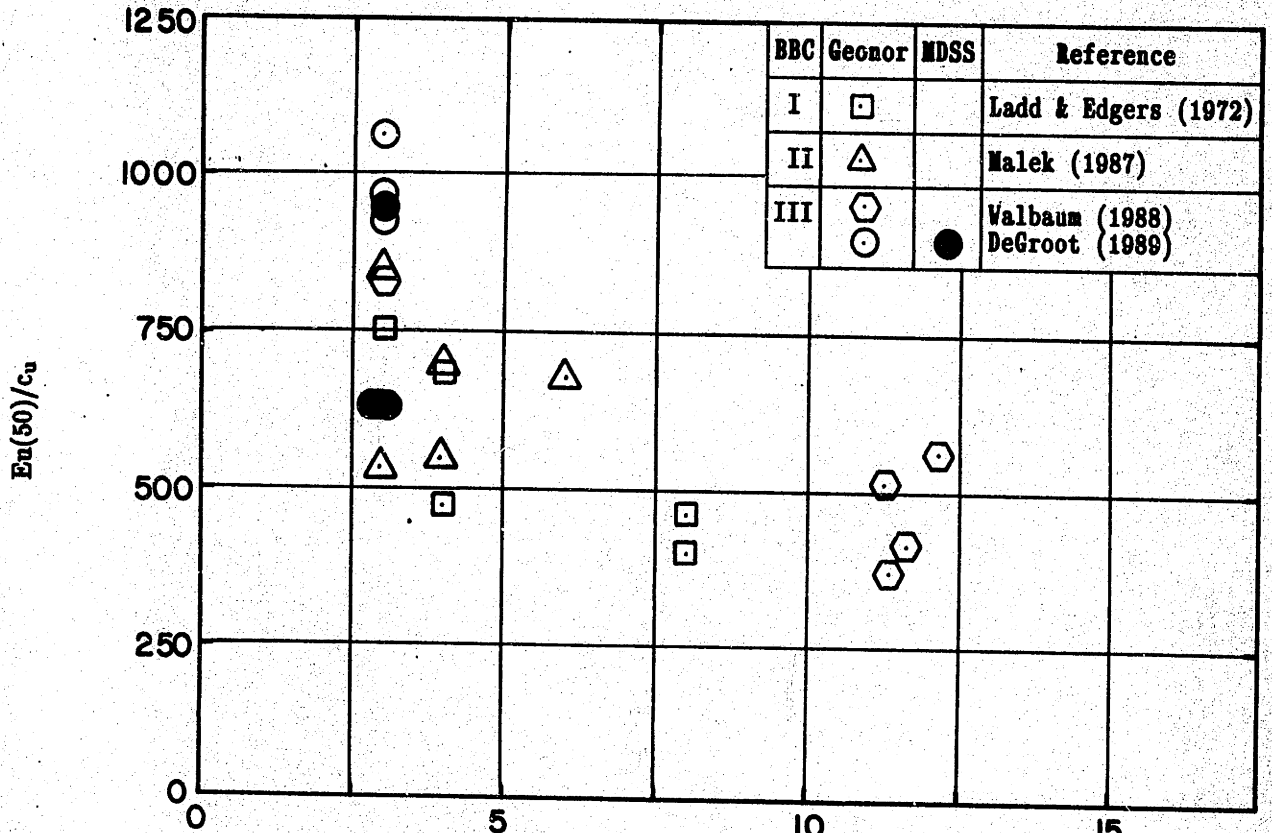

Figure 4.8: Normalized Young's Modulus $Eu(50)/c_u$ versus Vertical Consolidation Stress for CK_oU Direct Simple Shear Tests Conducted at MIT on Boston Blue Clay.

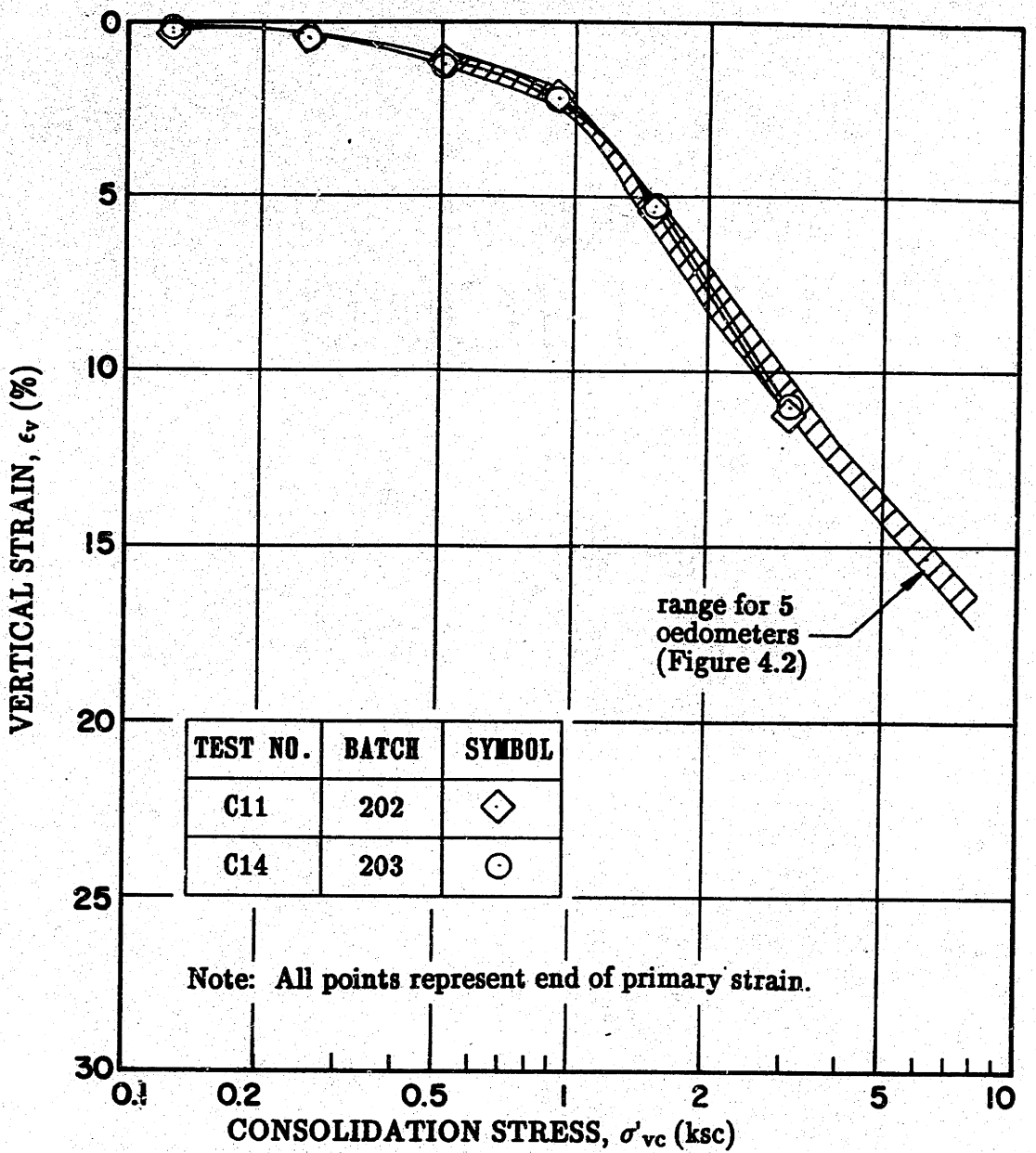

Figure 4.9: Compression Curves for CK_0UMDSS Tests on BBC and Range of Results from Oedometer Tests.

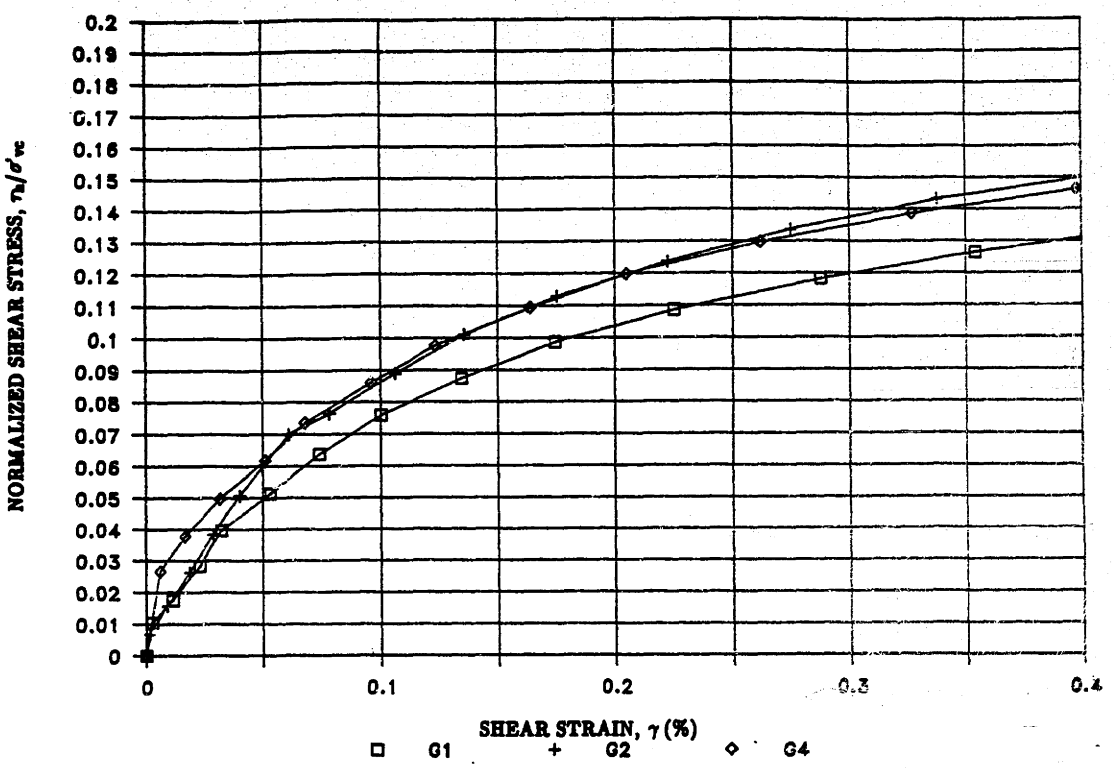

(a)

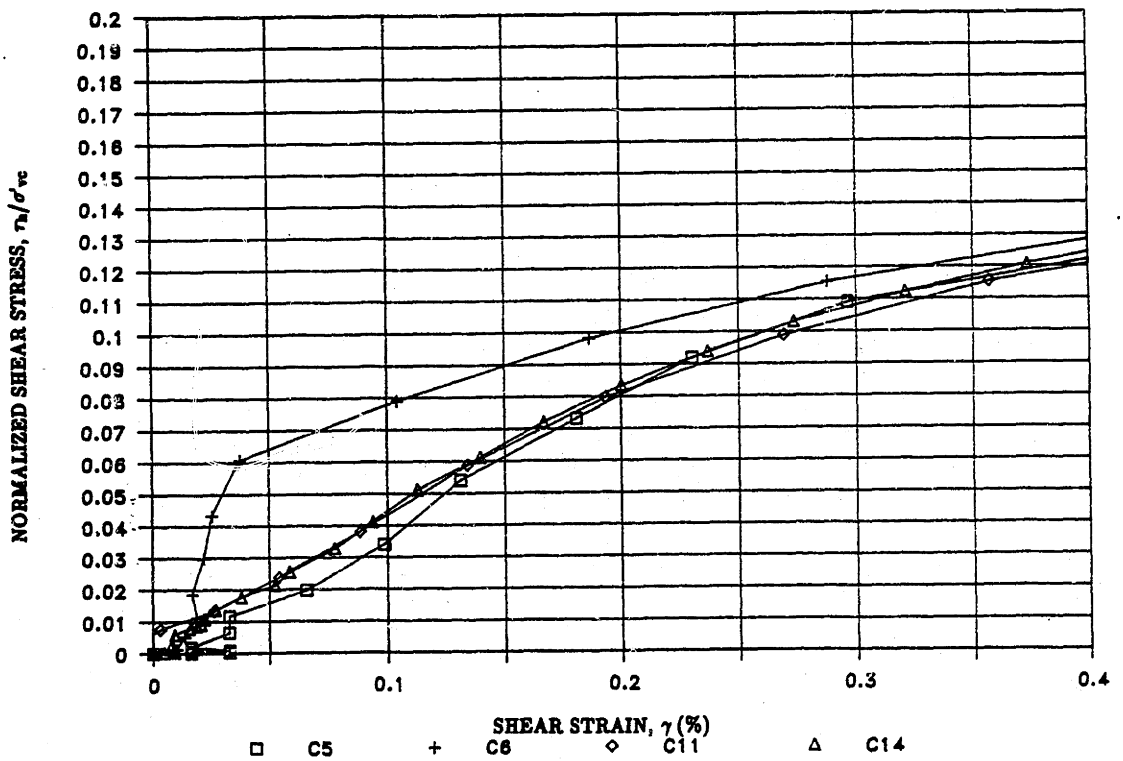

(b)

Figure 4.10: Shear Stress–Strain Curves up to $\gamma = 0.4\%$ for CK_oU Direct Simple Shear Tests on BBC: (a) Geonor DSS; (b) MDSS.

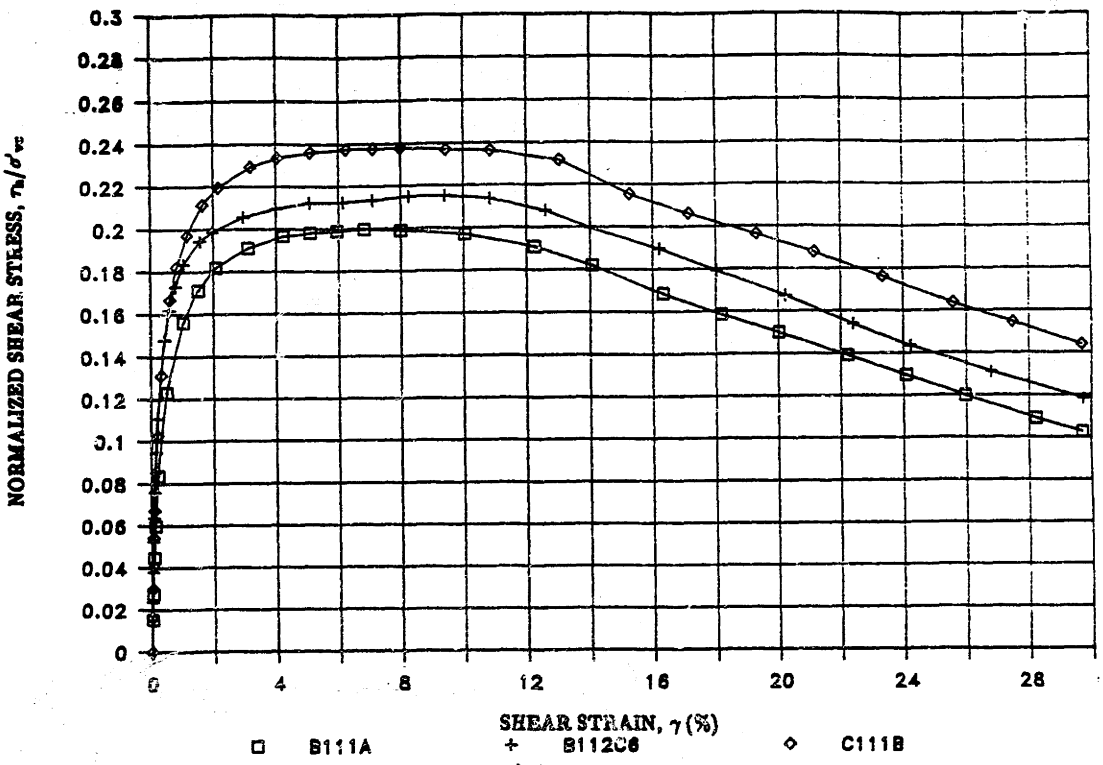

(a)

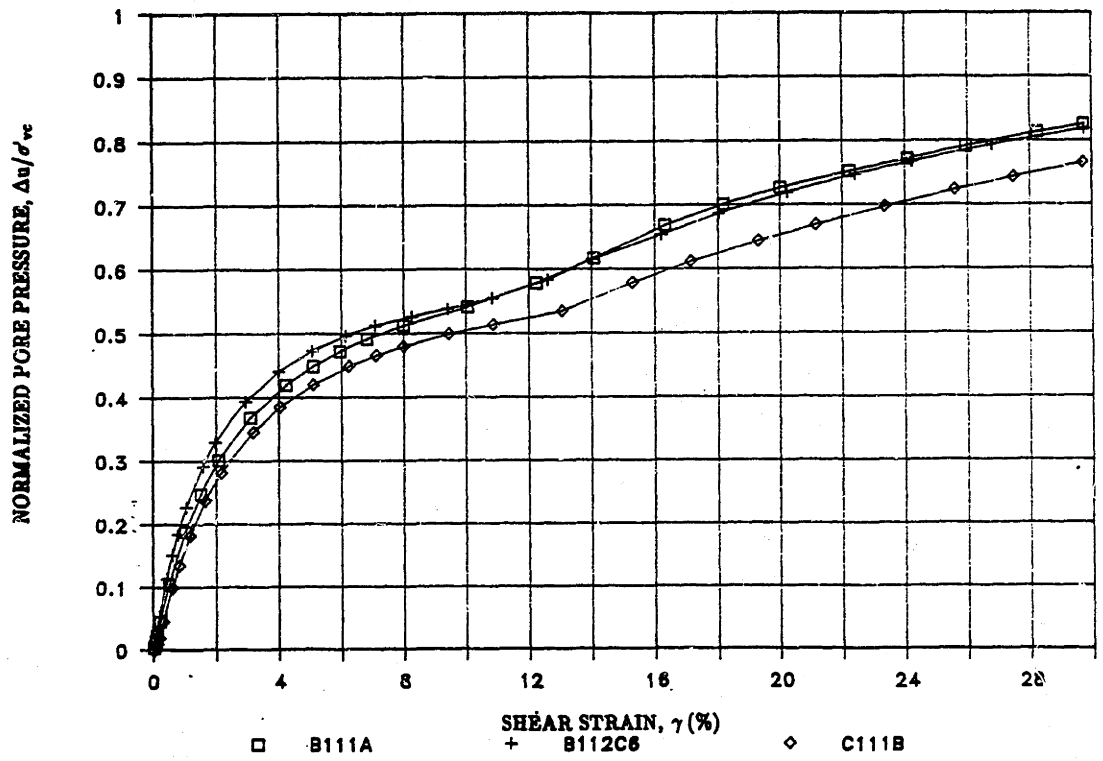

(b)

Figure 4.11: Results of CK_oU Direct Simple Shear Tests on BBC Using the Marshall Silva DSS: (a) Shear Stress–Strain Curves; (b) Pore Pressure versus Shear Strain (Tests by R.S. Ladd).

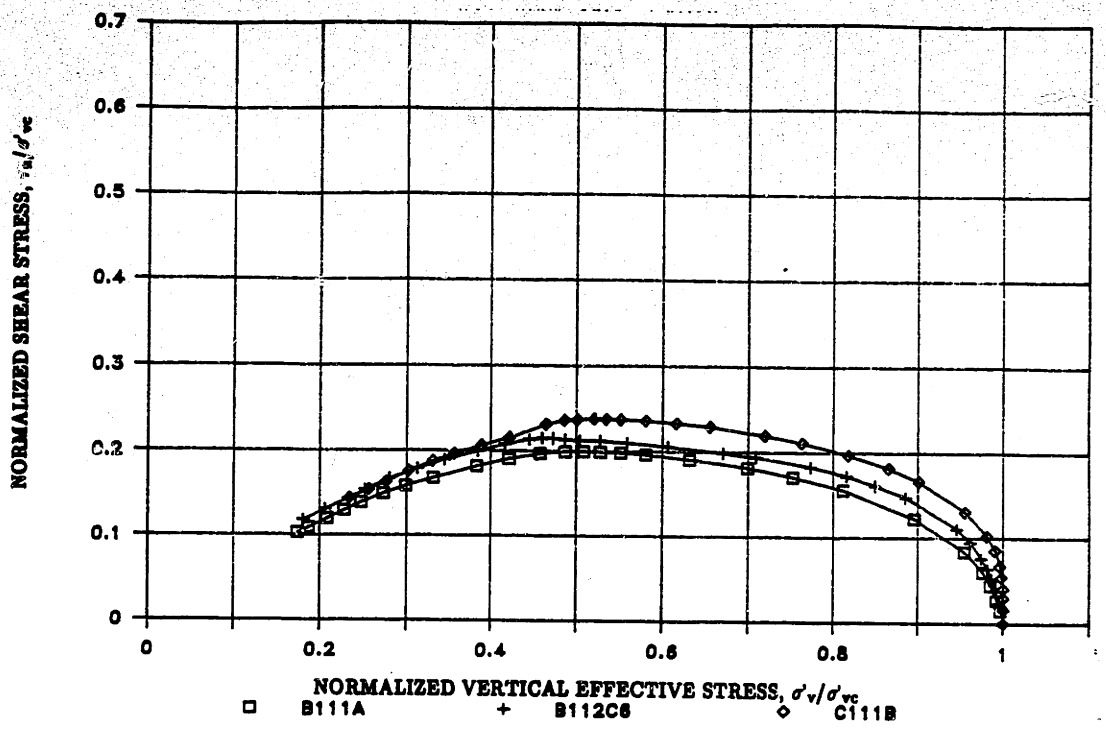

(a)

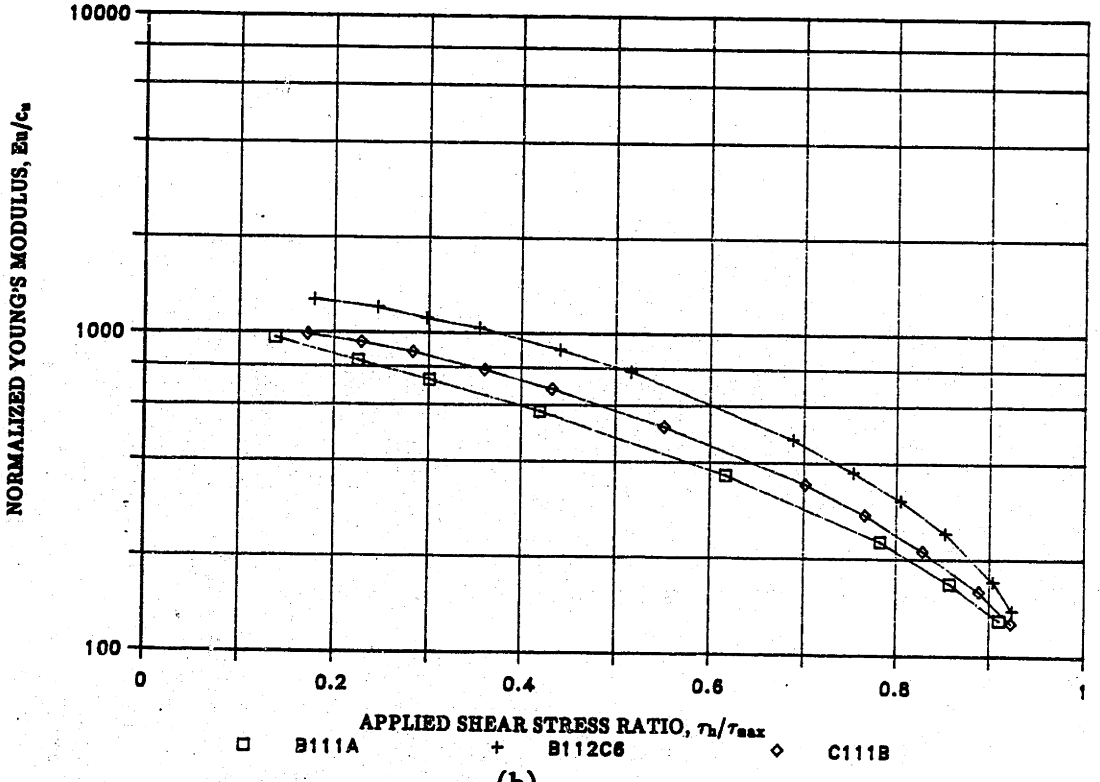

(b)

Figure 4.12: Results of CK_0U Direct Simple Shear Tests on BBC Using the Marshall Silva DSS: (a) Stress Paths; (b) Normalized Young's Modulus versus Applied Shear Stress Ratio (Tests by R.S. Ladd).

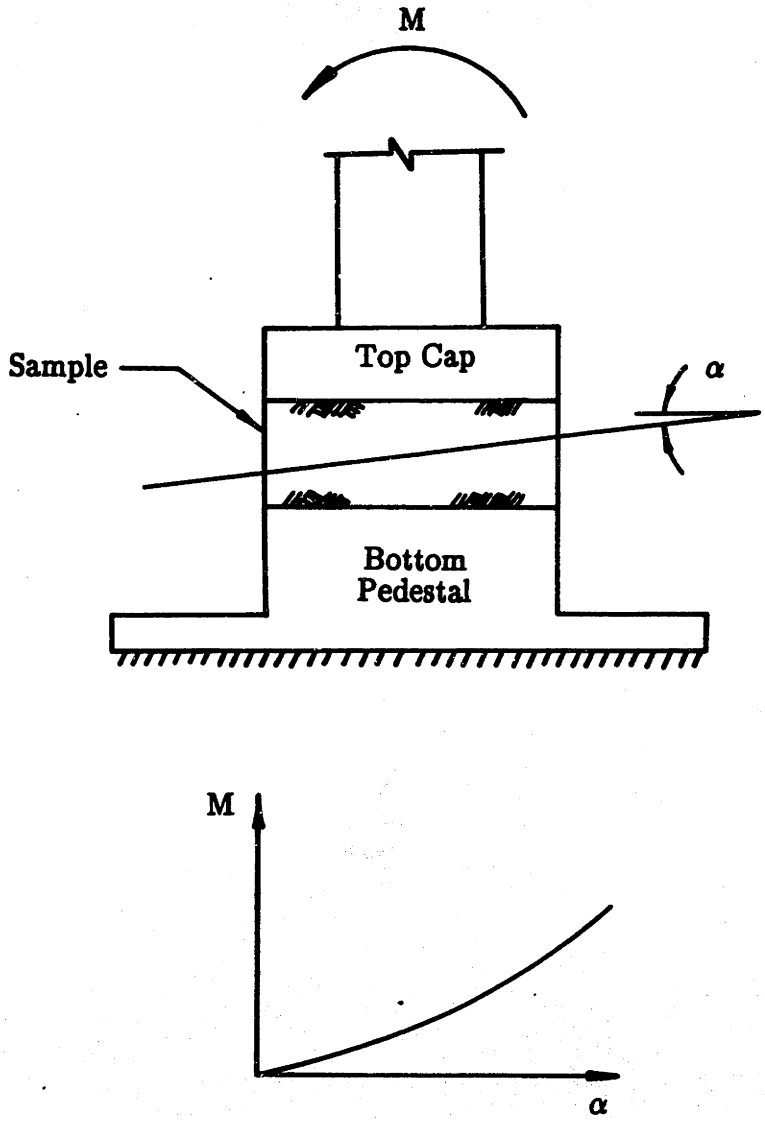

Figure 4.13: Schematic of Definition of Moment–Rotation Relationship for Geonor DSS and MDSS for Determining Their Relative Rotational Stiffness.

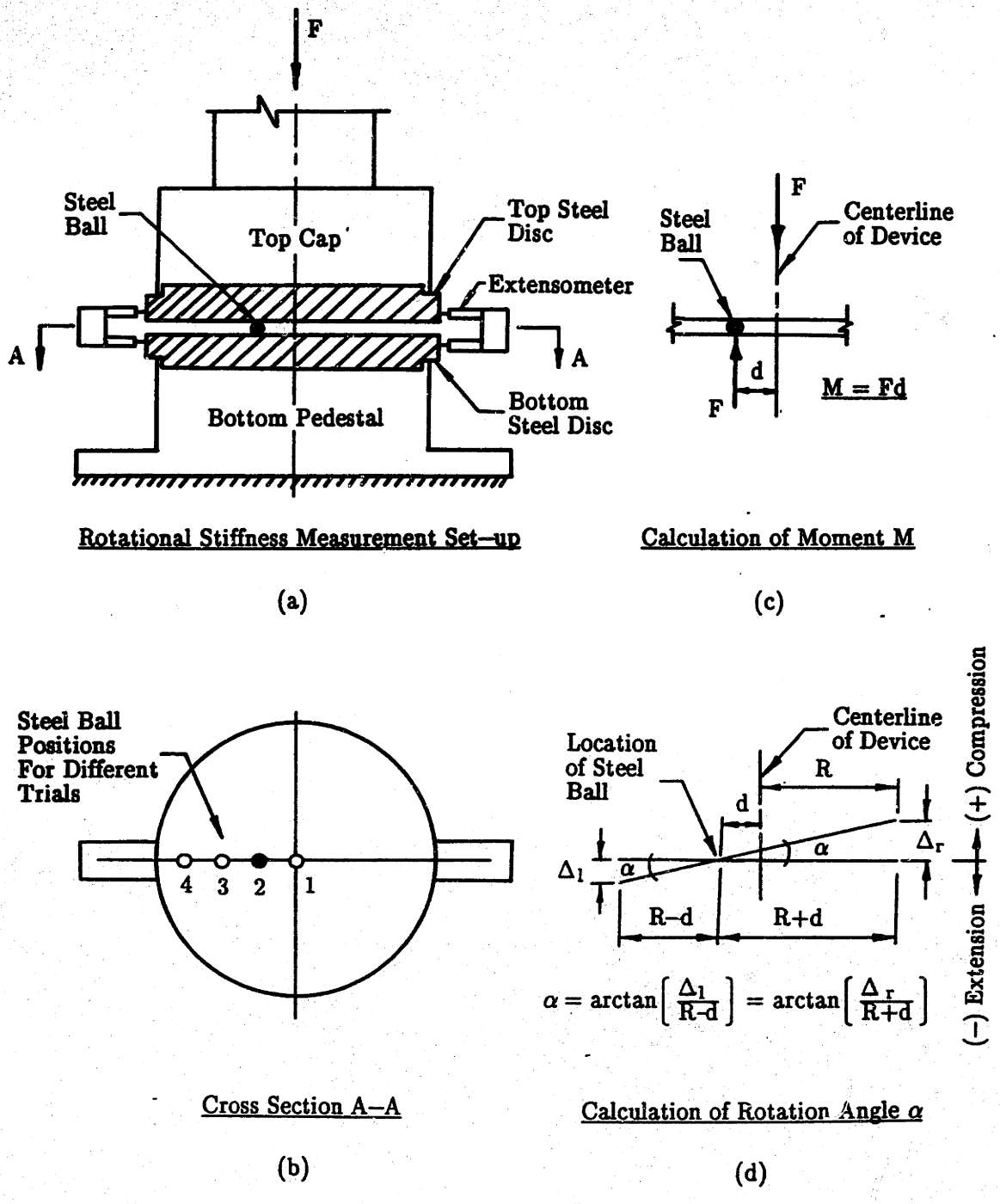

Figure 4.14: Detail of Rotational Stiffness Measurement Technique: (a) Schematic of Equipment Set–up; (b) Cross Section of Steel Disc With Location of Different Position for the Steel Ball; (c) Calculation of Bending Moment; (d) Calculation of Rotation Angle α Based on Extensometer Measurements.

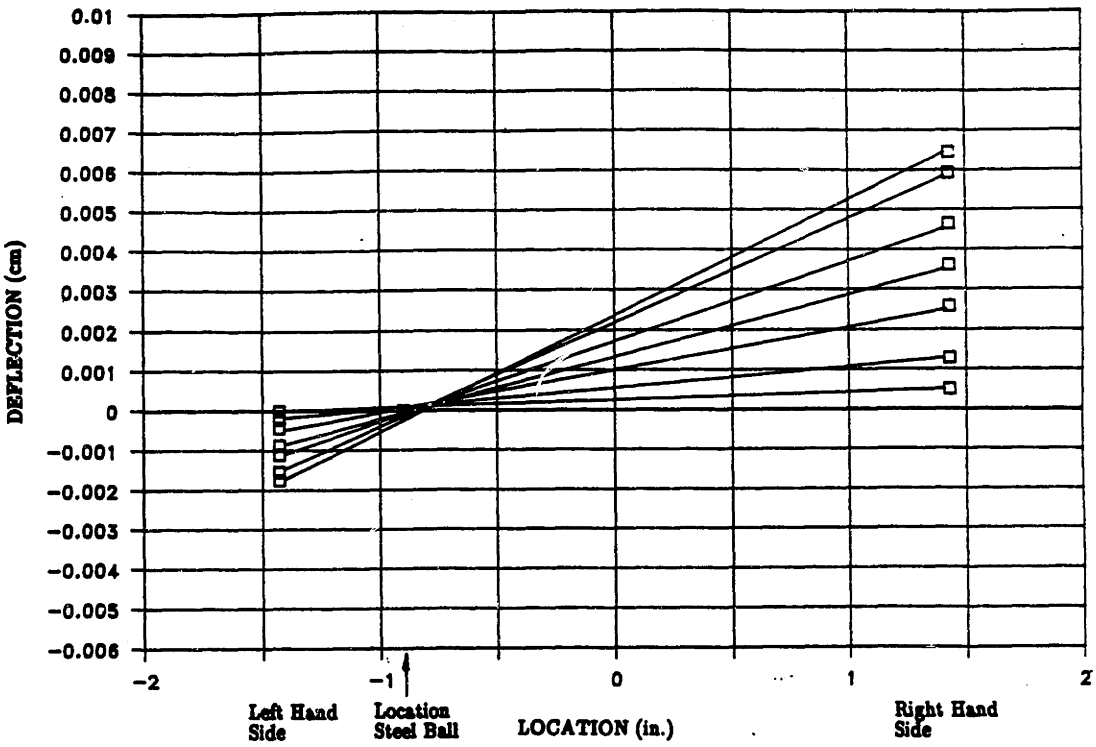

(a)

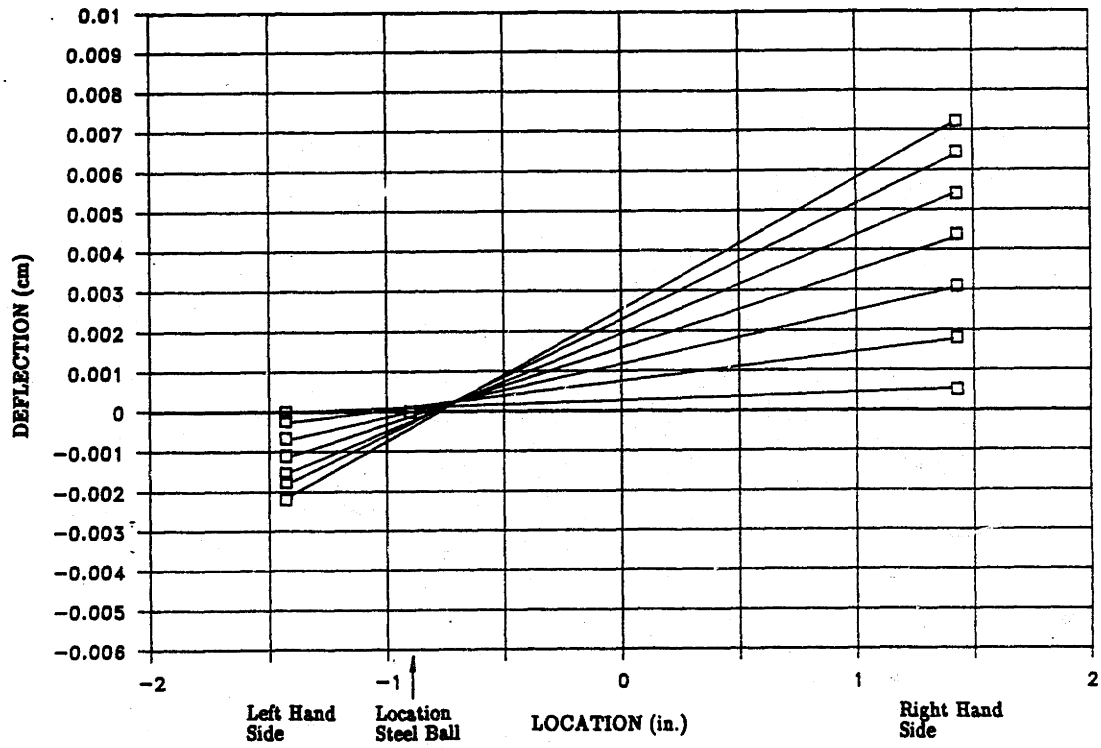

(b)

Figure 4.15: Rotational Deformation of the Vertical Loading Frame Based on Extensometer Measurements for Different Vertical Loads with the Steel Ball in Position 4 (Figure 4.14): (a) Geonor DSS; (b) MDSS.

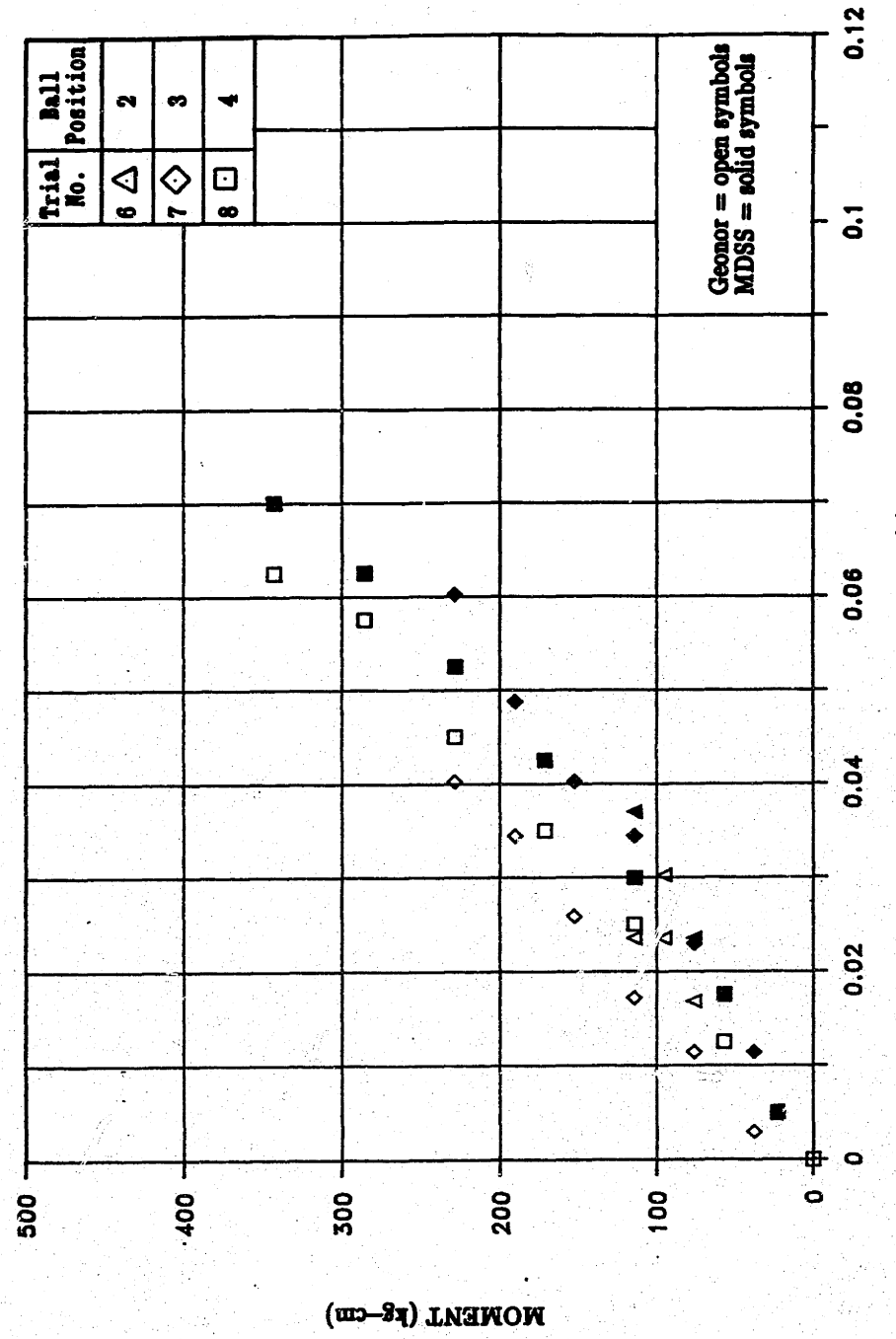

Figure 4.16: Measured Rotational Stiffness of the Geonor DSS and MDSS.

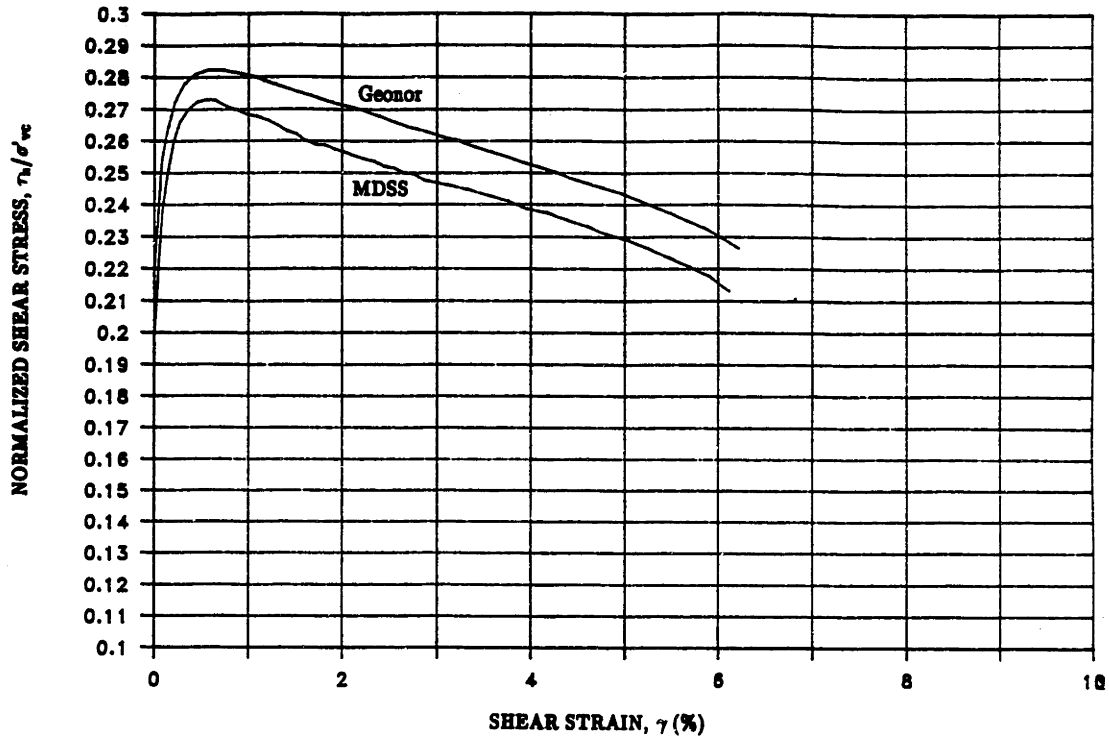

(a)

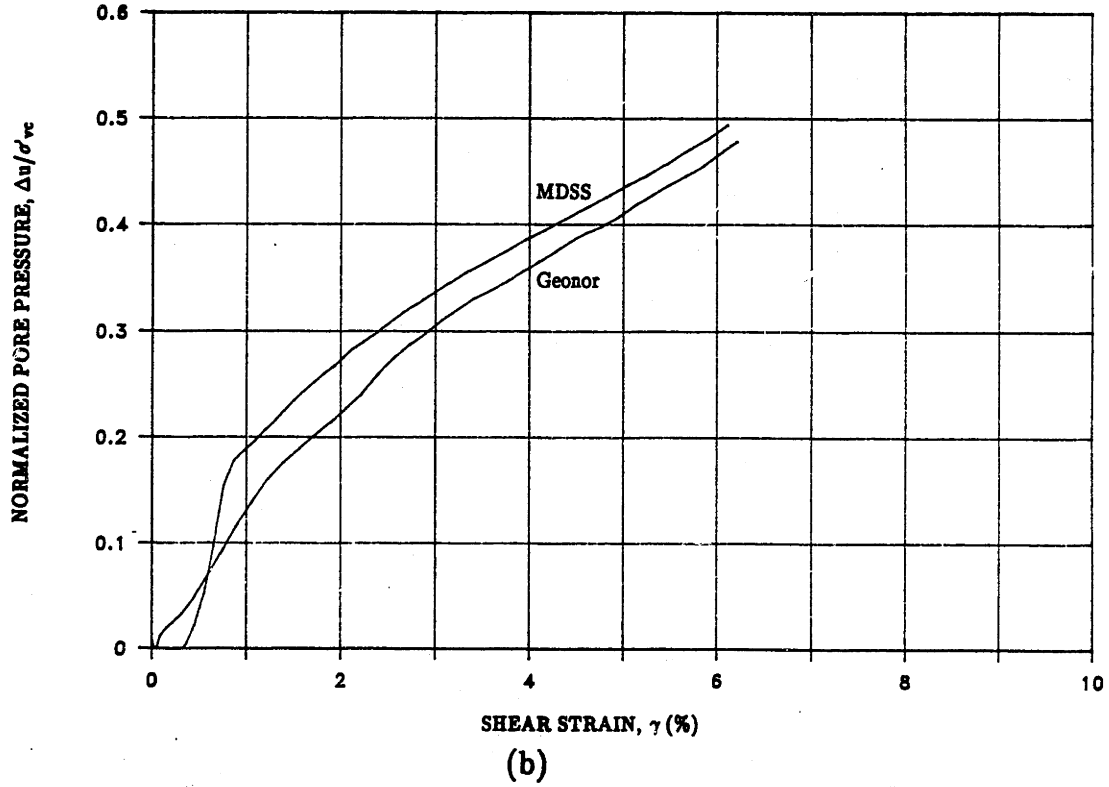

(b)

Figure 4.17: Comparison of Geonor DSS and MDSS Results for CAU Direct Simple Shear Test on BBC at $\theta = 0°$ and $\tau_{hc}/\sigma'_{vc} = 0.2$: (a) Shear Stress–Stain Curves; (b) Pore Pressure versus Shear Strain.

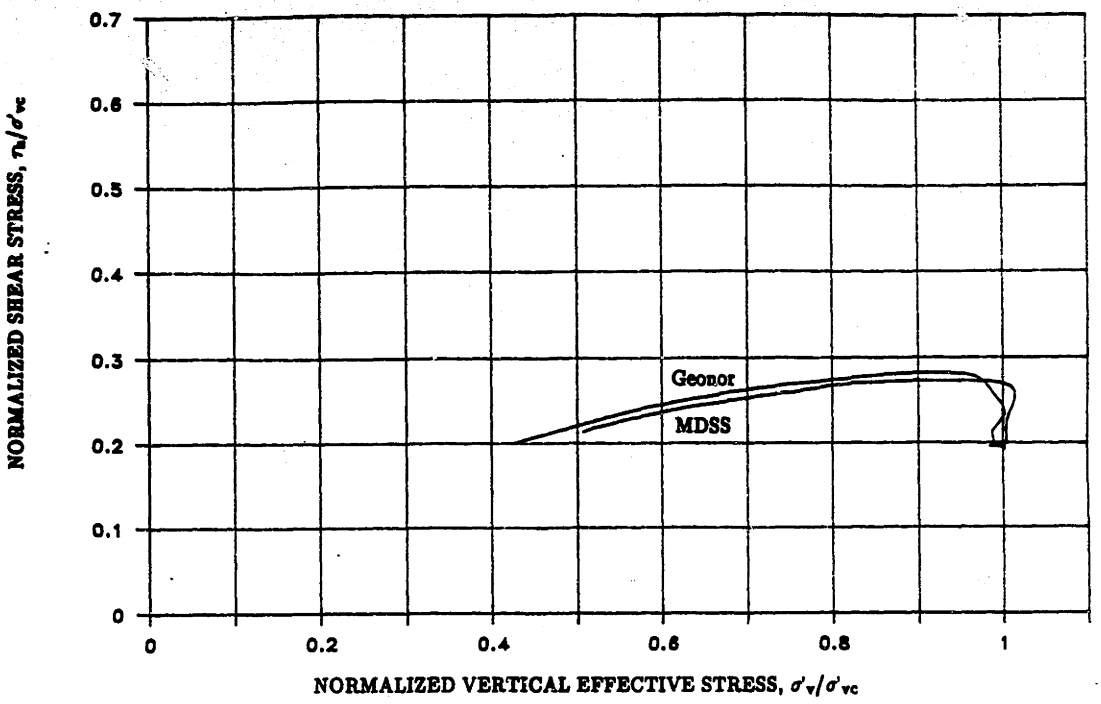

(a)

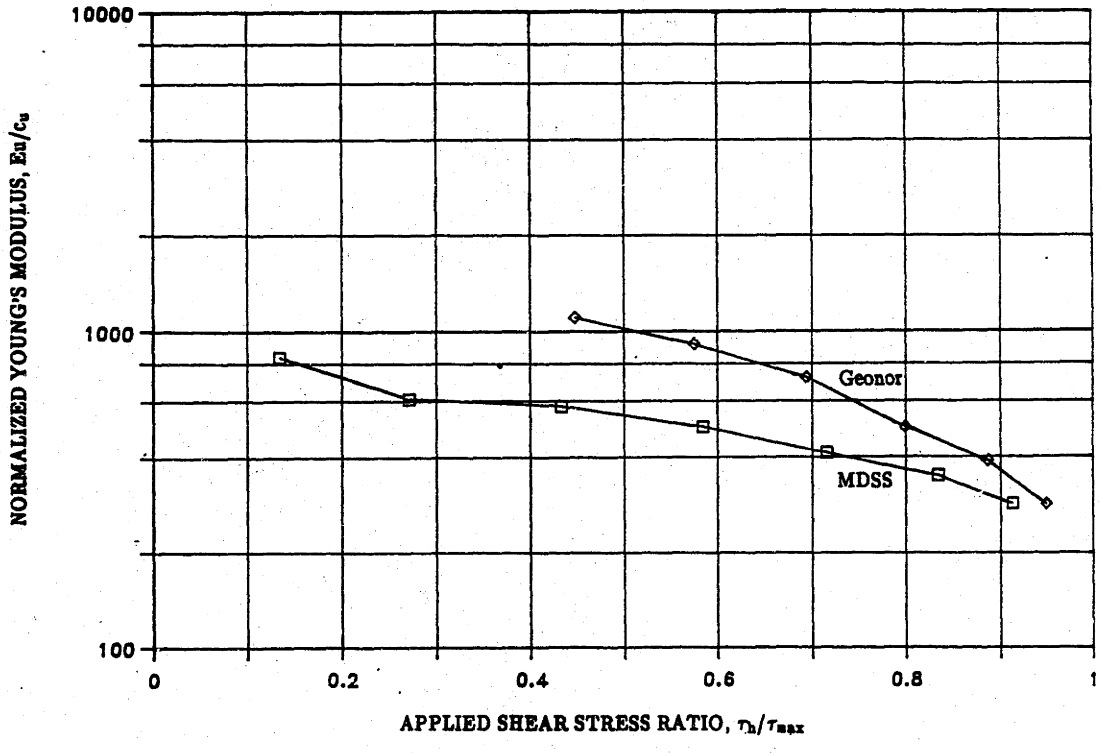

(b)

Figure 4.18: Comparison of Geonor DSS and MDSS Results for CAU Direct Simple Shear Test on BBC at $\theta = 0°$ and $\tau_{hc}/\sigma'_{vc} = 0.2$: (a) Stress Paths; (b) Normalized Young's Modulus versus Applied Shear Stress Ratio.

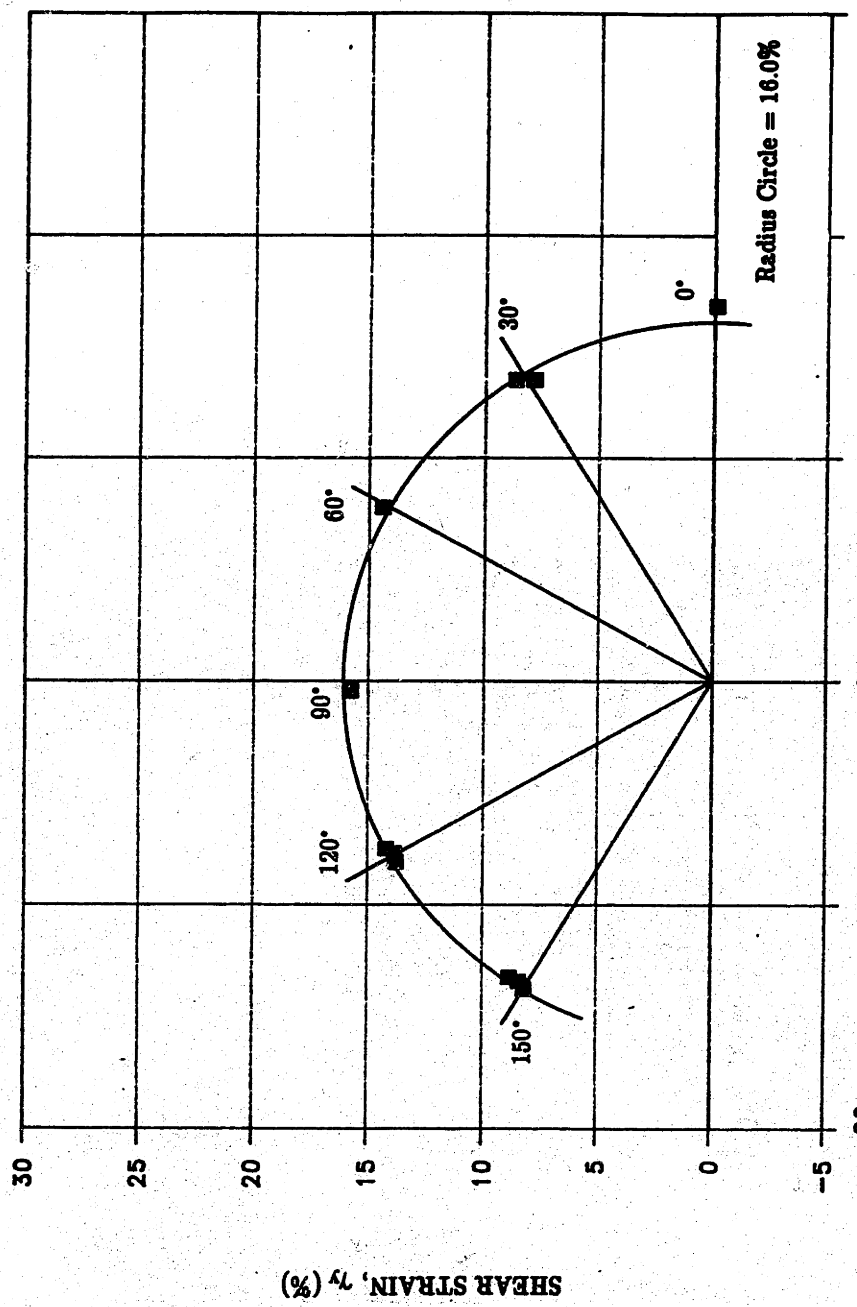

Figure 4.19: Total Shear Strain at End of Application of σ_{vo} and τ_1 for θ Tests on Rubber.

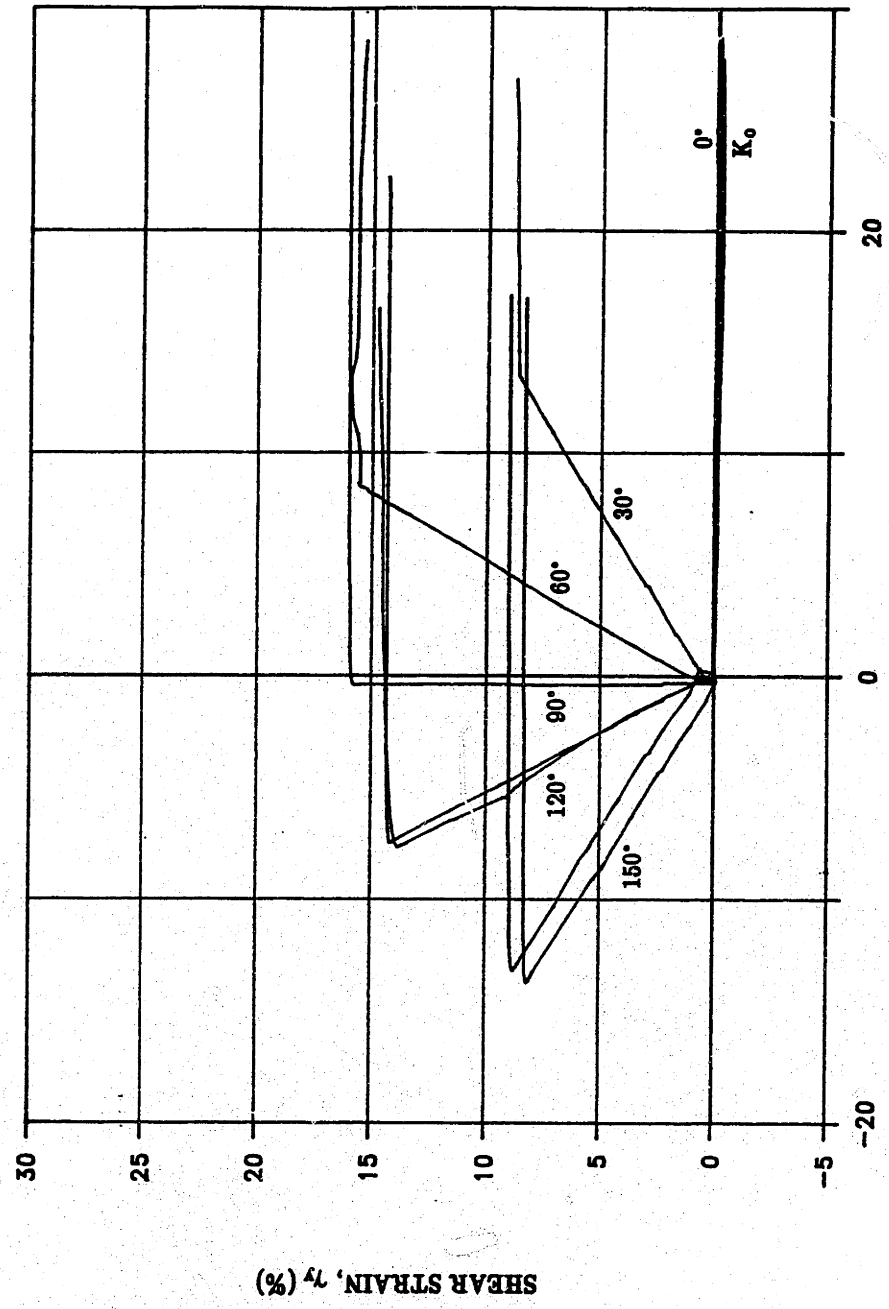

Figure 4.20: Shear Strain Paths for θ Tests on Rubber.

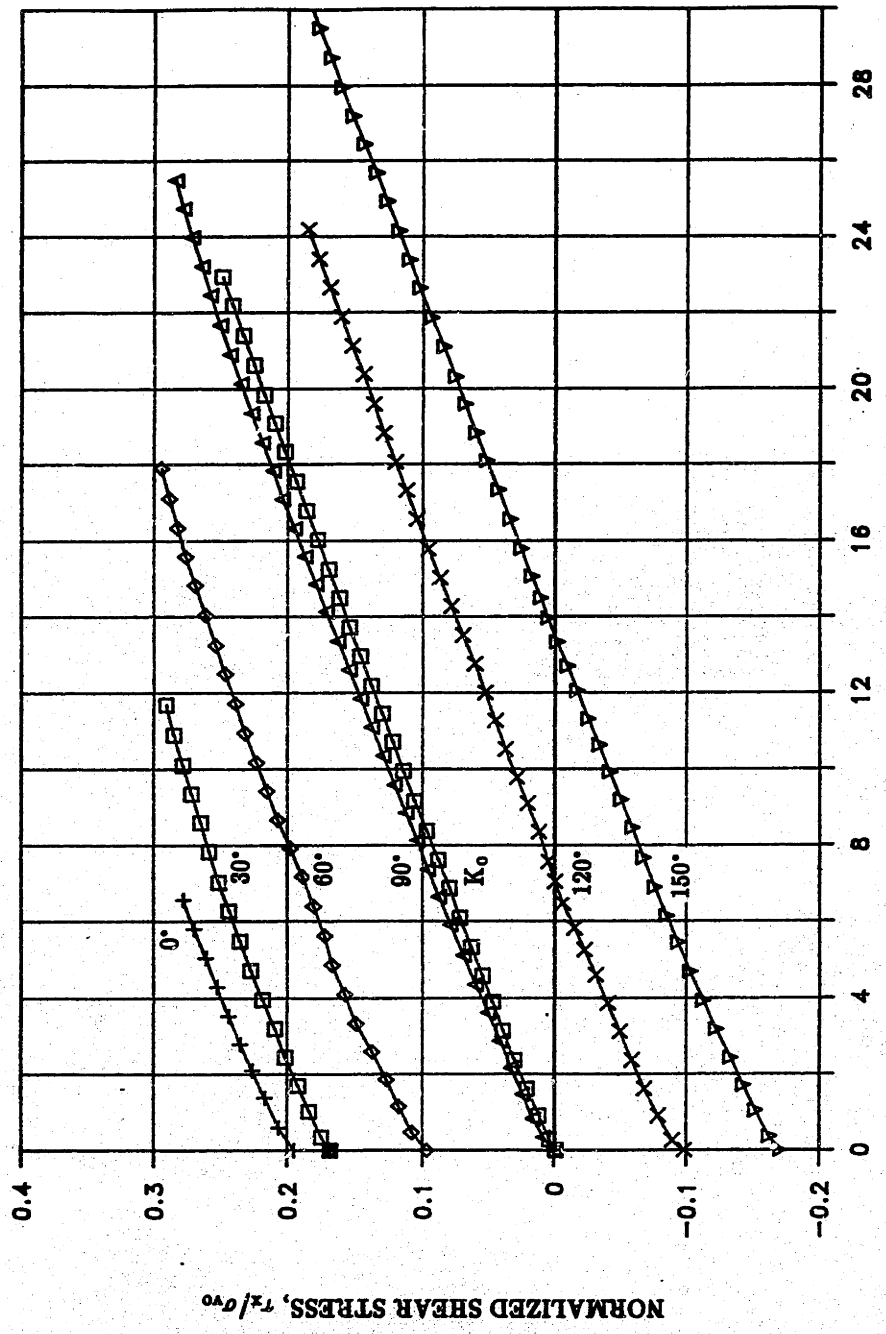

Figure 4.21: Incremental Shear Resistance τ_x versus Incremental Shear Strain γ_x for Several θ Tests and a K_o Test on Rubber.

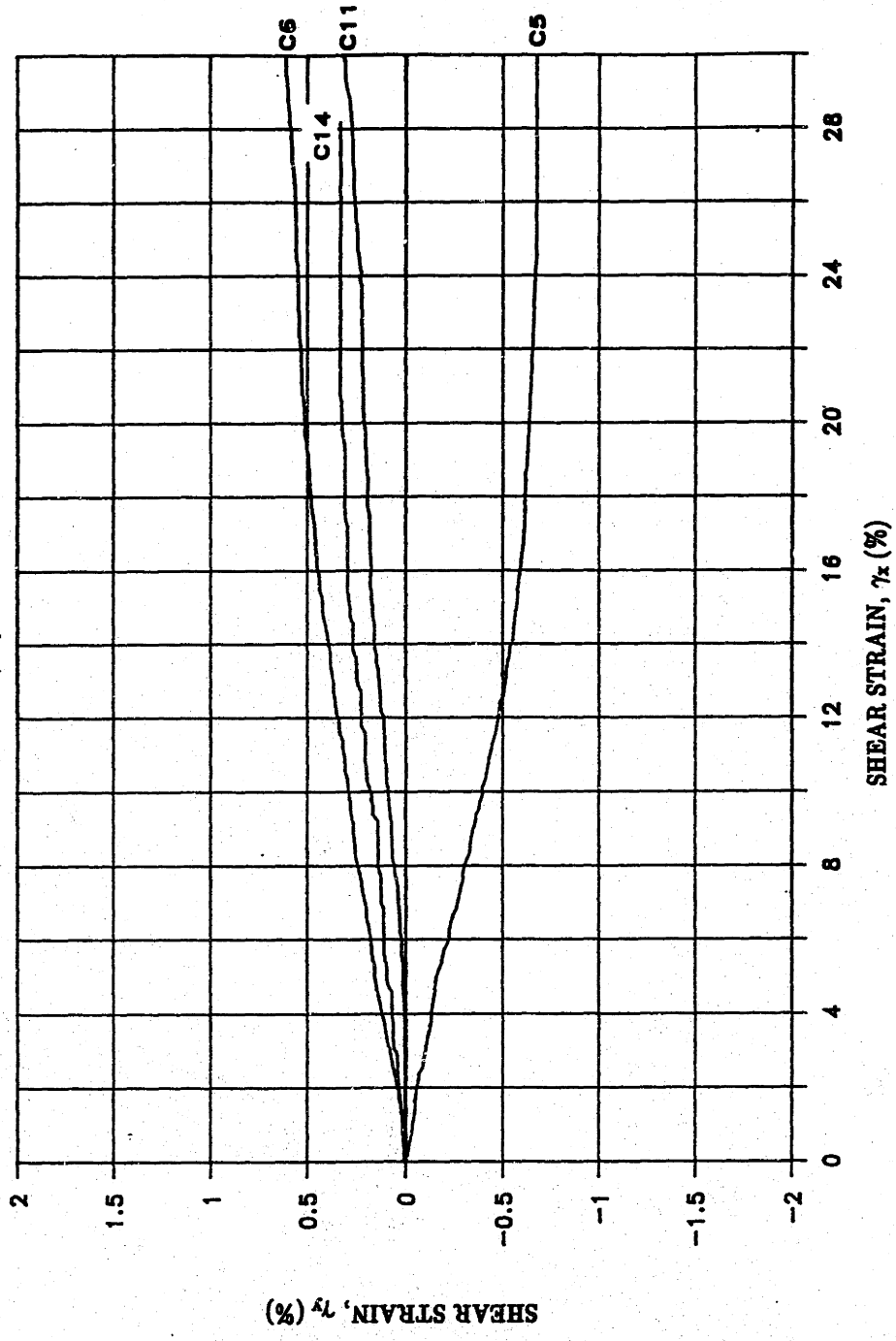

Figure 4.22: Shear Strain Paths During Undrained Shear for CK_oUMDSS Tests on BBC.

CHAPTER 5

MULTIDIRECTIONAL DIRECT SIMPLE SHEAR BEHAVIOR OF ANISOTROPICALLY CONSOLIDATED BOSTON BLUE CLAY

5.1 INTRODUCTION

An experimental test program was conducted on BBC with the objective of simulating the stress conditions acting at representative elements within the foundation soil of an offshore Arctic gravity structure. Samples of BBC were anisotropically consolidated under a vertical normal stress and horizontal shear stress and subsequently sheared undrained by application of a second horizontal shear stress acting at an angle θ relative to the consolidation shear stress. The stresses were applied in this manner to represent the gravity loading and ice loading forces acting on the foundation soil of an Arctic structure.

Fourteen CAU tests were performed as part of the laboratory test program. Five tests were conducted in the Geonor DSS under conditions of $\theta = 0°$ and 180° and at different anisotropic consolidation stress levels (τ_{hc}/σ'_{vc} = 0.0, 0.1 and 0.2; see Table 5.2). Nine tests were conducted in the MDSS to study the influence of varying θ on the behavior of samples subjected to the same anisotropic consolidation stress level ($\tau_{hc}/\sigma'_{vc} = 0.2$). Tests were run at $\theta = 0°$, 30°, 60°, 90°, 120° and 150° (Table 5.4). These data, combined with the θ =180° tests run in the Geonor DSS, give a complete set of results for investigating the dependency of BBC's behavior on the angle θ between the consolidation shear stress (gravity loading) and the undrained shear stress (ice loading).

Tests conducted as part of this experimental program reproduce the stress conditions acting on a wide range of representative elements within the foundation soil of an offshore Arctic gravity structure. The results provide information for assessing

the importance of conducting special direct simple shear tests for design of such structures. This chapter gives a presentation and evaluation of the results of the CAU test program conducted on BBC.

The chapter begins with a discussion of the procedure used during anisotropic consolidation and a presentation of the consolidation results. This is followed by a presentation of the results of the undrained shear portion of the CAU tests conducted in the Geonor DSS and the MDSS. The chapter concludes with the evaluation and synthesis of the results.

5.2 BEHAVIOR OF BBC DURING ANISOTROPIC CONSOLIDATION (GRAVITY LOADING)

The time interval between set–down of an offshore Arctic structure and subsequent application of the design ice loading force can be roughly estimated using historical and present environmental data (e.g., ice records, wind patterns, etc.). This information is needed for predicting the degree of consolidation obtainable by the foundation soil before the structure is subjected to its design ice load. The rate of consolidation is controlled by the soil type, thickness of the soil layer and the boundary drainage conditions. Since the gain in undrained shear strength of the soil is directly dependent on its degree of consolidation, it is important to be able to estimate this for design purposes. Clearly, the most critical case would be for a structure subjected to the design ice load immediately after set–down, although this would be unlikely for typical conditions within the Beaufort Sea. The time required to reach a certain degree of consolidation (and therefore strength gain) might also be enhanced using artificial drainage (e.g., wick drains).

While it is apparent that the degree of consolidation obtainable by the foundation soil before application of the design ice load will vary from case to case, it was decided for the first experimental test program using the MDSS that the soil

would be allowed to fully consolidate under the gravity loading stresses. The samples were then sheared undrained, which for the ice loading, represents the critical design case.

5.2.1 Anisotropic Consolidation Procedure

Table 5.1 shows the loading schedule used for the CK_oU direct simple shear tests performed on BBC as part of this thesis. Figure 5.1 is a plot of the sample height versus log time deflection curve for σ'_{vc} = 0.9, 1.5 and 3 ksc for CK_oU test C11 (σ'_p = 1 ksc).[1] Using Casagrande's log time construction gives the end of primary consolidation (t_{100}) equal to approximately 6, 79 and 25 minutes for σ'_{vc} = 0.9, 1.5 and 3.0 ksc respectively.

Using the CK_oU consolidation results as a guide, horizontal shear stress increments during anisotropic consolidation were applied after the specimen reached approximately t_{100} under the corresponding vertical stress increment. The samples were trimmed as for the CK_oU tests and then loaded with small increments of vertical and horizontal consolidation stresses to prevent undrained overstressing of the specimen. The horizontal shear stress was applied in two equal increments for each vertical stress level in order to reach the nominal τ_{hc}/σ'_{vc} value for the specific test. The two increments were applied at t = 20 min (step 2) and 30 min (step 3) after application of the vertical stress increment. In general, each σ'_{vc} increment and its two corresponding τ_{hc}/σ'_{vc} increments remained on the specimen for a total time of about 100 minutes except for the final increment which was left on for 24 hrs. The first application of a horizontal shear stress increment was not applied until the specimen was consolidated up to σ'_{vc} = 0.5 ksc. Table 5.1 presents the loading schedule used for

---

[1]The CAU loading schedule was determined on the basis of the results of the first CK_oU tests performed for this study on BBC in the Geonor DSS (G1 and G2). However, the vertical strains in these tests are inaccurate (see Section 4.3.1). Although this problem does not significantly influence the determination of t_{100}, the results of test C11 are presented here since they represent an accurate set of deflection log time curves.

anisotropic consolidation and Figure 5.2 plots stress paths of the consolidation phase for tests performed with $\tau_{hc}/\sigma'_{vc} = 0.0$ (K_o), 0.1 and 0.2.

5.2.2 Anisotropic Consolidation Results

Figure 5.3 is a representative plot of the incremental volumetric strain and shear strain versus log time for $\sigma'_{vc} = 2.5$ to 3.0 ksc for tests with $\tau_{hc}/\sigma'_{vc} = 0.1$ and 0.2. Also shown in the figure is the time at which the increments of horizontal shear stress were applied to the specimens. The plot displays several aspects of the influence of anisotropic consolidation on the behavior of the tests specimens including:

1. Application of a horizontal consolidation shear stress to a sample results in an increase in the volumetric (i.e., vertical) strain compared to K_o consolidated specimens.
2. Application of increments of either vertical or horizontal consolidation stresses results in an increase in both the volumetric strain and shear strain.

The change in shape of the volumetric strain curve due to application of an increment of horizontal shear stress is shown in Figure 5.3a. At the time of application of the increments of horizontal shear stress (steps 2 and 3 as shown in the figure) the volumetric strain curve changes slope from its original path (shown by the dotted line in the figure). It is clear from the curves plotted in this figure that the sample, at the end of consolidation, will have a higher volumetric strain than a K_o consolidated specimen. This effect is less pronounced for the $\tau_{hc}/\sigma'_{vc} = 0.1$ test.

The influence of an increment of vertical stress on the horizontal shear strain is shown in Figure 5.3b. The plot shows that before application of the first stage of horizontal shear stress the sample already experiences some horizontal shear strain. As in the case for volumetric strains, this effect is less pronounced for the test with $\tau_{hc}/\sigma'_{vc} = 0.1$.

The deflection versus log time curves for each of the increments during anisotropic consolidation cannot be interpreted using Casagrande's log time

construction to find t_{100}. The load increment ratios of the vertical stress increments are very low (see Table 5.1) and as a result many of the curves will not display the characteristic break from primary consolidation to secondary consolidation required to perform Casagrande's log time construction. In addition, the application of horizontal shear stress increments changes the slope of the deflection log time curve, particularly for tests with higher τ_{hc}/σ'_{vc} ratios as clearly shown in Figure 5.3. As a result it is not possible to compute the coefficient of consolidation for the CAU tests using conventional procedures.

Figure 5.4 is a plot of the compression curves for tests with τ_{hc}/σ'_{vc} = 0.0 (i.e., K_o), 0.1 and 0.2 (data are tabulated in Appendix H). Since it is not possible to determine the end of primary consolidation using conventional procedures the compression curves are plotted using the measured vertical strain at a fixed time interval (t = 100 minutes). The curves for K_o consolidation and τ_{hc}/σ'_{vc} = 0.2 represent the average curve for the tests run with these conditions (C11 and C14 for K_o and C7, C8, C10, C12, C13, C15, C16 and C17 for τ_{hc}/σ'_{vc} = 0.2)[2]. The curve for τ_{hc}/σ'_{vc} = 0.1 is from test G8 (the only other test conducted with this stress ratio, test G3, has inaccurate consolidation strains).

The data plotted in Figure 5.4 show that anisotropic consolidation results in an increase in the measured vertical strains during consolidation compared to K_o consolidation. The compression curves for the K_o and τ_{hc}/σ'_{vc} = 0.2 tests are nearly parallel in the virgin compression region indicating that most of the additional increase in vertical strains during anisotropic consolidation occurs at stress levels around the preconsolidation pressure. Ideally, the curve for τ_{hc}/σ'_{vc} = 0.10 should plot between the K_o and τ_{hc}/σ'_{vc} = 0.20 curves, but Figure 5.4 shows that it does not. However,

---

[2]Test C9 (θ =120°) was subjected to an irregular loading sequence due to a power failure. Hence, the consolidation results of this test are not included in this section but its undrained shear behavior will be used in this chapter.

this test had fairly large vertical strains up to σ'_{vc} = 0.5 ksc compared to the other types of tests. This indicates that the sample may have had a seating problem and/or experienced some disturbance prior to consolidation (also this is the result of one test which is not the case for the average curves for the K_o and τ_{hc}/σ'_{vc} = 0.20 tests). By considering only the incremental vertical strains beyond σ'_{vc} = 0.5 ksc, the τ_{hc}/σ'_{vc} = 0.1 test plots in between and parallel to the K_o and τ_{hc}/σ'_{vc} = 0.2 curves.

Figure 5.5 is a plot of the applied shear stress versus consolidation shear strain for all of the anisotropically consolidated Geonor DSS and MDSS tests (data are tabulated in Appendix H).[3] The strain values are plotted at t = 100 minutes after the start of each consolidation increment. The results show that there is a significant influence of τ_{hc} on the magnitude of the consolidation shear strain. At the end of consolidation tests with τ_{hc}/σ'_{vc} = 0.2 (τ_h final = 0.6ksc) have an average γ_t = 17.5% ± 1.9SD (n = 11) compared with γ_t = 6.8% for the two tests with τ_{hc}/σ'_{vc} = 0.10 (τ_h final = 0.3ksc). There appears to be little effect of τ_{hc}/σ'_{vc} ranging from 0.1 to 0.2 on τ_{hc} versus γ (compare curves for τ_{hc}/σ'_{vc} = 0.1 and 0.2 from τ_{hc} = 0 to 0.3 ksc in Figure 5.5).

The data plotted in Figure 5.5 for τ_{hc}/σ'_{vc} = 0.2 displays a considerable amount of scatter in the final shear strains. Furthermore it appears that the scatter is not random, as is more clearly shown in Table 5.3 and Figure 5.6 which is a plot of the final consolidation shear strain for tests conducted at the different θ angles. The circle plotted in the Figure represents the average shear strain of γ_t = 17.5% for all of the Geonor and MDSS tests. Focusing on the MDSS results, it appears that the tests conducted at θ = 120° and 150° experience less consolidation shear strain than those tests performed with θ = 0° to 90°. This indicates that there may be some inherent mechanical problem with the MDSS. However, tests conducted at θ = 120° and 150°

[3]Consolidation shear strain is based on the preconsolidation sample height.

(C13, C15, and C16) used specimens from batch 203 whereas most of the tests with θ = 0° to 90° (C7, C8, C10 and C12) were on specimens from batch 202. The use of material from two different batches may lead to some variability in the response of the different soil specimens and hence to differences in the consolidation shear strains.

When the first set of tests conducted at θ = 120° and 150° did not have final shear strains similar to the tests with θ = 0° to 90°, a second set of tests were performed at θ = 120° and 150° (C15 and C16) which also had shear strains different from the tests with θ = 0° to 90°. Test C17 was also a repeat test conducted at θ = 60° on a specimen from batch 203 with the objective of trying to determine if the cause of the difference in consolidation shear strains was due to a mechanical problem with the MDSS or due to batch variability. The results of this test proved to be inconclusive. The incremental shear strains near the preconsolidation pressure were less for this specimen than the other batch 202 test specimens, yet the final consolidation shear strains were similar to that found for the tests with θ = 0° to 90°.

Given the discrepancy found among the consolidation shear results, a detailed study of the data was performed and is presented in Appendix F. The objective of the Appendix was to study the anisotropic consolidation results and to decide if any concluding statements could be made about the two possible causes for the discrepancy in shear strains – specifically, whether it is due to variability between the specimens from the two different batches and/or due to inherent mechanical problems with the MDSS.

The data presented in Appendix F did not conclusively resolve the issue of why there are differences in the final consolidation shear strains. However, based on the analysis presented in the Appendix and the results of the tests conducted on rubber presented in Chapter 4, the following observations can be made:

1. Chapter 4 presented results for rubber which clearly showed that the set–up procedures, horizontal loading and strain measuring systems

in the MDSS are working properly and produce accurate and reliable results;

2. The consolidation shear strains for the tests on BBC show some inconsistencies among the various test angles θ and in general the angle of deformation of the specimens does not correspond as accurately to the test angle θ as was found for the tests on rubber (compare Figures 4.19 and 5.6). There does not appear to be a consistent trend between the deviation in the applied θ and measured θ with the final magnitude of the total consolidation shear strain γ_t (Table 5.3);

3. The vertical compression curves and incremental vertical strain data showed very little variation among the different CAU tests on BBC indicating that the vertical compression behavior is independent of the batch from which the specimens were taken as well as the test angle θ. Ideally this is what would be expected;

4. An analysis of the final and incremental consolidation shear strain data conducted in Appendix F was inconclusive. The final shear strain data appear to indicate that the lower consolidation shear strains found for the tests conducted at $\theta = 120°$ and 150° are not consistent with the data measured for tests conducted at $\theta = 0°$ to 90° independent of which batch the specimens came from. However, differences in the incremental shear strains around the preconsolidation pressure indicate that the response of the specimens depends in part on which batch they came from and not exclusively on the test angle θ;

5. Comparison of measurements of the top cap deformation during consolidation for tests on BBC and rubber in Appendix F showed that the MDSS deforms in a similar manner independent of whether the material is clay or rubber and does not exhibit any unusual response in terms of deformation for the BBC tests at $\theta = 120°$ and 150°.

The reason why tests conducted on BBC at $\theta = 120°$ and 150° exhibit smaller shear strains than tests conducted at $\theta = 0°$ to 90° remains uncertain. However, inspite of this, the undrained shear response of the tests with $\theta = 120°$ and 150° will be used with the $\theta = 0°$ to 90° for studying the undrained shear behavior of BBC with $\tau_{hc}/\sigma'_{vc} = 0.2$ as a function of the test angle θ.

5.2.3 Summary

The results presented in this section show that anisotropic consolidation leads to an increase in the vertical strain of a specimen compared to K_o consolidation. Application of increments of either vertical or horizontal consolidation stresses results in an increase in both the vertical strain and shear strain. For a given vertical

consolidation stress (σ'_{vc}) this influence increases with higher consolidation stress ratios (τ_{hc}/σ'_{vc}; see Figure 5.3). Increasing the consolidation shear stress results in a significant increase in the consolidation shear strain (e.g. $\gamma_t \cong 6.8\%$ and 17.5% for τ_{hc}(final) = 0.3 ($\tau_{hc}/\sigma'_{vc} = 0.1$) and 0.6 ($\tau_{hc}/\sigma'_{vc} = 0.2$) respectively).

In general, the vertical compression curve of an anisotropically consolidated specimen plots parallel and lower (i.e. higher ϵ_v at the same σ'_{vc}) during virgin compression than a K_o consolidated sample (Figure 5.4). Most of the difference in vertical strain between K_o and anisotropic consolidation occurs at stress levels around the preconsolidation pressure.

Results of the final consolidation shear strain data, plotted in Figure 5.6 show that tests conducted at $\theta = 120°$ and 150° exhibit smaller shear strains than tests conducted at $\theta = 0°$ to 90°. A comprehensive study of this discrepancy, presented in Appendix F, proved to be inconclusive. Differences in the final consolidation strain could not be solely explained in terms of the source material for each test (i.e., batch #) nor the deviation in the applied θ and measured θ (i.e., Δ in Table 5.3). This issue can only be resolved by conducting a comprehensive test program with BBC repeating many of the tests at all of the different θ angles with specimens from the same batch which is beyond the scope of the present work.

5.3 GEONOR CAUDSS UNDRAINED SHEAR RESULTS FOR BBC (ICE LOADING)

Five Geonor CAUDSS tests were conducted to investigate the influence of the orientation and magnitude of the consolidation shear stress on the undrained shear behavior of BBC. Two tests were conducted with $\theta = 0°$ ($\tau_{hc}/\sigma'_{vc} = 0.1$ and 0.2) and three tests with $\theta = 180°$ (one at $\tau_{hc}/\sigma'_{vc} = 0.1$ and two at $\tau_{hc}/\sigma'_{vc} = 0.2$). These test data, combined with the results of the CK_oUDSS tests, give a full set of results for the undrained shear behavior of BBC as τ_{hc}/σ'_{vc} acting along the same orientation varies

from –0.2 to 0.2. The five CAUDSS tests are summarized in Table 5.2 and Figures 5.10 to 5.14 present plots of the stress–strain curves, pore–pressure versus shear strain, stress paths and undrained Young's modulus. Also included in the Table and Figures are the average results of the three Geonor CK_oUDSS tests presented in Chapter 4.

The normalized shear stress–strain curves plotted in Figure 5.10 show a considerable influence of the magnitude and orientation of the consolidation shear stress on the undrained shear behavior.[4] For tests with $\theta = 0°$, increasing τ_{hc}/σ'_{vc} from 0 to 0.2 results in a significant increase in the total peak shear resistance ($(\tau_h/\sigma'_{vc})_{max}$ = 0.283 for $\tau_{hc}/\sigma'_{vc} = 0.2$ versus $(\tau_h/\sigma'_{vc})_{max} = 0.201$ for CK_oU) and a large decrease in the shear strain at failure ($\gamma_f = 0.6\%$ for $\tau_{hc}/\sigma'_{vc} = 0.2$ versus $\gamma_f = 5.1\%$ for CK_oU). Increasing the consolidation shear stress results in a more brittle response and a higher rate of strain softening as clearly shown in Figure 5.10 for tests G3 and G5. Conversely, conducting undrained shear in the opposite direction, (i.e., $\theta = 180°$) results in a less brittle (more ductile) behavior with a significant increase in the shear strain at failure ($\gamma_f \cong 24.5\%$ for $\theta = 180°$ and $\tau_{hc}/\sigma'_{vc} = 0.2$). It also results in an increase in the peak shear resistance compared to K_o consolidation, with the tests at θ = 180° and $\tau_{hc}/\sigma'_{vc} = 0.1$ and 0.2 having higher $(\tau_h/\sigma'_{vc})_{max}$ values than the CK_oU tests. In fact, the two tests with $\theta = 180°$ and $\tau_{hc}/\sigma'_{vc} = 0.2$ have a higher peak shear resistance than test G3 with $\theta = 0°$ and $\tau_{hc}/\sigma'_{vc} = 0.1$.

It is not clear what one would expect for the measured peak shear resistance of the tests with $\theta = 180°$ compared to a K_o consolidated sample. However, the much higher measured shear resistance of the two tests conducted at $\theta = 180°$ and τ_{hc}/σ'_{vc} = 0.2 compared to the K_o undrained shear strength is surprising. While the shear stress–strain curves for these two tests look relatively normal, the stress paths do not (Figure 5.12). The stress paths have conventional shapes up until the sample

[4]For all CAU Geonor DSS and MDSS tests the undrained shear strain, computed to correspond with the application of τ_2, is based on the preshear sample height.

approaches what would normally be considered its peak shear resistance (i.e., where the slope of the stress path approaches a horizontal line). At this point the stress path changes slope, with a significant increase in shear resistance with relatively little change in the pore pressure. Furthermore, this stage of the test (from the beginning of the change in slope of the stress path to the peak shear resistance) involves considerable straining of the sample. For example, in test G7 the change in slope of the stress path occurs at approximately $\sigma'_v/\sigma'_{vc} = 0.59$, which corresponds to $\gamma = 5.5\%$, while the peak shear resistance does not occur until $\gamma = 23.3\%$.

When the results of test G6 were obtained it was decided that something may have gone wrong during the test and that it should be repeated. Hence, test G7 was conducted with the same consolidation stress conditions as test G6 and, as clearly seen in Figure 5.12, this sample also had an unusual stress path. Because of the nature of tests with $\theta = 180°$ (i.e., the sample is consolidated in one direction and subsequently sheared undrained in the opposite direction back through the neutral axis of the device), it was suspected that the unusual results obtained for tests G6 and G7 may in part be due to an influence of the DSS device and hence do not entirely reflect the "true" simple shear behavior of these samples. This subject is explored in detail in Appendix G : "Discussion on Reversal of Applied Shear Stress in Direct Simple Shear Tests". The following paragraphs present a summary of the findings of Appendix G.

As part of the investigation into the unusual behavior found for Tests G6 and G7, several DSS and MDSS tests were conducted on a rubber specimen. These tests clearly reflected the nonuniform state of stress which develops in simple shear specimens as summarized in Figure 5.7. For this elastic material, gaps developed at the upper leading edge and lower trailing edge of the specimen during shear. These gaps caused a substantial decrease in the vertical stress required to maintain the sample height constant during shear. Under ideal simple shear conditions this would not occur for an elastic incompressible material such as the rubber sample.

In fact, for a DSS test with $\theta = 180°$ application of the second shear stress τ_2, results in a vertical stress curve which is parabolic and symmetric with respect to the neutral axis of the DSS (i.e., X coordinate = 0; Figure 5.7). In this type of test the gaps which develop during application of τ_1 start to close upon reversal of the shear stress due to τ_2 acting in the opposite direction. As the gaps close, the effective area of the specimen increases, thereby resulting in a decrease in the vertical stress and a tendency for the specimen to expand in the vertical direction. In response to this behavior the constant height servo control system increases the vertical force to maintain the sample height constant. The rate of increase in the vertical stress monotonically decreases as the X coordinate approaches zero ($\gamma = 0$) and the reverse phenomenon occurs as the sample passes through the neutral axis of the device.

These data dramatically show the influence of the development of gaps due to the nonuniform state of stress on the behavior of an elastic specimen in a direct simple shear device. The results lead one to question if and how this condition influences the behavior of clay specimens tested in a simple shear apparatus. The following paragraphs provide a summary of the results from an investigation on this subject reported in Appendix G.

The results of three cyclic Geonor DSS tests performed on cohesive samples at the conventional undrained shear rate of strain ($\dot{\gamma} = 5\%$/hour) are also presented in Appendix G. One test was on normally consolidated BBC and the other two were on San Francisco Bay Mud (SFBM) at OCR = 1.5 and 4.1. These tests displayed some interesting characteristics as the samples strained towards and past the neutral axis of the device during the first reversal stage of the applied shear stress (the samples were allowed to strain well beyond their peak shear resistance before the shear stress was reversed). In all three tests the vertical stress and shear resistance reached a peak value during the reversal stage almost exactly when the sample strained through the neutral axis of the device (Figures G.5 and G.6, Appendix G). Furthermore, the

vertical stress and shear resistance values during the reversal stage were symmetric about the neutral axis. The fact that three DSS tests on two different soils at three different OCR's and stress levels exhibit this type of behavior is more than coincidental (see Figure 5.8). Symmetry of the normalized vertical stress about the neutral axis of the device for all three different test conditions is suggestive of behavior that is not exclusively dependent on the type of soil and stress conditions, but also on the DSS apparatus itself.

Based on the results of the tests on rubber and the cyclic tests on clay specimens it is hypothesized that the behavior of samples tested in a direct simple shear apparatus can be strongly influenced by the device. Specifically, as concluded in Appendix G, during undrained shear the DSS apparatus causes the vertical stress acting on a sample to decrease as it strains away from the neutral axis of the device. This device induced reduction in σ'_v results in a corresponding decrease in the shear resistance and therefore a measured degree of strain softening which is greater than the "true" soil response (Figure 5.9). The opposite occurs when a sample strains towards the neutral axis such as during the undrained shear phase of a $\theta = 180°$ test. Hence, while the measured shear resistance of a sample is primarily due to the simple shear response of the sample, there is also a component which is induced by the device.

This hypothesis was also used to postulate that CAU tests with $\theta = 180°$ can exhibit some unusual behavior in the measured results depending on the magnitude of the consolidation shear strain γ_c, as illustrated in the following two examples for the effect of shear (strain) reversal on the behavior of normally consolidated specimens:

(a) Low γ_c:

At the beginning of undrained shear, the sample has a high rate of development of pore pressure (i.e., the sample exhibits contractive behavior and thus the vertical stress is reduced to maintain the sample's volume constant). Because of the relatively low value of γ_c, the rate of pore pressure development is still high as the

specimen strains through the neutral axis. This tends to mask the influence of the device on the vertical stress. Once the sample strains through the neutral axis the simple shear response of the sample and the influence of the device coincide (i.e., the soil continues to contract and the influence of the device also causes some additional contractive behavior, both resulting in a decrease in the vertical stress required to maintain the volume constant). Eventually the sample reaches its peak shear resistance and begins to strain soften.

(b) High γ_c:

In this case the sample also has an initially high rate of development of positive pore pressure. However, as the sample approaches the neutral axis the rate of development of pore pressure decreases significantly to a point where the influence of the device on the sample becomes more obvious in the measured results. The device causes the vertical stress to increase as the specimen strains towards the neutral axis thus resulting in a proportional increase in the shear resistance. The device–induced behavior continues to compete with the contractive simple shear response of the sample until it passes through the neutral axis. Once this occurs the influence of the device reverses itself and the sample eventually reaches its peak shear resistance.

This postulate was used in Appendix G to evaluate the results of six CAUDSS tests with $\theta = 180°$ (including tests G6, G7 and G8 of this thesis). It was indeed found that the unusual behavior in some of the tests with $\theta = 180°$ is more evident the higher γ_c is during consolidation.

The implication of the hypothesis presented in Appendix G and summarized here is that the direct simple shear device not only influences CAU tests with $\theta > 90°$, but in general influences the results of all direct simple shear tests. This raises the question that if the measured results of direct simple shear tests do not reflect the "true" simple shear behavior of a sample, can they be corrected? While the development of such a correction (if it is even possible) is beyond the scope of the

present work, it does not rule out adjusting the measured undrained strengths from CAU tests with $\theta > 90°$ for design purposes. From the Geonor DSS test results with $\theta = 180°$ presented here (and the MDSS tests with $\theta = 120°$ and $150°$ presented in the next section) it is not at all evident how even a crude adjustment could be made. Most of the tests have stress paths that do not display any dramatic changes in their shape as the samples approach their peak shear resistance. This, however, is not the case for tests G6 and G7. For these tests a crude adjustment could involve taking the shear resistance to be approximately equal to the value measured at the point where the slope of the stress path changes abruptly as the sample approaches its peak measured shear resistance. While this procedure is not very elegant, it is at least conservative compared to blindly using the measured peak shear resistance. Of course one could argue that if a correction is applied to the measured shear resistance of some of the tests with $\theta > 90°$, then CK_oU and MDSS tests with $\theta \leq 90°$ should also be considered for a correction. But again, how to apply even a crude correction to these type of tests is not evident. Furthermore, correcting the peak shear resistance of these tests involves increasing the measured value which clearly is not a conservative approach such as that suggested for the CAU tests with $\theta > 90°$.

The last set of results to present in this section is the undrained modulus. Figure 5.13 is a plot of the normalized Young's modulus E_u/c_u versus applied shear stress ratio for the four CAUDSS tests and the average of the CK_oUDSS tests. As pointed out in Footnote 5 of Chapter 4, the undrained Young's modulus and the applied shear stress ratio are computed based on the incremental shear stress applied after anisotropic consolidation using the following equation:

$$E_u/c_u = (3(\Delta\tau_h)/\gamma)/c_u \qquad 5.1$$

where:

$$\Delta\tau_h = \tau_h - \tau_{hc}$$

$c_u = (\tau_h)_{max}$

and the applied shear stress ratio is computed as $\Delta\tau_h/(\Delta\tau_h)_{max}$.

At applied stress ratios larger than 0.5, the curves plotted in Figure 5.13 show a gradual trend. Higher normalized modulus values are measured for Tests G3 and G5 with $\theta = 0°$ and $\tau_{hc}/\sigma'_{vc} = 0.1$ and 0.2 respectively. The curves progressively plot lower in the figure, with the lowest values being for Tests G6 and G7 with $\theta = 180°$ and $\tau_{hc}/\sigma'_{vc} = 0.2$.

While the normalized modulus values plotted in Figure 5.13 show a trend with the direction and magnitude of the applied consolidation shear stress the results can be somewhat misleading. For example, $\theta = 0°$ tests involve very small $\Delta\tau_h$, whereas $\theta = 180°$ tests involve very large changes in τ_h. Another way of presenting modulus values is to plot the log of the normalized undrained Young's modulus E_u/σ'_{vc} versus the log of the shear strain γ. These values are plotted in Figure 5.14 for the CAU and CK_oU tests which show the type of trend expected for CAUDSS tests. Generally a sample will display a high modulus upon reversal of the applied shear stress (i.e., tests with $\theta = 180°$) compared to applying an incremental shear stress in the same direction as an existing shear stress (i.e., $\theta = 0°$). This is clearly shown in Figure 5.14 with tests G6 and G7 conducted with $\theta = 180°$ having the highest modulus values and test G5 with $\theta = 0°$ having the lowest values. The average results for the CK_oU tests plot directly in between the CAU tests with $\theta = 0°$ and 180°. Figure 5.14 also shows that all of the curves are nearly linear at higher shear strains. The values plotted in Figure 5.14 can be readily converted to shear modulus (G) since for undrained shear E = 3G and hence dividing the value of the Young's modulus by three gives the shear modulus.

5.4 CAUMDSS UNDRAINED SHEAR RESULTS FOR BBC (ICE LOADING)

Nine CAUMDSS tests were conducted to investigate the influence of the test angle θ on the undrained shear behavior of BBC. All tests were run with the same

consolidation stress ratio, $\tau_{hc}/\sigma'_{vc} = 0.2$. Two tests were performed at angle $\theta = 60°$, 120° and 150° and one test was performed at angle $\theta = 0°$, 30° and 90°. These tests, combined with the two tests conducted at $\theta = 180°$ and $\tau_{hc}/\sigma'_{vc} = 0.2$ in the Geonor DSS, give a full set of results for investigating the undrained behavior of BBC as a function of θ. The nine CAUMDSS tests are summarized in Table 5.4 and Figures 5.15 to 5.19 present plots of the shear stress–strain curves, pore pressure versus shear strain, stress paths and undrained Young's modulus. The stress–strain–modulus data presented in these figures are based on the shear stress applied during undrained shear (i.e., τ_2 acting parallel to the X coordinate).

The stress–strain curves plotted in Figure 5.15 show a dramatic influence of the test angle θ on the undrained shear behavior. As θ varies from 0° to 120°, the peak shear resistance decreases significantly ($(\tau_x/\sigma'_{vc})_{max} = 0.273$ and 0.150 for $\theta = 0°$ and 120° respectively), while the shear strain at the peak shear resistance increases significantly ($\gamma_f = 0.55\%$ and 5.6% for $\theta = 0°$ and 120 ° respectively). The samples tested with $\theta \leq 60°$ exhibit a very brittle response, with a high rate of strain softening. Tests C13 and C16 with $\theta = 150°$ have a higher peak shear resistance than tests with $\theta = 90°$ and 120° and in addition have a very large shear strain at failure.

The stress paths plotted in Figure 5.17 also reflect the trend in the peak shear resistance with θ. They also show that there is a very consistent trend with θ in the normalized vertical stress at failure. For Test C7 with $\theta = 0°$, the sample almost immediately reached its peak shear resistance with a very high normalized vertical stress ratio. Conversely, Tests C13 and C16 with $\theta = 150°$ undergo considerable shear strain before the peak shear resistance is reached and have a very low normalized vertical stress ($\sigma'_v/\sigma'_{vc} = 0.948$ and 0.424 for $\theta = 0°$ and 150° respectively). For all of the intermediate test angles, the normalized vertical stress at peak shear resistance gradually decreases as θ varies from 0° to 150°.

Figure 5.16 shows that for $\gamma_x \leq 4\%$ there is a trend in the rate of pore pressure development as a function of the test angle θ. In general, as θ increases so does the initial rate of pore pressure development. This is a result of the fact that as θ increases the rate of applied undrained shear stress increases (see shear stress–strain curves in Figure 5.15) and hence the rate of shear–induced pore pressure also increases. Overall, however, the change in pore pressure does not vary significantly among the different tests. Some of the pore pressure curves display an irregularity at the beginning of shear which is likely due to a seating problem. The cycles in the pore pressure curves for Tests C13 and C16 at $\theta = 150°$ are due to periodic instabilities in the data acquisition and constant height servo control systems (e.g., buildup of static electricity) and do not affect the overall results of the tests.

Figure 5.18 is a plot of the normalized Young's modulus E_u/c_u versus applied shear stress ratio. The Young's modulus and applied shear stress ratio are computed based on the incremental shear stress applied after consolidation using Equation 5.1 but with $\gamma = \gamma_x$ and $\tau_h = \tau_x$. The results exhibit a lot of scatter and do not display a consistent trend in the magnitude of the normalized modulus as a function of the test angle θ. As pointed out in the previous section on the Geonor CAUDSS tests, the data plotted in Figure 5.18 can be misleading. The modulus values are replotted in Figure 5.19 with the log of the normalized Young's modulus E_u/σ'_{vc} versus the log of the shear strain. This plot, like Figure 5.14 for the Geonor CAUDSS tests presented in the previous section, reflects the type of trend expected. Tests with a reversal in the applied X shear stress during undrained shear (i.e., $\theta = 120°$ and $150°$) should have a higher modulus compared to applying the incremental shear stress in the same direction as the existing consolidation shear stress (i.e., $\theta = 0°$, $30°$ and $60°$). This is clearly shown in Figure 5.19, with Tests C13 and C16 ($\theta = 150°$) having the highest values and Test C7 ($\theta = 0°$) having the lowest. At higher shear strains Test C12 ($\theta = 90°$) ,with zero shear strain acting in the X direction at the end of consolidation, plots

directly in between the tests conducted at $\theta = 60°$ and $120°$. At higher shear strains most of the curves are nearly linear.

Figure 5.20 plots the shear strain paths for all of the tests from the beginning of consolidation to the end of undrained shear. The figure clearly shows the gradual increase in the shear strain between the end of consolidation and the peak shear resistance as the test angle θ increases from 0° to 150°. All of these tests were conducted with the consolidation shear stress acting on the sample during undrained shear. As a result, once a sample strains beyond its peak τ_x shear resistance the consolidation shear stress dominates the orientation of the strain path.[5] For example, the strain paths for samples with $\theta = 0°$, 30° and 60° ultimately approach an orientation equal to the direction of application of the consolidation shear stress (i.e., θ). In the case for $\theta = 90°$, 120° and 150° the strain path eventually approaches an orientation equal to 90°. This happens because during strain softening the τ_x component of the horizontal shear stress continues to decrease while the constant τ_y of the horizontal consolidation shear stress remains acting on the sample. These eventual orientations of the strain paths, however, are not shown in the paths plotted in Figure 5.20 because, in order to preserve the wire–reinforced membrane and the displacement transducers, it is not desirable to allow the sample to reach a point of catastrophic failure. Thus, once the rate of strain during the strain softening stage of a test started to increase dramatically, the test was terminated.

The most significant feature of Figure 5.20 is the orientation of the strain paths during undrained shear. For a perfectly elastic material the strain paths will all be parallel to the X axis, which was confirmed for the tests on rubber presented in Chapter 4 (Figure 4.19). Figure 5.20 shows that under the stress conditions used, the

---

[5]During undrained shear τ_2 is applied at a constant rate of strain while τ_{hc} is stress controlled and remains constant during undrained shear. Once a sample reaches its peak τ_x shear resistance and begins to strain soften, it will eventually fail catastrophically because τ_{hc} remains constant.

BBC specimens did not exhibit elastic behavior. It is interesting to note that the specimens clearly do not exhibit elastic behavior, even at the beginning of shear. In spite of the incremental undrained shear stress acting parallel to the X axis, all of the samples have a component of shear strain in the Y direction from the beginning of shear. This is shown in Figures 5.21a and 5.21b which are plots of the strain paths excluding the consolidation phase of each test (these two figures are the same plots except with different scales). Figure 5.21 shows that while the largest component of shear strain is in the X direction, all of the samples exhibit a significant component of shear strain in the Y direction. The figure also shows that for $\gamma_x \geq 0.5\%$ the test with the largest component of consolidation shear stress acting in the Y direction (C12 with $\theta = 90^\circ$) has the highest rate of increase in the Y shear strain component. In addition, tests at $\theta = 30^\circ$ & 150° and $\theta = 60^\circ$ & 120° have similar strain paths during the early stages of shear. This is expected since these pairs of tests have the same component of shear stress acting in the Y direction during undrained shear. However, the tests at $\theta \leq 60^\circ$ reach a peak shear resistance at a significantly lower shear strain than the tests at $\theta \geq 120^\circ$ and as a result the strain paths begin to deviate at larger strain levels as shown in Figure 5.21. This figure also shows the trend in the magnitude of the Y shear strain with the magnitude of the Y component of the consolidation shear stress (i.e., highest for $\theta = 90^\circ$ and smallest for $\theta = 30^\circ/150^\circ$).

An additional aspect of the data presented in this section which is interesting to note is the consistency of the results for the tests repeated at $\theta = 60^\circ$, 120° and 150°. As discussed in Section 5.2 and Appendix F, these tests were primarily repeated to provide additional data for determining the cause of the differences in consolidation shear strain among the different CAUMDSS tests. They, however, also provide an important check on the repeatability of results for tests conducted in the MDSS. The tabulated data and figures presented in this section show that the repeat tests gave results that are nearly identical to the original tests conducted at $\theta = 60^\circ$, 120° and

150°. The shear strain paths are also nearly identical if they are superimposed to a common origin (this was originally done in Figure 5.21 but since the paths were so similar the curves for the repeat tests were removed to provide clarity in the figure). This consistency of results was also found for the CK_oUMDSS tests presented in Chapter 4. The CK_oU and CAU test results show that, for BBC and the stress conditions used, the MDSS displays remarkable repeatability in the undrained shear results.

5.5 DISCUSSION AND SYNTHESIS OF RESULTS

5.5.1 Anisotropic Consolidation

The results of anisotropic consolidation of BBC showed that application of a horizontal shear stress leads to an increase in the vertical strain compared to K_o consolidation. This behavior is expected since, for a normally consolidated cohesive soil, application of a horizontal shear stress will induce positive pore pressures. This increment of pore pressure results in an increase in the consolidation shear strain and the vertical consolidation strain. Also, the increase in τ_{hc}/σ'_{vc} leads to an increase in σ'_{1c} and therefore an expected increase in the vertical consolidation strain. However, since the state of stress and hence σ'_{1c} cannot be computed for a DSS specimen it is not possible to check if σ'_{1c} versus ϵ_v is unique. The amount of increase in ϵ_v appears to be linearly dependent on the consolidation stress ratio τ_{hc}/σ'_{vc} as shown in Figure 5.22. The data for Test G8 with $\tau_{hc}/\sigma'_{vc} = 0.1$ plotted in this figure was adjusted to account for the probable seating errors experienced at the beginning of consolidation as discussed in Section 5.2.2. For the value plotted in Figure 5.22, the incremental vertical strain for Test G8 was set equal to the average of the CK_oU and CAU tests at $\sigma'_{vc} = 0.25$ ksc (this is before any anisotropic consolidation increments were applied in the CAU tests). This adjustment is justified in that the CK_oU tests (C11 and C14)

and all nine CAUMDSS tests with $\tau_{hc}/\sigma'_{vc} = 0.2$ had an ϵ_v significantly less than the 1.36% measured in Test G8 at $\sigma'_{vc} = 0.25$ ksc. The average ϵ_v for the CK_oU and CAU tests at $\sigma'_{vc} = 0.25$ ksc is equal to 0.53%, hence the adjusted ϵ_v at the end of consolidation for Test G8 is equal to 12.4% (consolidation data are tabulated in this Chapter and Appendix H). While the variation of ϵ_v with τ_{hc}/σ'_{vc} is linear, the increase in ϵ_v from K_o consolidation to anisotropic consolidation with $\tau_{hc}/\sigma'_{vc} = 0.2$ is not very large (approximately 2% vertical strain in the normally consolidated range). Figure 5.22 shows that the γ_c versus τ_{hc}/σ'_{vc} relationship is concave upward reflecting the significant increase in γ_c as τ_{hc}/σ'_{vc} varies from 0.0 to 0.2.

5.5.2 Behavior of BBC as a Function of Consolidation Stress Ratio ($\theta = 0°$ and $180°$)

The results of the Geonor CAUDSS tests on BBC showed that there is a significant influence of the consolidation stress ratio (τ_{hc}/σ'_{vc}) on the undrained behavior of the soil. Increasing the consolidation stress ratio from –0.2 ($\theta = 180°$) to 0.2 ($\theta = 0°$) results in a change in the peak shear resistance and a significant variation in the vertical stress ratio (σ'_v/σ'_{vc}) and shear strain at the peak shear resistance. There is also a decrease in the stiffness of the soil (undrained Young's modulus, E_u) as the applied undrained shear stress varies from reversing the direction of shear acting on a sample ($\theta = 180°$) to acting in the same direction ($\theta = 0°$; see Figure 5.11).

The results of the Geonor CAUDSS test program are summarized in Figures 5.23 to 5.26[6]. Figure 5.23 shows a parabolic increase in the peak shear resistance as τ_{hc}/σ'_{vc} varies from 0.0 (K_o) to 0.2. The measured data also shows an increase in the peak shear resistance as τ_{hc}/σ'_{vc} varies from 0.0 to –0.2, but with a much lower rate of increase compared to the $\theta = 0°$ tests. It was suggested in Appendix G and Section 5.3 that the measured peak shear resistance from CAUDSS tests with $\theta = 180°$ may be suspect due to problems inherent with the device. While this hypothesis was not

[6]In the summary plots, data for tests at $\tau_{hc}/\sigma'_{vc} = -0.2$ ($\theta = 180°$) and CK_oUDSS tests are plotted at their average value.

conclusive, it was recommended that tests with $\theta = 180°$, which display peculiarities in the stress path before reaching the measured peak shear resistance, be adjusted. In this experimental program, Tests G6 and G7 did exhibit unusual behavior in the stress path before reaching the measured peak shear resistance. This is shown in Figure 5.12 and again in Figure 5.27 which also includes an adjusted stress path (dotted line) and a reduced peak shear resistance to be used for subsequent analysis (adjusted peak τ_h/σ'_{vc} = 0.21 and 0.215 for Tests G6 and G7 respectively). The figure also includes the shear strain at various stages during the two tests and the point at which the samples passed through the neutral axis of the device (X = 0.0). The adjusted peak shear resistance values for Tests G6 and G7 are also plotted in Figure 5.23 (dotted symbol).

Figure 5.24 shows the applied undrained shear stress required to reach the peak shear resistance versus the consolidation stress ratio. The plot shows the significant decrease in the applied shear stress required to reach failure as τ_{hc}/σ'_{vc} varies from –0.2 to 0.2. It also shows that there is a consistent trend in the variation of the incremental shear stress to failure as τ_{hc}/σ'_{vc} varies from –0.2 to 0.2. The adjusted peak shear resistance for Tests G6 and G7 is also plotted in the Figure.

Figure 5.25 is a plot of the shear strain required to reach the peak shear resistance versus the consolidation stress ratio. The data display a very consistent trend with a large decrease in the strain at failure as τ_{hc}/σ'_{vc} varies from –0.2 to 0.2. In fact, Test G5 with $\tau_{hc}/\sigma'_{vc} = 0.2$ ($\theta = 0°$) requires remarkably little shear strain to reach the peak shear resistance ($\gamma_f = 0.57\%$ versus $\cong 24.6\%$ for $\tau_{hc}/\sigma'_{vc} = 0.2$). The plot also reflects an increase in the tendency of the samples to exhibit brittle behavior as τ_{hc}/σ'_{vc} varies from –0.2 to 0.2.

The final summary plot for the Geonor CAUDSS tests, Figure 5.26, is the normalized pore pressure ($\Delta u/\sigma'_{vc}$) at failure versus the consolidation stress ratio. With the notable exception of the tests with $\tau_{hc}/\sigma'_{vc} = -0.2$ (G6 and G7), these data also show a consistent trend with a linear relationship between $\Delta u/\sigma'_{vc}$ at peak τ_h

versus τ_{hc}/σ'_{vc}. Figure 5.26 clearly shows that the pore pressure at peak τ_h is strongly dependent on τ_{hc}/σ'_{vc}. As τ_{hc}/σ'_{vc} increases from –0.1 to 0.2 $\Delta u/\sigma'_{vc}$ at peak τ_h decreases significantly. The data points for Tests G6 and G7 do not agree with the trend in $\Delta u/\sigma'_{vc}$ based on the tests at different τ_{hc}/σ'_{vc} ratios. Like the measured peak shear resistance, this represents the influence of the apparatus on this type of test and that under ideal conditions the sample would not only have a lower peak shear resistance but also a higher normalized pore pressure ratio at the peak shear resistance.

5.5.3 Behavior of BBC as a Function of the Test Angle θ

The results of the CAUMDSS test program on BBC showed that there is a significant dependence of the undrained shear behavior of the soil on the test angle θ. Nine CAUMDSS tests were conducted at θ ranging from 0° to 150° in 30° increments with $\tau_{hc}/\sigma'_{vc} = 0.2$. These tests, combined with the Geonor CAUDSS tests with $\theta =$ 180° and $\tau_{hc}/\sigma'_{vc} = 0.2$ provide a full set of results for $\theta = 0°$ to 180°. The results of these tests, presented in Section 5.4, are summarized in Figures 5.28 to 5.32[7]

Figure 5.28 shows the variation of the maximum normalized X shear stress ($(\tau_x/\sigma'_{vc})_{max}$) as a function of the test angle θ. This plot shows the most significant result of the CAUMDSS test program, namely the very large variation in the undrained strength of BBC as θ varies from 0° to 180°. It is also significant that the variation is a smooth one with no abrupt changes in the plot of $(\tau_x/\sigma'_{vc})_{max}$ versus θ. The maximum τ_x/σ'_{vc} occurs at $\theta = 0°$, while the minimum is at $\theta = 120°$ ($\tau_x/\sigma'_{vc} =$ 0.273 and 0.150 for $\theta = 0°$ and 120° respectively). The reduction in $(\tau_x/\sigma'_{vc})_{max}$ as θ varies from 0° to 120° is approximately 55%. Beyond $\theta = 120°$ the trend reverses itself and $(\tau_x/\sigma'_{vc})_{max}$ increases for $\theta = 150°$ and 180°. Two points are plotted for the Geonor DSS tests at $\theta = 180°$; one represents the measured data and the other one (dotted symbol) represents the recommended adjustment in the measured shear stress

[7]In the summary plots, data for the pairs of tests conducted at $\theta = 60°$, 120°, 150° and 180° are plotted at their average value.

as discussed in the previous section. Figure 5.29 plots the incremental shear stress applied during undrained shear in the X direction (τ_2) required to reach failure as a function of the test angle θ. Like Figure 5.28, this plot displays a smooth and significant variation in the X shear stress required to cause failure as θ varies from 0° to 180°. The minimum value occurs at $\theta = 0°$ and 30° and the maximum occurs at $\theta = 180°$, with the value at $\theta = 180°$ equal to approximately 5.5 times larger than the $\theta = 0°$ and 30° values. The measured and adjusted values for the Geonor DSS tests at $\theta = 180°$ are both included in the plot.

Figure 5.30 plots the normalized maximum total shear stress ($(\tau_t/\sigma'_{vc})_{max}$) as a function of the test angle θ which also exhibits a significant variation with θ.[8] The normalized total shear stress at failure for $\theta = 0°$, 30° and 60° slightly decreases but once θ increases to 90° the value of $(\tau_t/\sigma'_{vc})_{max}$ gradually decreases to a minimum at $\theta = 150°$. In this plot the adjusted value for the Geonor DSS tests at $\theta = 180°$ does not fit the trend in the MDSS tests as θ varies from 60° to 150°. Extrapolating the linear curve fitted to these data points to $\theta = 180°$ gives a value of $(\tau_t/\sigma'_{vc})_{max}$ equal to 0.19 compared to the adjusted value of 0.21. One could speculate that the adjusted value is too high, however, the Geonor DSS generally gives a strength which is approximately 0.01 higher than the MDSS (e.g., for $\theta = 0°$ $(\tau_t/\sigma'_{vc})_{max} = 0.273$ and 0.283 for the MDSS and Geonor DSS respectively). Considering this factor makes the adjusted value at $\theta = 180°$ better fit the trend in the MDSS data.

Figure 5.31 is a plot of the normalized vertical effective stress (σ'_v/σ'_{vc}) at failure versus the test angle θ. This plot also exhibits a significant and smooth variation in the results as θ varies from 0° to 150°. The tests at $\theta = 0°$ develop very little pore pressure before reaching failure. As θ increases the magnitude of pore

[8] τ_t is the vector sum of τ_x and τ_y. τ_y is applied during consolidation and remains constant during undrained shear; see Table 5.4 for values of τ_y/σ'_{vc} which increase from zero at $\theta = 0°$ and 180° to a maximum of 0.2 at $\theta = 90°$.

pressure development increases significantly, such that for $\theta = 150°$ the normalized vertical effective stress is approximately 45% less than for the tests at $\theta = 0°$. For these data the results of the Geonor DSS tests at $\theta = 180°$ also do not fit the trend in the MDSS data very well. The Geonor and MDSS tests at $\theta = 0°$ have almost identical results, whereas the Geonor DSS results at $\theta = 180°$ appear to be too high. Again this may be a case of the influence of the Geonor apparatus on the test results as discussed for this particular type of test in the previous section. These data for the Geonor DSS tests at $\theta = 180°$ also did not fit the trend in the results of $\Delta u/\sigma'_{vc}$ versus τ_{hc}/σ'_{vc} for the Geonor CAUDSS tests plotted in Figure 5.26. It could very well be that under true simple shear conditions the samples tested with $\theta = 180°$ would develop more pore pressure (i.e., lower σ'_v/σ'_{vc}) before the peak shear resistance is reached.

The final summary plot Figure 5.31 plots the total shear strain (γ_t) at failure versus the test angle θ. As in all of the previous plots, there is a significant variation in $(\gamma_t)_f$ as θ varies from 0° to 180°. For test angles less than 90°, the total shear strain at failure is very small and does not increase much as θ varies from 0° to 90°. However, beyond 90° the magnitude of $(\gamma_t)_f$ increases significantly reaching a maximum at $\theta = 180°$. (Note: the influence of the DSS device on results of $\theta = 180°$ tests may result in a measured γ_t at failure which is too high). This plot also reflects the substantial changes in the behavior of the soil as θ varies from 0° to 180°. At low θ angles the soil is extremely brittle and requires very little shear strain to reach failure whereas at higher θ angles the soil becomes much more ductile with very large shear strains at failure.

The measured and adjusted results presented in these summary plots for the $\theta = 180°$ tests warrant additional discussion. The material presented in Appendix G and summarized in Section 5.3 suggest that the parameters at failure for $\theta = 180°$ tests do not reflect true simple shear behavior. It was further suggested that the peak shear

resistance be adjusted to account for this as was done in Figure 5.27 for Geonor Tests G6 and G7. However, the procedure used to make the adjustment is not very pleasing because it appears to be rather arbitrary. Furthermore, it does not provide an adjustment for a specimen's behavior during the entire test including estimates of the parameters at failure (e.g., γ_f, $(\sigma'_v/\sigma'_{vc})_f$, etc.). It is not satisfactory to estimate the parameters at failure based on trends in the $\theta = 0°$ to 150° tests as plotted in Figures 5.28 to 5.32 because this involves extrapolating the trend to $\theta = 180°$ (i.e., it would not be as tenuous if the trend fitting involved an interpolation rather than an extrapolation). The $\theta = 0°$ to 150° results do, however, confirm the direction in which an adjustment should be made. For Tests G6 and G7 with $\tau_{hc}/\sigma'_v = 0.2$ this involves reducing the measured values of $(\tau_h/\sigma'_{vc})_f$, $(\sigma'_v/\sigma'_{vc})_f$ and γ_f. At this point discussing the use of a more rational procedure to correct the $\theta = 180°$ tests requires previewing material presented in Chapter 6. In this chapter, results of predictions using the MIT–E3 constitutive soil model are compared with the measured data presented here. Overall, the model is found to provide satisfactory to excellent predictions of the test results thus justifying its use as a guide for evaluating the $\theta = 180°$ results. As presented in Chapter 6, the model predicts a normalized peak shear resistance for Tests G6 and G7 equal to 0.2 compared with the average measured value of 0.24 and the recommended adjusted value of 0.21.

The summary plots in Figure 5.26 to 5.32 show dramatic differences in the soil response as the test angle θ varies from 0° to 180°. Not only are the differences dramatic but the results exhibit a remarkably smooth variation as a function of θ. The implication of these test results is that designing the foundation of an offshore Arctic gravity structure subjected to ice loading requires incorporating the results of these type of tests in the design process. Given the complicated nature and variation of the stress conditions within the foundation soil during ice loading of a structure, such an

analysis will require using numerical techniques (i.e., Finite Element Method with realistic constitutive soil model). Thorough and reliable predictions for the foundation performance will presumably require the use of a soil model which is able to reproduce the main behavioral features of the experimental results presented in this chapter.

TABLE 5.1: K_o and Anisotropic Consolidation Loading Schedules

Inc. No.	K_o		Anisotropic Consolidation τ_{hc}/σ'_{vc} = 0.2						
			Step 1, t=0		Step 2, t=20min		Step 3, t=30min		Duration Incr. Ave±1SD†
	σ'_{vc}*	LIR	σ'_{vc}	LIR	τ_{hc}	τ_{hc}/σ'_{vc}	τ_{hc}	τ_{hc}/σ'_{vc}	
1	0.125	-	0.125	-	-	-	-	-	-
2	0.25	1	0.25	1	-	-	-	-	-
3	0.5	1	0.5	1	0.05	0.1	0.1	0.2	86±12
4	0.9	0.8	1.0	1	0.15	0.150	0.2	0.2	109±17
5	1.5	0.7	1.5	0.5	0.25	0.167	0.3	0.2	107±16
6	3.0	1	2.0	0.33	0.35	0.175	0.4	0.2	894±109
7			2.5	0.25	0.45	0.180	0.5	0.2	176±46
8			3.0	0.20	0.55	0.183	0.6	0.2	1430±66

Notes:

1. All stresses in KSC.
2. LIR = load increment ratio.
3. † duration in minutes. Data for all CAUMDSS tests except C9 and C12 (n=7).
4. * increments generally applied at end of primary consolidation.

TABLE 5.2: Summary of Geonor CAUDSS Tests on OCR=1 Boston Blue Clay

Test No. θ (°)	Batch No. w_c(%)	Consolidation $\frac{\tau_{hc}}{\sigma'_{vc}}$	t_c (days)	ϵ_v (%)	γ_x (%)	At Peak τ_h γ_x (%)	$\frac{\tau_h}{\sigma'_{vc}}$	$\frac{\sigma'_v}{\sigma'_{vc}}$	Remarks
G3 0	201 42.0	0.097	1.06	15.0	7.4	1.8	0.223	0.762	inaccurate ϵ_y data
G5 0	201 42.1	0.193	0.92	16.8	18.4	0.57	0.283	0.933	inaccurate ϵ_v data
G8 180	203 40.4	-0.103	1.00	13.2	-6.2	11.8	0.207	0.429	corrected ϵ_v=14.2%
G6 180	202 41.6	-0.200	1.11	15.6	-16.5	25.9	0.232	0.440	innacurate ϵ_v data
G7 180	203 40.5	-0.201	0.97	13.9	-17.2	23.3	0.251	0.481	
Average CK_oUDSS		0.0	-	-	-	5.1	0.201	0.558	Average of 4 tests see Table 4.4

Notes:

1. All tests had σ'_{vc} = 3.0 ksc.
2. $t_c \equiv$ duration of last consolidation increment.
3. τ_{hc} is corrected for membrane and bearing friction using Eq. E.2
4. $\epsilon_v \equiv$ vertical strain at the end of consolidation.

TABLE 5.3: Summary of End of Consolidation Strains for CAUMDSS Tests on OCR=1 Boston Blue Clay

Test No.	θ (°)	Batch No. w_c (%)	ϵ_v (%)	γ_x (%)	γ_y (%)	γ_t (%)	Arctan (γ_y/γ_x)	Δ Arctan - θ
C7	0	202 42.0	13.9	19.6	-1.3	19.6	-3.8	-3.8
C10	30	202 41.1	13.1	16.8	8.7	18.9	27.4	-2.6
C8	60	202 41.3	13.2	8.5	17.4	19.4	64.0	4.0
C17	60	203 40.7	14.6	6.7	17.3	18.6	68.8	8.8
C12	90	202 41.3	13.4	0.9	18.9	18.9	87.1	-2.9
C9	120	202 41.5	14.3	-4.7	13.0	13.9	109.8	-10.2
C15	120	203 41.0	13.4	-6.0	14.5	15.7	112.5	-7.5
C13	150	203 40.7	12.9	-11.5	9.3	14.8	141.1	-8.9
C16	150	203 41.2	13.1	-12.3	6.8	14.1	151.1	1.1
Ave. ±1SD (n=8)			13.5			17.5		-0.8
Excluding Test C9			±0.6			±2.2		±6.0

Notes:

1. See Figure 3.1 for definitions of θ, γ_x and γ_y.
2. $\gamma_t = (\gamma_x^2 + \gamma_y^2)^{0.5}$.
3. All tests have σ'_{vc} = 3.0 ksc.
4. All tests have nominal τ_{hc}/σ'_{vc} = 0.2.
5. C9 had loading problems due to power failure.

TABLE 5.4: Summary of CAUMDSS Tests on OCR=1 Boston Blue Clay

Test No. θ (°)	Batch No. w_c (%)	Consolidation τ_{hc}/σ'_{vc} X	Consolidation τ_{hc}/σ'_{vc} Y	t_c (days)	ϵ_v (%)	γ_t (%)	At Maximum τ_x: γ_x (%)	γ_y (%)	γ_t (%)	$\frac{\tau_x}{\sigma'_{vc}}$	$\frac{\tau_t}{\sigma'_{vc}}$	$\frac{\sigma'_v}{\sigma'_{vc}}$
C7 0	202 42.0	0.194	0.0	0.97	13.9	19.6	0.55	0.06	0.55	0.273	0.273	0.948
C10 30	202 41.1	0.168	0.097	0.96	13.1	18.9	0.47	0.09	0.48	0.252	0.270	0.893
C8 60	202 41.3	0.097	0.168	0.94	13.2	19.4	0.98	0.45	1.08	0.209	0.268	0.816
C17 60	203 40.7	0.097	0.168	1.01	14.6	18.6	0.67	0.21	0.70	0.206	0.267	0.874
C12 90	202 41.3	0.0	0.194	0.96	13.4	18.9	1.89	1.21	2.24	0.154	0.248	0.715
C9 120	202 41.5	-0.098	0.169	0.95	14.3	13.9	4.60	2.88	5.43	0.153	0.228	0.563
C15 120	203 41.0	-0.098	0.169	1.01	13.4	15.7	5.14	2.73	5.82	0.148	0.225	0.526
C13 150	203 40.7	-0.169	0.098	0.97	12.9	14.8	15.88	4.21	16.43	0.185	0.209	0.412
C16 150	203 41.2	-0.169	0.098	1.08	13.1	14.1	14.84	3.61	15.27	0.182	0.207	0.435

Notes:

1. See Figure 3.1 for definitions of θ, γ_x, γ_y, τ_x and τ_y.
2. All tests had σ'_{vc} = 3.0 ksc and nominal τ_{hc}/σ'_{vc} = 0.20.
3. τ_{hc} corrected for membrane resistance and bearing friction using Eq. B.2.
4. t_c ≡ duration of last consolidation increment.
5. ϵ_v, γ_t ≡ vertical strain and horizontal shear strain at end of consolidation.
6. $\gamma_t = (\gamma_x^2 + \gamma_y^2)^{0.5}$
7. $\tau_t = (\tau_x^2 + \tau_y^2)^{0.5}$

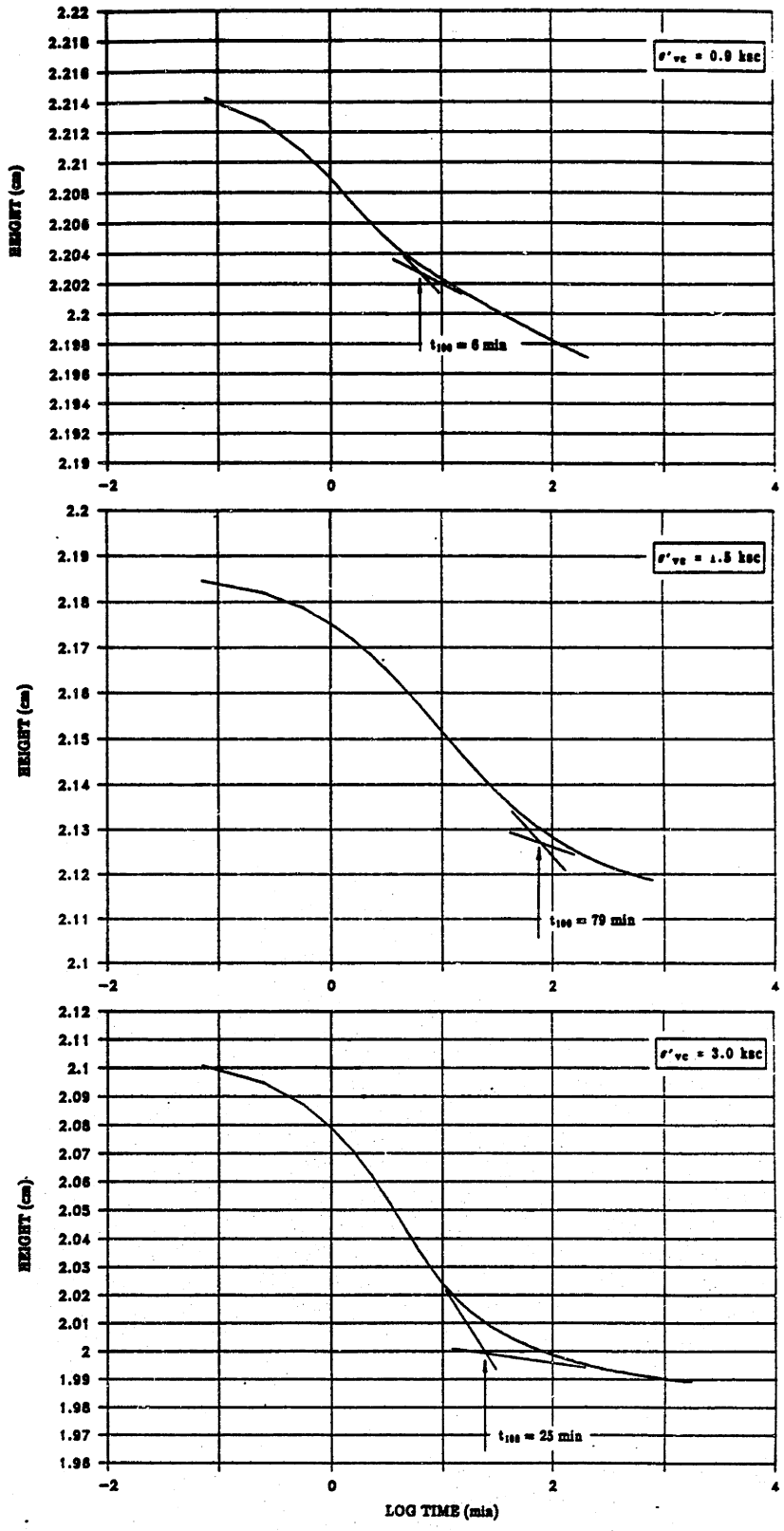

Figure 5.1: Sample Height Versus Log Time Deflection Curves for σ'_{vc} = 0.9, 1.5 and 3 ksc from CK_oUMDSS Test C11.

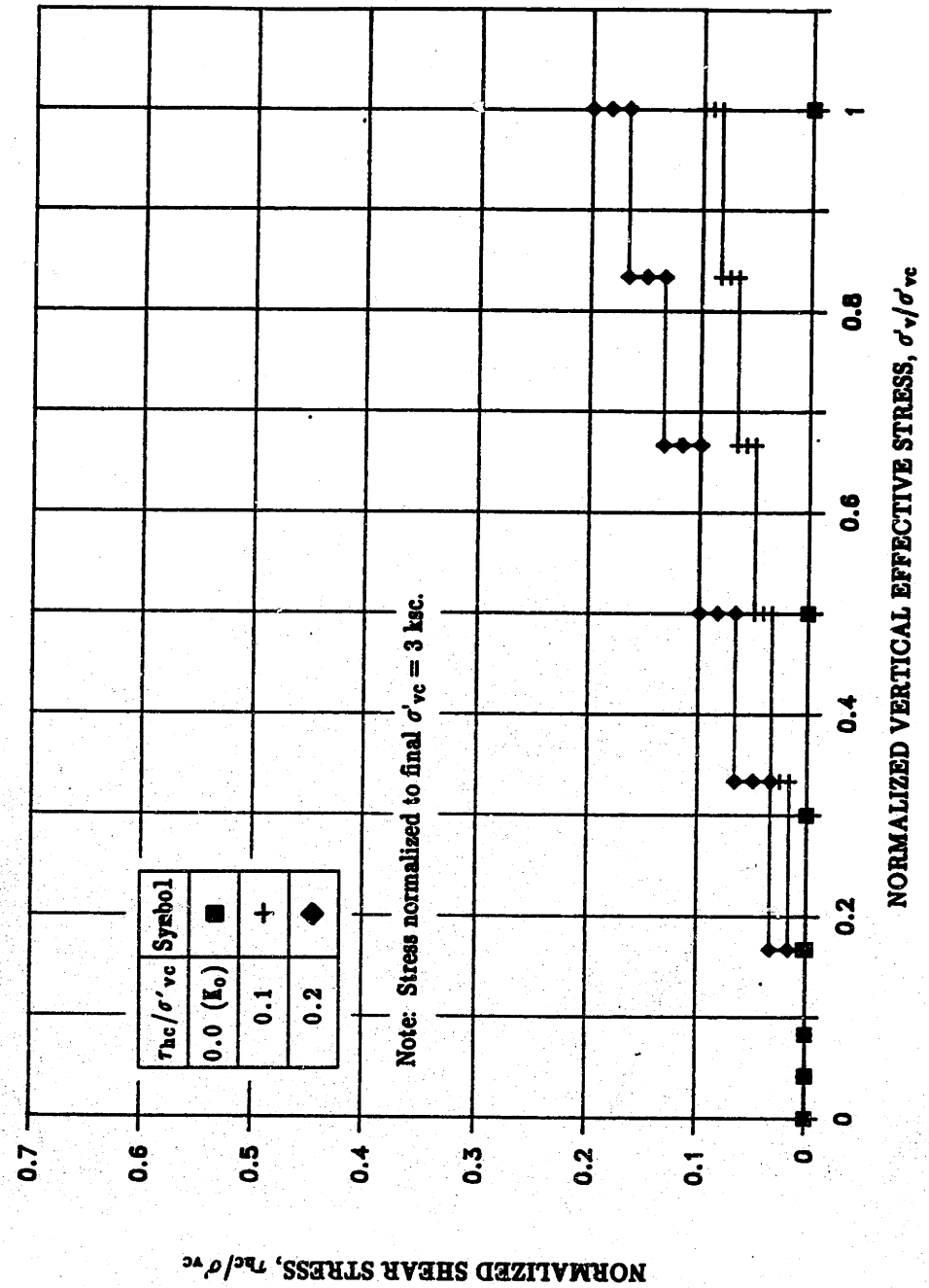

Figure 5.2: Consolidation Stress Paths for K_o and Anisotropic Consolidation (see Table 5.1).

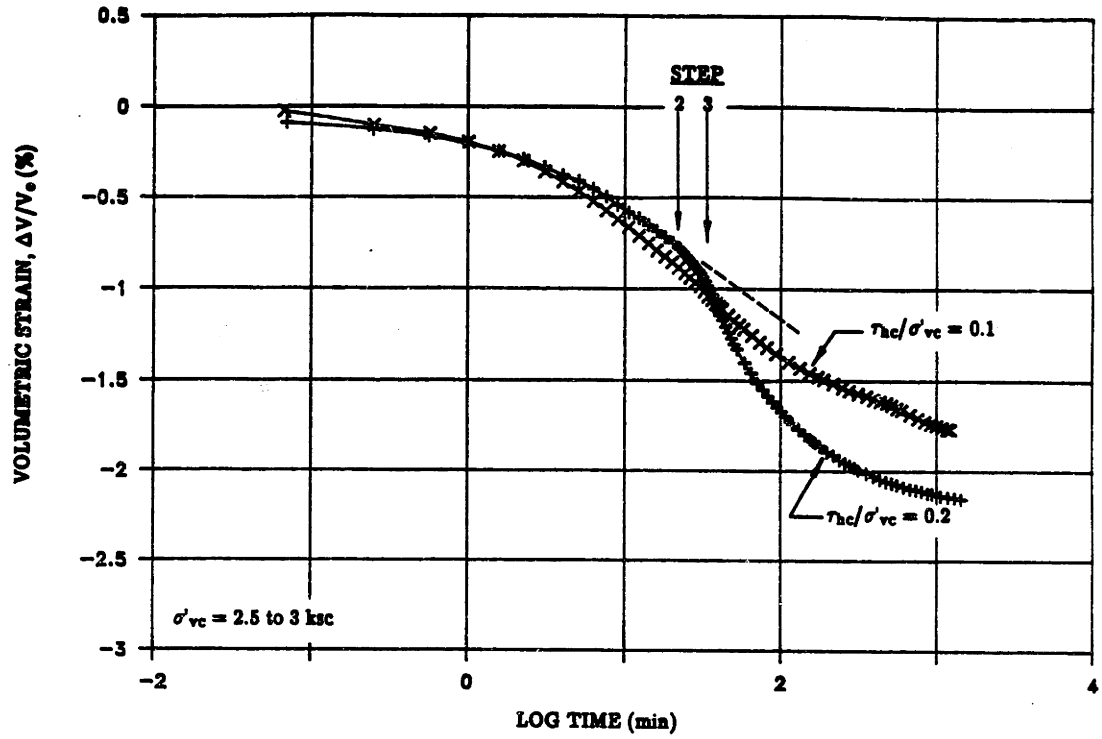

(a)

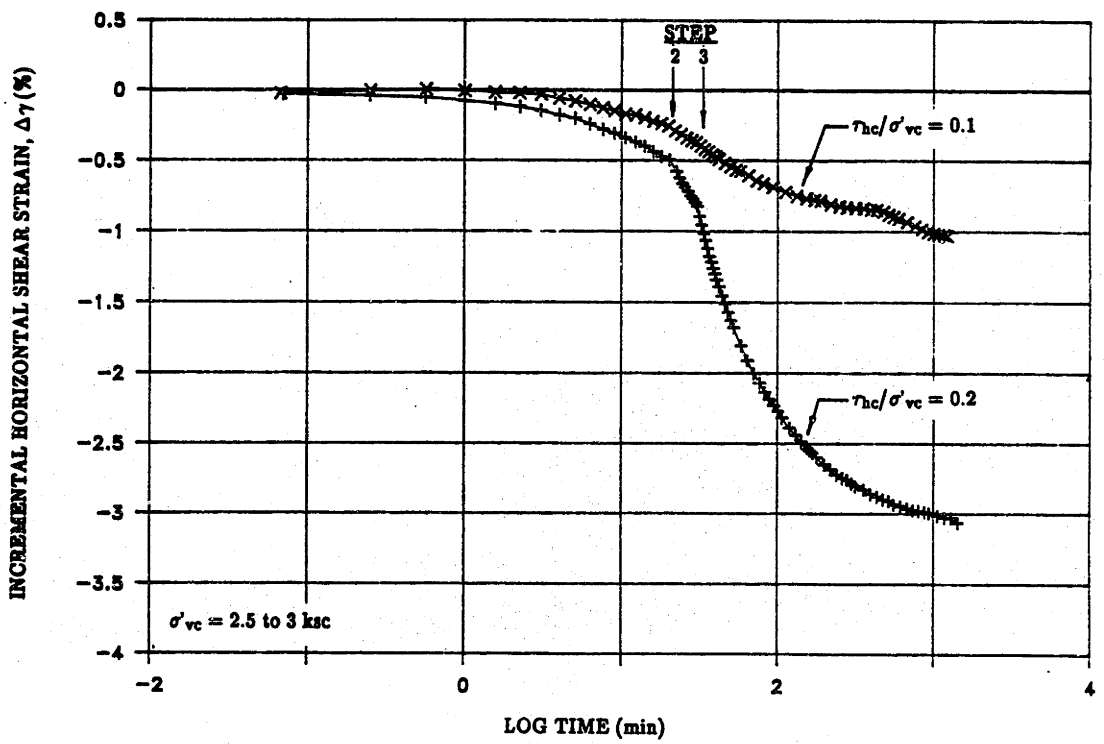

(b)

Figure 5.3: Representative Plots of Incremental (a) Volumetric Strain and (b) Shear Strain During Anisotropic Consolidation for Tests With $\tau_{hc}/\sigma'_{vc} = 0.1$ and 0.2.

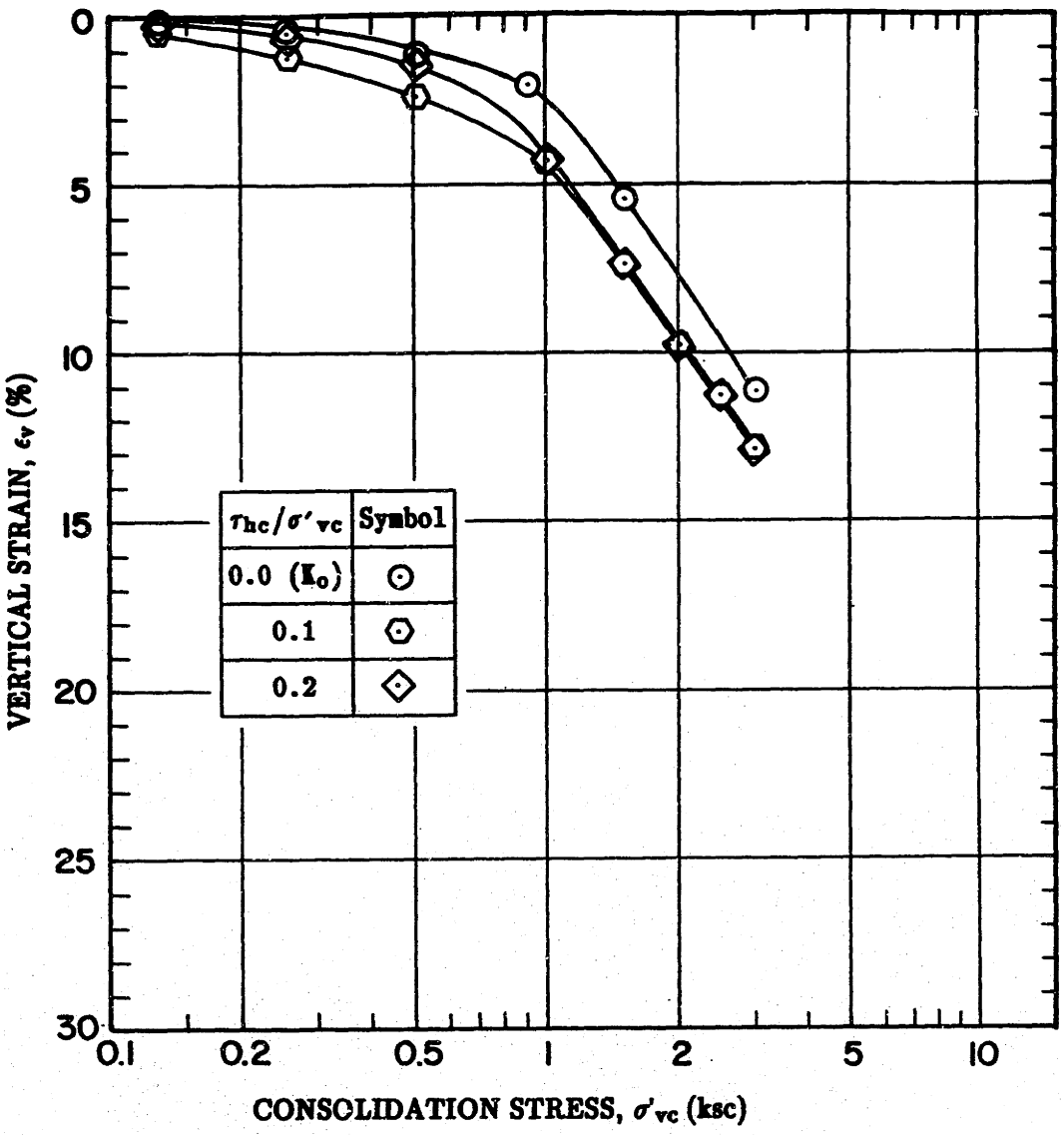

Figure 5.4: Compression Curves for K_o and Anisotropic Consolidation of BBC.

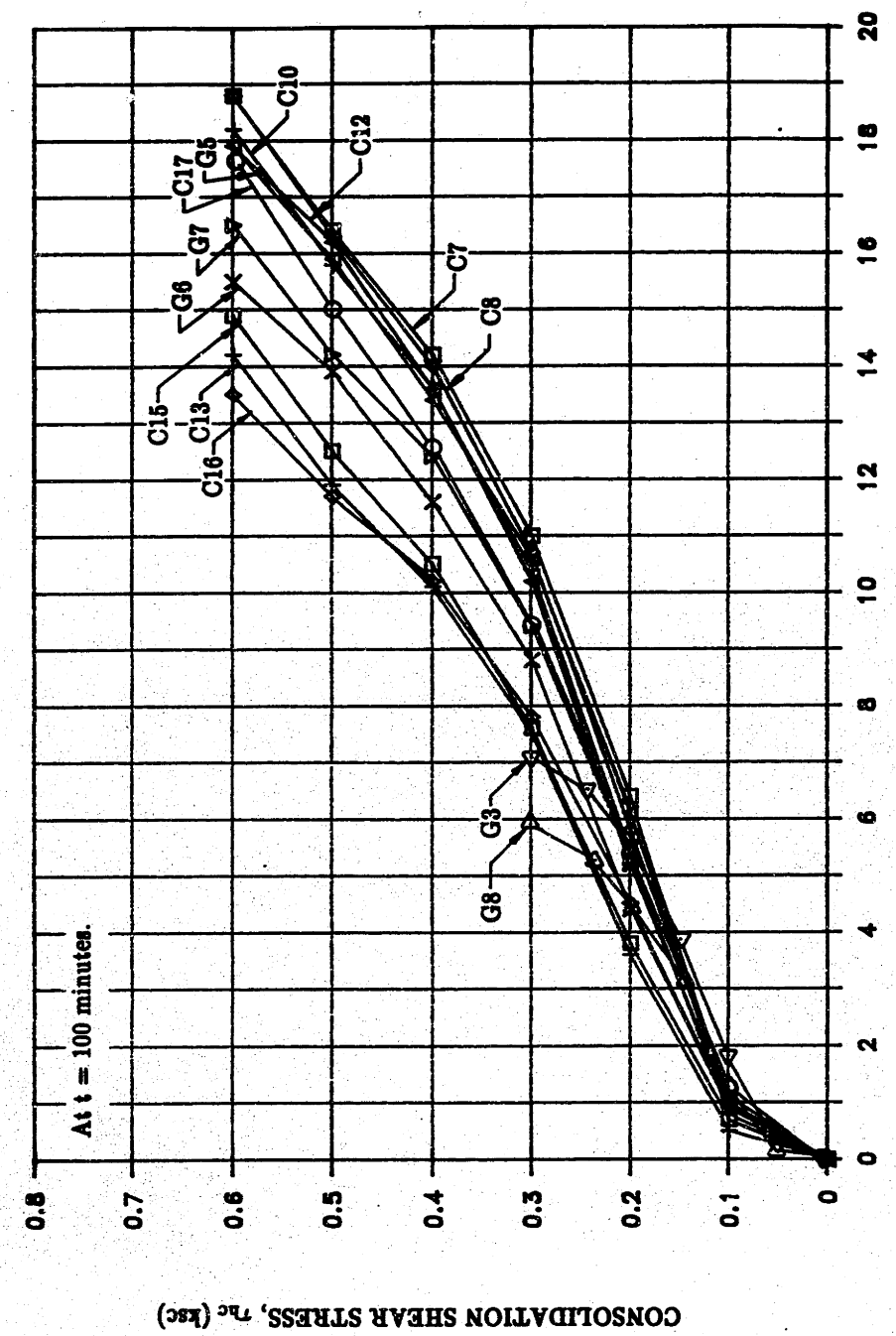

Figure 5.5: Total Shear Strain Versus Shear Stress During Anisotropic Consolidation from CAUMDSS and Geonor CAUDSS Tests on BBC (data tabulated in Appendix H).

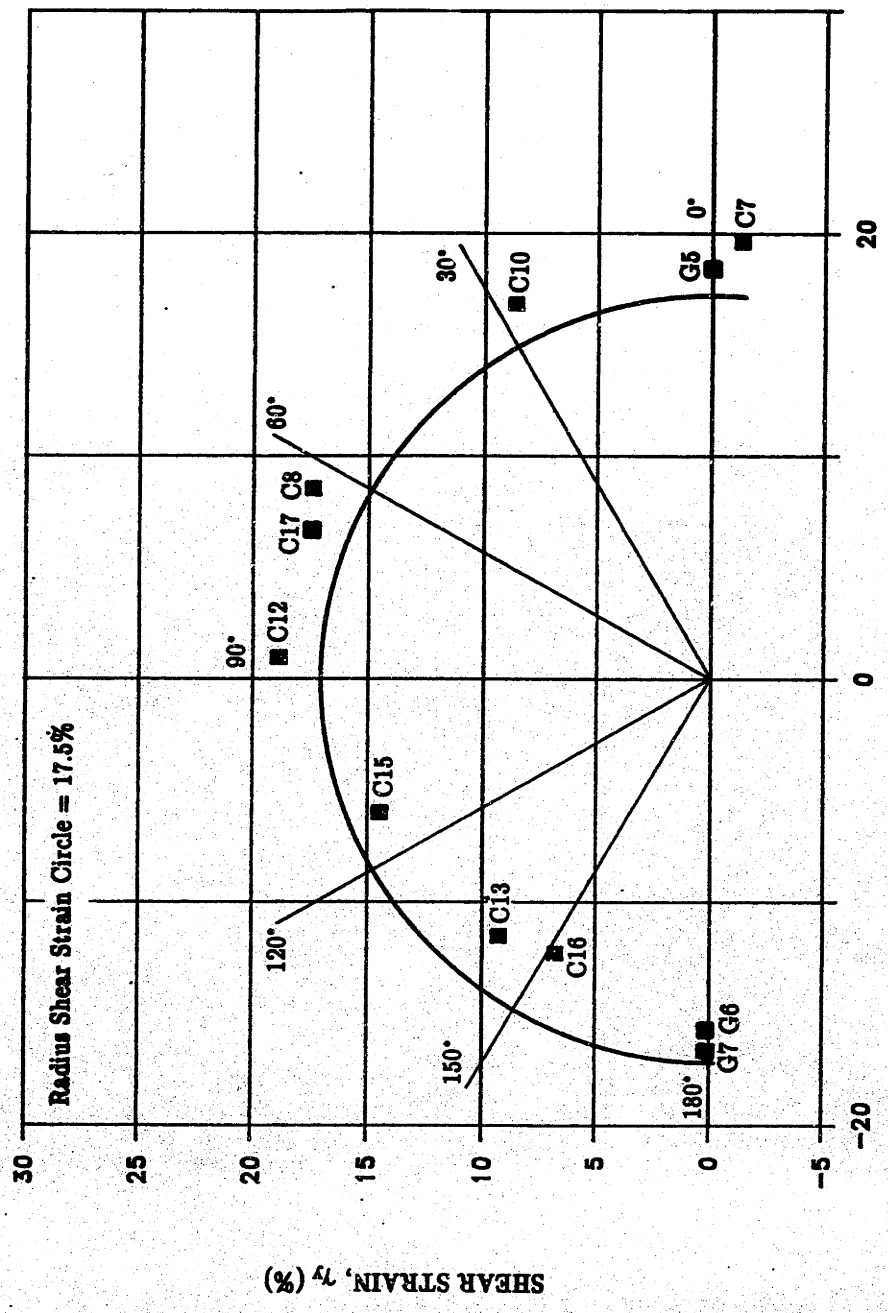

Figure 5.6: End of Consolidation Shear Strain for CAUMDSS and Geonor CAUDSS Tests on BBC With $\tau_{hc}/\sigma'_{vc} = 0.2$.

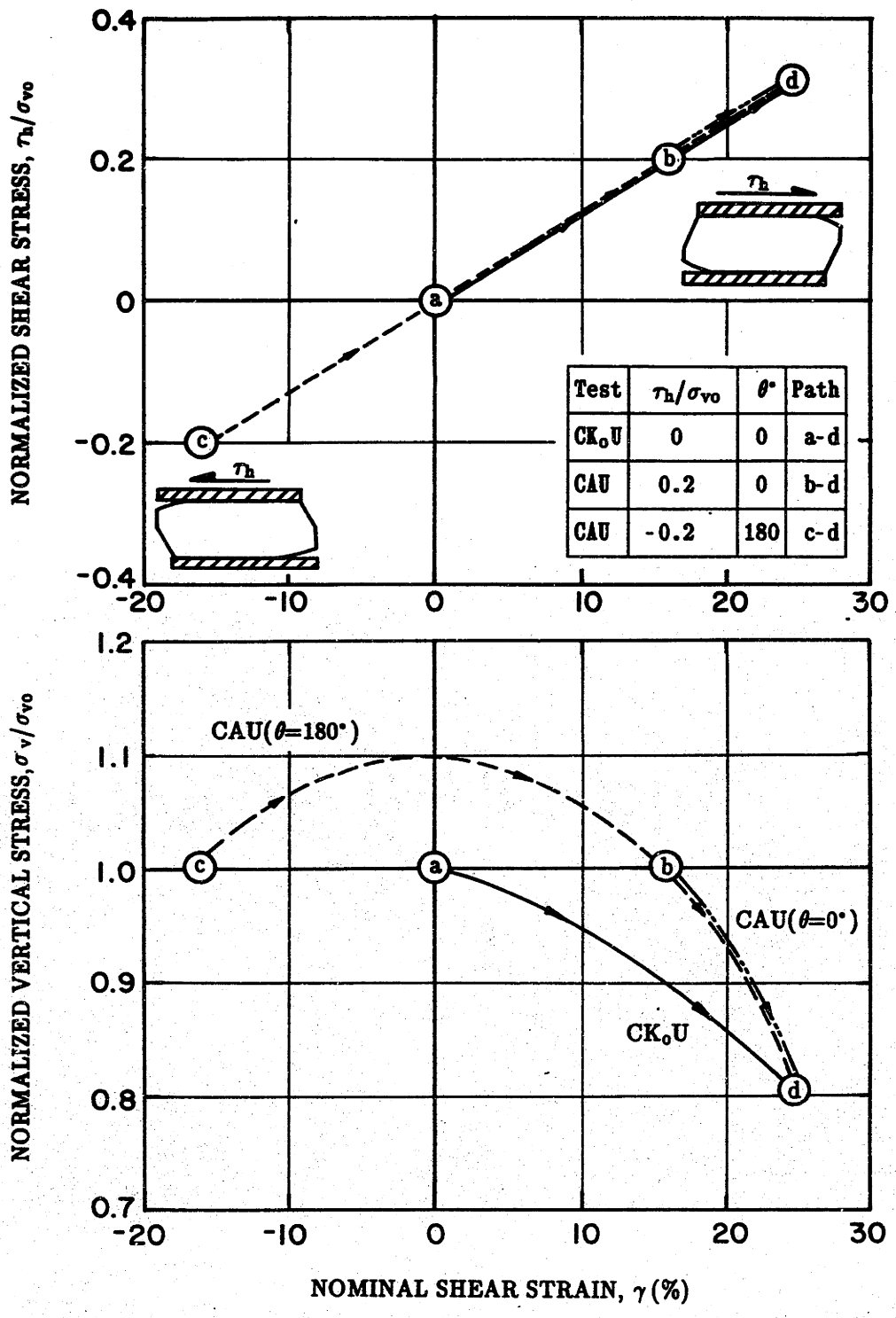

Figure 5.7: Summary of Effect of Shear Strain on Variation of Vertical Stress for DSS Tests on Rubber (idealization of data presented in Appendix G).

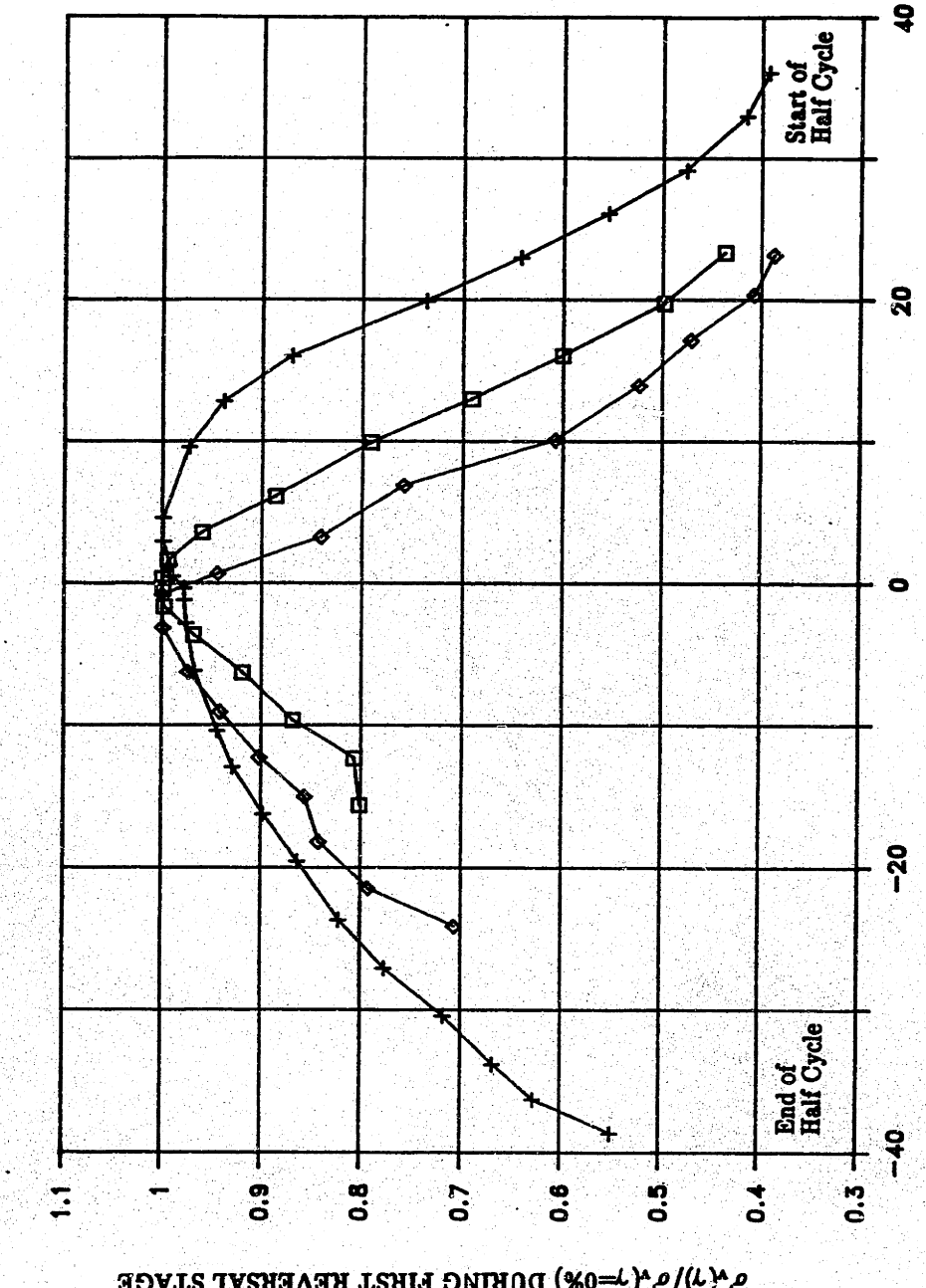

Figure 5.8: Vertical Stress During the First Reversal Stage (Normalized by σ'_v at $\gamma = 0\%$) versus Shear Strain for Undrained Cyclic Geonor DSS Tests at $\dot{\gamma} = 5\%$/hour on BBC and SFBM (same as Figure G.7).

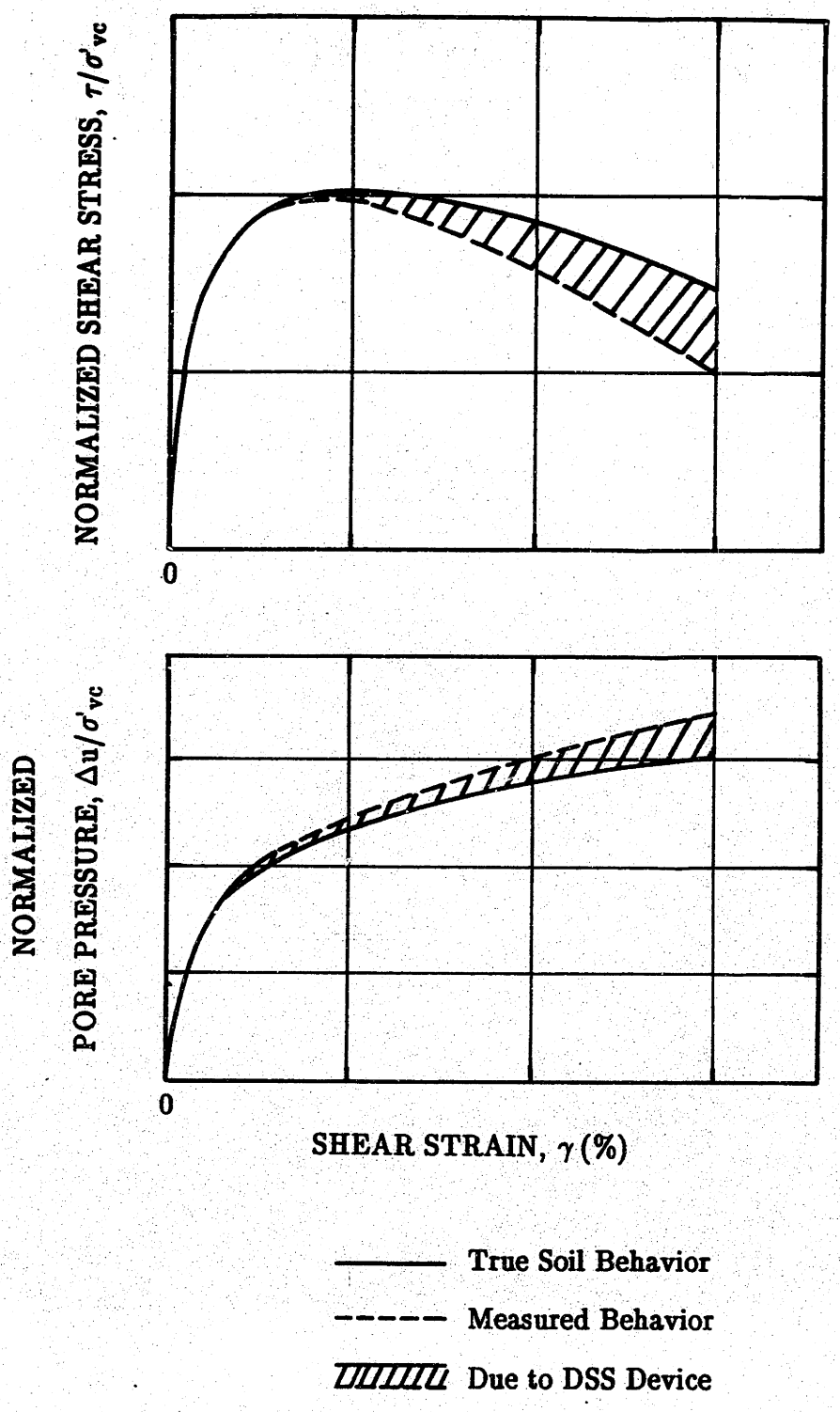

Figure 5.9: Schematic of Hypothesis Showing Influence of DSS Apparatus on the Behavior of a Sample in a DSS Test (same as Figure G.8).

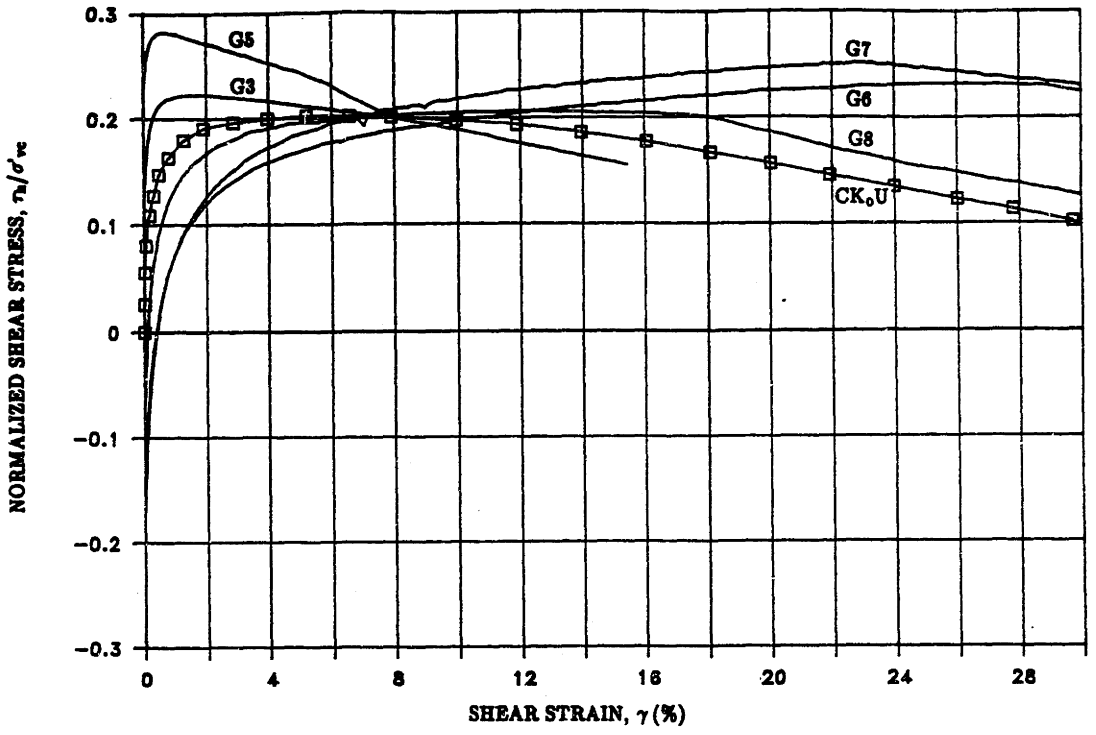

Figure 5.10: Shear Stress–Strain Curves for Geonor CAUDSS Tests on BBC.

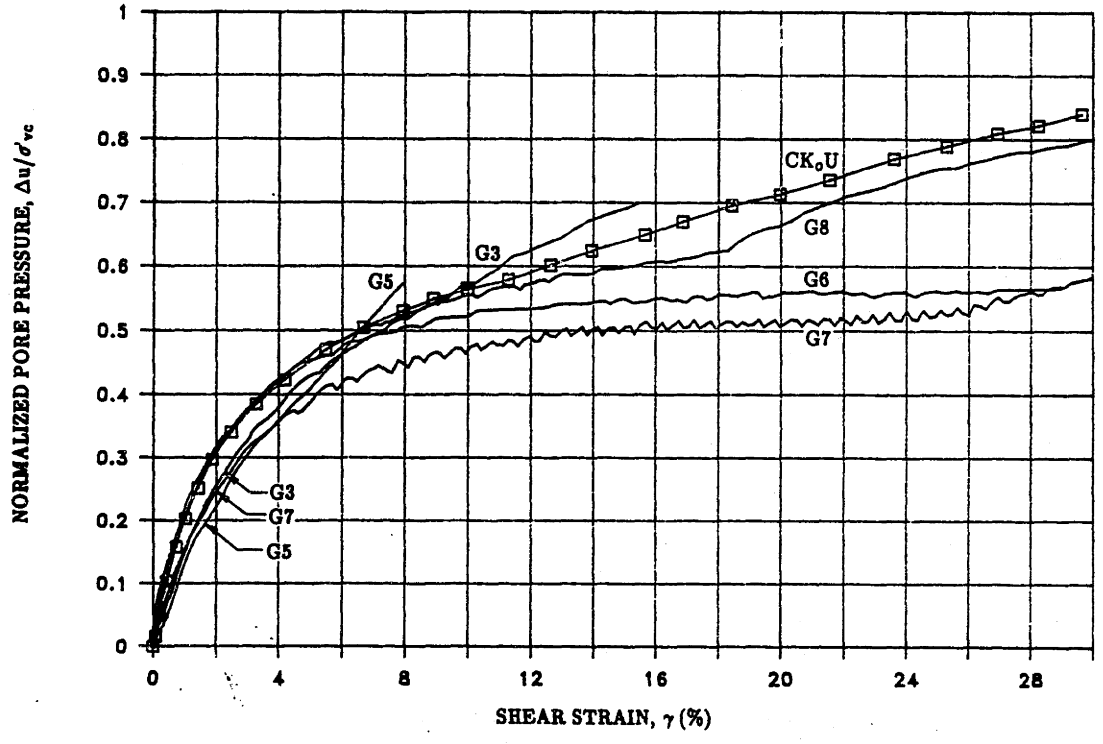

Figure 5.11: Normalized Pore Pressure Versus Shear Strain for Geonor CAUDSS Tests on BBC.

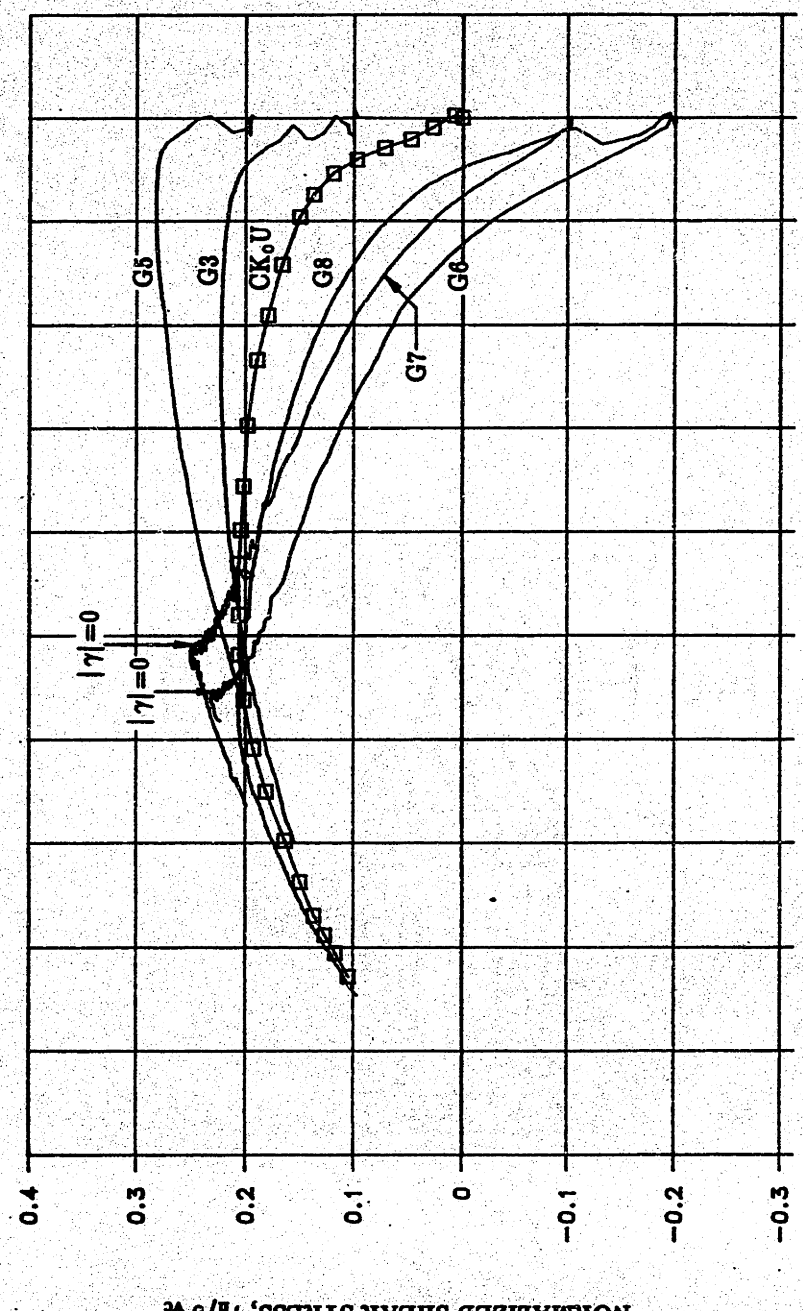

Figure 5.12: Stress Paths for Geonor CAUDSS Tests on BBC.

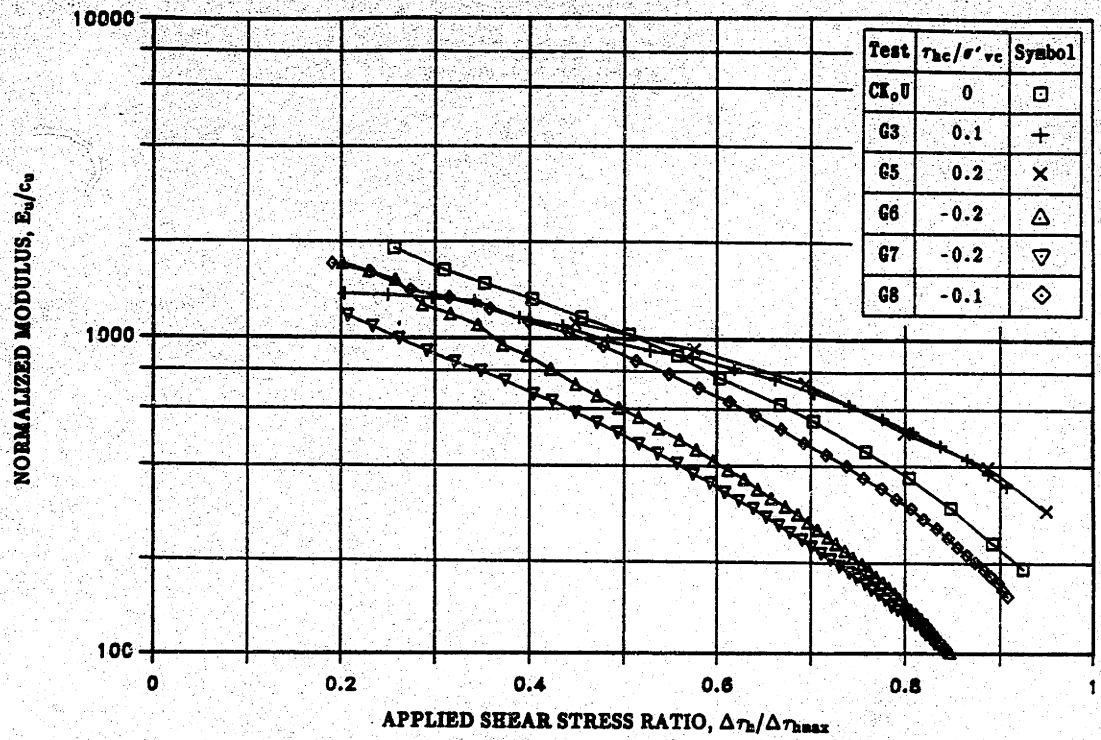

Figure 5.13: Normalized Undrained Young's Modulus E_u/c_u Versus Applied Shear Stress Ratio for Geonor CAUDSS Tests on BBC.

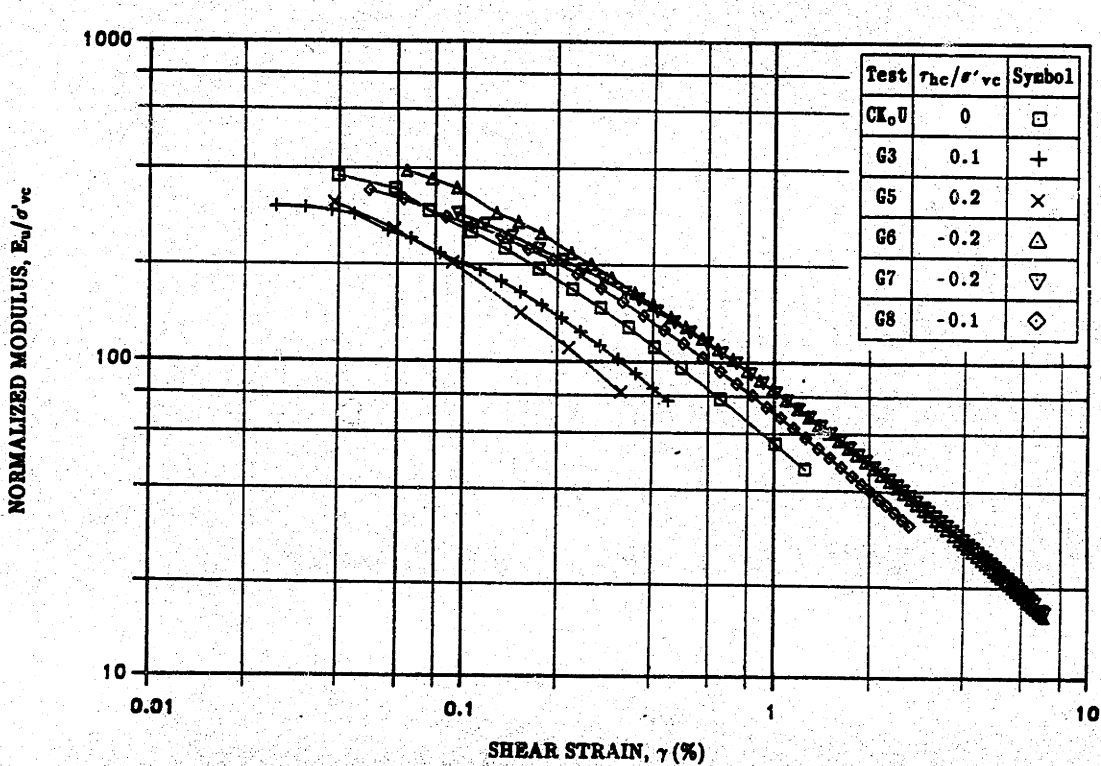

Figure 5.14: Normalized Undrained Young's Modulus E_u/σ'_{vc} Versus Shear Strain for Geonor CAUDSS Tests on BBC.

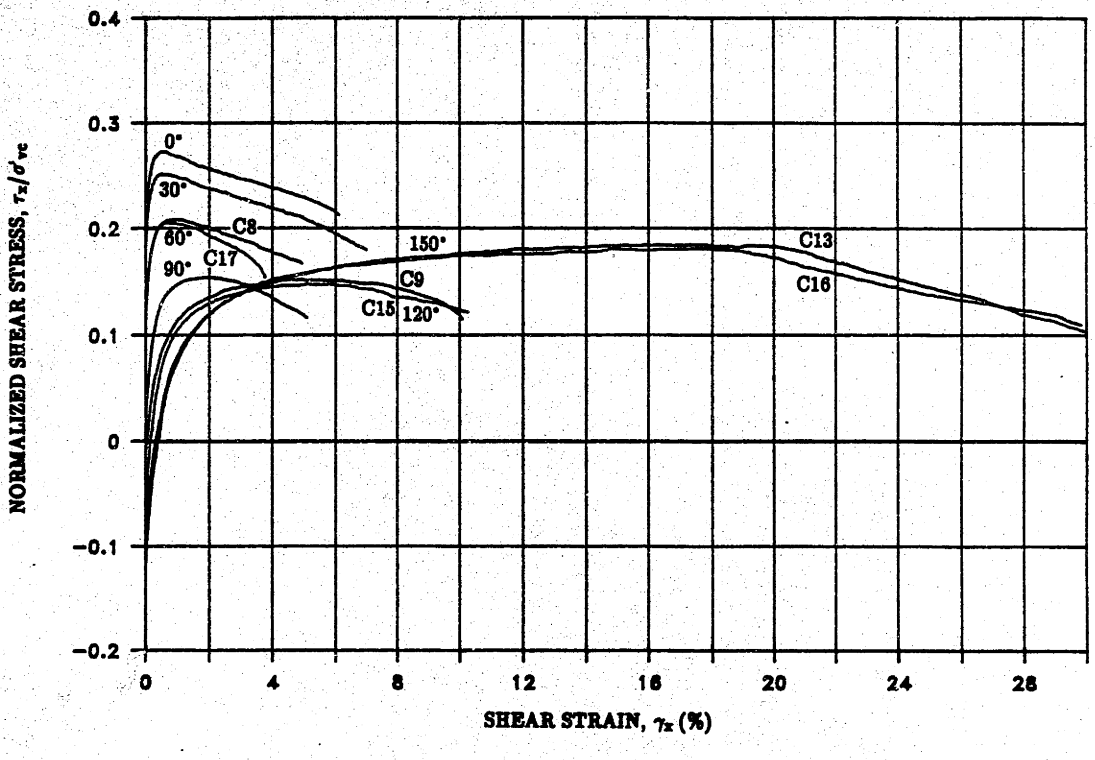

Figure 5.15: Shear Stress–Strain Curves for CAUMDSS Tests on BBC.

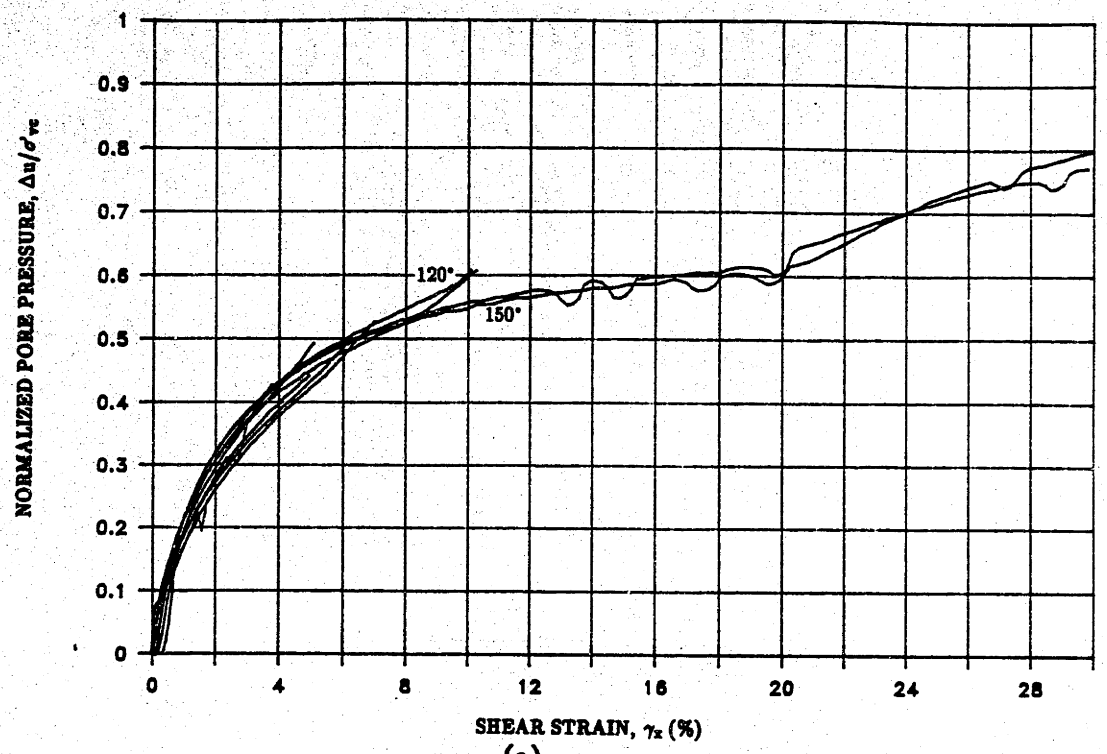

(a)

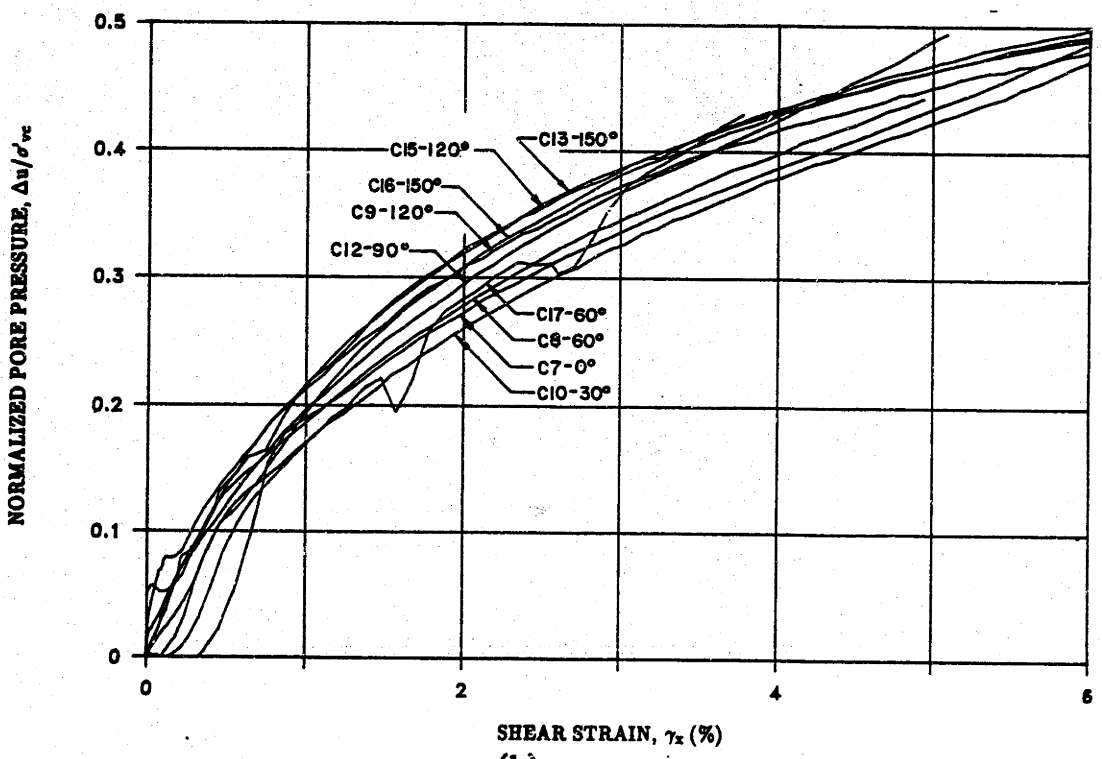

(b)

Figure 5.16: Normalized Pore Pressure Versus Shear Strain for CAUMDSS Tests on BBC: (a) Small Scale; (b) Large Scale.

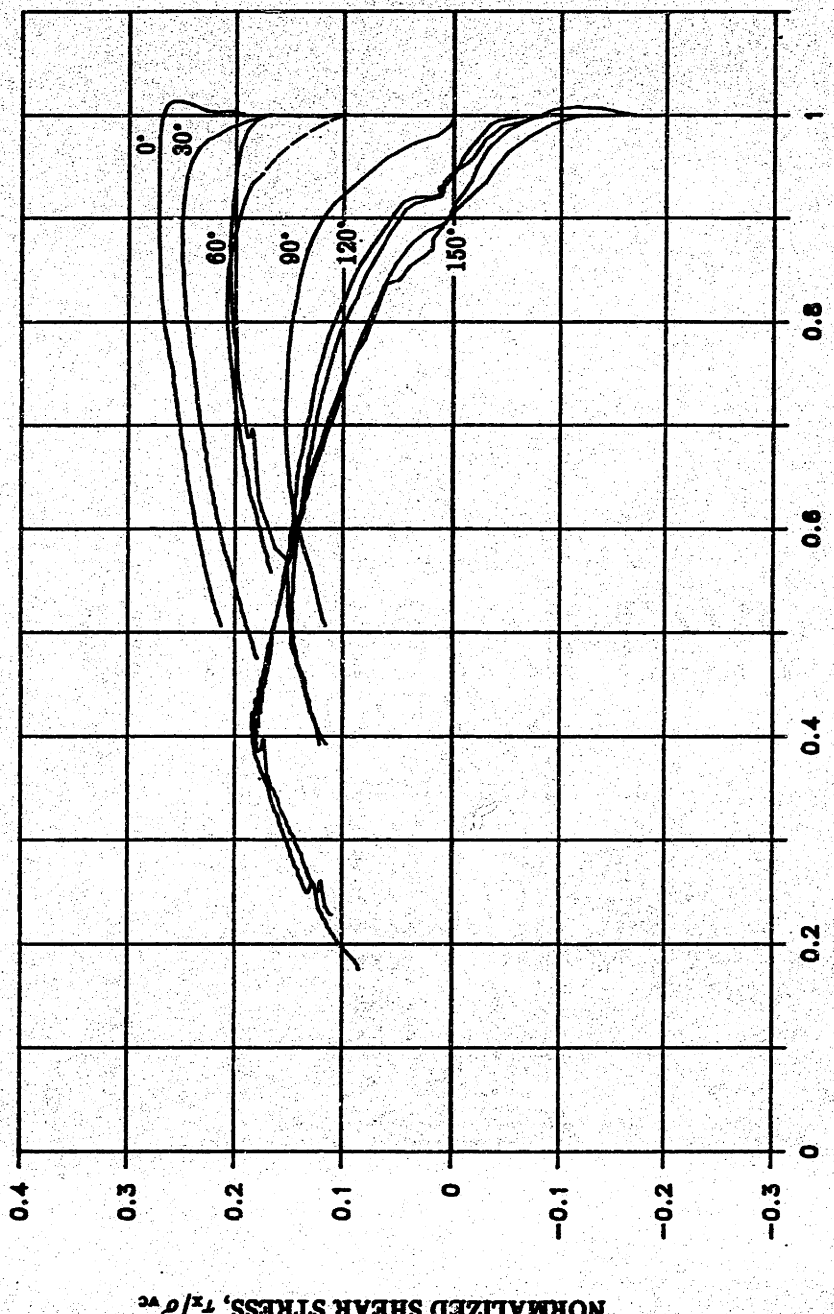

Figure 5.17: Stress Paths for CAUMDSS Tests on BBC.

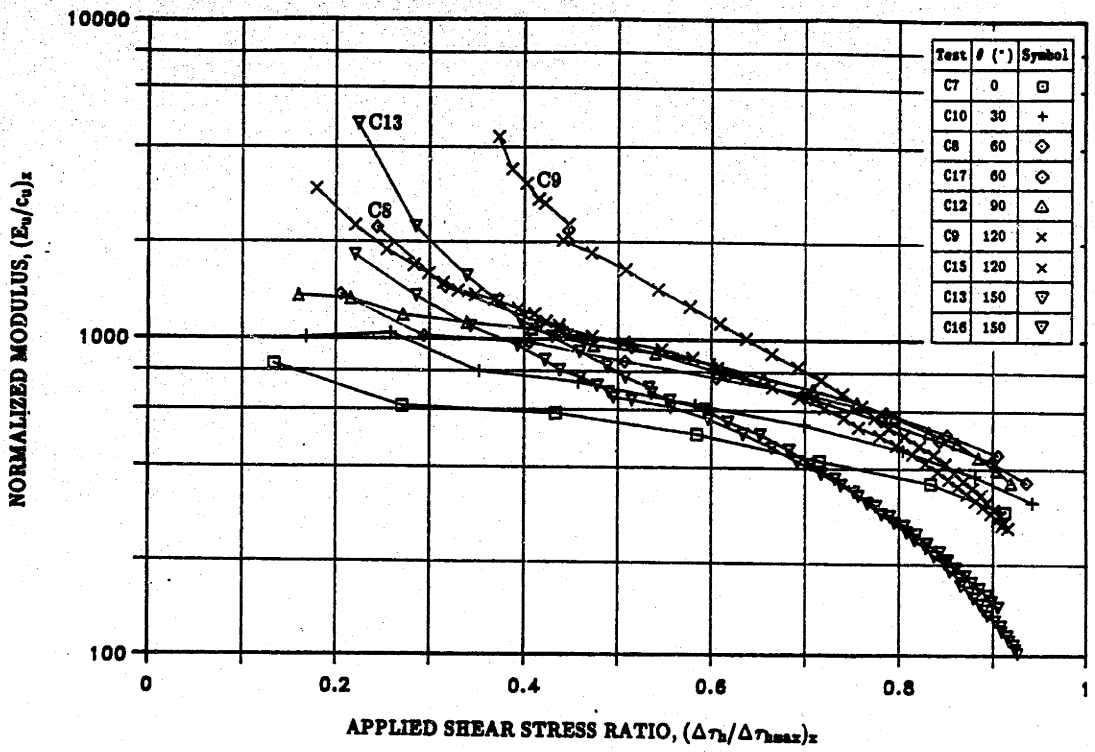

Figure 5.18: Normalized Undrained Young's Modulus $(E_u/c_u)_x$ Versus Applied Shear Stress Ratio for CAUMDSS Tests on BBC.

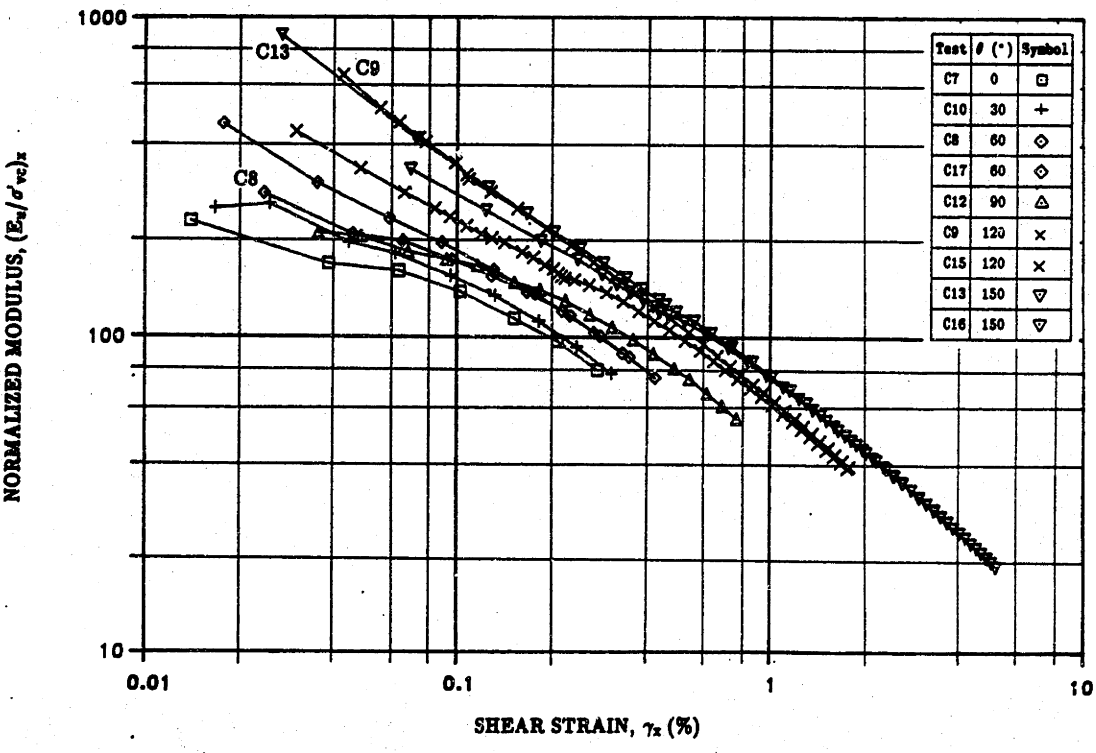

Figure 5.19: Normalized Undrained Young's Modulus $(E_u/\sigma'_{vc})_x$ Versus Shear Strain for CAUMDSS Tests on BBC.

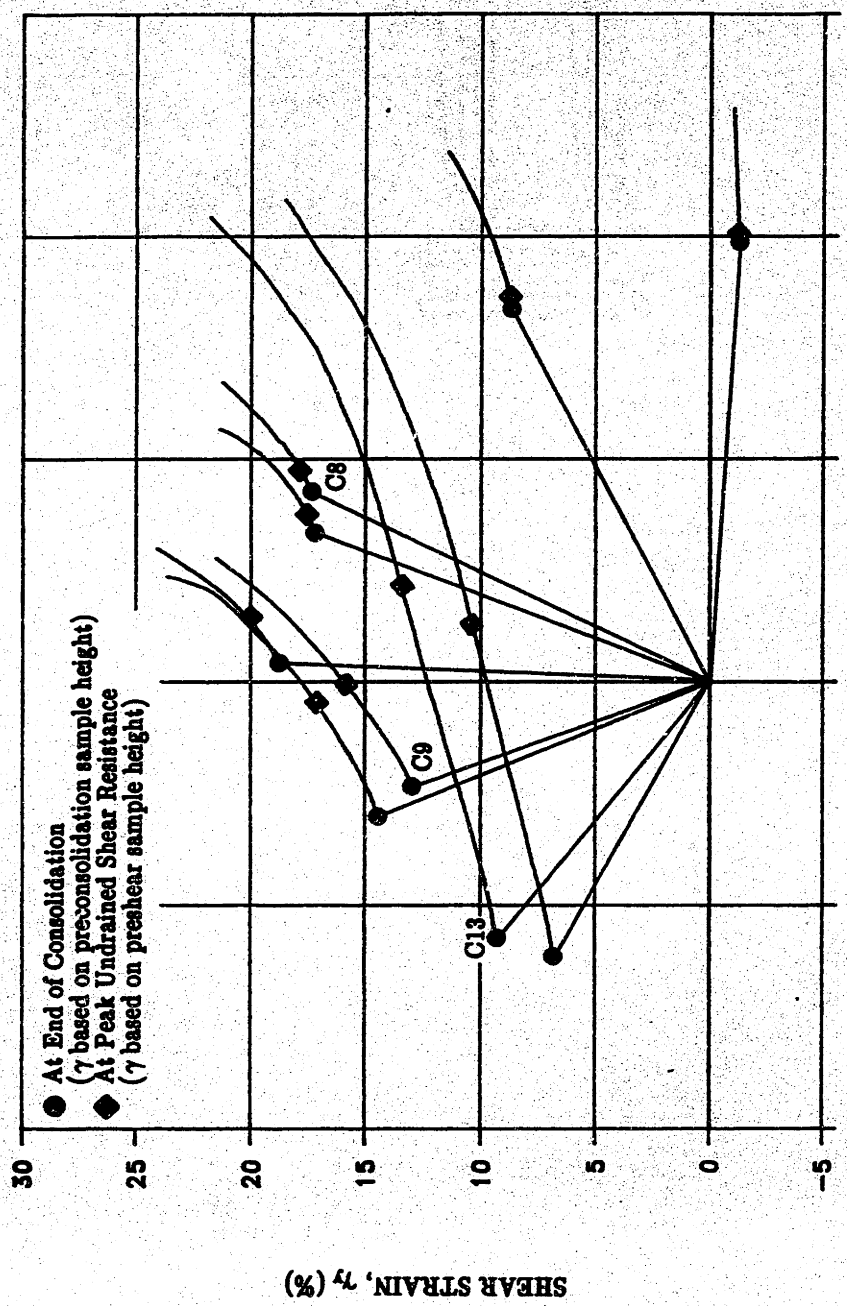

Figure 5.20: Shear Strain Paths for CAUMDSS Tests on BBC.

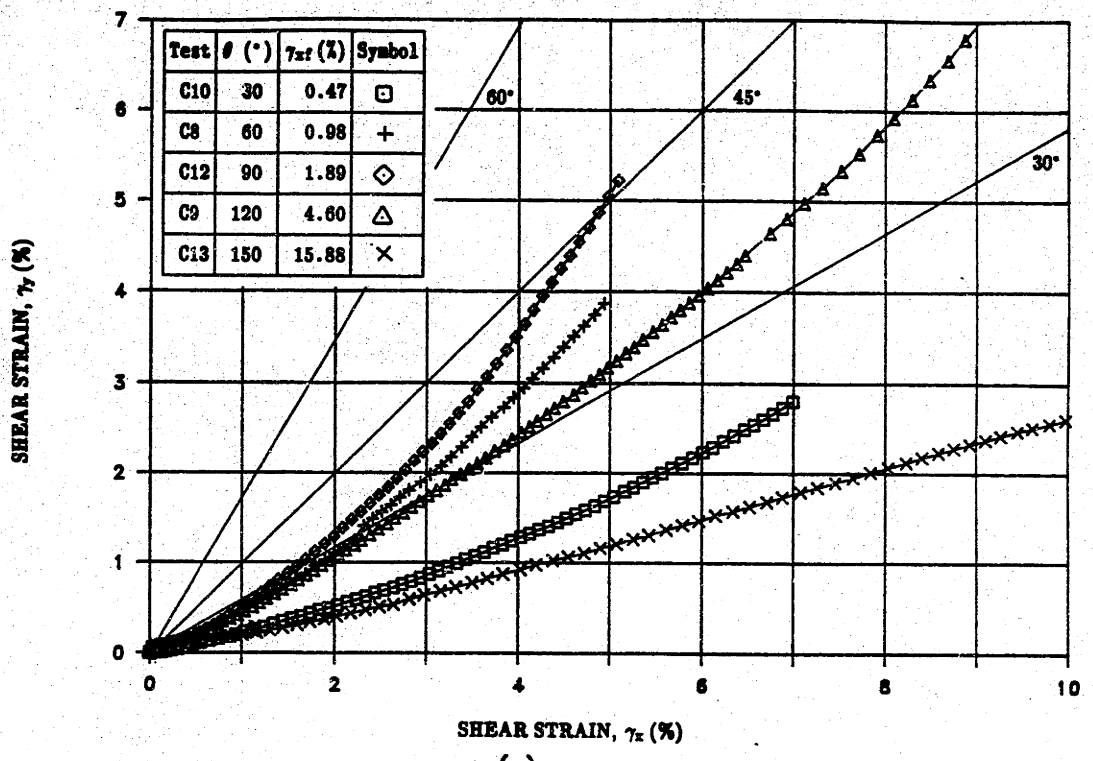

(a)

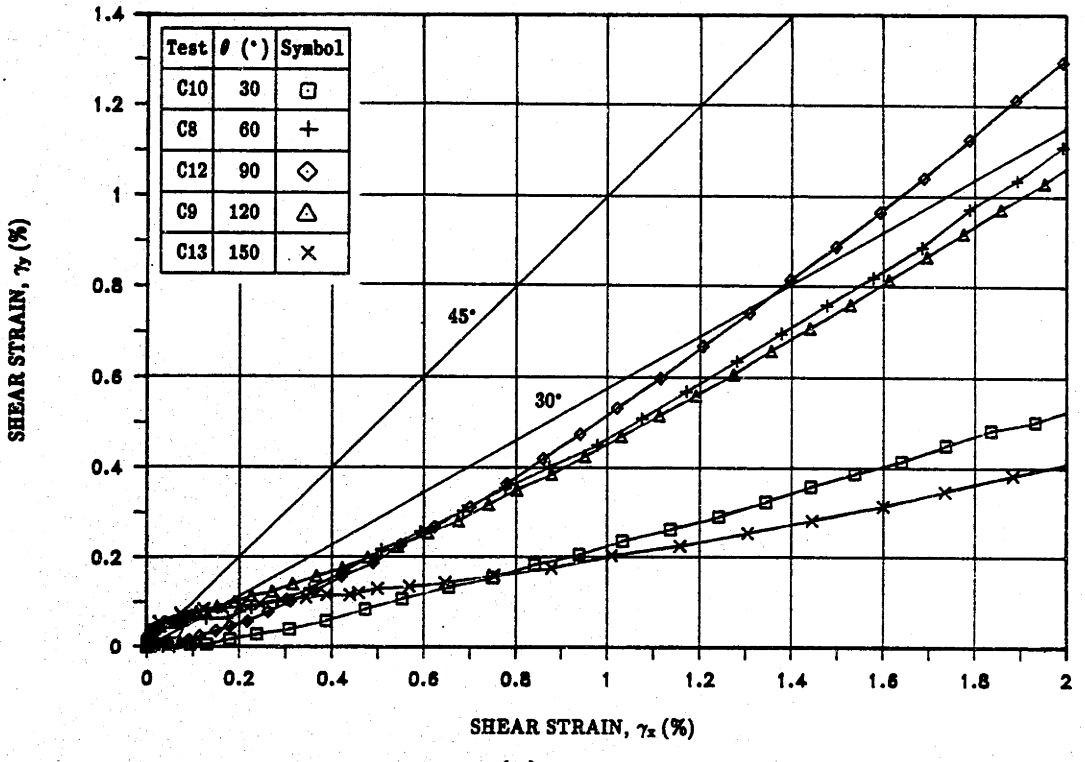

(b)

Figure 5.21: Shear Strain Paths During Undrained Shear for CAUMDSS Tests on BBC: (a) Small Scale; (b) Large Scale.

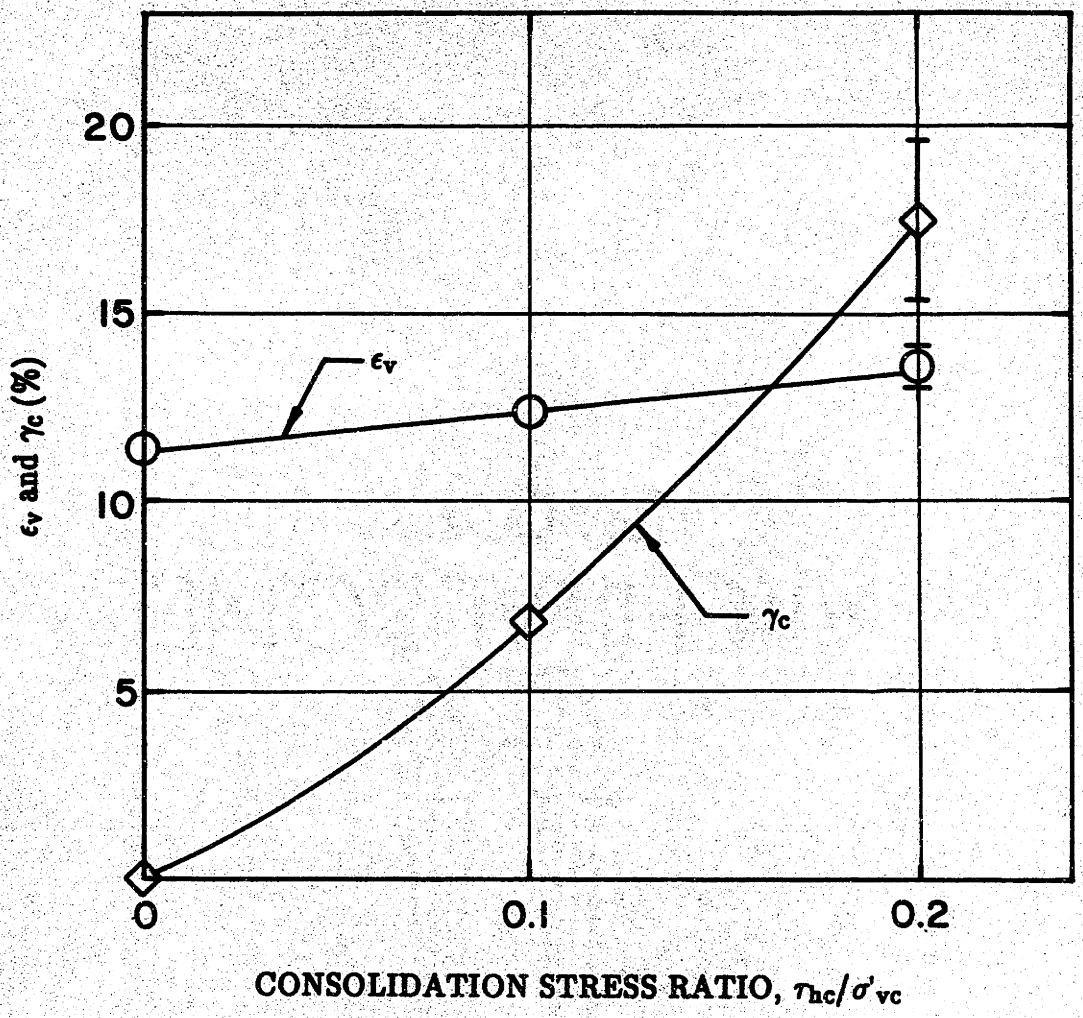

Figure 5.22: Consolidation Strains, ϵ_v and γ_c Versus Consolidation Stress Ratio for CAUMDSS and Geonor CAUDSS Test on BBC (plotted data = average ± 1SD).

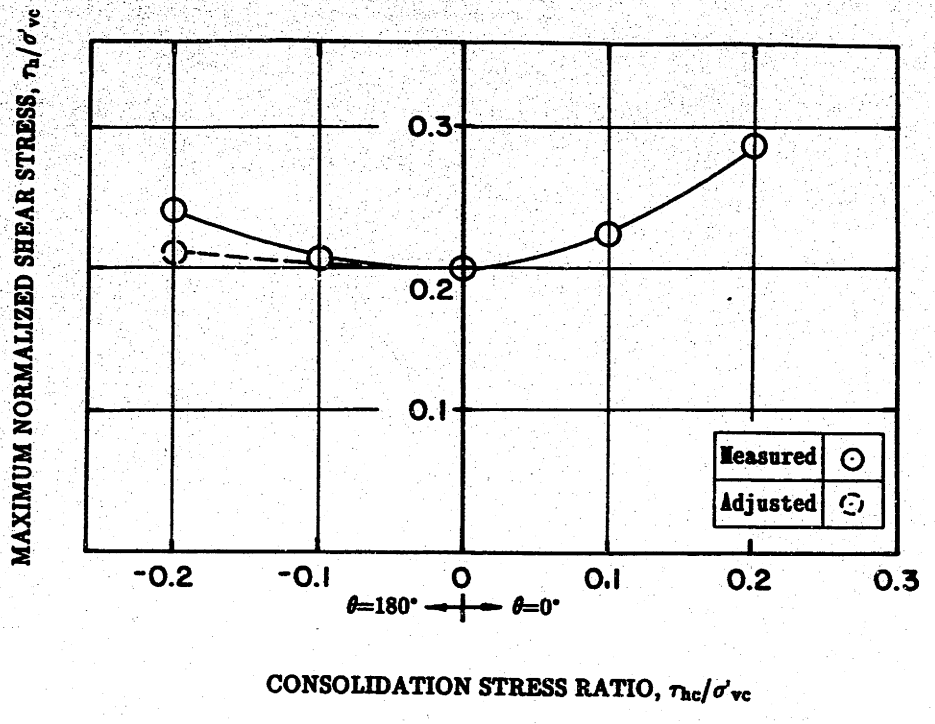

Figure 5.23: Peak Shear Stress Resistance Versus Consolidation Stress Ratio for Geonor CAUDSS Tests on BBC.

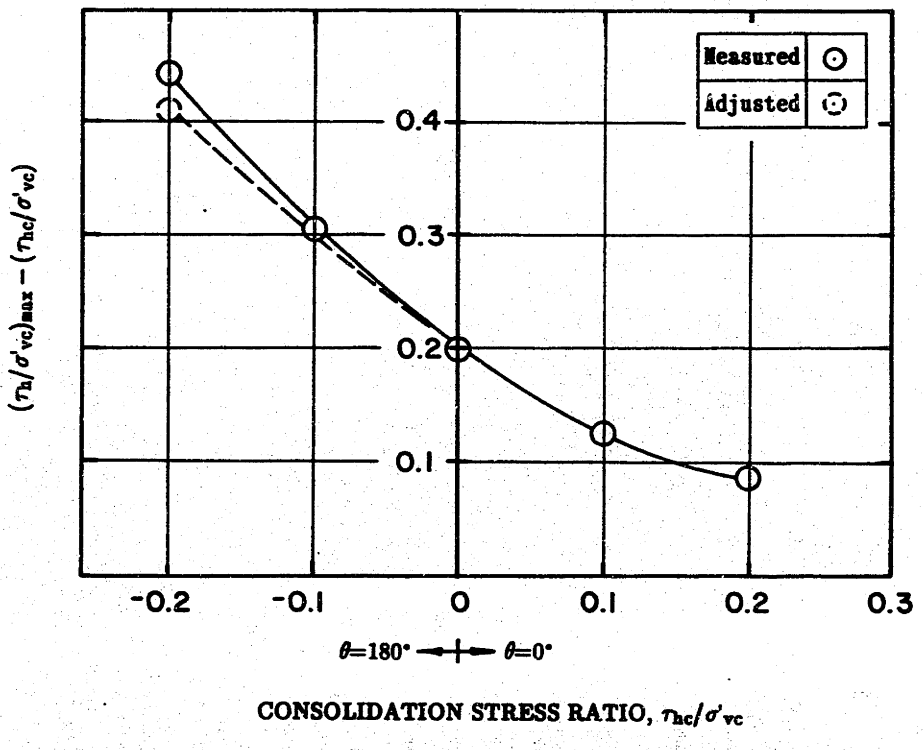

Figure 5.24: Incremental Undrained Shear Stress Required to Reach Peak Shear Stress Resistance Versus Consolidation Stress Ratio for Geonor CAUDSS Tests on BBC.

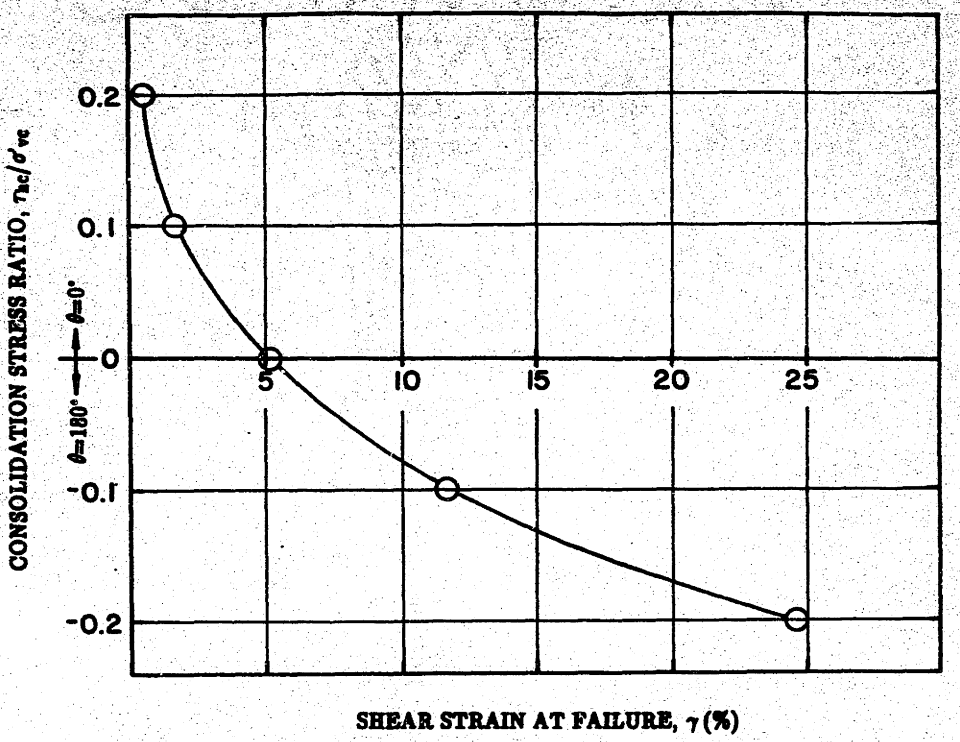

Figure 5.25: Shear Strain at Failure Versus Consolidation Stress Ratio for Geonor CAUDSS Tests on BBC.

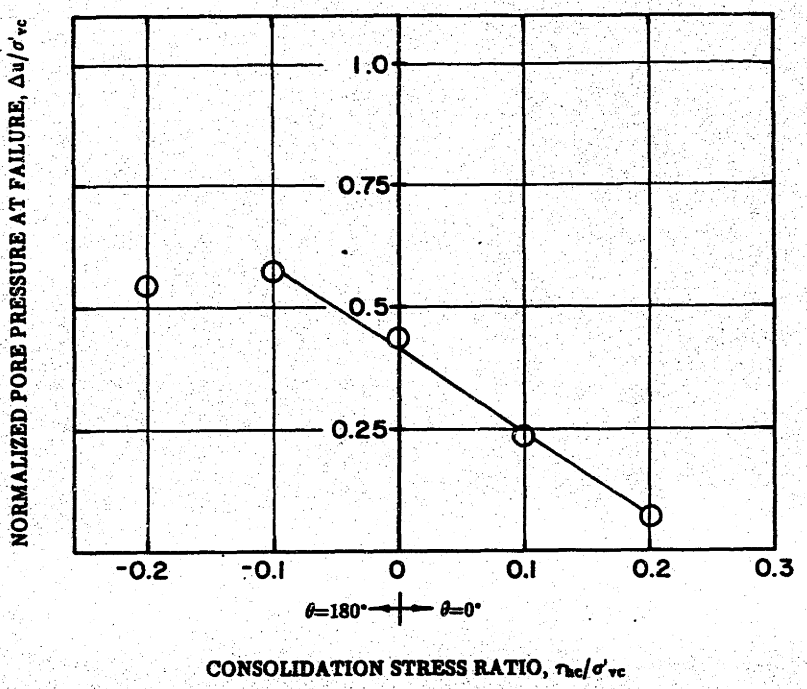

Figure 5.26: Normalized Pore Pressure at Failure Versus Consolidation Stress Ratio for Geonor CAUDSS Tests on BBC.

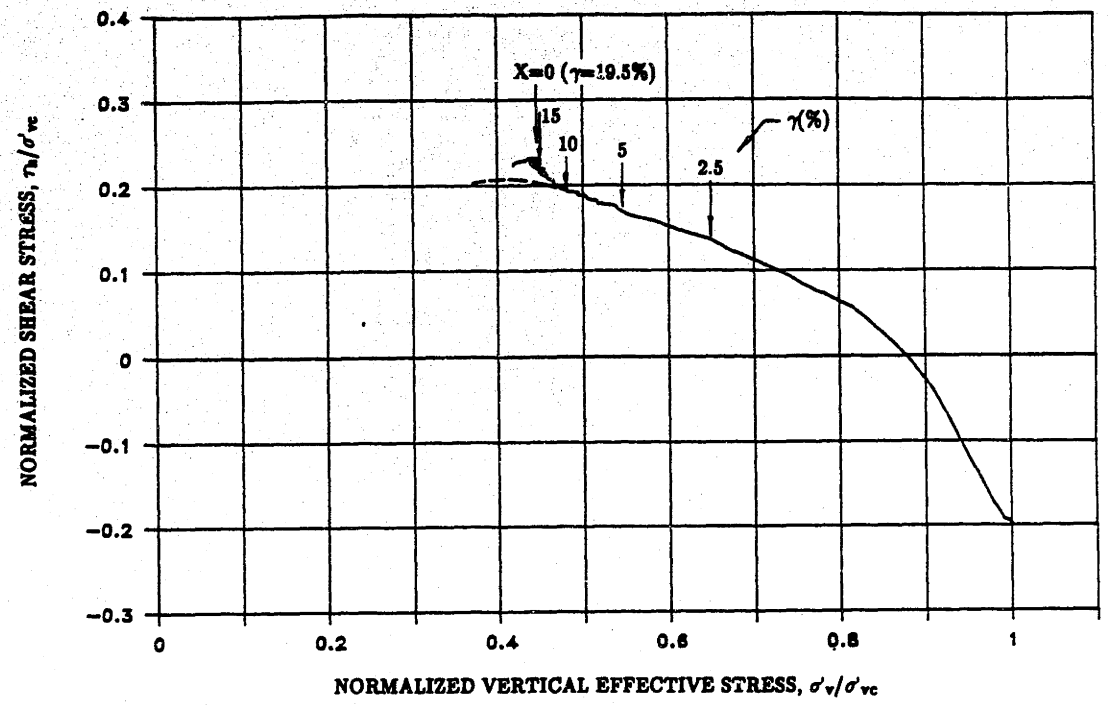

(a)

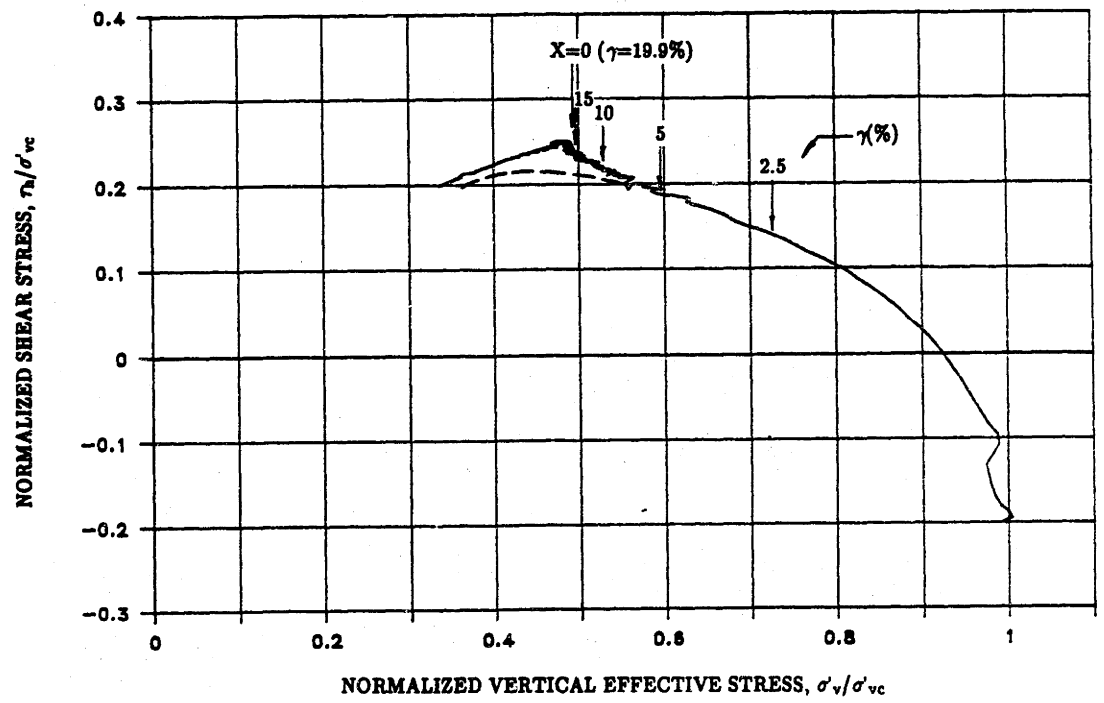

(b)

Figure 5.27: Adjusted Stress Paths for Geonor $\theta = 180°$ CAUDSS Tests With $\tau_{hc}/\sigma'_{vc} = 0.2$: (a) Test G6; (b) Test G7 (——— measured path; – – – adjusted path).

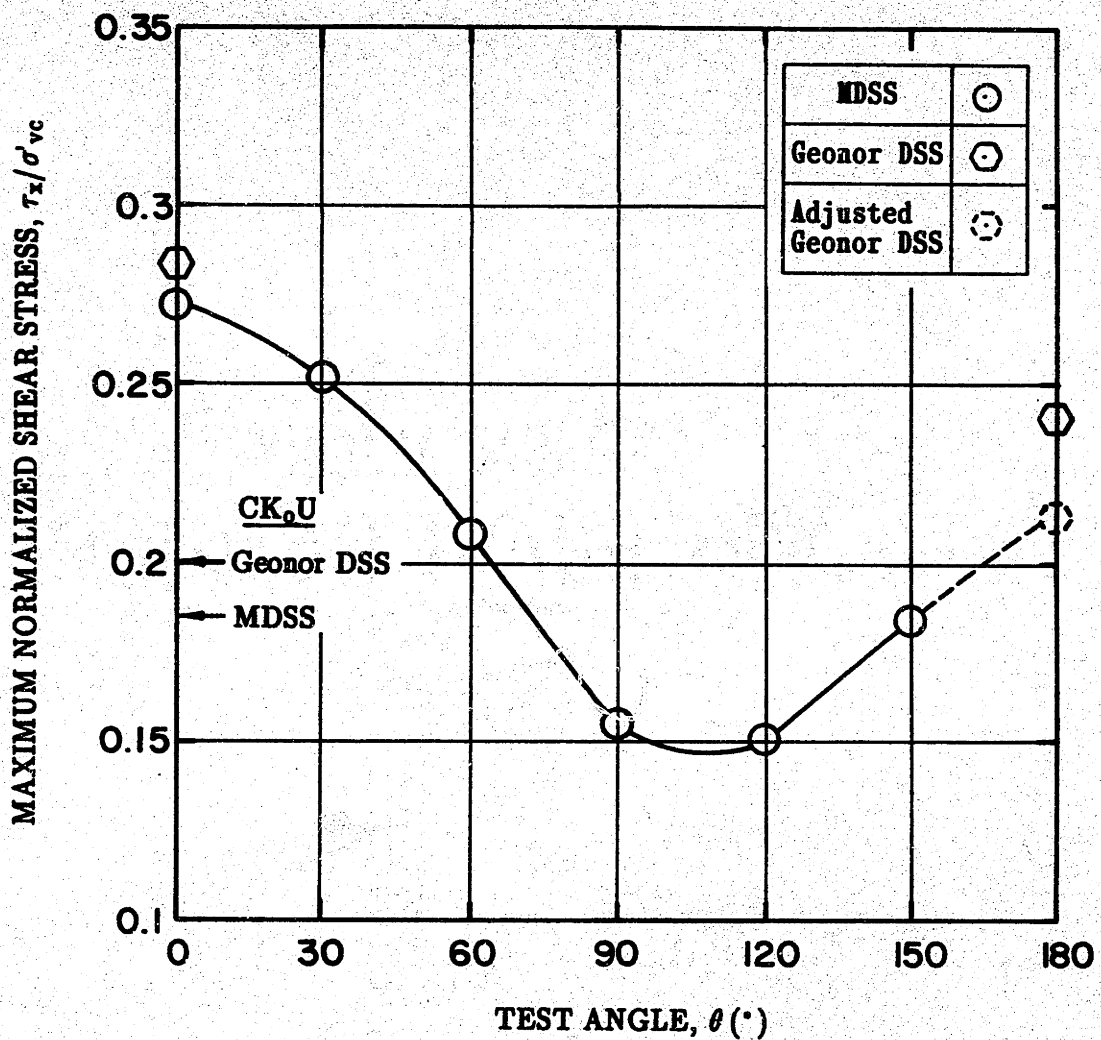

Figure 5.28: Maximum Normalized Shear Stress τ_x/σ'_{vc} Versus Test Angle θ for CAUMDSS and Geonor CAUDSS Tests on BBC.

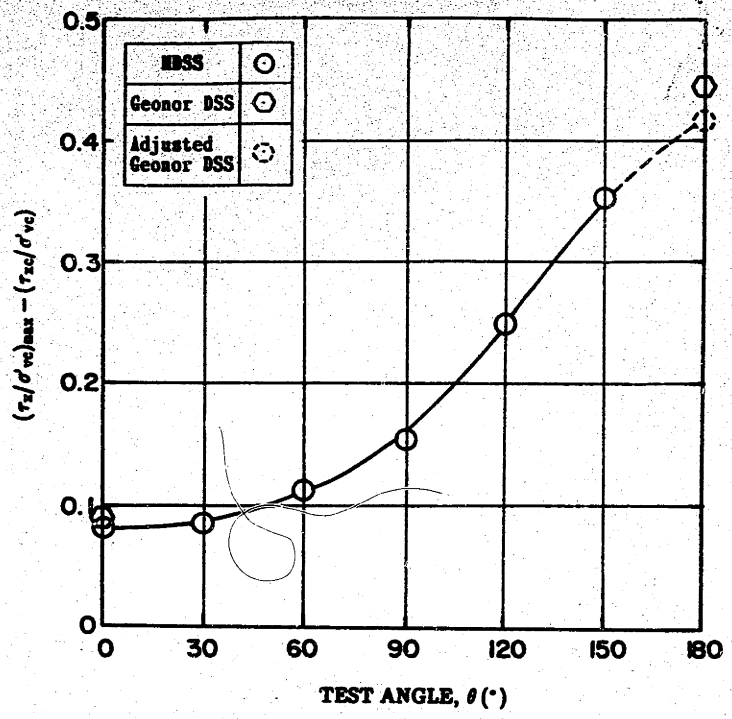

Figure 5.29: Incremental Undrained Shear Stress Required to Reach Peak Shear Stress Resistance Versus Test Angle θ for CAUMDSS and Geonor CAUDSS Tests on BBC.

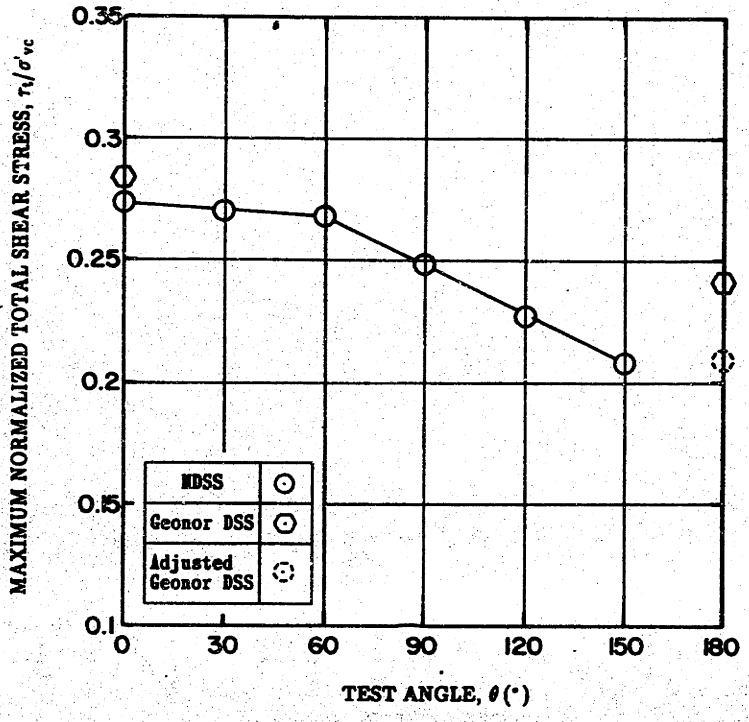

Figure 5.30: Maximum Normalized Total Shear Stress Versus Test Angle θ for CAUMDSS and Geonor CAUDSS Tests on BBC.

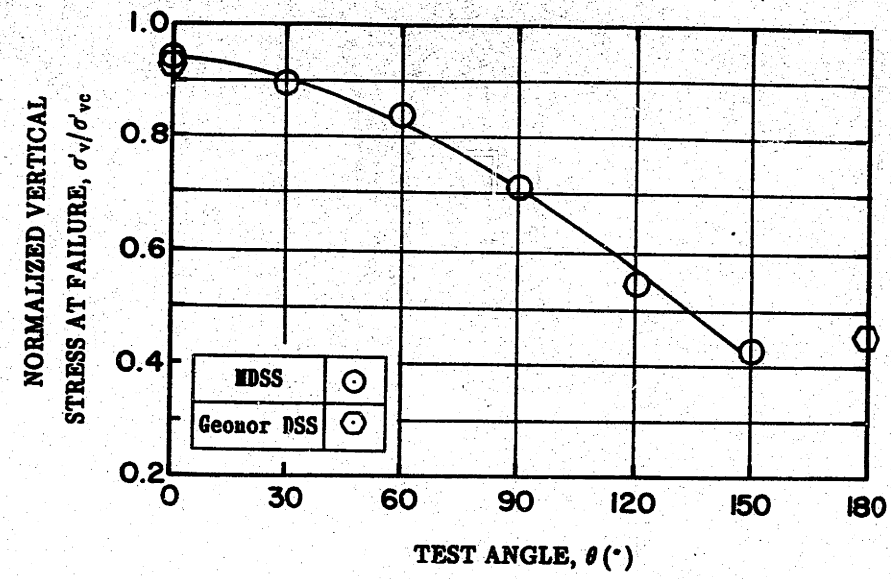

Figure 5.31: Normalized Vertical Effective Stress at Failure Versus Test Angle θ for CAUMDSS and Geonor CAUDSS Tests on BBC.

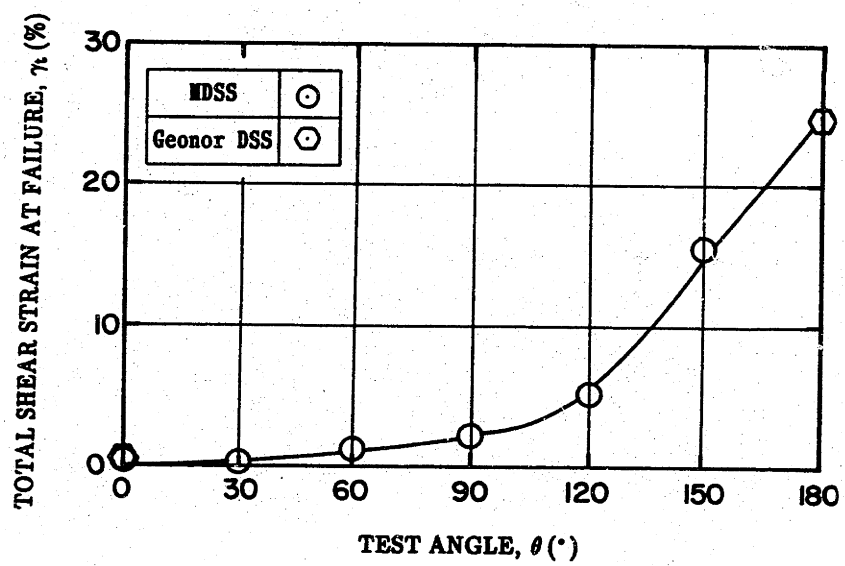

Figure 5.32: Total Shear Strain at Failure Versus Test Angle θ for CAUMDSS and Geonor CAUDSS Tests on BBC.

CHAPTER 6

PREDICTION OF MULTIDIRECTIONAL DIRECT SIMPLE SHEAR TEST RESULTS USING MIT–E3 SOIL MODEL

6.1 INTRODUCTION

The results of the Multidirectional Direct Simple Shear (MDSS) test program on BBC presented in Chapter 5 showed that there are dramatic differences in the soil's response as a function of the consolidation stress ratio (τ_{hc}/σ'_{vc}) and test angle theta (θ). This implies that designing the foundation of an offshore Arctic gravity structure requires incorporating the results of these type of tests in the design process. Since, the stress conditions within the foundation soil are very complex, it will not be possible to fully evaluate the problem only on the basis of experimental tests and simple analyses. Realistic predictions of the foundation soil's deformation and stability will also require the use of numerical techniques such as the Finite Element Method (FEM). However, finite element analysis are not very reliable if the constitutive model that is used to represent the behavior of the soil is unrealistic. Clearly in the case of analyzing the foundation of an offshore Arctic structure using simple constitutive models (e.g., linear elastic, elasto–plastic, etc.) would be unrealistic. At the very least one needs to use a model which can capture the basic behavioral patterns of the soil under the complex stress conditions that exist within the foundation of the structure.

The objective of this chapter is to present and compare MIT–E3 predictions with the Multidirectional Direct Simple Shear test results. The most recent version of the model was developed at MIT (Whittle; 1987, 1989) to describe the behavior of soils with varying overconsolidation and under both monotonic and cyclic loading. The chapter begins with a description of the model, discussion of required input parameters and a summary of an evaluation of the model conducted by Whittle. MIT–E3

predictions are compared with the experimental results of the CAUMDSS and Geonor CAUDSS test programs presented in Chapter 5. The model is then used to predict the MDSS response of BBC at different consolidation stress ratios and at OCR = 4. These predictions are repeated for an Arctic soil (Soft Zone Area of Harrison Bay). The chapter concludes with a recommended procedure for using the MDSS and the MIT–E3 model for analyzing the foundation stability and deformation of an offshore Arctic gravity structure.

6.2 MIT–E3 SOIL MODEL (abstracted from Whittle, 1987)

6.2.1 Historical Perspective

The first generalized constitutive soil model was developed at Cambridge University in the 1960's. It was based on the concepts of critical state soil mechanics (Schofield and Worth, 1968) and modeled the behavior of soil using plasticity theory. The work at Cambridge led to the development of the Modified Cam Clay model (Roscoe and Burland, 1968) which is able to predict the behavior of isotropically consolidated triaxial compression tests during drained and undrained shear. However, the model is too simplistic for most natural clays since it does not take into account some important features of soil behavior such as anisotropy and strain softening. These issues were addressed by Kavvadas (1982) who developed the MIT–E1 soil model for describing the behavior of normally consolidated clays. It is based on the Modified Cam Clay model but is able to give more realistic predictions of soil anisotropy and strain softening. However, like the Modified Cam Clay model, the MIT–E1 model assumes that stress–strain behavior within the yield surface (i.e., overconsolidation states) is linear–elastic and therefore cannot realistically predict the behavior of overconsolidated soils. Using the Modified Cam Clay and MIT–E1 models

as a framework, the MIT–E3 model was developed to overcome these shortcomings so that it can provide realistic predictions for overconsolidated soils.

6.2.2 Description of the MIT–E3 Model

The MIT–E3 model describes the mechanical behavior of normally consolidated and overconsolidated clays using a formulation which consists of three distinct parts: 1) a Perfectly Hysteretic model; 2) an Elasto–Plastic model for normally consolidated clays and 3) a Bounding Surface Plasticity model. The basic assumptions used in the model consist of:

1. There is a distinction between unloading and reloading events such that the load history of a clay cannot be described fully by its overconsolidation ratio (i.e., new state variables are introduced to account for the past load history);
2. A load cycle in effective stress space always involves some plastic (irrecoverable) strain components. Thus there is no purely elastic (reversible) range of behavior described by the model;
3. Coupling of the shear and volumetric behaviors is controlled by the bounding surface plasticity formulation;
4. The anisotropic behavior of the overconsolidated clay is related to the preferred directions of the normally consolidated clay via the bounding surface model;
5. The perfectly hysteretic model controls the non–linearity at small strain levels.

The model is rate independent (i.e., creep effects are not considered) and applies to clays which exhibit normalized behavior. The three key components of the model can be summarized as:

(I) The Perfectly Hysteretic Model

This model describes a closed, symmetric hysteresis loop between stress reversal points. Non–linearity is related to the most recent stress reversal point as defined from the strain history imposed on the sample. As a result, the perfectly hysteretic model retains only a limited memory of the load history. Functions describing non–linearity are developed from the measured behavior in hydrostatic

swelling and undrained shearing at small strain levels.

(II) The Normally Consolidated Model

Normally consolidated behavior is described by a simplified version of the MIT–E1 model and includes:

1. A yield surface represented by a distorted ellipsoid. The surface can change in size homothetically, reflecting changes in the void ratio (density hardening) and also rotates in stress space to describe the evolving directions of anisotropy;

2. Critical state failure conditions are defined by a conical surface whose magnitude and orientation reflect the critical state strength anisotropy;

3. The model uses a non–associated flow rule such that all radial effective stress paths have the same virgin compression index.

The new version of the model improves predictions of the volumetric behavior of normally consolidated clay and also uses a smaller number of input parameters than its predecessor.

(III) Bounding Surface Plasticity Model

This model introduces plastic strains for overconsolidated stress states. The plastic behavior for a state inside the bounding surface is uniquely related to that of an image point on the surface (which is defined using a radial mapping rule). Functions are introduced to relate both the flow direction and the elasto–plastic modulus (at the current stress state) to the corresponding values at the image point. The model describes a smooth transition for stress paths approaching the bounding surface.

6.2.3 Input Parameters

The MIT–E3 model requires 15 input parameters as shown in Table 6.1. Most of the parameters can be determined from standard laboratory tests. Seven of the parameters are deterministic and eight are determined from predefined parametric studies. Whittle (1987) recommends the following procedure for establishing the input

parameters:

1. κ determines the elastic bulk modulus at small strain levels (i.e., those which occur immediately following a stress reversal). In concept, κ can be estimated from the modulus measured immediately after reversal of loading in an oedometer or triaxial test. However, practical difficulties due to inaccuracy of small strain measurements and secondary compression of clays invalidate this approach. Instead, it is recommended that κ be estimated from the results of either resonant column tests or from measurements of the in–situ elastic shear wave velocity using techniques such as crosshole or downhole techniques.

2. λ is the slope of the Virgin Consolidation Line (VCL) of a normally consolidated clay in e–$\log_e\sigma'$ space, which can also be determined directly from an oedometer test plotted in e–$\log\sigma'_v$ space.

3. (2G/K) is the ratio of the tangential elastic shear modulus to the bulk modulus, which is related to the Poisson's ratio, ν, of the soil skeleton:

$$2G/K = 3(1-2\nu)/(1+\nu) \tag{6.1}$$

For one–dimensional (K_o) swelling, it is assumed that the effective stress path is initially linear (assuming there are no plastic strains). If the OCR at $K_o = 1$ is known (OCR_1), then (2G/K) can be determined from the expression:

$$2G/K = \frac{(1 - K_{onc})OCR_1}{(1/3)(1 + 2K_{onc})OCR_1 - 1} \tag{6.2}$$

4. ϕ'_{tc} and ϕ'_{te} are friction angles at the critical state condition measured in K_o consolidated triaxial compression and extension modes of shearing.

5. $(K_o)_{nc}$, the coefficient of lateral earth pressure at rest for normally consolidated clay, can be measured during K_o consolidation in either a triaxial test (with no lateral straining) or an oedometer with lateral stress measurement.

6. c, S_t are determined by a parametric study of the model behavior in undrained triaxial compression and extension tests for a K_o normally consolidated clay.

7. ψ_o is the parameter which controls the changes in anisotropy due to straining (i.e., rotational hardening of the model). There is limited experimental evidence giving the location of the yield surface for soils and almost no information on how the yield surface rotates during subsequent loading. It is recommended that, until more data becomes available, ψ_o should be determined from parametric studies such as those described in Whittle (1987).

8. C, n are the parameters used to describe the non–linearity in the volumetric response for the perfectly hysteretic formulation. Values of C

and n are selected to match the swelling behavior in an oedometer or CRSC test.

9. ω, h and γ are used to complete the perfectly hysteretic formulation and to specify the mapping laws for the bounding surface plasticity. ω can be estimated from small strain measurements of the variation in secant modulus with strain level in undrained shear tests. However, in general, such data are not readily available, and in practice, all three constants must be estimated from parametric studies: Two types of tests are used to assess the parameters: a) hydrostatic or K_o unload and reload cycles and b) undrained shear tests in triaxial compression for overconsolidated clays.

Table 6.2 is a list of the input parameters selected by Whittle (1987) for Boston Blue Clay. These parameters were used to perform the MIT–E3 predictions of CAUMDSS tests on BBC presented in the following section.

6.2.4 Model Evaluation

Using the input parameters for BBC listed in Table 6.2, Whittle (1987) conducted an evaluation of the MIT–E3 model by comparing predictions with the results of laboratory tests conducted during the past 20 years at MIT. The results are summarized as follows:

(I) Conventional Monotonic Undrained Shear

Model predictions of CK_oU shear tests in a) triaxial compression and extension, b) plane strain active and passive and c) direct simple shear modes were compared to experimental data for OCR's up to 8. Overall it was found that MIT–E3 gives very good predictions of the major features of behavior including the undrained shear strength, stress–strain behavior and development of shear induced pore pressure (effective stress paths). Model predictions of the non–linearity at small strains are in excellent agreement with measured data. As OCR increased (OCR's greater than 4 to 8) the model tended to overpredict the measured shear strength and stress obliquities, possibly due in part to measurement difficulties associated with the development of shear planes in laboratory tests.

(II) Directional Shear Cell

The Directional Shear Cell (DSC) is a plane strain stress controlled device which has the unique capability of controlling the application of principal stress directions in the plane of loading (see Section 2.4.1.5). Undrained shear tests have been conducted on BBC at OCR = 4 with the major principal stress orientation (δ) varying from 0° to 90° (Germaine, 1982). The tests were used to determine the undrained anisotropic behavior of overconsolidated clay caused by a K_o consolidated history. The MIT–E3 predictions of the tests agreed well with the measured stress–strain and effective stress path data for all δ angles. This result confirms the ability of the new model to describe anisotropic behavior caused by the previous consolidation stress history and also the non–linear stress–strain response of the overconsolidated clay. The DSC results provide an excellent test of the predictive capabilities of the model and represent a unique component of the evaluation process.

(III) Undrained Cyclic Direct Simple Shear

Malek (1987) conducted an extensive series of undrained, cyclic direct simple shear tests on Boston Blue Clay as part of research at MIT into the behavior of friction piles supporting Tension Leg Platforms. The principal variables for the stress–controlled cyclic loading portion of the program included the average shear stress, the cyclic shear stress and the overconsolidation ratio (OCR = 1 , 2 and 4). Comparison of MIT–E3 predictions with the measured data showed:

1. Excellent predictions of the number of cycles to failure provided that the effects of shear rate on the monotonic undrained shear strength are properly accounted for.

2. Very good predictions of shear strains are obtained throughout cyclic shearing.

3. The shear–induced pore pressures are reasonably well estimated but are regarded as the least reliable component of the model predictions due, in large part, to the sensitivity of pore pressure accumulation to rate effects.

The detailed evaluation process showed that MIT–E3 is a practical model which provides good predictions of the behavior of normally consolidated and overconsolidated clays including the effects of anisotropy caused by the stress history of the clay.

6.3 MIT–E3 PREDICTIONS OF CAUMDSS TEST RESULTS FOR NORMALLY CONSOLIDATED BBC

6.3.1 Introduction

In this section, MIT–E3 predictions of the Multidirectional Direct Simple Shear behavior of normally consolidated BBC are compared with the experimental results presented in Chapter 5. The model was run using the input parameters selected for BBC by Whittle (1987) which are listed in Table 6.2. The model was used to make predictions of the undrained shear behavior of the test specimens. The state of stress at the end of anisotropic consolidation was used as input to the model for describing part of the initial values of the state variables (i.e., the initial effective stress tensor). This section begins with a comparison of model predictions with results of the Geonor CAUDSS test program and is followed by a similar comparison of model predictions with results of the CAUMDSS test program. The section concludes with an evaluation and synthesis of the MIT–E3 predictions and a summary of additional predictions for CAUMDSS tests which were not performed.

6.3.2 Predictions of Geonor CAUDSS Undrained Shear Results

Chapter 5 presented the results of five Geonor CAUDSS tests which were conducted to study the influence of the orientation and magnitude of the consolidation shear stress on the undrained shear behavior of BBC. The tests were conducted with consolidation stress ratios, τ_{hc}/σ'_{vc} = 0.2(θ=0°), 0.1(θ=0°), 0.0(K_o), –0.1(θ=180°) and –0.2(θ=180°). Figures 6.1 to 6.4 are plots of the experimental results and the MIT–E3 predictions for the range of consolidation stress ratios listed above. The

figures include plots of the stress–strain curves, stress paths and log normalized secant modulus versus log shear strain curves. Table 6.3 summarizes the MIT–E3 predictions for each test including the consolidation stress ratio and the shear strain, shear resistance and effective stress ratio at the maximum horizontal shear resistance.

The stress–strain curves and stress paths (Figures 6.1 and 6.3) show that the model predicts similar trends in the peak shear resistance and shear strain and effective stress ratio at failure as that found in the experiments. The model captures the significant increase in the peak shear resistance and decrease in shear strain at failure as τ_{hc}/σ'_{vc} increases from 0 to 0.2. The predicted curves display some strain softening for the tests with $\tau_{hc}/\sigma'_{vc} = 0.0$ and 0.1 but, unlike the experimental results, the prediction for the test with $\tau_{hc}/\sigma'_{vc} = 0.2$ shows very little strain softening. For tests with $\tau_{hc}/\sigma'_{vc} = -0.1$ and -0.2, the model predicts a lower shear resistance and significantly lower shear strain at failure than the experimental results. However, as discussed in Chapter 5 and Appendix G, the results of the $\theta = 180°$ experimental tests are suspect (especially for $\tau_{hc}/\sigma'_{vc} = -0.2$) and a comparison of the "adjusted" experimental results and the model predictions is presented in Section 6.3.4: Evaluation and Synthesis of MIT–E3 Predictions.

Figure 6.2 compares predicted and measured normalized pore pressure versus shear strain data. The comparison between predicted and measured results for the CK_oUDSS test and the CAUDSS test with $\tau_{hc}/\sigma'_{vc} = -0.1$ is excellent. The predicted curve for the CAU test with $\tau_{hc}/\sigma'_{vc} = -0.2$ compares well with Test G7 but not G6. The predicted curves for $\tau_{hc}/\sigma'_{vc} = 0.1$ and 0.2 tend to deviate from the experimental data because for these stress conditions, once the peak shear resistance is reached the soil is very near its critical state. This is particularly the case for $\tau_{hc}/\sigma'_{vc} = -0.2$ where at $\gamma = 2\%$, the predicted pore pressure versus shear strain curve becomes horizontal. For the case of $\tau_{hc}/\sigma'_{vc} = 0.1$, after some strain softening the pore pressure curve begins to also become horizontal as it approaches the critical state. This is not

the case for experimental Tests G3 and G5 (τ_{hc}/σ'_{vc} = 0.1 and 0.2 respectively) where once the peak shear resistance is reached the samples exhibit significant strain softening.

Figure 6.4 presents predicted log–log plots of the normalized Young's modulus (E_u/σ'_{vc}) versus shear strain γ as a function of the consolidation stress ratio. For these data, MIT–E3 predictions and the experimental results compare very well both in terms of trend and magnitude. The only major difference is that at low shear strains the model does not predict higher modulus values for tests where the applied shear stress is reversed compared to those where the applied stress always acts in the same direction (i.e., τ_{hc}/σ'_{vc} = –0.2 and 0.2 respectively). However, the predicted curves for τ_{hc}/σ'_{vc} = 0.2 and –0.2 cross over at $\gamma \cong 0.08\%$ and thereafter display the same trend as the experimental results.

6.3.3 Prediction of CAUMDSS Undrained Shear Results

The results of the CAUMDSS test program on BBC presented in Chapter 5 showed that there is a significant dependence on the undrained shear behavior of BBC as a function of the test angle θ. Results were presented for tests conducted in the MDSS with τ_{hc}/σ'_{vc} = 0.2 and at θ ranging from 0° to 150° in 30° increments. Figures 6.5 to 6.9 compare plots of the experimental results and the MIT–E3 predictions. The figures include plots of stress–strain curves, stress paths, pore pressure versus shear strain curves, log normalized modulus versus log shear strain curves and strain paths (Note: the applied (ice loading) shear stress acts along the X axis of the MDSS and E_u is computed in terms of τ_x and γ_x during undrained shear). Table 6.5 summarizes the MIT–E3 predictions.

The stress–strain curves and stress paths show that the model predicts similar trends in the peak shear resistance and shear strain and effective stress ratio at failure as a function of θ. While the trends are very similar, the model predictions of peak

shear resistance are higher than the measured results. In addition, the experimental stress–strain curves show a significant increase in the brittleness (i.e., low strain at peak followed by pronounced strain softening) of the specimens as θ decreases from 180° to 0°, which the model does not predict (however, a significant portion of the measured strain softening at low θ angles may be due to the device, as discussed in Chapter 5 and Appendix G, rather than true soil behavior). Most of the predicted stress–strain curves display essentially no strain softening after the peak shear resistance is reached. This indicates that for all the tests the predicted peak shear resistance occurs very close to the critical state condition and therefore further shearing results in no change in the shear resistance.

The predictions of pore pressure development plotted in Figure 6.6 show marked differences from the measured data. However, the differences reflect the fact that, in the predictions, the peak resistance essentially coincides with the critical state condition. Thus, while the initial rate of pore pressure development is the same for all test angles, as is essentially the case for the experimental results, once the peak shear resistance is reached the model predicts no change in pore pressure and hence effective stress and undrained strength with continued shearing. In the case of the experimental tests the samples tend to undergo significant strain softening and a continuous increase in the magnitude of the pore pressure.

The MIT–E3 predictions of normalized modulus versus shear strain compare remarkably well with the experimental results (Figure 6.8). At shear strains greater than approximately 0.1% the magnitude and trend in the predicted curves are very similar to the experimental results. At a given shear strain (for $\gamma_x \geq 0.1\%$), the value of the normalized modulus gradually increases from a minimum for $\theta = 0°$ to a maximum for $\theta = 180°$. It is interesting that the modulus curves from the model predictions all intersect at $\gamma \cong 0.07\%$. This implies that the increase in shear resistance is independent of the test angle θ at $\gamma \cong 0.07\%$ but is different for $\gamma < 0.07\%$ and >

0.07%. It is not clear why the model predictions result in this intersection of the modulus–shear strain curves.

The measured and predicted strain paths are plotted in Figure 6.9 for tests with $\theta = 30°$, $60°$, $90°$, $120°$ and $150°$. While the model predictions display similar trends compared to the experimental results, it, however, predicts a significantly less magnitude in the Y component of shear strain. Like the experimental results, the MIT–E3 predictions show that the test with the largest component of consolidation shear stress acting in the Y direction ($\theta = 90°$) has the highest rate of increase in the Y component of shear strain. Furthermore, tests at $\theta = 30°$ & $150°$ and $60°$ & $120°$ have, as expected, nearly identical strain paths since, for these pairs of tests, the component of the consolidation shear stress in the Y direction is the same throughout the test.

6.3.4 Synthesis and Evaluation of MIT–E3 Predictions

(I) Behavior of BBC as a Function of Consolidation Stress Ratio

The results of the Geonor CAUDSS test program and the MIT–E3 predictions are summarized in Figures 6.10 to 6.12. Figure 6.10 plots the measured and predicted peak shear resistance as a function of the consolidation stress ratio.[1] The results compare very well with nearly identical shapes for the measured and predicted curves. The model predicts slightly higher strengths for positive consolidation stress ratios and slightly lower values for negative consolidation stress ratios.

Figure 6.11 plots the predicted and measured shear strain at failure versus the consolidation stress ratio. For these data the model predictions follow a similar trend compared to the experimental results, but for negative consolidation stress ratios the magnitudes are significantly different. However, as pointed out in Section 5.5 of

---

[1]Peak values of τ_x/σ'_{vc} plotted in the figures presented in this section for the two tests conducted with $\theta = 180°$ represent their average "adjusted" value of 0.21 as outlined in Section 5.5 of Chapter 5.

Chapter 5, the measured values of γ_f for $\theta = 180°$ tests are too high due to the influence of the device. Results from the K_o consolidated test compare reasonably well while results for tests with positive consolidation stress ratios show excellent agreement.

Predictions of the normalized pore pressure at failure as a function of consolidation stress ratio displays a slightly different shaped curve than the experimental results (Figure 6.12). With the exception of the results for $\tau_{hc}/\sigma'_{vc} = -0.2$, the measured data show a linear relationship between $\Delta u/\sigma'_{vc}$ at peak shear resistance versus τ_{hc}/σ'_{vc}. The MIT–E3 predictions on the other hand have a concave curve of $\Delta u/\sigma'_{vc}$ as a function of τ_{hc}/σ'_{vc}. However, the measured and predicted results at some of the individual τ_{hc}/σ'_{vc} ratios compare very well (i.e. $\tau_{hc}/\sigma'_{vc} = 0.0$ and 0.1). The measured value for $\tau_{hc}/\sigma'_{vc} = -0.2$ is plotted with a marker indicating that this value is to low for the reasons discussed in Section 5.5.2 of Chapter 5. It was suggested in that section that, like the measured peak shear resistance, this value may be incorrect due to the influence of the apparatus on this type of test ($\theta \approx 180°$) and that under ideal conditions the sample would not only have a lower peak shear resistance but also a higher normalized pore pressure ratio at the peak shear resistance.

(II) Behavior of BBC as a Function of the Test Angle θ

The results of the CAUMDSS test program and the MIT–E3 predictions are summarized in Figures 6.13 to 6.18.[2] Figure 6.13 shows the variation of the maximum normalized X shear stress $(\tau_x/\sigma'_{vc})_{max}$ as a function of the test angle θ. This plot shows the most significant result of the CAUMDSS test program which is the large variation in the undrained shear behavior of BBC as θ varies from 0° to 180°. The results of the MIT–E3 predictions, plotted in the same figure, show an even more

[2]In the summary plots, the plotted value for the pairs of tests conducted at $\theta = 60°$, 120°, and 150° is their average value. The $\theta = 0°$ value is that of MDSS Test C7 and the $\theta = 180°$ value is the average "adjusted" value of the two Geonor DSS Tests G6 and G7.

significant result in that the model predictions compare very well with the experimental data. While the model overpredicts the strength for tests with $\theta \leq 90°$, just the fact that the variation of the predicted strength with θ (i.e., trend) is nearly identical to the measured data is remarkable. The similarity in trends between the measured and predicted results is more evident in Figure 6.14 which plots the maximum X shear stress normalized by the $(\tau_x)_{max}$ value for $\theta = 0°$ (with this normalization the value at $\theta = 0°$ is equal to one). In this plot the experimental and model results are almost identical for all test angles except $\theta = 150°$ and $180°$. The excellent agreement between the normalized measured data and normalized MIT–E3 predictions is truly exceptional.

Figure 6.15 is a plot of the measured and predicted maximum normalized total shear stress versus the test angle θ. Like the X shear stress data, the model predictions display the same trend as the experimental results and give almost identical values for $\theta = 120°$ and $150°$.

MIT–E3 predictions of the normalized vertical effective stress ratio at $(\tau_x)_{max}$ as a function of θ do not compare as well with the trend in the measured data as shown in Figure 6.16. The curve of predicted results is initially concave and becomes convex with the inflection point occurring at $\theta = 90°$. The curve representing the measured data displays a gradual increase in its negative slope as θ increases. However, the predicted values for $\theta = 60°$, $90°$ and $120°$ are nearly identical to the measured results. Like the pore pressure data plotted in Figure 6.12, the value for $\theta = 180°$ is plotted with a marker indicating that the measured value is questionable and the true value is probably less.

Figure 6.17 shows that for tests with $\theta \leq 120°$ the predicted total shear strain at failure compares very well with the measured results. Actually the measured and predicted values for $\theta = 150°$ do not differ by very much but the trends in the data differ significantly as θ increases beyond $120°$. This is mainly a result of the large

magnitude of the measured total shear strain for $\theta = 180°$ which, as pointed out in Part (I) of this section, is considered to be too high. Excluding this test from the plot shows that overall the agreement between the model and experimental data for $\theta = 0°$ to 150° is excellent.

The final summary plot, Figure 6.18, is a superposition of Figures 6.8a and 6.8b showing the predicted and measured normalized modulus versus shear strain. The plotted curves represent the upper and lower bounds of the modulus values for all of the test angles. For both the measured and predicted curves, the lower and upper bounds correspond to $\theta = 0°$ and 180° respectively. Results for all other test angles lie in between these bounds with the modulus values gradually increasing (at a given shear strain) as θ increases from 0° to 180°. The plot shows that there is excellent agreement between the predicted and measured values for $\theta = 180°$. The predicted values for $\theta = 0°$ are larger than the measured values but considering the sensitivity of experimentally determining modulus values the comparison is quite good. In addition, the results for this test angle represent the largest deviation between the measured and experimental results. The agreement steadily improves as θ increases from 0° to 180°. Overall, the comparison is remarkably good. The only peculiarity with the predicted values, as mentioned is Section 6.3.3, is that all the curves intersect at $\gamma \cong 0.07\%$ and reverse their trend at $\gamma \leq 0.07\%$ with the upper and lower bounds becoming 0° and 180° respectively.

The summary plots presented in Figures 6.13 to 6.18 show satisfactory to excellent agreement between the MIT–E3 predictions and the experimental data. The most important result found from the experimental program was that there are dramatic differences in the soil response as the test angle θ varies from 0° to 180°. These variations were predicted remarkably well by the model, particularly for the most important design parameters such as the peak shear resistance and undrained Young's modulus. This is very significant since accurate prediction of trends in the

experimental results is much more important than accurate predictions of absolute magnitudes. Ideally one wants accurate predictions of both trend and magnitude, but differences in magnitudes are much easier to adjust for than differences in trend. This is clearly shown in Figures 6.13 and 6.14; Figure 6.13 shows that while the model overpredicts the peak X shear stress for $\theta < 120°$, normalizing the data results in excellent agreement with the experimental results as shown in Figure 6.14

The only major variation between the MIT–E3 predictions and experimental results is in the post peak pore pressure and strain softening behavior of the soil (Figures 6.5 and 6.6). As discussed in Section 6.3.3, the predicted peak shear resistance for all θ angles with $\tau_{hc}/\sigma'_{vc} = 0.2$ coincides with the critical state condition and therefore the stress strain curve is horizontal once the peak shear resistance is reached. In the experimental results, strain softening is significant, particularly for $\theta \leq 90°$. This could potentially be a problem if the model were used under conditions where the foundation soil is expected to undergo large shear strains. However, it is highly questionable if the measured strain softening behavior is truly representative of the post peak simple shear behavior of the soil. Appendix A points out that there is some preliminary evidence (in Airey, et al., 1985) which indicates that simple shear tests develop rupture planes near the peak shear resistance and therefore conventional interpretation of the post peak test results can be misleading. Furthermore, Chapter 5 and Appendix G present evidence which indicates that strain softening behavior as measured in a Direct Simple Shear test is due in part to the nonuniformity of stress imposed by the device and not exclusively due to the fundamental behavior of the soil. Hence, the validity of the degree of strain softening measured in the experimental tests is suspect. It would be more appropriate to evaluate the large strain behavior of the soil using a device which is better suited for this task such a ring shear apparatus. The main point of this discussion is that it is plausible that under actual conditions the soil will still exhibit some strain softening, but not as much as that measured in the

experimental tests. On the other hand the model predictions of the post peak behavior appear to be unrealistic as one would expect some strain softening to occur. It is likely that the true strain softening behavior of the soil lies in between the experimental results and the model predictions. Needless to say, this topic warrants additional research, particularly on the experimental side with respect to investigating the influence of the direct simple shear device per se on the stress–strain behavior of the soil.

6.3.5 MIT–E3 Predictions of CAUMDSS Tests on Normally Consolidated BBC for $\tau_{hc}/\sigma'_{vc} = 0.1$ and 0.3.

This section presents additional MIT–E3 predictions for CAUMDSS tests on normally consolidated BBC for different consolidation stress ratios. Given the very good to excellent agreement between the experimental and predicted results for $\tau_{hc}/\sigma'_{vc} = 0.2$ it will be interesting to study model predictions for $\tau_{hc}/\sigma'_{vc} = 0.1$ and 0.3. Tables 6.4 and 6.6 summarizes the MIT–E3 predictions for CAUMDSS tests with $\tau_{hc}/\sigma'_{vc} = 0.1$ and 0.3 respectively. Figures 6.19 to 6.21 present summary plots of $(\tau_x)_{max}$, $\tau_x(\theta)_{max}/\tau_x(\theta=0)_{max}$, and effective vertical stress ratio at $(\tau_x)_{max}$ versus the test angle θ. Figure 6.22 summarizes the variation of the undrained modulus as a function of θ and τ_{hc}/σ'_{vc}.

Figure 6.19 shows that there is a significant influence of the consolidation stress ratio on the relationship between $(\tau_x)_{max}/\sigma'_{vc}$ and the test angle θ. Decreasing τ_{hc}/σ'_{vc} from 0.2 to 0.1 results in significantly less variation in $(\tau_x)_{max}/\sigma'_{vc}$ as a function of θ with a maximum value of 0.247 at $\theta = 0°$ and a minimum of 0.190 at $\theta = 120°$, 150° and 180°. Conversely, increasing τ_{hc}/σ'_{vc} from 0.2 to 0.3 results in a significant increase in the variation of $(\tau_x)_{max}/\sigma'_{vc}$ as a function of θ. Once again the maximum value which occurs at $\theta = 0°$ equals 0.372 and, similar to the $\tau_{hc}/\sigma'_{vc} = 0.2$ tests, the minimum occurs at $\theta = 120°$, but is significantly smaller than the value of $(\tau_x)_{max}/\sigma'_{vc}$ for $\tau_{hc}/\sigma'_{vc} = 0.2$ (0.103 versus 0.158). It is interesting to note that all

three curves of $(\tau_x)_{max}/\sigma'_{vc}$ approximately intersect at $\theta = 60°$ and 150° and in addition the values do not differ by very much at $\theta = 180°$. The dramatic variation in $(\tau_x)_{max}/\sigma'_{vc}$ as a function of θ and τ_{hc}/σ'_{vc} is more clearly featured in Figure 6.20 which plots $\tau_x(\theta)_{max}/\tau_x(\theta=0°)_{max}$ versus θ. The figure shows the significant changes in $(\tau_x)_{max}$ as a function of θ and also the increase in the variation as τ_{hc}/σ'_{vc} increases from 0.1 to 0.3.

The shear stress–strain curves (not plotted here) for tests with $\tau_{hc}/\sigma'_{vc} = 0.1$ display some strain softening after the peak shear resistance is reached (this is plotted for $\theta = 0°$ and 180° in Figure 6.1). This is not, however, the case for predictions of tests with $\tau_{hc}/\sigma'_{vc} = 0.2$ and 0.3 where the peak shear resistance essentially coincides with the critical state condition.

The normalized vertical effective stress at failure also displays significant changes as a function of the test angle θ. Figure 6.21 shows that the largest decrease in the vertical effective stress at $(\tau_x)_{max}$ (for a given θ) occurs for tests with $\tau_{hc}/\sigma'_{vc} = 0.1$. Tests with the highest consolidation stress ratio reach the peak shear resistance very quickly for small θ angles ($\theta \leq 60°$) with very little development of pore pressure. The difference in the effective stress ratio at $(\tau_x)_{max}$ as a function of τ_{hc}/σ'_{vc} is largest for small θ angles and gradually decreases as θ approaches 150° where for $\theta \geq 150°$ the results become nearly independent of τ_{hc}/σ'_{vc}.

All of the normalized modulus versus shear strain curves fall within a relatively narrow band as shown in Figure 6.22. For $\gamma \geq 0.03\%$, the band is bounded at the top and bottom by curves for tests with $\tau_{hc}/\sigma'_{vc} = 0.3$ and $\theta = 180°$ and 0° respectively. All other combinations of τ_{hc}/σ'_{vc} ranging from 0 to 0.3 and θ ranging from 0° to 180° produce curves which lie within these bounds. The data plotted in the Figure show that as the τ_{hc}/σ'_{vc} increases from 0.1 to 0.3, the spread in the band containing the curves for $\theta = 0°$ and 180° increases. Unlike the curves for $\tau_{hc}/\sigma'_{vc} = 0.2$, the curves for $\tau_{hc}/\sigma'_{vc} = 0.1$ and 0.3 do not intersect in this plot. As stated in the

previous section it is unclear why the curves for $\tau_{hc}/\sigma'_{vc} = 0.2$ intersect.

In summary, the MIT–E3 predictions for CAUMDSS tests with $\tau_{hc}/\sigma'_{vc} = 0.1$ and 0.3 also display significant variations in the behavior of BBC as a function of the test angle θ. As expected, the variation with θ increases with an increase of τ_{hc}/σ'_{vc} to 0.3 and decreases with a decrease in τ_{hc}/σ'_{vc} to 0.1 (which is approaching the K_o condition). The most dramatic variation with θ, as was found in the experimental results, is in the value of $(\tau_x)_{max}/\sigma'_{vc}$, particularly for tests with $\tau_{hc}/\sigma'_{vc} = 0.2$ and 0.3.

6.4 MIT–E3 PREDICTIONS OF CAUMDSS BEHAVIOR OF OCR=4 BBC.

In this section, MIT–E3 predictions of the CAUMDSS behavior of overconsolidated BBC are studied. The predictions are presented to assess the degree of dependency of overconsolidated BBC on the test angle θ and the consolidation stress ratio τ_{hc}/σ'_{vc}. The section begins with a comparison of the predicted MIT–E3 response for a CK_oUDSS test on OCR=4 BBC with experimental data from Ladd and Edgers (1972) for the same type of test. This is followed by a presentation of MIT–E3 predictions of the CAUMDSS behavior of OCR=4 BBC.

6.4.1 Comparison of Experimental Results and MIT–E3 Predictions for a CK_oUDSS Test on OCR=4 BBC.

Ladd and Edgers (1972) present the results of three CK_oUDSS tests conducted on BBC at OCR = 4. The samples were loaded to a state of stress corresponding to OCR = 4 using the SHANSEP procedure (i.e., load sample to $\sigma'_{vc} \cong (1.5 - 2.0)\sigma'_p$ and then unload to OCR = 4). Figure 6.23 to 6.26 present the range of results obtained from the three tests and MIT–E3 predictions of the stress–strain curve, stress path, normalized pore pressure versus shear strain and normalized undrained modulus versus shear strain.

Figure 6.23 shows that the predicted stress–strain curve gives a maximum shear resistance which is approximately 15% higher than the experimental results. This is also shown in the stress paths plotted in Figure 6.25. While the difference in predicted and measured undrained strength is not significantly large, the shapes of the stress paths are very different. The difference in the stress paths is a result of the large deviation in the predicted and measured pore pressure data. This is clearly shown in the normalized pore pressure versus shear strain data plotted in Figure 6.24. The data show that while both the model and experimental results exhibit dilative behavior at the beginning of shear, the rate of negative pore pressure development is quite different. In addition, the model predicts that the sample will continuously dilate throughout the test. This is not the case for the experimental results which show a reversal in the development of negative pore pressure, with the pore pressure eventually becoming positive. Figure 6.26 shows excellent agreement between the measured and predicted normalized modulus versus shear strain data.

Overall, the results presented here show that the MIT–E3 model provides good to excellent predictions of undrained shear strength and undrained modulus data. This is not the case for the predicted development of pore pressure during shear. These results were presented to give some perspective of the model's capabilities to predict the direct simple shear behavior of overconsolidated BBC before presenting the results of MIT–E3 predictions of the CAUMDSS behavior of overconsolidated BBC.

6.4.2 Predicted Behavior of OCR=4 BBC as a Function of θ and τ_{hc}/σ'_{vc}

Three sets of predictions were made of the multidirectional direct simple shear behavior of OCR = 4 BBC. Based on the measured CK_oUDSS strength of approximately 0.6 (see Figure 6.23) the predictions presented here were made for consolidation stress ratios equal to the CK_oUDSS shear strength, 50% greater and 50% less (i.e. τ_{hc}/σ'_{vc} = 0.6, 0.9 and 0.3). The results are summarized in Tables 6.7 to 6.9.

Figures 6.27 to 6.30 present detailed results for $\tau_{hc}/\sigma'_{vc} = 0.6$ including stress–strain curves, stress paths, pore pressure versus shear strain curves and undrained modulus versus shear strain. Figure 6.31 to 6.33 present summary plots of $(\tau_x)_{max}/\sigma'_{vc}$, $\tau_x(\theta)_{max}/\tau_x(\theta=0^\circ)_{max}$, and the vertical effective stress ratio at $(\tau_x)_{max}$ as a function of θ for all three consolidation stress ratios.

The stress–strain curves and stress paths plotted in Figures 6.27 and 6.29 for $\tau_{hc}/\sigma'_{vc} = 0.6$ show that there is a significant variation in $(\tau_x)_{max}/\sigma'_{vc}$ as a function of θ. For all test angles, the model predicts the development of negative pore pressure throughout the tests as shown in the normalized pore pressure versus shear strain data plotted in Figure 6.28. The pore pressure data show that there is a significant dependency of the development of negative pore pressure during shear on the test angle θ. The maximum and minimum rates of pore pressure development are for $\theta = 0^\circ$ and 180°, respectively. The pore pressure data and stress paths show that as θ increases from 0° to 180°, the stress paths have a larger vertical portion from the beginning of shear (i.e., no change in vertical effective stress ≡ elastic response). In the extreme case, $\theta = 180^\circ$, the effective stress does not change until τ_x/σ'_{vc} reaches 0.2 from an initial value of –0.6. The normalized undrained modulus versus shear strain curves plotted in Figure 6.30 show that there is very little dependency on θ until γ approaches 1%, at which point the dispersion among the different curves becomes noticeably larger. Similar to normally consolidated BBC, the modulus data plot within upper and lower bounds which are the curves for $\theta = 180^\circ$ and 0° respectively.

Summary Figure 6.31 shows that there is a significant variation in $(\tau_x)_{max}/\sigma'_{vc}$ as a function of θ and τ_{hc}/σ'_{vc}. Similar to the normally consolidated results, the largest variation occurs for the highest consolidation stress ratio. For all three consolidation stress ratios the maximum and minimum values of $(\tau_x)_{max}/\sigma'_{vc}$ occur at $\theta = 0^\circ$ and 120° respectively. It is interesting to note that all three curves intersect at $\theta = 60^\circ$ and 180°. Figure 6.32 plots $\tau_x(\theta)_{max}$ normalized by $\tau_x(\theta=0^\circ)_{max}$ and shows

the dramatic changes in the maximum shear resistance as a function of θ. For example, with $\tau_{hc}/\sigma'_{vc} = 0.9$ the value of $(\tau_x)_{max}$ at $\theta = 0°$ is 4.5 times greater than the value at $\theta = 120°$. The trends in the data plotted in Figure 6.32 are very similar to those plotted for normally consolidated BBC in Figure 6.20[3]. This is shown in Figure 6.34 which plots both the NC and OCR=4 $\tau_x(\theta)_{max}/\tau_x(\theta=0°)_{max}$ predictions. Up to $\theta = 90°$, the NC and OCR = 4 normalized values of $(\tau_x)_{max}$ are identical at all three consolidation stress ratios. From $\theta = 120°$ to 180°, there is some deviation in the NC and OCR=4 data at the two higher consolidation stress ratios. However, the deviation is not very significant and in general, the results indicate that the value of $\tau_x(\theta)_{max}/\tau_x(\theta=0°)_{max}$ is independent of OCR for the same consolidation stress ratio (i.e., consolidation stress ratios equal to the same percentage of the CK_oUDSS strength at each OCR).

Figure 6.33 shows that there is also a large variation in the vertical effective stress ratio at $(\tau_x)_{max}$ as a function of θ and τ_{hc}/σ'_{vc}. For a given consolidation stress ratio, the test with $\theta = 0°$ develops the largest negative pore pressure and with $\theta = 180°$ develops the least. As the consolidation stress ratio increases the magnitude of negative pore pressure at $(\tau_x)_{max}$ increases. The only exceptions to this are for tests with $\theta = 150°$ and 180° where the pore pressure at $(\tau_x)_{max}$ is nearly independent of τ_{hc}/σ'_{vc}.

Figure 6.35 plots predictions of the shear strain at failure γ_{xf} as a function of the test angle θ at three different consolidation stress ratios for both NC and OCR=4 BBC. The OCR=4 results show that there is little variation in γ_{xf} as a function of both θ and the consolidation stress ratio. The NC results, however, display a significant variation with θ and the consolidation stress ratio. For the intermediate

---

[3]The consolidation stress ratios for the normally consolidated BBC data plotted in Figure 6.20 are also approximately equal to the CK_oUDSS shear strength, 50% greater and 50% less (i.e., $\tau_{hc}/\sigma'_{vc} = 0.2$, 0.3 and 0.1).

and high consolidation stress ratios, γ_{xf} for NC BBC is lower than that for OCR=4 BBC up to $\theta = 90°$; for $\theta \geq 120°$ the opposite occurs.

In summary, the MIT–E3 predictions of the CAUMDSS behavior of OCR = 4 BBC show that there is a significant variation in the response of the soil as a function of both the test angle θ and the consolidation stress ratio τ_{hc}/σ'_{vc}. The variation in $(\tau_x)_{max}$ displays very similar trends compared to the results for normally consolidated BBC. Furthermore, for consolidation stress ratios approximately equal to the undrained shear strength, 50% greater and 50% less, the magnitude of variation of $(\tau_x)_{max}$ is nearly identical to that predicted for normally consolidated BBC . The major difference between the predicted behavior of normally consolidated and overconsolidated BBC is in the development of pore pressure during shear and the shear strain at failure γ_{xf}. For OCR = 4 BBC the model predicts development of negative pore pressure throughout shear for all test angles and consolidation stress ratios.

6.5 MIT–E3 PREDICTIONS OF CAUMDSS BEHAVIOR OF OCR=1 HARRISON BAY SZA ARCTIC SILT

In this section, MIT–E3 predictions of the CAUMDSS behavior of normally consolidated Harrison Bay "Soft Zone Ares" (SZA) Arctic silt are studied. As outlined in Section 2.2.3, MIT conducted an extensive series of laboratory tests on this material. Figures 2.5 to 2.9 present partial results of the test program including plots of Atterberg limits, clay fraction, salt concentration, stress history profile and undrained shear strength profile. The deposit consists essentially of two layers of ML–MH clayey silts. The lower layer material has a finer grained silt fraction, higher clay content, and lower OCR and undrained shear strength. MIT–E3 predictions presented in this section are for the lower soft layer material.

6.5.1 Selection of MIT–E3 Input Parameters

The MIT–E3 input parameters for this material, listed in Table 6.2, were determined using the experimental data presented by Ayan (1985) and Yin (1985). Data from oedometer and lateral stress oedometer tests reported by Yin were used to determine seven of the parameters (e_o, λ, 2G/K, $(K_o)_{nc}$, C, n and h; Table 6.1). K_o consolidated triaxial compression and extension tests reported by Ayan (1985) were used to determine an additional six parameters (κ, ϕ'_{tc}, ϕ'_{te}, c, S_t and ω). The value of ψ_o was set equal to 100 based on the recommendations of Whittle (1987). The final input parameter γ was selected based on OCR=2 CK_oUDSS data and is explained in the following paragraph.

Table 6.2 presents a comparison of the MIT–E3 input parameters used for Boston Blue Clay and SZA Arctic silt. Variations in the selected parameters reflect differences in the behavior of the two soils. The normally consolidated value of K_o is larger for SZA Arctic silt, whereas BBC has higher values of the critical state triaxial compression and extension friction angles. SZA Arctic silt is less sensitive than BBC and this is reflected in its lower value of S_t. Larger values of κ and ω were selected for SZA Arctic silt because its small strain stiffness is less than that of BBC. SZA Arctic silt exhibits larger volumetric strains during K_o swelling and has less recoverable strains during K_o unload–reload cycles, which results in lower values of C and h respectively. No direct information is available to determine the value of γ for SZA Arctic silt (Whittle (1987) recommends using data from a CK_oUTC test at OCR = 2; Table 6.1). The final value selected was based primarily on the influence of γ on predictions of the peak undrained shear resistance of a CK_oUDSS test at OCR = 2 (comparison was made with data from Yin (1985)).

6.5.2 Comparison of Experimental Results and MIT–E3 Predictions for a CK_oUDSS Test on OCR=1 SZA Arctic Silt

Yin (1985) presents results of five CK_oUDSS tests conducted on normally consolidated SZA Arctic silt. Figures 6.36 to 6.39 present the average of the experimental results and MIT–E3 predictions of the normalized stress–strain curve, stress path, normalized pore pressure versus shear strain and normalized modulus versus shear strain.

Figure 6.36 shows that the predicted normalized stress–strain curve is nearly identical to the average curve of the experimental results (predicted and measured value of $(\tau_h/\sigma'_{vc})_{max}$ = 0.247 and 0.240 respectively). The predicted and measured shear strain at failure are equal to 7.2% and 9.6%. Figure 6.38 plots the predicted and measured stress paths which are also nearly identical. The main difference between the two paths is that the model predicts a lower vertical effective stress ratio at failure (0.655 versus 0.586 for the experimental results). This is also shown in the plot of normalized pore pressure versus shear strain (Figure 6.37) where the predicted curve lies below the curve representing the measured data. Figure 6.39 plots the normalized Young's modulus (E_u/σ'_{vc}) versus shear strain and shows very good agreement between the predicted and measured results.

Overall, the results presented here show that the MIT–E3 model provides very good predictions of the CK_oUDSS behavior of normally consolidated SZA Arctic silt. These results were presented to give some perspective of the model's ability to predict the CK_oUDSS behavior of SZA Arctic silt before presenting predictions of its CAUMDSS behavior.

6.5.3 Predicted Behavior of OCR=1 SZA Arctic Silt as a Function of θ and τ_{hc}/σ'_{vc}

Three sets of predictions were made of the Multidirectional Direct Simple Shear behavior of OCR=1 SZA Arctic silt (τ_{hc}/σ'_{vc} = 0.1 , 0.2 and 0.3). Tables 6.10 to 6.12 summarize the results. Figures 6.40 to 6.43 present detailed results for τ_{hc}/σ'_{vc}

= 0.2 including stress–strain curves, stress paths, pore pressure versus shear strain and undrained modulus versus shear strain. Figure 6.44 to 6.47 present summary plots of $(\tau_x)_{max}/\sigma'_{vc}$, $\tau_x(\theta)_{max}/\tau_x(\theta=0^\circ)_{max}$, the vertical effective stress ratio (σ'_v/σ'_{vc}) at $(\tau_x)_{max}$ and normalized modulus versus shear strain as a function of θ for all three consolidation stress ratios.

The stress–strain curves and stress paths plotted in Figures 6.40 and 6.42 for $\tau_{hc}/\sigma'_{vc} = 0.2$ show that there is a significant variation in $(\tau_x)_{max}/\sigma'_{vc}$ as a function of the test angle θ. The predicted stress–strain curves for SZA Arctic silt show that it is less brittle than BBC with $\tau_{hc}/\sigma'_{vc} = 0.2$ (Figure 6.5b; γ_x at $(\tau_x)_{max}$ for SZA Arctic silt is significantly greater than that of BBC for $\theta \leq 120^\circ$). Figure 6.41 plots the normalized pore pressure versus shear strain curves for the different θ angles and shows that SZA Arctic silt develops less pore pressure at $(\tau_x)_{max}$ than BBC (Figure 6.6b). There is very little difference in the predicted modulus versus shear strain data (Figure 6.43) among the different test angles until γ_x exceeds 0.1%. For higher values of γ, the modulus values display a gradual variation with θ and plot within upper and lower bounds which are the curves for $\theta = 180^\circ$ and 0° respectively. The modulus values for this soil are less than the predicted values for BBC (Figure 6.8b) until γ_x exceeds about 1%.

Summary Figure 6.44 shows that there is a significant variation in $(\tau_x)_{max}/\sigma'_{vc}$ as a function of θ and τ_{hc}/σ'_{vc}. Similar to the normally consolidated BBC results (Figure 6.19), the largest variation occurs for the highest consolidation stress ratio. For $\tau_{hc}/\sigma'_{vc} = 0.2$ and 0.3 the maximum and minimum values of $(\tau_x)_{max}/\sigma'_{vc}$ occur at $\theta = 0^\circ$ and 120° respectively. For $\tau_{hc}/\sigma'_{vc} = 0.1$ the maximum value of $(\tau_x)_{max}/\sigma'_{vc}$ also occurs at $\theta = 0^\circ$ with the minimum value at $\theta = 180^\circ$. Figure 6.45 plots $\tau_x(\theta)_{max}$ normalized by $\tau_x(\theta=0^\circ)_{max}$ and shows the dramatic changes in the maximum shear resistance as a function of θ. The trends in the data plotted in this figure are very similar to those for normally consolidated and OCR = 4 BBC (Figures 6.20 and 6.32

respectively).

Figure 6.46 shows that there is also a large variation in the vertical effective stress ratio at $(\tau_x)_{max}$ as a function of the consolidation stress ratio. The variation in σ'_v/σ'_{vc} at $(\tau_x)_{max}$ as a function of θ increases with an increase in the consolidation stress ratio. The trends in these results are also similar to those for normally consolidated BBC plotted in Figure 6.21.

All of the normalized modulus versus shear strain curves fall within a relatively narrow band as shown in Figure 6.47. The band is bounded at the top and bottom by curves for tests with $\tau_{hc}/\sigma'_{vc} = 0.3$ and $\theta = 180°$ and 0° respectively. All other combinations of τ_{hc}/σ'_{vc} ranging from 0.1 to 0.3 and θ ranging from 0° to 180° produce curves which lie within these bounds. The data plotted in the figure show that as τ_{hc}/σ'_{vc} increases from 0.1 to 0.3 the spread in the band containing curves for θ = 0° and 180° increases.

In summary, the MIT–E3 predictions of the CAUMDSS behavior of normally consolidated SZA Arctic silt show that there is a significant variation in the response of the soil as a function of both the consolidation stress ratio τ_{hc}/σ'_{vc} and the test angle θ. The trends in the predicted behavior as a function of τ_{hc}/σ'_{vc} and θ are very similar to that found for normally consolidated BBC.

6.6 FOUNDATION DESIGN USING MIT–E3 AND THE MDSS

The results presented in Section 6.3 showed that the MIT–E3 model provides very good to excellent predictions of the CAUMDSS behavior of normally consolidated BBC. This is particularly the case for predictions of two of the most important features of the soil's behavior for design, namely the variation in $(\tau_x)_{max}/\sigma'_{vc}$ and undrained Young's modulus with θ. Both model predictions and experimental results show that there are dramatic differences in the response of normally consolidated BBC as a function of the test angle θ (with $\tau_{hc}/\sigma'_{vc} = 0.2$). MIT–E3 predictions for

overconsolidated BBC and normally consolidated Harrison Bay SZA Arctic silt also showed significant variations in the behavior of these two soils as a function of θ and the consolidation stress ratio. The model predictions and experimental data clearly indicate that these behavioral trends must be considered when predicting the stability and deformation of an offshore Arctic gravity structure during ice loading.

Section 2.3 and Figures 2.21 and 2.23 showed the complicated state of stress within the foundation soil of an Arctic structure during ice loading. Clearly it is not possible to run an experimental test program which alone would provide ample information for design purposes. This type of geotechnical problem requires the use of numerical techniques such as the finite element method (FEM). The excellent performance of the MIT–E3 model in predicting the CAUMDSS behavior of BBC suggests that it can be used as the constitutive model in a finite element code for this problem.[4] The following steps outline a suggested procedure for assessing the foundation stability and deformation of an offshore Arctic gravity structure using the MDSS and the finite element method with MIT–E3 as its constitutive model.[5] Table 6.13 summarizes these steps in a flowchart.

(I) Site Characterization

The first task involved in the design process is to conduct a geotechnical characterization of the foundation soil at a prospective site. This should involve both in situ testing and laboratory testing of field samples. In situ tests such as the piezocone can provide important information regarding stratigraphy and spatial variation in undrained strength. The general objective of the site characterization program is to determine the stress history and basic strength–deformation–consolidation properties of a deposit. Incremental oedometer and/or constant rate of

---

[4]This is currently being done at MIT for other research purposes using the Finite Element Code ABAQUS.

[5]As pointed out in Section 6.2.2, the MIT–E3 model only applies to clays which exhibit normalized behavior.

strain consolidation tests provide an estimate of the deposit's stress history (i.e., σ'_p data) and compressibility–flow characteristics. Undrained strength–deformation properties require a program of CK_oU testing with different modes of failure to assess anisotropic behavior (e.g., CK_oUDSS and CK_oUTC/E). Depending on the nature of the soil, OCR and quality of undisturbed samples the CK_oU testing program would usually use the SHANSEP procedure as outlined in Table 2.1. The laboratory test program should also take into consideration the experimental data necessary for determining the input parameters for the MIT–E3 soil model (Table 6.1).

(II) MIT–E3 Input Parameters and Predictions

The MIT–E3 input parameters are determined using information from the laboratory test program. Once the input parameters are selected predictions of the CK_oUDSS and CAUMDSS behavior of the soil can be made. The CAUMDSS predictions should be performed for several different consolidation stress ratios (τ_{hc}/σ'_{vc}) and for θ ranging from 0° to 180°. All predictions should be conducted at an appropriate OCR determined from the stress history information in Step I and the predicted increase in the vertical consolidation stress σ'_{vc} due to gravity loads from the platform.

(III) Special CAUMDSS Experimental Test Program

On the basis of the MIT–E3 predictions conducted in Step II, several key CAUMDSS tests should be conducted on the soil to verify/adjust the model predictions. It is significant that MIT–E3 predictions for three soils (NC & OC BBC and NC SZA Arctic Silt) all lead to the same basic variation in undrained strength versus θ (Figure 6.34 for BBC and 6.45 for SZA Arctic Silt). This suggests that the MDSS test program can be "standardized" such that for all soils a predetermined number of tests be conducted at a limited number of θ angles and at the same consolidation stress ratio (computed as a percentage of the CK_oUDSS shear strength). For example, Figure 6.13 shows the experimental results and model predictions of

$(\tau_x)_{max}/\sigma'_{vc}$ for CAUMDSS tests on normally consolidated BBC with $\tau_{hc}/\sigma'_{vc} = 0.2$. Based on the model predictions plotted in Figure 6.13, it would be sufficient to run about three CAUMDSS tests (e.g. $\theta = 0°$, $60°$ and $120°$) to verify the trend and magnitude of $(\tau_x)_{max}/\sigma'_{vc}$ as a function of the test angle θ. For the particular example of NC BBC in Figure 6.13, the three experimental tests would verify that the model correctly predicts the trend in $(\tau_x)_{max}/\sigma'_{vc}$ but overpredicts the magnitude at low θ angles.. In this case it would be necessary to normalize the predictions relative to the experimental results (Figure 6.14). Once the results from the selected CAUMDSS tests verify that the model is producing acceptable predictions, then the final design process can begin using the finite element method.

(IV) Gravity Loading: Finite Element Method With MIT–E3

The behavior of most offshore Arctic structures during gravity loading can be analyzed assuming axisymmetric conditions. The initial state of stress is determined from the site characterization data. The finite element code with MIT–E3 is used to determine the state of stress and strain levels and also to compute deformations.

(V) Consolidation: Finite Element Method With MIT–E3

Consolidation analysis of the foundation soil after gravity loading requires a fully coupled analysis (i.e., pore pressure dissipation is computed considering the associated soil deformation and changes in total stress during consolidation). The finite element method with MIT–E3 can be used to solve this nonlinear consolidation problem. The degree of consolidation of the foundation soil will be a function of the estimated duration between set–down of a structure and when the horizontal ice load first becomes critical.

(VI) Ice Loading: Finite Element Method With MIT–E3

This is a three dimensional problem requiring a 3–dimensional finite element mesh to represent the geometry of the foundation soil. The initial state of stress before ice loading is taken directly from the consolidation analysis conducted in Step V. The

finite element method with MIT–E3 is used to estimate the factor of safety and especially the deformations due to application of the design ice load.

The procedure outlined in this section is very sophisticated but so are the geotechnical aspects of assessing the stability and deformation of an offshore Arctic structure. It is a complex problem necessitating the use of advanced analysis techniques. This is particularly the case in Step VI with respect to the ice loading problem. It is a three dimensional finite element problem requiring the use of a constitutive model, like MIT–E3, which can produce reliable predictions of the behavior of soils subjected to the stresses resulting from the combination of gravity and ice loads.

6.7 SUMMARY

The MIT–E3 soil model was developed at MIT (Whittle, 1987, 1989) to describe the behavior of soils with varying overconsolidation and under both monotonic and cyclic loading. The model uses a formulation which consists of three distinct parts: 1) a Perfectly Hysteretic model; 2) an Elasto–Plastic model for normally consolidated clays and 3) a Bounding Surface Plasticity model. The model requires 15 input parameters, most of which can be determined from standard laboratory tests (Table 6.1). A very detailed evaluation of the model by Whittle, (1987) found that it provides good to excellent predictions of the behavior of normally consolidated and overconsolidated resedimented Boston Blue Clay under monotonic undrained shear (e.g. TC/E, PSC/E and DSS) and undrained cyclic direct simple shear. The model also performed extremely well in predicting the pronounced effects of inherent anisotropy as measured by Directional Shear Cell (DSC) tests on BBC at OCR = 4.

In this chapter, MIT–E3 predictions of the Multidirectional Direct Simple Shear behavior of normally consolidated BBC were compared with the experimental results presented in Chapter 5. The comparisons showed satisfactory to excellent

agreement between experimental results and MIT–E3 predictions of very significant changes in soil behavior as a function of θ (=direction of ice loading). This was particularly the case for the two most important design parameters: the undrained peak shear resistance (Figures 6.13 and 6.14) and secant values of Young's modulus versus shear strain (Figure 6.18). The major variation between the model predictions and experimental results was in the post peak excess pore pressure and hence strain softening behavior of the soil. The predicted peak shear resistance for all θ angles with $\tau_{hc}/\sigma'_{vc} = 0.2$ coincided with the critical state condition and therefore the stress–strain curves were horizontal once the peak shear resistance was reached (Figure 6.5b). This was not the case for the experimental results, in particular at low θ angles (Figure 6.5a). However, the results in Chapter 5 and Appendix G indicate that a significant portion of the strain softening observed in either the DSS or MDSS devices may be caused by the apparatus. Hence the actual strain softening behavior probably lies between the measured and predicted results.

Given the very good agreement between the experimental results and MIT–E3 predictions, the model was used to predict the CAUMDSS response of BBC at different consolidation stress ratios and at OCR = 4. In both cases the model predicted dramatic changes in the behavior of BBC as a function of the test angle θ and the consolidation stress ratio τ_{hc}/σ'_{vc}. This was particularly the case for the variation of the peak shear resistance $(\tau_x)_{max}/\sigma'_{vc}$ as shown in Figures 6.19 and 6.31 for normally consolidated and overconsolidated BBC respectively (also Figure 6.34).

MIT–E3 predictions were also made for the CAUMDSS behavior of normally consolidated Harrison Bay SZA Arctic silt. The input parameters for this soil were derived from the laboratory test program conducted at MIT on samples from Harrison Bay (Table 6.2). The model predictions for Arctic silt also showed dramatic changes in its behavior as a function of θ and τ_{hc}/σ'_{vc} as is clearly shown for variations in peak strength plotted in Figures 6.44 and 6.45.

Results from the MDSS test program conducted with BBC showed that ice loading of an offshore Arctic structure leads to significant changes in soil behavior. Predicting foundation performance of these structures is very complex and require using a finite element code having a suitable soil model. The model must be capable of producing reliable predictions of the dramatic changes in soil behavior due to ice loading. Detailed comparisons presented in this chapter between the MDSS experimental results and those predicted by the MIT–E3 constitutive model found satisfactory to excellent agreement between the measured and predicted results. This suggests that the MDSS and a finite element code with MIT–E3 as its constitutive model can together be used as a reliable design tool for offshore Arctic gravity structures.

TABLE 6.1: Input Parameters for the MIT–E3 Soil Model (after Whittle, 1987).

Parameter	Role	How to Obtain
e_o	MIT-E1 NC clays	Void ratio at reference state of VCL of NC clay.
κ		Determines small strain modulus from resonant column or in situ elastic shear wave velocity.
λ		Slope of VCL in e-$\log_e\sigma'$ space from oedometer.
2G/K		From K_o swelling in lateral stress oedometer.
ϕ'_{tc}		Critical state friction angles from CK_oUC/E tests on normally consolidated clay.
ϕ'_{te}		
$(K_o)_{nc}$		Measured in lateral stress oedometer or CK_oUC/E.
c		Parametric study of undrained strength in CK_oUC/E tests.
S_t		Parametric study of sensitivity in CK_oUC/E tests.
ψ_o		Rotation rate of yield surface.
C	Perfectly Hysteretic Model	Parametric study of swelling in oedometer tests.
n		
ω		Estimate stiffness at small strains in CK_oUC for overconsolidated clay.
γ	Bounding Surface Plasticity	Parametric study of CK_oUC test at OCR = 2.
h		Parametric study of unload reload cycles in hydrostatic or oedometer tests.

TABLE 6.2: MIT–E3 Input Parameters for Boston Blue Clay and Harrison Bay SZA Arctic Silt.

Parameter	BBC	Arctic Silt
e_o	1.12	1.33
κ	0.001	0.0035
λ	0.184	0.201
2G/K	1.05	0.89
ϕ'_{tc}	33.4°	29.2°
ϕ'_{te}	45.9°	33.0°
$(K_o)_{nc}$	0.48	0.59
c	0.866	0.866
S_t	4.5	2.0
ϕ_o	100.0	100.0
C	22.0	5.0
n	1.60	1.5
ω	0.07	1.0
γ	0.5	5.0
h	0.2	0.01

TABLE 6.3: MIT–E3 Predictions of CAUDSS Behavior of Normally Consolidated BBC

Test Angle θ (°)	τ_{hc}/σ'_{vc}	At τ_h Maximum		
		γ_x (%)	τ_h/σ'_{vc}	σ_v'/σ'_{vc}
CK_oU	0	3.02	0.209	0.618
0	0.2	0.96	0.311	0.815
0	0.1	1.72	0.247	0.708
180	-0.1	5.02	0.191	0.555
180	-0.2	12.02	0.203	0.522

TABLE 6.4: MIT–E3 Predictions of CAUMDSS Behavior of Normally Consolidated BBC With $\tau_{hc}/\sigma'_{vc} = 0.1$.

Test Angle θ (°)	τ_{hc}/σ'_{vc}		At τ_x Maximum							
	X	Y	γ_x (%)	γ_y (%)	γ_t (%)	$\frac{\tau_x}{\sigma'_{vc}}$	$\frac{\tau_y}{\sigma'_{vc}}$	$\frac{\tau_t}{\sigma'_{vc}}$	$\frac{\tau_x(\theta)}{\tau_x(\theta=0°)}$	$\frac{\sigma'_v}{\sigma'_{vc}}$
0	0.100	0	1.72	0	1.72	0.247	0	0.247	1.0	0.708
30	0.087	0.050	1.81	0.16	1.82	0.239	0.050	0.244	0.968	0.700
60	0.050	0.087	2.00	0.31	2.02	0.220	0.087	0.236	0.891	0.685
90	0	0.100	2.77	0.51	2.82	0.201	0.100	0.224	0.814	0.639
120	-0.050	0.087	3.97	0.65	4.02	0.190	0.087	0.209	0.769	0.590
150	-0.087	0.050	4.80	0.44	4.82	0.190	0.050	0.196	0.769	0.562
180	-0.100	0	5.02	0	5.02	0.191	0	0.191	0.773	0.555

Notes:

1. See Figure 3.1 for definitions of θ, γ_x, γ_y, τ_x and τ_y.
2. $\gamma_t = \left(\gamma_x^2 + \gamma_y^2\right)^{1/2}$.
3. $\tau_t = \left(\tau_x^2 + \tau_y^2\right)^{1/2}$.

TABLE 6.5: MIT–E3 Predictions of CAUNDSS Behavior of Normally Consolidated BBC With $\tau_{hc}/\sigma'_{vc} = 0.2$.

Test Angle θ (°)	τ_{hc}/σ'_{vc}		At τ_x Maximum							
	X	Y	γ_x (%)	γ_y(%)	γ_t (%)	$\frac{\tau_x}{\sigma'_{vc}}$	$\frac{\tau_y}{\sigma'_{vc}}$	$\frac{\tau_t}{\sigma'_{vc}}$	$\frac{\tau_x(\theta)}{\tau_x(\theta=0°)}$	$\frac{\sigma'_v}{\sigma'_{vc}}$
0	0.200	0	0.96	0	0.96	0.311	0	0.311	1.0	0.815
30	0.173	0.100	1.07	0.16	1.08	0.290	0.100	0.307	0.932	0.804
60	0.100	0.173	1.42	0.40	1.48	0.234	0.173	0.291	0.752	0.770
90	0	0.200	2.66	0.93	2.82	0.178	0.200	0.268	0.572	0.693
120	-0.100	0.173	7.43	2.44	7.82	0.158	0.173	0.234	0.508	0.606
150	-0.173	0.100	11.84	2.04	12.01	0.185	0.100	0.210	0.595	0.539
180	-0.200	0	12.02	0	12.02	0.203	0	0.203	0.653	0.522

Notes:

1. See Figure 3.1 for definitions of θ, γ_x, γ_y, τ_x and τ_y.
2. $\gamma_t = \left(\gamma_x^2 + \gamma_y^2\right)^{1/2}$.
3. $\tau_t = \left(\tau_x^2 + \tau_y^2\right)^{1/2}$.

TABLE 6.6: MIT–E3 Predictions of CAUMDSS Behavior of Normally Consolidated BBC With $\tau_{hc}/\sigma'_{vc} = 0.3$.

Test Angle θ (°)	τ_{hc}/σ'_{vc}		At τ_x Maximum							
	X	Y	γ_x (%)	γ_y (%)	γ_t (%)	$\frac{\tau_x}{\sigma'_{vc}}$	$\frac{\tau_y}{\sigma'_{vc}}$	$\frac{\tau_t}{\sigma'_{vc}}$	$\frac{\tau_x(\theta)}{\tau_x(\theta=0°)}$	$\frac{\sigma'_v}{\sigma'_{vc}}$
0	0.300	0	0.32	0	0.32	0.372	0	0.372	1.0	0.940
30	0.260	0.150	0.38	0.05	0.38	0.337	0.150	0.369	0.906	0.932
60	0.150	0.260	0.62	0.16	0.64	0.246	0.260	0.358	0.661	0.904
90	0	0.300	1.38	0.52	1.48	0.142	0.300	0.332	0.382	0.837
120	-0.150	0.260	18.96	7.03	20.22	0.103	0.260	0.279	0.277	0.708
150	-0.260	0.150	21.06	3.89	21.42	0.179	0.150	0.233	0.481	0.591
180	-0.300	0	22.02	0	22.02	0.225	0	0.225	0.605	0.570

Notes:

1. See Figure 3.1 for definitions of θ, γ_x, γ_y, τ_x and τ_y.
2. $\gamma_t = \left(\gamma_x^2 + \gamma_y^2\right)^{1/2}$.
3. $\tau_t = \left(\tau_x^2 + \tau_y^2\right)^{1/2}$.

TABLE 6.7: MIT–E3 Predictions of CAUMDSS Behavior of OCR = 4 BBC With $\tau_{hc}/\sigma'_{vc} = 0.3$.

Test Angle θ (°)	τ_{hc}/σ'_{vc}		At τ_x Maximum							
	X	Y	γ_x (%)	γ_y (%)	γ_t (%)	$\frac{\tau_x}{\sigma'_{vc}}$	$\frac{\tau_y}{\sigma'_{vc}}$	$\frac{\tau_t}{\sigma'_{vc}}$	$\frac{\tau_x(\theta)}{\tau_x(\theta=0°)}$	$\frac{\sigma'_v}{\sigma'_{vc}}$
0	0.300	0	5.62	0	5.62	0.810	0	0.810	1.0	1.746
30	0.260	0.150	5.59	0.59	5.62	0.785	0.150	0.799	0.969	1.714
60	0.150	0.260	5.52	1.00	5.61	0.722	0.260	0.768	0.891	1.625
90	0	0.300	5.49	1.11	5.60	0.655	0.300	0.720	0.809	1.497
120	-0.150	0.260	5.73	0.90	5.80	0.618	0.260	0.670	0.763	1.374
150	-0.260	0.150	6.20	0.49	6.22	0.621	0.150	0.639	0.767	1.296
180	-0.300	0	6.62	0	6.62	0.630	0	0.630	0.778	1.278

Notes:

1. See Figure 3.1 for definitions of θ, γ_x, γ_y, τ_x and τ_y.
2. $\gamma_t = \left(\gamma_x^2 + \gamma_y^2\right)^{1/2}$.
3. $\tau_t = \left(\tau_x^2 + \tau_y^2\right)^{1/2}$.

TABLE 6.8: MIT–E3 Predictions of CAUMDSS Behavior of OCR = 4 BBC With $\tau_{hc}/\sigma'_{vc} = 0.6$.

Test Angle θ (°)	τ_{hc}/σ'_{vc}		At τ_x Maximum							
	X	Y	γ_x (%)	γ_y (%)	γ_t (%)	$\frac{\tau_x}{\sigma'_{vc}}$	$\frac{\tau_y}{\sigma'_{vc}}$	$\frac{\tau_t}{\sigma'_{vc}}$	$\frac{\tau_x(\theta)}{\tau_x(\theta=0°)}$	$\frac{\sigma'_v}{\sigma'_{vc}}$
0	0.600	0	4.22	0	4.22	0.970	0	0.970	1.0	2.094
30	0.520	0.300	4.32	0.94	4.42	0.904	0.300	0.953	0.932	2.035
60	0.300	0.520	4.26	1.74	4.60	0.742	0.520	0.906	0.765	1.898
90	0	0.600	4.29	2.08	4.77	0.560	0.600	0.821	0.577	1.680
120	-0.300	0.520	4.66	1.63	4.94	0.459	0.520	0.694	0.473	1.395
150	-0.520	0.300	6.92	1.01	6.99	0.526	0.300	0.605	0.542	1.242
180	-0.600	0	8.42	0	8.42	0.598	0	0.598	0.616	1.215

Notes:

1. See Figure 3.1 for definitions of θ, γ_x, γ_y, τ_x and τ_y.
2. $\gamma_t = (\gamma_x^2 + \gamma_y^2)^{1/2}$.
3. $\tau_t = (\tau_x^2 + \tau_y^2)^{1/2}$.

TABLE 6.9: MIT–E3 Predictions of CAUMDSS Behavior of OCR = 4 BBC With $\tau_{hc}/\sigma'_{vc} = 0.9$.

Test Angle θ (°)	τ_{hc}/σ'_{vc}		At τ_x Maximum							
	X	Y	γ_x (%)	γ_y (%)	γ_t (%)	$\frac{\tau_x}{\sigma'_{vc}}$	$\frac{\tau_y}{\sigma'_{vc}}$	$\frac{\tau_t}{\sigma'_{vc}}$	$\frac{\tau_x(\theta)}{\tau_x(\theta=0°)}$	$\frac{\sigma'_v}{\sigma'_{vc}}$
0	0.900	0	3.62	0	3.62	1.119	0	1.119	1.0	2.249
30	0.780	0.450	3.42	1.18	3.62	1.016	0.450	1.111	0.908	2.223
60	0.450	0.780	2.95	2.08	3.61	0.747	0.780	1.079	0.668	2.136
90	0	0.900	2.89	2.72	3.97	0.431	0.900	0.998	0.385	1.983
120	-0.450	0.780	2.45	3.65	4.40	0.247	0.780	0.817	0.221	1.582
150	-0.780	0.450	6.97	1.49	7.13	0.387	0.450	0.593	0.346	1.220
180	-0.900	0	7.42	0	7.42	0.589	0	0.589	0.526	1.115

Notes:

1. See Figure 3.1 for definitions of θ, γ_x, γ_y, τ_x and τ_y.
2. $\gamma_t = (\gamma_x^2 + \gamma_y^2)^{1/2}$.
3. $\tau_t = (\tau_x^2 + \tau_y^2)^{1/2}$.

TABLE 6.10: MIT–E3 Predictions of CAUMDSS Behavior of OCR = 1 Harrison Bay SZA Arctic Silt With $\tau_{hc}/\sigma'_{vc} = 0.1$.

Test Angle θ (°)	τ_{hc}/σ'_{vc}		At τ_x Maximum							
	X	Y	γ_x (%)	γ_y(%)	γ_t (%)	$\frac{\tau_x}{\sigma'_{vc}}$	$\frac{\tau_y}{\sigma'_{vc}}$	$\frac{\tau_t}{\sigma'_{vc}}$	$\frac{\tau_x(\theta)}{\tau_x(\theta=0°)}$	$\frac{\sigma'_v}{\sigma'_{vc}}$
0	0.100	0	5.62	0	5.62	0.280	0	0.280	1.0	0.720
30	0.087	0.050	5.80	0.43	5.82	0.273	0.050	0.278	0.975	0.714
60	0.050	0.087	6.36	0.84	6.42	0.256	0.087	0.270	0.914	0.696
90	0	0.100	7.13	1.10	7.21	0.238	0.100	0.258	0.850	0.671
120	-0.050	0.087	8.14	1.11	8.22	0.227	0.087	0.243	0.811	0.641
150	-0.087	0.050	8.79	0.69	8.82	0.224	0.050	0.230	0.800	0.622
180	-0.100	0	9.02	0	9.02	0.223	0	0.223	0.796	0.616

Notes:

1. See Figure 3.1 for definitions of θ, γ_x, γ_y, τ_x and τ_y.
2. $\gamma_t = (\gamma_x^2 + \gamma_y^2)^{1/2}$.
3. $\tau_t = (\tau_x^2 + \tau_y^2)^{1/2}$.

TABLE 6.11: MIT–E3 Predictions of CAUMDSS Behavior of OCR = 1 Harrison Bay SZA Arctic Silt With $\tau_{hc}/\sigma'_{vc} = 0.2$.

Test Angle θ (°)	τ_{hc}/σ'_{vc}		At τ_x Maximum							
	X	Y	γ_x (%)	γ_y (%)	γ_t (%)	$\frac{\tau_x}{\sigma'_{vc}}$	$\frac{\tau_y}{\sigma'_{vc}}$	$\frac{\tau_t}{\sigma'_{vc}}$	$\frac{\tau_x(\theta)}{\tau_x(\theta=0°)}$	$\frac{\sigma'_v}{\sigma'_{vc}}$
0	0.200	0	5.82	0	5.82	0.329	0	0.329	1.0	0.822
30	0.173	0.100	6.18	0.73	6.22	0.310	0.100	0.326	0.942	0.813
60	0.100	0.173	7.64	1.67	7.82	0.263	0.173	0.315	0.799	0.785
90	0	0.200	10.62	2.90	11.01	0.216	0.200	0.294	0.657	0.730
120	-0.100	0.173	11.08	2.73	11.41	0.199	0.173	0.264	0.605	0.659
150	-0.173	0.100	10.91	1.48	11.01	0.207	0.100	0.230	0.629	0.623
180	-0.200	0	11.22	0	11.22	0.213	0	0.213	0.647	0.612

Notes:

1. See Figure 3.1 for definitions of θ, γ_x, γ_y, τ_x and τ_y.
2. $\gamma_t = \left(\gamma_x^2 + \gamma_y^2\right)^{1/2}$.
3. $\tau_t = \left(\tau_x^2 + \tau_y^2\right)^{1/2}$.

TABLE 6.12: MIT–E3 Predictions of CAUMDSS Behavior of OCR = 1 Harrison Bay SZA Arctic Silt With $\tau_{hc}/\sigma'_{vc} = 0.3$.

Test Angle θ (°)	τ_{hc}/σ'_{vc}		At τ_x Maximum							
	X	Y	γ_x (%)	γ_y (%)	γ_t (%)	$\frac{\tau_x}{\sigma'_{vc}}$	$\frac{\tau_y}{\sigma'_{vc}}$	$\frac{\tau_t}{\sigma'_{vc}}$	$\frac{\tau_x(\theta)}{\tau_x(\theta=0°)}$	$\frac{\sigma'_v}{\sigma'_{vc}}$
0	0.300	0	0.94	0	0.94	0.378	0	0.378	1.0	0.948
30	0.260	0.150	1.09	0.11	1.10	0.345	0.150	0.376	0.913	0.941
60	0.150	0.260	1.78	0.36	1.82	0.258	0.260	0.367	0.683	0.916
90	0	0.300	3.85	1.12	4.01	0.166	0.300	0.343	0.439	0.856
120	-0.150	0.260	11.60	3.14	12.02	0.150	0.260	0.300	0.397	0.747
150	-0.260	0.150	11.91	1.61	12.02	0.205	0.150	0.254	0.542	0.686
180	-0.300	0	12.02	0	12.02	0.226	0	0.269	0.598	0.684

Notes:

1. See Figure 3.1 for definitions of θ, γ_x, γ_y, τ_x and τ_y.
2. $\gamma_t = (\gamma_x^2 + \gamma_y^2)^{1/2}$.
3. $\tau_t = (\tau_x^2 + \tau_y^2)^{1/2}$.

TABLE 6.13: Suggested Procedure for Foundation Design of Offshore Arctic Gravity Structures Using MIT–E3 Soil Model and the MDSS.

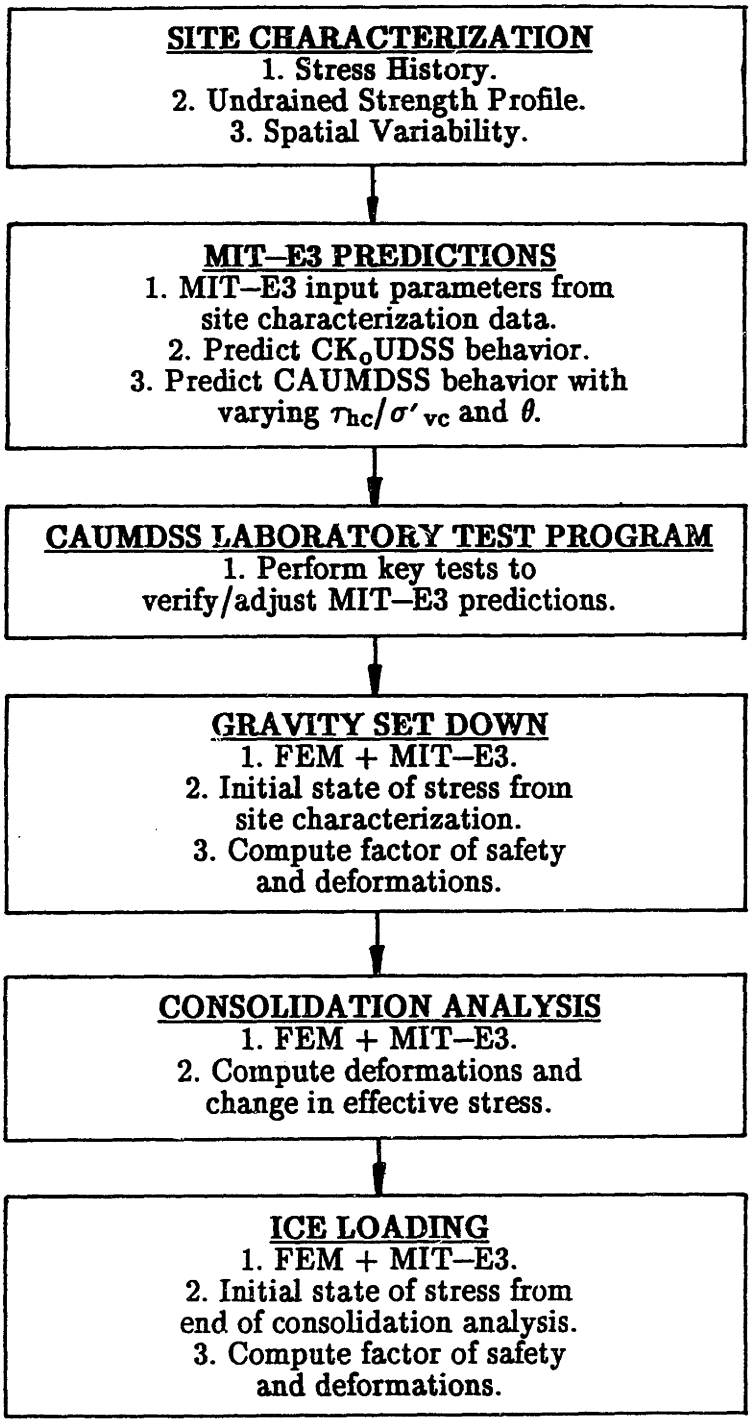

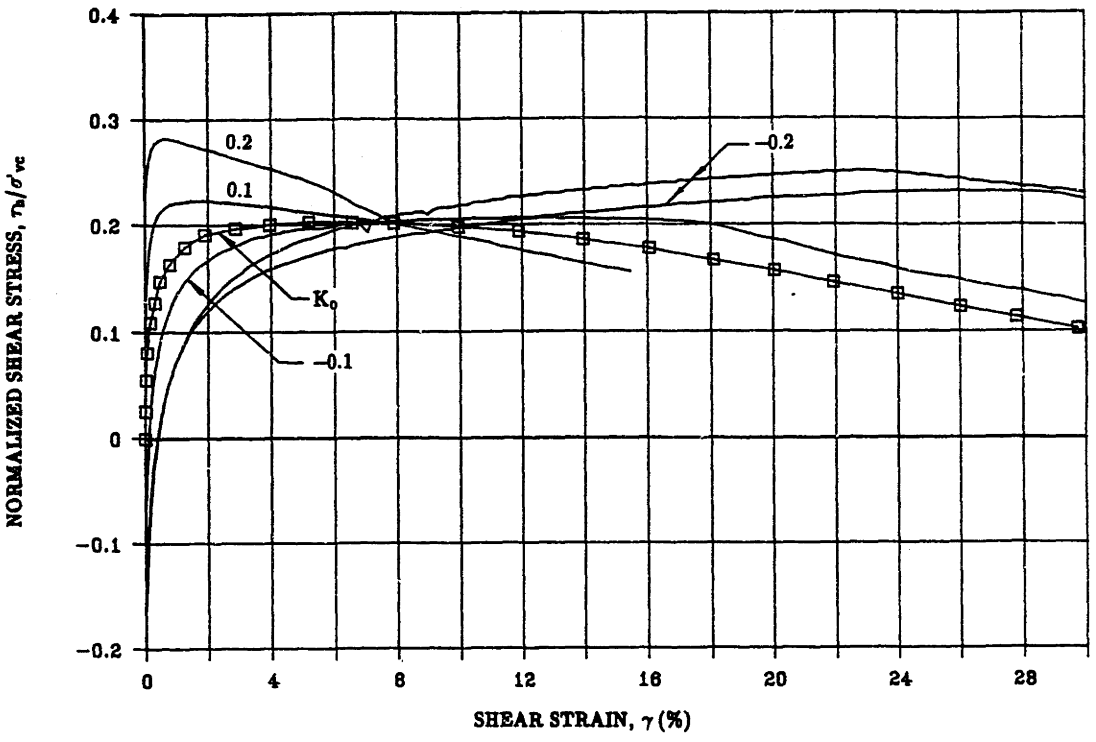

(a)

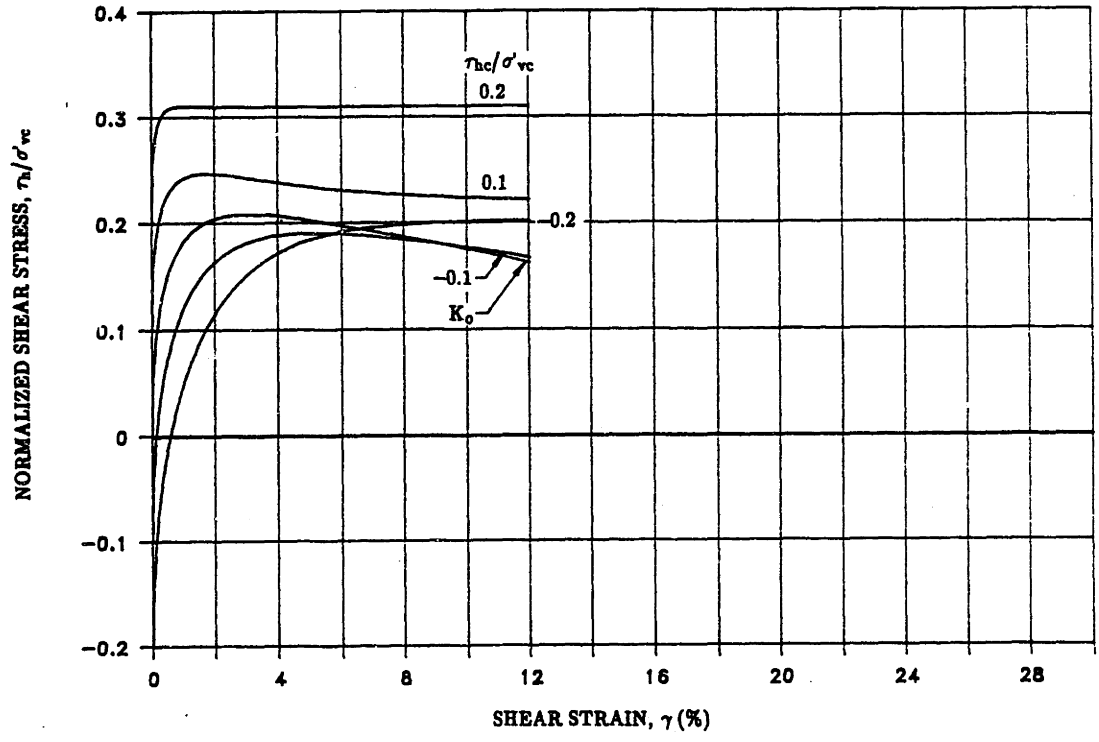

(b)

Figure 6.1: Shear Stress–Strain Curves for CAUDSS Behavior of BBC: (a) Experimental Results; (b) MIT–E3 Predictions.

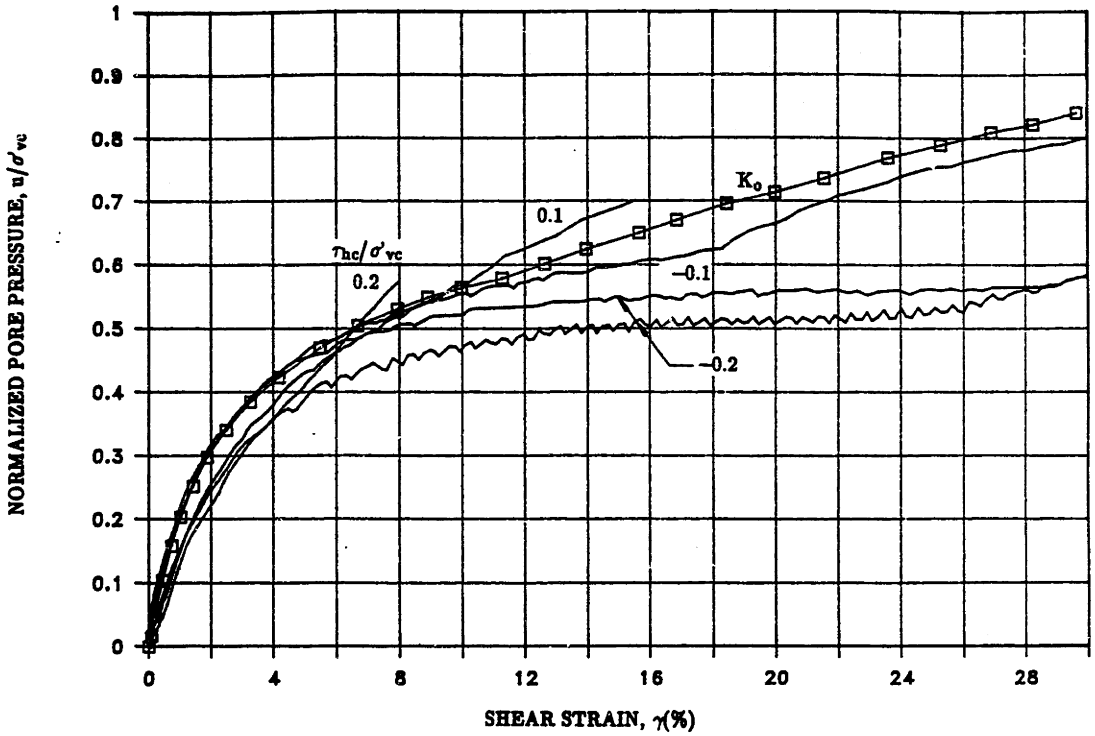

(a)

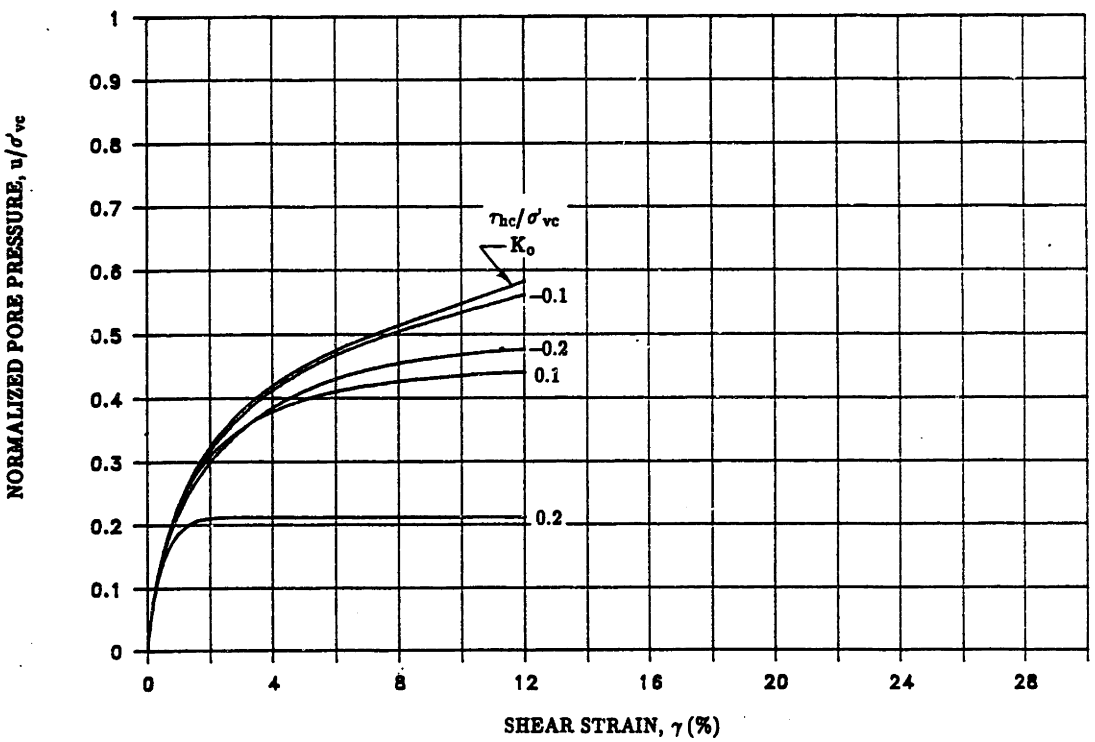

(b)

Figure 6.2: Pore Pressure Versus Shear Strain for CAUDSS Behavior of BBC: (a) Experimental Results; (b) MIT–E3 Predictions.

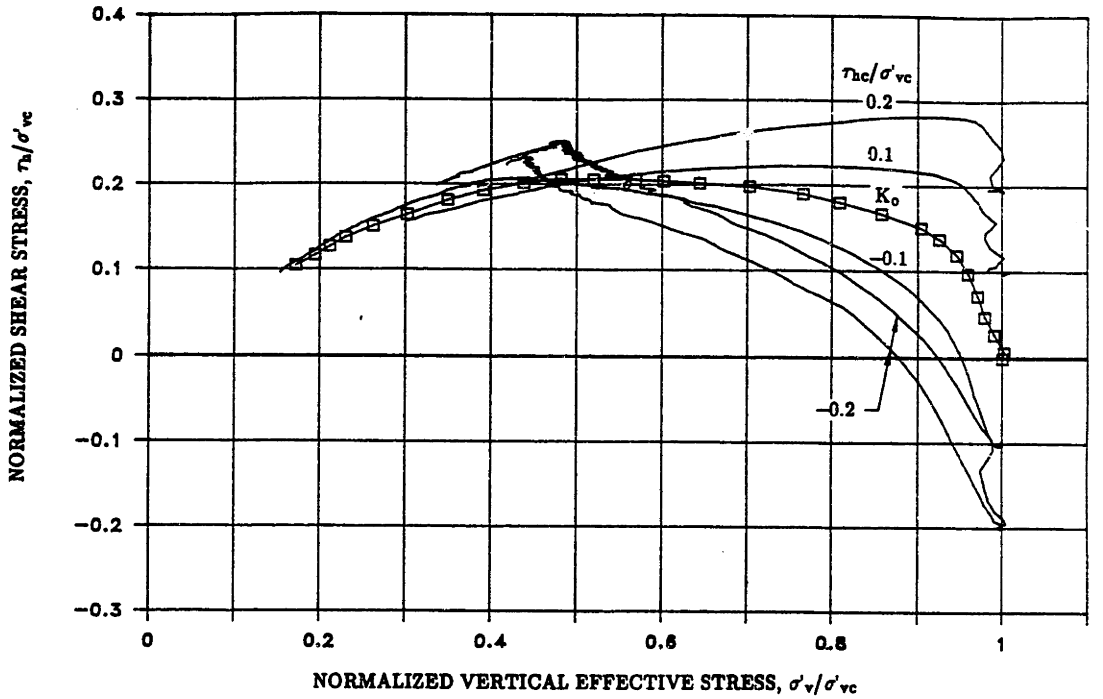

(a)

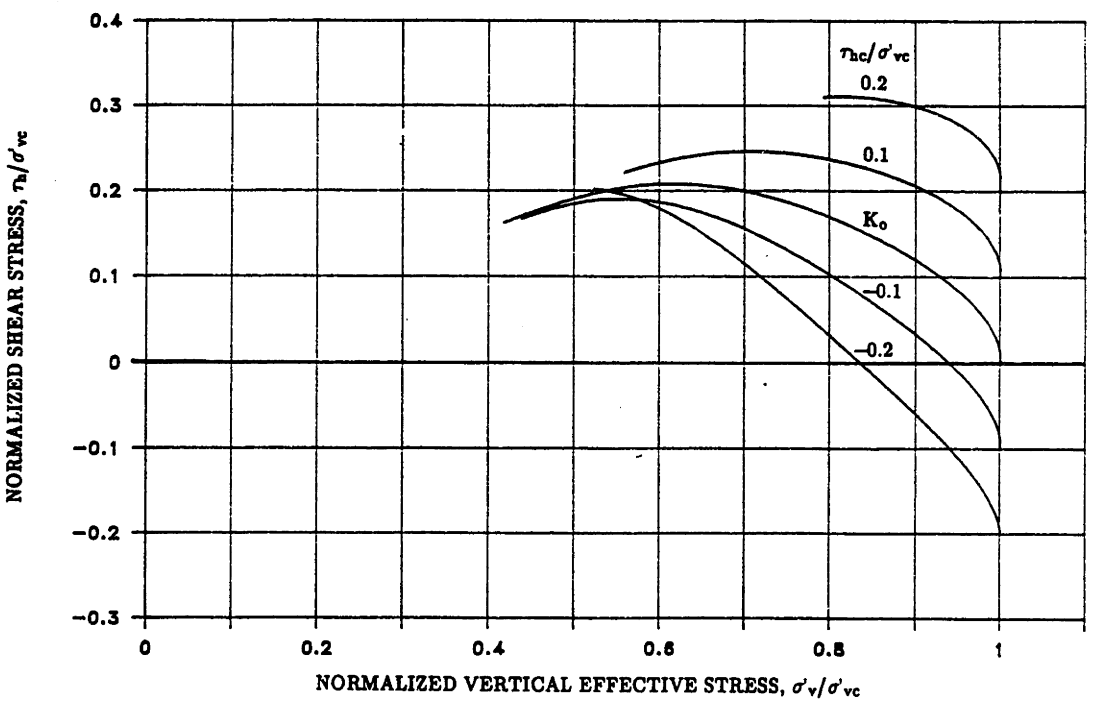

(b)

Figure 6.3: Stress Paths for CAUDSS Behavior of BBC: (a) Experimental Results; (b) MIT–E3 Predictions.

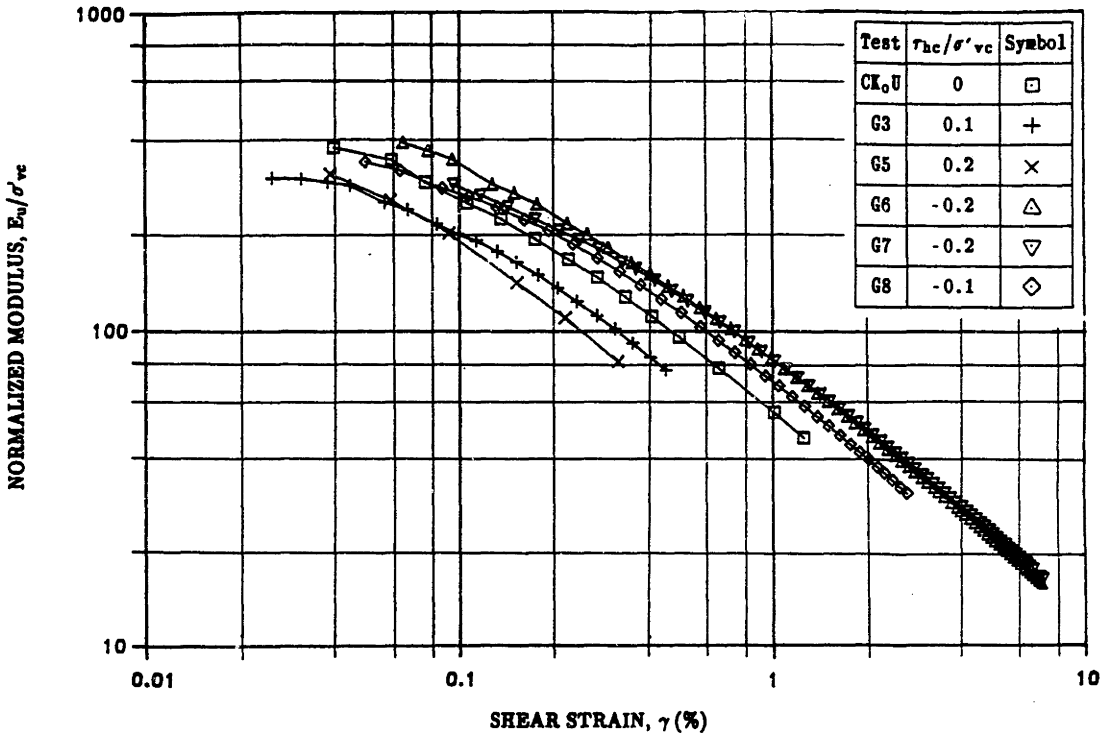

(a)

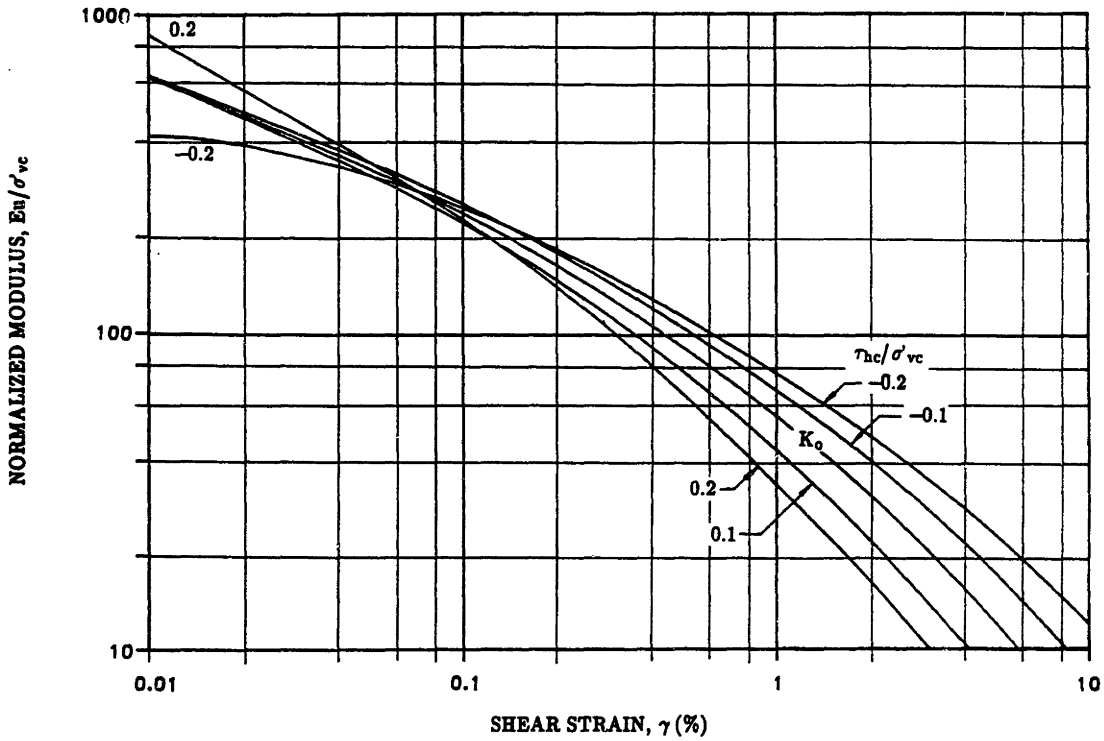

(b)

Figure 6.4: Normalized Modulus Curves for CAUDSS Behavior of BBC: (a) Experimental Results; (b) MIT–E3 Predictions.

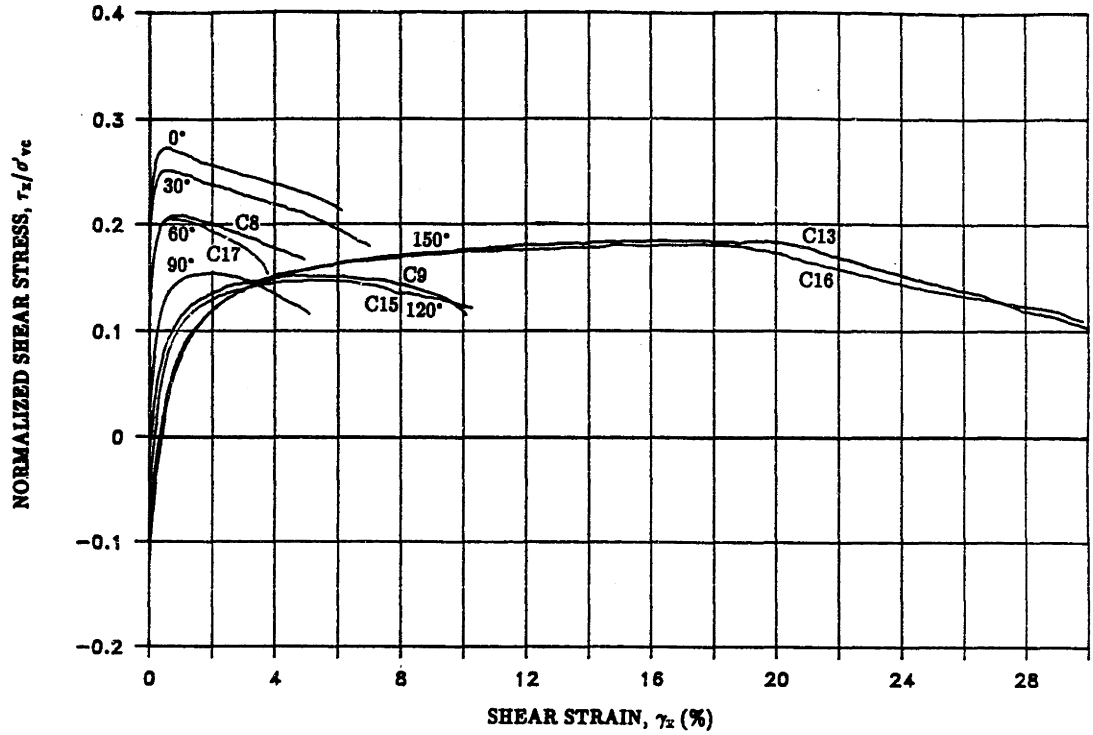

(a)

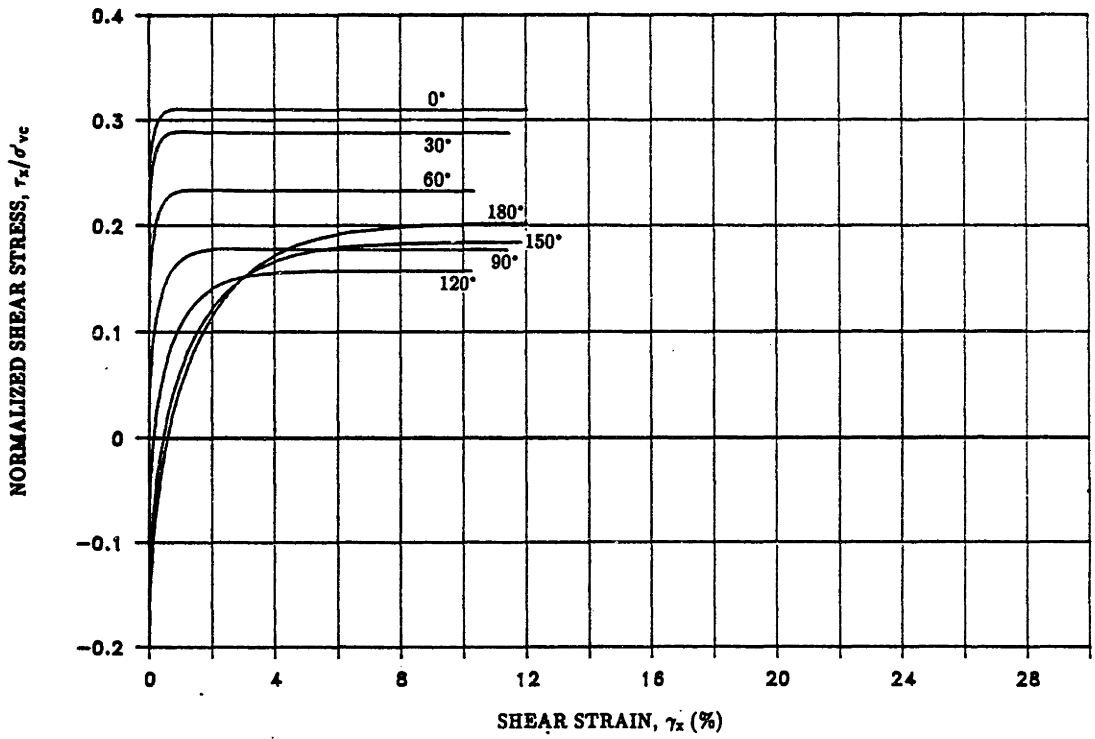

(b)

Figure 6.5: Shear Stress–Strain Curves for CAUMDSS Behavior of BBC With $\tau_{hc}/\sigma'_{vc} = 0.2$: (a) Experimental Results; (b) MIT–E3 Predictions.

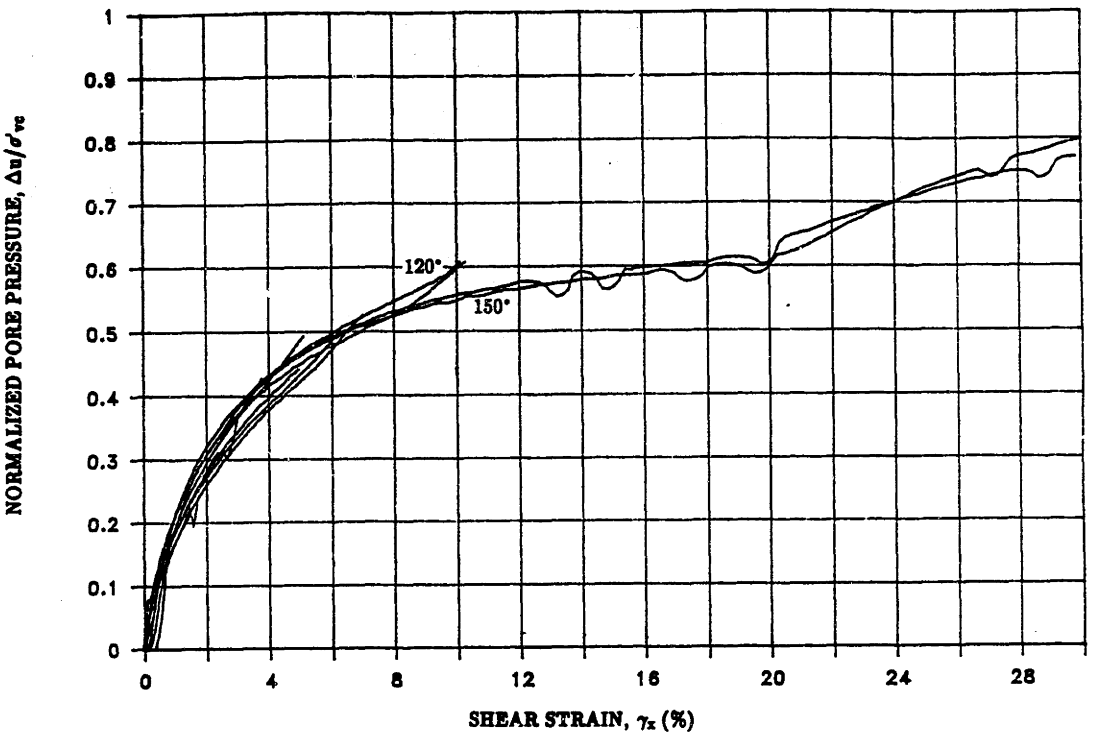

(a)

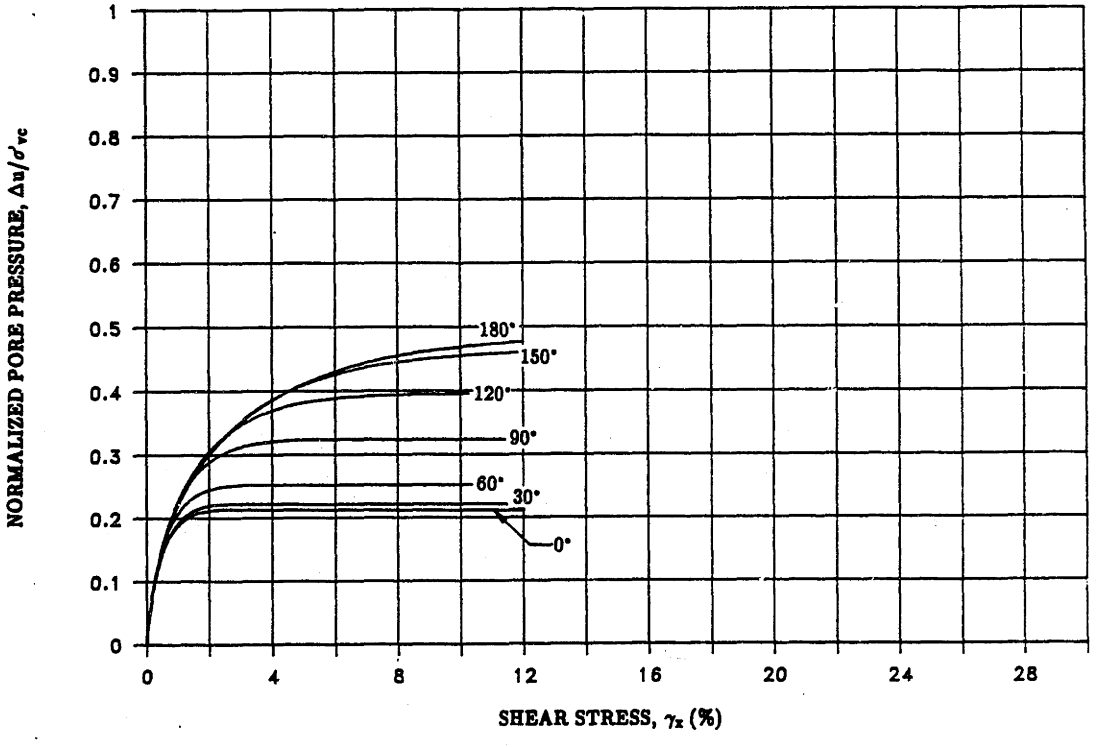

(b)

Figure 6.6: Pore Pressure versus Shear Strain Curves for CAUMDSS Behavior of BBC with $\tau_{hc}/\sigma'_{vc} = 0.2$: (a) Experimental Results; (b) MIT–E3 Predictions.

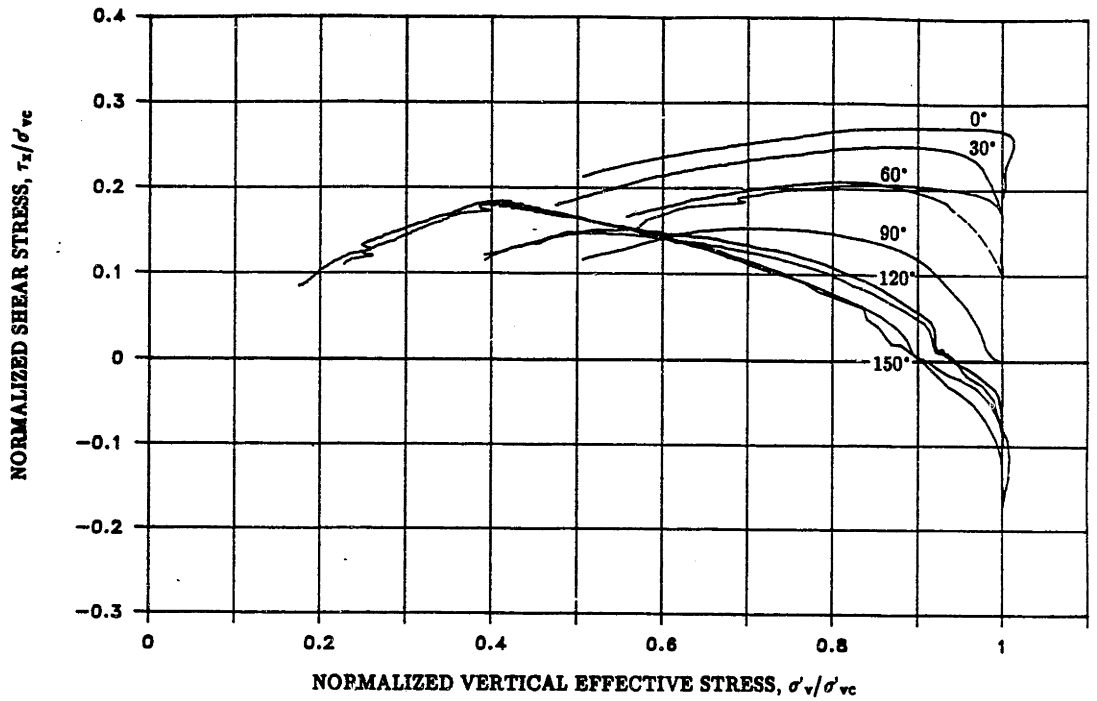

(a)

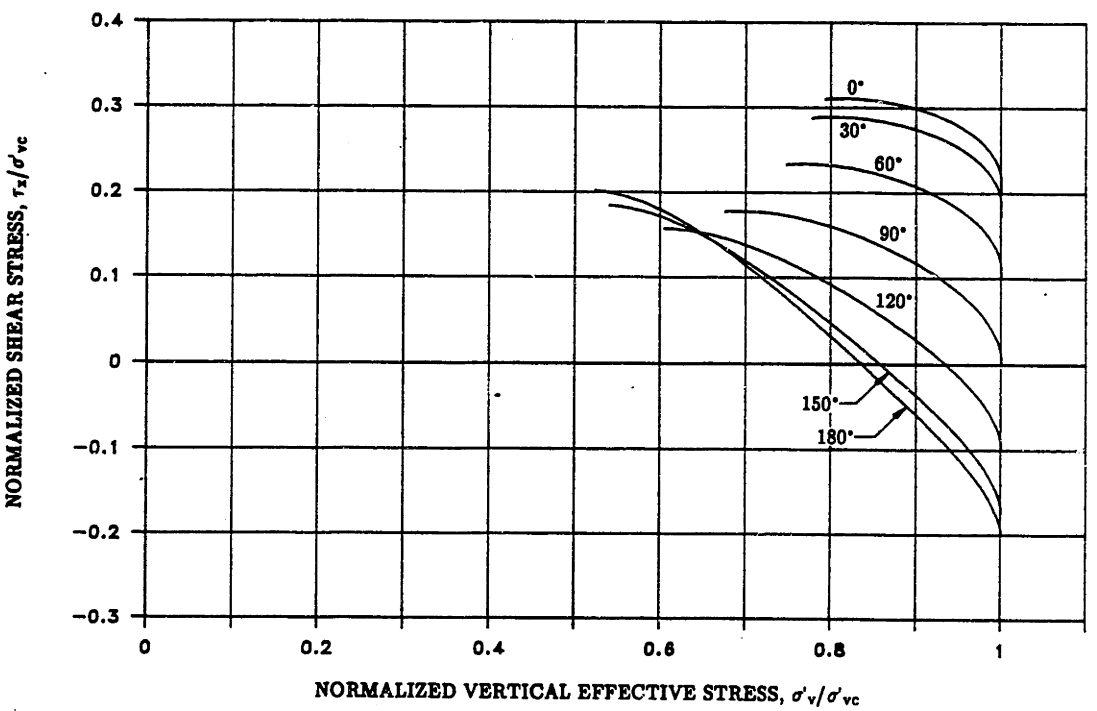

(b)

Figure 6.7: Stress Paths for CAUMDSS Behavior of BBC With $\tau_{hc}/\sigma'_{vc} = 0.2$: (a) Experimental Results; (b) MIT–E3 Predictions.

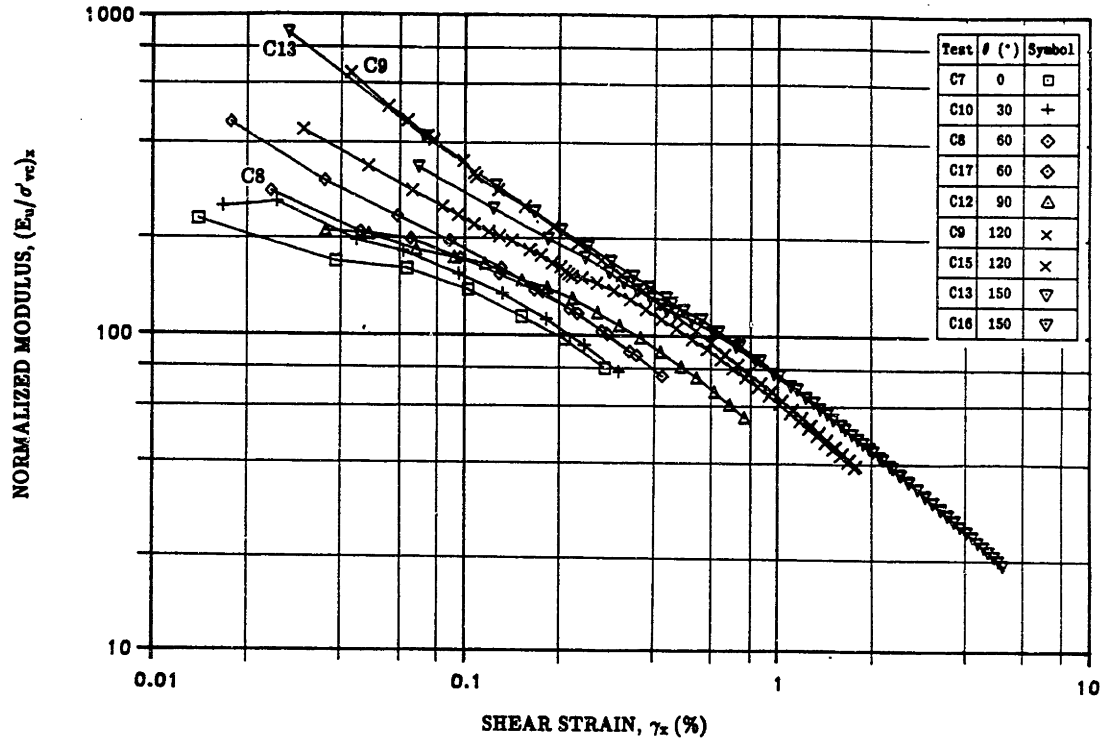

(a)

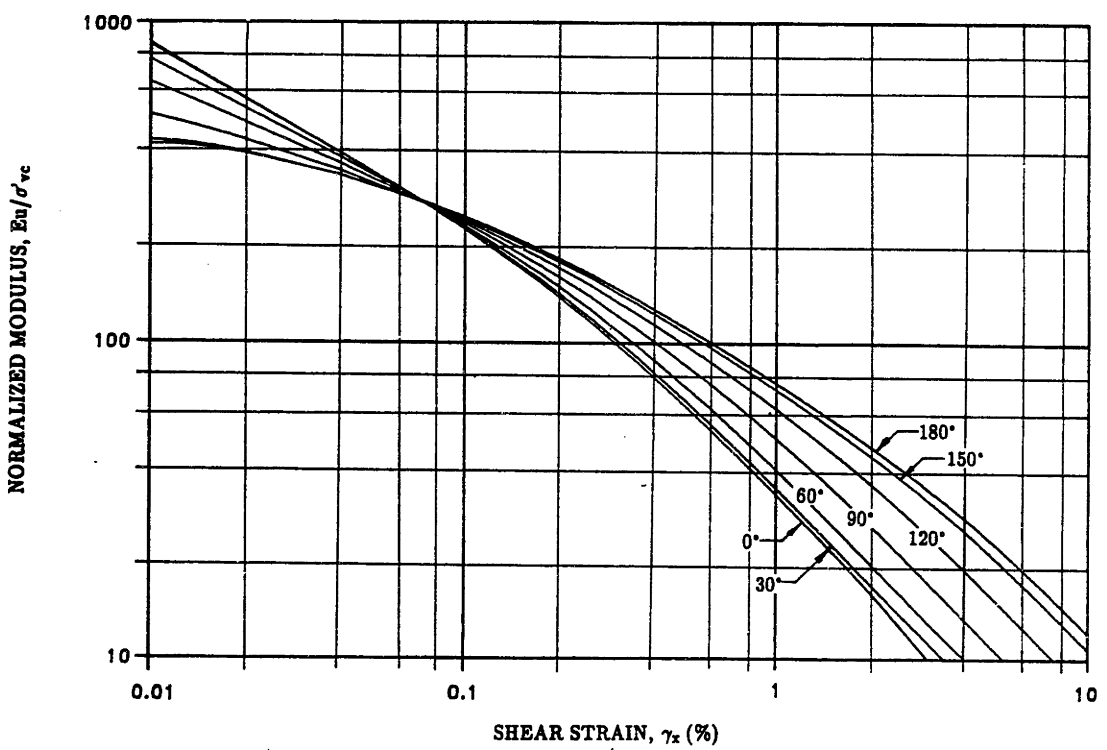

(b)

Figure 6.8: Normalized Modulus Curves for CAUMDSS Behavior of BBC With $\tau_{hc}/\sigma'_{vc} = 0.2$: (a) Experimental Results; (b) MIT–E3 Predictions.

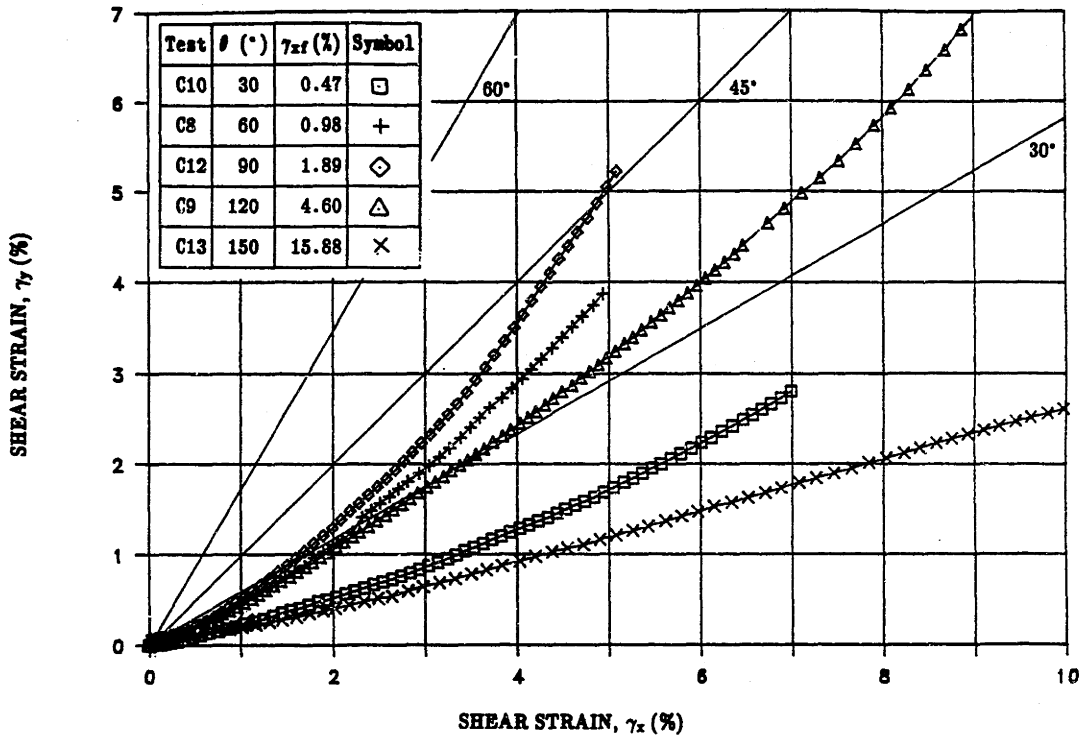

(a)

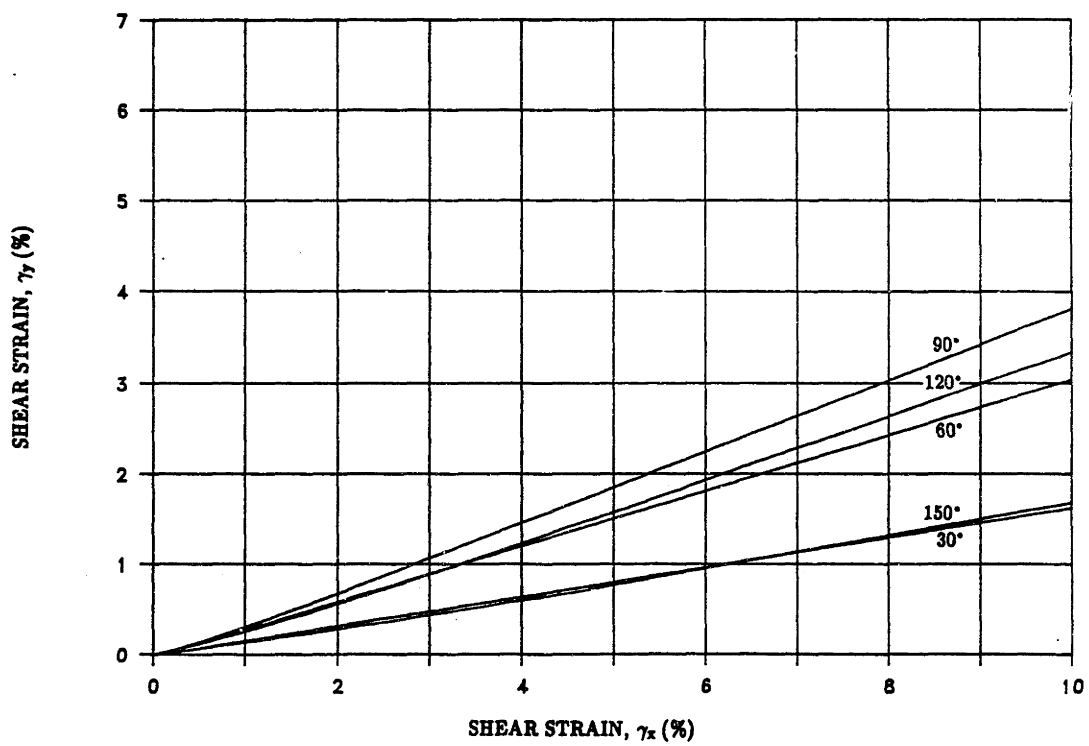

(b)

Figure 6.9: Shear Strain Paths for CAUMDSS Behavior of BBC With $\tau_{hc}/\sigma'_{vc} = 0.2$: (a) Experimental Results; (b) MIT–E3 Predictions.

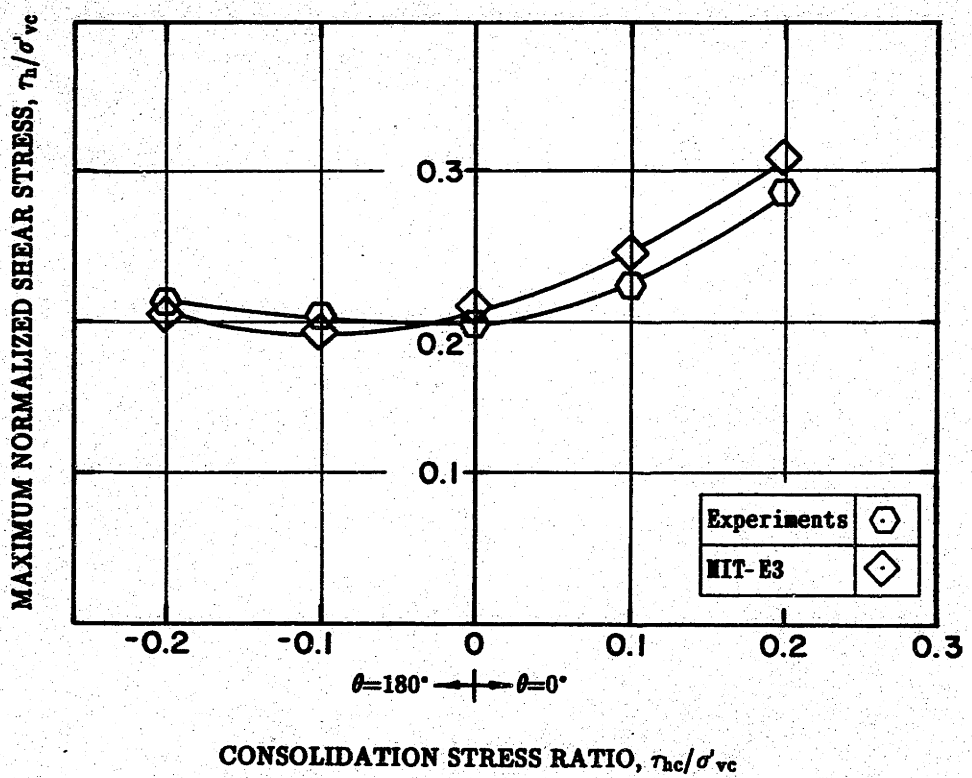

Figure 6.10: Measured and Predicted Peak Shear Resistance Versus Consolidation Stress Ratio for CAUDSS Behavior of BBC.

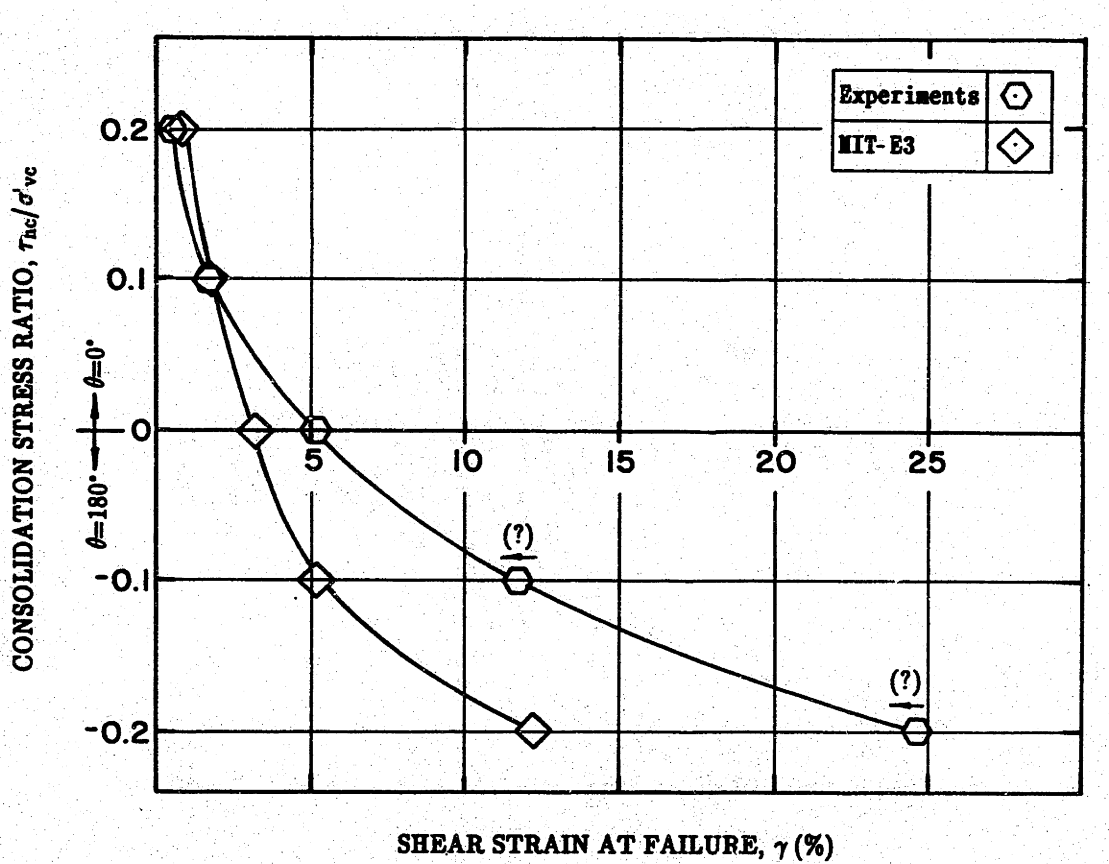

Figure 6.11: Measured and Predicted Shear Strain at Failure Versus Consolidation Stress Ratio for CAUDSS Behavior of BBC.

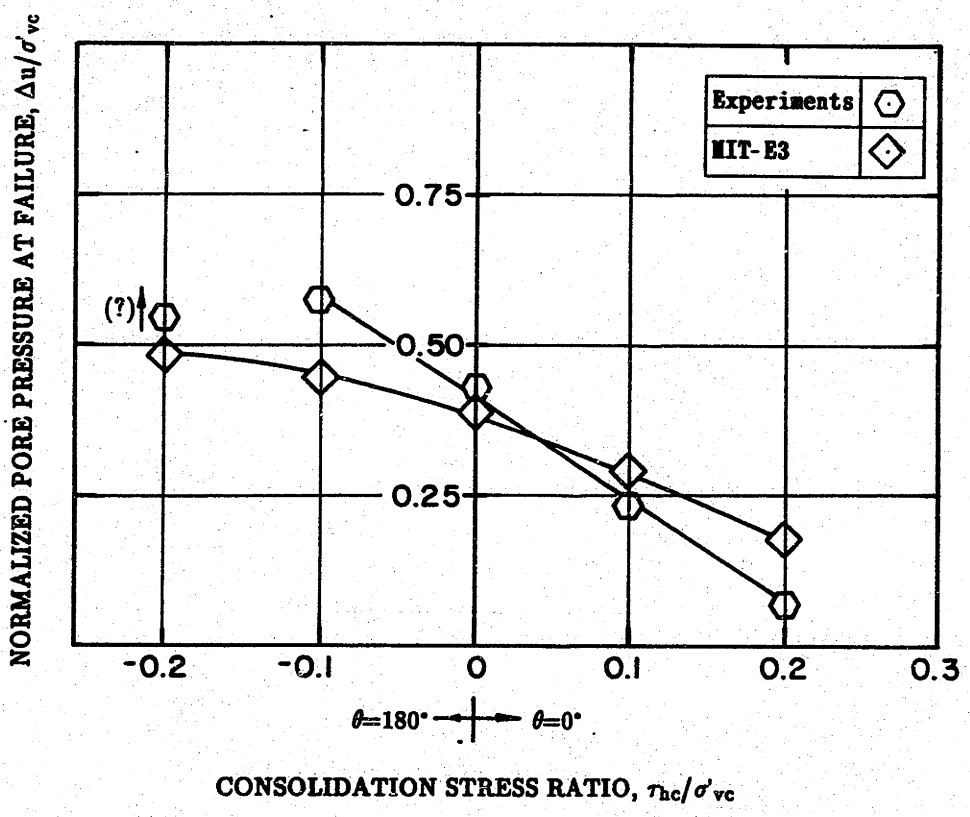

Figure 6.12: Measured and Predicted Pore Pressure at Failure Versus Consolidation Stress Ratio for CAUDSS Behavior of BBC.

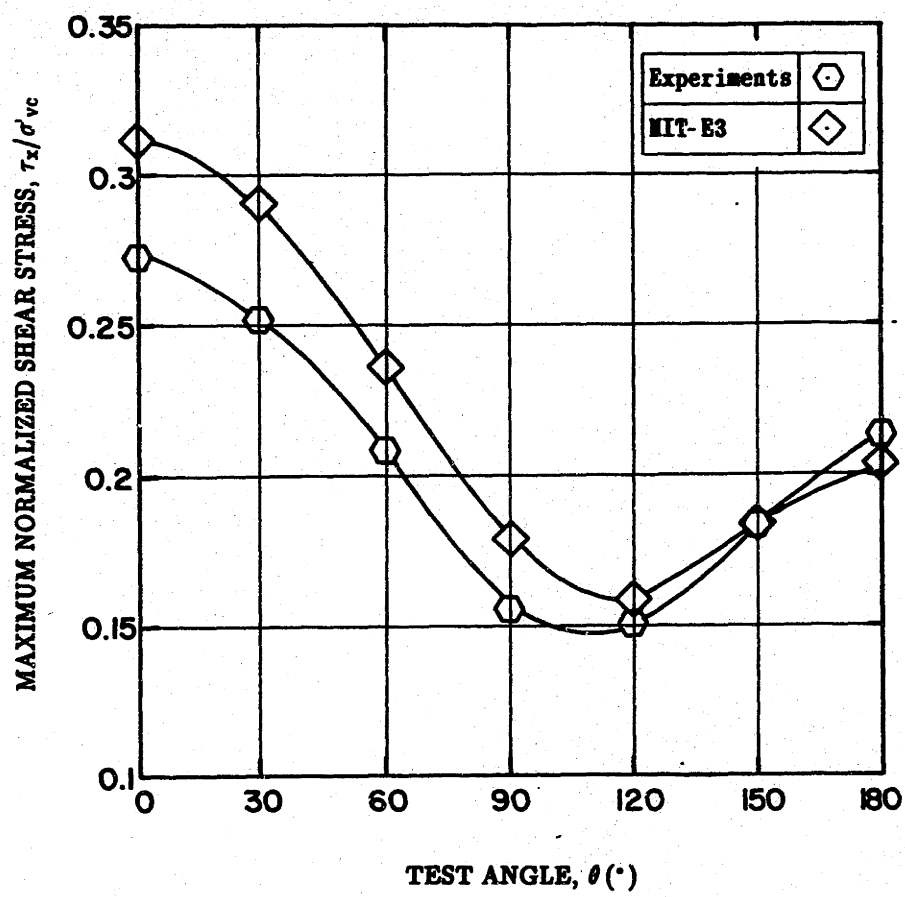

Figure 6.13: Measured and Predicted Maximum Shear Resistance τ_x/σ'_{vc} Versus Test Angle θ for CAUMDSS Behavior of BBC With $\tau_{hc}/\sigma'_{vc} = 0.2$.

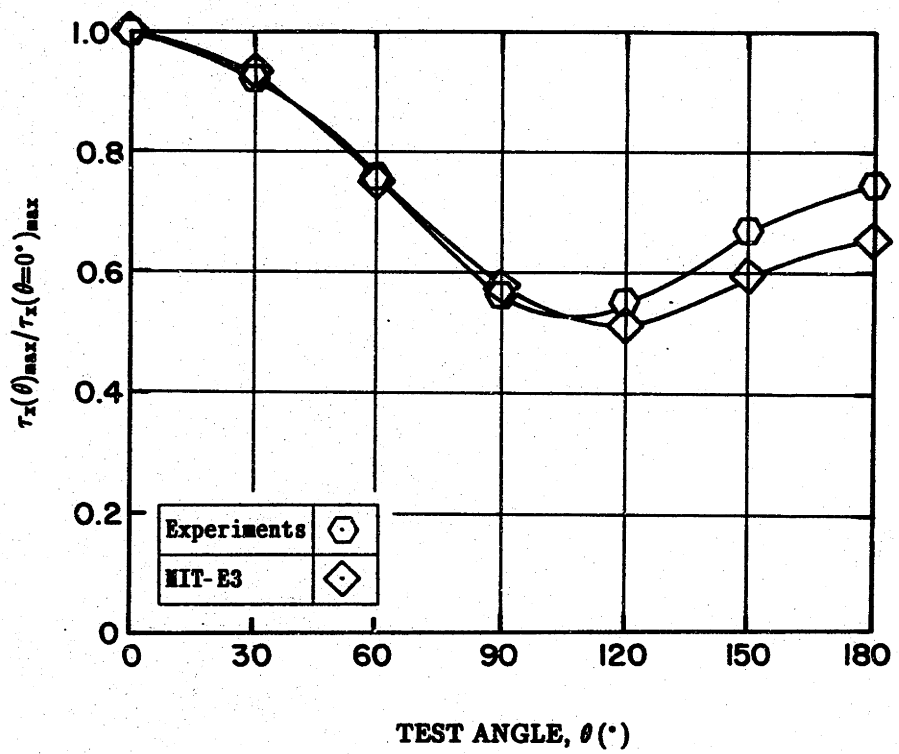

Figure 6.14: Measured and Predicted $\tau_x(\theta)_{max}/\tau_x(\theta=0^\circ)_{max}$ Versus Test Angle θ for CAUMDSS Behavior of BBC With $\tau_{hc}/\sigma'_{vc} = 0.2$.

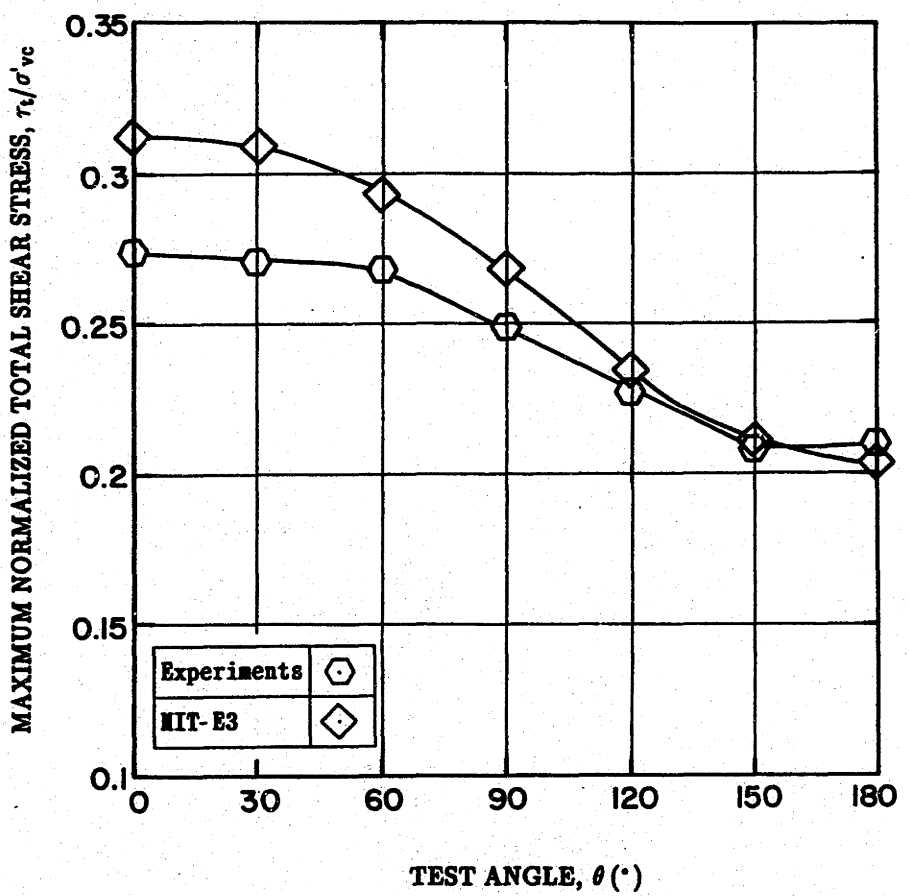

Figure 6.15: Measured and Predicted Maximum Total Shear Resistance τ_t/σ'_{vc} Versus Test Angle θ for CAUMDSS Behavior of BBC With $\tau_{hc}/\sigma'_{vc} = 0.2$.

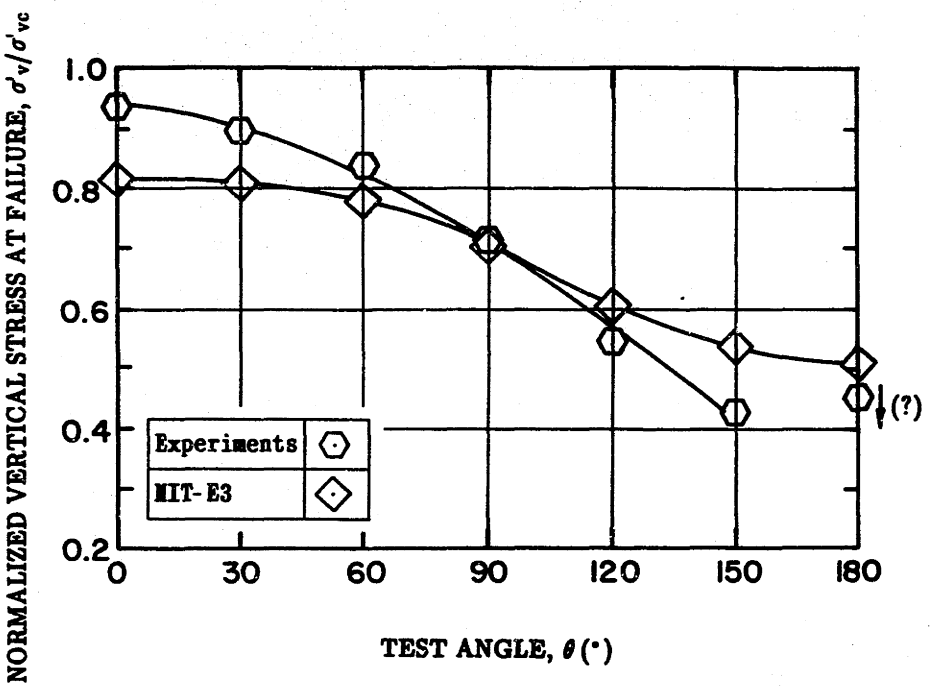

Figure 6.16: Measured and Predicted Vertical Effective Stress Ratio at Failure Versus Test Angle θ for CAUMDSS Behavior of BBC With $\tau_{hc}/\sigma'_{vc} = 0.2$.

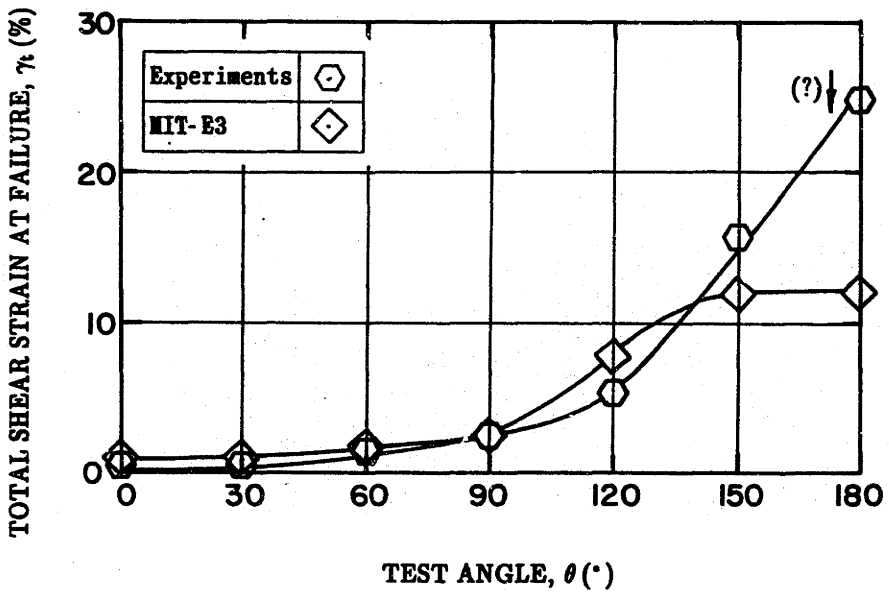

Figure 6.17: Measured and Predicted Total Shear Strain at Failure Versus Test Angle θ for CAUMDSS Behavior of BBC With $\tau_{hc}/\sigma'_{vc} = 0.2$.

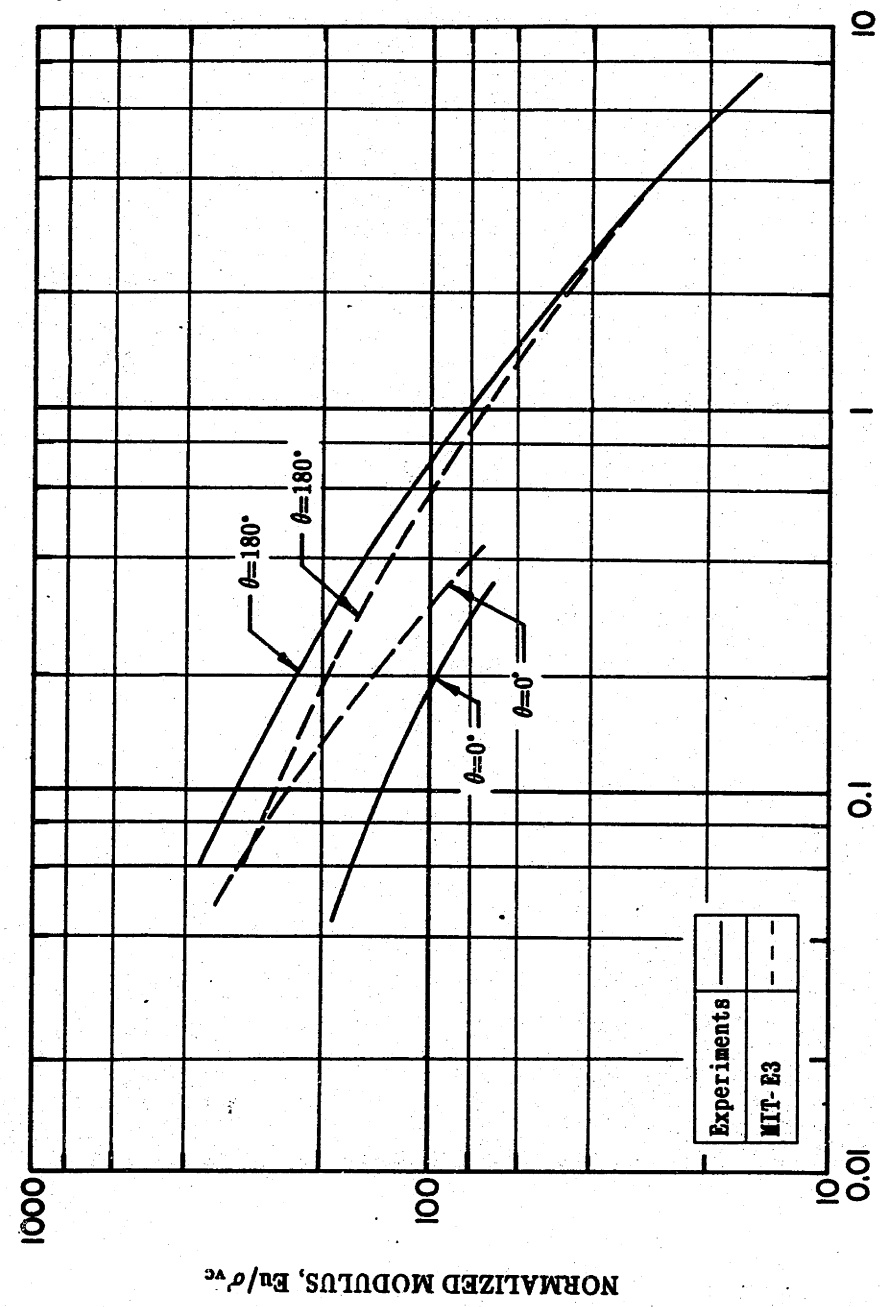

Figure 6.18: Measured and Predicted Normalized Modulus Curves as a Function of θ for CAUMDSS Behavior of BBC With $\tau_{hc}/\sigma'_{vc} = 0.2$.

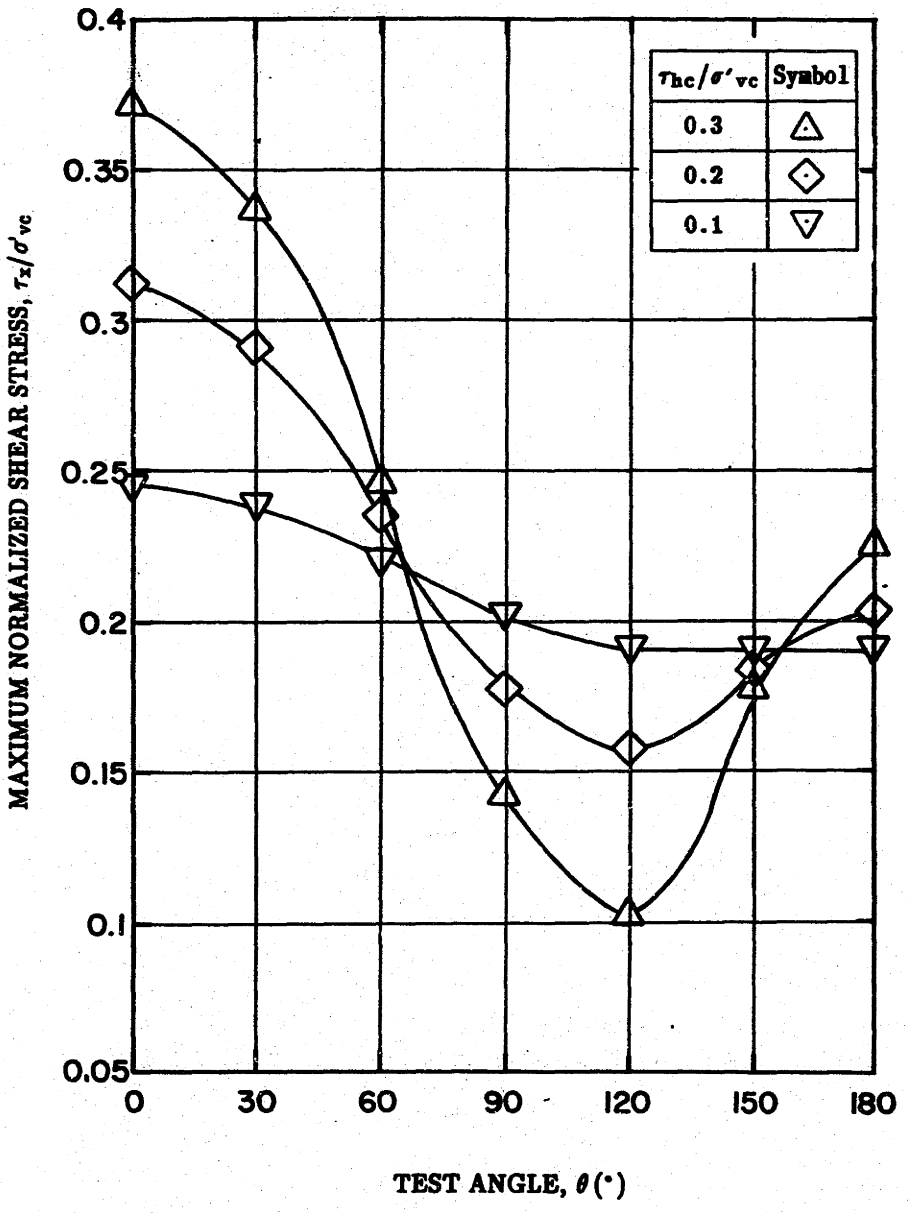

Figure 6.19: MIT–E3 Predictions of Maximum Shear Stress τ_x/σ'_{vc} Versus Test Angle θ for CAUMDSS Behavior of OCR=1 BBC.

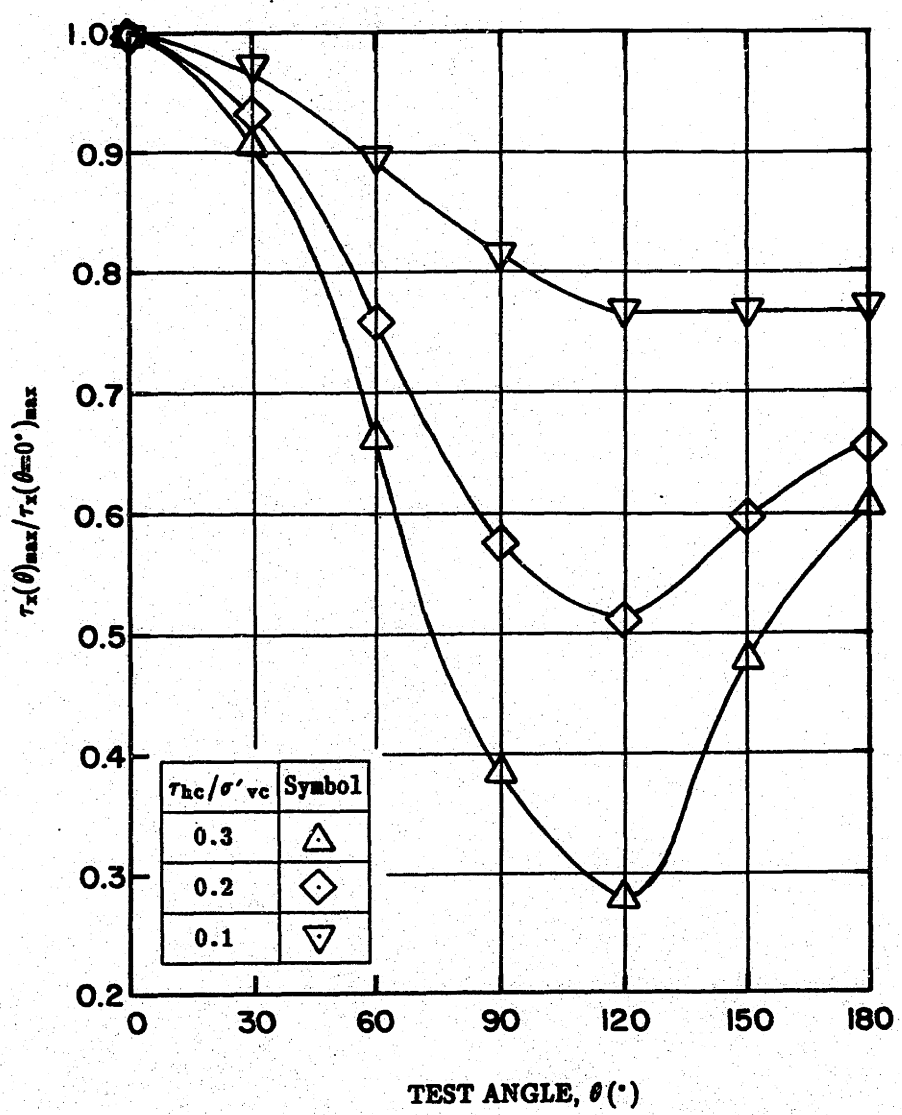

Figure 6.20: MIT–E3 Predictions of $\tau_x(\theta)_{max}/\tau_x(\theta=0^\circ)_{max}$ Versus Test Angle θ for CAUMDSS Behavior of OCR=1 BBC.

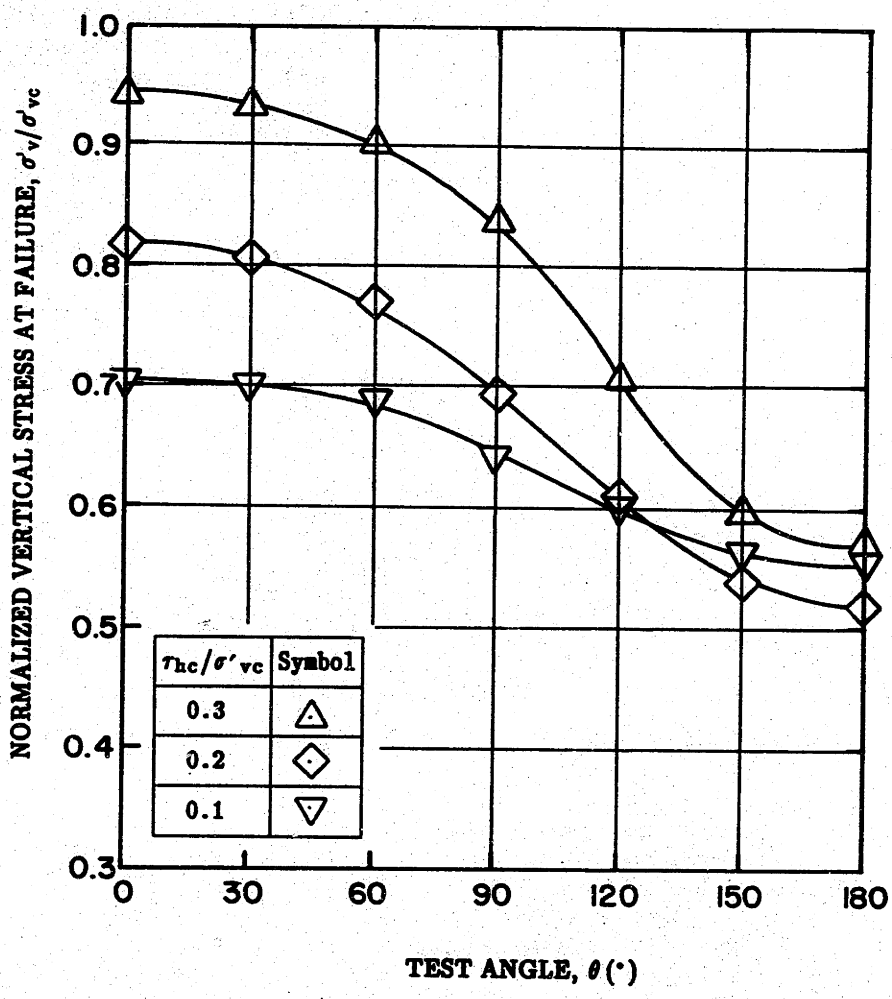

Figure 6.21: MIT–E3 Predictions of Vertical Effective Stress Ratio at Failure Versus Test Angle θ for CAUMDSS Behavior of OCR=1 BBC.

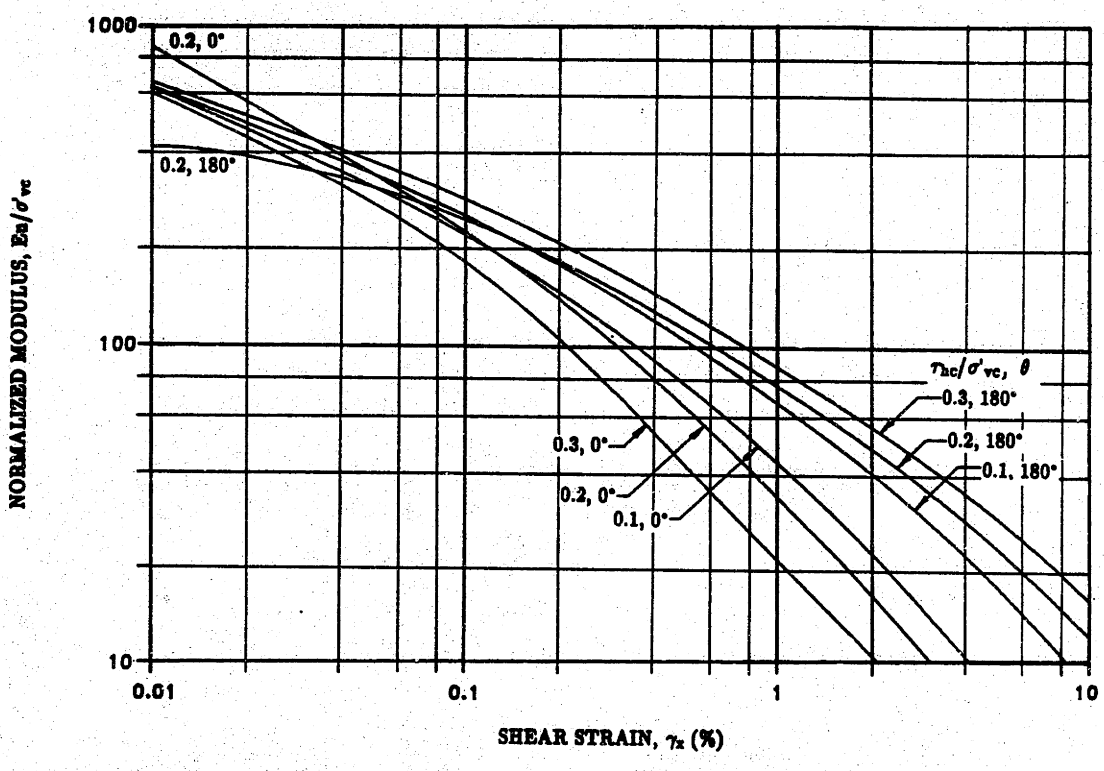

Figure 6.22: MIT–E3 Predictions of Normalized Modulus Curves as a Function of θ and τ_{hc}/σ'_{vc} for CAUMDSS Behavior of OCR=1 BBC.

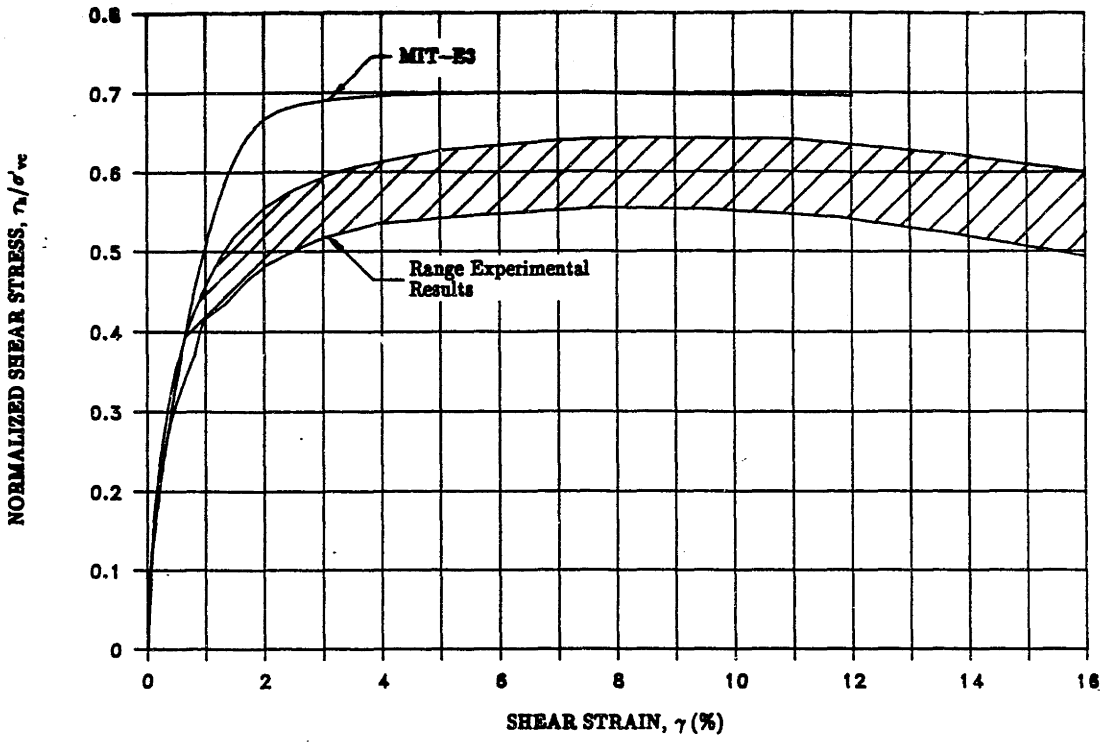

Figure 6.23: Measured and Predicted Shear Stress–Strain Curves for CK_0UDSS Test on OCR=4 BBC.

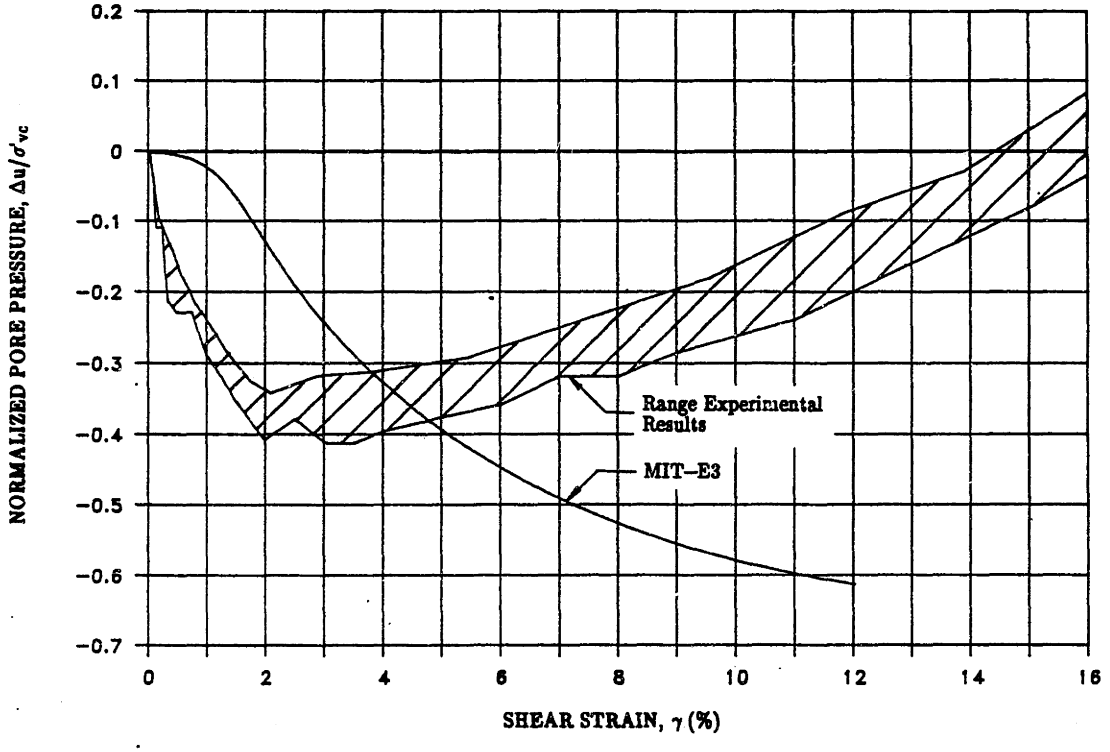

Figure 6.24: Measured and Predicted Pore Pressure versus Shear Strain Curves for CK_0UDSS Test on OCR=4 BBC.

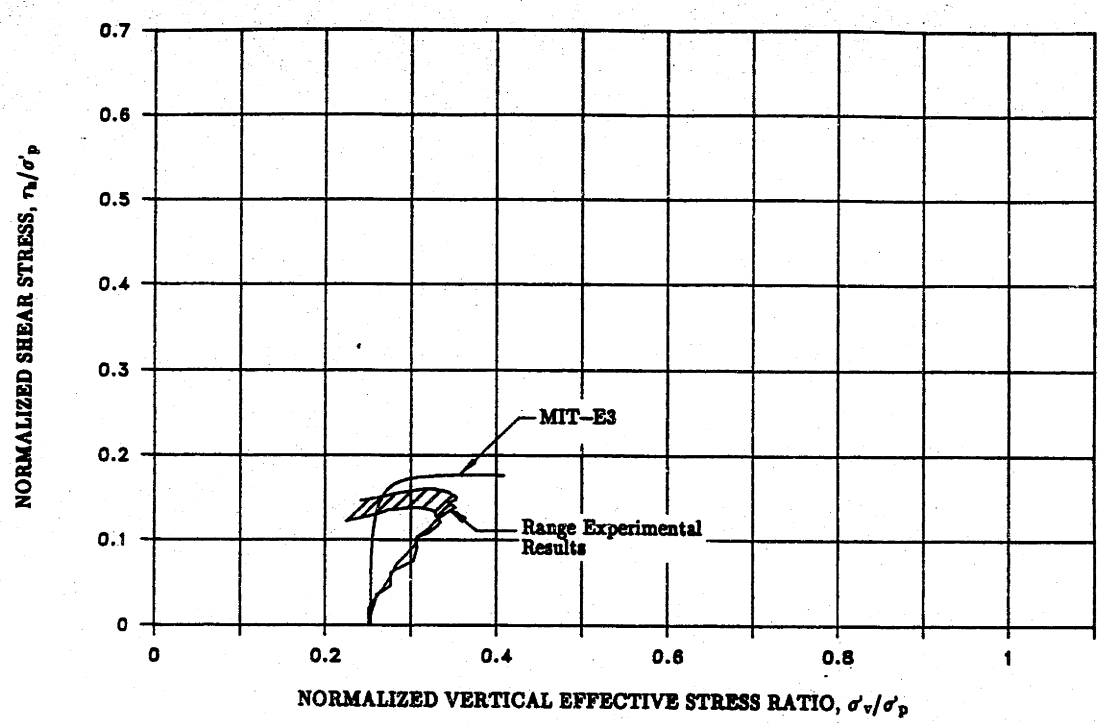

Figure 6.25: Measured and Predicted Stress Paths for CK_oUDSS Test on OCR=4 BBC.

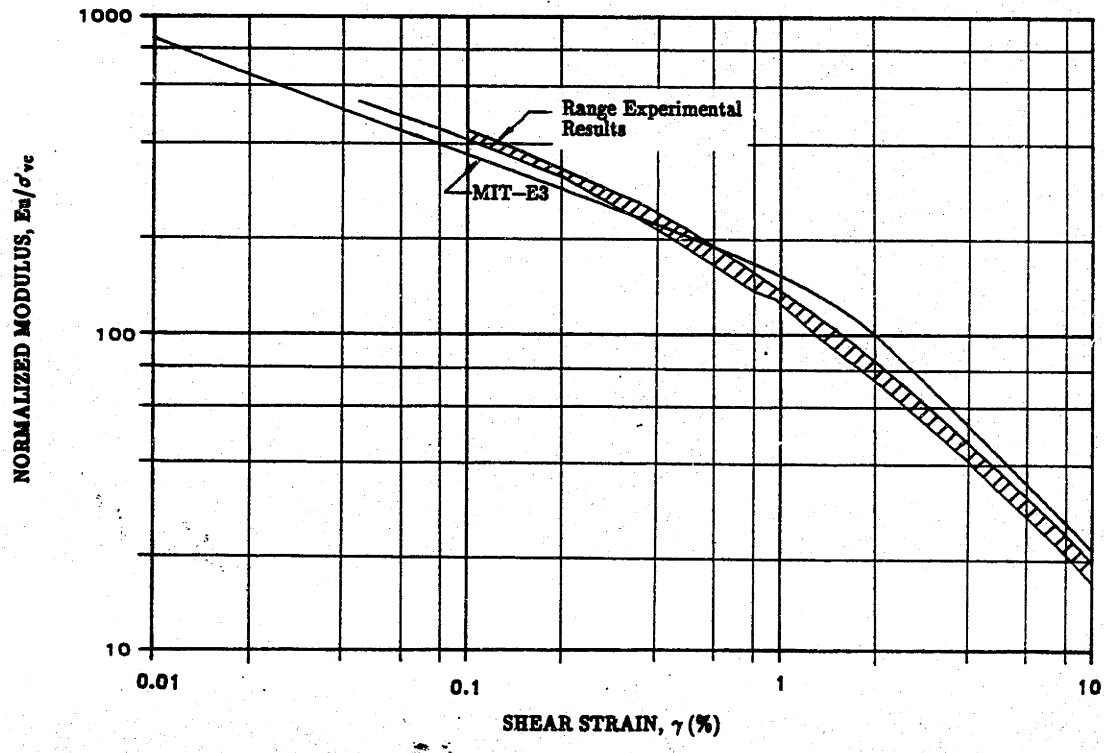

Figure 6.26: Measured and Predicted Normalized Modulus Curves for CK_oUDSS Test on OCR=4 BBC.

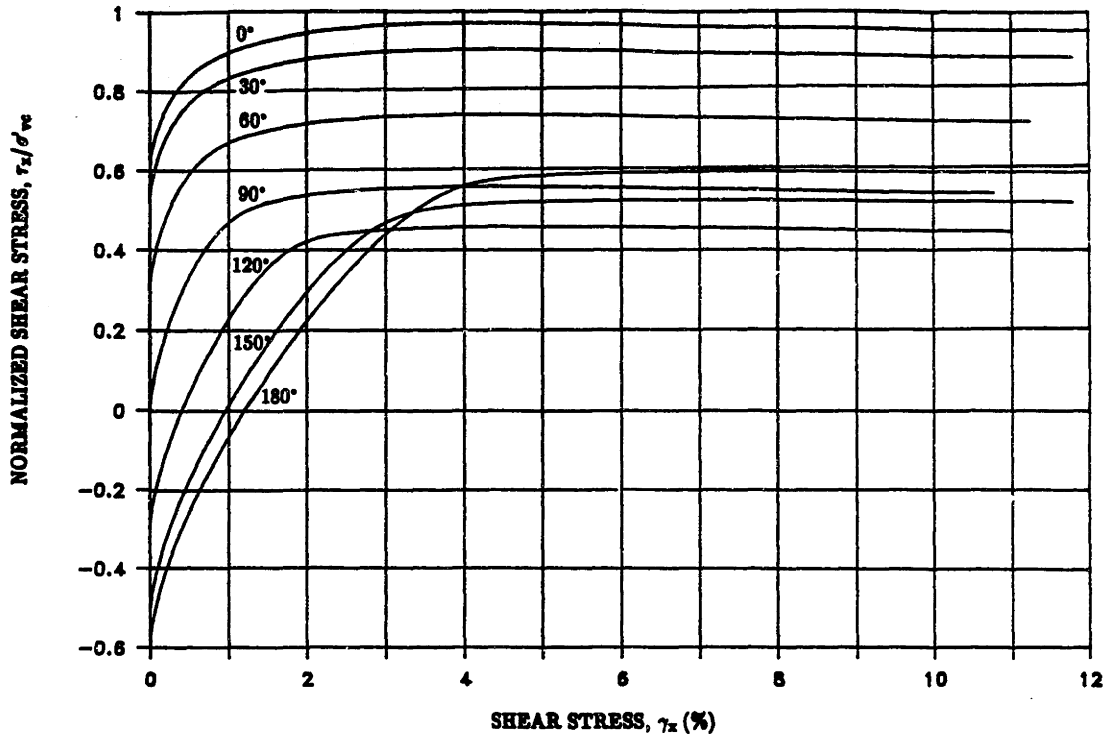

Figure 6.27: MIT–E3 Predictions of Shear Stress–Strain Curves as a Function of θ for CAUMDSS Behavior of OCR=4 BBC With $\tau_{hc}/\sigma'_{vc} = 0.6$.

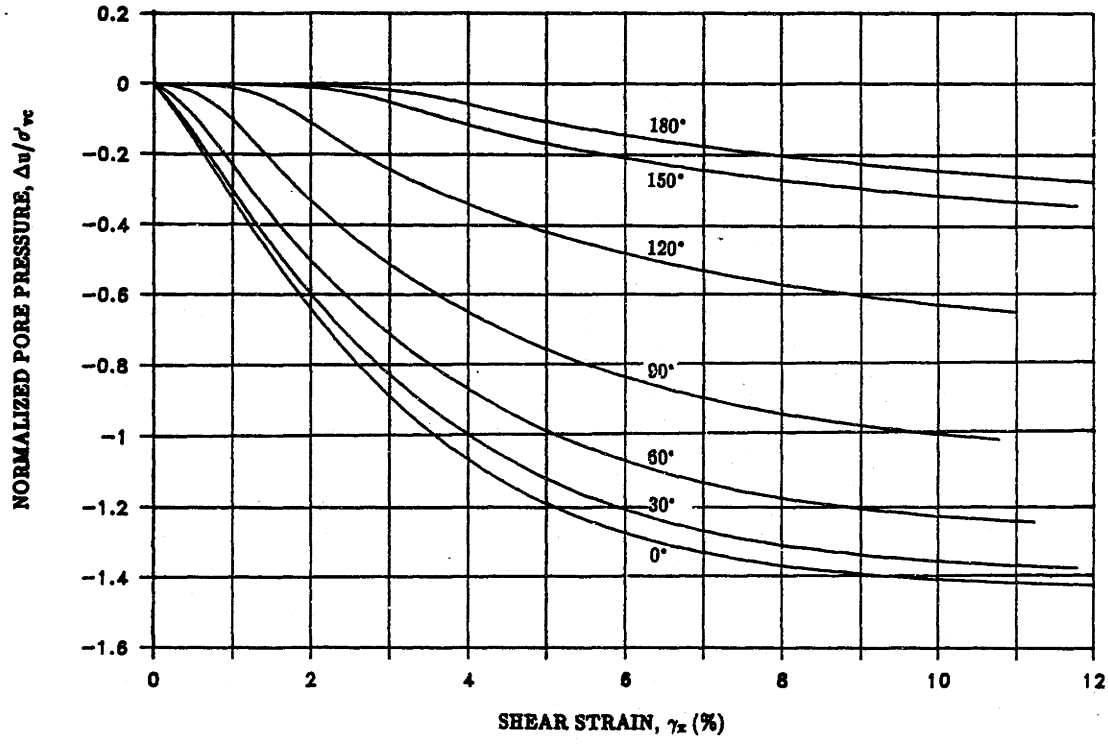

Figure 6.28: MIT–E3 Predictions of Pore Pressure Versus Shear Strain Curves as a Function of θ for CAUMDSS Behavior of OCR=4 BBC With $\tau_{hc}/\sigma'_{vc} = 0.6$.

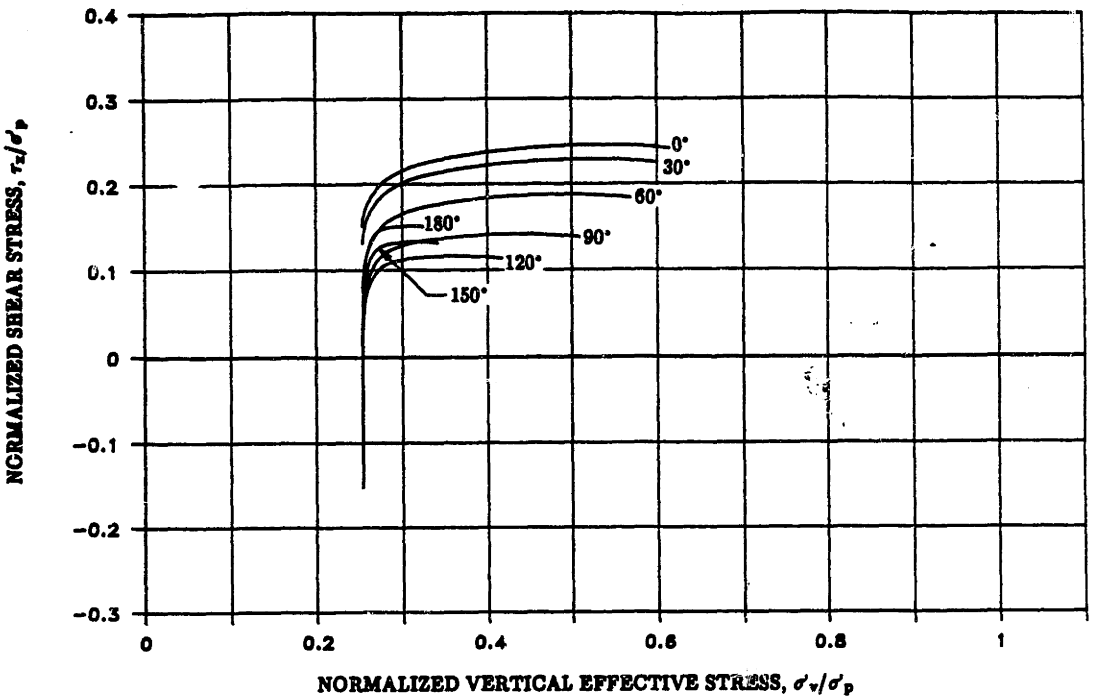

Figure 6.29: MIT–E3 Predictions of Stress Paths as a Function of θ for CAUMDSS Behavior of OCR=4 BBC With $\tau_{hc}/\sigma'_{vc} = 0.6$.

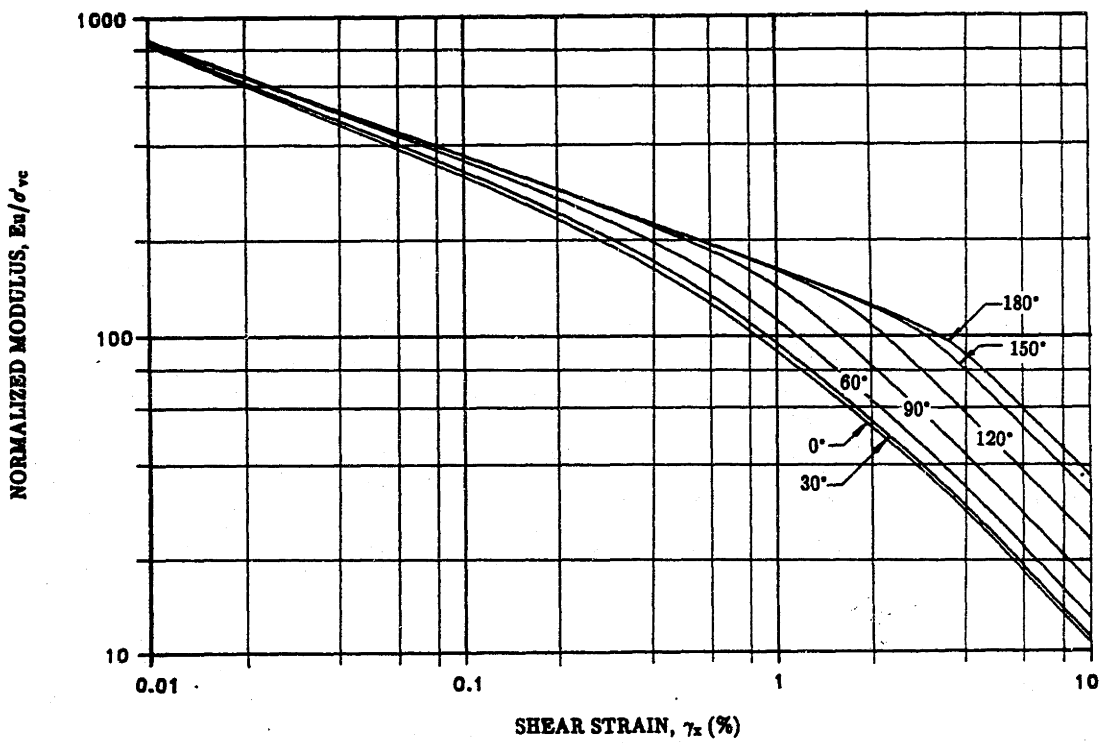

Figure 6.30: MIT–E3 Predictions of Normalized Modulus Curves as a Function of θ for CAUMDSS Behavior of OCR=4 BBC With $\tau_{hc}/\sigma'_{vc} = 0.6$.

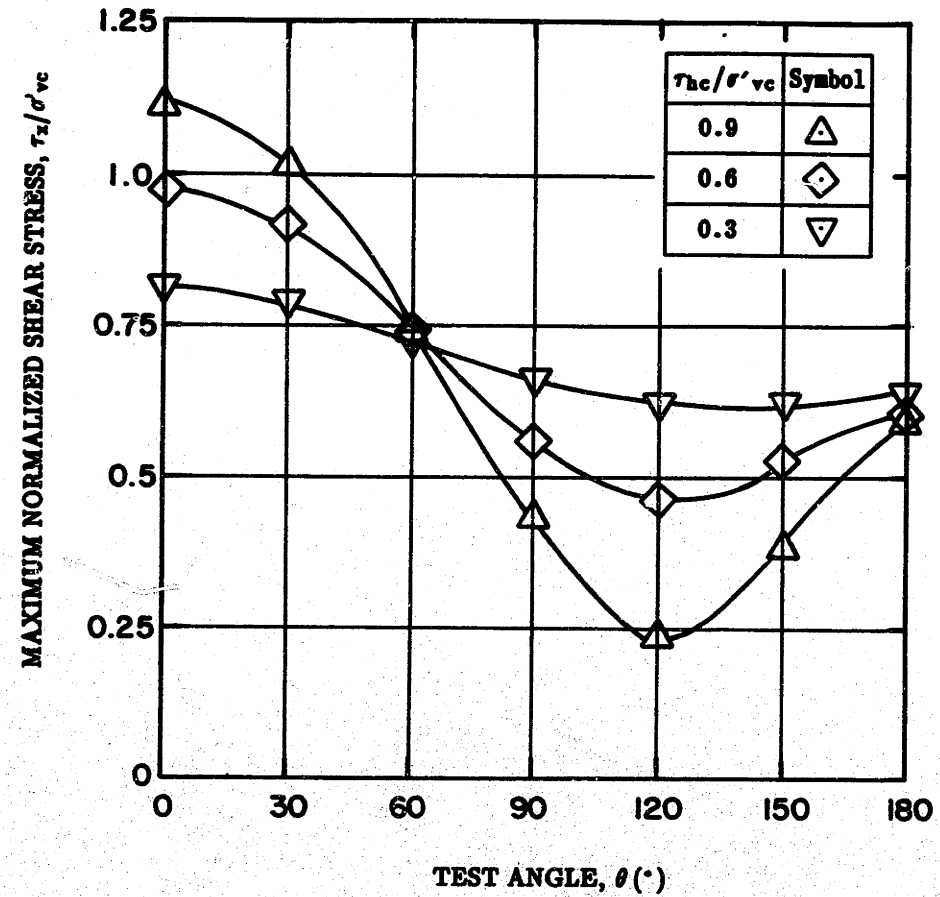

Figure 6.31: MIT–E3 Predictions of Maximum Shear Stress τ_x/σ'_{vc} Versus Test Angle θ for CAUMDSS Behavior of OCR=4 BBC.

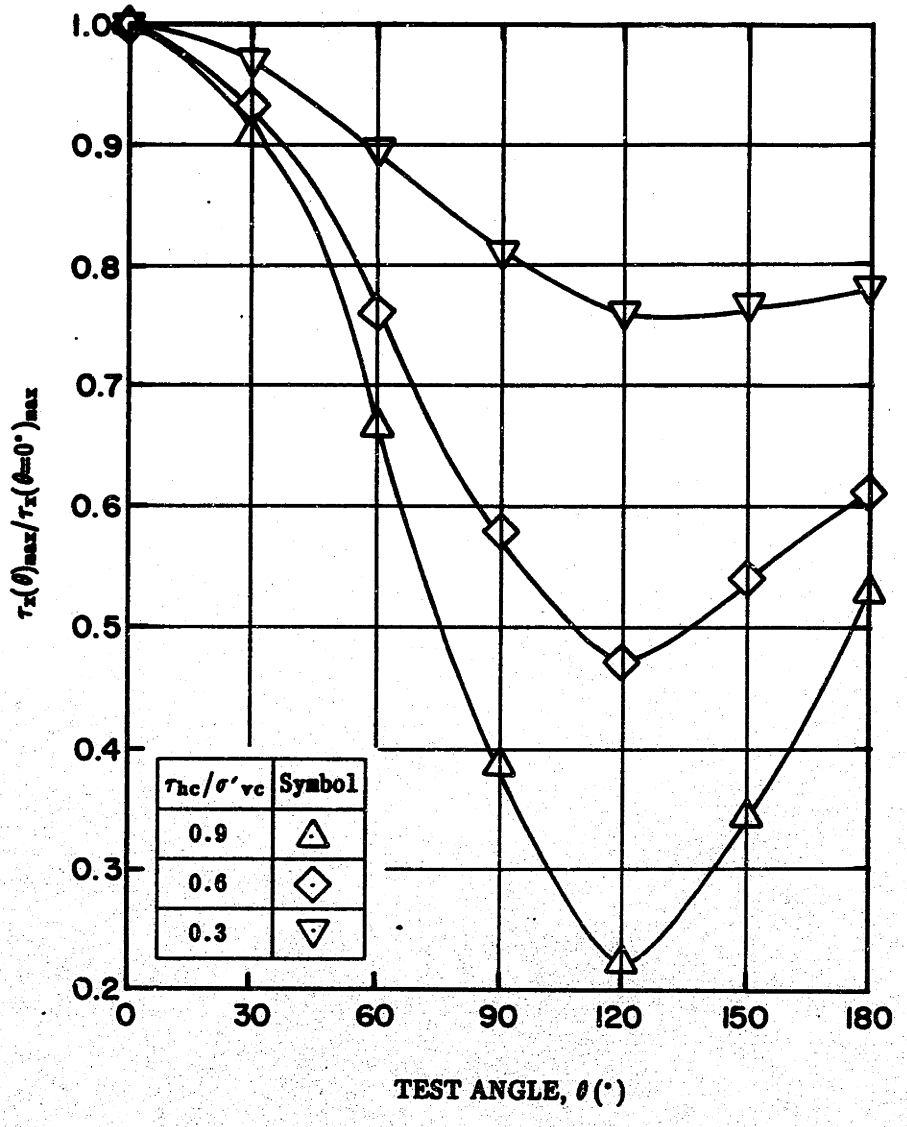

Figure 6.32: MIT–E3 Predictions of $\tau_x(\theta)_{max}/\tau_x(\theta=0^\circ)_{max}$ Versus Test Angle θ for CAUMDSS Behavior of OCR=4 BBC.

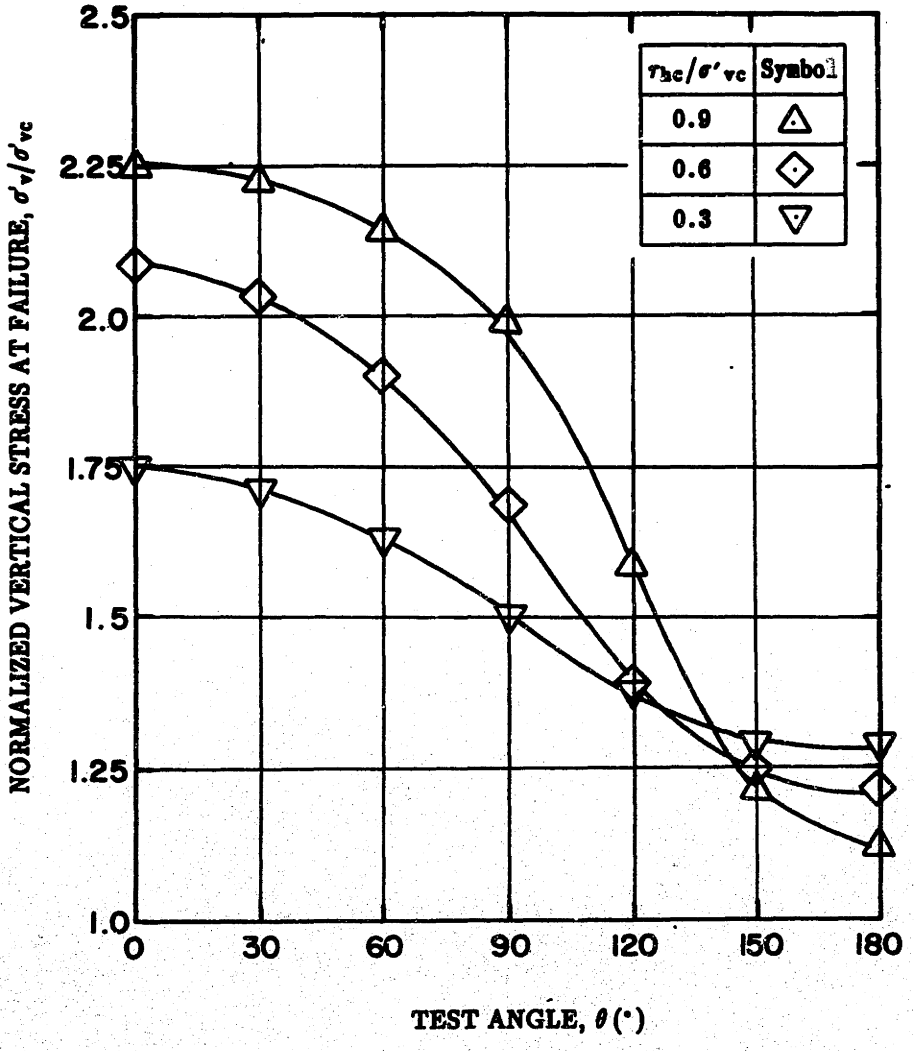

Figure 6.33: MIT–E3 Predictions of Vertical Effective Stress Ratio at Failure Versus Test Angle θ for CAUMDSS Behavior of OCR=4 BBC.

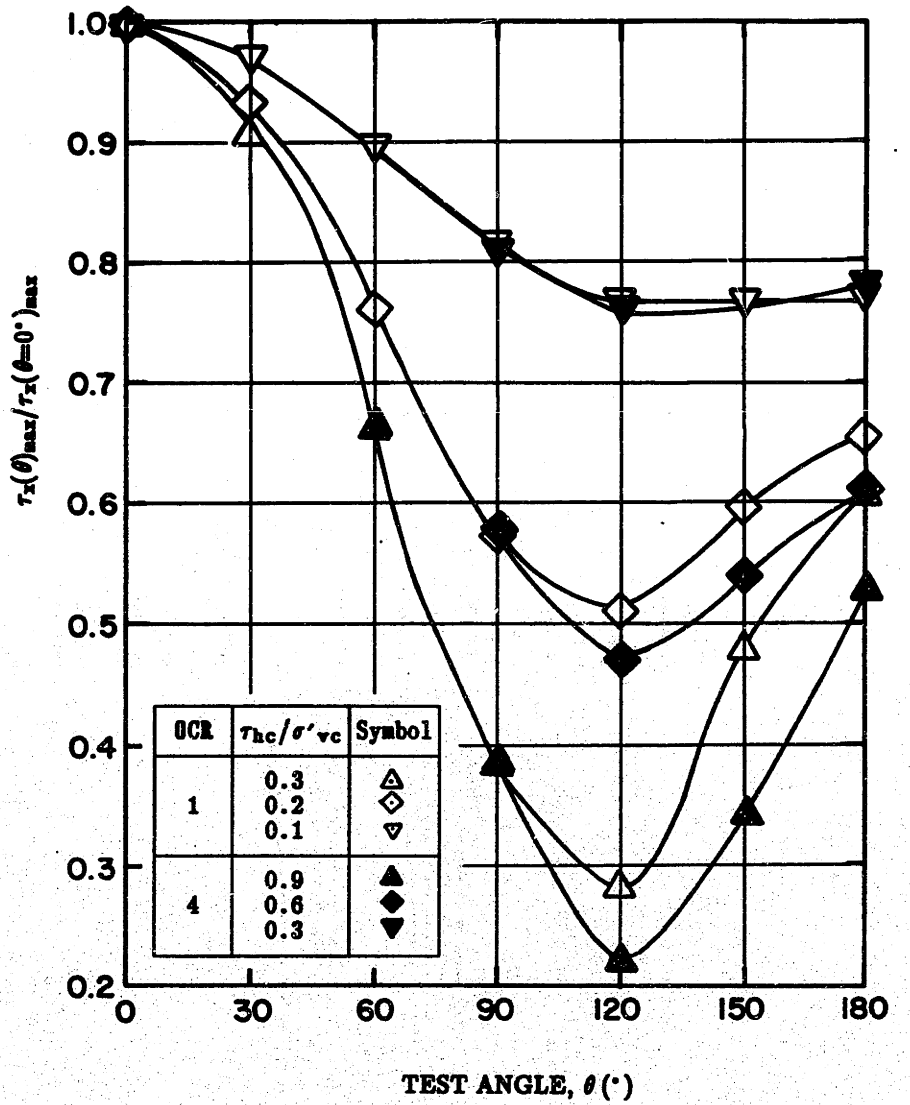

Figure 6.34: MIT–E3 Predictions of $\tau_x(\theta)_{max}/\tau_x(\theta=0^\circ)_{max}$ Versus Test Angle θ for CAUMDSS Behavior of OCR = 1 and 4 BBC.

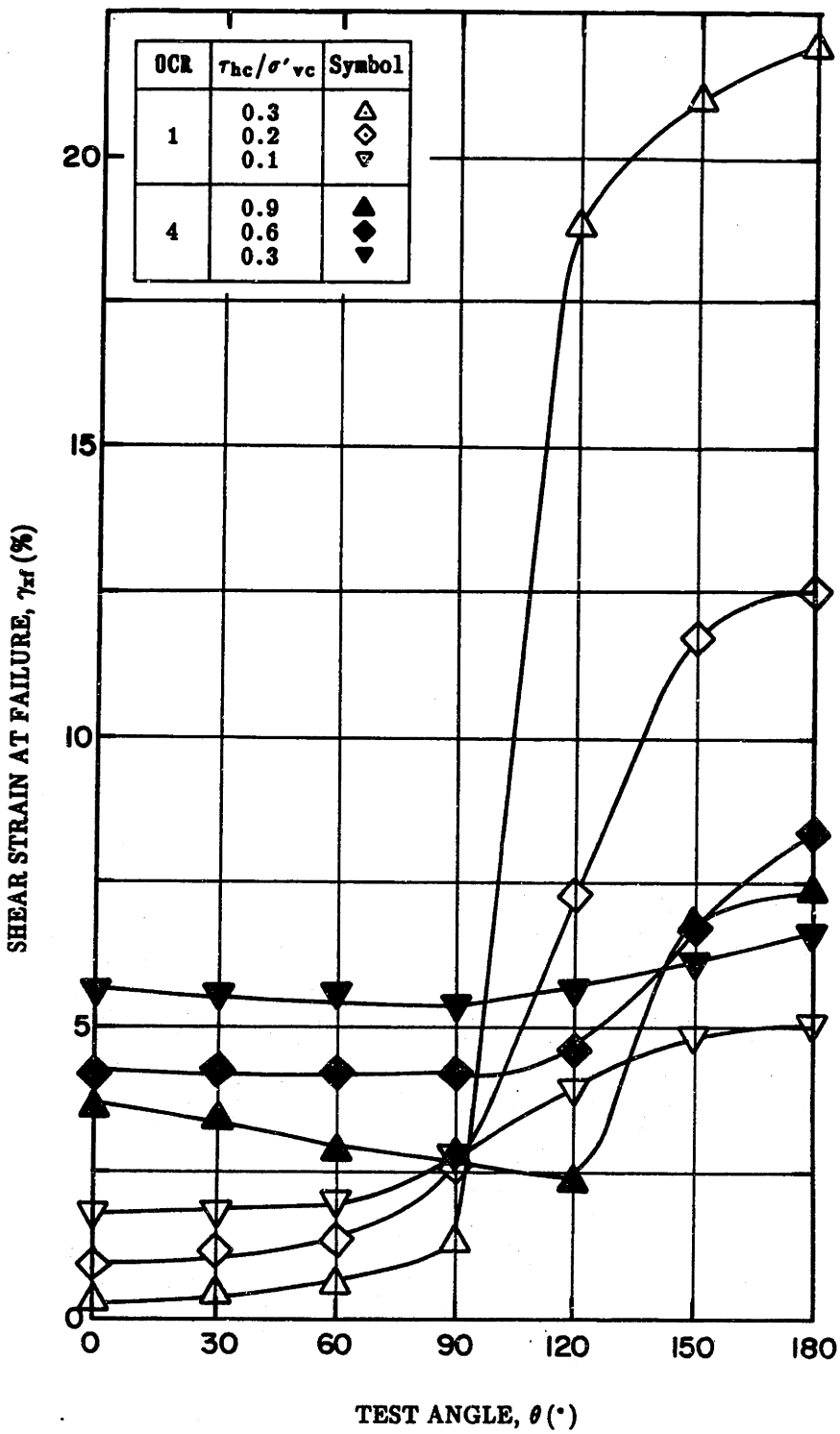

Figure 6.35: MIT–E3 Predictions of Shear Strain at Failure γ_{xf} Versus Test Angle θ for CAUMDSS Behavior of OCR = 1 and 4 BBC.

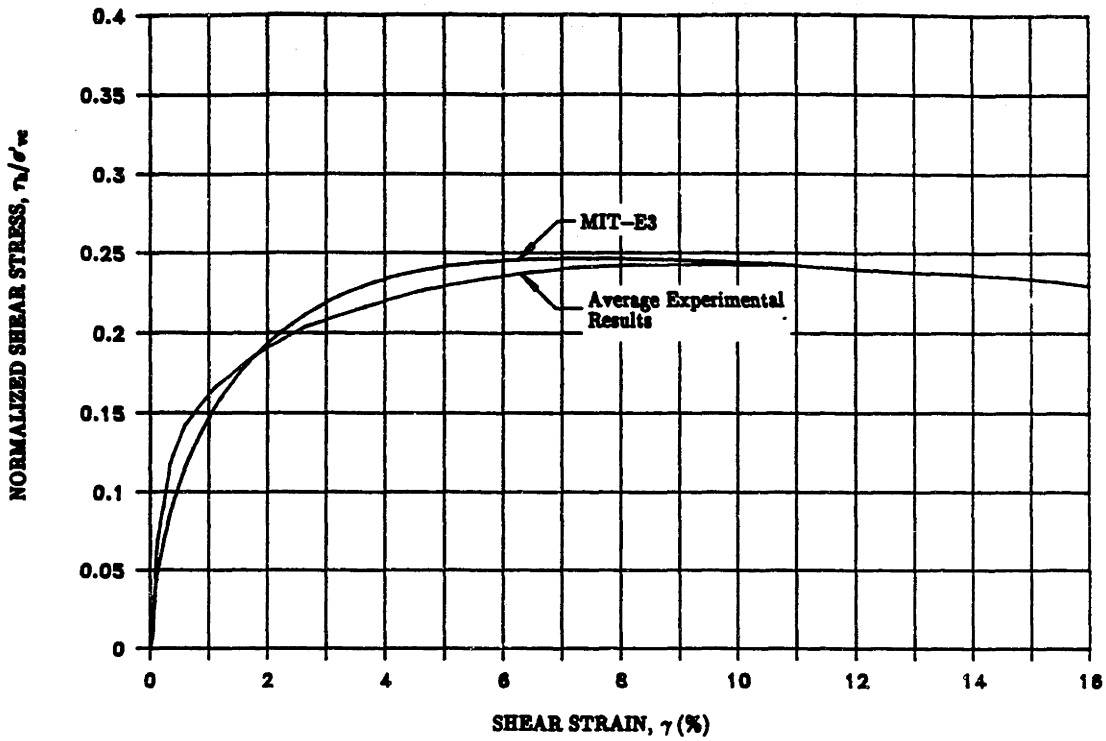

Figure 6.36: Measured and Predicted Shear Stress–Strain Curves for CK_0UDSS Test on Harrison Bay SZA Arctic Silt.

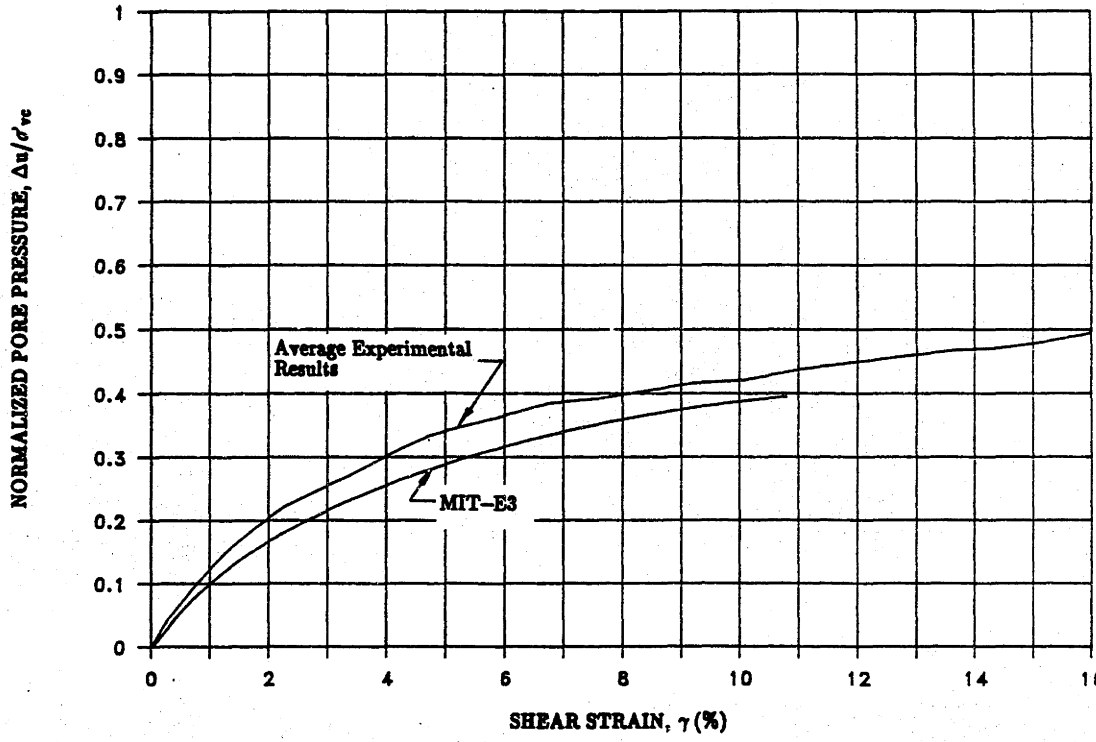

Figure 6.37: Measured and Predicted Pore Pressure versus Shear Strain Curves for CK_0UDSS Test on Harrison Bay SZA Arctic Silt.

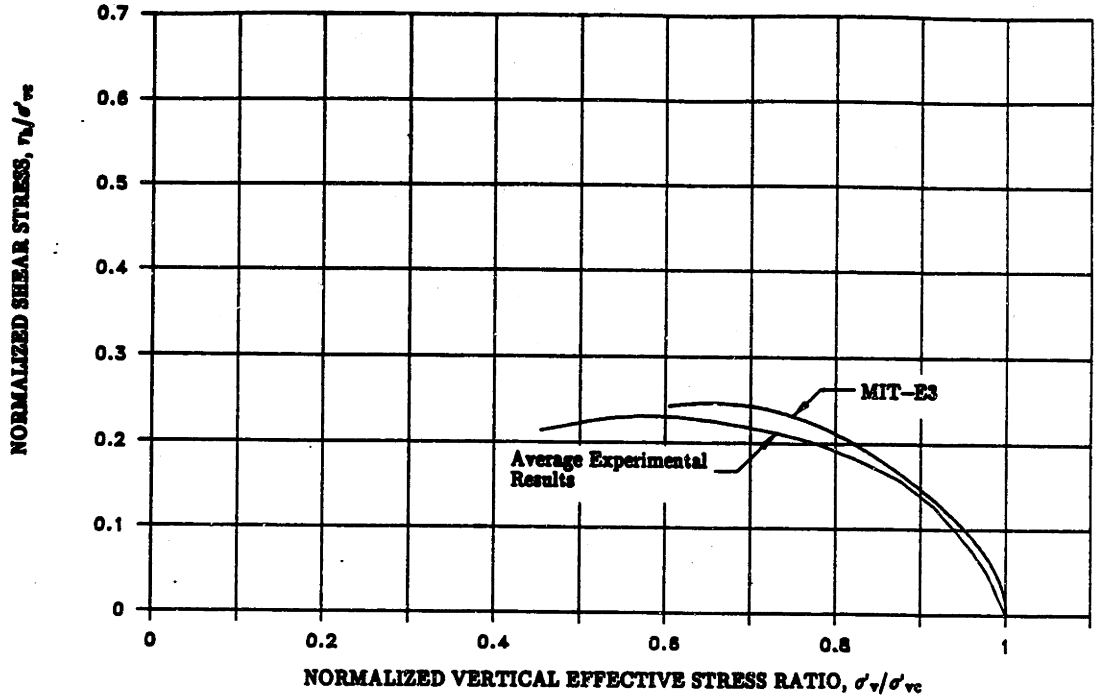

Figure 6.38: Measured and Predicted Stress Paths for CK_oUDSS Test on Harrison Bay SZA Arctic Silt.

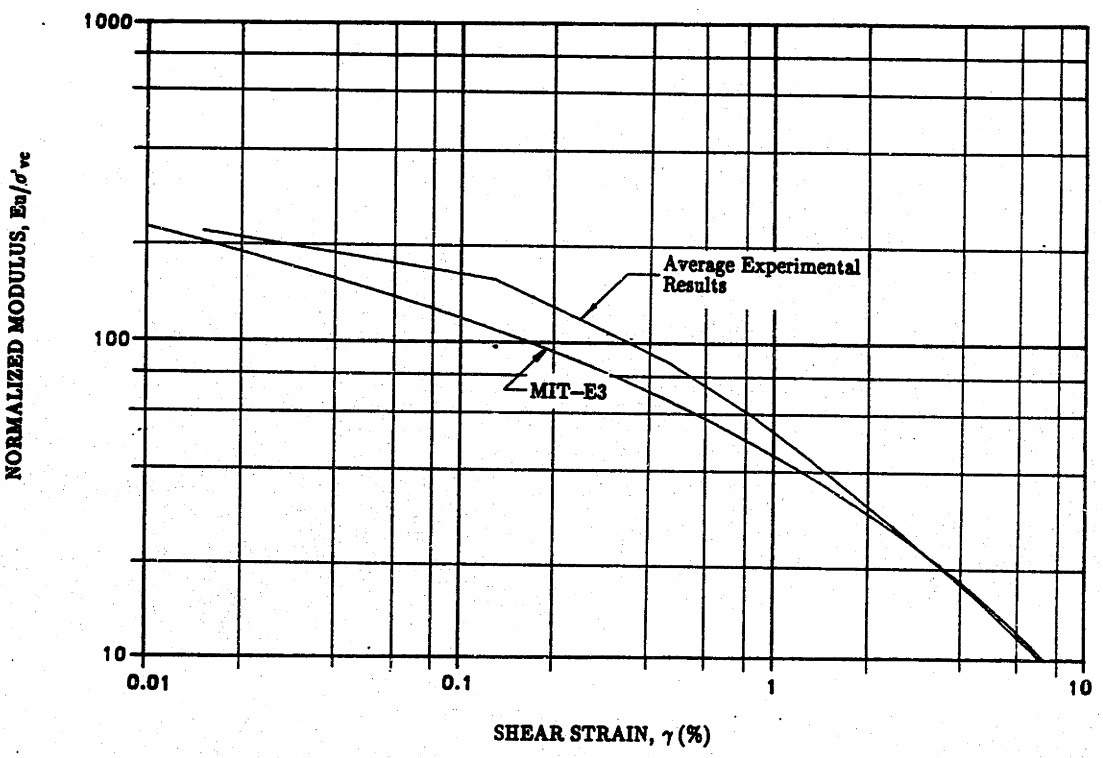

Figure 6.39: Measured and Predicted Normalized Modulus Curves for CK_oUDSS Test on Harrison Bay SZA Arctic Silt.

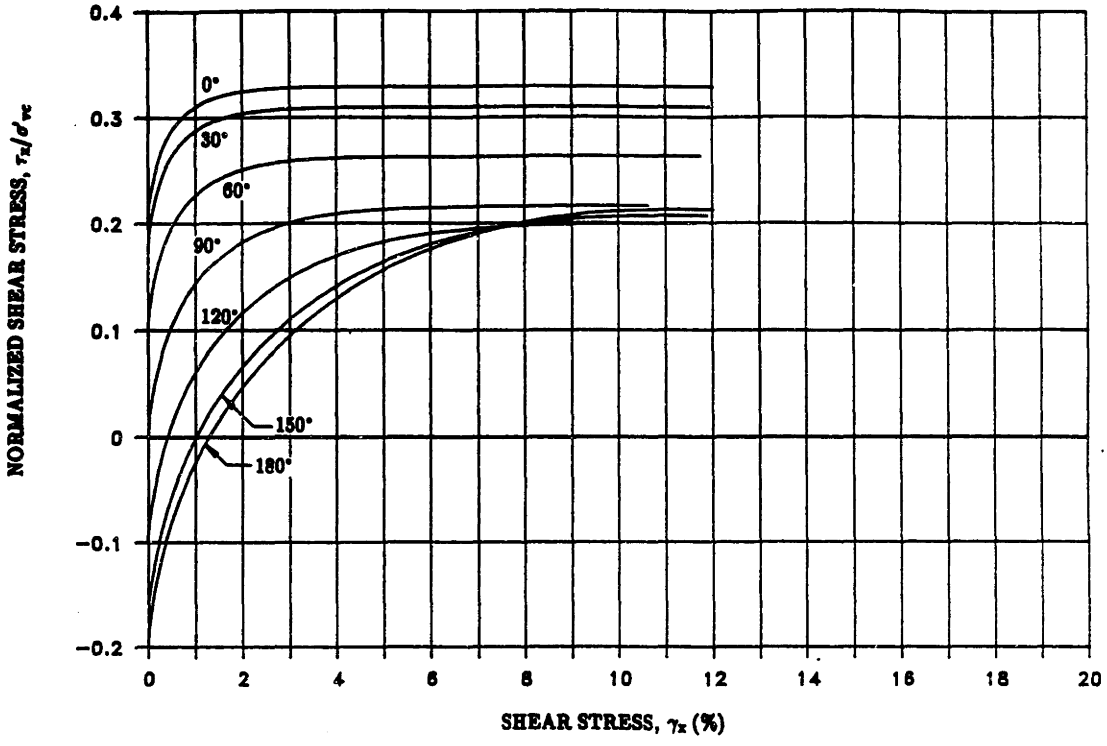

Figure 6.40: MIT–E3 Predictions of Shear Stress–Strain Curves as a Function of θ for CAUMDSS Behavior of Harrison Bay SZA Arctic Silt With $\tau_{hc}/\sigma'_{vc} = 0.2$.

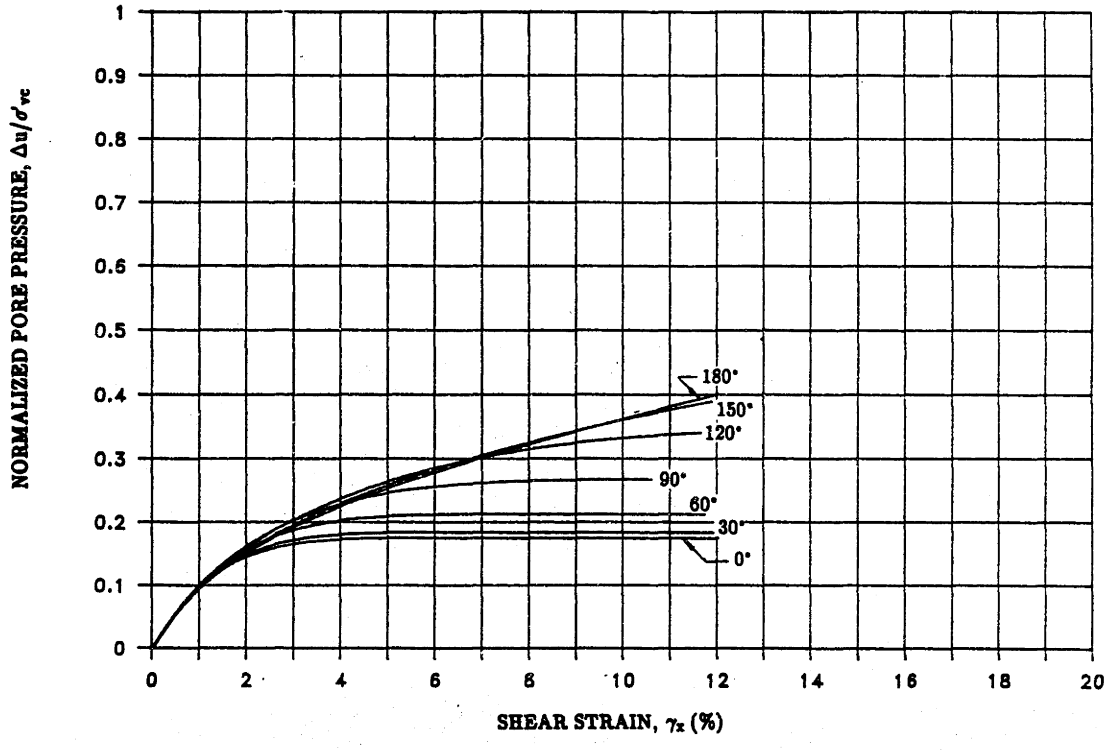

Figure 6.41: MIT–E3 Predictions of Pore Pressure versus Shear Strain Curves as a Function of θ for CAUMDSS Behavior of Harrison Bay SZA Arctic Silt With $\tau_{hc}/\sigma'_{vc} = 0.2$.

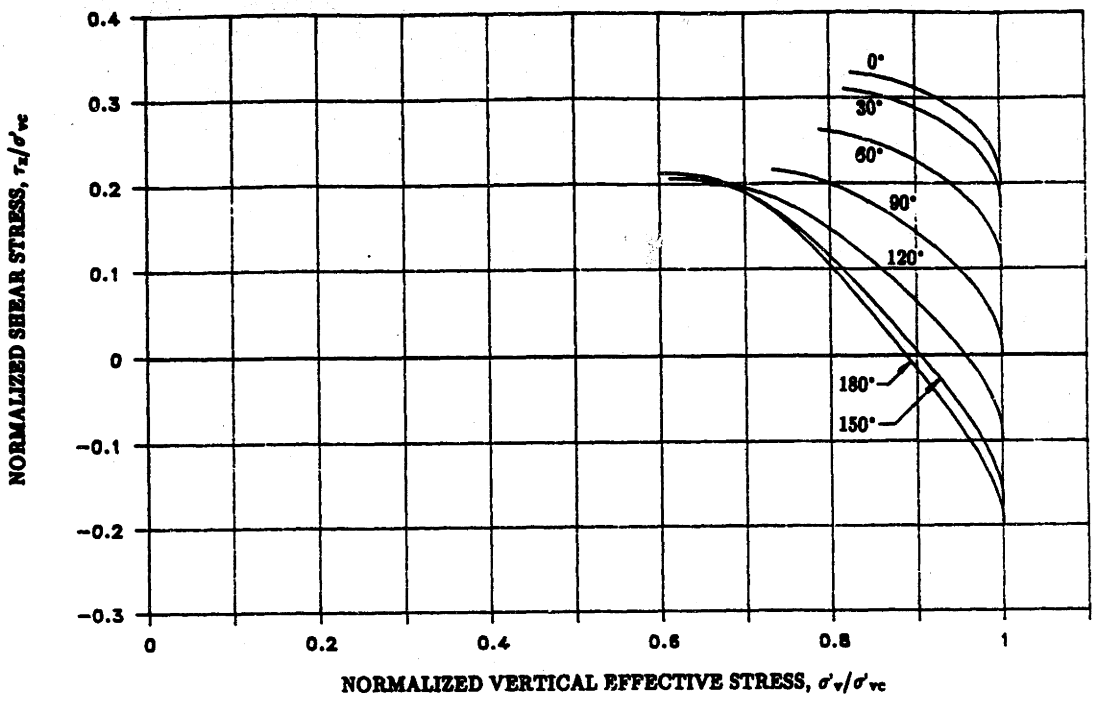

Figure 6.42: MIT–E3 Predictions of Stress Paths as a Function of θ for CAUMDSS Behavior of Harrison Bay SZA Arctic Silt With $\tau_{hc}/\sigma'_{vc} = 0.2$.

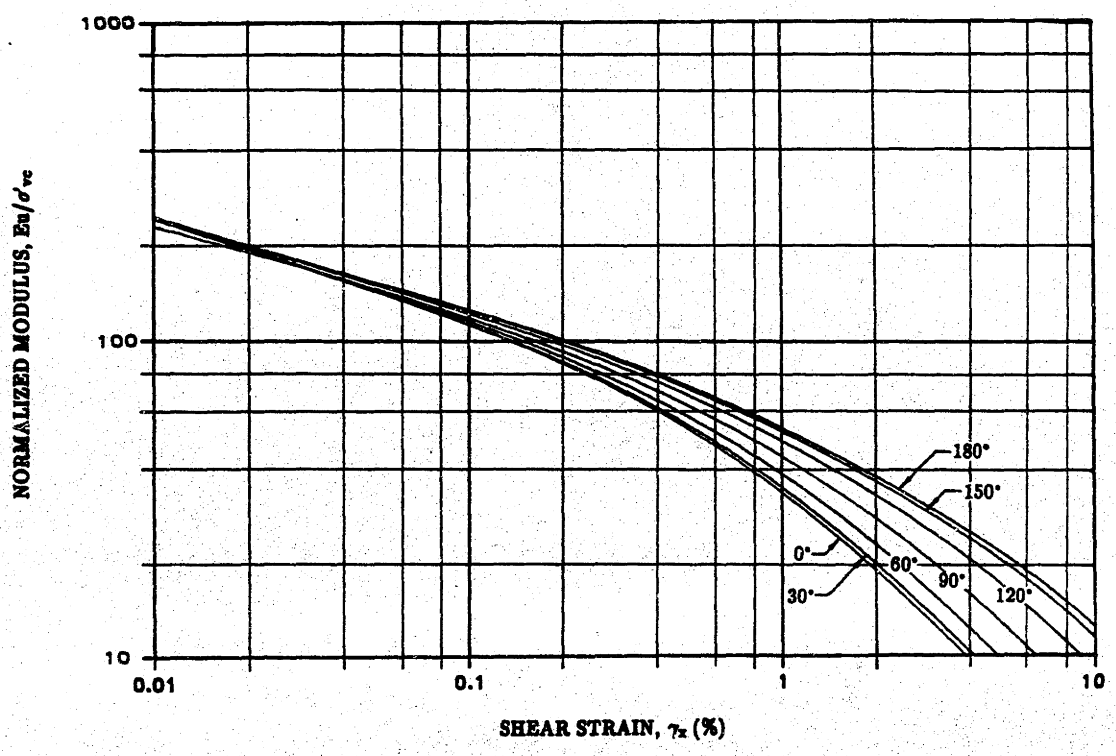

Figure 6.43: MIT–E3 Predictions of Normalized Modulus Curves as a Function of θ for CAUMDSS Behavior of Harrison Bay SZA Arctic Silt With $\tau_{hc}/\sigma'_{vc} = 0.2$.

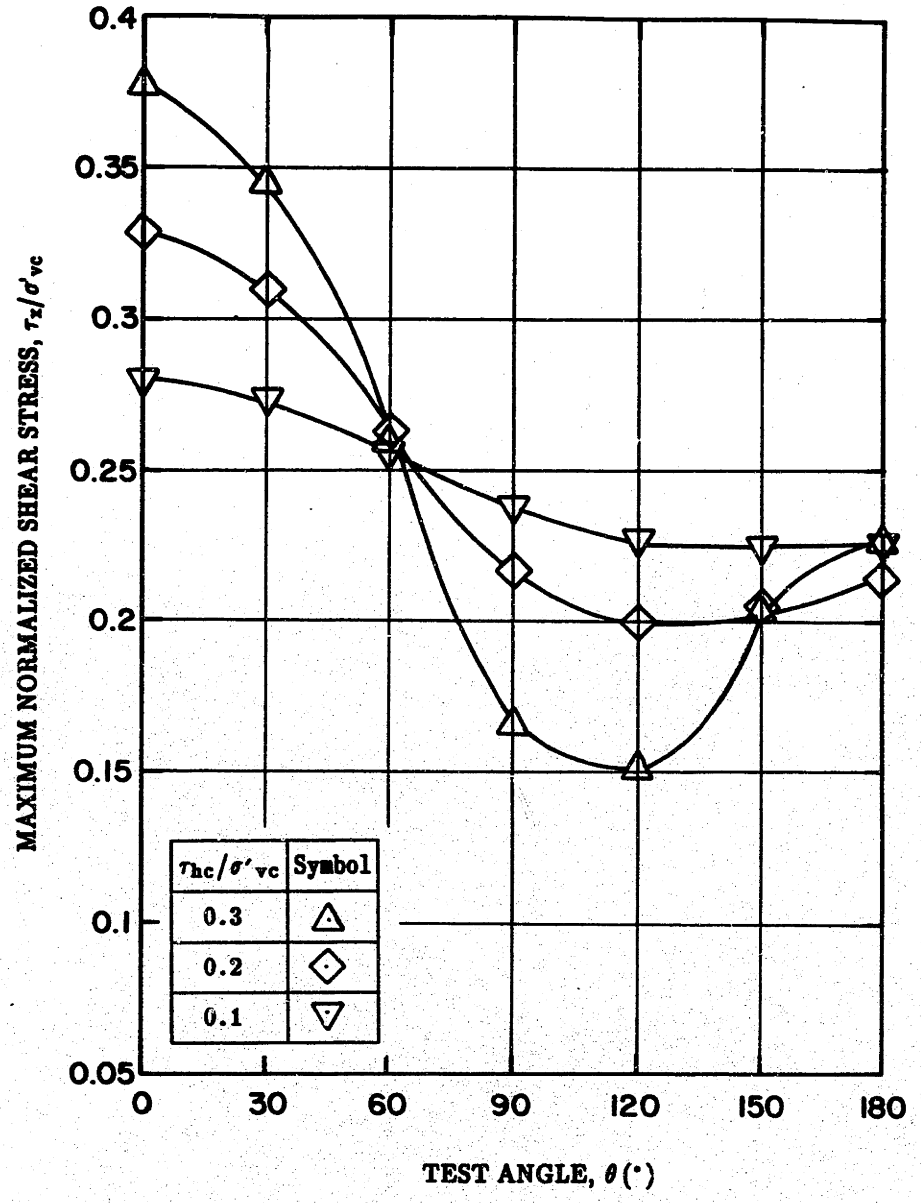

Figure 6.44: MIT–E3 Predictions of Maximum Shear Stress τ_x/σ'_{vc} Versus Test Angle θ for CAUMDSS Behavior of OCR=1 Harrison Bay SZA Arctic Silt.

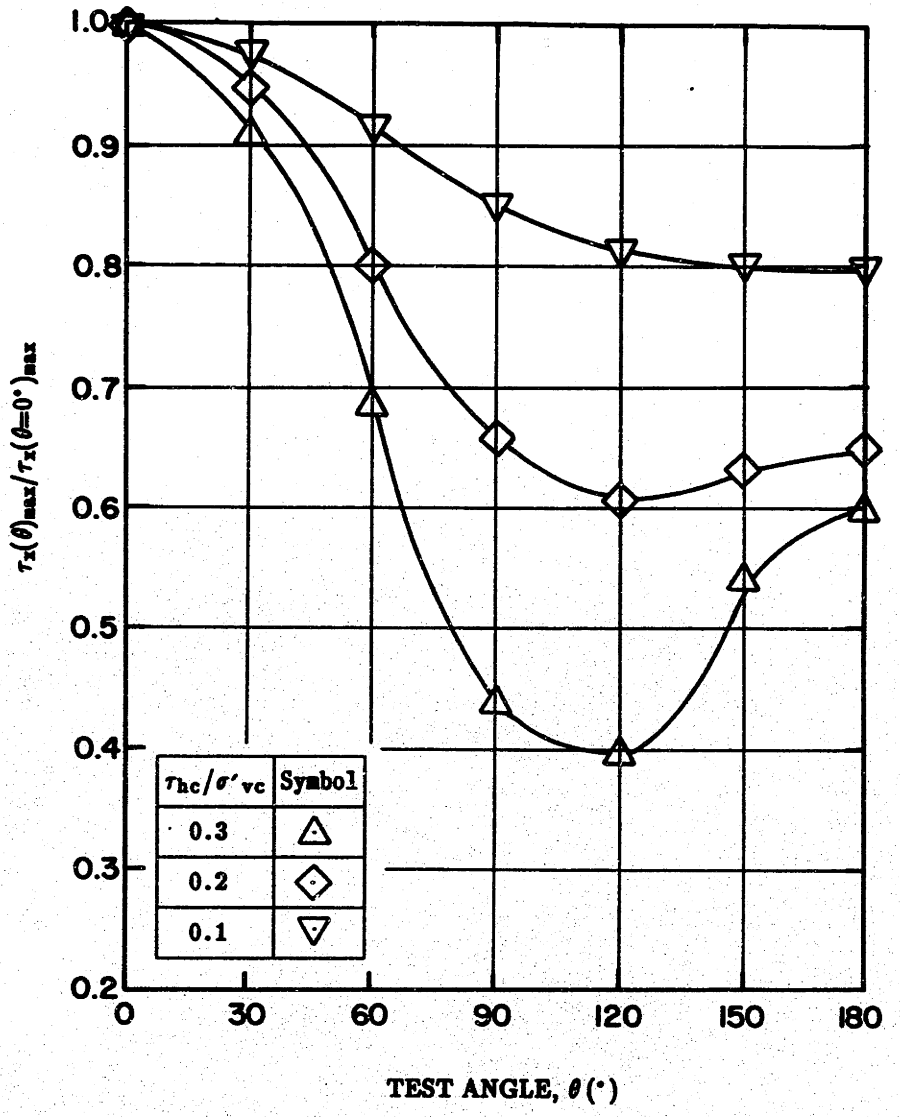

Figure 6.45: MIT–E3 Predictions of $\tau_x(\theta)_{max}/\tau_x(\theta=0^\circ)_{max}$ Versus Test Angle θ for CAUMDSS Behavior of OCR=1 Harrison Bay SZA Arctic Silt.

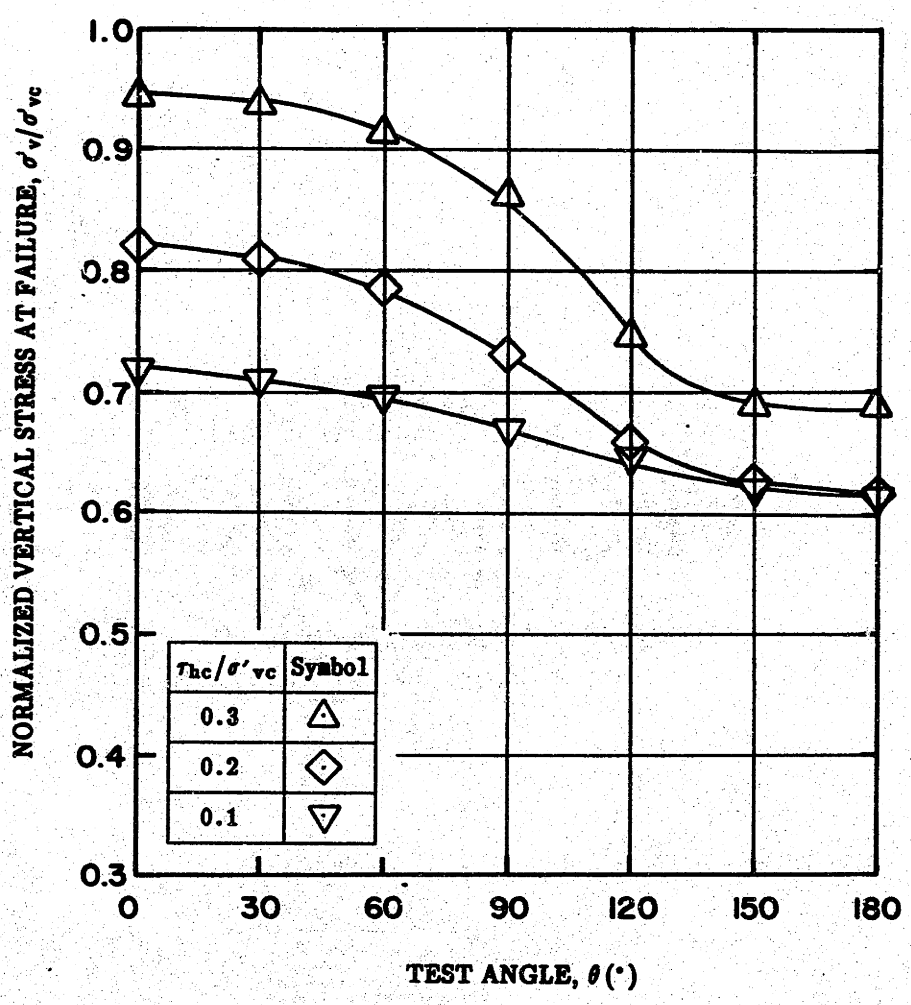

Figure 6.46: MIT–E3 Predictions of Vertical Effective Stress Ratio at Failure Versus Test Angle θ for CAUMDSS Behavior of OCR=1 Harrison Bay SZA Arctic Silt.

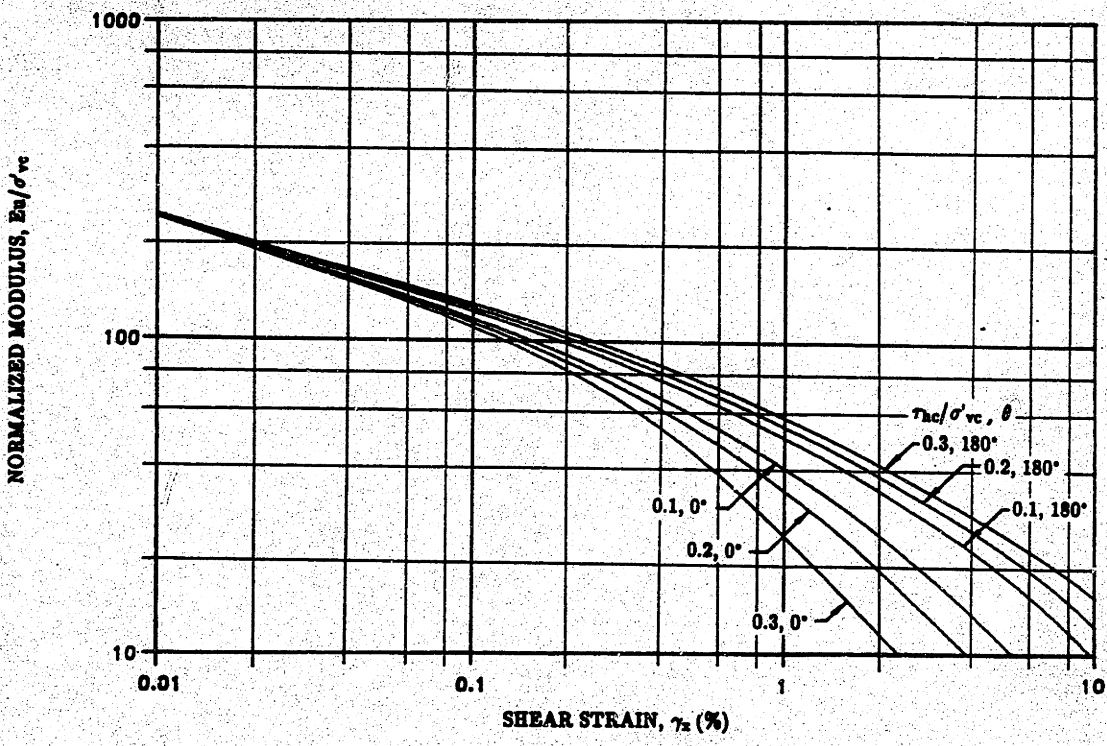

Figure 6.47: MIT–E3 Predictions of Normalized Modulus Curves as a Function of θ for CAUMDSS Behavior of OCR=1 Harrison Bay SZA Arctic Silt.

CHAPTER 7

SUMMARY, CONCLUSIONS AND RECOMMENDATIONS

7.1 BACKGROUND

The Center for Scientific Excellence in Offshore Engineering was established at MIT in September, 1983 by a five–year Grant of $2 million from the Standard Oil Company (now BP America, Inc.) with three principal objectives: 1) to conduct coordinated interdisciplinary research in Arctic offshore engineering in partnership with industry; 2) to support students engaged in offshore engineering research; and 3) to develop a scientific interchange program. The Center involved faculty and graduate students from the Departments of Civil Engineering and Ocean Engineering. They conducted research encompassing ice and structural, geotechnical, risk and reliability and hydrodynamic aspects of Arctic offshore engineering.

In 1987, BP reduced the Grant to $1.7 million due to the drastic drop in oil prices and concurrently opened the Center to other oil companies that led to a proposal for Consortium Cooperative Research in Arctic Offshore Engineering and Construction starting in 1988. Consortium members for 1989 include seven companies (Amoco Production Company; ARCO Alaska, Inc.; BP Exploration, Inc.; Chevron Oil Field Research Company; Conoco, Inc.; Exxon Production Research Company and Mobil Research and Development Corp.) to support interdisciplinary research in the areas of ice mechanics, ice–structure interaction, geotechnical engineering and hydrodynamic modeling.

The Center's program in geotechnical engineering initially sponsored research in two main areas: 1) engineering properties of Arctic silts, and 2) theoretical procedures for assessing the foundation stability of Arctic gravity structures. Research

on the first topic started at the time of the Center's inception, and studies in the second topic commenced in September of 1984.

7.1 1 General Research Objectives

Ultimately the aim of the Center's research in experimental geotechnical engineering is to develop recommended procedures for measuring the engineering properties of Arctic silts which are necessary for the safe and economical foundation design of offshore structures. Specifically the program addresses the following issues (Sauls, et al., 1984):

1. Why Arctic silts exhibit unique behavior compared to other offshore sediments, which negates reliance on past empirical correlations;
2. What types of in situ and laboratory test programs should be used to develop reliable estimates of the initial strength–deformation properties needed to predict the performance of gravity structures during and after set down;
3. What type of laboratory shear tests should be used to obtain strength–deformation properties needed to evaluate foundation performance against massive horizontal forces due to ice loading.

Evaluation of these experimental results (together with available field performance) and input from industry co–sponsors will provide the basis for developing guidelines for recommended practice. The research program initiated to achieve these objectives was divided into three phases of investigation:

1. Geology and composition of deposits;
2. Basic strength–deformation properties as a function of temperature, stress history and failure mode;
3. Foundation performance against ice loading.

7.1.2 Prior Research Activities

The first experimental program on measuring the engineering properties of Arctic silts used 15 undisturbed tube samples provided to MIT by the Standard Oil Production Company (SPOC) in January 1984. All of the samples were located within

or near the "Soft Zone Area" (SZA) of Harrison Bay (Figure 1.2). The results of this program plus a summary of research by MIT on the geology of Harrison Bay are contained in the research report by Sauls, et al. (1984).

In April 1984, SPOC sponsored a special program of undisturbed sampling and in situ testing near the edge of Mukluk Island (Figure 1.2). The samples were taken from an area where the water depth is 50 feet and the subsea profile consists of a 25 ft thick Holocene deposit overlying relict permafrost. The deposit was found to consist of essentially two layers: an upper layer of highly overconsolidated low plasticity silt and a lower layer of soft uniform clayey silt. Results of research conducted on these samples are contained in the MIT Master's theses by Ayan (1985) and Yin (1985).

SPOC sponsored further geotechnical exploration programs at four sites in Smith Bay (Figure 1.2) in early 1985, that were executed by The Earth Technology Corporation (TETC). The Center worked with SPOC to evaluate the results of the geotechnical program and assist SPOC and its design consultant (EBA Engineering Consultants Ltd., Canada) in development of a site specific design. Samples from Smith Bay were sent to MIT for a special test program at one site to supplement data obtained by TETC, plus additional testing at a second site to further MIT's research objectives. The Smith Bay deposits consist of Pleistocene silty clay, in contrast to the Holocene clayey silts encountered at Harrison Bay. Also, the effects of ice gouging have significantly affected the stress history and strength profiles at one site in Smith Bay. The results of this investigation are presented in an MIT Master's thesis by Young (1986).

Both the Mukluk Proximal in Harrison Bay and the Smith Bay geotechnical exploration programs included piezocone penetration tests (PCPT). The PCPT data collected from these sites in the Beaufort Sea provided a unique opportunity to: 1) assess the performance of the piezocone in Arctic silts, and 2) evaluate the applicability of existing methods of piezocone data interpretation for Arctic silts. The results of this

last investigation are contained in an MIT Master's thesis by de la Huerta (1987).

7.2 ISSUES AFFECTING THE FOUNDATION PERFORMANCE OF OFFSHORE ARCTIC GRAVITY STRUCTURES

7.2.1 Offshore Arctic Environment

Sea ice is the most important environmental factor affecting the design of gravity platforms in the offshore Arctic region. The characteristics of sea ice and its movement are the main items of concern for design. Depending on a structure's location and configuration lateral ice forces may reach 50,000 to 200,000 tons (Gerwick, 1983).

The subsea profile within the offshore Alaskan continental shelf of the Beaufort Sea often consists of Arctic silts overlying relict permafrost. Results from research conducted at MIT and summarized in Section 2.2, clearly show that there are substantial differences in the nature of Arctic silts. The soil can vary from Holocene ML–MH clayey silt (Harrison Bay SZA) to Pleistocene CL–CH silty clay (Smith Bay). The preconsolidation pressure σ'_p and undrained shear strength c_u can decrease with depth as in the SZA of Harrison Bay (Figures 2.8 and 2.9) or increase with depth as is the case in Smith Bay (Figures 2.14 to 2.18). In addition, MIT also found that strengths from conventional c_u tests (e.g., UUC, field vane and miniature vane) varies from reasonable to several times too high (Figures 2.17 and 2.18).

7.2.2 Set Down Conditions (Gravity Loading)

The foundation conditions for Arctic gravity structures are unique because of the horizontal ice loads and also because the foundation's soil layer is thin compared to the width of a typical structure. In the case of vertical gravity loads, the large ratio of the structure width to the depth of soil layer ($B/H \geq 15$, see Figure 2.20) makes traditional bearing capacity analyses inappropriate for design. For Arctic gravity structures the mechanism of failure consists of soil squeezing between the rigid

structure and permafrost underlying the foundation soil layer.

Upon initial set–down of an Arctic gravity structure, the foundation soil will be subjected to significant radial shear stresses which may be accompanied by large radial deformations due to lateral squeezing (Figure 2.21a). During this process the direction (given by the angle δ) of the major principal stress will rotate. The magnitude of rotation will depend on the location of a soil element relative to the centerline of the structure and its depth within the foundation layer. The magnitude and direction of the horizontal shear stress at a soil element will also depend on the element's location within the soil layer (Figure 2.21a).

7.2.3 Ice Loading

Ice loads will impose an inclined and eccentric load on the foundation of an Arctic gravity structure. However, the sliding mode of failure becomes predominant when the horizontal ice load is a large fraction of the horizontal sliding resistance of the foundation soil (Vivatrat and Watt, 1983). In this case, application of the ice load causes incremental horizontal shear stresses within the foundation soil all acting essentially in the same direction (Figure 2.21b). These can produce large rotations and even reversal in the direction of the horizontal shear stress acting at soil elements within the foundation soil (Figure 2.23). At a given depth, the incremental shear stress τ_2 required to resist the horizontal ice force varies as a function of a soil element's location with respect to the center of the structure and its orientation relative to the ice force (r and θ respectively; Figure 2.23).

7.2.4 Experimental Requirements

In order to experimentally simulate, at the element level, the stress conditions acting within the foundation of an offshore Arctic gravity structure a testing device must be able to apply a vertical stress and two independent horizontal shear stresses to a soil specimen (Figure 2.24). The vertical stress (σ_v) and the first shear stress (τ_1)

represent the stresses imposed on an element within the foundation soil under gravity loading. The second shear stress (τ_2), which must be applied at an angle θ relative to the first shear stress τ_1, represents the ice loading force.

The horizontal mode of shearing in the Geonor Direct Simple Shear (DSS) apparatus is especially relevant to both the gravity and ice loading conditions (Figure 2.29a). However, the device can be used to simulate the stress conditions due to combined gravity and ice loading for only those elements where the first and second horizontal shear stress act in the same direction ($\theta = 0^\circ$) or in the opposite direction ($\theta = 180^\circ$; Figure 2.29b). It cannot, nor can any other existing soil testing apparatus, be used to simulate conditions for all those elements where θ is in between 0 and 180 degrees. The Geonor DSS, as outlined in Section 2.4.1.6, does offer several appealing features that were used as the basis for designing a special simple shear device, the Multidirectional Direct Simple Shear (MDSS) apparatus, with capabilities to test soil specimens with θ ranging in 30° increments from 0 to 150 degrees.

7.3 THE MULTIDIRECTIONAL DIRECT SIMPLE SHEAR APPARATUS

7.3.1 Description of the MDSS

The MDSS uses the same size circular soil sample (2.3cm x 35 cm^2), wire reinforcement membrane and trimming procedures as used for the Geonor DSS. The sample is consolidated under both a vertical stress σ'_{vc} and a horizontal shear stress τ_1 which represent the gravity loading stresses (if the sample is allowed to fully consolidate during application of τ_1, then this shear stress is also referred to as the horizontal consolidation shear stress, τ_{hc}). The sample is then sheared undrained by applying a second independent horizontal shear stress τ_2 at an angle θ relative to τ_1 (Figure 3.1). The first shear stress and the vertical stress are applied to the sample using pneumatic cylinders while the second shear stress is applied using a variable speed gear drive system at a constant rate of strain (Figure 3.2). The second shear

stress is always applied from the same orientation which is parallel to the X axis (Figure 3.1). The location of the first shear stress cylinder can be varied, therefore enabling tests to be conducted at different θ angles. The heart of the MDSS is a set of main bearing plates (Figure 3.2) which allow the bottom of the sample to displace freely in a horizontal plane (while the top remains fixed). An array of direct current displacement transducers (DCDT) are used to measure the vertical strain and the X and Y components of the total shear strain (Figure 3.3).

7.3.2 Computer Control Software

The MDSS uses a Hewlett Packard Vectra personal computer for automatic application of the consolidation stresses and for data acquisition (Figure 3.4). The consolidation stresses (σ'_{vc} and τ_1) are controlled by pressure regulators which respond to signals from the computer thus enabling these forces to be applied and monitored automatically. Undrained shear is conducted in the MDSS by maintaining the volume of the sample constant during shear. The sample is assumed to be confined laterally by the wire–reinforced membrane and, therefore, only the height needs to be kept constant to run a constant volume test. The sample height is kept constant by varying the vertical stress acting on it during shear. Changes in the vertical stress required to keep the height constant are assumed to be equal to the pore pressure that would develop if the test was truly undrained with pore pressure measurement. Constant volume shear is performed in the MDSS using a Proportional plus Integral plus Derivative (PID) controller system which monitors the sample height with a DCDT; when an infinitesimal change in the sample height is detected the computer adjusts the vertical stress by sending a new signal to the pressure regulator which controls the σ'_v pneumatic cylinder. Figure 3.5 is a schematic of the main software program MDSSTEST which is used for computer control and data acquisition during an MDSS test.

7.4 EXPERIMENTAL EVALUATION OF THE MDSS DEVICE AND TESTING PROCEDURES

An experimental evaluation of the MDSS and testing procedures was conducted with the following objectives:

1. Determine if the same types of shear test run on soil specimens in the MDSS and the widely used Geonor DSS apparatus produce the same results;
2. Verify the kinematics of the new testing device.

The first objective of the evaluation program was to conduct tests on clay specimens in the MDSS which could also be performed in a standard DSS apparatus so that direct comparison of the results could be made. Specifically, the Geonor DSS is capable of performing two types of tests that can also be run in the MDSS. This includes standard CK_oUDSS tests, which are routinely performed in the Geonor DSS, and CAUDSS tests with $\theta = 0°$.[1] The second objective of the evaluation program was to check the kinematics of the MDSS. This evaluation was particularly important for two reasons: (1) it was necessary to determine if the first shear stress (τ_1) is applied at the correction orientation for each of the different θ angles, and (2) verify that the sample set–up procedure and strain measurement system are working properly and produce repeatable results.

The soil used in this research for the proof tests and the main MDSS testing program was resedimented Boston Blue Clay (BBC), which is an illitic glacio–marine CL clay. Resedimented BBC has been studied and tested extensively at MIT, making it an excellent reference material for research purposes. Batches of BBC used at MIT are basically prepared by consolidating a dilute slurry of soil in a 30 cm diameter cylindrical container to a maximum stress of 1 ksc. At the end of consolidation the cake of clay is trimmed, sealed and stored in a humid room. The BBC samples used

---

[1]The acronym CAU is used to designate tests with $\tau_1=\tau_{hc}>0$ in contrast to regular CK_oU tests with $\tau_1=\tau_{hc}=0$.

for this research were prepared using the procedure described by Germaine (1982) which produces high quality, uniform and saturated samples.

7.4.1 K_o Consolidation

The MDSS uses a wire–reinforced membrane which allows samples to be consolidated under K_o conditions (i.e., the wire–reinforced membrane is assumed to not allow any lateral deformation). As a result, the MDSS should produce the same consolidation results as that obtained in an oedometer test. Figure 4.9 plots the compression curve from the consolidation phase of two CK_oUMDSS tests on BBC and the range of results for five oedometer tests on BBC. The data plotted in this figure show that the K_o consolidation data obtained in the MDSS compare very well with those of the oedometers. Similar agreement was found for values of the time to end of primary (t_p), coefficient of consolidation (c_v) and rate of secondary compression ($C\alpha\epsilon$).

7.4.2 CK_oUDSS Behavior of BBC

Results from CK_oUMDSS tests on normally consolidated BBC agree well with those obtained in the Geonor DSS. Figure 4.3 compares the normalized stress–strain curves for three Geonor DSS tests and four MDSS tests all having $\sigma'_{vc} = 3$ ksc. The undrained strength ratio from the four MDSS tests equals 0.185, which is 7% lower than from the three Geonor tests (0.201). Unlike the Geonor results, the MDSS shear stress–shear strain curves have remarkably little scatter. The average strain at failure for tests in the two devices is almost identical; 4.8% for the MDSS and 5.1% for the Geonor. In general, the MDSS shear stress–shear strain curves are identical in shape to the Geonor curves, except that they are shifted slightly lower.

Results from a procedure developed to evaluate the relative stiffness of the two devices indicate that the Geonor DSS is slightly more rigid than the MDSS. This combined with the fact that the MDSS has an additional degree of freedom (necessary to conduct tests at different θ angles) may be the reasons why the undrained strength

ratio is lower in the MDSS than that measured in the Geonor DSS.

The Normalized undrained secant Young's modulus values do not compare very well at low applied stress ratios (i.e., at the beginning of shear; Figure 4.6). Inspection of the initial portion of the MDSS shear stress–strain curves (Figure 4.10) indicates that there was a seating problem with the CK_0U tests run in this device and is a probable cause for obtaining lower undrained modulus values.

7.4.3 CAUDSS Behavior of BBC

Figure 4.17 plots the shear stress–shear strain curves from CAU tests at $\theta = 0^\circ$ and $\tau_{hc}/\sigma'_{vc} = 0.2$ performed both in the Geonor DSS and the MDSS. In this type of test the sample is consolidated with a horizontal shear stress equal to 20% of the vertical consolidation stress and subsequently sheared undrained by application of an additional horizontal shear stress acting in the same direction as the consolidation shear stress (i.e., $\theta = 0^\circ$). The MDSS and Geonor DSS results compare very well except for modulus values (Figure 4.18b). Like the CK_0U tests, the MDSS undrained strength ratio was lower (3.5%) than that measured in the Geonor DSS and the modulus values were considerably less, except near the peak shear resistance. With the exception of the modulus values, the CAU test results are very satisfactory because the MDSS, in a test for which the device was specifically designed, produced results nearly identical to those measured for the same type of test run in the Geonor DSS.

7.4.4 Kinematic Proof Tests

In the MDSS, an elastic material should deform in the direction of any applied incremental horizontal shear stress. If the material is loaded in one direction and then subjected to a second horizontal shear stress acting in another direction, the sample should incrementally deform in the direction of application of the second shear stress. This provides an important check on the kinematics of the MDSS because the orientation of the applied horizontal shear stress is known and hence the expected

orientation of the shear strain path of a specimen is also known and can be compared with measurements made in the MDSS.

The kinematic proof tests with an elastic material proved to be very successful (Figures 4.19 and 4.20). The test results showed that the rubber specimen deformed in the direction of the applied τ_1 for different θ angles and also that the γ_t and ϵ_v at the end of application of τ_1 and σ_v are independent of θ. Furthermore, during subsequent application of the second horizontal shear stress τ_2, the specimen deformed parallel to the X axis showing the elastic nature of the rubber which the MDSS clearly captured with repeatability. These kinematic proof tests gave excellent results, confirming that the application of τ_1, sample set–up procedure and strain measurement system in the MDSS are working properly and produce repeatable results.

7.5 SOIL BEHAVIOR IN UNDRAINED DIRECT SIMPLE SHEAR

Appendix A presented a state–of–the–art review of undrained direct simple shear testing of normally consolidated cohesive soils. It also included a comprehensive study of results from over 100 CK_oUDSS tests conducted during the past 20 years at MIT on over 30 different of soils.

The influence of the nonuniform state of stress caused by the DSS device on the measured behavior of test specimens was investigated in Appendix G and summarized in Chapter 5. Several constant height tests were conducted on an elastic specimen (rubber) in the Geonor DSS and MDSS which clearly reflected the nonuniform state of stress which develops in DSS specimens. For this elastic material, gaps developed at the upper leading edge and lower trailing edge of the specimen during shear (Figures 5.7 and G.1). These gaps caused a substantial decrease in the vertical stress required to maintain the sample height constant during shear. Under ideal simple shear conditions this would not occur for an elastic material such as the rubber sample.

In fact, for a DSS test with $\theta = 180°$, application of the second shear stress τ_2 resulted in a normalized vertical stress curve which is parabolic and symmetric with respect to the neutral axis of the DSS (i.e., path c–d in Figure 5.7). In this type of test the gaps which develop during application of τ_1 start to close upon reversal of the shear stress due to τ_2 acting in the opposite direction. As the gaps close, the effective area of the specimen increases, thereby resulting in a decrease in the vertical stress and a tendency for the specimen to expand in the vertical direction. In response to this behavior the constant height servo control system increases the vertical force to maintain the sample height constant. The rate of increase in the vertical stress monotonically decreases as the X coordinate approaches zero ($\gamma = 0\%$) and the reverse phenomenon occurs as the sample passes through the neutral axis of the device.

The results of three cyclic Geonor DSS tests performed on cohesive samples (OCR=1 BBC; OCR= 1.5 and 4.1 San Francisco Bay Mud) at the conventional undrained shear rate of strain ($\dot{\gamma} = 5\%$/hour) displayed some interesting characteristics as the samples strained towards and past the neutral axis of the device during the first reversal stage of the applied shear stress (the samples were allowed to strain well beyond their peak shear resistance before the shear stress was reversed). In all three tests the vertical stress and shear resistance reached a peak value during the reversal stage when the sample was exactly at the neutral axis of the device (Figures G.5 and G.6). Furthermore, the vertical stress and shear resistance values during the reversal stage were nearly symmetric about the neutral axis. The fact that three DSS tests on two different soils at three different OCR's and stress levels exhibit this type of behavior is more than coincidental (Figure 5.8). Symmetry of the normalized vertical stress about the neutral axis of the device for all three different test conditions is suggestive of behavior that is not exclusively dependent on the type of soil and stress conditions but also on the DSS apparatus itself.

Based on the results of the tests on rubber and the cyclic tests on clay

specimens it was hypothesized that the behavior of samples tested in a direct simple shear apparatus can be strongly influenced by the device. Specifically, during undrained shear the DSS apparatus causes the vertical stress acting on a sample to decrease as it strains away from the neutral axis of the device and the opposite occurs when a sample strains towards the neutral axis. This hypothesis implies that the pronounced strain softening always observed at large strains is at least partially due to the nonuniform vertical stress caused by the DSS device (Figure 5.9). Furthermore, the results of CAU $\theta = 180°$ tests may exhibit unusual behavior since in this type of test the sample strains back towards and through the neutral axis of the device during undrained shear (this was found to be the case for the $\theta = 180°$ tests with $\tau_{hc}/\sigma'_{vc} = 0.2$; see tests G6 and G7 stress paths in Figure 5.12).

7.6 MULTIDIRECTIONAL DIRECT SIMPLE SHEAR BEHAVIOR OF ANISOTROPICALLY CONSOLIDATED BOSTON BLUE CLAY

An experimental test program was conducted on BBC with the objective of reproducing the gravity loading and ice loading forces acting at representative elements within the foundation soil of an offshore Arctic gravity structure. Samples of BBC were anisotropically consolidated under a vertical normal stress (σ'_{vc}) and horizontal shear stress ($\tau_1 \equiv \tau_{hc}$) and subsequently sheared undrained by application of a second horizontal shear stress (τ_2) acting at an angle θ relative to the consolidation shear stress.

7.6.1 Behavior of BBC as a Function of Consolidation Stress Ratio ($\theta = 0$ and $180°$)

The results of the Geonor CAUDSS tests on BBC showed that there is a significant influence of the consolidation stress ratio (τ_{hc}/σ'_{vc}) on the undrained behavior of the soil (Figures 5.10 to 5.12). Increasing the consolidation stress ratio from 0 (K_o) to 0.2 ($\theta = 0°$) results in an increase in the peak shear resistance (Figures 5.10 and 5.23). Decreasing τ_{hc}/σ'_{vc} from 0.2 ($\theta = 0°$) to –0.2 ($\theta = 180°$) results in a

significant increase in the shear strain and normalized pore pressure ($\Delta u/\sigma'_{vc}$) at the peak shear resistance (Figures 5.25 and 5.26). There is also a decrease in the normalized undrained secant Young's modulus, E_u/σ'_{vc} at a given shear strain γ_x, as the applied undrained stress ratio varies from reversing the direction of shear acting on a sample ($\theta = 180°$) to acting in the same direction ($\theta = 0°$; Figure 5.14).

Summary Figure 5.23 shows the parabolic increase in the peak shear resistance as τ_{hc}/σ'_{vc} varies from 0 to 0.2 in the $\theta = 0°$ tests. In Contrast, the $\theta = 180°$ tests show little change in the peak shear resistance as τ_{hc}/σ'_{vc} varies from 0 to –0.2. The value for $\tau_{hc}/\sigma'_{vc} = -0.2$ represents an adjusted value because the two tests conducted at this consolidation stress ratio exhibited peculiarities in the stress path before reaching the measured peak shear resistance (Figure 5.12). This adjustment was made (Figure 5.27) because it is believed that the behavior of the samples in these two tests were in part influenced by the nonuniform state of stress caused by the DSS device (as discussed in Appendix G and summarized in Section 7.5). However, the procedure used to make the adjustment, as outlined in Chapter 5, is not very pleasing in that it appears to be rather arbitrary. Furthermore, it does not provide an adjustment for specimen behavior during the entire test, including estimates of other parameters at failure (e.g., γ_f, $(\sigma'_v/\sigma'_{vc})_f$, etc). Results of predictions using the MIT–E3 constitutive soil model, presented in Chapter 6 and summarized in the next section (7.7), were found to provide satisfactory to excellent predictions of the experimental data and therefore it is recommended that the model be used as a guide for evaluating the $\theta = 180°$ tests. As presented in Chapter 6, the model predicts a normalized peak shear resistance $(\tau_x/\sigma'_{vc})_{max}$ for a $\theta = 180°$ test with $\tau_{hc}/\sigma'_{vc} = 0.2$ equal to 0.2 compared with the average measured value of 0.24 (Tests G6 and G7) and the Chapter 5 recommended adjusted value of 0.21 (Figure 5.27).

7.6.2 Behavior of BBC as a Function of the Test Angle θ

The results of the CAUMDSS test program on BBC showed that there is a significant dependence of the undrained shear behavior of the soil on the test angle θ. At low θ angles the soil is extremely brittle and requires very little shear strain to reach failure, whereas at higher θ angles the soil becomes much more ductile with very large shear strains at failure (Figure 5.15.and 5.17)

There is a very large variation in the undrained strength of BBC as θ varies from 0° to 180° (Figure 5.28). It is also significant that the variation is a smooth one with no abrupt changes in the plot of $(\tau_x/\sigma'_{vc})_{max}$ versus θ. The maximum τ_x/σ'_{vc} occurs at $\theta = 0°$, while the minimum is at $\theta = 120°$. The reduction in $(\tau_x/\sigma'_{vc})_{max}$ as θ varies from 0° to 120° is approximately 55%.

The normalized vertical effective stress (σ'_v/σ'_{vc}) at failure exhibits a smooth but significant decrease as θ varies from 0° to 150° (Figure 5.31). The tests at $\theta = 0°$ develop very little pore pressure before reaching failure. As θ increases the magnitude of pore pressure development increases significantly, such that for $\theta = 150°$ the normalized vertical effective stress at $(\tau_x)_{max}$ is approximately 45% less than that for the tests at $\theta = 0°$.

The strain paths (Figure 5.20) for these tests showed that the BBC specimens clearly did not exhibit elastic behavior. For an elastic material the strain paths will all be parallel to the X axis, which was confirmed for the tests on rubber (Figure 4.20). In spite of the incremental undrained shear stress acting parallel to the X axis, all of the $\theta = 30°$ to 150° tests on BBC have a component of shear strain in the Y direction from the beginning of shear.

The preceeding CAUMDSS test data on normally consolidated BBC show dramatic differences in the soil response as a function of the test angle θ. Not only are the differences dramatic but the results exhibit a remarkably smooth variation as a function of θ. The implication of these test results is that designing the foundation of

an offshore Arctic gravity structure subjected to ice loading requires incorporating the results of these types of tests in the design process. Given the complicated nature and variation of the stress conditions within the foundation soil during ice loading of a structure, such an analysis will require using numerical techniques (i.e., Finite Element Method with realistic constitutive soil model). Thorough and reliable predictions for the foundation performance will require the use of a soil model which is able to reproduce the main behavioral features of the experimental results presented in Chapter 5 and summarized here.

7.7 PREDICTION OF MULTIDIRECTIONAL DIRECT SIMPLE SHEAR TEST RESULTS USING MIT–E3 SOIL MODEL

7.7.1 MIT–E3 Soil Model

The MIT–E3 soil model described in Chapter 6 was developed at MIT (Whittle, 1987, 1989) to describe the drained and undrained behavior of soils with varying overconsolidation and under both monotonic and cyclic loading. The model uses a formulation which consists of three distinct parts: 1) a perfectly hysteretic model; 2) an elasto–plastic model for normally consolidated clays and 3) a bounding surface plasticity model. The model requires 15 input parameters, most of which can be determined from standard laboratory tests (Table 6.1). A very detailed evaluation of the model by Whittle (1987) found that it provides good to excellent predictions of the behavior of normally consolidated and overconsolidated resedimented Boston Blue Clay (BBC) under monotonic undrained shear (e.g., CK_oUTC/E, PSC/E and DSS) and undrained cyclic direct simple shear. The model also performed extremely well in predicting the pronounced effects of inherent anisotropy as measured by Directional Shear Cell (DSC) tests on BBC at OCR = 4.

7.7.2 MIT–E3 Predictions

In Chapter 6, MIT–E3 predictions of the Multidirectional Direct Simple Shear

behavior of normally consolidated BBC were compared with the experimental results presented in Chapter 5. The MIT–E3 predictions and the very significant measured changes in soil behavior showed very good to excellent agreement. This was particularly the case for the two more important design parameters: the undrained peak shear resistance (Figure 6.13 and 6.14) and the secant values of Young's modulus versus shear strain (Figure 6.18). The major variation between the model predictions and experimental results was in the post peak excess pore pressure and hence strain softening behavior of the soil. The predicted peak shear resistance for all θ angles with $\tau_{hc}/\sigma'_{vc} = 0.2$ coincided with the critical state condition and therefore the shear stress–shear strain curves were horizontal once the peak shear resistance was reached (Figure 6.5b). This was not the case for the experimental results, in particular for low θ angles (Figure 6.5a). However, the results in Chapter 5 and Appendix G indicate that a significant portion of the strain softening observed in the DSS and MDSS devices may be caused by the apparatus. Hence, the actual strain softening behavior probably lies between the measured and predicted results.

Given the very good agreement between the experimental results and MIT–E3 predictions, the model was used to predict the CAUMDSS response of OCR = 1 and 4 BBC at different consolidation stress ratios. In both cases the model predicted dramatic changes in the behavior of BBC as a function of the test angle θ and the consolidation stress ratio τ_{hc}/σ'_{vc}. This was particularly the case for the variation of the peak shear resistance $(\tau_x/\sigma'_{vc})_{max}$ as shown in Figures 6.19 & 6.20 and 6.31 & 6.32 for normally consolidated and overconsolidated BBC, respectively. Furthermore, the trends in the OCR = 4 peak shear resistance data are very similar to the normally consolidated results as shown in Figure 6.34. In fact, the values of $\tau_x(\theta)_{max}/\tau_x(\theta=0^\circ)_{max}$ are essentially identical up to $\theta = 90^\circ$ and then exhibit some deviation at $\theta = 120^\circ$ to 180°. However, the deviation is not very significant and in general, the results indicate that the value of $\tau_x(\theta)_{max}/\tau_x(\theta=0^\circ)_{max}$ is independent of

OCR for the same consolidation stress ratio (i.e., consolidation stress ratio equal to the same percentage of the CK_oUDSS strength at each OCR). The major difference between the predicted behavior of OCR = 1 and 4 BBC is in the development of shear induced pore pressures (OCR = 1 exhibits contractive behavior while OCR = 4 exhibits dilative behavior) and the shear strain at failure γ_{xf} (Figure 6.35).

MIT–E3 predictions were also made for the CAUMDSS behavior of normally consolidated Harrison Bay "Soft Zone Area" (SZA) Arctic silt. The input parameters for this soil were derived from the laboratory test program conducted at MIT on samples from Harrison Bay. The model predictions for this Arctic silt also showed dramatic changes in its behavior as a function of θ and τ_{hc}/σ'_{vc}, as is clearly shown for variation is peak strength plotted in Figures 6.44 and 6.45. The trends in $(\tau_x/\sigma'_{vc})_{max}$ for this soil are also similar to that predicted for OCR = 1 and 4 BBC.

7.7.3 Foundation Design Using MIT–E3 and the MDSS

The experimental results presented in Chapter 5 showed that ice loading on an offshore Arctic gravity structure leads to very complex changes in soil behavior as measured in the MDSS. However, experimental tests alone will not be sufficient for design. This type of geotechnical problem requires the use of numerical techniques such as the Finite Element Method (FEM). Detailed comparisons presented in Chapter 6 between the MDSS experimental results and those predicted by MIT–E3 found satisfactory to excellent agreement between the measured and predicted results. On this basis it was concluded that the MDSS and a finite element code with MIT–E3 as its constitutive model can together be used as a reliable design tool for offshore Arctic gravity structures. Table 6.13 gives a suggested procedure for foundation design of these structures using the MIT–E3 model and the MDSS. The procedure outlined in Table 6.13 is very sophisticated but so are the geotechnical aspects of this problem, particularly for the case of ice loading.

7.8 FUTURE RESEARCH

Recommendations for future research in this project are divided into the following three categories: (1) The MDSS Device, (2) Experimental Programs and (3) Recommended Design Procedure.

7.8.1 The MDSS

(a) The MDSS produced peak shear resistance values that were consistently lower than those measured in the Geonor DSS. Additional tests should be performed on different soils and at different stress levels (i.e., σ'_{vc}) to determine if the deviation is independent of soil type and stress level. If it is found that the deviation is dependent on stress level (i.e., deviation increases with increase in σ'_{vc}) then this would further indicate that it is a difference in the stiffness of the two devices that is a primary cause for the difference in measured strength.

(b) One disappointing aspect of the MDSS's performance was the measured secant Young's modulus values during undrained shear. The MDSS produced values which were more scattered and lower than measured in the Geonor DSS. The initial portions of the CK_oUDSS shear stress–strain curves of tests performed in the MDSS indicated that there was a seating problem in most of these tests. The technique used to measured γ in the MDSS should be reevaluated along with the procedure used to seat the sample to determine if an improvement can be developed to get better modulus values.

(c) The CAUMDSS tests on normally consolidated BBC with $\tau_{hc}/\sigma'_{vc} = 0.2$ gave consolidation results (i.e., during application τ_{hc} and σ'_{vc}) which indicated that there may be a dependency of the consolidation shear strain γ_* on the test angle θ. An investigation of this problem (Appendix F) proved to be inconclusive in that the source of the discrepancy could not be attributed to batch variability of the BBC samples

and/or the device itself. Additional tests should be conducted similar to those already performed to provide additional information for determining if γ_t is or is not dependent on θ and/or variability in the soil samples.

7.8.2 Experimental Programs

The following test programs should be performed to continue the investigation into the behavior of soil specimens subjected to combined gravity and ice loading forces.

1. Conducted a few additional tests on normally consolidated BBC at different consolidated stress ratios than used in this thesis (e.g., τ_{hc}/σ'_{vc}=0.1).
2. Perform a test program on overconsolidated BBC similar to that conducted in this thesis for normally consolidated BBC.
3. Perform a test program on a different soil such as an Arctic silt to confirm if basic behavior trends are similar to that found for OCR =1 and 4 BBC.
4. Continue investigation on influence of nonuniform state of stress in the DSS device to determine if a correction procedure for measured test data can be developed.

7.8.3 Recommended Design Procedure

Continue evaluation of MIT–E3 predictions as results from the experimental programs suggested in items 1 to 3 above become available. Analyze the state of stress within the foundation of an offshore Arctic gravity structure during gravity and ice loading using a suitable finite element code with MIT–E3 as its constitutive model (this work is contingent on the model being successfully implemented into ABAQUS which is currently being done for other research purposes at MIT). Results from these two tasks, together with the existing evaluation of MIT–E3 performed for this thesis, should ultimately be used to develop the final recommended foundation design procedure for offshore Arctic structures using MIT–E3 and the MDSS.

CHAPTER 8

REFERENCES

Note:

ASCE	= American Society of Civil Engineers
ASTM	= American Society for Testing and Materials
CGJ	= Canadian Geotechnical Journal
GTJ	= Geotechnical Testing Journal
ICSMFE	= International Conference on Soil Mechanics and Foundation Engineering
ISSMFE	= International Society for Soil Mechanics and Foundation Engineering
JGE	= Journal of Geotechnical Engineering
JGED	= Journal of the Geotechnical Engineering Division
JSMFD	= Journal of the Soil Mechanics and Foundations Division
MIT	= Massachusetts Institute of Technology
STP	= Special Technical Publication
USGS	= United States Geological Survey

Airey, D.W. and Wood, D.M. (1984), "Discussion on 'Specimen Size Effect in Simple Shear Test'," JGED, ASCE, Vol. 110, No. GT3, pp. 439–442.

Airey, D.W., Budhu, M. and Wood, D.M. (1985), "Some Aspects of the Behavior of Soils in Simple Shear," Developments in Soil Mechanics and Foundation Engineering, P.K. Banerjee and R. Butterfield, Eds., Vol. 2, Elsevier, London

Airey, D.W. and Wood, D.M. (1987), "An Evaluation of Direct Simple Shear Tests on Clay," Géotechnique, Vol. 37, No. 1, pp. 25–25.

Alaska Oil and Gas Association (1986), "What Types of Structures are used for Offshore Exploration Drilling?," Alaskan Update, Piper, R. (ed.), Vol. 4, No. 2, pp.4–7.

Alpan, I. (1967), "The Empirical Evaluation of the Coefficient K_o and K_{or}," Soil and Foundation, Vol. 7, No. 1, pp. 31–40.

Ansell, P. and Brown, S.F. (1978), "A Cyclic Simple Shear Apparatus for Dry Granular Material, " GTJ, Vol. 1, No. 2, pp. 82–92.

Arthur, J.R.F., Chua, K.S. and Dunstan, T. (1977), "Induced Anisotropy in a Sand," Géotechnique, Vol. 27, No. 1, pp. 13–36.

Arthur, J.P.F., Bekenstein, S., Germaine, J.T. and Ladd, C.C. (1981), "Stress Path Tests with Controlled Rotation of Principal Stress Directions," ASTM Symposium on Laboratory Shear Strength of Soil, STP No. 740, pp. 516–540.

Ayan, K.D.J. (1985), "Undrained Triaxial Strength–Deformation Behavior of Harrison Bay Arctic Silts," Master's Thesis, Department of Civil Engineering, MIT, Cambridge, MA.

Azzouz, A.S. and Baligh, M.M. (1984), "Behavior of Friction Piles in Plastic Empire Clays: Volume 3," Research Report No. R84–14, Department of Civil Engineering, MIT, Cambridge, MA.

Baligh, M.M., Azzouz, A.S., Wissa, A.E.Z., Martin, R.T. and Morrison, M.J. (1981), "The piezocone penetrometer," Proc. Natl. Conf. on Cone Penetration Testing and Experience, ASCE, St. Louis, pp. 247–263.

Baligh, M.M., and Azzouz, A.S. (1985a), "Stability Analysis for Gravity Arctic Structures," Technical Progress Report No. 3, Submitted to Standard Oil Production Company, Dallas, TX.

Baligh, M.M., and Azzouz, A.S. (1985b), "Stability Analysis for Gravity Arctic Structures," Technical Progress Report No. 4, Submitted to Standard Oil Production Company, Dallas, TX.

Baligh, M.M., Azzouz, A.S., Chin, C.T. and Elghaib, M.K. (1987), "Stability of Rigid Gravity Arctic Structures," Proc. Sixth International Offshore Mechanics and Arctic Engineering Symposium, Houston, TX., Vol. I, pp. 357–363.

Bathe, K.J. (1976), "ADINA – A Finite Element Program for Automatic Dynamic Incremental Nonlinear Analysis," Acoustics and Vibration Laboratory Report No. 82448–1, Department of Mechanical Engineering, MIT, Cambridge, MA.

Barnes, P.W. and Reimnitz E. (1974), "Sedimentary Processes on Arctic Shelves off the Northern Coast of Alaska," in The Coast and Shelf of the Beaufort Sea, J. Read and J.E. Sater (eds.), Arctic Institute of North America, Arlington, Virginia, pp. 439–476.

Bea, R.G., Puskar, F.J., Barnes, P.W. and Reimnitz, E. (1985), "The Role of Ice Gouging in Determining Global Forces on Arctic Structures," Proc. ACSE Specialty Conference Arctic '85, San Francisco, pp. 251–265.

Bishop, A.W. (1971), "Shear Strength for Undisturbed and Remolded Soil Specimens," Proc. Roscoe Memorial Symp., Ed. Parry, R.H.G, G.T. Foulis & Co., Henley–on–Thames, pp. 3–58.

Bjerrum, L. (1954), "Theoretical and Experimental Investigations on the Shear Strength of Soils, " Norwegian Geotechnical Institute Publication No. 5, Oslo, 113 pp.

Bjerrum, L. (1967), "Engineering Geology of Norwegian Normally Consolidated Marine Clays as Related to Settlements of Buildings," 7th Rankine Lecture, Géotechnique, Vol. 17, No. 2, pp. 81–118.

Bjerrum, L. (1972), "Embankments on Soft Ground: State–of–the–Art–Report," Proceedings ASCE Specialty Conference on Performance of Earth and Earth Supported Structures; Lafayette, IN., Vol. II, pp. 1–54.

Bjerrum, L. (1973), "Problems of Soil Mechanics and Construction on Soft Clays: State–of–the–Art–Report," Proceedings 8th ICSMFE, Moscow, Vol. III.4, pp. 109–159

Bjerrum, L., and Landva, A. (1966), "Direct Simple Shear Tests on Norwegian Quick Clay," Géotechnique, Vol. 16, No. 1, pp. 1–20.

Borin, D.L. (1973), "The Behaviour of Saturated Kaolin in the Simple Shear Apparatus," PhD Thesis, Cambridge University.

Brooker, E.W. and Ireland, H.O. (1965), "Earth Pressures at Rest Related to Stress History," CGJ, Vol. 11, No. 1, pp. 1–15.

Budhu, M. (1979), "Simple Shear Deformation of Sands," PhD Thesis, Cambridge University.

Budhu, M. (1984a), "Discussion on 'Specimen Size Effect in Simple Shear Test'," JGED, ASCE, Vol. 110, No. GT3, pp. 442–445.

Budhu, M. (1984b), "Non–Uniformities Imposed by Simple Shear Apparatus," CGJ, Vol. 21, No. 1, pp. 125–137.

Budhu, M. (1985), "Lateral Stresses Observed in Two Simple Shear Apparatus," JGE, Vol. 111, No. 6 , pp. 698–711.

Budhu, M. (1988), "A New Simple Shear Apparatus," GTJ, Vol. 11, No. 4, pp. 281–287.

Casagrande, A. (1936), "The Determination of the Preconsolidation Load and its Practical Significance," Proc. 1st ICSMFE, Cambridge, MA. pp. 60–64.

Casagrande, A. (1979), "Liquefaction and Cyclic Deformation of Sands: A critical Review," Harvard Soil Mechanics Series No. 88, Harvard University, Cambridge, MA., 51p.

Casagrande, A. and Carillo, N. (1944), "Shear Failure in Anisotropic Materials," Proc. Boston Soc. of Civil Engr., Vol. 31, pp. 74–87.

Casagrande, A. and Rendon, F. (1978), "Gyratory Shear Apparatus Design and Testing Procedures, Technical Report S–78–15, Corps of Engineers Waterways Experimental Station, Vicksburg, Mississippi.

Chamberlain, E.J., Sellman, P.V., Blouin, S.E., Hopkins, D.M. and Lewellen, R.I. (1978), "Engineering Properties of Subsea Permafrost in the Prudhoe Bay Region of the Beaufort Sea," Proceedings of the Third International Conference on Permafrost, Vol. I, Edmonton, Alberta, pp. 630–635.

Christian, J.T. (1981), "Discussion of 'State of the Art: Laboratory Strength Testing of Soils'," Laboratory Shear Strength of Soils, ASTM STP 740, R.N. Yong and F.C. Townsend, Eds., ASTM, pp. 638–640.

Cole, E.R.L. (1967), "The Behaviour of Soils in The Simple Shear Apparatus," PhD Thesis, Cambridge University.

Croasdale, K.R. and Marcelus, R.W. (1978), "Ice and Wave Action on Artificial Islands in the Beaufort Sea," Can. J. Civil Eng., Vol. 5, March, pp. 98–113.

de Josselin de Jong, G. (1971), Discussion: Session 2. Strain Strain Behaviour of Soils, Proc. Roscoe Memorial Symp., Ed. Parry, R.H.G, G.T. Foulis & Co., Henley–on–Thames, pp. 258–261.

De La Huerta, C.G. (1987), "Analysis of Piezocone Penetration Test Data in Arctic Silts," Master's Thesis, Department of Civil Engineering, MIT, Cambridge, MA.

De Ruiter, J. (1981), "Current Penetrometer Practice," Cone Penetration Testing and Experience., ASCE National Convention, St. Louis, Missouri.

De Ruiter, J. and Richards, A.F. (1983), "Marine Geotechnical Investigations – a Mature Technology," Proc. ASCE Conference on Geotechnical Practice in Offshore Engineering, Austin , TX.

Dingle, P.J. (1982), "Constructing Artificial Islands in Canada's Beaufort Sea," Ocean Industry, June, pp. 29–31.

Disman, S.H. (1968), "Direct Simple Shear Tests on Three Saturated Clays," Master's Thesis, Department of Civil Engineering, MIT, Cambridge, MA.

Duncan, J.M. and Dunlop, P. (1969), "Behavior of Soils in Simple Shear," Proc. 7th. ICSMFE, Mexico, pp. 101–109.

Dyvik, R., Zimmie, T.F. and Floess, C.H.L. (1981), "Lateral Stress Measurements in Direct Simple Shear Device," Laboratory Shear Strength of Soil, ASTM STP No. 740, R.N. Yong and F.C. Townsend, Eds., pp. 191–206.

Dyvik, R. and Zimmie, T.F. (1983), "Lateral Stress Measurements During Static and Cyclic Direct Simple Shear Testing," NGI Publication No. 149, pp. 1–8.

Dyvik, R., Berre, T., Lacasse, S., and Raadim, B. (1987), "Comparison of Truly Undrained and Constant Volume Direct Simple Shear Tests," Géotechnique, Vol. 37, No. 1, pp. 3–10.

Edgers, L. (1967), "The Effect of Simple Shear Stress System on the Strength of Saturated Clay," Master's Thesis, Department of Civil Engineering, MIT, Cambridge, MA.

Finn, W.D.L., Pickering, D.Y. and Bransby, P.L. (1971), "Sand Liquefaction in Triaxail and Simple Shear Tests, JSMFD, ASCE, Vol. 97, No. SM4, pp. 639–659.

Franke, E., Kiekbusch, M. and Schuppener, B. (1979), "A New Direct Simple Shear Device," GTJ, Vol. 2, No. 4, pp. 190–199.

Gedney, R. (1988), "Design and Implementation of a Computer Controlled Servosystem for Automating Materials Testing," Master's Thesis, Department of Mechanical Engineering, MIT, Cambridge, MA.

Germaine, J.T. (1982), "Development of the Directional Shear Cell for Measuring Cross Anisotropic Clay Properties," Doctor of Science Thesis, Department of Civil Engineering, MIT, Cambridge, MA.

Gerwick, B.C. Jr. (1983), "Oil Rigs Designed to Combat Arctic Ice," Civil Engineering, ASCE, NY., December, pp. 38–41.

Grantz A. and Dinter, D.A. (1980), "Constraints of Geologic Processes on Western Beaufort Sea Oil Developments," Oil and Gas Journal, May 5th, pp. 304–319.

Hansen, J.B. and Gibson, R.E. (1949), "Undrained Shear Strengths of Anisotropically Consolidated Clays," Géotechnique, Vol. 1, No. 3, pp. 189–204.

Hara, A. and Kiyota (1977), "Dynamic Shear Tests of Soils for Seismic Analysis," Proc. 9th ICSMFE, Tokyo, Vol. 2, pp. 247–250.

Hight, D.W., Gens, A. and Symes, M.J.P.R. (1983), "The Development of a New Hollow Cylinder for Investigating the Effects of Principal Stress Rotations in Soils," Géotechnique, Vol. 33, No. 4, pp. 355–384.

Hill, R. (1950), Plasticity, Oxford University Press, 356p.

Idriss, I.M., Moriwaki, Y., Wright, S.G., Doyle, E.H. and Ladd, R.S. (1980), "Behavior of Normally Consolidated Clay Under Simulated Earthquake and Ocean Wave Loading Conditions, Proc. Int. Symp. Soils Under Cyclic and Transient Loading, G.N. Pande and O.C. Zienkiewcz, Vol. 1, pp. 437–495, Balkema, Rotterdam

Ishihara, K. and Yamazaki, F. (1980), "Cyclic Simple Shear Tests on Saturated Sand in Multi–Directional Loading," Soils and Foundations, Vol. 20, No. 1, pp. 45–59.

Ishihara, K. and Nagase, H. (1985), "Multi–Directional Irregular Loading Tests on Sand," Advances in the Art of Testing Soil Under Cyclic Conditions, ASCE, pp. 99–119.

Jaky, J. (1944), "The Coefficient of Earth Pressure at Rest," Jour. Soc. of Hungarian Architects and Engineers, Budapest, Hungary, Oct., pp. 191–196.

Jamiolkowski, M., Ladd, C.C., Germaine, J.T., and Lancellotta, R. (1985), "New Developments in Field and Laboratory Testing of Soils," Proc. XI ICSMFE, San Francisco, Vol. I, pp. 57–153.

Kavvadas, M. (1982), "Non–Linear Consolidation around Driven Piles in Clay," Ph.D. Thesis, Department of Civil Engineering, MIT, Cambridge, MA., 666p.

Kenny, T.C. (1964), "Sea–Level Movements and the Geologic Histories of the Post–Glacial Marine Soils at Boston, Nicolet, Ottawa and Oslo," Géotechnique, Vol. 14, No. 3, pp. 203–230.

Kjellman, W. (1951), "Testing the Shear Strength of Clay in Sweden," Géotechnique, Vol. 2, No. 3, pp. 225–232.

Koutsoftas, D. and Ladd, C.C. (1985), "Design Strengths for an Offshore Clay," ASCE, JGED, Vol. 111, No. 3, pp. 337–355.

Lacasse, S.M., Connell, D.H. and Ladd, C.C. (1972), "Interim Report on the Shear Strength of Connecticut Valley Varved Clays," Research Report No. R72–16, Department of Civil Engineering, MIT, Cambridge, MA., 121p.

Lacasse, S. and Vucetic, M. (1981), "Discussion of 'State of the Art: Laboratory Strength Testing of Soils'," Laboratory Shear Strength of Soils, ASTM STP 740, R.N. Yong and F.C. Townsend, Eds., ASTM, pp. 633–637.

Ladd, C.C. (1973), Discussion, Proc. 8th ICSMFE, Moscow, Vol. 4, No. 2, pp. 108–115.

Ladd, C.C. (1981), "Discussion of 'State of the Art: Laboratory Strength Testing of Soils'," Laboratory Shear Strength of Soils, ASTM STP 740, R.N. Yong and F.C. Townsend, Eds., ASTM, pp. 643–652.

Ladd, C.C. (1984), "Strength–Deformation Properties of Arctic Silts," Proposal prepared for MIT Sea Grant Program, Department of Civil Engineering, MIT., 25p.

Ladd, C.C. (1985), "Stability Evaluation During Staged Construction," in Recent Developments in Measurement and Modeling of Clay Behavior for Foundation Design, MIT Special Summer Course 1.60S, Department of Civil Engineering, MIT, Cambridge, MA.

Ladd, C.C. (1988), "Stability Evaluation During Staged Construction," 22nd Terzaghi Lecture, ASCE, draft version.

Ladd, C.C. and Edgers, L. (1972), "Consolidated–Undrained Direct Simple Shear Tests on Saturated Clays," MIT Research Report R72–82, No. 284, Department of Civil Engineering, MIT, Cambridge, MA., 354p.

Ladd, C.C. and Foott, R. (1974), "New Design Procedure for Stability of Soft Clays," ASCE, JGED, Vol. 100, No. GT7, pp. 763–786.

Ladd, C.C., Foott, R., Ishihara, K., Schlosser, F., and Poulos, H.G. (1977), "Stress–Deformation and Strength Characteristics, State–of–the–Art Report," Proc. 9th ICSMFE, Tokyo, Vol. 2, pp. 421–494.

Ladd, C.C., Azzouz, A.S., Martin, R.T., Day, R.W. and Malek, A.M. (1980), "Evaluation of Compositional and Engineering Properties of Offshore Venezuelan Soils, Volume 1: Orinoco Clay," Research Report No. R80–14, No. 665, Department of Civil Engineering, MIT, Cambridge, MA., 286p.

Ladd, C.C., Malek, A.M., Martin, R.T. and Mishu, R. (1981), "Evaluation of Compositional and Engineering Properties of Offshore Venezuelan Soils, Volume 2: North of Paria Stiff Clays," Research Report No. R81–21, No. 706, Department of Civil Engineering, MIT, Cambridge, MA., 217p.

Ladd, C.C. and Azzouz, A.S. (1983), "Stress History and Strength of Stiff Offshore Clays," in Geotechnical Practice in Offshore Engineering, S.G. Wright (ed.), ASCE, New York, pp. 65–80.

Ladd, C.C., Einstein, H.H., Martin, R.T., Germaine, J.T., and Novich, B.E. (1984), "Engineering Properties of Arctic Silts: Technical Progress Report No. 1," Center for Scientific Excellence in Offshore Engineering, MIT, Cambridge, MA.

Ladd, C.C., Weaver, J.S., Germaine, J.T., and Sauls, D.P. (1985), "Strength Deformation Properties of Arctic Silt," Proc. ACSE Specialty Conference Arctic '85, San Francisco, pp. 820–829.

Larrson, R. (1980), "Undrained Shear Strength in Stability Calculation of Embankments and Foundations on Soft Clays," CGJ, Vol. 17, No. 4, pp. 591–602.

Leonards, G.A. and Altschaeffl, A.G. (1964), "Compressibility of Clay," ASCE, JSMFD, Vol. 90, No. SM5, pp. 61–66.

Lucks, A.S. (1970), "The Influence of Particle Shape on the Strength of Granular Material," Doctor of Philosophy Thesis, Department of Civil Engineering, MIT, Cambridge, MA.

Lucks, A.S., Christian, J.T., Brandow, G.E. and Høeg, K. (1972), "Stress Conditions in NGI Simple Shear Test," JSMFD, ASCE, Vol. 98, No. SM1, pp. 155–160.

Madsen, O.S. (1978), "Wave–Induced Pore Pressure and Effective Stresses in a Porous Bed," Géotechnique, Vol. 28, No. 4, pp. 377–393

Malek, A.M. (1987), "Cyclic Behavior of Clay in Undrained Simple Shearing and Application to Offshore Tension Piles," Doctor of Science Thesis, Department of Civil Engineering, MIT, Cambridge, MA.

Mesri, G. and Choi, Y.K. (1985), "Settlement Analysis of Embankments on Soft Clays," JGE, Vol. 111, No. 4, pp. 441–464.

Mishu, R., Ladd, C.C., Martin, R.T. and Spikula, D.R. (1982), "Evaluation of Compositional and Engineering Properties of Offshore Venezuelan Soils, Volume 3: Tuy Cariaco Clays," Research Report No. R82–31, No. 735, Department of Civil Engineering, MIT, Cambridge, MA., 332p.

Mitchell, J.K. (1976), Fundamentals of Soil Behavior, John Wiley and Sons, New York, 422p.

Nadarajah, V. (1973), "Stress Strain Properties of Lightly Overconsolidated Clays," PhD Thesis, Cambridge University.

Ochiai, H. (1975), "The Behavior of Sands in Direct Shear Tests," Journal of JSSMFE, Vol. 15, No. 4, pp. 93–100.

Ochiai, H. (1976a), "The Coefficient of Earth Pressure at Rest of Sands," Journal of JSSMFE, Vol. 16, No. 2, pp. 105–111.

Ochiai, H. (1976b), "Discussion, 'On the Relation $\tau/\sigma_n = \kappa\tan\psi$ in the Simple Shear Test," Soils and Foundations, Vol. 16, No. 3, pp. 81–85.

Ochiai, H. (1981), "A Method for Calculating the Undrained Strength Ratio, c_u/p, of Normally Consolidated Clay Measured in the Simple Shear Apparatus," Soils and Foundations, Vol. 21, No. 1, pp. 109–115.

Oda, M. and Konishi, J. (1974), "Rotation of Principal Stresses in Granular Material During Simple Shear," Soils and Foundations, Vol. 14, No. 4, pp. 39–53.

O.T.A. (1985), Oil and Gas Technologies for the Arctic and Deepwater, Office of Technology Assessment, U.S. Congress,Washington, D.C., OTA–O–270.

Ogata, K. (1970), Modern Control Theory, Prentice–Hall, Inc., New York.

O'Neill, D.A. (1985), "Undrained Strength Anisotropy of an Overconsolidated Thixotropic Clay, S.M. Thesis, Dept. of Civil Eng., MIT, Cambridge, MA, 360p.

Peacock, W.H. and Seed, H.B. (1968), "Sand Liquefaction Under Cyclic Loading Simple Shear Conditions," JSMFD, ASCE, Vol. 94, No. SM3, pp. 689–708.

Prévost, J.H. and Høeg, K. (1976), "Re–analysis of Simple Shear Soil Testing," CGJ, Vol. 13, No. 4, pp. 418–429.

Randolph, M.F. and Wroth, C.P. (1981), "Application of the Failure State in Undrained Simple Shear to the Shaft Capacity of Driven Piles,", Géotechnique, Vol. 31, No. 1, pp. 143–157.

Reimnitz, E, Kempema, E., Ross, R. and Minkler, P. (1980), "Overconsolidated Surficial Deposits," USGS Open File Report No. 80–2010.

Roscoe, K.H. (1953), "An Apparatus for the Application of Simple Shear to Soil Samples," Proc. 3rd ICSMFE, London, Vol. 1, pp. 186–191.

Roscoe, K.H., Bassett, R.H. and Cole, E.R.L. (1967), "Principal Axes Observed During SImple Shear of a Sand," Proc. Geotechnical Conf., Olso, Vol. 1, pp. 231–237.

Roscoe, K.H. and Burland, J.B. (1968), "On the Generalized Behavior of 'wet' Clay," in Engineering Plasticity, Eds. J. Heyman and F. Leckie, Cambridge University Press, Cambridge, pp. 535–609.

Saada, A.S. and Townsend, F.C. (1981), "State of the Art: Laboratory Strength Testing of Soils," Laboratory Shear Strength of Soil, ASTM STP 740, R.N. Yong and F.C. Townsend, Eds., pp. 7–77.

Sauls, D.P., Germaine, J.T. and Ladd, C.C. (1984), "Strength Deformation Properties of Harrison Bay Arctic Silts," MIT Research Report R84–18, No. 773, Department of Civil Engineering, MIT, Cambridge, MA. 318p.

Seah, T.H. (1989), personal communication.

Schofield, A.N. and Wroth, C.P. (1968), Critical State Soil Mechanics, McGraw Hill, London, 310p.

Shaw, P. and Brown, S.F. (1986), "Cyclic Simple Shear Testing of Granular Materials," GTJ, Vol. 9, No. 4, pp. 213–220.

Shen, C.K., Saligh, K. and Herrmann, L.R. (1978), "An Analysis of NGI Simple Shear Apparatus for Cyclic Soil Testing.," in Dynamic Geotechnical Testing, ASTM STP 654, ASTM, pp. 148–162.

Shibuya, S. and Hight, D.W. (1987), "On The Stress Path in Simple Shear," Géotechnique, Vol. 37, No. 4, pp. 511–515.

Sidney, R., Strom, J.A. and Pyke, R.M. (1978), "Discussion on Measurement of Dynamic Soil Properties," Proc. Specialty Conf. Earthquake and Soil Dynamics, Pasadena, Vol. 3, pp. 1478–1481.

Silver, M.L., Tatsuoka, F., Phukunhaphan, A. and Avramidis, A.S. (1980), "Cyclic Undrained Strength of Sand by Triaxial Test and Simple Shear," Proc. 7th World Conference Earthquake Engineering, Istanbul, Vol. 3. pp. 281–288.

Stroud, M.A. (1971), "The Behavior of Sand at Low Stress Levels in the Simple SHear Apparatus," PhD Thesis, Cambridge University.

Symes, M.J.P.R. (1983), "Rotation of Principal Stresses in Sand," Doctor of Philosophy Thesis, Department of Civil Engineering, Imperial College of Science and Technology, London.

Symes, M.J.P.R., Gens, A. and Hight, D.W. (1984), "Undrained Anisotropy and Principal Stress Rotation in Saturated Sand," Géotechnique, Vol. 34, No. 1, pp. 11–27.

Tatsuoka, F. and Silver, M. (1981), "Undrained Stress–Strain Behavior of Sand Under Irregular Loading," Soils and Foundations, Vol. 21, No. 1, pp. 51–56.

Taylor, D.W. (1953), "A Direct Shear Test With Drainage Control," ASTM STP 131, pp. 63–74.

U.S. Army Corps of Engineers (1970), "Stability of Earth and Rock Fill Dams," Engineering Manual EM 1110–2–1902, Office of the Chief of Engineers, Washington, D.C.

Vivatrat, V. and Watt, B.J. (1983), "Stability of Arctic Gravity Structures," Proc. ACSE Specialty Conference on Geotechnical Practice in Offshore Engineering, Austin, TX. pp. 267–287.

Vucetic, M. (1984), "Discussion of 'An Evaluation of Laboratory Testing Techniques in Soil Mechanics'," Soils and Foundations, Vol. 24, No. 2 pp. 112–117.

Vucetic, M. and Lacasse, S. (1982), "Specimen Size Effect in Simple Shear Test," JGED, Vol. 108, No. GT12, pp. 1567–1585.

Vucetic, M. and Lacasse, S. (1984), "Specimen Size Effect in Simple Shear Test: Closure," JGE, Vol. 110, No. GT3, pp. 439–453.

Walbaum, M. (1988), "Procedure for Investigation of Sample Disturbance Using the Direct Simple Shear Apparatus," Master's Thesis, Department of Civil Engineering, MIT, Cambridge, MA.

Wang, J.L., Vivatrat, V. and Ruser, J.R. (1984), "Geotechnical Properties of Alaska OCS Marine Silts," Proc. Offshore Technology Conference, Houston, TX., Vol. 4.

Watt, B.J. (1982), "Hydrocarbon Extraction in Arctic Frontiers, State–of–the–Art Paper", Proceedings 3rd International Conference on the Behavior of Offshore Structures, Cambridge, MA, Vol. 1, pp. 71–91.

Weeks, W.F., Barnes, P.W., Rearic, D.M. and Reimnitz E. (1983), "Statistical Aspects of Ice Gouging on the Alaskan Shelf of the Beaufort Sea," Cold Regions Research and Engineering Laboratory Report No. 83–21, U.S. Army Corps of Engineers, Hanover, NH., 40p.

Whittle, A.J. (1987), "A Constitutive Model for Overconsolidated Clays with Application to the Cyclic Loading of Friction Piles," Sc.D. Thesis, Department of Civil Engineering, MIT, Cambridge, MA, 641p.

Whittle, A.J. (1989a), "A Model for Predicting the Behaviour of Overconsolidated Clays: Part 1 Formulation," submitted for publication in Géotechnique.

Whittle, A.J. (1989b), "A Model for Predicting the Behaviour of Overconsolidated Clays: Part 2 Evaluation," submitted for publication in Géotechnique.

Williams, C.E. (1973), "Undrained Creep Behavior of Atchafalaya Clay From CU Direct–Simple Shear Tests," Master's Thesis, Department of Civil Engineering, MIT, Cambridge, MA.

Wood, D.M., Drescher, A. and Budhu, M. (1979), "On the Determination of the Stress State in the Simple Shear Apparatus," GTJ, ASTM, Vol. 2, No. 4, pp. 211–222.

Wright, D.K., Gilbert, P.A. and Saada, A.S. (1978), "Shear Devices for Determining Dynamic Soil Properties," Proc. ASCE Specialty Conference on Earthquake Engineering and Soil Dynamics, Vol. 2, pp. 1056–1075.

Wroth, C.P. (1984), "The Interpretation of In Situ Soil Tests," Géotechnique, Vol. 34, No. 4, pp. 449–489.

Wroth, C.P. (1987), "The Behavior of Normally Consolidated Clay as Observed in Undrained Direct Simple Shear Tests," Géotechnique, Vol. 37, No.1, pp. 37–43.

Yin, E.Y–P. (1985), "Consolidation and Direct Simple Shear Behavior of Harrison Bay Arctic Silts," Master's Thesis, Department of Civil Engineering, MIT, Cambridge, MA.

Young, G.A. (1986), "The Strength Deformation Properties of Smith Bay Arctic Silts," Master's Thesis, Department of Civil Engineering, MIT, Cambridge, MA.

APPENDIX A

DIRECT SIMPLE SHEAR TESTING OF COHESIVE SOILS

A.1 INTRODUCTION

The direct simple shear apparatus was developed to provide a soil testing device which can evaluate the stress–strain behavior of soils under simple shear strain conditions. It enables soil specimens to be tested wherein the major principal stress axis rotates during shear while the sample is kept under a condition of plane strain. Since its inception the direct simple shear apparatus has been used to study a variety of practical engineering problems. Several examples of this include:

1. Behavior of soil within the foundation of an embankment (Figure A.1);
2. Shearing of soil elements adjacent to a pile shaft (Figure A.2);
3. Dynamic loads on highway bases (Figure A.3);
4. Liquefaction behavior of soils;
5. Cyclic loads on foundation piles of offshore structures subjected to wind and wave loads (Figure A.4);
6. Interface studies between soil and other construction materials.

The purpose of this appendix is to provide an overview of the current state of the art of simple shear testing with particular emphasis on monotonic testing of normally consolidated cohesive soils.

A.2 DEFINITIONS

When an element is subjected to two equal and opposite principal stresses with the third principal stress remaining zero, the element is said to be in a state of pure shear stress. If the orientation of the element is rotated 45° then the element faces will be subjected only to shear force tractions (Figure A.5). The term pure shear can also be used to refer to a state of pure shear strain. It is a plane strain condition

where a uniform contraction in one direction is accompanied by a uniform extension in another direction under the condition that the element's volume remains constant. If a material is isotropic, then a pure shear stress condition is also a pure shear strain condition.

The term simple shear refers only to a state of strain. It is a plane strain state where under constant volume conditions an element deforms only in one direction (Figure A.6a). Throughout the deformation, the height of the element remains constant therefore requiring the sides to elongate. For small strains, a pure shear condition is equal to a simple shear strain plus a rotation. (Figure A.6b)

A.3 REVIEW OF EXISTING SIMPLE SHEAR DEVICES

The first direct shear apparatus capable of uniformly deforming a soil specimen was built in 1936 at the Royal Swedish Geotechnical Institute (SGI; Kjellman, 1951). The SGI apparatus used a circular soil specimen (6 cm diameter by 2 cm high) which is placed between a lower and upper grooved plate (Figure A.7). The specimen is confined laterally by a rubber membrane and a series of stacked aluminum rings. The ring spacing is small enough to allow vertical compression of the sample while minimizing lateral expansion of the membrane. Lead weights are used to apply both the vertical stress and horizontal shear stress to the sample. The sample is sheared under stress controlled conditions.

In the early 1960's, the Norwegian Geotechnical Institute (NGI) developed a simple shear device based on the SGI apparatus (Bjerrum and Landva, 1966). The new device was designed to K_o consolidate undisturbed sensitive clay specimens and to allow the specimen to strain in simple shear. These conditions are satisfied by confining a circular specimen (8 cm diameter by 1 cm height) within a wire–reinforced rubber membrane which allows the sample to deform vertically and horizontally with minimal changes in diameter (Figure A.8b). A special trimming apparatus was also

developed so that soft sensitive clays could be prepared with minimal disturbance. Constant volume tests are run by varying the normal force acting on a sample via a screw–controlled loading system. This device is sold commercially by Geonor as the Direct Simple Shear (DSS) apparatus.[1] MIT currently uses the Geonor Model 4 DSS which is described in more detail in Appendix E.

In 1953, Cambridge University developed a simple shear apparatus which can impose simple shear strain to a rectangular (6 cm square by 2 cm high) sand specimen while also permitting the measurement of volume changes during shear (Roscoe, 1953). The apparatus deforms an initially cuboidal sample into a parallelepiped shape by allowing two initially vertical sides of the box containing the sample to rotate as the top or bottom face displaces horizontally (Figure A.8a). Since 1953, seven versions of the Cambridge simple shear device have been developed (Mk1 to Mk7). The newer models have been elaborately instrumented to measure normal and shear forces along the faces of the sample and are also capable of testing cohesive soils (Figure A.9). Cambridge has also developed a fully instrumented circular simple shear apparatus (Figure A.10).

Since the late 1960's, many other types of simple shear devices have been developed. Several were primarily built to conduct cyclic tests on soil samples, including those described by Peacock and Seed (1968), Finn, et al. (1971), Hara and Kiyota (1977), Ansell and Brown (1978), Sidney, et al. (1978) and Idriss, et al. (1980). Several other devices are equipped with pressure chambers as described by Franke, et al. (1979), Silver, et al. (1980) and Tatsuoka and Silver (1981). Some special simple shear devices were developed to study multidirectional cyclic loading of sand samples for liquefaction studies, including those reported by Casagrande (1979) and Ishihara and Yamazaki (1980).

---

[1]From here on the NGI type DSS will be referred to as the Geonor simple shear device or the Geonor DSS.

A.4 UNIFORMITY OF STRESS AND STRAIN

From the beginning of its inception the simple shear apparatus has been known to be unable to impose uniform normal and shear stresses to a test specimen. In 1951, Kjellman wrote:

> "Since shearing forces are applied only on the top and bottom surfaces, it is required for equilibrium that the normal forces on these surfaces be eccentric ... thus, the normal stresses on the top and bottom surfaces must be unevenly distributed. The shearing stresses on these surfaces must also be unevenly distributed since they must be zero close to the front and rear of the specimen. Consequently, the stress system ... is heterogeneous, and differs from the system of pure shear."

This problem mainly arises from the fact that all existing simple shear devices cannot impose complementary shear forces to the specimen sides (Figure A.11). Roscoe (1953) emphasized this point by stating:

> "... it is apparent that it is not likely that any apparatus can be made which will impose uniform simple shear stress together with the complementary shear stress upon the surfaces of a sample."

Many studies have been conducted to determine the state of stress within a soil sample tested in a simple shear device. This section will discuss some of these studies including both theoretical and experimental analysis.

A.4.1 Theoretical and Numerical Analysis

Roscoe (1953) conducted a mathematical analysis of the Cambridge apparatus for an elastic material. The results show that the application of a shear force to the top and bottom faces is counterbalanced by a couple due to normal stresses acting on the sample faces minus a couple formed due to normal stresses acting on the sample sides. The development of the counteracting couple on the faces causes tension zones to develop at the upper leading edge and the lower trailing edge. These tension zones can be overcome if a sufficiently large normal stress is applied to the sample (this analysis was conducted with zero normal stress initially acting on the specimen). The

results also show that the shear stress on the sample faces is approximately uniform across only the middle third of each face. These results are shown schematically in Figure A.12.

Duncan and Dunlop (1969) used a finite element analysis with a nonlinear and anisotropic stress–strain constitutive relationship to study the stress conditions within the Cambridge simple shear apparatus. Based on Roscoe's study with an elastic material they point out that for horizontal equilibrium the shear stress varies throughout the height of the sample. It increases from the top and bottom towards the middle, reaching a maximum value at the mid height. For Roscoe's analysis the difference between the average values of shear stress at the top and at the mid height is equal to 7%. For the nonlinear finite element analysis the difference ranges from 4% to 8%, with the largest difference corresponding to small values of shear strain. They also found that the stress conditions in simple shear specimens are nonuniform and that progressive failure takes place. Yet they conclude that this has little or no effect on the ultimate simple shear resistance of San Francisco Bay Mud (SFBM) but may have a pronounced effect on the behavior of brittle soils.

Lucks, et al. (1972) used a three dimensional finite element method with linear elastic isotropic material properties and with the assumption of infinitesimal strains to study the stress conditions in the Geonor simple shear apparatus. Their results (shown in Figure A.13) indicate that local stress concentrations occur at the edges of an elastic material in the apparatus. However, overall 70% of the sample has a uniform stress condition and the horizontal shear stress acting at the mid height of the sample is uniform over the central 80% of the sample. Finally they conclude that it is reasonable to assume that the test is measuring the horizontal shear stress and that progressive yielding is of minimum importance unless the soil is significantly strain softening.

Prevost and Hoeg (1976) mathematically investigated the effects of slippage on the stress distribution of a specimen in the Cambridge simple shear apparatus using

an isotropic elastic soil model. Figure A.14 shows the results for the case of no slippage ($\lambda = 0$) between the top and bottom surfaces and the soil (this is the same as Roscoe's analysis). The figure also shows results for two additional cases where the center point on the top and bottom faces of the specimen moves only 80% ($\lambda = 0.2$) and 50% ($\lambda = 0.5$) of the horizontal displacement of the edges of the specimen (δ). The results show large variations in the stress distributions due to slippage, but the analysis represents an extreme case. It is highly unlikely that the center of a soil specimen will displace only 50% of the displacement of its edges and also for an elasto–plastic soil the stress concentrations will be much less as the soil yields. Furthermore, as pointed out by Lacasse and Vucetic (1981), slippage in most cases can be detected by studying the experimental stress–strain curve for a test (e.g., see Mishu, et al. 1982).

Shen, et al. (1978) conducted a parametric study of the Geonor simple shear apparatus using a three dimensional elastic finite element analysis of a nonaxisymetrically loaded axisymetric solid. The cases investigated used different combinations of material properties, membrane stiffness, specimen geometry and boundary displacements. The study concluded that the uniformity of the shear strain distribution in the sample improves as the:

1. specimen height–diameter ratio is decreased;
2. percent of wire–reinforcement increases;
3. elastic modulus of the soil decreases;
4. Poisson's ratio of the soil decreases;
5. applied horizontal displacement is increased.

Saada and Townsend (1981), in their state of the art paper on laboratory testing of soil, used St. Venant's principle and the results of photoelastic studies carried out by Wright, et al. (1978) to describe theoretically and experimentally the

elastic stress distribution for simple shear tests on square and circular specimens. From their analysis they conclude that the stress distribution in the sample is far from uniform and based on the photoelastic studies can change by as much as 47 percent. They further conclude that the simple shear apparatus is of no value for research purposes. Christian (1981), however, points out that the photoelastic experiments show the horizontal shear stresses are unsymmetrically distributed about the center of the sample, which is impossible for an isotropic, elastic, axially symmetric body loaded by displacing a rigid top platen uniformly in the horizontal direction.

A.4.2 Experimental Results

Vucetic and Lacasse (1982) performed a laboratory investigation of the influences of height to diameter ratio and membrane stiffness on the behavior of clay in the Geonor simple shear apparatus. The study included 21 strain–controlled constant volume tests on undisturbed specimens of the medium–stiff Haga CL clay. Figure A.15 shows a summary of their results for tests conducted at OCR = 1 and 10 with three different height to diameter ratios (0.32, 0.20 and 0.14 with the height remaining constant at 1.6 cm) and two different membranes (constantan (B) and the stiffer nickel alloy (A) reinforcement). The results show that for the clay tested the height to diameter ratio has no significant influence on the soil strength as measured in the Geonor simple shear device. Furthermore, the results are not sensitive to the stiffness of the wire reinforcement used in the membranes. In the closure to their paper, Vucetic and Lacasse (1984) present additional data from static and cyclic DSS tests conducted on 20 cm^2 and 50 cm^2 Drammen Clay specimens (Figure A.16). The results from most of these tests also show minimal differences in the soil's behavior between the two specimen sizes.

Based on their results Vucetic and Lacasse conclude that the theoretical elastic analysis of the simple shear device presents a pessimistic view of the expected

influence of stress nonuniformities. They state that such analyses cannot take into account the influence of soil yield during shear which will reduce the predicted stress concentrations. The authors end their paper by stating, "the direct simple shear test is ... believed to yield useful results and represents one of the valuable tools available today to define the complex stress–strain behavior of soils in engineering practice."

Many experimental studies have been conducted on the stress uniformity of sand specimens tested in the Cambridge simple shear apparatus (Airey and Wood, 1984; Budhu, 1984a; Budhu, 1984b; Airey, et al., 1985). The Cambridge devices (Figure A.9 and A.10) are elaborately instrumented so that the normal and shear stresses can be measured at several locations on the top and bottom faces of a specimen. Most of the results indicate that there are significant nonuniformities in the stress distributions both at the end of one–dimensional compression and at maximum shear stress.

A limited number of tests have been performed on clay samples with encouraging results (Airey and Wood, 1984; Airey, et al., 1985; Airey and Wood, 1987). Figure A.17 shows the normal and shear stress distributions measured along the principal third load cells for a constant volume test on normally consolidated kaolin in the Cambridge circular simple shear apparatus. For each load cell the vertical force, the eccentricity of the vertical force and the shear force can be determined. At the ends of the sample the normal stress distribution is estimated by fitting the measured normal forces and eccentricities to a quintic polynomial. The normal stress distribution at the end of one–dimensional consolidation ($\alpha = 0.0$) is approximately uniform while at $\gamma = 10\%$ and 20% shear strain ($\alpha = 0.1$ and 0.2) the distribution is fairly uniform. These results are much better than those measured for sands as concluded by Airey, et al. (1985) who state, "it has become clear for tests on clays in the simple shear apparatus that uniformity of boundary stresses and internal deformations is very much better than that for tests on sands." Airey and Wood

(1987) reinforce this conclusion by stating that, provided rupture planes do not develop in the test specimen, the stress–strain behavior from direct simple shear tests on clays can be presented with confidence.

A.4.3 Summary

All of the initial studies on the uniformity of stress in the simple shear apparatus were conducted using theoretical or numerical analysis assuming elastic behavior of the specimen. These studies shed light on the nature of the stress variation in the simple shear apparatus, but also tended to exaggerate the situation. For an elastic material, the stress concentrations at the specimen edges represent an extreme case. This would not be expected for a plastic material such as clay that yields, as clearly shown by Airey and Woods' (1987) test on Kaolin (Figure A.17) and Vucetic and Lacasse's (1982, 1984)) data from constant volume DSS tests on clay specimens with different height to diameter ratios (Figures A.15 and A.16). Furthermore, Airey and Wood justifiably argue that the uniformity of stress and strain is better in the DSS than in a standard triaxial apparatus at large strains with rough ends wherein considerable bulging of the sample may occur as the test approaches failure. Yet triaxial test results do not receive the same degree of suspicion as simple shear test results.

A.5 STATE OF STRESS AT FAILURE

Determining the state of stress at failure in the simple shear apparatus has received more attention than any other topic of simple shear testing. The basic problem is that in most simple shear devices there is not enough information to construct the Mohr's circle of stress at failure. For example, in the Geonor DSS only the vertical stress (σ'_v) and shear stress (τ_h) on a horizontal plane are known (this only fixes one point on Mohr's circle of stress). It is only in the more sophisticated devices

like those developed at Cambridge University that the complete state of stress can be determined. However, the Cambridge devices are clearly suited only for research purposes while the more practical Geonor type device is much more commonly used in practice. It is therefore important to be able to evaluate the state of stress in this type of device.

The state of stress at failure in a specimen can be represented by a unique Mohr's circle of stress. The maximum value of shear stress acting within the specimen is equal to the radius of Mohr's circle. This definition is often used to represent the undrained shear strength from tests on saturated cohesive soils as given by the following equation:

$$c_u = 0.5(\sigma_1 - \sigma_3)_f \qquad \text{A.1}$$

where:

c_u = undrained shear strength

σ_1 = major principal stress

σ_3 = minor principal stress

$(\sigma_1 - \sigma_2)_f$ = principal stress difference at failure (peak value)

Although this definition is not ideal because it does not take into account the value of the intermediate principal stress σ_2, it is what is most commonly used. Others (Ladd, 1988; Wroth, 1987 and USACE Design Manual, 1970) argue that for certain types of undrained strength analyses, it is more appropriate to use the available undrained shear strength on the most realistic potential failure surface (i.e., $c_u = 0.5(\sigma_1 - \sigma_3)\cos\phi'$; see Figure A.18). However, with respect to interpreting simple shear tests, the issue is determining Mohr's circle of stress and not the definition of undrained shear strength for analysis.

The purpose of this section is to review the various failure conditions that have been proposed for simple shear test results. While the main focus of this Appendix is on undrained simple shear testing of cohesive soils, results of drained tests

conducted on sands in the Cambridge devices will be presented. Wood, et al. (1979) recommend a procedure for determining the state of stress within the central part of a sample in the Cambridge rectangular apparatus (e.g., Mk7). The procedure uses equilibrium of forces to determine the stress tensor (σ_{ij}) based on measurements from the array of load cells in the device (Figure A.9). The stress state is calculated within the central part of the specimen because this is the region which is least influenced by the nonuniformities of stress at the ends. This procedure allows the orientation of the principal stress, principal stress increment and principal strain increment to be determined.

A.5.1 Failure Conditions

Seven approaches have been proposed to determine Mohr's circle of stress at failure for tests in the Geonor–type direct simple shear device. Each procedure makes an assumption with respect to determining the orientation of the major principal stress at failure, thereby allowing σ_1' and σ_3' to be calculated. Figure A.19 shows Mohr's circle of stress for the initial and failure conditions in a direct simple shear test. The initial stresses conform to a K_0 condition and the Mohr–Coulomb failure criterion is assumed to be valid (i.e., the stresses on the failure plane at failure, τ_{ff} and σ'_{ff}, correspond to the point of tangency between Mohr's circle at failure and the failure envelope). Table A.1 presents results of the computed state of stress for a representative DSS test on a normally consolidated Boston Blue Clay specimen using the different failure criteria.

(a) Failure Criterion I – Applied Stress System is Pure Shear

Roscoe (1953) and Duncan and Dunlop (1969) suggested that the applied stress system is one of pure shear (Figure A.20). In pure shear the total horizontal and vertical stresses remain constant during shear and therefore the ratio σ'_h/σ'_v is also assumed to be constant. This procedure produces the highest values of q_f/σ'_{vc} and friction angle ϕ'. It involves the least amount of rotation of the principal stresses and

gives a resultant failure plane which deviates the most from the horizontal plane (Ladd and Edgers, 1972).

Ladd and Edgers (1972) and Ochiai (1981) used this assumption to demonstrate the state of stress it predicts for DSS tests on several different clays. They show that for normally consolidated clays the procedure predicts totally unrealistic friction angles (e.g., $\phi' > 80°$ for Boston Blue Clay). Furthermore, the assumption of constant σ'_h/σ'_v during shear appears to also be unreasonable. Dyvik and Zimmie (1983) present results for tests on three different clays in the Geonor DSS where σ'_h/σ'_v starts at K_o (equal to 0.5, 0.54 and 0.65 for the three clays) and monotonically approaches 1 with increasing shear strain.[2]

(b) Failure Criterion II – Horizontal Plane is Plane of Maximum Obliquity (Failure Plane)

Here the assumption made is that the horizontal plane is the failure plane (rupture surface; Figure A.21). In this case $\tau_h = \tau_{ff}$ and $\sigma'_{vf} = \sigma'_{ff}$ and the major principal stress is oriented at an angle of $45 + \phi'/2$ with respect to the horizontal (i.e. $\sigma'_{hf} > \sigma'_{vf}$). This is the assumption usually made for interpreting the results of drained direct shear box tests.

Roscoe, et al. (1967) ran drained tests in the Cambridge Mk6 simple shear apparatus on dense and medium–loose sand. From the load cell array measurements they determined, for the central third of the specimen, the orientation to the horizontal of the major principal stress (ψ), major principal stress increment (χ), major principal strain increment (ξ), maximum shear stress (β), and the maximum obliquity (ω). These results, plotted in Figure A.22, clearly show that the plane of maximum obliquity (i.e. the failure plane) is not horizontal.

Figure A.23 shows the ruptures observed in a drained (constant load) test in

---

[2] σ'_h was determined using a specially instrumented wire–reinforced membrane. The procedure will be discussed in more detail in Section A.6.

the Cambridge circular simple shear apparatus on Kaolin (Airey, et al., 1985). Thin threads of lead paste were injected into the sample before shear and subsequently radiographed to show the step discontinuities in the paste. The ruptures shown occurred around the peak shear stress and extend across the center of the sample at an angle of 5–15° to the horizontal.

These test results suggest that the assumption that the horizontal plane in a DSS specimen is the plane of maximum obliquity is incorrect. It also gives a friction angle at failure that is too low to be reasonable (Table A.1 for normally consolidated BBC). Results like those presented by Airey, et al. but for CK_oUDSS tests on normally consolidated natural clays would be useful and, if similar to those presented above, would clearly eliminate this failure criterion from further consideration.

(c) Failure Criterion III – Horizontal Plane is a Plane of Maximum Shear Stress

For this assumption the major principal stress is inclined at an angle of 45° to the horizontal (Figure A.24). Furthermore, if the preshear initial state of stress is isotropic, then this assumption is equivalent to assuming the applied stress system is pure shear. For an undrained test, this assumption is the same as assuming coincidence of the principal axes of strain increment and stress as discussed in failure criterion VII.

Roscoe, et al. (1967) showed this assumption to be justified for their drained test on medium–loose sand, but not for the test on dense sand (Figure A.22). They also state that "data from undrained tests suggests that this assumption is reasonable whatever the void ratio; this result would be expected for a plastic material in a constant volume test if it was isotropic but not if anisotropic." However, they do not present any of the results from their undrained tests on sands. No data has been published for tests on natural clays in the Cambridge type devices to indicate whether, for these materials, the horizontal plane is indeed the plane of maximum shear stress.

(d) Failure Criterion IV – Assume Mohr–Coulomb Failure Envelope

In this case the Mohr circle at failure must pass through the measured normal and shear stresses on the horizontal plane (σ'_{vc} and τ_h) and be tangent to the assumed Mohr–Coulomb envelope (Figure A.25). The smaller of the two possible Mohr's circles is the more reasonable state of stress (Ladd and Edgers, 1972). If the larger circle is selected, σ'_h/σ'_v would be significantly greater than 1 which is unlikely.

(e) Failure Criterion V – Failure Occurs on Vertical Planes

de Josselin de Jong (1971) proposed this criterion using a book–stack analogy as shown in Figure A.26. The externally observed simple shear deformation can be produced by failure along horizontal planes, but the same external effect is found by failure along vertical planes with a subsequent clockwise rotation. Externally there is no difference, but in terms of stress there is. For the horizontal failure plane the major principal stress is orientated at $45 + \phi'/2$, while for vertical failure planes the major principal stress is orientated at $45 - \phi'/2$ (Figure A.27). The vertical failure plane produces the smaller shear stress and de Josselin de Jong concludes that the soil will choose this mode of deformation.

Randolph and Wroth (1981), Wroth (1984) and Wroth (1987) suggest that de Josselin de Jong's failure criterion is applicable to interpreting the results of undrained direct simple shear tests on normally consolidated clay. They support their hypothesis by showing the results of a simple shear test conducted by Borin (1973) on kaolin in the Cambridge simple shear apparatus. As shown in Figure A.28 the stress path plotted indicates that, at failure, one plane of maximum obliquity is approximately vertical (it is important to emphasize that the location of the origin of planes O_p for this criterion is at the opposite side of Mohr's circle compared to criterion II which assumes the failure plane is horizontal; Figures A.27 and A.21). Based on this observation, Randolph and Wroth used the vertical failure plane hypothesis and the

Modified Cam Clay soil model (Roscoe and Burland, 1968) to derive a relationship between $(\tau_h/\sigma'_{vc})_f$ and ϕ' for normally or lightly overconsolidated clays. They compare theoretical with experiment results (mostly data from Ladd and Edgers, 1972) and found the agreement to be reasonably good. They therefore concluded "that failure in a simple shear test is initiated by the formation of rupture planes parallel to the initial direction of the major principal stress (i.e., vertical)." Figure A.29 shows a plot of Randolph and Wroth's theoretical predictions and experimental results from MIT for $(\tau_h/\sigma'_{vc})_f$ versus ψ for CK_oU direct simple shear tests on normally consolidated clays.[3] The plot shows that at low undrained shear strength ratios the agreement is very good but the predictions reach a theoretical limit at $(\tau_h/\sigma'_{vc})_f = 0.222$, whereas experimentally many soils have DSS strengths higher than this ratio.

Airey, et al. (1985) point out that de Josselin de Jong's theory only makes sense if ruptures occur along zero extension directions (i.e., vertical or horizontal) and are planes along which the maximum stress obliquity is mobilized. They present test results (Figure A.23) which show that the ruptures that do develop are approximately 5–15° to the horizontal therefore questioning de Josselin de Jong's postulate.

(f) Failure Criterion VI – Linear Relationship Between τ_h/σ'_v and $\kappa\tan\delta$

Oda and Konishi (1974) proposed that a unique relationship exits between the effective stress ratio acting on a horizontal plane (τ_h/σ'_v) and the orientation of the major principal stress from the vertical δ, such that,

$$\tau_h/\sigma'_v = \kappa\tan\delta \qquad \text{A.2}$$

The material constant κ is expressed by the following equation (Ochiai, 1975, 1976a, 1976b),

$$\kappa = 1 - K_o = \sin\phi_{cv} = \frac{2\sin\phi_u}{(1+\sin\phi_u)} \qquad \text{A.3}$$

[3] $\psi = \arctan(\tau_h/\sigma'_v)$ at maximum τ_h.

where:

K_o = earth pressure coefficient at rest;

ϕ_{cv} = internal friction angle at the critical void ratio;

ϕ_u = interparticle friction angle.

Equation A.2 inherently assumes that $\sigma'_3 = K_o\sigma'_v$ throughout a test. Using Equations A.2 and A.3 certain relationships for the major and minor principal stresses can be derived from consideration of Mohr's circle of stress (Figure A.30). Ochiai (1981) used these equations to propose the following relationship for computing the undrained strength ratio q_f/σ'_{vc} for simple shear tests on normally consolidated soils:

$$\frac{q_f}{\sigma'_{vc}} = \frac{\beta^2(1 - K_o)^2 + ((\tau_h)_{max}/\sigma'_{vc})^2}{2\beta(1 - K_o)} \qquad \text{A.4}$$

where:

$(\tau_h)_{max}$ = maximum measured horizontal shear stress;

$\beta = \frac{\sigma'_{vc} - u}{\sigma'_{vc}} = 1 - \frac{u}{\sigma'_{vc}}$;

u = excess pore pressure.

and

$$\sin\phi' = \frac{\beta^2(1 - K_o)^2 + ((\tau_h)_{max}/\sigma'_{vc})^2}{\beta^2(1 - K_o^2) + ((\tau_h)_{max}/\sigma'_{vc})^2} \qquad \text{A.5}$$

Using Equation A.4 and $K_o = 0.5$ Ochiai predicts that the normalized undrained simple shear strength of BBC should be 0.213 with a friction angle of 25.2°.

Airey, et al. (1985) present data from many drained simple shear tests in the Cambridge devices on Leighton Buzzard sand (Cole, 1967; Stroud, 1971; Budhu, 1979) which is plotted in Figure A.31. The data shows that there is indeed a linear relationship between τ_{xy}/σ_{yy} ($= \tau_h/\sigma'_{vc}$ for drained test) and $\tan\delta$. The relationship is independent of vertical stress, initial void ratio and holds true for loading and unloading. Wood, et al. (1979) and Airey, et al. (1985) propose using this relationship for predicting the state of stress in the Geonor DSS apparatus. But the data shown in

Figure A.31 do not all represent states of failure in the soil and in fact it is not clear whether any of the points represent a failure condition.

Borin (1973) tested kaolin in the Cambridge rectangular simple shear device and also found that before the peak shear stress a relation like Equation A.2 exists with $\kappa = 0.4$ (Figure A.32). From Equation A.3 this corresponds to a K_o value of 0.6 which is slightly lower than the value of 0.64 quoted by Nadarajah (1973) for kaolin. However, Airey, et al. point out that Equation A.2 only applied to monotonic loading of normally consolidated kaolin which is a much more restrictive set of circumstances than for sand. Again the data presented in Figure A.32 are for conditions before peak and it is not clear if the relationship holds at the peak horizontal shear resistance.

This procedure is simple to use for normally consolidated clays provided that a reliable estimate of K_o can be made (which is not a trivial task) and that the relationship in Equation A.2 holds for each soil tested up to the measured peak shear stress. It is clear that more data needs to be obtained on natural cohesive soils to determine how valid this relationship is for different soils.

(g) Failure Criterion VII – Coincidence of Principal Axes of Strain Increment and Stress

For an isotropic elastic material, the incremental strain depends on the change in stress and the principal axes of incremental stress and of elastic incremental strain coincide. In the case of a perfectly plastic isotropic material, the incremental plastic strains depend on the current state of stress and the principal axes of strain increment and stress coincide. This is one of the classical postulates of the theory of plasticity (Hill, 1950). In the case of undrained direct simple shear tests, assuming coincidence of principal axes of strain increment and stress give the same results (Figure A.33) as Failure Criterion III – the failure plane is the plane of maximum shear stress (Figure A.24)

Roscoe, et al. (1967) showed that, for drained simple shear tests on Leighton

Buzzard sand in the Cambridge rectangular device, between the minimum void ratio and peak stress ratio conditions, the principal axes of strain increment and stress coincide (Figure A.22). Budhu (1979) conducted a drained cyclic test on Leighton Buzzard sand (Figure A.34) which showed that at small strains and on stress reversal the behavior is generally elastic ($\xi = \chi$) while plastic at larger strain levels ($\xi = \psi$). The only data for clays are that measured by Borin (1973) on kaolin which, according to Airey, et al. (1985), show fairly convincingly that the relationship between the principal axes of stress (ψ), stress increment (χ) and strain increment (ξ) found for sands does not exist for kaolin.

A.5.2 Discussion

Table A.1 presents the state of stress for an undrained test on normally consolidated BBC in the Geonor DSS using the different failure criteria. Figure A.35 shows the predicted friction angle ϕ' as a function of the measured τ_h/σ'_v at peak τ_h for four of the failure criteria. Based on these results and data presented in the preceding section for each of the failure criteria, the following observations can be made:

1. The assumption that applied shear stresses are pure shear (I) results in the highest q_f/σ'_{vo}, the least amount of rotation of the principal axes and gives unrealistically high friction angles ϕ';

2. Assuming a horizontal failure plane (II) yields the largest ratio of $(\sigma'_h/\sigma'_v)_f$ (in fact it predicts $\sigma'_{hf} > \sigma'_{vf}$), largest rotation of the principal axes and an unreasonably small friction angle ϕ'. Results from drained tests by Roscoe, et al. (1967) and Airey, et al. (1985) on kaolin indicate that using this assumption is incorrect;

3. Some of the experimental data on sands indicate that assuming the horizontal plane is the plane of maximum shear stress (III) is reasonable. No data has been published for natural clays. While this assumption appears to be reasonable the measured τ_h may not be the actual maximum shear stress within the sample. If this is the case, predictions for q_f/σ'_{vc} and ϕ' are conservative;

4. Assuming the friction angle ϕ' (IV) is a tenuous failure criterion to use because of the need to select a reasonable friction angle. This cannot be done without confidence unless considerable additional laboratory results

for the soil being tested are available and can produce a reliable estimate for ϕ';

5. Assuming the failure plane is vertical (V) appears to give very good results for low undrained shear strengths (as shown in Figure A.29) which also corresponds to low values of ψ (= arctan (τ_h/σ'_v)). However, this criterion reaches a theoretical limit at $(\tau_h/\sigma'_{vc})_{max} \cong 0.22$ whereas half of the experimental data plotted in Figure A.29 exceed this value. Furthermore, it predicts a very large increase in ϕ' for values of $\tau_h/\sigma'_v \geq 0.3$ ($\psi = 16.7°$) as shown in Figure A.35;

6. Assuming $\tau_h/\sigma'_v = \kappa\tan\delta$ (VI) appears to give reasonable results that do not differ much from assuming the horizontal plane is the plane of maximum shear stress. However, the method cannot be recommended without showing that the relationship holds at $(\tau_h)_{max}$ for a variety of natural clays. Furthermore, it requires a value of K_o which is not easy to obtain;

7. Assuming coincidence of the principal axes of strain increment and stress (VII) has been shown to exist (at higher shear strains) for drained direct simple tests on sands. However, there is no experimental evidence indicating that this assumption is valid for natural clays. In the case of undrained tests, using this criterion gives the same results as assuming the horizontal plane is the plane of maximum shear stress (III).

Ladd and Edgers (1972) in their review of the state of stress at failure in CK_oU direct simple shear tests conclude that the undrained shear strength based on $(\tau_h)_{max}$ lies between q_f and $\tau_{ff} = q_f\cos\phi'$. They further state that the test cannot be used to evaluate Mohr–Coulomb failure envelopes, except at very large shear strains. Wroth (1987) also concludes that $(\tau_h)_{max}$ is less than q_f and further states that simple shear tests produce a complex pattern of behavior where the maximum values of shear stress acting on different planes in the specimen vary widely and occur at different stages of the test.

A.5.3 Rupture Planes

It is interesting to investigate whether clays actually develop rupture surfaces in direct simple shear tests. Airey and Wood (1987) used a combination of lead shot and lead thread markers along the central plane of kaolin samples, tested in the Cambridge circular simple shear device, to check for the existence of ruptures. Based on their results they concluded that ruptures develop in all simple shear tests and that

the behavior of clays can be divided into three parts:

1. Part 1 is concerned with the behavior before ruptures develop when the stresses and strains in the sample are relatively uniform;
2. The second part is concerned with the conditions of failure and the development of ruptures;
3. The final part is the behavior of the ruptured material.

Once the sample reaches Part 2, continued shearing no longer represents the behavior of the intact soil but provides information on the ruptured soil for which correct interpretation is unclear. Unfortunately, without radiography, ruptures are virtually impossible to detect. Near the peak τ_h the stress–strain curve of normally consolidated clays are flat and do not provide any information to determine when and if a rupture occurred.

A.5.4 Summary

There is still no conclusive evidence which allows a specific failure criterion to be chosen for interpreting the state of stress at failure in a direct simple shear test. It is not possible to determine the Mohr–Coulomb failure envelope based on the measurements currently made in the Geonor type DSS. Some interesting results have been obtained from drained tests on sands and kaolin in the Cambridge simple shear devices and provide some insight into which failure criteria are most reasonable. However, there are no data of this type yet available for CK_oU tests on natural clays. Hence, the situation has not significantly improved since Ladd and Edgers (1972) wrote their report on CK_oUDSS tests on saturated clays. After two decades we can only draw the same conclusion that the undrained shear strength based on peak τ_h lies between q_f and $\tau_{ff} = q_f \cos\phi'$. We can only use the undrained shear strength (i.e. peak τ_h) measured in the DSS with confidence for certain field situations because it gives good agreement with the strengths estimated from back analysis of foundation failures (Ladd, 1981 and 1988). These data will be presented and discussed in Section A.9.

A.6 MEASUREMENT OF RADIAL STRESS IN THE GEONOR DSS APPARATUS

Geonor manufactures calibrated wire–reinforced membranes for the purpose of measuring the radial stress, σ_r, acting on a soil specimen in the Geonor DSS apparatus. The calibrated membranes operate on a strain gauge principle where small changes in the length of the reinforcing wire will result in a change in its electrical resistance. The membranes are calibrated by subjecting them to a known air or water pressure within a calibration cylinder (Dyvik, et al., 1981).

A.6.1 Determination of Coefficient of Earth Pressure at Rest (K_o)

If it is assumed that the wire–reinforced membrane does not allow lateral strains to occur during consolidation, then the sample is consolidated under K_o conditions. Hence, in principle, the specially calibrated membranes can be used to directly determine the K_o value of samples consolidated in the Geonor DSS.

Dyvik and Zimmie (1983) used calibrated membranes to determine the K_o values for three different marine clays. They concluded that the membranes worked satisfactorily and that the measured K_o values agree well with various indirect determinations of K_o (e.g., Jaky, 1944; Brooker and Ireland, 1965; Alpan, 1967). Airey and Wood (1987) also measured K_o values for kaolin in the Geonor apparatus and found satisfactory comparison with the average value of K_o obtained at Cambridge in a variety of other apparatuses. Their data does, however, show that K_o appears to continuously increase after the preconsolidation pressure was exceeded, when generally it should be expected to remain constant. They conclude that this behavior is due to the membrane allowing small lateral deformations, thus violating the K_o condition. While this does not appear to explain the problem since an increase in the lateral strain presumably results in a decrease in σ'_h and hence a decrease in K_o, it does emphasize that the ratio of the membrane stiffness to soil stiffness is very important

for obtaining satisfactory values. If the stiffness ratio is too small, then incorrect values of K_o will be measured.

A.6.2 Determination of State of Stress Using Measured σ_r

Dyvik and Zimmie (1983) claim that measurement of the lateral stress in the Geonor DSS apparatus greatly increases the knowledge of the state of stress within the soil specimen. Their procedure assumes that σ'_r measured during shear is equal to σ'_h acting on a plane perpendicular to the plane of shear deformation of an infinitesimal element of soil at the center of the specimen. They also assume that the measured boundary values of σ'_v and τ_h also act on this infinitesimal element and therefore Mohr's circle of stress can be computed (Figure A.36). Once Mohr's circle of stress is defined, then the magnitude and orientation of the principal stresses can be computed.

Budhu (1985) conducted a series of CD tests on dense and loose Leighton Buzzard sand in both the Cambridge Mk7 device and the Cambridge specially instrumented Cylindrical Simple Shear Apparatus (CSSA; Figures A.9 and A.10). The objective of the test program was to determine if the radial stress measured in the Geonor type DSS is equal to the horizontal stress acting on a plane perpendicular to the plane of shear deformation (σ_x) or the intermediate principal stress (σ_2) or neither. Values of σ_x and σ_2 were computed for the tests run in the Mk7 device and compared directly with σ_r measured in the "Geonor type" CSSA. The results shown in Figure A.37 indicate that the radial stress measured during shear in the circular CSSA is equal to neither the intermediate principal stress nor the horizontal normal stress on the plane perpendicular to the plane of shear deformation. Thus, measurement of the radial stress in the Geonor DSS cannot be used to calculate the state of stress of specimens tested in this type of device.

Budhu's results clearly question the validity of the procedure used by Dyvik and Zimmie for computing the state of stress in the Geonor DSS based on

measurements of σ_r. However, Budhu's data come from CD tests conducted on sands and further research is needed to determine if the same results hold for CU tests on cohesive materials. Airey and Wood (1987) do not recommend using specially reinforced membranes to estimate radial stress and further state that they can only be relied upon to give qualitative information on tests run under different conditions (i.e., different overconsolidation ratios).

A.6.3 Summary

It appears that the specially instrumented membranes are useful for estimating K_o of soils in the Geonor DSS device and therefore provides even more information on the properties of a specimen during the consolidation phase of a test. However, one must keep in mind the potential problems that may arise depending on the relative stiffness of the membrane and the soil. Budhu's research indicates that using the membrane to determine the state of stress of a sample during shear is incorrect.

A.7 CONSTANT VOLUME TESTING

Undrained shear is conducted in most simple shear devices by maintaining the volume of the sample constant during shear. In the case of the Geonor DSS the sample is assumed to be confined laterally by the wire–reinforced rubber membrane and therefore, only the height needs to be kept constant to run a constant volume test. The sample height is kept constant by varying the vertical stress acting on it. Changes in vertical stress to keep the height constant are assumed to be equal to the pore pressure that would develop if the specimen were sealed and pore pressure measured.

Taylor (1953) and Bjerrum (1954) first used the constant volume procedure for conducting undrained direct shear box tests because of the difficulties of preventing drainage during this type of test. (Note: Taylor presented conclusive data showing that "rapid" shearing (e.g., failure in a few minutes) of clay in direct box shear tests

cannot prevent significant drainage and hence the normal stress must be varied when using this device to simulate CU test conditions). Bjerrum and Landva (1966) proposed using this procedure to measure the undrained direct simple shear response of soils in the Geonor DSS. However, until recently little evidence has been presented in the literature which confirms that the constant volume procedure is valid.

Dyvik, et al. (1987) describe a new chamber developed for NGI's direct simple shear device that enables undrained tests with pore pressure measurements to be run (Figure A.38). Tests were conducted on normally consolidated Drammen clay and compared with results obtained from conventional constant volume direct simple shear tests. Figure A.39 shows the results of two constant volume tests and two undrained tests conducted in the new chamber. While the results show a slight variation in the normalized shear stress, the pore pressure plots are almost identical. Based on these results and comparison with prior CK_0UDSS data on the clay that showed similar scatter, Dyvik, et al. conclude that "static constant volume tests on normally consolidated clays will produce the same results as truly undrained tests. The assumption that the change in applied vertical stress is equal to the pore pressure which would have developed in an undrained test is therefore valid. This conclusion applies to saturated soils."

Airey and Wood (1987) point out that for there to be similarity between an undrained and constant volume test, an apparatus has to impose a uniform deformation with no volume change. Using lead shot and radiography they found for a constant volume test on OCR = 1 kaolin that the shear strains were uniform and the volumetric strains zero up to $\gamma = 11\%$, at which point localization in the deformation occurred (peak τ_h based on boundary measurement occurred around $\gamma = 10\%$). This supports the results of Dyvik, et al. However, Airey and Wood further state that, once ruptures formed (which they maintain will develop in all simple shear tests but are not easy to detect), the constant volume condition can only be maintained in an overall

sense. They observed that the rupture planes compressed while the intact soil dilated slightly. They concluded their analysis by stating, "clearly the behavior determined from the direct simple shear apparatus after rupture should be analyzed as a boundary value problem; it no longer represents constant volume simple shear." While this maybe the case, it is questionable what useful information one would derive from analyzing the results of an "undrained" test after ruptures develop. The evaluation and interpretation of these data has the same limitations as occur in all types of shear tests. However, in some tests, such as triaxial compression, one can usually detect initial formation of rupture surfaces whereas in the DSS it is much more difficult and there is no data to show if and when they occur in CK_oUDSS tests on normally consolidated natural clays.

A.8 DEVELOPMENT OF SIMPLE SHEAR DEVICES WITH CAMBRIDGE TYPE LOAD CELLS

Cambridge University developed special load cells for their fully instrumented rectangular and circular simple shear apparatuses. The load cells are actually contact stress transducers and are directly in contact with a specimen in the devices. The transducers can be used to measure simultaneously shear load, vertical load, and eccentricity of the vertical load (Figures A.9 and A.10). One advantage of using such load cells in a Geonor type DSS is that compliance errors due to bearing friction and the wire–reinforced membrane do not need to be accounted for. Secondly, if a single load cell of this type were placed in contact with the center of a sample, then the shear resistance of the soil would be measured within the most uniform state of stress region of the specimen.

Airey and Wood (1987) conducted tests on OCR = 1 kaolin in the Cambridge CSSA and in the Geonor DSS. Figure A.40 shows the stress–strain curves for a constant volume test conducted in the CSSA. The two curves represent data

calculated from the central contact stress transducer (sample core) and from the average boundary measurements (average). While the curves have a similar shape, the shear resistance based on average shear stress is about 8% less than the sample core measurement. Figure A.41 shows the stress ratio–shear strain responses and stress paths for constant volume tests conducted in the CSSA and the Geonor DSS. Values for the normalized undrained strength ratio $(\tau_h/\sigma'_{vc})_{max}$ were found to be 0.175 and 0.152 based on the CSSA sample core measurement and average stress measurement in the Geonor DSS respectively. This represents a difference of 13%. The dotted lines in Figure A.41 for the CSSA data start where rupture in the sample was detected and is shown to emphasize that the response is no longer undrained simple shear. Airey and Wood conclude that the normalized strength determined from the average stress (as in the Geonor DSS) underestimates the "true" undrained simple shear strength based on sample core measurement.

Airey and Wood's results are significant and may eventually lead to a new generation of Geonor type simple shear devices which make use of contact stress transducers at the middle of a specimen. Unfortunately, the transducers are quite tedious to calibrate (Dyvik, et al., 1987) and, when testing wet material, they are less convenient because of the need to prevent moisture from the soil penetrating to the strain gauges on the load cell (Airey, et al., 1985).

Budhu (1988) describes a new simple shear apparatus that tests 70mm by 70mm by 20mm rectangular clay samples (Figure A.42). The device uses a single Cambridge type load cell in contact with the central region of the specimen which measures shear and vertical forces and pore pressures. The specimen is confined in a stack of Teflon coated aluminum plates wherein two strain gauges are installed so that the lateral stress can be measured on two mutually perpendicular sides of the specimen. Assuming that the measured values of lateral stress acting at the boundary correspond to those acting within the mid region of the sample enables the complete

state of stress to be computed at the sample core (Figure A.43). It was Budhu's intention to develop a new device which incorporates the simplicity of the Geonor DSS with that of the Cambridge devices' ability to compute the complete state of stress. Unfortunately, the apparatus requires square specimens which are more difficult to prepare than undisturbed circular specimens using the Geonor trimming apparatus. In addition, standard U.S. tube samples are 3 in. diameter (45 cm^2) which are too small to be tested in this apparatus. However, it will be interesting to obtain more data for clays tested in this device and, in particular, to make comparisons with results obtained for the same soil in the Geonor DSS.

A.9 SUMMARY OF CK_oUDSS TESTS RUN AT MIT ON NORMALLY CONSOLIDATED COHESIVE SOILS

No research laboratory has conducted CK_oUDSS tests on a larger variety of undisturbed cohesive soils than MIT. Ladd and Edgers (1972) present data from tests run at MIT on resedimented Boston Blue Clay and six undisturbed natural clays. However, since 1972 many other soils have been tested at MIT and it is therefore the objective of this section to update the data set published by Ladd and Edgers. The results presented in this section are limited to CK_oUDSS tests on normally consolidated soils. The main purpose of presenting these data is to provide a summary of the results measured for many different cohesive soils and to show how the data varies depending on the type of soil being tested.

A.9.1 Geonor CK_oUDSS Test Results for Normally Consolidated Cohesive Soils

Table A.2a to A.2d present a summary of over 25 different cohesive soils tested at MIT. The Table gives average and standard deviation values for the plasticity index (Ip) of each soil and several measured parameters at the peak shear resistance. All of the tests were conducted using the Geonor DSS and generally

followed the test procedures outlined in Appendix E. All soils were loaded during consolidation into the normally consolidated range (generally σ'_{vc} = (1.5 to 2)σ'_p as recommended by the SHANSEP procedure; see Table 2.1 and Ladd and Foott, 1974) and sheared undrained at $\dot{\gamma}$ = 5%/hour. Also included in the Table is the normalized secant Young's modulus at 50 percent of the peak shear resistance, $E_u(50)/c_u$. This value is computed using the following equation:

$$E_u = 2(1 + \nu)G \qquad \text{A.6}$$

where:

G = shear modulus = τ_h/γ

ν = Poisson's ratio.

Since the tests are undrained, ν = 0.5 and Equation A.6 reduces to:

$$E_u = 3(\tau_h/\gamma) \qquad \text{A.7}$$

The bottom of Table A.2d gives the mean, standard deviation and coefficient of variation (COV) for each of the values listed for the peak shear resistance. Figures A.44 – A.47 present histograms of the undrained strength ratio (τ_h/σ'_{vc} at maximum τ_h) and the shear strain, stress ratio and ψ angle at peak maximum τ_h for the 100 tests summarized in Table A.2. (Note: Table A.2 presents averages of the measured values for each of the different soils, while the mean values at the end of Table A.2, the histograms and some of the figures to follow actually use all of the individual values of the 100 tests run at MIT.)

The tabulated data and histograms show that for cohesive soils the Geonor DSS measures a large variation of undrained strength ratios. Excluding the varved clay, this range is equal to 0.18 to 0.30. This is quite contradictory to the belief of some researchers and practitioners who criticize the DSS because it seems to measure the same strength independent of the soil type. For comparison, CK_oU triaxial compression tests, according to Ladd, (1988) on a variety of normally consolidated clays and silts (excluding varved clays) gives a range for q_f/σ'_{vc} of 0.27 to 0.37 with an

average of 0.32 ± 0.03SD and COV = 9.4%. This variation is smaller than that measured in the DSS (Average = 0.23 ± 0.03SD with COV = 14.3%).

The shear strain and ψ angle at peak τ_h display a large variation among the different soils, ranging from approximately 2% to 23% with a mean = 10.1% ± 4.0SD and 12° to 29° with a mean = 21.1° ± 3.3SD respectively. This is not the case for the stress ratio at peak σ'_v/σ'_{vc}, which has very little variation as clearly shown in Figure A.46 (this parameter has the smallest COV = 8.5%; Table A.2d). This is a somewhat peculiar result because it indicates that all of the different soils develop almost the same equivalent pore pressure at peak shear resistance. This is also shown in Figure A.48 which clearly indicates that there is no correlation between the stress ratio at peak τ_h and the plasticity index.

Figure A.29 shows that there is a strong correlation between the undrained strength ratio and the ψ angle. This correlation, however, is a direct result of the fact that the vertical stress ratio at failure is almost independent of the soil type as discussed in the previous paragraph. In other words, since $(\sigma'_v/\sigma'_{vc})_f$ does not vary by much among the different soils then obviously ψ increases with increasing $(\tau_h)_{max}$.

Figure A.49 shows that there is a fairly strong correlation between the shear strain at peak τ_h and the plasticity index. In general it is expected that higher plasticity soils reach a failure state at higher shear strains. There is much less correlation between the measured undrained strength ratio and the shear strain at failure (Figure A.50). This is also the case for the ψ angle versus shear strain at failure (Figure A.51).

Figure A.52 shows a plot of the normalized secant value of Young's modulus versus the shear stress level (τ_h/c_u) for six of the soils listed in Table A.2. The figure shows that while the trends are quite similar, the absolute values of E_u/c_u decrease significantly with increasing plasticity and organic content of the soil, thus showing a large variation of the measured Young's modulus with soil type. In addition, Ladd, et

al. (1977) state that the deformation observed during construction of embankments on five of these soils were in general accord with those expected based on the measured CK_oUDSS E_u/c_u values.

Figure A.53 shows the most significant result from all the data discussed in this section. The figure plots undrained strength ratio versus plasticity for 29 of the soils listed in Table A.2 and the average value of the in–situ c_u back calculated from case histories of loading failures divided by the estimated in situ preconsolidation pressure, σ'_p, from 27 case histories. The field data are from Larsson (1980) and most of the cases involve embankment failures, including many of those used to develop Bjerrum's (1972) field vane correction factor. The figure shows that there is a slight trend in undrained strength ratio versus plasticity for the CK_oUDSS results whereas the field data shows a stronger trend. However, the DSS data generally falls within the range of values from the field data. This is very significant because according to Ladd (1981), "no other laboratory test, and certainly not CIU or CK_oU triaxial compression tests, has been shown to produce comparable results."

Ladd (1988) reanalyzed these data in terms of each of the soil's location with respect to Casagrande's plasticity chart (Figure A.54). Based on distinguishing between inorganic clays (above Casagrande's A–line) and organic clays and silts (below the A–line), Ladd makes the following conclusion with respect to the field data and Geonor CK_oUDSS test results:

> "For inorganic clays with Ip = 25 ± 15%, good agreement exists between strengths back calculated from field failures and those obtained ... from DSS tests (τ_h). Silts and organic clays appear to have higher, but more scattered, normalized strengths, with Larsson's results generally showing larger values than predicted from DSS data."

A.10 STRAIN SOFTENING BEHAVIOR OF CK_oUDSS TESTS

This section discusses the strain softening behavior that is prevalent in all of the normally consolidated CK_oUDSS tests summarized in Table A.2. The analysis

presented in this section should be viewed upon as a cursory investigation of a subject which, in the author's opinion, is worthy of a Ph.D. dissertation. The objective is to provide some insight into the nature of strain softening in the DSS, as well as some concluding remarks.

Every normally consolidated cohesive soil tested at MIT in the Geonor DSS has exhibited strain softening behavior. In fact, many of the tests summarized in Table A.2 exhibit a near linear negative slope of shear stress versus shear strain starting within a few percent shear strain of the peak shear resistance. In addition, no soil has shown any indication that the post peak stress–strain curve is reaching the "Critical State Line" (CSL) let alone the residual strength of the soil. The basis for this conclusion is the observed shape of the shear stress–strain curve and that the obliquity (τ_h/σ'_v) very seldom approaches a constant value at large shear strains and is often still increasing at the end of most tests where γ has already reached 30%.

Figure A.55 is a plot of $\tau_h/(\tau_h)_{max}$ versus shear strain beyond peak shear resistance (i.e. $\gamma - \gamma_f$, for $\gamma > \gamma_f$) for 90 of the tests summarized in Table A.2. The symbols are plotted at values of $(\gamma - \gamma_f) > 0$ which is computed at 5% intervals using γ = 5%, 10%, 15%, ..., etc. (e.g., if γ_f = 8.5%, values of τ/τ_{max} are plotted at $(\gamma - \gamma_f)$ equal to 10–8.5=2.5%, 15–8.5=7.5%, ..., etc.).[4] The symbols for each individual test are not joined to avoid making the figure more cluttered. It is clear from this figure that not only all of the soils tested exhibit strain softening behavior but they also strain soften by different amounts. In general, it is not unreasonable to expect that different soil types will exhibit differences in their strain softening behavior. For example, the solid symbols in the figure represent tests performed on the Arctic soils from Harrison Bay and Smith Bay which show that these soils tend to strain soften

[4]Standard MIT CK_0UDSS tests are conducted up to γ = 30%, hence all these strain softening data are readily available. It is, however, not standard procedure at many other laboratories such as NGI which often terminates a test once the peak shear resistance $(\tau_h)_{max}$ is reached.

more than most of the other soils tested at MIT. Thus the obvious question is; is it possible to correlate the degree of strain softening to soil type using certain common soil properties such as plasticity index? It is also important to question if the measurements made past the peak shear resistance truly represent strain softening of the intact soil under uniform simple shear conditions (providing ruptures do not occur). The remainder of this section will discuss strain softening observed in the DSS by addressing these two questions.

A.10.1 Question 1: Can Strain Softening in Geonor CK_oUDSS Tests on Normally Consolidated Cohesive Soils be Correlated With Soil Type?

Bishop (1971) defined a brittleness index (I_b) to describe the drop from peak to the residual strength of a soil as given by the following equation for undrained shear strength:

$$I_b = \frac{(c_u)_f - (c_u)_r}{(c_u)_f} \qquad \text{A.8}$$

where:

I_b = Brittleness Index;

$(c_u)_f$ = Undrained shear strength;

$(c_u)_r$ = Undrained residual strength.

Bishop evaluated the brittleness index for some soils using a ring shear apparatus which allows large displacements, necessary to reach the residual strength, between two horizontal surfaces of an annular soil sample. An example of a typical result is given in Figure A.56 for remolded Blue London Clay which required a Δ of 17.3 cm (Δ is the relative displacement at the mean diameter of the annular sample) to reach the residual strength. (Note: the time required to reach failure and the residual strength for this test suggests that this was a "rapid undrained" shear test. Regardless of this, the test data is presented here primary to illustrate the Brittleness Index concept).

In the case of CK_oUDSS tests we cannot use the brittleness index to describe

how much a soil strain softens when it reaches its residual strength. The problem, as discussed at the beginning of this section, is that soils do not reach their residual shear strength in the DSS. However, as a first approximation to analyze MIT's test data, a pseudo brittleness index will be used as a strain softening index to see if it shows a correlation between strain softening behavior and soil type. The reduction in shear resistance at $\gamma = 25\%$ will be compared with the plasticity and liquidity indices of the soils tested at MIT.[5] The pseudo brittleness factor is described schematically in Figure A.57a and is calculated using the following equation:

$$I_{pb} = \frac{(\tau_h)_{max} - (\tau_h)_{\gamma=25}}{(\tau_h)_{max}} \qquad A.9$$

where:

I_{pb} = Pseudo Brittleness Index;

$(\tau_h)_{max}$ = maximum shear resistance;

$(\tau_h)_{\gamma=25}$ = shear stress at $\gamma = 25\%$.

If $I_{pb} = 0$, a soil exhibits no strain softening between its peak shear resistance and $\gamma = 25\%$; conversely, for $I_{pb} = 1$ a soil has strain softened to zero shear resistance.

Figure A.58 and A.59 are plots of the I_{pb} versus liquidity index and plasticity index respectively for most of the tests summarized in Table A.2. Figure A.58 shows that there is no correlation between the I_{pb} and liquidity index and furthermore it also shows that the Arctic soils do not cluster within a unique region of the plot with respect to the I_{pb}. Figure A.59 shows that there is a moderate correlation between the I_{pb} and plasticity index. The plot indicates that higher plasticity soils tend to strain soften less up to $\gamma = 25\%$. However, the correlation presented by Figure A.59 can be misleading. This is shown in Figure A.60a which is a plot of the stress strain curves for three of the tests summarized in Table A.2. The three soils range from a high plasticity clay (Atchafalaya) to a sensitive soil with low plasticity (Portsmouth). As

[5] $\gamma = 25\%$ was selected because most of the tests were terminated between 25 and 30 percent shear strain.

expected and shown in Section A.9, the higher a soil's plasticity the larger the strain at failure and therefore at $\gamma = 25\%$ a higher plasticity soil is likely to have undergone less strain softening than a lower plasticity soil which reached its peak shear resistance at a much lower shear strain. Thus, for describing the absolute degree of strain softening of a soil with respect to the amount of total shear strain to which it is subjected, the I_{pb} versus plasticity index correlation is useful. However, for describing the rate or degree of strain softening that a soil exhibits once its peak shear resistance is reached, the correlation is not useful.

Given the results found for the I_{pb} index, it appears that a strain softening index which incorporates the slope of the post peak stress–strain curve should also be investigated. Thus, a second index was selected as described schematically in Figure A.57b and is computed as follows:

$$S\gamma = \frac{(1 - (\tau_h)\gamma/(\tau_h)_{max})}{\gamma - \gamma_f}, \text{ for } \gamma > \gamma_f \qquad \text{A.10}$$

where:

$S\gamma$ = slope of the stress strain curve from γ_f to γ;

γ_f = shear strain at maximum shear resistance (in absolute units);

γ = shear strain (in absolute units);

$(\tau_h)_{max}$ = maximum shear resistance;

$(\tau_h)\gamma$ = shear stress at shear strain γ.

The actual post peak stress–strain slope is almost always negative, but Equation A.10 is arranged so that $S\gamma$ values are always positive. The shear strains in the equation are in absolute units so that an $S\gamma = 1$ represents a stress–strain curve where a soil loses one percent of its peak shear resistance per one percent shear strain. As shown in Figure A.60a, many stress–strain curves are not straight lines just beyond the peak shear resistance. Thus to capture this characteristic, $S\gamma$ values can be calculated for different values of $\gamma - \gamma_f$ (e.g., S_5, S_{10}, etc.) and then averaged. Although this may not

be an ideal parameter, it still gives an indication of the relative difference in the slope of the post peak stress–strain curves for different soils. This is shown by a simple example in Figure A.57c. In the figure, soils B and C lose the same amount of shear resistance at $(\gamma - \gamma_f) = 15\%$; however, soil B throughout the post peak stress–strain curve up to this point exhibits less strain softening than soil C. This is reflected by its lower average $S\gamma$ (1.5 versus 2). This index does not work very well if the post peak stress–strain curves of different soils tend to cross each other. For example, in Figure A.57c soil B's stress–strain curve would have to fall significantly below soil C beyond $(\gamma - \gamma_f) = 15\%$ before its average $S\gamma$ value is greater than 2 (this is the constant value for soil C because its curve is straight). Fortunately, most soils tested in the DSS tend to exhibit gradual increases in the slope of the post peak stress–strain curves.

The S_5, S_{10} and S_{15} values were computed for most of the soils summarized in Table A.2. Figures A.61 and A.62 are plots of the average of S_5, S_{10} and S_{15} for the different tests versus plasticity and liquidity indices. Figure A.61 confirms the observation made from Figure A.55 that the Arctic soils tend to have steeper strain softening slopes than many of the other soils as seen by their high average S_5, S_{10} and S_{15} values. However, in general there appears to be no correlation between the average S_5, S_{10} and S_{15} values and plasticity index. Upon first inspection this is not the case for average S_5, S_{10} and S_{15} values versus liquidity index (Figure A.62). There appears to be a moderate degree of correlation between average S_5, S_{10} and S_{15} and liquidity index. However, in this case, the Arctic soils tend to cluster around a region of the plot which distinguishes them from the other soils and in fact removing their values from the data set gives a new linear regression which indicates that there is little correlation between average S_5, S_{10} and S_{15} and liquidity index for all of the non–Arctic soils (dashed line in Figure A.62). This is shown clearly by the stress–strain curves of the three soils plotted in Figure A.60b. The slope of the Arctic soil (Harrison Bay) is steeper than the other two soils and is reflected by its higher

average S_5, S_{10} and S_{15} value (1.73). Yet, the higher plasticity Atchafalaya clay and the very different sensitive Portsmouth Sensitive clay (sensitivity = 11 based on field vane data, Ladd and Edgers, 1972) exhibit nearly identical post peak behavior (average S_5, S_{10} and S_{15} equal to 1.26 and 1.19 respectively) which is consistent with the lack of correlation found in Figures A.61 and A.62.

A.10.2 Question 2: Does the Post Peak Behavior of CK_oUDSS Tests on Cohesive Soils Truly Represent Strain Softening of Intact Soil Under Uniform Simple Shear Conditions?

Results from theoretical studies presented in Section A.4 show that the DSS device imposes a nonuniform state of stress to test specimens. Data presented in Appendix G strongly suggests that this nonuniform state of stress is responsible for a significant portion of the degree of strain softening measured in a constant volume direct simple shear test. Question 2 of this section will be answered in the following paragraphs by presenting a summary of the findings of Appendix G. Readers are referred to Appendix G for a detailed discussion of this material.

Results from several constant height tests were conducted on an elastic specimen (rubber) in the Geonor DSS and the MDSS which clearly reflected the nonuniform state of stress which develops in DSS specimens. For this elastic material, gaps developed at the upper leading edge and lower trailing edge of the specimen during shear (Figure 5.7 and G.1). These gaps caused a substantial decrease in the vertical stress required to maintain the sample height constant during shear. Under ideal simple shear conditions this would not occur for an elastic material such as the rubber sample.

In fact, for a DSS test with $\theta = 180°$ application of the second shear stress τ_2, resulted in a normalized vertical stress curve which is parabolic and symmetric with respect to the neutral axis of the DSS (i.e., X coordinate = 0; Figure 5.7)[6]. In this

[6]As described in the main text, a $\theta = 180°$ test is one in which two independent

type of test the gaps which develop during application of τ_1 start to close upon reversal of the shear stress due to τ_2 acting in the opposite direction. As the gaps close, the effective area of the specimen increases, thereby resulting in a decrease in the vertical stress and a tendency for the specimen to expand in the vertical direction. In response to this behavior the constant height servo control system increases the vertical force to maintain the sample height constant. The rate of increase in the vertical stress monotonically decreases as the X coordinate approaches zero ($\gamma = 0\%$) and the reverse phenomenon occurs as the sample passes through the neutral axis of the device.

The results of three cyclic Geonor DSS tests performed on cohesive samples (OCR=1 BBC; OCR=1.5 and 4.1 San Francisco Bay Mud) at the conventional undrained shear rate of strain ($\dot{\gamma} = 5\%$/hour) displayed some interesting characteristics as the samples strained towards and past the neutral axis of the device during the first reversal stage of the applied shear stress (the samples were allowed to strain well beyond their peak shear resistance before the shear stress was reversed). In all three tests the vertical stress and shear resistance reached a peak value during the reversal stage when the sample was exactly at the neutral axis of the device (Figures G.5 and G.6). Furthermore, the vertical stress and shear resistance values during the reversal stage were symmetric about the neutral axis. The fact that three DSS tests on two different soils at three different OCR's and stress levels exhibit this type of behavior is more than coincidental (Figure 5.8). Symmetry of the normalized vertical stress about the neutral axis of the device for all three different test conditions is suggestive of behavior that is not exclusively dependent on the type of soil and stress conditions but also on the DSS apparatus itself.

Based on the results of the tests on rubber and the cyclic tests on clay specimens it was hypothesized in Appendix G that the behavior of samples tested in a

---

horizontal shear stresses are imposed to the sample (τ_1 and τ_2) and act in opposite directions.

direct simple shear apparatus can be strongly influenced by the device. Specifically, during undrained shear the DSS apparatus causes the vertical stress acting on a sample to decrease as it strains away from the neutral axis of the device and the opposite occurs when a sample strains towards the neutral axis. This hypothesis implies that the pronounced strain softening always observed at large strains is at least partially due to the nonuniform vertical stress caused by the DSS device (Figure 5.9).

Airey and Wood (1987) state that ruptures develop in all simple shear tests. If this is the case, then the measured post rupture behavior of the sample cannot be used to represent the simple shear behavior of intact soil and it is not clear how to analyze the measured data. If indeed all simple shear tests develop ruptures, the problem is that they are virtually impossible to detect in the Geonor DSS. Even with major modifications (i.e., using radiography), detecting the development of ruptures and their orientation during a test would not be very easy and certainly would not become a routine testing procedure. While it is plausible that some soils do indeed develop ruptures, Airey and Wood's statement is a strong one.

Regardless of whether ruptures occur or not, the data presented in Appendix G and summarized here clearly indicate that the strain softening behavior measured in the DSS does not truly represent an intact soil's post peak simple shear behavior. Thus one cannot unequivocally recommend using the measured strain softening data for design. Unfortunately, many designers, for lack of adequate information, are forced to make assumptions in their analysis which do not realistically represent the field situation (e.g., extensive use of elastic and rigid perfectly plastic soil models in finite element analysis). The same situation holds for design problems where strain softening data are required and the available laboratory data is from DSS tests. In such cases, the temptation is to use the measured data for design (e.g., strain compatibility approach presented by Koutsoftas and Ladd, 1985). While the evidence summarized in

this section indicate that this is not realistic, it is a conservative approach.

A.10.3 Summary

Based on the discussion presented in the previous sections, the following statements/opinions are offered on the strain softening behavior of cohesive soils as measured in Geonor CK_0UDSS testing:

1. All normally consolidated cohesive soils exhibit strain softening behavior when tested in the Geonor DSS. This in itself is not surprising since it is commonly accepted that most undisturbed normally consolidated cohesive soils exhibit strain softening behavior in an undrained shear test;

2. Data presented in Appendix G and summarized in this section clearly indicate that the measured strain softening response of a DSS specimen is in part due to the nonuniform state of stress imposed by the device. It is still, however, unclear to what degree the device influences the measured strain softening behavior;

3. There appears to be little correlation between the nature of a soil's strain softening behavior, as represented by the two strain softening indices presented in Section A.10.1, and the plasticity and liquidity indices. It is still unclear why the Arctic soils tested at MIT tend to strain soften more than most other soils;

4. If ruptures do occur in all simple shear tests, then the post rupture data do not represent the behavior of the intact soil and proper interpretation of the data is unclear. Unfortunately, little research has focused on detecting the presence of ruptures in a DSS test.

It is clear from the discussion presented in this section that the issue of strain softening in the DSS is complex. Much research (e.g., detection of ruptures and continuation of work presented in Appendix G) is still required to resolve this issue and it is hoped that the material presented in this section will have at least shed some light on the subject. Until more insight is provided through additional research, it is not recommended that the strain softening behavior of soils, as measured in the DSS, be used for design purposes.

A.11 SUMMARY AND CONCLUSIONS

The direct simple shear apparatus was developed to provide a soil testing device which can evaluate the stress–strain behavior of soils under simple shear strain conditions. It has the unique ability to test soil specimens wherein the major principal stress is free to rotate during shear while the sample is kept in a condition of plane strain. Direct simple shear devices cannot, however, impose complementary shear stresses to the sides of a specimen (Figure A.11) and as a result, a condition of nonuniform stress and strain occur within the specimen. This initially lead to considerable criticism of the device to the point of questioning its usefulness as an apparatus for evaluating the behavior of soils. However, in addition to theoretical analysis, several experimental programs have shown quite convincingly that for plastic soils the degree of uniformity of stress and strain in the device is acceptable up to the peak shear resistance (Figures A.15 to A.17).

In the commonly used Geonor DSS, only the vertical effective stress (σ'_v) and the shear stress (τ_h) on a horizontal plane are known. This is not enough information to determine Mohr's circle of stress and, therefore, at peak horizontal shear resistance the undrained maximum shear stress, $q_f = 0.5(\sigma_1 - \sigma_3)$, of the soil cannot be calculated. Seven failure criteria have been proposed to estimate Mohr's circle of stress at failure for samples tested in the Geonor DSS (Figures A.20, A.21, A.24, A.25, A.27, A.30, A.33 and Table A.1). Each criterion makes an assumption which determines the orientation of the major principal stress at failure thereby allowing σ'_1 and σ'_3 to be calculated. The basic problem, however, is that there is still insufficient evidence to indicate which of the proposed failure criteria are correct. While a considerable amount of interesting data has been obtained from the specially instrumented Cambridge simple shear devices where the complete state of stress can be computed, the data have not conclusively indicated which failure criteria are the most appropriate. In spite of the lack of sufficient information, the material presented in

Section A.5 does allow the following statements to be made with respect to the state of stress at $(\tau_h)_{max}$ for CK_oUDSS tests on normally consolidated cohesive soils:

1. The undrained shear strength based on $(\tau_h)_{max}$ probably lies between q_f and $\tau_{ff} = q_f \cos\phi'$ (Ladd and Edgers, 1972);
2. Assuming that the applied stress system is one of pure shear (I) or that the failure plane is horizontal (II) is unreasonable;
3. The vertical effective stress ratio σ'_v/σ'_{vc} at $(\tau_h)_{max}$ lies within a narrow band based on data from over 30 different soils ($\sigma_v'/\sigma'_{vc} = 0.598 \pm 0.051SD$ for n = 100; Table A.2d). As a result there is a strong correlation between ψ (= $\arctan(\tau_h/\sigma'_v)$) and $(\tau_h/\sigma'_{vc})_{max}$ (Figure A.29);
4. Assuming the failure plane is vertical (V) compares well with experimental results for values of the undrained strength ratio $(\tau_h/\sigma'_{vc})_{max}$ less than 0.22 which represents approximately 50% of the test data tabulated in Table A.2 (Figure A.29).

Some researchers have used specially instrumented wire–reinforced membranes to measure the radial stress (σ'_r) of a sample in the Geonor DSS. Experimental evidence indicates that the special membranes can be used successfully to evaluate the coefficient of earth pressure at rest (K_o) of a sample during virgin consolidation and subsequent rebound. They also have been used to "evaluate" the state of stress within a specimen during shear by assuming that the measured radial stress is equal to the horizontal stress acting on a plane perpendicular to the plane of shear deformation (Figure A.36). However, some experimental results have shown that for sand, the measured radial stress is equal to neither the horizontal stress acting on a plane perpendicular to the plane of shear deformation nor the intermediate principal stress, thus questioning the validity of this procedure (Figure A.37).

Dyvik, et al. (1987) and Airey and Wood (1987) have recently provided experimental evidence which confirms the validity of conducting undrained tests by maintaining the volume of the specimen constant during shear. More specifically, Dyvik, et al. found that for tests on a normally consolidated clay, the assumption that the change in applied vertical stress required to maintain the volume constant is equal

to the pore pressure which would have developed in a truly undrained test is valid (Figures A.39 to A.41).

Every normally consolidated soil tested at MIT in the Geonor DSS has exhibited strain softening behavior. This appendix reviewed two strain softening indices to see if there is any correlation between the post peak stress–strain behavior and soil type (Figure A.57). For the indices chosen the degree of strain softening of the different soils does not appear to be related to their plasticity and liquidity indices. Data from tests on an elastic material (rubber) and two cohesive soils (BBC and SFBM) presented in Appendix G and summarized in Section A.10 clearly indicate that the measured strain softening response of a DSS specimen is in part due to the nonuniform state of stress imposed by the device. It is, however, still unclear to what degree the device influences the measured strain softening behavior.

In spite of some of its problems the Geonor DSS offers important practical advantages compared with other shear devices for design problems involving clays. Experience obtained over 20 years of DSS testing performed in conjunction with design problems involving construction of embankments, tanks, etc., suggests that DSS testing offers the following advantages:

1. During consolidation, prior to shear, one easily obtains the same compression curve and coefficient of consolidation data as gained from conventional incremental oedometer tests (Ladd, 1981);

2. The measured values of maximum horizontal shear stress (τ_h max.) give a fairly reliable estimate of the undrained shear strength (c_u) appropriate for undrained stability and bearing capacity analysis, for example, Figures A.53 and A.54;

3. The measured value of undrained Young's modulus (E_u) gives a good indication of potential displacements due to in situ undrained shear deformations (Figure A.52; Ladd, 1981; Ladd, et al., 1977);

4. Tests are easy to run and less liable to experimental problems and, most important for testing expensive Arctic soils, uses little soil compared to triaxial testing and other shear devices.

Since its inception in the 1960's, some of the doubts associated with the Geonor DSS have been resolved. The device has proven itself to be a practical apparatus which provides valuable information for design purposes, particularly in applications for which its horizontal failure mode is well suited. It is, however, clear that many uncertainties still need to be resolved. Some of the more important ones include: determining a suitable failure criterion for evaluating the state of stress at failure, determining the degree to which the measured strain softening behavior is influenced by the device and verify if ruptures do indeed develop in all simple shear tests on natural soils.

TABLE A.1: State of Stress in Geonor CK_oUDSS Test on a Normally Consolidated BBC Specimen Using Different Assumptions (after Ladd and Edgers, 1972).

Failure Criterion	Assumption	At Failure (Maximum τ_h)							
		q_f/σ'_{vc}	τ_{ff}/σ'_{vc}	p'_f/σ'_{vc}	$(\sigma'_1/\sigma'_3)_f$	$(\sigma'_h/\sigma'_v)_f$	$\phi'_f{}^\circ$	$\theta_p{}^\circ$	$\theta_f{}^\circ$
I	Applied Stresses Are Pure Shear	0.320	Indeter.	0.320	∞	0.5	90.0	19.3	Indeter.
II	Horizontal Failure Plane	0.212	0.200	0.640	1.99	1.246	19.3	54.7	0
III	$\tau_h = q_f$	0.200	0.187	0.570	2.08	1	20.6	45.0	10.3
IV	$\phi'_f = 30^\circ$	0.230	0.199	0.459	3.00	0.611	30.0	30.4	29.6
V	Vertical Failure Plane	0.236	0.200	0.445	3.26	0.561	32.0	29.0	90.0
VI	$\tau_h/\sigma'_v = \kappa\tan\phi$	0.213	0.193	0.498	2.49	0.747	25.3	35.1	22.6
VII	Plasticity Theory	0.200	0.187	0.570	2.08	1	20.6	45.0	10.3

Notes:

a) Measured Data: at $(\tau_h)_{max}$, $\tau_h/\sigma'_{vc}=0.200$ and $\sigma'_v/\sigma'_{vc}=0.570$; assume $K_o=0.5$.
b) See Figure A.19 for definition of stresses and angles.

TABLE A.2a: Summary of Normally Consolidated CK_oUDSS Tests Run on Cohesive Soils at MIT.

Soil (Classification)	Plasticity		At Peak τ_h					$\frac{E_u(50)}{c_u}$	Remarks/Source
	No.	I_p (%)	No.	γ (%)	τ/σ'_{vc}	σ'_v/σ'_{vc}	ϕ °		
San Fransico Bay Mud (CH)	1	25.2	3	8.6 ±1.4	0.220 ±0.007	0.582 ±0.027	20.7 ±1.5	330 (n=2)	MIT, 1985
Great Salt Lake (CH)	4	31.3 ±8.3	4	6.3 ±2.4	0.236 ±0.011	0.571 ±0.057	22.6 ±1.6	625 ±175	MIT, 1985
Omaha (CH)	3	43.0 ±17.4	3	11.9 ±4.1	0.218 ±0.002	0.583 ±0.026	20.5 ±0.6	330 ±130	MIT, 1985
Klamath Falls Oregon (MH)	2	84.1 ±1.1	2	11.7 ±0.7	0.263 ±0.007	0.581 ±0.021	24.4 ±0.2	210 ±10	MIT, 1986
Bombay, India (MH)	4	43.9 ±8.9	4	12.3 ±2.0	0.243 ±0.006	0.634 ±0.023	21.0 ±0.3	250 ±55	MIT, 1982
Franklin, N.H. (ML)	4	5.5 ±3.1	4	5.1 ±0.6	0.223 ±0.025	0.592 ±0.076	20.8 ±2.1	700 (n=2)	MIT, 1983
Empire, Lousiana (CH)	3	54.2 ±4.1	3	13.6 ±1.3	0.209 ±0.009	0.666 ±0.023	17.4 ±1.3	190 ±10	Azzouz and Baligh (1984)
Boston Blue Clay (CL)	*	21±3	5	6.1 ±1.8	0.197 ±0.009	0.561 ±0.017	19.4 ±0.9	550 ±155	Ladd and Edgers (1972)

Notes:

1. All values are mean ± 1 standard deviation unless * appears in No. column then value is mean ± range.
2. MIT in source column ≡ MIT Geotechnical Laboratory files; unpublished.

TABLE A.2b: Summary of Normally Consolidated CK_oUDSS Tests Run on Cohesive Soils at MIT.

Soil (Classification)	Plasticity		At Peak τ_h					$\frac{E_u(50)}{c_u}$	Remarks/Source
	No.	I_p (%)	No.	γ (%)	τ/σ'_{vc}	σ'_v/σ'_{vc}	ϕ' °		
Portsmouth Sensitive(CL)	*	15±3	2	1.8 ±0.3	0.201 ±0.005	0.641 ±0.016	17.4 ±0.1	950 ±70	Ladd and Edgers (1972)
Portland, Marine Clay (CL)	*	20±4	4	4.0 ±1.0	0.208 ±0.030	0.556 ±0.045	20.6 ±2.6	630 ±105	Ladd and Edgers (1972)
Maine Organic (CH)	*	34±8	3	10.6 ±4.8	0.294 ±0.015	0.593 ±0.105	25.5 ±3.4	380 ±55	Ladd and Edgers (1972)
Bangkok (CH)	*	41±9	2	7.9 ±1.2	0.268 ±0.000	0.581 ±0.000	24.1 ±1.1	425 ±90	Ladd and Edgers (1972)
Atchafalaya Lousiana (CH)	*	75±10	3	21.0 ±2.3	0.243 ±0.017	0.555 ±0.058	23.9 ±3.8	155 ±15	Williams (1973)
AGS, New Jersey (CH)	3	38.0 ±7.0	2	11.9 ±1.4	0.254 ±0.007	0.595 ±0.026	23.1 ±1.6	275 ±35	Koutsoftas and Ladd (1985)
Connecticut Valley Varved Clay	-	-	5	6.5 ±1.9	0.168 ±0.011	0.628 ±0.021	14.8 ±1.0	510 ±70	Lacasse, et al. (1972)
Harrison Bay Alaska (ML-MH)	8	18.3 ±4.2	9	11.0 ±2.7	0.243 ±0.009	0.606 ±0.060	21.9 ±1.6	320 ±110	lower material Yin (1985)

Notes:

1. All values are mean ± 1 standard deviation unless * appears in No. column then value is mean ± range.
2. MIT in source column ≡ MIT Geotechnical Laboratory files; unpublished.

TABLE A.2c: Summary of Normally Consolidated CK_oUDSS Tests Run on Cohesive Soils at MIT.

Soil (Classification)	Plasticity		At Peak τ_h					$\frac{E_u(50)}{c_u}$	Remarks/Source
	No.	I_p (%)	No.	γ (%)	τ/σ'_{vc}	σ'_v/σ'_{vc}	ϕ °		
Harrison Bay Alaska (ML)	1	9.7	2	11.3 ±1.3	0.303 ±0.009	0.560 ±0.008	28.4 ±0.4	275 ±30	upper material Yin (1985)
Smith Bay, Alaska Site T (CL-CH)	5	24.8 ±5.0	7	13.8 ±2.3	0.267 ±0.022	0.592 ±0.014	24.3 ±1.8	270 ±50	Young (1986)
Smith Bay, Alaska Site W (CL-CH)	4	24.4 ±3.2	6	10.9 ±1.9	0.257 ±0.026	0.657 ±0.045	21.4 ±0.9	240 ±70	Young (1986)
Venezuela Orinoco <70′ (CH)	4	42.8 ±6.8	5	11.8 ±3.1	0.235 ±0.007	0.596 ±0.024	21.6 ±0.7	310 ±35	Ladd, et al. (1980)
Venezuela Orinoco >70′ (OH)	4	47.3 ±7.6	4	11.1 ±2.2	0.200 ±0.005	0.620 ±0.031	17.9 ±0.9	250 ±40	Ladd, et al. (1980)
Venezuela North of Paria(CH)	2	47.5 ±2.4	3	9.6 ±0.9	0.185 ±0.006	0.646 ±0.003	16.0 ±0.5	260 ±5	Ladd, et al. (1981)
Venezuela Tuy Cariaco	3	29.5 ±2.8	3	11.3 ±0.8	0.197 ±0.016	0.632 ±0.027	17.4 ±1.5	255 ±60	Boring C1 Mishu, et al. (1982)
Venezuela Tuy Cariaco	2	49.1 ±1.1	2	13.2 ±1.1	0.234 ±0.018	0.599 ±0.012	21.3 ±1.8	275 ±10	Boring C2 Mishu, et al. (1982)

Notes:

1. All values are mean ± 1 standard deviation unless * appears in No. column then value is mean ± range.
2. MIT in source column ≡ MIT Geotechnical Laboratory files; unpublished.

TABLE A.2d: Summary of Normally Consolidated CK_oUDSS Tests Run on Cohesive Soils at MIT.

Soil (Classification)	Plasticity		At Peak τ_h					$\frac{E_u(50)}{c_u}$	Remraks/Source
	No.	I_p (%)	No.	γ (%)	τ/σ'_{vc}	σ'_v/σ'_{vc}	ϕ °		
Venezuela Tuy Cariaco	2	20.0 ±7.8	3	6.0 ±1.0	0.213 ±0.007	0.559 ±0.043	21.0 ±2.1	355 ±50	Boring C3 Mishu, et al. (1982)
Great Salt Lake (CH)	*	30±10	3	9.1 ±3.1	0.252 ±0.003	0.528 ±0.049	25.6 ±2.3	640 (n=2)	MIT, 1987
Draw-7, MA. (CH w/shells)	2	30.5 ±5.2	2	11.8 ±5.8	0.243 ±0.004	0.513 ±0.049	25.4 ±1.8	445 ±65	MIT, 1987
Alabama	1	56	2	10.4 ±0.8	0.180 ±0.006	0.628 ±0.048	16.0 ±0.6	305 ±50	MIT, 1988
Omaha	*	60±10	2	-	0.237 ±0.001	-	-	-	Ladd (1981)
Trieste Clay (w/shells)	1	55	-	-	0.30 ±0.01	-	-	-	Ladd (1981)
Mean ± S.D.			100	10.1 ±4.0	0.230 ±0.033	0.598 ±0.051	21.1 ±3.3		Excluding Omaha(1981) and Trieste Clay
COV				39.6%	14.3%	8.5%	15.6%		

Notes:

1. All values are mean ± 1 standard deviation unless * appears in No. column then value is mean ± range.
2. MIT in source column ≡ MIT Geotechnical Laboratory files; unpublished.
3. COV = Standard Deviation/Mean.

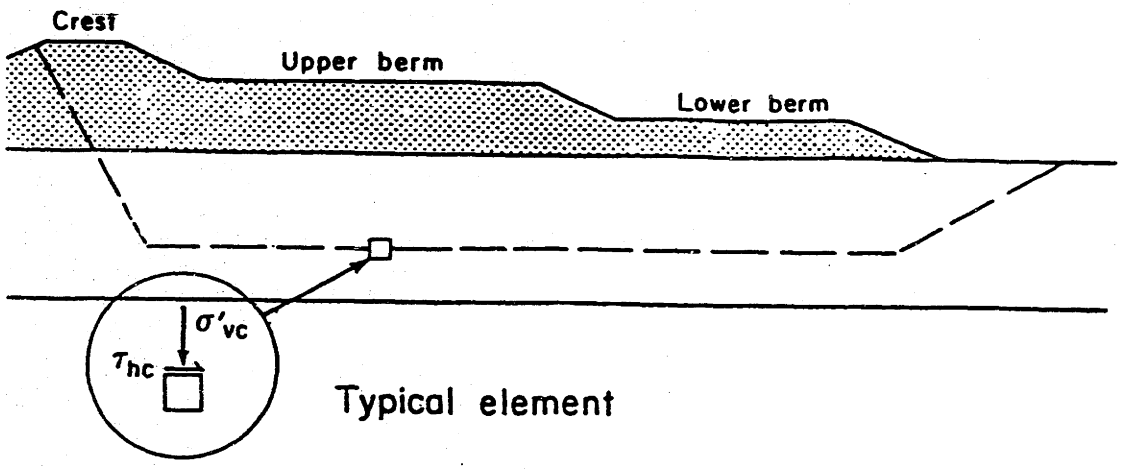

Figure A.1: Simple Shear Representation of an Element Within the Foundation of an Embankment (from Ladd, 1985).

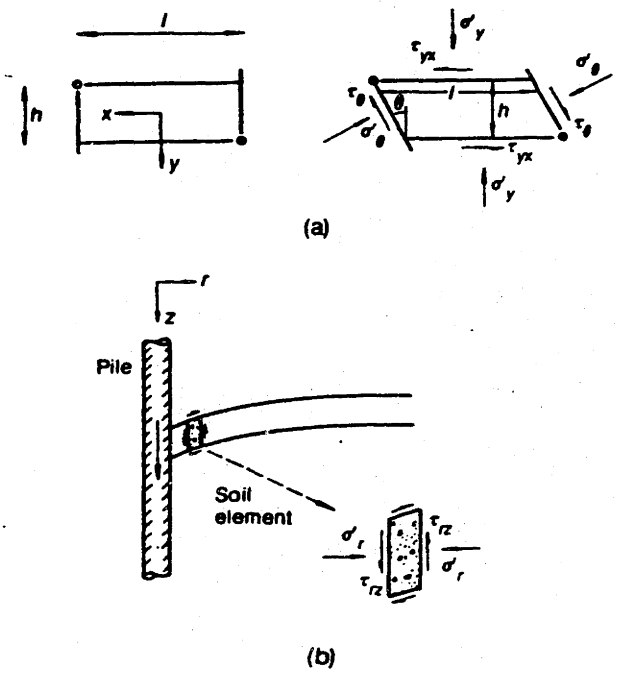

Figure A.2: Deformation in Simple Shear: (a) Simple Shear Apparatus; (b) Axially Loaded Pile (from Randolph and Wroth, 1981).

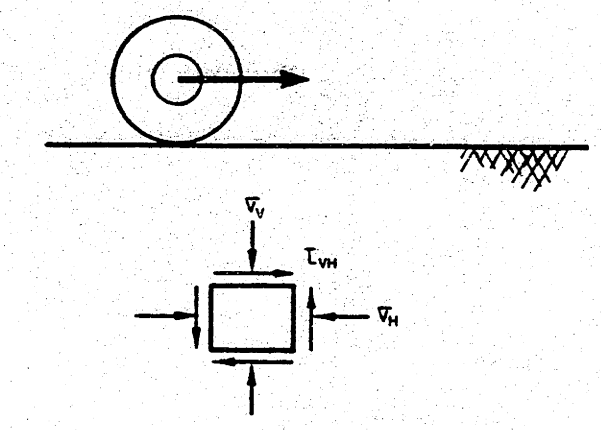

(a) Typical pavement element

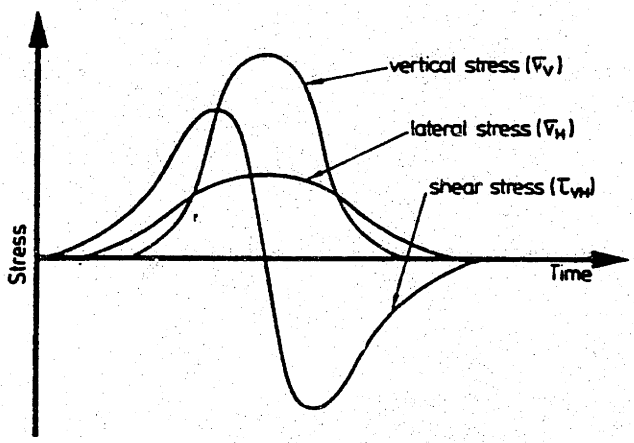

(b) Stress variations with time

Figure A.3: Stress Conditions Under a Rolling Wheel (from Shaw and Brown, 1986).

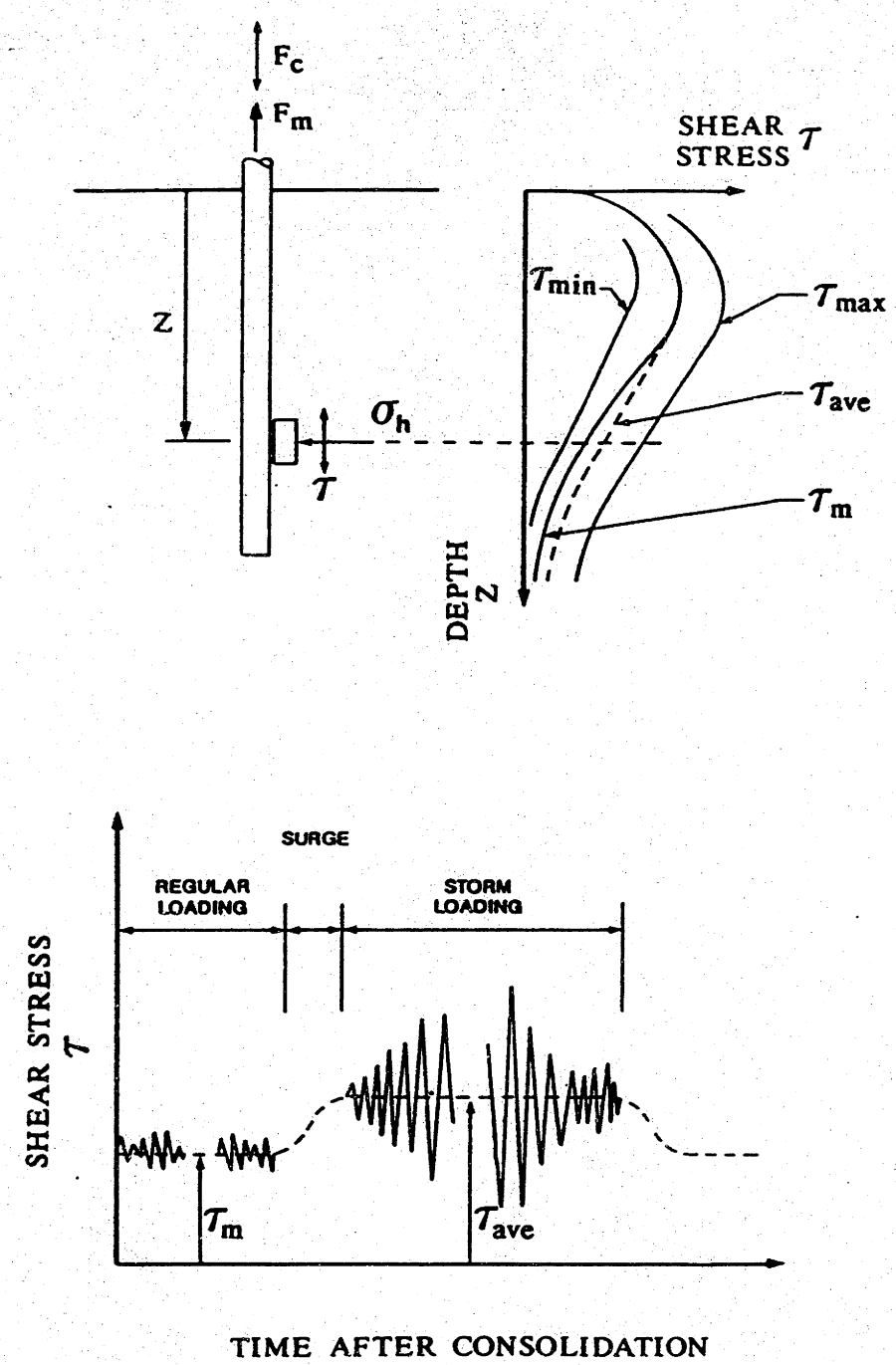

Figure A.4: Cyclic Loads on Foundation Piles of Offshore Structures Subjected to Wind and Wave Loads (from Malek, 1987).

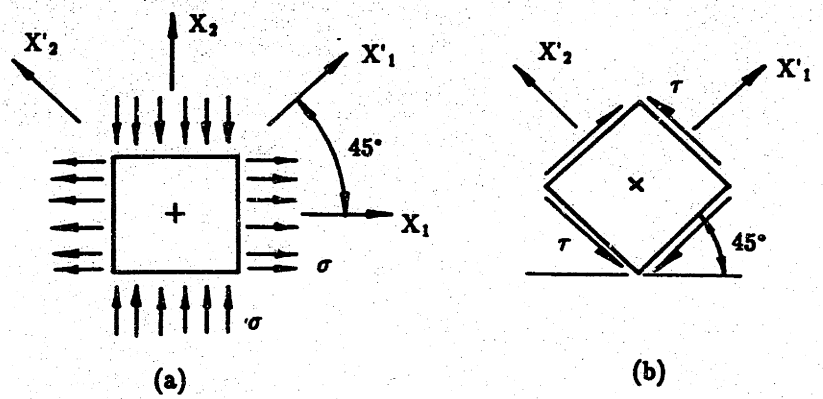

Figure A.5: (a) Pure Shear Stresses at a point; (b) Axes Rotated by 45 Degrees (after Saada and Townsend, 1981).

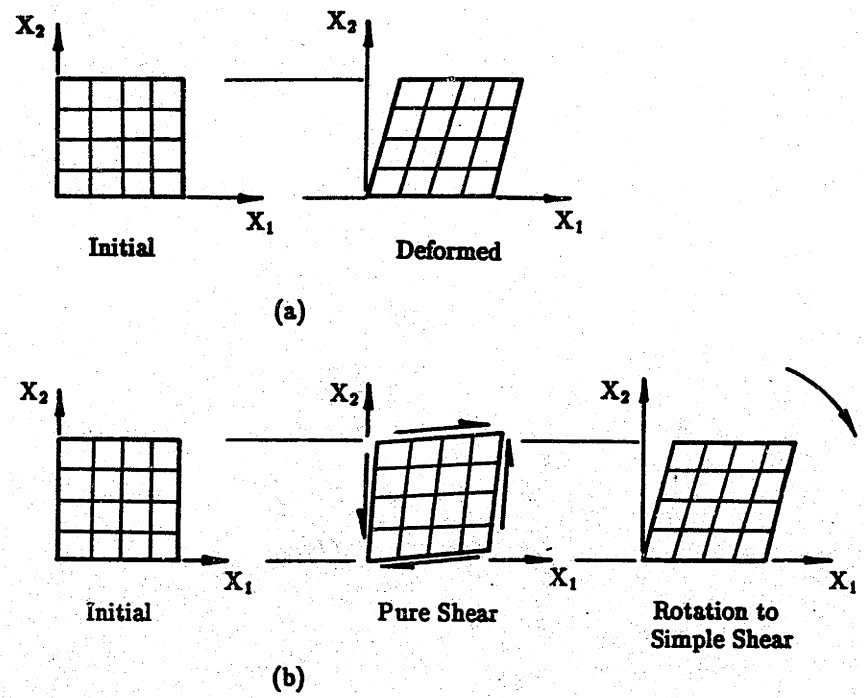

Figure A.6: (a) Simple Shear Strain Condition; (b) Rotation of Pure Shear to Simple Shear Strain Condition (after Saada and Townsend, 1981).

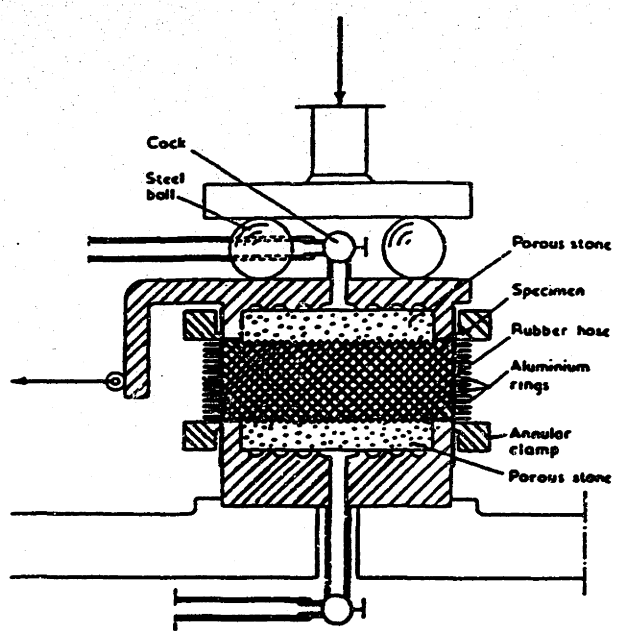

Figure A.7: Cross–Section of the SGI Simple Shear Apparatus (Kjellman, 1951).

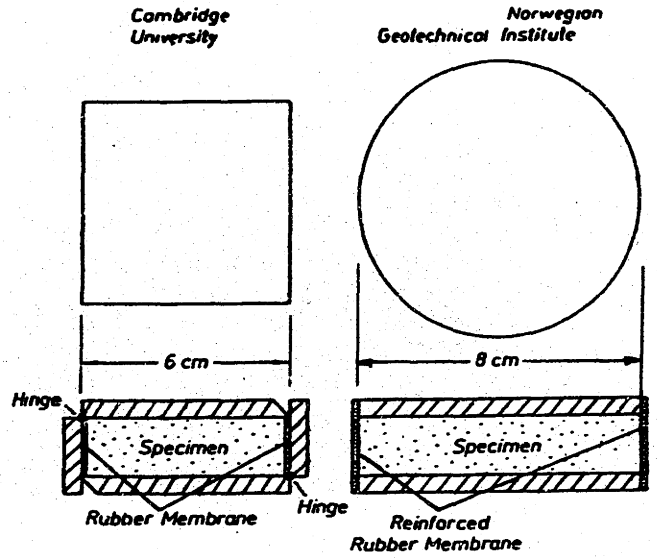

Figure A.8: Schematics of: (a) Cambridge University Direct Simple Shear Device; (b) NGI Direct Simple Shear Device (after Franke, et al., 1979).

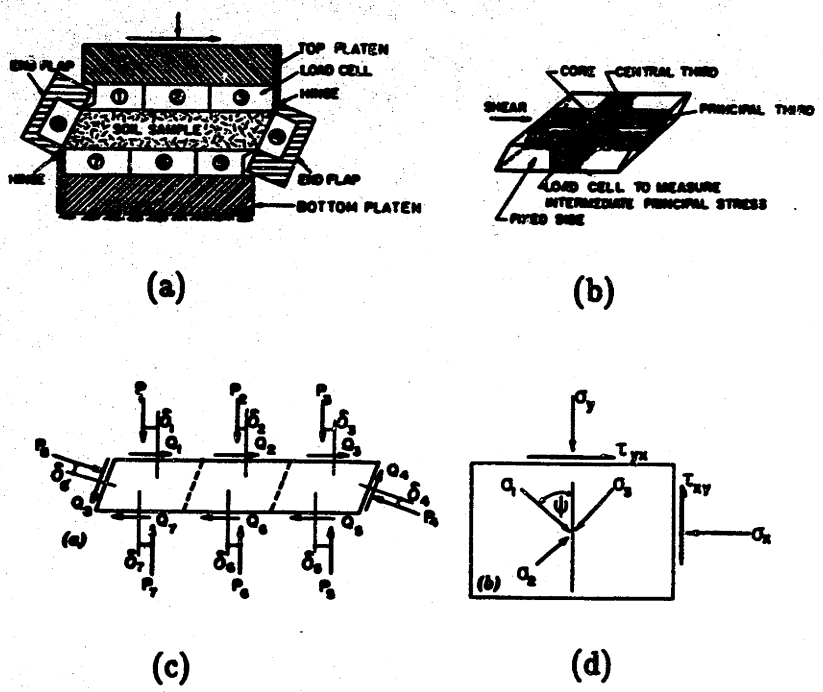

Figure A.9: Cambridge University Mk7 Simple Shear Apparatus: (a) Cross–Section; (b) Arrangement of Load Transducers; (c) Typical Set of Forces Measured; (d) Stresses Deduced for Sample Core (after Budhu, 1985).

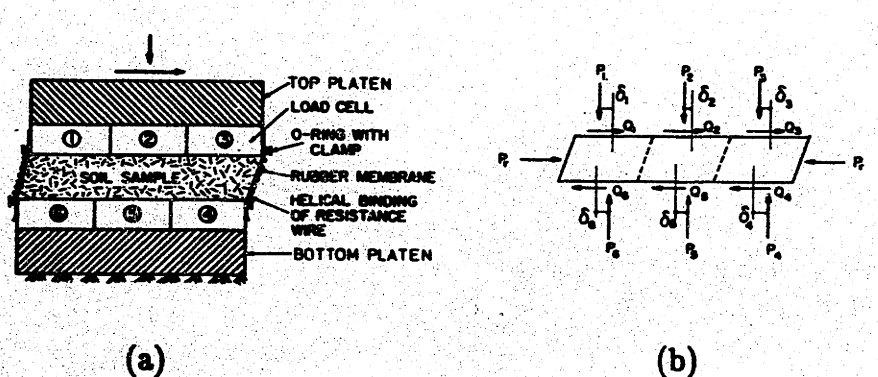

Figure A.10: Cambridge University Cylindrical Simple Shear Apparatus (CSSA): (a) Cross–Section; (b) Typical Set of Forces Measured (after Budhu, 1985).

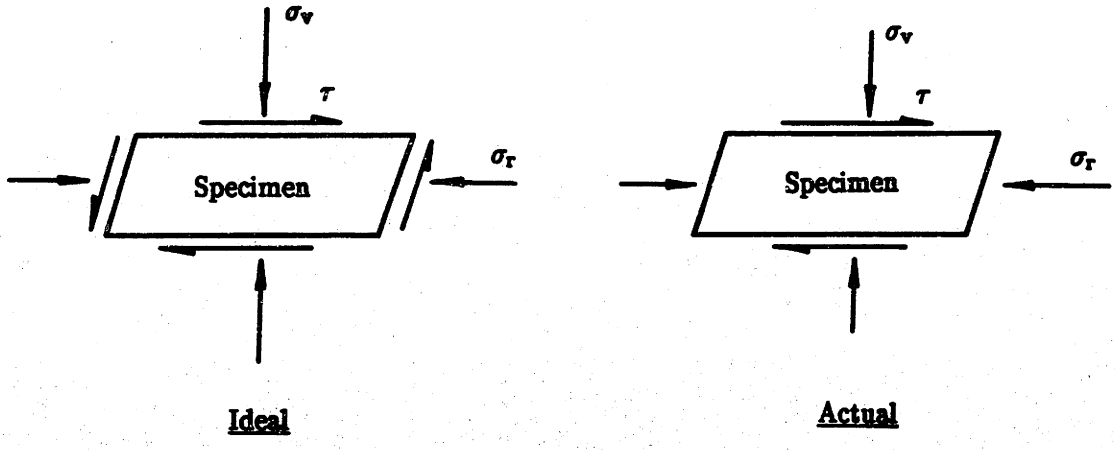

Figure A.11: Comparison of Ideal Set of Stresses Imposed to a Simple Shear Specimen Versus Stresses Which can Realistically be Imposed.

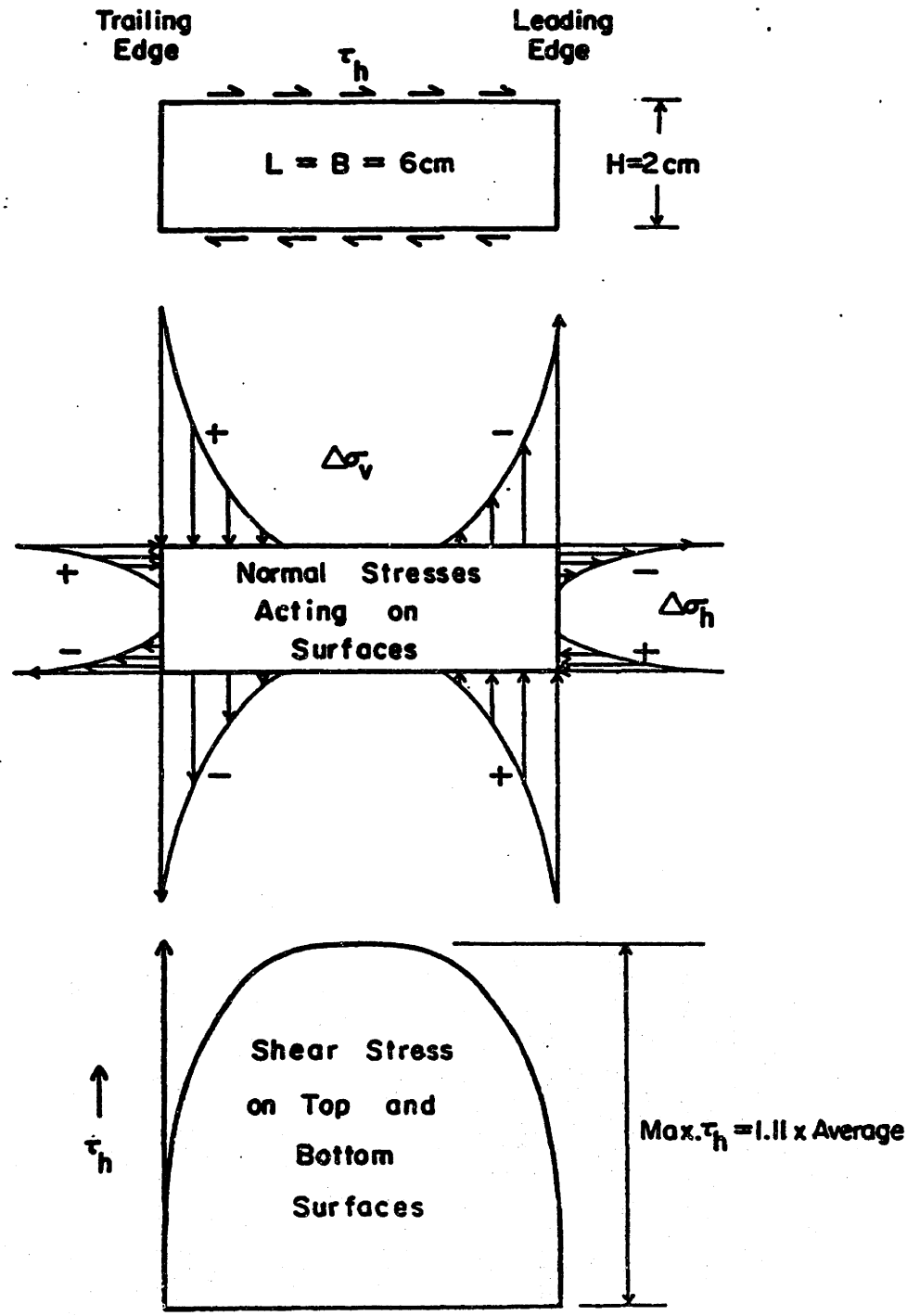

Figure A.12: Elastic Stresses in Cambridge Simple Shear Apparatus Computed by Roscoe (1953; from Ladd and Edgers, 1972).

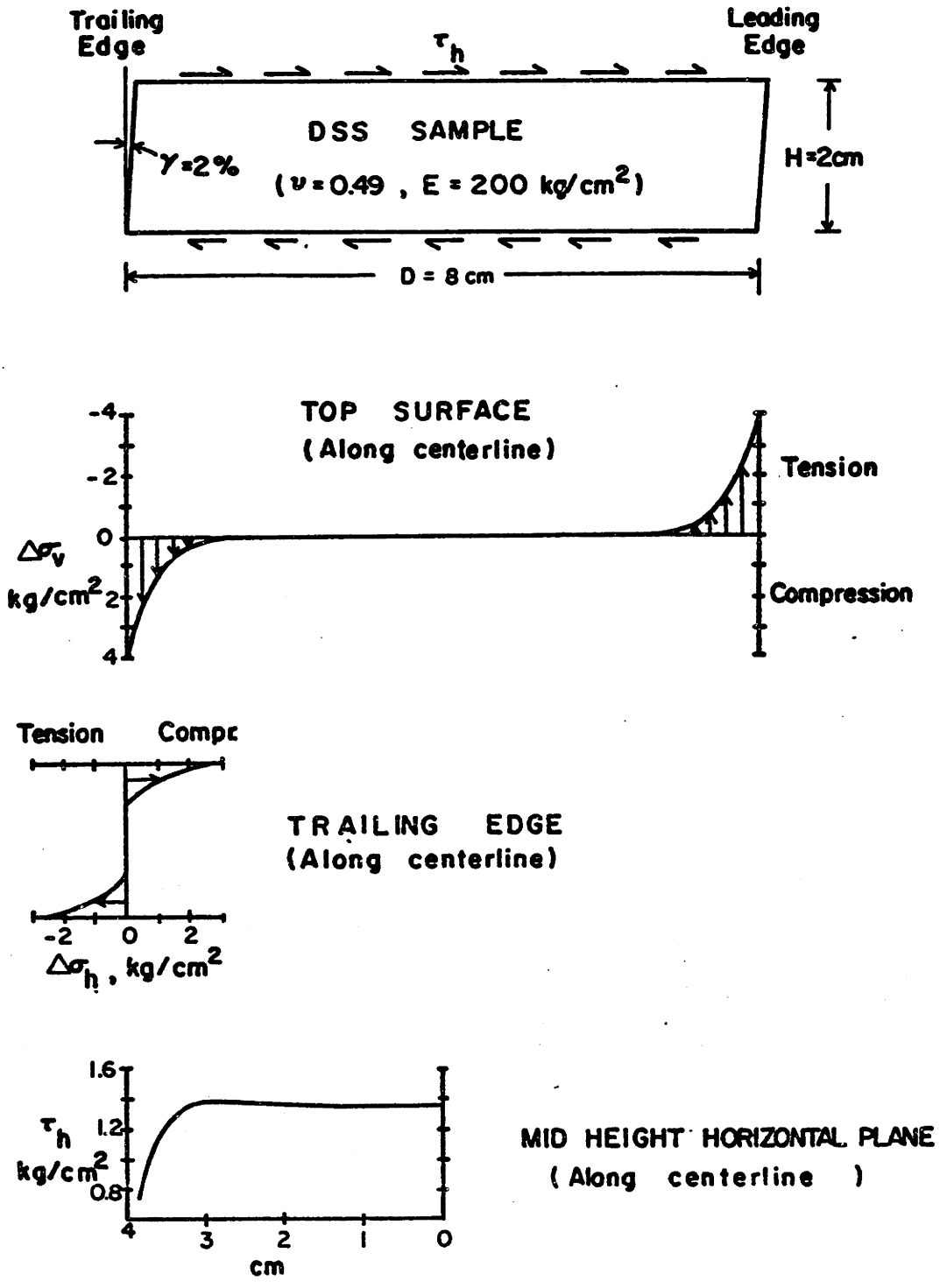

Figure A.13: Elastic Stresses in Geonor Direct Simple Shear Apparatus Computed by Lucks, et al. (1972; from Ladd and Edgers, 1972).

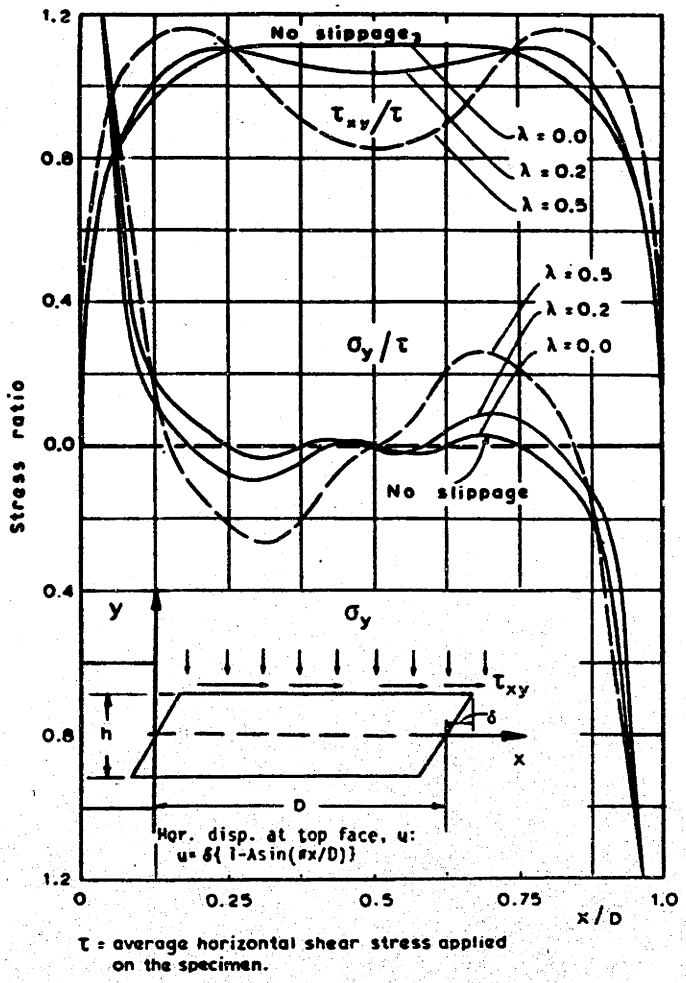

τ = average horizontal shear stress applied on the specimen.

Figure A.14: Distribution of Shear and Normal Stresses on Top Face of Specimen in Cambridge University Apparatus due to Slippage Computed by Prevost and Hoeg (1976; from Lacasse and Vucetic, 1981).

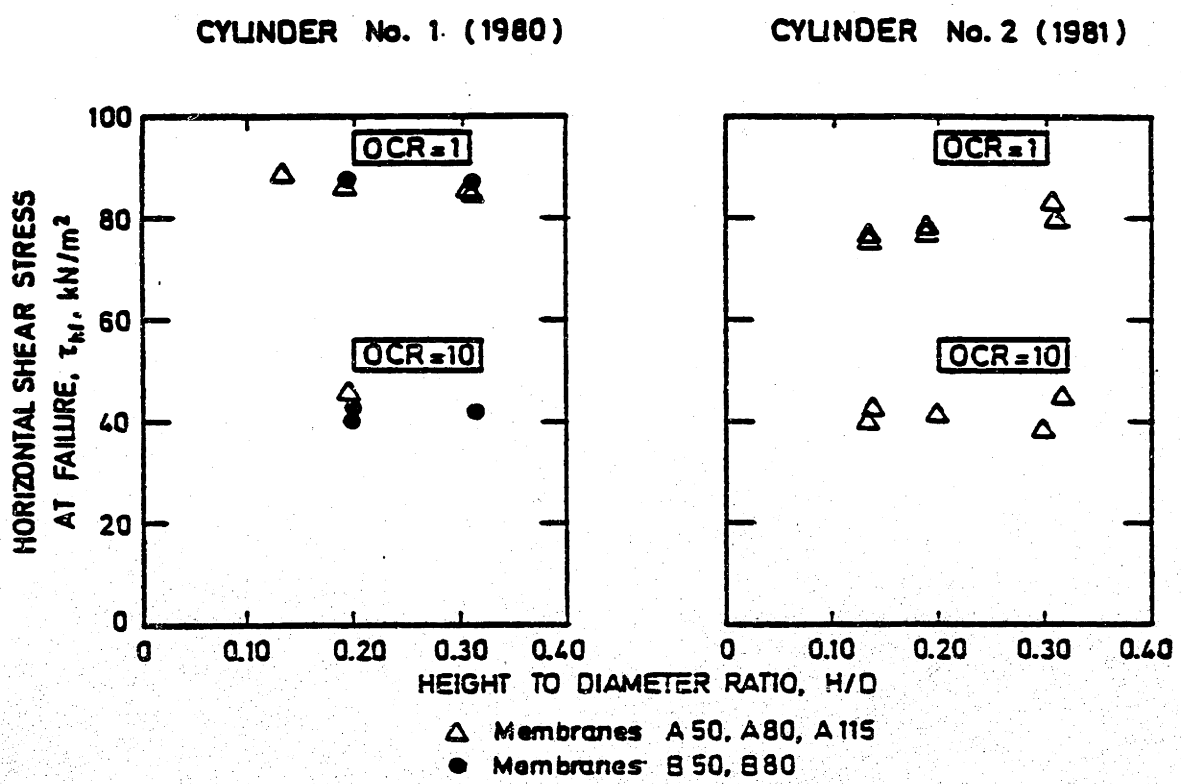

Figure A.15: Influence of Height to Diameter Ratio and Membrane Type on Measured Peak Horizontal Shear Stress from Geonor DSS Tests on Haga Clay (from Vucetic and Lacasse, 1982).

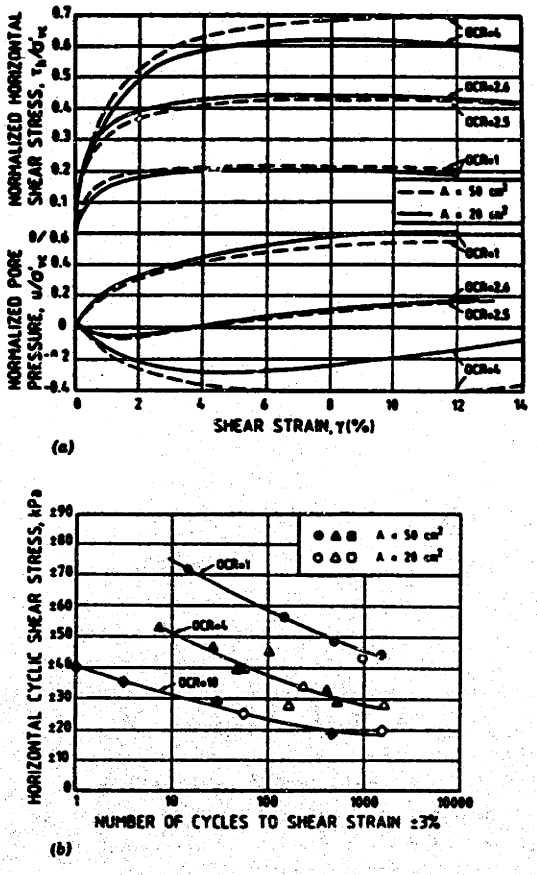

Figure A.16: Constant Volume Geonor DSS Tests on Drammen Clay Specimens with Cross–Sectional Areas of 20 and 50 cm²: (a) Static Tests; (b) Cyclic Tests (from Vucetic and Lacasse, 1984).

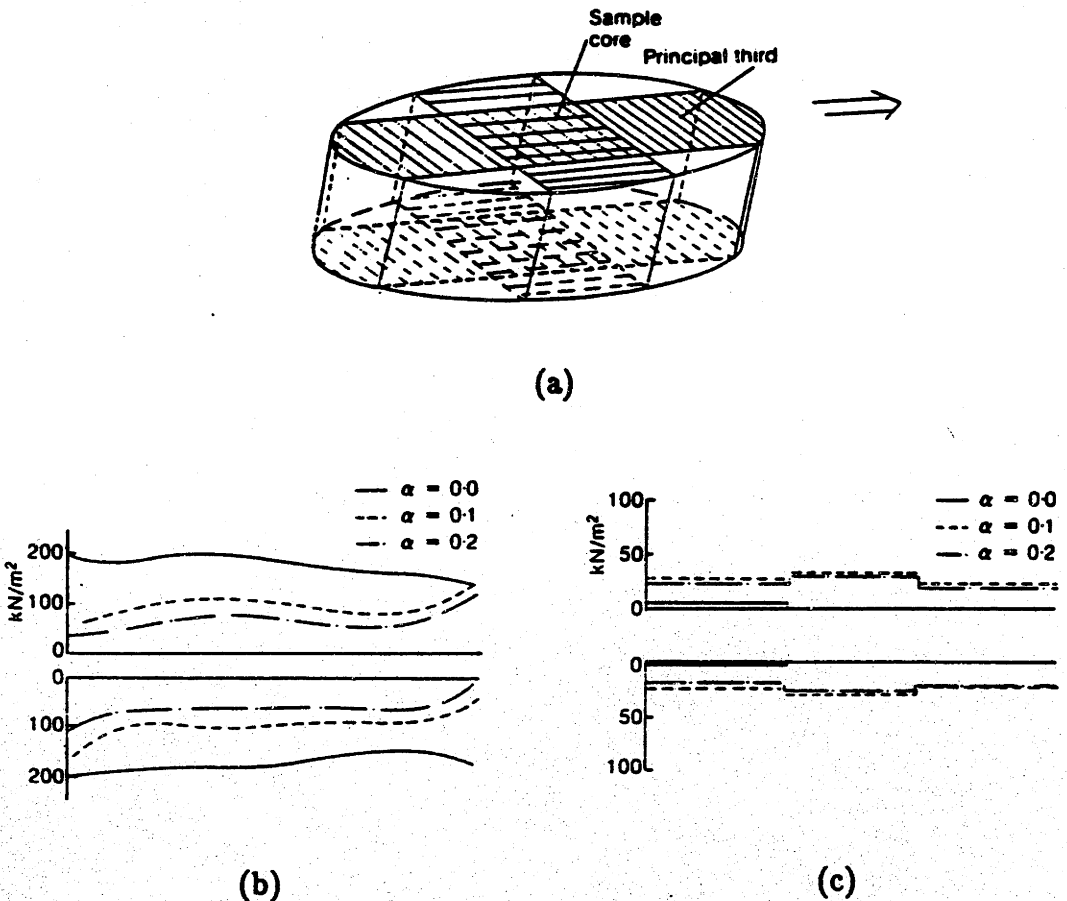

Figure A.17: Stress Distributions on the Principal Third for a Constant Volume Test on Kaolin in the Cambridge CSSA: (a) Principal Third Load Cells; (b) Normal Stress; (c) Shear Stress (α = shear distortion γ_{yx}; after Airey and Wood, 1987).

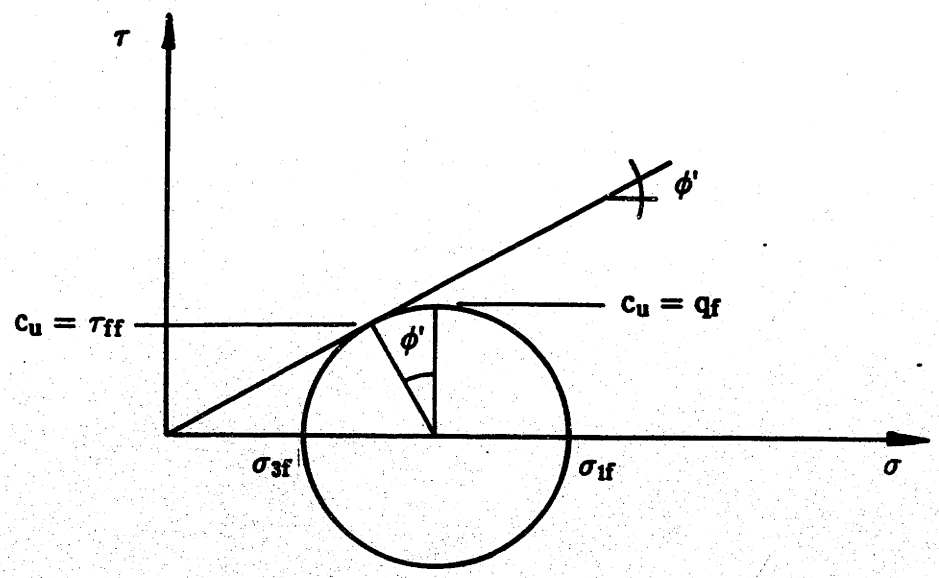

$$\tau_{ff} = q_f \cos\phi' \qquad q_f = 0.5(\sigma_1 - \sigma_3)_f$$

Figure A.18: Alternate Definitions of the Undrained Shear Strength: (1) Radius of Mohr's Circle of Stress at Failure, $c_u = q_f$; (2) Shear Stress on the Failure Plane at Failure, $c_u = \tau_{ff} = q_f \cos\phi'$.

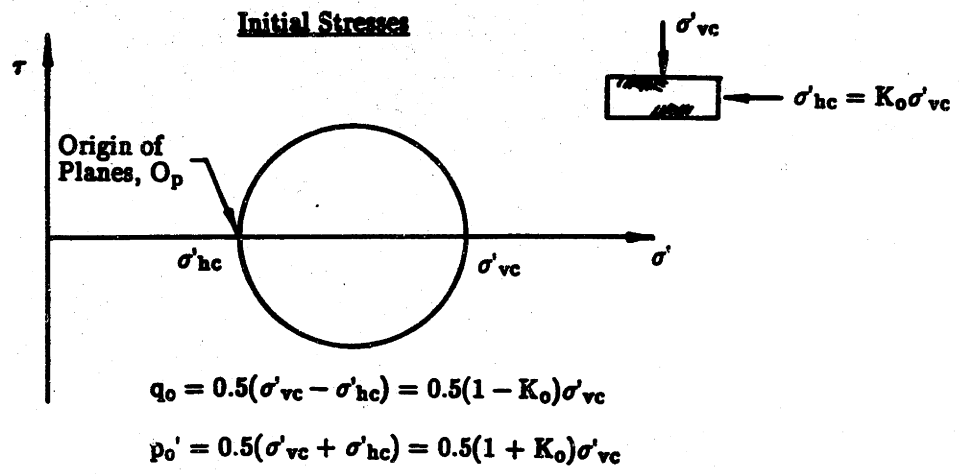

$$q_o = 0.5(\sigma'_{vc} - \sigma'_{hc}) = 0.5(1 - K_o)\sigma'_{vc}$$

$$p_o' = 0.5(\sigma'_{vc} + \sigma'_{hc}) = 0.5(1 + K_o)\sigma'_{vc}$$

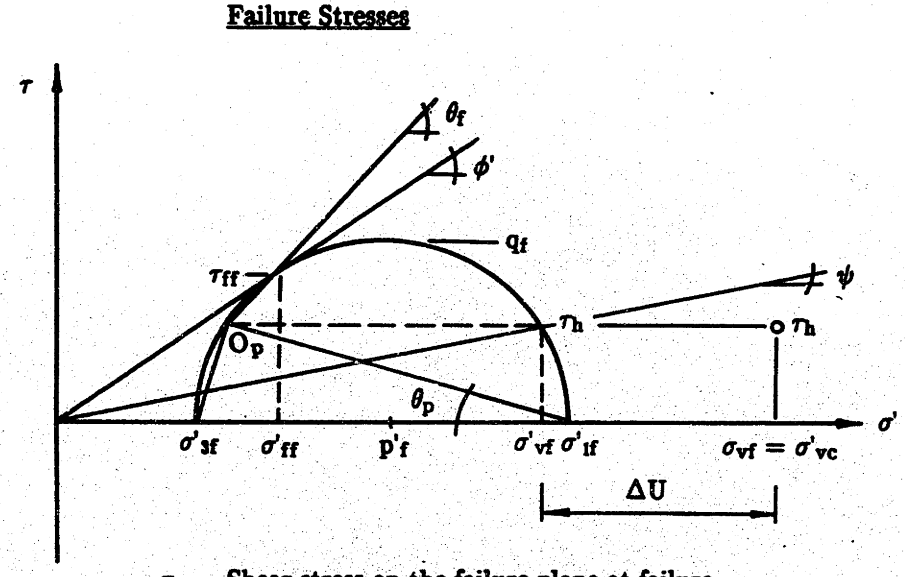

τ_{ff} = Shear stress on the failure plane at failure.

θ_f = Orientation of the failure plane.

θ_p = Orientation of the plane on which σ'_1 acts.

Figure A.19: Definition of Stresses and Angles for Initial and Failure States in the Direct Simple Shear Test (after Ladd and Edgers, 1972).

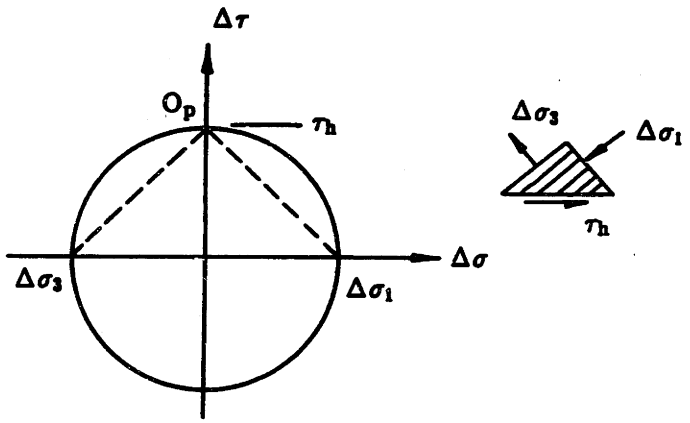

Applied Stresses for Pure Shear

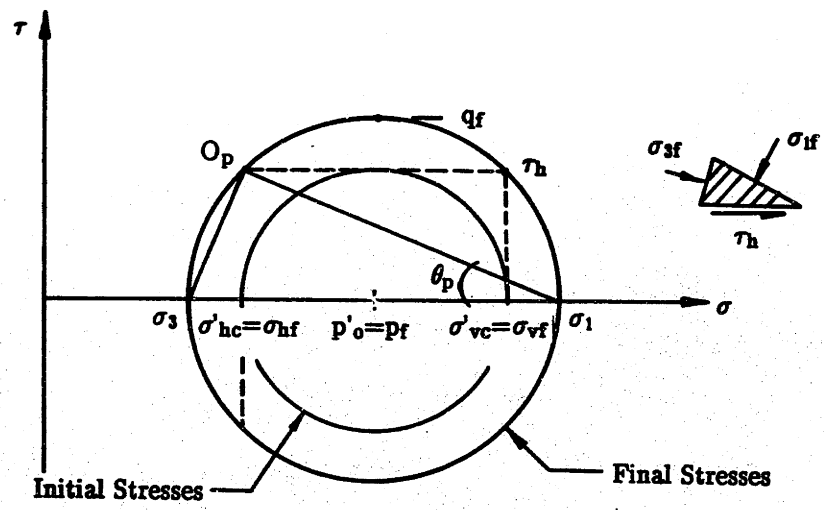

$$q_f/\sigma'_{vc} = \sqrt{\frac{(1 - K_o)^2}{4} + (\tau_h/\sigma'_{vc})^2}$$

$$\tau_{ff} = q_f \cos\phi' \qquad p'_f/\sigma'_{vc} = (p'_o - \Delta U)/\sigma'_{vc}$$

$$\sin\phi' = q_f/p'_f \qquad \theta_f = 45^\circ = \phi'/2 - \theta_p$$

$$\tan\theta_p = \frac{\tau_h/\sigma'_{vc}}{0.5(1 - K_o) + q_f/\sigma'_{vc}}$$

Figure A.20: Direct Simple Shear Failure Criterion I: Applied Stress System is Pure Shear (after Ladd and Edgers, 1972).

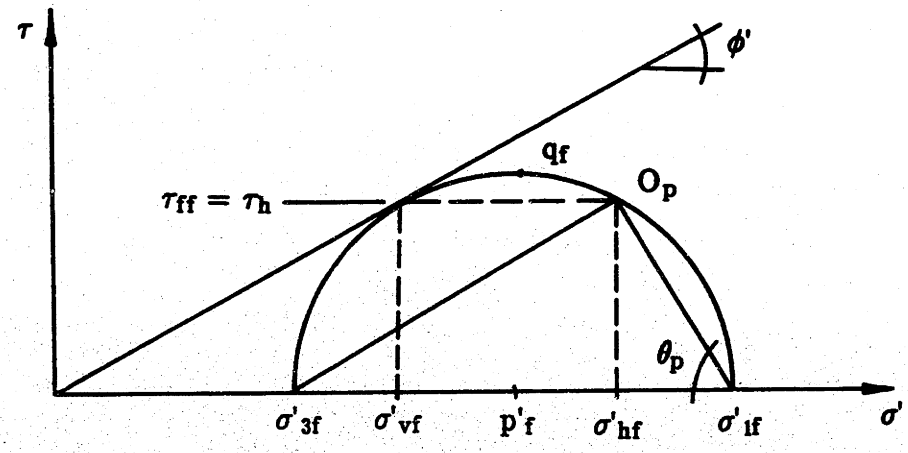

$$q_f/\sigma'_{vc} = \frac{\tau_h/\sigma'_{vc}}{\cos\phi'} \qquad \tau_{ff} = \tau_h$$

$$p'_f/\sigma'_{vc} = \sigma'_{vf}/\sigma'_{vc} + (\tau_h/\sigma'_{vc})\tan\phi'$$

$$\sigma'_{hf}/\sigma'_{vf} > 1 \qquad \tan\phi' = \tau_h/\sigma'_{vf}$$

$$\theta_p = 45^\circ + \phi'/2 \qquad \theta_f = 0^\circ$$

Figure A.21: Direct Simple Shear Failure Criterion II: Horizontal Plane is Failure Plane.

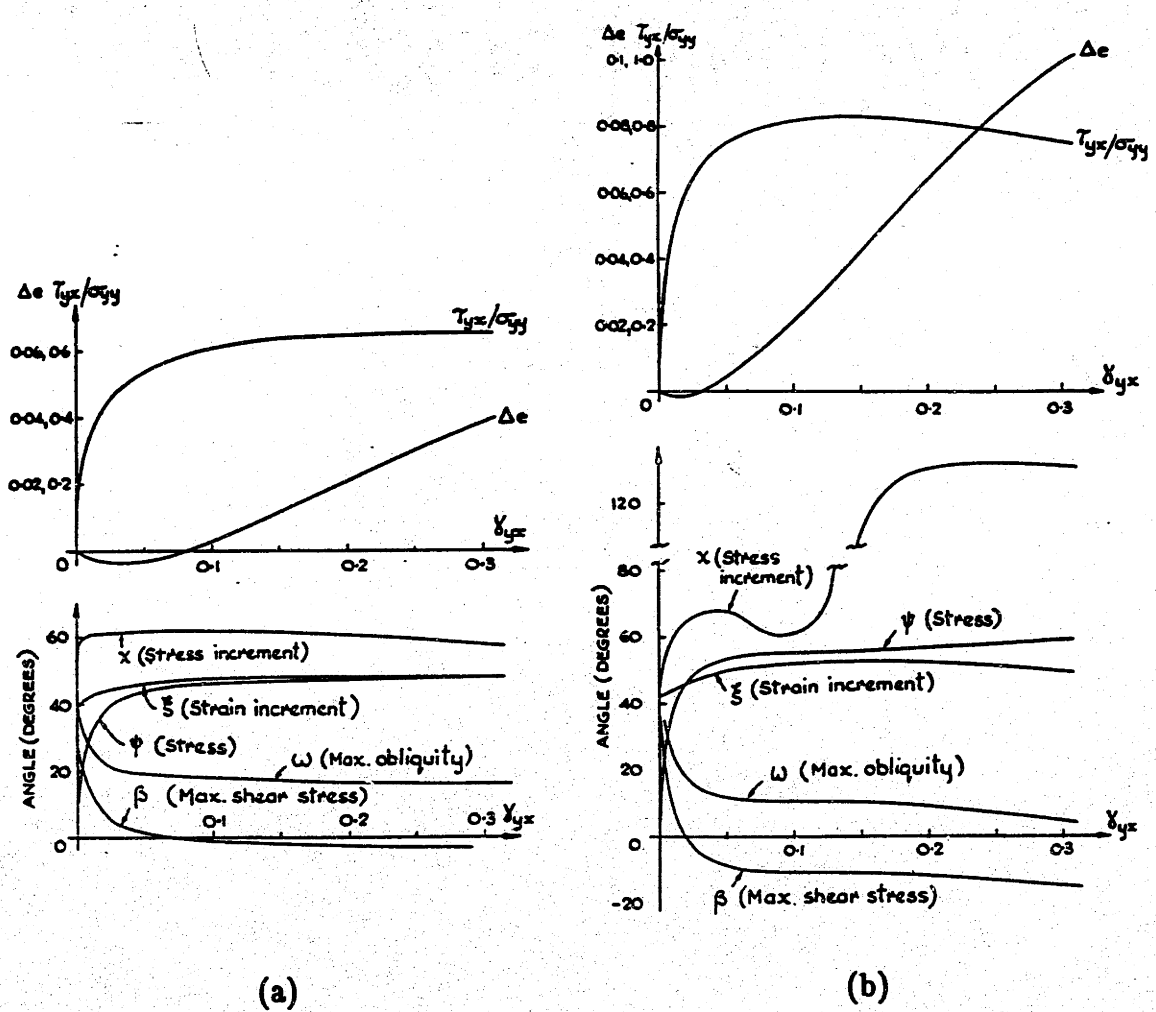

Figure A.22: Stress Ratio on Horizontal Plane in Central Third, Average Voids Ratio Change for Whole Sample and Inclination to Horizontal of Major Principal Planes of Stress (ψ), Stress Increment (χ), Strain Increment (ξ), as Well as Planes of Maximum Shear Stress (β) and Maximum Obliquity (ω) for drained tests in the Cambridge DSS on: (a) Medium Loose Sand (e_0=0.68); (b) Dense Sand (e_0=0.53; after Roscoe, et al., 1967).

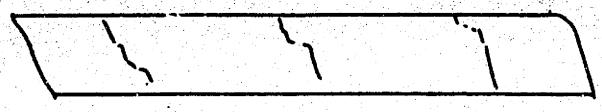

Figure A.23: Ruptures Observed in Radiograph of Simple Shear Test on Kaolin (sketches of radiographs of threads of lead paste; after Airey, et al., 1985).

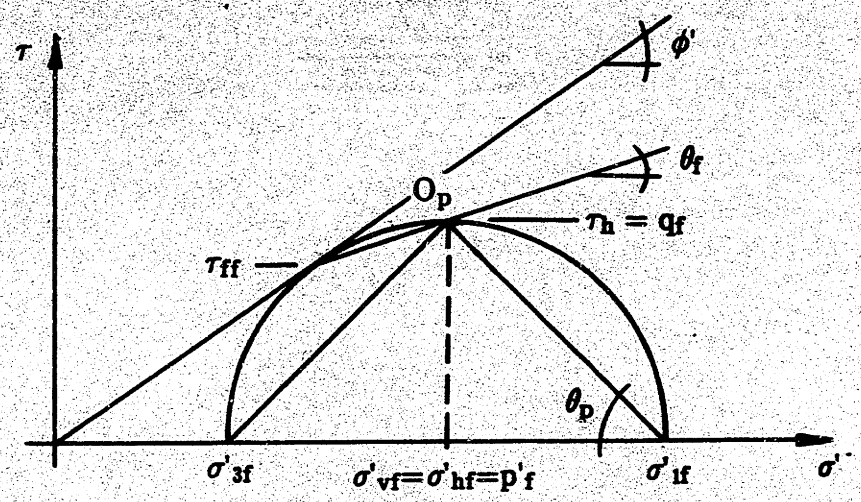

$q_f/\sigma'_{vc} = \tau_h/\sigma'_{vc}$ $\qquad$ $\tau_{ff} = q_f \cos\phi'$

$p'_f/\sigma'_{vc} = \sigma'_{vf}/\sigma'_{vc}$

$\sigma'_{hf}/\sigma'_{vf} = 1$ $\qquad$ $\sin\phi' = \tau_h/\sigma'_{vf}$

$\theta_p = 45°$ $\qquad$ $\theta_f = \phi'/2$

Figure A.24: Direct Simple Shear Failure Criterion III: Horizontal Plane is Plane of Maximum Shear Stress.

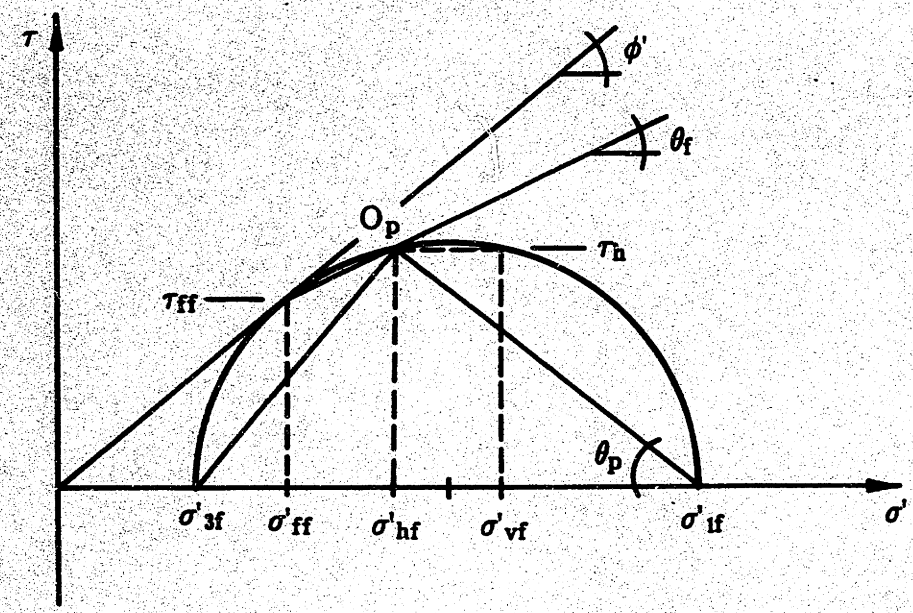

$$q_f/\sigma'_{vc} = (\tau_{ff}/\sigma'_{vc})/\cos\phi'$$

$$p'_f/\sigma'_{vc} = \sigma'_{ff}/\sigma'_{vc} + (q_f/\sigma'_{vc})\sin\phi'$$

$$\sigma'_{3f} = p'_f - q_f$$

ϕ' = assumed $\qquad\qquad \theta_f = 45^\circ + \phi'/2 - \theta_p$

$$\tan\theta_p = \tau_h/(\sigma'_{vf} - \sigma'_{3f})$$

Figure A.25: Direct Simple Shear Failure Criterion IV: Assume Mohr–Coulomb Failure Envelope.

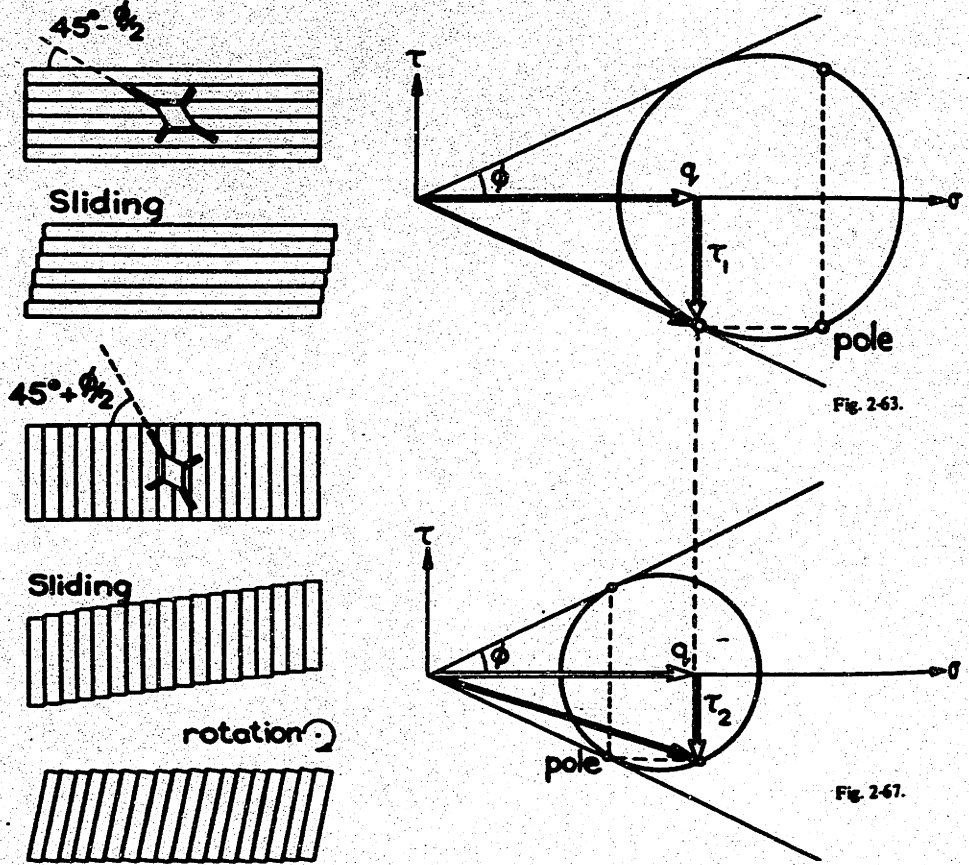

Figure A.26: Book Stack Analogy of Simple Shear Deformation Produced by Sliding on Either Horizontal or Vertical Planes (from de Josselin de Jong, 1971).

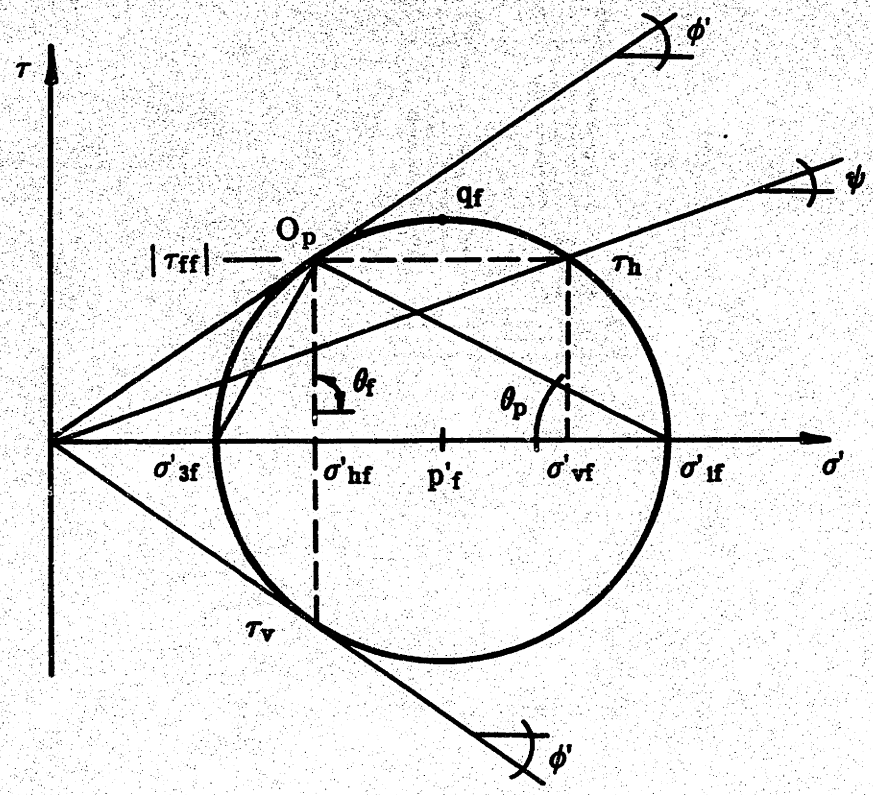

$$q_f/\sigma'_{vc} = \frac{\tau_h/\sigma'_{vc}}{\cos\phi'} \qquad \tau_h/\sigma'_{vf} = \frac{\sin\phi'\cos\phi'}{1+\sin^2\phi'}$$

$$\tau_{ff} = q_f\cos\phi' \qquad p'_f/\sigma'_{vc} = \sigma'_v/\sigma'_{vc} - (\tau_h/\sigma'_{vc})\tan\phi'$$

$$\theta_p = 45^\circ - \phi'/2 \qquad \psi = \arctan(\tau_h/\sigma'_{vf})$$

$$\theta_f = 90^\circ$$

Figure A.27: Direct Simple Shear Failure Criterion V: Failure Occurs on Vertical Planes.

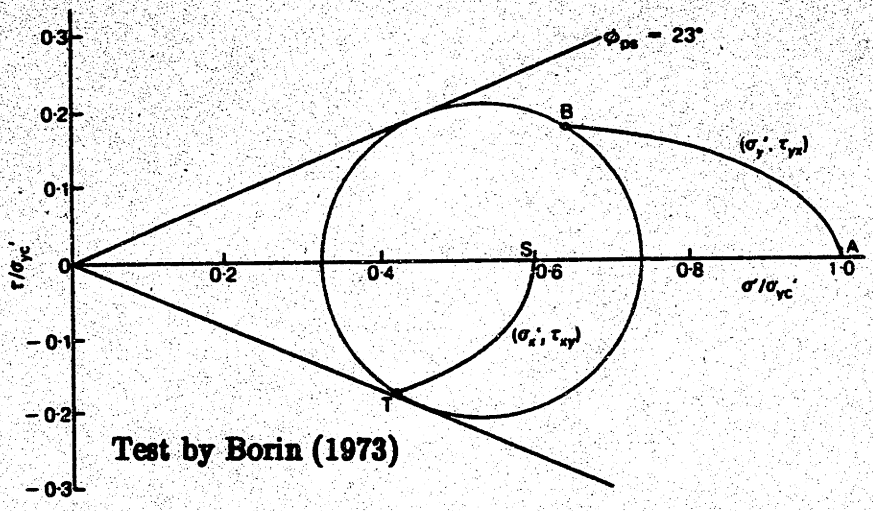

Figure A.28: Effective Stress Paths and the Failure State From a CK_0UDSS Test on Normally Consolidated Kaolin (from Wroth, 1987).

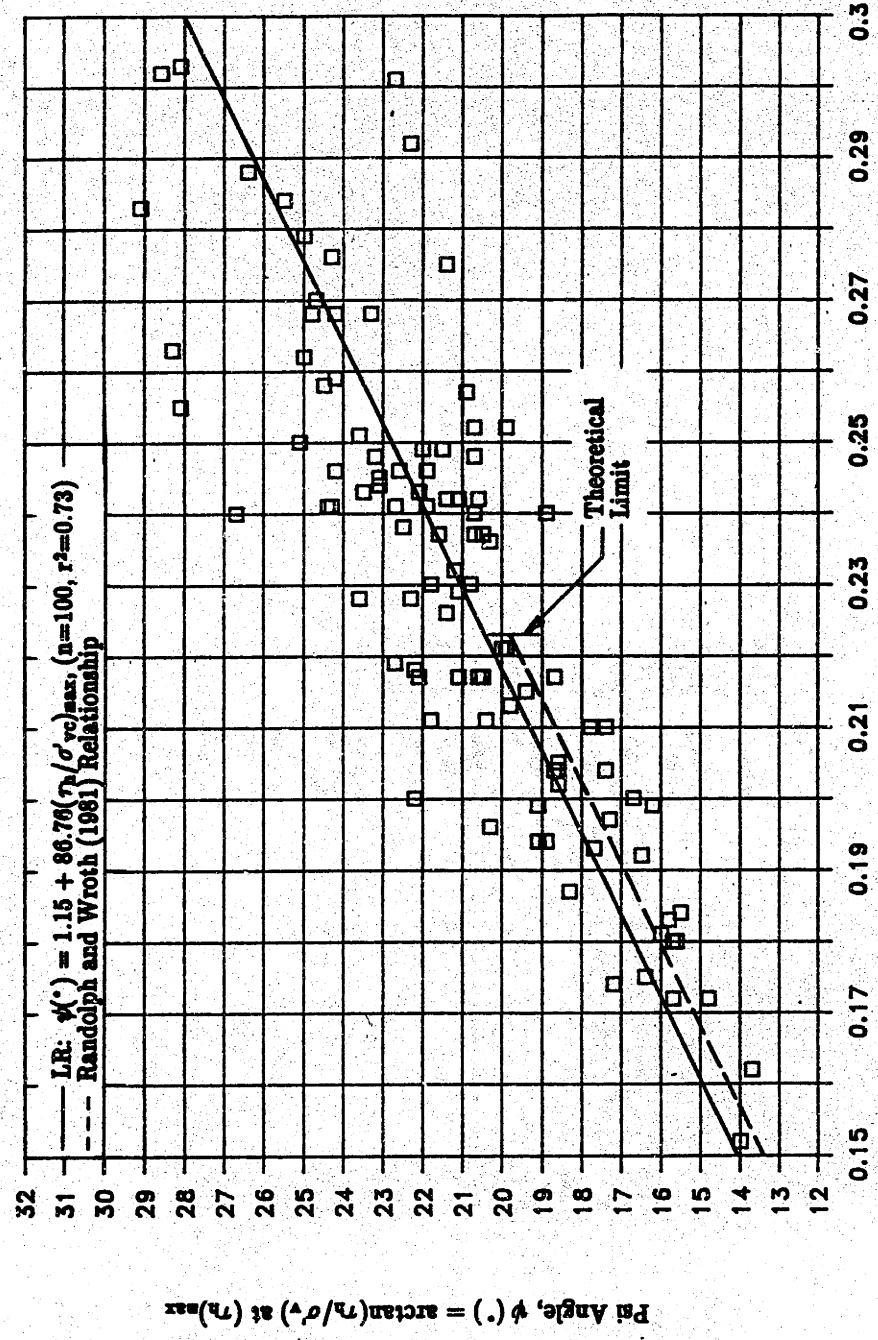

Figure A.29: Psi Angle Versus Undrained Strength Ratio for CK_oUDSS Test Results on Normally Consolidated Cohesive Soils (data summarized in Table A.2).

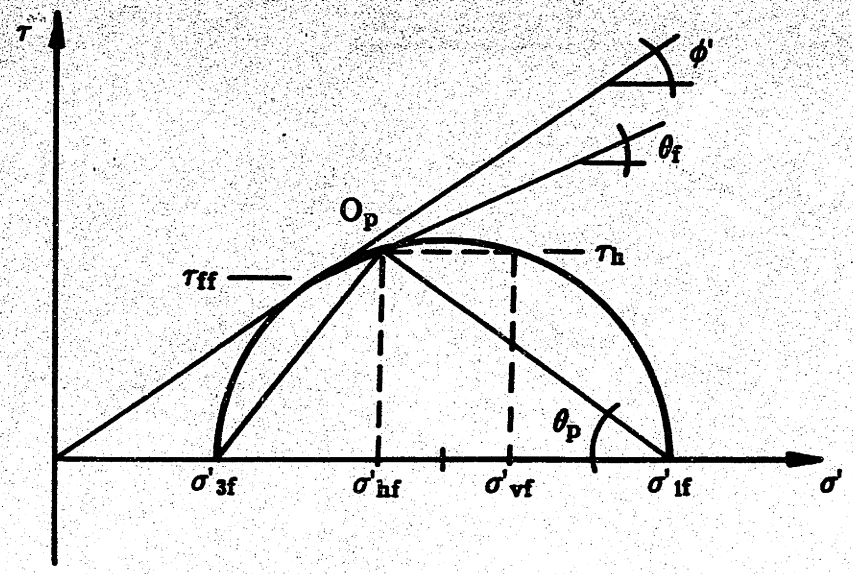

$$\tau_h/\sigma'_v = \kappa\tan\delta \qquad \theta_p = \delta \qquad \kappa = 1 - K_o$$

$$\beta = 1 - \Delta U/\sigma'_{vc} \qquad \tau_{ff} = q_f\cos\phi'$$

$$\sigma'_3/\sigma'_{vc} = K_o\beta \qquad \theta_f = 45^\circ + \phi'/2 - \theta_p$$

$$q_f/\sigma'_{vc} = \frac{\beta^2(1 - K_o)^2 + (\tau_h/\sigma'_{vc})^2}{2\beta(1 - K_o)}$$

$$\sigma'_1/\sigma'_{vc} = \frac{\beta^2(1 - K_o) + (\tau_h/\sigma'_{vc})^2}{\beta(1 - K_o)}$$

$$\sin\phi' = \frac{\beta^2(1 - K_o)^2 + (\tau_h/\sigma'_{vc})^2}{\beta^2(1 - K_o^2) + (\tau_h/\sigma'_{vc})^2}$$

$$p'_f/\sigma'_{vc} = 0.5(\sigma'_1/\sigma'_{vc} + \sigma'_3/\sigma'_{vc})$$

$$\tan\theta_p = \frac{\tau_h}{(\sigma'_{vf} - \sigma'_{3f})}$$

Figure A.30: Direct Simple Shear Failure Criterion VI: Linear Relationship Between τ_h/σ'_v and $\kappa\tan\delta$.

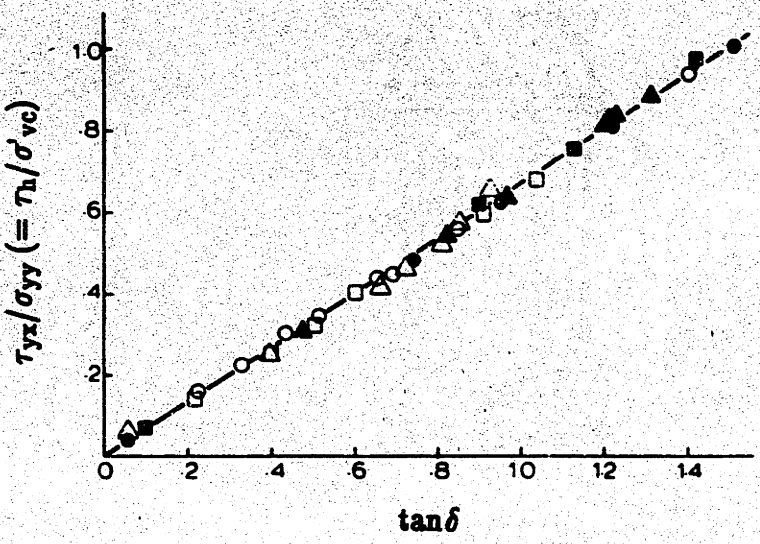

Figure A.31: Linear Relationship Between R=τ_{xy}/σ_{yy} (=τ_h/σ'_{vc}) and Tanδ Supported by Data From a Wide Range of Different Drained Simple Shear Tests on Leighton Buzzard Sand (from Airey, et al., 1985).

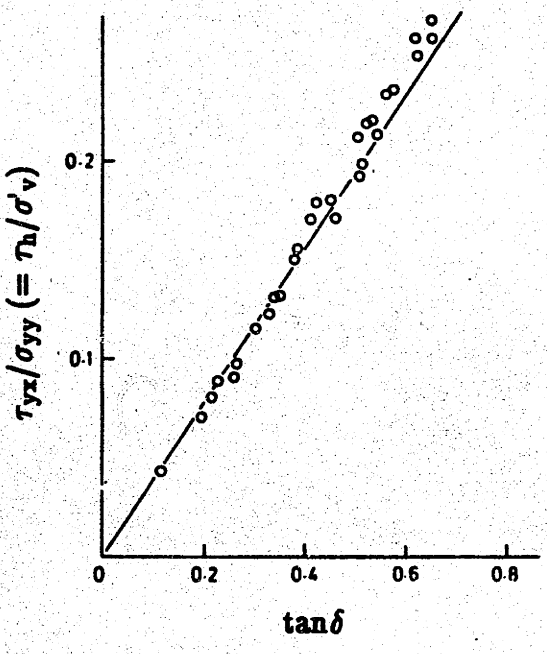

Figure A.32: Relationship Between R=τ_{xy}/σ_{yy} (=τ_h/σ'_v) and Tanδ for CU Simple Shear Tests on Normally Consolidated Kaolin (from Airey, et al., 1985).

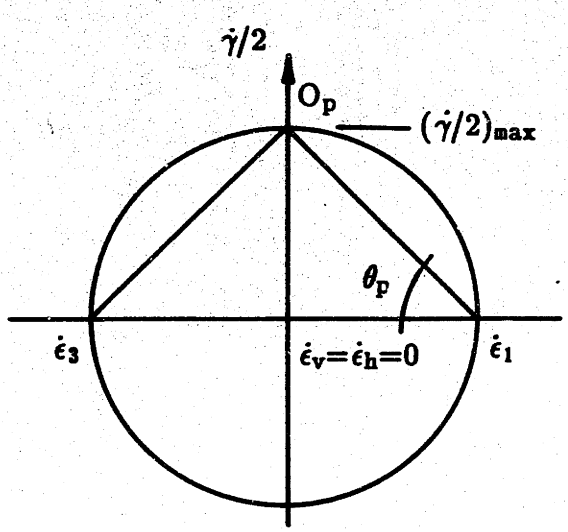

Mohr's Circle of Strain Increment (undrained test)

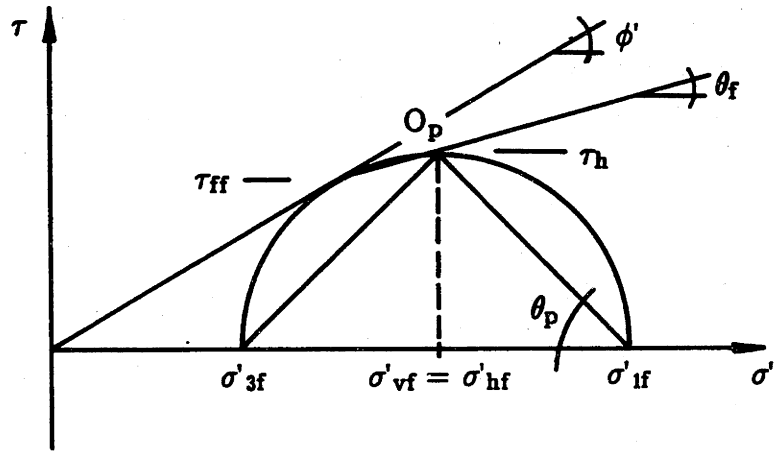

$q_f/\sigma'_{vc} = \tau_h/\sigma'_{vc}$ $\qquad$ $\tau_{ff} = q_f \cos\phi'$

$p'_f/\sigma'_{vc} = \sigma'_{vf}/\sigma'_{vc}$

$\sigma'_{hf}/\sigma'_{vf} = 1$

$\sin\phi' = \tau_h/\sigma'_{vf}$ $\qquad$ $\theta_p = 45°$

$\theta_f = \phi'/2$

Figure A.33: Direct Simple Shear Failure Criterion VII: Coincidence of Principal Axes of Strain Increment and Stress.

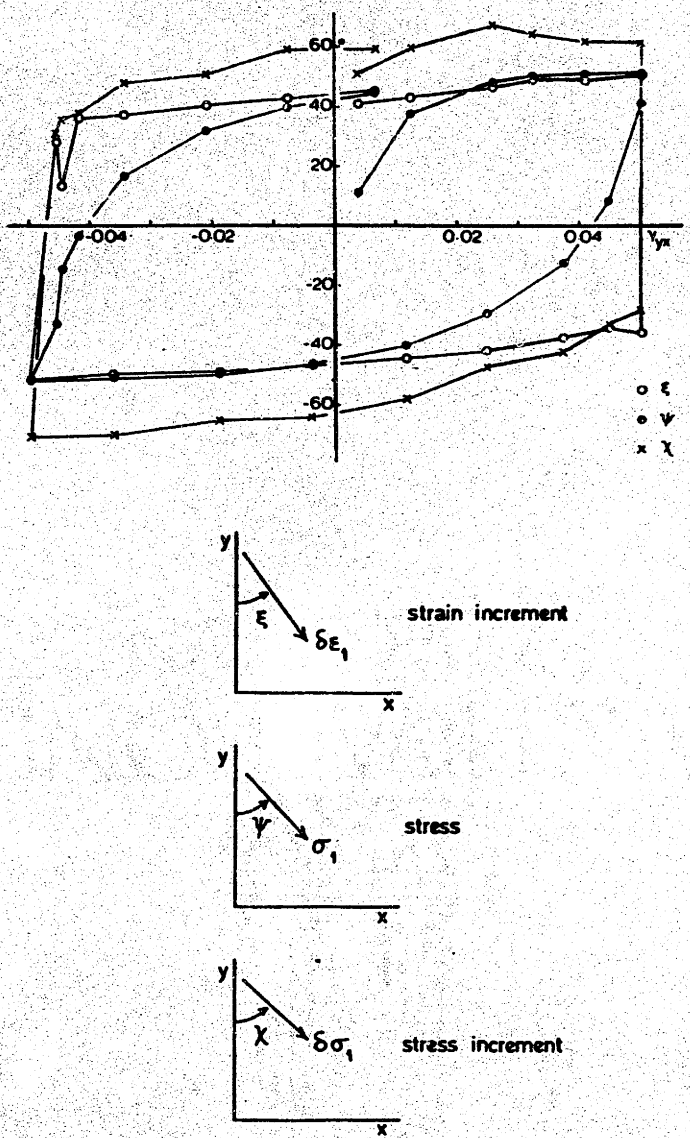

Figure A.34: Variation of Angles ξ, ψ and χ With Shear Distortion α $(= \gamma_{yx})$ for Cyclic Simple Shear Test on Dense Sand by Budhu (1979; from Airey, et al., 1985).

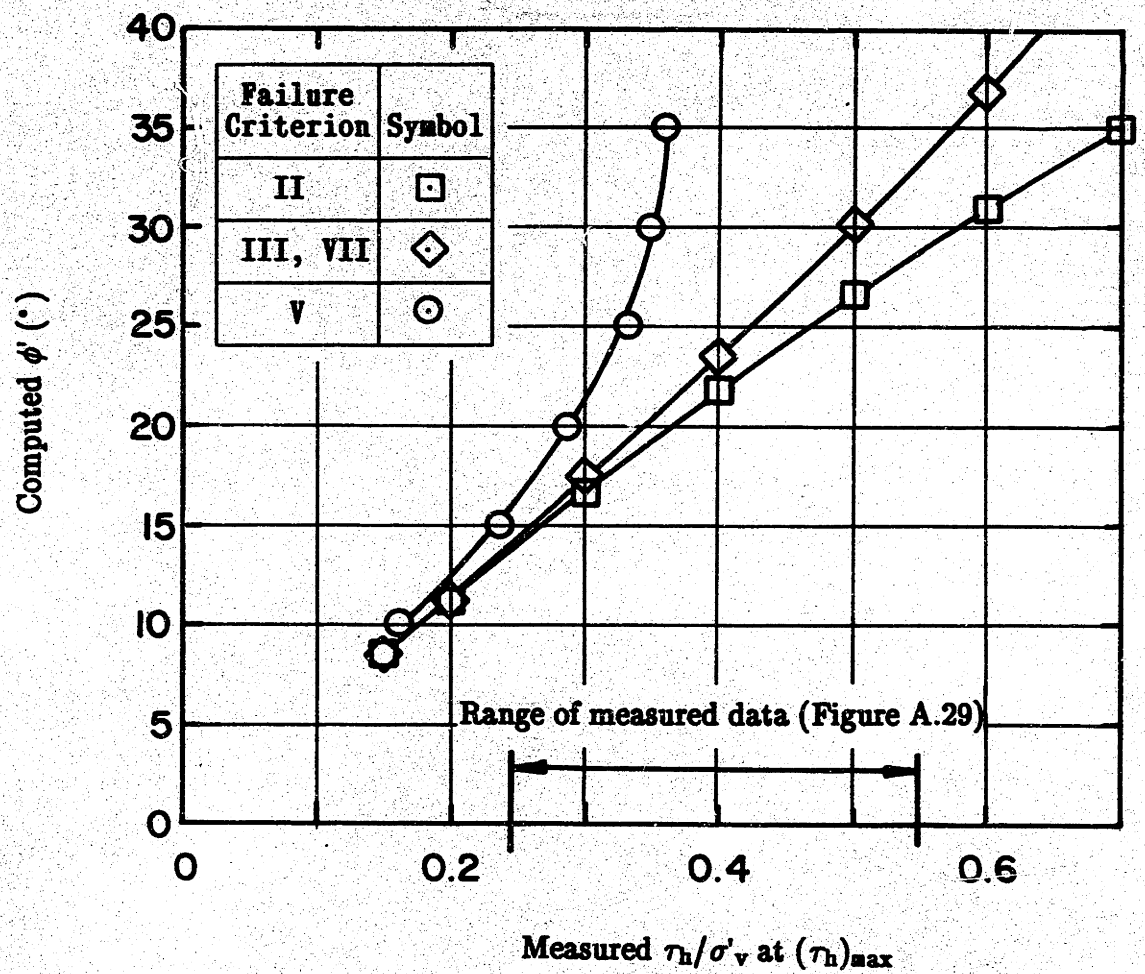

Figure A.35: Predicted ϕ' Versus Obliquity (τ_h/σ'_v) at Maximum Horizontal Shear Resistance for Direct Simple Shear Failure Criteria II, III, V and VII (see Table A.1 for reference).

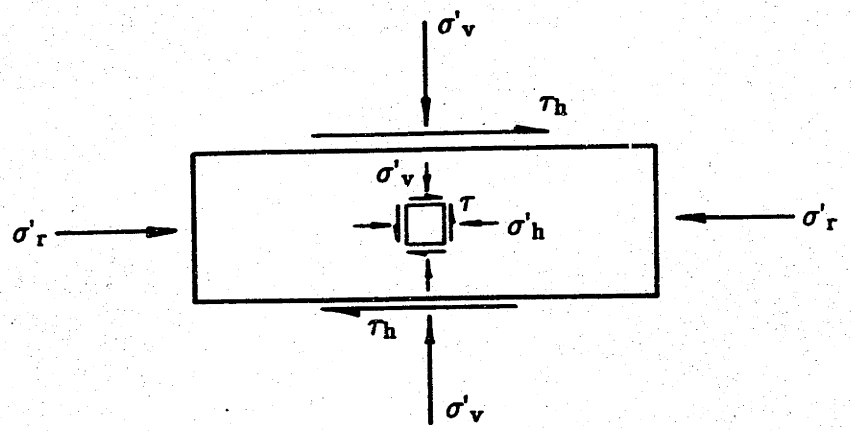

(a)

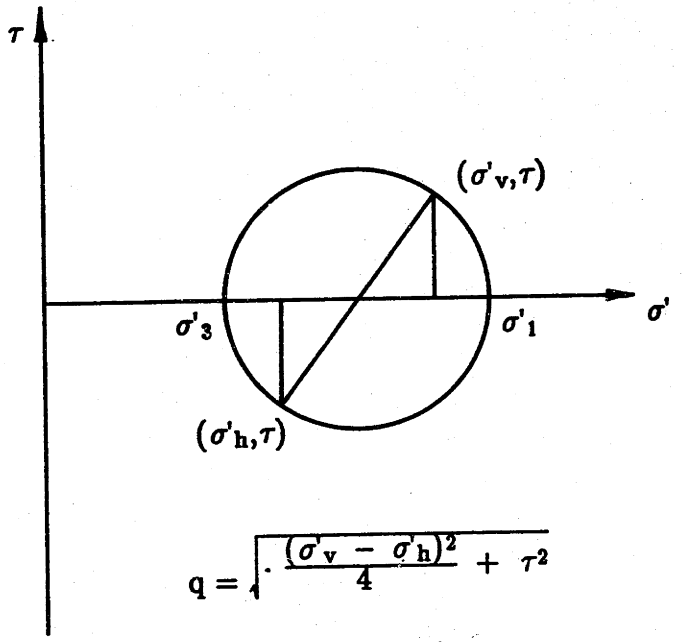

(b)

Figure A.36: Determination of State of Stress in the Geonor DSS Using Measurement of the Radial Stress σ'_r: (a) Measured Boundary Stresses and Stresses Assumed to be Acting on an Infinitesimal Element at the Center of the Sample; (b) Mohr's Circle of Stress for Infinitesimal Element at Center of Sample.

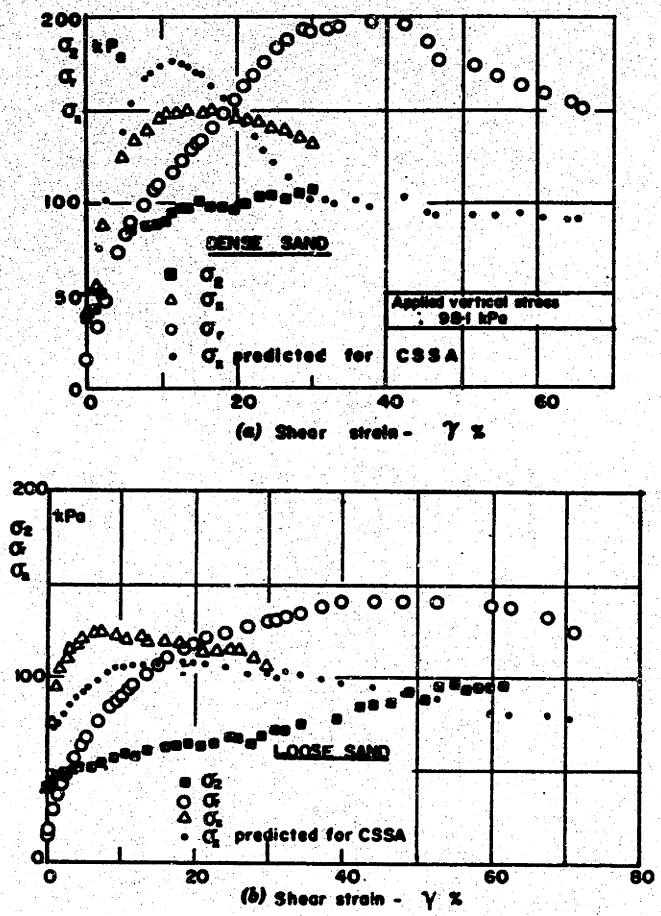

Figure A.37: Variation of Lateral Stresses During Monotonic CD Simple Shear Tests: (a) Dense Sand; (b) Loose Sand (from Budhu, 1985).

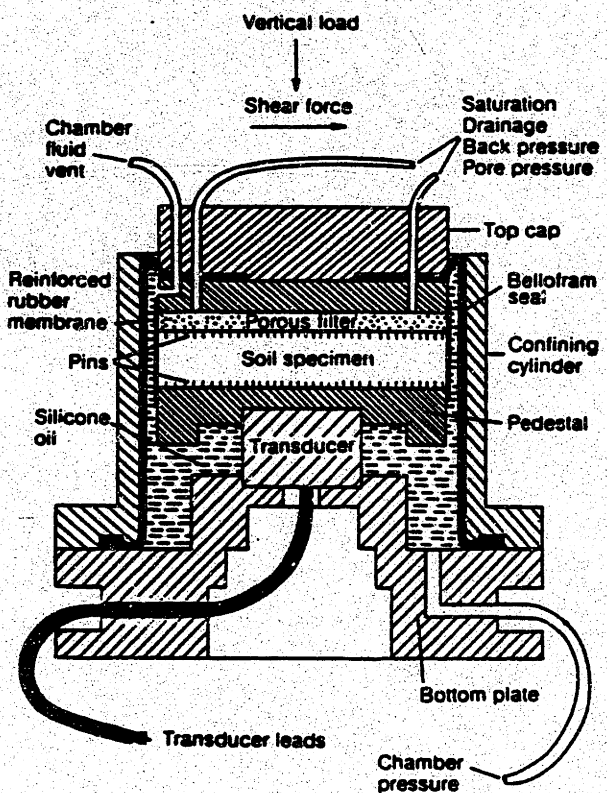

Figure A.38: Cross–Section of the NGI Direct Simple Shear Pressure Chamber (from Dyvik, et al., 1987).

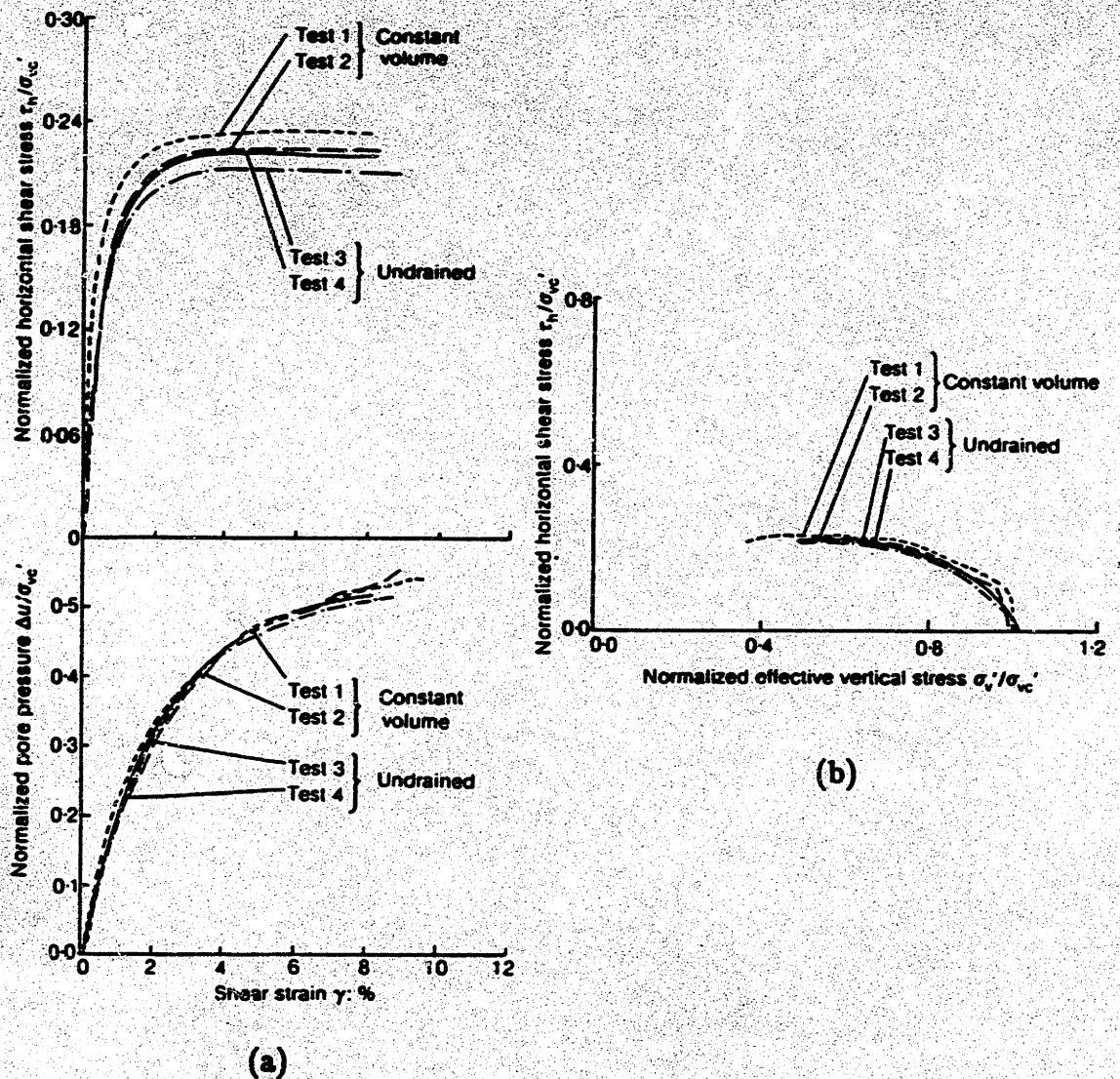

Figure A.39: Comparison of Constant Volume and Undrained Direct Simple Shear Test Results: (a) Normalized Horizontal Shear Stress and Normalized Pore Pressure Versus Shear Strain; (b) Normalized Effective Stress Path (from Dyvik, et al., 1987).

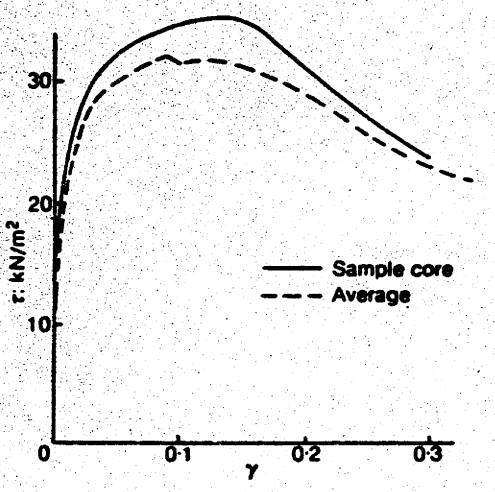

Figure A.40: CK_0U Shear Stress–Strain Curves for Kaolin Determined from the Cambridge CSSA (from Airey and Wood, 1987).

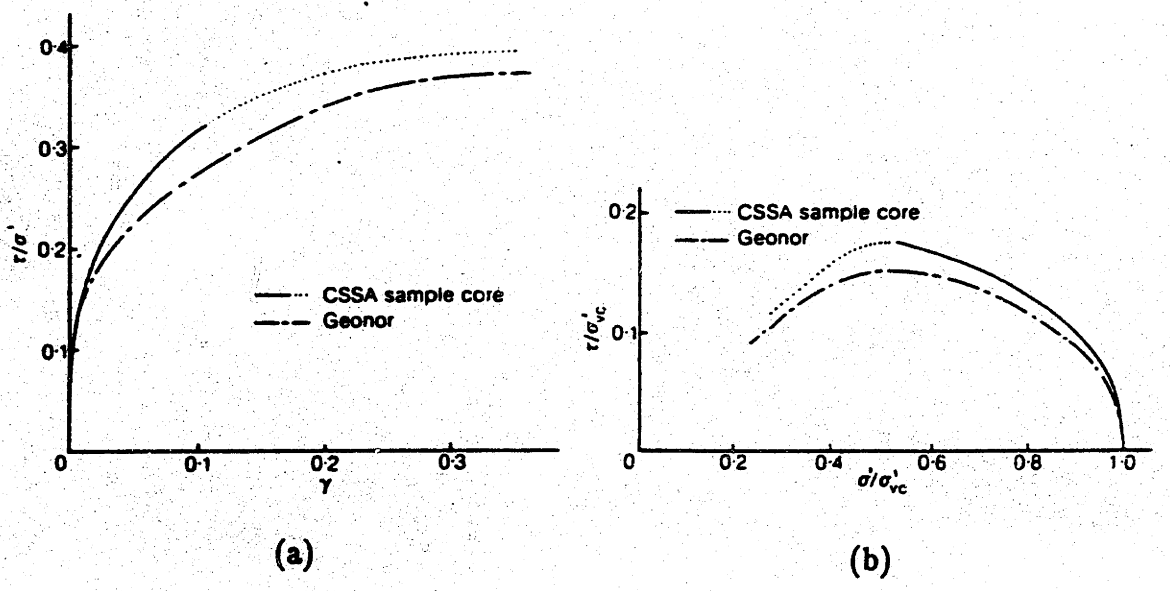

Figure A.41: CK_0U Constant Volume Simple Shear Tests on Kaolin: (a) Shear Stress–Strain Curves; (b) Normalized Effective Stress Paths (from Airey and Wood, 1987).

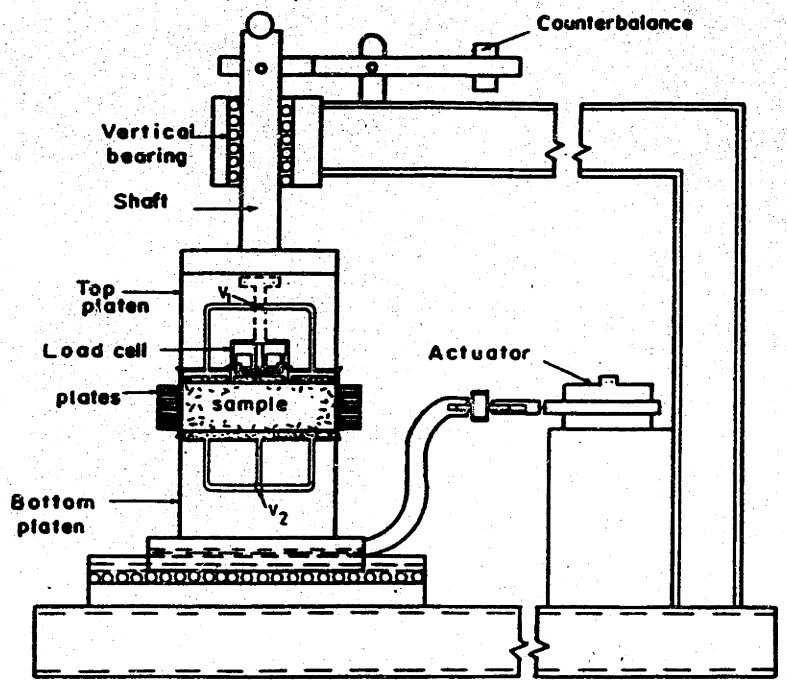

Figure A.42: Cross–Section of New Simple Shear Device Incorporating a Single Cambridge Type Load Cell (from Budhu, 1988).

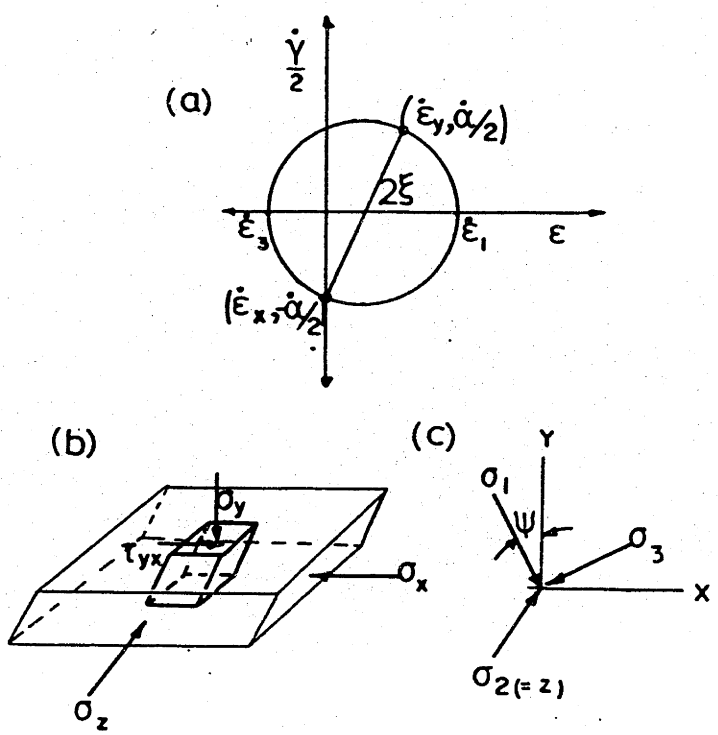

Figure A.43: Strains and Stresses from the New Simple Shear Device Described by Budhu (1988; Figure A.42): (a) Mohr's Circle of Strain Increment; (b) Measured Stresses; (c) Stresses Deduced for Specimen Core (from Budhu, 1988).

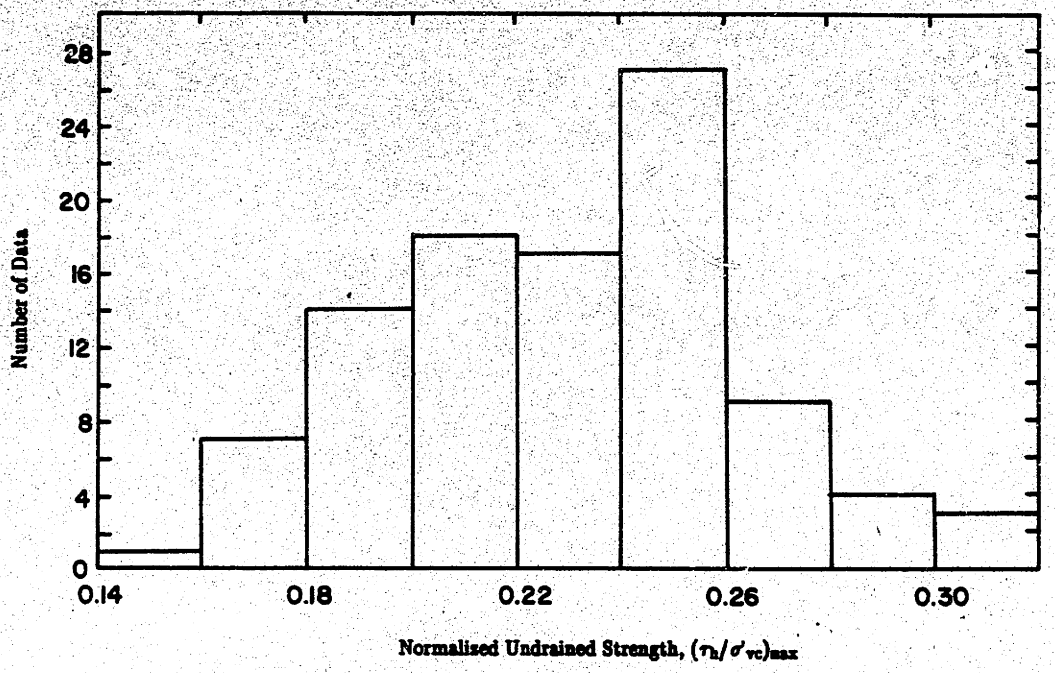

Figure A.44: Histogram of Normalized Undrained Strength for 100 Normally Consolidated CK_oUDSS Tests on a Variety of Cohesive Soils (Mean = 0.230 ± 0.033SD).

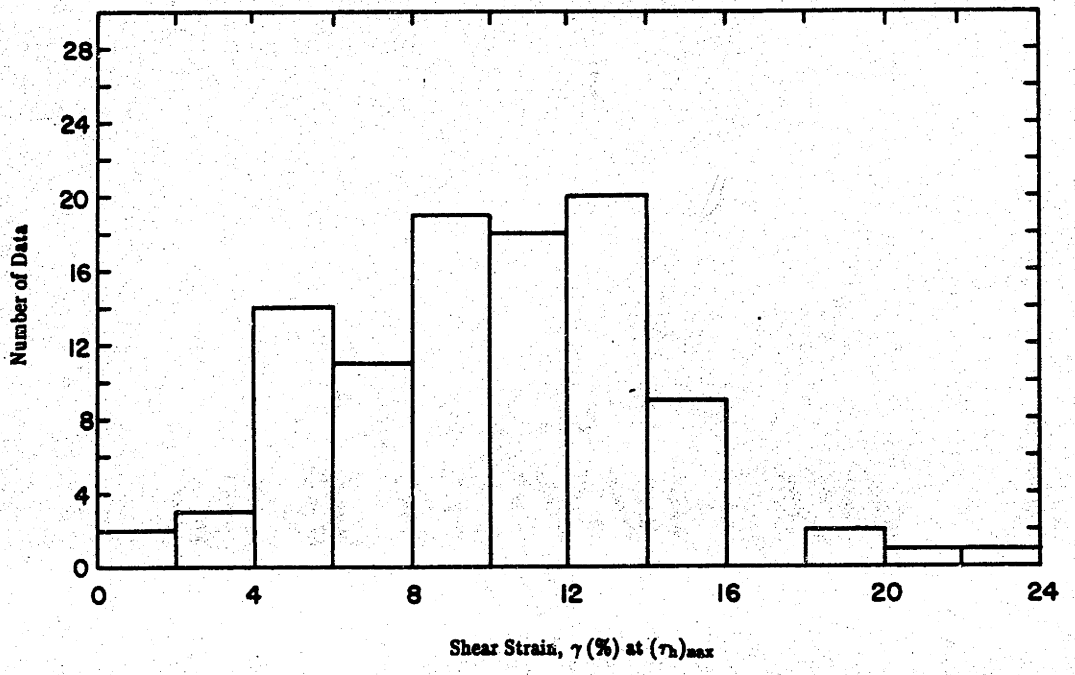

Figure A.45: Histogram of Shear Strain at $(\tau_h)_{max}$ for 100 Normally Consolidated CK_oUDSS Tests on a Variety of Cohesive Soils (Mean = 10.1% ± 4.0SD).

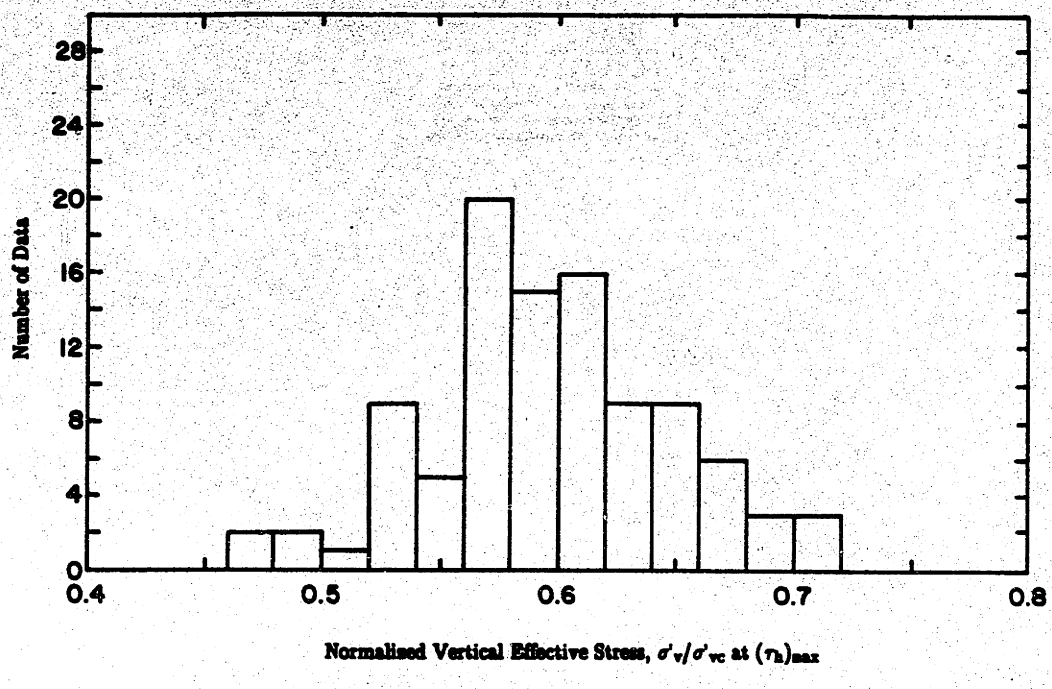

Figure A.46: Histogram of Normalized Vertical Effective Stress at $(\tau_h)_{max}$ for 100 Normally Consolidated CK_oUDSS Tests on a Variety of Cohesive Soils (Mean = 0.598 ± 0.051SD).

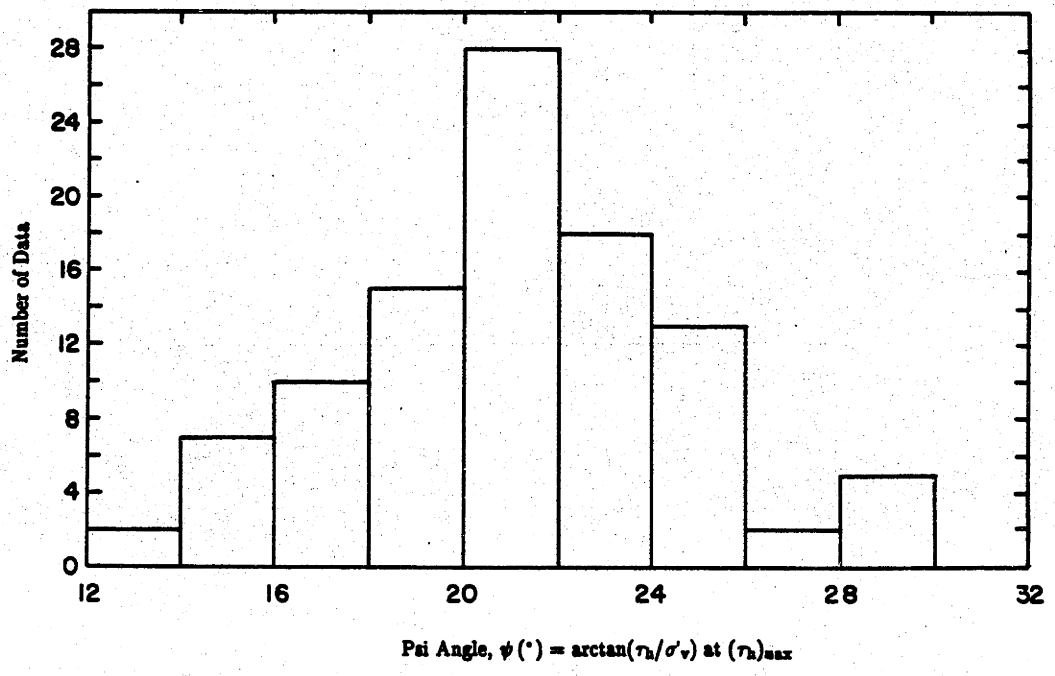

Figure A.47: Histogram of Psi Angle at $(\tau_h)_{max}$ for 100 Normally Consolidated CK_oUDSS Tests on a Variety of Cohesive Soils (Mean = 21.1° ± 3.3SD).

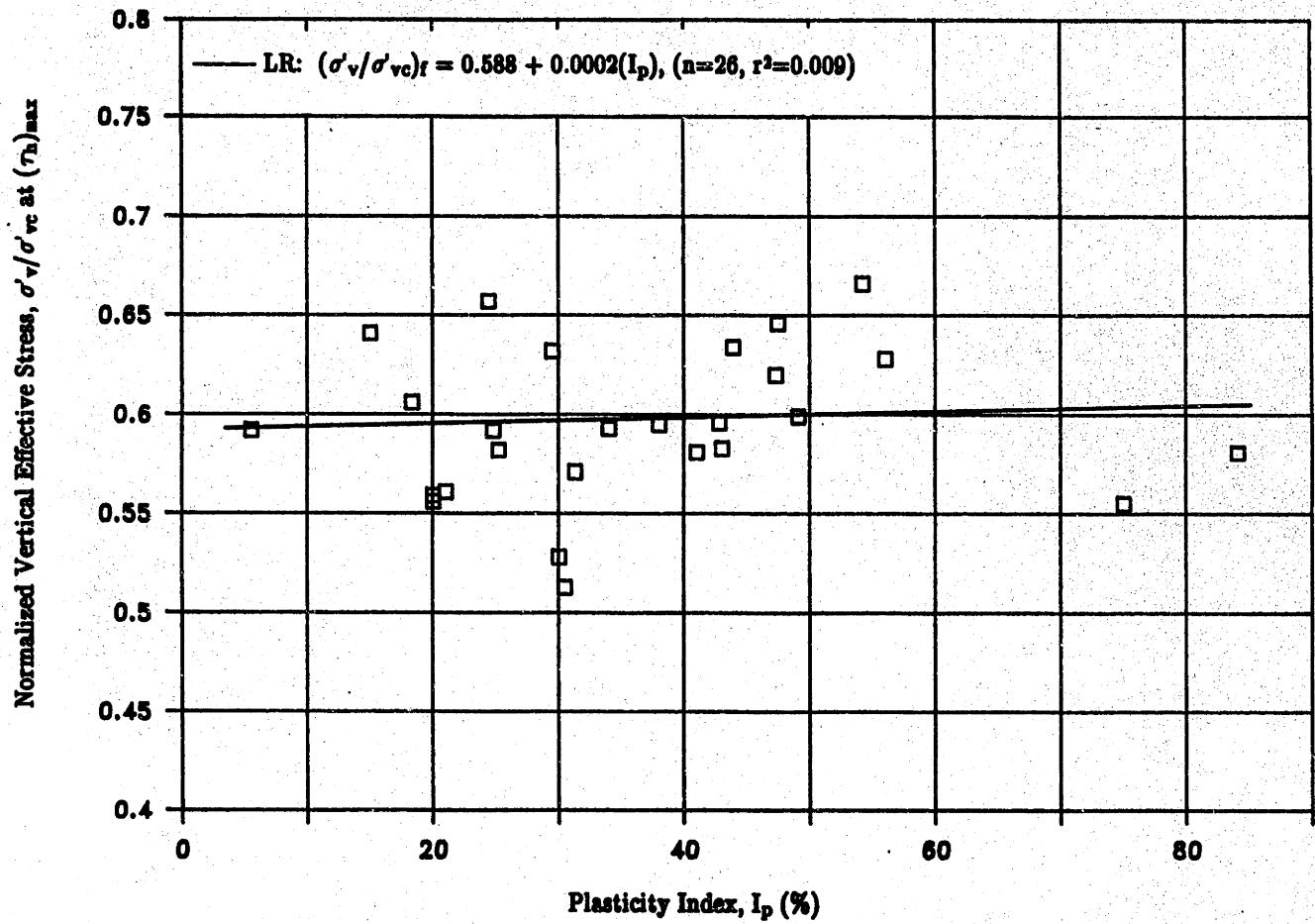

Figure A.48: Normalized Vertical Effective Stress at $(\tau_h)_{max}$ Versus Plasticity Index for Normally Consolidated CK_oUDSS Tests on Cohesive Soils (data from Table A.2).

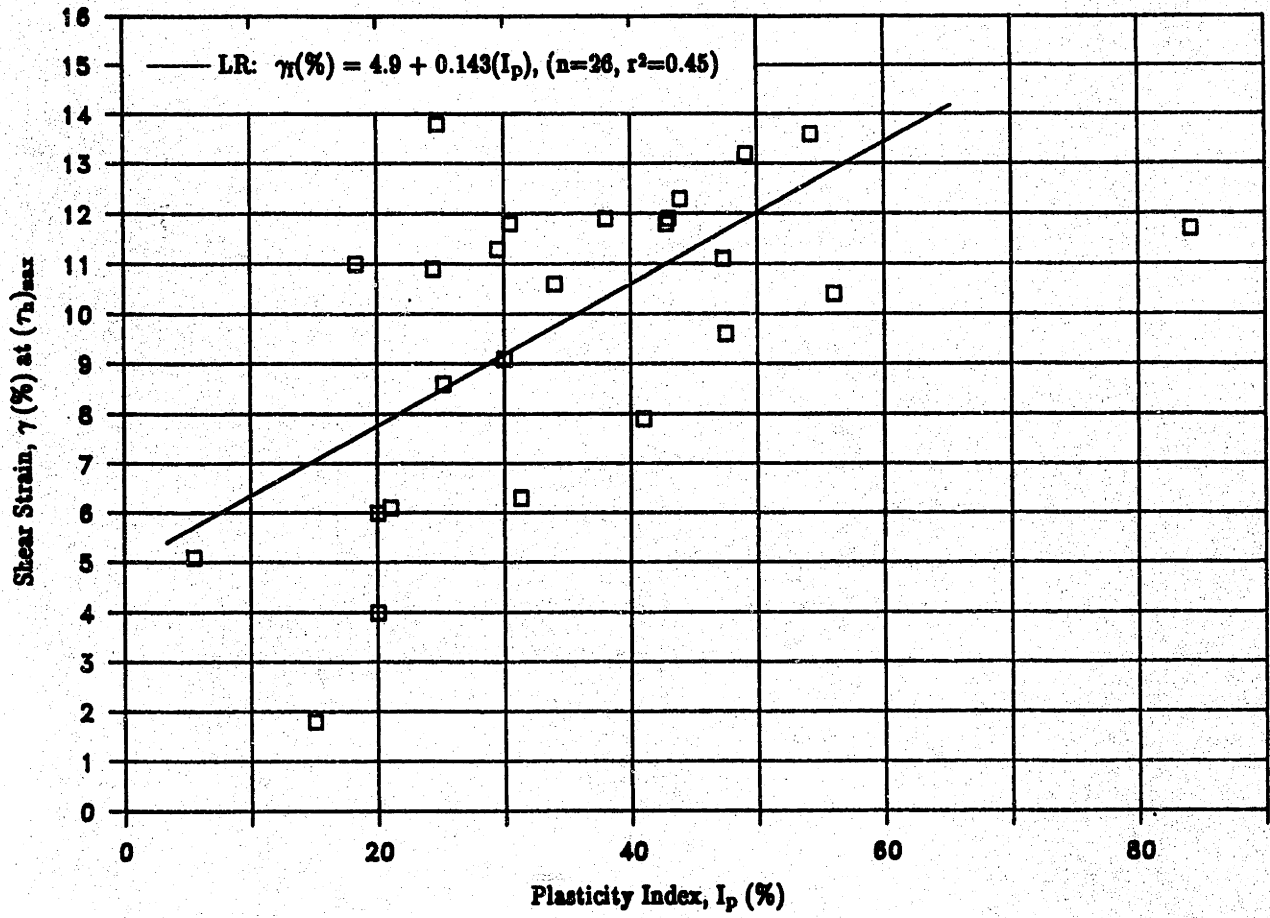

Figure A.49: Shear Strain at $(\tau_h)_{max}$ Versus Plasticity Index for Normally Consolidated CK_oUDSS Tests on Cohesive Soils (data from Table A.2).

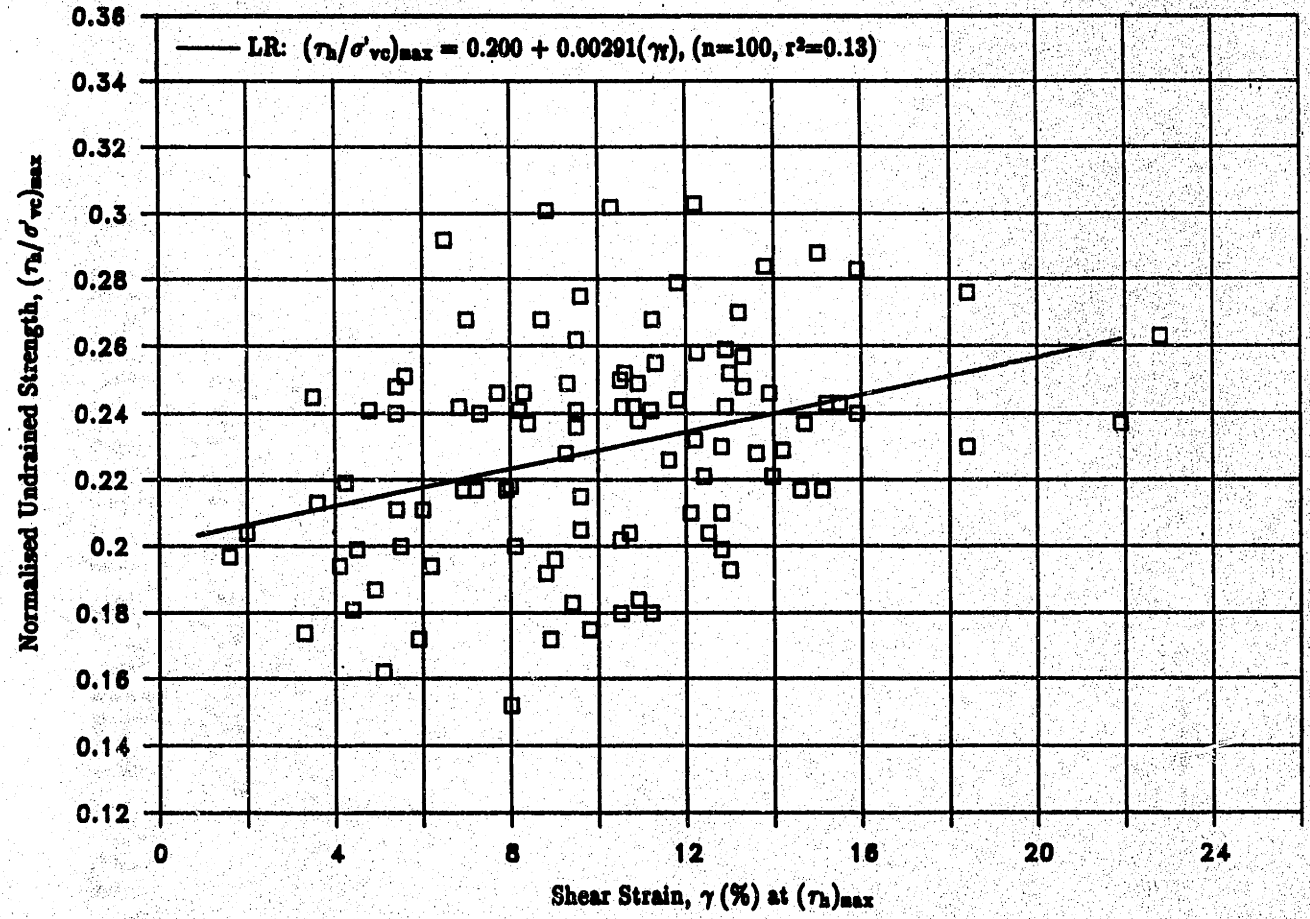

Figure A.50: Normalized Undrained Strength Versus Shear Strain at $(\tau_h)_{max}$ for Normally Consolidated CK_oUDSS Tests on Cohesive Soils (data from Table A.2).

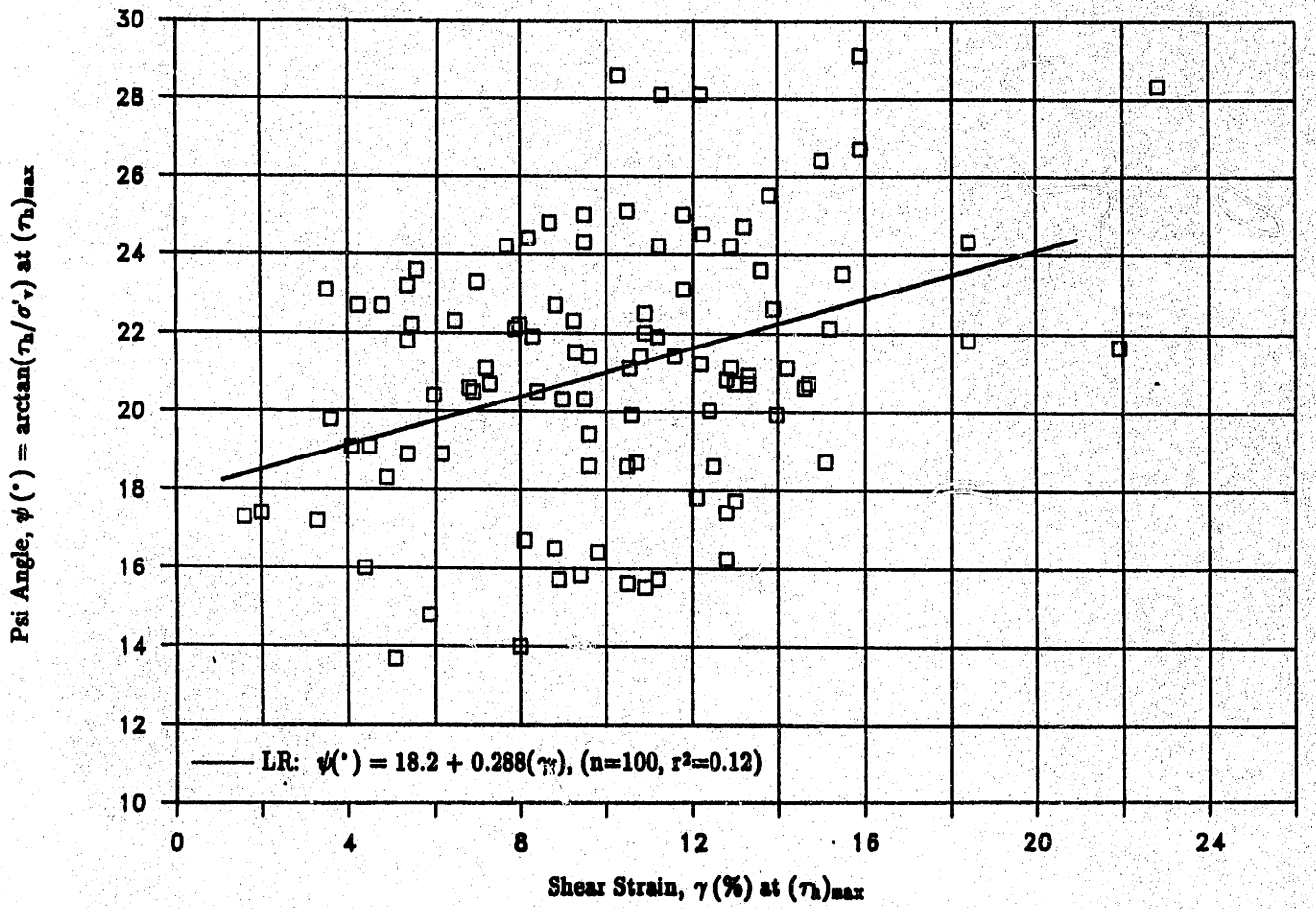

Figure A.51: Psi Angle Versus Shear Strain at $(\tau_h)_{max}$ for Normally Consolidated CK_oUDSS Tests on Cohesive Soils (data from Table A.2).

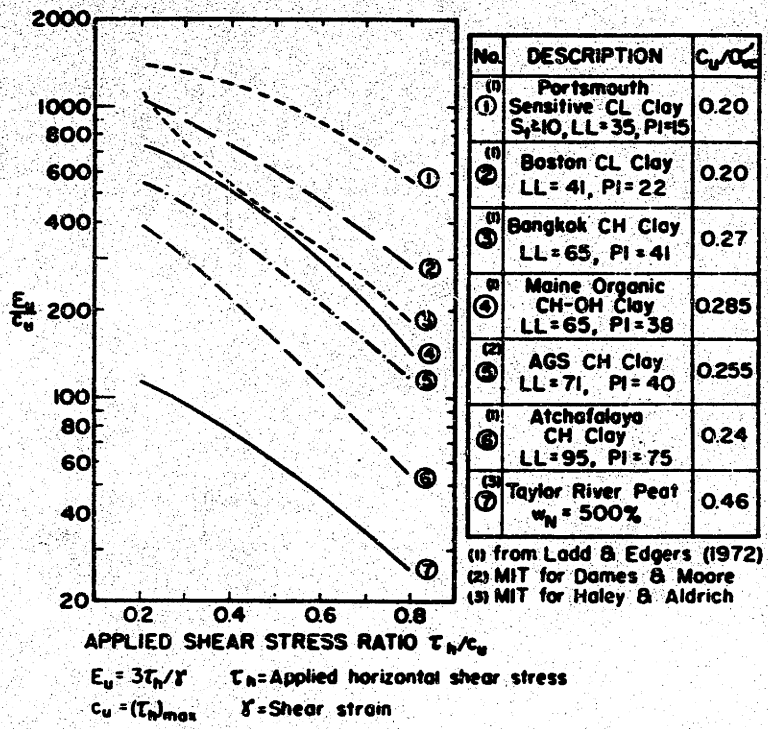

Figure A.52: Normalized Secant Young's Modulus Versus Applied Shear Stress Ratio from CK_0UDSS Tests on Seven Normally Consolidated Soils (from Ladd, et al., 1977).

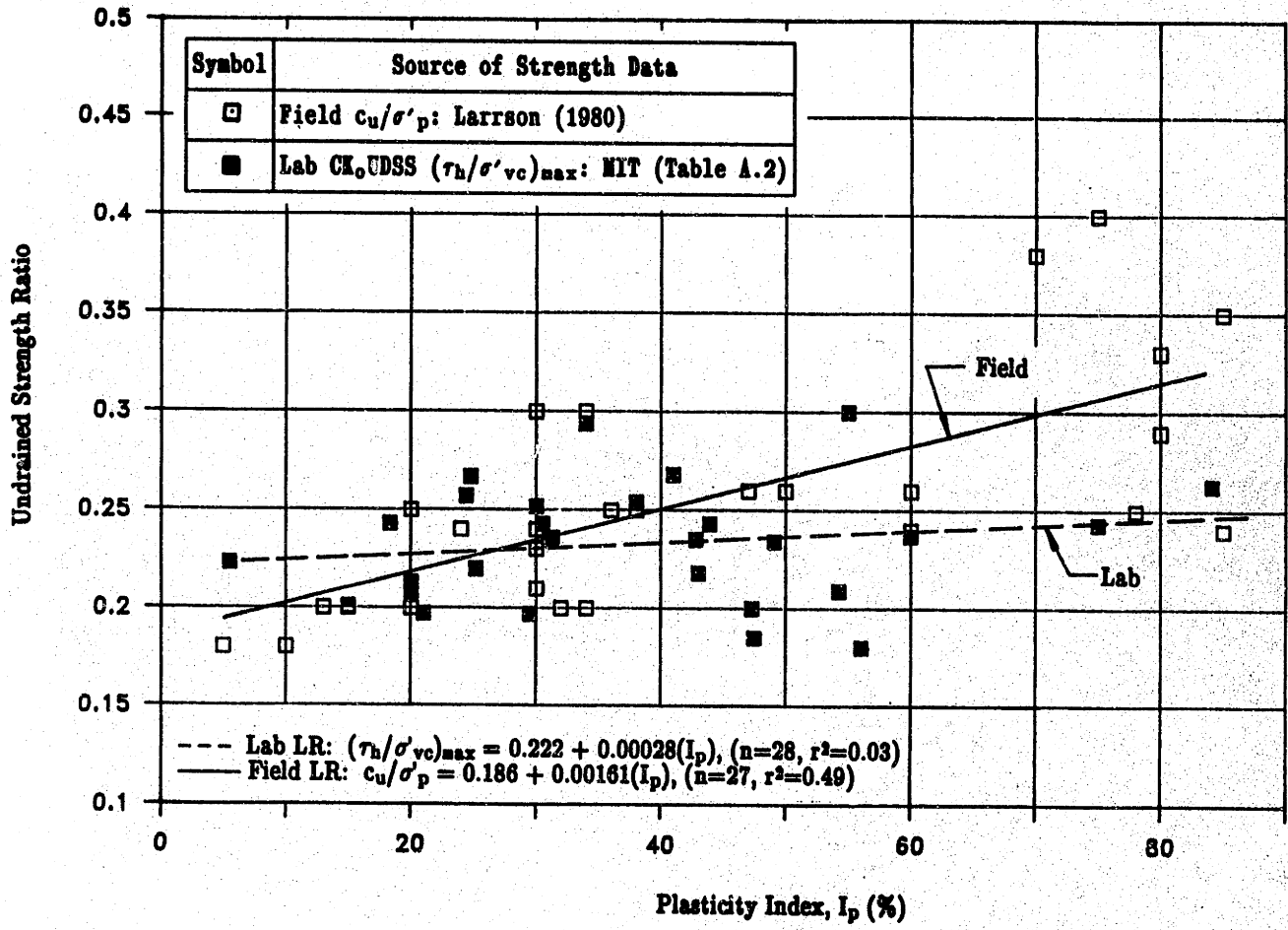

Figure A.53: Comparison of Field and Laboratory Normalized Undrained Shear Strengths for Non–Varved Cohesive Soils (OCR=1 for Laboratory CK_oUDSS Tests; after Ladd, 1981).

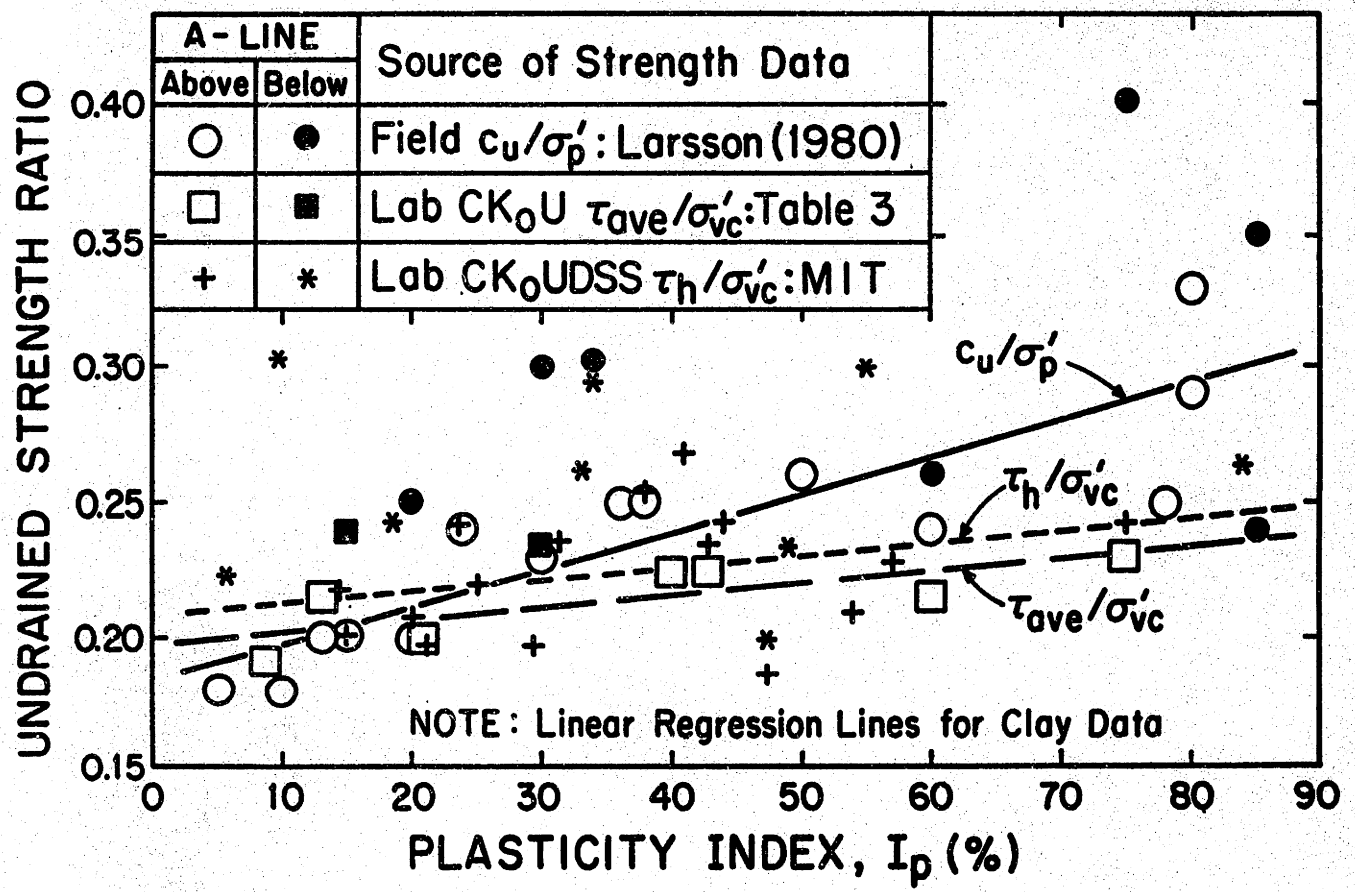

Figure A.54: Comparison of Field and Laboratory Undrained Strength Ratios for Non–Varved Sedimentary Soils (OCR=1 for Laboratory CK_oU Testing; from Ladd, 1988).

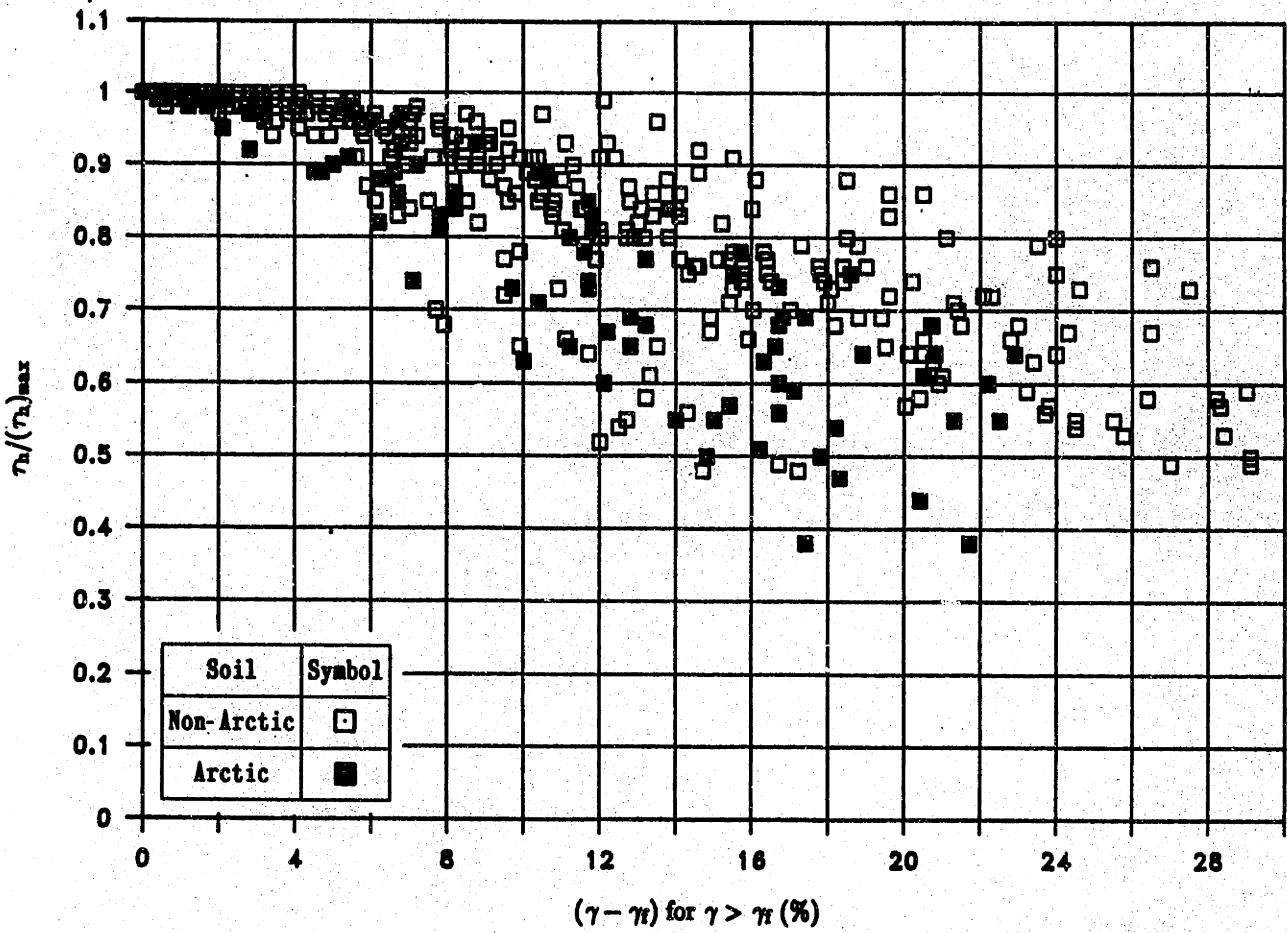

Figure A.55: $\tau_h/(\tau_h)_{max}$ Versus Shear Strain Beyond $(\tau_h)_{max}$ for Normally Consolidated CK_oUDSS Tests on a Variety of Cohesive Soils.

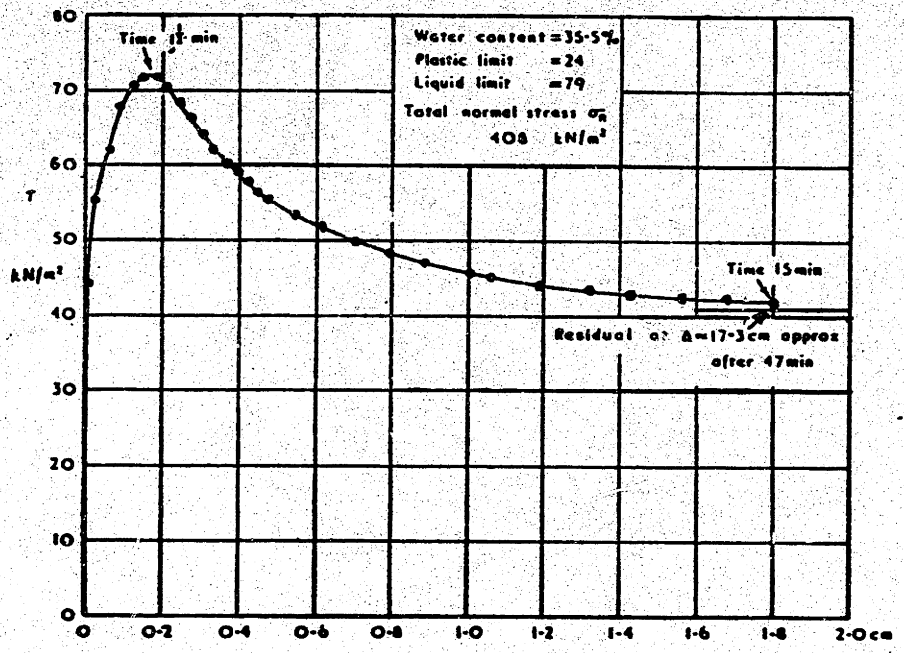

Figure A.56: Stress–Displacement Relationship for "Rapid Undrained" Ring Shear Test on Freshly Remolded Blue London Clay (from Bishop, 1971).

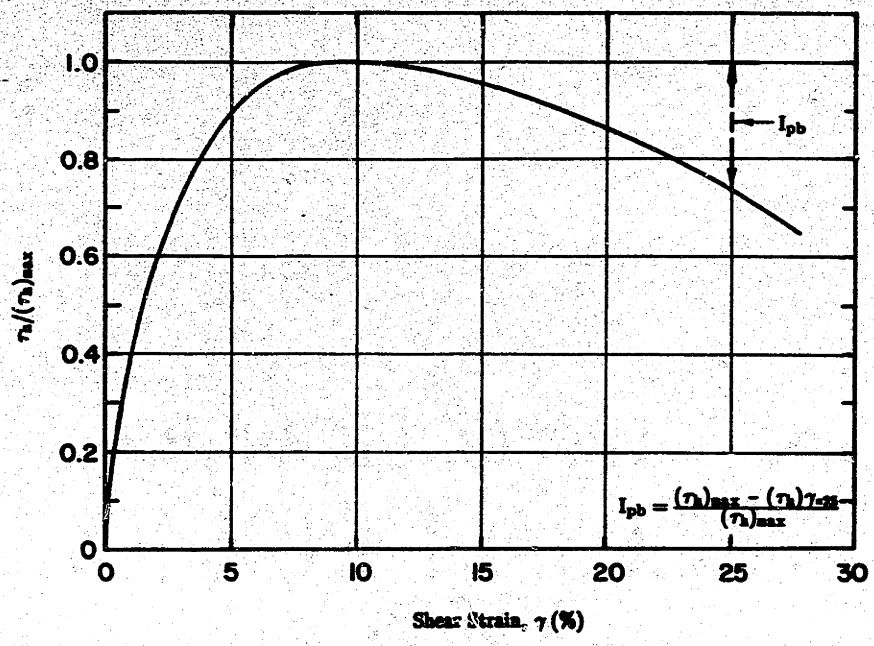

(a)

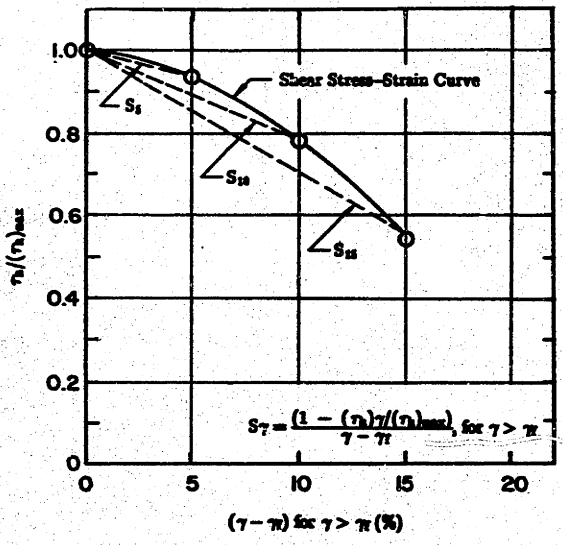

(b)

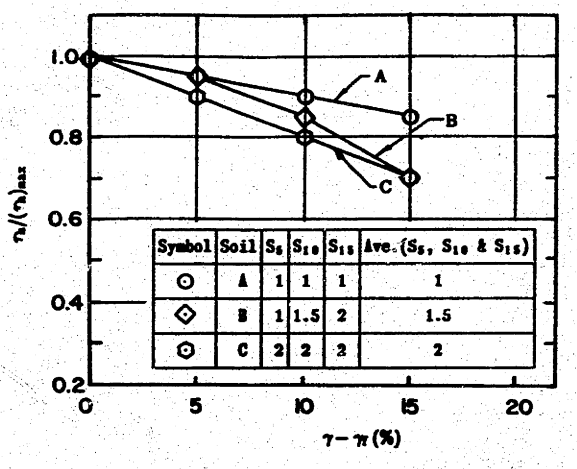

Symbol	Soil	S_5	S_{10}	S_{15}	Ave. (S_5, S_{10} & S_{15})
⊙	A	1	1	1	1
◇	B	1	1.5	2	1.5
⊙	C	2	2	2	2

(c)

Figure A.57: Strain Softening Indices: (a) Pseudo Brittleness Index, I_{pb}; (b) Shear Stress–Strain Slope, $S\gamma$; (c) Example of $S\gamma$ Values for Three Hypothetical Shear Stress–Strain Curves.

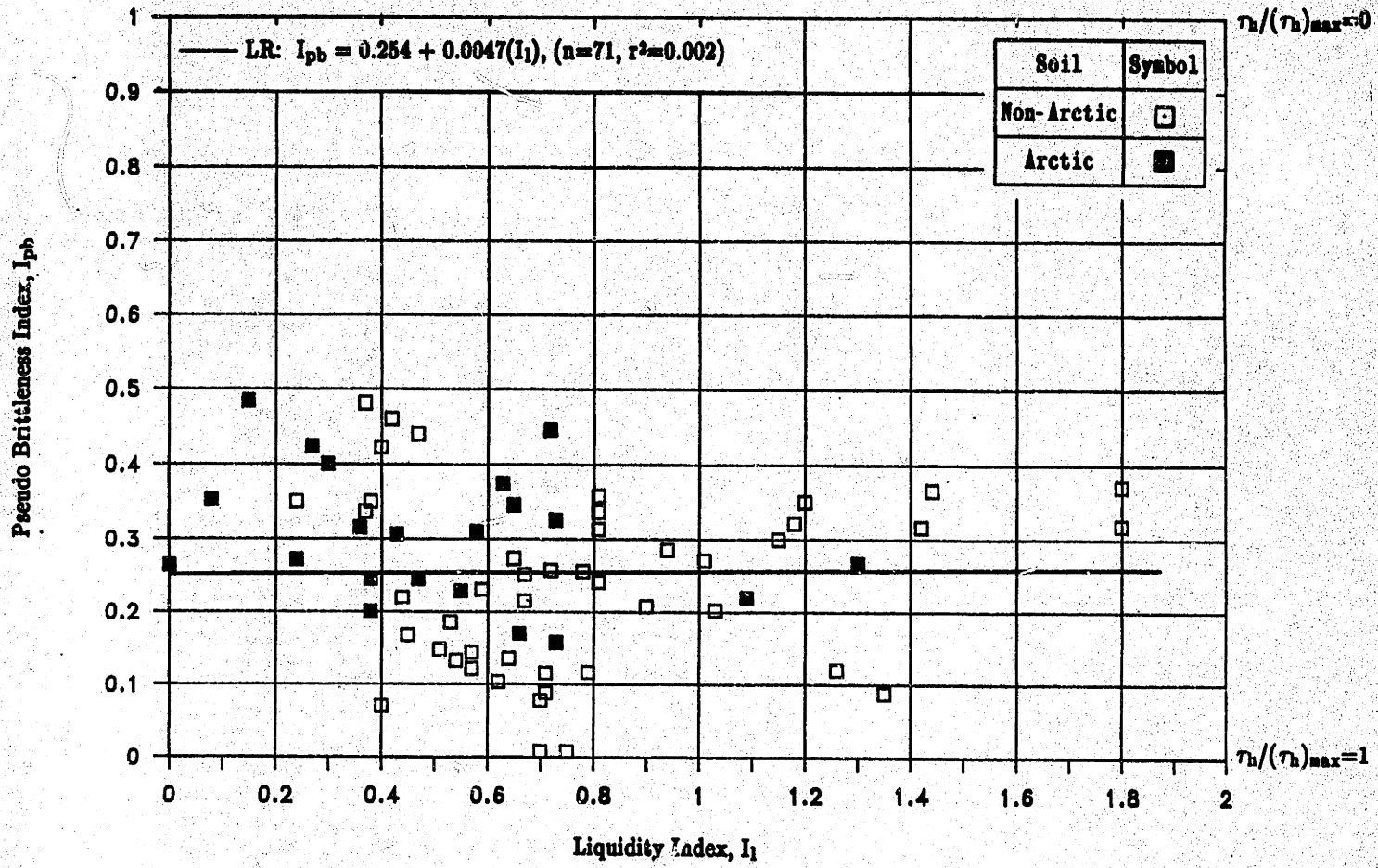

Figure A.58: Pseudo Brittleness Index Versus Liquidity Index for Normally Consolidated CK_oUDSS Tests on a Variety of Cohesive Soils.

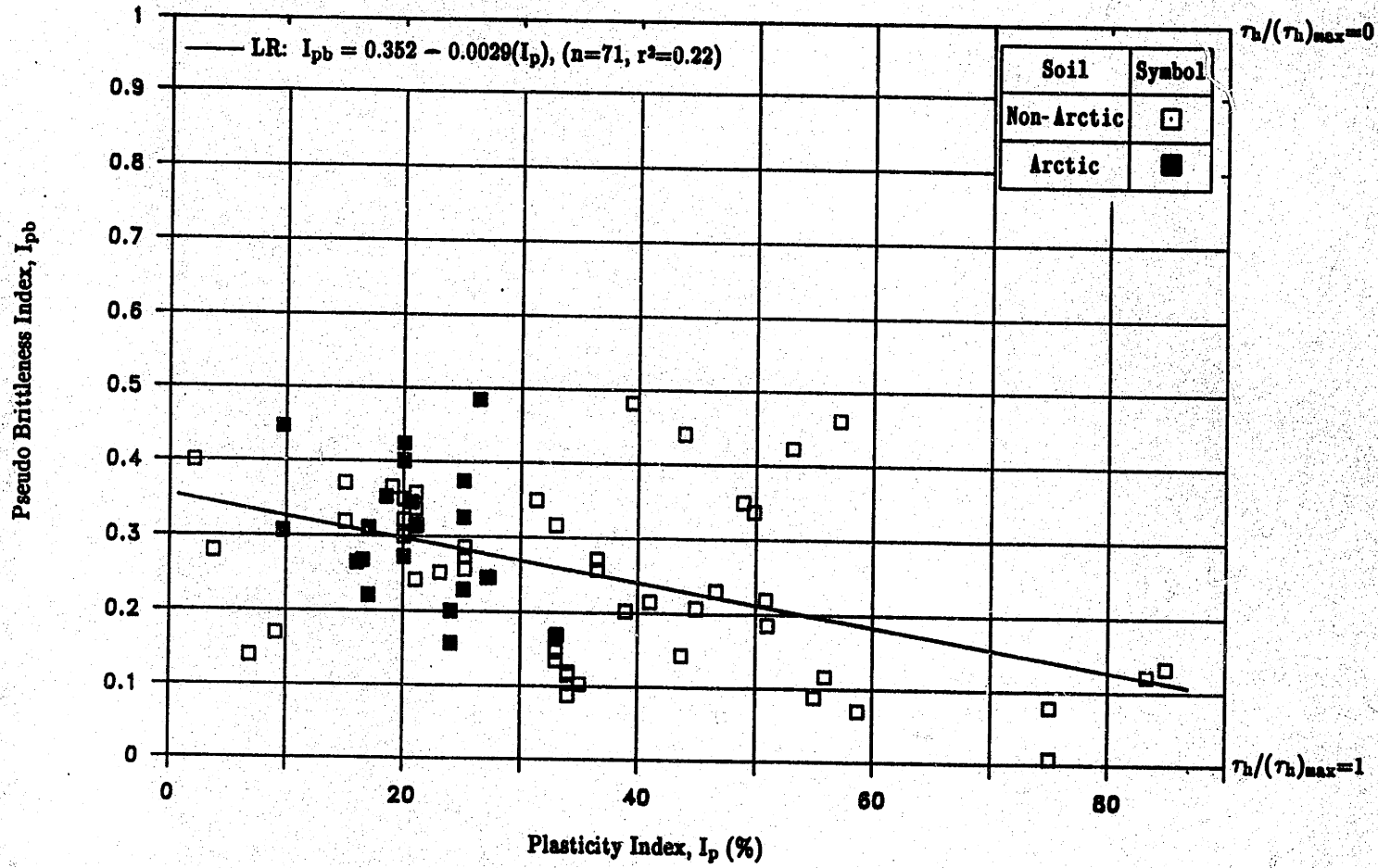

Figure A.59: Pseudo Brittleness Index Versus Plasticity Index for Normally Consolidated CK_oUDSS Tests on a Variety of Cohesive Soils.

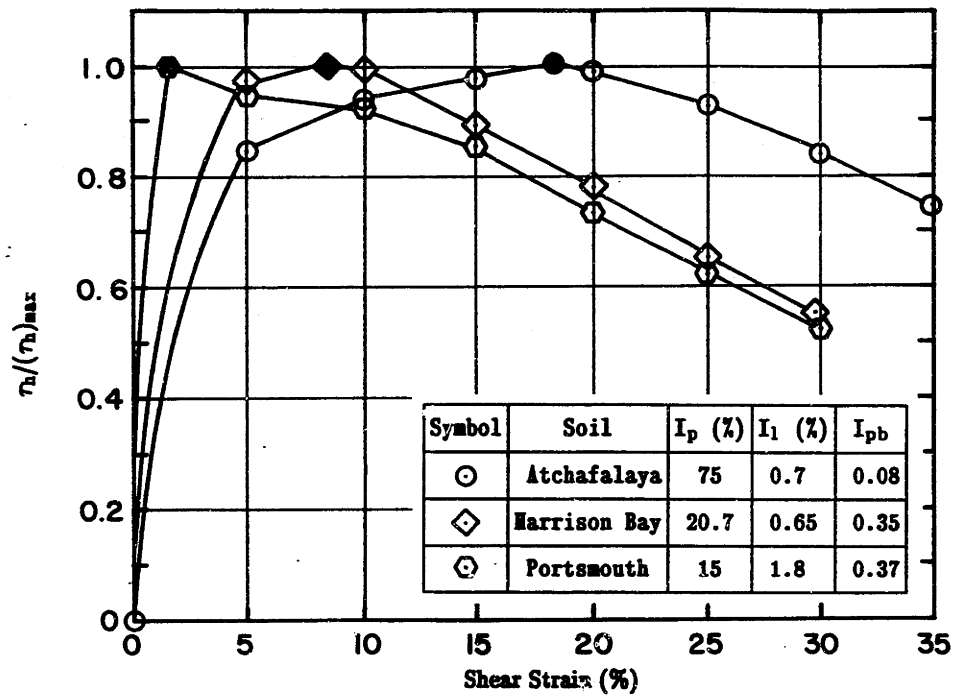

(a)

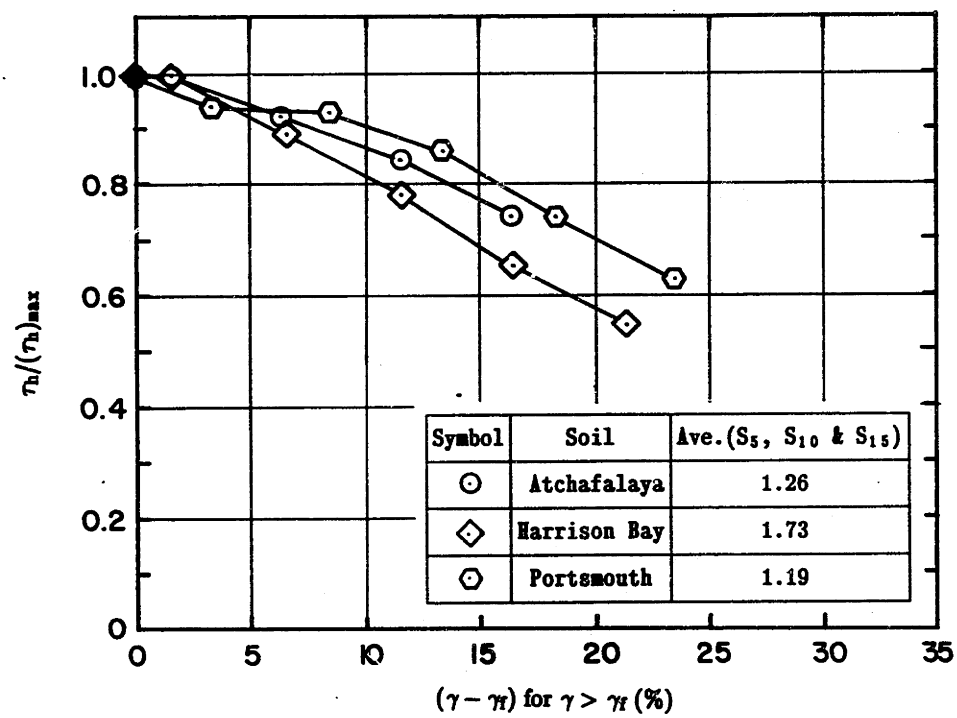

(b)

Figure A.60: Shear Stress–Strain Data from CK_oUDSS Tests on Three Normally Consolidated Cohesive Soils Illustrating Two Strain Softening Indices: (a) Pseudo Brittleness Index, I_{pb}; (b) Shear Stress–Strain Slope, $S\gamma$.

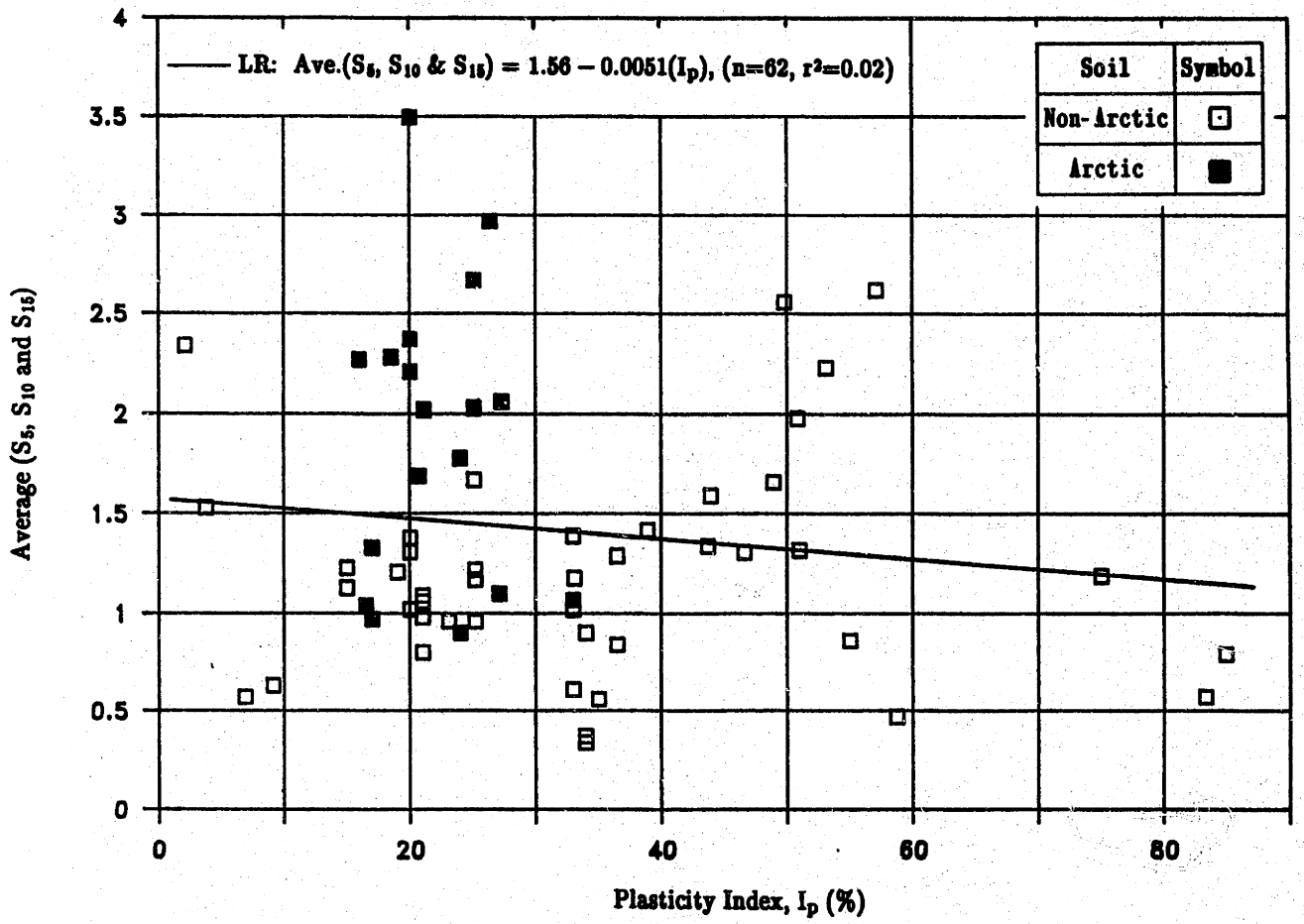

Figure A.61: Average of Strain Softening Slope Indices S_5, S_{10} and S_{15} Versus Plasticity Index for Normally Consolidated CK_oUDSS Tests on a Variety of Cohesive Soils.

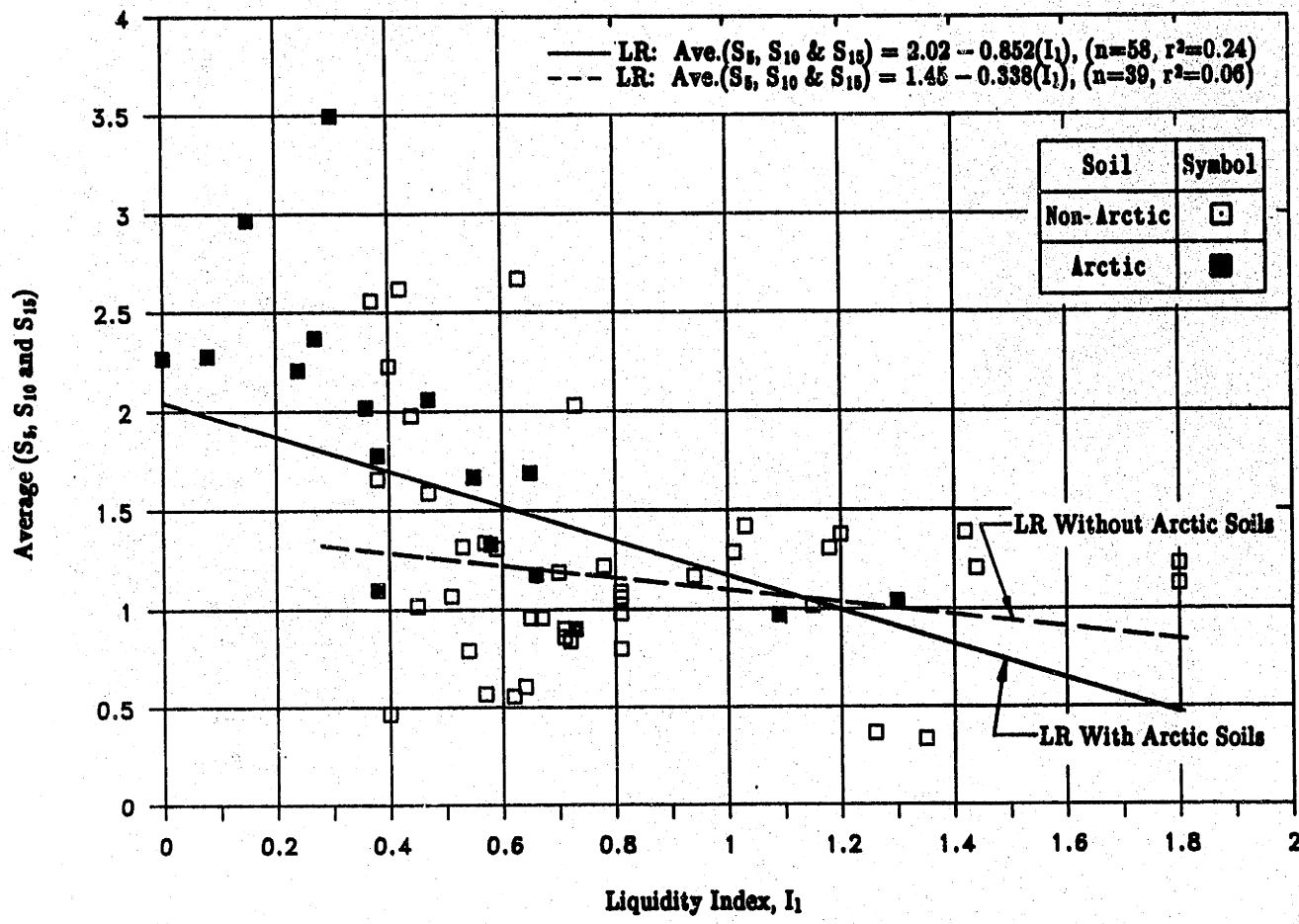

Figure A.62: Average of Strain Softening Slope Indices S_5, S_{10} and S_{15} Versus Liquidity Index for Normally Consolidated CK_oUDSS Tests on a Variety of Cohesive Soils.

APPENDIX B
DESCRIPTION OF THE MDSS

B.1 INTRODUCTION

The MDSS is capable of applying a vertical stress and two independent horizontal shear stresses to a circular sample (usually 2.3 cm by 6.68 cm diameter). For cohesive soils the vertical stress and the first horizontal shear stress are usually applied under drained conditions (i.e., anisotropic consolidation). The second horizontal shear stress is applied at a constant rate of strain and is usually used to test samples in undrained conditions. The first horizontal shear stress can be applied at an angle theta (θ) relative to the second horizontal shear stress ranging from 0 to 150 degrees in 30° increments.

The device has a set of coordinate axes for reference in describing directions of displacements and stresses as shown in Figure 3.1. All structural members and connections were designed with a maximum vertical force of 800 kg and a maximum horizontal shear force of 400 kg. Some of the structural components were designed against ultimate failure (with a factor of safety) while others were designed with maximum deformation as the controlling criterion.

The following sections describe the main features of the MDSS. The computer and data acquisition system are described in Chapter 3 and the software programs used for testing and data reduction are listed in Appendix C.

B.2 SAMPLE ENCLOSURE

Samples tested in the MDSS are contained between a top cap and a bottom pedestal (Figure B.1). The bottom pedestal is bolted to a circular cage which rests on the main bearing plates. These consist of two square hardened steel plates and a ball

bearing retainer. One plate is bolted to the base of the MDSS with the ball bearing retainer resting on top of it followed by the second steel plate.

The top cap is held stationary in the horizontal plane by bolting it to the stainless steel disc of the vertical stress loading system described in Section B.3. The top cap is free to displace in the vertical direction as is necessary during consolidation of a sample. It also provides a fixed top boundary condition for conducting simple shear tests on samples. The bottom bearing plates allow the sample to deform freely in any direction on a horizontal plane (i.e., the bottom of the sample is displaced in simple shear strain relative to the top of the sample). The bearing plate assembly is the heart of the MDSS allowing both conventional K_o consolidated and special anisotropically consolidated tests at various theta angles in the device. After consolidation the samples can be sheared at a constant rate of strain either drained or undrained.

The circular cage, which contains the sample and rests on the top bearing plate, is used to transfer the first and second shear stresses to the sample. The cage consists of a base plate and a circular wall. Several screws around the bottom perimeter of the cage thread through the cage wall and bear against a round track along the perimeter of the base plate. When the screws are loosened this allows the circular wall of the cage to rotate freely around the base plate. This is used to properly align the circular wall at the theta angle chosen for a particular test. Once the wall is properly aligned with the base by lining up the scribe mark inside the wall with the scribe mark for a selected theta angle on the base, the screws are tightened. Once this is done, the flexible connector which is used to transmit the first shear stress to the sample can be threaded into the circular cage at the correct theta angle. The second shear stress is transmitted to the sample during shear through a special applicator which pushes on the side of the cage along an axis through the mid–height of the

sample. This applicator and the first shear stress flexible connector are described in more detail in Section B.4

The bottom pedestal is made of brass and is fastened to the base of the circular cage using three screws. The pedestal has two drainage lines and contains a porous stone for drainage and transfer of shear stress to the sample. The top cap is also made of brass, has two drainage lines and a porous stone. The water is contained by a plexiglas container which sits on a large diameter brass disc that is bolted to the base of the bottom pedestal. The brass disc contains two o–rings to prevent leakage out of the water bath.

B.3 VERTICAL STRESS LOADING SYSTEM

Vertical stress is applied to a sample in the MDSS with a Bellofram diaphragm air cylinder (Figure B.2). The air cylinder has a piston which is threaded into a connector which attaches it to the top of a Data Instruments load cell. The bottom of the load cell is connected to a 1.25" diameter hardened steel Thompson shaft. This shaft is guided by a Thompson adjustable diameter twin pillow block (i.e., two Thompson linear ball bushings set in a pillow block). A stainless steel circular disc, which is used to connect the vertical loading system to the top cap of the sample, is threaded to the bottom of the shaft. The circular disc is the same diameter as the top cap (area = 35 cm^2) and is connected to it with four screws.

The vertical stress reaction is provided by the superstructure of the device. It consists of two steel vertical uprights, a steel cross brace which supports the twin pillow block and a 4"x4"x$^1/_8$" steel channel which supports the Bellofram air cylinder. The vertical uprights are bolted to the base of the MDSS which is a 41"x12"x2" aluminum block.

The connectors used to attach the load cell to the vertical loading system are specially designed to allow some tension force across the load cell and also to work as

moment breaks for compressive forces. The tension force acts on the load cell when there is no sample in the device and the Thompson shaft and the circular stainless steel disc hang freely on the bottom of the load cell. The moment break is necessary for correctly measuring compressive forces if the loading system is slightly misaligned. The moment break is provided by a 0.75" diameter steel ball which is placed above and below the load cell. The whole load system is kept in place by two small brass rods that pass through the middle of the steel ball and the two threaded screws that serve as a cradle for the steel ball (see Figure B.3). The brass rod has a spring on each end and a threaded end piece which keeps the springs in place. When a tensile force acts on the vertical loading system the force is taken by the two springs thus holding the system intact and in compression until it is subjected to a compressive force.

Air pressure in the Bellofram cylinder is controlled by a Fairchild voltage to pneumatic transducer/regulator. The Fairchild transducer supplies air pressure directly proportional to a voltage applied to the transducer. The transducer proportionally converts a 1 to 9 volt DC input voltage to a 3 to 15 psi output pressure. The output pressure can be multiplied or reduced and also have either a positive or negative bias adjustment to obtain the final output pressure applied to the air cylinder. The final output pressure can range from 0 to 150 psi. All air pressure used by the MDSS is supplied by the central air compressor in MIT's Geotechnical Laboratory.

B.4 HORIZONTAL SHEAR STRESS LOADING SYSTEMS

Two independent horizontal shear stresses can be applied to a specimen in the MDSS. The first shear stress is stress–controlled while the second shear stress is applied at a constant rate of strain. For cohesive soils the first shear stress is usually applied under drained conditions (i.e., during consolidation) and the second shear stress is applied during undrained shear. The second shear stress always acts along the X axis while the first shear stress is applied at an angle theta relative to the X axis

(Figure 3.1). The loading systems used to apply these shear stresses are described in the following two sections and shown in Figure B.4.

B.4.1 Stress Controlled Loading System

The first horizontal shear stress is applied to a specimen using a pneumatic cylinder. The cylinder is constructed of aluminum and plexiglas and uses a Bellofram diaphragm (Figure B.5). The cylinder piston shaft is guided by a Thompson linear bearing bushing and is connected to a loading bracket. At the other end of the bracket a flexible connector is used to transfer the shear force from the bracket to the circular cage containing the sample. The connector is made of $^1/_{16}$" diameter aircraft cable with a screw fastened at each end. One end is threaded into the circular cage and the other is connected to the loading bracket.

The pneumatic cylinder is supported by a circular aluminum frame which is mounted on a track consisting of three Thompson pillow blocks. The pillow blocks slide along 0.5" diameter Thompson shafts which are mounted on the aluminum base of the MDSS. The frame is connected to the ball spline shaft of the constant rate of strain loading system which is described in the following section. The connection is made with a 0.5" diameter Thompson shaft which is threaded into the circular frame at one end and attached to the ball spline shaft by an aluminum locking bracket at the other end. The 0.5" diameter shaft is guided by a Thompson pillow block. This system provides the reaction support for the first shear stress and also allows the frame to displace along the X direction during application of the second shear stress. Hence, during application of the second shear stress the frame will displace the same amount as the bottom of the sample. Thus the orientation of the first shear stress relative to the X axis (i.e., theta) remains approximately constant during undrained shear.

The pneumatic cylinder can be positioned at different locations on the circular frame so that the first shear stress can be applied at various theta angles relative to the

X axis. Tests can be run at theta equal to 0, 30, 60, 90, 120 and 150 degrees. The 90 degree test uses a separate loading bracket which has two flexible connectors to transfer the first shear stress to the circular cage. This special bracket is required to get around the vertical upright of the MDSS superstructure (one connector is positioned on each side of the vertical upright).

Air pressure in the pneumatic cylinder is controlled using the same type of Fairchild voltage to pneumatic transducer/regulator as described for the vertical loading system. The pressure in the cylinder is monitored by a Data Instruments 50 psi pressure transducer. The air cylinder is calibrated so that the force it produces is known as a function of the air pressure reading on the transducer.

B.4.2 Constant Rate of Strain Loading System

The constant rate of strain loading system is powered by an Insco electric motor which has an output speed of 30 rpm. The motor output is geared by an Insco multi–speed changer (ratio 1:1 to 1:60) and an Insco step function reducer (ratios 1:1 to 1:1000). The torque output is increased by a Boston Gear worm gear. The worm gear's rotary motion is converted to a horizontal thrust by a Beaver Precision ball–screw and ball–spline. This is the original gear drive system used by Lucks (1970) for MIT's direct shear box device.

The horizontal force is measured by a Data Instruments load cell that is connected to the ball spline shaft using the same type of assembly as the vertical load system (Figure B.3). The load cell assembly is connected to a 0.5" diameter Thompson steel shaft which is guided by a pillow block consisting of two Thompson linear ball bushing bearings. A special load applicator is connected to the end of the Thompson shaft which transfers the horizontal force to the circular cage containing the sample. The load applicator applies the horizontal force for τ_2 while allowing the circular cage to move in any horizontal direction in a region forward of a perpendicular

line to the applicator. This allows the sample to displace freely during undrained shear. This freedom of movement is required because samples anisotropically consolidated at some angle theta (during first shear) will not strain along a path which is parallel to the direction of application of the undrained second shear stress (i.e., the X axis). The strain path would be parallel to the direction of the applied second shear stress if the sample is an elastic material.

B.5 INSTRUMENTATION

The MDSS uses load cells, displacement transducers and a pressure transducer to measure forces and displacements experienced by a sample. All of the transducers are connected to an instrumentation box which provides an excitation voltage to the transducers, feeds the response lines to the data acquisition system and also allows direct visual measurements of each transducer to be made by plugging a voltage meter into the box. The type and location of the transducers used to measure forces and displacements are described in the following two sections.

B.5.1 Forces

Three independent stresses can be applied to samples in the MDSS. The vertical stress is measured using a 1000 lbs Data Instruments load cell. The second shear stress, which is usually applied to produce undrained shear, is measured with a 500 lbs Data Instruments load cell. The first horizontal shear stress, which is usually applied with drainage (consolidation), is measured with a 50 psi Data Instruments pressure transducer. The air cylinder, used for the first shear stress, is calibrated so that the force it produces is known as a function of the air pressure reading on the transducer.

B.5.2 Displacements

In the MDSS the sample can deform vertically and in any horizontal direction.

The horizontal deformation takes place with the bottom of the sample moving relative to its top (i.e., the top cap is held fixed against horizontal displacement). To properly calculate sample strains, three displacement measurements are made: vertical, horizontal in the X direction, and horizontal in the Y direction. With these measurements the vertical strain ϵ_v and the resultant total shear strain γ_t can be computed.

Vertical displacements are measured using two Collins displacement transducers (± 0.125") that are attached at opposite sides of the top cap (Figure 3.3). Two transducers are required because, upon application of a horizontal shear stress to the sample, the top cap will undergo some rotation. Therefore, two measurements and a linear interpolation are made to get the measured deformation of the sample center. The transducers are held in place with two plexiglas retainers that are fastened to the top cap.

X and Y displacements of the sample bottom relative to its top are made with two Collins displacement transducers (± 0.125" for X and ± 0.375" for Y). These measurements are made relative to two perpendicular flats on the top cap (Figure 3.3). The transducers are held in place with two plexiglas retainers that are fastened to the brass disc which also holds the water bath.

One additional Collins displacement transducer (± 0.125") is used for the constant height servo control system. Its location and operation are described in more detail in Appendix D.

B.6 ALIGNMENT

The key to making correct measurements for the X and Y displacements during a test is to properly align the sample in the MDSS. The base plate of the main bearing plates is bolted to the base of the device and contains two 0.375" diameter holes at diametrically opposite ends of the plate. This plate is properly oriented with

the X–Y axis of the device. The ball bearing retainer plate, top bearing plate, base of the circular cage and the large diameter brass disc all have two 0.375" diameter alignment holes drilled through them. Hence, all of the assembly can be properly oriented by passing a 0.375" diameter rod through both of the alignment holes in each piece and down to the bottom bearing plate.

The bottom pedestal is aligned relative to the base of the circular cage by two 0.125" diameter pins. The top cap is aligned relative to the X and Y axis using the Geonor trimming jig. The jig has several scribe marks on it so that when the membrane is being placed around the sample the top cap can be placed in its proper orientation relative to the bottom pedestal. Once the membrane is in place it holds the top cap in the correct orientation relative to the bottom pedestal while the sample enclosure is placed in the device. This alignment procedure is particularly important since the top cap contains the two perpendicular flats that are used by the X and Y displacement transducers (Figure 3.3a).

B.7 CORRECTIONS

Two types of corrections are made to the reduced data of an MDSS test. During consolidation the measured vertical strains are corrected for the apparatus compressibility. The undrained shear resistance data are corrected for the frictional resistance of the horizontal loading system and the resistance of the membrane.

B.7.1 Apparatus Compressibility

The compressibility of the vertical loading system is measured using a steel disc in place of a soil sample. The system is subjected to several load–unload cycles to get repeatable measurements for the load versus deflection relation of the device (Figure D.1). Most of the apparatus compressibility is due to the compliance of the porous stones and in fact, if they are warped, their compressibility can be large.

Hence, in the MDSS the porous stones are routinely checked to ensure that they are as flat as possible.

Using the load versus deflection relationship for the device all vertical consolidation displacements are corrected automatically by the main program MDSSTEST as the data are being reduced for a given consolidation increment. The load deflection relationship is also used during constant volume undrained shear where the program corrects for the apparatus compressibility due to changes in vertical stress required to maintain the sample height constant.

B.7.2 Friction and Membrane Resistance

B.7.2.1 CK_oUMDSS Tests

During undrained shear the horizontal loading system has frictional resistance due to the main bearing plates and the horizontal loading piston linear bearings and also horizontal resistance due to the membrane. Measurements of these resistances were made using several large steel ball bearings in place of a sample. The membrane was installed with the top cap and bottom pedestal with three $^3/_4$ " diameter steel balls in the middle. The balls were subjected to a small seating load to keep the system intact. The steel balls have a minimal rolling friction and thus the frictional and membrane resistance were measured by applying a horizontal load and measuring the resistance. The resistance versus displacement curves displayed an initial intercept at zero displacement and a linear slope of resistance versus displacement. The results suggest that the resistance contains an initial frictional component and the linearly increasing resistance with displacement due to the membrane. For the MDSS the best fit relationship was found to be:

$$MC(ksc) = 0.0017 + 0.00075(\gamma_t \text{ in percent}) \qquad (B.1)$$

where:

MC = resistance correction (ksc)

The first part of the right hand side of Equation B.1 represents the frictional component and the second part of the equation represents the membrane resistance. The correction is applied directly to the measurements made by the horizontal load cell during CK_oU tests to get the corrected shear resistance of the sample. This is done in the reduction program MDSSCKO.

B.7.7.2 CAUMDSS Tests ($0^\circ \leq \theta \leq 150^\circ$)

The friction and membrane resistance corrections are more complicated for CAU tests that are consolidated under a first shear stress at some angle theta. First, the horizontal shear force applied during consolidation has to be corrected for friction and the membrane resistance. Second, an additional friction and membrane correction has to be made during undrained shear where the sample strains along a path in the X–Y plane (the actual path depends on the test angle theta). In the corrections derived for these tests the membrane resistance is assumed to be isotropic in the X–Y plane.

(1) Correction of Horizontal Consolidation Shear Stress

The actual horizontal shear stress τ_{hc} acting on the sample at the end of anisotropic consolidation is computed using the following equation:

$$(\tau_{hc})_{cor} = (\tau_{hc})_{nom} - 0.00136 - 0.0394R \qquad (B.2)$$

where:

$(\tau_{hc})_{cor}$ = corrected horizontal shear stress at end of consolidation (ksc)

$(\tau_{hc})_{nom}$ = applied horizontal shear stress at end of consolidation (ksc)

0.00136 = frictional resistance of the main bearing plates (ksc)

$R = \sqrt{X_c^2 + Y_c^2}$

X_c = consolidation displacement along X axis (cm)

Y_c = consolidation displacement along Y axis (cm)

(2) Correction to τ_x During Undrained Shear

Once undrained shear starts, the horizontal resistance measured by the constant rate of strain horizontal loading system load cell has to be corrected for changes in the bearing plate friction and membrane resistance. The membrane resistance in the Y direction is ignored because it would make the correction more complicated and, in any event, its value would be small since most of the prepeak shear strain of the sample during undrained shear occurs in the X direction. The following equation is used to calculate τ_x during undrained shear:

$$\tau_x = (\tau_{hc})_{nom}(\cos\theta) + HLC - 0.0017 - 0.0394X_s \qquad (B.3)$$

where:

τ_x = sample shear resistance in the X direction (ksc)

$(\tau_{hc})_{nom}$ = applied horizontal shear stress at end of consolidation (ksc)

θ = test angle theta

HLC = horizontal load cell reading (ksc)

0.0017 = main bearing plate and horizontal loading piston friction (ksc)

X_s = X coordinate of sample w.r.t. neutral axis of device (cm)

From this equation the total shear resistance of the sample is computed as:

$$\tau_t = \sqrt{\tau_x^2 + \tau_y^2} \qquad (B.4)$$

where:

$$\tau_y = (\tau_{hc})_{cor}(\sin\theta) \qquad (B.5)$$

TABLE B.1: Sample Enclosure Parts List (Figure B.1)

Part No	Description
1	$1^1/_4$" diameter Thompson shaft for application of σ_v
2	Stainless steel circular disc
3	Top Cap
4	Drainage line
5	Porous stones
6	Plexiglas water bath
7	O-ring
8	Screw for flexible τ_1 connector
9	$^1/_{16}$" diameter aircraft cable for τ_1 connector
10	Planer bearing plates - two steel plates and one brass ball bearing retainer
11	Special τ_2 force applicator
12	$^1/_2$" diameter Thompson shaft for application τ_2
13	Alignment pins
14	Side wall of circular cage
15	Screws connecting circular cage wall to its base
16	Circular cage base
17	Large circular brass disc
18	Geonor wire-reinforced rubber membrane

TABLE B.2: Vertical Loading System Parts List (Figure B.2)

Part No	Description
1	Air pressure value
2	9 in^2 Bellofram Super Cylinder Air cylinder
3	Bellofram air cylinder piston rod
4	4"x4"x$^1/_2$" steel channel
5	Threaded brass coupling
6	Moment break connector (see Figure B.3)
7	1000 lbs Data Instruments load cell
8	21.4"x4"x$^3/_4$" Steel vertical upright
9	$1^1/_4$" diameter Thompson hardened steel shaft
10	Locking bracket for vertical shaft
11	$1^1/_4$" adjustable diameter Thompson Twin Pillow Block
12	11.5"x7.5"x$^3/_4$" steel cross brace
13	Stainless steel circular disc
14	Top cap
15	Sample
16	Bottom pedestal
17	Circular cage
18	Main bearing plates
19	41"x12"x2" MDSS aluminum base

TABLE B.3: Moment Break Connector Parts List (Figure B.3)

Part No	Description
1	Bellofram Air Cylinder piston shaft
2	Threaded brass coupling
3	$^1/_2$" diameter 1" long threaded bolt, with 0.22" diameter hole through its center (up to 0.8") and 0.125" diameter hole at its curved end
4	0.22" diameter brass end piece with $^1/_{16}$" diameter threads through its center
5	$^3/_{16}$" diameter $^1/_4$" long steel spring
6	2" long $^1/_{16}$" diameter brass rod with threaded ends
7	$^3/_4$" diameter steel ball with $^1/_8$" diameter hole through its center
8	1000 lbs Data Instruments load cell
9	Same as part number 3 except $1^1/_4$"long
10	$1^1/_4$" diameter Thompson hardened steel shaft

TABLE B.4: Plan View Parts List (Figure B.4)

Part No	Description
1	Insco electric motor
2	Bearing block with sterling flanged ball bearing
3	Insco multi-speed changer
4	Bearing block with sterling flanged ball bearing
5	Bearing block with sterling flanged ball bearing
6	Shaft coupling
7	Insco step function reducer
8	Econalign flexible coupling
9	Drive package mounting plate
10	Boston Gear flanged cartridge ball bearing
11	Boston Gear cast iron worm gear
12	$^1/_2$" diameter worm gear shaft
13	Boston Gear flanged cartridge ball bearing
14	Worm gear bearing plate
15	Beaver precision heat treated screw
16	Boston Gear pillow block
17	Pillow block spacer
18	Beaver precision ball screw
19	Ball screw housing

TABLE B.4: — continued

Part No	Description
20	Beaver precision ball spline
21	Ball spline housing
22	Beaver precision heat treated spline shaft
23	Aluminum locking bracket
24	$^1/_2$" diameter Thompson shaft
25	Moment break connector (see Figure B.3)
26	500 lbs Data Instruments load cell
27	Thompson $^1/_2$" adjustable diameter pillow block
28	Threaded brass coupling
29	Twin pillow block with two $^1/_2$" Thompson Super Ball Bushing Bearings
30	$^1/_2$" diameter Thompson shaft
31	Special load applicator for τ_2 shear force
32	Threaded block connecting $^1/_2$" diameter Thompson shaft to large circular frame
33	$^1/_2$" diameter Thompson shaft mounted on V support
34	Thompson $^1/_2$" open pillow block
35	Large circular loading frame for applying τ_1 force
36	Alignment hole for τ_1 pneumatic piston (i.e. @ θ = 0, 30, 60, 90, 120, and 150 degrees)

TABLE B.4: – continued

Part No	Description
37	21.4"x4"x$^3/_4$" steel vertical upright
38	Circular cage
39	Z1 DCDT with plexiglas holder
40	Planar Bearing plates
41	Large circular brass disc
42	PLexiglas water bath
43	Top cap
44	$1^1/_4$" diameter Thompson shaft
45	Alignment pin hole
46	Thompson $1^1/_4$" adjustable diameter twin pillow block
47	11.5"x7.5"x$^3/_4$" steel cross brace
48	Z2 DCDT and plexiglas holder
49	Y DCDT and plexiglas holder
50	X DCDT and plexiglas holder
51	$^1/_{16}$" diameter aircraft cable for τ_1 connector
52	τ_1 pneumatic cylinder (see Figure B.5)
53	τ_1 loading bracket
54	41"x12"x2" MDSS aluminum base

TABLE B.5: τ_1 Pneumatic Cylinder Parts List (Figure B.5)

Part No	Description
1	$^1/_{16}$" diameter aircraft cable for τ_1 connector
2	Large aluminum circular reaction frame
3	Screw for positioning τ_1 cylinder at a selected test angle θ
4	Loading bracket: consists of two $^1/_4$" diameter rods and two $^1/_2$"x$^1/_2$"x4.5" aluminum bars
5	$^3/_8$" diameter Thompson piston connected to the pneumatic cylinder's piston head
6	$^1/_2$" diameter Thompson shaft
7	Thompson low shaft rail
8	Thompson $^1/_2$" diameter open pillow block

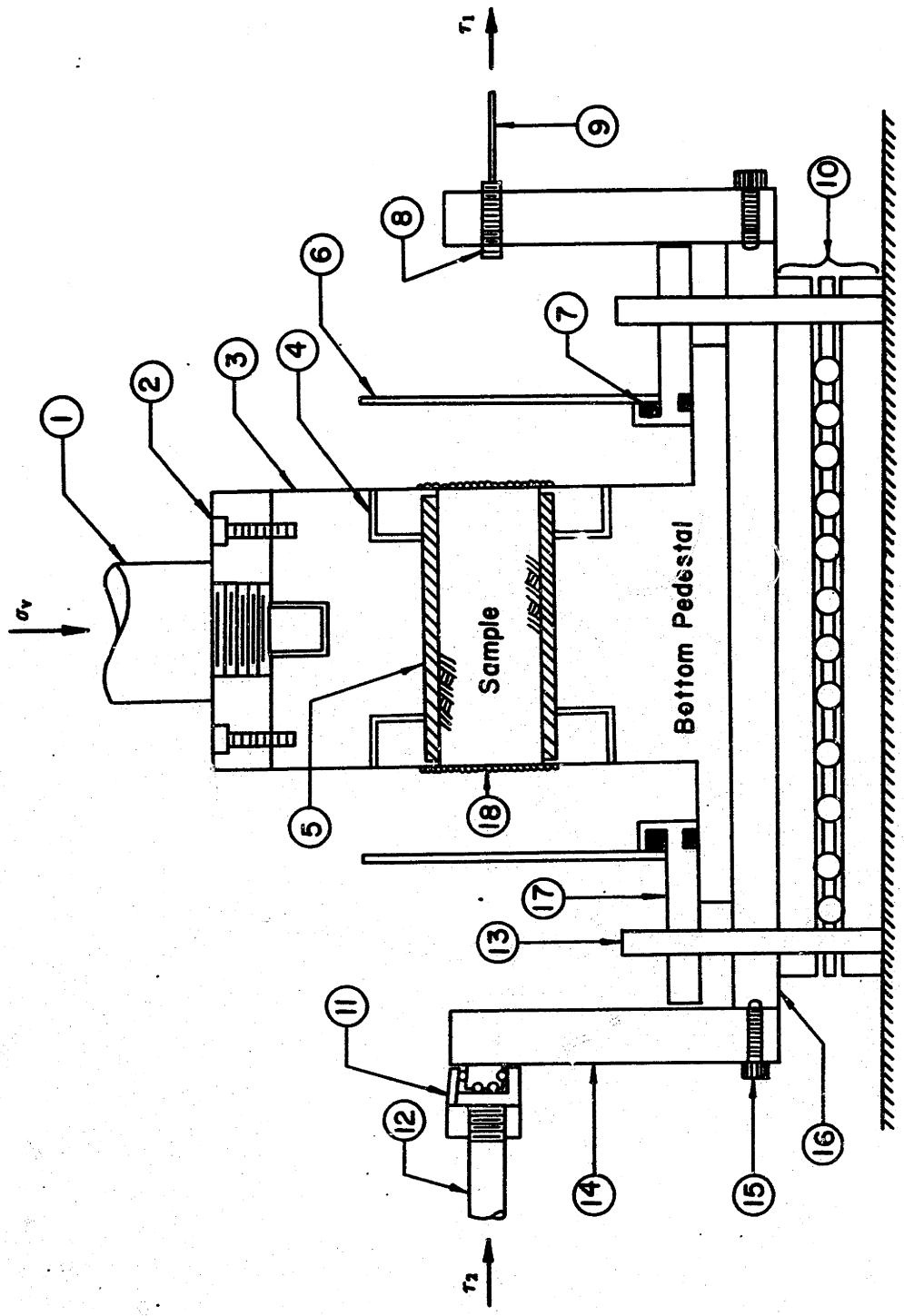

Figure B.1: MDSS Sample Enclosure (see Table B.1 for Parts List).

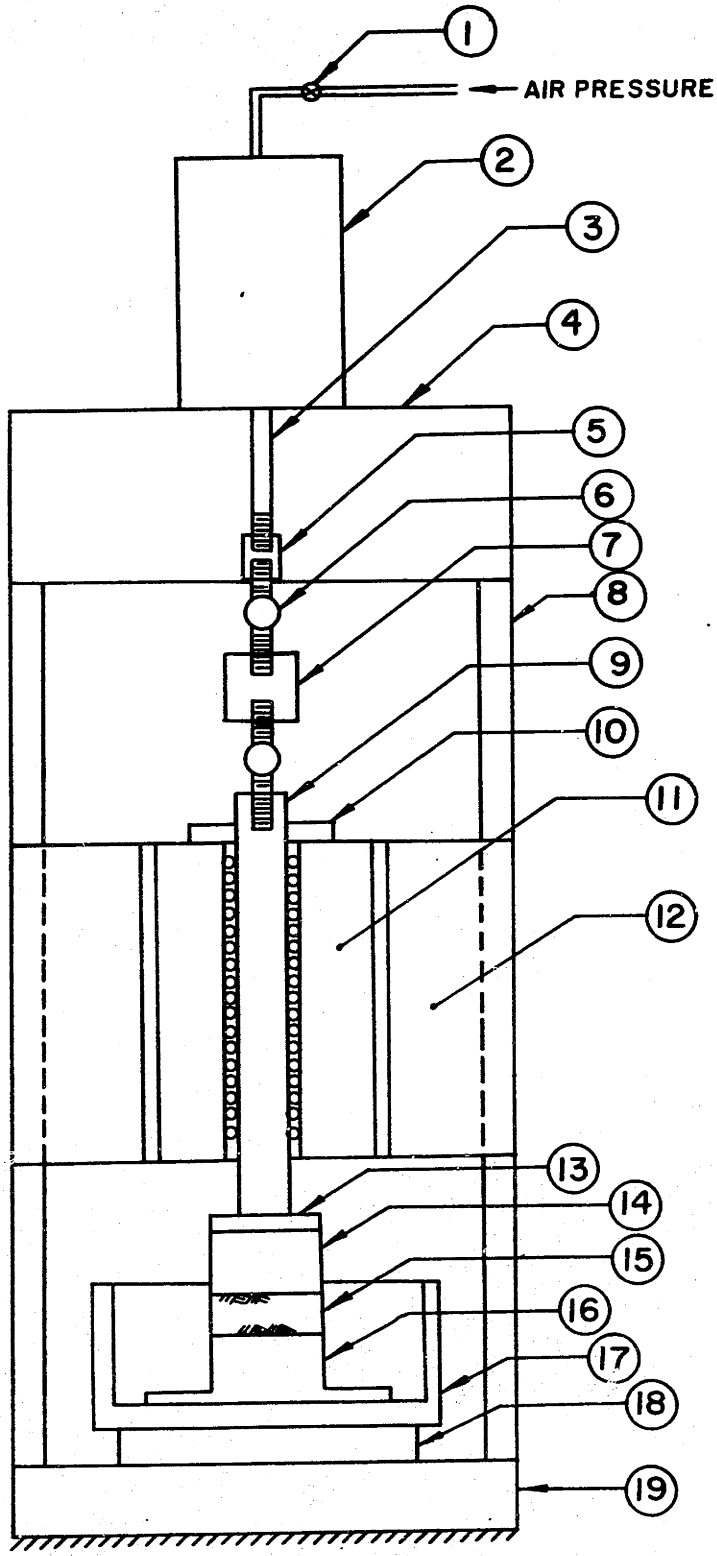

Figure B.2: MDSS Vertical Stress Loading System (see Table B.2 for Parts List).

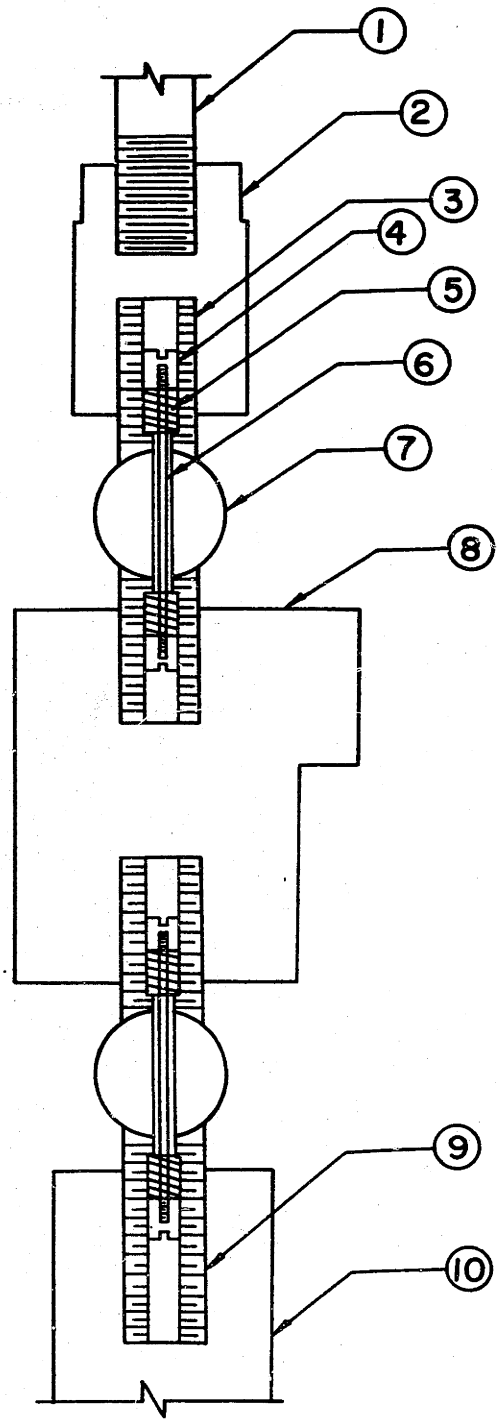

Figure B.3: MDSS Moment Break Connectors (see Table B.3 for Parts List).

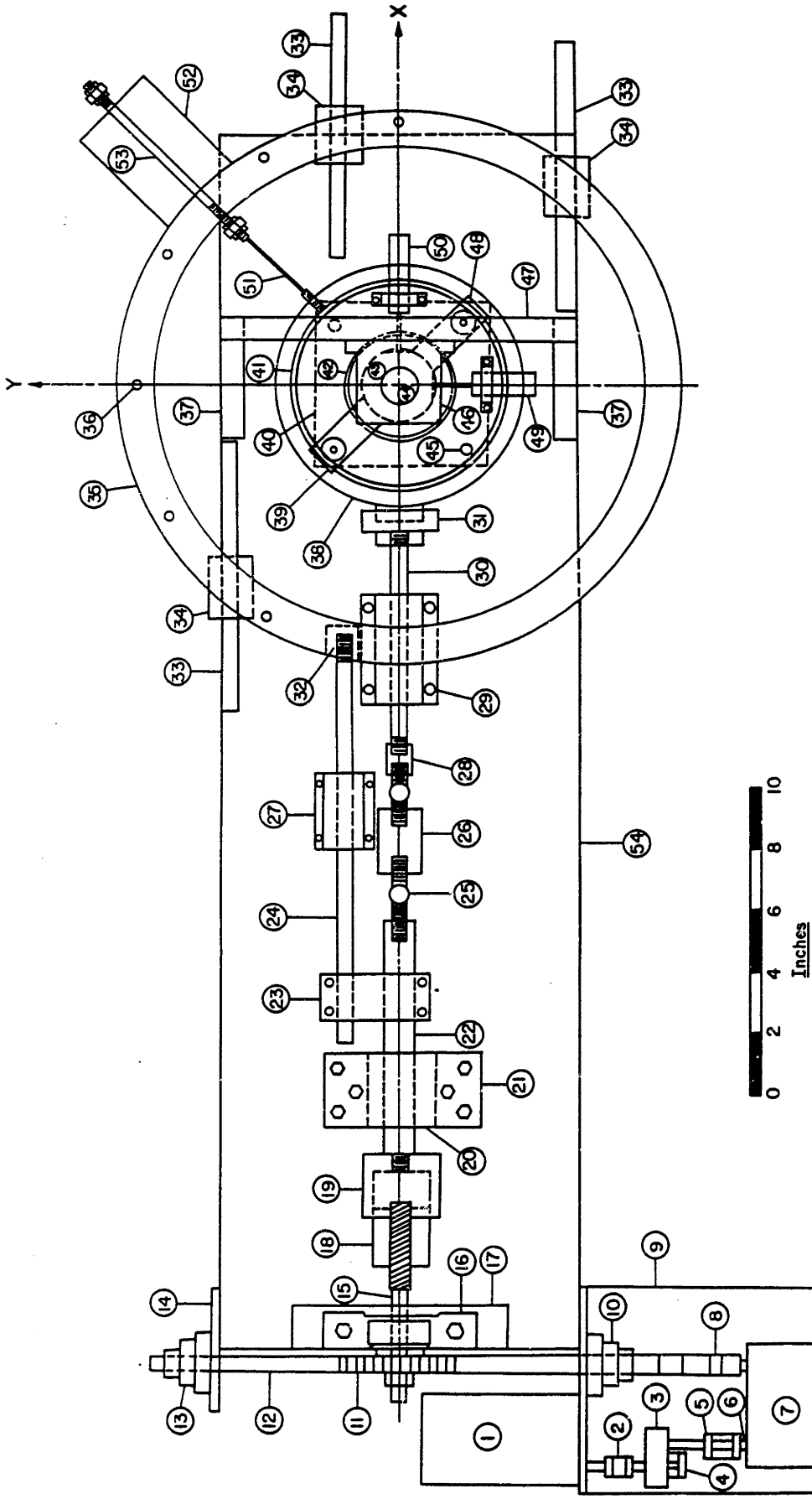

Figure B.4: Plan View of the MDSS Excluding Top Part of Vertical Stress Loading System (see Table B.4 for Parts List).

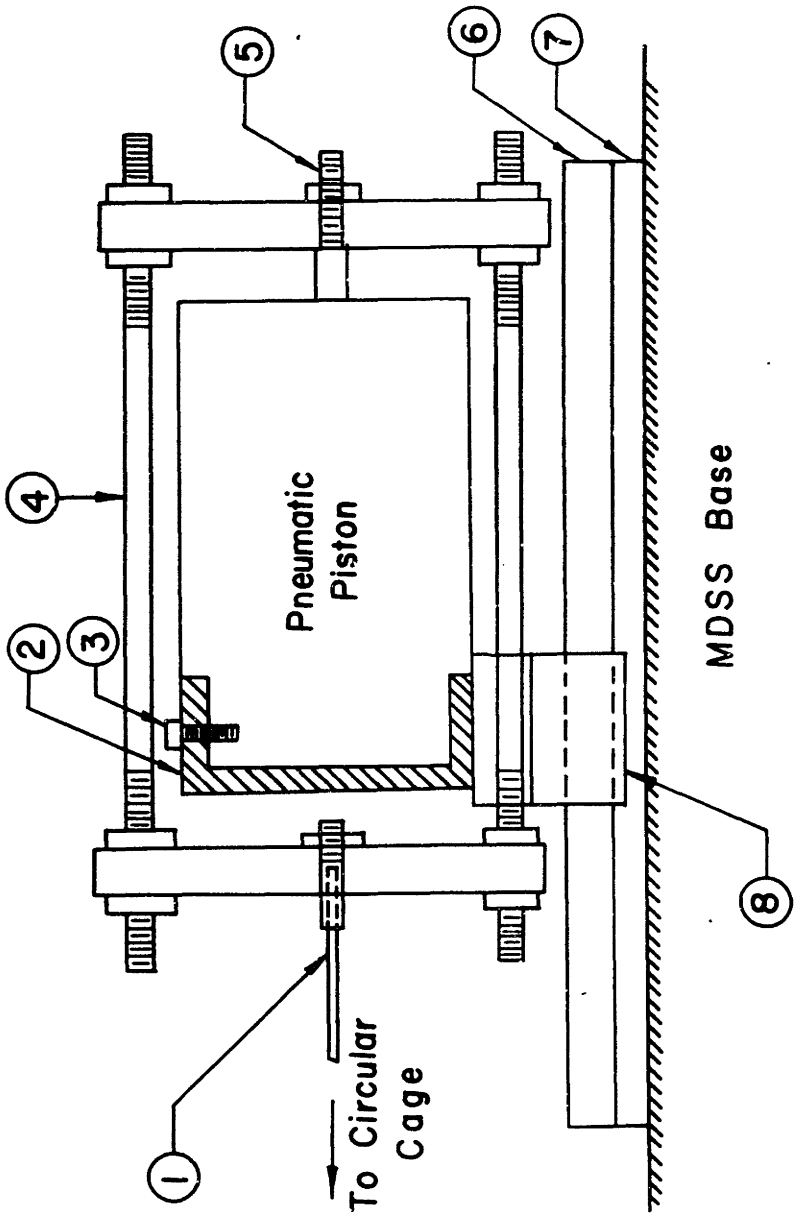

Figure B.5: MDSS First Shear Stress Pneumatic Cylinder (see Table B.5 for Parts List).

APPENDIX C

MDSS TEST AND DATA ACQUISITION SOFTWARE

This appendix contains a listing of the three main software programs used to conduct tests in the MDSS. All of the programs are written in BASIC.

C.1 MDSSTEST

This program is the main testing program for running automated MDSS tests. The code included in the program, as outlined in Chapter 3, allows samples to be tested by operator commands executed from the computer keyboard (e.g., application of seating load, application of consolidation increments σ'_{vc} and τ_{hc}, undrained shear constant height servo control, etc.). It also stores raw data and prints out reduced data of stress and strain during consolidation increments.

The first section of the program (up to line 1000) is supplied by HP PC Instruments software. This part of the code enables the remainder of the program to communicate through call statements with the PC Instruments modules. This software and the special call statements available for each PC Instrument Module are documented in the HP PC Instruments System Owner's Guide for the HP Vectra PC and the individual Owner's Guide for each module. The remaining section of the code was developed at MIT for this thesis research. The program has many subroutines and is structured as shown schematically in Figure 3.5

C.2 MDSSCKO

This program reduces the undrained shear data for K_o consolidated MDSS tests. The program reduces the data while correcting for the frictional and membrane

resistances. The beginning of the code is interactive allowing the user to check and make any necessary changes to the transducer zero readings and calibration factors.

C.3 MDSSCAU

This program reduces the undrained shear data for CAUMDSS tests conducted at some angle theta. The program is similar to MDSSCKO but has additional statements for calculating the total shear resistance of the sample, taking into account the magnitude and angle θ of the consolidation shear stress τ_1 acting on the sample, and the special friction and membrane corrections required.

```
1 DEF SEG:CLEAR ,&HFE00:GOTO 4 'Begin PCIB Program Shell: MDSSTEST BY DJD 1988
2 GOTO 1000 ' User program
3 GOTO 900 ' Error handling
4 I=&HFE00 ' Copyright Hewlett-Packard 1984,1985
5 PCIB.DIR$=ENVIRON$("PCIB")
6 I$=PCIB.DIR$+"\PCIBILC.BLD"
7 BLOAD I$,I
8 CALL I(PCIB.DIR$,I%,J%):PCIB.SEG=I%
9 IF J%=0 THEN GOTO 13
10 PRINT "Unable to load.";
11 PRINT "   (Error #";J%;")"
12 END
13 '
14 DEF SEG=PCIB.SEG:O.S=5:C.S=10:I.V=15
15 I.C=20:L.P=25:LD.FILE=30
16 GET.MEM=35:L.S=40:PANELS=45:DEF.ERR=50
17 PCIB.ERR$=STRING$(64,32) : PCIB.NAME$=STRING$(16,32)
18 CALL DEF.ERR(PCIB.ERR,PCIB.ERR$,PCIB.NAME$,PCIB.GLBERR) : PCIB.BASERR=255
19 ON ERROR GOTO 3
20 J=-1
21 I$=PCIB.DIR$+"\PCIB.SYN"
22 CALL O.S(I$)
23 IF PCIB.ERR<>0 THEN ERROR PCIB.BASERR
24 I=0
25 CALL I.V(I,READ.REGISTER,READ.SELFID,DEFINE,INITIALIZE.SYSTEM)
26 IF PCIB.ERR<>0 THEN ERROR PCIB.BASERR
27 CALL I.V(I,ENABLE.SYSTEM,DISABLE.SYSTEM,INITIALIZE,POWER.ON)
28 IF PCIB.ERR<>0 THEN ERROR PCIB.BASERR
29 CALL I.V(I,MEASURE,OUTPUT,START,HALT)
30 IF PCIB.ERR<>0 THEN ERROR PCIB.BASERR
31 CALL I.V(I,ENABLE.INT.TRIGGER,DI  BLE.INT.TRIGGER,ENABLE.OUTPUT,DISABLE.OUTPU
T)
32 IF PCIB.ERR<>0 THEN ERROR PCIB.BASERR
33 CALL I.V(I,CHECK.DONE,GET.STATUS,SET.FUNCTION,SET.RANGE)
34 IF PCIB.ERR<>0 THEN ERROR PCIB.BASERR
35 CALL I.V(I,SET.MODE,WRITE.CAL,READ.CAL,STORE.CAL)
36 IF PCIB.ERR<>0 THEN ERROR PCIB.BASERR
37 CALL I.V(I,DELAY,SAVE.SYSTEM,J,J)
38 IF PCIB.ERR<>0 THEN ERROR PCIB.BASERR
39 I=2
40 I=3
41 CALL I.V(I,ZERO.OHMS,SET.SPEED,J,J)
42 IF PCIB.ERR<>0 THEN ERROR PCIB.BASERR
43 CALL I.C(I,DCVOLTS,ACVOLTS,OHMS,R200MILLI)
44 IF PCIB.ERR<>0 THEN ERROR PCIB.BASERR
45 CALL I.C(I,R2,R20,R200,R2KILO)
46 IF PCIB.ERR<>0 THEN ERROR PCIB.BASERR
```

```
47 CALL I.C(I,R20KILO,R200KILO,R2MEGA,R20MEGA)
48 IF PCIB.ERR<>0 THEN ERROR PCIB.BASERR
49 CALL I.C(I,AUTOM,R2.5,R12.5,J)
50 IF PCIB.ERR<>0 THEN ERROR PCIB.BASERR
51 I=5
52 CALL I.C(I,R1,R5,R10,J)
53 IF PCIB.ERR<>0 THEN ERROR PCIB.BASERR
54 CALL C.S
55 IF PCIB.ERR<>0 THEN ERROR PCIB.BASERR
56 I$=PCIB.DIR$+"\PCIB.PLD"
57 CALL L.P(I$)
58 IF PCIB.ERR<>0 THEN ERROR PCIB.BASERR
59 I$="DMM.01":I=3:J=0:K=0:L=1
60 CALL DEFINE(DMM.01,I$,I,J,K,L)
61 IF PCIB.ERR<>0 THEN ERROR PCIB.BASERR
62 I$="VDAC.A.01":I=5:J=0:K=2:L=1
63 CALL DEFINE(VDAC.A.01,I$,I,J,K,L)
64 IF PCIB.ERR<>0 THEN ERROR PCIB.BASERR
65 I$="VDAC.B.01":I=5:J=1:K=2:L=1
66 CALL DEFINE(VDAC.B.01,I$,I,J,K,L)
67 IF PCIB.ERR<>0 THEN ERROR PCIB.BASERR
68 I$="Relay.Mux.01":I=2:J=0:K=5:L=1
69 CALL DEFINE(RELAY.MUX.01,I$,I,J,K,L)
70 IF PCIB.ERR<>0 THEN ERROR PCIB.BASERR
800 I$=ENVIRON$("PANELS")+"\PANELS.EXE"
801 CALL L.S(I$)
899 GOTO 2
900 IF ERR=PCIB.BASERR THEN GOTO 903
901 PRINT "BASIC error #";ERR;" occurred in line ";ERL
902 STOP
903 TMPERR=PCIB.ERR:IF TMPERR=0 THEN TMPERR=PCIB.GLBERR
904 PRINT "PC Instrument error #";TMPERR;" detected at line ";ERL
905 PRINT "Error: ";PCIB.ERR$
906 IF LEFT$(PCIB.NAME$,1)<>CHR$(32) THEN PRINT "Instrument: ";PCIB.NAME$
907 STOP
908 COMMON PCIB.DIR$,PCIB.SEG
909 COMMON LD.FILE,GET.MEM,PANELS,DEF.ERR
910 COMMON PCIB.BASERR,PCIB.ERR,PCIB.ERR$,PCIB.NAME$,PCIB.GLBERR
911 COMMON READ.REGISTER,READ.SELFID,DEFINE,INITIALIZE.SYSTEM,ENABLE.SYSTEM,DISA
BLE.SYSTEM,INITIALIZE,POWER.ON,MEASURE,OUTPUT,START,HALT,ENABLE.INT.TRIGGER,DISA
BLE.INT.TRIGGER,ENABLE.OUTPUT,DISABLE.OUTPUT,CHECK.DONE,GET.STATUS
912 COMMON SET.FUNCTION,SET.RANGE,SET.MODE,WRITE.CAL,READ.CAL,STORE.CAL,DELAY,SA
VE.SYSTEM,ZERO.OHMS,SET.SPEED
913 COMMON DCVOLTS,ACVOLTS,OHMS,R200MILLI,R2,R20,R200,R2KILO,R20KILO,R200KILO,R2
MEGA,R20MEGA,AUTOM,R2.5,R12.5,R1,R5,R10
914 COMMON DMM.01,VDAC.A.01,VDAC.B.01,RELAY.MUX.01
999 'End PCIB Program Shell
```

```
1000 REM *** start of application program
1020 REM *** for consolidation phase of conventional DSS testing
1030 DIM DATAV(8),SL(20),SD(20)
1060 CALL ENABLE.OUTPUT(RELAY.MUX.01)
1063 CALL SET.FUNCTION(DMM.01,DCVOLTS)
1070 CALL SET.SPEED(DMM.01,R12.5)
1080 CALL DISABLE.INT.TRIGGER(DMM.01)
1090 K=0!
1200 KEY 8, "INTERV"
1210 KEY (8) ON
1220 ON KEY(8) GOSUB 5490
1230 KEY 10, "STOP"
1240 KEY (10) ON
1250 ON KEY(10) GOSUB 9650
1260 KEY 9, "END"
1270 KEY (9) ON
1280 ON KEY(9) GOSUB 5160
1290 KEY 7, "INCREM"
1300 KEY (7) ON
1310 ON KEY(7) GOSUB 2810
1320 KEY 6, "SHEAR"
1330 KEY (6) ON
1340 ON KEY(6) GOSUB 6510
1350 KEY 5, "PRINT"
1360 KEY (5) ON
1370 ON KEY(5) GOSUB 8000
1380 KEY 1, " Thc"
1390 KEY (1) ON
1400 ON KEY(1) GOSUB 10350
1410 KEY 3, "T SEAT"
1420 KEY (3) ON
1430 ON KEY(3) GOSUB 10010
1440 KEY 2, ""
1450 KEY 4, ""
1460 DELTA.VOLTS=0!
1470 FILE.CODE=0!
1480 INC.NUMBER=0!
1490 SHEAR.FLAG=0!
1500 VSTRESS=.03          'FOR COMPUTING FIRST L.I.R. (0.3KSC=SEATING LOAD)
1510 GOSUB 5980           'APPLY TOP CAP SEATING LOAD
1520 GOSUB 1800           'PRELIMINARY INPUT DATA
1530 GOSUB 2810           'CONSOLIDATION INCREMENT DATA
1540 GOSUB 5490           'TIME INTERVAL AND POWER-UP
1550 REM *** time trigger section for readings and servo loop
1560 GOSUB 3240
1570 GOSUB 3420
1580 REM
```

```
1590 IF DTRIG >= STRIGG THEN TRIGGER=STRIGG:XON=1 ELSE TRIGGER=DTRIG:XON=0
1600 IF TRIGGER < 1! GOTO 1740
1610 ITRIGG%=TRIGGER
1620 ON TIMER(ITRIGG%) GOSUB 1740
1630 TIMER ON
1640 II=1:KK=1
1650 WHILE II
1660 IF REFDATE$<>DATE$ THEN GOSUB 5840
1670 PRINT " ";
1680 FOR KLM=1 TO 500
1690 REM
1700 NEXT KLM
1710 WEND
1720 GOTO 1560
1730 REM
1740 IF XON < .5 THEN GOSUB 3500 ELSE GOSUB 3900
1750 IF TRIGGER < 1! GOTO 1560
1760 TIMER OFF
1770 II=0
1780 RETURN
1790 CLS
1800 REM ***************************************************************
1810 REM ***  PRELIMINARY INPUT DATA SUBROUTINE
1820 REM ***************************************************************
1830 SWITCH=0
1840 CLS
1850 INPUT " *** ENTER THE TEST NAME : "; TEST$
1860 INPUT " *** IS THE PRELIMINARY INPUT DATA IN A FILE(Y/N)? ";M$
1870 IF M$="N" THEN 1980
1880 ON ERROR GOTO 0
1890 ON ERROR GOTO 11200
1900 INPUT " *** ENTER THE FILE NAME : "; FILENAM$
1910 OPEN "I",#2 ,FILENAM$
1920 INPUT #2, VINPUT,ZOVLC,CFVLC,CFPT,CFVSR,CFHSR,AVL
1930 INPUT #2, ZOZ1,CFZ1,ZOY,CFY,ZOX,CFX,ZOZ2,CFZ2,H.INITIAL
1940 CLOSE #2
1950 ON ERROR GOTO 0
1960 ON ERROR GOTO 3
1970 IF M$<>"N" THEN 2230
1980 CLS
1990 PRINT " *** PRELIMINARY INPUT DATA REQUIRED  ****
2000 PRINT "     (UNITS: V,cm/V/V,cm,mV,kg/mV/V))
2010 PRINT ""
2020 PRINT "    1. FOR VERTICAL DISPLACEMENT TRANSDUCER, Z1:"
2030 INPUT "        1. ZERO READING:  ", ZOZ1
2040 INPUT "        2. CALIBRATION FACTOR: ",CFZ1
2050 IF SWITCH=1 THEN 2230
```

```
 2060 PRINT "    2. FOR VERTICAL DISPLACEMENT TRANSDUCER, Z2:"
2070 INPUT "        1. ZERO READING: ",ZOZ2
2080 INPUT "        2. CALIBRATION FACTOR: ",CFZ2
2090 IF SWITCH=1 THEN 2230
2100 PRINT "    3. FOR HORIZONTAL DISPLACEMENT TRANSDUCER, X:"
2110 INPUT "        1. ZERO READING: ", ZOX
2120 INPUT "        2. CALIBRATION FACTOR: ", CFX
2130 IF SWITCH=1 THEN 2230
2140 PRINT "    4. FOR HORIZONTAL DISPLACEMENT TRANSDUCER, Y:"
2150 INPUT "        1. ZERO READING: ",ZOY
2160 INPUT "        2. CALIBRATION FACTOR: ",CFY
2170 IF SWITCH=1 THEN 2230
2180 PRINT "    5. FOR THE VERTICAL STRESS LOAD CELL, INPUT:"
2190 INPUT "         1. ZERO READING: ", ZOVLC
2200 INPUT "         2. CALIBRATION FACTOR: ", CFVLC
2210 IF SWITCH=1 GOTO 2230
2220 INPUT "    6. INITIAL SAMPLE HEIGHT: ",H.INITIAL
2230 CLS
2240 PRINT " *** ECHO OF PRELIMINARY INPUT DATA ***"
2250 PRINT "     (UNITS: V,cm/V/V,cm,mV,kg/mV/V)
2260 PRINT ""
2270 PRINT "    1. VERTICAL DISP. TRANSDUCER, Z1:"
2280 PRINT "            ZERO: "; ZOZ1
2290 PRINT "              CF: "; CFZ1
2300 PRINT "    2. VERTICAL DISP. TRANSDUCER, Z2:"
2310 PRINT "            ZERO: "; ZOZ2
2320 PRINT "              CF: "; CFZ2
2330 PRINT "    3. HORIZONTAL DISP. TRANSDUCER, X:"
2340 PRINT "            ZERO: ";ZOX
2350 PRINT "              CF: "; CFX
2360 PRINT "    4. HORIZONTAL DISP. TRANSDUCER, Y:"
2370 PRINT "            ZERO: ";ZOY
2380 PRINT "              CF: "; CFY
2390 PRINT "    5. VERTICAL STRESS LOAD CELL:"
2400 PRINT "              ZERO: "; ZOVLC
2410 PRINT "                CF: "; CFVLC
2420 PRINT "    6. INITIAL SAMPLE HEIGHT: "; H.INITIAL
2430 PRINT ""
2440 PRINT ""
2450 INPUT " *** DO YOU WANT TO MAKE ANY CORRECTIONS (Y/N)? ",CORR$
2460 IF CORR$="N" THEN 2520
2470 SWITCH=1
2480 INPUT " *** WHICH ITEM NUMBER IS INCORRECT (1,2,...,6)? ",ITNUM
2490 IF ITNUM>6 THEN 2480
2500 CLS
2510 ON ITNUM GOTO 2020,2060,2100,2140,2180,2220
2520 CLS
```

```
2530 PRINT ""
2540 INPUT " *** WOULD YOU LIKE A HARDCOPY OF THE INITIAL READING (Y/N)? " ;HC$
2550 IF HC$ = "N" THEN 2800
2560 LPRINT ""
2570 LPRINT " INITIAL READINGS AND CALIBRATION FACTORS "
2580 LPRINT "     (UNITS: V,cm/V/V,cm,mV,kg/mV/V)
2590 LPRINT "  TEST NAME : "; TEST$
2600 LPRINT "  DATE      : "; DATE$
2610 LPRINT "  TIME      : "; TIME$
2620 LPRINT ""
2630 LPRINT "    1. VERTICAL DISP. TRANSDUCER, Z1:"
2640 LPRINT "            ZERO: "; ZOZ1
2650 LPRINT "              CF: "; CFZ1
2660 LPRINT "    2. VERTICAL DISP. TRANSDUCER, Z2:"
2670 LPRINT "            ZERO: "; ZOZ2
2680 LPRINT "              CF: "; CFZ2
2690 LPRINT "    3. HORIZONTAL DISP. TRANSDUCER, X:"
2700 LPRINT "            ZERO: ";ZOX
2710 LPRINT "              CF: "; CFX
2720 LPRINT "    4. HORIZONTAL DISP. TRANSDUCER, Y:"
2730 LPRINT "            ZERO: ";ZOY
2740 LPRINT "              CF: "; CFY
2750 LPRINT "    5. VERTICAL STRESS LOAD CELL:"
2760 LPRINT "              ZERO: "; ZOVLC
2770 LPRINT "                CF: "; CFVLC
2780 LPRINT "    6. INITIAL INPUT VOLTAGE: "; VINPUT
2790 LPRINT "    7. INITIAL SAMPLE HEIGHT: "; H.INITIAL
2800 RETURN
2810 REM ************************************************************
2820 REM *** NEW VERTICAL CONSOLIDATION INCREMENT DATA
2830 REM ************************************************************
2840 CLS
2850 INPUT " *** ARE YOU SURE YOU WANT APPLY A NEW INCREMENT(Y/N)? ";INCM$
2860 IF INCM$ <> "Y" THEN RETURN
2870 FIRST.PASS=0!
2880 SWITCH=0
2890 VSTRESS.1=VSTRESS
2900 IF FILE.CODE < .5 THEN FILE.CODE=1! ELSE CLOSE #1:TIMER OFF
2910 PRINT ""
2920 REM
2930 PRINT " *** INPUT DATA FOR VERTICAL CONSOLIDATION INCREMENT *** "
2940 PRINT "                    (UNITS: KSC)"
2950 PRINT ""
2960 INPUT "     1. VERTICAL STRESS: ", VSTRESS
2970 IF SWITCH=1 GOTO 3000
2980 INPUT "     2. GAIN ON VERTICAL STRESS REGULATOR: ", VSGAIN
2990 LIR=(VSTRESS-VSTRESS.1)/VSTRESS.1
```

```
3000 CLS
3010 PRINT " *** CAREFULLY CHECK THESE NUMBERS ****
3020 PRINT "            (UNITS: KSC)"
3030 PRINT ""
3040 PRINT "    1. VERTICAL STRESS: "; VSTRESS
3050 PRINT "    2. GAIN ON VERTICAL STRESS REGULATOR: "; VSGAIN
3060 PRINT "    3. L.I.R. OF NEW INCREMENT: "; LIR
3070 PRINT ""
3080 INPUT " *** ARE THER ANY CORRECTIONS (Y/N)? ", COOR$
3090 IF COOR$="N" THEN 3150
3100 SWITCH=1
3110 INPUT " *** WHICH ITEM NUMBER IS INCORRECT (1 or 2)? ", ITNUM
3120 IF ITNUM>4 GOTO 3110
3130 CLS
3140 ON ITNUM GOTO 2960,2980
3150 IF VSTRESS>8! OR VSTRESS<.1 THEN 3000
3160 PRINT "":PRINT ""
3170 INPUT " *** SELECT A FILE NAME FOR THE DATA: ", FILEN$
3180 OPEN "O", #1, FILEN$
3190 D$=DATE$
3200 T$=TIME$
3210 INC.NUMBER=INC.NUMBER+1
3220 WRITE #1,TEST$,INC.NUMBER,D$,T$,VSTRESS
3230 RETURN 1540
3240 REM ************************************************
3250 REM ** DATA UPDATING SUBROUTINE **
3260 REM ************************************************
3270 IF REFDATE$<>DATE$ THEN GOSUB 5840
3280 IF(TIMFLAG > .5) THEN GOTO 3360
3290 IF(DFLIP > .5) THEN GOTO 3320
3300 ADATA=ADATA+1
3310 DTEMP=DTREF-DOFFSET+ADATA*INTDATA
3320 DTRIG=DTEMP-TIMER
3330 IF DTRIG < 1!  THEN DTRIG=0!
3340 RETURN
3350 REM
3360 IF DFLIP > .5  THEN GOTO 3390
3370 INTDATA=INTDATA+.25
3380 DTEMP=DTREF-DOFFSET+(INTDATA^2)*60!
3390 DTRIG=DTEMP-TIMER
3400 IF DTRIG < 1! THEN DTRIG=0!
3410 RETURN
3420 REM ************************************************
3430 REM ** SERVO UPDATING SUBROUTINE
3440 REM ************************************************
3450 IF(SFLIF > .5) THEN GOTO 3470
3460 STEMP=TIMER+INTSERVO
```

```
3470 STRIGG=STEMP-TIMER
3480 IF STRIGG < 1!  THEN STRIGG=0!
3490 RETURN
3500 REM ***************************************************
3510 REM ** DATA READING SUBROUTINE
3520 REM ***************************************************
3530 PRINT ""
3540 SETT=.2                        'DELAY TIME FOR READINGS
3550 ATDATA=(TIMER-REF.TIME+DTT)/60!
3560 '*************************************
3570 CALL SET.RANGE(DMM.01,R20)
3580 FOR NUM=1 TO 4
3590 CALL OUTPUT(RELAY.MUX.01,NUM)
3600 CALL DELAY(SETT)
3610 CALL MEASURE(DMM.01,VOLTS)
3620 DATAV(NUM)=VOLTS
3630 NEXT NUM
3640 '*************************************
3650 CALL SET.RANGE(DMM.01,R200MILLI)
3660 FOR NUM=6 TO 8
3670 CALL OUTPUT(RELAY.MUX.01,NUM)
3680 IF NUM=6 THEN CALL DELAY(SETT)
3690 CALL DELAY(SETT)
3700 CALL MEASURE(DMM.01,VOLTS)
3710 DATAV(NUM)=VOLTS
3720 NEXT NUM
3730 '*************************************
3740 CALL SET.RANGE(DMM.01,R2)
3750 NUM=5
3760 CALL OUTPUT(RELAY.MUX.01,NUM)
3770 CALL DELAY(SETT)
3780 CALL MEASURE(DMM.01,VOLTS)
3790 DATAV(NUM)=VOLTS
3800 VLMV=1000*DATAV(6) : HLMV=1000*DATAV(7)
3810 PRINT USING "####.##";ATDATA;
3820 PRINT USING "+##.###";DATAV(1),DATAV(2),DATAV(3),DATAV(4);
3830 PRINT USING "+##.####";DATAV(5);
3840 PRINT USING "+####.##";1000*DATAV(8),VLMV,HLMV;
3850 PRINT USING "+###.###";DAC.VER.VOLT
3860 WRITE #1,ATDATA,DATAV(1),DATAV(2),DATAV(3),DATAV(4),DATAV(5),DATAV(6),DATAV
(7),DATAV(8),DELTA.VOLTS
3870 DFLIP=0
3880 SFLIP=1
3890 RETURN
3900 REM ***************************************************
3910 REM ** SERVO READING SUBROUTINE
3920 REM ***************************************************
```

```
 3930 PRINT ""
3940 Z$="SERVO"
3950 ATDATA=(TIMER-REF.TIME+DTT)/60!
3960 PRINT Z$,ATDATA
3970 REM ******* first check the input voltage
3980 CALL SET.RANGE(DMM.01,R20)
3990 NN=1
4000 CALL OUTPUT(RELAY.MUX.01,NN)
4010 SETT=.2
4020 CALL DELAY(SETT)
4030 CALL MEASURE(DMM.01,VINPUT)
4040 IF VINPUT>5! THEN 4080
4050 PRINT ********* INPUT VOLTAGE IS LESS THAN 5 VOLTS, IT IS = ";VINPUT
4060 STOP
4070 GOTO 3970
4080 REM      Compare measured voltage to required voltage
4090 REM      check vertical stress first
4100 CALL SET.RANGE(DMM.01,R200MILLI)
4110 NN=6
4120 CALL OUTPUT(RELAY.MUX.01,NN)
4130 ICHECK=0
4140 SETT=.2
4150 PRINT " ********* VERTICAL STRESS CHECK:"
4160 II=1
4170 WHILE II
4180 CALL DELAY(SETT)
4190 CALL MEASURE(DMM.01,VOLTS)
4200 DELTA.VOLTS=REQ.VER.VOLT-VOLTS
4210 IF ABS(DELTA.VOLTS) < .0001 THEN ICHECK=ICHECK+1
4220 PRINT "VLC       : ";
4230 PRINT USING "####.##"; 1000*VOLTS;
4240 PRINT "      DAC.VER.VOLT :";
4250 PRINT USING "###.###"; DAC.VER.VOLT
4260 PRINT "ICHECK : "; ICHECK
4270 IF ICHECK > 3 THEN 4310
4280 DAC.VER.VOLT=DAC.VER.VOLT+(DELTA.VOLTS*40!)
4290 CALL OUTPUT(VDAC.A.01,DAC.VER.VOLT)
4300 WEND
4310 IF HSTRESS < .01 THEN 4510   'ie. do not check unless there is a Thc stress
4320 PRINT " ********** HORIZONTAL STRESS CHECK:"
4330 NN=8
4340 CALL OUTPUT(RELAY.MUX.01,NN)
4350 ICHECK=0
4360 II=1
4370 WHILE II
4380 CALL DELAY(SETT)
4390 CALL MEASURE(DMM.01,VOLTS)
```

```
4400 DELTA.VOLTS=REQ.HOR.VOLT-VOLTS
4410 IF ABS(DELTA.VOLTS) < .00005 THEN ICHECK=ICHECK+1
4420 PRINT "HPT       : ";
4430 PRINT USING "####.##"; 1000*VOLTS;
4440 PRINT "      DAC.HOR.VOLT :";
4450 PRINT USING "###.###"; DAC.HOR.VOLT
4460 PRINT "ICHECK : "; ICHECK
4470 IF ICHECK > 3 THEN 4510
4480 DAC.HOR.VOLT=DAC.HOR.VOLT+(DELTA.VOLTS*40!)
4490 CALL OUTPUT(VDAC.B.01,DAC.HOR.VOLT)
4500 WEND
4510 PRINT " ************** OUT OF SERVO CHECK"
4520 SFLIP=0
4530 DFLIP=1
4540 RETURN
4550 REM ***************************************************
4560 REM ** POWER UP SUBROUTINE **
4570 REM ***************************************************
4580 T1=TIMER          'need this in addition to 4410 for FIRST.PASS>0.5
4590 IF FIRST.PASS>.5 THEN 5080
4600 REM ******* first check the input voltage
4610 CALL SET.RANGE(DMM.01,R20)
4620 NN=1
4630 CALL OUTPUT(RELAY.MUX.01,NN)
4640 SETT=.3
4650 CALL DELAY(SETT)
4660 CALL MEASURE(DMM.01,VINPUT)
4670 IF VINPUT>5! THEN 4710
4680 PRINT "******** INPUT VOLTAGE IS LESS THAN 5 VOLTS, IT IS = ";VINPUT
4690 STOP
4700 GOTO 4600
4710 REM
4720 VFORCE=(VSTRESS*35!)-1.15                'Wt. top cap=1.150kg
4730 REQ.VER.VOLT=(VFORCE*VINPUT/CFVLC+ZOVLC)/1000!
4740 VER.AIR.PRESS=VFORCE/AVL
4750 REM **  lines for initial power up of stresses
4760 DAC.VER.VOLT=(VER.AIR.PRESS*CFVSR/VSGAIN)+1!
4770 VALPHA=120!
4780 IF VSGAIN < 3 THEN 4800
4790 VALPHA=120!/(VSGAIN-1)
4800 PRINT "VINPUT        : "; VINPUT
4810 PRINT "REQ.VER.VOLT  : "; REQ.VER.VOLT
4820 PRINT "DAC.VER.VOLT  : "; DAC.VER.VOLT
4830 NN=6
4840 CALL OUTPUT(RELAY.MUX.01,NN)
4850 CALL SET.RANGE(DMM.01,R200MILLI)
4860 II=1
```

```
4870 SETT=.15
4875 WAITT=.75
4880 ICHECK=0
4890 REM   vertical stress
4900 T1=TIMER
4910 CALL OUTPUT(VDAC.A.01,DAC.VER.VOLT)
4915 BEEP
4920 CALL DELAY(WAITT)
4930 WHILE II
4940 CALL DELAY(SETT)                  'need trial and error with this
4950 CALL MEASURE(DMM.01,VOLTS)
4960 DELTA.VOLTS=REQ.VER.VOLT-VOLTS
4970 IF ABS(DELTA.VOLTS) < .0003 THEN ICHECK=ICHECK+1
4980 PRINT "VLC       : ";
4990 PRINT USING "####.##"; 1000*VOLTS;
5000 PRINT "      DAC.VER.VOLT  : ";
5010 PRINT USING "###.###"; DAC.VER.VOLT
5020 PRINT "ICHECK : "; ICHECK
5030 IF ICHECK > 3 THEN 5070
5040 DAC.VER.VOLT=DAC.VER.VOLT+(DELTA.VOLTS*VALPHA)
5050 CALL OUTPUT(VDAC.A.01,DAC.VER.VOLT)
5060 WEND
5070 PRINT "OUT OF POWER UP"
5080 DTREF=T1+1!        ' T1 from begining of subroutine or the middle
5090 BEEP
5100 IF FIRST.PASS>.5 THEN 5130
5110 START.TIME=DTREF:REF.TIME=DTREF
5120 FIRST.PASS=1!
5130 TIMER OFF
5140 JJ=0
5150 RETURN
5160 REM ************************************************************
5170 REM ** END PROGRAM AND CLOSE DATA FILE **
5180 REM ************************************************************
5190 PRINT ""
5200 INPUT "  *** ARE YOU SURE YOU WANT TO END THE PROGRAM (Y/N)? "; M$
5210 IF M$ <> "Y" THEN RETURN
5220 TIMER OFF
5230 CLOSE #1
5240 '*********************************************
5250 INPUT "  *** DO YOU NEED TO REDUCE THE HORIZONTAL STRESS(Y/N)? "; M3$
5260 IF M3$="N" THEN 5360
5270 CLS
5280 PRINT " *** TIME TO REDUCE THE REGULATOR VOLTAGE, SET GAIN=1.0 "
5290 PRINT " *** CURRENT DAC OUTPUT B VOLTAGE = ";DAC.HOR.VOLT
5300 INPUT " *** DO YOU WANT TO CHANGE THIS VALUE(Y/N)? "; MR$
5310 IF MR$="N" THEN 5360
```

```
5320 INPUT " *** ENTER NEW VOLTAGE VALUE :"; DAC.HOR.VOLT
5330 CALL OUTPUT(VDAC.B.01,DAC.HOR.VOLT)
5340 GOTO 5290
5350 '*****************************************
5360 INPUT "  *** DO YOU NEED TO REDUCE THE VERTICAL STRESS(Y/N)? "; M3$
5370 IF M3$="N" THEN 5460
5380 CLS
5390 PRINT " *** TIME TO REDUCE THE REGULATOR VOLTAGE, SET GAIN=1.0 "
5400 PRINT " *** CURRENT DAC OUTPUT A VOLTAGE = ";DAC.VER.VOLT
5410 INPUT " *** DO YOU WANT TO CHANGE THIS VALUE(Y/N)? "; MR$
5420 IF MR$="N" THEN 5460
5430 INPUT " *** ENTER NEW VOLTAGE VALUE :"; DAC.VER.VOLT
5440 CALL OUTPUT(VDAC.A.01,DAC.VER.VOLT)
5450 GOTO 5400
5470 PRINT "THE END"
5480 END
5490 REM ************************************************************
5500 REM ** TIME INTERVAL SUBROUTINE **
5510 REM ************************************************************
5520 IF FIRST.PASS < .5 THEN DTT=0!:DDAYS=0! ELSE TIMER OFF
5530 OFFSET.DAYS=0!     ' reset reference for servo and data triggers
5540 DOFFSET=0!         '     "          "            "            "
5550 TIMFLAG=0
5560 ADATA=0            ' increment counter for data readings
5570 CLS
5580 PRINT " *** INPUT TIME INTERVAL FOR DATA READINGS AND THE "
5590 PRINT "     SERVO LOOP.  FORMAT:  HOURS,MINUTES,SECONDS"
5600 PRINT "     USE 00,00,00 FOR VARIABLE INCREMENTS DURING"
5610 PRINT "     CONSOLIDATION."
5620 PRINT ""
5630 INPUT "     1. FOR DATA READINGS: ", DHRS,DMIN,DSEC
5640 INPUT "     2. FOR SERVO LOOP   : ", SHRS,SMIN,SSEC
5650 REFDATE$=DATE$
5660 IF DHRS<>0 OR DMIN<>0 OR DSEC<>0 THEN 5700
5670 TIMFLAG=1
5680 INTDATA=0
5690 GOTO 5710
5700 INTDATA=(DHRS*3600 + DMIN*60 + DSEC)
5710 INTSERVO=(SHRS*3600 + SMIN*60 + SSEC)
5720 IF FIRST.PASS < .5 THEN REF.TIME=TIMER 'just need this to get ATDATA=0
5730 GOSUB 3500     ' take the a set of channel readings
5740 ON TIMER(5) GOSUB 4550
5750 TIMER ON
5760 JJ=1
5770 WHILE JJ
5780 REM
5790 WEND
```

```
 5800 DFLIP=0
5810 SFLIP=0
5820 RETURN 1550
5830 REM
5840 REM ***************************************************
5850 REM ** 24 HOUR TIMER UPDATE **
5860 REM ***************************************************
5870 TIMER STOP
5880 REFDATE$=DATE$
5890 DDAYS=DDAYS+1
5900 OFFSET.DAYS=OFFSET.DAYS+1!
5910 DOFFSET=OFFSET.DAYS*86400!                    ' for servo and data triggers
5920 DTT=(DDAYS-1!)*86400! + (86400!-START.TIME)  ' for time of data readings
5930 DFLIP=0!
5940 SFLIP=0!
5950 REF.TIME=0!
5960 II=0
5970 RETURN
5980 REM ***************************************************************
5990 REM ** SUBROUTINE TO APPLY THE VERTICAL SEATING LOAD
6000 REM ***************************************************************
6010 CLS
6020 SETT=2!
6030 CALL SET.RANGE(VDAC.A.01,R10)
6040 VSTART=1!
6050 CALL OUTPUT(VDAC.A.01,VSTART)
6060 CALL ENABLE.OUTPUT(VDAC.A.01)
6070 NN=6
6080 CALL OUTPUT(RELAY.MUX.01,NN)
6090 CALL SET.RANGE(DMM.01,R200MILLI)
6100 PRINT "CURRENT DAC VOLTAGE: "; VSTART
6110 INPUT "INPUT NEW VALUE    : "; VSTART
6120 CALL OUTPUT(VDAC.A.01,VSTART)
6130 CALL DELAY(SETT)
6140 CALL MEASURE(DMM.01,VOLTS)
6150 PRINT ""
6160 PRINT "VERTICAL LOAD CELL READING (mv) : "; 1000*VOLTS
6170 INPUT "CONTINUE INCREASING LOAD (Y/N)? : "; M$
6180 IF M$ <> "N" THEN 6100
6190 INPUT "ENTER C WHEN READY TO READ DCDT ZEROS : "; M$
6200 IF M$ <> "C" THEN 6190
6210 SETT=.5
6220 CALL SET.RANGE(DMM.01,R20)
6230 FOR NUM=1 TO 4
6240 CALL OUTPUT(RELAY.MUX.01,NUM)
6250 CALL DELAY(SETT)
6260 CALL MEASURE(DMM.01,VOLTS)
```

```
6270 DATAV(NUM)=VOLTS
6280 NEXT NUM
6290 NUM=5
6300 CALL SET.RANGE(DMM.01,R2)
6310 CALL OUTPUT(RELAY.MUX.01,NUM)
6320 CALL DELAY(SETT)
6330 CALL MEASURE(DMM.01,VOLTS)
6340 DATAV(NUM)=VOLTS
6350 ZOZ1=DATAV(2):ZOZ2=DATAV(3):ZOY=DATAV(4):ZOX=DATAV(5)
6360 INPUT " *** ENTER THE VERTICAL LOAD CELL ZERO (mV): ";ZOVLC
6370 INPUT " *** ENTER THE INITIAL SAMPLE HEIGHT (cm): ";H.INITIAL
6380 INPUT " *** ENTER A FILE NAME TO STORE THE PRELIM DATA : "; FPRELIM$
6390 OPEN "O",#1,FPRELIM$
6400 REM store calibration factors
6410 CFVLC=13.70491:CFVSR=9.6658:AVL=58.064:CFPT=2.4528:CFHSR=.267
6420 CFZ1=.28883:CFY=-.261:CFX=-1.81917:CFZ2=.29569
6430 WRITE #1,DATAV(1),ZOVLC,CFVLC,CFPT,CFVSR,CFHSR,AVL
6440 WRITE #1,ZOZ1,CFZ1,ZOY,CFY,ZOX,CFX,ZOZ2,CFZ2,H.INITIAL
6450 CLOSE #1
6460 INPUT " DO YOU NEED TO APPLY THE Thc FORCE (Y/N)? : "; T$
6470 IF T$="Y" THEN GOSUB 10010   'only need this if program crashed
6480 INPUT " *** ENTER C WHEN READY TO CONTINUE : "; M$
6490 IF M$ <> "C" THEN 6480
6500 RETURN
6510 REM ************************************************************
6520 REM **  SHEARING SUBROUTINE
6530 REM ************************************************************
6540 TIMER OFF
6550 CLS
6560 INPUT " DO YOU WANT TO START SHEARING (Y/N)? : "; M$
6570 IF M$ <> "Y" THEN RETURN 1540         ' GO BACK TO TIME INTERVAL SUB.
6580 SHEAR.FLAG=1!
6590 DAC.VER.IN=DAC.VER.VOLT
6600 KEY(8) OFF
6610 KEY 8, "INTERV"
6620 ON KEY(8) GOSUB 7890
6630 KEY(8) ON
6640 KEY(5) OFF
6650 KEY 5, "CUTOFF"
6660 ON KEY(5) GOSUB 9810
6670 KEY(5) ON
6680 KEY 1, "  K  "
6690 ON KEY(1) GOSUB 9350
6700 KEY(1) ON
6710 KEY 2, "  A  "
6720 ON KEY(2) GOSUB 9450
6730 KEY(2) ON
```

```
6740 KEY 3, "  B  "
6750 ON KEY(3) GOSUB 9550
6760 KEY(3) ON
6770 KEY(4) OFF
6780 KEY 4, "  C  "
6790 ON KEY(4) GOSUB 9710
6800 KEY(4) ON
6802 K=25:A=.01:B=.1:C=.001:CUTOFF=.02
6803 PRINT " *** SERVO CONTROL VARIABLES ***"
6804 PRINT "      K, A, B, C, & CUTOFF"
6805 PRINT USING  "+####.###";K,A,B,C,CUTOFF
6806 PRINT "":PRINT ""
6810 '        GOSUB 9350    ' select value for gain K
6820 '        GOSUB 9450    ' select value for gain A
6830 '        GOSUB 9550    ' select value for gain B
6840 '        GOSUB 9710    ' select value for gain C
6850 '        GOSUB 9810    ' select value for CUTOFF
6860 GOSUB 9910    ' enter CF for the Z DCDT
6870 INPUT " SELECT NAME FOR DATA FILE           : "; FILEN$
6880 INPUT " SELECT NAME FOR THE TEST            : "; TESTN$
6890 CLOSE #1
6900 OPEN "O", #1, FILEN$
6910 D$=DATE$
6920 T$=TIME$
6930 WRITE #1, TESTN$,D$,T$
6950 WRITE #1, ZOVLC,CFVLC,CFZ1,CFZ2,CFY,CFX
6960 REM *************  SET INITIAL TIME VARIABLES
6970 DTT=0!
6980 ATDATA=0!
6990 PRINT " PRESS FUNCTION KEY 8 TO SELECT TIME INTERVAL FOR READINGS"
7000 JJ=1
7010 WHILE JJ
7020 WEND
7030 PRINT " *** PREPARE DEVICE FOR PRESHEAR READINGS. "
7040 PRINT "":PRINT "" :PRINT ""
7045 PRINT " *** MAKE SURE THE CONSTANT HEIGHT DCDT IS CONNECTED !!!! ***"
7050 PRINT " *** MAKE SURE THE CONSTANT HEIGHT DCDT IS WITHIN +/-200 mV ***"
7060 PRINT "":PRINT "" :PRINT ""
7070 PRINT " MAKE SURE THE PINS ARE REMOVED  !!!!!!!!!!!"
7080 PRINT " MAKE SURE THE MOTOR SPEED IS CORRECT !!!!!!!"
7090 INPUT " WHEN READY ENTER C, WAIT 10 SECONDS THEN TURN ON THE MOTOR : "; M$
7100 IF M$ <> "C" THEN 7030
7110 REM  preshear readings
7120 SETT=.5
7130 CALL SET.RANGE(DMM.01,AUTOM)
7140 FOR NUM=1 TO 8
7150 CALL OUTPUT(RELAY.MUX.01,NUM)
```

```
7160 CALL DELAY(SETT)
7170 CALL MEASURE(DMM.01,VOLTS)
7180 DATAV(NUM)=VOLTS
7190 NEXT NUM
7200 VINPUT=DATAV(1)
7210 WRITE #1,ATDATA,DATAV(1),DATAV(2),DATAV(3),DATAV(4),DATAV(5),DATAV(6),DATAV
(7),DATAV(8),DELTA.VOLTS
7220 PRINT USING "+##.####";ATDATA,DATAV(1),DATAV(2),DATAV(3),DATAV(4),DATAV(5),
DATAV(8);
7230 PRINT USING "+####.##";1000*DATAV(6),1000*DATAV(7),DAC.VER.VOLT
7240 REM                  compute reference for stone deflections
7250 VER.LOAD=(DATAV(6)*1000!-ZOVLC)*CFVLC/VINPUT+1.15
7260 GOSUB 8950          ' read stone deflection data
7270 KL=1
7280 KL=KL+1
7290 IF VER.LOAD > SL(KL) THEN 7280
7300 REF.STNS=(SD(KL)-SD(KL-1))/(SL(KL)-SL(KL-1))*(VER.LOAD-SL(KL-1))+SD(KL-1)
7310 REM read reference voltage for constant height DCDT
7320 SDELAY=1!
7330 SDEL1=.3
7340 HZ=8
7350 REM  take average of three readings for the reference voltages
7360 ZSUM=0!
7370 CALL SET.RANGE(DMM.01,R200MILLI)
7380 CALL OUTPUT(RELAY.MUX.01,HZ)
7390 CALL DELAY(SDEL1)
7400 FOR NM=1 TO 3
7410 CALL MEASURE(DMM.01,VOLTZ)
7420 ZSUM=ZSUM+VOLTZ
7430 NEXT NM
7440 REFZO=ZSUM/3!
7450 IN.1=DAC.VER.VOLT : IN.2=DAC.VER.VOLT
7460 P.1=REFZO : P.2=REFZO : DV=0!
7470 PRINT "REFERENCE VOLTAGE:  REFZO = "; REFZO
7480 REM *************  START TIMER FOR DATA READINGS
7490 DATA.TIME=TIMER+INT.DATA
7500 REF.TIME=TIMER
7510 REM  *************  START OF SERVO LOOP
7520 II=1
7530 DV.1=DV
7540 CALL ENABLE.INT.TRIGGER(DMM.01)
7550 CALL OUTPUT(RELAY.MUX.01,HZ)
7560 CALL DELAY(SDEL1)
7570 CALL SET.RANGE(DMM.01,R200MILLI)
7580 REM  *************  COMPUTE STONE CORRECTION
7590 VER.LOAD=(DATAV(6)*1000!-ZOVLC)*CFVLC/DATAV(1)+1.15
7600 KL=1
```

```
 7610 KL=KL+1
7620 IF VER.LOAD > SL(KL) THEN 7610
7630 DEFS=(SD(KL)-SD(KL-1))/(SL(KL)-SL(KL-1))*(VER.LOAD-SL(KL-1))+SD(KL-1)
7640 DS=DEFS-REF.STNS
7650 DV=DS*DATAV(1)/CFZ
7660 DV.COUNT=0!
7670 DV.SLOPE=(DV-DV.1)/DV.SUM
7680 WHILE II
7690 CALL MEASURE(DMM.01,P)
7700 DV.COUNT=DV.COUNT+1
7710 REFZ=REFZO+DV.1+(DV.SLOPE*DV.COUNT)
7720 XE=REFZ-P:PRINT USING "###.####";XE;
7730 IN=(1!-C)*IN.1 + C*IN.2 + K*REFZ*(A+A*C) - K*(P*(1+B)+P.1*(C-1!+A-2*B)+P.2*
(A*C-C+B))
7740 IF ABS(IN-IN.1) < CUTOFF THEN 7760
7750 IF (IN-IN.1)<0! THEN IN=IN.1-.002:PRINT "$"; ELSE IN=IN.1+.002:PRINT "#";
7760 DAC.VER.VOLT=IN
7770 IF DAC.VER.VOLT>9! THEN PRINT " VER.DAC OVER LIMIT ": STOP
7780 IF DAC.VER.VOLT<1.2 THEN PRINT " VER.DAC UNDER LIMIT ": STOP
7790 CALL OUTPUT(VDAC.A.01,DAC.VER.VOLT)
7800 P.2=P.1 : P.1=P
7810 IN.2=IN.1 :IN.1=IN
7820 IF TIMER > DATA.TIME THEN 7840
7830 WEND
7840 CALL DISABLE.INT.TRIGGER(DMM.01)
7850 DELTA.VOLTS=XE : GOSUB 3500                    'DATA READINGS
7860 'GOSUB 5040  FOR SERVO CHECK OF HORIZONTAL SHEAR STRESS
7870 DATA.TIME=DATA.TIME+INT.DATA
7880 GOTO 7520
7890 REM ************************************************************
7900 REM **  TIME INTERVAL SUB FOR SHEARING
7910 REM ************************************************************
7920 JJ=0
7930 CLS
7940 PRINT "  *** SELECT TIME INTERVAL FOR DATA READINGS DURING SHEAR."
7950 INPUT "      FORMAT : HOURS,MINUTES,SECONDS : ", SDHRS,SDMIN,SDSEC
7960 INT.DATA=(SDHRS*3600! + SDMIN*60! +SDSEC)
7970 DATA.TIME=TIMER+INT.DATA
7980 DV.SUM=450*INT.DATA/60!   'SERVO LOOP MAKES APPROX. 450 CHECKS PER MIN.
7990 RETURN
8000 REM ************************************************************
8010 REM *** PRINT FILE SUBROUTINE
8020 REM ************************************************************
8030 TIMER OFF
8040 CLS
8050 PRINT ""
8060 PRINT " *** THERE ARE TWO PRINTING OPTIONS:"
```

```
8070 PRINT "      1. PRINT CHANNEL READINGS"
8080 PRINT "      2. PRINT CALCULATED DISPLACEMENTS AND STAINS"
8090 PRINT ""
8100 INPUT "  DO YOU WANT TO PRINT CHANNEL READINGS (Y/N)? : ",M$
8110 IF M$="N" THEN 8360
8120 INPUT " ENTER NAME OF FILE TO BE PRINTED : ", FILENAM$
8130 INPUT " IS THIS AN ACTIVE FILE (Y/N)? ", ACTIVE$
8140 ON ERROR GOTO 0
8150 ON ERROR GOTO 11200
8160 IF ACTIVE$="N" THEN OPEN "I",#2,FILENAM$ ELSE CLOSE #1:OPEN "I",#2,FILENAM$
8170 INPUT #2, T$,INCN,DT$,TM$,VST
8180 LPRINT "":LPRINT "":LPRINT ""
8190 LPRINT "   TEST NAME   : "; T$
8200 LPRINT "   DATE        : "; DT$
8210 LPRINT "   TIME        : "; TM$
8220 LPRINT "   INC. NUMBER : "; INCN
8230 LPRINT "   VER. STRESS (KSC) : "; VST
8240 LPRINT ""
8250 LPRINT "   UNITS: (MIN,VOLTS,mVOLTS)
8260 LPRINT "   TIME    Vin     Z1      Z2        Y       X       VLC      HLC
   PY"
8270 IF EOF(2) THEN 8340
8280 INPUT #2, TIM,D1,D2,D3,D4,D5,D6,D7,D8,D9
8290 LPRINT USING "####.##"; TIM;
8300 LPRINT USING "+###.###"; D1,D2,D3,D4;
8310 LPRINT USING "+###.####"; D5;
8320 LPRINT USING "+#####.##"; 1000*D6,1000*D7,1000*D8
8330 GOTO 8270
8340 PRINT "END OF FILE"
8350 IF ACTIVE$="N" THEN CLOSE #2 ELSE CLOSE #2:OPEN "A",#1,FILENAM$
8360 PRINT "":PRINT ""
8370 INPUT " DO YOU WANT TO PRINT DISPLACEMENTS AND STRAINS (Y/N)? ", MD$
8380 IF MD$="N" THEN 8900
8390 IF M$="Y" THEN 8420
8400 INPUT " ENTER NAME OF FILE : ", FILENAM$
8410 INPUT " IS THIS AN ACTIVE FILE (Y/N)? ",ACTIVE$
8420 IF ACTIVE$="N" THEN OPEN "I",#2,FILENAM$ ELSE CLOSE #1:OPEN "I",#2,FILENAM$
8430 INPUT " DO YOU WANT TO STORE THE DATA ON DRIVE B FOR PLOTTING (Y/N)? ",MC$
8440 IF MC$="N" THEN 8490
8442 ON ERROR GOTO 0
8444 ON ERROR GOTO 11300
8450 PRINT "":PRINT " *** MAKE SURE THERE IS A DISC IN DRIVE B ***"
8460 PRINT "":PRINT " ENTER A FILE NAME FOR THE NEW FILE.  IT MUST BE DIFFERENT"
8470 INPUT " THAN THE SOURCE FILE NAME AND IT MUST BEGIN WITH B: ",COPYN$
8480 OPEN "O",#3,COPYN$
8490 A$= "  +#.##### +#.##### +##.### +##.##### +##.### +##.##### +##.### +##.##
###"
```

```
8500 GOSUB 9150    'read stone deflection data
8510 INPUT #2, T$,INCN,DT$,TM$,VST
8520 IF MC$="N" THEN 8540
8530 WRITE #3,T$,INCN,DT$,TM$,VST
8540 LPRINT "":LPRINT "":LPRINT ""
8550 LPRINT "  TEST NAME   : "; T$
8560 LPRINT "  DATE        : "; DT$
8570 LPRINT "  TIME        : "; TM$
8580 LPRINT "  INC. NUMBER : "; INCN
8590 LPRINT "  VER. STRESS (KSC) : "; VST
8600 LPRINT "  INITIAL SAMPLE HEIGHT (CM) :" ; H.INITIAL
8610 LPRINT ""
8620 LPRINT "  UNITS: (MIN,CM,%)
8630 LPRINT "                    Z1                    Y                X"
8640 LPRINT "  TIME     DISP    HEIGHT   STRAIN    DISP    STRAIN    DISP    STR
AIN   DELTA.Z"
8650 VL=VST*35!
8660 KL=1
8670 KL=KL+1
8680 IF VL>SL(KL) THEN 8670
8690 DSTONES=(SD(KL)-SD(KL-1))/(SL(KL)-SL(KL-1))*(VL-SL(KL-1))+SD(KL-1)
8700 IF EOF(2) THEN 8870
8710 INPUT #2, TIM,D1,D2,D3,D4,D5,D6,D7,D8,D9
8720 DISP.Z1=(D2-ZOZ1)*CFZ1/D1
8730 DISP.Z2=(D3-ZOZ2)*CFZ2/D1
8740 DISP.Y =(D4-ZOY)*CFY/D1
8750 DISP.X =(D5-ZOX)*CFX/D1
8760 DELTA.Z=DISP.Z1-DISP.Z2
8770 DISP.VER=.5188361*DISP.Z1+(1!-.5188361)*DISP.Z2-DSTONES
8780 HEIGHT=H.INITIAL-DISP.VER
8790 STRAIN.VER=DISP.VER/H.INITIAL*100!
8800 STRAIN.X =DISP.X/H.INITIAL*100!
8810 STRAIN.Y =DISP.Y/H.INITIAL*100!
8820 LPRINT USING "####.##";TIM;
8830 LPRINT USING A$;DISP.VER,HEIGHT,STRAIN.VER,DISP.Y,STRAIN.Y,DISP.X,STRAIN.X,
DELTA.Z
8840 IF MC$="N" THEN 8860
8850 WRITE #3, TIM,DISP.VER,HEIGHT,STRAIN.VER,DISP.Y,STRAIN.Y,DISP.X,STRAIN.X,DE
LTA.Z
8860 GOTO 8700
8870 PRINT "END OF FILE"
8880 CLOSE #3
8890 IF ACTIVE$="N" THEN CLOSE #2 ELSE CLOSE #2:OPEN "A",#1,FILENAM$
8900 ON ERROR GOTO 0
8910 ON ERROR GOTO 3
8920 II=0:DFLIP=1:$FLIP=1
8930 RETURN
```

```
8940 END
8950 REM ************************************************************
8960 REM *STONE DEFLECTION DATA; FOR SHEAR  -measured 9/17/1987 djd
8970 REM ************************************************************
8980 REM load(kg) vs deflection(cm)
8990 SL(1)=0! : SD(1)=0!
9000 SL(2)=4.375 : SD(2)=.00267
9010 SL(3)=8.75 : SD(3)=.004251
9020 SL(4)=17.5 : SD(4)=.005831
9030 SL(5)=26.25 : SD(5)=.006867
9040 SL(6)=35!: SD(6)=.007575
9050 SL(7)=52.5 : SD(7)=.00872
9060 SL(8)=70! : SD(8)=.009537
9070 SL(9)=105! : SD(9)=.010846
9080 SL(10)=140! : SD(10)=.011827
9090 SL(11)=175! : SD(11)=.012644
9100 SL(12)=210! : SD(12)=.013298
9110 SL(13)=350! : SD(13)=.014
9120 SL(14)=999
9130 P=14
9140 RETURN
9150 REM ************************************************************
9160 REM *STONE DEFLECTION DATA; FOR CONSOLIDATION -measured 9/17/1987 djd
9170 REM ********* average of z1 and z2 values    *********************
9180 REM load(kg) vs deflection(cm)
9190 SL(1)=0! : SD(1)=0!
9200 SL(2)=4.375 : SD(2)=.001454
9210 SL(3)=8.75 : SD(3)=.00302
9220 SL(4)=17.5 : SD(4)=.004296
9230 SL(5)=26.25 : SD(5)=.005277
9240 SL(6)=35!: SD(6)=.005647
9250 SL(7)=52.5 : SD(7)=.006443
9260 SL(8)=70! : SD(8)=.007107
9270 SL(9)=105! : SD(9)=.008063
9280 SL(10)=140! : SD(10)=8.833001E-03
9290 SL(11)=175! : SD(11)=.009549
9300 SL(12)=210! : SD(12)=.010158
9310 SL(13)=350! : SD(13)=.013
9320 SL(14)=999
9330 P=14
9340 RETURN
9350 REM ************************************************************************
9360 REM *  GAIN VALUE K
9370 REM ************************************************************************
9380 PRINT "":PRINT ""
9390 PRINT " *** CURRENT VALUE OF K : ";K
9400 INPUT " *** INPUT NEW VALUE ";K
```

```
 9410 PRINT " *** NEW VALUE OF K =";K
9420 INPUT " *** IS THIS CORRECT (Y/N) ";MALPHA$
9430 IF MALPHA$<>"Y" THEN 9380
9440 RETURN
9450 REM ************************************************************************
9460 REM *  GAIN VALUE A
9470 REM ************************************************************************
9480 PRINT "":PRINT ""
9490 PRINT " *** CURRENT VALUE OF A : ";A
9500 INPUT " *** INPUT NEW VALUE " ;A
9510 PRINT " *** NEW VALUE OF A = ";A
9520 INPUT " *** IS THIS CORRECT (Y/N) ";MSBETA$
9530 IF MSBETA$<>"Y" THEN 9480
9540 RETURN
9550 REM ************************************************************************
9560 REM *  GAIN VALUE B
9570 REM ************************************************************************
9580 PRINT "":PRINT ""
9590 PRINT " *** CURRENT VALUE OF B : ";B
9600 INPUT " *** INPUT NEW VALUE ";B
9610 PRINT " *** NEW VALUE OF B =";B
9620 INPUT " *** IS THIS CORRECT (Y/N) ";MSGAIN$
9630 IF MSGAIN$<>"Y" THEN 9590
9640 RETURN
9650 REM ************************************************************************
9660 REM  TEMPORARY PAUSE SUBROUTINE
9670 REM ************************************************************************
9680 PRINT " **** PAUSE IN THE EXECUTION, ENTER CONT TO CONTINUE ****"
9690 STOP
9700 RETURN
9710 REM ************************************************************************
9720 REM *  GAIN VALUE C
9730 REM ************************************************************************
9740 PRINT "":PRINT ""
9750 PRINT " *** CURRENT VALUE OF C : ";C
9760 INPUT " *** INPUT NEW VALUE ";C
9770 PRINT " *** NEW VALUE OF C =";C
9780 INPUT " *** IS THIS CORRECT (Y/N) ";MSGAIN$
9790 IF MSGAIN$<>"Y" THEN 9740
9800 RETURN
9810 REM ************************************************************************
9820 REM *  CUTOFF VOLTAGE FOR STABILIZING THE REGULATOR
9830 REM ************************************************************************
9840 PRINT "":PRINT ""
9850 PRINT " *** CURRENT CUTOFF VALUE : ";CUTOFF
9860 INPUT " *** INPUT NEW VALUE ";CUTOFF
9870 PRINT " *** NEW CUTOFF VALUE =";CUTOFF
```

```
9880 INPUT " *** IS THIS CORRECT (Y/N) ";MSGAIN$
9890 IF MSGAIN$<>"Y" THEN 9850
9900 RETURN
9910 REM ************************************************************************
9920 REM *  CF FOR THE Z DCDT
9930 REM ************************************************************************
9940 PRINT "":PRINT ""
9950 INPUT " *** ENTER Z DCDT CF ";CFZ
9960 PRINT " *** Z DCDT CF =";CFZ
9970 INPUT " *** IS THIS CORRECT (Y/N) ";MSGAIN$
9980 IF MSGAIN$<>"Y" THEN 9950
9990 RETURN
10000 END
10010 REM ************************************************************
10020 REM ** SUBROUTINE TO APPLY THE HORIZONTAL SHEAR SEATING LOAD
10030 REM ************************************************************
10040 CLS
10050 INPUT "*** ARE YOU SURE YOU WANT TO SET-UP THE Thc PISTON (Y/N)? ";INCM$
10060 IF INCM$ <> "Y" THEN RETURN
10070 TIMER OFF
10080 CLS
10090 PRINT ""
10100 PRINT " *** MAKE SURE YOU REMOVE THE PINS ****"
10110 PRINT ""
10120 SETT=2!
10130 CALL SET.RANGE(VDAC.B.01,R10)
10140 HSTART=1!
10150 CALL OUTPUT(VDAC.B.01,HSTART)
10160 CALL ENABLE.OUTPUT(VDAC.B.01)
10170 NN=8
10180 CALL OUTPUT(RELAY.MUX.01,NN)
10190 CALL SET.RANGE(DMM.01,R200MILLI)
10200 PRINT "CURRENT DAC VOLTAGE: "; HSTART
10210 INPUT "INPUT NEW VALUE    : "; HSTART
10220 CALL OUTPUT(VDAC.B.01,HSTART)
10230 CALL DELAY(SETT)
10240 CALL MEASURE(DMM.01,VOLTS)
10250 PRINT ""
10260 PRINT "HOR. SHEAR P.T. READING (mv)    : "; 1000*VOLTS
10270 INPUT "CONTINUE INCREASING LOAD (Y/N)? : "; M$
10280 IF M$ <> "N" THEN 10200
10290 INPUT "ENTER THE P.T. ZERO (mv) : "; ZOPT
10300 PRINT " ZOPT= "; ZOPT
10310 INPUT " IS THIS VALUE CORRECT(Y/N)? :"; P$
10320 IF P$ <> "Y" THEN 10290
10330 I1=0:DFLIP=1:SFLIP=1
10340 RETURN
```

```
10350 REM*****************************************************************
10360 REM    APPLICATION OF CONSOLIDATION SHEAR STRESS
10370 REM*****************************************************************
10380 CLS
10390 INPUT " *** ARE YOU SURE YOU WANT A NEW Thc INCREMENT (Y/N)? ";INCM$
10400 IF INCM$ <> "Y" THEN RETURN
10410 TIMER OFF
10420 REM   ********** first check the input voltage
10430 CALL SET.RANGE(DMM.01,R20)
10440 NN=1
10450 CALL OUTPUT(RELAY.MUX.01,NN)
10460 SETT=.2
10470 CALL DELAY(SETT)
10480 CALL MEASURE(DMM.01,VINPUT)
10490 IF VINPUT>5! THEN 10530
10500 PRINT "******** INPUT VOLTAGE IS LESS THAN 5 VOLTS, IT IS = ";VINPUT
10510 STOP
10520 GOTO 10420
10530 SWITCH=0
10540 PRINT ""
10550 PRINT " *** INPUT DATA FOR Thc INCREMENT ***"
10560 PRINT "           (UNITS: KSC)"
10570 PRINT ""
10580 INPUT "        1. HORIZONTAL SHEAR STRESS: ",HSTRESS
10590 IF SWITCH=1 GOTO 10620
10600 INPUT "        2. GAIN ON THE HORIZ STRESS REGULATOR: ",HSGAIN
10610 REM
10620 CLS
10630 STRESS.RATIO=HSTRESS/VSTRESS
10640 PRINT " *** CAREFULLY CHECK THESE NUMBERS ***"
10650 PRINT "           (UNITS: KSC)"
10660 PRINT ""
10670 PRINT "        1. HORIZONTAL SHEAR STRESS: ",HSTRESS
10680 PRINT "        2. GAIN ON THE HORIZ STRESS REGULATOR: ",HSGAIN
10690 PRINT "        3. HORIZONTAL TO VERTICAL STESS RATIO: ",STRESS.RATIO
10700 PRINT ""
10710 INPUT " *** ARE THERE ANY CORRECTIONS (Y/N)? ",COOR$
10720 IF COOR$="N" THEN 10780
10730 SWITCH=1
10740 INPUT " *** WHICH NUMBER IS INCORRECT (1 or 2)? ",ITUM
10750 IF ITUM>2 THEN 10740
10760 CLS
10770 ON ITUM GOTO 10580,10600
10780 IF HSTRESS>2.4 OR HSTRESS<.01 THEN 10620
10790 PRINT ""
10800 PRINT " *** PRESS ANY KEY WHEN READY"
10810 INPUT "     THE LOAD WILL BE APPLIED IN 5sec ";R$
```

```
10820 HWAIT=5!
10830 CALL DELAY(HWAIT)
10840 BEEP
10850 NUM=8
10860 CALL SET.RANGE(DMM.01,R200MILLI)
10870 CALL OUTPUT(RELAY.MUX.01,NUM)
10880 HOR.AIR.PRESS=HSTRESS*35!*2.205/2.881     'EFFECTIVE AREA PISTON=2.881
10890 REQ.HOR.VOLT=(HOR.AIR.PRESS*VINPUT/CFPT+ZOPT)/1000!
10900 DAC.HOR.VOLT=(CFHSR*HOR.AIR.PRESS)/(HSGAIN-1) + 3!
10910 HALPHA=100            '********* MAY NEED TO PLAY WITH THIS
10920 PRINT "    REQ.HOR.VOLT  :"; REQ.HOR.VOLT
10930 PRINT "    DAC.HOR.VOLT  :"; DAC.HOR.VOLT
10940 NN=8
10950 CALL OUTPUT(RELAY.MUX.01,NN)
10960 CALL SET.RANGE(DMM.01,R200MILLI)
10970 KH=1
10980 SETT=.15
10990 ICHECK=0
11000 REM ****** SERVO LOOP TO APPLY THE HORIZONTAL STRESS
11010 CALL OUTPUT(VDAC.B.01,DAC.HOR.VOLT)
11020 WHILE HH
11030 CALL DELAY(SETT)
11040 CALL MEASURE(DMM.01,VOLTS)
11050 DELTA.VOLTS=REQ.HOR.VOLT-VOLTS
11060 IF ABS(DELTA.VOLTS) < .0001 THEN ICHECK=ICHECK+1
11070 PRINT "PT       :";
11080 PRINT USING "####.##"; 1000*VOLTS;
11090 PRINT "      DAC.HOR.VOLT  : ";
11100 PRINT USING "###.###"; DAC.HOR.VOLT
11110 PRINT "ICHECK   :";ICHECK
11120 IF ICHECK > 3 THEN 11170
11130 DAC.HOR.VOLT=DAC.HOR.VOLT+(DELTA.VOLTS*HALPHA)
11140 CALL OUTPUT(VDAC.B.01,DAC.HOR.VOLT)
11150 WEND
11160 BEEP
11170 PRINT " *** OUT OF POWER UP"
11180 II=0:DFLIP=1:SFLIP=1
11190 RETURN
11200 REM ************************************************************************
11210 REM   PARTIAL ERROR HANDLING SUBROUTINE
11215 REM     - for reading prel*.dat file and consolidation channel reading
11217 REM       files c*con*.dat.  All have the name FILENAM$
11220 REM ************************************************************************
11230 PRINT "BASIC error # ";ERR;"occurred in line ";ERL
11240 INPUT " ENTER THE CORRECT FILE NAME:"; FILENAM$
11250 INPUT " ENTER C WHEN READY TO CONTINUE :"; CE$
11260 RESUME
```

```
 11270 RETURN
11300 REM ************************************************************************
11310 REM   PARTIAL ERROR HANDLING SUBROUTINE
11315 REM     - for opening the consolidation strains output data file
11317 REM       c*con*.prn on the B: drive.  All have the name COPYN$.
11320 REM ************************************************************************
11330 PRINT "BASIC error # ";ERR;"occurred in line ";ERL
11340 INPUT " ENTER THE CORRECT FILE NAME:"; COPYN$
11350 INPUT " ENTER C WHEN READY TO CONTINUE :"; CE$
11360 RESUME
11370 RETURN
```

```
10 REM
20 REM MDSS REDUCTION PROGRAM MDSSCKO   BY DJD 1988
30 REM
40 DIM VIN(300),Z1(300),Z2(300),X(300),Y(300),VLC(300),HLC(300),DV(300)
50 DIM GX(300),TH.SHEAR(300),EU(300),MC(300),DELTA.H(300),DELTA.U(300)
60 DIM VS(300),MS(20),MR(20),SL(20),SD(20),Z(300),DELTA.Z(300)
70 CLS
80 INPUT " *** ENTER NAME OF THE DATA FILE : "; FILENAM$
90 OPEN "I",#1,FILENAM$
100 INPUT #1, TESTN$,D$,T$
110 INPUT #1, ZOVLC,CFVLC,CFZ1,CFZ2,CFY,CFX
120 PRINT "":PRINT "":PRINT ""
130 INPUT " *** DO YOU WANT TO PRINT DATA READINGS (Y/N)? "; M1$
140 IF M1$="N" THEN 370
150 LPRINT "":LPRINT ""
160 LPRINT "   TEST NAME : "; TESTN$
170 LPRINT "   DATE      : "; D$
180 LPRINT ""
190 LPRINT "   CHANNEL READINGS DURING SHEAR"
200 LPRINT "   UNITS : (MIN,VOLTS,mVOLTS)
210 LPRINT "   TIME    Vin     Z1      Z2      Z       Y       X     VLC
 HLC    DV"
220 LPRINT "   (MIN)   (V)    (V)     (V)     (V)     (V)     (V)     (mV)
(mV)   (mv)"
230 IC=1
240 IF EOF(1) THEN 350
250 REM FOR IC=1 TO 4
260 INPUT #1, TIM,VIN(IC),Z1(IC),Z2(IC),Y(IC),X(IC),VLC(IC),HLC(IC),Z(IC),DV(IC)
270 VLC(IC)=1000!*VLC(IC):HLC(IC)=1000!*HLC(IC)
280 LPRINT USING "####.##"; TIM;
290 LPRINT USING "+###.###"; VIN(IC),Z1(IC),Z2(IC);
300 LPRINT USING "+###.####";Z(IC),Y(IC),X(IC);
310 LPRINT USING "+###.##"; VLC(IC),HLC(IC),1000*DV(IC)
320 IC=IC+1
330 GOTO 240
340 REM NEXT IC
350 PRINT " *** END OF FILE "
360 FILELEN=IC-1
370 INPUT " *** DO YOU WANT TO REDUCE THE DATA (Y/N)? "; M2$
380 IF M2$="N" THEN 2660
390 PRINT "":PRINT ""
400 PRINT " *** MAKE SURE THAT THE MEMBRANE AND STONE DEFLECTION"
410 PRINT "     CORRECTIONS STORED IN THE PROGRAM ARE CORRECT."
420 INPUT "     PRESS ANY LETTER KEY TO CONTINUE. "; M$
430 IF M1$="Y" THEN 510
440 IC=1
450 IF EOF(1) THEN 500
```

```
460 INPUT #1, TIM,VIN(IC),Z1(IC),Z2(IC),Y(IC),X(IC),VLC(IC),HLC(IC),Z(IC),DV(IC)
470 VLC(IC)=1000!*VLC(IC):HLC(IC)=1000!*HLC(IC)
480 IC=IC+1
490 GOTO 450
500 FILELEN=IC-1
510 REM  assign and compute additional zeros/variables
520 GOSUB 2680    ' stone deflections
530 ZOZ1=Z1(1)
540 ZOZ2=Z2(1)
550 ZOHLC=HLC(1)
560 ZOX=X(1)
570 ZOY=Y(1)
580 ZOZ=Z(1)
590 OCR=1!
600 TC=1.15
610 AREA=35!      'cm^2
620 TMAX=0!
630 CFHLC=6.70298
640 CFZ=.3014
650 VL=(VLC(1)-ZOVLC)*CFVLC/VIN(1)+TC
660 VS(1)=VL/AREA
670 V.C.S=VS(1)
680 K=1
690 K=K+1
700 IF VL>SL(K) THEN 690
710 DSTONES=(SD(K)-SD(K-1))/(SL(K)-SL(K-1))*(VL-SL(K-1))+SD(K-1)
720 S1=DSTONES
730 REM
740 PRINT " *** REDUCTION DATA ****
750 PRINT ""
760 PRINT "   1. TEST NAME : "; TESTN$
770 PRINT "   2. DATE      : "; D$
780 PRINT "   3. OCR       : "; OCR
790 PRINT "   4. VER. CONSOLIDATION STRESS (KSC) : "; V.C.S
800 PRINT "   5. HOR. CONSOLIDATION STRESS (KSC) : "; H.C.S
810 PRINT "   6. PRE-SHEAR SAMPLE HEIGHT (cm)    : "; H.SHEAR
820 PRINT "":PRINT "":PRINT ""
830 INPUT " *** PRESS ANY LETTER KEY TO CONTINUE: "; M$
840 CLS
850 PRINT "":PRINT ""
860 PRINT "   7. VERTICAL STRESS LOAD CELL:"
870 PRINT "            ZERO: "; ZOVLC
880 PRINT "              CF: "; CFVLC
890 PRINT "   8. HORIZONTAL SHEAR LOAD CELL:"
900 PRINT "            ZERO: "; ZOHLC
910 PRINT "              CF: "; CFHLC
920 PRINT "   9. HORIZONTAL DISP. TRANSDUCER, X:"
```

```
930 PRINT "            ZERO: "; ZOX
940 PRINT "              CF: "; CFX
950 PRINT "  10. HORIZONTAL DISP. TRANSDUCER, Y:"
960 PRINT "            ZERO: "; ZOY
970 PRINT "              CF: "; CFY
980 PRINT "  11. VERTICAL DISP. TRANSDUCER, Z1:"
990 PRINT "            ZERO: "; ZOZ1
1000 PRINT "             CF: "; CFZ1
1010 PRINT "  12. VERTICAL DISP. TRANSDUCER, Z2:"
1020 PRINT "            ZERO: "; ZOZ2
1030 PRINT "             CF: "; CFZ2
1040 PRINT "  13. CONSTANT HEIGHT TRANSDUCER, Z:"
1050 PRINT "            ZERO: "; ZOZ
1060 PRINT "             CF: "; CFZ
1070 PRINT ""
1080 INPUT "  *** ARE THERE ANY CORRECTIONS? "; M$
1090 IF M$="N" THEN 1550
1100 INPUT "  *** WHICH ITEM NUMBER IS INCORRECT (1,2,...,13)? "; ITNUM
1110 IF ITNUM>13 THEN 1100
1120 CLS
1130 PRINT "":PRINT ""
1140 ON ITNUM GOTO 1150,1170,1190,1210,1230,1250,1270,1310,1350,1390,1430,1470,1
510
1150 INPUT "   1. TEST NAME : "; TESTN$
1160 GOTO 740
1170 INPUT "   2. DATE      : "; D$
1180 GOTO 740
1190 INPUT "   3. OCR       : "; OCR
1200 GOTO 740
1210 INPUT "   4. VER. CONSOLIDATION STRESS (KSC) : "; V.C.S
1220 GOTO 740
1230 INPUT "   5. HOR. CONSOLIDATION STRESS (KSC) : "; H.C.S
1240 GOTO 740
1250 INPUT "   6. PRE-SHEAR SAMPLE HEIGHT (cm)    : "; H.SHEAR
1260 GOTO 740
1270 PRINT "   7. VERTICAL STRESS LOAD CELL:"
1280 INPUT "            ZERO: "; ZOVLC
1290 INPUT "              CF: "; CFVLC
1300 GOTO 740
1310 PRINT "   8. HORIZONTAL SHEAR LOAD CELL:"
1320 INPUT "            ZERO: "; ZOHLC
1330 INPUT "              CF: "; CFHLC
1340 GOTO 740
1350 PRINT "   9. HORIZONTAL DISP. TRANSDUCER, X:"
1360 INPUT "            ZERO: "; ZOX
1370 INPUT "              CF: "; CFX
1380 GOTO 740
```

```
1390 PRINT "  10. HORIZONTAL DISP. TRANSDUCER, Y:"
1400 INPUT "            ZERO: "; ZOY
1410 INPUT "              CF: "; CFY
1420 GOTO 740
1430 PRINT "  11. VERTICAL DISP. TRANSDUCER, Z1:"
1440 INPUT "            ZERO: "; ZOZ1
1450 INPUT "              CF: "; CFZ1
1460 GOTO 740
1470 PRINT "  12. VERTICAL DISP. TRANSDUCER, Z2:"
1480 INPUT "            ZERO: "; ZOZ2
1490 INPUT "              CF: "; CFZ2
1500 GOTO 740
1510 PRINT "  13. CONSTANT HEIGHT TRANSDUCER, Z:"
1520 INPUT "            ZERO: "; ZOZ
1530 INPUT "              CF: "; CFZ
1540 GOTO 740
1550 REM print reduction data
1560 'GOTO 4305   TEMPORARY ****************
1570 LPRINT "":LPRINT ""
1580 LPRINT "*************************************************************************
*************
1590 LPRINT ""
1600 LPRINT "                          Ko CONSOLIDATED MOSS TEST"
1610 LPRINT "                            MIT GEOTECHNICAL LAB"
1620 LPRINT ""
1630 LPRINT "*************************************************************************
*************
1640 LPRINT ""
1650 LPRINT "   FILE NAME: "; FILENAM$
1660 LPRINT ""
1670 LPRINT "-----------------------------------------------------------------
-----------"
1680 LPRINT ""
1690 LPRINT "                          REDUCTION DATA"
1700 LPRINT "                     UNITS: (kg,cm,mVOLTS,VOLTS)"
1710 LPRINT ""
1720 LPRINT "   1. TEST NAME : "; TEST N$
1730 LPRINT "   2. DATE      : "; D$
1740 LPRINT "   3. OCR       : "; OCR
1750 LPRINT "   4. VER. CONSOLIDATION STRESS (KSC) : ";
1760 LPRINT USING "+##.###"; V.C.S
1770 LPRINT "   5. HOR. CONSOLIDATION STRESS (KSC) : ";
1780 LPRINT USING "+##.###"; H.C.S
1790 LPRINT "   6. PRE-SHEAR SAMPLE HEIGHT (cm)    : ";
1800 LPRINT USING "+##.####"; H.SHEAR
1810 LPRINT ""
1820 LPRINT "   7. VERTICAL STRESS LOAD CELL:"
```

```
 1840 LPRINT "              CF: "; CFVLC
1850 LPRINT "   8. HORIZONTAL SHEAR LOAD CELL:"
1860 LPRINT "            ZERO: "; ZOHLC
1870 LPRINT "              CF: "; CFHLC
1880 LPRINT "   9. HORIZONTAL DISP. TRANSDUCER, X:"
1890 LPRINT "            ZERO: "; ZOX
1900 LPRINT "              CF: "; CFX
1910 LPRINT "  10. HORIZONTAL DISP. TRANSDUCER, Y:"
1920 LPRINT "            ZERO: "; ZOY
1930 LPRINT "              CF: "; CFY
1940 LPRINT "  11. VERTICAL DISP. TRANSDUCER, Z1:"
1950 LPRINT "            ZERO: "; ZOZ1
1960 LPRINT "              CF: "; CFZ1
1970 LPRINT "  12. VERTICAL DISP. TRANSDUCER, Z2:"
1980 LPRINT "            ZERO: "; ZOZ2
1990 LPRINT "              CF: "; CFZ2
2000 LPRINT "  13. CONSTANT HEIGHT TRANSDUCER, Z:"
2010 LPRINT "            ZERO: "; ZOZ
2020 LPRINT "              CF: "; CFZ
2030 LPRINT ""
2040 REM
2050 LPRINT "":LPRINT "":LPRINT ""
2060 LPRINT " Pt. Str.X   Str.Y  TauH   DelU    SigV    TauH   TauH     Eu     T
auH    SigV "
2070 LPRINT " No.  (%)     (%)   ----   ----    ----    ----   ----     --     -
---    ---- "
2080 LPRINT "                    SigVc  SigVc   SigVc   SigV    Su      Su     S
igVm   SigVm "
2090 CLOSE #1
2100 INPUT " *** ENTER A FILE NAME FOR THE REDUCED DATA : "; FILOUT$
2110 OPEN "O", #1, FILOUT$
2120 FOR I= 1 TO FILELEN
2130 GX(I)=(X(I)-ZOX)*CFX/VIN(I)/H.SHEAR*100!
2140 REM *** menbrane and friction correction - changed 2/9/1988
2150 REM *** friction=0.0017 ksc/% strain
2160 REM *** membrane correction=0.00075 ksc/% strain
2170 MC(I)=.0017+.00075*GX(I)
2180 TH.SHEAR(I)=(HLC(I)-ZOHLC)*CFHLC/VIN(I)/AREA-MC(I)
2190 IF GX(I)=0! THEN EU(I)=9999 : GOTO 2230
2200 EU(I)=300!*TH.SHEAR(I)/GX(I)
2210 IF EU(I)>9999 THEN EU(I)=9999!
2220 IF EU(I)<-9999 THEN EU(I)=-9999
2230 IF TH.SHEAR(I)>T.MAX THEN T.MAX=TH.SHEAR(I)
2240 NEXT I
2250 A$= "### +##.### +##.### +.### +#.###  +#.###  +.###  +#.### +####.#  +#.##
#  +#.###"
2260 FOR I=1 TO FILELEN
```

```
2270 VL=(VLC(I)-ZOVLC)*CFVLC/VIN(I)+TC
2280 VS(I)=VL/AREA
2290 DELTA.U(I)=V.C.S-VS(I)
2300 REM *** stone defections
2310 K=1
2320 K=K+1
2330 IF VL>SL(K) THEN 2320
2340 DSTONES=(SD(K)-SD(K-1))/(SL(K)-SL(K-1))*(VL-SL(K-1))+SD(K-1)
2350 DZ1=(Z1(I)-ZOZ1)*CFZ1/VIN(I)
2360 DZ1.EDGE=(.743151*DZ1+(1!-.743151)*DZ2)-(DSTONES-S1)
2370 DZ2=(Z2(I)-ZOZ2)*CFZ2/VIN(I)
2380 DZ2.EDGE=(.294521*DZ1+(1!-.294521)*DZ2)-(DSTONES-S1)
2390 DMIDDLE=.5188361*DZ1+(1!-.5188361)*DZ2
2400 DMID.STN=DMIDDLE-(DSTONES-S1)
2410 DELTA.H(I)=DMID.STN/H.SHEAR*100!
2420 DELTA.Z(I)=DV(I)*CFZ/VIN(I)/H.SHEAR*100!
2430 GY=(Y(I)-ZOY)*CFY/VIN(I)/H.SHEAR*100!
2440 TH.N=TH.SHEAR(I)/V.C.S
2450 DELTAU.N=DELTA.U(I)/V.C.S
2460 VS.N=VS(I)/V.C.S
2470 TH.VS.N=TH.SHEAR(I)/VS(I)
2480 TH.SU.N=TH.SHEAR(I)/T.MAX
2490 EU.N=EU(I)/T.MAX
2500 IF EU.N>9999! THEN EU.N=9999!
2510 IF EU.N<-9999! THEN EU.N=-9999!
2520 OT=TH.N/OCR
2530 OS=VS.N/OCR
2540 LPRINT USING A$;I,GX(I),GY,TH.N,DELTAU.N,VS.N,TH.VS.N,TH.SU.N,EU.N,OT,OS
2550 WRITE #1,I,GX(I),GY,TH.N,DELTAU.N,VS.N,TH.VS.N,TH.SU.N,EU.N,OT,OS,DZ1.EDGE,
DZ2.EDGE,DMID.STN,DV(I)
2560 NEXT I
2570 CLOSE #1
2580 LPRINT "":LPRINT "":LPRINT "":LPRINT ""
2590 LPRINT " Pt.    Str.X     SigV     TauH     DelU      Eu      Membr    Delta
.H    Delta.Z"
2600 LPRINT " No.     (%)                                        Corr      (%)
       (%)"
2610 B$=   "###    +##.###   ##.###   +#.###   +#.###  +####.#  +#.###    +#.###
     +#.###"
2620 REM
2630 FOR I= 1 TO FILELEN
2640 LPRINT USING B$;I,GX(I),VS(I),TH.SHEAR(I),DELTA.U(I),EU(I),MC(I),DELTA.H(I)
,DELTA.Z(I)
2650 NEXT I
2660 PRINT "":PRINT "":PRINT "  *** THE END ****
2670 END
2680 REM ************************************************************************
```

```
2690 REM * STONE DEFLECTIONS - measured by DJD 9/17/1987
2700 REM ************************************************************************
2710 REM load(kg) vs deflection(cm)
2720 SL(1)=0! : SD(1)=0!
2730 SL(2)=4.375 : SD(2)=.00267
2740 SL(3)=8.75  : SD(3)=.004251
2750 SL(4)=17.5  : SD(4)=.005831
2760 SL(5)=26.25 : SD(5)=.006867
2770 SL(6)=35!   : SD(6)=.007575
2780 SL(7)=52.5  : SD(7)=.00872
2790 SL(8)=70!   : SD(8)=.009537
2800 SL(9)=105! : SD(9)=.010846
2810 SL(10)=140!: SD(10)=.011827
2820 SL(11)=175!: SD(11)=.012644
2830 SL(12)=210!: SD(12)=.013298
2840 SL(13)=350! : SD(13)=.014
2850 SL(14)=999
2860 P=14
2870 RETURN
```

```
10 REM
20 REM MDSS REDUCTION PROGRAM MDSSCAU  BY DJD 1988
30 REM
40 DIM VIN(300),Z1(300),Z2(300),X(300),Y(300),VLC(300),HLC(300),DV(300)
50 DIM GX(300),TH.SHEAR(300),EU(300),X.SHEAR(300),DELTA.H(300),DELTA.U(300)
60 DIM VS(300),SL(20),SD(20),Z(300),DELTA.Z(300)
70 CLS
80 INPUT " *** ENTER NAME OF THE DATA FILE : "; FILENAM$
90 OPEN "I",#1,FILENAM$
100 INPUT #1, TESTN$,D$,T$
110 INPUT #1, ZOVLC,CFVLC,CFZ1,CFZ2,CFY,CFX
120 PRINT "":PRINT "":PRINT ""
130 INPUT " *** DO YOU WANT TO PRINT DATA READINGS (Y/N)? "; M1$
140 IF M1$="N" THEN 370
150 LPRINT "":LPRINT ""
160 LPRINT "   TEST NAME : "; TESTN$
170 LPRINT "   DATE      : "; D$
180 LPRINT ""
190 LPRINT "   CHANNEL READINGS DURING SHEAR"
200 LPRINT "   UNITS : (MIN,VOLTS,mVOLTS)
210 LPRINT "   TIME    Vin     Z1      Z2       Z        Y        X      VLC
 HLC    DV"
220 LPRINT "   (MIN)   (V)    (V)     (V)      (V)      (V)      (V)     (mV)
(mV)   (mv)"
230 IC=1
240 IF EOF(1) THEN 350
250 REM FOR IC=1 TO 4
260 INPUT #1, TIM,VIN(IC),Z1(IC),Z2(IC),Y(IC),X(IC),VLC(IC),HLC(IC),Z(IC),DV(IC)
270 VLC(IC)=1000!*VLC(IC):HLC(IC)=1000!*HLC(IC)
280 LPRINT USING "####.##"; TIM;
290 LPRINT USING "+###.###"; VIN(IC),Z1(IC),Z2(IC);
300 LPRINT USING "+###.####";Z(IC),Y(IC),X(IC);
310 LPRINT USING "+###.##"; VLC(IC),HLC(IC),1000*DV(IC)
320 IC=IC+1
330 GOTO 240
340 REM NEXT IC
350 PRINT " *** END OF FILE "
360 FILELEN=IC-1
370 INPUT " *** DO YOU WANT TO REDUCE THE DATA (Y/N)? "; M2$
380 IF M2$="N" THEN 2760
390 PRINT "":PRINT ""
400 PRINT " *** MAKE SURE THAT THE MEMBRANE AND STONE DEFLECTION"
410 PRINT "     CORRECTIONS STORED IN THE PROGRAM ARE CORRECT."
420 INPUT "     PRESS ANY LETTER KEY TO CONTINUE. "; M$
430 IF M1$="Y" THEN 510
440 IC=1
450 IF EOF(1) THEN 500
```

```
460 INPUT #1, TIM,VIN(IC),Z1(IC),Z2(IC),Y(IC),X(IC),VLC(IC),HLC(IC),Z(IC),DV(IC)
470 VLC(IC)=1000!*VLC(IC):HLC(IC)=1000!*HLC(IC)
480 IC=IC+1
490 GOTO 450
500 FILELEN=IC-1
510 REM  assign and compute additional zeros/variables
520 GOSUB 2780    ' stone deflections
530 ZOZ1=Z1(1)
540 ZOZ2=Z2(1)
550 ZOHLC=HLC(1)
560 ZOX=X(1)
570 ZOY=Y(1)
580 ZOZ=Z(1)
590 OCR=1!
600 TC=1.15
610 AREA=35!      'cm^2
620 TMAX=0!
630 CFHLC=6.70298
640 CF2=.3014
650 VL=(VLC(1)-ZOVLC)*CFVLC/VIN(1)+TC
660 VS(1)=VL/AREA
670 V.C.S=VS(1)
680 K=1
690 K=K+1
700 IF VL>SL(K) THEN 690
710 DSTONES=(SD(K)-SD(K-1))/(SL(K)-SL(K-1))*(VL-SL(K-1))+SD(K-1)
720 S1=DSTONES
730 REM
740 PRINT " *** REDUCTION DATA ****"
750 PRINT ""
760 PRINT "   1. TEST NAME : "; TESTN$
770 PRINT "   2. DATE      : "; D$
780 PRINT "   3. OCR       : "; OCR
790 PRINT "   4. VER. CONSOLIDATION STRESS (KSC) : "; V.C.S
800 PRINT "   5. HOR. CONSOLIDATION STRESS (KSC) : "; H.C.S
810 PRINT "   6. PRE-SHEAR SAMPLE HEIGHT (cm)    : "; H.SHEAR
820 PRINT "":PRINT "":PRINT ""
830 INPUT " *** PRESS ANY LETTER KEY TO CONTINUE: "; M$
840 CLS
850 PRINT "":PRINT ""
860 PRINT "   7. VERTICAL STRESS LOAD CELL:"
870 PRINT "            ZERO: "; ZOVLC
880 PRINT "              CF: "; CFVLC
890 PRINT "   8. HORIZONTAL SHEAR LOAD CELL:"
900 PRINT "            ZERO: "; ZOHLC
910 PRINT "              CF: "; CFHLC
920 PRINT "   9. HORIZONTAL DISP. TRANSDUCER, X:"
```

```
930 PRINT "            ZERO: "; ZOX
940 PRINT "              CF: "; CFX
950 PRINT "  10. HORIZONTAL DISP. TRANSDUCER, Y:"
960 PRINT "            ZERO: "; ZOY
970 PRINT "              CF: "; CFY
980 PRINT "  11. VERTICAL DISP. TRANSDUCER, Z1:"
990 PRINT "            ZERO: "; ZOZ1
1000 PRINT "             CF: "; CFZ1
1010 PRINT "  12. VERTICAL DISP. TRANSDUCER, Z2:"
1020 PRINT "            ZERO: "; ZOZ2
1030 PRINT "             CF: "; CFZ2
1040 PRINT "  13. CONSTANT HEIGHT TRANSDUCER, Z:"
1050 PRINT "            ZERO: "; ZOZ
1060 PRINT "             CF: "; CFZ
1070 PRINT ""
1080 INPUT "  *** ARE THERE ANY CORRECTIONS? "; M$
1090 IF M$="N" THEN 1550
1100 INPUT "  *** WHICH ITEM NUMBER IS INCORRECT (1,2,...,13)? "; ITNUM
1110 IF ITNUM>13 THEN 1100
1120 CLS
1130 PRINT "":PRINT ""
1140 ON ITNUM GOTO 1150,1170,1190,1210,1230,1250,1270,1310,1350,1390,1430,1470,1
510
1150 INPUT "   1. TEST NAME : "; TESTN$
1160 GOTO 740
1170 INPUT "   2. DATE      : "; D$
1180 GOTO 740
1190 INPUT "   3. OCR       : "; OCR
1200 GOTO 740
1210 INPUT "   4. VER. CONSOLIDATION STRESS (KSC) : "; V.C.S
1220 GOTO 740
1230 INPUT "   5. HOR. CONSOLIDATION STRESS (KSC) : "; H.C.S
1240 GOTO 740
1250 INPUT "   6. PRE-SHEAR SAMPLE HEIGHT (cm)    : "; H.SHEAR
1260 GOTO 740
1270 PRINT "   7. VERTICAL STRESS LOAD CELL:"
1280 INPUT "            ZERO: "; ZOVLC
1290 INPUT "              CF: "; CFVLC
1300 GOTO 740
1310 PRINT "   8. HORIZONTAL SHEAR LOAD CELL:"
1320 INPUT "            ZERO: "; ZOHLC
1330 INPUT "              CF: "; CFHLC
1340 GOTO 740
1350 PRINT "   9. HORIZONTAL DISP. TRANSDUCER, X:"
1360 INPUT "            ZERO: "; ZOX
1370 INPUT "              CF: "; CFX
1380 GOTO 740
```

```
1390 PRINT "  10. HORIZONTAL DISP. TRANSDUCER, Y:"
1400 INPUT "            ZERO: "; ZOY
1410 INPUT "              CF: "; CFY
1420 GOTO 740
1430 PRINT "  11. VERTICAL DISP. TRANSDUCER, Z1:"
1440 INPUT "            ZERO: "; ZOZ1
1450 INPUT "              CF: "; CFZ1
1460 GOTO 740
1470 PRINT "  12. VERTICAL DISP. TRANSDUCER, Z2:"
1480 INPUT "            ZERO: "; ZOZ2
1490 INPUT "              CF: "; CFZ2
1500 GOTO 740
1510 PRINT "  13. CONSTANT HEIGHT TRANSDUCER, Z:"
1520 INPUT "            ZERO: "; ZOZ
1530 INPUT "              CF: "; CFZ
1540 GOTO 740
1550 REM print reduction data
1560 REM
1570 LPRINT "":LPRINT ""
1580 LPRINT "*************************************************************************
*************
1590 LPRINT ""
1600 LPRINT "           ANISOTROPICALLY CONSOLIDATED MDSS TEST"
1610 LPRINT "                    MIT GEOTECHNICAL LAB"
1620 LPRINT ""
1630 LPRINT "*************************************************************************
*************
1640 LPRINT ""
1650 LPRINT "   FILE NAME: "; FILENAM$
1660 LPRINT ""
1670 LPRINT "-------------------------------------------------------------------
------------"
1680 LPRINT ""
1690 LPRINT "                        REDUCTION DATA"
1700 LPRINT "                  UNITS: (kg,cm,mVOLTS,VOLTS)"
1710 LPRINT ""
1720 LPRINT "   1. TEST NAME : "; TEST N$
1730 LPRINT "   2. DATE      : "; D$
1740 LPRINT "   3. OCR       : "; OCR
1750 LPRINT "   4. VER. CONSOLIDATION STRESS (KSC) : ";
1760 LPRINT USING "+##.###"; V.C.S
1770 LPRINT "   5. HOR. CONSOLIDATION STRESS (KSC) : ";
1780 LPRINT USING "+##.###"; H.C.S
1790 LPRINT "   6. PRE-SHEAR SAMPLE HEIGHT (cm)    : ";
1800 LPRINT USING "+##.####"; H.SHEAR
1810 LPRINT ""
1820 LPRINT "   7. VERTICAL STRESS LOAD CELL:"
```

```
 1840 LPRINT "              CF: "; CFVLC
1850 LPRINT "   8. HORIZONTAL SHEAR LOAD CELL:"
1860 LPRINT "            ZERO: "; ZOHLC
1870 LPRINT "              CF: "; CFHLC
1880 LPRINT "   9. HORIZONTAL DISP. TRANSDUCER, X:"
1890 LPRINT "            ZERO: "; ZOX
1900 LPRINT "              CF: "; CFX
1910 LPRINT "  10. HORIZONTAL DISP. TRANSDUCER, Y:"
1920 LPRINT "            ZERO: "; ZOY
1930 LPRINT "              CF: "; CFY
1940 LPRINT "  11. VERTICAL DISP. TRANSDUCER, Z1:"
1950 LPRINT "            ZERO: "; ZOZ1
1960 LPRINT "              CF: "; CFZ1
1970 LPRINT "  12. VERTICAL DISP. TRANSDUCER, Z2:"
1980 LPRINT "            ZERO: "; ZOZ2
1990 LPRINT "              CF: "; CFZ2
2000 LPRINT "  13. CONSTANT HEIGHT TRANSDUCER, Z:"
2010 LPRINT "            ZERO: "; ZOZ
2020 LPRINT "              CF: "; CFZ
2030 REM *** additional input data required
2040 PRINT "":PRINT ""
2050 INPUT "   ENTER TEST ANGLE THETA (degrees): ";THETA
2060 INPUT "   ENTER TOTAL X DISPLACEMENT DURING CONSOLIDATION (cm): "; X.CON
2070 INPUT "   ENTER NAME OF FILE FOR REDUCED DATA: ";FILERED$
2080 CLOSE #1
2090 OPEN "O", #1, FILERED$
2100 LPRINT "  14. TEST ANGLE THETA: "; THETA
2110 LPRINT "      TOTAL X DISP. DURING CONSOLIDATION: "; X.CON
2120 LPRINT ""
2130 REM
2140 LPRINT "":LPRINT "":LPRINT ""
2150 LPRINT " Pt. Str.X   Str.Y  TauH   DelU    SigV    TauH   TauH     Eu     T
auH    SigV "
2160 LPRINT " No.  (%)     (%)   ----   ----    ----    ----   ----     --     -
---    ---- "
2170 LPRINT "                    SigVc  SigVc   SigVc   SigV    Su      Su     S
igVm   SigVm "
2180 THETA.RAD=THETA*3.1416/180!   'convert theta to radians
2190 FOR I= 1 TO FILELEN
2200 GX(I)=(X(I)-ZOX)*CFX/VIN(I)/H.SHEAR*100!
2210 X.SHEAR(I)=X.CON+(X(I)-ZOX)*CFX/VIN(I)
2220 REM *** menbrane and friction correction - changed 2/9/1988
2230 REM *** friction=0.0017 ksc
2240 REM *** membrane resistance=0.0394 ksc/cm
2250 REM *** corrections are made to the x component only
2260 TH.SHEAR(I)=(H.C.S)*COS(THETA.RAD)+((HLC(I)-ZOHLC)*CFHLC/VIN(I)/AREA)-.0017
-.0394*X.SHEAR(I)
```

```
2270 DELTA.TH=TH.SHEAR(I)-TH.SHEAR(1)
2280 IF GX(I)=0! THEN EU(I)=9999 : GOTO 2320
2290 EU(I)=300!*DELTA.TH/GX(I)
2300 IF EU(I)>9999 THEN EU(I)=9999!
2310 IF EU(I)<-9999 THEN EU(I)=-9999
2320 IF TH.SHEAR(I)>T.MAX THEN T.MAX=TH.SHEAR(I)
2330 NEXT I
2340 DELTA.TH=T.MAX-TH.SHEAR(1)
2350 A$= "### +##.### +##.### +.### +#.###  +#.###  +.###  +#.### +####.#  +#.##
#  +#.###"
2360 FOR I=1 TO FILELEN
2370 VL=(VLC(I)-ZOVLC)*CFVLC/VIN(I)+TC
2380 VS(I)=VL/AREA
2390 DELTA.U(I)=V.C.S-VS(I)
2400 REM *** stone defections
2410 K=1
2420 K=K+1
2430 IF VL>SL(K) THEN 2420
2440 DSTONES=(SD(K)-SD(K-1))/(SL(K)-SL(K-1))*(VL-SL(K-1))+SD(K-1)
2450 DZ1=(Z1(I)-ZOZ1)*CFZ1/VIN(I)
2460 DZ1.EDGE=(.743151*DZ1+(1!-.743151)*DZ2)-(DSTONES-S1)
2470 DZ2=(Z2(I)-ZOZ2)*CFZ2/VIN(I)
2480 DZ2.EDGE=(.294521*DZ1+(1!-.294521)*DZ2)-(DSTONES-S1)
2490 DMIDDLE=.5188361*DZ1+(1!-.5188361)*DZ2
2500 DMID.STN=DMIDDLE-(DSTONES-S1)
2510 DELTA.H(I)=DMID.STN/H.SHEAR*100!
2520 DELTA.Z(I)=DV(I)*CFZ/VIN(I)/H.SHEAR*100!
2530 GY=(Y(I)-ZOY)*CFY/VIN(I)/H.SHEAR*100!
2540 TH.N=TH.SHEAR(I)/V.C.S
2550 DELTAU.N=DELTA.U(I)/V.C.S
2560 VS.N=VS(I)/V.C.S
2570 TH.VS.N=TH.SHEAR(I)/VS(I)
2580 TH.SU.N=(TH.SHEAR(I)-TH.SHEAR(1))/DELTA.TH
2590 EU.N=EU(I)/DELTA.TH
2600 IF EU.N>9999! THEN EU.N=9999!
2610 IF EU.N<-9999! THEN EU.N=-9999!
2620 OT=TH.N/OCR
2630 OS=VS.N/OCR
2640 LPRINT USING A$;I,GX(I),GY,TH.N,DELTAU.N,VS.N,TH.VS.N,TH.SU.N,EU.N,OT,OS
2650 WRITE #1,I,GX(I),GY,TH.N,DELTAU.N,VS.N,TH.VS.N,TH.SU.N,EU.N,OT,OS,DZ1.EDGE,
DZ2.EDGE,DMID.STN,DV(I)
2660 NEXT I
2670 CLOSE #1
2680 LPRINT "":LPRINT "":LPRINT "":LPRINT ""
2690 LPRINT " Pt.    Str.X    X.Coor.  SigV     TauH     DelU      Eu    Delta.H
    Delta.Z"
2700 LPRINT " No.     (%)      (cm)                                    (%)
```

```
      (%)"
2710 B$=   "###    +##.###   #.####   ##.###   +#.###   +#.###  +####.#  +#.###
    +#.###"
2720 REM
2730 FOR I= 1 TO FILELEN
2740 LPRINT USING B$;I,GX(I),X.SHEAR(I),VS(I),TH.SHEAR(I),DELTA.U(I),EU(I),DELTA
.H(I),DELTA.Z(I)
2750 NEXT I
2760 PRINT "":PRINT "":PRINT "  *** THE END ****
2770 END
2780 REM ************************************************************************
2790 REM * STONE DEFLECTIONS - measured by DJD 9/17/1987
2800 REM ************************************************************************
2810 REM load(kg) vs deflection(cm)
2820 SL(1)=0! : SD(1)=0!
2830 SL(2)=4.375 : SD(2)=.00267
2840 SL(3)=8.75  : SD(3)=.004251
2850 SL(4)=17.5  : SD(4)=.005831
2860 SL(5)=26.25 : SD(5)=.006867
2870 SL(6)=35!   : SD(6)=.007575
2880 SL(7)=52.5  : SD(7)=.00872
2890 SL(8)=70!   : SD(8)=.009537
2900 SL(9)=105!  : SD(9)=.010846
2910 SL(10)=140!: SD(10)=.011827
2920 SL(11)=175!: SD(11)=.012644
2930 SL(12)=210!: SD(12)=.013298
2940 SL(13)=350! : SD(13)=.014
2950 SL(14)=999
2960 P=14
2970 RETURN
```

APPENDIX D
CONSTANT HEIGHT CONTROL AND SAMPLE DEFORMATION DURING UNDRAINED SHEAR

D.1 INTRODUCTION

This appendix discusses measured deformation of specimens during undrained shear of K_o consolidated resedimented BBC tests conducted in the Geonor and MDSS devices. The discussion focuses on how the height of the sample is monitored during shear and some of the measurements made. The servo control system used to maintain constant height during undrained shear in the Geonor is described in Appendix E. The final version of the servo control system used for the MDSS is described in Chapter 3. This appendix discusses some of the changes made to the original design of the MDSS in order to get the constant height servo control system to work properly. The test conditions for all of the CK_oU tests described in this appendix are summarized in Table 4.4 for the Geonor tests and Table 4.5 for the MDSS tests.

D.2 APPARATUS COMPRESSIBILITY

The compressibility of the vertical loading system is measured using a steel disc in place of a soil sample. The system is subjected to several load–unload cycles to get repeatable measurements for the load–deflection relationship of the device. Most of the apparatus compressibility is due to compliance of the porous stones. The load–deflection relationship is used during constant volume (undrained) shear to correct for the apparatus compressibility. For a typical CK_oUDSS test on a normally consolidated specimen the sample will tend to contract during shear and as a result the vertical stress is reduced to maintain the sample height constant (i.e., constant volume shear). As the vertical stress is reduced the porous stones will expand and if this is not

taken into account they will expand into the sample. Hence, while the distance between the top cap and bottom pedestal may be constant, the sample actually experiences some compression during shear. To avoid this problem, the apparatus compressibility is usually taken into account during undrained shear. In the MDSS, the corrections are made automatically by a computer whereas for the Geonor DSS used for this thesis, the corrections must be made manually by the operator (Note: as described in Appendix E, the constant volume control for the Geonor DSS is automatic but incorporating the apparatus compressibility correction during shear is not).

Figure D.1 is a plot of the apparatus compressibility measured for both the MDSS and the Geonor DSS. The figure shows that there is a large decrease in the slope of the curves as the stress level increases. Much of the initial deflection is due to seating of the vertical load system. However, CK_oUDSS tests on normally consolidated cohesive soils do not involve this part of the curve since at the beginning of undrained shear the sample is already at a higher stress level (equal to σ'_{vc}). Once undrained shear starts and the vertical stress decreases, changes in the apparatus compressibility are computed starting from σ'_{vc} and moving back towards the origin. For example, most CK_oUDSS tests conducted for this thesis were consolidated to σ'_{vc} = 3 ksc and at the end of undrained shear had $\sigma'_v/\sigma'_{vc} \cong 0.2$ or $\sigma'_v = 0.6$ ksc. Hence that portion of the load–deflection curve from $\sigma'_{vc} = 3$ ksc back down to $\sigma'_{vc} = 0.6$ ksc represents the component of the apparatus compressibility that needs to be accounted for during undrained shear.

D.3 GEONOR DSS

In the Geonor DSS, vertical deformations of a sample are measured using a direct current displacement transducer (DCDT) which is attached to the top loading platen of the apparatus. The DCDT is located on an axis through the middle of the sample and perpendicular to the direction of the applied horizontal shear force (see

Figure D.2). During constant volume shear, a second DCDT is used for the constant height servo control system. This DCDT is positioned adjacent to the sample on the opposite side of where the horizontal shear force is applied (Figure D.2). It monitors the height changes in the top loading platen which is directly connected to the top cap of the sample. The vertical displacement DCDT is not used for the constant height servo control because it does not have the necessary sensitivity (the vertical deformation DCDT must have a sufficient range to measure deformations during consolidation whereas the constant height DCDT only needs to cover a very small range and, therefore, a more sensitive transducer can be used). The constant height DCDT is positioned at the back side of the sample because it cannot be conveniently placed at any other location. Ideally, it should be placed along the same axis as the vertical deformation DCDT (i.e., perpendicular to the direction of the applied horizontal shear force so that as the loading platen rotates during shear about an axis perpendicular to the direction of shear the DCDT reading will not be biased by this rotation).

Constant volume tests in the Geonor DSS are typically run without correcting for the apparatus compressibility during shear. The correction can be made manually if someone continuously monitors the test and makes the appropriate adjustments. The constant height DCDT is connected directly to the servo control box and its output during undrained shear is not recorded. However, the vertical displacement DCDT output is recorded and used as a check of the sample height during shear. Figure D.3 is a plot of the sample height deflection during shear as measured by the vertical deformation DCDT for Tests G1, G2, and G4. The values for deflection in Figure D.3 do not take into account the apparatus compressibility. The maximum deflection at peak shear resistance ($\gamma \simeq 5\%$) is approximately –0.0004 cm (for Test G4). This represents 0.02% of the preshear sample height.

The data plotted in Figure D.3 represent the vertical displacement of the

sample during undrained shear without taking into account the apparatus compressibility. In principle, the vertical expansion of the apparatus during undrained shear will cause some compression of the sample which is not reflected in Figure D.3.[1] If the apparatus compressibility were to be taken into account then at the peak shear resistance ($\gamma \cong 5.0\%$, $\sigma'_v/\sigma'_{vc} \cong 0.56$ and $\sigma'_{vc} = 3$ ksc) the correction is equal to 0.0013 cm (Figure D.1) which represents a vertical expansion of the apparatus or compression of the sample. Adding this to –0.0004 cm gives a sample deflection equal to 0.0009 cm or 0.045% of the preshear sample height.

D.4 MDSS

The MDSS was designed with two vertical displacement DCDT's for measuring the sample height during consolidation and shear. Since the top cap does undergo some slight rotation during application of the applied horizontal shear force, the two DCDT's are placed at opposite sides of the top cap as shown in Figure D.4. Changes in the sample height are computed by linear interpolation using values from the two vertical displacement DCDT's (Z1 and Z2). The original servo control system used for Tests C1 and C4 also used these two DCDT's in order to maintain the height of the sample constant during shear. Unfortunately, the data acquisition system (specifically the multiplexer) can only read the two DCDT's and the vertical load cell every 1.5 secs. (the load cell was read to make corrections for the apparatus compressibility). When the new servo control system was being developed it was decided that the servo control loop required a much quicker response time. Hence, a third vertical DCDT (Collins ± 0.125 in.) was added to the system to serve as the constant height DCDT during undrained shear. This DCDT is attached to the vertical load piston which is connected to the top cap of the sample. It monitors the position

[1]The Geonor DSS tests were run without making the manual correction for the apparatus compressibility during undrained shear.

of the piston relative to the structural frame of the device and is positioned along an axis through the middle of the sample perpendicular to the direction of the applied shear force (see Figure D.4).

With only one DCDT to monitor, the data acquisition system is able to take a reading every 0.15 secs, hence providing an order of magnitude increase in the speed at which the constant height servo control loop can operate. In addition, the precision of the DCDT reading was increased by two orders of magnitude (from 1 mv to 0.01 mv). Corrections for the apparatus compressibility during shear are updated every time a full set of data readings is taken, which is usually every 1 to 2 minutes (i.e., the vertical load cell is read only when a full set of data readings is taken and therefore the correction for compressibility of the apparatus is made at that time). The two vertical displacement DCDT's are read during each set of full data readings and are used as a check of the sample height.

The new servo control system therefore, consisted of relocating the constant height DCDT, thus allowing an increase in the speed of the constant height DCDT readings, increasing the precision of the readings and using a Proportional Plus Integral Plus Derivative (PID) controller for the software (see Chapter 3). With this set–up three qualitative criteria are used to determine if the servo control system is working properly during a test:

1. Check if the constant height DCDT is able to maintain its position during the test within acceptable limits.

2. If condition 1 is met, then check if the *computed* deflection of the center of the sample based on measurements from the two witness DCDT's Z1 and Z2 is within acceptable limits.

3. If conditions 1 and 2 pass, then check if changes in vertical stress required to maintain the sample height constant during shear are reasonable. For example, the pore pressure plot does not contain any severe oscillations or "no–action" sections.

For all of the CK_oU tests run in the MDSS with the new constant height servo control system (C5, C6, C11, and C14), the system was able to maintain the constant height DCDT's position within 0.6 μm or 0.003% of the sample height. This, however, represents the maximum error whereas the average error during a test was typically within 0.1 μm or 0.0005% of the sample height (see Figure D.5). The X DCDT error plotted in Figure G.5 was computed using the following equation:

$$\text{X DCDT Error} = \Delta Z_m - \Delta Z_r \qquad \text{(D.1)}$$

where:

ΔZ_m = measured change in constant height DCDT voltage.
ΔZ_r = required change in constant height DCDT voltage to account for the apparatus compressibility.

If the X DCDT Error is positive then the system is behind in correcting for the apparatus compressibility and the sample is being compressed. The reverse holds if the X DCDT Error is negative. Figure G.6 is the same plot as Figure D.5 for Test C14 which was conducted without correcting for the apparatus compressibility. Hence, in this figure the X DCDT Error is computed using equation D.1 with $\Delta Z_r = 0.0$. Figures D.5 and D.6 are nearly identical and show that the constant height servo control system responded similarly whether it was required to maintain the X DCDT reading constant (Test C14) or to maintain a reading which takes into account the apparatus compressibility (Test C6).

Figures D.7 and D.8 are plots of the computed deflection of the top of the sample versus shear strain for Tests C6 and C14 respectively. This data is computed by using linear interpolation of the readings of the two vertical displacement transducers Z1 and Z2. Again like the plots of the X DCDT error, the results are very similar regardless of whether or not the apparatus compressibility was taken into account during shear. In Figure D.7 the data is computed using the Z1 and Z2 DCDT readings and the apparatus compressibility correction to determine the "true" sample

deformation during shear since the correction was used during this test. In the case of Figure D.8 for Test C14 which was run without the apparatus compressibility, the deflection curves are computed using only the measured data from Z1 and Z2. Thus, in principle, Figure D.8 does not represent the "true" sample deformation during shear. Figure D.9 is a plot of the computed sample deformation for Test C14 if the expansion of the stones is accounted for in making the deformation computations.

The interesting observation that comes from this data is that while the "true" sample deformation for Test C14 (Figure D.9) is significantly different than Test C6, (Figure D.7) the normalized strength (c_u/σ'_{vc}, where $c_u = \tau_h(max)$) only differs by 0.003. In the case of Test C6, at $\gamma_f \cong 5\%$ sample deformation equals 0.0005 cm or 0.025% of the sample height compared to 0.0018 cm or 0.09% for Test C14. This indicates that for BBC and the stress level used in these tests ($\sigma'_{vc} = 3$ ksc), correcting for the apparatus compressibility during undrained shear only results in an insignificant change in the measured strength ($\simeq$ 1.6%). Further evidence of this is found from the results of Test C5 and C11, which were conducted without and with the apparatus compressibility during shear respectively. Test C5 had a normalized undrained strength which is identical to that of Test C14 while Test C11 had a normalized strength which is only 0.005 less than Tests C5 and C14.

With the Z1 and Z2 displacement measurements, it should be possible to correlate the computed sample deflections during shear with the measured normalized shear strength.[2] For example, Test C4, which was run with the original constant height servo control system operating at a very slow rate, has an unusually high normalized strength and, therefore, its deflection versus shear strain results should be different from the other tests. This is clearly shown in Figure D.10 which is a plot of

---

[2]The Z1 and Z2 readings cannot be used to compute the rotation of the top cap during shear since they do not lie along the axis of the applied shear stress. With the present set–up, a third reading at another orientation relative to Z1 and Z2 would be required to compute the plane of rotation of the top cap.

computed center of sample deflection versus shear strain for all six CK_oUMDSS tests except C5 (in this plot the sample deformation is computed using only the Z1 and Z2 DCDT measurements without adjusting for the apparatus compressibility for Test C1, C6 and C11). For all of these tests 75% of the peak horizontal shear resistance was reached at $\gamma = 0.5\%$.

The sample deflection results for Test C1 (which was also run with the original constant height servo control system but at a faster rate than that used for C4) does not differ significantly from Tests C6, C11 and C14 yet this test also had a higher normalized shear strength. This test, however, had some servo control problems before the peak shear resistance was reached. The deflection plot shows some initial compression at the beginning of the test ($\gamma < 0.1\%$) and also the normalized pore pressure plot (Figure 3.7) shows that the servo control system periodically stopped unloading the vertical stress after $\gamma = 2\%$ when normally this does not occur.

Figure D.10 also shows that Test C4 had larger than normal negative shear strains at the beginning of shear. Generally a test may have a few initial readings that indicate a very small negative shear strain which is may be due to inaccurate determination of the preshear displacement transducer reading and/or slight electronic fluctuations in the reading that do not represent actual sample displacements. The problem with Test C4 was that the sample was initially sheared at a very fast rate of strain. During the first minute of the test the sample was loaded to at least 20% of the usual shear strength of BBC. This rapid loading also caused the servo control program to fail because the Z1 and Z2 displacement transducers went out of range (for this test the Z1 and Z2 transducers were used for the constant height servo control and the rapid loading deflected the transducers out of the ± 200 mv range). Once the servo program failed, the horizontal force was unloaded and the sample was allowed to sit for two hours before reshearing. Throughout the initial shear and the subsequent two hour time period the vertical stress on the sample did not change (σ'_{vc} = 4.0 ksc). It is

possible that the initial shear force that was rapidly applied to the sample may have also contributed to its unusually high strength (i.e., like a 0 degree CAU test, but loaded quickly and then unloaded before subsequent undrained shear in the same direction). It is not clear whether the negative shear strains are actual sample strains or due to a mechanical problem such as a shift in the DCDT post position during reshearing of the sample.

The computed center of sample deformation during Test C5 indicates that this sample was compressed during shear (see Figure D.11). Given the results found for Test C4 one would expect that the measured strength for Test C5 would be higher than C6, C11, and C14, but this is not the case. During Test C5 the Z2 displacement transducer displaced approximately 0.002 cm less than that measured for Test C14 yet the Z1 transducer displaced exactly as that for Test C14. This is shown in Figure D.12 which is a plot of the measured Z1 and Z2 DCDT deflections versus shear strain for Tests C5, C6, C11 and C14. The values for Tests C6 and C11 deviate from Test C14 (and also Z1 for Test C5) by an amount equal to the apparatus compressibility which was used during shear for these two tests. This indicates that there was a mechanical problem with the set–up of the Z2 transducer during Test C5. Hence, the computed center of sample deformation would be erroneous and in this case would indicate that the sample was consolidating during shear when in fact it probably was not. Further evidence of this can be seen by comparing the deflection versus shear strain plots for Tests C1 and C4 (Figures D.13 and D.14). Once Test C4 reached $\gamma > 4\%$ and the servo control system finally started to catch up with the behavior of the sample, the Z1 and Z2 displacements were similar to that of Test C1. Yet the sample in Test C4 clearly compressed during the initial stages of the test as shown in this Figure D.14 and Figure D.10)

Figure D.15 shows the deflection versus shear strain plot for two drained DSS tests run on BBC by Edgers (1967). At $\gamma = 5\%$, which is the normal shear strain at

failure for an undrained test, the drained samples compress approximately 0.03 cm or 1.63% of the sample height. Figure D.16 is an expanded plot of Figure D.15 and can be compared with the deflection versus shear strain plot for CK_oUMDSS Test C4. It shows that for $\gamma < 0.1\%$, Test C4 actually compressed more than the drained tests.

D.5 SUMMARY

This appendix showed that for CK_oU tests run in the MDSS there was a correlation between the computed deflection of the sample center and the measured undrained shear strength. It is evident that the original constant height servo control system used for Tests C1 and C4 was not satisfactory. This is particularly true for Test C4 where the sample clearly compressed during the initial stages of the test and subsequently resulted in a high measured undrained shear strength.

The new constant height servo control system works very well as was shown in the results obtained for Tests C5, C6, C11 and C14. They also indicate that for the test conditions used, correcting for the apparatus compressibility during shear leads to insignificant changes in the measured undrained strength.

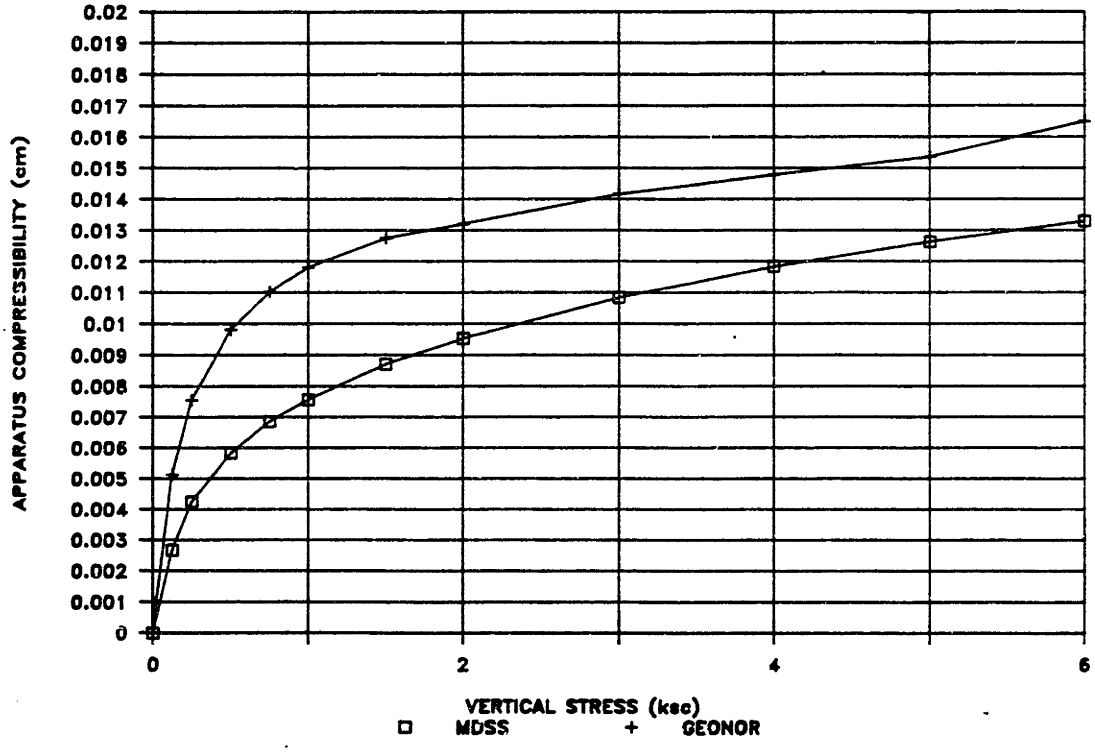

Figure D.1: Apparatus Compressibility Curves for the MDSS and Geonor DSS.

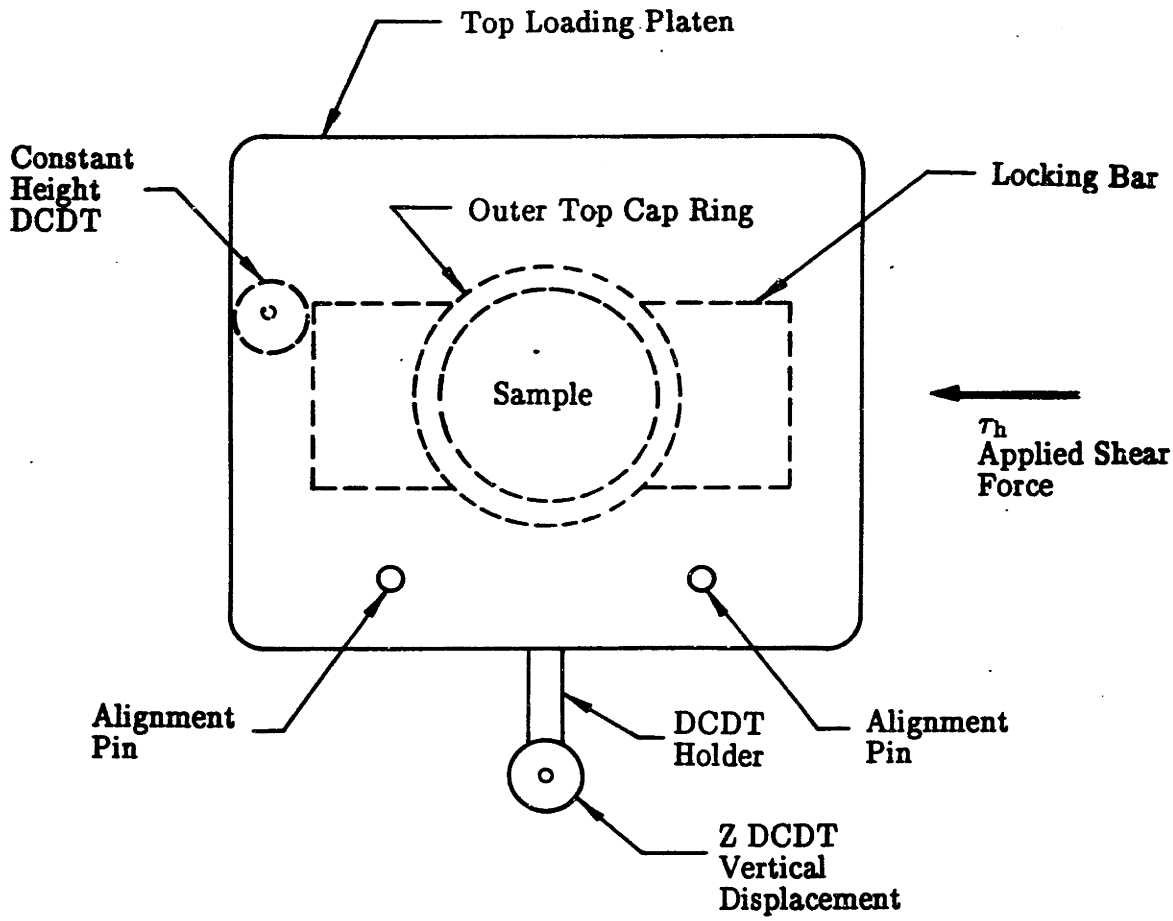

Figure D.2: Location of Vertical Displacement and Constant Height DCDT's in the Geonor DSS.

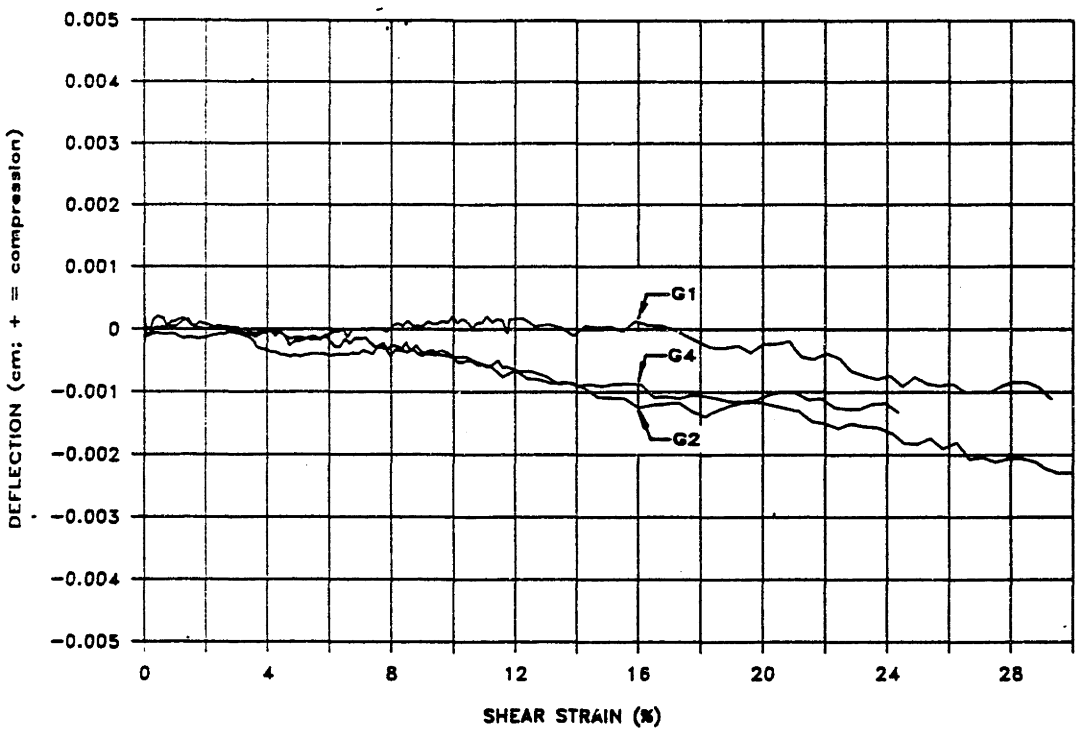

Figure D.3: Sample Height Deflection for Geonor CK_0UDSS Tests G1, G2 and G4.

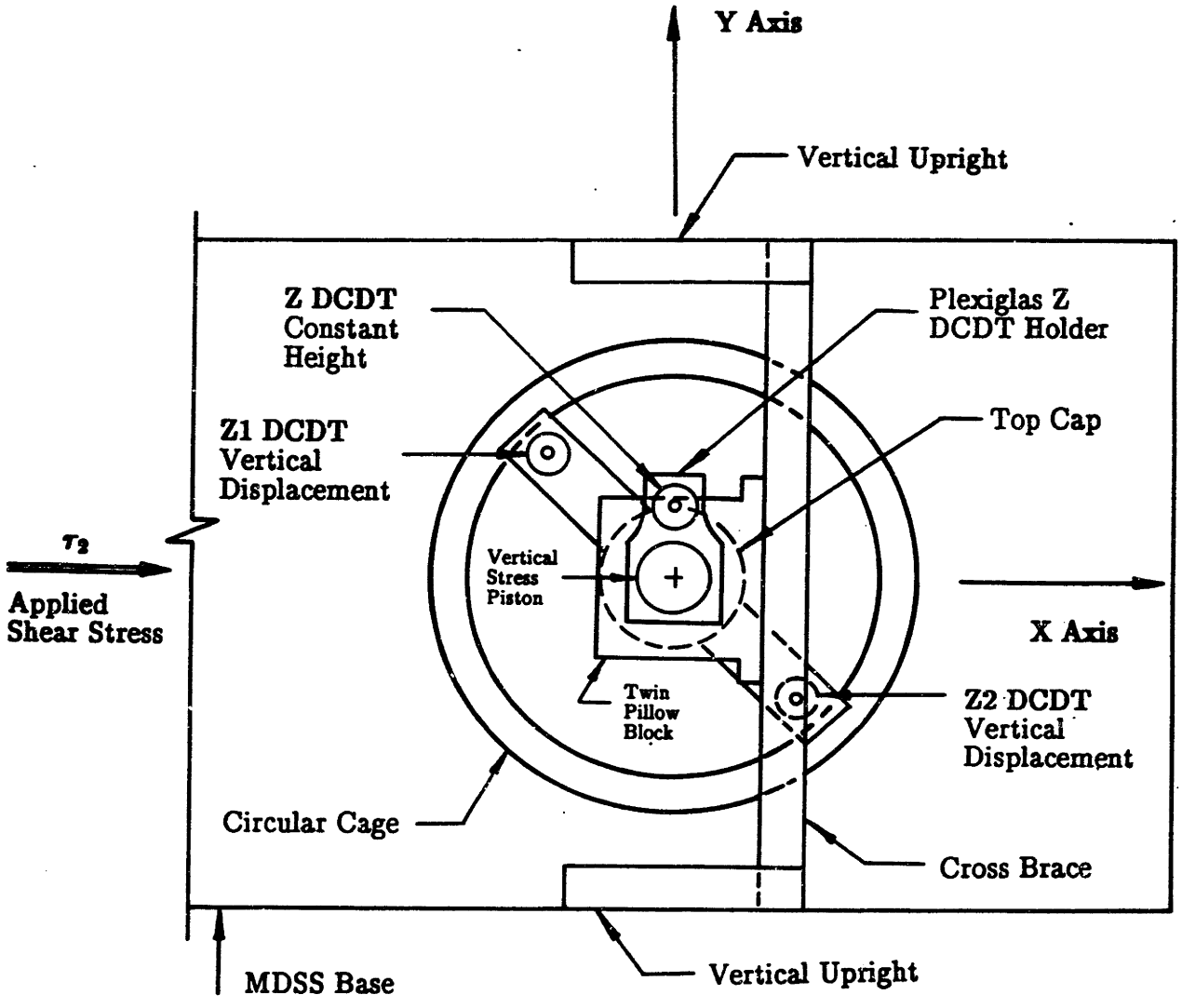

Plan View

Scale Approx. 1" = 3"

Figure D.4: Location of the MDSS Vertical Displacement and Constant Height DCDT's.

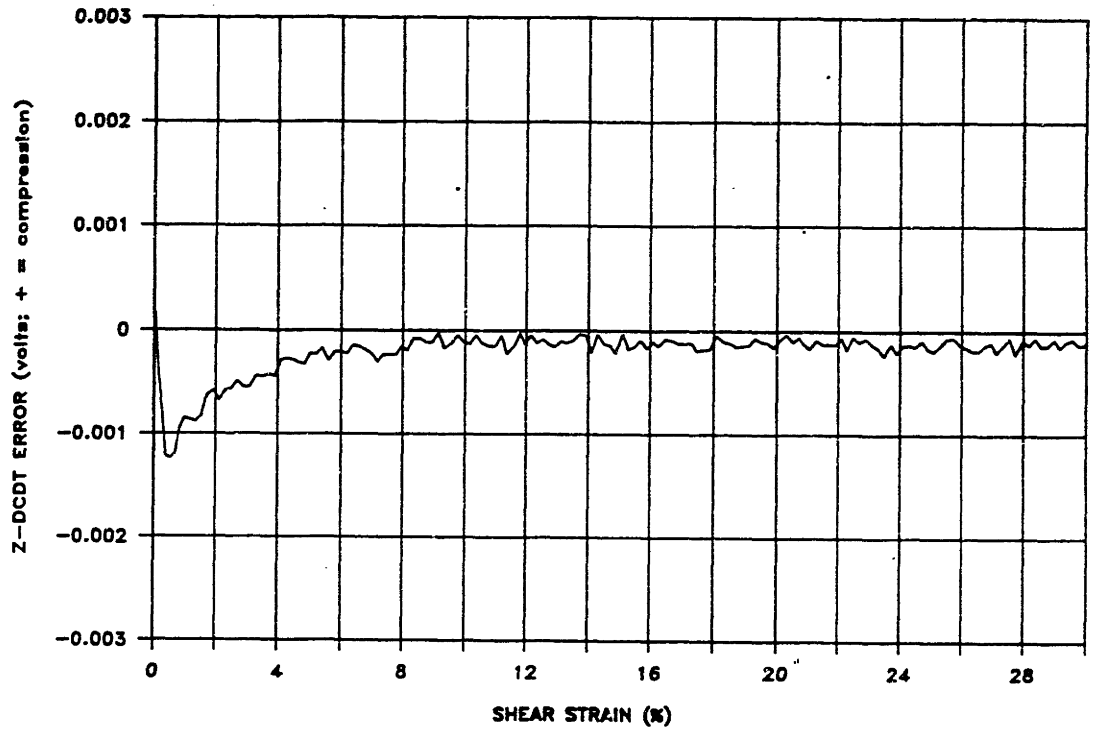

Figure D.5: Constant Height DCDT Error During Undrained Shear for CK_oUMDSS Test C6 (apparatus compressibility correction used during shear; 1 mVolt = 0.5 μm).

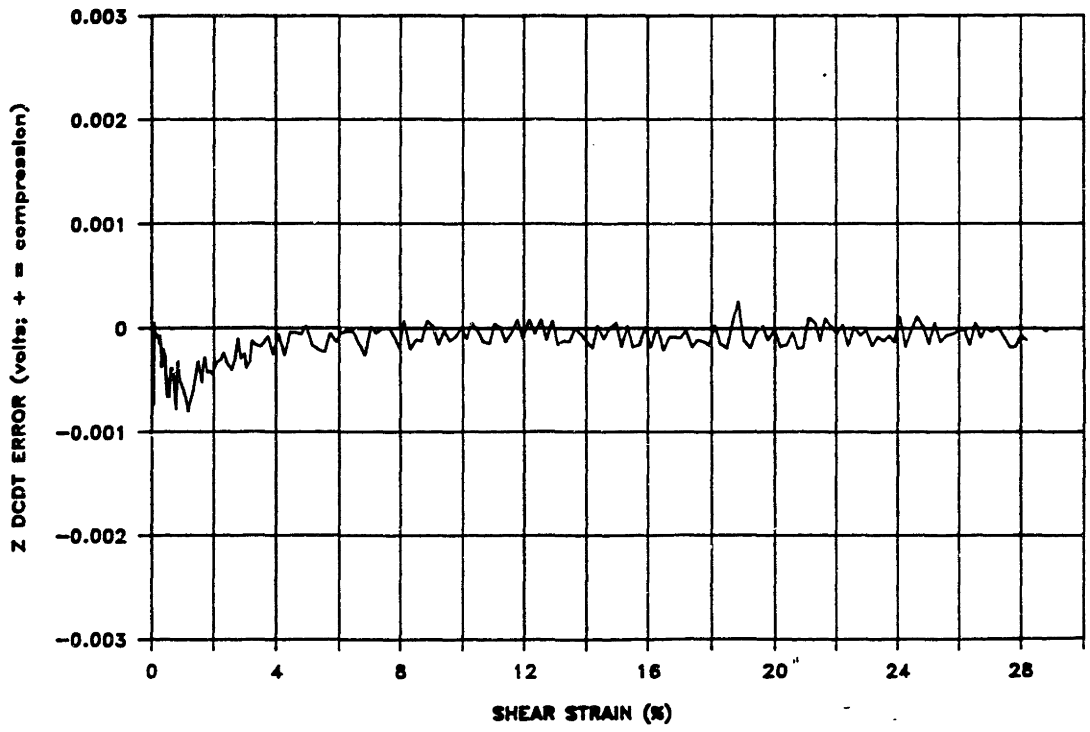

Figure D.6: Constant Height DCDT Error During Undrained Shear for CK_oUMDSS Test C14 (apparatus compressibility correction not used during shear; 1 mVolt = 0.5 μm).

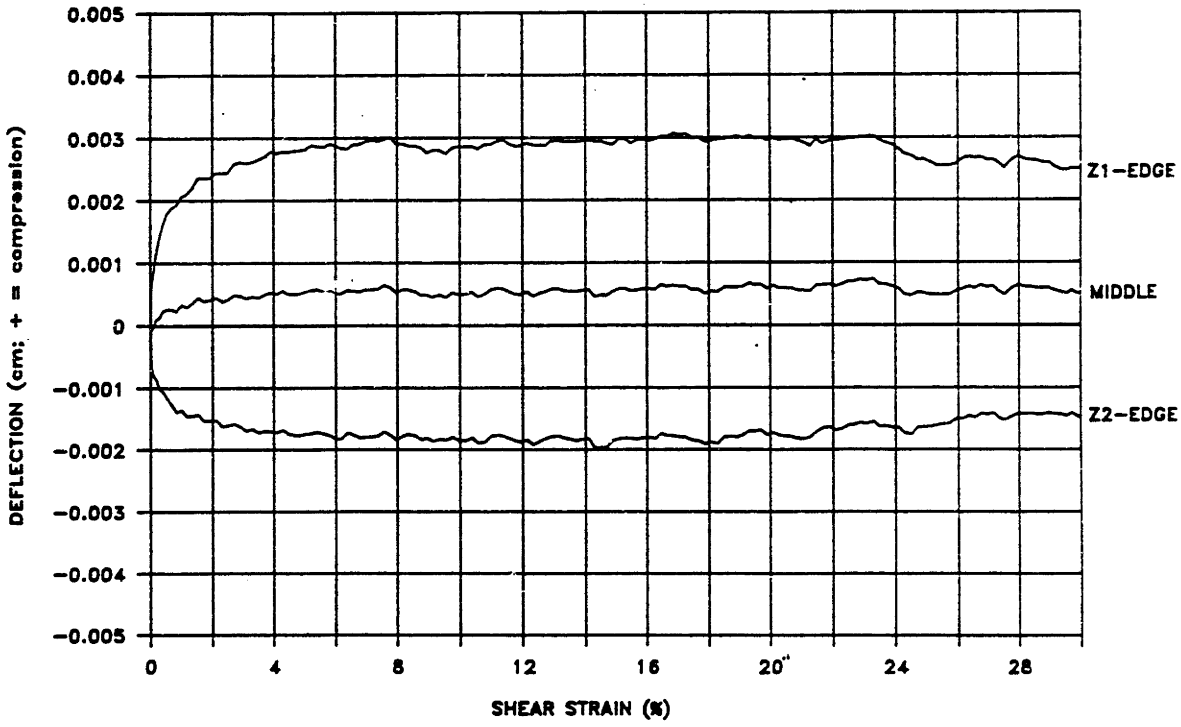

Figure D.7: Computed Deflection of Top of Sample During Undrained Shear for CK_oUMDSS Test C6 (apparatus compressibility used during shear).

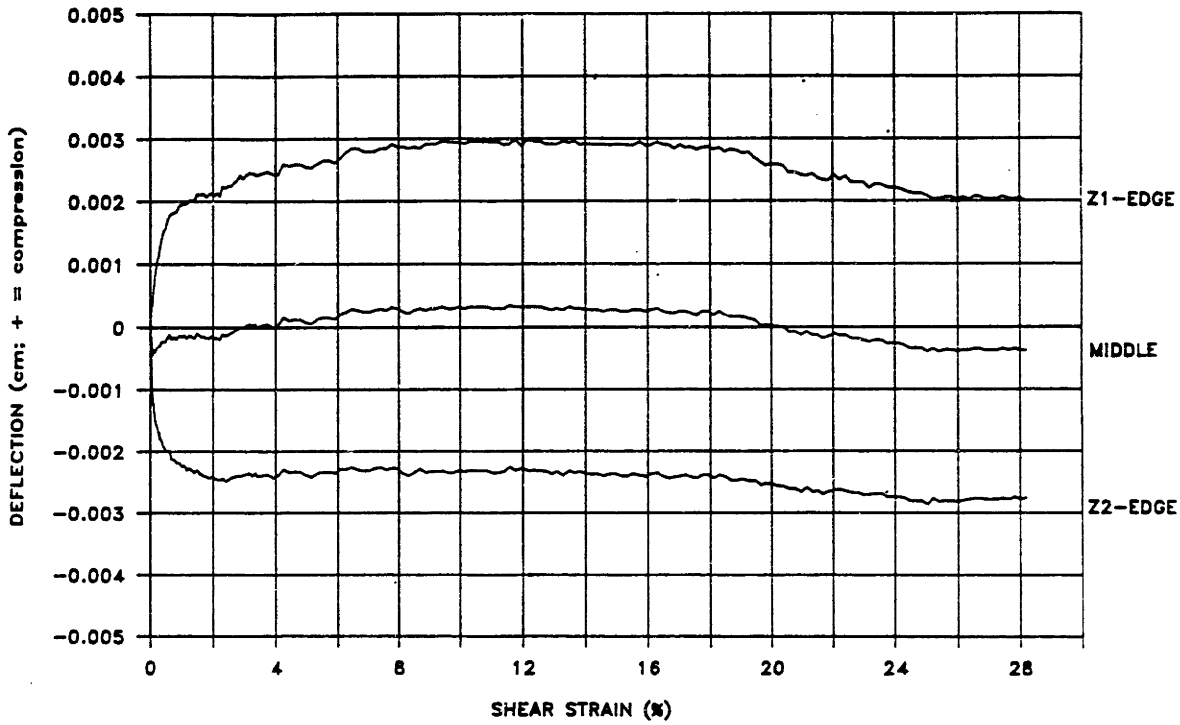

Figure D.8: Computed Deflection of Top of Sample During Undrained Shear for CK_0UMDSS Test C14 (apparatus compressibility not used during shear).

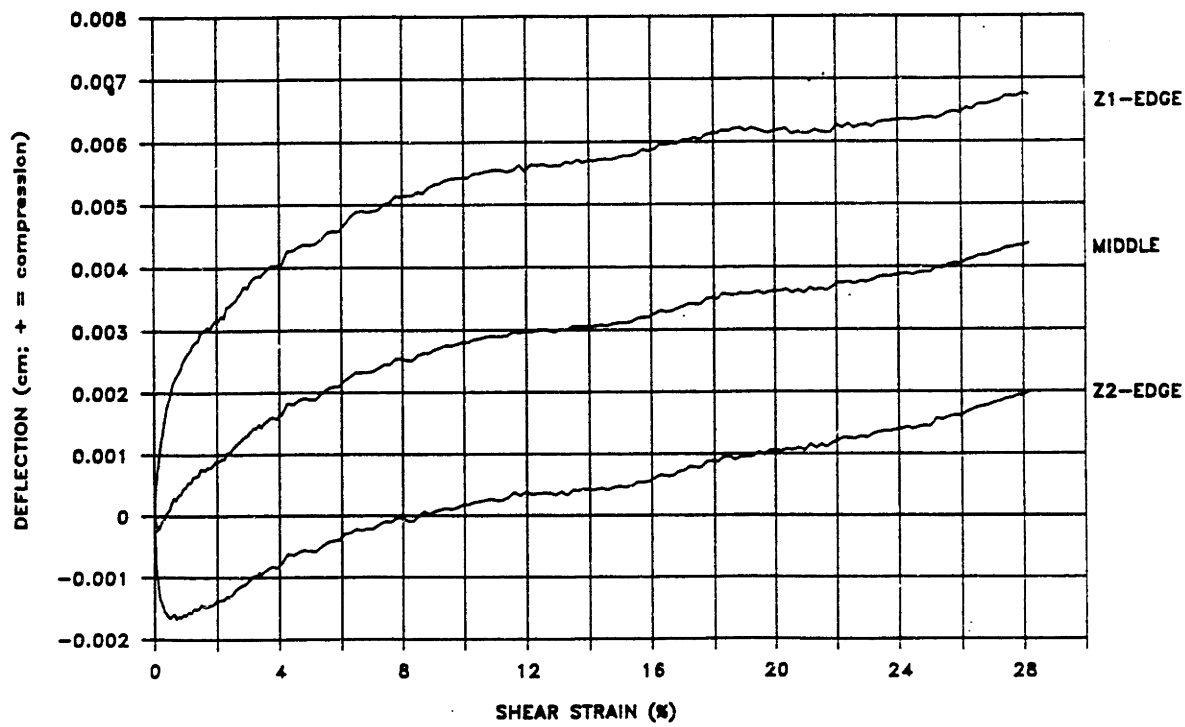

Figure D.9: Computed Deflection of Top of Sample During Undrained Shear for CK_0UMDSS Test C14 (apparatus compressibility <u>not</u> used during shear but <u>included</u> in computation of the top of sample deflection).

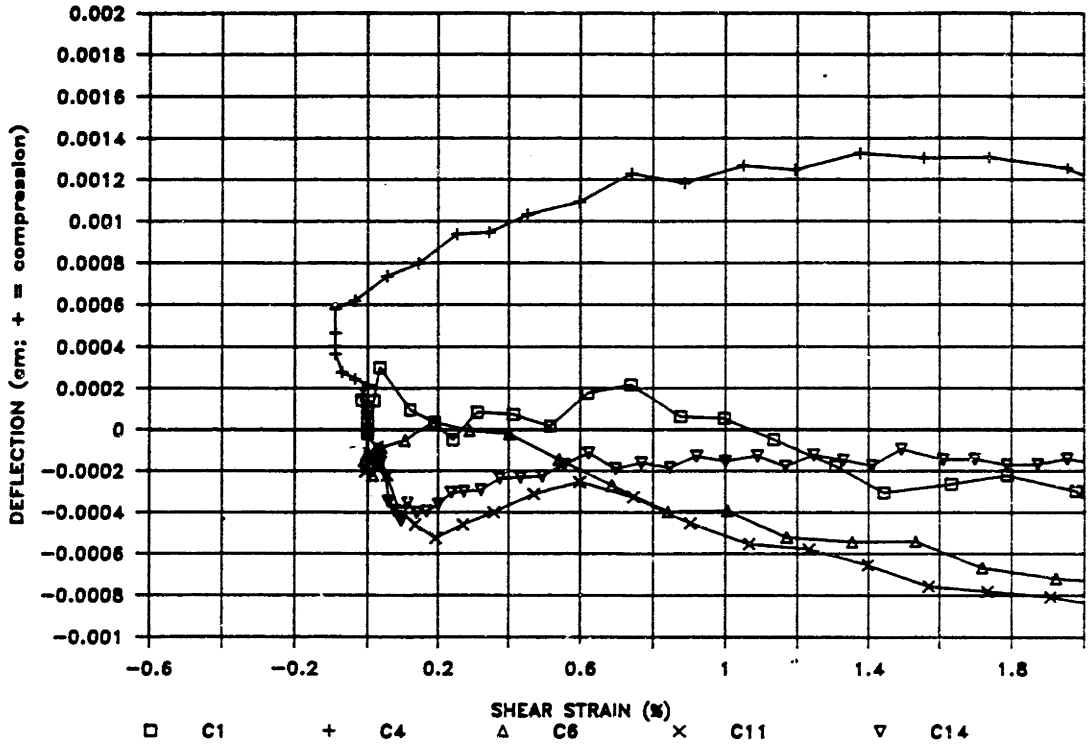

Figure D.10: Computed Center of Sample Deflection for CK_0UMDSS Tests C1, C4, C6, C11 and C14.

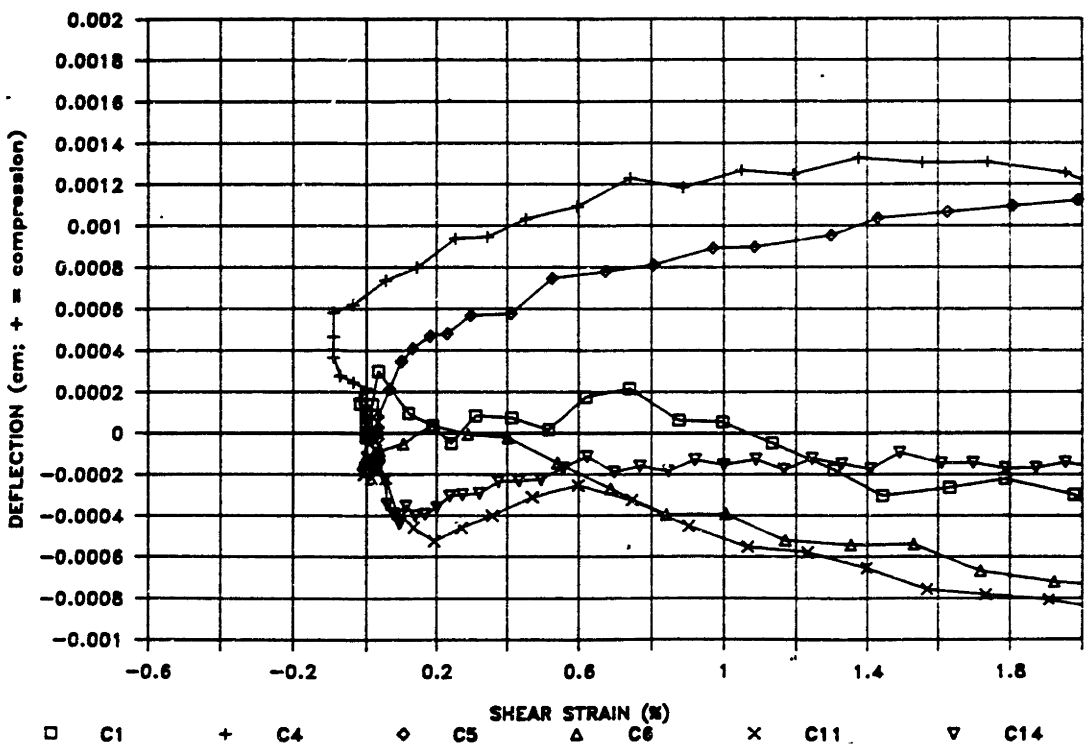

Figure D.11: Computed Center of Sample Deflection for all CK_0UMDSS Tests.

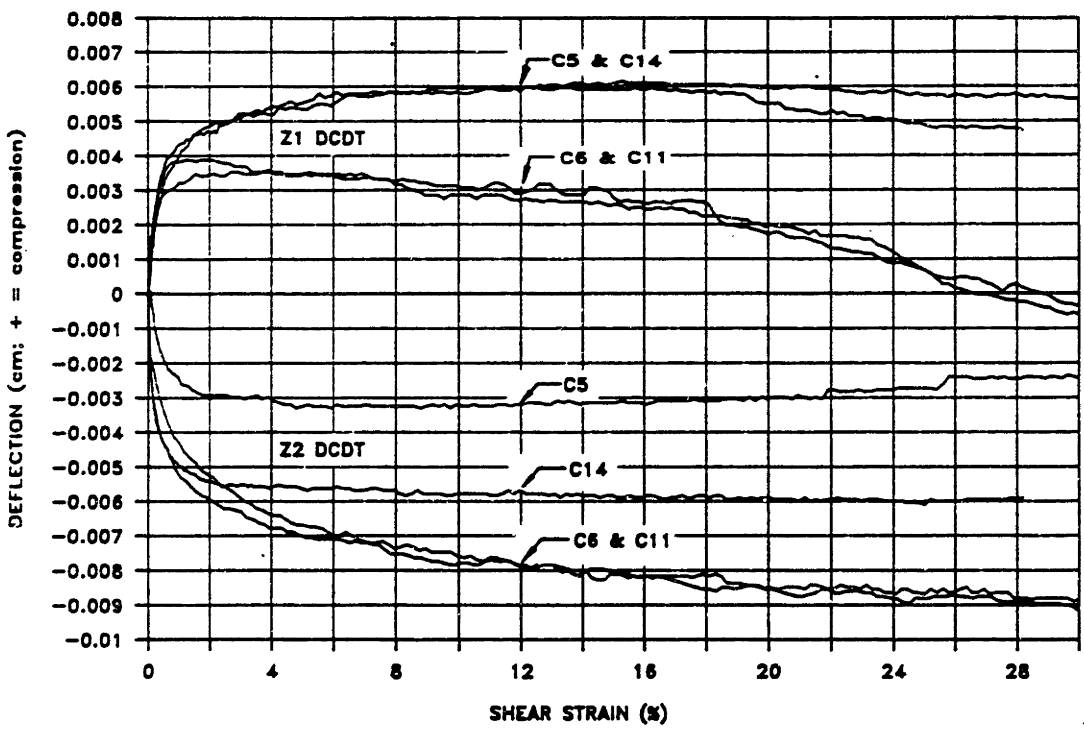

Figure D.12: Measured Z1 and Z2 DCDT Displacement During Undrained Shear for CK_oUMDSS Tests C5, C6, C11 and C14.

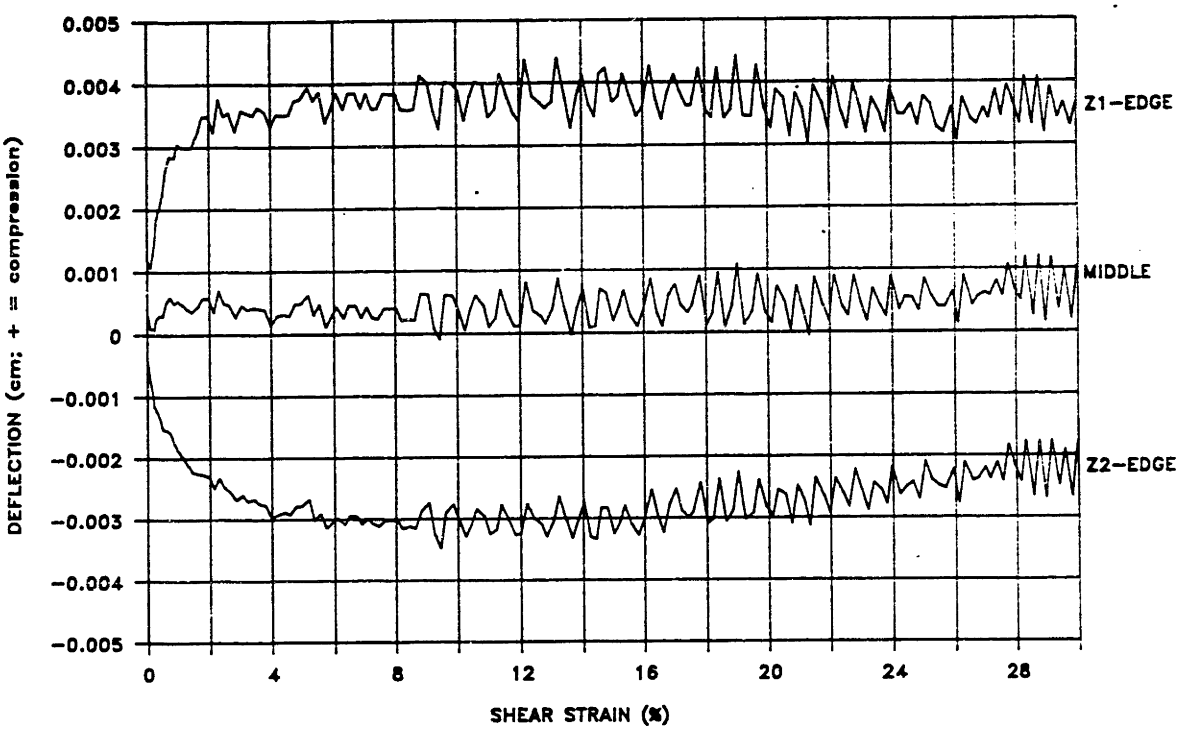

Figure D.13: Computed Deflection of Top of Sample During Undrained Shear for CK_oUMDSS Test C1.

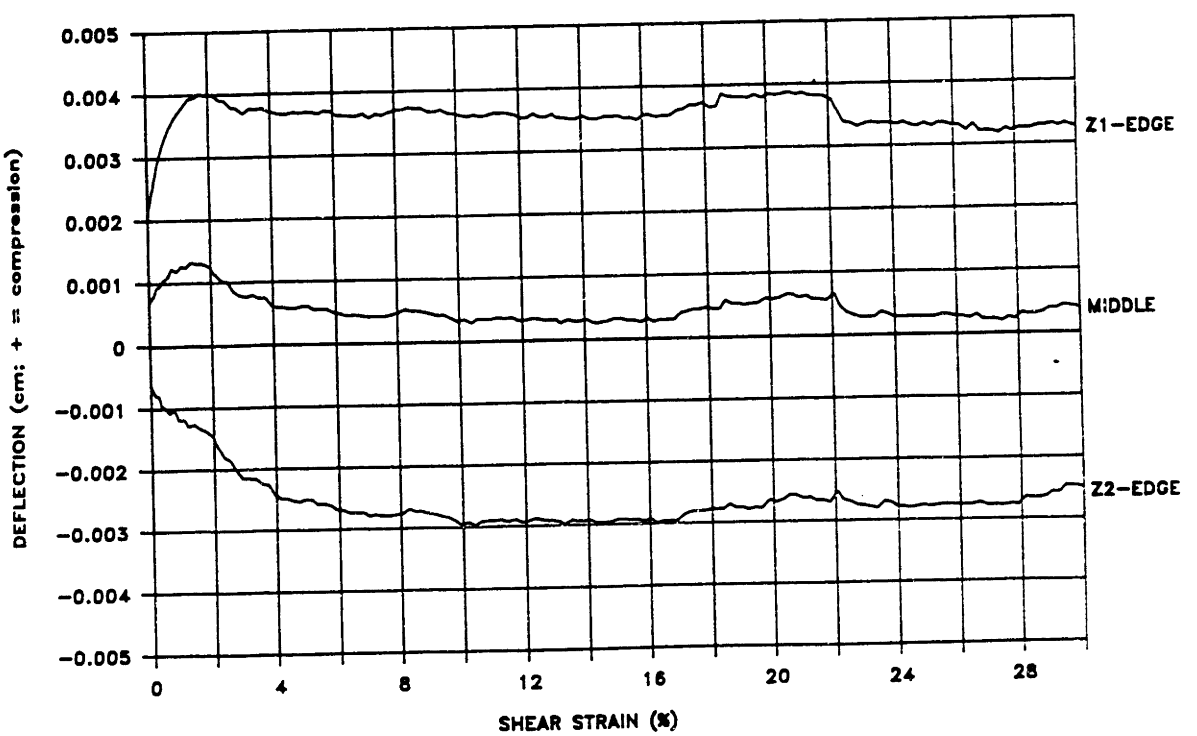

Figure D.14: Computed Deflection of Top of Sample During Undrained Shear for CK_oUMDSS Test C4.

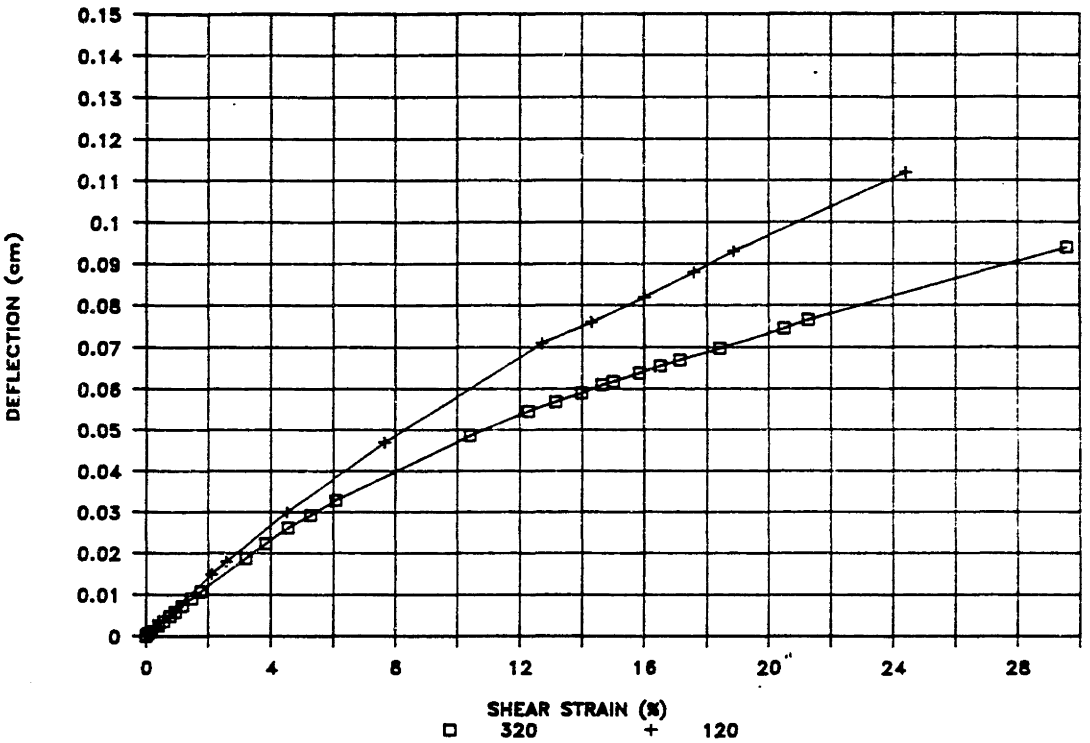

Figure D.15: Deflection Versus Shear Strain for Drained DSS Tests on BBC (from Edgers, 1967).

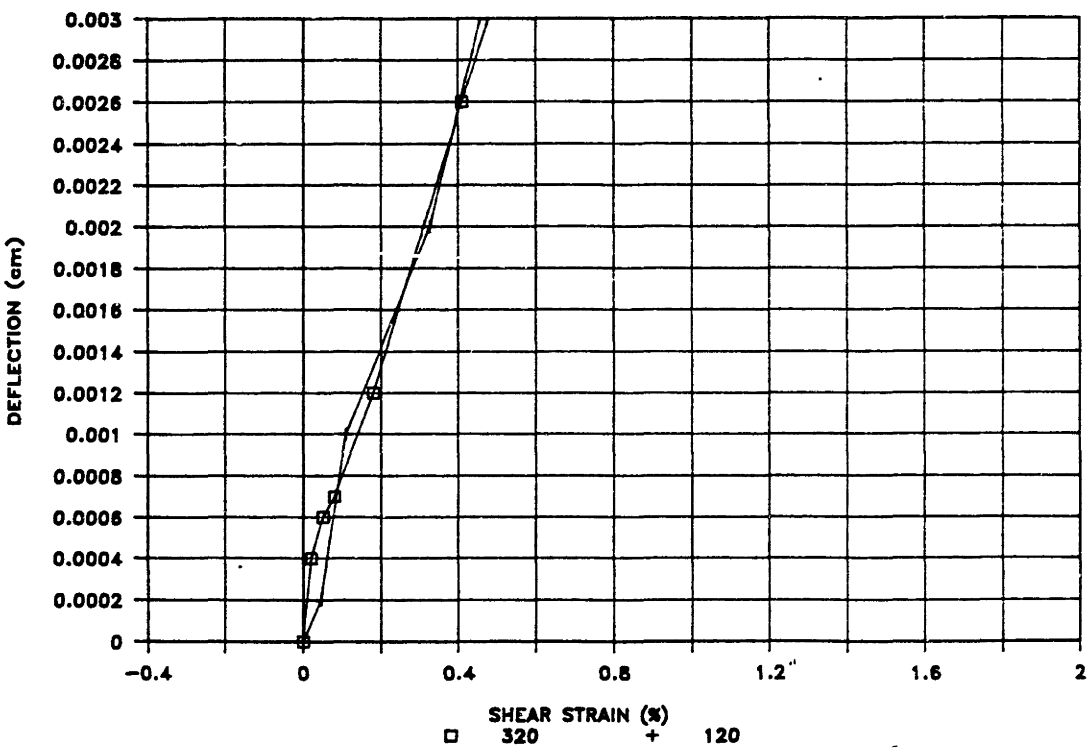

Figure D.16: Figure D.15 Plotted to Same Scale as Figures D.10 and D.11.

APPENDIX E

GEONOR DIRECT SIMPLE SHEAR APPARATUS

The Geonor Model 4 Direct Simple Shear (DSS) apparatus has been used extensively for direct simple shear research and testing at MIT. The Geonor Model 4 is similar to the original apparatus developed at the Norwegian Geotechnical Institute as described by Bjerrum and Landva (1966). This appendix describes the Geonor DSS and testing procedures used at MIT for this research.

E.1 DESCRIPTION

Figure E.1 and E.2 schematically show the original Geonor Model 4 DSS device. The original device was designed for testing samples with an area of 50 cm^2. This, however, is incompatible with the diameter of sampling tubes typically used in North America (3" diameter or 45 cm^2) hence a 35 cm^2 sample with an approximate height of 2.3 cm is used at MIT. The sample is confined by a circular wire–reinforced rubber membrane between a top cap and the bottom pedestal. Both the top cap and bottom pedestal contain porous stones allowing drainage to take place in both directions. The stones also provide the frictional interface for transferring the horizontal shear force during testing to the sample. The sample is surrounded by a plexiglas water bath.

E.1.2 Consolidation and Undrained Shear

Increments of vertical stress are applied to the sample using dead weights loaded onto a lever arm acting on the sample. The lever arm ratio is approximately 1:10 and the vertical load is measured with a proving ring and a displacement transducer (DCDT). The DCDT measures the deflection of the proving ring under

load thus allowing readings to be taken by a data acquisition system. Vertical displacements are measured using a dial gauge/DCDT assembly which is connected to the top loading platen adjacent to the sample. The DCDT is connected to the dial gauge so that vertical displacement readings can also be made with the data acquisition system. The increments of vertical stress are normally applied during consolidation (i.e., drained conditions) and the consolidation is under K_o conditions because of the confining reinforced rubber membrane. The apparatus can also be used to run special anisotropically consolidated (CAU) tests – the procedure is described in more detail in section E.2.2.

The sample is sheared by application of a horizontal force to the top cap (i.e., the top of the sample moves relative to the bottom in a simple shear strain mode). The force is applied by an AC motor and gear box and is usually applied at a constant rate of strain, although stress control testing is possible. The horizontal force is measured by a proving ring which also has a DCDT connected to it. The proving ring has some compliance and therefore the strain rate is not truly constant particularly at the beginning of a test. The horizontal displacement of the sample top relative to its fixed bottom is measured using a DCDT.

Shearing can be performed under drained or undrained conditions. Drained tests are performed by deforming the sample under constant vertical stress at a strain rate which is sufficiently slow to allow dissipation of excess pore pressure. Undrained shear is conducted by maintaining the volume of the sample constant during shear. The sample is assumed to be laterally confined by the rubber membrane and therefore, only the height needs to be kept constant to run a constant volume test. The sample height is kept constant by varying the vertical stress acting on it. Changes in vertical stress required to keep the height constant are assumed to be equal to the pore pressure that would develop if the test was truly undrained with pore pressure

measurements. Dyvik, et al. (1987) showed that for normally consolidated clay this assumption is valid.

The sample height is maintained constant during undrained shear in the Geonor DSS using a servo control system consisting of a DCDT, a controller box and an Electrocraft analog motor. The DCDT (Collins ± 0.125") is placed adjacent to the sample (as described in Appendix D) and monitors movements in the top loading platen which is connected to the sample top cap. The control box compares the DCDT reading to a reference voltage and sends the difference (i.e., voltage error) through an amplifier to the Electrocraft motor driver. The motor driver turns the motor at a rate which is proportional to the voltage error. The motor in turn drives a worm–screw mechanism that is connected to the lever arm which applies the vertical load to the sample. Hence, the vertical load acting on the sample can be automatically changed in response to changes in the sample height. This is a closed loop analog feedback system and is shown schematically in Figure E.3. The control box was built by MIT's Geotechnical Laboratory Director, Dr. John T. Germaine.

The system does not correct for the apparatus compressibility during shear. This can be done manually by gradually adjusting the reference voltage of the constant height DCDT according to the vertical stress acting on the sample and the load deflection curve (i.e., apparatus compressibility) of the device. However, this is not typically done as a standard procedure. Appendix D discusses the measured sample deformation during shear for the three CK_oU tests (G1, G2, and G4) run in the Geonor apparatus for this research and reports the maximum sample deflection at the peak shear resistance to be 0.004 cm or 0.02% of the sample height.

E.1.3 Data Acquisition, Reduction and Corrections

Transducer readings during consolidation and shear are recorded by MIT's central data acquisition system. The latest version of this system (installed August

1988) consists of an NEC APCIV Power Mate 1 personal computer[1] and Hewlett Packard # 3497A data acquisition control unit. All readings are triggered and taken by the central data acquisition's main software program and are subsequently transferred to $5^1/_4$" floppy disks for reduction and plotting. The data reduction program for CK_oU and CAU tests are very similar to the MDSS programs MDSSCKO and MDSSCAU listed in Appendix C and therefore are not included here.

Corrections are made to the measured data for apparatus compressibility during consolidation and for piston friction and membrane resistance during undrained shear. These corrections are similar to that used for tests conducted in the MDSS which are described in more detail in Section B.7 of Appendix B. The following is a summary of the corrections made for tests run in the Geonor DSS:

(a) Apparatus Compressibility

Using the measured load deflection relationship of the apparatus all consolidation displacements are corrected for the apparatus compressibility as the data are being reduced for each consolidation increment.

(b) Friction and Membrane Resistance

For CK_oUDSS tests, the measured horizontal resistance of a sample during undrained shear is corrected for the frictional and membrane resistance using the following equation:

$$MC(ksc) = 0.004 + 0.00075(\gamma \text{ in percent}) \qquad (E.1)$$

where:

MC = shear resistance correction (ksc)

The first part of the right hand side of Equation E.1 represents the frictional component and the second part of the equation represents the membrane resistance.

---

[1]The NEC Power Mate 1 is an IBM PC/AT compatible.

For anisotropically consolidated tests run in the Geonor, two corrections are made – one at the end of consolidation and one during undrained shear:

(1) Correction of Horizontal Consolidation Shear Stress

The actual horizontal shear stress τ_{hc} acting on the sample at the end of anisotropic consolidation is computed using the following equation:

$$(\tau_{hc})_{cor} = (\tau_{hc})_{nom} - 0.004 - 0.00075(\gamma_{con}) \qquad \text{(E.2)}$$

where:

$(\tau_{hc})_{cor}$ = corrected horizontal shear stress at end of consolidation (ksc)

$(\tau_{hc})_{nom}$ = applied horizontal shear stress at end of consolidation (ksc)

0.004 = horizontal loading system friction (ksc)

γ_{con} = % shear strain at end of consolidation

(2) Correction to τ During Undrained Shear

The total shear resistance of the sample during undrained shear is computed using the following equation:

$$\tau_t = (\tau_{hc})_{nom}(\cos\theta) + HLC - 0.004 - 0.0394X_s \qquad \text{(E.3)}$$

where:

θ = test angle theta (equal to either 0° or 180°)

HLC = horizontal shear stress proving ring reading

X_s = X coordinate of sample w.r.t. neutral axis of the device (cm)

E.2 TESTING PROCEDURES

This section describes the testing procedures used for cohesive soils in the Geonor DSS. All samples tested for this thesis came from batches of resedimented Boston Blue Clay (BBC). The procedure for preparation of the batches of BBC is given by Germaine (1982). Section 4.2 summarizes the batching procedure and describes the test soil in more detail.

E.2.1 Sample Preparation and Set–Up

Each specimen of BBC is unwrapped from its protective wax and aluminum coating and trimmed in MIT's humid room. Three or four water contents of approximately 15 g each are cut from the corners of the specimen. The sample is then carefully placed on the bottom pedestal and into the Geonor trimming jig. The edges of the sample are trimmed using the Geonor cutting shoe which cuts the sample into a circular shape of 35 cm^2. The cutting shoe also allows the top and bottom of the sample to be smoothly trimmed with a wire saw to an approximate height of 2.3 cm. The sample is then transferred to the testing laboratory where a vacuum pump is used to place the wire–reinforced membrane around it. Before the vacuum is released, the top cap is placed on the sample. Once this is complete the sample height is measured with a micrometer. The sample is then placed in the apparatus below the vertical loading platen and secured in place. The vertical and horizontal DCDT's are adjusted and a seating load is applied to the sample. At this stage the DCDT zero readings are taken.

E.2.2 Consolidation

Samples in the Geonor DSS are typically consolidated under K_o conditions. The device does however have the additional capability of conducting anisotropically consolidated tests where a horizontal shear force is applied to the sample during consolidation. This force always acts in the same direction whereas the motor used for shearing the sample can either push or pull the sample. Hence, the anisotropic consolidation force can act in the same direction as the undrained shear force (0 degree test) or act in the opposite direction (180 degree test).

K_o Consolidation:

Vertical consolidation increments are applied to the sample through application of dead weights on the vertical loading system lever arm. The

deformation–time data are recorded by the data acquisition system and can be simultaneously plotted for consolidation analysis. Consolidation increments are left on the sample usually between the end of primary and 24 hrs. (end of primary is determined from plots of deformation versus log time). The final consolidation increment is left on for 24 hrs. Before application of the final consolidation increment, the pins which hold the vertical loading platens in place are removed and the top cap is horizontally locked in place (this allows the top of the sample to displace relative to the bottom during shear).

CAU Consolidation:

Anisotropic consolidation is performed using dead weights attached to a hanger which acts on the horizontal loading yoke (see Figure E.1). The sample is placed in the device like K_o consolidated samples and is subjected to a few increments of vertical stress. The pins holding the top platens in place are then removed and the horizontal shear force is applied to the sample using dead weights placed on the hanger. The pre–undrained shear loading of either a 0 degree or a 180 degree test is the same and consists of the following steps:

- disconnect horizontal shear force proving ring;
- place sample in device and apply first few increments of vertical stress;
- remove pins from top loading platen and tighten horizontal locking bolts around the sample top cap;
- apply increments of vertical stress (σ'_{vc}) and horizontal shear stress (τ_1) to sample according to planned schedule (for an example see Table 5.1);
- leave last consolidation increment on sample for 24 hrs;
- reattach horizontal shear force proving ring and prepare sample for undrained shear.

The data acquisition system records all the appropriate transducers so that the consolidation data can be reduced to get the time–stress–strain results for each

increment (i.e., ϵ_v and γ versus time for each σ'_{vc} and τ_1 increment).

E.2.3 Undrained Shear

Once the sample has been consolidated then the undrained shear phase is ready to begin. The constant height DCDT is placed in its position adjacent to the sample and the control box is turned on and allowed to warm up for approximately 1 hour. The vertical loading lever arm is pinned in place so that the dead weights can be removed. The Electrocraft motor is connected to the worm–gear which controls the force acting through the lever arm thus allowing the vertical stress to be changed in response to changes in the sample height. Finally, the motor is turned on and the sample is sheared at a constant rate of strain of approximately 5% per hour.

For the CAU consolidated tests the same set–up procedure is used except that the horizontal consolidation shear force is left acting on the sample during shear (the horizontal proving is disconnected before anisotropic consolidation and is reconnected prior to undrained shear). For the 0 degree test, the analog motor shears the sample in the same direction as the horizontal consolidation shear force acts and conversely the motor shears in the opposite direction of the horizontal consolidation shear force for the 180 degree test (the analog motor can either push or pull the sample).

The data acquisition system is used to take readings of all the transducer channels typically every one to four minutes.

E.2.4 End of Test

At the end of undrained shear, the sample is manually brought back to its preshear configuration (i.e., X coordinate $\cong$ 0) and allowed to sit overnight under just a vertical stress seating load. The following day the sample is removed from the device and a final water content is taken.

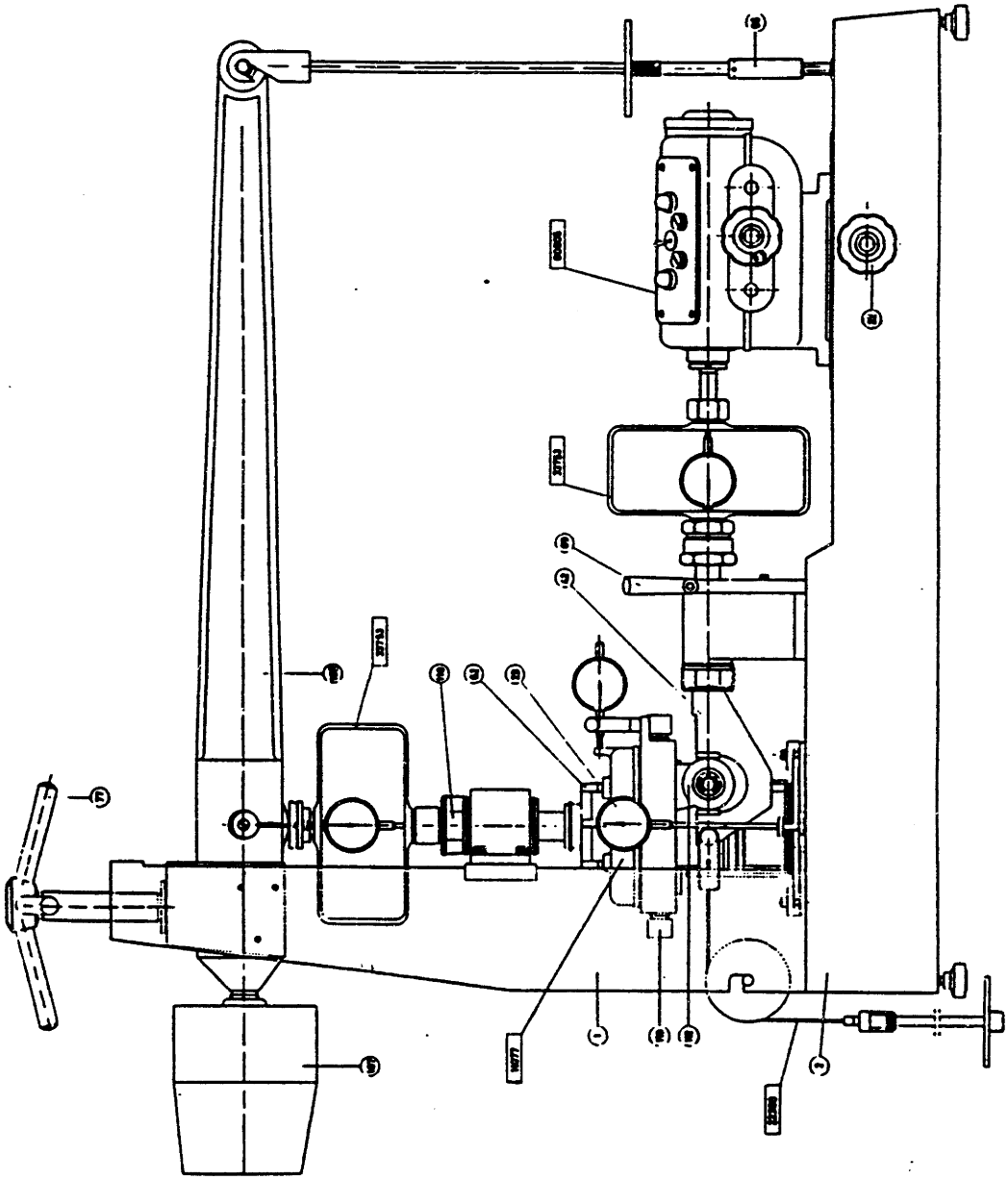

Figure E.1: Geonor Model 4 Direct Simple Shear Device (Geonor DSS Manual).

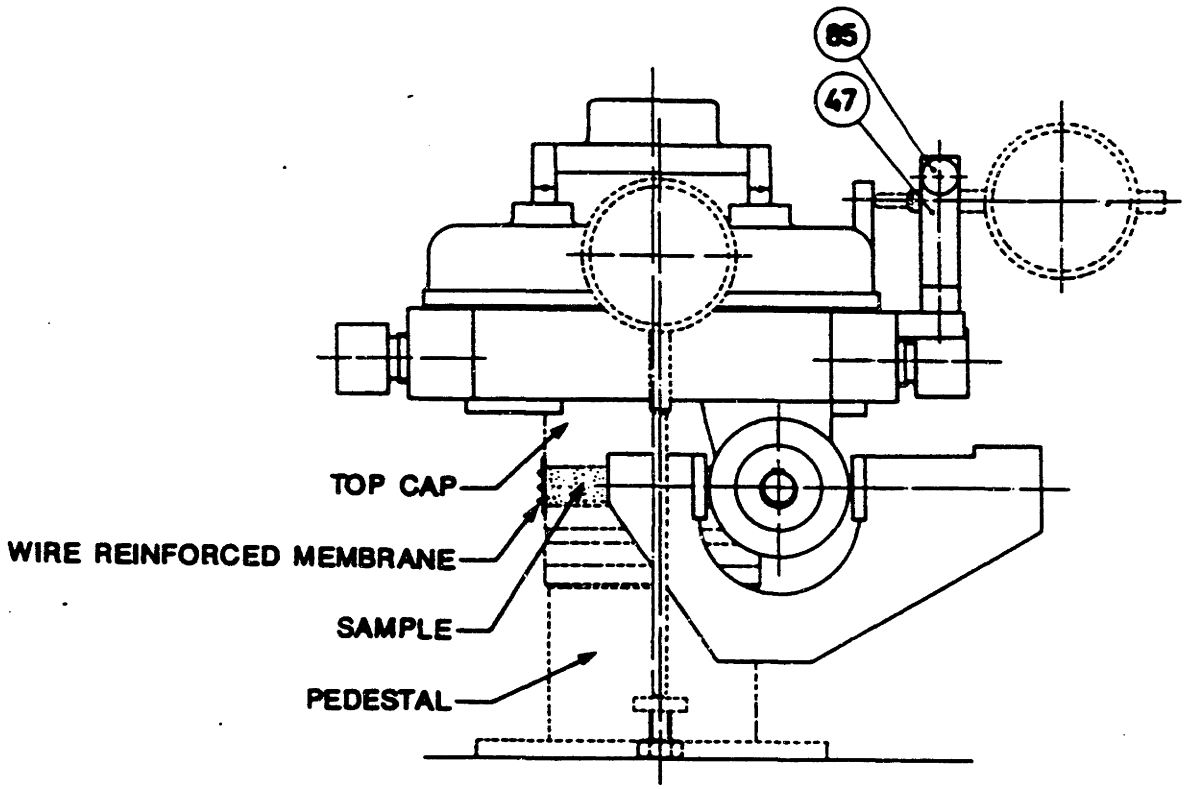

Figure E.2: Sample Loading Assembly (Geonor DSS Manual).

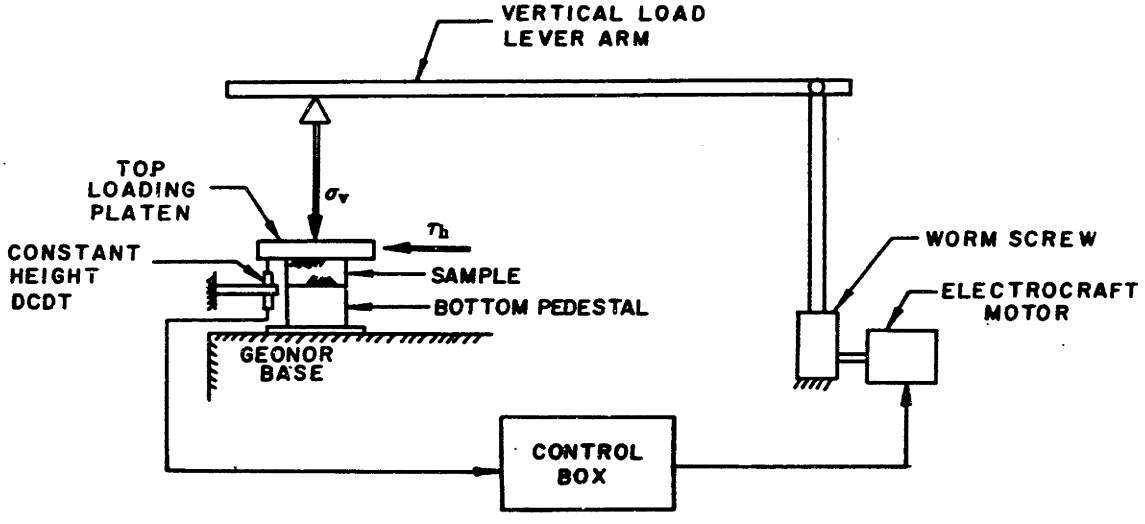

Figure E.3: Schematic of Geonor Constant Height Control Servo System.

APPENDIX F

DISCUSSION ON ANISOTROPIC CONSOLIDATION OF BBC IN THE MDSS

This appendix discusses the results of the anisotropic consolidation phase of tests conducted on BBC in the MDSS. The consolidation results presented in Chapter 5 indicate that the pattern of shear strains measured during anisotropic consolidation may not be consistent. In general, it appears that tests conducted at θ angles of 120 and 150 degrees do not exhibit the same magnitude of shear strain as found for tests conducted at θ equal to 0°, 30°, 60° and 90°. This discrepancy may be due to variability in the batch soil and/or inherent mechanical problems with the MDSS. The objective of this appendix is to study the anisotropic consolidation results and to decide if any concluding statements about the two possible causes for the discrepancy can be made.

F.1 OVERVIEW

Tests performed in the MDSS on the same type of material and at the same stress conditions should result in the same strains (ϵ_v and γ_t) independent of the test angle θ.[1] The excellent results found for the kinematic proof tests with rubber, presented in Chapter 4, clearly showed that this is the case for the device. It does not, however, appear to be the case for tests performed with BBC. Tests conducted on BBC at $\theta = 0°$, 30°, 60° and 90° have very similar vertical and shear strains during anisotropic consolidation. The first set of tests run at $\theta = 120°$ and 150° did not have final shear strains similar to the tests run at $\theta = 0°$ to 90°. Hence a second set of tests were performed at $\theta = 120°$ and 150° which also had shear strains different from the $\theta = 0°$ to 90° tests.

---

[1]Assuming the material is isotropic in the horizontal plane.

It was also decided that some additional rubber tests should be conducted in conjunction with the repeat tests on BBC at $\theta = 120^\circ$ (C15) and 150° (C16). Tests with rubber were conducted both before and after the two repeat tests on BBC (R24 and R26 for C15; R23 and R27 for C16). The results were found to be accurate, consistent and repeatable and are presented in Chapter 4 along with the other tests performed on rubber. All rubber tests were subjected to the same magnitude of stresses applied to the soil samples ($\sigma'_{vc} = 3.0$ ksc and $\tau_{hc}/\sigma'_{vc} = 0.2$). This, combined with the fact that the vertical and shear strains in the rubber specimens are of the same order of magnitude as the BBC specimens, eliminates several possible explanations for the different consolidation shear strains obtained for the BBC tests at $\theta = 120^\circ$ and 150°. These include: incorrect calibration factors for the displacement transducers and load cells, incorrect magnitude of the applied vertical force and horizontal shear force, and problems with inaccurate sliding of the main bearing plates.

The initial tests conducted on BBC at $\theta = 0^\circ$ to 90° were on specimens from batch 202 while the initial tests with $\theta = 120^\circ$ and 150° were conducted on specimens from batch 203. This indicated that differences in the measured shear strains may be due to sample variability between the two batches hence a second test at $\theta = 60^\circ$ was performed using a specimen from batch 203.

The consolidation strain results for the MDSS tests are analyzed in more detail in the following two sections.[2]

F.2 VERTICAL CONSOLIDATION STRAINS

The compression curves plotted in Figure 5.4 of Chapter 5 show that anisotropically consolidated specimens exhibit larger vertical strains than a K_o

[2]Test C9 ($\theta = 120^\circ$) is not included in the consolidation results presented in this appendix because the specimen was subjected to an irregular loading pattern during consolidation as a result of a power failure.

consolidated specimen. In addition, the virgin compression slopes are nearly parallel indicating that most of the difference in the vertical strains occur at stress levels around the preconsolidation pressure. Figure F.1 is a plot of the individual compression curves for the CAU tests conducted on BBC in the MDSS at τ_{hc}/σ'_{vc} = 0.2. The results show that there is very little variation in vertical strains among the different tests. The four tests conducted on batch 202 soil (C7, C8, C10 and C12) have at σ'_{vc} = 3 ksc an average ϵ_v (at t = 100 min) equal to 12.9% ± 0.3SD compared to 13.0% ± 0.8SD for the four tests on batch 203 soil (C13, C15, C16 and C17). The three tests conducted at θ = 120° and 150° (C13, C15 and C16) have an average ϵ_v = 12.6% ± 0.2SD. These results show that the final vertical strains display very little variation between the two batches and between tests conducted at θ = 0° to 90° and those at θ = 120° and 150°.

Figure F.2 is a plot of the incremental vertical strains measured at t = 100 min for the CAU tests.[3] The results show very little variation at all stress levels except at σ'_{vc} = 1.0 ksc which is approximately the preconsolidation pressure of the test specimens. Tests C13 (θ = 150°) and C15 (θ = 120°) have the smallest increment of vertical strain from σ'_{vc} = 0.5 to 1.0 ksc. Both of these samples are from batch 203, however, tests C16 (θ = 150°) and C17 (θ = 60°) are also from batch 203 and have incremental vertical strains at σ'_{vc} = 1.0 ksc very similar to the batch 202 specimens. Also the results for test C16 (θ = 150°) show that all tests conducted at θ = 120° and 150° do not have smaller incremental vertical strains at σ'_{vc} = 1.0 ksc.

In analyzing these data it is important to keep in perspective the changes in vertical strain due to anisotropic consolidation. Anisotropic consolidation induces a completely different stress state within a specimen compared with K_o consolidation,

---

[3]Test C12 (θ = 90°) is excluded from this plot because in this test the consolidation increments were applied at a different time schedule than the other tests. This does not affect the final consolidation strains but does influence the incremental strains.

yet the data plotted in Figure 5.4 show that the vertical strains are only about 1.5 to 2% (% strain and not % difference) larger than K_o consolidated specimens. Therefore, the CAU tests at θ = 120° and 150°, despite having an average γ_t approximately 4% less than the θ = 0° to 90° tests (14.9% versus 19.1%), will not have vertical strains that differ from the θ = 0° to 90° tests. In other words, it is highly unlikely that the differences in consolidation shear strains among the CAU tests will result in a noticeable variation in the vertical consolidation strains.

F.3 CONSOLIDATION SHEAR STRAINS

Figure F.3 is a plot of the final consolidation shear strain for the CAU tests run in the MDSS. This is the same as Figure 5.6 of Chapter 5 with the addition of several average shear strain circles including one that represents the average of the four tests on batch 202 soil (γ_t = 19.2% ±0.4SD for tests C7, C8, C10 and C12) and one for batch 203 specimens (γ_t = 15.8% ±2.0SD for tests C13, C15, C16 and C17). The average shear strain circles indicate that the batch 202 specimens have a larger shear strain than specimens from batch 203. However, it also shows that the tests conducted at θ = 120° and 150° have the lowest final shear strain, all plotting on or inside the γ_t = 15.8% circle. Test C17 (θ = 60°) plots outside the γ_t = 15.8% circle and in fact is much closer to the average shear strain circle for the batch 202 specimens. Recomputing the average shear strain circles to include all tests with θ = 0° to 90° gives γ_t = 19.1% ±0.4SD (C7, C8, C10, C12 and C17) and tests with θ = 120° and 150° (C13, C15 and C16) gives γ_t = 14.9% ±0.8SD. The recomputed circles strongly indicate that tests conducted at $\theta > 90°$ experience less shear strain during anisotropic consolidation than tests conducted at $\theta \leq 90°$, independent of which batch the specimens came from. If this is the case, then the difference in consolidation shear strains may not be due to sample variability but due to a problem with the mechanics of the MDSS. Yet the data are limited and certainly not conclusive. Evidence to the

contrary is found in a plot of the incremental shear strain versus shear stress shown in Figure F.4. Figure F.4a shows that the batch 202 specimens have the largest incremental shear strains at $\tau_{hc} = 0.2$ and 0.3 (this corresponds to $\sigma'_{vc} = 1$ and 1.5 ksc; i.e., around the preconsolidation pressure) compared to the batch 203 specimens. Figure F.4b is the same plot showing the average incremental strains at each stress level for the batch 202 specimens (C7, C8 and C10), batch 203 specimens (C13, C15, C16 and C17) and test C17. The data plotted in the figure shows that although the batch 203 specimens have a lower incremental shear strain at all stress levels the most significant difference occurs at stress increments around the preconsolidation pressure. This would be expected if there was some variability between the two batches. Furthermore, test C17 ($\theta = 60°$, batch 203) compares well with the batch 202 specimens at $\tau_{hc} \geq 0.4$ ksc, but has lower incremental shear strains at stress increments near the preconsolidation pressure.

The data presented in this section appear to be inconclusive. The final shear strain for test C17 indicates that the lower shear strains found for the $\theta = 120°$ and 150° test are not a function of batch variability. Yet, differences in the incremental shear strains around the preconsolidation pressure indicate that the response of the specimens depends in part on which batch they come from and not exclusively on the test angle θ.

F.4 MEASURED TOP CAP DEFLECTION DURING CONSOLIDATION

The kinematic proof tests on rubber presented in Section 4.6 of Chapter 4 gave excellent results and confirmed that the set–up procedure and strain measuring system in the MDSS are working properly and produce repeatable results. Some data from these tests can be used to compare with the results obtained for the CAU tests on BBC. Specifically, the measured deflection of the top cap during consolidation for the tests on BBC can be compared with the results obtained for the tests conducted at the

same stress level on rubber. This measurement is made with the two vertical displacement transducers Z1 and Z2 (see Figure 3.3). The difference in vertical displacement measured by these two transducers is defined as ΔZ where,

$$\Delta Z = Z1 - Z2 \qquad \text{F.1}$$

Ideally, ΔZ should be zero for CK_oU tests but this is rarely the case. The value of ΔZ is influenced by several factors including; alignment of the vertical loading system, set–up and tightness of the top cap bolts, set–up of the displacement transducers and conditions of the porous stones and wire–reinforced membrane. In CAU tests all these variables still exist but the magnitude and sign of ΔZ is primarily controlled by the magnitude of the consolidation shear force and its orientation (i.e., θ angle). Table F.1 gives a summary of the type of trends expected in the value of ΔZ as a function of the tests angle θ for the CAU tests. Theoretically, tests at $\theta = 120°$ and $150°$ should have the maximum ΔZ , tests at $\theta = 30°$ and $60°$ should have the minimum ΔZ and tests at $\theta = 0°$ and $90°$ should have equal and opposite ΔZ's and be in between the values for $\theta = 120°/150°$ and $\theta = 30°/60°$. Table F.2 is a summary of the ΔZ measured at the end of consolidation for all of the tests on BBC and rubber. It should be kept in mind that the reported values of ΔZ do not represent the absolute rotation of the top cap. The absolute rotation angle should theoretically be independent of θ for tests conducted at the same stress level. Since the vertical displacement transducers are always set up at a fixed orientation ($\theta \cong 135°$, see sketch in Table F.1), the ΔZ trends and measurements given in Tables F.1 and F.2 are those for a line in the plane of rotation of the top cap at an orientation of $|\theta - 135°|$ relative to the test angle θ. For the displacement transducer limited to a fixed orientation, the ΔZ measurements will most closely represent the absolute rotation of the top cap for tests at $\theta = 120°$ and $150°$ and least represent it for tests at $\theta = 30°$ and $60°$ (as listed

in Table F.1). The objective of presenting the measured ΔZ values here is to make comparisons between the rubber and clay tests and not to estimate the absolute rotation of the top cap.

With the exception of one clay test, all the CK_oU tests resulted in a negative ΔZ which most likely indicates a slight misalignment of the vertical loading system. For the CAU tests, most of the data for both the rubber and clay tests confirm the trends expected in Table F.1. The $\theta = 0°$ test has a positive ΔZ while the tests at $\theta = 90°$, $120°$ and $150°$ all have negative ΔZ's, with the $\theta = 120°$ and $150°$ tests having the maximum values. The $\theta = 0°$ and $90°$ results are opposite in sign but not equal. This result is not surprising given the negative ΔZ measured for the CK_oU tests (i.e., if the device has an inherent negative ΔZ then the $0°$ value will decrease and the $90°$ value will increase). The data show that there is very little difference between the results found for the rubber and clay tests. This indicates that the vertical loading system of the MDSS is not deforming in an unusual manner during the tests on clay, particularly for those tests at angles of $\theta = 120°$ and $150°$.

The data presented in this section do not resolve the question of why the tests conducted on BBC at $\theta = 120°$ and $150°$ experience less consolidation shear strain than those conducted at $\theta = 0°$ to $90°$. However, they do show that the MDSS deforms in a similar manner under an applied stress state independent of whether the material is clay or rubber and does not exhibit any unusual response in terms of deformation for the tests conducted on BBC at $\theta = 120°$ and $150°$.

F.5 UNDRAINED SHEAR RESULTS OF REPEAT TESTS ON BBC AT $\theta = 60°$, $120°$ and $150°$

All three pairs of repeat tests on BBC with $\tau_{hc}/\sigma'_{vc} = 0.2$ do not have identical shear strain at the end of consolidation (Figure F.3). The magnitude of the vector difference between the end of consolidation total shear strain γ_t for the three

test pairs equals 2.6%, 2.0% and 1.8% (% shear strain) for θ = 150°, 120° and 60° respectively.[4] Given that the repeat tests have these vector differences in γ_t, at the end of consolidation, it is interesting to check if the undrained shear behavior of the pairs of repeat tests display any differences.

The results of the repeat tests are presented in more detail in Chapter 5 but Table F.3 gives a brief summary of the undrained shear parameters at the peak τ_x shear resistance. The data listed in the table clearly show that the results for the repeat tests at all three theta angles compare very well with the first set of tests conducted at these angles. In fact, as shown in Chapter 5, the stress–strain curves and stress paths of all three pairs of tests are nearly identical. Furthermore, if the undrained shear strain paths are superimposed with a common origin they are also almost identical.

These data show that there is remarkably little variation in the undrained shear response for each of the pairs of repeat tests inspite of deviations in the magnitude of the vector difference between γ_t for each of the three pairs ranging from 1.8% to 2.6%. This clearly indicates that it is the orientation θ and magnitude of the applied consolidation stress ratio τ_{hc}/σ'_{vc} which determines a sample's undrained shear behavior (i.e., variations in the magnitude and orientation of γ_t between samples with the same θ and τ_{hc}/σ'_{vc} did not result in differences in their undrained shear response). This implies that the 4.2% (% strain) difference in the average magnitude of γ_t between the θ = 0° to 90° and θ =120° and 150° tests (Figure F.3; 19.1% versus 14.9%) should not be considered significant enough to preclude using the θ = 120° and 150° undrained shear results for further analysis. In other words, the tests conducted

---

[4]From vector analysis the difference in magnitude of γ_t for two tests A and B is computed as: $\|{}^a\underline{\gamma}_t\| - \|{}^b\underline{\gamma}_t\| = ({}^a\gamma_x{}^2 + {}^a\gamma_y{}^2)^{0.5} - ({}^b\gamma_x{}^2 + {}^b\gamma_y{}^2)^{0.5}$. The magnitude of the vector difference of γ_t between two tests is computed as: $\|{}^a\underline{\gamma}_t - {}^b\underline{\gamma}_t\| = [({}^a\gamma_x - {}^b\gamma_x)^2 + ({}^a\gamma_y - {}^b\gamma_y)^2]^{0.5}$. Under ideal conditions two specimens of the same soil subjected to the same θ and τ_{hc}/σ'_{vc} should have the same magnitude of γ_t and the magnitude of the vector difference between their γ_t's should be equal to zero.

at $\theta = 120°$ and 150° should be used together with those at $\theta = 0°$ to 90° for studying the undrained shear behavior of BBC with $\tau_{hc}/\sigma'_{vc} = 0.2$ as a function of the test angle θ.

F.6 SUMMARY AND CONCLUSIONS

The objective of this appendix was to determine if the differences in the final consolidation shear strain during anisotropic consolidation of BBC specimens in the MDSS are due to variability between the batches from which the specimens were taken from and/or due to inherent problems with the mechanics of the MDSS. While the data presented in this appendix did not conclusively resolve the issue, they did provide some additional insight into the problem. It was not expected that carefully studying the consolidation data would result in a resolution of the problem because it appears that the only way to do this would be to conduct an extensive series of tests at all of the different test angles θ. However, this would be a very time–consuming exercise which would not be very practical.

Based on the results presented in this appendix and Chapter 4, the following observations can be made with respect to the differences in the consolidation shear strains for the CAU tests conducted on BBC in the MDSS:

1. Chapter 4 presented results for rubber which clearly showed that the set–up procedures, horizontal loading system and strain measuring system in the MDSS are working properly and produce accurate and reliable results.

2. The consolidation shear strains for the tests on BBC show some inconsistencies among the various test angles θ and in general the angle of deformation of the specimens does not correspond as accurately to the test angle θ as was found for the tests on rubber. There does not appear to be a consistent trend between the deviation in the applied θ and measured θ with the final magnitude of the end of consolidation total shear strain γ_t.

3. The vertical compression curves and incremental vertical strain data showed very little variation among the different CAU tests on BBC indicating that the vertical compression behavior is independent of the

batch which the specimens were taken from as well as the test angle θ.

4. An analysis of the final and incremental consolidation shear strain data was inconclusive. The final shear strain data appear to indicate that the lower consolidation shear strains found for the tests conducted at θ = 120° and 150° are not consistent with the data measured for tests conducted at θ = 0° to 90° independent of which batch the specimens came from. However, differences in the incremental shear strains around the preconsolidation pressure indicate that the response of the specimens depends in part on which batch they came from and not exclusively on the test angle theta.

5. Comparison of measurements of the top cap deformation during consolidation for tests on BBC and rubber showed that the MDSS deforms in a similar manner independent of whether the material is clay or rubber and does not exhibit any unusual response in terms of deformation for the BBC tests at θ = 120° and 150°.

The reason why the tests conducted on BBC at θ = 120° and 150° exhibit smaller shear strains than tests conducted at θ = 0° to 90° remains uncertain. However, in spite of this, the undrained shear response of the tests with θ =120° and 150° will be used with the θ = 0° to 90° tests for studying the the undrained shear behavior of BBC with τ_{hc}/σ'_{vc} = 0.2 as a function of the test angle θ.

TABLE F.1: Expected Magnitude and Orientation of ΔZ During Anisotropic Consolidation in the MDSS

Test Angle θ (°)	ΔZ = Z1 - Z2	
	Orientation	Magnitude
0	+	average
30	+/-	minimum
60	+/-	minimum
90	-	average
120	-	maximum
150	-	maximum

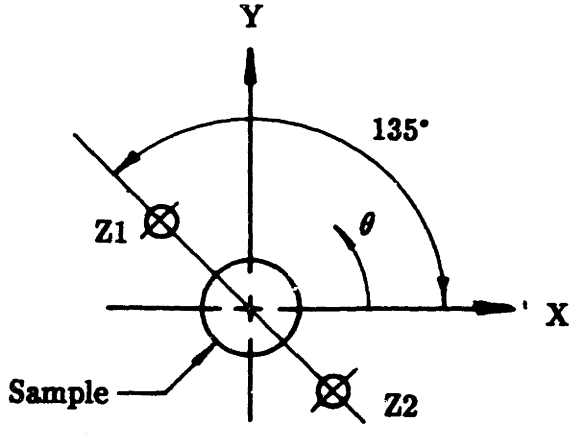

Orientation of Z1 and Z2
Displacement Transducers

TABLE F.2: ΔZ at the End of Application of τ_1 for BBC and Rubber Tests in the MDSS

Test Angle θ (°)	Rubber		BBC	
	Test	ΔZ (cm)	Test	ΔZ (cm)
CK_oU	R28	-0.0033	C5 C6 C11 C14	+0.0036 -0.0041 -0.0052 -0.0058
0	R18	+0.0044	C7	+0.0023
30	R30	-0.0024	C10	-0.0037
60	R19	-0.0068	C17	-0.0086
90	R21	-0.0157	C12	-0.0176
120	R20 R24 R26	-0.0226 -0.0165 -0.0216 Ave. = -0.0202	C9 C15	-0.0203 -0.0214 Ave. = -0.0209
150	R23 R27 R22	-0.0124 -0.0151 -0.0174 Ave. = -0.0150	C13 C16	-0.0152 -0.0194 Ave. = -0.0173

Notes:
1. σ'_{vc} = 3.0 ksc and τ_{hc} = 0.6 ksc.
2. ΔZ = Z1 - Z2 (cm).

TABLE F.3: Undrained Shear Results of CAUMDSS Repeat Tests on OCR = 1 BBC with $\tau_{hc}/\sigma'_{vc} = 0.2$ and $\theta = 60°$, 120° and 150°

Test No.	Theta (°)	Cons. $\Delta\gamma_t$ (%)	At Peak τ_x				
			γ_x (%)	γ_y (%)	γ_t (%)	$\frac{\tau_x}{\sigma'_{vc}}$	$\frac{\sigma'_v}{\sigma'_{vc}}$
C8	60		0.98	0.45	1.08	0.268	0.816
C17	60	2.0	0.67	0.21	0.70	0.267	0.874
C9	120		4.6	2.9	5.4	0.153	0.563
C15	120	2.4	5.1	2.7	5.8	0.148	0.526
C13	150		15.9	4.2	16.4	0.185	0.412
C16	150	2.7	14.8	3.6	15.2	0.182	0.435

Notes:

1. See Table 5.5 in Chapter 5 for more detailed results.
2. $\Delta\gamma_t = \|{}^a\gamma_t - {}^b\gamma_t\| = [({}^a\gamma_x - {}^b\gamma_x)^2 + ({}^a\gamma_y - {}^b\gamma_y)^2]^{0.5}$ for two tests A and B.

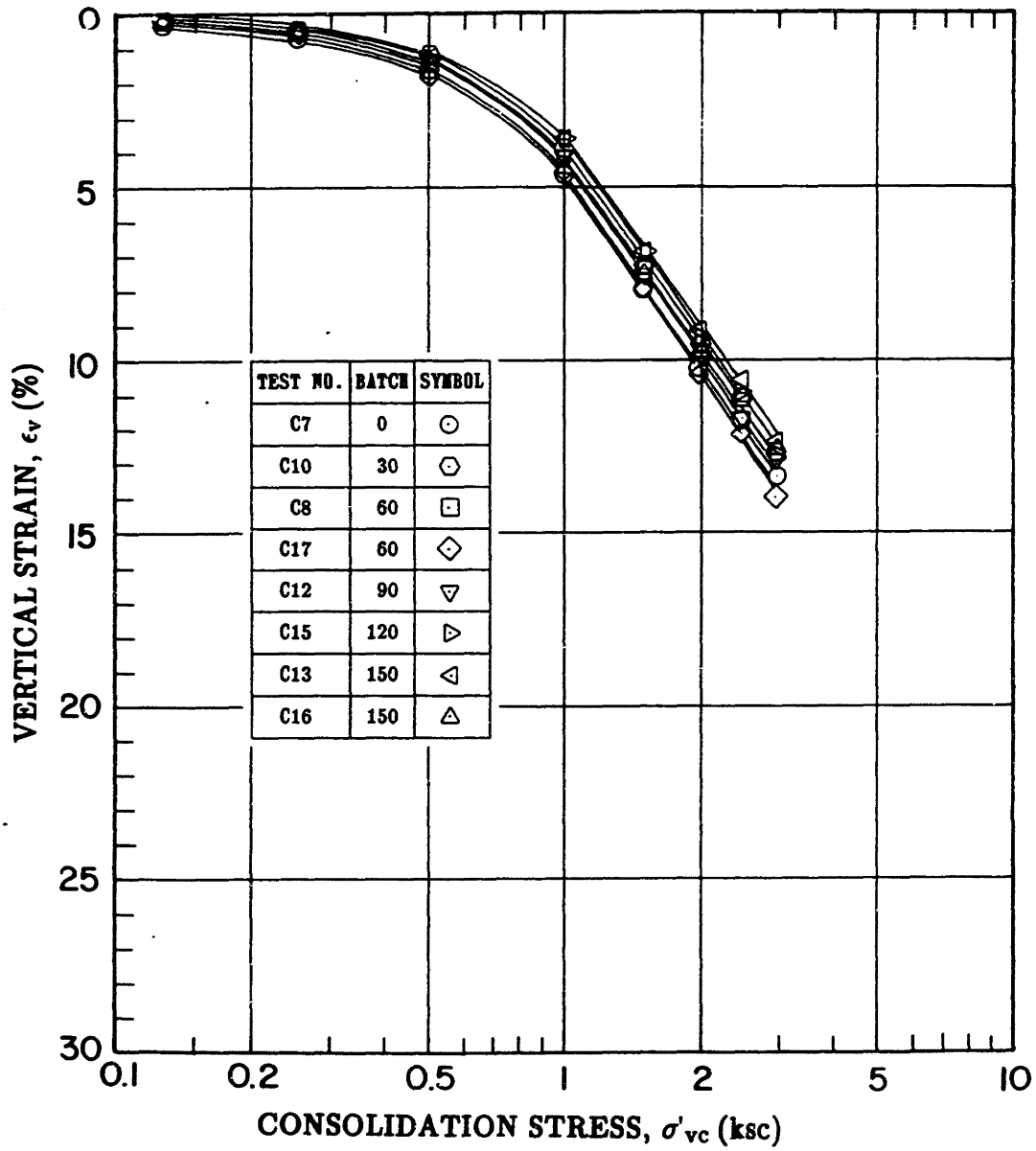

Points Plotted At:
1. t_f for $\sigma'_{vc} \leq 0.25$ ksc.
2. t = 100 min. for $\sigma'_{vc} \geq 0.5$ ksc.

Figure F.1: Compression Curves for CAUMDSS Tests on BBC with $\tau_{hc}/\sigma'_{vc} = 0.2$ (tabulated data in Appendix H).

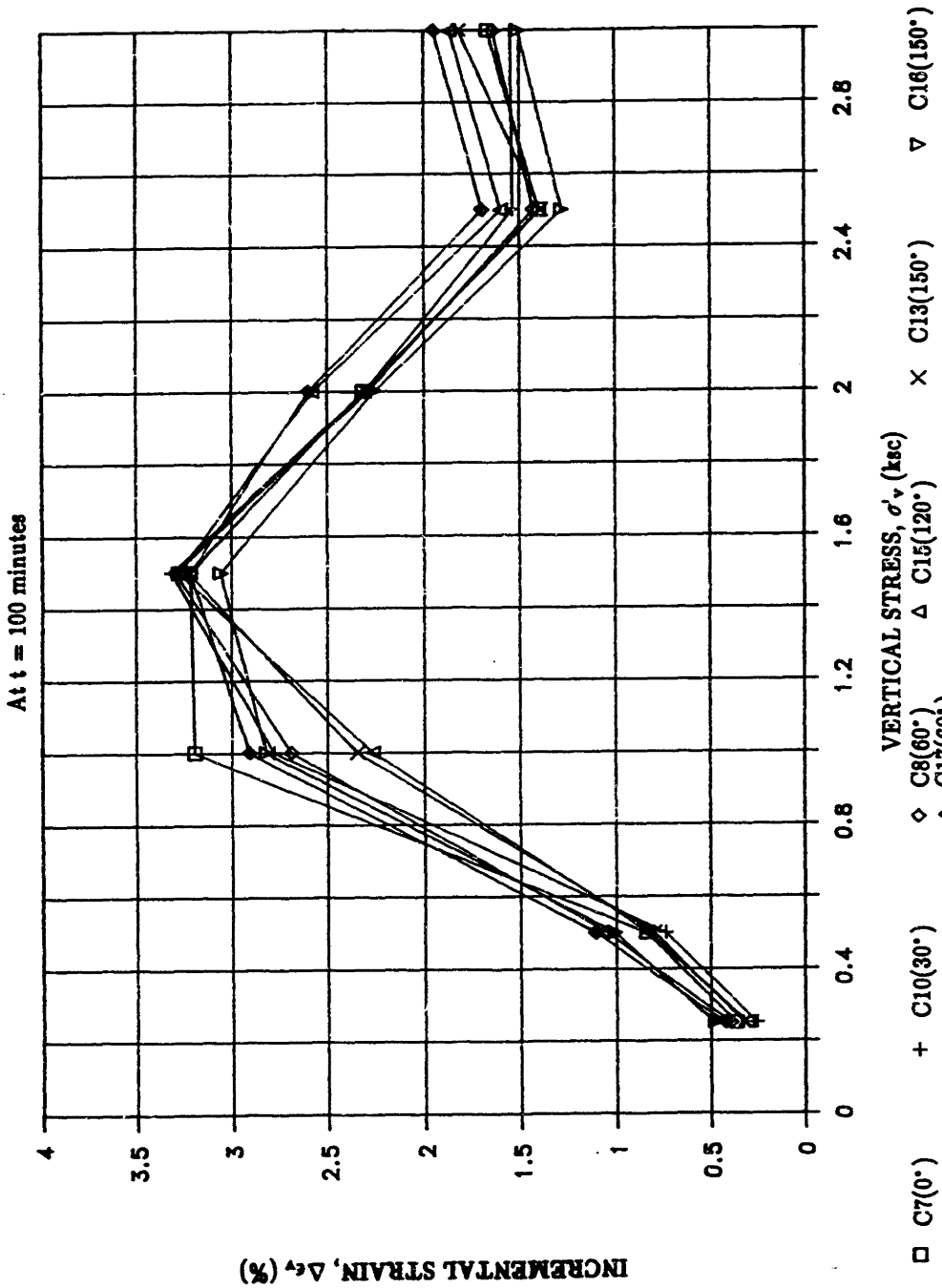

Figure F.2: Incremental Vertical Consolidation Strains for CAUMDSS Tests on BBC with $\tau_{hc}/\sigma'_{vc} = 0.2$.

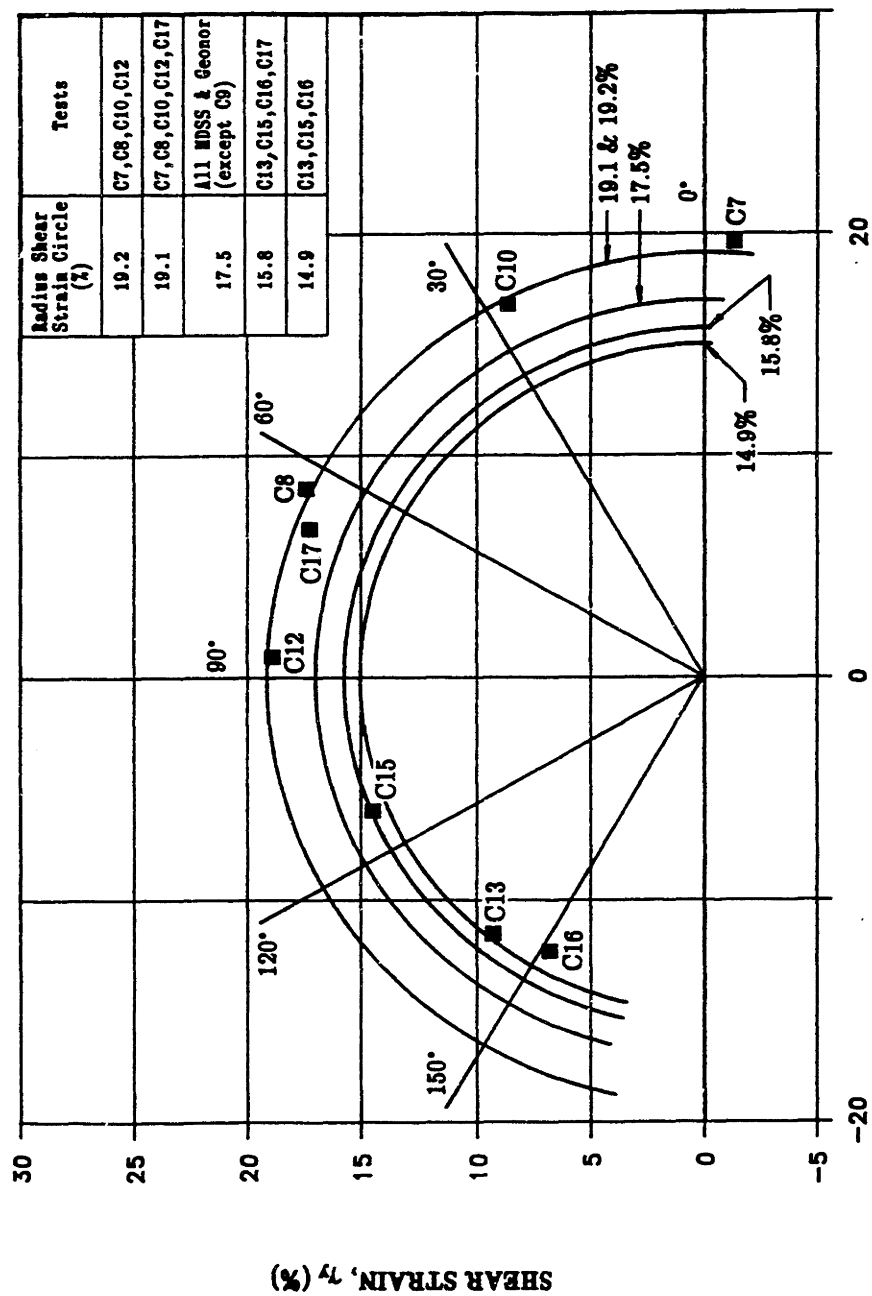

Figure F.3: End of Consolidation Shear Strain for CAUMDSS Tests on BBC with $\tau_{hc}/\sigma'_{vc} = 0.2$.

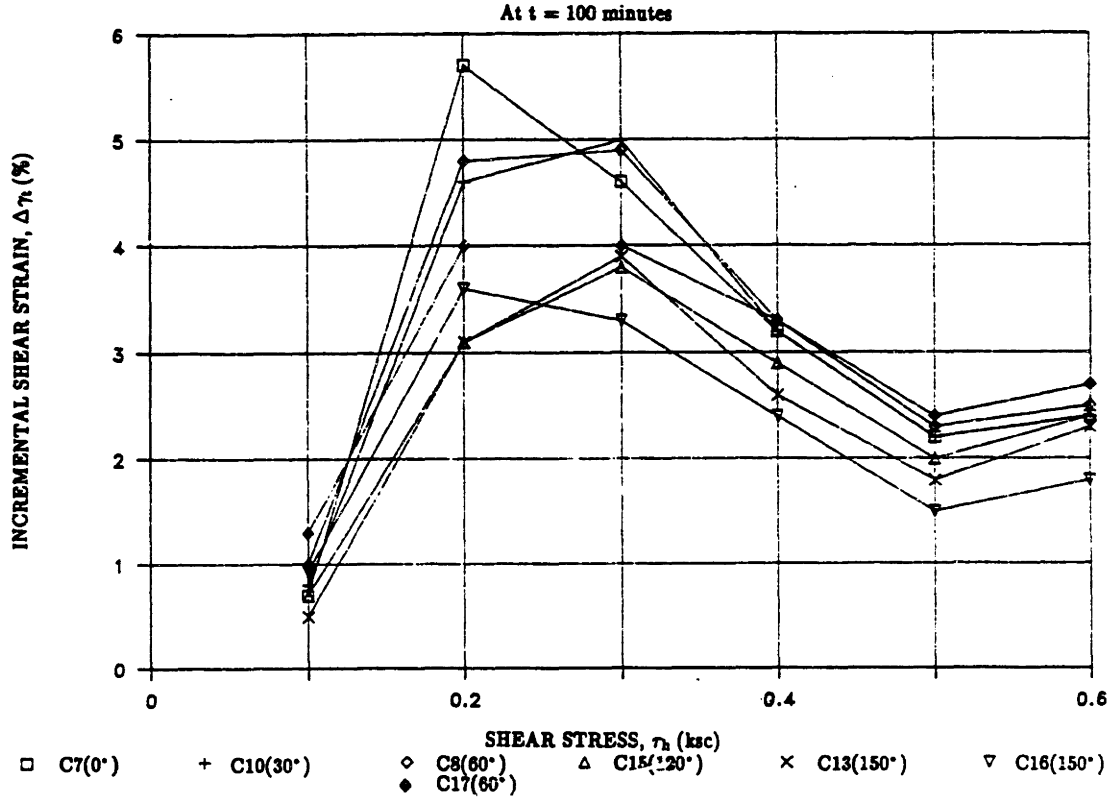

(a)

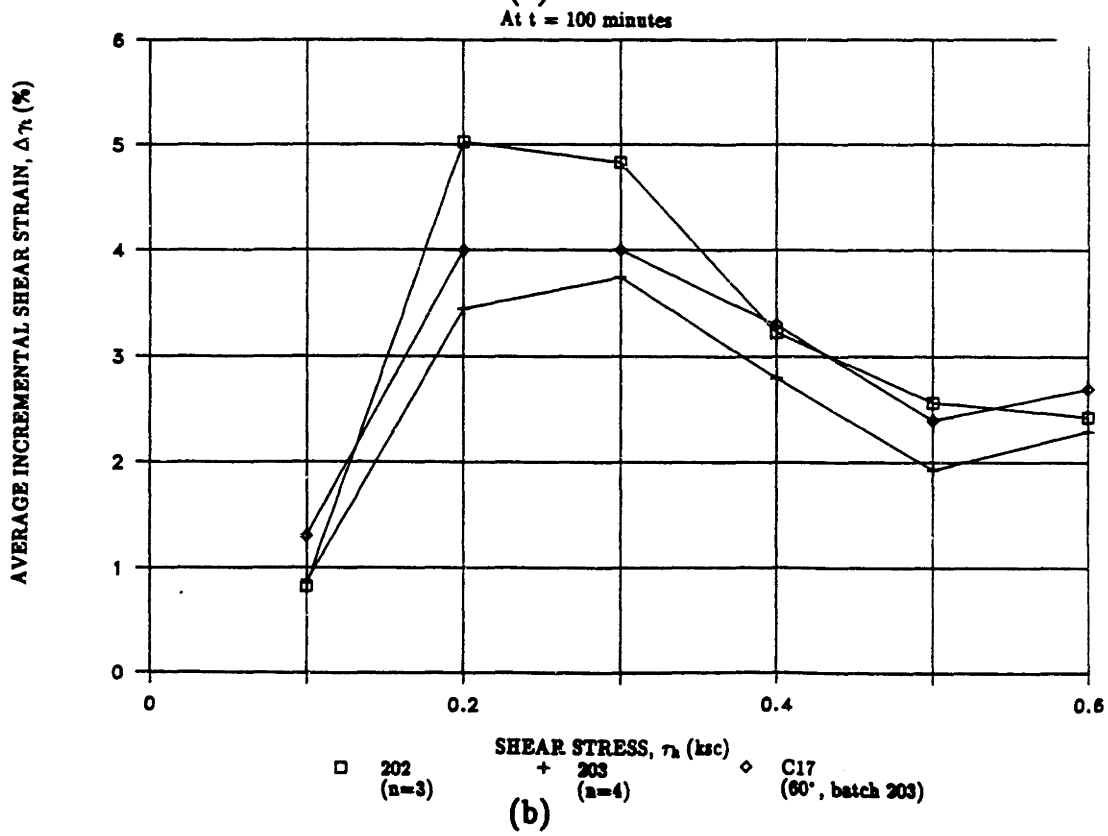

(b)

Figure F.4: Consolidation Shear Strain versus Shear Stress for CAUMDSS Tests on BBC with $\tau_{hc}/\sigma'_{vc} = 0.2$: (a) Incremental Shear Strains; (b) Average Incremental Shear Strains for Tests from Batches 202 and 203.

APPENDIX G

DISCUSSION ON REVERSAL OF APPLIED SHEAR STRESS IN DIRECT SIMPLE SHEAR TESTS

G.1 INTRODUCTION

Section 2.4.1.6 of Chapter 2 discussed the ability of the Geonor DSS to apply two independent horizontal shear stresses to a test specimen. The first shear stress is applied under stress controlled conditions while the second is usually applied under strain controlled conditions. Both forces can be applied in the same direction ($\theta = 0°$) or in opposite directions ($\theta = 180°$; see Figure 2.29b). Generally, this feature of the Geonor DSS is used to run anisotropically consolidated undrained direct simple shear tests (CAUDSS). Specimens are subjected to a vertical stress and a horizontal shear stress during consolidation and then subsequently sheared undrained by application of the second horizontal shear stress.

Section 5.3 of Chapter 5 presented results of two CAUDSS tests on BBC with $\theta = 180°$ and $\tau_{hc}/\sigma'_{vc} = 0.2$ (tests G6 and G7). The stress paths of these two tests display some unusual features near the peak shear resistance. The stress paths have fairly conventional shapes until the sample approaches what would generally be considered its peak shear resistance (i.e., the slope of the stress paths were approaching a horizontal line). At this point the slope of the stress paths changed such that the sample developed a significant increase in shear resistance with relatively little change in effective stress. This behavior was unexpected, which tends to make one question if it represents real soil behavior or an undesirable influence of the testing device. The objective of this Appendix is to investigate whether it can be determined if the peculiar behavior of these test specimens near their peak shear resistance is caused by problems with the direct simple shear apparatus.

The Appendix begins with a presentation of the results of a series of tests conducted with an elastic material (rubber). This is followed by a discussion of the results of four cyclic DSS tests on two different clays (BBC and San Francisco Bay Mud; SFBM) which were conducted at the conventional rate of undrained shear (γ = 5%/hour). The results of the rubber and cyclic tests are used to postulate a reason for the unusual behavior of some of the CAUDSS test conducted with $\theta = 180°$ in the Geonor DSS.

G.2 RESULTS OF DSS TESTS CONDUCTED WITH RUBBER

Several tests in the Geonor DSS and the MDSS were performed using a rubber material because of its elastic properties. Rubber is also an incompressible material and therefore does not undergo volume changes like soils do (i.e., $\nu = 0.5$). Hence, if a sample of perfectly elastic rubber were subjected to pure shear conditions there would be no volume changes.[1] However, in the Geonor DSS and MDSS, specimens are subjected to simple shear strain conditions without complementary shear stresses acting on the sides of the specimen, resulting in a nonuniform state of stress. In fact, theoretical studies using elastic material properties (Appendix A, Section A.5) predict that tensile zones develop at the upper leading edge and lower trailing edge of specimens under simple shear strain conditions (see Figures A.12 and A.13).

The development of tensile zones in the DSS apparatus for an elastic material was verified using a rubber specimen. The rubber was subjected to a vertical stress of 3 ksc in the DSS and then sheared under constant height conditions (the sample was not confined in the wire–reinforced membrane). Figure G.1 shows a schematic cross–section of the rubber specimen at shear strains less and greater than 10%. The sketches in Figure G.1 show that at small shear strains a gap opens up at the lower

---

[1]Actually a material does not have to be incompressible for this condition to hold. An elastic material subjected to a pure shear state of stress (i.e., $\Delta\sigma_{oct} = 0$) will have $\Delta\epsilon_{vol} = 0$ independent of the value of ν.

trailing edge, while the sample was pinched at the upper leading edge. Furthermore, the specimen did not have straight and parallel edges from the top surface to the bottom surface, as required for simple shear strain conditions to exist. At higher shear strains the top leading edge also developed a gap that, along with the lower trailing edge gap, kept getting bigger with increasing shear (a file folder $\cong$ 0.025 inches thick could easily be inserted in the gap)

The stress–strain curve of a constant height direct simple shear test conducted in the MDSS on the rubber specimen is shown in Figure G.2a. In spite of the development of gaps, the stress–strain relationship is almost linear because the specimen is well within its elastic range and is able to redistribute the shear stress to the area of the specimen remaining in contact with the top cap and the bottom pedestal. The influence of the gaps is reflected in the vertical stress versus the X coordinate plotted in Figure G.2b (X = 0 in the Figure represents the neutral position of the MDSS which corresponds to $\gamma = 0$). In this figure the continuous decrease in the vertical stress required to maintain the specimen's height constant during shear is similar to the behavior of a normally consolidated cohesive soil (i.e., the soil tends to develop positive pore pressure $\rightarrow$ contractive behavior). However, the rubber specimen is an incompressible elastic material which ideally should not require a change in the vertical stress to maintain its height constant under simple shear strain conditions.
Yet in a DSS test the stress conditions are not uniform; gaps develop and the effective area of the specimen decreases. This results in an increase in the vertical stress acting on the sample remaining in contact with the top cap and bottom pedestal. The increase in vertical stress causes the rubber to want to undergo vertical compression. This is detected by the constant height servo control system which decreases the vertical load acting on the specimen. The vertical load continuously decreases during shear as the effective area of the specimen decreases due to the increase in the size of the gaps.

Section 4.6 of Chapter 4 described a series of tests conducted on rubber which were used as part of the kinematic proof tests of the MDSS. The vertical stress response during constant height shear (application of τ_2) of some of these tests is plotted in Figure G.3, along with the same type of test conducted on rubber in the Geonor DSS with $\theta = 180°$. The results plotted in this Figure for the tests with $\theta = 0°$ to 90° reflect the same trends as found for the MDSS test with $\tau_1 = 0$ plotted in Figure G.2. During application of τ_1, the samples presumably develop gaps which continue to increase in the X direction during application of τ_2. Hence, all of the curves show a significant decrease in the vertical force required to maintain the specimen's height constant during shear (τ_2). Of even more interest is the curves for the tests at $\theta =$ 120°, 150° and 180°. In these tests the vertical stress curves are parabolic and symmetric about the neutral axis of the MDSS and the Geonor DSS (i.e., X = 0). In these tests the gaps which develop during application of τ_1 start to close upon reversal of the shear stress due to τ_2 acting parallel to the X axis. As the gaps close, the effective area of the specimen increases, thereby resulting in a decrease in the average vertical stress and a tendency for the specimen to expand in the vertical direction. In response to this behavior, the constant height servo control system increases the vertical force to maintain the sample height constant. The rate of increase in the vertical stress monotonically decreases as the X coordinate approaches zero and the reverse phenomenon occurs as the sample passes through the neutral axis of the device. This effect is clearly more pronounced for those tests where the specimen strains the largest in the negative X direction during application of τ_1 (e.g., compare $\theta = 150°$ and 180° with $\theta = 120°$).

These results dramatically show the influence of the development of gaps due to the nonuniform state of stress on the behavior of an elastic specimen in a direct simple shear device. The results lead one to question if and how this condition influences the behavior of clay specimens tested in a simple shear apparatus. This will

be explored in the next two sections.

G.3 RESULTS OF CYCLIC DSS TESTS ON CLAY SPECIMENS TESTED WITH $\dot{\gamma} = 5\%$/HOUR

This section discusses the results of four cyclic direct simple shear tests conducted on BBC and SFBM. All four specimens were consolidated under K_o conditions and subsequently sheared undrained at the conventional rate of 5%/hour.

Figure G.4a is a plot of the stress–strain curve for a cyclic Geonor DSS test on normally consolidated BBC II conducted by Malek (1987). The specimen was cycled with $\tau_h/s_u = 0.85$ and required 2.25 cycles to reach failure. Before the specimen failed the stress–strain curve displayed the characteristic hysteresis shape of cyclic tests on soils. Figure G.4b is a plot of the normalized vertical stress during undrained shear. This plot shows a continuous decrease in the vertical effective stress (equivalent to development of positive pore pressure) as the number of cycles increases.

Figure G.5a is a plot of the stress–strain curve of a Geonor DSS test also conducted on a normally consolidated BBC III sample (Batch 205). In this case, the sample was K_o consolidated to $\sigma'_{vc} = 6$ ksc and then sheared undrained well beyond the peak shear resistance before reversing the direction of the applied shear force.[2] During initial loading, the normalized undrained shear strength was equal to 0.184 at $\gamma = 6.2\%$. Upon reversal, the maximum normalized shear resistance was equal to –0.133 and occurred at approximately $\gamma = 0\%$ (i.e., the neutral axis of the device). The variation in the normalized vertical effective stress is plotted in Figure G.5b. During initial loading the normalized vertical stress decreased in response to the contractive behavior of the sample. But upon reversal of the applied shear stress, the vertical stress gradually increased with the increase in the negative shear resistance and decrease in the shear strain. The increase in vertical stress reached a maximum at

[2]This test was performed by MIT graduate student Mr. I. Ahmed in 1989.

exactly $\gamma = 0\%$. The vertical stress then began to gradually decrease as the sample strained beyond the neutral axis of the device. The vertical stress response during the reversal cycle is also essentially symmetric about $\gamma = 0\%$.

This same type of behavior was observed in two Geonor DSS tests on SFBM conducted by MIT's Geotechnical Laboratory Director Dr. J.T. Germaine in 1985. Figure G.6 is a plot of the normalized shear stress and normalized vertical stress versus shear strain for the two tests. Both specimens were overconsolidated using the SHANSEP technique with OCR's equaling 1.5 and 4.1 for tests DSS–5 and DSS–6 respectively. In both tests the increase in vertical stress and shear stress during reversal of the applied shear stress reached a maximum at approximately $\gamma = 0\%$ and both curves display a symmetric shape about $\gamma = 0\%$.

Figure G.7 is a plot of the normalized vertical stress during reversal of the applied shear stress for the three tests described in the previous paragraphs. The value of the maximum vertical effective stress during the reversal cycle (usually near $\gamma = 0\%$) was used to normalize the data. The results plotted in Figure G.7 reflect the concave and near symmetric shape of the normalized vertical stress versus shear strain during the reversal stage. The fact that three DSS tests on two different soils at three different OCR's and stress levels exhibit this type of behavior during the reversal stage of the first cycle is more than coincidental. Symmetry of the normalized vertical stress about the neutral axis of the DSS device for all of the three different test conditions is suggestive of behavior that is not exclusively dependent on the type of soil and stress conditions, but also strongly dependent on the DSS apparatus itself.

There is no apparent soil behavioral reason why the vertical stress should reach a maximum while a sample is passing through the neutral plane of the device during the reversal stage. This did not occur in the cyclic test on BBC plotted in Figure G.4 because in this test the specimen was not initially strained beyond failure. The sample was loaded up to 85% of its maximum shear resistance and experienced

relatively small shear strains. The normalized vertical stress plot does, however, begin to show similar characteristics as the other three tests during cycle number 2. But clearly during the first cycle the vertical stress continuously decreases as the sample passes through the neutral axis of the device.

The results of the DSS tests on rubber presented in Section G.2 display the same characteristics in the vertical stress behavior as the clay tests when the specimens strained through the neutral axis of the device (e.g., $\theta = 180^{\circ}$ in Figure G.3). The response of the rubber specimens is explainable in terms of the reduction in their effective area as gaps develop during shear. It is unlikely that such gaps develop in the tests on clay specimens, but the similarity in the vertical stress plots between the rubber tests and clay tests (during the reversal cycle) suggest that the normal stress distribution in the clay specimens is influenced by the apparatus. The clay specimens undergo an apparatus–induced dilative behavior as the samples strain towards the neutral axis during the reversal cycle. This causes the servo control system to increase the vertical stress to maintain the sample height constant and hence results in an increase in the shear resistance. Once the sample passes through the neutral axis, the reverse occurs and the vertical stress and shear resistance decrease.

This device–induced behavior will not be evident in the measured results unless the sample has been sheared to a state where the rate of development of shear–induced pore pressure is relatively low. In other words, if the specimen is in a state where it is developing significant shear–induced pore pressures, as during the first cycle of the test on BBC plotted in Figure G.4, the measured response will reflect basic soil behavior rather than the tendency of the apparatus to influence the specimen's behavior. However, if a sample is in a state where it is not developing significant shear–induced pore pressure, then the influence of the device will dominate the measured response of the specimen as seen during the reversal cycle of the two tests on SFBM and the test on BBC.

The implication of this hypothesis is that the shear resistance of a clay specimen during a standard CK_oUDSS tests is not exclusively dependent on the soil type and stress conditions. This may particularly be the case during the post peak stage of a test where the specimen continuously strains away from the neutral axis of the device and the rate of pore pressure development is significantly less than the pre–peak stage of the test. The influence of the apparatus on the measured shear resistance could be considered to have a convex shape symmetric with respect to the neutral axis of the device. As the shear strain increases, the reduction in shear resistance of a test specimen due to the influence of the apparatus on the reduction in σ'_v increases as shown schematically in Figure G.8.

The notion that the DSS apparatus causes a device–induced reduction in shear resistance leads one to wonder if a correction to the measured data could be developed. Before such a correction could be developed, however, it is necessary to obtain experimental evidence which would leave little doubt that the device–induced reduction in shear resistance hypothesis is valid. One possible way to do this would be to conduct tests like that performed on the SFBM specimens but with many more cycles. Presumably after several cycles the shear resistance of the soil will have reduced to the residual value.[3] If at this stage the stress–strain curve continues to exhibit a maximum shear resistance each time the specimen passes through the neutral axis of the device and is symmetric about the neutral axis, then that should leave little doubt about the influence of the device as shown schematically in Figure G.9.

If the same phenomenon was observed in a variety of tests on different soils and the normalized stress–strain curves were parallel as shown in Figure G.10, then it

---

[3]This was tried with the BBC test plotted in Figure G.5. Unfortunately, the vertical stress becomes very low in these type of tests and may cause slippage between the top cap and the specimen. This is what happened during the BBC test and once it occurred continued shearing involved displacement of the top cap relative to the top of the specimen.

may be possible to develop a correction. If, however, they are not parallel then how to make a correction is not evident. Even if a correction to the stress–strain data could be made, it could not be used if ruptures occur during the test (see discussion on ruptures in simple shear tests in Appendix A). Once a rupture develops the measured post rupture response of the specimen does not represent the behavior of the intact soil and proper interpretation of the data is unclear. Making a correction to the stress–strain data under these circumstances would be nonsensical.

The development of a correction procedure (if it is even possible) to account for the influence of the device on the shear resistance of specimens tested in simple shear is beyond the scope of the present work. However, the data presented in this and the previous section suggest that the hypothesis proposed here may be valid. The objective of the remainder of this Appendix is to use this hypothesis to explain the unusual response found for the DSS tests on BBC with $\theta = 180^\circ$ and $\tau_{hc}/\sigma'_{vc} = 0.2$ as described in Chapter 5.

G.4 EVALUATION OF GEONOR CAUDSS TESTS ON COHESIVE SOILS WITH $\theta = 180^\circ$

The undrained direct simple shear response of an anisotropically consolidated sample depends on its OCR, soil type and consolidation stress ratio (τ_{hc}/σ'_{vc}). However, the results presented in the previous section suggest that there may be an additional influence on the behavior of a sample which is due to the device. This may be particularly evident in the results of tests conducted with $\theta = 180^\circ$ where the sample strains through the neutral axis of the device during undrained shear. This section will use this hypothesis to postulate how the device may undesirably influence the undrained shear behavior of CAUDSS tests conducted with $\theta = 180^\circ$. The postulate will then be used to evaluate the results of six CAUDSS tests performed with $\theta = 180^\circ$.

In the previous section it was hypothesized that the behavior of samples tested in a simple shear apparatus may be influenced by the device. Specifically, it was proposed that during undrained shear the device causes the vertical stress acting on a sample to increase as it strains towards the neutral axis of the device and the opposite occurs when a sample strains away from the neutral axis. The increase in vertical stress as the sample strains towards the neutral axis results in an increase in shear resistance of the sample. Hence, while the measured shear resistance of a sample is primarily due to the simple shear response of the sample, there is also a component which is induced by the device. It was further proposed that the influence of the device on the measured experimental results will be most evident if the sample is in a state where the rate of development of shear–induced pore pressure is relatively low.

Most CK_oU and CAU direct simple shear tests on normally consolidated cohesive specimens have an initially high rate of development of positive pore pressure.[4] This rate, however, decreases as a sample approaches its peak shear resistance and typically becomes constant thereafter (at a rate significantly less than the initial rate). For CAU tests with $\theta = 180°$, the rate of pore pressure development as the sample strains through the neutral axis of the device depends on the magnitude of the consolidation shear strain γ_c. The higher γ_c during consolidation, the lower the rate of pore pressure development will be as the sample strains through the neutral axis during undrained shear. The reasoning behind this hypothesis is explained as follows.

For all CAU tests with $\theta = 180°$ (and also MDSS tests with $\theta = 120°$ and $150°$), the influence of the device on the behavior of a sample exists independent of the magnitude of γ_c. However, whether this influence will be clearly evident in the

[4]It is important to keep in mind that undrained direct simple shear tests are typically run as constant volume tests and the pore pressure is assumed to be equal to the change in vertical stress required to maintain the sample volume constant.

measured results during undrained shear depends on the rate of pore pressure development and as a result is dependent on γ_c. The dependency on γ_c is explained as follows for the case of two CAU tests on a normally consolidated cohesive soil with $\theta = 180°$; during anisotropic consolidation one has a low γ_c and the other has a high γ_c:

(a) Low γ_c:

At the beginning of undrained shear the sample has a high rate of development of pore pressure (i.e., the sample exhibits contractive behavior and thus the vertical stress is reduced to maintain the sample's volume constant). Because of the relatively low value of γ_c the rate of pore pressure development is still high as the specimen strains through the neutral axis. This tends to mask the influence of the device on the vertical stress. Once the sample strains through the neutral axis, the simple shear response of the sample and the influence of the device coincide (i.e., the soil continues to contract and the influence of the device also causes some additional contractive behavior, both resulting in a decrease in the vertical stress required to maintain the volume constant). Eventually the sample reaches its peak shear resistance and begins to strain soften.

(b) High γ_c:

In this case the sample also has an initially high rate of development of positive pore pressure. However, as the sample approaches the neutral axis the rate of development of pore pressure decreases significantly to a point where the influence of the device on the sample becomes more explicit in the measured results. The device causes the vertical stress to increase as the specimen approaches the neutral axis, thus resulting in a proportional increase in the shear resistance. The device–induced behavior continues to compete with the contractive simple shear response of the sample until it passes through the neutral axis. Once this occurs, the influence of the device reverses itself and the sample eventually reaches its peak shear resistance.

It was pointed out in the previous section that the influence of the device affects the behavior of all types of simple shear tests (e.g., CK_oU, CAU, etc.). The postulate outlined in the preceeding paragraphs was restricted to describing the influence of the device on the results of CAU tests with $\theta = 180°$. It will now be used to evaluate the results of six CAUDSS tests performed with $\theta = 180°$.

Table G.1 is a summary of six CAU tests with $\theta = 180°$ conducted in the Geonor DSS. Tests G6, G7 and G8 were conducted on BBC as part of this thesis and are also summarized in Chapter 5. Tests 604 and 801 were also conducted on BBC by Disman (1968) and test S36–5 was on an Arctic Silt (Sauls, et al., 1984). Figures G.11 and G.12 are plots of the stress–strain curve, pore pressure versus shear strain, and the stress paths for the six tests. The data from these tests will be used to test the hypothesis presented in the previous paragraphs on the results of CAU tests with $\theta = 180°$.

Test G8 with $\tau_{hc}/\sigma'_{vc} = 0.1$ and $\gamma_c = 6.2\%$ reached a peak shear resistance at $\gamma = 11.8\%$[5] which is 4.6% shear strain beyond the neutral axis of the device (i.e. on the opposite side of the direction of γ_c). The stress–strain curve and stress path for this test do not exhibit any unusual characteristics before the peak shear resistance is reached. The sample passed through the neutral axis of the device at $\gamma = 7.2\%$ when the rate of pore pressure was still relatively high. Tests G6 and G7, with $\tau_{hc}/\sigma'_{vc} = 0.2$ had $\gamma_c = 16.5\%$ and 17.2% respectively. Test G6 reached a peak shear resistance at $\gamma = 25.9\%$, which is 6.4% shear strain beyond the neutral axis and Test G7 had $\gamma = 23.3\%$ or 3.3% beyond the neutral axis. Both tests exhibited unusual behavior as the samples approached their peak shear resistance. This is clearly shown in the stress paths plotted in Figure G.12. In both tests the neutral axis of the device was reached

[5] γ_c is based on the preconsolidation sample height and γ is based on the preshear sample height. For all tests, γ is equal to zero at the start of undrained shear and for tests with $\theta = 180°$, γ is in the opposite direction of γ_c.

at a stage where the rate of development of pore pressure was very low (neutral axis reached at $\gamma = 19.5\%$ and 20.0% for tests G6 and G7 respectively compared to $\gamma =$ 7.2% for test G8). Only when the samples strained beyond the neutral axis did they reach a peak shear resistance and begin to strain soften.

Tests 604 and 801 were performed in 1968 at MIT on resedimented BBC by Disman (1968). Test 604 with $\tau_{hc}/\sigma'_{vc} = 0.2$ and $\gamma_c = 14.8\%$ did not exhibit any unusual behavior during undrained shear whereas test 801 with $\tau_{hc}/\sigma'_{vc} = 0.3$ and γ_c = 25% displayed very unusual behavior near the peak shear resistance which is clearly shown in the stress path plotted in Figure G.12. Test 801 actually dilated (causing a reversal in the direction of the stress path) before the peak shear resistance. Test 604 reached a peak shear resistance at $\gamma = 13.9\%$, which is 3.4% before the neutral axis of the device was reached, and test 801 had $\gamma = 28.4\%$ or 1.1% before the neutral axis.

In principle the behavior of these two tests is consistent with the postulate about the influence of the device presented at the beginning of this section. Test 801 with the unusual undrained shear behavior before its peak shear resistance had a significantly higher γ_c than test 604. However, in both cases, the peak shear resistance was reached before the sample strained back through the neutral axis. This is not entirely consistent with the predicted sample response and the results of tests G6, G7 and G8. A probable reason for this is the fact that these tests were conducted using manual control unlike tests G6, G7 and G8 which were performed using the automatic constant volume servo control system currently used at MIT for undrained tests in the Geonor DSS (see Appendix E for a description). The automatic system is more sensitive and has a continuous response period compared to manual control. Presumably test 604 should exhibit behavior similar to tests G6 and G7 since all three were conducted on BBC at the same consolidation stress ratio. It is possible that during test 604 the changes in vertical stress induced by the device were not of a sufficient magnitude to be detected during manual control. The operator would expect

the specimen to continuously contract thereby requiring the vertical stress to be continuously decreased throughout the test. Any subtle changes in the sample height due to the device which require an increase in vertical stress may not be considered significant and were not reacted to by the operator. In the case of test 801 with the very large consolidation shear strain, the rate of development of positive pore pressure was such that the influence of the device manifested itself to a degree where the operator reacted to it and started to decrease the rate of unloading of the vertical stress and eventually began to reload the sample. It is likely that with manual control the reloading cycle was a result of overshooting while decreasing the rate of decrease in the vertical stress. While this reasoning involves a lot of speculation the fact remains that for these two tests the sample with the higher γ_c exhibited unusual behavior as it strained towards the neutral axis of the device.

Test S36–5 on the Arctic Silt sample has a consolidation shear strain equal to 6.4%. The shear strain at failure was equal to 17.1% which is 10.2% shear strain beyond the neutral axis of the device. In this test with low γ_c, the undrained shear results did not exhibit any unusual behavior.

The major issue that arises from this discussion on the results of CAU tests with $\theta = 180^\circ$ is: if the measured results do not reflect the "true" undrained direct simple shear behavior of a sample, can they be corrected? As discussed in the previous section, the development of such a correction (if it is even possible) is beyond the scope of the present work. However, this does not rule out adjusting the measured undrained strength from CAU tests with $\theta > 90^\circ$ for design purposes. From the Geonor DSS test results with $\theta = 180^\circ$ presented here and the MDSS tests with $\theta = 120^\circ$ and 150° presented in Chapter 5 it is not at all evident how even a crude but simple adjustment could be made. Most of the tests have stress paths that do not display any dramatic changes in their shape as the sample approaches its peak shear resistance. This, however, is not the case for tests G6 and G7. For these tests a crude adjustment could

involve taking the shear resistance to be approximately equal to the value measured at the point where the slope of the stress paths changes abruptly as the sample approaches the peak measured shear resistance. While this procedure is not very elegant, it is conservative compared to blindly using the measured peak shear resistance. Of course one could argue that if a correction is applied to the measured shear resistance of some of the tests with $\theta = 180°$, then CK_oU and MDSS tests with $\theta \leq 90°$ should also be considered for a correction. But again, how to apply even a crude correction to these types of tests is not evident. Furthermore, correcting the peak shear resistance of these tests involves increasing the measured value, which clearly is not a conservative approach such as that suggested for the CAU tests with $\theta = 180°$.

G.5 SUMMARY

The direct simple shear tests performed on a rubber sample clearly reflected the nonuniform state of stress which develops in simple shear specimens. For this elastic material, gaps developed at the upper leading edge and lower trailing edge of the specimen during shear (Figure G.1). These gaps caused a change in the vertical stress required to maintain the sample height constant during shear. Under ideal simple shear conditions this would not occur for an elastic incompressible material such as the rubber sample.

The results of three cyclic tests performed on cohesive samples at the conventional undrained shear rate of strain ($\dot{\gamma} = 5\%$/hour) displayed some interesting characteristics as the samples strained towards and past the neutral axis of the device during the first reversal stage of the applied shear stress (these samples were allowed to strain well beyond their peak shear resistance before the shear stress was reversed). In all three tests, the vertical stress and shear resistance reached a peak value during the reversal stage when the sample was almost exactly at the neutral axis of the device (Figures G5 and G6). Furthermore, the vertical stress and shear resistance values

during the reversal stage were symmetric about the neutral axis. The fact that three DSS tests on two different soils at three different OCR's and stress levels exhibit this type of behavior is more than coincidental. Symmetry of the normalized vertical stress about the neutral axis of the device for all of the three different test conditions (Figure G.7) is suggestive of behavior that is not exclusively dependent on the type of soil and stress conditions but also on the DSS apparatus itself.

Based on the results of the tests on rubber and the cyclic tests on clay specimens it was hypothesized that the behavior of samples tested in a direct simple shear apparatus can be influenced by the device. It was proposed that during undrained shear the device causes the vertical stress acting on a sample to increase as it strains towards the neutral axis of the device and the opposite occurs when a sample strains away from the neutral axis. The increase in vertical stress as the sample strains towards the neutral axis results in an increase in shear resistance of the sample. Hence, while the measured shear resistance of a sample is primarily due to the simple shear response of the sample, there is also a component which is induced by the device (Figure G.8). It was further proposed that the influence of the device is only detectable in the measured experimental results if the sample is in a state where the rate of development of pore pressure is relatively low.

This hypothesis was used to postulate that CAU tests with $\theta = 180°$ may exhibit some unusual behavior in the measured results depending on the magnitude of the consolidation shear strain γ_c. The higher the γ_c, the lower the rate of development of pore pressure in a normally consolidated sample as it strains towards the neutral axis of the device. Under these circumstances the influence of the device may explicitly manifest itself in the measured results. This postulate was used to explain the unusual behavior of CAUDSS tests G6 and G7 performed on BBC. It was further suggested that the peak measured shear resistance of these samples be reduced for design purposes.

The primary objective of this Appendix was to determine if the unusual behavior of CAUDSS tests G6 and G7 could be explained in terms of deficiencies with the direct simple shear apparatus. The results and discussion presented here suggest that there is indeed a problem with the DSS that not only influences CAU tests with $\theta = 180^{\circ}$ but in general influences the results of all direct simple shear tests (e.g., measured strain softening response in DSS tests is to high particularly as γ approaches large values). This is a significant finding that clearly warrants additional research along the lines suggested in Section G.3.

Table G.1: Summary of Geonor CAUDSS Tests With $\theta = 180°$

Test No.	w_n (%)	Consolidation				At Maximum τ_h			$\gamma(\%)^*$ @ X=0	Soil Type Reference
		σ'_{vc} (ksc)	$\frac{\tau_{hc}}{\sigma'_{vc}}$	ϵ_v (%)	γ_c (%)	γ (%)	$\frac{\tau_h}{\sigma'_{vc}}$	$\frac{\sigma'_v}{\sigma'_{vc}}$		
G8	40.4	3.0	0.1	13.2	6.2	11.8	0.207	0.429	7.2	Boston Blue Clay This Thesis; Ch. 5
G6	41.6	3.0	0.2	15.6†	16.5	25.9	0.232	0.440	19.5	Boston Blue Clay This Thesis; Ch. 5
G7	40.5	3.0	0.2	13.9	17.2	23.3	0.251	0.481	19.9	Boston Blue Clay This Thesis; Ch. 5
604	38.7	3.0	0.2	14.2	14.8	13.9	0.177	0.452	17.3	Boston Blue Clay Ladd & Edgers (1972)
801-	37.9	3.0	0.3	15.2	25.0	28.4	0.283	0.560	29.5	Boston Blue Clay Ladd & Edgers (1972)
S36-5	33.7	4.0	0.2	7.0	6.4	17.1	0.222	0.645	6.9	Arctic Silt Sauls et. al. (1984)

Notes:

1. τ_{hc}/σ'_{vc} values are nominal.
2. ϵ_v and γ_c are strains at the end of consolidation.
3. † inaccurate value (see Section 4.3.1, Ch. 4).
4. * value of undrained shear strain as sample passes through neutral axis (X=0).

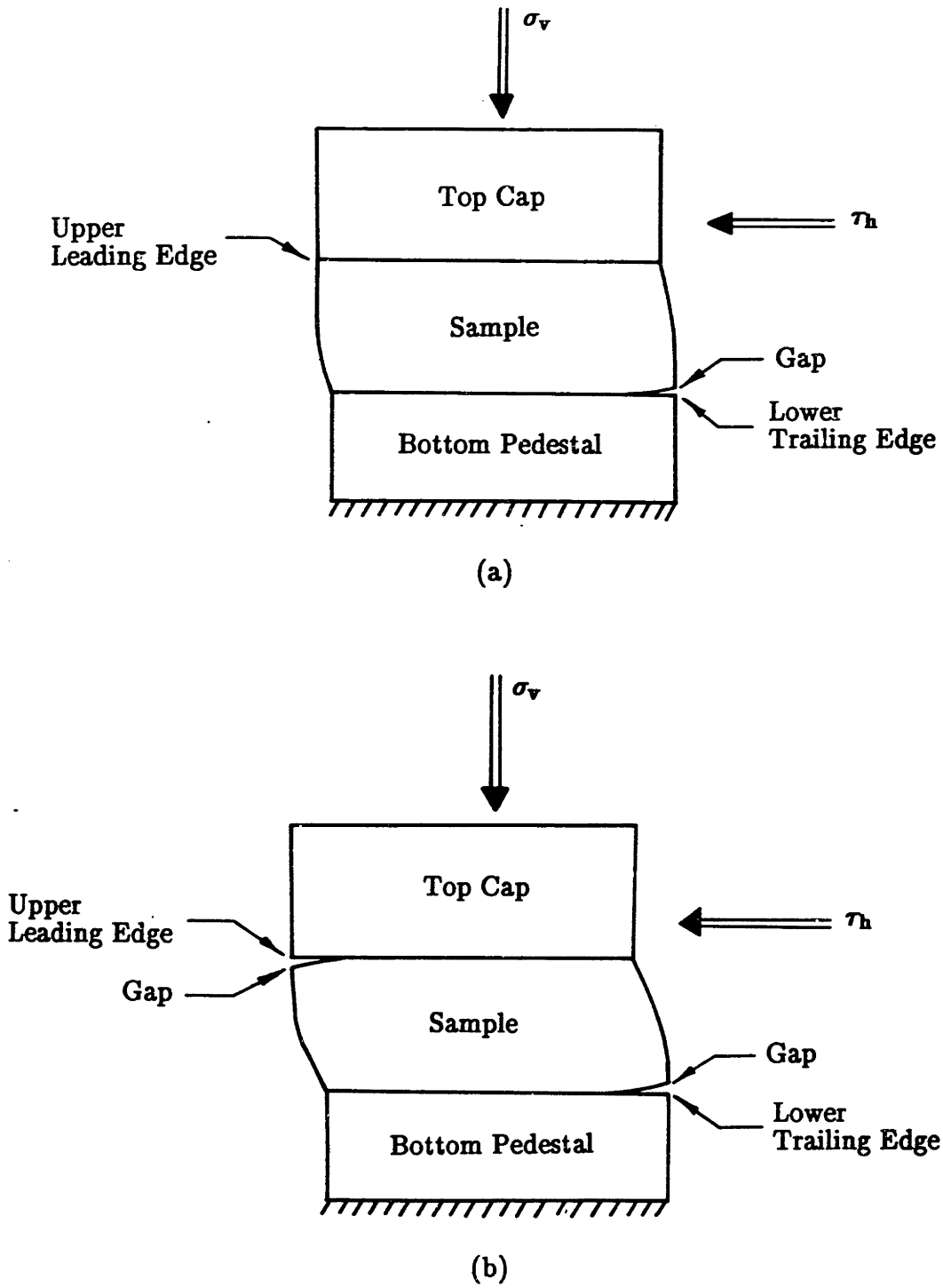

Figure G.1: Schematic of Deformed Shape of a Rubber Specimen Under Constant Height Direct Simple Shear Conditions: (a) $\gamma <$ 10%; (b) $\gamma >$ 10%.

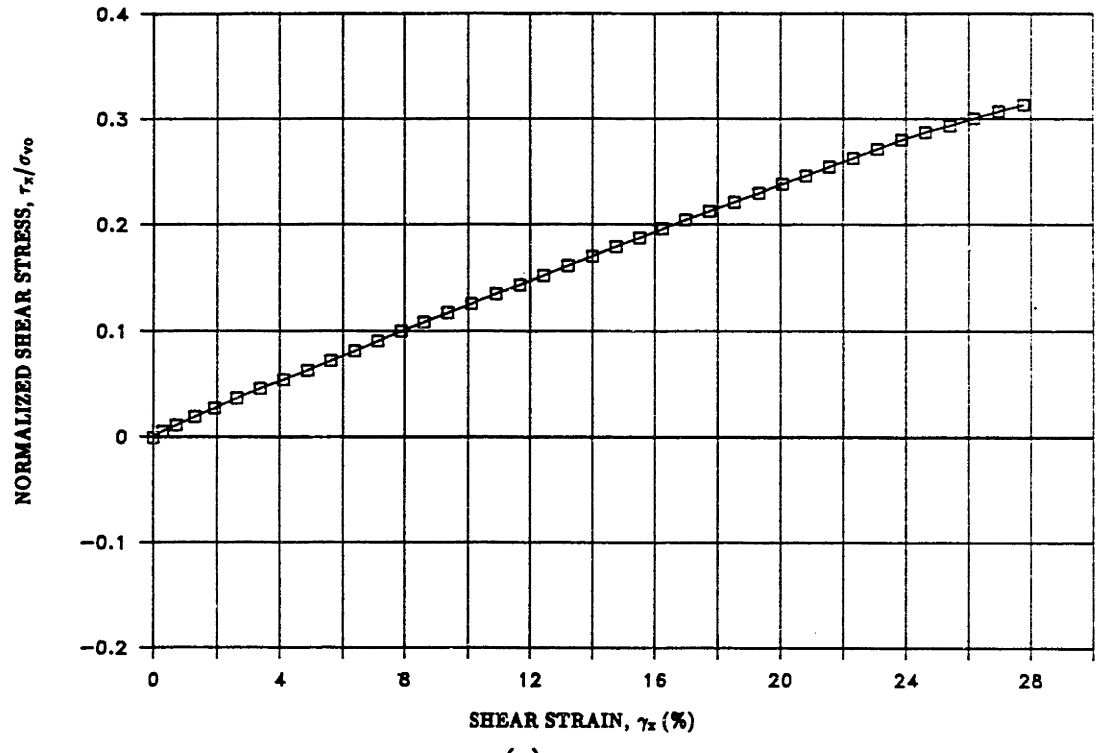

(a)

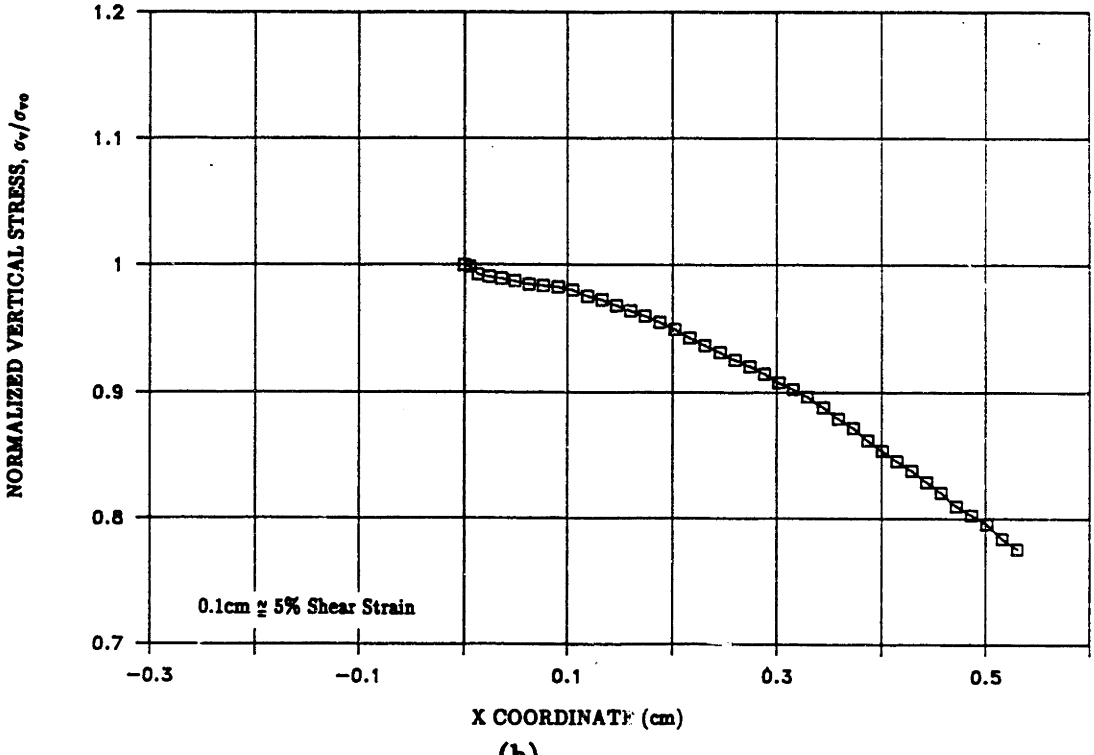

(b)

Figure G.2: Results of a Constant Height MDSS Test on a Rubber Specimen: (a) Shear Stress–Strain Curve; (b) Vertical Stress versus X Coordinate.

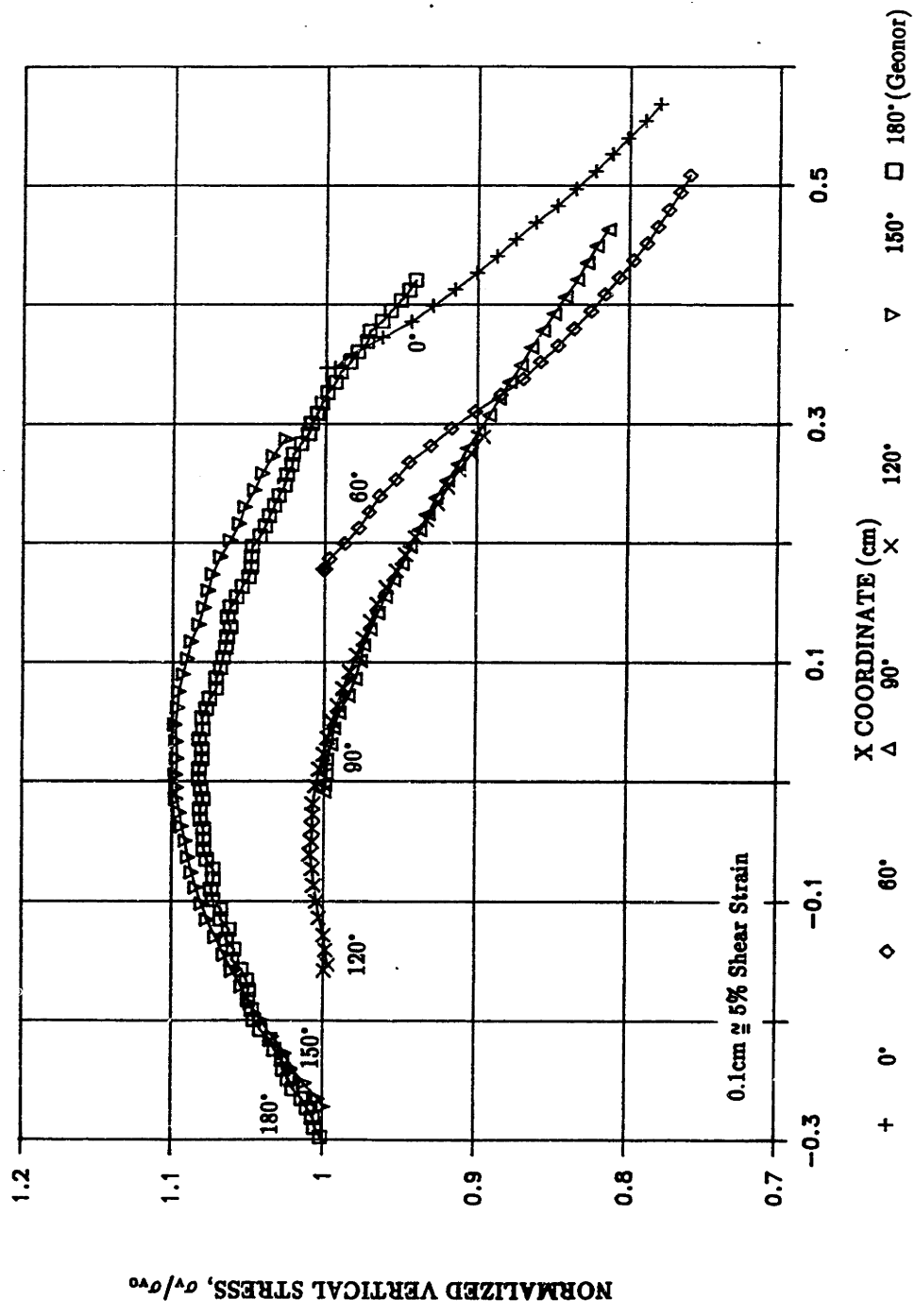

Figure G.3: Normalized Vertical Stress versus X Coordinate for Constant Height MDSS Tests on Rubber at Different θ Angles With $\tau_1/\sigma_{vo} = 0.2$.

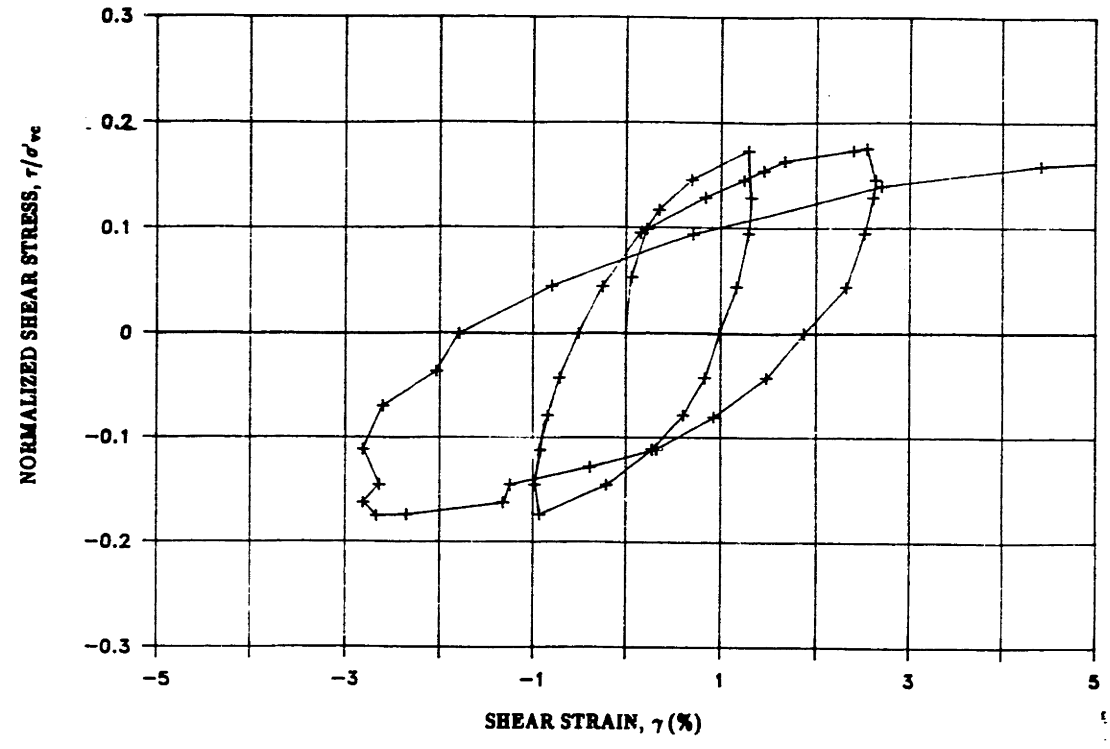

(a)

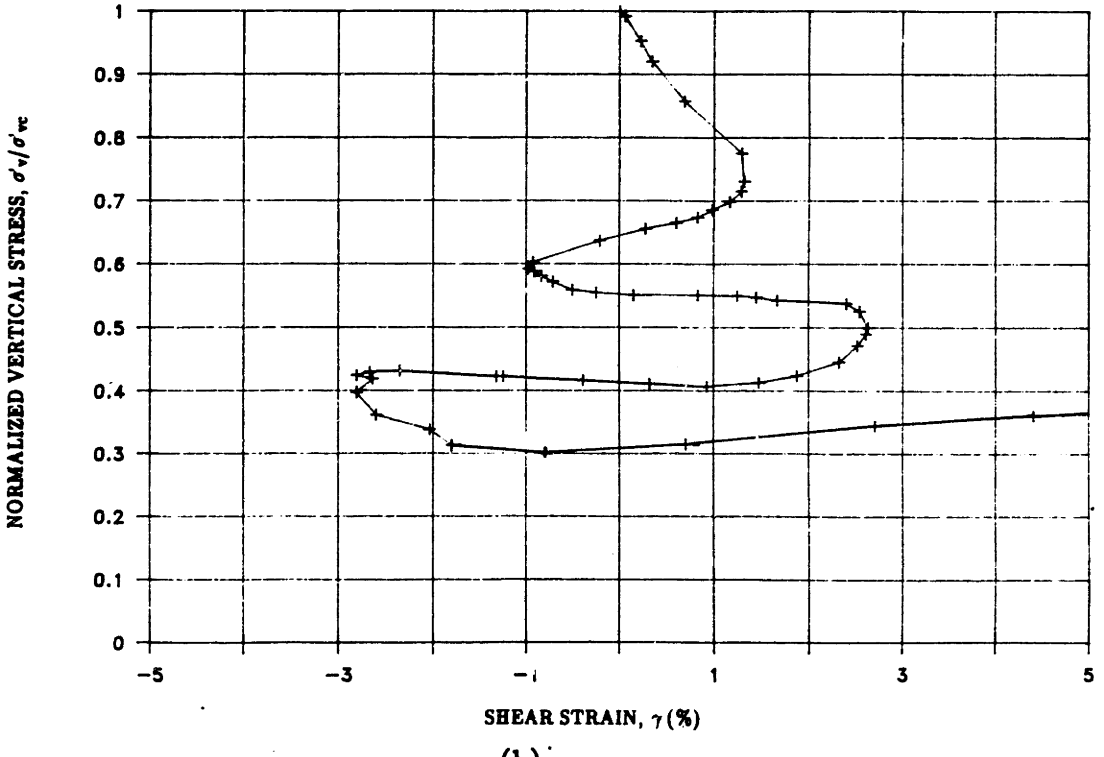

(b)

Figure G.4: Results of an Undrained Cyclic Geonor DSS Test on BBC at $\dot{\gamma} = 5\%$/hour: (a) Shear Stress–Strain Curve; (b) Normalized Vertical Effective Stress versus Shear Strain (after Malek, 1987).

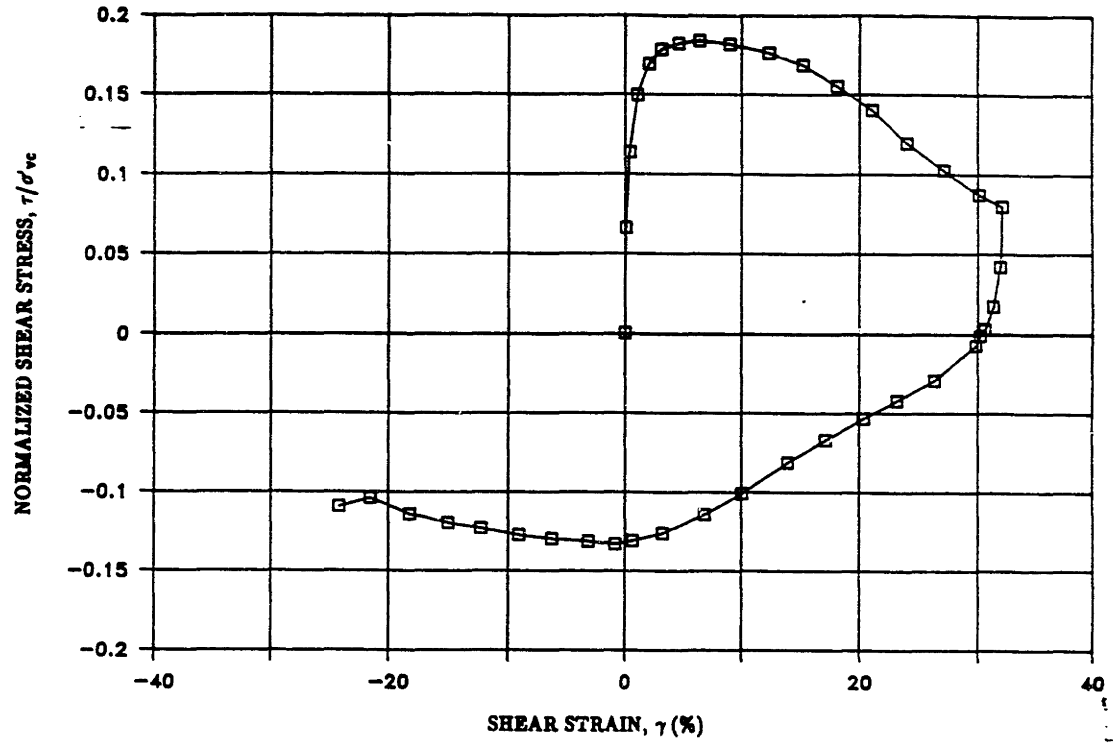

(a)

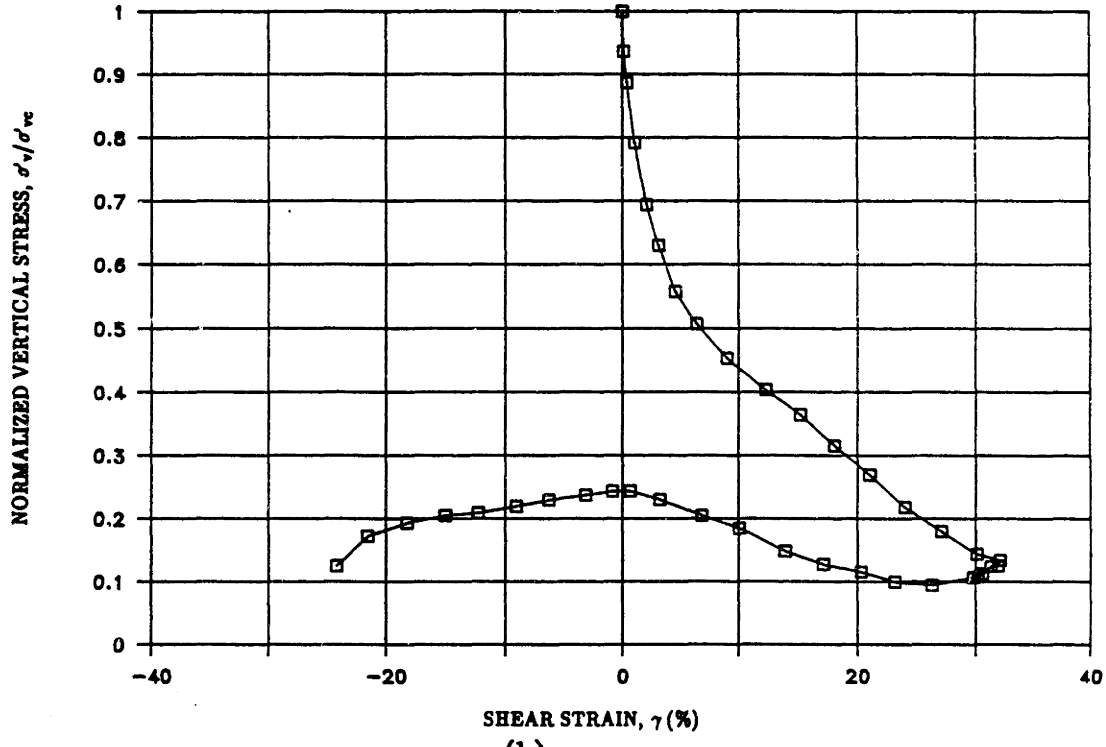

(b)

Figure G.5: Results of Undrained Cyclic Geonor DSS Test No. 16 on OCR = 1 BBC at $\dot{\gamma} = 5\%$/hour: (a) Shear Stress–Strain Curve; (b) Normalized Vertical Effective Stress versus Shear Strain.

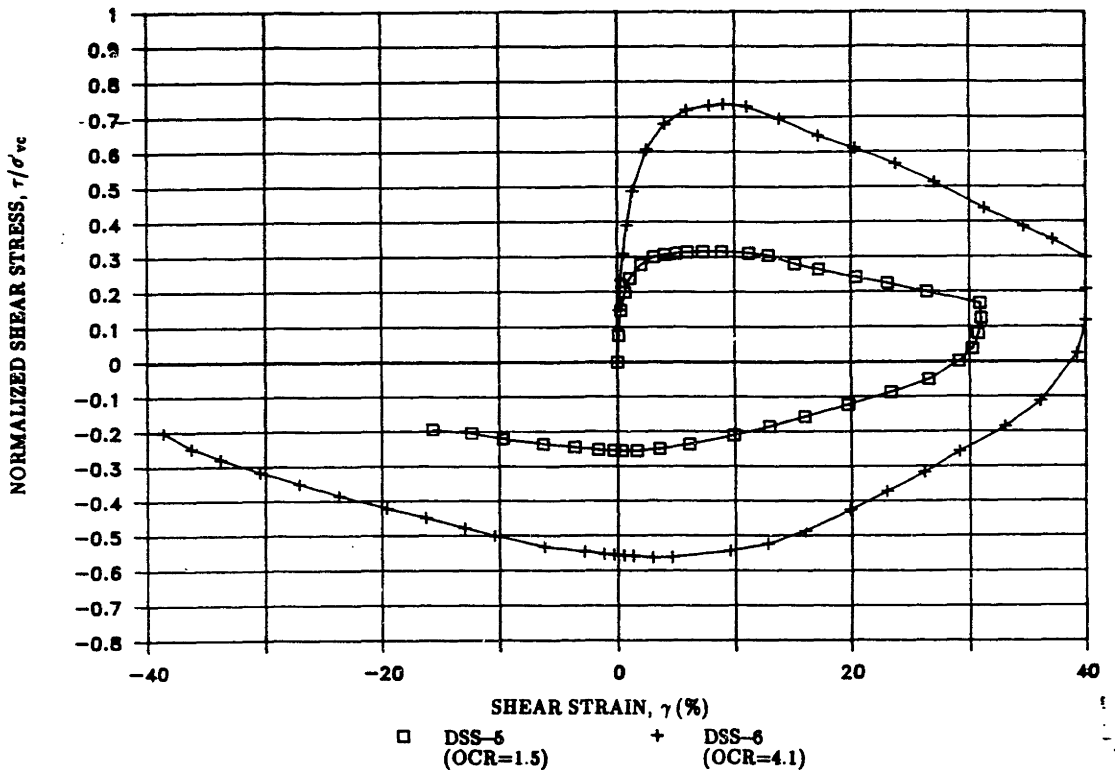

(a)

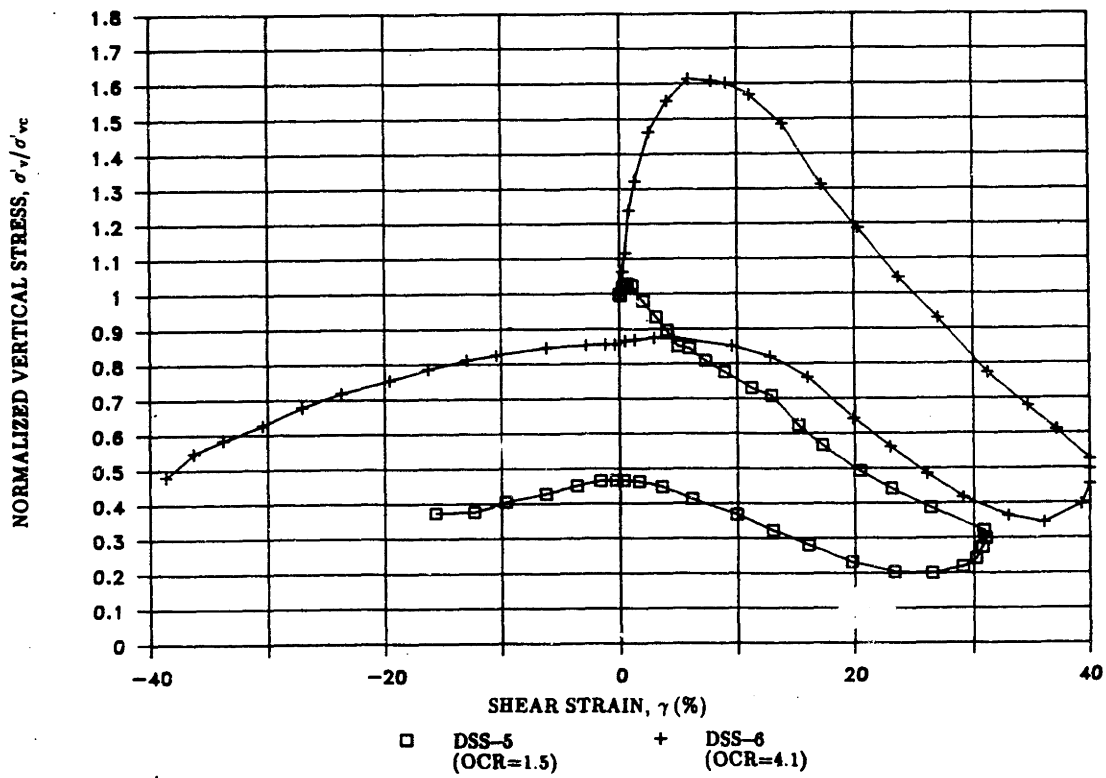

(b)

Figure G.6: Results of Undrained Cyclic Geonor DSS Tests on San Francisco Bay Mud (SFBM) at $\dot{\gamma} = 5\%$/hour: (a) Shear Stress-Strain Curve; (b) Normalized Vertical Effective Stress versus Shear Strain.

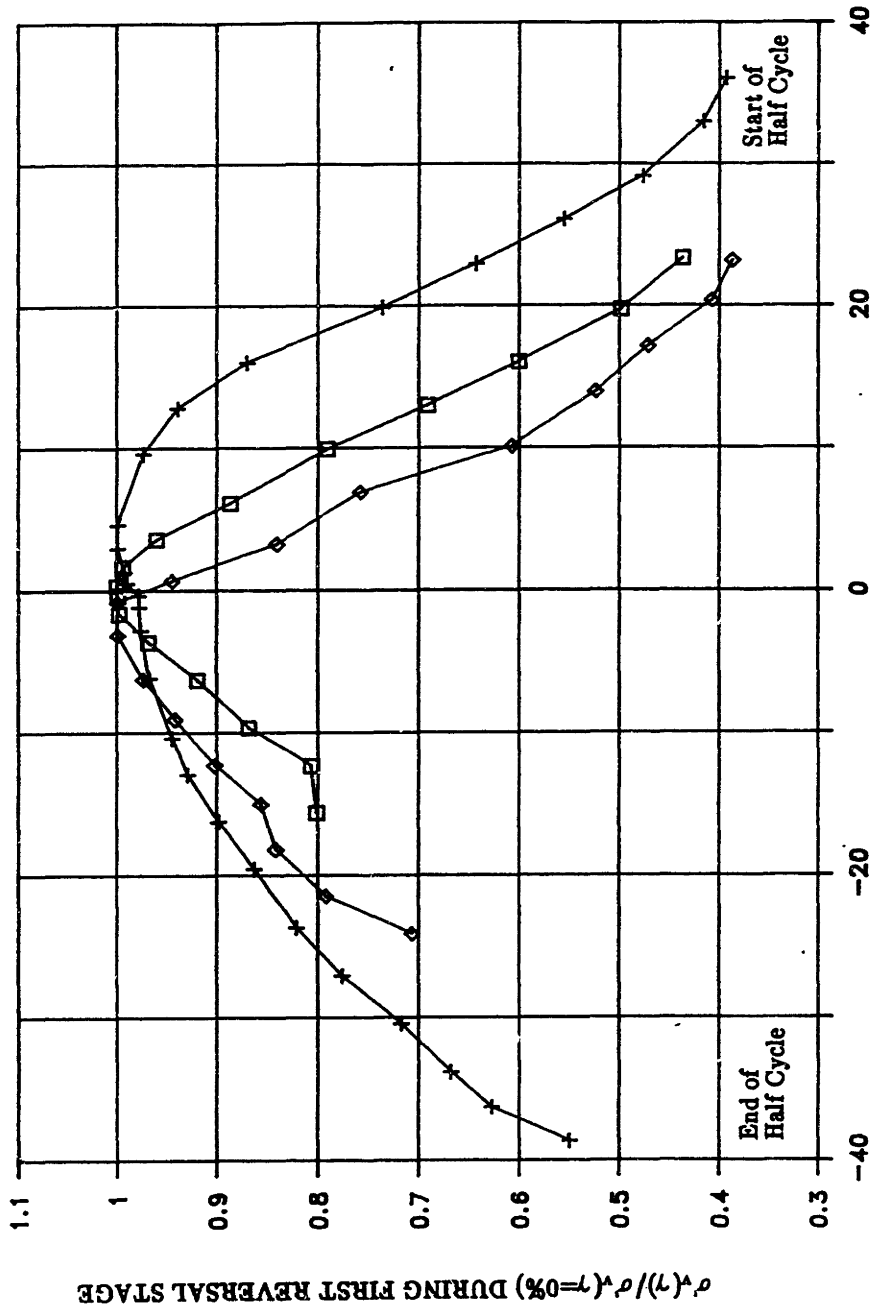

Figure G.7: Vertical Stress During the First Reversal Stage (Normalized by σ'_v at $\gamma = 0\%$) versus Shear Strain for Undrained Cyclic Geonor DSS Tests at $\dot{\gamma} = 5\%$/hour on BBC and SFBM.

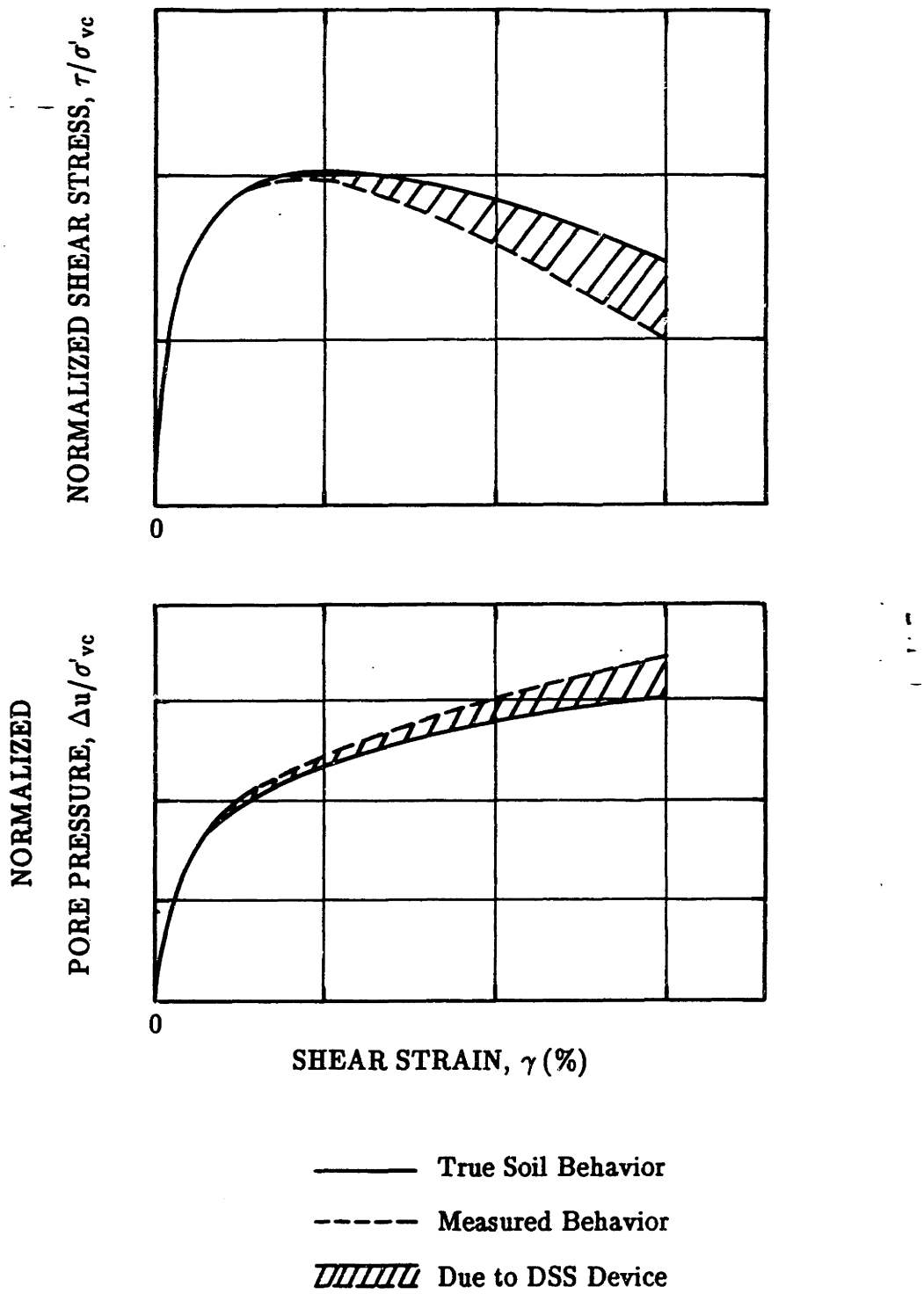

Figure G.8: Schematic of Hypothesis Showing Influence of DSS Apparatus on the Behavior of a Sample in a DSS Test.

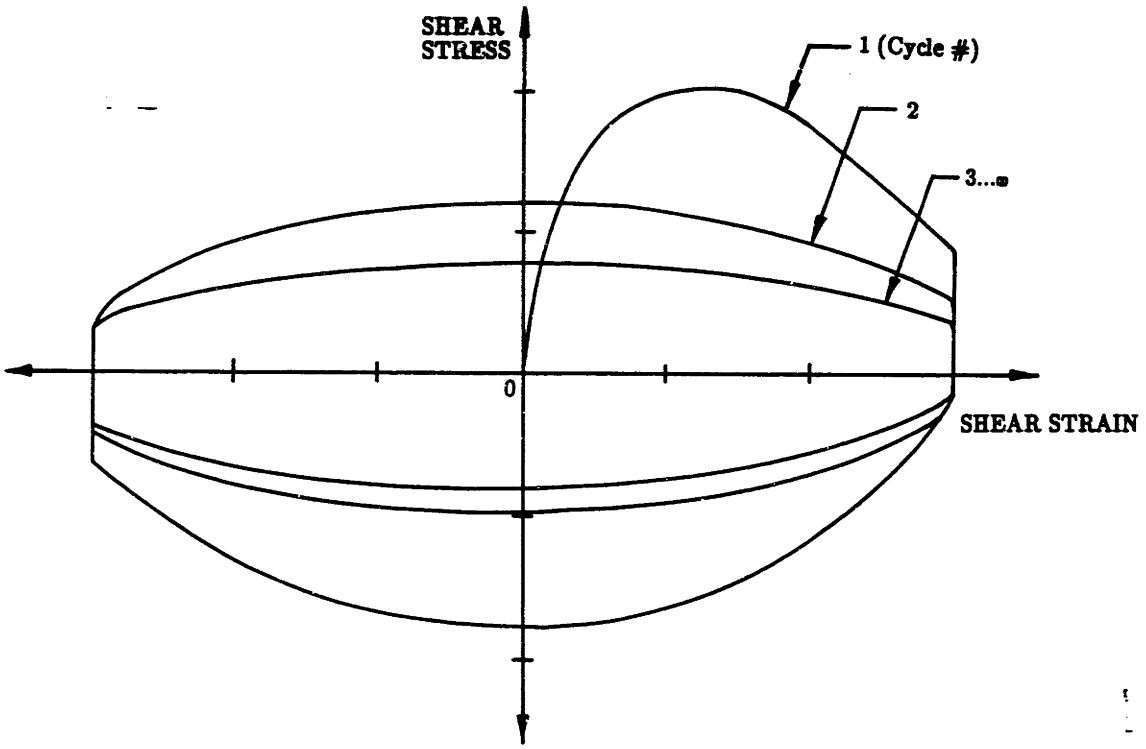

Figure G.9: Schematic of Cyclic Shear Stress–Strain Curve for a DSS Test Indicating an Influence of the Device on the Measured Shear Resistance Visible Once the Sample Reaches a Steady State Response.

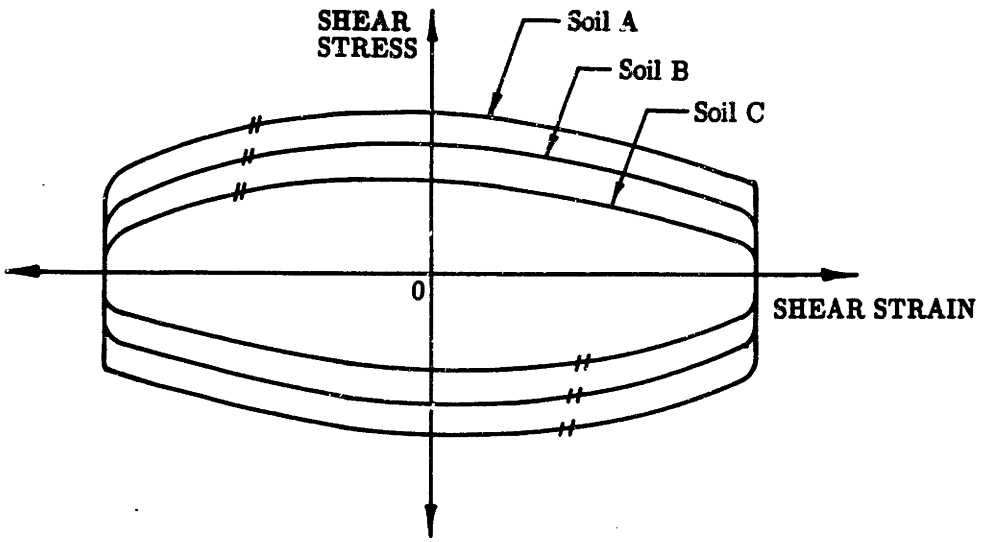

Figure G.10: Schematic of Steady State Shear Stress–Strain Curves for Cyclic DSS Tests on Three Different Soils Indicating a Similar Influence of the Device on the Shear Stress–Strain Response.

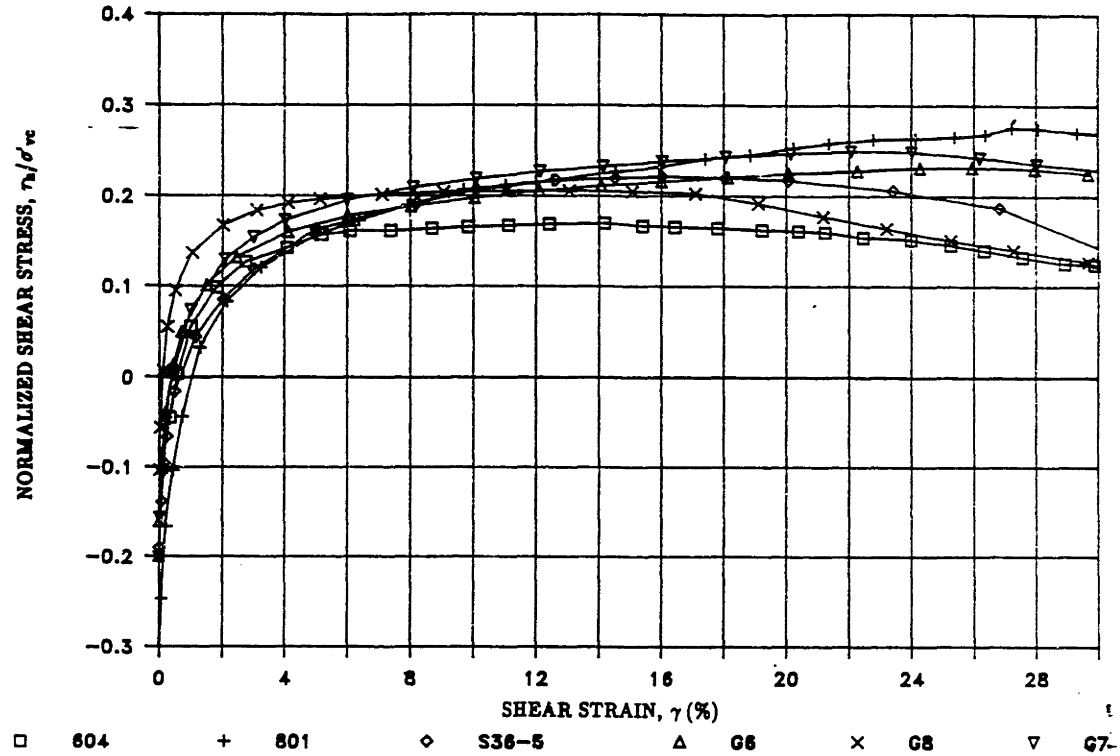

(a)

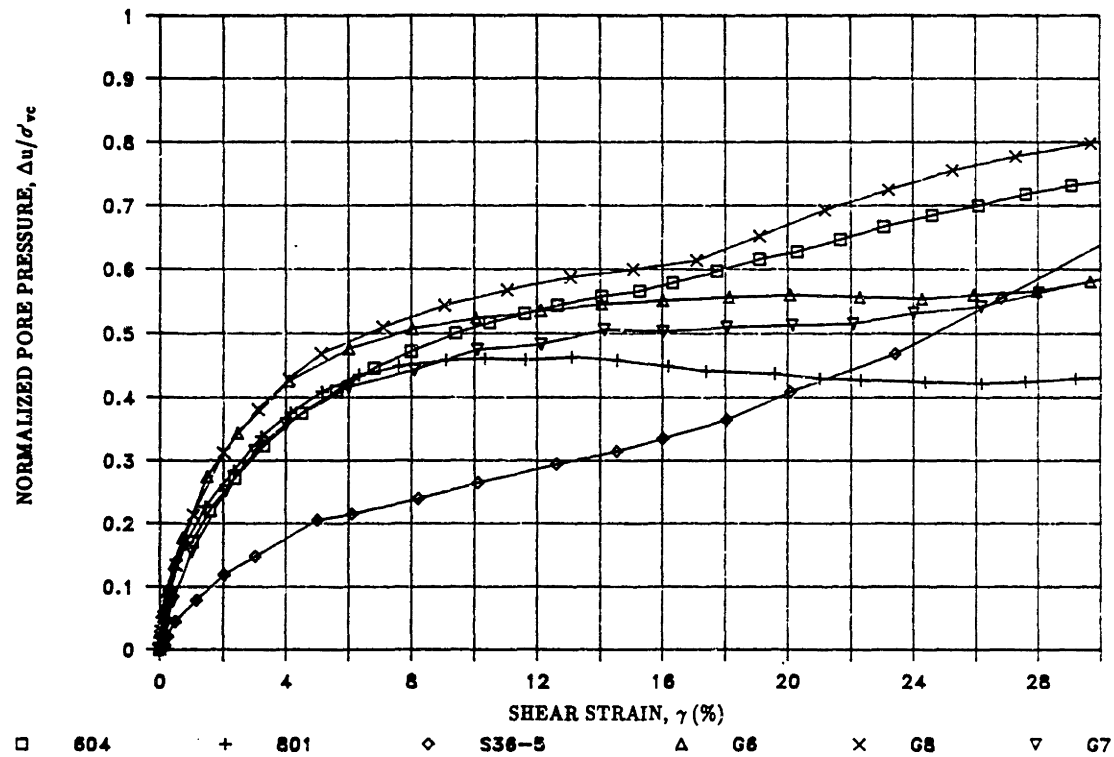

(b)

Figure G.11: Results of Six Geonor CAUDSS Tests With $\theta = 180°$: (a) Shear Stress–Strain Curves; (b) Pore Pressure versus Shear Strain (Note: γ based on preshear sample height, see Footnote No. 5 of this Appendix).

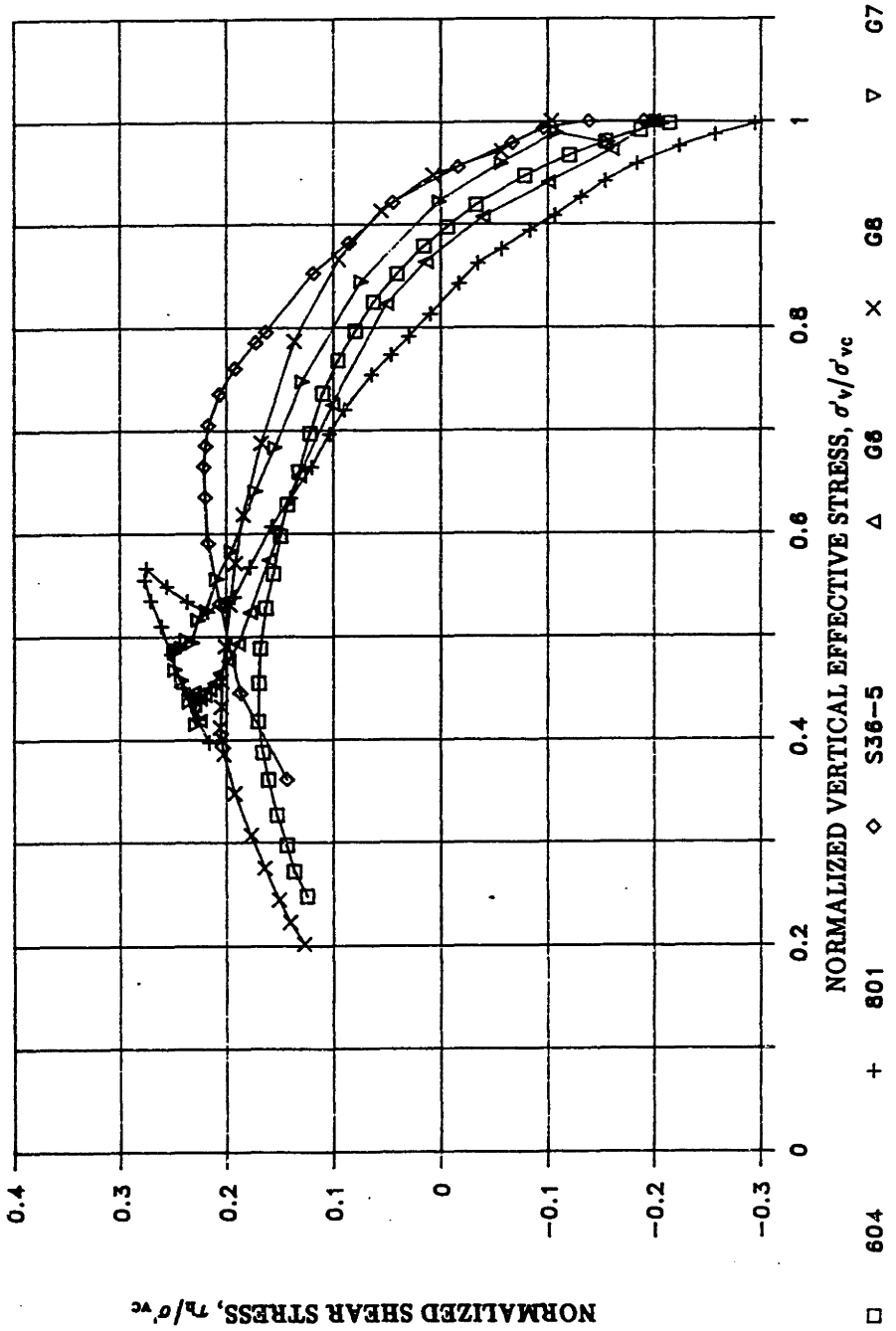

Figure G.12: Stress Paths for Six Geonor CAUDSS Tests With $\theta = 180°$.

APPENDIX H

CONSOLIDATION AND UNDRAINED SHEAR DATA FROM GEONOR DSS AND MDSS TESTS ON BBC

1. **TABLE H.1:** List of Geonor DSS and MDSS Tests on BBC.
2. **TABLE H.2:** Summary of Initial Conditions for Geonor DSS and MDSS Tests on BBC.
3. **TABLE H.3:** Summary of Consolidation Strains From CK_oUMDSS Tests on BBC.
4. **TABLE H.4:** Summary of Anisotropic Consolidation Strains From Geonor CAUDSS Tests on BBC.
5. **TABLE H.5:** Summary of Anisotropic Consolidation Strains From CAUMDSS Tests on BBC.
6. Undrained Shear Results of Geonor DSS Tests on BBC.
7. Undrained Shear Results of MDSS Tests on BBC.

TABULATED UNDRAINED SHEAR DATA

Notes:

1. Corrected preshear components of the consolidation shear stress (τ_x and τ_y) for CAUMDSS tests are tabulated in Table 5.4.

2. Headings in the tabulated undrained shear data in this appendix correspond to the following symbols:

   Str. X = γ_x

   SigV = σ'_v

   SigVc = σ'_{vc}

   TauH = τ_h

   DelU = Δu

   X.Coor. = X coordinate of the horizontal displacement relative to the neutral axis (X = 0) of the device.

3. Additional headings for MDSS tests:

   Str. Y = γ_y

   TauH = τ_x

TABLE H.1: List of Geonor DSS and MDSS Tests on BBC

Geonor DSS					MDSS				
Test No.	Test Type	σ'_{vc} (ksc)	θ (°)	$\frac{\tau_{hc}}{\sigma'_{vc}}$	Test No.	Test Type	σ'_{vc} (ksc)	θ (°)	$\frac{\tau_{hc}}{\sigma'_{vc}}$
G1	CK_oU	3.0	-	-	C1	CK_oU	4.0	-	-
G2	CK_oU	3.0	-	-	C4	CK_oU	4.0	-	-
G3	CAU	3.0	0	0.10	C5	CK_oU	3.0	-	-
G4	CK_oU	3.0	-	-	C6	CK_oU	3.0	-	-
G5	CAU	3.0	0	0.20	C7	CAU	3.0	0	0.20
G6	CAU	3.0	180	0.20	C8	CAU	3.0	60	0.20
G7	CAU	3.0	180	0.20	C9	CAU	3.0	120	0.20
G8	CAU	3.0	180	0.10	C10	CAU	3.0	30	0.20
					C11	CK_oU	3.0	-	-
					C12	CAU	3.0	90	0.20
					C13	CAU	3.0	150	0.20
					C14	CK_oU	3.0	-	-
					C15	CAU	3.0	120	0.20
					C16	CAU	3.0	150	0.20
					C17	CAU	3.0	60	0.20

TABLE H.2: Summary of Initial Conditions for Geonor DSS and MDSS Tests on BBC

Geonor DSS				MDSS			
Test No.	w (%)	e_o	Height (cm)	Test No.	w (%)	e_o	Height (cm)
G1	41.1	1.1446	2.2504	C1	41.8	1.1641	2.1950
G2	40.8	1.1363	2.1920	C4	41.3	1.1502	2.0913
G3	42.0	1.1697	2.2962	C5	41.6	1.1586	2.3199
G4	41.0	1.1419	2.2403	C6	41.2	1.1474	2.2047
G5	42.1	1.1725	2.2682	C7	42.0	1.1697	2.1615
G6	41.6	1.1586	2.1394	C8	41.3	1.1502	2.1184
G7	40.5	1.1279	1.9863	C9	41.5	1.1558	2.2327
G8	40.4	1.1251	2.2454	C10	41.1	1.1446	2.2657
				C11	40.7	1.1335	2.2487
				C12	41.3	1.1502	2.2200
				C13	40.7	1.1335	2.3376
				C14	40.9	1.1391	2.3097
				C15	41.0	1.1419	2.2369
				C16	41.2	1.1474	2.2911
				C17	40.7	1.1335	2.2335

Notes:

1. Height = initial sample height.
2. e_o based on Gw = Se with G = 2.785 and S = 100%.

TABLE H.3: Summary of Consolidation Strains from CK_oUMDSS Tests on BBC

Inc. No.	σ'_{vc} (ksc)	Test Number			
		C11		C14	
		ϵ_{100}	ϵ_f	ϵ_{100}	ϵ_f
1	0.125	-	0.15	0.14	0.15
2	0.25	0.44	0.47	0.49	0.54
3	0.5	1.06	1.14	1.24	1.32
4	0.9	2.04	2.30	2.15	2.36
5	1.5	5.46	5.78	5.31	5.60
6	3.0	11.15	11.53	10.81	11.15

Notes:

1. All strains in percent.
2. ϵ_{100} = strain at end of primary consolidation.
3. ϵ_f = strain at end of increment.
4. Data for tests C1, C4, C5 and C6 not accurate (see Section 4.3.1 of Chapter 4).

TABLE H.4: Summary of Anisotropic Consolidation Strains From Geonor CAUDSS Tests on BBC

Inc No.	σ'_{vc} (ksc)	Test Number (θ)						
		G3 (0°) γ (%)	G5 (0°) γ (%)	G6 (180°) γ (%)	G7 (180°) ϵ_v(%)	G7 (180°) γ(%)	G8 (180°) ϵ_v(%)	G8 (180°) γ(%)
1	0.125	-	-	-	0.43	-	0.54	-
2	0.25	-	-	-	0.98	-	1.36	-
3	0.5	0.42	1.05	0.85	2.27	1.01	2.36	0.16
4	1	1.78	6.14	4.34	4.96	5.28	4.45	1.33
5	1.5	3.91	10.62	8.81	8.07	9.48	7.46	3.12
6	2	5.43	13.37	11.65	10.39	12.40	9.88	4.41
7	2.5	6.51	15.96	13.96	11.71	14.17	11.37	5.11
8	3	7.11	17.86	15.57	13.51	16.50	12.82	5.91

Notes:

1. All data at t = 100 minutes.
2. ϵ_v data for tests G3, G5, and G6 not accurate (see Section 4.3.1 of Chapter 4).
3. Consolidation Stress Ratios for $\sigma'_{vc} \geq 0.5$ ksc:
   (a) $\tau_{hc}/\sigma'_{vc} = 0.1$ for Tests G3 and G8.
   (b) $\tau_{hc}/\sigma'_{vc} = 0.2$ for Tests G5, G6 and G7.

TABLE H.5a: Summary of Anisotropic Consolidation Strains From CAUMDSS Tests on BBC

Inc. No.	σ'_{vc} (ksc)	Test Number (θ)															
		C7 (θ = 0°)				C10 (θ = 30°)				C8 (θ = 60°)				C17 (θ = 60°)			
		ϵ_v	γ_x	γ_y	γ_t	ϵ_v	γ_x	γ_y	γ_t	ϵ_v	γ_x	γ_y	γ_t	ϵ_v	γ_x	γ_y	γ_t
1	0.125	0.37	-	-	-	0.13	-	-	-	0.15	-	-	-	0.22	-	-	-
2	0.25	0.74	-	-	-	0.39	-	-	-	0.40	-	-	-	0.65	-	-	-
3	0.5	1.58	0.68	0.09	0.69	1.13	0.61	0.47	0.77	1.45	0.10	1.02	1.02	1.76	0.44	1.20	1.28
4	1	4.78	6.37	-0.20	6.37	3.91	4.82	2.52	5.44	4.14	2.31	5.30	5.78	4.67	1.90	4.97	5.32
5	1.5	8.00	11.03	-0.67	11.05	7.23	9.22	4.72	10.36	7.44	4.53	9.68	10.69	7.89	3.30	8.72	9.32
6	2	10.32	14.18	-0.89	14.21	9.54	12.06	6.17	13.55	9.73	6.06	12.58	13.96	10.49	4.45	11.77	12.58
7	2.5	11.72	16.34	-1.11	16.38	11.08	14.10	7.26	15.86	11.16	7.06	14.65	16.26	12.19	5.32	14.14	15.01
8	3	13.39	18.73	-1.27	18.77	12.63	16.18	8.34	18.20	12.80	8.19	16.92	18.80	14.14	6.38	16.55	17.74

Notes:

1. ϵ_v, γ_x, γ_y and γ_t in % strain.
2. $\gamma_t = (\gamma_x^2 + \gamma_y^2)^{1/2}$
3. All data at t_f for $\sigma'_{vc} \leq 0.25$ ksc and at t = 100 minutes for $\sigma'_{vc} \geq 0.5$ ksc.
4. $\tau_{hc}/\sigma'_{vc} = 0.2$ for $\sigma'_{vc} \geq 0.5$ ksc.

TABLE H.5b: Summary of Anisotropic Consolidation Strains From CAUMDSS Tests on BBC

Inc. No.	σ'_{vc} (ksc)	Test Number (θ)															
		C12 (θ = 90°)				C15 (θ = 120°)				C13 (θ = 150°)				C16 (θ = 150°)			
		ϵ_v	γ_x	γ_y	γ_t	ϵ_v	γ_x	γ_y	γ_t	ϵ_v	γ_x	γ_y	γ_t	ϵ_v	γ_x	γ_y	γ_t
1	0.125	0.27	-	-	-	0.14	-	-	-	0.18	-	-	-	0.22	-	-	-
2	0.25	0.61	-	-	-	0.45	-	-	-	0.51	-	-	-	0.70	-	-	-
3	0.5	1.43	0.00	1.00	1.00	1.28	-0.10	0.67	0.68	1.31	-0.32	0.41	0.52	1.71	-0.78	0.50	0.93
4	1	4.10	0.22	5.25	5.25	3.55	-1.28	3.51	3.74	3.66	-2.72	2.32	3.58	4.53	-3.88	2.26	4.49
5	1.5	7.54	0.44	10.15	10.16	6.83	-2.67	7.07	7.56	6.89	-5.75	4.82	7.50	7.59	-6.83	3.85	7.84
6	2	9.96	0.66	13.57	13.59	9.41	-3.78	9.74	10.45	9.20	-7.80	6.46	10.13	9.85	-8.96	4.98	10.25
7	2.5	11.74	0.81	16.18	16.20	11.01	-4.63	11.64	12.53	10.59	-9.20	7.54	11.90	11.13	-10.24	5.67	11.70
8	3	12.79	0.90	17.85	17.87	12.88	-5.65	13.83	14.94	12.41	-11.01	8.92	14.17	12.64	-11.78	6.52	13.46

Notes:

1. ϵ_v, γ_x, γ_y and γ_t in % strain.
2. $\gamma_t = (\gamma_x^2 + \gamma_y^2)^{1/2}$
3. All data at t_f for $\sigma'_{vc} \leq 0.25$ ksc and at t = 100 minutes for $\sigma'_{vc} \geq 0.5$ ksc.
4. $\tau_{hc}/\sigma'_{vc} = 0.2$ for $\sigma'_{vc} \geq 0.5$ ksc.

****

Ko CONSOLIDATED GEONOR DIRECT SIMPLE SHEAR TEST

MIT GEOTECHNICAL LAB

****

FILE NAME: DSSG1.PRN

REDUCTION DATA

UNITS: (kg,cm,mVOLTS,VOLTS)

1. TEST NAME : DSS-G1
2. DATE : 7/9/1987
3. OCR : 1
4. VER. CONSOLIDATION STRESS (KSC) : +2.984
5. HOR. CONSOLIDATION STRESS (KSC) : +0.000
6. PRE-SHEAR SAMPLE HEIGHT (cm) : +1.9122
7. VERTICAL STRESS LOAD CELL:
   ZERO: -.41
   CF: -361.54
8. HORIZONTAL SHEAR LOAD CELL:
   ZERO: -1.9225
   CF: -173.8
9. HORIZONTAL DISP. TRANSDUCER, X:
   ZERO: .64607
   CF: 2.2815
10. VERTICAL HEIGHT TRANSDUCER, Z:
    ZERO: .71609
    CF: 2.1089

Pt. No.	Str.Y (%)	SigV (ksc)	TauH (ksc)	Eu (ksc)	TauH / SigVc	DelU / SigVc	SigV / SigVc	TauH / SigV	TauH / Cu	Eu / Cu
1	+0.000	2.984	+0.000	+9999.0	+0.000	+0.000	+1.000	+.000	+0.000	+9999.0
2	-0.003	2.983	-0.000	+30.0	-0.000	+0.000	+1.000	-.000	-0.000	+52.7
3	+0.002	2.983	+0.013	+1622.4	+0.004	+0.000	+1.000	+.004	+0.023	+2850.2
4	+0.000	2.958	+0.022	+9999.0	+0.007	+0.009	+0.991	+.007	+0.038	+9999.0
5	+0.003	2.957	+0.031	+3302.8	+0.010	+0.009	+0.991	+.011	+0.055	+5802.4
6	+0.012	2.996	+0.052	+1365.2	+0.018	-0.004	+1.004	+.018	+0.092	+2398.3
7	+0.023	2.968	+0.084	+1087.5	+0.028	+0.005	+0.995	+.028	+0.148	+1910.5
8	+0.033	2.929	+0.118	+1086.7	+0.040	+0.018	+0.982	+.040	+0.208	+1909.2
9	+0.053	2.910	+0.153	+862.6	+0.051	+0.025	+0.975	+.053	+0.269	+1515.4
10	+0.074	2.896	+0.191	+770.3	+0.064	+0.029	+0.971	+.066	+0.335	+1353.2
11	+0.100	2.885	+0.227	+677.5	+0.076	+0.033	+0.967	+.079	+0.398	+1190.3
12	+0.135	2.869	+0.261	+580.9	+0.087	+0.039	+0.961	+.091	+0.458	+1020.6
13	+0.175	2.849	+0.295	+506.6	+0.099	+0.045	+0.955	+.103	+0.518	+890.1
14	+0.225	2.833	+0.324	+431.8	+0.109	+0.051	+0.949	+.114	+0.570	+758.6
15	+0.288	2.814	+0.353	+368.3	+0.118	+0.057	+0.943	+.125	+0.620	+647.1
16	+0.354	2.780	+0.377	+319.7	+0.126	+0.068	+0.932	+.136	+0.663	+561.6
17	+0.434	2.724	+0.401	+277.3	+0.134	+0.087	+0.913	+.147	+0.704	+487.2
18	+0.521	2.672	+0.420	+242.3	+0.141	+0.104	+0.896	+.157	+0.739	+425.6
19	+0.615	2.616	+0.438	+213.6	+0.147	+0.123	+0.877	+.167	+0.770	+375.2
20	+0.712	2.552	+0.455	+191.7	+0.153	+0.145	+0.855	+.178	+0.800	+336.8
21	+0.820	2.503	+0.469	+171.6	+0.157	+0.161	+0.839	+.187	+0.824	+301.5
22	+0.930	2.461	+0.481	+155.2	+0.161	+0.175	+0.825	+.196	+0.846	+272.7
23	+1.053	2.423	+0.492	+140.1	+0.165	+0.188	+0.812	+.203	+0.864	+246.1
24	+1.178	2.389	+0.501	+127.7	+0.168	+0.199	+0.801	+.210	+0.881	+224.3
25	+1.298	2.350	+0.510	+117.7	+0.171	+0.213	+0.787	+.217	+0.895	+206.9
26	+1.430	2.301	+0.517	+108.5	+0.173	+0.229	+0.771	+.225	+0.909	+190.6
27	+1.556	2.250	+0.523	+100.9	+0.175	+0.246	+0.754	+.233	+0.919	+177.2
28	+1.695	2.204	+0.528	+93.5	+0.177	+0.261	+0.739	+.240	+0.928	+164.3

TEST NAME : DSS-G1

Pt. No.	Str.Y (%)	SigV (ksc)	TauH (ksc)	Eu (ksc)	TauH / SigVc	DelU / SigVc	SigV / SigVc	TauH / SigV	TauH / Cu	Eu / Cu
29	+1.832	2.172	+0.534	+87.5	+0.179	+0.272	+0.728	+.246	+0.939	+153.8
30	+1.968	2.134	+0.539	+82.1	+0.181	+0.285	+0.715	+.252	+0.946	+144.3
31	+2.112	2.109	+0.544	+77.2	+0.182	+0.293	+0.707	+.258	+0.955	+135.7
32	+2.253	2.076	+0.547	+72.8	+0.183	+0.304	+0.696	+.263	+0.960	+127.9
33	+2.402	2.042	+0.551	+68.8	+0.185	+0.316	+0.684	+.270	+0.967	+120.8
34	+2.541	2.005	+0.554	+65.4	+0.186	+0.328	+0.672	+.276	+0.973	+114.9
35	+2.685	1.976	+0.556	+62.1	+0.186	+0.338	+0.662	+.281	+0.976	+109.0
36	+2.833	1.953	+0.559	+59.2	+0.187	+0.346	+0.654	+.286	+0.982	+103.9
37	+2.978	1.924	+0.560	+56.5	+0.188	+0.355	+0.645	+.291	+0.985	+99.2
38	+3.137	1.896	+0.562	+53.8	+0.188	+0.364	+0.636	+.297	+0.988	+94.5
39	+3.281	1.868	+0.564	+51.6	+0.189	+0.374	+0.626	+.302	+0.991	+90.6
40	+3.447	1.842	+0.565	+49.2	+0.189	+0.383	+0.617	+.307	+0.992	+86.4
41	+3.588	1.816	+0.565	+47.3	+0.189	+0.391	+0.609	+.311	+0.993	+83.0
42	+3.753	1.806	+0.567	+45.3	+0.190	+0.395	+0.605	+.314	+0.996	+79.6
43	+3.910	1.783	+0.568	+43.6	+0.190	+0.402	+0.598	+.319	+0.998	+76.6
44	+4.070	1.757	+0.569	+41.9	+0.191	+0.411	+0.589	+.324	+0.999	+73.6
45	+4.232	1.736	+0.569	+40.3	+0.191	+0.418	+0.582	+.328	+1.000	+70.9
46	+4.391	1.717	+0.569	+38.9	+0.191	+0.425	+0.575	+.331	+0.999	+68.3
47	+4.545	1.688	+0.569	+37.6	+0.191	+0.434	+0.566	+.337	+1.000	+66.0
48	+4.713	1.675	+0.569	+36.2	+0.191	+0.439	+0.561	+.340	+1.000	+63.7
49	+4.865	1.659	+0.569	+35.1	+0.191	+0.444	+0.556	+.343	+0.999	+61.6
50	+5.018	1.645	+0.569	+34.0	+0.191	+0.449	+0.551	+.346	+0.999	+59.7
51	+5.176	1.624	+0.569	+33.0	+0.191	+0.456	+0.544	+.350	+0.999	+57.9
52	+5.328	1.605	+0.569	+32.0	+0.191	+0.462	+0.538	+.354	+0.999	+56.2
53	+5.485	1.590	+0.568	+31.1	+0.190	+0.467	+0.533	+.357	+0.998	+54.6
54	+5.641	1.578	+0.568	+30.2	+0.190	+0.471	+0.529	+.360	+0.998	+53.0
55	+5.795	1.564	+0.567	+29.4	+0.190	+0.476	+0.524	+.363	+0.997	+51.6
56	+5.963	1.559	+0.568	+28.6	+0.190	+0.478	+0.522	+.364	+0.997	+50.2
57	+6.120	1.542	+0.568	+27.8	+0.190	+0.483	+0.517	+.368	+0.998	+48.9
58	+6.284	1.526	+0.567	+27.1	+0.190	+0.488	+0.512	+.372	+0.996	+47.6
59	+6.438	1.515	+0.567	+26.4	+0.190	+0.492	+0.508	+.374	+0.996	+46.4
60	+6.591	1.505	+0.567	+25.8	+0.190	+0.495	+0.505	+.377	+0.996	+45.3
61	+6.754	1.502	+0.568	+25.2	+0.190	+0.497	+0.503	+.378	+0.997	+44.3
62	+6.911	1.482	+0.567	+24.6	+0.190	+0.503	+0.497	+.382	+0.995	+43.2
63	+7.069	1.469	+0.567	+24.0	+0.190	+0.508	+0.492	+.386	+0.996	+42.3
64	+7.225	1.454	+0.565	+23.5	+0.190	+0.513	+0.487	+.389	+0.993	+41.2
65	+7.384	1.441	+0.565	+23.0	+0.190	+0.517	+0.483	+.392	+0.993	+40.4
66	+7.545	1.430	+0.565	+22.5	+0.189	+0.521	+0.479	+.395	+0.992	+39.5
67	+7.706	1.419	+0.564	+22.0	+0.189	+0.524	+0.476	+.398	+0.992	+38.6
68	+7.862	1.409	+0.564	+21.5	+0.189	+0.528	+0.472	+.400	+0.991	+37.8
69	+8.042	1.422	+0.564	+21.0	+0.189	+0.524	+0.476	+.397	+0.991	+36.9
70	+8.193	1.388	+0.564	+20.6	+0.189	+0.535	+0.465	+.406	+0.990	+36.3
71	+8.368	1.379	+0.562	+20.1	+0.188	+0.538	+0.462	+.408	+0.987	+35.4
72	+8.524	1.387	+0.564	+19.8	+0.189	+0.535	+0.465	+.406	+0.990	+34.8
73	+8.689	1.358	+0.562	+19.4	+0.188	+0.545	+0.455	+.414	+0.987	+34.1
74	+8.842	1.354	+0.561	+19.0	+0.188	+0.546	+0.454	+.415	+0.986	+33.5
75	+9.009	1.347	+0.561	+18.7	+0.188	+0.549	+0.451	+.417	+0.986	+32.8
76	+9.172	1.343	+0.560	+18.3	+0.188	+0.550	+0.450	+.417	+0.984	+32.2

TEST NAME : DSS-G1

Pt. No.	Str.Y (%)	SigV (ksc)	TauH (ksc)	Eu (ksc)	TauH / SigVc	DelU / SigVc	SigV / SigVc	TauH / SigV	TauH / Cu	Eu / Cu
77	+9.337	1.332	+0.559	+18.0	+0.187	+0.553	+0.447	+.420	+0.982	+31.6
78	+9.501	1.328	+0.558	+17.6	+0.187	+0.555	+0.445	+.420	+0.980	+30.9
79	+9.655	1.323	+0.558	+17.3	+0.187	+0.557	+0.443	+.422	+0.980	+30.4
80	+9.823	1.313	+0.556	+17.0	+0.186	+0.560	+0.440	+.423	+0.976	+29.8
81	+9.964	1.311	+0.556	+16.7	+0.186	+0.561	+0.439	+.424	+0.976	+29.4
82	+10.127	1.293	+0.554	+16.4	+0.186	+0.567	+0.433	+.428	+0.973	+28.8
83	+10.292	1.311	+0.554	+16.2	+0.186	+0.561	+0.439	+.423	+0.974	+28.4
84	+10.449	1.283	+0.553	+15.9	+0.185	+0.570	+0.430	+.431	+0.971	+27.9
85	+10.619	1.279	+0.552	+15.6	+0.185	+0.571	+0.429	+.431	+0.970	+27.4
86	+10.769	1.281	+0.551	+15.4	+0.185	+0.571	+0.429	+.430	+0.969	+27.0
87	+10.939	1.271	+0.550	+15.1	+0.184	+0.574	+0.426	+.433	+0.967	+26.5
88	+11.089	1.277	+0.551	+14.9	+0.185	+0.572	+0.428	+.431	+0.967	+26.2
89	+11.263	1.263	+0.549	+14.6	+0.184	+0.577	+0.423	+.435	+0.964	+25.7
90	+11.422	1.263	+0.549	+14.4	+0.184	+0.577	+0.423	+.435	+0.965	+25.3
91	+11.581	1.253	+0.547	+14.2	+0.183	+0.580	+0.420	+.437	+0.961	+24.9
92	+11.742	1.248	+0.546	+14.0	+0.183	+0.582	+0.418	+.438	+0.960	+24.5
93	+11.831	1.253	+0.545	+13.8	+0.183	+0.580	+0.420	+.435	+0.957	+24.3
94	+12.247	1.248	+0.543	+13.3	+0.182	+0.582	+0.418	+.435	+0.954	+23.4
95	+12.661	1.211	+0.539	+12.8	+0.181	+0.594	+0.406	+.445	+0.947	+22.4
96	+13.070	1.197	+0.536	+12.3	+0.180	+0.599	+0.401	+.448	+0.942	+21.6
97	+13.481	1.193	+0.534	+11.9	+0.179	+0.600	+0.400	+.448	+0.938	+20.9
98	+13.893	1.168	+0.528	+11.4	+0.177	+0.608	+0.392	+.452	+0.928	+20.0
99	+14.295	1.172	+0.526	+11.0	+0.176	+0.607	+0.393	+.449	+0.925	+19.4
100	+14.705	1.146	+0.524	+10.7	+0.176	+0.616	+0.384	+.458	+0.921	+18.8
101	+15.110	1.138	+0.519	+10.3	+0.174	+0.619	+0.381	+.456	+0.912	+18.1
102	+15.512	1.118	+0.514	+9.9	+0.172	+0.625	+0.375	+.460	+0.903	+17.5
103	+15.917	1.119	+0.511	+9.6	+0.171	+0.625	+0.375	+.456	+0.897	+16.9
104	+16.339	1.104	+0.504	+9.3	+0.169	+0.630	+0.370	+.457	+0.886	+16.3
105	+16.753	1.100	+0.501	+9.0	+0.168	+0.631	+0.369	+.456	+0.881	+15.8
106	+17.160	1.071	+0.494	+8.6	+0.165	+0.641	+0.359	+.461	+0.867	+15.2
107	+17.581	1.047	+0.488	+8.3	+0.164	+0.649	+0.351	+.466	+0.857	+14.6
108	+17.988	1.032	+0.482	+8.0	+0.161	+0.654	+0.346	+.467	+0.846	+14.1
109	+18.386	1.012	+0.477	+7.8	+0.160	+0.661	+0.339	+.472	+0.839	+13.7
110	+18.797	0.992	+0.472	+7.5	+0.158	+0.668	+0.332	+.476	+0.829	+13.2
111	+19.208	0.975	+0.467	+7.3	+0.157	+0.673	+0.327	+.479	+0.821	+12.8
112	+19.622	0.962	+0.462	+7.1	+0.155	+0.677	+0.323	+.480	+0.812	+12.4
113	+20.021	0.954	+0.460	+6.9	+0.154	+0.680	+0.320	+.482	+0.808	+12.1
114	+20.419	0.949	+0.456	+6.7	+0.153	+0.682	+0.318	+.480	+0.801	+11.8
115	+20.828	0.940	+0.453	+6.5	+0.152	+0.685	+0.315	+.481	+0.795	+11.5
116	+21.246	0.902	+0.445	+6.3	+0.149	+0.698	+0.302	+.493	+0.781	+11.0
117	+21.656	0.887	+0.440	+6.1	+0.147	+0.703	+0.297	+.496	+0.773	+10.7
118	+22.078	0.870	+0.435	+5.9	+0.146	+0.708	+0.292	+.499	+0.763	+10.4
119	+22.457	0.864	+0.429	+5.7	+0.144	+0.710	+0.290	+.497	+0.754	+10.1
120	+22.864	0.830	+0.422	+5.5	+0.142	+0.722	+0.278	+.509	+0.742	+9.7
121	+23.279	0.810	+0.416	+5.4	+0.139	+0.728	+0.272	+.513	+0.731	+9.4
122	+23.689	0.795	+0.410	+5.2	+0.137	+0.734	+0.266	+.516	+0.720	+9.1
123	+24.096	0.784	+0.405	+5.0	+0.136	+0.737	+0.263	+.516	+0.711	+8.9
124	+24.505	0.770	+0.397	+4.9	+0.133	+0.742	+0.258	+.516	+0.698	+8.5

TEST NAME : DSS-G1

Pt. No.	Str.Y (%)	SigV (ksc)	TauH (ksc)	Eu (ksc)	TauH / SigVc	DelU / SigVc	SigV / SigVc	TauH / SigV	TauH / Cu	Eu / Cu
125	+24.903	0.751	+0.395	+4.8	+0.133	+0.748	+0.252	+.526	+0.695	+8.4
126	+25.308	0.734	+0.387	+4.6	+0.130	+0.754	+0.246	+.528	+0.681	+8.1
127	+25.711	0.721	+0.380	+4.4	+0.127	+0.758	+0.242	+.527	+0.668	+7.8
128	+26.114	0.705	+0.375	+4.3	+0.126	+0.764	+0.236	+.531	+0.658	+7.6
129	+26.538	0.683	+0.368	+4.2	+0.123	+0.771	+0.229	+.538	+0.646	+7.3
130	+26.941	0.665	+0.362	+4.0	+0.121	+0.777	+0.223	+.545	+0.637	+7.1
131	+27.339	0.651	+0.356	+3.9	+0.119	+0.782	+0.218	+.548	+0.626	+6.9
132	+27.720	0.641	+0.353	+3.8	+0.118	+0.785	+0.215	+.550	+0.619	+6.7
133	+28.125	0.628	+0.347	+3.7	+0.116	+0.790	+0.210	+.552	+0.609	+6.5
134	+28.515	0.622	+0.341	+3.6	+0.114	+0.792	+0.208	+.548	+0.599	+6.3
135	+28.892	0.607	+0.334	+3.5	+0.112	+0.797	+0.203	+.550	+0.586	+6.1
136	+29.292	0.585	+0.326	+3.3	+0.109	+0.804	+0.196	+.558	+0.573	+5.9

****

Ko CONSOLIDATED GEONOR DIRECT SIMPLE SHEAR TEST

MIT GEOTECHNICAL LAB

****

FILE NAME: DSSG2.PRN

REDUCTION DATA

UNITS: (kg,cm,mVOLTS,VOLTS)

1. TEST NAME : DSS-G2
2. DATE : 7/21/1987
3. OCR : 1
4. VER. CONSOLIDATION STRESS (KSC) : +2.990
5. HOR. CONSOLIDATION STRESS (KSC) : +0.000
6. PRE-SHEAR SAMPLE HEIGHT (cm) : +1.8560
7. VERTICAL STRESS LOAD CELL:
   ZERO: 1.043
   CF: -343.29
8. HORIZONTAL SHEAR LOAD CELL:
   ZERO: -1.9461
   CF: -170.77
9. HORIZONTAL DISP. TRANSDUCER, X:
   ZERO: .63663
   CF: 2.2815
10. VERTICAL HEIGHT TRANSDUCER, Z:
    ZERO: .3301
    CF: 2.1089

Pt. No.	Str.Y (%)	SigV (ksc)	TauH (ksc)	Eu (ksc)	TauH / SigVc	DelU / SigVc	SigV / SigVc	TauH / SigV	TauH / Cu	Eu / Cu
1	+0.000	2.990	+0.000	+9999.0	+0.000	+0.000	+1.000	+.000	+0.000	+9999.0
2	+0.002	2.994	+0.007	+1360.1	+0.002	-0.001	+1.001	+.002	+0.011	+2135.7
3	+0.004	2.971	+0.008	+601.2	+0.003	+0.007	+0.993	+.003	+0.012	+944.0
4	+0.001	2.947	+0.008	+2070.4	+0.003	+0.014	+0.986	+.003	+0.012	+3250.9
5	+0.000	2.933	+0.008	+9999.0	+0.003	+0.019	+0.981	+.003	+0.013	+9999.0
6	+0.000	2.921	+0.013	+9999.0	+0.004	+0.023	+0.977	+.005	+0.021	+9999.0
7	+0.001	2.905	+0.021	+4621.2	+0.007	+0.028	+0.972	+.007	+0.032	+7256.3
8	+0.009	2.939	+0.047	+1515.7	+0.016	+0.017	+0.983	+.016	+0.074	+2380.0
9	+0.019	2.955	+0.079	+1245.6	+0.026	+0.012	+0.988	+.027	+0.124	+1955.8
10	+0.029	2.918	+0.115	+1187.7	+0.038	+0.024	+0.976	+.039	+0.180	+1865.0
11	+0.040	2.888	+0.152	+1127.7	+0.051	+0.034	+0.966	+.053	+0.239	+1770.7
12	+0.061	2.864	+0.209	+1026.6	+0.070	+0.042	+0.958	+.073	+0.329	+1611.9
13	+0.078	2.856	+0.229	+875.4	+0.076	+0.045	+0.955	+.080	+0.359	+1374.6
14	+0.106	2.837	+0.266	+751.8	+0.089	+0.051	+0.949	+.094	+0.418	+1180.4
15	+0.136	2.811	+0.303	+667.5	+0.101	+0.060	+0.940	+.108	+0.475	+1048.1
16	+0.175	2.778	+0.338	+577.8	+0.113	+0.071	+0.929	+.122	+0.530	+907.3
17	+0.223	2.741	+0.370	+498.6	+0.124	+0.083	+0.917	+.135	+0.581	+782.9
18	+0.275	2.701	+0.400	+436.6	+0.134	+0.097	+0.903	+.148	+0.628	+685.6
19	+0.338	2.660	+0.428	+380.5	+0.143	+0.111	+0.889	+.161	+0.672	+597.5
20	+0.410	2.616	+0.451	+330.6	+0.151	+0.125	+0.875	+.173	+0.709	+519.0
21	+0.501	2.557	+0.478	+285.7	+0.160	+0.145	+0.855	+.187	+0.750	+448.6
22	+0.577	2.510	+0.494	+257.0	+0.165	+0.161	+0.839	+.197	+0.776	+403.6
23	+0.672	2.462	+0.511	+228.1	+0.171	+0.177	+0.823	+.208	+0.802	+358.2
24	+0.778	2.411	+0.527	+203.0	+0.176	+0.194	+0.806	+.218	+0.827	+318.8
25	+0.890	2.368	+0.540	+181.9	+0.181	+0.208	+0.792	+.228	+0.848	+285.6
26	+1.007	2.327	+0.553	+164.9	+0.185	+0.222	+0.778	+.238	+0.869	+258.9
27	+1.128	2.279	+0.563	+149.7	+0.188	+0.238	+0.762	+.247	+0.884	+235.1
28	+1.252	2.223	+0.573	+137.2	+0.192	+0.257	+0.743	+.258	+0.899	+215.4

TEST NAME : DSS-G2

Pt. No.	Str.Y (%)	SigV (ksc)	TauH (ksc)	Eu (ksc)	TauH / SigVc	DelU / SigVc	SigV / SigVc	TauH / SigV	TauH / Cu	Eu / Cu
29	+1.384	2.168	+0.581	+125.8	+0.194	+0.275	+0.725	+.268	+0.912	+197.6
30	+1.520	2.120	+0.587	+116.0	+0.196	+0.291	+0.709	+.277	+0.922	+182.1
31	+1.658	2.084	+0.593	+107.3	+0.198	+0.303	+0.697	+.285	+0.931	+168.5
32	+1.802	2.052	+0.598	+99.5	+0.200	+0.314	+0.686	+.291	+0.938	+156.3
33	+1.949	2.013	+0.601	+92.5	+0.201	+0.327	+0.673	+.299	+0.944	+145.3
34	+2.114	1.973	+0.600	+85.1	+0.201	+0.340	+0.660	+.304	+0.942	+133.7
35	+2.263	1.951	+0.604	+80.0	+0.202	+0.347	+0.653	+.309	+0.948	+125.6
36	+2.404	1.933	+0.608	+75.8	+0.203	+0.354	+0.646	+.314	+0.954	+119.1
37	+2.562	1.910	+0.610	+71.5	+0.204	+0.361	+0.639	+.320	+0.959	+112.3
38	+2.704	1.880	+0.613	+68.1	+0.205	+0.371	+0.629	+.326	+0.963	+106.9
39	+2.852	1.857	+0.618	+65.0	+0.207	+0.379	+0.621	+.333	+0.971	+102.1
40	+3.001	1.828	+0.620	+62.0	+0.207	+0.389	+0.611	+.339	+0.974	+97.3
41	+3.156	1.805	+0.623	+59.2	+0.208	+0.396	+0.604	+.345	+0.978	+92.9
42	+3.310	1.782	+0.625	+56.6	+0.209	+0.404	+0.596	+.351	+0.981	+88.9
43	+3.469	1.754	+0.625	+54.1	+0.209	+0.414	+0.586	+.357	+0.982	+84.9
44	+3.622	1.746	+0.628	+52.0	+0.210	+0.416	+0.584	+.360	+0.986	+81.6
45	+3.774	1.727	+0.628	+49.9	+0.210	+0.422	+0.578	+.364	+0.986	+78.4
46	+3.935	1.706	+0.630	+48.1	+0.211	+0.429	+0.571	+.369	+0.990	+75.5
47	+4.095	1.692	+0.630	+46.2	+0.211	+0.434	+0.566	+.372	+0.990	+72.5
48	+4.249	1.678	+0.632	+44.6	+0.211	+0.439	+0.561	+.377	+0.992	+70.0
49	+4.402	1.674	+0.633	+43.1	+0.212	+0.440	+0.560	+.378	+0.994	+67.7
50	+4.562	1.629	+0.634	+41.7	+0.212	+0.455	+0.545	+.389	+0.995	+65.4
51	+4.724	1.603	+0.634	+40.3	+0.212	+0.464	+0.536	+.396	+0.996	+63.2
52	+4.880	1.606	+0.634	+39.0	+0.212	+0.463	+0.537	+.395	+0.995	+61.2
53	+5.037	1.607	+0.635	+37.8	+0.212	+0.463	+0.537	+.395	+0.998	+59.4
54	+5.194	1.581	+0.637	+36.8	+0.213	+0.471	+0.529	+.403	+1.000	+57.7
55	+5.365	1.580	+0.637	+35.6	+0.213	+0.472	+0.528	+.403	+1.000	+55.9
56	+5.526	1.555	+0.637	+34.6	+0.213	+0.480	+0.520	+.409	+1.000	+54.3
57	+5.693	1.537	+0.636	+33.5	+0.213	+0.486	+0.514	+.414	+0.998	+52.6
58	+5.852	1.544	+0.636	+32.6	+0.213	+0.484	+0.516	+.412	+0.999	+51.2
59	+6.017	1.513	+0.635	+31.6	+0.212	+0.494	+0.506	+.420	+0.997	+49.7
60	+6.186	1.493	+0.635	+30.8	+0.212	+0.501	+0.499	+.425	+0.997	+48.3
61	+6.347	1.490	+0.633	+29.9	+0.212	+0.502	+0.498	+.425	+0.994	+47.0
62	+6.508	1.499	+0.634	+29.2	+0.212	+0.499	+0.501	+.423	+0.996	+45.9
63	+6.671	1.469	+0.633	+28.5	+0.212	+0.509	+0.491	+.431	+0.994	+44.7
64	+6.836	1.483	+0.634	+27.8	+0.212	+0.504	+0.496	+.428	+0.996	+43.7
65	+6.998	1.465	+0.633	+27.2	+0.212	+0.510	+0.490	+.432	+0.995	+42.6
66	+7.163	1.452	+0.633	+26.5	+0.212	+0.514	+0.486	+.436	+0.994	+41.6
67	+7.321	1.436	+0.633	+25.9	+0.212	+0.520	+0.480	+.441	+0.994	+40.7
68	+7.490	1.420	+0.631	+25.3	+0.211	+0.525	+0.475	+.444	+0.991	+39.7
69	+7.654	1.425	+0.631	+24.7	+0.211	+0.523	+0.477	+.443	+0.991	+38.8
70	+7.819	1.408	+0.630	+24.2	+0.211	+0.529	+0.471	+.448	+0.990	+38.0
71	+7.985	1.393	+0.630	+23.7	+0.211	+0.534	+0.466	+.452	+0.989	+37.1
72	+8.145	1.405	+0.630	+23.2	+0.211	+0.530	+0.470	+.449	+0.990	+36.5
73	+8.314	1.391	+0.630	+22.7	+0.211	+0.535	+0.465	+.453	+0.989	+35.7
74	+8.471	1.397	+0.630	+22.3	+0.211	+0.533	+0.467	+.451	+0.990	+35.0
75	+8.636	1.371	+0.629	+21.9	+0.210	+0.542	+0.458	+.459	+0.988	+34.3
76	+8.801	1.382	+0.630	+21.5	+0.211	+0.538	+0.462	+.456	+0.989	+33.7

TEST NAME : DSS-G2

Pt. No.	Str.Y (%)	SigV (ksc)	TauH (ksc)	Eu (ksc)	TauH / SigVc	DelU / SigVc	SigV / SigVc	TauH / SigV	TauH / Cu	Eu / Cu
77	+8.962	1.353	+0.627	+21.0	+0.210	+0.548	+0.452	+.463	+0.984	+33.0
78	+9.132	1.356	+0.627	+20.6	+0.210	+0.547	+0.453	+.463	+0.985	+32.4
79	+9.293	1.350	+0.627	+20.3	+0.210	+0.549	+0.451	+.465	+0.985	+31.8
80	+9.470	1.347	+0.627	+19.9	+0.210	+0.550	+0.450	+.465	+0.984	+31.2
81	+9.635	1.343	+0.627	+19.5	+0.210	+0.551	+0.449	+.467	+0.985	+30.7
82	+9.805	1.324	+0.625	+19.1	+0.209	+0.557	+0.443	+.472	+0.982	+30.0
83	+9.971	1.314	+0.625	+18.8	+0.209	+0.561	+0.439	+.476	+0.981	+29.5
84	+10.144	1.328	+0.624	+18.4	+0.209	+0.556	+0.444	+.470	+0.979	+29.0
85	+10.309	1.310	+0.623	+18.1	+0.208	+0.562	+0.438	+.475	+0.978	+28.4
86	+10.449	1.317	+0.623	+17.9	+0.208	+0.560	+0.440	+.473	+0.978	+28.1
87	+10.616	1.300	+0.622	+17.6	+0.208	+0.565	+0.435	+.478	+0.977	+27.6
88	+10.784	1.283	+0.620	+17.2	+0.207	+0.571	+0.429	+.483	+0.973	+27.1
89	+10.951	1.288	+0.620	+17.0	+0.207	+0.569	+0.431	+.481	+0.973	+26.7
90	+11.117	1.281	+0.617	+16.7	+0.206	+0.572	+0.428	+.482	+0.969	+26.2
91	+11.286	1.278	+0.617	+16.4	+0.206	+0.573	+0.427	+.483	+0.969	+25.8
92	+11.449	1.285	+0.617	+16.2	+0.206	+0.570	+0.430	+.480	+0.969	+25.4
93	+11.612	1.258	+0.616	+15.9	+0.206	+0.579	+0.421	+.490	+0.967	+25.0
94	+11.719	1.270	+0.615	+15.8	+0.206	+0.575	+0.425	+.485	+0.966	+24.7
95	+12.126	1.251	+0.614	+15.2	+0.205	+0.582	+0.418	+.491	+0.964	+23.8
96	+12.548	1.240	+0.609	+14.6	+0.204	+0.585	+0.415	+.491	+0.957	+22.9
97	+12.972	1.210	+0.604	+14.0	+0.202	+0.595	+0.405	+.500	+0.949	+21.9
98	+13.394	1.184	+0.599	+13.4	+0.200	+0.604	+0.396	+.506	+0.941	+21.1
99	+13.807	1.159	+0.594	+12.9	+0.199	+0.612	+0.388	+.513	+0.933	+20.3
100	+14.249	1.132	+0.586	+12.3	+0.196	+0.622	+0.378	+.518	+0.920	+19.4
101	+14.687	1.096	+0.575	+11.7	+0.192	+0.634	+0.366	+.525	+0.903	+18.4
102	+15.129	1.078	+0.567	+11.2	+0.190	+0.639	+0.361	+.526	+0.890	+17.6
103	+15.558	1.047	+0.559	+10.8	+0.187	+0.650	+0.350	+.534	+0.878	+16.9
104	+16.002	1.008	+0.548	+10.3	+0.183	+0.663	+0.337	+.544	+0.861	+16.1
105	+16.424	0.984	+0.543	+9.9	+0.182	+0.671	+0.329	+.552	+0.853	+15.6
106	+16.846	0.966	+0.536	+9.5	+0.179	+0.677	+0.323	+.555	+0.841	+15.0
107	+17.284	0.942	+0.529	+9.2	+0.177	+0.685	+0.315	+.562	+0.831	+14.4
108	+17.728	0.905	+0.520	+8.8	+0.174	+0.697	+0.303	+.574	+0.816	+13.8
109	+18.154	0.892	+0.511	+8.4	+0.171	+0.702	+0.298	+.573	+0.802	+13.2
110	+18.579	0.884	+0.507	+8.2	+0.169	+0.704	+0.296	+.573	+0.795	+12.8
111	+18.998	0.869	+0.501	+7.9	+0.167	+0.709	+0.291	+.576	+0.786	+12.4
112	+19.420	0.853	+0.496	+7.7	+0.166	+0.715	+0.285	+.581	+0.779	+12.0
113	+19.847	0.839	+0.488	+7.4	+0.163	+0.719	+0.281	+.581	+0.766	+11.6
114	+20.271	0.821	+0.481	+7.1	+0.161	+0.726	+0.274	+.586	+0.755	+11.2
115	+20.700	0.810	+0.475	+6.9	+0.159	+0.729	+0.271	+.586	+0.745	+10.8
116	+21.135	0.795	+0.467	+6.6	+0.156	+0.734	+0.266	+.587	+0.733	+10.4
117	+21.564	0.767	+0.457	+6.4	+0.153	+0.744	+0.256	+.596	+0.718	+10.0
118	+22.008	0.753	+0.446	+6.1	+0.149	+0.748	+0.252	+.593	+0.701	+9.6
119	+22.432	0.730	+0.439	+5.9	+0.147	+0.756	+0.244	+.600	+0.689	+9.2
120	+22.863	0.718	+0.432	+5.7	+0.144	+0.760	+0.240	+.601	+0.678	+8.9
121	+23.290	0.697	+0.423	+5.5	+0.142	+0.767	+0.233	+.608	+0.665	+8.6
122	+23.705	0.678	+0.417	+5.3	+0.140	+0.773	+0.227	+.616	+0.655	+8.3
123	+24.145	0.659	+0.409	+5.1	+0.137	+0.780	+0.220	+.620	+0.641	+8.0
124	+24.565	0.640	+0.400	+4.9	+0.134	+0.786	+0.214	+.625	+0.628	+7.7

TEST NAME : DSS-G2

Pt. No.	Str.Y (%)	SigV (ksc)	TauH (ksc)	Eu (ksc)	TauH / SigVc	DelU / SigVc	SigV / SigVc	TauH / SigV	TauH / Cu	Eu / Cu
125	+24.996	0.630	+0.394	+4.7	+0.132	+0.789	+0.211	+.627	+0.619	+7.4
126	+25.400	0.627	+0.389	+4.6	+0.130	+0.790	+0.210	+.620	+0.611	+7.2
127	+25.815	0.601	+0.383	+4.4	+0.128	+0.799	+0.201	+.637	+0.601	+7.0
128	+26.237	0.602	+0.377	+4.3	+0.126	+0.799	+0.201	+.626	+0.592	+6.8
129	+26.674	0.573	+0.367	+4.1	+0.123	+0.808	+0.192	+.640	+0.576	+6.5
130	+27.088	0.562	+0.362	+4.0	+0.121	+0.812	+0.188	+.643	+0.568	+6.3
131	+27.512	0.551	+0.354	+3.9	+0.118	+0.816	+0.184	+.643	+0.556	+6.1
132	+27.914	0.544	+0.349	+3.7	+0.117	+0.818	+0.182	+.641	+0.547	+5.9
133	+28.324	0.534	+0.344	+3.6	+0.115	+0.821	+0.179	+.643	+0.540	+5.7
134	+28.735	0.522	+0.337	+3.5	+0.113	+0.825	+0.175	+.645	+0.529	+5.5
135	+29.147	0.517	+0.331	+3.4	+0.111	+0.827	+0.173	+.641	+0.520	+5.4
136	+29.551	0.502	+0.325	+3.3	+0.109	+0.832	+0.168	+.648	+0.511	+5.2
137	+29.950	0.495	+0.320	+3.2	+0.107	+0.835	+0.165	+.647	+0.503	+5.0
138	+30.368	0.485	+0.314	+3.1	+0.105	+0.838	+0.162	+.648	+0.493	+4.9
139	+30.783	0.471	+0.306	+3.0	+0.102	+0.842	+0.158	+.649	+0.480	+4.7
140	+31.185	0.470	+0.300	+2.9	+0.100	+0.843	+0.157	+.639	+0.472	+4.5
141	+31.578	0.465	+0.290	+2.8	+0.097	+0.845	+0.155	+.623	+0.455	+4.3

****

ANISOTROPICALLY CONSOLIDATED GEONOR DIRECT SIMPLE SHEAR TEST
MIT GEOTECHNICAL LAB

****

FILE NAME: DSSG3.PRN

REDUCTION DATA
UNITS: (kg,cm,VOLTS)

1. TEST NAME : DSS-G3
2. DATE : 7-26-1987
3. OCR : 1
4. VER. CONSOLIDATION STRESS (KSC) : +2.980
5. HOR. CONSOLIDATION STRESS (KSC) : +0.300
6. PRE-SHEAR SAMPLE HEIGHT (cm) : +1.9511
7. VERTICAL STRESS LOAD CELL:
   ZERO: 1.043
   CF: -343.29
8. HORIZONTAL SHEAR LOAD CELL:
   ZERO: -1.951
   CF: -176.64
9. HORIZONTAL DISP. TRANSDUCER, X:
   ZERO: 1.01263
   CF: 2.2815
10. CONSTANT HEIGHT TRANSDUCER, Z:
    ZERO: .35813
    CF: 2.1089
11. TEST ANGLE THETA: 0
    TOTAL X DISP. DURING CONSOLIDATION: .1701

Pt. No.	Str.X (%)	X.Coor. (cm)	SigV (ksc)	TauH (ksc)	Eu (ksc)	TauH ---- SigVc	DelU ---- SigVc	SigV ---- SigVc	TauH ---- SigV	TauH ---- Cu	Eu -- Cu
1	+0.000	+0.170	2.980	+0.289	+9999.0	+.097	+0.000	+1.000	+.097	+0.000	+9999.0
2	+0.003	+0.170	2.988	+0.289	+21.3	+.097	-0.003	+1.003	+.097	+0.000	+56.8
3	+0.004	+0.170	2.983	+0.290	+28.5	+.097	-0.001	+1.001	+.097	+0.001	+76.0
4	+0.010	+0.170	3.007	+0.300	+327.8	+.101	-0.009	+1.009	+.100	+0.028	+872.1
5	+0.008	+0.170	3.010	+0.300	+381.7	+.101	-0.010	+1.010	+.100	+0.029	+1015.5
6	+0.010	+0.170	2.975	+0.300	+324.8	+.101	+0.001	+0.999	+.101	+0.029	+864.3
7	+0.010	+0.170	2.948	+0.300	+343.2	+.101	+0.011	+0.989	+.102	+0.030	+913.0
8	+0.009	+0.170	2.933	+0.301	+376.2	+.101	+0.016	+0.984	+.103	+0.030	+1000.9
9	+0.006	+0.170	2.925	+0.301	+543.5	+.101	+0.018	+0.982	+.103	+0.031	+1446.1
10	+0.007	+0.170	2.933	+0.313	+954.2	+.105	+0.016	+0.984	+.107	+0.063	+2538.9
11	+0.014	+0.170	2.957	+0.317	+600.0	+.106	+0.008	+0.992	+.107	+0.075	+1596.5
12	+0.014	+0.170	2.969	+0.333	+941.9	+.112	+0.004	+0.996	+.112	+0.115	+2506.2
13	+0.022	+0.171	2.985	+0.349	+819.4	+.117	-0.002	+1.002	+.117	+0.159	+2180.2
14	+0.025	+0.171	2.958	+0.365	+905.0	+.123	+0.007	+0.993	+.124	+0.203	+2407.9
15	+0.031	+0.171	2.935	+0.383	+897.4	+.129	+0.015	+0.985	+.131	+0.250	+2387.7
16	+0.038	+0.171	2.924	+0.401	+876.6	+.135	+0.019	+0.981	+.137	+0.297	+2332.4
17	+0.045	+0.171	2.916	+0.417	+854.8	+.140	+0.021	+0.979	+.143	+0.341	+2274.4
18	+0.058	+0.171	2.921	+0.435	+756.7	+.146	+0.020	+0.980	+.149	+0.389	+2013.4
19	+0.069	+0.171	2.942	+0.453	+715.3	+.152	+0.013	+0.987	+.154	+0.435	+1903.3
20	+0.084	+0.172	2.958	+0.470	+643.6	+.158	+0.007	+0.993	+.159	+0.482	+1712.4
21	+0.099	+0.172	2.934	+0.488	+599.0	+.164	+0.015	+0.985	+.166	+0.528	+1593.8
22	+0.113	+0.172	2.913	+0.505	+571.0	+.169	+0.022	+0.978	+.173	+0.574	+1519.4
23	+0.132	+0.173	2.902	+0.522	+527.5	+.175	+0.026	+0.974	+.180	+0.619	+1403.4
24	+0.153	+0.173	2.894	+0.538	+488.4	+.181	+0.029	+0.971	+.186	+0.662	+1299.4

TEST NAME : DSS-G3

Pt. No.	Str.X (%)	X.Coor. (cm)	SigV (ksc)	TauH (ksc)	Eu (ksc)	TauH ---- SigVc	DelU ---- SigVc	SigV ---- SigVc	TauH ---- SigV	TauH ---- Cu	Eu -- Cu
25	+0.178	+0.174	2.880	+0.554	+444.3	+.186	+0.033	+0.967	+.192	+0.703	+1182.0
26	+0.206	+0.174	2.871	+0.568	+405.0	+.191	+0.037	+0.963	+.198	+0.741	+1077.6
27	+0.237	+0.175	2.858	+0.581	+368.1	+.195	+0.041	+0.959	+.203	+0.775	+979.3
28	+0.274	+0.175	2.846	+0.593	+333.1	+.199	+0.045	+0.955	+.208	+0.808	+886.2
29	+0.312	+0.176	2.833	+0.604	+302.4	+.203	+0.049	+0.951	+.213	+0.837	+804.6
30	+0.357	+0.177	2.815	+0.614	+273.6	+.206	+0.055	+0.945	+.218	+0.865	+728.0
31	+0.406	+0.178	2.794	+0.623	+246.4	+.209	+0.062	+0.938	+.223	+0.888	+655.5
32	+0.454	+0.179	2.767	+0.630	+225.3	+.211	+0.071	+0.929	+.228	+0.907	+599.3
33	+0.516	+0.180	2.747	+0.637	+202.1	+.214	+0.078	+0.922	+.232	+0.925	+537.6
34	+0.573	+0.181	2.724	+0.642	+184.6	+.215	+0.086	+0.914	+.236	+0.938	+491.1
35	+0.633	+0.182	2.695	+0.645	+168.7	+.217	+0.095	+0.905	+.239	+0.948	+448.8
36	+0.695	+0.184	2.665	+0.650	+155.6	+.218	+0.106	+0.894	+.244	+0.959	+414.0
37	+0.763	+0.185	2.635	+0.653	+143.2	+.219	+0.116	+0.884	+.248	+0.969	+381.0
38	+0.830	+0.186	2.603	+0.655	+132.1	+.220	+0.126	+0.874	+.252	+0.973	+351.6
39	+0.897	+0.188	2.571	+0.656	+122.8	+.220	+0.137	+0.863	+.255	+0.977	+326.8
40	+0.966	+0.189	2.544	+0.659	+114.9	+.221	+0.146	+0.854	+.259	+0.984	+305.6
41	+1.040	+0.190	2.517	+0.660	+107.1	+.222	+0.155	+0.845	+.262	+0.987	+284.9
42	+1.110	+0.192	2.489	+0.661	+100.4	+.222	+0.165	+0.835	+.265	+0.989	+267.2
43	+1.182	+0.193	2.462	+0.662	+94.6	+.222	+0.174	+0.826	+.269	+0.991	+251.7
44	+1.257	+0.195	2.435	+0.663	+89.1	+.222	+0.183	+0.817	+.272	+0.994	+237.1
45	+1.332	+0.196	2.408	+0.663	+84.2	+.223	+0.192	+0.808	+.275	+0.995	+224.0
46	+1.402	+0.197	2.388	+0.664	+80.1	+.223	+0.199	+0.801	+.278	+0.996	+213.1
47	+1.474	+0.199	2.363	+0.665	+76.4	+.223	+0.207	+0.793	+.281	+0.999	+203.4
48	+1.553	+0.200	2.339	+0.665	+72.5	+.223	+0.215	+0.785	+.284	+0.999	+193.0
49	+1.629	+0.202	2.312	+0.664	+69.0	+.223	+0.224	+0.776	+.287	+0.997	+183.6
50	+1.710	+0.203	2.288	+0.665	+65.9	+.223	+0.232	+0.768	+.291	+0.999	+175.3
51	+1.791	+0.205	2.269	+0.665	+62.9	+.223	+0.239	+0.761	+.293	+1.000	+167.5
52	+1.856	+0.206	2.248	+0.665	+60.7	+.223	+0.245	+0.755	+.296	+1.000	+161.6
53	+1.939	+0.208	2.230	+0.664	+58.1	+.223	+0.252	+0.748	+.298	+0.998	+154.5
54	+2.020	+0.210	2.213	+0.665	+55.8	+.223	+0.257	+0.743	+.300	+0.999	+148.4
55	+2.103	+0.211	2.195	+0.664	+53.5	+.223	+0.263	+0.737	+.303	+0.997	+142.3
56	+2.181	+0.213	2.175	+0.663	+51.3	+.222	+0.270	+0.730	+.305	+0.993	+136.6
57	+2.262	+0.214	2.157	+0.662	+49.4	+.222	+0.276	+0.724	+.307	+0.991	+131.5
58	+2.338	+0.216	2.138	+0.661	+47.7	+.222	+0.282	+0.718	+.309	+0.990	+127.0
59	+2.421	+0.217	2.120	+0.661	+46.0	+.222	+0.288	+0.712	+.312	+0.989	+122.5
60	+2.500	+0.219	2.099	+0.659	+44.4	+.221	+0.296	+0.704	+.314	+0.984	+118.1
61	+2.578	+0.220	2.079	+0.659	+43.0	+.221	+0.302	+0.698	+.317	+0.984	+114.5
62	+2.659	+0.222	2.064	+0.658	+41.6	+.221	+0.307	+0.693	+.319	+0.982	+110.8
63	+2.739	+0.224	2.046	+0.657	+40.3	+.221	+0.313	+0.687	+.321	+0.979	+107.2
64	+2.816	+0.225	2.032	+0.656	+39.1	+.220	+0.318	+0.682	+.323	+0.977	+104.1
65	+2.896	+0.227	2.020	+0.657	+38.1	+.220	+0.322	+0.678	+.325	+0.978	+101.3
66	+2.973	+0.228	2.008	+0.656	+37.0	+.220	+0.326	+0.674	+.327	+0.976	+98.5
67	+3.056	+0.230	1.989	+0.655	+35.9	+.220	+0.332	+0.668	+.329	+0.973	+95.5
68	+3.130	+0.231	1.969	+0.654	+35.0	+.220	+0.339	+0.661	+.332	+0.971	+93.1
69	+3.213	+0.233	1.953	+0.654	+34.0	+.219	+0.345	+0.655	+.335	+0.969	+90.5
70	+3.291	+0.234	1.938	+0.652	+33.1	+.219	+0.350	+0.650	+.337	+0.966	+88.1
71	+3.425	+0.237	1.922	+0.651	+31.7	+.219	+0.355	+0.645	+.339	+0.963	+84.4
72	+3.448	+0.237	1.920	+0.651	+31.5	+.218	+0.356	+0.644	+.339	+0.963	+83.8

TEST NAME : DSS-G3

Pt. No.	Str.X (%)	X.Coor. (cm)	SigV (ksc)	TauH (ksc)	Eu (ksc)	TauH ---- SigVc	DelU ---- SigVc	SigV ---- SigVc	TauH ---- SigV	TauH ---- Cu	Eu -- Cu
73	+3.525	+0.239	1.912	+0.651	+30.8	+.218	+0.358	+0.642	+.340	+0.962	+81.9
74	+3.622	+0.241	1.901	+0.649	+29.8	+.218	+0.362	+0.638	+.341	+0.958	+79.3
75	+3.686	+0.242	1.891	+0.649	+29.3	+.218	+0.365	+0.635	+.343	+0.957	+77.9
76	+3.769	+0.244	1.880	+0.649	+28.6	+.218	+0.369	+0.631	+.345	+0.956	+76.1
77	+3.832	+0.245	1.871	+0.648	+28.1	+.218	+0.372	+0.628	+.346	+0.955	+74.7
78	+3.989	+0.248	1.847	+0.646	+26.8	+.217	+0.380	+0.620	+.350	+0.949	+71.3
79	+4.149	+0.251	1.815	+0.644	+25.6	+.216	+0.391	+0.609	+.355	+0.943	+68.2
80	+4.310	+0.254	1.782	+0.641	+24.5	+.215	+0.402	+0.598	+.360	+0.937	+65.2
81	+4.478	+0.257	1.757	+0.639	+23.4	+.214	+0.410	+0.590	+.364	+0.931	+62.4
82	+4.637	+0.261	1.735	+0.637	+22.5	+.214	+0.418	+0.582	+.367	+0.925	+59.8
83	+4.804	+0.264	1.716	+0.634	+21.6	+.213	+0.424	+0.576	+.370	+0.918	+57.3
84	+4.968	+0.267	1.697	+0.633	+20.7	+.212	+0.430	+0.570	+.373	+0.914	+55.2
85	+5.125	+0.270	1.686	+0.630	+19.9	+.211	+0.434	+0.566	+.374	+0.907	+53.1
86	+5.286	+0.273	1.681	+0.629	+19.3	+.211	+0.436	+0.564	+.374	+0.905	+51.3
87	+5.439	+0.276	1.660	+0.627	+18.6	+.210	+0.443	+0.557	+.378	+0.899	+49.6
88	+5.605	+0.279	1.635	+0.625	+18.0	+.210	+0.451	+0.549	+.383	+0.895	+47.9
89	+5.766	+0.283	1.619	+0.624	+17.4	+.209	+0.457	+0.543	+.385	+0.890	+46.3
90	+5.931	+0.286	1.601	+0.621	+16.8	+.209	+0.463	+0.537	+.388	+0.884	+44.7
91	+6.093	+0.289	1.591	+0.620	+16.3	+.208	+0.466	+0.534	+.390	+0.880	+43.3
92	+6.256	+0.292	1.573	+0.617	+15.7	+.207	+0.472	+0.528	+.392	+0.872	+41.8
93	+6.417	+0.295	1.563	+0.616	+15.3	+.207	+0.476	+0.524	+.394	+0.870	+40.7
94	+6.574	+0.298	1.545	+0.614	+14.8	+.206	+0.481	+0.519	+.397	+0.864	+39.4
95	+6.738	+0.302	1.528	+0.612	+14.4	+.206	+0.487	+0.513	+.401	+0.860	+38.3
96	+6.897	+0.305	1.515	+0.610	+13.9	+.205	+0.491	+0.509	+.402	+0.853	+37.1
97	+7.063	+0.308	1.502	+0.608	+13.5	+.204	+0.496	+0.504	+.405	+0.848	+36.0
98	+7.218	+0.311	1.494	+0.607	+13.2	+.204	+0.498	+0.502	+.406	+0.844	+35.1
99	+7.377	+0.314	1.485	+0.605	+12.9	+.203	+0.502	+0.498	+.408	+0.841	+34.2
100	+7.542	+0.317	1.456	+0.603	+12.5	+.202	+0.511	+0.489	+.414	+0.835	+33.2
101	+7.706	+0.320	1.443	+0.599	+12.1	+.201	+0.516	+0.484	+.415	+0.824	+32.1
102	+7.865	+0.324	1.433	+0.598	+11.8	+.201	+0.519	+0.481	+.417	+0.821	+31.3
103	+8.028	+0.327	1.431	+0.595	+11.4	+.200	+0.520	+0.480	+.416	+0.814	+30.4
104	+8.115	+0.328	1.429	+0.595	+11.3	+.200	+0.520	+0.480	+.416	+0.813	+30.1
105	+8.525	+0.336	1.383	+0.588	+10.5	+.197	+0.536	+0.464	+.425	+0.794	+28.0
106	+8.932	+0.344	1.357	+0.581	+9.8	+.195	+0.545	+0.455	+.428	+0.777	+26.1
107	+9.336	+0.352	1.337	+0.575	+9.2	+.193	+0.551	+0.449	+.430	+0.761	+24.4
108	+9.718	+0.360	1.290	+0.568	+8.6	+.190	+0.567	+0.433	+.440	+0.741	+22.9
109	+10.129	+0.368	1.280	+0.561	+8.1	+.188	+0.571	+0.429	+.439	+0.724	+21.4
110	+10.533	+0.376	1.238	+0.554	+7.5	+.186	+0.584	+0.416	+.447	+0.705	+20.1
111	+10.940	+0.384	1.202	+0.547	+7.1	+.184	+0.597	+0.403	+.455	+0.686	+18.8
112	+11.373	+0.392	1.146	+0.535	+6.5	+.180	+0.615	+0.385	+.467	+0.655	+17.3
113	+11.776	+0.400	1.128	+0.529	+6.1	+.177	+0.621	+0.379	+.469	+0.637	+16.2
114	+12.188	+0.408	1.102	+0.521	+5.7	+.175	+0.630	+0.370	+.473	+0.617	+15.2
115	+12.596	+0.416	1.079	+0.513	+5.3	+.172	+0.638	+0.362	+.476	+0.597	+14.2
116	+13.003	+0.424	1.055	+0.508	+5.0	+.170	+0.646	+0.354	+.482	+0.582	+13.4
117	+13.419	+0.432	1.016	+0.498	+4.7	+.167	+0.659	+0.341	+.490	+0.556	+12.4
118	+13.820	+0.440	0.979	+0.491	+4.4	+.165	+0.671	+0.329	+.502	+0.537	+11.7
119	+14.228	+0.448	0.959	+0.485	+4.1	+.163	+0.678	+0.322	+.506	+0.520	+11.0
120	+14.638	+0.456	0.937	+0.477	+3.8	+.160	+0.685	+0.315	+.508	+0.498	+10.2

****

Ko CONSOLIDATED GEONOR DIRECT SIMPLE SHEAR TEST
MIT GEOTECHNICAL LAB

****

FILE NAME: DSSG4.PRN

REDUCTION DATA
UNITS: (kg,cm,mVOLTS,VOLTS)

1. TEST NAME : GDSS-G4
2. DATE : 7/30/1987
3. OCR : 1
4. VER. CONSOLIDATION STRESS (KSC) : +2.981
5. HOR. CONSOLIDATION STRESS (KSC) : +0.000
6. PRE-SHEAR SAMPLE HEIGHT (cm) : +1.9253
7. VERTICAL STRESS LOAD CELL:
   ZERO: 1.044
   CF: -343.29
8. HORIZONTAL SHEAR LOAD CELL:
   ZERO: 1.9758
   CF: -169.73
9. HORIZONTAL DISP. TRANSDUCER, X:
   ZERO: .2219
   CF: 2.2815
10. VERTICAL HEIGHT TRANSDUCER, Z:
    ZERO: .48342
    CF: 2.1089

Pt. No.	Str.Y (%)	SigV (ksc)	TauH (ksc)	Eu (ksc)	TauH / SigVc	DelU / SigVc	SigV / SigVc	TauH / SigV	TauH / Cu	Eu / Cu
1	+0.000	2.981	+0.000	+9999.0	+0.000	+0.000	+1.000	+.000	+0.000	+9999.0
2	-0.002	2.981	-0.000	+11.1	-0.000	+0.000	+1.000	-.000	-0.000	+18.1
3	-0.002	2.988	+0.006	-771.3	+0.002	-0.002	+1.002	+.002	+0.010	-1260.4
4	-0.001	3.007	+0.011	-3192.7	+0.004	-0.009	+1.009	+.004	+0.019	-5217.3
5	-0.000	2.961	+0.011	-7982.3	+0.004	+0.007	+0.993	+.004	+0.019	-9999.0
6	-0.002	2.914	+0.012	-1474.4	+0.004	+0.022	+0.978	+.004	+0.019	-2409.4
7	-0.003	2.898	+0.011	-1071.1	+0.004	+0.028	+0.972	+.004	+0.018	-1750.3
8	-0.003	2.912	+0.011	-1191.2	+0.004	+0.023	+0.977	+.004	+0.018	-1946.5
9	-0.005	2.938	+0.011	-652.4	+0.004	+0.015	+0.985	+.004	+0.018	-1066.1
10	-0.001	2.929	+0.011	-3020.9	+0.004	+0.017	+0.983	+.004	+0.018	-4936.5
11	-0.004	2.902	+0.012	-908.3	+0.004	+0.026	+0.974	+.004	+0.019	-1484.3
12	-0.005	2.881	+0.017	-1004.7	+0.006	+0.034	+0.966	+.006	+0.027	-1641.8
13	-0.004	2.880	+0.026	-2102.7	+0.009	+0.034	+0.966	+.009	+0.042	-3436.0
14	-0.001	2.911	+0.051	-9999.0	+0.017	+0.024	+0.976	+.017	+0.083	-9999.0
15	+0.006	2.907	+0.079	+3826.0	+0.027	+0.025	+0.975	+.027	+0.130	+6252.1
16	+0.017	2.894	+0.113	+1992.7	+0.038	+0.029	+0.971	+.039	+0.184	+3256.2
17	+0.032	2.919	+0.148	+1392.1	+0.050	+0.021	+0.979	+.051	+0.242	+2274.9
18	+0.051	2.925	+0.184	+1077.5	+0.062	+0.019	+0.981	+.063	+0.301	+1760.8
19	+0.068	2.896	+0.219	+964.4	+0.074	+0.028	+0.972	+.076	+0.358	+1575.9
20	+0.096	2.877	+0.257	+801.2	+0.086	+0.035	+0.965	+.089	+0.419	+1309.2
21	+0.124	2.855	+0.291	+707.7	+0.098	+0.042	+0.958	+.102	+0.476	+1156.5
22	+0.164	2.840	+0.326	+596.8	+0.109	+0.047	+0.953	+.115	+0.533	+975.2
23	+0.205	2.825	+0.357	+522.7	+0.120	+0.052	+0.948	+.126	+0.584	+854.2
24	+0.262	2.792	+0.387	+443.6	+0.130	+0.063	+0.937	+.139	+0.632	+724.9
25	+0.327	2.766	+0.413	+379.6	+0.139	+0.072	+0.928	+.149	+0.675	+620.3
26	+0.398	2.730	+0.436	+328.9	+0.146	+0.084	+0.916	+.160	+0.713	+537.5
27	+0.479	2.686	+0.457	+286.6	+0.153	+0.099	+0.901	+.170	+0.747	+468.3
28	+0.569	2.636	+0.476	+251.1	+0.160	+0.116	+0.884	+.181	+0.778	+410.4

TEST NAME : GDSS-G4

Pt. No.	Str.Y (%)	SigV (ksc)	TauH (ksc)	Eu (ksc)	TauH / SigVc	DelU / SigVc	SigV / SigVc	TauH / SigV	TauH / Cu	Eu / Cu
29	+0.664	2.592	+0.494	+223.1	+0.166	+0.130	+0.870	+.190	+0.807	+364.5
30	+0.769	2.548	+0.508	+198.0	+0.170	+0.145	+0.855	+.199	+0.830	+323.6
31	+0.879	2.503	+0.521	+177.7	+0.175	+0.160	+0.840	+.208	+0.851	+290.5
32	+0.996	2.444	+0.531	+160.0	+0.178	+0.180	+0.820	+.217	+0.868	+261.5
33	+1.116	2.396	+0.541	+145.6	+0.182	+0.196	+0.804	+.226	+0.885	+237.9
34	+1.239	2.356	+0.550	+133.2	+0.185	+0.210	+0.790	+.233	+0.899	+217.7
35	+1.366	2.314	+0.558	+122.5	+0.187	+0.224	+0.776	+.241	+0.911	+200.2
36	+1.499	2.273	+0.565	+113.0	+0.189	+0.237	+0.763	+.248	+0.923	+184.7
37	+1.635	2.233	+0.570	+104.5	+0.191	+0.251	+0.749	+.255	+0.931	+170.8
38	+1.773	2.197	+0.576	+97.4	+0.193	+0.263	+0.737	+.262	+0.940	+159.2
39	+1.912	2.165	+0.579	+90.8	+0.194	+0.274	+0.726	+.267	+0.946	+148.4
40	+2.050	2.129	+0.583	+85.4	+0.196	+0.286	+0.714	+.274	+0.953	+139.5
41	+2.191	2.101	+0.587	+80.4	+0.197	+0.295	+0.705	+.279	+0.959	+131.3
42	+2.336	2.076	+0.591	+75.8	+0.198	+0.303	+0.697	+.284	+0.965	+123.9
43	+2.478	2.048	+0.594	+71.9	+0.199	+0.313	+0.687	+.290	+0.970	+117.5
44	+2.627	2.018	+0.597	+68.1	+0.200	+0.323	+0.677	+.296	+0.975	+111.3
45	+2.772	1.987	+0.599	+64.8	+0.201	+0.334	+0.666	+.302	+0.979	+106.0
46	+2.919	1.958	+0.601	+61.8	+0.202	+0.343	+0.657	+.307	+0.982	+101.0
47	+3.070	1.925	+0.603	+58.9	+0.202	+0.354	+0.646	+.313	+0.985	+96.3
48	+3.219	1.897	+0.603	+56.2	+0.202	+0.364	+0.636	+.318	+0.986	+91.9
49	+3.371	1.867	+0.605	+53.8	+0.203	+0.374	+0.626	+.324	+0.988	+87.9
50	+3.521	1.844	+0.605	+51.6	+0.203	+0.382	+0.618	+.328	+0.989	+84.3
51	+3.674	1.828	+0.607	+49.5	+0.204	+0.387	+0.613	+.332	+0.991	+80.9
52	+3.823	1.800	+0.607	+47.6	+0.204	+0.396	+0.604	+.337	+0.992	+77.9
53	+3.978	1.785	+0.609	+45.9	+0.204	+0.401	+0.599	+.341	+0.995	+75.0
54	+4.130	1.763	+0.609	+44.3	+0.204	+0.408	+0.592	+.346	+0.996	+72.3
55	+4.281	1.742	+0.610	+42.7	+0.204	+0.415	+0.585	+.350	+0.996	+69.8
56	+4.436	1.723	+0.611	+41.3	+0.205	+0.422	+0.578	+.354	+0.998	+67.5
57	+4.589	1.704	+0.610	+39.9	+0.205	+0.428	+0.572	+.358	+0.997	+65.2
58	+4.747	1.691	+0.611	+38.6	+0.205	+0.433	+0.567	+.362	+0.999	+63.1
59	+4.898	1.672	+0.611	+37.4	+0.205	+0.439	+0.561	+.365	+0.998	+61.2
60	+5.060	1.658	+0.612	+36.3	+0.205	+0.444	+0.556	+.369	+1.000	+59.3
61	+5.216	1.644	+0.612	+35.2	+0.205	+0.448	+0.552	+.372	+1.000	+57.5
62	+5.376	1.631	+0.612	+34.1	+0.205	+0.453	+0.547	+.375	+0.999	+55.8
63	+5.533	1.616	+0.612	+33.2	+0.205	+0.458	+0.542	+.379	+1.000	+54.2
64	+5.689	1.601	+0.611	+32.2	+0.205	+0.463	+0.537	+.382	+0.999	+52.7
65	+5.847	1.589	+0.611	+31.4	+0.205	+0.467	+0.533	+.385	+0.999	+51.2
66	+6.005	1.577	+0.611	+30.5	+0.205	+0.471	+0.529	+.387	+0.998	+49.8
67	+6.164	1.565	+0.611	+29.7	+0.205	+0.475	+0.525	+.390	+0.998	+48.6
68	+6.317	1.552	+0.610	+29.0	+0.205	+0.479	+0.521	+.393	+0.997	+47.4
69	+6.474	1.538	+0.610	+28.2	+0.205	+0.484	+0.516	+.396	+0.996	+46.2
70	+6.631	1.526	+0.609	+27.6	+0.204	+0.488	+0.512	+.399	+0.995	+45.0
71	+6.788	1.518	+0.608	+26.9	+0.204	+0.491	+0.509	+.401	+0.994	+43.9
72	+6.946	1.509	+0.609	+26.3	+0.204	+0.494	+0.506	+.403	+0.995	+43.0
73	+7.097	1.505	+0.608	+25.7	+0.204	+0.495	+0.505	+.404	+0.993	+42.0
74	+7.260	1.480	+0.607	+25.1	+0.204	+0.503	+0.497	+.410	+0.992	+41.0
75	+7.416	1.469	+0.605	+24.5	+0.203	+0.507	+0.493	+.412	+0.989	+40.0
76	+7.578	1.471	+0.606	+24.0	+0.203	+0.507	+0.493	+.412	+0.990	+39.2

TEST NAME : GDSS-G4

Pt. No.	Str.Y (%)	SigV (ksc)	TauH (ksc)	Eu (ksc)	TauH / SigVc	DelU / SigVc	SigV / SigVc	TauH / SigV	TauH / Cu	Eu / Cu
77	+7.732	1.453	+0.604	+23.4	+0.203	+0.513	+0.487	+.416	+0.988	+38.3
78	+7.895	1.439	+0.603	+22.9	+0.202	+0.517	+0.483	+.419	+0.985	+37.4
79	+8.049	1.444	+0.602	+22.4	+0.202	+0.515	+0.485	+.417	+0.984	+36.7
80	+8.207	1.429	+0.601	+22.0	+0.202	+0.521	+0.479	+.421	+0.983	+35.9
81	+8.368	1.407	+0.600	+21.5	+0.201	+0.528	+0.472	+.426	+0.980	+35.1
82	+8.527	1.399	+0.598	+21.0	+0.201	+0.531	+0.469	+.427	+0.977	+34.4
83	+8.687	1.400	+0.599	+20.7	+0.201	+0.530	+0.470	+.428	+0.979	+33.8
84	+8.847	1.381	+0.597	+20.3	+0.200	+0.537	+0.463	+.433	+0.976	+33.1
85	+9.012	1.371	+0.597	+19.9	+0.200	+0.540	+0.460	+.435	+0.976	+32.5
86	+9.173	1.372	+0.596	+19.5	+0.200	+0.540	+0.460	+.434	+0.974	+31.8
87	+9.204	1.367	+0.596	+19.4	+0.200	+0.541	+0.459	+.436	+0.974	+31.7
88	+9.610	1.352	+0.594	+18.5	+0.199	+0.546	+0.454	+.440	+0.971	+30.3
89	+10.008	1.325	+0.592	+17.7	+0.198	+0.555	+0.445	+.447	+0.967	+29.0
90	+10.405	1.307	+0.591	+17.0	+0.198	+0.561	+0.439	+.452	+0.966	+27.8
91	+10.803	1.295	+0.588	+16.3	+0.197	+0.565	+0.435	+.454	+0.961	+26.7
92	+11.201	1.279	+0.586	+15.7	+0.197	+0.571	+0.429	+.458	+0.958	+25.7
93	+11.603	1.247	+0.583	+15.1	+0.195	+0.582	+0.418	+.467	+0.952	+24.6
94	+12.008	1.238	+0.580	+14.5	+0.195	+0.585	+0.415	+.469	+0.948	+23.7
95	+12.407	1.217	+0.577	+14.0	+0.194	+0.592	+0.408	+.474	+0.943	+22.8
96	+12.805	1.202	+0.575	+13.5	+0.193	+0.597	+0.403	+.478	+0.939	+22.0
97	+13.218	1.182	+0.571	+13.0	+0.191	+0.604	+0.396	+.483	+0.932	+21.2
98	+13.628	1.168	+0.567	+12.5	+0.190	+0.608	+0.392	+.486	+0.927	+20.4
99	+14.037	1.149	+0.561	+12.0	+0.188	+0.614	+0.386	+.488	+0.916	+19.6
100	+14.441	1.142	+0.557	+11.6	+0.187	+0.617	+0.383	+.488	+0.911	+18.9
101	+14.855	1.113	+0.551	+11.1	+0.185	+0.627	+0.373	+.495	+0.900	+18.2
102	+15.257	1.096	+0.546	+10.7	+0.183	+0.632	+0.368	+.499	+0.893	+17.6
103	+15.664	1.074	+0.542	+10.4	+0.182	+0.640	+0.360	+.504	+0.885	+17.0
104	+16.080	1.048	+0.536	+10.0	+0.180	+0.648	+0.352	+.511	+0.875	+16.3
105	+16.497	1.014	+0.528	+9.6	+0.177	+0.660	+0.340	+.521	+0.863	+15.7
106	+16.909	0.992	+0.524	+9.3	+0.176	+0.667	+0.333	+.528	+0.856	+15.2
107	+17.329	0.981	+0.518	+9.0	+0.174	+0.671	+0.329	+.528	+0.847	+14.7
108	+17.735	0.963	+0.514	+8.7	+0.172	+0.677	+0.323	+.533	+0.840	+14.2
109	+18.146	0.944	+0.507	+8.4	+0.170	+0.683	+0.317	+.537	+0.828	+13.7
110	+18.559	0.922	+0.500	+8.1	+0.168	+0.691	+0.309	+.542	+0.817	+13.2
111	+18.973	0.905	+0.494	+7.8	+0.166	+0.697	+0.303	+.546	+0.807	+12.8
112	+19.391	0.892	+0.487	+7.5	+0.163	+0.701	+0.299	+.545	+0.795	+12.3
113	+19.807	0.877	+0.481	+7.3	+0.161	+0.706	+0.294	+.549	+0.786	+11.9
114	+20.217	0.858	+0.474	+7.0	+0.159	+0.712	+0.288	+.552	+0.775	+11.5
115	+20.626	0.843	+0.468	+6.8	+0.157	+0.717	+0.283	+.556	+0.765	+11.1
116	+21.051	0.823	+0.460	+6.6	+0.154	+0.724	+0.276	+.559	+0.751	+10.7
117	+21.471	0.804	+0.452	+6.3	+0.152	+0.730	+0.270	+.562	+0.739	+10.3
118	+21.889	0.788	+0.445	+6.1	+0.149	+0.736	+0.264	+.564	+0.727	+10.0
119	+22.301	0.767	+0.437	+5.9	+0.147	+0.743	+0.257	+.570	+0.714	+9.6
120	+22.719	0.753	+0.431	+5.7	+0.145	+0.747	+0.253	+.572	+0.704	+9.3
121	+23.129	0.737	+0.423	+5.5	+0.142	+0.753	+0.247	+.574	+0.691	+9.0
122	+23.543	0.720	+0.416	+5.3	+0.139	+0.758	+0.242	+.577	+0.679	+8.7
123	+23.959	0.706	+0.408	+5.1	+0.137	+0.763	+0.237	+.579	+0.668	+8.4
124	+24.353	0.676	+0.401	+4.9	+0.134	+0.773	+0.227	+.593	+0.655	+8.1

****

ANISOTROPICALLY CONSOLIDATED GEONOR DIRECT SIMPLE SHEAR TEST
MIT GEOTECHNICAL LAB

****

FILE NAME: DSSG5.PRN

REDUCTION DATA
UNITS: (kg,cm,VOLTS)

1. TEST NAME : DSS-G5
2. DATE : 8/27/1987
3. OCR : 1
4. VER. CONSOLIDATION STRESS (KSC) : +3.001
5. HOR. CONSOLIDATION STRESS (KSC) : +0.600
6. PRE-SHEAR SAMPLE HEIGHT (cm) : +1.9130
7. VERTICAL STRESS LOAD CELL:
   ZERO: 1.05
   CF: -343.74
8. HORIZONTAL SHEAR LOAD CELL:
   ZERO: 1.9856
   CF: -172.82
9. HORIZONTAL DISP. TRANSDUCER, X:
   ZERO: 1.4116
   CF: 2.2815
10. CONSTANT HEIGHT TRANSDUCER, Z:
    ZERO: .41436
    CF: 2.1089
11. TEST ANGLE THETA: 0
    TOTAL X DISP. DURING CONSOLIDATION: .41758

Pt. No.	Str.X (%)	X.Coor. (cm)	SigV (ksc)	TauH (ksc)	Eu (ksc)	TauH / SigVc	DelU / SigVc	SigV / SigVc	TauH / SigV	TauH / Cu	Eu / Cu
1	+0.000	+0.418	3.001	+0.580	+9999.0	+.193	+0.000	+1.000	+.193	+0.000	+9999.0
2	-0.002	+0.418	3.000	+0.579	+74.3	+.193	+0.000	+1.000	+.193	-0.002	+276.8
3	-0.004	+0.417	3.006	+0.583	-230.0	+.194	-0.002	+1.002	+.194	+0.012	-856.9
4	-0.006	+0.417	3.008	+0.586	-281.7	+.195	-0.002	+1.002	+.195	+0.023	-1049.7
5	-0.004	+0.417	2.975	+0.590	-701.9	+.196	+0.009	+0.991	+.198	+0.038	-2615.2
6	-0.004	+0.417	2.958	+0.590	-695.7	+.196	+0.014	+0.986	+.199	+0.037	-2592.1
7	-0.009	+0.417	2.949	+0.590	-351.2	+.196	+0.017	+0.983	+.200	+0.038	-1308.4
8	-0.006	+0.417	2.972	+0.590	-463.8	+.196	+0.009	+0.991	+.198	+0.037	-1728.3
9	-0.004	+0.417	3.002	+0.590	-695.7	+.196	-0.000	+1.000	+.196	+0.037	-2592.1
10	-0.022	+0.417	2.999	+0.589	-129.4	+.196	+0.001	+0.999	+.196	+0.035	-482.1
11	-0.004	+0.417	2.966	+0.603	-1664.3	+.201	+0.012	+0.988	+.203	+0.089	-6201.3
12	-0.015	+0.417	2.956	+0.636	-1116.3	+.212	+0.015	+0.985	+.215	+0.209	-4159.4
13	+0.011	+0.418	2.984	+0.667	+2439.4	+.222	+0.006	+0.994	+.224	+0.326	+9089.2
14	+0.039	+0.418	3.006	+0.700	+928.5	+.233	-0.002	+1.002	+.233	+0.447	+3459.8
15	+0.060	+0.419	2.996	+0.734	+767.6	+.245	+0.002	+0.998	+.245	+0.575	+2860.3
16	+0.093	+0.419	2.967	+0.766	+603.2	+.255	+0.011	+0.989	+.258	+0.694	+2247.5
17	+0.153	+0.421	2.945	+0.794	+420.7	+.265	+0.018	+0.982	+.270	+0.799	+1567.5
18	+0.218	+0.422	2.928	+0.818	+328.2	+.272	+0.024	+0.976	+.279	+0.887	+1223.1
19	+0.319	+0.424	2.902	+0.834	+239.7	+.278	+0.033	+0.967	+.288	+0.950	+893.2
20	+0.437	+0.426	2.861	+0.844	+181.1	+.281	+0.047	+0.953	+.295	+0.984	+674.7
21	+0.573	+0.429	2.801	+0.848	+140.5	+.283	+0.067	+0.933	+.303	+1.000	+523.4
22	+0.731	+0.432	2.731	+0.847	+110.0	+.282	+0.090	+0.910	+.310	+0.998	+409.8
23	+0.888	+0.435	2.656	+0.845	+89.6	+.282	+0.115	+0.885	+.318	+0.988	+333.9
24	+1.054	+0.438	2.586	+0.841	+74.5	+.280	+0.138	+0.862	+.325	+0.975	+277.5

TEST NAME : DSS-G5

Pt. No.	Str.X (%)	X.Coor. (cm)	SigV (ksc)	TauH (ksc)	Eu (ksc)	TauH ---- SigVc	DelU ---- SigVc	SigV ---- SigVc	TauH ---- SigV	TauH ---- Cu	Eu -- Cu
25	+1.222	+0.441	2.520	+0.835	+62.8	+.278	+0.160	+0.840	+.331	+0.952	+233.8
26	+1.386	+0.444	2.473	+0.830	+54.3	+.277	+0.176	+0.824	+.336	+0.935	+202.3
27	+1.564	+0.448	2.432	+0.825	+47.1	+.275	+0.190	+0.810	+.339	+0.916	+175.6
28	+1.728	+0.451	2.394	+0.821	+41.9	+.274	+0.202	+0.798	+.343	+0.900	+156.3
29	+1.896	+0.454	2.358	+0.817	+37.5	+.272	+0.214	+0.786	+.346	+0.884	+139.8
30	+2.060	+0.457	2.319	+0.813	+34.0	+.271	+0.227	+0.773	+.351	+0.870	+126.8
31	+2.224	+0.460	2.279	+0.809	+31.0	+.270	+0.241	+0.759	+.355	+0.856	+115.5
32	+2.394	+0.463	2.223	+0.804	+28.2	+.268	+0.259	+0.741	+.362	+0.837	+104.9
33	+2.558	+0.467	2.177	+0.798	+25.7	+.266	+0.275	+0.725	+.367	+0.815	+95.6
34	+2.732	+0.470	2.139	+0.793	+23.4	+.264	+0.287	+0.713	+.371	+0.795	+87.3
35	+2.903	+0.473	2.107	+0.789	+21.6	+.263	+0.298	+0.702	+.374	+0.780	+80.6
36	+3.066	+0.476	2.071	+0.784	+20.0	+.261	+0.310	+0.690	+.378	+0.762	+74.5
37	+3.239	+0.480	2.039	+0.781	+18.6	+.260	+0.321	+0.679	+.383	+0.749	+69.4
38	+3.413	+0.483	2.009	+0.774	+17.1	+.258	+0.331	+0.669	+.385	+0.726	+63.8
39	+3.581	+0.486	1.987	+0.770	+15.9	+.257	+0.338	+0.662	+.387	+0.709	+59.4
40	+3.749	+0.489	1.963	+0.765	+14.8	+.255	+0.346	+0.654	+.390	+0.691	+55.3
41	+3.918	+0.493	1.934	+0.760	+13.8	+.253	+0.355	+0.645	+.393	+0.673	+51.5
42	+4.086	+0.496	1.908	+0.756	+13.0	+.252	+0.364	+0.636	+.396	+0.658	+48.3
43	+4.260	+0.499	1.879	+0.751	+12.1	+.250	+0.374	+0.626	+.400	+0.639	+45.0
44	+4.443	+0.503	1.848	+0.745	+11.2	+.248	+0.384	+0.616	+.403	+0.615	+41.6
45	+4.609	+0.506	1.824	+0.740	+10.5	+.247	+0.392	+0.608	+.406	+0.600	+39.0
46	+4.777	+0.509	1.805	+0.736	+9.8	+.245	+0.398	+0.602	+.408	+0.583	+36.6
47	+4.963	+0.513	1.777	+0.731	+9.2	+.244	+0.408	+0.592	+.412	+0.565	+34.2
48	+5.129	+0.516	1.746	+0.725	+8.5	+.242	+0.418	+0.582	+.416	+0.543	+31.8
49	+5.312	+0.519	1.717	+0.719	+7.9	+.239	+0.428	+0.572	+.419	+0.518	+29.3
50	+5.484	+0.522	1.689	+0.712	+7.3	+.237	+0.437	+0.563	+.422	+0.495	+27.1
51	+5.654	+0.526	1.664	+0.706	+6.7	+.235	+0.445	+0.555	+.424	+0.470	+24.9
52	+5.848	+0.529	1.635	+0.699	+6.1	+.233	+0.455	+0.545	+.427	+0.443	+22.7
53	+6.031	+0.533	1.600	+0.690	+5.5	+.230	+0.467	+0.533	+.431	+0.411	+20.5
54	+6.217	+0.537	1.565	+0.680	+4.8	+.227	+0.478	+0.522	+.434	+0.374	+18.0
55	+6.419	+0.540	1.528	+0.669	+4.2	+.223	+0.491	+0.509	+.438	+0.335	+15.7
56	+6.596	+0.544	1.492	+0.660	+3.6	+.220	+0.503	+0.497	+.442	+0.298	+13.6
57	+6.779	+0.547	1.464	+0.652	+3.2	+.217	+0.512	+0.488	+.445	+0.268	+11.9
58	+6.967	+0.551	1.434	+0.644	+2.8	+.215	+0.522	+0.478	+.449	+0.241	+10.4
59	+7.158	+0.555	1.405	+0.636	+2.4	+.212	+0.532	+0.468	+.453	+0.212	+8.9
60	+7.342	+0.558	1.376	+0.629	+2.0	+.210	+0.542	+0.458	+.458	+0.186	+7.6
61	+7.531	+0.562	1.340	+0.620	+1.6	+.207	+0.554	+0.446	+.463	+0.151	+6.0
62	+7.734	+0.566	1.310	+0.612	+1.3	+.204	+0.563	+0.437	+.467	+0.120	+4.7
63	+7.921	+0.569	1.283	+0.602	+0.9	+.201	+0.572	+0.428	+.469	+0.085	+3.2
64	+8.109	+0.573	1.268	+0.596	+0.6	+.198	+0.577	+0.423	+.470	+0.060	+2.2
65	+8.301	+0.576	1.223	+0.588	+0.3	+.196	+0.593	+0.407	+.481	+0.031	+1.1
66	+8.540	+0.581	1.196	+0.585	+0.2	+.195	+0.601	+0.399	+.489	+0.019	+0.7
67	+8.822	+0.586	1.158	+0.572	-0.2	+.191	+0.614	+0.386	+.494	-0.027	-0.9
68	+9.197	+0.594	1.109	+0.569	-0.3	+.190	+0.631	+0.369	+.514	-0.037	-1.2

****

ANISOTROPICALLY CONSOLIDATED GEONOR DIRECT SIMPLE SHEAR TEST
MIT GEOTECHNICAL LAB

****

FILE NAME: DSSG6.PRN

REDUCTION DATA
UNITS: (kg,cm,VOLTS)

1. TEST NAME : DSS-G6
2. DATE : 9/28/1987
3. OCR : 1
4. VER. CONSOLIDATION STRESS (KSC) : +2.966
5. HOR. CONSOLIDATION STRESS (KSC) : +0.600
6. PRE-SHEAR SAMPLE HEIGHT (cm) : +1.8057
7. VERTICAL STRESS LOAD CELL:
   ZERO: 1.08
   CF: -343.7
8. HORIZONTAL SHEAR LOAD CELL:
   ZERO: 1.9942
   CF: 170.47
9. HORIZONTAL DISP. TRANSDUCER, X:
   ZERO: 2.1673
   CF: -2.2815
10. CONSTANT HEIGHT TRANSDUCER, Z:
    ZERO: .28282
    CF: 2.1089
11. TEST ANGLE THETA: 180
    TOTAL X DISP. DURING CONSOLIDATION: -.35215

Pt. No.	Str.X (%)	X.Coor. (cm)	SigV (ksc)	TauH (ksc)	Eu (ksc)	TauH / SigVc	DelU / SigVc	SigV / SigVc	TauH / SigV	TauH / Cu	Eu / Cu
1	+0.000	-0.352	2.966	-0.590	+9999.0	-.199	+0.000	+1.000	-.199	+0.000	+7818.8
2	-0.036	-0.353	2.965	-0.591	+5.6	-.199	+0.000	+1.000	-.199	-0.001	+4.4
3	-0.030	-0.353	2.962	-0.584	-58.0	-.197	+0.001	+0.999	-.197	+0.004	-45.4
4	-0.025	-0.353	2.955	-0.576	-171.6	-.194	+0.004	+0.996	-.195	+0.011	-134.2
5	-0.021	-0.353	2.936	-0.567	-344.6	-.191	+0.010	+0.990	-.193	+0.018	-269.4
6	-0.023	-0.353	2.922	-0.541	-649.0	-.182	+0.015	+0.985	-.185	+0.039	-507.5
7	-0.018	-0.352	2.900	-0.510	-1325.6	-.172	+0.022	+0.978	-.176	+0.063	-1036.5
8	+0.005	-0.352	2.884	-0.474	+7613.7	-.160	+0.028	+0.972	-.165	+0.090	+5953.6
9	+0.016	-0.352	2.865	-0.441	+2805.0	-.149	+0.034	+0.966	-.154	+0.117	+2193.4
10	+0.034	-0.352	2.847	-0.403	+1639.0	-.136	+0.040	+0.960	-.142	+0.146	+1281.6
11	+0.046	-0.351	2.826	-0.367	+1464.9	-.124	+0.047	+0.953	-.130	+0.174	+1145.5
12	+0.066	-0.351	2.808	-0.333	+1168.2	-.112	+0.053	+0.947	-.118	+0.201	+913.5
13	+0.080	-0.351	2.789	-0.297	+1101.1	-.100	+0.059	+0.941	-.107	+0.229	+861.0
14	+0.096	-0.350	2.772	-0.261	+1031.8	-.088	+0.065	+0.935	-.094	+0.257	+806.8
15	+0.128	-0.350	2.753	-0.224	+860.7	-.075	+0.072	+0.928	-.081	+0.286	+673.1
16	+0.150	-0.349	2.733	-0.186	+805.3	-.063	+0.079	+0.921	-.068	+0.316	+629.7
17	+0.178	-0.349	2.712	-0.149	+744.1	-.050	+0.086	+0.914	-.055	+0.345	+581.8
18	+0.221	-0.348	2.691	-0.115	+644.4	-.039	+0.093	+0.907	-.043	+0.371	+503.9
19	+0.255	-0.348	2.668	-0.082	+597.2	-.028	+0.100	+0.900	-.031	+0.397	+467.0
20	+0.299	-0.347	2.641	-0.050	+542.7	-.017	+0.109	+0.891	-.019	+0.422	+424.4
21	+0.353	-0.346	2.618	-0.017	+486.5	-.006	+0.117	+0.883	-.007	+0.448	+380.5
22	+0.403	-0.345	2.590	+0.012	+447.8	+.004	+0.127	+0.873	+.005	+0.471	+350.2
23	+0.463	-0.344	2.561	+0.043	+410.2	+.014	+0.137	+0.863	+.017	+0.495	+320.7
24	+0.517	-0.343	2.530	+0.070	+382.5	+.024	+0.147	+0.853	+.028	+0.516	+299.1

TEST NAME : DSS-G6

Pt. No.	Str.X (%)	X.Coor. (cm)	SigV (ksc)	TauH (ksc)	Eu (ksc)	TauH ---- SigVc	DelU ---- SigVc	SigV ---- SigVc	TauH ---- SigV	TauH ---- Cu	Eu -- Cu
25	+0.586	-0.342	2.500	+0.098	+352.1	+.033	+0.157	+0.843	+.039	+0.538	+275.3
26	+0.659	-0.340	2.470	+0.126	+326.0	+.042	+0.167	+0.833	+.051	+0.560	+254.9
27	+0.732	-0.339	2.441	+0.149	+303.1	+.050	+0.177	+0.823	+.061	+0.578	+237.0
28	+0.818	-0.337	2.409	+0.172	+279.6	+.058	+0.188	+0.812	+.072	+0.596	+218.6
29	+0.898	-0.336	2.367	+0.193	+261.6	+.065	+0.202	+0.798	+.082	+0.612	+204.5
30	+0.985	-0.334	2.323	+0.215	+245.2	+.072	+0.217	+0.783	+.092	+0.629	+191.7
31	+1.085	-0.333	2.277	+0.233	+227.6	+.079	+0.232	+0.768	+.102	+0.644	+178.0
32	+1.185	-0.331	2.240	+0.252	+213.2	+.085	+0.245	+0.755	+.113	+0.659	+166.7
33	+1.286	-0.329	2.209	+0.270	+200.8	+.091	+0.255	+0.745	+.122	+0.673	+157.0
34	+1.388	-0.327	2.179	+0.287	+189.6	+.097	+0.265	+0.735	+.132	+0.686	+148.3
35	+1.495	-0.325	2.150	+0.302	+178.9	+.102	+0.275	+0.725	+.140	+0.697	+139.9
36	+1.603	-0.323	2.121	+0.314	+169.3	+.106	+0.285	+0.715	+.148	+0.707	+132.4
37	+1.717	-0.321	2.093	+0.328	+160.5	+.111	+0.294	+0.706	+.157	+0.718	+125.5
38	+1.826	-0.319	2.062	+0.340	+152.8	+.115	+0.305	+0.695	+.165	+0.727	+119.4
39	+1.947	-0.317	2.033	+0.352	+145.2	+.119	+0.315	+0.685	+.173	+0.737	+113.5
40	+2.068	-0.315	2.005	+0.362	+138.2	+.122	+0.324	+0.676	+.181	+0.745	+108.1
41	+2.195	-0.313	1.979	+0.374	+131.8	+.126	+0.333	+0.667	+.189	+0.754	+103.1
42	+2.323	-0.310	1.963	+0.385	+125.9	+.130	+0.338	+0.662	+.196	+0.762	+98.5
43	+2.453	-0.308	1.946	+0.394	+120.3	+.133	+0.344	+0.656	+.202	+0.769	+94.1
44	+2.581	-0.306	1.928	+0.403	+115.4	+.136	+0.350	+0.650	+.209	+0.776	+90.3
45	+2.706	-0.303	1.909	+0.410	+110.9	+.138	+0.356	+0.644	+.215	+0.782	+86.7
46	+2.838	-0.301	1.880	+0.419	+106.7	+.141	+0.366	+0.634	+.223	+0.789	+83.4
47	+2.979	-0.298	1.852	+0.426	+102.3	+.144	+0.376	+0.624	+.230	+0.794	+80.0
48	+3.114	-0.296	1.827	+0.434	+98.6	+.146	+0.384	+0.616	+.237	+0.801	+77.1
49	+3.246	-0.294	1.806	+0.440	+95.2	+.148	+0.391	+0.609	+.244	+0.806	+74.5
50	+3.381	-0.291	1.788	+0.448	+92.1	+.151	+0.397	+0.603	+.250	+0.811	+72.0
51	+3.522	-0.289	1.769	+0.454	+89.0	+.153	+0.404	+0.596	+.257	+0.817	+69.6
52	+3.711	-0.285	1.749	+0.462	+85.1	+.156	+0.410	+0.590	+.264	+0.823	+66.5
53	+3.857	-0.283	1.729	+0.468	+82.3	+.158	+0.417	+0.583	+.271	+0.827	+64.4
54	+3.967	-0.281	1.719	+0.471	+80.3	+.159	+0.420	+0.580	+.274	+0.830	+62.8
55	+4.108	-0.278	1.702	+0.476	+77.9	+.161	+0.426	+0.574	+.280	+0.834	+60.9
56	+4.249	-0.275	1.678	+0.480	+75.6	+.162	+0.434	+0.566	+.286	+0.837	+59.1
57	+4.402	-0.273	1.658	+0.485	+73.3	+.164	+0.441	+0.559	+.293	+0.841	+57.3
58	+4.548	-0.270	1.643	+0.490	+71.2	+.165	+0.446	+0.554	+.298	+0.844	+55.7
59	+4.694	-0.267	1.630	+0.494	+69.3	+.167	+0.450	+0.550	+.303	+0.848	+54.2
60	+4.837	-0.265	1.625	+0.498	+67.5	+.168	+0.452	+0.548	+.307	+0.851	+52.8
61	+4.979	-0.262	1.617	+0.502	+65.8	+.169	+0.455	+0.545	+.310	+0.854	+51.5
62	+5.122	-0.260	1.611	+0.507	+64.2	+.171	+0.457	+0.543	+.315	+0.858	+50.2
63	+5.264	-0.257	1.604	+0.510	+62.7	+.172	+0.459	+0.541	+.318	+0.860	+49.0
64	+5.412	-0.254	1.600	+0.514	+61.2	+.173	+0.461	+0.539	+.321	+0.864	+47.9
65	+5.555	-0.252	1.597	+0.518	+59.8	+.175	+0.462	+0.538	+.324	+0.866	+46.8
66	+5.708	-0.249	1.591	+0.523	+58.5	+.176	+0.464	+0.536	+.329	+0.870	+45.7
67	+5.854	-0.246	1.575	+0.526	+57.2	+.177	+0.469	+0.531	+.334	+0.873	+44.7
68	+6.012	-0.244	1.552	+0.528	+55.8	+.178	+0.477	+0.523	+.340	+0.875	+43.6
69	+6.169	-0.241	1.538	+0.531	+54.5	+.179	+0.482	+0.518	+.345	+0.877	+42.6
70	+6.331	-0.238	1.532	+0.529	+53.0	+.178	+0.484	+0.516	+.345	+0.875	+41.5
71	+6.470	-0.235	1.530	+0.535	+52.2	+.180	+0.484	+0.516	+.350	+0.880	+40.8
72	+6.616	-0.233	1.528	+0.538	+51.2	+.181	+0.485	+0.515	+.352	+0.882	+40.0

TEST NAME : DSS-G6

Pt. No.	Str.X (%)	X.Coor. (cm)	SigV (ksc)	TauH (ksc)	Eu (ksc)	TauH ---- SigVc	DelU ---- SigVc	SigV ---- SigVc	TauH ---- SigV	TauH ---- Cu	Eu -- Cu
73	+6.771	-0.230	1.522	+0.542	+50.2	+.183	+0.487	+0.513	+.356	+0.885	+39.2
74	+6.919	-0.227	1.507	+0.544	+49.2	+.183	+0.492	+0.508	+.361	+0.887	+38.4
75	+7.076	-0.224	1.499	+0.547	+48.2	+.184	+0.495	+0.505	+.365	+0.889	+37.7
76	+7.229	-0.222	1.494	+0.549	+47.3	+.185	+0.496	+0.504	+.367	+0.891	+37.0
77	+7.391	-0.219	1.493	+0.552	+46.4	+.186	+0.497	+0.503	+.370	+0.893	+36.3
78	+7.548	-0.216	1.491	+0.556	+45.6	+.187	+0.497	+0.503	+.373	+0.896	+35.6
79	+7.705	-0.213	1.486	+0.558	+44.7	+.188	+0.499	+0.501	+.375	+0.898	+35.0
80	+7.860	-0.210	1.470	+0.560	+43.9	+.189	+0.504	+0.496	+.381	+0.899	+34.3
81	+8.018	-0.207	1.462	+0.561	+43.1	+.189	+0.507	+0.493	+.384	+0.900	+33.7
82	+8.182	-0.204	1.460	+0.564	+42.3	+.190	+0.508	+0.492	+.386	+0.902	+33.1
83	+8.332	-0.202	1.459	+0.566	+41.6	+.191	+0.508	+0.492	+.388	+0.904	+32.5
84	+8.485	-0.199	1.468	+0.569	+41.0	+.192	+0.505	+0.495	+.388	+0.906	+32.0
85	+8.645	-0.196	1.453	+0.570	+40.3	+.192	+0.510	+0.490	+.393	+0.908	+31.5
86	+8.800	-0.193	1.442	+0.571	+39.6	+.193	+0.514	+0.486	+.396	+0.908	+31.0
87	+8.957	-0.190	1.428	+0.573	+38.9	+.193	+0.518	+0.482	+.401	+0.909	+30.5
88	+9.112	-0.188	1.423	+0.574	+38.3	+.194	+0.520	+0.480	+.404	+0.910	+30.0
89	+9.262	-0.185	1.421	+0.577	+37.8	+.194	+0.521	+0.479	+.406	+0.912	+29.5
90	+9.417	-0.182	1.420	+0.578	+37.2	+.195	+0.521	+0.479	+.407	+0.914	+29.1
91	+9.575	-0.179	1.419	+0.581	+36.7	+.196	+0.521	+0.479	+.410	+0.916	+28.7
92	+9.732	-0.176	1.417	+0.583	+36.1	+.196	+0.522	+0.478	+.411	+0.917	+28.3
93	+9.894	-0.173	1.417	+0.586	+35.6	+.197	+0.522	+0.478	+.413	+0.919	+27.9
94	+10.051	-0.171	1.412	+0.588	+35.2	+.198	+0.524	+0.476	+.416	+0.921	+27.5
95	+10.224	-0.168	1.395	+0.589	+34.6	+.199	+0.530	+0.470	+.422	+0.922	+27.0
96	+10.386	-0.165	1.388	+0.590	+34.1	+.199	+0.532	+0.468	+.425	+0.923	+26.7
97	+10.553	-0.162	1.387	+0.592	+33.6	+.200	+0.532	+0.468	+.427	+0.924	+26.3
98	+10.685	-0.159	1.386	+0.594	+33.2	+.200	+0.533	+0.467	+.429	+0.926	+26.0
99	+10.835	-0.156	1.385	+0.596	+32.8	+.201	+0.533	+0.467	+.430	+0.927	+25.7
100	+11.000	-0.154	1.384	+0.598	+32.4	+.202	+0.533	+0.467	+.432	+0.929	+25.3
101	+11.157	-0.151	1.383	+0.599	+32.0	+.202	+0.534	+0.466	+.433	+0.930	+25.0
102	+11.307	-0.148	1.382	+0.602	+31.6	+.203	+0.534	+0.466	+.435	+0.932	+24.7
103	+11.487	-0.145	1.381	+0.604	+31.2	+.204	+0.534	+0.466	+.437	+0.933	+24.4
104	+11.633	-0.142	1.380	+0.605	+30.8	+.204	+0.535	+0.465	+.439	+0.935	+24.1
105	+11.807	-0.139	1.379	+0.607	+30.4	+.205	+0.535	+0.465	+.440	+0.936	+23.8
106	+11.952	-0.136	1.378	+0.608	+30.1	+.205	+0.535	+0.465	+.442	+0.937	+23.5
107	+12.121	-0.133	1.377	+0.611	+29.7	+.206	+0.536	+0.464	+.443	+0.939	+23.2
108	+12.278	-0.130	1.376	+0.612	+29.4	+.206	+0.536	+0.464	+.444	+0.940	+23.0
109	+12.429	-0.128	1.375	+0.614	+29.1	+.207	+0.536	+0.464	+.446	+0.941	+22.7
110	+12.593	-0.125	1.370	+0.615	+28.7	+.207	+0.538	+0.462	+.449	+0.943	+22.5
111	+12.759	-0.122	1.361	+0.617	+28.4	+.208	+0.541	+0.459	+.453	+0.944	+22.2
112	+12.928	-0.119	1.357	+0.618	+28.0	+.208	+0.542	+0.458	+.455	+0.945	+21.9
113	+13.088	-0.116	1.357	+0.620	+27.7	+.209	+0.542	+0.458	+.457	+0.946	+21.7
114	+13.250	-0.113	1.357	+0.622	+27.4	+.210	+0.542	+0.458	+.458	+0.948	+21.5
115	+13.411	-0.110	1.356	+0.622	+27.1	+.210	+0.543	+0.457	+.459	+0.948	+21.2
116	+13.571	-0.107	1.355	+0.624	+26.8	+.210	+0.543	+0.457	+.461	+0.950	+21.0
117	+13.731	-0.104	1.355	+0.624	+26.5	+.210	+0.543	+0.457	+.461	+0.949	+20.7
118	+13.892	-0.101	1.354	+0.627	+26.3	+.211	+0.544	+0.456	+.463	+0.951	+20.5
119	+14.056	-0.098	1.347	+0.627	+26.0	+.211	+0.546	+0.454	+.466	+0.952	+20.3
120	+14.218	-0.095	1.344	+0.628	+25.7	+.212	+0.547	+0.453	+.467	+0.953	+20.1

TEST NAME : DSS-G6

Pt. No.	Str.X (%)	X.Coor. (cm)	SigV (ksc)	TauH (ksc)	Eu (ksc)	TauH ---- SigVc	DelU ---- SigVc	SigV ---- SigVc	TauH ---- SigV	TauH ---- Cu	Eu -- Cu
121	+14.376	-0.093	1.344	+0.629	+25.4	+.212	+0.547	+0.453	+.468	+0.953	+19.9
122	+14.535	-0.090	1.356	+0.631	+25.2	+.213	+0.543	+0.457	+.466	+0.955	+19.7
123	+14.697	-0.087	1.345	+0.633	+25.0	+.214	+0.546	+0.454	+.471	+0.957	+19.5
124	+14.861	-0.084	1.335	+0.633	+24.7	+.214	+0.550	+0.450	+.474	+0.957	+19.3
125	+15.025	-0.081	1.335	+0.635	+24.5	+.214	+0.550	+0.450	+.475	+0.958	+19.1
126	+15.190	-0.078	1.347	+0.635	+24.2	+.214	+0.546	+0.454	+.472	+0.958	+18.9
127	+15.347	-0.075	1.353	+0.639	+24.0	+.215	+0.544	+0.456	+.472	+0.961	+18.8
128	+15.509	-0.072	1.347	+0.640	+23.8	+.216	+0.546	+0.454	+.475	+0.962	+18.6
129	+15.680	-0.069	1.347	+0.641	+23.6	+.216	+0.546	+0.454	+.476	+0.963	+18.4
130	+15.839	-0.066	1.338	+0.641	+23.3	+.216	+0.549	+0.451	+.479	+0.963	+18.2
131	+16.006	-0.063	1.330	+0.642	+23.1	+.216	+0.552	+0.448	+.482	+0.963	+18.1
132	+16.170	-0.060	1.328	+0.643	+22.9	+.217	+0.552	+0.448	+.484	+0.964	+17.9
133	+16.336	-0.057	1.335	+0.643	+22.7	+.217	+0.550	+0.450	+.482	+0.965	+17.7
134	+16.489	-0.054	1.343	+0.647	+22.5	+.218	+0.547	+0.453	+.482	+0.967	+17.6
135	+16.649	-0.052	1.338	+0.647	+22.3	+.218	+0.549	+0.451	+.483	+0.967	+17.4
136	+16.813	-0.049	1.344	+0.649	+22.1	+.219	+0.547	+0.453	+.483	+0.969	+17.3
137	+16.968	-0.046	1.350	+0.652	+22.0	+.220	+0.545	+0.455	+.483	+0.971	+17.2
138	+17.141	-0.043	1.327	+0.652	+21.7	+.220	+0.553	+0.447	+.491	+0.971	+17.0
139	+17.310	-0.040	1.322	+0.652	+21.5	+.220	+0.554	+0.446	+.493	+0.971	+16.8
140	+17.472	-0.037	1.322	+0.651	+21.3	+.220	+0.554	+0.446	+.493	+0.971	+16.7
141	+17.631	-0.034	1.336	+0.654	+21.2	+.220	+0.550	+0.450	+.489	+0.973	+16.5
142	+17.788	-0.031	1.332	+0.655	+21.0	+.221	+0.551	+0.449	+.492	+0.974	+16.4
143	+17.962	-0.028	1.316	+0.655	+20.8	+.221	+0.556	+0.444	+.498	+0.974	+16.3
144	+18.142	-0.025	1.315	+0.656	+20.6	+.221	+0.557	+0.443	+.499	+0.974	+16.1
145	+18.306	-0.022	1.316	+0.656	+20.4	+.221	+0.556	+0.444	+.499	+0.975	+16.0
146	+18.463	-0.019	1.319	+0.657	+20.3	+.222	+0.555	+0.445	+.498	+0.975	+15.8
147	+18.627	-0.016	1.321	+0.659	+20.1	+.222	+0.555	+0.445	+.499	+0.977	+15.7
148	+18.787	-0.013	1.312	+0.660	+20.0	+.222	+0.558	+0.442	+.503	+0.977	+15.6
149	+18.930	-0.010	1.312	+0.661	+19.8	+.223	+0.558	+0.442	+.504	+0.979	+15.5
150	+19.100	-0.007	1.303	+0.662	+19.7	+.223	+0.560	+0.440	+.508	+0.979	+15.4
151	+19.262	-0.004	1.304	+0.662	+19.5	+.223	+0.560	+0.440	+.507	+0.979	+15.2
152	+19.422	-0.001	1.329	+0.666	+19.4	+.224	+0.552	+0.448	+.501	+0.982	+15.2
153	+19.579	+0.001	1.323	+0.667	+19.3	+.225	+0.554	+0.446	+.504	+0.983	+15.1
154	+19.741	+0.004	1.322	+0.669	+19.1	+.225	+0.554	+0.446	+.506	+0.984	+15.0
155	+19.903	+0.007	1.314	+0.668	+19.0	+.225	+0.557	+0.443	+.509	+0.984	+14.8
156	+20.071	+0.010	1.304	+0.669	+18.8	+.225	+0.560	+0.440	+.513	+0.984	+14.7
157	+20.236	+0.013	1.305	+0.669	+18.7	+.226	+0.560	+0.440	+.513	+0.985	+14.6
158	+20.388	+0.016	1.305	+0.670	+18.5	+.226	+0.560	+0.440	+.513	+0.985	+14.5
159	+20.552	+0.019	1.305	+0.670	+18.4	+.226	+0.560	+0.440	+.513	+0.985	+14.4
160	+20.639	+0.021	1.303	+0.670	+18.3	+.226	+0.561	+0.439	+.514	+0.985	+14.3
161	+20.990	+0.027	1.296	+0.671	+18.0	+.226	+0.563	+0.437	+.517	+0.986	+14.1
162	+21.314	+0.033	1.313	+0.673	+17.8	+.227	+0.557	+0.443	+.513	+0.988	+13.9
163	+21.647	+0.039	1.302	+0.674	+17.5	+.227	+0.561	+0.439	+.518	+0.988	+13.7
164	+21.961	+0.044	1.298	+0.673	+17.3	+.227	+0.562	+0.438	+.519	+0.988	+13.5
165	+22.278	+0.050	1.315	+0.677	+17.1	+.228	+0.557	+0.443	+.515	+0.991	+13.3
166	+22.611	+0.056	1.306	+0.678	+16.8	+.229	+0.560	+0.440	+.519	+0.992	+13.2
167	+22.950	+0.062	1.326	+0.682	+16.6	+.230	+0.553	+0.447	+.515	+0.995	+13.0

TEST NAME : DSS-G6

Pt. No.	Str.X (%)	X.Coor. (cm)	SigV (ksc)	TauH (ksc)	Eu (ksc)	TauH / SigVc	DelU / SigVc	SigV / SigVc	TauH / SigV	TauH / Cu	Eu / Cu
168	+23.287	+0.068	1.309	+0.683	+16.4	+.230	+0.559	+0.441	+.522	+0.996	+12.8
169	+23.620	+0.074	1.303	+0.683	+16.2	+.230	+0.561	+0.439	+.524	+0.996	+12.6
170	+23.944	+0.080	1.302	+0.685	+16.0	+.231	+0.561	+0.439	+.526	+0.997	+12.5
171	+24.272	+0.086	1.323	+0.687	+15.8	+.232	+0.554	+0.446	+.519	+0.998	+12.3
172	+24.609	+0.092	1.303	+0.688	+15.6	+.232	+0.561	+0.439	+.528	+0.999	+12.2
173	+24.945	+0.098	1.297	+0.688	+15.4	+.232	+0.563	+0.437	+.530	+0.999	+12.0
174	+25.282	+0.104	1.304	+0.688	+15.2	+.232	+0.560	+0.440	+.527	+0.999	+11.9
175	+25.609	+0.110	1.295	+0.688	+15.0	+.232	+0.563	+0.437	+.531	+0.999	+11.7
176	+25.942	+0.116	1.304	+0.689	+14.8	+.232	+0.560	+0.440	+.528	+1.000	+11.6
177	+26.279	+0.122	1.297	+0.687	+14.6	+.232	+0.563	+0.437	+.529	+0.999	+11.4
178	+26.610	+0.128	1.304	+0.686	+14.4	+.231	+0.560	+0.440	+.526	+0.998	+11.3
179	+26.941	+0.134	1.290	+0.687	+14.2	+.232	+0.565	+0.435	+.532	+0.998	+11.1
180	+27.286	+0.141	1.288	+0.685	+14.0	+.231	+0.566	+0.434	+.532	+0.997	+11.0
181	+27.619	+0.147	1.288	+0.685	+13.9	+.231	+0.566	+0.434	+.532	+0.997	+10.8
182	+27.958	+0.153	1.287	+0.684	+13.7	+.231	+0.566	+0.434	+.531	+0.996	+10.7
183	+28.293	+0.159	1.288	+0.683	+13.5	+.230	+0.566	+0.434	+.530	+0.996	+10.6
184	+28.624	+0.165	1.286	+0.683	+13.3	+.230	+0.566	+0.434	+.531	+0.995	+10.4
185	+28.966	+0.171	1.282	+0.681	+13.2	+.229	+0.568	+0.432	+.531	+0.994	+10.3
186	+29.327	+0.177	1.254	+0.675	+12.9	+.228	+0.577	+0.423	+.538	+0.989	+10.1
187	+29.685	+0.184	1.241	+0.668	+12.7	+.225	+0.581	+0.419	+.538	+0.984	+9.9
188	+30.026	+0.190	1.239	+0.664	+12.5	+.224	+0.582	+0.418	+.536	+0.981	+9.8
189	+32.335	+0.232	1.226	+0.034	+5.8	+.011	+0.587	+0.413	+.028	+0.488	+4.5

****

ANISOTROPICALLY CONSOLIDATED GEONOR DIRECT SIMPLE SHEAR TEST
MIT GEOTECHNICAL LAB

****

FILE NAME: DSSG7.PRN

REDUCTION DATA
UNITS: (kg,cm,VOLTS)

1. TEST NAME : DSS-G7
2. DATE : 12/16/1987
3. OCR : 1
4. VER. CONSOLIDATION STRESS (KSC) : +2.944
5. HOR. CONSOLIDATION STRESS (KSC) : +0.600
6. PRE-SHEAR SAMPLE HEIGHT (cm) : +1.7099
7. VERTICAL STRESS LOAD CELL:
   ZERO: 1.085
   CF: -342.65
8. HORIZONTAL SHEAR LOAD CELL:
   ZERO: -.32516
   CF: 169.21
9. HORIZONTAL DISP. TRANSDUCER, X:
   ZERO: 2.0357
   CF: -2.2815
10. CONSTANT HEIGHT TRANSDUCER, Z:
    ZERO: .21239
    CF: 2.1089
11. TEST ANGLE THETA: 180

TOTAL X DISP. DURING CONSOLIDATION: -.3416

Pt. No.	Str.X (%)	X.Coor. (cm)	SigV (ksc)	TauH (ksc)	Eu (ksc)	TauH / SigVc	DelU / SigVc	SigV / SigVc	TauH / SigV	TauH / Cu	Eu / Cu
1	+0.000	-0.342	2.944	-0.591	+9999.0	-.201	+0.000	+1.000	-.201	+0.000	+7513.9
2	-0.007	-0.342	2.943	-0.590	-5.6	-.201	+0.000	+1.000	-.201	+0.000	-4.2
3	+0.000	-0.342	2.933	-0.589	+9999.0	-.200	+0.004	+0.996	-.201	+0.001	+7513.9
4	-0.002	-0.342	2.920	-0.587	-458.3	-.199	+0.008	+0.992	-.201	+0.003	-344.4
5	+0.002	-0.342	2.928	-0.584	+786.8	-.198	+0.005	+0.995	-.200	+0.005	+591.3
6	+0.002	-0.342	2.955	-0.572	+2363.0	-.194	-0.004	+1.004	-.193	+0.014	+1775.7
7	+0.002	-0.342	2.947	-0.556	+4335.4	-.189	-0.001	+1.001	-.189	+0.026	+3257.9
8	+0.007	-0.341	2.915	-0.529	+2574.2	-.180	+0.010	+0.990	-.181	+0.046	+1934.4
9	+0.017	-0.341	2.894	-0.495	+1703.8	-.168	+0.017	+0.983	-.171	+0.071	+1280.3
10	+0.034	-0.341	2.883	-0.460	+1171.6	-.156	+0.021	+0.979	-.159	+0.098	+880.4
11	+0.050	-0.341	2.874	-0.425	+988.6	-.144	+0.024	+0.976	-.148	+0.124	+742.9
12	+0.065	-0.340	2.866	-0.388	+941.3	-.132	+0.026	+0.974	-.135	+0.152	+707.3
13	+0.077	-0.340	2.892	-0.352	+934.0	-.120	+0.018	+0.982	-.122	+0.179	+701.9
14	+0.096	-0.340	2.911	-0.316	+860.9	-.107	+0.011	+0.989	-.108	+0.206	+647.0
15	+0.117	-0.340	2.906	-0.280	+793.5	-.095	+0.013	+0.987	-.096	+0.233	+596.3
16	+0.144	-0.339	2.872	-0.242	+727.8	-.082	+0.024	+0.976	-.084	+0.262	+546.9
17	+0.175	-0.339	2.846	-0.203	+666.1	-.069	+0.033	+0.967	-.071	+0.291	+500.5
18	+0.208	-0.338	2.823	-0.164	+614.5	-.056	+0.041	+0.959	-.058	+0.320	+461.8
19	+0.242	-0.337	2.803	-0.127	+575.8	-.043	+0.048	+0.952	-.045	+0.349	+432.7
20	+0.278	-0.337	2.783	-0.093	+537.7	-.032	+0.055	+0.945	-.033	+0.374	+404.0
21	+0.330	-0.336	2.755	-0.053	+488.5	-.018	+0.064	+0.936	-.019	+0.404	+367.1
22	+0.364	-0.335	2.738	-0.027	+465.2	-.009	+0.070	+0.930	-.010	+0.424	+349.5
23	+0.419	-0.334	2.715	+0.006	+427.4	+.002	+0.078	+0.922	+.002	+0.448	+321.2
24	+0.474	-0.333	2.692	+0.037	+397.1	+.012	+0.086	+0.914	+.014	+0.471	+298.4

TEST NAME : DSS-G7

Pt. No.	Str.X (%)	X.Coor. (cm)	SigV (ksc)	TauH (ksc)	Eu (ksc)	TauH ---- SigVc	DelU ---- SigVc	SigV ---- SigVc	TauH ---- SigV	TauH ---- Cu	Eu -- Cu
25	+0.534	-0.332	2.666	+0.066	+369.2	+.023	+0.094	+0.906	+.025	+0.494	+277.5
26	+0.605	-0.331	2.632	+0.096	+340.3	+.033	+0.106	+0.894	+.037	+0.516	+255.8
27	+0.675	-0.330	2.602	+0.123	+317.4	+.042	+0.116	+0.884	+.047	+0.537	+238.5
28	+0.751	-0.329	2.574	+0.151	+296.0	+.051	+0.126	+0.874	+.059	+0.557	+222.4
29	+0.838	-0.327	2.546	+0.174	+274.0	+.059	+0.135	+0.865	+.068	+0.575	+205.9
30	+0.921	-0.326	2.516	+0.198	+256.8	+.067	+0.145	+0.855	+.079	+0.593	+193.0
31	+1.012	-0.324	2.485	+0.218	+239.8	+.074	+0.156	+0.844	+.088	+0.608	+180.2
32	+1.103	-0.323	2.454	+0.239	+225.7	+.081	+0.166	+0.834	+.097	+0.624	+169.6
33	+1.199	-0.321	2.424	+0.260	+212.8	+.088	+0.176	+0.824	+.107	+0.639	+159.9
34	+1.302	-0.319	2.399	+0.279	+200.3	+.095	+0.185	+0.815	+.116	+0.653	+150.5
35	+1.412	-0.317	2.371	+0.296	+188.4	+.101	+0.195	+0.805	+.125	+0.666	+141.6
36	+1.517	-0.316	2.342	+0.312	+178.4	+.106	+0.204	+0.796	+.133	+0.678	+134.1
37	+1.627	-0.314	2.312	+0.328	+169.4	+.111	+0.215	+0.785	+.142	+0.690	+127.3
38	+1.740	-0.312	2.279	+0.342	+160.8	+.116	+0.226	+0.774	+.150	+0.701	+120.9
39	+1.852	-0.310	2.251	+0.356	+153.3	+.121	+0.235	+0.765	+.158	+0.711	+115.2
40	+1.969	-0.308	2.225	+0.369	+146.2	+.125	+0.244	+0.756	+.166	+0.721	+109.9
41	+2.091	-0.306	2.201	+0.382	+139.5	+.130	+0.252	+0.748	+.174	+0.731	+104.8
42	+2.214	-0.304	2.176	+0.395	+133.6	+.134	+0.261	+0.739	+.182	+0.741	+100.4
43	+2.340	-0.302	2.149	+0.406	+127.8	+.138	+0.270	+0.730	+.189	+0.749	+96.0
44	+2.465	-0.299	2.124	+0.418	+122.7	+.142	+0.278	+0.722	+.197	+0.758	+92.2
45	+2.589	-0.297	2.097	+0.426	+117.8	+.145	+0.288	+0.712	+.203	+0.764	+88.5
46	+2.721	-0.295	2.067	+0.438	+113.4	+.149	+0.298	+0.702	+.212	+0.773	+85.2
47	+2.848	-0.293	2.038	+0.446	+109.2	+.152	+0.308	+0.692	+.219	+0.779	+82.1
48	+3.013	-0.290	2.012	+0.456	+104.2	+.155	+0.317	+0.683	+.227	+0.786	+78.3
49	+3.120	-0.288	1.997	+0.464	+101.4	+.158	+0.322	+0.678	+.233	+0.793	+76.2
50	+3.259	-0.286	1.981	+0.474	+98.0	+.161	+0.327	+0.673	+.239	+0.800	+73.6
51	+3.403	-0.283	1.965	+0.482	+94.6	+.164	+0.333	+0.667	+.246	+0.806	+71.1
52	+3.551	-0.281	1.949	+0.490	+91.3	+.166	+0.338	+0.662	+.251	+0.812	+68.6
53	+3.702	-0.278	1.930	+0.498	+88.2	+.169	+0.344	+0.656	+.258	+0.818	+66.3
54	+3.853	-0.276	1.910	+0.504	+85.2	+.171	+0.351	+0.649	+.264	+0.822	+64.0
55	+4.006	-0.273	1.889	+0.511	+82.5	+.174	+0.358	+0.642	+.270	+0.828	+62.0
56	+4.154	-0.271	1.867	+0.515	+79.9	+.175	+0.366	+0.634	+.276	+0.831	+60.0
57	+4.305	-0.268	1.852	+0.522	+77.6	+.177	+0.371	+0.629	+.282	+0.836	+58.3
58	+4.456	-0.265	1.841	+0.528	+75.3	+.179	+0.375	+0.625	+.287	+0.841	+56.6
59	+4.607	-0.263	1.853	+0.535	+73.3	+.182	+0.371	+0.629	+.289	+0.846	+55.1
60	+4.748	-0.260	1.842	+0.542	+71.5	+.184	+0.374	+0.626	+.294	+0.851	+53.8
61	+4.903	-0.258	1.814	+0.545	+69.5	+.185	+0.384	+0.616	+.301	+0.854	+52.2
62	+5.061	-0.255	1.786	+0.550	+67.6	+.187	+0.393	+0.607	+.308	+0.857	+50.8
63	+5.214	-0.252	1.760	+0.553	+65.8	+.188	+0.402	+0.598	+.314	+0.859	+49.4
64	+5.377	-0.250	1.739	+0.557	+64.1	+.189	+0.409	+0.591	+.321	+0.863	+48.1
65	+5.530	-0.247	1.725	+0.561	+62.5	+.191	+0.414	+0.586	+.325	+0.865	+46.9
66	+5.691	-0.244	1.717	+0.566	+61.0	+.192	+0.417	+0.583	+.329	+0.869	+45.8
67	+5.834	-0.242	1.742	+0.572	+59.8	+.194	+0.408	+0.592	+.328	+0.874	+44.9
68	+5.990	-0.239	1.716	+0.577	+58.5	+.196	+0.417	+0.583	+.336	+0.877	+43.9
69	+6.152	-0.236	1.691	+0.579	+57.0	+.197	+0.426	+0.574	+.343	+0.879	+42.9
70	+6.313	-0.234	1.689	+0.581	+55.7	+.198	+0.426	+0.574	+.344	+0.881	+41.9
71	+6.468	-0.231	1.705	+0.587	+54.6	+.200	+0.421	+0.579	+.345	+0.885	+41.1
72	+6.626	-0.228	1.681	+0.590	+53.5	+.201	+0.429	+0.571	+.351	+0.887	+40.2

TEST NAME : DSS-G7

Pt. No.	Str.X (%)	X.Coor. (cm)	SigV (ksc)	TauH (ksc)	Eu (ksc)	TauH ---- SigVc	DelU ---- SigVc	SigV ---- SigVc	TauH ---- SigV	TauH ---- Cu	Eu -- Cu
73	+6.789	-0.226	1.659	+0.593	+52.3	+.202	+0.436	+0.564	+.358	+0.890	+39.3
74	+7.043	-0.221	1.640	+0.569	+49.4	+.193	+0.443	+0.557	+.347	+0.871	+37.1
75	+7.150	-0.219	1.629	+0.590	+49.5	+.200	+0.447	+0.553	+.362	+0.887	+37.2
76	+7.315	-0.217	1.643	+0.600	+48.8	+.204	+0.442	+0.558	+.365	+0.895	+36.7
77	+7.459	-0.214	1.656	+0.606	+48.1	+.206	+0.437	+0.563	+.366	+0.900	+36.2
78	+7.593	-0.212	1.663	+0.612	+47.5	+.208	+0.435	+0.565	+.368	+0.904	+35.7
79	+7.784	-0.208	1.608	+0.611	+46.3	+.208	+0.454	+0.546	+.380	+0.903	+34.8
80	+7.950	-0.206	1.623	+0.613	+45.4	+.208	+0.449	+0.551	+.378	+0.905	+34.1
81	+8.096	-0.203	1.637	+0.618	+44.8	+.210	+0.444	+0.556	+.377	+0.908	+33.6
82	+8.275	-0.200	1.594	+0.620	+43.9	+.210	+0.459	+0.541	+.389	+0.909	+33.0
83	+8.440	-0.197	1.590	+0.620	+43.0	+.211	+0.460	+0.540	+.390	+0.909	+32.3
84	+8.605	-0.194	1.611	+0.625	+42.4	+.212	+0.453	+0.547	+.388	+0.914	+31.8
85	+8.775	-0.192	1.582	+0.626	+41.6	+.213	+0.463	+0.537	+.396	+0.914	+31.3
86	+8.971	-0.188	1.568	+0.619	+40.4	+.210	+0.467	+0.533	+.395	+0.909	+30.4
87	+9.115	-0.186	1.574	+0.628	+40.1	+.213	+0.465	+0.535	+.399	+0.916	+30.1
88	+9.259	-0.183	1.597	+0.634	+39.7	+.215	+0.458	+0.542	+.397	+0.920	+29.8
89	+9.424	-0.180	1.572	+0.638	+39.1	+.217	+0.466	+0.534	+.406	+0.923	+29.4
90	+9.596	-0.178	1.552	+0.637	+38.4	+.216	+0.473	+0.527	+.410	+0.922	+28.8
91	+9.771	-0.175	1.552	+0.639	+37.7	+.217	+0.473	+0.527	+.412	+0.924	+28.4
92	+9.919	-0.172	1.574	+0.643	+37.3	+.218	+0.465	+0.535	+.408	+0.927	+28.0
93	+10.091	-0.169	1.544	+0.645	+36.7	+.219	+0.475	+0.525	+.418	+0.928	+27.6
94	+10.266	-0.166	1.531	+0.646	+36.1	+.219	+0.480	+0.520	+.422	+0.929	+27.1
95	+10.424	-0.163	1.557	+0.649	+35.7	+.221	+0.471	+0.529	+.417	+0.932	+26.8
96	+10.589	-0.161	1.540	+0.652	+35.2	+.222	+0.477	+0.523	+.424	+0.934	+26.5
97	+10.761	-0.158	1.521	+0.652	+34.6	+.221	+0.483	+0.517	+.429	+0.934	+26.0
98	+10.929	-0.155	1.534	+0.654	+34.2	+.222	+0.479	+0.521	+.426	+0.935	+25.7
99	+11.084	-0.152	1.539	+0.658	+33.8	+.224	+0.477	+0.523	+.428	+0.938	+25.4
100	+11.261	-0.149	1.515	+0.660	+33.3	+.224	+0.485	+0.515	+.436	+0.940	+25.0
101	+11.427	-0.146	1.517	+0.660	+32.8	+.224	+0.485	+0.515	+.435	+0.940	+24.7
102	+11.589	-0.143	1.542	+0.666	+32.5	+.226	+0.476	+0.524	+.432	+0.944	+24.4
103	+11.766	-0.140	1.510	+0.667	+32.1	+.227	+0.487	+0.513	+.442	+0.945	+24.1
104	+11.948	-0.137	1.495	+0.666	+31.5	+.226	+0.492	+0.508	+.445	+0.944	+23.7
105	+12.111	-0.135	1.520	+0.669	+31.2	+.227	+0.484	+0.516	+.440	+0.946	+23.4
106	+12.271	-0.132	1.517	+0.672	+30.9	+.228	+0.485	+0.515	+.443	+0.949	+23.2
107	+12.456	-0.129	1.478	+0.672	+30.4	+.228	+0.498	+0.502	+.455	+0.949	+22.8
108	+12.623	-0.126	1.494	+0.672	+30.0	+.228	+0.492	+0.508	+.450	+0.949	+22.6
109	+12.786	-0.123	1.499	+0.676	+29.7	+.230	+0.491	+0.509	+.451	+0.952	+22.3
110	+12.956	-0.120	1.473	+0.676	+29.3	+.230	+0.500	+0.500	+.459	+0.952	+22.0
111	+13.135	-0.117	1.460	+0.675	+28.9	+.229	+0.504	+0.496	+.463	+0.951	+21.7
112	+13.291	-0.114	1.494	+0.679	+28.6	+.231	+0.493	+0.507	+.454	+0.954	+21.5
113	+13.456	-0.112	1.476	+0.682	+28.4	+.232	+0.499	+0.501	+.462	+0.956	+21.3
114	+13.638	-0.108	1.454	+0.681	+28.0	+.231	+0.506	+0.494	+.468	+0.956	+21.0
115	+13.798	-0.106	1.491	+0.684	+27.7	+.232	+0.494	+0.506	+.459	+0.957	+20.8
116	+13.968	-0.103	1.464	+0.685	+27.4	+.233	+0.503	+0.497	+.468	+0.959	+20.6
117	+14.138	-0.100	1.455	+0.685	+27.1	+.233	+0.506	+0.494	+.471	+0.959	+20.3
118	+14.298	-0.097	1.491	+0.690	+26.9	+.234	+0.493	+0.507	+.463	+0.962	+20.2
119	+14.478	-0.094	1.460	+0.690	+26.5	+.234	+0.504	+0.496	+.473	+0.962	+19.9
120	+14.655	-0.091	1.455	+0.690	+26.2	+.234	+0.506	+0.494	+.474	+0.962	+19.7

TEST NAME : DSS-G7

Pt. No.	Str.X (%)	X.Coor. (cm)	SigV (ksc)	TauH (ksc)	Eu (ksc)	TauH ---- SigVc	DelU ---- SigVc	SigV ---- SigVc	TauH ---- SigV	TauH ---- Cu	Eu -- Cu
121	+14.817	-0.088	1.480	+0.694	+26.0	+.236	+0.497	+0.503	+.469	+0.966	+19.6
122	+14.995	-0.085	1.453	+0.694	+25.7	+.236	+0.506	+0.494	+.477	+0.965	+19.3
123	+15.172	-0.082	1.448	+0.694	+25.4	+.236	+0.508	+0.492	+.479	+0.965	+19.1
124	+15.327	-0.080	1.485	+0.698	+25.2	+.237	+0.496	+0.504	+.470	+0.968	+18.9
125	+15.509	-0.076	1.445	+0.698	+24.9	+.237	+0.509	+0.491	+.483	+0.968	+18.7
126	+15.686	-0.073	1.429	+0.696	+24.6	+.236	+0.515	+0.485	+.487	+0.967	+18.5
127	+15.854	-0.071	1.454	+0.698	+24.4	+.237	+0.506	+0.494	+.480	+0.968	+18.3
128	+16.014	-0.068	1.462	+0.702	+24.2	+.238	+0.503	+0.497	+.480	+0.971	+18.2
129	+16.196	-0.065	1.433	+0.701	+23.9	+.238	+0.513	+0.487	+.489	+0.970	+18.0
130	+16.361	-0.062	1.467	+0.705	+23.7	+.239	+0.502	+0.498	+.480	+0.973	+17.8
131	+16.526	-0.059	1.446	+0.706	+23.5	+.240	+0.509	+0.491	+.488	+0.974	+17.7
132	+16.717	-0.056	1.425	+0.705	+23.3	+.240	+0.516	+0.484	+.495	+0.974	+17.5
133	+16.880	-0.053	1.455	+0.706	+23.0	+.240	+0.506	+0.494	+.485	+0.974	+17.3
134	+17.041	-0.050	1.453	+0.711	+22.9	+.242	+0.507	+0.493	+.489	+0.978	+17.2
135	+17.220	-0.047	1.420	+0.709	+22.6	+.241	+0.518	+0.482	+.499	+0.977	+17.0
136	+17.385	-0.044	1.456	+0.712	+22.5	+.242	+0.505	+0.495	+.489	+0.979	+16.9
137	+17.557	-0.041	1.445	+0.714	+22.3	+.243	+0.509	+0.491	+.495	+0.981	+16.8
138	+17.739	-0.038	1.425	+0.713	+22.0	+.242	+0.516	+0.484	+.500	+0.980	+16.6
139	+17.909	-0.035	1.456	+0.716	+21.9	+.243	+0.505	+0.495	+.492	+0.982	+16.4
140	+18.074	-0.033	1.441	+0.717	+21.7	+.243	+0.510	+0.490	+.497	+0.982	+16.3
141	+18.254	-0.029	1.426	+0.716	+21.5	+.243	+0.516	+0.484	+.502	+0.982	+16.1
142	+18.431	-0.026	1.429	+0.716	+21.3	+.243	+0.515	+0.485	+.501	+0.982	+16.0
143	+18.589	-0.024	1.450	+0.721	+21.2	+.245	+0.507	+0.493	+.497	+0.985	+15.9
144	+18.768	-0.021	1.429	+0.720	+20.9	+.245	+0.515	+0.485	+.504	+0.985	+15.7
145	+18.941	-0.018	1.443	+0.720	+20.8	+.245	+0.510	+0.490	+.499	+0.985	+15.6
146	+19.106	-0.015	1.441	+0.722	+20.6	+.245	+0.511	+0.489	+.501	+0.986	+15.5
147	+19.285	-0.012	1.417	+0.721	+20.4	+.245	+0.519	+0.481	+.509	+0.986	+15.3
148	+19.450	-0.009	1.450	+0.724	+20.3	+.246	+0.507	+0.493	+.499	+0.988	+15.2
149	+19.618	-0.006	1.436	+0.725	+20.1	+.246	+0.512	+0.488	+.505	+0.989	+15.1
150	+19.800	-0.003	1.420	+0.725	+19.9	+.246	+0.518	+0.482	+.511	+0.989	+15.0
151	+19.970	-0.000	1.450	+0.726	+19.8	+.247	+0.507	+0.493	+.501	+0.990	+14.9
152	+20.142	+0.003	1.435	+0.728	+19.6	+.247	+0.513	+0.487	+.508	+0.991	+14.8
153	+20.321	+0.006	1.419	+0.727	+19.5	+.247	+0.518	+0.482	+.512	+0.990	+14.6
154	+20.503	+0.009	1.422	+0.727	+19.3	+.247	+0.517	+0.483	+.512	+0.990	+14.5
155	+20.666	+0.012	1.447	+0.730	+19.2	+.248	+0.509	+0.491	+.505	+0.993	+14.4
156	+20.850	+0.015	1.418	+0.730	+19.0	+.248	+0.518	+0.482	+.514	+0.992	+14.3
157	+21.025	+0.018	1.428	+0.730	+18.8	+.248	+0.515	+0.485	+.511	+0.992	+14.2
158	+21.188	+0.021	1.443	+0.733	+18.7	+.249	+0.510	+0.490	+.508	+0.994	+14.1
159	+21.372	+0.024	1.416	+0.733	+18.6	+.249	+0.519	+0.481	+.517	+0.994	+14.0
160	+21.544	+0.027	1.418	+0.732	+18.4	+.249	+0.518	+0.482	+.516	+0.994	+13.8
161	+21.712	+0.030	1.445	+0.736	+18.3	+.250	+0.509	+0.491	+.510	+0.997	+13.8
162	+21.894	+0.033	1.411	+0.735	+18.2	+.250	+0.521	+0.479	+.521	+0.996	+13.6
163	+22.071	+0.036	1.426	+0.735	+18.0	+.250	+0.516	+0.484	+.516	+0.996	+13.5
164	+22.233	+0.039	1.441	+0.738	+17.9	+.251	+0.511	+0.489	+.512	+0.998	+13.5
165	+22.417	+0.042	1.401	+0.736	+17.8	+.250	+0.524	+0.476	+.525	+0.997	+13.3
166	+22.585	+0.045	1.427	+0.738	+17.6	+.251	+0.515	+0.485	+.517	+0.998	+13.3
167	+22.751	+0.047	1.427	+0.740	+17.5	+.251	+0.515	+0.485	+.519	+1.000	+13.2

TEST NAME : DSS-G7

Pt. No.	Str.X (%)	X.Coor. (cm)	SigV (ksc)	TauH (ksc)	Eu (ksc)	TauH ---- SigVc	DelU ---- SigVc	SigV ---- SigVc	TauH ---- SigV	TauH ---- Cu	Eu -- Cu
168	+22.939	+0.051	1.396	+0.738	+17.4	+.251	+0.526	+0.474	+.529	+0.999	+13.1
169	+23.106	+0.053	1.432	+0.739	+17.3	+.251	+0.513	+0.487	+.516	+0.999	+13.0
170	+23.284	+0.057	1.415	+0.740	+17.1	+.251	+0.519	+0.481	+.523	+1.000	+12.9
171	+23.473	+0.060	1.386	+0.735	+16.9	+.250	+0.529	+0.471	+.531	+0.996	+12.7
172	+23.648	+0.063	1.423	+0.736	+16.8	+.250	+0.517	+0.483	+.517	+0.997	+12.6
173	+23.812	+0.066	1.422	+0.737	+16.7	+.250	+0.517	+0.483	+.518	+0.998	+12.6
174	+24.009	+0.069	1.378	+0.733	+16.5	+.249	+0.532	+0.468	+.532	+0.994	+12.4
175	+24.189	+0.072	1.415	+0.732	+16.4	+.249	+0.519	+0.481	+.517	+0.994	+12.3
176	+24.363	+0.075	1.419	+0.733	+16.3	+.249	+0.518	+0.482	+.516	+0.994	+12.2
177	+24.560	+0.078	1.376	+0.729	+16.1	+.248	+0.533	+0.467	+.530	+0.992	+12.1
178	+24.740	+0.081	1.406	+0.727	+16.0	+.247	+0.523	+0.477	+.517	+0.990	+12.0
179	+24.918	+0.084	1.403	+0.728	+15.9	+.247	+0.524	+0.476	+.519	+0.991	+11.9
180	+25.107	+0.088	1.377	+0.724	+15.7	+.246	+0.532	+0.468	+.526	+0.988	+11.8
181	+25.288	+0.091	1.396	+0.722	+15.6	+.245	+0.526	+0.474	+.517	+0.986	+11.7
182	+25.461	+0.094	1.393	+0.722	+15.5	+.245	+0.527	+0.473	+.519	+0.986	+11.6
183	+25.650	+0.097	1.363	+0.718	+15.3	+.244	+0.537	+0.463	+.527	+0.984	+11.5
184	+25.829	+0.100	1.386	+0.717	+15.2	+.244	+0.529	+0.471	+.517	+0.983	+11.4
185	+25.996	+0.103	1.399	+0.717	+15.1	+.244	+0.525	+0.475	+.513	+0.983	+11.3
186	+26.192	+0.106	1.348	+0.715	+15.0	+.243	+0.542	+0.458	+.531	+0.981	+11.2
187	+26.381	+0.109	1.355	+0.710	+14.8	+.241	+0.540	+0.460	+.524	+0.977	+11.1
188	+26.558	+0.113	1.367	+0.711	+14.7	+.241	+0.535	+0.465	+.520	+0.978	+11.0
189	+26.740	+0.116	1.336	+0.709	+14.6	+.241	+0.546	+0.454	+.531	+0.977	+11.0
190	+26.938	+0.119	1.314	+0.704	+14.4	+.239	+0.554	+0.446	+.536	+0.973	+10.8
191	+27.114	+0.122	1.332	+0.702	+14.3	+.239	+0.547	+0.453	+.527	+0.972	+10.8
192	+27.284	+0.125	1.335	+0.703	+14.2	+.239	+0.547	+0.453	+.526	+0.972	+10.7
193	+27.466	+0.128	1.315	+0.702	+14.1	+.238	+0.553	+0.447	+.534	+0.971	+10.6
194	+27.654	+0.131	1.301	+0.698	+14.0	+.237	+0.558	+0.442	+.537	+0.968	+10.5
195	+27.839	+0.134	1.294	+0.696	+13.9	+.236	+0.560	+0.440	+.538	+0.967	+10.4
196	+28.021	+0.138	1.285	+0.693	+13.7	+.236	+0.563	+0.437	+.539	+0.965	+10.3
197	+28.198	+0.141	1.302	+0.694	+13.7	+.236	+0.558	+0.442	+.533	+0.965	+10.3
198	+28.368	+0.143	1.301	+0.694	+13.6	+.236	+0.558	+0.442	+.533	+0.965	+10.2
199	+28.556	+0.147	1.279	+0.692	+13.5	+.235	+0.566	+0.434	+.541	+0.964	+10.1
200	+28.742	+0.150	1.267	+0.690	+13.4	+.234	+0.570	+0.430	+.544	+0.962	+10.0
201	+28.932	+0.153	1.266	+0.686	+13.2	+.233	+0.570	+0.430	+.542	+0.959	+9.9
202	+29.105	+0.156	1.268	+0.686	+13.2	+.233	+0.569	+0.431	+.542	+0.960	+9.9
203	+29.287	+0.159	1.251	+0.685	+13.1	+.233	+0.575	+0.425	+.547	+0.958	+9.8
204	+29.475	+0.162	1.244	+0.683	+13.0	+.232	+0.578	+0.422	+.549	+0.957	+9.7
205	+29.661	+0.166	1.235	+0.679	+12.8	+.231	+0.580	+0.420	+.550	+0.954	+9.7
206	+29.847	+0.169	1.229	+0.678	+12.7	+.230	+0.582	+0.418	+.551	+0.953	+9.6
207	+30.025	+0.172	1.221	+0.675	+12.6	+.229	+0.585	+0.415	+.553	+0.951	+9.5
208	+30.213	+0.175	1.215	+0.673	+12.5	+.229	+0.587	+0.413	+.554	+0.949	+9.4
209	+30.393	+0.178	1.206	+0.671	+12.5	+.228	+0.590	+0.410	+.556	+0.948	+9.4
210	+30.578	+0.181	1.202	+0.669	+12.4	+.227	+0.592	+0.408	+.556	+0.946	+9.3
211	+30.759	+0.184	1.198	+0.667	+12.3	+.227	+0.593	+0.407	+.557	+0.945	+9.2
212	+30.942	+0.187	1.196	+0.665	+12.2	+.226	+0.594	+0.406	+.556	+0.944	+9.1
213	+31.124	+0.191	1.192	+0.664	+12.1	+.226	+0.595	+0.405	+.557	+0.943	+9.1
214	+31.310	+0.194	1.187	+0.663	+12.0	+.225	+0.597	+0.403	+.558	+0.942	+9.0
215	+31.502	+0.197	1.177	+0.660	+11.9	+.224	+0.600	+0.400	+.561	+0.939	+8.9
216	+31.690	+0.200	1.169	+0.656	+11.8	+.223	+0.603	+0.397	+.561	+0.937	+8.9
217	+31.870	+0.203	1.167	+0.654	+11.7	+.222	+0.604	+0.396	+.560	+0.935	+8.8
218	+32.048	+0.206	1.156	+0.653	+11.6	+.222	+0.607	+0.393	+.564	+0.934	+8.7
219	+32.234	+0.210	1.155	+0.650	+11.5	+.221	+0.608	+0.392	+.563	+0.932	+8.7

220	+32.413	+0.213	1.152	+0.649	+11.5	+.221	+0.609	+0.391	+.564	+0.932	+8.6
221	+32.593	+0.216	1.154	+0.648	+11.4	+.220	+0.608	+0.392	+.561	+0.931	+8.6
222	+32.778	+0.219	1.145	+0.648	+11.3	+.220	+0.611	+0.389	+.566	+0.931	+8.5
223	+32.963	+0.222	1.139	+0.645	+11.2	+.219	+0.613	+0.387	+.566	+0.928	+8.4
224	+33.147	+0.225	1.133	+0.644	+11.2	+.219	+0.615	+0.385	+.568	+0.927	+8.4
225	+33.334	+0.228	1.127	+0.641	+11.1	+.218	+0.617	+0.383	+.569	+0.926	+8.3
226	+33.515	+0.231	1.125	+0.640	+11.0	+.217	+0.618	+0.382	+.569	+0.924	+8.3
227	+33.700	+0.235	1.118	+0.638	+10.9	+.217	+0.620	+0.380	+.571	+0.923	+8.2
228	+33.886	+0.238	1.115	+0.636	+10.9	+.216	+0.621	+0.379	+.570	+0.922	+8.2
229	+34.071	+0.241	1.112	+0.635	+10.8	+.216	+0.622	+0.378	+.571	+0.921	+8.1
230	+34.258	+0.244	1.111	+0.631	+10.7	+.214	+0.623	+0.377	+.568	+0.918	+8.0
231	+34.439	+0.247	1.109	+0.631	+10.6	+.214	+0.623	+0.377	+.569	+0.918	+8.0
232	+34.625	+0.250	1.071	+0.626	+10.5	+.213	+0.636	+0.364	+.584	+0.914	+7.9
233	+34.835	+0.254	1.056	+0.618	+10.4	+.210	+0.641	+0.359	+.585	+0.908	+7.8
234	+35.009	+0.257	1.067	+0.616	+10.3	+.209	+0.638	+0.362	+.577	+0.906	+7.8
235	+35.186	+0.260	1.065	+0.615	+10.3	+.209	+0.638	+0.362	+.578	+0.906	+7.7
236	+35.369	+0.263	1.059	+0.615	+10.2	+.209	+0.640	+0.360	+.581	+0.906	+7.7
237	+35.554	+0.266	1.056	+0.613	+10.2	+.208	+0.641	+0.359	+.581	+0.905	+7.6
238	+35.733	+0.269	1.061	+0.614	+10.1	+.209	+0.640	+0.360	+.579	+0.905	+7.6
239	+35.925	+0.273	1.048	+0.612	+10.0	+.208	+0.644	+0.356	+.584	+0.903	+7.5
240	+36.116	+0.276	1.043	+0.609	+10.0	+.207	+0.646	+0.354	+.584	+0.902	+7.5
241	+36.293	+0.279	1.040	+0.606	+9.9	+.206	+0.647	+0.353	+.583	+0.900	+7.4
242	+36.478	+0.282	1.035	+0.605	+9.8	+.205	+0.648	+0.352	+.584	+0.898	+7.4
243	+36.655	+0.285	1.032	+0.603	+9.8	+.205	+0.649	+0.351	+.584	+0.897	+7.3
244	+36.835	+0.288	1.030	+0.602	+9.7	+.204	+0.650	+0.350	+.584	+0.896	+7.3
245	+37.017	+0.291	1.026	+0.601	+9.7	+.204	+0.651	+0.349	+.586	+0.896	+7.3
246	+37.209	+0.295	1.020	+0.598	+9.6	+.203	+0.653	+0.347	+.586	+0.893	+7.2
247	+37.396	+0.298	1.017	+0.597	+9.5	+.203	+0.655	+0.345	+.587	+0.892	+7.2
248	+37.582	+0.301	1.009	+0.594	+9.5	+.202	+0.657	+0.343	+.588	+0.890	+7.1
249	+37.777	+0.304	0.996	+0.591	+9.4	+.201	+0.662	+0.338	+.594	+0.888	+7.1
250	+37.979	+0.308	0.988	+0.586	+9.3	+.199	+0.665	+0.335	+.593	+0.884	+7.0

****

ANISOTROPICALLY CONSOLIDATED GEONOR DIRECT SIMPLE SHEAR TEST
MIT GEOTECHNICAL LAB

****

FILE NAME: DSSG8.PRN

REDUCTION DATA
UNITS: (kg,cm,VOLTS)

1. TEST NAME : DSS-G8
2. DATE : 6/3/1988
3. OCR : 1
4. VER. CONSOLIDATION STRESS (KSC) : +2.893
5. HOR. CONSOLIDATION STRESS (KSC) : +0.300
6. PRE-SHEAR SAMPLE HEIGHT (cm) : +1.9483
7. VERTICAL STRESS LOAD CELL:
   ZERO: 1.071
   CF: -343.3
8. HORIZONTAL SHEAR LOAD CELL:
   ZERO: -.72031
   CF: 169.21
9. HORIZONTAL DISP. TRANSDUCER, X:
   ZERO: 1.2764
   CF: -2.2815
10. CONSTANT HEIGHT TRANSDUCER, Z:
    ZERO: .43961
    CF: 2.1089
11. TEST ANGLE THETA: 180
    TOTAL X DISP. DURING CONSOLIDATION: -.13966

Pt. No.	Str.X (%)	X.Coor. (cm)	SigV (ksc)	TauH (ksc)	Eu (ksc)	TauH / SigVc	DelU / SigVc	SigV / SigVc	TauH / SigV	TauH / Cu	Eu / Cu
1	+0.000	-0.140	2.893	-0.298	+9999.0	-.103	+0.000	+1.000	-.103	+0.000	+9999.0
2	+0.000	-0.140	2.894	-0.298	+9999.0	-.103	-0.000	+1.000	-.103	+0.000	+9999.0
3	-0.004	-0.140	2.893	-0.298	-18.8	-.103	+0.000	+1.000	-.103	+0.000	-21.0
4	+0.002	-0.140	2.892	-0.298	+14.6	-.103	+0.000	+1.000	-.103	+0.000	+16.3
5	+0.004	-0.140	2.886	-0.298	+0.4	-.103	+0.002	+0.998	-.103	+0.000	+0.4
6	+0.002	-0.140	2.880	-0.298	+18.3	-.103	+0.005	+0.995	-.104	+0.000	+20.4
7	+0.004	-0.140	2.871	-0.298	+1.0	-.103	+0.008	+0.992	-.104	+0.000	+1.1
8	+0.008	-0.139	2.858	-0.285	+484.1	-.098	+0.012	+0.988	-.100	+0.015	+539.3
9	+0.008	-0.139	2.846	-0.263	+1281.2	-.091	+0.016	+0.984	-.092	+0.040	+1427.4
10	+0.017	-0.139	2.834	-0.231	+1208.4	-.080	+0.020	+0.980	-.081	+0.075	+1346.3
11	+0.027	-0.139	2.822	-0.196	+1120.9	-.068	+0.025	+0.975	-.070	+0.114	+1248.8
12	+0.044	-0.139	2.809	-0.163	+921.7	-.056	+0.029	+0.971	-.058	+0.151	+1026.9
13	+0.050	-0.139	2.795	-0.128	+1014.8	-.044	+0.034	+0.966	-.046	+0.190	+1130.6
14	+0.065	-0.138	2.784	-0.092	+952.2	-.032	+0.038	+0.962	-.033	+0.230	+1060.8
15	+0.088	-0.138	2.772	-0.053	+835.7	-.018	+0.042	+0.958	-.019	+0.274	+931.0
16	+0.107	-0.138	2.759	-0.016	+789.8	-.006	+0.046	+0.954	-.006	+0.314	+879.9
17	+0.132	-0.137	2.742	+0.022	+727.0	+.008	+0.052	+0.948	+.008	+0.357	+809.9
18	+0.162	-0.137	2.723	+0.059	+663.4	+.021	+0.059	+0.941	+.022	+0.399	+739.1
19	+0.193	-0.136	2.700	+0.097	+614.2	+.034	+0.067	+0.933	+.036	+0.441	+684.2
20	+0.231	-0.135	2.673	+0.131	+556.9	+.045	+0.076	+0.924	+.049	+0.478	+620.4
21	+0.275	-0.134	2.643	+0.162	+501.6	+.056	+0.086	+0.914	+.061	+0.513	+558.9
22	+0.324	-0.133	2.613	+0.194	+456.2	+.067	+0.097	+0.903	+.074	+0.548	+508.3
23	+0.378	-0.132	2.580	+0.223	+413.3	+.077	+0.108	+0.892	+.086	+0.581	+460.4
24	+0.441	-0.131	2.543	+0.252	+374.2	+.087	+0.121	+0.879	+.099	+0.613	+416.9

TEST NAME : DSS-G8

Pt. No.	Str.X (%)	X.Coor. (cm)	SigV (ksc)	TauH (ksc)	Eu (ksc)	TauH ---- SigVc	DelU ---- SigVc	SigV ---- SigVc	TauH ---- SigV	TauH ---- Cu	Eu -- Cu
25	+0.509	-0.130	2.504	+0.277	+339.5	+.096	+0.134	+0.866	+.111	+0.641	+378.3
26	+0.586	-0.128	2.466	+0.302	+307.1	+.104	+0.148	+0.852	+.122	+0.669	+342.1
27	+0.670	-0.127	2.425	+0.323	+278.3	+.112	+0.162	+0.838	+.133	+0.693	+310.1
28	+0.757	-0.125	2.388	+0.344	+254.9	+.119	+0.174	+0.826	+.144	+0.716	+284.0
29	+0.847	-0.123	2.348	+0.364	+234.6	+.126	+0.188	+0.812	+.155	+0.738	+261.4
30	+0.946	-0.121	2.310	+0.380	+215.2	+.131	+0.201	+0.799	+.164	+0.756	+239.8
31	+1.044	-0.119	2.275	+0.397	+199.8	+.137	+0.214	+0.786	+.175	+0.775	+222.6
32	+1.152	-0.117	2.239	+0.411	+184.9	+.142	+0.226	+0.774	+.184	+0.791	+206.0
33	+1.259	-0.115	2.200	+0.425	+172.5	+.147	+0.239	+0.761	+.193	+0.807	+192.2
34	+1.381	-0.113	2.161	+0.437	+159.9	+.151	+0.253	+0.747	+.202	+0.820	+178.1
35	+1.500	-0.110	2.125	+0.450	+149.6	+.155	+0.266	+0.734	+.212	+0.833	+166.6
36	+1.632	-0.108	2.088	+0.460	+139.4	+.159	+0.278	+0.722	+.220	+0.845	+155.3
37	+1.767	-0.105	2.053	+0.469	+130.3	+.162	+0.290	+0.710	+.228	+0.855	+145.1
38	+1.892	-0.103	2.021	+0.478	+123.1	+.165	+0.302	+0.698	+.237	+0.865	+137.2
39	+2.019	-0.100	1.990	+0.486	+116.5	+.168	+0.312	+0.688	+.244	+0.874	+129.8
40	+2.151	-0.098	1.962	+0.494	+110.5	+.171	+0.322	+0.678	+.252	+0.883	+123.2
41	+2.274	-0.095	1.936	+0.501	+105.4	+.173	+0.331	+0.669	+.259	+0.891	+117.5
42	+2.414	-0.093	1.909	+0.508	+100.2	+.175	+0.340	+0.660	+.266	+0.898	+111.6
43	+2.555	-0.090	1.877	+0.512	+95.1	+.177	+0.351	+0.649	+.273	+0.903	+106.0
44	+2.690	-0.087	1.850	+0.517	+90.9	+.179	+0.361	+0.639	+.279	+0.908	+101.3
45	+2.828	-0.085	1.827	+0.523	+87.1	+.181	+0.368	+0.632	+.286	+0.915	+97.0
46	+2.964	-0.082	1.805	+0.527	+83.6	+.182	+0.376	+0.624	+.292	+0.920	+93.1
47	+3.104	-0.079	1.790	+0.533	+80.4	+.184	+0.381	+0.619	+.298	+0.927	+89.6
48	+3.232	-0.077	1.771	+0.538	+77.6	+.186	+0.388	+0.612	+.304	+0.932	+86.5
49	+3.384	-0.074	1.748	+0.544	+74.7	+.188	+0.396	+0.604	+.311	+0.939	+83.2
50	+3.526	-0.071	1.724	+0.547	+71.9	+.189	+0.404	+0.596	+.317	+0.942	+80.1
51	+3.671	-0.068	1.701	+0.549	+69.2	+.190	+0.412	+0.588	+.323	+0.944	+77.1
52	+3.811	-0.065	1.680	+0.550	+66.8	+.190	+0.419	+0.581	+.327	+0.945	+74.4
53	+3.958	-0.063	1.666	+0.554	+64.6	+.191	+0.424	+0.576	+.332	+0.949	+72.0
54	+4.103	-0.060	1.653	+0.557	+62.5	+.192	+0.429	+0.571	+.337	+0.953	+69.7
55	+4.247	-0.057	1.639	+0.558	+60.5	+.193	+0.434	+0.566	+.340	+0.954	+67.4
56	+4.385	-0.054	1.621	+0.562	+58.9	+.194	+0.440	+0.560	+.347	+0.959	+65.6
57	+4.530	-0.051	1.606	+0.564	+57.1	+.195	+0.445	+0.555	+.351	+0.961	+63.6
58	+4.678	-0.049	1.591	+0.567	+55.5	+.196	+0.450	+0.550	+.356	+0.964	+61.8
59	+4.826	-0.046	1.575	+0.568	+53.8	+.196	+0.456	+0.544	+.360	+0.965	+60.0
60	+4.981	-0.043	1.555	+0.569	+52.3	+.197	+0.462	+0.538	+.366	+0.967	+58.2
61	+5.131	-0.040	1.536	+0.570	+50.8	+.197	+0.469	+0.531	+.371	+0.967	+56.6
62	+5.298	-0.036	1.519	+0.570	+49.2	+.197	+0.475	+0.525	+.375	+0.968	+54.8
63	+5.445	-0.034	1.509	+0.570	+47.9	+.197	+0.479	+0.521	+.378	+0.968	+53.3
64	+5.595	-0.031	1.497	+0.570	+46.6	+.197	+0.483	+0.517	+.381	+0.968	+51.9
65	+5.741	-0.028	1.501	+0.573	+45.6	+.198	+0.481	+0.519	+.382	+0.971	+50.8
66	+5.889	-0.025	1.493	+0.574	+44.4	+.198	+0.484	+0.516	+.384	+0.972	+49.5
67	+6.040	-0.022	1.489	+0.576	+43.5	+.199	+0.485	+0.515	+.387	+0.975	+48.4
68	+6.190	-0.019	1.479	+0.578	+42.5	+.200	+0.489	+0.511	+.391	+0.977	+47.3
69	+6.344	-0.016	1.464	+0.579	+41.5	+.200	+0.494	+0.506	+.396	+0.978	+46.3
70	+6.494	-0.013	1.450	+0.580	+40.6	+.200	+0.499	+0.501	+.400	+0.979	+45.2
71	+6.647	-0.010	1.438	+0.581	+39.7	+.201	+0.503	+0.497	+.404	+0.980	+44.2
72	+6.802	-0.007	1.427	+0.583	+38.9	+.201	+0.507	+0.493	+.408	+0.982	+43.3

TEST NAME : DSS-G8

Pt. No.	Str.X (%)	X.Coor. (cm)	SigV (ksc)	TauH (ksc)	Eu (ksc)	TauH ---- SigVc	DelU ---- SigVc	SigV ---- SigVc	TauH ---- SigV	TauH ---- Cu	Eu -- Cu
73	+6.953	-0.004	1.421	+0.583	+38.0	+.201	+0.509	+0.491	+.410	+0.982	+42.4
74	+7.103	-0.001	1.418	+0.584	+37.3	+.202	+0.510	+0.490	+.412	+0.984	+41.5
75	+7.246	+0.002	1.418	+0.585	+36.6	+.202	+0.510	+0.490	+.413	+0.985	+40.8
76	+7.381	+0.004	1.408	+0.587	+36.0	+.203	+0.513	+0.487	+.417	+0.986	+40.1
77	+7.543	+0.007	1.405	+0.588	+35.2	+.203	+0.515	+0.485	+.419	+0.987	+39.3
78	+7.696	+0.010	1.390	+0.588	+34.6	+.203	+0.520	+0.480	+.423	+0.988	+38.5
79	+7.847	+0.013	1.379	+0.588	+33.9	+.203	+0.523	+0.477	+.427	+0.988	+37.8
80	+7.999	+0.016	1.369	+0.589	+33.3	+.203	+0.527	+0.473	+.430	+0.988	+37.1
81	+8.151	+0.019	1.363	+0.589	+32.7	+.204	+0.529	+0.471	+.432	+0.989	+36.4
82	+8.296	+0.022	1.357	+0.590	+32.1	+.204	+0.531	+0.469	+.434	+0.990	+35.8
83	+8.443	+0.025	1.350	+0.591	+31.6	+.204	+0.533	+0.467	+.438	+0.991	+35.2
84	+8.591	+0.028	1.342	+0.592	+31.1	+.204	+0.536	+0.464	+.441	+0.992	+34.6
85	+8.753	+0.031	1.332	+0.593	+30.6	+.205	+0.540	+0.460	+.445	+0.994	+34.1
86	+8.909	+0.034	1.325	+0.593	+30.0	+.205	+0.542	+0.458	+.447	+0.993	+33.4
87	+9.063	+0.037	1.320	+0.592	+29.5	+.205	+0.544	+0.456	+.449	+0.993	+32.9
88	+9.213	+0.040	1.314	+0.592	+29.0	+.205	+0.546	+0.454	+.451	+0.993	+32.3
89	+9.360	+0.043	1.312	+0.593	+28.6	+.205	+0.547	+0.453	+.452	+0.994	+31.8
90	+9.510	+0.046	1.307	+0.594	+28.2	+.205	+0.548	+0.452	+.455	+0.994	+31.4
91	+9.666	+0.049	1.298	+0.594	+27.7	+.205	+0.551	+0.449	+.458	+0.994	+30.9
92	+9.822	+0.052	1.290	+0.595	+27.3	+.206	+0.554	+0.446	+.461	+0.995	+30.4
93	+9.976	+0.055	1.285	+0.594	+26.9	+.205	+0.556	+0.444	+.462	+0.995	+29.9
94	+10.130	+0.058	1.284	+0.595	+26.5	+.206	+0.556	+0.444	+.464	+0.996	+29.5
95	+10.273	+0.060	1.296	+0.596	+26.1	+.206	+0.552	+0.448	+.460	+0.996	+29.1
96	+10.429	+0.064	1.284	+0.597	+25.8	+.206	+0.556	+0.444	+.465	+0.997	+28.7
97	+10.581	+0.066	1.270	+0.596	+25.4	+.206	+0.561	+0.439	+.470	+0.997	+28.3
98	+10.737	+0.070	1.258	+0.596	+25.0	+.206	+0.565	+0.435	+.474	+0.996	+27.8
99	+10.897	+0.073	1.252	+0.596	+24.6	+.206	+0.567	+0.433	+.476	+0.996	+27.4
100	+11.042	+0.075	1.249	+0.595	+24.3	+.206	+0.568	+0.432	+.477	+0.996	+27.1
101	+11.200	+0.079	1.248	+0.596	+24.0	+.206	+0.568	+0.432	+.477	+0.997	+26.7
102	+11.347	+0.081	1.248	+0.596	+23.6	+.206	+0.569	+0.431	+.477	+0.996	+26.3
103	+11.497	+0.084	1.247	+0.597	+23.4	+.206	+0.569	+0.431	+.479	+0.997	+26.0
104	+11.643	+0.087	1.261	+0.598	+23.1	+.207	+0.564	+0.436	+.474	+0.999	+25.7
105	+11.796	+0.090	1.241	+0.599	+22.8	+.207	+0.571	+0.429	+.483	+1.000	+25.4
106	+11.949	+0.093	1.234	+0.599	+22.5	+.207	+0.573	+0.427	+.485	+1.000	+25.1
107	+12.108	+0.096	1.230	+0.599	+22.2	+.207	+0.575	+0.425	+.487	+0.999	+24.8
108	+12.262	+0.099	1.221	+0.599	+21.9	+.207	+0.578	+0.422	+.490	+0.999	+24.5
109	+12.418	+0.102	1.216	+0.598	+21.7	+.207	+0.580	+0.420	+.492	+0.999	+24.1
110	+12.580	+0.105	1.226	+0.598	+21.4	+.207	+0.576	+0.424	+.488	+0.999	+23.8
111	+12.733	+0.108	1.209	+0.598	+21.1	+.207	+0.582	+0.418	+.494	+0.998	+23.5
112	+12.894	+0.112	1.197	+0.598	+20.8	+.207	+0.586	+0.414	+.499	+0.998	+23.2
113	+13.047	+0.115	1.191	+0.596	+20.6	+.206	+0.588	+0.412	+.501	+0.997	+22.9
114	+13.205	+0.118	1.190	+0.596	+20.3	+.206	+0.589	+0.411	+.501	+0.997	+22.6
115	+13.357	+0.121	1.194	+0.596	+20.1	+.206	+0.587	+0.413	+.499	+0.996	+22.4
116	+13.513	+0.124	1.193	+0.595	+19.8	+.206	+0.588	+0.412	+.499	+0.996	+22.1
117	+13.670	+0.127	1.193	+0.596	+19.6	+.206	+0.588	+0.412	+.500	+0.996	+21.9
118	+13.826	+0.130	1.192	+0.596	+19.4	+.206	+0.588	+0.412	+.500	+0.996	+21.6
119	+13.987	+0.133	1.188	+0.596	+19.2	+.206	+0.589	+0.411	+.502	+0.996	+21.4
120	+14.138	+0.136	1.176	+0.595	+19.0	+.206	+0.593	+0.407	+.506	+0.995	+21.1

TEST NAME : DSS-G8

Pt. No.	Str.X (%)	X.Coor. (cm)	SigV (ksc)	TauH (ksc)	Eu (ksc)	TauH ---- SigVc	DelU ---- SigVc	SigV ---- SigVc	TauH ---- SigV	TauH ---- Cu	Eu -- Cu
121	+14.293	+0.139	1.167	+0.594	+18.7	+.205	+0.596	+0.404	+.509	+0.994	+20.9
122	+14.442	+0.142	1.167	+0.593	+18.5	+.205	+0.597	+0.403	+.508	+0.994	+20.6
123	+14.596	+0.145	1.166	+0.593	+18.3	+.205	+0.597	+0.403	+.509	+0.994	+20.4
124	+14.746	+0.148	1.164	+0.593	+18.1	+.205	+0.598	+0.402	+.510	+0.994	+20.2
125	+14.899	+0.151	1.162	+0.593	+18.0	+.205	+0.598	+0.402	+.511	+0.993	+20.0
126	+15.061	+0.154	1.157	+0.593	+17.8	+.205	+0.600	+0.400	+.513	+0.994	+19.8
127	+15.214	+0.157	1.154	+0.593	+17.6	+.205	+0.601	+0.399	+.514	+0.993	+19.6
128	+15.367	+0.160	1.152	+0.593	+17.4	+.205	+0.602	+0.398	+.515	+0.993	+19.4
129	+15.520	+0.163	1.147	+0.593	+17.2	+.205	+0.604	+0.396	+.517	+0.993	+19.2
130	+15.676	+0.166	1.139	+0.592	+17.0	+.205	+0.606	+0.394	+.520	+0.992	+19.0
131	+15.829	+0.169	1.136	+0.592	+16.9	+.205	+0.607	+0.393	+.521	+0.992	+18.8
132	+15.990	+0.172	1.133	+0.592	+16.7	+.204	+0.609	+0.391	+.522	+0.992	+18.6
133	+16.147	+0.175	1.132	+0.591	+16.5	+.204	+0.609	+0.391	+.522	+0.991	+18.4
134	+16.306	+0.178	1.135	+0.591	+16.4	+.204	+0.608	+0.392	+.520	+0.991	+18.2
135	+16.463	+0.181	1.133	+0.591	+16.2	+.204	+0.608	+0.392	+.521	+0.990	+18.0
136	+16.620	+0.184	1.127	+0.589	+16.0	+.203	+0.610	+0.390	+.522	+0.988	+17.8
137	+16.776	+0.187	1.123	+0.588	+15.9	+.203	+0.612	+0.388	+.524	+0.988	+17.7
138	+16.933	+0.190	1.120	+0.588	+15.7	+.203	+0.613	+0.387	+.525	+0.987	+17.5
139	+17.091	+0.193	1.117	+0.587	+15.5	+.203	+0.614	+0.386	+.526	+0.987	+17.3
140	+17.249	+0.196	1.112	+0.586	+15.4	+.202	+0.616	+0.384	+.527	+0.985	+17.1
141	+17.406	+0.199	1.105	+0.585	+15.2	+.202	+0.618	+0.382	+.529	+0.984	+17.0
142	+17.566	+0.203	1.097	+0.584	+15.1	+.202	+0.621	+0.379	+.532	+0.983	+16.8
143	+17.723	+0.206	1.092	+0.582	+14.9	+.201	+0.623	+0.377	+.533	+0.981	+16.6
144	+17.876	+0.209	1.089	+0.581	+14.8	+.201	+0.624	+0.376	+.534	+0.980	+16.5
145	+18.284	+0.217	1.082	+0.575	+14.3	+.199	+0.626	+0.374	+.531	+0.973	+16.0
146	+18.695	+0.225	1.038	+0.566	+13.9	+.196	+0.641	+0.359	+.546	+0.964	+15.5
147	+19.106	+0.233	1.006	+0.557	+13.4	+.192	+0.652	+0.348	+.553	+0.953	+15.0
148	+19.522	+0.241	0.983	+0.546	+13.0	+.189	+0.660	+0.340	+.555	+0.941	+14.5
149	+19.925	+0.249	0.972	+0.540	+12.6	+.187	+0.664	+0.336	+.556	+0.935	+14.1
150	+20.335	+0.257	0.949	+0.534	+12.3	+.185	+0.672	+0.328	+.562	+0.927	+13.7
151	+20.748	+0.265	0.912	+0.524	+11.9	+.181	+0.685	+0.315	+.574	+0.916	+13.2
152	+21.169	+0.273	0.888	+0.515	+11.5	+.178	+0.693	+0.307	+.579	+0.906	+12.8
153	+21.577	+0.281	0.868	+0.505	+11.2	+.175	+0.700	+0.300	+.582	+0.895	+12.5
154	+21.988	+0.289	0.842	+0.495	+10.8	+.171	+0.709	+0.291	+.588	+0.884	+12.1
155	+22.395	+0.297	0.828	+0.487	+10.5	+.168	+0.714	+0.286	+.589	+0.875	+11.7
156	+22.791	+0.304	0.812	+0.481	+10.3	+.166	+0.719	+0.281	+.592	+0.868	+11.4
157	+23.201	+0.312	0.796	+0.476	+10.0	+.164	+0.725	+0.275	+.597	+0.862	+11.2
158	+23.609	+0.320	0.778	+0.468	+9.7	+.162	+0.731	+0.269	+.602	+0.854	+10.9
159	+24.015	+0.328	0.753	+0.459	+9.5	+.159	+0.740	+0.260	+.610	+0.844	+10.5
160	+24.428	+0.336	0.735	+0.451	+9.2	+.156	+0.746	+0.254	+.613	+0.835	+10.2
161	+24.834	+0.344	0.718	+0.444	+9.0	+.154	+0.752	+0.248	+.619	+0.828	+10.0
162	+25.246	+0.352	0.708	+0.438	+8.8	+.152	+0.755	+0.245	+.620	+0.821	+9.8
163	+25.642	+0.360	0.705	+0.436	+8.6	+.151	+0.756	+0.244	+.618	+0.818	+9.6
164	+26.049	+0.368	0.686	+0.429	+8.4	+.148	+0.763	+0.237	+.625	+0.810	+9.3
165	+26.460	+0.376	0.673	+0.421	+8.2	+.146	+0.767	+0.233	+.626	+0.802	+9.1
166	+26.856	+0.384	0.659	+0.414	+8.0	+.143	+0.772	+0.228	+.629	+0.794	+8.9
167	+27.261	+0.391	0.644	+0.408	+7.8	+.141	+0.777	+0.223	+.633	+0.787	+8.7

TEST NAME : DSS-G8

Pt. No.	Str.X (%)	X.Coor. (cm)	SigV (ksc)	TauH (ksc)	Eu (ksc)	TauH ---- SigVc	DelU ---- SigVc	SigV ---- SigVc	TauH ---- SigV	TauH ---- Cu	Eu -- Cu
168	+27.663	+0.399	0.633	+0.402	+7.6	+.139	+0.781	+0.219	+.636	+0.780	+8.5
169	+28.052	+0.407	0.632	+0.399	+7.5	+.138	+0.782	+0.218	+.632	+0.777	+8.3
170	+28.470	+0.415	0.617	+0.391	+7.3	+.135	+0.787	+0.213	+.634	+0.768	+8.1
171	+28.867	+0.423	0.606	+0.384	+7.1	+.133	+0.791	+0.209	+.634	+0.761	+7.9
172	+29.270	+0.431	0.602	+0.380	+7.0	+.131	+0.792	+0.208	+.632	+0.756	+7.7
173	+29.682	+0.439	0.583	+0.370	+6.8	+.128	+0.798	+0.202	+.635	+0.745	+7.5
174	+30.084	+0.446	0.572	+0.364	+6.6	+.126	+0.802	+0.198	+.637	+0.738	+7.4
175	+30.496	+0.454	0.565	+0.356	+6.4	+.123	+0.805	+0.195	+.631	+0.729	+7.2
176	+30.877	+0.462	0.560	+0.352	+6.3	+.122	+0.806	+0.194	+.627	+0.724	+7.0
177	+31.298	+0.470	0.537	+0.341	+6.1	+.118	+0.814	+0.186	+.635	+0.712	+6.8
178	+31.707	+0.478	0.528	+0.335	+6.0	+.116	+0.818	+0.182	+.636	+0.706	+6.7
179	+32.090	+0.486	0.528	+0.334	+5.9	+.115	+0.817	+0.183	+.633	+0.705	+6.6
180	+32.492	+0.493	0.521	+0.330	+5.8	+.114	+0.820	+0.180	+.633	+0.700	+6.5
181	+32.890	+0.501	0.511	+0.324	+5.7	+.112	+0.823	+0.177	+.633	+0.693	+6.3
182	+33.292	+0.509	0.504	+0.320	+5.6	+.111	+0.826	+0.174	+.635	+0.689	+6.2
183	+33.692	+0.517	0.490	+0.313	+5.4	+.108	+0.831	+0.169	+.639	+0.681	+6.1
184	+34.079	+0.524	0.483	+0.310	+5.4	+.107	+0.833	+0.167	+.640	+0.677	+6.0
185	+34.500	+0.533	0.468	+0.302	+5.2	+.104	+0.838	+0.162	+.646	+0.669	+5.8
186	+34.891	+0.540	0.466	+0.299	+5.1	+.103	+0.839	+0.161	+.642	+0.666	+5.7
187	+35.285	+0.548	0.459	+0.295	+5.0	+.102	+0.841	+0.159	+.642	+0.661	+5.6
188	+35.687	+0.556	0.452	+0.291	+5.0	+.100	+0.844	+0.156	+.642	+0.656	+5.5
189	+36.002	+0.562	0.444	+0.280	+4.8	+.097	+0.847	+0.153	+.632	+0.645	+5.4
190	+36.010	+0.562	0.443	+0.277	+4.8	+.096	+0.847	+0.153	+.625	+0.641	+5.3
191	+36.014	+0.562	0.444	+0.276	+4.8	+.095	+0.847	+0.153	+.621	+0.640	+5.3
192	+36.019	+0.562	0.444	+0.275	+4.8	+.095	+0.846	+0.154	+.620	+0.639	+5.3

****

Ko CONSOLIDATED MDSS TEST
MIT GEOTECHNICAL LAB

****

FILE NAME: DSSC5.PRN

REDUCTION DATA
UNITS: (kg,cm,mVOLTS,VOLTS)

1. TEST NAME : DSSC5
2. DATE : 09-03-1987
3. OCR : 1
4. VER. CONSOLIDATION STRESS (KSC) : +3.004
5. HOR. CONSOLIDATION STRESS (KSC) : +0.000
6. PRE-SHEAR SAMPLE HEIGHT (cm) : +1.9838
7. VERTICAL STRESS LOAD CELL:
   ZERO: .35
   CF: 13.70491
8. HORIZONTAL SHEAR LOAD CELL:
   ZERO: -2
   CF: 6.70298
9. HORIZONTAL DISP. TRANSDUCER, X:
   ZERO: 1.097
   CF: -1.81917
10. HORIZONTAL DISP. TRANSDUCER, Y:
    ZERO: -1.61
    CF: .261
11. VERTICAL DISP. TRANSDUCER, Z1:
    ZERO: .556
    CF: .28883
12. VERTICAL DISP. TRANSDUCER, Z2:
    ZERO: .39
    CF: .29569

Pt. No.	Str.X (%)	Str.Y (%)	SigV (ksc)	TauH (ksc)	Eu (ksc)	TauH / SigVc	DelU / SigVc	SigV / SigVc	TauH / SigV	TauH / Cu	Eu / Cu
1	+0.000	+0.000	3.004	-0.002	+9999.0	-.001	+0.000	+1.000	-.001	-0.003	+9999.0
2	+0.016	+0.002	3.004	-0.001	-25.0	-.000	-0.000	+1.000	-.000	-0.002	-44.0
3	+0.016	+0.002	2.997	-0.001	-18.7	-.000	+0.002	+0.998	-.000	-0.002	-33.0
4	+0.016	+0.002	2.990	-0.000	-6.2	-.000	+0.005	+0.995	-.000	-0.001	-10.9
5	+0.033	+0.002	2.984	-0.001	-9.5	-.000	+0.007	+0.993	-.000	-0.002	-16.7
6	+0.016	+0.002	2.981	+0.000	+6.4	+.000	+0.008	+0.992	+.000	+0.001	+11.2
7	+0.016	+0.000	2.979	+0.000	+0.1	+.000	+0.008	+0.992	+.000	+0.000	+0.2
8	+0.033	+0.002	2.976	+0.001	+6.2	+.000	+0.009	+0.991	+.000	+0.001	+10.9
9	+0.016	+0.005	2.973	+0.004	+75.3	+.001	+0.010	+0.990	+.001	+0.007	+132.8
10	+0.033	+0.002	2.975	+0.018	+162.8	+.006	+0.010	+0.990	+.006	+0.032	+287.4
11	+0.033	+0.002	2.970	+0.034	+306.9	+.011	+0.011	+0.989	+.011	+0.059	+541.7
12	+0.066	+0.002	2.976	+0.058	+264.6	+.019	+0.009	+0.991	+.019	+0.102	+466.9
13	+0.099	+0.000	2.974	+0.101	+306.8	+.034	+0.010	+0.990	+.034	+0.178	+541.5
14	+0.132	+0.000	2.967	+0.161	+367.9	+.054	+0.012	+0.988	+.054	+0.285	+649.3
15	+0.181	-0.009	2.957	+0.219	+363.2	+.073	+0.016	+0.984	+.074	+0.387	+640.9
16	+0.230	-0.009	2.939	+0.275	+358.7	+.092	+0.022	+0.978	+.094	+0.486	+633.0
17	+0.296	-0.012	2.909	+0.327	+331.5	+.109	+0.032	+0.968	+.112	+0.577	+585.0
18	+0.411	-0.017	2.861	+0.371	+270.7	+.123	+0.048	+0.952	+.130	+0.655	+477.7
19	+0.526	-0.019	2.812	+0.410	+233.4	+.136	+0.064	+0.936	+.146	+0.723	+411.8
20	+0.674	-0.024	2.748	+0.438	+194.6	+.146	+0.085	+0.915	+.159	+0.772	+343.5
21	+0.806	-0.031	2.686	+0.460	+171.4	+.153	+0.106	+0.894	+.171	+0.813	+302.4
22	+0.970	-0.035	2.622	+0.479	+148.0	+.159	+0.127	+0.873	+.183	+0.845	+261.2
23	+1.086	-0.038	2.557	+0.494	+136.5	+.164	+0.149	+0.851	+.193	+0.872	+240.9
24	+1.299	-0.045	2.498	+0.507	+117.0	+.169	+0.168	+0.832	+.203	+0.894	+206.5
25	+1.431	-0.047	2.448	+0.518	+108.7	+.173	+0.185	+0.815	+.212	+0.915	+191.8

TEST NAME : DSSC5

Pt. No.	Str.X (%)	Str.Y (%)	SigV (ksc)	TauH (ksc)	Eu (ksc)	TauH ---- SigVc	DelU ---- SigVc	SigV ---- SigVc	TauH ---- SigV	TauH ---- Cu	Eu -- Cu
26	+1.628	-0.050	2.397	+0.529	+97.4	+.176	+0.202	+0.798	+.221	+0.933	+171.9
27	+1.809	-0.054	2.342	+0.536	+88.9	+.178	+0.220	+0.780	+.229	+0.946	+156.8
28	+1.990	-0.057	2.292	+0.541	+81.6	+.180	+0.237	+0.763	+.236	+0.955	+144.0
29	+2.187	-0.064	2.237	+0.546	+74.9	+.182	+0.255	+0.745	+.244	+0.964	+132.2
30	+2.369	-0.068	2.192	+0.550	+69.7	+.183	+0.270	+0.730	+.251	+0.971	+123.0
31	+2.550	-0.087	2.147	+0.550	+64.7	+.183	+0.285	+0.715	+.256	+0.971	+114.2
32	+2.730	-0.092	2.105	+0.553	+60.7	+.184	+0.299	+0.701	+.263	+0.975	+107.1
33	+2.928	-0.097	2.070	+0.555	+56.8	+.185	+0.311	+0.689	+.268	+0.979	+100.3
34	+3.109	-0.104	2.036	+0.558	+53.8	+.186	+0.322	+0.678	+.274	+0.984	+94.9
35	+3.306	-0.111	1.999	+0.560	+50.8	+.187	+0.335	+0.665	+.280	+0.989	+89.7
36	+3.520	-0.118	1.964	+0.561	+47.8	+.187	+0.346	+0.654	+.286	+0.990	+84.4
37	+3.668	-0.123	1.935	+0.563	+46.0	+.187	+0.356	+0.644	+.291	+0.993	+81.2
38	+3.881	-0.130	1.906	+0.564	+43.6	+.188	+0.366	+0.634	+.296	+0.995	+76.9
39	+4.064	-0.132	1.878	+0.564	+41.6	+.188	+0.375	+0.625	+.300	+0.995	+73.4
40	+4.245	-0.137	1.852	+0.567	+40.1	+.189	+0.383	+0.617	+.306	+1.000	+70.7
41	+4.408	-0.142	1.825	+0.566	+38.5	+.188	+0.393	+0.607	+.310	+0.999	+68.0
42	+4.622	-0.149	1.799	+0.567	+36.8	+.189	+0.401	+0.599	+.315	+1.000	+64.9
43	+4.803	-0.153	1.780	+0.566	+35.4	+.188	+0.408	+0.592	+.318	+0.999	+62.4
44	+4.984	-0.156	1.760	+0.565	+34.0	+.188	+0.414	+0.586	+.321	+0.998	+60.1
45	+5.165	-0.165	1.743	+0.563	+32.7	+.188	+0.420	+0.580	+.323	+0.994	+57.8
46	+5.362	-0.182	1.728	+0.563	+31.5	+.187	+0.425	+0.575	+.326	+0.993	+55.5
47	+5.543	-0.189	1.706	+0.562	+30.4	+.187	+0.432	+0.568	+.330	+0.992	+53.7
48	+5.724	-0.196	1.681	+0.562	+29.5	+.187	+0.440	+0.560	+.334	+0.992	+52.0
49	+5.939	-0.212	1.661	+0.561	+28.4	+.187	+0.447	+0.553	+.338	+0.990	+50.0
50	+6.119	-0.219	1.650	+0.561	+27.5	+.187	+0.451	+0.549	+.340	+0.989	+48.5
51	+6.300	-0.224	1.629	+0.561	+26.7	+.187	+0.458	+0.542	+.344	+0.990	+47.1
52	+6.497	-0.231	1.613	+0.560	+25.9	+.187	+0.463	+0.537	+.347	+0.989	+45.7
53	+6.663	-0.241	1.604	+0.561	+25.3	+.187	+0.466	+0.534	+.350	+0.990	+44.6
54	+6.843	-0.257	1.586	+0.562	+24.6	+.187	+0.472	+0.528	+.354	+0.992	+43.5
55	+7.056	-0.267	1.572	+0.561	+23.8	+.187	+0.477	+0.523	+.357	+0.989	+42.1
56	+7.237	-0.274	1.562	+0.557	+23.1	+.185	+0.480	+0.520	+.357	+0.983	+40.8
57	+7.453	-0.283	1.547	+0.557	+22.4	+.185	+0.485	+0.515	+.360	+0.983	+39.6
58	+7.632	-0.293	1.533	+0.557	+21.9	+.186	+0.490	+0.510	+.364	+0.984	+38.7
59	+7.831	-0.295	1.519	+0.557	+21.3	+.185	+0.494	+0.506	+.366	+0.983	+37.6
60	+8.028	-0.304	1.505	+0.556	+20.8	+.185	+0.499	+0.501	+.369	+0.981	+36.7
61	+8.208	-0.314	1.490	+0.556	+20.3	+.185	+0.504	+0.496	+.373	+0.981	+35.8
62	+8.389	-0.328	1.482	+0.555	+19.9	+.185	+0.507	+0.493	+.375	+0.980	+35.0
63	+8.585	-0.333	1.468	+0.554	+19.3	+.184	+0.511	+0.489	+.377	+0.977	+34.1
64	+8.767	-0.337	1.459	+0.554	+18.9	+.184	+0.514	+0.486	+.379	+0.977	+33.4
65	+8.965	-0.345	1.450	+0.553	+18.5	+.184	+0.517	+0.483	+.381	+0.975	+32.6
66	+9.162	-0.354	1.442	+0.552	+18.1	+.184	+0.520	+0.480	+.383	+0.973	+31.9
67	+9.377	-0.361	1.434	+0.551	+17.6	+.183	+0.523	+0.477	+.384	+0.972	+31.1
68	+9.540	-0.375	1.424	+0.550	+17.3	+.183	+0.526	+0.474	+.386	+0.970	+30.5
69	+9.721	-0.380	1.414	+0.548	+16.9	+.183	+0.529	+0.471	+.388	+0.968	+29.9
70	+9.917	-0.392	1.404	+0.548	+16.6	+.182	+0.533	+0.467	+.390	+0.967	+29.3
71	+10.132	-0.394	1.394	+0.545	+16.1	+.182	+0.536	+0.464	+.391	+0.962	+28.5
72	+10.297	-0.404	1.381	+0.545	+15.9	+.181	+0.540	+0.460	+.395	+0.962	+28.0
73	+10.494	-0.413	1.370	+0.544	+15.6	+.181	+0.544	+0.456	+.397	+0.961	+27.5

TEST NAME : DSSC5

Pt. No.	Str.X (%)	Str.Y (%)	SigV (ksc)	TauH (ksc)	Eu (ksc)	TauH / SigVc	DelU / SigVc	SigV / SigVc	TauH / SigV	TauH / Cu	Eu / Cu
74	+10.708	-0.420	1.362	+0.543	+15.2	+.181	+0.547	+0.453	+.399	+0.958	+26.8
75	+10.905	-0.427	1.353	+0.540	+14.9	+.180	+0.550	+0.450	+.399	+0.953	+26.2
76	+11.103	-0.437	1.343	+0.539	+14.6	+.179	+0.553	+0.447	+.401	+0.951	+25.7
77	+11.282	-0.444	1.330	+0.538	+14.3	+.179	+0.557	+0.443	+.405	+0.950	+25.3
78	+11.481	-0.453	1.318	+0.536	+14.0	+.178	+0.561	+0.439	+.406	+0.945	+24.7
79	+11.664	-0.465	1.310	+0.534	+13.7	+.178	+0.564	+0.436	+.408	+0.943	+24.3
80	+11.857	-0.472	1.300	+0.533	+13.5	+.177	+0.567	+0.433	+.410	+0.940	+23.8
81	+12.043	-0.477	1.291	+0.531	+13.2	+.177	+0.570	+0.430	+.411	+0.938	+23.4
82	+12.219	-0.484	1.286	+0.530	+13.0	+.176	+0.572	+0.428	+.412	+0.935	+22.9
83	+12.419	-0.486	1.280	+0.528	+12.8	+.176	+0.574	+0.426	+.413	+0.933	+22.5
84	+12.597	-0.503	1.274	+0.528	+12.6	+.176	+0.576	+0.424	+.414	+0.931	+22.2
85	+12.795	-0.507	1.264	+0.525	+12.3	+.175	+0.579	+0.421	+.415	+0.926	+21.7
86	+12.978	-0.512	1.258	+0.523	+12.1	+.174	+0.581	+0.419	+.415	+0.922	+21.3
87	+13.173	-0.517	1.252	+0.522	+11.9	+.174	+0.583	+0.417	+.417	+0.922	+21.0
88	+13.373	-0.519	1.240	+0.519	+11.6	+.173	+0.587	+0.413	+.418	+0.916	+20.5
89	+13.554	-0.526	1.232	+0.517	+11.4	+.172	+0.590	+0.410	+.419	+0.912	+20.2
90	+13.735	-0.533	1.225	+0.513	+11.2	+.171	+0.592	+0.408	+.419	+0.905	+19.8
91	+13.932	-0.538	1.216	+0.511	+11.0	+.170	+0.595	+0.405	+.420	+0.902	+19.4
92	+14.097	-0.552	1.208	+0.509	+10.8	+.169	+0.598	+0.402	+.421	+0.898	+19.1
93	+14.310	-0.555	1.200	+0.504	+10.6	+.168	+0.600	+0.400	+.420	+0.890	+18.7
94	+14.524	-0.557	1.186	+0.503	+10.4	+.167	+0.605	+0.395	+.424	+0.887	+18.3
95	+14.708	-0.562	1.173	+0.499	+10.2	+.166	+0.610	+0.390	+.426	+0.881	+18.0
96	+14.883	-0.566	1.161	+0.497	+10.0	+.165	+0.614	+0.386	+.428	+0.877	+17.7
97	+15.083	-0.573	1.152	+0.494	+9.8	+.164	+0.616	+0.384	+.429	+0.871	+17.3
98	+15.281	-0.576	1.140	+0.490	+9.6	+.163	+0.621	+0.379	+.430	+0.865	+17.0
99	+15.465	-0.578	1.126	+0.490	+9.5	+.163	+0.625	+0.375	+.435	+0.864	+16.8
100	+15.659	-0.583	1.115	+0.485	+9.3	+.162	+0.629	+0.371	+.435	+0.856	+16.4
101	+15.873	-0.588	1.100	+0.484	+9.1	+.161	+0.634	+0.366	+.440	+0.854	+16.1
102	+16.057	-0.590	1.087	+0.480	+9.0	+.160	+0.638	+0.362	+.442	+0.847	+15.8
103	+16.251	-0.595	1.072	+0.477	+8.8	+.159	+0.643	+0.357	+.445	+0.841	+15.5
104	+16.435	-0.600	1.066	+0.475	+8.7	+.158	+0.645	+0.355	+.446	+0.839	+15.3
105	+16.630	-0.604	1.053	+0.472	+8.5	+.157	+0.649	+0.351	+.448	+0.832	+15.0
106	+16.827	-0.607	1.039	+0.469	+8.4	+.156	+0.654	+0.346	+.451	+0.827	+14.8
107	+17.005	-0.609	1.027	+0.468	+8.2	+.156	+0.658	+0.342	+.455	+0.825	+14.6
108	+17.219	-0.613	1.015	+0.465	+8.1	+.155	+0.662	+0.338	+.458	+0.821	+14.3
109	+17.422	-0.611	1.002	+0.463	+8.0	+.154	+0.667	+0.333	+.462	+0.816	+14.1
110	+17.613	-0.613	0.987	+0.459	+7.8	+.153	+0.671	+0.329	+.465	+0.810	+13.8
111	+17.797	-0.614	0.982	+0.456	+7.7	+.152	+0.673	+0.327	+.465	+0.805	+13.6
112	+18.011	-0.614	0.973	+0.453	+7.5	+.151	+0.676	+0.324	+.466	+0.799	+13.3
113	+18.143	-0.616	0.963	+0.450	+7.4	+.150	+0.679	+0.321	+.467	+0.793	+13.1
114	+18.390	-0.616	0.947	+0.446	+7.3	+.148	+0.685	+0.315	+.471	+0.787	+12.8
115	+18.623	-0.616	0.936	+0.441	+7.1	+.147	+0.688	+0.312	+.471	+0.778	+12.5
116	+18.801	-0.623	0.928	+0.437	+7.0	+.146	+0.691	+0.309	+.471	+0.771	+12.3
117	+19.015	-0.625	0.912	+0.433	+6.8	+.144	+0.696	+0.304	+.474	+0.764	+12.1
118	+19.199	-0.628	0.902	+0.430	+6.7	+.143	+0.700	+0.300	+.477	+0.759	+11.9
119	+19.409	-0.632	0.892	+0.427	+6.6	+.142	+0.703	+0.297	+.478	+0.753	+11.6
120	+19.574	-0.630	0.883	+0.423	+6.5	+.141	+0.706	+0.294	+.479	+0.746	+11.4

TEST NAME : DSSC5

Pt. No.	Str.X (%)	Str.Y (%)	SigV (ksc)	TauH (ksc)	Eu (ksc)	TauH ---- SigVc	DelU ---- SigVc	SigV ---- SigVc	TauH ---- SigV	TauH ---- Cu	Eu -- Cu
121	+19.768	-0.635	0.871	+0.419	+6.4	+.140	+0.710	+0.290	+.481	+0.740	+11.2
122	+19.985	-0.635	0.861	+0.417	+6.3	+.139	+0.713	+0.287	+.484	+0.736	+11.0
123	+20.166	-0.637	0.849	+0.414	+6.2	+.138	+0.717	+0.283	+.488	+0.731	+10.9
124	+20.351	-0.637	0.840	+0.412	+6.1	+.137	+0.720	+0.280	+.490	+0.726	+10.7
125	+20.561	-0.640	0.828	+0.407	+5.9	+.135	+0.724	+0.276	+.492	+0.718	+10.5
126	+20.745	-0.637	0.820	+0.402	+5.8	+.134	+0.727	+0.273	+.490	+0.710	+10.3
127	+20.923	-0.644	0.811	+0.398	+5.7	+.133	+0.730	+0.270	+.491	+0.703	+10.1
128	+21.120	-0.647	0.803	+0.394	+5.6	+.131	+0.733	+0.267	+.491	+0.696	+9.9
129	+21.334	-0.644	0.790	+0.391	+5.5	+.130	+0.737	+0.263	+.494	+0.689	+9.7
130	+21.498	-0.649	0.776	+0.387	+5.4	+.129	+0.742	+0.258	+.498	+0.682	+9.5
131	+21.712	-0.649	0.765	+0.382	+5.3	+.127	+0.745	+0.255	+.499	+0.674	+9.3
132	+21.910	-0.651	0.760	+0.378	+5.2	+.126	+0.747	+0.253	+.497	+0.667	+9.1
133	+22.091	-0.654	0.749	+0.372	+5.1	+.124	+0.751	+0.249	+.497	+0.657	+8.9
134	+22.288	-0.654	0.742	+0.368	+5.0	+.123	+0.753	+0.247	+.496	+0.650	+8.7
135	+22.489	-0.656	0.730	+0.364	+4.9	+.121	+0.757	+0.243	+.499	+0.642	+8.6
136	+22.699	-0.658	0.718	+0.359	+4.7	+.119	+0.761	+0.239	+.499	+0.633	+8.4
137	+22.880	-0.661	0.706	+0.355	+4.7	+.118	+0.765	+0.235	+.504	+0.627	+8.2
138	+23.077	-0.658	0.695	+0.352	+4.6	+.117	+0.769	+0.231	+.506	+0.621	+8.1
139	+23.275	-0.661	0.683	+0.348	+4.5	+.116	+0.773	+0.227	+.509	+0.614	+7.9
140	+23.472	-0.663	0.676	+0.345	+4.4	+.115	+0.775	+0.225	+.510	+0.608	+7.8
141	+23.637	-0.665	0.667	+0.343	+4.4	+.114	+0.778	+0.222	+.514	+0.606	+7.7
142	+23.818	-0.665	0.661	+0.341	+4.3	+.113	+0.780	+0.220	+.515	+0.601	+7.6
143	+24.003	-0.668	0.655	+0.337	+4.2	+.112	+0.782	+0.218	+.516	+0.595	+7.4
144	+24.180	-0.670	0.647	+0.334	+4.1	+.111	+0.784	+0.216	+.516	+0.589	+7.3
145	+24.344	-0.673	0.639	+0.330	+4.1	+.110	+0.787	+0.213	+.516	+0.582	+7.2
146	+24.537	-0.675	0.635	+0.329	+4.0	+.110	+0.789	+0.211	+.518	+0.581	+7.1
147	+24.788	-0.673	0.628	+0.327	+4.0	+.109	+0.791	+0.209	+.520	+0.577	+7.0
148	+24.986	-0.675	0.617	+0.323	+3.9	+.107	+0.795	+0.205	+.523	+0.569	+6.8
149	+25.199	-0.675	0.611	+0.319	+3.8	+.106	+0.797	+0.203	+.523	+0.563	+6.7
150	+25.380	-0.673	0.597	+0.316	+3.7	+.105	+0.801	+0.199	+.530	+0.558	+6.6
151	+25.611	-0.673	0.589	+0.313	+3.7	+.104	+0.804	+0.196	+.531	+0.552	+6.5
152	+25.808	-0.673	0.584	+0.309	+3.6	+.103	+0.806	+0.194	+.529	+0.545	+6.3
153	+25.984	-0.675	0.576	+0.306	+3.5	+.102	+0.808	+0.192	+.531	+0.539	+6.2
154	+26.203	-0.675	0.569	+0.303	+3.5	+.101	+0.810	+0.190	+.532	+0.534	+6.1
155	+26.384	-0.675	0.558	+0.299	+3.4	+.100	+0.814	+0.186	+.537	+0.528	+6.0
156	+26.597	-0.675	0.549	+0.296	+3.3	+.099	+0.817	+0.183	+.539	+0.522	+5.9
157	+26.795	-0.673	0.541	+0.294	+3.3	+.098	+0.820	+0.180	+.543	+0.518	+5.8
158	+26.976	-0.675	0.534	+0.291	+3.2	+.097	+0.822	+0.178	+.545	+0.513	+5.7
159	+27.168	-0.675	0.527	+0.288	+3.2	+.096	+0.824	+0.176	+.547	+0.509	+5.6
160	+27.349	-0.675	0.524	+0.285	+3.1	+.095	+0.826	+0.174	+.545	+0.504	+5.5
161	+27.568	-0.675	0.517	+0.282	+3.1	+.094	+0.828	+0.172	+.545	+0.497	+5.4
162	+27.749	-0.673	0.509	+0.278	+3.0	+.093	+0.831	+0.169	+.547	+0.491	+5.3
163	+27.946	-0.673	0.503	+0.275	+3.0	+.092	+0.832	+0.168	+.546	+0.485	+5.2
164	+28.111	-0.673	0.498	+0.273	+2.9	+.091	+0.834	+0.166	+.549	+0.482	+5.1
165	+28.308	-0.673	0.492	+0.270	+2.9	+.090	+0.836	+0.164	+.549	+0.477	+5.1
166	+28.506	-0.675	0.484	+0.267	+2.8	+.089	+0.839	+0.161	+.550	+0.471	+5.0
167	+28.686	-0.673	0.475	+0.264	+2.8	+.088	+0.842	+0.158	+.556	+0.466	+4.9
168	+28.900	-0.673	0.470	+0.261	+2.7	+.087	+0.844	+0.156	+.555	+0.460	+4.8
169	+29.065	-0.673	0.460	+0.260	+2.7	+.086	+0.847	+0.153	+.565	+0.458	+4.7
170	+29.279	-0.673	0.451	+0.257	+2.6	+.086	+0.850	+0.150	+.571	+0.454	+4.7

TEST NAME :-DSSC5

Pt. No.	Str.X (%)	Str.Y (%)	SigV (ksc)	TauH (ksc)	Eu (ksc)	TauH ---- SigVc	DelU ---- SigVc	SigV ---- SigVc	TauH ---- SigV	TauH ---- Cu	Eu -- Cu
171	+29.460	-0.673	0.441	+0.253	+2.6	+.084	+0.853	+0.147	+.574	+0.447	+4.6
172	+29.657	-0.675	0.438	+0.251	+2.5	+.084	+0.854	+0.146	+.574	+0.444	+4.5
173	+29.854	-0.673	0.435	+0.248	+2.5	+.082	+0.855	+0.145	+.570	+0.437	+4.4
174	+30.052	-0.673	0.428	+0.246	+2.5	+.082	+0.858	+0.142	+.575	+0.434	+4.3
175	+30.249	-0.673	0.425	+0.243	+2.4	+.081	+0.859	+0.141	+.572	+0.429	+4.3
176	+30.419	-0.666	0.420	+0.241	+2.4	+.080	+0.860	+0.140	+.574	+0.426	+4.2
177	+30.616	-0.670	0.417	+0.239	+2.3	+.080	+0.861	+0.139	+.574	+0.422	+4.1
178	+30.808	-0.670	0.411	+0.237	+2.3	+.079	+0.863	+0.137	+.576	+0.418	+4.1

Ko CONSOLIDATED MDSS TEST
MIT GEOTECHNICAL LAB

FILE NAME: DSSC6.PRN

REDUCTION DATA
UNITS: (kg,cm,mVOLTS,VOLTS)

1. TEST NAME : DSSC6
2. DATE : 09-21-1987
3. OCR : 1
4. VER. CONSOLIDATION STRESS (KSC) : +2.990
5. HOR. CONSOLIDATION STRESS (KSC) : +0.000
6. PRE-SHEAR SAMPLE HEIGHT (cm) : +1.9064
7. VERTICAL STRESS LOAD CELL:
   ZERO: .2
   CF: 13.70491
8. HORIZONTAL SHEAR LOAD CELL:
   ZERO: -2.04
   CF: 6.70298
9. HORIZONTAL DISP. TRANSDUCER, X:
   ZERO: 1.4203
   CF: -1.81917
10. HORIZONTAL DISP. TRANSDUCER, Y:
   ZERO: 2.592
   CF: .261
11. VERTICAL DISP. TRANSDUCER, Z1:
   ZERO: .05975
   CF: .28883
12. VERTICAL DISP. TRANSDUCER, Z2:
   ZERO: .8279
   CF: .29569
13. CONSTANT HEIGHT TRANSDUCER, Z:
   ZERO: .14781
   CF: .3014

Pt. No.	Str.X (%)	Str.Y (%)	SigV (ksc)	TauH (ksc)	Eu (ksc)	TauH / SigVc	DelU / SigVc	SigV / SigVc	TauH / SigV	TauH / Cu	Eu / Cu
1	+0.000	+0.000	2.990	-0.002	+9999.0	-.001	+0.000	+1.000	-.001	-0.003	+9999.0
2	-0.009	+0.000	2.990	-0.001	+23.2	-.000	+0.000	+1.000	-.000	-0.001	+42.1
3	-0.002	+0.000	2.986	-0.001	+177.2	-.000	+0.001	+0.999	-.000	-0.002	+320.8
4	+0.002	+0.002	2.979	-0.001	-177.7	-.000	+0.004	+0.996	-.000	-0.002	-321.6
5	+0.003	+0.000	2.977	-0.001	-89.0	-.000	+0.004	+0.996	-.000	-0.002	-161.0
6	+0.009	+0.002	2.972	-0.001	-23.7	-.000	+0.006	+0.994	-.000	-0.001	-42.9
7	+0.010	+0.000	2.962	+0.002	+60.5	+.001	+0.010	+0.990	+.001	+0.004	+109.5
8	+0.014	+0.000	2.959	+0.014	+308.7	+.005	+0.011	+0.989	+.005	+0.026	+558.8
9	+0.019	-0.002	2.955	+0.032	+509.1	+.011	+0.012	+0.988	+.011	+0.058	+921.4
10	+0.017	-0.002	2.959	+0.054	+951.3	+.018	+0.011	+0.989	+.018	+0.098	+1721.8
11	+0.022	+0.000	2.962	+0.088	+1181.1	+.029	+0.009	+0.991	+.030	+0.159	+2137.6
12	+0.026	+0.002	2.971	+0.128	+1497.2	+.043	+0.006	+0.994	+.043	+0.232	+2709.7
13	+0.038	+0.005	2.976	+0.180	+1434.0	+.060	+0.005	+0.995	+.061	+0.326	+2595.3
14	+0.104	+0.002	2.972	+0.235	+675.9	+.079	+0.006	+0.994	+.079	+0.426	+1223.4
15	+0.187	-0.005	2.946	+0.293	+471.0	+.098	+0.015	+0.985	+.099	+0.530	+852.4
16	+0.288	-0.005	2.891	+0.345	+359.6	+.115	+0.033	+0.967	+.119	+0.624	+650.9
17	+0.402	-0.005	2.797	+0.385	+286.7	+.129	+0.065	+0.935	+.137	+0.696	+519.0
18	+0.541	+0.000	2.680	+0.421	+233.6	+.141	+0.104	+0.896	+.157	+0.762	+422.7
19	+0.688	+0.002	2.586	+0.446	+194.6	+.149	+0.135	+0.865	+.173	+0.808	+352.3
20	+0.841	+0.007	2.508	+0.465	+165.9	+.155	+0.161	+0.839	+.185	+0.841	+300.3
21	+1.005	+0.010	2.436	+0.481	+143.7	+.161	+0.185	+0.815	+.198	+0.871	+260.1
22	+1.172	+0.017	2.368	+0.494	+126.4	+.165	+0.208	+0.792	+.209	+0.894	+228.8

TEST NAME : DSSC6

Pt. No.	Str.X (%)	Str.Y (%)	SigV (ksc)	TauH (ksc)	Eu (ksc)	TauH ---- SigVc	DelU ---- SigVc	SigV ---- SigVc	TauH ---- SigV	TauH ---- Cu	Eu -- Cu
23	+1.354	+0.022	2.302	+0.507	+112.2	+.169	+0.230	+0.770	+.220	+0.917	+203.1
24	+1.532	+0.027	2.237	+0.515	+100.9	+.172	+0.252	+0.748	+.230	+0.933	+182.6
25	+1.719	+0.034	2.182	+0.523	+91.4	+.175	+0.270	+0.730	+.240	+0.947	+165.3
26	+1.923	+0.039	2.130	+0.531	+82.9	+.178	+0.287	+0.713	+.249	+0.961	+150.0
27	+2.121	+0.049	2.081	+0.536	+75.8	+.179	+0.304	+0.696	+.258	+0.970	+137.2
28	+2.315	+0.056	2.031	+0.541	+70.1	+.181	+0.321	+0.679	+.266	+0.979	+126.9
29	+2.508	+0.064	1.988	+0.544	+65.0	+.182	+0.335	+0.665	+.273	+0.984	+117.6
30	+2.700	+0.071	1.947	+0.546	+60.7	+.183	+0.349	+0.651	+.281	+0.988	+109.8
31	+2.898	+0.079	1.906	+0.545	+56.4	+.182	+0.362	+0.638	+.286	+0.986	+102.1
32	+3.098	+0.088	1.870	+0.547	+53.0	+.183	+0.375	+0.625	+.293	+0.990	+95.9
33	+3.304	+0.096	1.834	+0.548	+49.8	+.183	+0.387	+0.613	+.299	+0.993	+90.1
34	+3.508	+0.103	1.798	+0.550	+47.1	+.184	+0.399	+0.601	+.306	+0.996	+85.2
35	+3.712	+0.111	1.766	+0.550	+44.4	+.184	+0.409	+0.591	+.311	+0.995	+80.4
36	+3.903	+0.118	1.738	+0.550	+42.3	+.184	+0.419	+0.581	+.317	+0.996	+76.5
37	+4.092	+0.125	1.713	+0.550	+40.3	+.184	+0.427	+0.573	+.321	+0.996	+73.0
38	+4.278	+0.133	1.689	+0.549	+38.5	+.184	+0.435	+0.565	+.325	+0.994	+69.7
39	+4.460	+0.140	1.668	+0.550	+37.0	+.184	+0.442	+0.558	+.330	+0.996	+67.0
40	+4.645	+0.147	1.642	+0.550	+35.5	+.184	+0.451	+0.549	+.335	+0.996	+64.3
41	+4.829	+0.152	1.620	+0.550	+34.1	+.184	+0.458	+0.542	+.339	+0.995	+61.8
42	+5.018	+0.160	1.604	+0.551	+32.9	+.184	+0.464	+0.536	+.343	+0.997	+59.6
43	+5.212	+0.160	1.585	+0.552	+31.8	+.185	+0.470	+0.530	+.348	+0.999	+57.5
44	+5.406	+0.165	1.565	+0.551	+30.6	+.184	+0.477	+0.523	+.352	+0.997	+55.4
45	+5.615	+0.172	1.547	+0.552	+29.5	+.184	+0.482	+0.518	+.356	+0.998	+53.3
46	+5.810	+0.174	1.531	+0.553	+28.5	+.185	+0.488	+0.512	+.361	+1.000	+51.6
47	+6.007	+0.179	1.510	+0.552	+27.6	+.185	+0.495	+0.505	+.365	+0.998	+49.9
48	+6.200	+0.184	1.496	+0.551	+26.7	+.184	+0.500	+0.500	+.368	+0.997	+48.2
49	+6.389	+0.189	1.481	+0.549	+25.8	+.183	+0.505	+0.495	+.370	+0.993	+46.6
50	+6.586	+0.199	1.465	+0.548	+25.0	+.183	+0.510	+0.490	+.374	+0.992	+45.2
51	+6.779	+0.201	1.450	+0.548	+24.3	+.183	+0.515	+0.485	+.378	+0.992	+43.9
52	+6.978	+0.204	1.435	+0.546	+23.5	+.183	+0.520	+0.480	+.381	+0.989	+42.5
53	+7.175	+0.214	1.420	+0.546	+22.8	+.182	+0.525	+0.475	+.384	+0.987	+41.3
54	+7.368	+0.224	1.406	+0.545	+22.2	+.182	+0.530	+0.470	+.388	+0.987	+40.2
55	+7.567	+0.226	1.391	+0.546	+21.6	+.183	+0.535	+0.465	+.392	+0.988	+39.2
56	+7.769	+0.231	1.383	+0.545	+21.0	+.182	+0.537	+0.463	+.394	+0.986	+38.1
57	+7.959	+0.241	1.366	+0.543	+20.5	+.182	+0.543	+0.457	+.398	+0.983	+37.1
58	+8.156	+0.251	1.354	+0.543	+20.0	+.181	+0.547	+0.453	+.401	+0.982	+36.1
59	+8.347	+0.258	1.343	+0.542	+19.5	+.181	+0.551	+0.449	+.403	+0.980	+35.2
60	+8.548	+0.258	1.331	+0.541	+19.0	+.181	+0.555	+0.445	+.406	+0.979	+34.3
61	+8.746	+0.263	1.321	+0.539	+18.5	+.180	+0.558	+0.442	+.408	+0.975	+33.5
62	+8.943	+0.268	1.313	+0.537	+18.0	+.180	+0.561	+0.439	+.409	+0.971	+32.6
63	+9.144	+0.268	1.302	+0.537	+17.6	+.179	+0.564	+0.436	+.412	+0.971	+31.9
64	+9.339	+0.275	1.288	+0.536	+17.2	+.179	+0.569	+0.431	+.416	+0.970	+31.2
65	+9.539	+0.280	1.281	+0.537	+16.9	+.180	+0.572	+0.428	+.419	+0.972	+30.6
66	+9.746	+0.283	1.274	+0.535	+16.5	+.179	+0.574	+0.426	+.420	+0.969	+29.8
67	+9.957	+0.290	1.263	+0.535	+16.1	+.179	+0.578	+0.422	+.423	+0.967	+29.1
68	+10.161	+0.295	1.252	+0.532	+15.7	+.178	+0.581	+0.419	+.425	+0.963	+28.4
69	+10.371	+0.297	1.244	+0.531	+15.4	+.178	+0.584	+0.416	+.427	+0.961	+27.8
70	+10.570	+0.309	1.233	+0.531	+15.1	+.177	+0.588	+0.412	+.430	+0.960	+27.3

TEST NAME : DSSC6

Pt. No.	Str.X (%)	Str.Y (%)	SigV (ksc)	TauH (ksc)	Eu (ksc)	TauH ---- SigVc	DelU ---- SigVc	SigV ---- SigVc	TauH ---- SigV	TauH ---- Cu	Eu -- Cu
71	+10.786	+0.310	1.226	+0.530	+14.7	+.177	+0.590	+0.410	+.432	+0.958	+26.7
72	+10.982	+0.312	1.217	+0.526	+14.4	+.176	+0.593	+0.407	+.432	+0.952	+26.0
73	+11.176	+0.322	1.208	+0.526	+14.1	+.176	+0.596	+0.404	+.435	+0.952	+25.5
74	+11.375	+0.322	1.198	+0.524	+13.8	+.175	+0.599	+0.401	+.437	+0.948	+25.0
75	+11.587	+0.334	1.189	+0.523	+13.5	+.175	+0.602	+0.398	+.440	+0.947	+24.5
76	+11.775	+0.339	1.182	+0.521	+13.3	+.174	+0.605	+0.395	+.440	+0.942	+24.0
77	+11.955	+0.341	1.172	+0.519	+13.0	+.173	+0.608	+0.392	+.442	+0.939	+23.6
78	+12.140	+0.354	1.166	+0.519	+12.8	+.173	+0.610	+0.390	+.445	+0.939	+23.2
79	+12.325	+0.356	1.161	+0.517	+12.6	+.173	+0.612	+0.388	+.446	+0.936	+22.8
80	+12.529	+0.359	1.152	+0.517	+12.4	+.173	+0.615	+0.385	+.449	+0.936	+22.4
81	+12.722	+0.368	1.141	+0.514	+12.1	+.172	+0.618	+0.382	+.450	+0.930	+21.9
82	+12.912	+0.368	1.135	+0.511	+11.9	+.171	+0.621	+0.379	+.450	+0.925	+21.5
83	+13.106	+0.373	1.129	+0.512	+11.7	+.171	+0.622	+0.378	+.454	+0.927	+21.2
84	+13.290	+0.378	1.120	+0.509	+11.5	+.170	+0.626	+0.374	+.455	+0.922	+20.8
85	+13.497	+0.383	1.115	+0.510	+11.3	+.171	+0.627	+0.373	+.458	+0.923	+20.5
86	+13.695	+0.383	1.107	+0.507	+11.1	+.170	+0.630	+0.370	+.458	+0.918	+20.1
87	+13.907	+0.388	1.099	+0.506	+10.9	+.169	+0.632	+0.368	+.460	+0.916	+19.8
88	+14.106	+0.396	1.092	+0.503	+10.7	+.168	+0.635	+0.365	+.461	+0.910	+19.4
89	+14.297	+0.403	1.084	+0.500	+10.5	+.167	+0.637	+0.363	+.461	+0.906	+19.0
90	+14.501	+0.410	1.076	+0.498	+10.3	+.167	+0.640	+0.360	+.463	+0.901	+18.6
91	+14.694	+0.418	1.067	+0.496	+10.1	+.166	+0.643	+0.357	+.465	+0.898	+18.3
92	+14.885	+0.427	1.061	+0.494	+10.0	+.165	+0.645	+0.355	+.466	+0.894	+18.0
93	+15.087	+0.427	1.054	+0.494	+9.8	+.165	+0.648	+0.352	+.469	+0.894	+17.8
94	+15.289	+0.432	1.042	+0.490	+9.6	+.164	+0.652	+0.348	+.471	+0.887	+17.4
95	+15.483	+0.440	1.034	+0.487	+9.4	+.163	+0.654	+0.346	+.471	+0.882	+17.1
96	+15.683	+0.442	1.028	+0.487	+9.3	+.163	+0.656	+0.344	+.474	+0.881	+16.9
97	+15.886	+0.445	1.015	+0.484	+9.1	+.162	+0.661	+0.339	+.477	+0.876	+16.5
98	+16.075	+0.454	1.008	+0.481	+9.0	+.161	+0.663	+0.337	+.477	+0.870	+16.2
99	+16.264	+0.454	1.000	+0.478	+8.8	+.160	+0.666	+0.334	+.478	+0.865	+16.0
100	+16.469	+0.459	0.992	+0.478	+8.7	+.160	+0.668	+0.332	+.482	+0.865	+15.8
101	+16.679	+0.462	0.983	+0.476	+8.6	+.159	+0.671	+0.329	+.484	+0.862	+15.5
102	+16.883	+0.462	0.976	+0.472	+8.4	+.158	+0.673	+0.327	+.483	+0.854	+15.2
103	+17.073	+0.464	0.965	+0.468	+8.2	+.157	+0.677	+0.323	+.485	+0.848	+14.9
104	+17.277	+0.467	0.955	+0.466	+8.1	+.156	+0.680	+0.320	+.488	+0.844	+14.7
105	+17.472	+0.474	0.947	+0.464	+8.0	+.155	+0.683	+0.317	+.490	+0.840	+14.4
106	+17.677	+0.481	0.937	+0.463	+7.8	+.155	+0.687	+0.313	+.494	+0.837	+14.2
107	+17.878	+0.484	0.930	+0.460	+7.7	+.154	+0.689	+0.311	+.495	+0.832	+14.0
108	+18.087	+0.486	0.921	+0.459	+7.6	+.153	+0.692	+0.308	+.498	+0.830	+13.8
109	+18.306	+0.491	0.913	+0.456	+7.5	+.152	+0.695	+0.305	+.499	+0.824	+13.5
110	+18.518	+0.491	0.903	+0.452	+7.3	+.151	+0.698	+0.302	+.501	+0.818	+13.3
111	+18.720	+0.494	0.893	+0.449	+7.2	+.150	+0.701	+0.299	+.503	+0.813	+13.0
112	+18.924	+0.499	0.887	+0.446	+7.1	+.149	+0.703	+0.297	+.503	+0.807	+12.8
113	+19.119	+0.501	0.880	+0.445	+7.0	+.149	+0.706	+0.294	+.505	+0.805	+12.6
114	+19.313	+0.506	0.872	+0.441	+6.9	+.148	+0.708	+0.292	+.506	+0.799	+12.4
115	+19.504	+0.509	0.862	+0.440	+6.8	+.147	+0.712	+0.288	+.511	+0.797	+12.3
116	+19.701	+0.516	0.858	+0.439	+6.7	+.147	+0.713	+0.287	+.512	+0.795	+12.1
117	+19.896	+0.516	0.846	+0.435	+6.6	+.145	+0.717	+0.283	+.514	+0.787	+11.9
118	+20.099	+0.516	0.839	+0.433	+6.5	+.145	+0.719	+0.281	+.516	+0.783	+11.7

TEST NAME : DSSC6

Pt. No.	Str.X (%)	Str.Y (%)	SigV (ksc)	TauH (ksc)	Eu (ksc)	TauH / SigVc	DelU / SigVc	SigV / SigVc	TauH / SigV	TauH / Cu	Eu / Cu
119	+20.288	+0.518	0.835	+0.430	+6.4	+.144	+0.721	+0.279	+.514	+0.777	+11.5
120	+20.494	+0.521	0.828	+0.428	+6.3	+.143	+0.723	+0.277	+.517	+0.775	+11.3
121	+20.703	+0.526	0.818	+0.424	+6.1	+.142	+0.726	+0.274	+.518	+0.768	+11.1
122	+20.891	+0.531	0.811	+0.420	+6.0	+.141	+0.729	+0.271	+.518	+0.760	+10.9
123	+21.076	+0.533	0.805	+0.419	+6.0	+.140	+0.731	+0.269	+.520	+0.758	+10.8
124	+21.276	+0.533	0.796	+0.416	+5.9	+.139	+0.734	+0.266	+.523	+0.754	+10.6
125	+21.485	+0.535	0.790	+0.414	+5.8	+.138	+0.736	+0.264	+.523	+0.748	+10.5
126	+21.684	+0.535	0.780	+0.411	+5.7	+.137	+0.739	+0.261	+.526	+0.743	+10.3
127	+21.896	+0.536	0.773	+0.410	+5.6	+.137	+0.741	+0.259	+.530	+0.741	+10.2
128	+22.091	+0.540	0.768	+0.406	+5.5	+.136	+0.743	+0.257	+.528	+0.734	+10.0
129	+22.279	+0.543	0.758	+0.402	+5.4	+.134	+0.747	+0.253	+.530	+0.727	+9.8
130	+22.473	+0.545	0.751	+0.400	+5.3	+.134	+0.749	+0.251	+.533	+0.724	+9.7
131	+22.671	+0.545	0.743	+0.397	+5.3	+.133	+0.751	+0.249	+.535	+0.719	+9.5
132	+22.879	+0.545	0.737	+0.394	+5.2	+.132	+0.754	+0.246	+.535	+0.713	+9.3
133	+23.084	+0.550	0.728	+0.390	+5.1	+.131	+0.756	+0.244	+.536	+0.706	+9.2
134	+23.290	+0.548	0.720	+0.388	+5.0	+.130	+0.759	+0.241	+.538	+0.701	+9.0
135	+23.485	+0.550	0.709	+0.384	+4.9	+.128	+0.763	+0.237	+.541	+0.695	+8.9
136	+23.690	+0.550	0.704	+0.381	+4.8	+.128	+0.765	+0.235	+.542	+0.690	+8.7
137	+23.907	+0.553	0.694	+0.379	+4.8	+.127	+0.768	+0.232	+.546	+0.686	+8.6
138	+24.109	+0.553	0.687	+0.375	+4.7	+.125	+0.770	+0.230	+.546	+0.679	+8.5
139	+24.299	+0.553	0.679	+0.372	+4.6	+.124	+0.773	+0.227	+.548	+0.674	+8.3
140	+24.503	+0.562	0.671	+0.369	+4.5	+.124	+0.775	+0.225	+.550	+0.668	+8.2
141	+24.700	+0.562	0.664	+0.365	+4.4	+.122	+0.778	+0.222	+.549	+0.660	+8.0
142	+24.907	+0.563	0.655	+0.361	+4.4	+.121	+0.781	+0.219	+.552	+0.654	+7.9
143	+25.112	+0.563	0.647	+0.358	+4.3	+.120	+0.784	+0.216	+.554	+0.649	+7.7
144	+25.323	+0.565	0.642	+0.355	+4.2	+.119	+0.785	+0.215	+.554	+0.643	+7.6
145	+25.525	+0.562	0.635	+0.352	+4.1	+.118	+0.788	+0.212	+.554	+0.637	+7.5
146	+25.722	+0.565	0.628	+0.350	+4.1	+.117	+0.790	+0.210	+.557	+0.633	+7.4
147	+25.948	+0.567	0.619	+0.347	+4.0	+.116	+0.793	+0.207	+.561	+0.629	+7.3
148	+26.167	+0.567	0.612	+0.343	+3.9	+.115	+0.795	+0.205	+.561	+0.622	+7.1
149	+26.368	+0.567	0.602	+0.339	+3.9	+.114	+0.799	+0.201	+.564	+0.614	+7.0
150	+26.559	+0.570	0.596	+0.335	+3.8	+.112	+0.801	+0.199	+.562	+0.606	+6.8
151	+26.741	+0.575	0.590	+0.333	+3.7	+.111	+0.803	+0.197	+.564	+0.602	+6.8
152	+26.941	+0.577	0.586	+0.330	+3.7	+.110	+0.804	+0.196	+.563	+0.597	+6.6
153	+27.143	+0.582	0.575	+0.329	+3.6	+.110	+0.808	+0.192	+.571	+0.595	+6.6
154	+27.340	+0.582	0.570	+0.324	+3.6	+.108	+0.809	+0.191	+.569	+0.586	+6.4
155	+27.527	+0.585	0.564	+0.322	+3.5	+.108	+0.811	+0.189	+.571	+0.582	+6.3
156	+27.746	+0.587	0.559	+0.318	+3.4	+.107	+0.813	+0.187	+.570	+0.576	+6.2
157	+27.978	+0.587	0.551	+0.315	+3.4	+.105	+0.816	+0.184	+.571	+0.570	+6.1
158	+28.172	+0.594	0.546	+0.311	+3.3	+.104	+0.818	+0.182	+.570	+0.563	+6.0
159	+28.370	+0.595	0.539	+0.309	+3.3	+.103	+0.820	+0.180	+.572	+0.559	+5.9
160	+28.574	+0.597	0.532	+0.308	+3.2	+.103	+0.822	+0.178	+.578	+0.557	+5.8
161	+28.771	+0.602	0.527	+0.304	+3.2	+.102	+0.824	+0.176	+.577	+0.551	+5.7
162	+28.968	+0.602	0.518	+0.301	+3.1	+.101	+0.827	+0.173	+.581	+0.544	+5.6
163	+29.163	+0.607	0.514	+0.299	+3.1	+.100	+0.828	+0.172	+.581	+0.540	+5.6
164	+29.358	+0.607	0.508	+0.296	+3.0	+.099	+0.830	+0.170	+.582	+0.536	+5.5
165	+29.559	+0.614	0.502	+0.293	+3.0	+.098	+0.832	+0.168	+.584	+0.531	+5.4
166	+29.751	+0.614	0.494	+0.291	+2.9	+.097	+0.835	+0.165	+.590	+0.527	+5.3

TEST NAME : DSSC6

Pt. No.	Str.X (%)	Str.Y (%)	SigV (ksc)	TauH (ksc)	Eu (ksc)	TauH / SigVc	DelU / SigVc	SigV / SigVc	TauH / SigV	TauH / Cu	Eu / Cu
167	+29.930	+0.617	0.489	+0.289	+2.9	+.097	+0.836	+0.164	+.590	+0.523	+5.2
168	+30.125	+0.617	0.484	+0.287	+2.9	+.096	+0.838	+0.162	+.593	+0.519	+5.2
169	+30.324	+0.619	0.478	+0.284	+2.8	+.095	+0.840	+0.160	+.593	+0.513	+5.1
170	+30.534	+0.619	0.480	+0.280	+2.8	+.094	+0.840	+0.160	+.584	+0.507	+5.0
171	+30.747	+0.624	0.472	+0.277	+2.7	+.093	+0.842	+0.158	+.588	+0.502	+4.9
172	+30.949	+0.631	0.461	+0.275	+2.7	+.092	+0.846	+0.154	+.597	+0.498	+4.8

****

ANISOTROPICALLY CONSOLIDATED MDSS TEST
MIT GEOTECHNICAL LAB

****

FILE NAME: DSSC7.PRN

REDUCTION DATA
UNITS: (kg,cm,mVOLTS,VOLTS)

1. TEST NAME : DSS-C7
2. DATE : 10-18-1987
3. OCR : 1
4. VER. CONSOLIDATION STRESS (KSC) : +2.999
5. HOR. CONSOLIDATION STRESS (KSC) : +0.600
6. PRE-SHEAR SAMPLE HEIGHT (cm) : +1.8622
7. VERTICAL STRESS LOAD CELL:
   ZERO: .64
   CF: 13.70491
8. HORIZONTAL SHEAR LOAD CELL:
   ZERO: -2.05
   CF: 6.70298
9. HORIZONTAL DISP. TRANSDUCER, X:
   ZERO: .3493
   CF: -1.81917
10. HORIZONTAL DISP. TRANSDUCER, Y:
    ZERO: -1.1267
    CF: .261
11. VERTICAL DISP. TRANSDUCER, Z1:
    ZERO: .143
    CF: .28883
12. VERTICAL DISP. TRANSDUCER, Z2:
    ZERO: .879
    CF: .29569
13. CONSTANT HEIGHT TRANSDUCER, Z:
    ZERO: .10512
    CF: .3014
14. TEST ANGLE THETA (degrees): 0

TOTAL X DISP. DURING CONSOLIDATION (cm): .4234

Pt. No.	Str.X (%)	Str.Y (%)	X.Coor. (cm)	SigV (ksc)	TauH (ksc)	Eu (ksc)	TauH / SigVc	DelU / SigVc	SigV / SigVc	TauH / SigV	TauH / Cu	Eu / Cu
1	+0.000	+0.000	+0.423	2.999	+0.582	+9999.0	+.194	+0.000	+1.000	+.194	+0.000	+9999.0
2	+0.002	+0.000	+0.423	3.002	+0.582	+58.6	+.194	-0.001	+1.001	+.194	+0.001	+246.2
3	+0.004	+0.000	+0.423	3.006	+0.597	+1293.6	+.199	-0.002	+1.002	+.198	+0.064	+5434.5
4	+0.014	+0.000	+0.424	3.011	+0.614	+683.5	+.205	-0.004	+1.004	+.204	+0.134	+2871.3
5	+0.039	-0.000	+0.424	3.006	+0.646	+502.4	+.215	-0.002	+1.002	+.215	+0.271	+2110.4
6	+0.065	+0.000	+0.425	3.013	+0.685	+476.6	+.228	-0.004	+1.004	+.227	+0.433	+2002.4
7	+0.102	+0.000	+0.425	3.030	+0.721	+410.5	+.240	-0.010	+1.010	+.238	+0.584	+1724.3
8	+0.151	-0.000	+0.426	3.040	+0.752	+339.0	+.251	-0.013	+1.013	+.247	+0.715	+1424.0
9	+0.207	-0.000	+0.427	3.039	+0.780	+287.9	+.260	-0.013	+1.013	+.257	+0.834	+1209.3
10	+0.279	-0.043	+0.429	3.021	+0.799	+233.9	+.266	-0.007	+1.007	+.264	+0.913	+982.7
11	+0.365	-0.046	+0.430	2.987	+0.811	+188.4	+.270	+0.004	+0.996	+.271	+0.962	+791.4
12	+0.459	-0.052	+0.432	2.934	+0.817	+154.0	+.273	+0.022	+0.978	+.279	+0.990	+646.9
13	+0.552	-0.057	+0.434	2.844	+0.820	+129.4	+.273	+0.052	+0.948	+.288	+1.000	+543.4
14	+0.659	-0.059	+0.436	2.707	+0.819	+107.9	+.273	+0.097	+0.903	+.302	+0.996	+453.1
15	+0.766	-0.064	+0.438	2.533	+0.813	+90.5	+.271	+0.155	+0.845	+.321	+0.971	+380.1
16	+0.871	-0.079	+0.440	2.464	+0.810	+78.6	+.270	+0.179	+0.821	+.329	+0.959	+330.2
17	+0.976	-0.081	+0.442	2.436	+0.806	+68.8	+.269	+0.188	+0.812	+.331	+0.941	+289.2
18	+1.087	-0.090	+0.444	2.409	+0.803	+61.2	+.268	+0.197	+0.803	+.333	+0.932	+257.3
19	+1.199	-0.095	+0.446	2.379	+0.800	+54.6	+.267	+0.207	+0.793	+.336	+0.916	+229.2
20	+1.304	-0.104	+0.448	2.353	+0.795	+49.1	+.265	+0.216	+0.784	+.338	+0.897	+206.3

TEST NAME : DSS-C7

Pt. No.	Str.X (%)	Str.Y (%)	X.Coor. (cm)	SigV (ksc)	TauH (ksc)	Eu (ksc)	TauH / SigVc	DelU / SigVc	SigV / SigVc	TauH / SigV	TauH / Cu	Eu / Cu
21	+1.407	-0.112	+0.450	2.323	+0.789	+44.2	+.263	+0.225	+0.775	+.340	+0.872	+185.8
22	+1.509	-0.115	+0.452	2.295	+0.787	+40.8	+.262	+0.235	+0.765	+.343	+0.862	+171.2
23	+1.613	-0.117	+0.453	2.269	+0.780	+36.9	+.260	+0.244	+0.756	+.344	+0.834	+155.1
24	+1.714	-0.119	+0.455	2.243	+0.777	+34.1	+.259	+0.252	+0.748	+.346	+0.819	+143.3
25	+1.820	-0.124	+0.457	2.219	+0.776	+32.1	+.259	+0.260	+0.740	+.350	+0.817	+134.7
26	+1.923	-0.133	+0.459	2.198	+0.772	+29.7	+.257	+0.267	+0.733	+.351	+0.800	+124.8
27	+2.028	-0.140	+0.461	2.175	+0.769	+27.8	+.257	+0.275	+0.725	+.354	+0.789	+116.7
28	+2.132	-0.144	+0.463	2.150	+0.766	+25.9	+.255	+0.283	+0.717	+.356	+0.775	+109.0
29	+2.233	-0.149	+0.465	2.131	+0.763	+24.3	+.254	+0.290	+0.710	+.358	+0.761	+102.2
30	+2.338	-0.152	+0.467	2.112	+0.761	+23.0	+.254	+0.296	+0.704	+.360	+0.753	+96.7
31	+2.447	-0.155	+0.469	2.090	+0.756	+21.4	+.252	+0.303	+0.697	+.362	+0.733	+89.9
32	+2.556	-0.162	+0.471	2.068	+0.755	+20.3	+.252	+0.310	+0.690	+.365	+0.727	+85.3
33	+2.660	-0.167	+0.473	2.047	+0.750	+19.0	+.250	+0.318	+0.682	+.366	+0.707	+79.7
34	+2.759	-0.174	+0.475	2.030	+0.749	+18.2	+.250	+0.323	+0.677	+.369	+0.702	+76.3
35	+2.862	-0.179	+0.477	2.014	+0.743	+17.0	+.248	+0.328	+0.672	+.369	+0.680	+71.2
36	+3.118	-0.192	+0.481	1.970	+0.738	+15.1	+.246	+0.343	+0.657	+.375	+0.659	+63.4
37	+3.325	-0.202	+0.485	1.935	+0.734	+13.8	+.245	+0.355	+0.645	+.379	+0.641	+57.8
38	+3.541	-0.205	+0.489	1.904	+0.729	+12.4	+.243	+0.365	+0.635	+.383	+0.617	+52.3
39	+3.756	-0.213	+0.493	1.873	+0.723	+11.3	+.241	+0.376	+0.624	+.386	+0.593	+47.4
40	+3.960	-0.229	+0.497	1.842	+0.716	+10.2	+.239	+0.386	+0.614	+.389	+0.564	+42.7
41	+4.168	-0.235	+0.501	1.813	+0.713	+9.4	+.238	+0.395	+0.605	+.393	+0.550	+39.6
42	+4.382	-0.251	+0.505	1.784	+0.706	+8.5	+.235	+0.405	+0.595	+.396	+0.521	+35.6
43	+4.603	-0.257	+0.509	1.753	+0.700	+7.7	+.233	+0.416	+0.584	+.399	+0.495	+32.3
44	+4.813	-0.264	+0.513	1.722	+0.692	+6.9	+.231	+0.426	+0.574	+.402	+0.464	+28.9
45	+5.031	-0.270	+0.517	1.690	+0.687	+6.3	+.229	+0.436	+0.564	+.407	+0.444	+26.5
46	+5.252	-0.279	+0.521	1.661	+0.679	+5.6	+.226	+0.446	+0.554	+.409	+0.410	+23.4
47	+5.466	-0.292	+0.525	1.627	+0.671	+4.9	+.224	+0.458	+0.542	+.412	+0.374	+20.5
48	+5.685	-0.299	+0.529	1.588	+0.662	+4.2	+.221	+0.470	+0.530	+.417	+0.338	+17.8
49	+5.906	-0.309	+0.533	1.555	+0.653	+3.6	+.218	+0.481	+0.519	+.420	+0.299	+15.2
50	+6.116	-0.313	+0.537	1.517	+0.639	+2.8	+.213	+0.494	+0.506	+.421	+0.242	+11.9
51	+6.363	-0.318	+0.542	1.480	+0.631	+2.3	+.210	+0.507	+0.493	+.426	+0.206	+9.7
52	+6.584	-0.325	+0.546	1.443	+0.624	+1.9	+.208	+0.519	+0.481	+.432	+0.176	+8.0
53	+6.807	-0.331	+0.550	1.410	+0.616	+1.5	+.205	+0.530	+0.470	+.437	+0.144	+6.3
54	+7.038	-0.337	+0.554	1.376	+0.607	+1.1	+.202	+0.541	+0.459	+.441	+0.105	+4.5
55	+7.275	-0.341	+0.559	1.340	+0.599	+0.7	+.200	+0.553	+0.447	+.447	+0.071	+2.9
56	+7.516	-0.345	+0.563	1.309	+0.591	+0.4	+.197	+0.564	+0.436	+.451	+0.039	+1.6
57	+7.764	-0.350	+0.568	1.279	+0.583	+0.1	+.195	+0.574	+0.426	+.456	+0.008	+0.3
58	+8.034	-0.355	+0.573	1.246	+0.577	-0.2	+.192	+0.585	+0.415	+.463	-0.019	-0.7
59	+8.438	-0.361	+0.581	1.196	+0.577	-0.2	+.192	+0.601	+0.399	+.482	-0.019	-0.7
60	+10.251	-0.384	+0.614	1.043	+0.575	-0.2	+.192	+0.652	+0.348	+.552	-0.027	-0.8

****

ANISOTROPICALLY CONSOLIDATED MDSS TEST
MIT GEOTECHNICAL LAB

****

FILE NAME: DSSC8.PRN

REDUCTION DATA
UNITS: (kg,cm,mVOLTS,VOLTS)

1. TEST NAME : DSS-C8
2. DATE : 10-28-1987
3. OCR : 1
4. VER. CONSOLIDATION STRESS (KSC) : +2.998
5. HOR. CONSOLIDATION STRESS (KSC) : +0.600
6. PRE-SHEAR SAMPLE HEIGHT (cm) : +1.8386
7. VERTICAL STRESS LOAD CELL:
   ZERO: .6
   CF: 13.70491
8. HORIZONTAL SHEAR LOAD CELL:
   ZERO: -1.84
   CF: 6.70298
9. HORIZONTAL DISP. TRANSDUCER, X:
   ZERO: 1.1095
   CF: -1.81917
10. HORIZONTAL DISP. TRANSDUCER, Y:
    ZERO: -3.352
    CF: -.261
11. VERTICAL DISP. TRANSDUCER, Z1:
    ZERO: -1.886
    CF: .28883
12. VERTICAL DISP. TRANSDUCER, Z2:
    ZERO: 1.389
    CF: .29569
13. CONSTANT HEIGHT TRANSDUCER, Z:
    ZERO: .08655
    CF: .3014
14. TEST ANGLE THETA (degrees): 60

TOTAL X DISP. DURING CONSOLIDATION (cm): .18028

Pt. No.	Str.X (%)	Str.Y (%)	X.Coor. (cm)	SigV (ksc)	TauH (ksc)	Eu (ksc)	TauH / SigVc	DelU / SigVc	SigV / SigVc	TauH / SigV	TauH / Cu	Eu / Cu
1	+0.000	+0.000	+0.180	2.998	+0.291	+9999.0	+.097	+0.000	+1.000	+.097	+0.000	+9999.0
2	-0.009	+0.003	+0.180	3.000	+0.290	+34.6	+.097	-0.001	+1.001	+.097	-0.003	+103.4
3	-0.009	+0.000	+0.180	2.996	+0.290	+34.6	+.097	+0.000	+1.000	+.097	-0.003	+103.4
4	-0.009	+0.000	+0.180	2.997	+0.290	+34.6	+.097	+0.000	+1.000	+.097	-0.003	+103.4
5	-0.009	+0.000	+0.180	2.997	+0.290	+34.6	+.097	+0.000	+1.000	+.097	-0.003	+103.4
6	-0.009	+0.000	+0.180	2.995	+0.291	+11.4	+.097	+0.001	+0.999	+.097	-0.001	+34.0
7	-0.009	+0.000	+0.180	2.987	+0.305	-453.2	+.102	+0.003	+0.997	+.102	+0.040	-1352.6
8	-0.007	-0.003	+0.180	2.981	+0.304	-522.9	+.101	+0.006	+0.994	+.102	+0.037	-1560.7
9	-0.011	+0.000	+0.180	2.974	+0.302	-290.6	+.101	+0.008	+0.992	+.101	+0.031	-867.3
10	-0.009	+0.000	+0.180	2.966	+0.300	-313.8	+.100	+0.010	+0.990	+.101	+0.028	-936.6
11	-0.009	+0.000	+0.180	2.954	+0.298	-220.9	+.099	+0.015	+0.985	+.101	+0.020	-659.3
12	-0.009	+0.000	+0.180	2.942	+0.296	-162.8	+.099	+0.018	+0.982	+.101	+0.014	-486.0
13	-0.009	+0.003	+0.180	2.929	+0.295	-128.0	+.098	+0.023	+0.977	+.101	+0.011	-382.0
14	-0.007	+0.000	+0.180	2.914	+0.295	-145.4	+.098	+0.028	+0.972	+.101	+0.010	-434.0
15	-0.007	+0.000	+0.180	2.896	+0.295	-159.9	+.098	+0.034	+0.966	+.102	+0.011	-477.3
16	-0.009	+0.000	+0.180	2.880	+0.308	-557.7	+.103	+0.039	+0.961	+.107	+0.049	-1664.6
17	-0.007	+0.000	+0.180	2.863	+0.328	-1568.3	+.110	+0.045	+0.955	+.115	+0.111	-4680.9
18	+0.002	+0.000	+0.180	2.845	+0.345	+9056.8	+.115	+0.051	+0.949	+.121	+0.160	+9999.0
19	+0.018	+0.000	+0.181	2.834	+0.373	+1381.7	+.124	+0.055	+0.945	+.132	+0.244	+4124.2
20	+0.036	+0.000	+0.181	2.825	+0.397	+896.9	+.133	+0.058	+0.942	+.141	+0.317	+2677.0

TEST NAME : DSS-C8

Pt. No.	Str.X (%)	Str.Y (%)	X.Coor. (cm)	SigV (ksc)	TauH (ksc)	Eu (ksc)	TauH / SigVc	DelU / SigVc	SigV / SigVc	TauH / SigV	TauH / Cu	Eu / Cu
21	+0.060	+0.000	+0.181	2.831	+0.431	+694.9	+.144	+0.055	+0.945	+.152	+0.417	+2074.0
22	+0.089	+0.061	+0.182	2.841	+0.464	+582.8	+.155	+0.052	+0.948	+.163	+0.515	+1739.5
23	+0.130	+0.064	+0.183	2.839	+0.498	+479.4	+.166	+0.053	+0.947	+.176	+0.618	+1431.0
24	+0.176	+0.066	+0.184	2.827	+0.528	+403.9	+.176	+0.057	+0.943	+.187	+0.706	+1205.6
25	+0.227	+0.089	+0.184	2.801	+0.553	+345.5	+.184	+0.066	+0.934	+.197	+0.781	+1031.1
26	+0.284	+0.104	+0.186	2.756	+0.574	+298.5	+.191	+0.081	+0.919	+.208	+0.844	+890.9
27	+0.352	+0.132	+0.187	2.696	+0.592	+257.0	+.198	+0.101	+0.899	+.220	+0.899	+767.0
28	+0.426	+0.171	+0.188	2.642	+0.605	+220.9	+.202	+0.118	+0.882	+.229	+0.937	+659.4
29	+0.508	+0.219	+0.190	2.601	+0.614	+190.4	+.205	+0.132	+0.868	+.236	+0.962	+568.4
30	+0.593	+0.260	+0.191	2.568	+0.618	+165.5	+.206	+0.143	+0.857	+.241	+0.976	+493.9
31	+0.685	+0.306	+0.193	2.540	+0.623	+145.4	+.208	+0.153	+0.847	+.245	+0.991	+434.0
32	+0.778	+0.357	+0.195	2.510	+0.625	+128.9	+.209	+0.163	+0.837	+.249	+0.997	+384.8
33	+0.874	+0.403	+0.196	2.478	+0.625	+114.7	+.209	+0.173	+0.827	+.252	+0.997	+342.5
34	+0.978	+0.451	+0.198	2.446	+0.626	+102.7	+.209	+0.184	+0.816	+.256	+1.000	+306.7
35	+1.076	+0.510	+0.200	2.415	+0.626	+93.2	+.209	+0.194	+0.806	+.259	+0.998	+278.2
36	+1.172	+0.571	+0.202	2.382	+0.624	+85.2	+.208	+0.205	+0.795	+.262	+0.993	+254.3
37	+1.282	+0.637	+0.204	2.349	+0.620	+77.0	+.207	+0.216	+0.784	+.264	+0.982	+229.8
38	+1.378	+0.698	+0.206	2.319	+0.617	+71.0	+.206	+0.226	+0.774	+.266	+0.973	+212.0
39	+1.477	+0.759	+0.207	2.291	+0.616	+65.9	+.205	+0.236	+0.764	+.269	+0.968	+196.6
40	+1.578	+0.820	+0.209	2.264	+0.612	+61.1	+.204	+0.245	+0.755	+.270	+0.959	+182.2
41	+1.685	+0.886	+0.211	2.236	+0.610	+56.7	+.203	+0.254	+0.746	+.273	+0.950	+169.2
42	+1.790	+0.970	+0.213	2.213	+0.606	+52.8	+.202	+0.262	+0.738	+.274	+0.941	+157.7
43	+1.893	+1.034	+0.215	2.188	+0.605	+49.7	+.202	+0.270	+0.730	+.276	+0.936	+148.4
44	+1.992	+1.108	+0.217	2.164	+0.601	+46.7	+.201	+0.278	+0.722	+.278	+0.925	+139.3
45	+2.095	+1.169	+0.219	2.141	+0.597	+43.8	+.199	+0.286	+0.714	+.279	+0.913	+130.8
46	+2.212	+1.248	+0.221	2.115	+0.596	+41.4	+.199	+0.294	+0.706	+.282	+0.910	+123.4
47	+2.315	+1.416	+0.223	2.092	+0.592	+39.0	+.198	+0.302	+0.698	+.283	+0.899	+116.4
48	+2.413	+1.493	+0.225	2.071	+0.587	+36.7	+.196	+0.309	+0.691	+.283	+0.882	+109.7
49	+2.512	+1.572	+0.226	2.051	+0.585	+35.0	+.195	+0.316	+0.684	+.285	+0.876	+104.6
50	+2.613	+1.648	+0.228	2.029	+0.580	+33.2	+.194	+0.323	+0.677	+.286	+0.863	+99.1
51	+2.713	+1.732	+0.230	2.010	+0.577	+31.6	+.192	+0.330	+0.670	+.287	+0.852	+94.2
52	+2.811	+1.811	+0.232	1.990	+0.575	+30.3	+.192	+0.336	+0.664	+.289	+0.847	+90.4
53	+2.939	+1.903	+0.234	1.972	+0.570	+28.5	+.190	+0.342	+0.658	+.289	+0.833	+85.0
54	+3.043	+1.989	+0.236	1.954	+0.567	+27.2	+.189	+0.348	+0.652	+.290	+0.824	+81.3
55	+3.158	+2.086	+0.238	1.936	+0.564	+25.9	+.188	+0.354	+0.646	+.291	+0.814	+77.3
56	+3.270	+2.186	+0.240	1.915	+0.562	+24.8	+.187	+0.361	+0.639	+.293	+0.807	+74.1
57	+3.383	+2.298	+0.242	1.896	+0.559	+23.7	+.186	+0.368	+0.632	+.295	+0.798	+70.8
58	+3.492	+2.412	+0.244	1.877	+0.553	+22.5	+.185	+0.374	+0.626	+.295	+0.782	+67.2
59	+3.593	+2.519	+0.246	1.860	+0.547	+21.3	+.182	+0.379	+0.621	+.294	+0.762	+63.7
60	+3.706	+2.632	+0.248	1.841	+0.543	+20.3	+.181	+0.386	+0.614	+.295	+0.750	+60.7
61	+3.835	+2.738	+0.251	1.826	+0.538	+19.3	+.180	+0.391	+0.609	+.295	+0.737	+57.7
62	+3.943	+2.845	+0.253	1.811	+0.536	+18.6	+.179	+0.396	+0.604	+.296	+0.731	+55.6
63	+4.052	+2.953	+0.255	1.795	+0.531	+17.7	+.177	+0.401	+0.599	+.296	+0.714	+52.9
64	+4.153	+3.057	+0.257	1.775	+0.527	+17.0	+.176	+0.408	+0.592	+.297	+0.704	+50.9
65	+4.265	+3.169	+0.259	1.761	+0.525	+16.4	+.175	+0.412	+0.588	+.298	+0.697	+49.1
66	+4.383	+3.288	+0.261	1.745	+0.521	+15.7	+.174	+0.418	+0.582	+.299	+0.686	+46.9
67	+4.492	+3.401	+0.263	1.732	+0.516	+15.0	+.172	+0.422	+0.578	+.298	+0.671	+44.8
68	+4.599	+3.521	+0.265	1.716	+0.511	+14.3	+.170	+0.428	+0.572	+.298	+0.655	+42.7

TEST NAME : DSS-C8

Pt. No.	Str.X (%)	Str.Y (%)	X.Coor. (cm)	SigV (ksc)	TauH (ksc)	Eu (ksc)	TauH / SigVc	DelU / SigVc	SigV / SigVc	TauH / SigV	TauH / Cu	Eu / Cu
69	+4.710	+3.635	+0.267	1.698	+0.510	+13.9	+.170	+0.434	+0.566	+.300	+0.652	+41.6
70	+4.831	+3.755	+0.269	1.686	+0.506	+13.3	+.169	+0.438	+0.562	+.300	+0.640	+39.7
71	+4.936	+3.879	+0.271	1.670	+0.500	+12.7	+.167	+0.443	+0.557	+.300	+0.624	+37.9
72	+5.042	+4.014	+0.273	1.653	+0.493	+12.0	+.164	+0.449	+0.551	+.298	+0.601	+35.8
73	+5.161	+4.144	+0.275	1.633	+0.485	+11.3	+.162	+0.455	+0.545	+.297	+0.579	+33.6
74	+5.264	+4.279	+0.277	1.614	+0.477	+10.6	+.159	+0.462	+0.538	+.296	+0.555	+31.6
75	+5.369	+4.417	+0.279	1.596	+0.470	+10.0	+.157	+0.468	+0.532	+.295	+0.535	+29.9
76	+5.483	+4.563	+0.281	1.577	+0.462	+9.3	+.154	+0.474	+0.526	+.293	+0.509	+27.9
77	+5.600	+4.711	+0.283	1.554	+0.454	+8.7	+.151	+0.481	+0.519	+.292	+0.486	+26.0
78	+5.708	+4.860	+0.285	1.529	+0.446	+8.1	+.149	+0.490	+0.510	+.291	+0.462	+24.3
79	+5.820	+5.031	+0.287	1.505	+0.436	+7.5	+.146	+0.498	+0.502	+.290	+0.434	+22.4
80	+5.960	+5.199	+0.290	1.475	+0.426	+6.8	+.142	+0.508	+0.492	+.289	+0.401	+20.2
81	+6.074	+5.387	+0.292	1.444	+0.414	+6.0	+.138	+0.518	+0.482	+.286	+0.365	+18.0
82	+6.219	+5.595	+0.295	1.412	+0.401	+5.3	+.134	+0.529	+0.471	+.284	+0.327	+15.8
83	+6.362	+5.834	+0.297	1.374	+0.385	+4.4	+.129	+0.541	+0.459	+.280	+0.281	+13.2
84	+6.521	+6.123	+0.300	1.335	+0.366	+3.5	+.122	+0.555	+0.445	+.274	+0.224	+10.3
85	+6.668	+6.467	+0.303	1.295	+0.344	+2.4	+.115	+0.568	+0.432	+.265	+0.157	+7.1
86	+6.848	+6.865	+0.306	1.252	+0.323	+1.4	+.108	+0.582	+0.418	+.258	+0.095	+4.2

****

ANISOTROPICALLY CONSOLIDATED MDSS TEST
MIT GEOTECHNICAL LAB

****

FILE NAME: DSSC9.PRN

REDUCTION DATA
UNITS: (kg,cm,mVOLTS,VOLTS)

1. TEST NAME : DSS-C9
2. DATE : 11-05-1987
3. OCR : 1
4. VER. CONSOLIDATION STRESS (KSC) : +2.998
5. HOR. CONSOLIDATION STRESS (KSC) : +0.600
6. PRE-SHEAR SAMPLE HEIGHT (cm) : +1.9135
7. VERTICAL STRESS LOAD CELL:
   ZERO: .6
   CF: 13.70491
8. HORIZONTAL SHEAR LOAD CELL:
   ZERO: -2
   CF: 6.70298
9. HORIZONTAL DISP. TRANSDUCER, X:
   ZERO: .6086
   CF: -1.81917
10. HORIZONTAL DISP. TRANSDUCER, Y:
    ZERO: -1.6787
    CF: -.261
11. VERTICAL DISP. TRANSDUCER, Z1:
    ZERO: -.03565
    CF: .28883
12. VERTICAL DISP. TRANSDUCER, Z2:
    ZERO: 1.7043
    CF: .29569
13. CONSTANT HEIGHT TRANSDUCER, Z:
    ZERO: .07231
    CF: .3014
14. TEST ANGLE THETA (degrees): 120

TOTAL X DISP. DURING CONSOLIDATION (cm): -.10475

Pt. No.	Str.X (%)	Str.Y (%)	X.Coor. (cm)	SigV (ksc)	TauH (ksc)	Eu (ksc)	TauH / SigVc	DelU / SigVc	SigV / SigVc	TauH / SigV	TauH / Cu	Eu / Cu
1	+0.000	+0.000	-0.105	2.998	-0.296	+9999.0	-.099	+0.000	+1.000	-.099	+0.000	+9999.0
2	+0.000	+0.008	-0.105	2.999	-0.296	+9999.0	-.099	-0.000	+1.000	-.099	-0.000	+9999.0
3	+0.002	+0.020	-0.105	2.997	-0.278	+3081.6	-.093	+0.000	+1.000	-.093	+0.023	+4090.9
4	+0.002	+0.020	-0.105	3.000	-0.262	+5800.6	-.088	-0.001	+1.001	-.087	+0.044	+7700.5
5	+0.000	+0.020	-0.105	2.997	-0.247	+9999.0	-.082	+0.000	+1.000	-.082	+0.064	+9999.0
6	-0.002	+0.018	-0.105	2.993	-0.229	-9999.0	-.076	+0.002	+0.998	-.077	+0.088	-9999.0
7	+0.002	+0.020	-0.105	2.993	-0.206	+9999.0	-.069	+0.002	+0.998	-.069	+0.119	+9999.0
8	+0.002	+0.020	-0.105	2.992	-0.178	+9999.0	-.059	+0.002	+0.998	-.060	+0.156	+9999.0
9	+0.005	+0.023	-0.105	2.985	-0.149	+8559.8	-.050	+0.004	+0.996	-.050	+0.195	+9999.0
10	+0.007	+0.025	-0.105	2.980	-0.121	+9999.0	-.040	+0.006	+0.994	-.041	+0.232	+9999.0
11	+0.005	+0.028	-0.105	2.968	-0.099	+9999.0	-.033	+0.010	+0.990	-.033	+0.261	+9999.0
12	+0.002	+0.033	-0.105	2.946	-0.082	+9999.0	-.027	+0.017	+0.983	-.028	+0.284	+9999.0
13	+0.009	+0.035	-0.105	2.923	-0.063	+8145.9	-.021	+0.025	+0.975	-.022	+0.309	+9999.0
14	+0.017	+0.043	-0.104	2.898	-0.043	+4423.3	-.014	+0.033	+0.967	-.015	+0.335	+5872.1
15	+0.031	+0.047	-0.104	2.870	-0.024	+2638.7	-.008	+0.043	+0.957	-.008	+0.360	+3503.0
16	+0.043	+0.055	-0.104	2.849	-0.015	+1965.1	-.005	+0.050	+0.950	-.005	+0.372	+2608.7
17	+0.057	+0.055	-0.104	2.828	-0.004	+1547.2	-.001	+0.057	+0.943	-.001	+0.387	+2054.0
18	+0.065	+0.060	-0.104	2.815	+0.007	+1396.1	+.002	+0.061	+0.939	+.003	+0.402	+1853.4
19	+0.075	+0.065	-0.103	2.803	+0.017	+1244.2	+.006	+0.065	+0.935	+.006	+0.415	+1651.7
20	+0.079	+0.067	-0.103	2.794	+0.022	+1208.4	+.007	+0.068	+0.932	+.008	+0.421	+1604.2

TEST NAME : DSS-C9

Pt. No.	Str.X (%)	Str.Y (%)	X.Coor. (cm)	SigV (ksc)	TauH (ksc)	Eu (ksc)	TauH / SigVc	DelU / SigVc	SigV / SigVc	TauH / SigV	TauH / Cu	Eu / Cu
21	+0.098	+0.072	-0.103	2.787	+0.041	+1034.6	+.014	+0.070	+0.930	+.015	+0.447	+1373.4
22	+0.106	+0.077	-0.103	2.779	+0.041	+949.2	+.014	+0.073	+0.927	+.015	+0.446	+1260.1
23	+0.108	+0.079	-0.103	2.768	+0.036	+921.6	+.012	+0.077	+0.923	+.013	+0.440	+1223.5
24	+0.127	+0.082	-0.102	2.759	+0.060	+840.9	+.020	+0.080	+0.920	+.022	+0.472	+1116.4
25	+0.154	+0.092	-0.102	2.761	+0.087	+744.4	+.029	+0.079	+0.921	+.032	+0.508	+988.3
26	+0.190	+0.102	-0.101	2.757	+0.113	+644.9	+.038	+0.080	+0.920	+.041	+0.543	+856.2
27	+0.228	+0.116	-0.100	2.743	+0.139	+571.8	+.046	+0.085	+0.915	+.051	+0.577	+759.1
28	+0.271	+0.126	-0.100	2.712	+0.163	+508.5	+.054	+0.095	+0.905	+.060	+0.609	+675.0
29	+0.315	+0.143	-0.099	2.676	+0.184	+456.6	+.061	+0.107	+0.893	+.069	+0.637	+606.2
30	+0.367	+0.161	-0.098	2.643	+0.205	+409.5	+.068	+0.118	+0.882	+.078	+0.664	+543.7
31	+0.421	+0.178	-0.097	2.613	+0.226	+371.0	+.075	+0.129	+0.871	+.086	+0.692	+492.5
32	+0.478	+0.202	-0.096	2.582	+0.245	+339.0	+.082	+0.139	+0.861	+.095	+0.717	+450.0
33	+0.545	+0.227	-0.094	2.552	+0.262	+306.9	+.087	+0.149	+0.851	+.103	+0.740	+407.4
34	+0.610	+0.256	-0.093	2.518	+0.277	+281.6	+.092	+0.160	+0.840	+.110	+0.760	+373.8
35	+0.675	+0.283	-0.092	2.492	+0.288	+259.1	+.096	+0.169	+0.831	+.115	+0.774	+344.0
36	+0.742	+0.320	-0.091	2.460	+0.299	+240.5	+.100	+0.179	+0.821	+.122	+0.790	+319.3
37	+0.802	+0.352	-0.089	2.431	+0.311	+227.0	+.104	+0.189	+0.811	+.128	+0.806	+301.4
38	+0.879	+0.387	-0.088	2.403	+0.323	+211.2	+.108	+0.198	+0.802	+.135	+0.822	+280.4
39	+0.953	+0.426	-0.087	2.376	+0.335	+198.6	+.112	+0.208	+0.792	+.141	+0.837	+263.6
40	+1.031	+0.470	-0.085	2.350	+0.344	+186.1	+.115	+0.216	+0.784	+.147	+0.849	+247.0
41	+1.114	+0.517	-0.083	2.324	+0.351	+174.3	+.117	+0.225	+0.775	+.151	+0.859	+231.4
42	+1.192	+0.561	-0.082	2.294	+0.359	+164.6	+.120	+0.235	+0.765	+.156	+0.868	+218.5
43	+1.275	+0.608	-0.080	2.270	+0.366	+155.7	+.122	+0.243	+0.757	+.161	+0.878	+206.7
44	+1.355	+0.660	-0.079	2.244	+0.373	+148.1	+.125	+0.251	+0.749	+.166	+0.888	+196.6
45	+1.439	+0.709	-0.077	2.223	+0.378	+140.3	+.126	+0.259	+0.741	+.170	+0.894	+186.2
46	+1.528	+0.760	-0.076	2.199	+0.383	+133.2	+.128	+0.266	+0.734	+.174	+0.901	+176.9
47	+1.612	+0.815	-0.074	2.169	+0.388	+127.3	+.130	+0.277	+0.723	+.179	+0.908	+168.9
48	+1.694	+0.866	-0.072	2.146	+0.391	+121.6	+.131	+0.284	+0.716	+.182	+0.912	+161.5
49	+1.776	+0.917	-0.071	2.123	+0.395	+116.6	+.132	+0.292	+0.708	+.186	+0.916	+154.7
50	+1.859	+0.972	-0.069	2.109	+0.399	+112.2	+.133	+0.297	+0.703	+.189	+0.923	+148.9
51	+1.951	+1.028	-0.067	2.088	+0.404	+107.5	+.135	+0.303	+0.697	+.193	+0.929	+142.8
52	+2.034	+1.085	-0.066	2.066	+0.407	+103.6	+.136	+0.311	+0.689	+.197	+0.933	+137.6
53	+2.123	+1.141	-0.064	2.051	+0.410	+99.7	+.137	+0.316	+0.684	+.200	+0.936	+132.3
54	+2.210	+1.195	-0.062	2.029	+0.412	+96.1	+.138	+0.323	+0.677	+.203	+0.940	+127.6
55	+2.294	+1.252	-0.061	2.012	+0.416	+93.1	+.139	+0.329	+0.671	+.207	+0.945	+123.6
56	+2.380	+1.308	-0.059	1.995	+0.421	+90.3	+.140	+0.335	+0.665	+.211	+0.951	+119.9
57	+2.476	+1.375	-0.057	1.982	+0.425	+87.3	+.142	+0.339	+0.661	+.214	+0.956	+115.8
58	+2.570	+1.436	-0.056	1.961	+0.427	+84.4	+.143	+0.346	+0.654	+.218	+0.960	+112.0
59	+2.659	+1.498	-0.054	1.947	+0.429	+81.7	+.143	+0.351	+0.649	+.220	+0.962	+108.5
60	+2.752	+1.559	-0.052	1.925	+0.432	+79.3	+.144	+0.358	+0.642	+.224	+0.966	+105.3
61	+2.840	+1.620	-0.050	1.907	+0.432	+76.8	+.144	+0.364	+0.636	+.226	+0.966	+102.0
62	+2.928	+1.687	-0.049	1.894	+0.433	+74.6	+.144	+0.368	+0.632	+.229	+0.967	+99.1
63	+3.019	+1.749	-0.047	1.878	+0.436	+72.7	+.146	+0.374	+0.626	+.232	+0.972	+96.5
64	+3.110	+1.808	-0.045	1.866	+0.436	+70.6	+.145	+0.377	+0.623	+.234	+0.971	+93.7
65	+3.198	+1.869	-0.044	1.854	+0.436	+68.7	+.146	+0.382	+0.618	+.235	+0.972	+91.1
66	+3.284	+1.935	-0.042	1.840	+0.440	+67.2	+.147	+0.386	+0.614	+.239	+0.976	+89.2
67	+3.373	+1.991	-0.040	1.824	+0.440	+65.4	+.147	+0.392	+0.608	+.241	+0.976	+86.9
68	+3.464	+2.051	-0.038	1.811	+0.440	+63.7	+.147	+0.396	+0.604	+.243	+0.977	+84.6

TEST NAME : DSS-C9

Pt. No.	Str.X (%)	Str.Y (%)	X.Coor. (cm)	SigV (ksc)	TauH (ksc)	Eu (ksc)	TauH / SigVc	DelU / SigVc	SigV / SigVc	TauH / SigV	TauH / Cu	Eu / Cu
69	+3.552	+2.110	-0.037	1.800	+0.442	+62.3	+.147	+0.400	+0.600	+.246	+0.979	+82.7
70	+3.646	+2.176	-0.035	1.789	+0.446	+61.0	+.149	+0.403	+0.597	+.249	+0.984	+81.0
71	+3.741	+2.248	-0.033	1.779	+0.448	+59.6	+.149	+0.407	+0.593	+.252	+0.987	+79.2
72	+3.839	+2.314	-0.031	1.770	+0.448	+58.1	+.149	+0.410	+0.590	+.253	+0.987	+77.1
73	+3.930	+2.380	-0.030	1.755	+0.449	+56.9	+.150	+0.414	+0.586	+.256	+0.989	+75.5
74	+4.026	+2.451	-0.028	1.742	+0.449	+55.5	+.150	+0.419	+0.581	+.258	+0.988	+73.6
75	+4.115	+2.515	-0.026	1.732	+0.450	+54.3	+.150	+0.422	+0.578	+.260	+0.989	+72.1
76	+4.206	+2.584	-0.024	1.724	+0.453	+53.4	+.151	+0.425	+0.575	+.263	+0.994	+70.9
77	+4.302	+2.660	-0.022	1.714	+0.455	+52.3	+.152	+0.428	+0.572	+.265	+0.996	+69.4
78	+4.396	+2.729	-0.021	1.707	+0.455	+51.2	+.152	+0.431	+0.569	+.266	+0.996	+68.0
79	+4.494	+2.803	-0.019	1.696	+0.456	+50.2	+.152	+0.434	+0.566	+.269	+0.998	+66.6
80	+4.596	+2.876	-0.017	1.687	+0.458	+49.2	+.153	+0.437	+0.563	+.271	+1.000	+65.3
81	+4.694	+2.955	-0.015	1.676	+0.456	+48.0	+.152	+0.441	+0.559	+.272	+0.997	+63.7
82	+4.787	+3.032	-0.013	1.662	+0.455	+47.0	+.152	+0.446	+0.554	+.274	+0.996	+62.4
83	+4.879	+3.103	-0.011	1.658	+0.456	+46.2	+.152	+0.447	+0.553	+.275	+0.998	+61.3
84	+4.977	+3.179	-0.010	1.647	+0.456	+45.3	+.152	+0.451	+0.549	+.277	+0.997	+60.1
85	+5.071	+3.253	-0.008	1.638	+0.453	+44.3	+.151	+0.454	+0.546	+.277	+0.994	+58.8
86	+5.167	+3.329	-0.006	1.626	+0.453	+43.5	+.151	+0.458	+0.542	+.279	+0.994	+57.7
87	+5.263	+3.403	-0.004	1.617	+0.454	+42.7	+.151	+0.461	+0.539	+.281	+0.995	+56.7
88	+5.359	+3.484	-0.002	1.609	+0.453	+41.9	+.151	+0.463	+0.537	+.282	+0.994	+55.6
89	+5.457	+3.567	-0.000	1.606	+0.453	+41.2	+.151	+0.464	+0.536	+.282	+0.994	+54.7
90	+5.561	+3.646	+0.002	1.594	+0.454	+40.4	+.151	+0.468	+0.532	+.285	+0.995	+53.7
91	+5.662	+3.730	+0.004	1.591	+0.452	+39.6	+.151	+0.469	+0.531	+.284	+0.993	+52.6
92	+5.757	+3.806	+0.005	1.579	+0.454	+39.0	+.151	+0.473	+0.527	+.287	+0.994	+51.8
93	+5.851	+3.887	+0.007	1.568	+0.454	+38.4	+.151	+0.477	+0.523	+.289	+0.994	+51.0
94	+5.957	+3.968	+0.009	1.561	+0.453	+37.7	+.151	+0.479	+0.521	+.290	+0.994	+50.1
95	+6.055	+4.048	+0.011	1.553	+0.453	+37.1	+.151	+0.482	+0.518	+.291	+0.993	+49.2
96	+6.161	+4.138	+0.013	1.551	+0.452	+36.4	+.151	+0.483	+0.517	+.292	+0.993	+48.3
97	+6.262	+4.221	+0.015	1.544	+0.452	+35.8	+.151	+0.485	+0.515	+.293	+0.992	+47.5
98	+6.369	+4.313	+0.017	1.540	+0.450	+35.1	+.150	+0.486	+0.514	+.292	+0.989	+46.6
99	+6.464	+4.409	+0.019	1.530	+0.449	+34.5	+.150	+0.490	+0.510	+.293	+0.988	+45.9
100	+6.734	+4.652	+0.024	1.509	+0.445	+33.0	+.148	+0.497	+0.503	+.295	+0.983	+43.8
101	+6.922	+4.814	+0.028	1.496	+0.443	+32.0	+.148	+0.501	+0.499	+.296	+0.981	+42.5
102	+7.108	+4.981	+0.031	1.478	+0.445	+31.3	+.148	+0.507	+0.493	+.301	+0.983	+41.5
103	+7.311	+5.154	+0.035	1.463	+0.444	+30.3	+.148	+0.512	+0.488	+.303	+0.981	+40.3
104	+7.514	+5.342	+0.039	1.451	+0.441	+29.4	+.147	+0.516	+0.484	+.304	+0.978	+39.0
105	+7.713	+5.534	+0.043	1.440	+0.438	+28.5	+.146	+0.520	+0.480	+.304	+0.973	+37.9
106	+7.912	+5.740	+0.047	1.425	+0.432	+27.6	+.144	+0.525	+0.475	+.303	+0.965	+36.6
107	+8.096	+5.931	+0.050	1.405	+0.428	+26.8	+.143	+0.531	+0.469	+.305	+0.961	+35.6
108	+8.289	+6.136	+0.054	1.392	+0.424	+26.1	+.142	+0.536	+0.464	+.305	+0.956	+34.6
109	+8.481	+6.351	+0.058	1.380	+0.419	+25.3	+.140	+0.540	+0.460	+.303	+0.948	+33.5
110	+8.683	+6.570	+0.061	1.360	+0.413	+24.5	+.138	+0.546	+0.454	+.304	+0.941	+32.5
111	+8.873	+6.799	+0.065	1.339	+0.408	+23.8	+.136	+0.553	+0.447	+.304	+0.933	+31.6
112	+9.063	+7.021	+0.069	1.321	+0.403	+23.1	+.134	+0.559	+0.441	+.305	+0.927	+30.7
113	+9.267	+7.258	+0.073	1.294	+0.397	+22.4	+.132	+0.568	+0.432	+.306	+0.919	+29.7
114	+9.461	+7.495	+0.076	1.269	+0.390	+21.7	+.130	+0.577	+0.423	+.307	+0.910	+28.9
115	+9.654	+7.770	+0.080	1.248	+0.380	+21.0	+.127	+0.584	+0.416	+.304	+0.897	+27.9
116	+9.855	+8.028	+0.084	1.225	+0.374	+20.4	+.125	+0.591	+0.409	+.305	+0.888	+27.0

TEST NAME : DSS-C9

Pt. No.	Str.X (%)	Str.Y (%)	X.Coor. (cm)	SigV (ksc)	TauH (ksc)	Eu (ksc)	TauH / SigVc	DelU / SigVc	SigV / SigVc	TauH / SigV	TauH / Cu	Eu / Cu
117	+10.054	+8.275	+0.088	1.195	+0.368	+19.8	+.123	+0.601	+0.399	+.308	+0.881	+26.3
118	+10.254	+8.520	+0.091	1.173	+0.364	+19.3	+.122	+0.609	+0.391	+.311	+0.876	+25.6
119	+10.460	+8.771	+0.095	1.151	+0.360	+18.8	+.120	+0.616	+0.384	+.312	+0.870	+24.9
120	+10.668	+9.062	+0.099	1.127	+0.350	+18.2	+.117	+0.624	+0.376	+.311	+0.857	+24.1
121	+10.888	+9.355	+0.104	1.105	+0.341	+17.5	+.114	+0.631	+0.369	+.309	+0.845	+23.3
122	+11.102	+9.656	+0.108	1.078	+0.331	+16.9	+.110	+0.640	+0.360	+.307	+0.832	+22.5
123	+11.316	+9.983	+0.112	1.059	+0.320	+16.3	+.107	+0.647	+0.353	+.302	+0.817	+21.7
124	+11.637	+11.040	+0.118	0.995	+0.246	+16.0	+.082	+0.668	+0.332	+.247	+0.719	+18.5
125	+11.859	+11.817	+0.122	0.937	+0.223	+13.1	+.074	+0.688	+0.312	+.238	+0.689	+17.4
126	+12.120	+12.670	+0.127	0.880	+0.201	+12.3	+.067	+0.706	+0.294	+.228	+0.659	+16.3
127	+14.904	+15.769	+0.180	0.388	-0.032	+5.3	-.011	+0.871	+0.129	-.083	+0.349	+7.0

****

ANISOTROPICALLY CONSOLIDATED MDSS TEST

MIT GEOTECHNICAL LAB

****

FILE NAME: DSSC10.PRN

REDUCTION DATA

UNITS: (kg,cm,mVOLTS,VOLTS)

1. TEST NAME : DSS-C10
2. DATE : 11-11-1987
3. OCR : 1
4. VER. CONSOLIDATION STRESS (KSC) : +2.997
5. HOR. CONSOLIDATION STRESS (KSC) : +0.600
6. PRE-SHEAR SAMPLE HEIGHT (cm) : +1.9693
7. VERTICAL STRESS LOAD CELL:
   ZERO: .62
   CF: 13.70491
8. HORIZONTAL SHEAR LOAD CELL:
   ZERO: -1.74
   CF: 6.70298
9. HORIZONTAL DISP. TRANSDUCER, X:
   ZERO: .03321
   CF: -1.81917
10. HORIZONTAL DISP. TRANSDUCER, Y:
    ZERO: .07929
    CF: -.261
11. VERTICAL DISP. TRANSDUCER, Z1:
    ZERO: -.12724
    CF: .28883
12. VERTICAL DISP. TRANSDUCER, Z2:
    ZERO: .7662
    CF: .29569
13. CONSTANT HEIGHT TRANSDUCER, Z:
    ZERO: .07006
    CF: .3014
14. TEST ANGLE THETA (degrees): 30

TOTAL X DISP. DURING CONSOLIDATION (cm): .38064

Pt. No.	Str.X (%)	Str.Y (%)	X.Coor. (cm)	SigV (ksc)	TauH (ksc)	Eu (ksc)	TauH / SigVc	DelU / SigVc	SigV / SigVc	TauH / SigV	TauH / Cu	Eu / Cu
1	+0.000	+0.000	+0.381	2.997	+0.505	+9999.0	+.168	+0.000	+1.000	+.168	+0.000	+9999.0
2	+0.000	+0.005	+0.381	2.998	+0.505	+1.1	+.168	-0.000	+1.000	+.168	+0.000	+4.3
3	+0.003	+0.008	+0.381	2.995	+0.518	+1154.9	+.173	+0.001	+0.999	+.173	+0.054	+4633.8
4	+0.008	+0.005	+0.381	2.990	+0.532	+951.0	+.177	+0.003	+0.997	+.178	+0.107	+3815.7
5	+0.017	+0.005	+0.381	2.983	+0.547	+751.1	+.182	+0.005	+0.995	+.183	+0.168	+3013.4
6	+0.025	+0.005	+0.381	2.978	+0.570	+774.1	+.190	+0.006	+0.994	+.191	+0.259	+3106.0
7	+0.045	+0.005	+0.382	2.967	+0.593	+587.3	+.198	+0.010	+0.990	+.200	+0.352	+2356.4
8	+0.063	+0.008	+0.382	2.958	+0.619	+541.7	+.207	+0.013	+0.987	+.209	+0.457	+2173.6
9	+0.095	+0.005	+0.383	2.940	+0.650	+460.5	+.217	+0.019	+0.981	+.221	+0.582	+1847.7
10	+0.131	+0.005	+0.383	2.924	+0.679	+399.2	+.227	+0.024	+0.976	+.232	+0.699	+1601.7
11	+0.181	+0.017	+0.384	2.898	+0.705	+332.7	+.235	+0.033	+0.967	+.243	+0.804	+1334.8
12	+0.239	+0.029	+0.385	2.863	+0.725	+276.0	+.242	+0.045	+0.955	+.253	+0.881	+1107.4
13	+0.308	+0.041	+0.387	2.814	+0.740	+228.7	+.247	+0.061	+0.939	+.263	+0.943	+917.6
14	+0.388	+0.060	+0.388	2.740	+0.750	+189.5	+.250	+0.086	+0.914	+.274	+0.982	+760.2
15	+0.472	+0.086	+0.390	2.675	+0.754	+158.4	+.252	+0.107	+0.893	+.282	+1.000	+635.4
16	+0.553	+0.110	+0.392	2.631	+0.754	+134.9	+.252	+0.122	+0.878	+.287	+0.998	+541.3
17	+0.654	+0.136	+0.394	2.596	+0.753	+113.9	+.251	+0.134	+0.866	+.290	+0.997	+457.0
18	+0.750	+0.158	+0.395	2.568	+0.753	+99.0	+.251	+0.143	+0.857	+.293	+0.994	+397.3
19	+0.841	+0.186	+0.397	2.540	+0.749	+87.0	+.250	+0.153	+0.847	+.295	+0.980	+349.2
20	+0.939	+0.207	+0.399	2.505	+0.748	+77.6	+.250	+0.164	+0.836	+.299	+0.975	+311.5

TEST NAME : DSS-C10

Pt. No.	Str.X (%)	Str.Y (%)	X.Coor. (cm)	SigV (ksc)	TauH (ksc)	Eu (ksc)	TauH / SigVc	DelU / SigVc	SigV / SigVc	TauH / SigV	TauH / Cu	Eu / Cu
21	+1.034	+0.238	+0.401	2.474	+0.746	+69.4	+.248	+0.174	+0.826	+.301	+0.960	+278.6
22	+1.138	+0.264	+0.403	2.440	+0.741	+62.2	+.247	+0.186	+0.814	+.304	+0.947	+249.7
23	+1.242	+0.293	+0.405	2.415	+0.741	+57.0	+.247	+0.194	+0.806	+.307	+0.946	+228.6
24	+1.345	+0.326	+0.407	2.386	+0.737	+51.8	+.246	+0.204	+0.796	+.309	+0.931	+207.7
25	+1.443	+0.359	+0.409	2.359	+0.731	+47.1	+.244	+0.213	+0.787	+.310	+0.909	+189.0
26	+1.538	+0.388	+0.411	2.325	+0.728	+43.5	+.243	+0.224	+0.776	+.313	+0.896	+174.7
27	+1.640	+0.414	+0.413	2.303	+0.724	+40.2	+.242	+0.232	+0.768	+.315	+0.881	+161.1
28	+1.737	+0.450	+0.415	2.278	+0.719	+37.0	+.240	+0.240	+0.760	+.316	+0.860	+148.4
29	+1.837	+0.483	+0.417	2.255	+0.717	+34.6	+.239	+0.248	+0.752	+.318	+0.850	+138.8
30	+1.932	+0.502	+0.419	2.231	+0.715	+32.5	+.238	+0.256	+0.744	+.320	+0.841	+130.6
31	+2.030	+0.535	+0.421	2.209	+0.712	+30.6	+.238	+0.263	+0.737	+.322	+0.831	+122.8
32	+2.133	+0.569	+0.423	2.187	+0.709	+28.7	+.237	+0.270	+0.730	+.324	+0.819	+115.1
33	+2.236	+0.599	+0.425	2.167	+0.708	+27.3	+.236	+0.277	+0.723	+.327	+0.815	+109.4
34	+2.337	+0.635	+0.427	2.145	+0.705	+25.6	+.235	+0.284	+0.716	+.329	+0.801	+102.9
35	+2.439	+0.671	+0.429	2.124	+0.701	+24.1	+.234	+0.291	+0.709	+.330	+0.787	+96.8
36	+2.540	+0.701	+0.431	2.105	+0.700	+23.1	+.234	+0.298	+0.702	+.333	+0.784	+92.6
37	+2.643	+0.733	+0.433	2.085	+0.696	+21.6	+.232	+0.304	+0.696	+.334	+0.765	+86.8
38	+2.738	+0.768	+0.435	2.071	+0.692	+20.5	+.231	+0.309	+0.691	+.334	+0.752	+82.4
39	+2.840	+0.799	+0.437	2.047	+0.689	+19.4	+.230	+0.317	+0.683	+.337	+0.738	+77.9
40	+2.938	+0.837	+0.438	2.028	+0.686	+18.5	+.229	+0.323	+0.677	+.338	+0.728	+74.3
41	+3.036	+0.880	+0.440	2.015	+0.682	+17.5	+.227	+0.328	+0.672	+.338	+0.710	+70.1
42	+3.133	+0.918	+0.442	1.993	+0.683	+17.0	+.228	+0.335	+0.665	+.343	+0.713	+68.3
43	+3.237	+0.960	+0.444	1.979	+0.678	+16.0	+.226	+0.340	+0.660	+.343	+0.694	+64.3
44	+3.333	+0.998	+0.446	1.960	+0.675	+15.3	+.225	+0.346	+0.654	+.344	+0.682	+61.4
45	+3.432	+1.041	+0.448	1.948	+0.673	+14.7	+.225	+0.350	+0.650	+.345	+0.674	+58.9
46	+3.528	+1.079	+0.450	1.932	+0.669	+14.0	+.223	+0.355	+0.645	+.346	+0.660	+56.1
47	+3.630	+1.120	+0.452	1.915	+0.668	+13.5	+.223	+0.361	+0.639	+.349	+0.654	+54.0
48	+3.726	+1.167	+0.454	1.902	+0.665	+12.9	+.222	+0.365	+0.635	+.350	+0.644	+51.9
49	+3.825	+1.205	+0.456	1.885	+0.661	+12.3	+.221	+0.371	+0.629	+.351	+0.627	+49.2
50	+3.922	+1.248	+0.458	1.867	+0.659	+11.8	+.220	+0.377	+0.623	+.353	+0.617	+47.2
51	+4.026	+1.291	+0.460	1.857	+0.656	+11.3	+.219	+0.381	+0.619	+.353	+0.606	+45.2
52	+4.128	+1.329	+0.462	1.842	+0.653	+10.8	+.218	+0.386	+0.614	+.355	+0.595	+43.2
53	+4.226	+1.374	+0.464	1.826	+0.651	+10.4	+.217	+0.391	+0.609	+.357	+0.586	+41.6
54	+4.333	+1.412	+0.466	1.816	+0.649	+10.0	+.216	+0.394	+0.606	+.357	+0.577	+40.0
55	+4.433	+1.457	+0.468	1.802	+0.644	+9.4	+.215	+0.399	+0.601	+.357	+0.556	+37.7
56	+4.529	+1.502	+0.470	1.789	+0.642	+9.0	+.214	+0.403	+0.597	+.359	+0.548	+36.3
57	+4.630	+1.550	+0.472	1.774	+0.640	+8.7	+.213	+0.408	+0.592	+.361	+0.541	+35.0
58	+4.732	+1.590	+0.474	1.760	+0.636	+8.3	+.212	+0.413	+0.587	+.361	+0.527	+33.4
59	+4.837	+1.640	+0.476	1.750	+0.635	+8.0	+.212	+0.416	+0.584	+.363	+0.521	+32.3
60	+4.941	+1.693	+0.478	1.734	+0.631	+7.6	+.211	+0.421	+0.579	+.364	+0.505	+30.7
61	+5.045	+1.742	+0.480	1.720	+0.626	+7.2	+.209	+0.426	+0.574	+.364	+0.486	+28.9
62	+5.161	+1.799	+0.482	1.706	+0.621	+6.7	+.207	+0.431	+0.569	+.364	+0.465	+27.0
63	+5.259	+1.849	+0.484	1.692	+0.618	+6.4	+.206	+0.435	+0.565	+.365	+0.452	+25.8
64	+5.362	+1.904	+0.486	1.679	+0.613	+6.0	+.205	+0.440	+0.560	+.365	+0.434	+24.3
65	+5.466	+1.957	+0.488	1.667	+0.610	+5.7	+.203	+0.444	+0.556	+.366	+0.420	+23.0
66	+5.567	+2.006	+0.490	1.648	+0.606	+5.4	+.202	+0.450	+0.550	+.368	+0.405	+21.9
67	+5.676	+2.063	+0.492	1.634	+0.602	+5.1	+.201	+0.455	+0.545	+.368	+0.387	+20.5
68	+5.782	+2.120	+0.495	1.616	+0.595	+4.7	+.198	+0.461	+0.539	+.368	+0.361	+18.7

TEST NAME : DSS-C10

Pt. No.	Str.X (%)	Str.Y (%)	X.Coor. (cm)	SigV (ksc)	TauH (ksc)	Eu (ksc)	TauH / SigVc	DelU / SigVc	SigV / SigVc	TauH / SigV	TauH / Cu	Eu / Cu
69	+5.895	+2.177	+0.497	1.595	+0.591	+4.4	+.197	+0.468	+0.532	+.370	+0.344	+17.5
70	+6.008	+2.241	+0.499	1.579	+0.585	+4.0	+.195	+0.473	+0.527	+.370	+0.320	+16.0
71	+6.115	+2.298	+0.501	1.558	+0.582	+3.8	+.194	+0.480	+0.520	+.373	+0.307	+15.1
72	+6.230	+2.362	+0.503	1.540	+0.574	+3.3	+.191	+0.486	+0.514	+.372	+0.275	+13.3
73	+6.348	+2.427	+0.506	1.519	+0.569	+3.0	+.190	+0.493	+0.507	+.375	+0.259	+12.2
74	+6.461	+2.493	+0.508	1.498	+0.562	+2.7	+.188	+0.500	+0.500	+.375	+0.231	+10.7
75	+6.567	+2.547	+0.510	1.484	+0.558	+2.4	+.186	+0.505	+0.495	+.376	+0.212	+9.7
76	+6.671	+2.607	+0.512	1.467	+0.552	+2.1	+.184	+0.511	+0.489	+.376	+0.189	+8.5
77	+6.772	+2.669	+0.514	1.451	+0.548	+1.9	+.183	+0.516	+0.484	+.378	+0.172	+7.6
78	+6.880	+2.735	+0.516	1.434	+0.545	+1.7	+.182	+0.522	+0.478	+.380	+0.160	+7.0
79	+6.992	+2.807	+0.518	1.420	+0.539	+1.5	+.180	+0.526	+0.474	+.380	+0.137	+5.9
80	+7.108	+2.882	+0.521	1.399	+0.537	+1.3	+.179	+0.533	+0.467	+.384	+0.128	+5.4
81	+7.236	+2.961	+0.523	1.380	+0.530	+1.0	+.177	+0.539	+0.461	+.384	+0.099	+4.1
82	+7.354	+3.034	+0.525	1.363	+0.524	+0.8	+.175	+0.545	+0.455	+.384	+0.075	+3.1
83	+7.471	+3.120	+0.528	1.348	+0.517	+0.5	+.173	+0.550	+0.450	+.384	+0.050	+2.0
84	+7.590	+3.203	+0.530	1.328	+0.511	+0.3	+.171	+0.557	+0.443	+.385	+0.026	+1.0
85	+7.713	+3.286	+0.533	1.312	+0.508	+0.1	+.169	+0.562	+0.438	+.387	+0.010	+0.4
86	+7.845	+3.372	+0.535	1.298	+0.502	-0.1	+.168	+0.567	+0.433	+.387	-0.011	-0.4
87	+7.996	+3.472	+0.538	1.277	+0.499	-0.2	+.167	+0.574	+0.426	+.391	-0.024	-0.9

****

Ko CONSOLIDATED MDSS TEST
MIT GEOTECHNICAL LAB

****

FILE NAME: DSSC11.PRN

REDUCTION DATA
UNITS: (kg,cm,mVOLTS,VOLTS)

1. TEST NAME : DSS-C11
2. DATE : 11-15-1987
3. OCR : 1
4. VER. CONSOLIDATION STRESS (KSC) : +2.996
5. HOR. CONSOLIDATION STRESS (KSC) : +0.000
6. PRE-SHEAR SAMPLE HEIGHT (cm) : +1.9893
7. VERTICAL STRESS LOAD CELL:
   ZERO: .63
   CF: 13.70491
8. HORIZONTAL SHEAR LOAD CELL:
   ZERO: -2.03
   CF: 6.70298
9. HORIZONTAL DISP. TRANSDUCER, X:
   ZERO: 1.4512
   CF: -1.81917
10. HORIZONTAL DISP. TRANSDUCER, Y:
    ZERO: 2.109
    CF: -.261
11. VERTICAL DISP. TRANSDUCER, Z1:
    ZERO: -.9113
    CF: .28883
12. VERTICAL DISP. TRANSDUCER, Z2:
    ZERO: -.3061
    CF: .29569
13. CONSTANT HEIGHT TRANSDUCER, Z:
    ZERO: .13077
    CF: .3014

Pt. No.	Str.X (%)	Str.Y (%)	SigV (ksc)	TauH (ksc)	Eu (ksc)	TauH ---- SigVc	DelU ---- SigVc	SigV ---- SigVc	TauH ---- SigV	TauH ---- Cu	Eu -- Cu
1	+0.000	+0.000	2.996	-0.002	+9999.0	-.001	+0.000	+1.000	-.001	-0.003	+9999.0
2	-0.007	+0.005	3.002	+0.009	-425.1	+.003	-0.002	+1.002	+.003	+0.017	-773.7
3	+0.003	+0.002	3.012	+0.021	+1948.6	+.007	-0.005	+1.005	+.007	+0.039	+3546.2
4	+0.026	+0.002	3.014	+0.038	+439.7	+.013	-0.006	+1.006	+.013	+0.070	+800.3
5	+0.054	+0.002	2.944	+0.070	+388.3	+.023	+0.017	+0.983	+.024	+0.127	+706.6
6	+0.089	+0.002	2.856	+0.113	+382.6	+.038	+0.047	+0.953	+.040	+0.205	+696.3
7	+0.134	+0.005	2.823	+0.175	+390.6	+.058	+0.058	+0.942	+.062	+0.319	+710.8
8	+0.193	+0.002	2.806	+0.238	+368.8	+.079	+0.063	+0.937	+.085	+0.433	+671.1
9	+0.269	+0.002	2.806	+0.296	+330.0	+.099	+0.063	+0.937	+.105	+0.538	+600.6
10	+0.357	+0.002	2.795	+0.345	+290.0	+.115	+0.067	+0.933	+.124	+0.629	+527.8
11	+0.469	+0.002	2.769	+0.387	+247.4	+.129	+0.076	+0.924	+.140	+0.704	+450.2
12	+0.598	+0.005	2.691	+0.422	+211.3	+.141	+0.102	+0.898	+.157	+0.767	+384.6
13	+0.746	+0.002	2.570	+0.449	+180.5	+.150	+0.142	+0.858	+.175	+0.817	+328.5
14	+0.903	+0.002	2.476	+0.470	+156.2	+.157	+0.174	+0.826	+.190	+0.856	+284.3
15	+1.066	+0.005	2.412	+0.486	+136.7	+.162	+0.195	+0.805	+.201	+0.884	+248.9
16	+1.233	+0.005	2.341	+0.497	+121.0	+.166	+0.219	+0.781	+.212	+0.905	+220.2
17	+1.398	+0.005	2.282	+0.507	+108.7	+.169	+0.238	+0.762	+.222	+0.922	+197.8
18	+1.569	+0.002	2.226	+0.514	+98.2	+.171	+0.257	+0.743	+.231	+0.934	+178.7
19	+1.733	+0.005	2.175	+0.515	+89.2	+.172	+0.274	+0.726	+.237	+0.938	+162.3
20	+1.907	+0.005	2.125	+0.521	+82.0	+.174	+0.291	+0.709	+.245	+0.949	+149.3
21	+2.084	+0.005	2.082	+0.526	+75.7	+.176	+0.305	+0.695	+.253	+0.957	+137.8
22	+2.267	+0.005	2.036	+0.531	+70.2	+.177	+0.320	+0.680	+.261	+0.966	+127.8

TEST NAME : DSS-C11

Pt. No.	Str.X (%)	Str.Y (%)	SigV (ksc)	TauH (ksc)	Eu (ksc)	TauH ---- SigVc	DelU ---- SigVc	SigV ---- SigVc	TauH ---- SigV	TauH ---- Cu	Eu -- Cu
23	+2.451	+0.002	1.997	+0.535	+65.4	+.178	+0.333	+0.667	+.268	+0.973	+119.1
24	+2.630	+0.005	1.956	+0.538	+61.4	+.180	+0.347	+0.653	+.275	+0.979	+111.7
25	+2.821	+0.005	1.917	+0.541	+57.5	+.181	+0.360	+0.640	+.282	+0.984	+104.7
26	+3.005	+0.007	1.882	+0.543	+54.2	+.181	+0.372	+0.628	+.289	+0.988	+98.7
27	+3.181	+0.007	1.850	+0.544	+51.3	+.182	+0.383	+0.617	+.294	+0.991	+93.4
28	+3.373	+0.005	1.821	+0.547	+48.7	+.183	+0.392	+0.608	+.301	+0.996	+88.6
29	+3.569	+0.005	1.789	+0.548	+46.0	+.183	+0.403	+0.597	+.306	+0.996	+83.8
30	+3.761	+0.007	1.758	+0.547	+43.6	+.183	+0.413	+0.587	+.311	+0.996	+79.4
31	+3.944	+0.007	1.734	+0.547	+41.6	+.183	+0.421	+0.579	+.316	+0.996	+75.8
32	+4.135	+0.007	1.713	+0.549	+39.9	+.183	+0.428	+0.572	+.321	+1.000	+72.6
33	+4.322	+0.009	1.689	+0.548	+38.0	+.183	+0.436	+0.564	+.324	+0.997	+69.2
34	+4.517	+0.014	1.668	+0.549	+36.4	+.183	+0.443	+0.557	+.329	+0.998	+66.3
35	+4.708	+0.016	1.647	+0.549	+35.0	+.183	+0.450	+0.550	+.333	+0.998	+63.6
36	+4.908	+0.016	1.630	+0.548	+33.5	+.183	+0.456	+0.544	+.336	+0.998	+61.0
37	+5.095	+0.016	1.607	+0.548	+32.2	+.183	+0.464	+0.536	+.341	+0.997	+58.7
38	+5.292	+0.016	1.587	+0.547	+31.0	+.183	+0.470	+0.530	+.345	+0.996	+56.5
39	+5.472	+0.019	1.569	+0.545	+29.9	+.182	+0.476	+0.524	+.348	+0.993	+54.4
40	+5.647	+0.024	1.554	+0.544	+28.9	+.182	+0.481	+0.519	+.350	+0.991	+52.6
41	+5.827	+0.021	1.536	+0.544	+28.0	+.182	+0.487	+0.513	+.354	+0.990	+51.0
42	+6.005	+0.021	1.523	+0.545	+27.2	+.182	+0.492	+0.508	+.358	+0.992	+49.5
43	+6.184	+0.028	1.507	+0.543	+26.3	+.181	+0.497	+0.503	+.360	+0.988	+48.0
44	+6.358	+0.028	1.498	+0.542	+25.6	+.181	+0.500	+0.500	+.362	+0.987	+46.6
45	+6.527	+0.031	1.486	+0.544	+25.0	+.181	+0.504	+0.496	+.366	+0.989	+45.5
46	+6.709	+0.033	1.472	+0.543	+24.3	+.181	+0.509	+0.491	+.369	+0.989	+44.2
47	+6.898	+0.035	1.463	+0.544	+23.7	+.182	+0.512	+0.488	+.372	+0.990	+43.1
48	+7.092	+0.038	1.445	+0.543	+23.0	+.181	+0.518	+0.482	+.376	+0.988	+41.8
49	+7.281	+0.040	1.435	+0.542	+22.3	+.181	+0.521	+0.479	+.378	+0.986	+40.6
50	+7.464	+0.042	1.421	+0.542	+21.8	+.181	+0.526	+0.474	+.381	+0.985	+39.6
51	+7.651	+0.049	1.410	+0.540	+21.2	+.180	+0.529	+0.471	+.383	+0.983	+38.5
52	+7.840	+0.056	1.401	+0.540	+20.7	+.180	+0.532	+0.468	+.386	+0.983	+37.6
53	+8.028	+0.059	1.400	+0.540	+20.2	+.180	+0.533	+0.467	+.386	+0.982	+36.7
54	+8.214	+0.071	1.383	+0.539	+19.7	+.180	+0.538	+0.462	+.389	+0.980	+35.8
55	+8.396	+0.071	1.372	+0.537	+19.2	+.179	+0.542	+0.458	+.391	+0.977	+34.9
56	+8.595	+0.071	1.361	+0.538	+18.8	+.179	+0.546	+0.454	+.395	+0.978	+34.2
57	+8.777	+0.073	1.350	+0.535	+18.3	+.179	+0.549	+0.451	+.397	+0.974	+33.3
58	+8.963	+0.075	1.340	+0.534	+17.9	+.178	+0.553	+0.447	+.398	+0.972	+32.5
59	+9.141	+0.073	1.335	+0.534	+17.5	+.178	+0.554	+0.446	+.400	+0.971	+31.9
60	+9.330	+0.078	1.327	+0.535	+17.2	+.178	+0.557	+0.443	+.403	+0.973	+31.3
61	+9.530	+0.082	1.317	+0.535	+16.8	+.179	+0.560	+0.440	+.406	+0.973	+30.6
62	+9.724	+0.087	1.308	+0.535	+16.5	+.179	+0.563	+0.437	+.409	+0.973	+30.0
63	+9.914	+0.089	1.308	+0.532	+16.1	+.178	+0.563	+0.437	+.407	+0.969	+29.3
64	+10.106	+0.089	1.307	+0.533	+15.8	+.178	+0.564	+0.436	+.408	+0.970	+28.8
65	+10.296	+0.099	1.311	+0.532	+15.5	+.178	+0.562	+0.438	+.406	+0.968	+28.2
66	+10.483	+0.099	1.325	+0.533	+15.3	+.178	+0.558	+0.442	+.402	+0.970	+27.8
67	+10.668	+0.101	1.372	+0.533	+15.0	+.178	+0.542	+0.458	+.389	+0.970	+27.3
68	+10.856	+0.106	1.421	+0.535	+14.8	+.179	+0.526	+0.474	+.376	+0.973	+26.9
69	+11.045	+0.106	1.421	+0.537	+14.6	+.179	+0.526	+0.474	+.378	+0.977	+26.5
70	+11.235	+0.111	1.392	+0.536	+14.3	+.179	+0.535	+0.465	+.385	+0.975	+26.0

TEST NAME : DSS-C11

Pt. No.	Str.X (%)	Str.Y (%)	SigV (ksc)	TauH (ksc)	Eu (ksc)	TauH / SigVc	DelU / SigVc	SigV / SigVc	TauH / SigV	TauH / Cu	Eu / Cu
71	+11.422	+0.111	1.293	+0.533	+14.0	+.178	+0.568	+0.432	+.412	+0.970	+25.5
72	+11.615	+0.111	1.227	+0.528	+13.6	+.176	+0.590	+0.410	+.430	+0.960	+24.8
73	+11.820	+0.113	1.223	+0.525	+13.3	+.175	+0.592	+0.408	+.429	+0.956	+24.3
74	+12.014	+0.113	1.237	+0.523	+13.1	+.175	+0.587	+0.413	+.423	+0.952	+23.8
75	+12.196	+0.127	1.270	+0.523	+12.9	+.175	+0.576	+0.424	+.412	+0.952	+23.4
76	+12.379	+0.129	1.363	+0.525	+12.7	+.175	+0.545	+0.455	+.385	+0.956	+23.2
77	+12.571	+0.129	1.368	+0.526	+12.6	+.176	+0.543	+0.457	+.385	+0.958	+22.9
78	+12.758	+0.134	1.339	+0.525	+12.3	+.175	+0.553	+0.447	+.392	+0.955	+22.5
79	+12.960	+0.136	1.253	+0.523	+12.1	+.175	+0.582	+0.418	+.417	+0.952	+22.0
80	+13.150	+0.139	1.181	+0.516	+11.8	+.172	+0.606	+0.394	+.437	+0.938	+21.4
81	+13.332	+0.141	1.169	+0.514	+11.6	+.171	+0.610	+0.390	+.440	+0.935	+21.0
82	+13.514	+0.151	1.169	+0.513	+11.4	+.171	+0.610	+0.390	+.439	+0.933	+20.7
83	+13.696	+0.151	1.176	+0.511	+11.2	+.171	+0.607	+0.393	+.435	+0.931	+20.4
84	+13.873	+0.158	1.204	+0.511	+11.1	+.171	+0.598	+0.402	+.424	+0.930	+20.1
85	+14.057	+0.162	1.299	+0.511	+10.9	+.171	+0.566	+0.434	+.394	+0.930	+19.9
86	+14.234	+0.162	1.313	+0.514	+10.8	+.172	+0.562	+0.438	+.392	+0.936	+19.7
87	+14.435	+0.162	1.292	+0.516	+10.7	+.172	+0.569	+0.431	+.399	+0.939	+19.5
88	+14.632	+0.165	1.242	+0.513	+10.5	+.171	+0.585	+0.415	+.413	+0.934	+19.1
89	+14.845	+0.172	1.132	+0.507	+10.2	+.169	+0.622	+0.378	+.448	+0.923	+18.7
90	+15.035	+0.172	1.108	+0.502	+10.0	+.167	+0.630	+0.370	+.453	+0.913	+18.2
91	+15.219	+0.176	1.109	+0.500	+9.8	+.167	+0.630	+0.370	+.451	+0.909	+17.9
92	+15.464	+0.176	1.114	+0.497	+9.7	+.166	+0.628	+0.372	+.447	+0.905	+17.6
93	+15.637	+0.181	1.114	+0.495	+9.5	+.165	+0.628	+0.372	+.445	+0.901	+17.3
94	+15.816	+0.179	1.115	+0.493	+9.4	+.165	+0.628	+0.372	+.442	+0.898	+17.0
95	+16.108	+0.176	1.112	+0.490	+9.1	+.163	+0.629	+0.371	+.440	+0.891	+16.6
96	+16.344	+0.179	1.113	+0.487	+8.9	+.162	+0.628	+0.372	+.437	+0.886	+16.3
97	+16.353	+0.179	1.113	+0.486	+8.9	+.162	+0.628	+0.372	+.437	+0.885	+16.2
98	+16.598	+0.183	1.114	+0.482	+8.7	+.161	+0.628	+0.372	+.433	+0.878	+15.9
99	+16.918	+0.183	1.113	+0.478	+8.5	+.160	+0.628	+0.372	+.429	+0.870	+15.4
100	+16.929	+0.183	1.113	+0.478	+8.5	+.160	+0.629	+0.371	+.430	+0.871	+15.4
101	+17.412	+0.186	1.113	+0.471	+8.1	+.157	+0.629	+0.371	+.423	+0.856	+14.8
102	+17.417	+0.183	1.113	+0.470	+8.1	+.157	+0.628	+0.372	+.422	+0.856	+14.7
103	+17.511	+0.186	1.113	+0.470	+8.0	+.157	+0.628	+0.372	+.422	+0.855	+14.6
104	+17.709	+0.195	1.113	+0.469	+7.9	+.156	+0.629	+0.371	+.421	+0.853	+14.4
105	+17.894	+0.195	1.098	+0.464	+7.8	+.155	+0.633	+0.367	+.423	+0.845	+14.2
106	+18.094	+0.195	1.034	+0.461	+7.6	+.154	+0.655	+0.345	+.446	+0.839	+13.9
107	+18.286	+0.195	0.949	+0.455	+7.5	+.152	+0.683	+0.317	+.479	+0.827	+13.6
108	+18.488	+0.191	0.930	+0.450	+7.3	+.150	+0.690	+0.310	+.484	+0.820	+13.3
109	+18.686	+0.198	0.922	+0.447	+7.2	+.149	+0.692	+0.308	+.484	+0.813	+13.0
110	+18.893	+0.202	0.919	+0.444	+7.1	+.148	+0.693	+0.307	+.483	+0.808	+12.8
111	+19.085	+0.205	0.919	+0.441	+6.9	+.147	+0.693	+0.307	+.479	+0.802	+12.6
112	+19.295	+0.205	0.913	+0.439	+6.8	+.146	+0.695	+0.305	+.480	+0.798	+12.4
113	+19.480	+0.207	0.886	+0.434	+6.7	+.145	+0.704	+0.296	+.489	+0.789	+12.2
114	+19.670	+0.207	0.877	+0.431	+6.6	+.144	+0.707	+0.293	+.491	+0.784	+12.0
115	+19.840	+0.209	0.867	+0.426	+6.4	+.142	+0.711	+0.289	+.492	+0.776	+11.7
116	+20.022	+0.214	0.863	+0.426	+6.4	+.142	+0.712	+0.288	+.493	+0.775	+11.6
117	+20.208	+0.212	0.860	+0.421	+6.3	+.141	+0.713	+0.287	+.490	+0.766	+11.4
118	+20.363	+0.219	0.849	+0.420	+6.2	+.140	+0.717	+0.283	+.494	+0.764	+11.2

TEST NAME : DSS-C11

Pt. No.	Str.X (%)	Str.Y (%)	SigV (ksc)	TauH (ksc)	Eu (ksc)	TauH ---- SigVc	DelU ---- SigVc	SigV ---- SigVc	TauH ---- SigV	TauH ---- Cu	Eu -- Cu
119	+20.545	+0.216	0.837	+0.417	+6.1	+.139	+0.721	+0.279	+.498	+0.758	+11.1
120	+20.741	+0.216	0.828	+0.416	+6.0	+.139	+0.724	+0.276	+.503	+0.757	+10.9
121	+20.952	+0.219	0.817	+0.412	+5.9	+.137	+0.727	+0.273	+.504	+0.749	+10.7
122	+21.144	+0.216	0.808	+0.408	+5.8	+.136	+0.730	+0.270	+.505	+0.742	+10.5
123	+21.321	+0.221	0.799	+0.404	+5.7	+.135	+0.733	+0.267	+.505	+0.735	+10.3
124	+21.509	+0.223	0.791	+0.402	+5.6	+.134	+0.736	+0.264	+.508	+0.731	+10.2
125	+21.709	+0.221	0.783	+0.400	+5.5	+.134	+0.739	+0.261	+.511	+0.728	+10.1
126	+21.901	+0.221	0.773	+0.396	+5.4	+.132	+0.742	+0.258	+.513	+0.721	+9.9
127	+22.091	+0.221	0.766	+0.394	+5.3	+.131	+0.744	+0.256	+.514	+0.717	+9.7
128	+22.297	+0.223	0.754	+0.391	+5.3	+.130	+0.748	+0.252	+.518	+0.711	+9.6
129	+22.505	+0.223	0.748	+0.387	+5.2	+.129	+0.750	+0.250	+.517	+0.704	+9.4
130	+22.706	+0.226	0.740	+0.383	+5.1	+.128	+0.753	+0.247	+.518	+0.698	+9.2
131	+22.906	+0.226	0.732	+0.381	+5.0	+.127	+0.756	+0.244	+.520	+0.693	+9.1
132	+23.111	+0.226	0.721	+0.378	+4.9	+.126	+0.759	+0.241	+.524	+0.687	+8.9
133	+23.313	+0.226	0.711	+0.374	+4.8	+.125	+0.763	+0.237	+.526	+0.680	+8.8
134	+23.516	+0.226	0.702	+0.371	+4.7	+.124	+0.766	+0.234	+.528	+0.674	+8.6
135	+23.711	+0.226	0.693	+0.366	+4.6	+.122	+0.769	+0.231	+.527	+0.665	+8.4
136	+23.897	+0.230	0.690	+0.363	+4.6	+.121	+0.770	+0.230	+.526	+0.660	+8.3
137	+24.082	+0.226	0.677	+0.360	+4.5	+.120	+0.774	+0.226	+.531	+0.655	+8.2
138	+24.270	+0.233	0.672	+0.357	+4.4	+.119	+0.776	+0.224	+.531	+0.650	+8.0
139	+24.454	+0.238	0.663	+0.353	+4.3	+.118	+0.779	+0.221	+.533	+0.642	+7.9
140	+24.639	+0.242	0.653	+0.350	+4.3	+.117	+0.782	+0.218	+.536	+0.638	+7.8
141	+24.824	+0.247	0.646	+0.348	+4.2	+.116	+0.784	+0.216	+.539	+0.633	+7.7
142	+25.021	+0.245	0.635	+0.345	+4.1	+.115	+0.788	+0.212	+.543	+0.628	+7.5
143	+25.219	+0.249	0.630	+0.341	+4.1	+.114	+0.790	+0.210	+.542	+0.621	+7.4
144	+25.413	+0.249	0.625	+0.339	+4.0	+.113	+0.791	+0.209	+.543	+0.617	+7.3
145	+25.600	+0.256	0.616	+0.335	+3.9	+.112	+0.794	+0.206	+.544	+0.609	+7.1
146	+25.787	+0.256	0.606	+0.331	+3.9	+.110	+0.798	+0.202	+.546	+0.602	+7.0
147	+25.972	+0.261	0.601	+0.329	+3.8	+.110	+0.799	+0.201	+.547	+0.598	+6.9
148	+26.172	+0.263	0.593	+0.324	+3.7	+.108	+0.802	+0.198	+.547	+0.590	+6.8
149	+26.357	+0.266	0.585	+0.321	+3.6	+.107	+0.805	+0.195	+.548	+0.584	+6.6
150	+26.536	+0.266	0.583	+0.319	+3.6	+.106	+0.806	+0.194	+.547	+0.580	+6.6
151	+26.733	+0.266	0.571	+0.316	+3.5	+.106	+0.809	+0.191	+.554	+0.576	+6.5
152	+26.920	+0.268	0.564	+0.314	+3.5	+.105	+0.812	+0.188	+.557	+0.572	+6.4
153	+27.111	+0.270	0.559	+0.312	+3.5	+.104	+0.813	+0.187	+.558	+0.568	+6.3
154	+27.300	+0.273	0.556	+0.309	+3.4	+.103	+0.814	+0.186	+.556	+0.562	+6.2
155	+27.498	+0.270	0.545	+0.306	+3.3	+.102	+0.818	+0.182	+.562	+0.557	+6.1
156	+27.690	+0.270	0.540	+0.301	+3.3	+.101	+0.820	+0.180	+.558	+0.548	+5.9
157	+27.879	+0.275	0.537	+0.299	+3.2	+.100	+0.821	+0.179	+.557	+0.545	+5.9
158	+28.077	+0.275	0.532	+0.298	+3.2	+.100	+0.822	+0.178	+.561	+0.543	+5.8
159	+28.279	+0.278	0.524	+0.296	+3.1	+.099	+0.825	+0.175	+.565	+0.538	+5.7
160	+28.472	+0.280	0.517	+0.293	+3.1	+.098	+0.827	+0.173	+.566	+0.533	+5.6
161	+28.664	+0.282	0.515	+0.291	+3.0	+.097	+0.828	+0.172	+.566	+0.530	+5.5
162	+28.864	+0.287	0.508	+0.289	+3.0	+.096	+0.830	+0.170	+.569	+0.526	+5.5
163	+29.059	+0.299	0.499	+0.286	+2.9	+.095	+0.833	+0.167	+.572	+0.520	+5.4
164	+29.236	+0.306	0.494	+0.284	+2.9	+.095	+0.835	+0.165	+.576	+0.518	+5.3
165	+29.434	+0.308	0.488	+0.281	+2.9	+.094	+0.837	+0.163	+.576	+0.511	+5.2
166	+29.628	+0.310	0.484	+0.278	+2.8	+.093	+0.838	+0.162	+.573	+0.505	+5.1

TEST NAME : DSS-C11

Pt. No.	Str.X (%)	Str.Y (%)	SigV (ksc)	TauH (ksc)	Eu (ksc)	TauH / SigVc	DelU / SigVc	SigV / SigVc	TauH / SigV	TauH / Cu	Eu / Cu
167	+29.823	+0.311	0.481	+0.277	+2.8	+.092	+0.840	+0.160	+.576	+0.504	+5.1
168	+30.025	+0.318	0.472	+0.275	+2.7	+.092	+0.842	+0.158	+.582	+0.501	+5.0
169	+30.230	+0.320	0.469	+0.270	+2.7	+.090	+0.843	+0.157	+.577	+0.492	+4.9

****

ANISOTROPICALLY CONSOLIDATED MDSS TEST
MIT GEOTECHNICAL LAB

****

FILE NAME: DSSC12.PRN

REDUCTION DATA
UNITS: (kg,cm,mVOLTS,VOLTS)

1. TEST NAME : DSSC12
2. DATE : 12-11-1987
3. OCR : 1
4. VER. CONSOLIDATION STRESS (KSC) : +2.997
5. HOR. CONSOLIDATION STRESS (KSC) : +0.600
6. PRE-SHEAR SAMPLE HEIGHT (cm) : +1.9227
7. VERTICAL STRESS LOAD CELL:
   ZERO: .64
   CF: 13.70491
8. HORIZONTAL SHEAR LOAD CELL:
   ZERO: -1.66
   CF: 6.70298
9. HORIZONTAL DISP. TRANSDUCER, X:
   ZERO: 1.4459
   CF: -1.81917
10. HORIZONTAL DISP. TRANSDUCER, Y:
    ZERO: -4.447
    CF: -.261
11. VERTICAL DISP. TRANSDUCER, Z1:
    ZERO: .2815
    CF: .28883
12. VERTICAL DISP. TRANSDUCER, Z2:
    ZERO: 1.2761
    CF: .29569
13. CONSTANT HEIGHT TRANSDUCER, Z:
    ZERO: .14807
    CF: .3014
14. TEST ANGLE THETA (degrees): 90

TOTAL X DISP. DURING CONSOLIDATION (cm): .02101

Pt. No.	Str.X (%)	Str.Y (%)	X.Coor. (cm)	SigV (ksc)	TauH (ksc)	Eu (ksc)	TauH / SigVc	DelU / SigVc	SigV / SigVc	TauH / SigV	TauH / Cu	Eu / Cu
1	+0.000	+0.000	+0.021	2.997	-0.003	+9999.0	-.001	+0.000	+1.000	-.001	+0.000	+9999.0
2	-0.008	-0.005	+0.021	2.998	-0.001	-48.8	-.000	-0.000	+1.000	-.000	+0.003	-104.9
3	-0.008	-0.002	+0.021	2.994	-0.001	-48.8	-.000	+0.001	+0.999	-.000	+0.003	-104.9
4	+0.002	-0.002	+0.021	2.991	-0.000	+364.1	-.000	+0.002	+0.998	-.000	+0.004	+782.6
5	+0.002	+0.000	+0.021	2.982	+0.002	+849.8	+.001	+0.005	+0.995	+.001	+0.010	+1826.8
6	+0.003	+0.000	+0.021	2.969	+0.008	+971.8	+.003	+0.009	+0.991	+.003	+0.024	+2089.1
7	+0.005	-0.002	+0.021	2.959	+0.016	+1093.1	+.005	+0.013	+0.987	+.005	+0.040	+2349.8
8	+0.010	-0.002	+0.021	2.948	+0.029	+930.9	+.010	+0.017	+0.983	+.010	+0.068	+2001.2
9	+0.019	+0.002	+0.021	2.936	+0.046	+772.7	+.015	+0.020	+0.980	+.016	+0.103	+1661.1
10	+0.036	+0.005	+0.022	2.928	+0.072	+627.3	+.024	+0.023	+0.977	+.025	+0.160	+1348.5
11	+0.049	+0.010	+0.022	2.919	+0.098	+613.3	+.033	+0.026	+0.974	+.034	+0.216	+1318.4
12	+0.070	+0.010	+0.022	2.906	+0.124	+546.3	+.041	+0.030	+0.970	+.043	+0.272	+1174.4
13	+0.092	+0.015	+0.023	2.887	+0.155	+517.1	+.052	+0.037	+0.963	+.054	+0.339	+1111.6
14	+0.115	+0.024	+0.023	2.868	+0.187	+493.6	+.062	+0.043	+0.957	+.065	+0.408	+1061.1
15	+0.151	+0.036	+0.024	2.840	+0.218	+438.5	+.073	+0.052	+0.948	+.077	+0.474	+942.7
16	+0.181	+0.046	+0.024	2.812	+0.249	+415.2	+.083	+0.062	+0.938	+.088	+0.540	+892.6
17	+0.219	+0.058	+0.025	2.786	+0.278	+384.4	+.093	+0.070	+0.930	+.100	+0.603	+826.3
18	+0.263	+0.080	+0.026	2.762	+0.303	+348.4	+.101	+0.078	+0.922	+.110	+0.656	+749.1
19	+0.310	+0.105	+0.027	2.740	+0.327	+318.7	+.109	+0.086	+0.914	+.119	+0.709	+685.0
20	+0.361	+0.127	+0.028	2.710	+0.349	+291.7	+.116	+0.096	+0.904	+.129	+0.755	+627.1

TEST NAME : DSSC12

Pt. No.	Str.X (%)	Str.Y (%)	X.Coor. (cm)	SigV (ksc)	TauH (ksc)	Eu (ksc)	TauH ---- SigVc	DelU ---- SigVc	SigV ---- SigVc	TauH ---- SigV	TauH ---- Cu	Eu -- Cu
21	+0.421	+0.161	+0.029	2.680	+0.367	+263.7	+.123	+0.106	+0.894	+.137	+0.795	+567.0
22	+0.490	+0.190	+0.030	2.645	+0.384	+236.8	+.128	+0.117	+0.883	+.145	+0.832	+509.0
23	+0.550	+0.229	+0.032	2.610	+0.399	+219.1	+.133	+0.129	+0.871	+.153	+0.863	+470.9
24	+0.624	+0.270	+0.033	2.573	+0.409	+197.8	+.136	+0.142	+0.858	+.159	+0.885	+425.2
25	+0.701	+0.314	+0.034	2.534	+0.418	+180.2	+.140	+0.154	+0.846	+.165	+0.905	+387.3
26	+0.780	+0.365	+0.036	2.500	+0.425	+164.5	+.142	+0.166	+0.834	+.170	+0.920	+353.7
27	+0.860	+0.421	+0.038	2.461	+0.432	+151.5	+.144	+0.179	+0.821	+.175	+0.934	+325.7
28	+0.941	+0.475	+0.039	2.432	+0.438	+140.3	+.146	+0.188	+0.812	+.180	+0.946	+301.5
29	+1.023	+0.533	+0.041	2.400	+0.444	+130.9	+.148	+0.199	+0.801	+.185	+0.959	+281.4
30	+1.116	+0.599	+0.042	2.370	+0.448	+121.1	+.150	+0.209	+0.791	+.189	+0.969	+260.4
31	+1.208	+0.669	+0.044	2.337	+0.452	+112.9	+.151	+0.220	+0.780	+.193	+0.977	+242.6
32	+1.309	+0.742	+0.046	2.306	+0.455	+104.8	+.152	+0.230	+0.770	+.197	+0.983	+225.3
33	+1.398	+0.815	+0.048	2.277	+0.456	+98.5	+.152	+0.240	+0.760	+.200	+0.987	+211.8
34	+1.498	+0.888	+0.050	2.243	+0.458	+92.3	+.153	+0.251	+0.749	+.204	+0.990	+198.4
35	+1.593	+0.964	+0.052	2.220	+0.458	+86.8	+.153	+0.259	+0.741	+.206	+0.990	+186.5
36	+1.689	+1.039	+0.053	2.194	+0.460	+82.1	+.154	+0.268	+0.732	+.210	+0.994	+176.6
37	+1.790	+1.124	+0.055	2.169	+0.461	+77.7	+.154	+0.276	+0.724	+.213	+0.996	+167.1
38	+1.891	+1.212	+0.057	2.143	+0.463	+73.8	+.154	+0.285	+0.715	+.216	+1.000	+158.6
39	+1.993	+1.295	+0.059	2.114	+0.463	+70.0	+.154	+0.295	+0.705	+.219	+1.000	+150.5
40	+2.086	+1.387	+0.061	2.089	+0.461	+66.7	+.154	+0.303	+0.697	+.221	+0.997	+143.4
41	+2.186	+1.482	+0.063	2.069	+0.460	+63.4	+.153	+0.310	+0.690	+.222	+0.994	+136.3
42	+2.286	+1.569	+0.065	2.042	+0.458	+60.5	+.153	+0.319	+0.681	+.224	+0.990	+130.0
43	+2.385	+1.665	+0.067	2.019	+0.458	+57.9	+.153	+0.326	+0.674	+.227	+0.990	+124.5
44	+2.482	+1.755	+0.069	2.001	+0.455	+55.3	+.152	+0.332	+0.668	+.227	+0.984	+118.9
45	+2.580	+1.845	+0.071	1.979	+0.454	+53.0	+.151	+0.340	+0.660	+.229	+0.980	+114.0
46	+2.677	+1.940	+0.072	1.959	+0.452	+51.0	+.151	+0.346	+0.654	+.231	+0.977	+109.5
47	+2.775	+2.037	+0.074	1.938	+0.451	+49.0	+.150	+0.353	+0.647	+.233	+0.975	+105.4
48	+2.868	+2.134	+0.076	1.919	+0.449	+47.2	+.150	+0.360	+0.640	+.234	+0.970	+101.5
49	+2.962	+2.239	+0.078	1.901	+0.446	+45.4	+.149	+0.366	+0.634	+.235	+0.964	+97.7
50	+3.058	+2.334	+0.080	1.885	+0.443	+43.7	+.148	+0.371	+0.629	+.235	+0.957	+93.9
51	+3.153	+2.443	+0.082	1.869	+0.441	+42.2	+.147	+0.377	+0.623	+.236	+0.954	+90.7
52	+3.252	+2.550	+0.084	1.852	+0.438	+40.7	+.146	+0.382	+0.618	+.237	+0.948	+87.4
53	+3.352	+2.672	+0.085	1.837	+0.435	+39.2	+.145	+0.387	+0.613	+.237	+0.941	+84.2
54	+3.452	+2.797	+0.087	1.819	+0.429	+37.5	+.143	+0.393	+0.607	+.236	+0.928	+80.7
55	+3.551	+2.933	+0.089	1.803	+0.424	+36.1	+.142	+0.398	+0.602	+.235	+0.918	+77.5
56	+3.659	+3.071	+0.091	1.782	+0.420	+34.7	+.140	+0.405	+0.595	+.236	+0.909	+74.6
57	+3.759	+3.215	+0.093	1.765	+0.415	+33.3	+.138	+0.411	+0.589	+.235	+0.897	+71.6
58	+3.864	+3.361	+0.095	1.747	+0.411	+32.1	+.137	+0.417	+0.583	+.235	+0.890	+69.1
59	+3.969	+3.507	+0.097	1.728	+0.406	+30.9	+.136	+0.423	+0.577	+.235	+0.879	+66.4
60	+4.066	+3.648	+0.099	1.710	+0.400	+29.7	+.133	+0.429	+0.571	+.234	+0.865	+63.8
61	+4.163	+3.804	+0.101	1.692	+0.394	+28.6	+.132	+0.436	+0.564	+.233	+0.853	+61.5
62	+4.263	+3.955	+0.103	1.673	+0.389	+27.6	+.130	+0.442	+0.558	+.233	+0.842	+59.3
63	+4.361	+4.103	+0.105	1.657	+0.384	+26.6	+.128	+0.447	+0.553	+.232	+0.831	+57.2
64	+4.462	+4.253	+0.107	1.635	+0.380	+25.7	+.127	+0.454	+0.546	+.232	+0.822	+55.3
65	+4.562	+4.398	+0.109	1.619	+0.376	+24.9	+.126	+0.460	+0.540	+.232	+0.814	+53.5
66	+4.660	+4.551	+0.111	1.603	+0.372	+24.1	+.124	+0.465	+0.535	+.232	+0.804	+51.8
67	+4.770	+4.707	+0.113	1.583	+0.368	+23.3	+.123	+0.472	+0.528	+.233	+0.798	+50.2
68	+4.874	+4.871	+0.115	1.559	+0.362	+22.5	+.121	+0.480	+0.520	+.233	+0.785	+48.3

TEST NAME : DSSC12

Pt. No.	Str.X (%)	Str.Y (%)	X.Coor. (cm)	SigV (ksc)	TauH (ksc)	Eu (ksc)	TauH ---- SigVc	DelU ---- SigVc	SigV ---- SigVc	TauH ---- SigV	TauH ---- Cu	Eu -- Cu
69	+4.979	+5.049	+0.117	1.536	+0.356	+21.6	+.119	+0.488	+0.512	+.232	+0.770	+46.4
70	+5.089	+5.224	+0.119	1.517	+0.350	+20.8	+.117	+0.494	+0.506	+.231	+0.757	+44.6
71	+5.202	+5.415	+0.121	1.492	+0.341	+19.8	+.114	+0.502	+0.498	+.229	+0.738	+42.6
72	+5.321	+5.629	+0.123	1.466	+0.332	+18.9	+.111	+0.511	+0.489	+.227	+0.720	+40.6
73	+5.449	+5.900	+0.126	1.433	+0.319	+17.7	+.106	+0.522	+0.478	+.222	+0.690	+38.0
74	+5.589	+6.235	+0.128	1.388	+0.297	+16.1	+.099	+0.537	+0.463	+.214	+0.644	+34.6
75	+5.735	+6.663	+0.131	1.342	+0.271	+14.3	+.091	+0.552	+0.448	+.202	+0.589	+30.8
76	+5.901	+7.238	+0.134	1.273	+0.240	+12.3	+.080	+0.575	+0.425	+.188	+0.520	+26.5

****

ANISOTROPICALLY CONSOLIDATED MDSS TEST
MIT GEOTECHNICAL LAB

****

FILE NAME: DSSC13.PRN

REDUCTION DATA
UNITS: (kg,cm,mVOLTS,VOLTS)

1. TEST NAME : DSS-C13
2. DATE : 01-20-1988
3. OCR : 1
4. VER. CONSOLIDATION STRESS (KSC) : +2.999
5. HOR. CONSOLIDATION STRESS (KSC) : +0.600
6. PRE-SHEAR SAMPLE HEIGHT (cm) : +2.0371
7. VERTICAL STRESS LOAD CELL:
   ZERO: .65
   CF: 13.70491
8. HORIZONTAL SHEAR LOAD CELL:
   ZERO: -1.58
   CF: 6.70298
9. HORIZONTAL DISP. TRANSDUCER, X:
   ZERO: 1.1476
   CF: -1.81917
10. HORIZONTAL DISP. TRANSDUCER, Y:
    ZERO: .2418
    CF: -.261
11. VERTICAL DISP. TRANSDUCER, Z1:
    ZERO: .5184
    CF: .28883
12. VERTICAL DISP. TRANSDUCER, Z2:
    ZERO: .8289
    CF: .29569
13. CONSTANT HEIGHT TRANSDUCER, Z:
    ZERO: .1256
    CF: .3014
14. TEST ANGLE THETA (degrees): 150
    TOTAL X DISP. DURING CONSOLIDATION (cm): -.26947

Pt. No.	Str.X (%)	Str.Y (%)	X.Coor. (cm)	SigV (ksc)	TauH (ksc)	Eu (ksc)	TauH / SigVc	DelU / SigVc	SigV / SigVc	TauH / SigV	TauH / Cu	Eu / Cu
1	+0.000	+0.000	-0.269	2.999	-0.509	+9999.0	-.170	+0.000	+1.000	-.170	+0.000	+9396.2
2	-0.005	+0.009	-0.270	2.999	-0.495	-922.6	-.165	-0.000	+1.000	-.165	+0.014	-867.0
3	-0.008	+0.027	-0.270	2.999	-0.451	-2187.9	-.150	-0.000	+1.000	-.150	+0.055	-2056.0
4	-0.008	+0.032	-0.270	2.997	-0.443	-2483.9	-.148	+0.001	+0.999	-.148	+0.062	-2334.1
5	-0.006	+0.043	-0.270	2.994	-0.340	-7914.8	-.113	+0.002	+0.998	-.114	+0.159	-7437.6
6	+0.027	+0.057	-0.269	2.970	-0.271	+2626.2	-.090	+0.010	+0.990	-.091	+0.224	+2467.8
7	+0.074	+0.075	-0.268	2.933	-0.206	+1237.5	-.069	+0.022	+0.978	-.070	+0.285	+1162.9
8	+0.125	+0.087	-0.267	2.888	-0.149	+865.8	-.050	+0.037	+0.963	-.052	+0.339	+813.6
9	+0.165	+0.089	-0.266	2.843	-0.114	+720.0	-.038	+0.052	+0.948	-.040	+0.372	+676.6
10	+0.202	+0.091	-0.265	2.802	-0.087	+628.3	-.029	+0.066	+0.934	-.031	+0.397	+590.4
11	+0.245	+0.098	-0.264	2.769	-0.053	+559.4	-.018	+0.077	+0.923	-.019	+0.429	+525.7
12	+0.291	+0.107	-0.264	2.737	-0.021	+503.1	-.007	+0.087	+0.913	-.008	+0.459	+472.8
13	+0.344	+0.112	-0.262	2.704	+0.011	+453.1	+.004	+0.098	+0.902	+.004	+0.489	+425.8
14	+0.387	+0.119	-0.262	2.674	+0.031	+418.5	+.010	+0.108	+0.892	+.012	+0.508	+393.3
15	+0.439	+0.119	-0.261	2.636	+0.058	+387.9	+.019	+0.121	+0.879	+.022	+0.533	+364.5
16	+0.458	+0.124	-0.260	2.606	+0.061	+373.4	+.020	+0.131	+0.869	+.023	+0.536	+350.9
17	+0.500	+0.133	-0.259	2.587	+0.081	+354.8	+.027	+0.137	+0.863	+.031	+0.555	+333.5
18	+0.568	+0.137	-0.258	2.558	+0.122	+333.0	+.041	+0.147	+0.853	+.048	+0.593	+313.0
19	+0.647	+0.147	-0.256	2.520	+0.148	+304.7	+.049	+0.160	+0.840	+.059	+0.617	+286.4
20	+0.752	+0.163	-0.254	2.505	+0.185	+277.0	+.062	+0.165	+0.835	+.074	+0.653	+260.3

TEST NAME : DSS-C13

Pt. No.	Str.X (%)	Str.Y (%)	X.Coor. (cm)	SigV (ksc)	TauH (ksc)	Eu (ksc)	TauH ---- SigVc	DelU ---- SigVc	SigV ---- SigVc	TauH ---- SigV	TauH ---- Cu	Eu -- Cu
21	+0.877	+0.179	-0.252	2.417	+0.218	+248.5	+.073	+0.194	+0.806	+.090	+0.683	+233.6
22	+1.010	+0.206	-0.249	2.345	+0.243	+223.5	+.081	+0.218	+0.782	+.104	+0.707	+210.0
23	+1.158	+0.227	-0.246	2.301	+0.270	+201.9	+.090	+0.233	+0.767	+.117	+0.732	+189.8
24	+1.305	+0.257	-0.243	2.246	+0.291	+183.9	+.097	+0.251	+0.749	+.129	+0.752	+172.8
25	+1.446	+0.284	-0.240	2.187	+0.306	+169.2	+.102	+0.271	+0.729	+.140	+0.766	+159.0
26	+1.599	+0.317	-0.237	2.140	+0.322	+155.9	+.107	+0.286	+0.714	+.150	+0.781	+146.5
27	+1.735	+0.349	-0.234	2.102	+0.337	+146.2	+.112	+0.299	+0.701	+.160	+0.795	+137.4
28	+1.883	+0.383	-0.231	2.067	+0.350	+137.0	+.117	+0.311	+0.689	+.169	+0.808	+128.7
29	+2.021	+0.413	-0.228	2.027	+0.360	+129.0	+.120	+0.324	+0.676	+.177	+0.817	+121.2
30	+2.168	+0.448	-0.225	1.998	+0.372	+122.0	+.124	+0.334	+0.666	+.186	+0.828	+114.6
31	+2.331	+0.482	-0.222	1.966	+0.382	+114.7	+.127	+0.344	+0.656	+.194	+0.838	+107.8
32	+2.488	+0.521	-0.219	1.929	+0.394	+108.9	+.131	+0.357	+0.643	+.204	+0.849	+102.3
33	+2.643	+0.542	-0.216	1.899	+0.399	+103.1	+.133	+0.367	+0.633	+.210	+0.854	+96.9
34	+2.811	+0.601	-0.212	1.868	+0.411	+98.2	+.137	+0.377	+0.623	+.220	+0.864	+92.3
35	+2.978	+0.647	-0.209	1.844	+0.412	+92.8	+.137	+0.385	+0.615	+.223	+0.866	+87.2
36	+3.150	+0.691	-0.205	1.818	+0.422	+88.7	+.141	+0.394	+0.606	+.232	+0.875	+83.3
37	+3.323	+0.739	-0.202	1.791	+0.427	+84.5	+.142	+0.403	+0.597	+.238	+0.880	+79.4
38	+3.497	+0.788	-0.198	1.768	+0.433	+80.9	+.144	+0.410	+0.590	+.245	+0.886	+76.0
39	+3.665	+0.836	-0.195	1.744	+0.438	+77.6	+.146	+0.418	+0.582	+.251	+0.890	+72.9
40	+3.833	+0.879	-0.191	1.724	+0.442	+74.5	+.147	+0.425	+0.575	+.257	+0.894	+70.0
41	+4.018	+0.930	-0.188	1.704	+0.451	+71.7	+.150	+0.432	+0.568	+.265	+0.902	+67.4
42	+4.197	+0.983	-0.184	1.686	+0.458	+69.1	+.153	+0.438	+0.562	+.271	+0.909	+65.0
43	+4.379	+1.029	-0.180	1.665	+0.459	+66.3	+.153	+0.445	+0.555	+.276	+0.910	+62.3
44	+4.551	+1.068	-0.177	1.649	+0.465	+64.2	+.155	+0.450	+0.550	+.282	+0.916	+60.4
45	+4.724	+1.109	-0.173	1.628	+0.467	+62.0	+.156	+0.457	+0.543	+.287	+0.918	+58.3
46	+4.901	+1.167	-0.170	1.615	+0.472	+60.0	+.157	+0.462	+0.538	+.292	+0.922	+56.4
47	+5.075	+1.215	-0.166	1.598	+0.474	+58.1	+.158	+0.467	+0.533	+.297	+0.924	+54.6
48	+5.255	+1.265	-0.162	1.583	+0.476	+56.3	+.159	+0.472	+0.528	+.301	+0.926	+52.9
49	+5.427	+1.313	-0.159	1.569	+0.481	+54.8	+.160	+0.477	+0.523	+.307	+0.931	+51.5
50	+5.611	+1.373	-0.155	1.555	+0.485	+53.1	+.162	+0.482	+0.518	+.312	+0.934	+49.9
51	+5.787	+1.426	-0.152	1.542	+0.485	+51.5	+.162	+0.486	+0.514	+.314	+0.934	+48.4
52	+5.963	+1.474	-0.148	1.531	+0.491	+50.3	+.164	+0.489	+0.511	+.320	+0.940	+47.3
53	+6.146	+1.536	-0.144	1.521	+0.494	+49.0	+.165	+0.493	+0.507	+.325	+0.942	+46.0
54	+6.333	+1.580	-0.140	1.506	+0.497	+47.7	+.166	+0.498	+0.502	+.330	+0.946	+44.8
55	+6.519	+1.635	-0.137	1.497	+0.499	+46.4	+.166	+0.501	+0.499	+.333	+0.947	+43.6
56	+6.704	+1.686	-0.133	1.483	+0.500	+45.2	+.167	+0.506	+0.494	+.337	+0.948	+42.4
57	+6.881	+1.741	-0.129	1.471	+0.503	+44.1	+.168	+0.509	+0.491	+.342	+0.951	+41.5
58	+7.073	+1.798	-0.125	1.465	+0.506	+43.0	+.169	+0.511	+0.489	+.345	+0.954	+40.5
59	+7.257	+1.853	-0.122	1.456	+0.508	+42.1	+.169	+0.515	+0.485	+.349	+0.956	+39.5
60	+7.451	+1.904	-0.118	1.448	+0.511	+41.1	+.170	+0.517	+0.483	+.353	+0.958	+38.6
61	+7.649	+1.957	-0.114	1.440	+0.512	+40.1	+.171	+0.520	+0.480	+.356	+0.960	+37.7
62	+7.837	+2.017	-0.110	1.428	+0.514	+39.2	+.171	+0.524	+0.476	+.360	+0.961	+36.8
63	+8.032	+2.074	-0.106	1.422	+0.514	+38.2	+.172	+0.526	+0.474	+.362	+0.962	+35.9
64	+8.224	+2.129	-0.102	1.411	+0.515	+37.4	+.172	+0.529	+0.471	+.365	+0.963	+35.1
65	+8.399	+2.186	-0.098	1.401	+0.518	+36.7	+.173	+0.533	+0.467	+.370	+0.965	+34.5
66	+8.581	+2.237	-0.095	1.394	+0.519	+35.9	+.173	+0.535	+0.465	+.372	+0.966	+33.8
67	+8.752	+2.290	-0.091	1.388	+0.520	+35.3	+.173	+0.537	+0.463	+.375	+0.967	+33.2
68	+8.930	+2.336	-0.088	1.385	+0.522	+34.6	+.174	+0.538	+0.462	+.377	+0.969	+32.5

TEST NAME : DSS-C13

Pt. No.	Str.X (%)	Str.Y (%)	X.Coor. (cm)	SigV (ksc)	TauH (ksc)	Eu (ksc)	TauH / SigVc	DelU / SigVc	SigV / SigVc	TauH / SigV	TauH / Cu	Eu / Cu
69	+9.102	+2.382	-0.084	1.376	+0.522	+34.0	+.174	+0.541	+0.459	+.380	+0.970	+32.0
70	+9.270	+2.430	-0.081	1.366	+0.524	+33.4	+.175	+0.545	+0.455	+.383	+0.971	+31.4
71	+9.446	+2.481	-0.077	1.364	+0.525	+32.8	+.175	+0.545	+0.455	+.385	+0.972	+30.9
72	+9.614	+2.524	-0.074	1.364	+0.523	+32.2	+.175	+0.545	+0.455	+.384	+0.971	+30.3
73	+9.795	+2.568	-0.070	1.361	+0.528	+31.8	+.176	+0.546	+0.454	+.388	+0.975	+29.9
74	+9.971	+2.616	-0.066	1.353	+0.530	+31.3	+.177	+0.549	+0.451	+.392	+0.977	+29.4
75	+10.149	+2.673	-0.063	1.343	+0.530	+30.7	+.177	+0.552	+0.448	+.394	+0.976	+28.9
76	+10.321	+2.719	-0.059	1.335	+0.531	+30.2	+.177	+0.555	+0.445	+.398	+0.978	+28.4
77	+10.496	+2.767	-0.056	1.334	+0.531	+29.7	+.177	+0.555	+0.445	+.399	+0.978	+28.0
78	+10.674	+2.830	-0.052	1.332	+0.533	+29.3	+.178	+0.556	+0.444	+.400	+0.979	+27.5
79	+10.860	+2.883	-0.048	1.330	+0.536	+28.9	+.179	+0.557	+0.443	+.403	+0.982	+27.1
80	+11.042	+2.937	-0.045	1.321	+0.535	+28.4	+.178	+0.560	+0.440	+.405	+0.982	+26.7
81	+11.220	+2.988	-0.041	1.314	+0.536	+28.0	+.179	+0.562	+0.438	+.408	+0.983	+26.3
82	+11.403	+3.032	-0.037	1.309	+0.538	+27.6	+.179	+0.564	+0.436	+.411	+0.984	+25.9
83	+11.585	+3.083	-0.033	1.303	+0.539	+27.1	+.180	+0.566	+0.434	+.414	+0.985	+25.5
84	+11.776	+3.131	-0.030	1.305	+0.542	+26.8	+.181	+0.565	+0.435	+.416	+0.988	+25.2
85	+11.956	+3.174	-0.026	1.303	+0.542	+26.4	+.181	+0.566	+0.434	+.416	+0.988	+24.8
86	+12.144	+3.227	-0.022	1.297	+0.543	+26.0	+.181	+0.567	+0.433	+.418	+0.989	+24.4
87	+12.323	+3.271	-0.018	1.292	+0.542	+25.6	+.181	+0.569	+0.431	+.419	+0.988	+24.0
88	+12.508	+3.326	-0.015	1.287	+0.542	+25.2	+.181	+0.571	+0.429	+.421	+0.988	+23.7
89	+12.692	+3.376	-0.011	1.282	+0.542	+24.9	+.181	+0.573	+0.427	+.423	+0.988	+23.4
90	+12.880	+3.423	-0.007	1.278	+0.543	+24.5	+.181	+0.574	+0.426	+.425	+0.989	+23.0
91	+13.070	+3.475	-0.003	1.275	+0.547	+24.2	+.182	+0.575	+0.425	+.429	+0.993	+22.8
92	+13.260	+3.524	+0.001	1.271	+0.547	+23.9	+.182	+0.576	+0.424	+.430	+0.993	+22.5
93	+13.446	+3.572	+0.004	1.270	+0.546	+23.6	+.182	+0.577	+0.423	+.430	+0.992	+22.1
94	+13.626	+3.620	+0.008	1.266	+0.549	+23.3	+.183	+0.578	+0.422	+.433	+0.994	+21.9
95	+13.807	+3.661	+0.012	1.263	+0.545	+22.9	+.182	+0.579	+0.421	+.431	+0.990	+21.5
96	+13.989	+3.707	+0.015	1.257	+0.548	+22.7	+.183	+0.581	+0.419	+.436	+0.994	+21.3
97	+14.174	+3.758	+0.019	1.255	+0.551	+22.4	+.184	+0.581	+0.419	+.439	+0.996	+21.1
98	+14.374	+3.813	+0.023	1.257	+0.551	+22.1	+.184	+0.581	+0.419	+.438	+0.996	+20.8
99	+14.567	+3.864	+0.027	1.255	+0.552	+21.9	+.184	+0.581	+0.419	+.440	+0.998	+20.5
100	+14.752	+3.912	+0.031	1.252	+0.552	+21.6	+.184	+0.582	+0.418	+.441	+0.997	+20.3
101	+14.945	+3.962	+0.035	1.245	+0.551	+21.3	+.184	+0.585	+0.415	+.443	+0.997	+20.0
102	+15.131	+4.021	+0.039	1.239	+0.553	+21.1	+.184	+0.587	+0.413	+.447	+0.998	+19.8
103	+15.321	+4.077	+0.043	1.236	+0.553	+20.8	+.185	+0.588	+0.412	+.448	+0.999	+19.6
104	+15.510	+4.123	+0.046	1.237	+0.553	+20.5	+.184	+0.588	+0.412	+.447	+0.998	+19.3
105	+15.699	+4.167	+0.050	1.236	+0.551	+20.3	+.184	+0.588	+0.412	+.446	+0.997	+19.0
106	+15.883	+4.208	+0.054	1.236	+0.555	+20.1	+.185	+0.588	+0.412	+.449	+1.000	+18.9
107	+16.067	+4.276	+0.058	1.234	+0.553	+19.8	+.184	+0.589	+0.411	+.448	+0.998	+18.6
108	+16.248	+4.327	+0.062	1.225	+0.554	+19.6	+.185	+0.592	+0.408	+.453	+1.000	+18.5
109	+16.428	+4.366	+0.065	1.216	+0.554	+19.4	+.185	+0.594	+0.406	+.455	+0.999	+18.2
110	+16.592	+4.398	+0.069	1.214	+0.553	+19.2	+.184	+0.595	+0.405	+.455	+0.998	+18.0
111	+16.769	+4.442	+0.072	1.221	+0.552	+19.0	+.184	+0.593	+0.407	+.452	+0.998	+17.8
112	+16.944	+4.500	+0.076	1.230	+0.553	+18.8	+.184	+0.590	+0.410	+.450	+0.998	+17.7
113	+17.127	+4.548	+0.079	1.253	+0.553	+18.6	+.184	+0.582	+0.418	+.441	+0.998	+17.5
114	+17.300	+4.598	+0.083	1.267	+0.555	+18.4	+.185	+0.578	+0.422	+.438	+1.000	+17.3
115	+17.483	+4.644	+0.087	1.268	+0.554	+18.2	+.185	+0.577	+0.423	+.437	+0.999	+17.1
116	+17.665	+4.686	+0.090	1.259	+0.554	+18.1	+.185	+0.580	+0.420	+.440	+0.999	+17.0

TEST NAME : DSS-C13

Pt. No.	Str.X (%)	Str.Y (%)	X.Coor. (cm)	SigV (ksc)	TauH (ksc)	Eu (ksc)	TauH / SigVc	DelU / SigVc	SigV / SigVc	TauH / SigV	TauH / Cu	Eu / Cu
117	+17.851	+4.740	+0.094	1.242	+0.553	+17.9	+.185	+0.586	+0.414	+.446	+0.999	+16.8
118	+18.038	+4.785	+0.098	1.203	+0.550	+17.6	+.183	+0.599	+0.401	+.457	+0.995	+16.6
119	+18.216	+4.833	+0.102	1.193	+0.551	+17.5	+.184	+0.602	+0.398	+.462	+0.996	+16.4
120	+18.397	+4.895	+0.105	1.187	+0.550	+17.3	+.183	+0.604	+0.396	+.463	+0.995	+16.2
121	+18.578	+4.952	+0.109	1.186	+0.550	+17.1	+.184	+0.605	+0.395	+.464	+0.996	+16.1
122	+18.759	+5.005	+0.113	1.190	+0.547	+16.9	+.182	+0.603	+0.397	+.460	+0.993	+15.9
123	+18.936	+5.044	+0.116	1.195	+0.547	+16.7	+.183	+0.601	+0.399	+.458	+0.993	+15.7
124	+19.129	+5.093	+0.120	1.205	+0.552	+16.6	+.184	+0.598	+0.402	+.458	+0.998	+15.6
125	+19.312	+5.138	+0.124	1.221	+0.553	+16.5	+.184	+0.593	+0.407	+.453	+0.998	+15.5
126	+19.511	+5.187	+0.128	1.233	+0.551	+16.3	+.184	+0.589	+0.411	+.446	+0.996	+15.3
127	+19.702	+5.266	+0.132	1.230	+0.553	+16.2	+.184	+0.590	+0.410	+.449	+0.998	+15.2
128	+19.892	+5.320	+0.136	1.217	+0.549	+16.0	+.183	+0.594	+0.406	+.451	+0.995	+15.0
129	+20.083	+5.374	+0.140	1.181	+0.549	+15.8	+.183	+0.606	+0.394	+.465	+0.995	+14.9
130	+20.281	+5.433	+0.144	1.146	+0.545	+15.6	+.182	+0.618	+0.382	+.476	+0.991	+14.7
131	+20.474	+5.502	+0.148	1.140	+0.543	+15.4	+.181	+0.620	+0.380	+.476	+0.989	+14.5
132	+20.667	+5.555	+0.152	1.133	+0.540	+15.2	+.180	+0.622	+0.378	+.477	+0.986	+14.3
133	+20.845	+5.604	+0.155	1.123	+0.535	+15.0	+.178	+0.626	+0.374	+.477	+0.982	+14.1
134	+21.032	+5.665	+0.159	1.111	+0.534	+14.9	+.178	+0.629	+0.371	+.480	+0.980	+14.0
135	+21.228	+5.734	+0.163	1.098	+0.528	+14.7	+.176	+0.634	+0.366	+.481	+0.975	+13.8
136	+21.415	+5.809	+0.167	1.082	+0.520	+14.4	+.173	+0.639	+0.361	+.481	+0.967	+13.6
137	+21.603	+5.873	+0.171	1.069	+0.516	+14.2	+.172	+0.644	+0.356	+.482	+0.963	+13.4
138	+21.801	+5.976	+0.175	1.057	+0.509	+14.0	+.170	+0.648	+0.352	+.482	+0.957	+13.2
139	+21.984	+6.009	+0.178	1.043	+0.507	+13.9	+.169	+0.652	+0.348	+.486	+0.955	+13.0
140	+22.168	+6.088	+0.182	1.026	+0.502	+13.7	+.168	+0.658	+0.342	+.490	+0.951	+12.9
141	+22.359	+6.153	+0.186	1.011	+0.500	+13.5	+.167	+0.663	+0.337	+.494	+0.948	+12.7
142	+22.562	+6.239	+0.190	0.995	+0.493	+13.3	+.164	+0.668	+0.332	+.495	+0.942	+12.5
143	+22.746	+6.320	+0.194	0.982	+0.488	+13.2	+.163	+0.673	+0.327	+.497	+0.937	+12.4
144	+22.939	+6.401	+0.198	0.971	+0.482	+13.0	+.161	+0.676	+0.324	+.496	+0.931	+12.2
145	+23.124	+6.477	+0.202	0.953	+0.477	+12.8	+.159	+0.682	+0.318	+.500	+0.927	+12.0
146	+23.305	+6.546	+0.205	0.939	+0.474	+12.7	+.158	+0.687	+0.313	+.505	+0.924	+11.9
147	+23.483	+6.619	+0.209	0.929	+0.470	+12.5	+.157	+0.690	+0.310	+.506	+0.920	+11.8
148	+23.671	+6.696	+0.213	0.915	+0.465	+12.3	+.155	+0.695	+0.305	+.508	+0.915	+11.6
149	+23.857	+6.777	+0.217	0.906	+0.461	+12.2	+.154	+0.698	+0.302	+.509	+0.912	+11.5
150	+24.044	+6.853	+0.220	0.894	+0.456	+12.0	+.152	+0.702	+0.298	+.510	+0.907	+11.3
151	+24.227	+6.923	+0.224	0.879	+0.452	+11.9	+.151	+0.707	+0.293	+.514	+0.903	+11.2
152	+24.414	+6.997	+0.228	0.869	+0.447	+11.7	+.149	+0.710	+0.290	+.514	+0.898	+11.0
153	+24.597	+7.079	+0.232	0.852	+0.444	+11.6	+.148	+0.716	+0.284	+.521	+0.896	+10.9
154	+24.789	+7.156	+0.236	0.840	+0.438	+11.5	+.146	+0.720	+0.280	+.521	+0.890	+10.8
155	+24.973	+7.234	+0.239	0.829	+0.435	+11.3	+.145	+0.724	+0.276	+.524	+0.887	+10.7
156	+25.157	+7.319	+0.243	0.821	+0.431	+11.2	+.144	+0.726	+0.274	+.525	+0.884	+10.5
157	+25.351	+7.397	+0.247	0.812	+0.425	+11.1	+.142	+0.729	+0.271	+.524	+0.878	+10.4
158	+25.535	+7.490	+0.251	0.799	+0.422	+10.9	+.141	+0.733	+0.267	+.528	+0.875	+10.3
159	+25.723	+7.579	+0.255	0.790	+0.417	+10.8	+.139	+0.737	+0.263	+.529	+0.871	+10.2
160	+25.908	+7.657	+0.258	0.780	+0.413	+10.7	+.138	+0.740	+0.260	+.529	+0.867	+10.0
161	+26.092	+7.739	+0.262	0.772	+0.412	+10.6	+.137	+0.743	+0.257	+.533	+0.865	+10.0
162	+26.286	+7.830	+0.266	0.764	+0.408	+10.5	+.136	+0.745	+0.255	+.535	+0.862	+9.8
163	+26.491	+7.928	+0.270	0.754	+0.403	+10.3	+.135	+0.749	+0.251	+.535	+0.858	+9.7
164	+26.699	+8.050	+0.274	0.744	+0.398	+10.2	+.133	+0.752	+0.248	+.535	+0.853	+9.6

TEST NAME : DSS-C13

Pt. No.	Str.X (%)	Str.Y (%)	X.Coor. (cm)	SigV (ksc)	TauH (ksc)	Eu (ksc)	TauH ---- SigVc	DelU ---- SigVc	SigV ---- SigVc	TauH ---- SigV	TauH ---- Cu	Eu -- Cu
165	+26.928	+8.200	+0.279	0.761	+0.389	+10.0	+.130	+0.746	+0.254	+.512	+0.844	+9.4
166	+27.124	+8.333	+0.283	0.778	+0.384	+9.9	+.128	+0.741	+0.259	+.494	+0.840	+9.3
167	+27.322	+8.472	+0.287	0.769	+0.378	+9.7	+.126	+0.743	+0.257	+.492	+0.834	+9.2
168	+27.517	+8.622	+0.291	0.740	+0.373	+9.6	+.124	+0.753	+0.247	+.504	+0.829	+9.0
169	+27.723	+8.766	+0.295	0.699	+0.366	+9.5	+.122	+0.767	+0.233	+.524	+0.823	+8.9
170	+27.915	+8.888	+0.299	0.682	+0.357	+9.3	+.119	+0.772	+0.228	+.523	+0.814	+8.7
171	+28.097	+9.033	+0.303	0.676	+0.355	+9.2	+.118	+0.775	+0.225	+.525	+0.812	+8.7
172	+28.281	+9.157	+0.307	0.671	+0.352	+9.1	+.117	+0.776	+0.224	+.524	+0.809	+8.6
173	+28.475	+9.281	+0.311	0.666	+0.348	+9.0	+.116	+0.778	+0.222	+.523	+0.806	+8.5
174	+28.678	+9.407	+0.315	0.656	+0.344	+8.9	+.115	+0.781	+0.219	+.524	+0.802	+8.4
175	+28.869	+9.536	+0.319	0.647	+0.341	+8.8	+.114	+0.784	+0.216	+.528	+0.799	+8.3
176	+29.068	+9.669	+0.323	0.641	+0.336	+8.7	+.112	+0.786	+0.214	+.524	+0.795	+8.2
177	+29.258	+9.807	+0.327	0.630	+0.331	+8.6	+.110	+0.790	+0.210	+.525	+0.789	+8.1
178	+29.455	+9.952	+0.331	0.622	+0.323	+8.5	+.108	+0.793	+0.207	+.519	+0.782	+8.0
179	+29.654	+10.096	+0.335	0.614	+0.320	+8.4	+.107	+0.795	+0.205	+.521	+0.779	+7.9
180	+29.860	+10.258	+0.339	0.606	+0.313	+8.3	+.104	+0.798	+0.202	+.517	+0.773	+7.8
181	+30.076	+10.428	+0.343	0.595	+0.308	+8.2	+.103	+0.802	+0.198	+.518	+0.768	+7.7
182	+30.283	+10.600	+0.347	0.589	+0.298	+8.0	+.100	+0.804	+0.196	+.507	+0.759	+7.5
183	+30.496	+10.786	+0.352	0.581	+0.295	+7.9	+.098	+0.806	+0.194	+.508	+0.756	+7.4
184	+30.686	+10.967	+0.356	0.575	+0.289	+7.8	+.096	+0.808	+0.192	+.503	+0.751	+7.3
185	+30.896	+11.160	+0.360	0.569	+0.284	+7.7	+.095	+0.810	+0.190	+.499	+0.745	+7.2
186	+31.078	+11.335	+0.364	0.560	+0.276	+7.6	+.092	+0.813	+0.187	+.493	+0.738	+7.1
187	+31.266	+11.512	+0.367	0.555	+0.273	+7.5	+.091	+0.815	+0.185	+.492	+0.735	+7.1
188	+31.453	+11.693	+0.371	0.552	+0.268	+7.4	+.089	+0.816	+0.184	+.484	+0.730	+7.0
189	+31.637	+11.875	+0.375	0.543	+0.263	+7.3	+.088	+0.819	+0.181	+.485	+0.726	+6.9
190	+31.822	+12.040	+0.379	0.536	+0.258	+7.2	+.086	+0.821	+0.179	+.481	+0.721	+6.8
191	+31.991	+12.196	+0.382	0.528	+0.257	+7.2	+.086	+0.824	+0.176	+.488	+0.721	+6.8
192	+32.165	+12.343	+0.386	0.526	+0.256	+7.1	+.085	+0.824	+0.176	+.487	+0.719	+6.7
193	+32.357	+12.527	+0.390	0.523	+0.254	+7.1	+.085	+0.826	+0.174	+.487	+0.718	+6.7

****

Ko CONSOLIDATED MDSS TEST
MIT GEOTECHNICAL LAB

****

FILE NAME: DSSC14.PRN

REDUCTION DATA
UNITS: (kg,cm,mVOLTS,VOLTS)

1. TEST NAME : MDSS-C14
2. DATE : 01-28-1988
3. OCR : 1
4. VER. CONSOLIDATION STRESS (KSC) : +2.994
5. HOR. CONSOLIDATION STRESS (KSC) : +0.000
6. PRE-SHEAR SAMPLE HEIGHT (cm) : +2.0522
7. VERTICAL STRESS LOAD CELL:
   ZERO: .69
   CF: 13.70491
8. HORIZONTAL SHEAR LOAD CELL:
   ZERO: -1.55
   CF: 6.70298
9. HORIZONTAL DISP. TRANSDUCER, X:
   ZERO: .7331
   CF: -1.81917
10. HORIZONTAL DISP. TRANSDUCER, Y:
    ZERO: .5599
    CF: -.261
11. VERTICAL DISP. TRANSDUCER, Z1:
    ZERO: -.2025
    CF: .28883
12. VERTICAL DISP. TRANSDUCER, Z2:
    ZERO: .6799
    CF: .29569
13. CONSTANT HEIGHT TRANSDUCER, Z:
    ZERO: .03187
    CF: .3014

Pt. No.	Str.X (%)	Str.Y (%)	SigV (ksc)	TauH (ksc)	Eu (ksc)	TauH ---- SigVc	DelU ---- SigVc	SigV ---- SigVc	TauH ---- SigV	TauH ---- Cu	Eu -- Cu
1	+0.000	+0.000	2.994	-0.001	+9999.0	-.000	+0.000	+1.000	-.000	-0.002	+9999.0
2	+0.005	+0.007	2.999	-0.001	-42.4	-.000	-0.002	+1.002	-.000	-0.001	-75.3
3	+0.010	+0.007	2.997	-0.000	-10.5	-.000	-0.001	+1.001	-.000	-0.001	-18.6
4	+0.008	+0.007	2.996	+0.007	+259.7	+.002	-0.001	+1.001	+.002	+0.012	+461.3
5	+0.010	+0.009	2.986	+0.016	+508.0	+.005	+0.003	+0.997	+.005	+0.029	+902.5
6	+0.016	+0.007	2.980	+0.022	+421.4	+.007	+0.005	+0.995	+.007	+0.040	+748.6
7	+0.019	+0.009	2.978	+0.025	+388.9	+.008	+0.005	+0.995	+.008	+0.044	+690.9
8	+0.021	+0.007	2.973	+0.026	+374.0	+.009	+0.007	+0.993	+.009	+0.046	+664.3
9	+0.022	+0.007	2.968	+0.031	+412.0	+.010	+0.009	+0.991	+.010	+0.054	+732.0
10	+0.027	+0.007	2.960	+0.039	+438.4	+.013	+0.011	+0.989	+.013	+0.070	+778.8
11	+0.038	+0.007	2.937	+0.051	+405.0	+.017	+0.019	+0.981	+.018	+0.091	+719.5
12	+0.052	+0.007	2.902	+0.063	+359.3	+.021	+0.031	+0.969	+.022	+0.112	+638.3
13	+0.059	+0.007	2.865	+0.075	+381.7	+.025	+0.043	+0.957	+.026	+0.133	+678.1
14	+0.078	+0.007	2.842	+0.097	+372.9	+.032	+0.051	+0.949	+.034	+0.172	+662.4
15	+0.094	+0.007	2.839	+0.122	+390.9	+.041	+0.052	+0.948	+.043	+0.217	+694.4
16	+0.113	+0.007	2.840	+0.152	+404.2	+.051	+0.051	+0.949	+.054	+0.270	+718.1
17	+0.140	+0.007	2.846	+0.182	+390.9	+.061	+0.050	+0.950	+.064	+0.324	+694.4
18	+0.167	+0.007	2.845	+0.215	+386.8	+.072	+0.050	+0.950	+.076	+0.382	+687.2
19	+0.200	+0.007	2.843	+0.249	+372.7	+.083	+0.050	+0.950	+.088	+0.442	+662.2
20	+0.237	+0.009	2.842	+0.281	+355.6	+.094	+0.051	+0.949	+.099	+0.499	+631.8
21	+0.273	+0.009	2.827	+0.308	+338.2	+.103	+0.056	+0.944	+.109	+0.547	+600.8
22	+0.321	+0.009	2.813	+0.336	+313.6	+.112	+0.060	+0.940	+.119	+0.596	+557.1

TEST NAME : MDSS-C14

Pt. No.	Str.X (%)	Str.Y (%)	SigV (ksc)	TauH (ksc)	Eu (ksc)	TauH ---- SigVc	DelU ---- SigVc	SigV ---- SigVc	TauH ---- SigV	TauH ---- Cu	Eu -- Cu
23	+0.374	+0.009	2.797	+0.361	+290.2	+.121	+0.066	+0.934	+.129	+0.642	+515.5
24	+0.432	+0.011	2.769	+0.386	+267.6	+.129	+0.075	+0.925	+.139	+0.685	+475.4
25	+0.493	+0.009	2.741	+0.406	+247.3	+.136	+0.085	+0.915	+.148	+0.722	+439.4
26	+0.555	+0.013	2.709	+0.423	+228.8	+.141	+0.095	+0.905	+.156	+0.751	+406.4
27	+0.623	+0.013	2.687	+0.440	+211.8	+.147	+0.102	+0.898	+.164	+0.781	+376.2
28	+0.698	+0.011	2.650	+0.452	+194.5	+.151	+0.115	+0.885	+.171	+0.804	+345.6
29	+0.769	+0.016	2.610	+0.464	+180.8	+.155	+0.128	+0.872	+.178	+0.824	+321.2
30	+0.847	+0.013	2.581	+0.473	+167.3	+.158	+0.138	+0.862	+.183	+0.840	+297.3
31	+0.920	+0.016	2.550	+0.482	+157.3	+.161	+0.148	+0.852	+.189	+0.857	+279.4
32	+1.001	+0.016	2.518	+0.491	+147.1	+.164	+0.159	+0.841	+.195	+0.872	+261.3
33	+1.089	+0.016	2.480	+0.499	+137.4	+.166	+0.172	+0.828	+.201	+0.886	+244.0
34	+1.168	+0.018	2.441	+0.501	+128.7	+.167	+0.185	+0.815	+.205	+0.890	+228.6
35	+1.246	+0.018	2.414	+0.507	+122.1	+.169	+0.194	+0.806	+.210	+0.901	+217.0
36	+1.329	+0.023	2.382	+0.512	+115.5	+.171	+0.205	+0.795	+.215	+0.909	+205.2
37	+1.410	+0.023	2.352	+0.518	+110.2	+.173	+0.214	+0.786	+.220	+0.920	+195.7
38	+1.493	+0.025	2.337	+0.523	+105.0	+.175	+0.220	+0.780	+.224	+0.929	+186.6
39	+1.612	+0.025	2.308	+0.528	+98.2	+.176	+0.229	+0.771	+.229	+0.937	+174.5
40	+1.699	+0.027	2.282	+0.531	+93.8	+.177	+0.238	+0.762	+.233	+0.943	+166.6
41	+1.787	+0.029	2.256	+0.528	+88.6	+.176	+0.246	+0.754	+.234	+0.937	+157.4
42	+1.872	+0.032	2.230	+0.531	+85.0	+.177	+0.255	+0.745	+.238	+0.943	+151.1
43	+1.955	+0.032	2.209	+0.534	+81.9	+.178	+0.262	+0.738	+.242	+0.948	+145.5
44	+2.046	+0.036	2.185	+0.536	+78.7	+.179	+0.270	+0.730	+.246	+0.953	+139.7
45	+2.136	+0.039	2.158	+0.541	+75.9	+.181	+0.279	+0.721	+.251	+0.961	+134.9
46	+2.224	+0.039	2.138	+0.542	+73.1	+.181	+0.286	+0.714	+.253	+0.963	+129.8
47	+2.308	+0.041	2.123	+0.542	+70.5	+.181	+0.291	+0.709	+.256	+0.964	+125.2
48	+2.402	+0.039	2.097	+0.546	+68.2	+.182	+0.300	+0.700	+.260	+0.970	+121.2
49	+2.494	+0.041	2.074	+0.547	+65.8	+.183	+0.307	+0.693	+.264	+0.971	+116.8
50	+2.580	+0.041	2.054	+0.548	+63.8	+.183	+0.314	+0.686	+.267	+0.974	+113.3
51	+2.674	+0.043	2.037	+0.550	+61.8	+.184	+0.320	+0.680	+.270	+0.978	+109.7
52	+2.770	+0.045	2.025	+0.552	+59.8	+.184	+0.324	+0.676	+.273	+0.981	+106.3
53	+2.864	+0.045	2.009	+0.552	+57.8	+.184	+0.329	+0.671	+.275	+0.981	+102.8
54	+2.963	+0.050	1.990	+0.554	+56.1	+.185	+0.335	+0.665	+.278	+0.983	+99.6
55	+3.051	+0.061	1.969	+0.553	+54.4	+.185	+0.342	+0.658	+.281	+0.982	+96.6
56	+3.145	+0.064	1.949	+0.552	+52.7	+.184	+0.349	+0.651	+.283	+0.981	+93.6
57	+3.230	+0.064	1.934	+0.553	+51.3	+.185	+0.354	+0.646	+.286	+0.982	+91.2
58	+3.319	+0.066	1.916	+0.554	+50.1	+.185	+0.360	+0.640	+.289	+0.984	+89.0
59	+3.408	+0.066	1.907	+0.554	+48.8	+.185	+0.363	+0.637	+.290	+0.984	+86.6
60	+3.498	+0.066	1.886	+0.555	+47.6	+.185	+0.370	+0.630	+.294	+0.986	+84.5
61	+3.732	+0.066	1.843	+0.554	+44.5	+.185	+0.385	+0.615	+.301	+0.984	+79.1
62	+3.896	+0.070	1.821	+0.555	+42.7	+.185	+0.392	+0.608	+.305	+0.986	+75.9
63	+4.066	+0.070	1.802	+0.557	+41.1	+.186	+0.398	+0.602	+.309	+0.989	+72.9
64	+4.244	+0.073	1.773	+0.557	+39.4	+.186	+0.408	+0.592	+.314	+0.990	+70.0
65	+4.426	+0.073	1.749	+0.558	+37.8	+.186	+0.416	+0.584	+.319	+0.991	+67.2
66	+4.600	+0.075	1.730	+0.559	+36.4	+.187	+0.422	+0.578	+.323	+0.992	+64.7
67	+4.778	+0.091	1.706	+0.559	+35.1	+.187	+0.430	+0.570	+.328	+0.994	+62.4
68	+4.954	+0.096	1.687	+0.560	+33.9	+.187	+0.437	+0.563	+.332	+0.995	+60.3
69	+5.150	+0.096	1.670	+0.563	+32.8	+.188	+0.442	+0.558	+.337	+1.000	+58.3
70	+5.354	+0.100	1.656	+0.563	+31.5	+.188	+0.447	+0.553	+.340	+0.999	+56.0

TEST NAME : MDSS-C14

Pt. No.	Str.X (%)	Str.Y (%)	SigV (ksc)	TauH (ksc)	Eu (ksc)	TauH ---- SigVc	DelU ---- SigVc	SigV ---- SigVc	TauH ---- SigV	TauH ---- Cu	Eu -- Cu
71	+5.545	+0.107	1.628	+0.560	+30.3	+.187	+0.456	+0.544	+.344	+0.995	+53.8
72	+5.724	+0.112	1.613	+0.558	+29.2	+.186	+0.461	+0.539	+.346	+0.991	+52.0
73	+5.906	+0.112	1.593	+0.559	+28.4	+.187	+0.468	+0.532	+.351	+0.992	+50.4
74	+6.101	+0.112	1.577	+0.557	+27.4	+.186	+0.473	+0.527	+.353	+0.990	+48.7
75	+6.274	+0.112	1.561	+0.557	+26.6	+.186	+0.479	+0.521	+.356	+0.989	+47.3
76	+6.464	+0.114	1.548	+0.557	+25.8	+.186	+0.483	+0.517	+.360	+0.989	+45.9
77	+6.661	+0.114	1.536	+0.556	+25.0	+.186	+0.487	+0.513	+.362	+0.987	+44.5
78	+6.846	+0.114	1.513	+0.555	+24.3	+.185	+0.495	+0.505	+.367	+0.986	+43.2
79	+7.032	+0.125	1.507	+0.554	+23.6	+.185	+0.497	+0.503	+.368	+0.985	+42.0
80	+7.216	+0.125	1.495	+0.552	+23.0	+.184	+0.501	+0.499	+.369	+0.981	+40.8
81	+7.399	+0.127	1.481	+0.551	+22.3	+.184	+0.505	+0.495	+.372	+0.978	+39.7
82	+7.588	+0.127	1.468	+0.550	+21.7	+.184	+0.510	+0.490	+.374	+0.976	+38.6
83	+7.769	+0.127	1.454	+0.549	+21.2	+.183	+0.514	+0.486	+.378	+0.975	+37.7
84	+7.957	+0.141	1.442	+0.546	+20.6	+.183	+0.519	+0.481	+.379	+0.971	+36.6
85	+8.129	+0.141	1.429	+0.547	+20.2	+.183	+0.523	+0.477	+.383	+0.972	+35.9
86	+8.310	+0.141	1.421	+0.546	+19.7	+.182	+0.525	+0.475	+.384	+0.970	+35.0
87	+8.488	+0.141	1.407	+0.546	+19.3	+.182	+0.530	+0.470	+.388	+0.969	+34.3
88	+8.680	+0.139	1.402	+0.546	+18.9	+.182	+0.532	+0.468	+.389	+0.969	+33.5
89	+8.869	+0.143	1.392	+0.545	+18.4	+.182	+0.535	+0.465	+.392	+0.968	+32.8
90	+9.047	+0.141	1.380	+0.542	+18.0	+.181	+0.539	+0.461	+.393	+0.963	+31.9
91	+9.222	+0.143	1.368	+0.543	+17.7	+.181	+0.543	+0.457	+.397	+0.965	+31.4
92	+9.405	+0.166	1.364	+0.542	+17.3	+.181	+0.545	+0.455	+.397	+0.962	+30.7
93	+9.586	+0.164	1.354	+0.540	+16.9	+.180	+0.548	+0.452	+.399	+0.959	+30.0
94	+9.766	+0.175	1.343	+0.539	+16.5	+.180	+0.551	+0.449	+.401	+0.957	+29.4
95	+9.953	+0.175	1.338	+0.537	+16.2	+.179	+0.553	+0.447	+.401	+0.953	+28.7
96	+10.138	+0.187	1.328	+0.536	+15.9	+.179	+0.556	+0.444	+.404	+0.953	+28.2
97	+10.320	+0.198	1.320	+0.537	+15.6	+.179	+0.559	+0.441	+.407	+0.955	+27.8
98	+10.505	+0.200	1.315	+0.535	+15.3	+.179	+0.561	+0.439	+.407	+0.950	+27.1
99	+10.689	+0.205	1.304	+0.535	+15.0	+.179	+0.564	+0.436	+.410	+0.951	+26.7
100	+10.864	+0.207	1.297	+0.532	+14.7	+.178	+0.567	+0.433	+.410	+0.946	+26.1
101	+11.042	+0.205	1.290	+0.532	+14.5	+.178	+0.569	+0.431	+.413	+0.946	+25.7
102	+11.224	+0.207	1.288	+0.532	+14.2	+.178	+0.570	+0.430	+.413	+0.945	+25.3
103	+11.395	+0.205	1.283	+0.531	+14.0	+.177	+0.572	+0.428	+.414	+0.943	+24.8
104	+11.584	+0.205	1.277	+0.530	+13.7	+.177	+0.574	+0.426	+.415	+0.942	+24.4
105	+11.776	+0.226	1.273	+0.529	+13.5	+.177	+0.575	+0.425	+.415	+0.940	+23.9
106	+11.970	+0.226	1.266	+0.529	+13.2	+.177	+0.577	+0.423	+.417	+0.939	+23.5
107	+12.160	+0.228	1.267	+0.528	+13.0	+.176	+0.577	+0.423	+.416	+0.937	+23.1
108	+12.352	+0.228	1.259	+0.527	+12.8	+.176	+0.579	+0.421	+.418	+0.936	+22.7
109	+12.550	+0.228	1.253	+0.526	+12.6	+.176	+0.581	+0.419	+.419	+0.934	+22.3
110	+12.724	+0.230	1.249	+0.523	+12.3	+.175	+0.583	+0.417	+.419	+0.929	+21.9
111	+12.907	+0.246	1.245	+0.522	+12.1	+.174	+0.584	+0.416	+.419	+0.928	+21.6
112	+13.088	+0.248	1.239	+0.522	+12.0	+.174	+0.586	+0.414	+.421	+0.927	+21.2
113	+13.271	+0.248	1.235	+0.520	+11.8	+.174	+0.588	+0.412	+.421	+0.925	+20.9
114	+13.464	+0.251	1.231	+0.519	+11.6	+.173	+0.589	+0.411	+.422	+0.922	+20.5
115	+13.642	+0.253	1.220	+0.516	+11.4	+.172	+0.592	+0.408	+.423	+0.917	+20.2
116	+13.817	+0.267	1.217	+0.516	+11.2	+.172	+0.593	+0.407	+.424	+0.916	+19.9
117	+14.006	+0.269	1.209	+0.516	+11.1	+.172	+0.596	+0.404	+.427	+0.917	+19.6
118	+14.194	+0.269	1.205	+0.514	+10.9	+.172	+0.597	+0.403	+.426	+0.913	+19.3

TEST NAME : MDSS-C14

Pt. No.	Str.X (%)	Str.Y (%)	SigV (ksc)	TauH (ksc)	Eu (ksc)	TauH ---- SigVc	DelU ---- SigVc	SigV ---- SigVc	TauH ---- SigV	TauH ---- Cu	Eu -- Cu
119	+14.382	+0.269	1.196	+0.513	+10.7	+.171	+0.600	+0.400	+.429	+0.912	+19.0
120	+14.574	+0.269	1.193	+0.512	+10.5	+.171	+0.602	+0.398	+.429	+0.910	+18.7
121	+14.767	+0.283	1.191	+0.510	+10.4	+.170	+0.602	+0.398	+.428	+0.906	+18.4
122	+14.961	+0.283	1.181	+0.508	+10.2	+.170	+0.606	+0.394	+.430	+0.902	+18.1
123	+15.141	+0.289	1.172	+0.504	+10.0	+.168	+0.609	+0.391	+.430	+0.896	+17.7
124	+15.334	+0.294	1.165	+0.503	+9.8	+.168	+0.611	+0.389	+.432	+0.894	+17.5
125	+15.524	+0.296	1.153	+0.501	+9.7	+.167	+0.615	+0.385	+.434	+0.889	+17.2
126	+15.723	+0.294	1.145	+0.498	+9.5	+.166	+0.618	+0.382	+.435	+0.884	+16.9
127	+15.907	+0.294	1.130	+0.496	+9.3	+.165	+0.622	+0.378	+.438	+0.880	+16.6
128	+16.093	+0.296	1.119	+0.493	+9.2	+.165	+0.626	+0.374	+.441	+0.876	+16.3
129	+16.289	+0.296	1.109	+0.491	+9.0	+.164	+0.630	+0.370	+.443	+0.872	+16.1
130	+16.484	+0.294	1.095	+0.487	+8.9	+.162	+0.634	+0.366	+.444	+0.864	+15.7
131	+16.669	+0.296	1.076	+0.483	+8.7	+.161	+0.641	+0.359	+.448	+0.857	+15.4
132	+16.840	+0.294	1.059	+0.481	+8.6	+.161	+0.646	+0.354	+.454	+0.854	+15.2
133	+17.020	+0.296	1.055	+0.476	+8.4	+.159	+0.648	+0.352	+.451	+0.846	+14.9
134	+17.206	+0.296	1.038	+0.473	+8.3	+.158	+0.653	+0.347	+.456	+0.841	+14.7
135	+17.386	+0.308	1.027	+0.469	+8.1	+.157	+0.657	+0.343	+.457	+0.833	+14.4
136	+17.564	+0.310	1.019	+0.466	+8.0	+.156	+0.660	+0.340	+.458	+0.828	+14.1
137	+17.746	+0.312	1.004	+0.463	+7.8	+.155	+0.665	+0.335	+.461	+0.822	+13.9
138	+17.931	+0.310	0.998	+0.459	+7.7	+.153	+0.667	+0.333	+.460	+0.815	+13.6
139	+18.112	+0.308	0.985	+0.458	+7.6	+.153	+0.671	+0.329	+.465	+0.813	+13.5
140	+18.293	+0.310	0.975	+0.453	+7.4	+.151	+0.674	+0.326	+.465	+0.806	+13.2
141	+18.481	+0.310	0.960	+0.452	+7.3	+.151	+0.679	+0.321	+.471	+0.802	+13.0
142	+18.672	+0.310	0.958	+0.448	+7.2	+.150	+0.680	+0.320	+.468	+0.796	+12.8
143	+10.858	+0.310	0.944	+0.446	+7.1	+.149	+0.685	+0.315	+.472	+0.792	+12.6
144	+19.055	+0.310	0.948	+0.443	+7.0	+.148	+0.683	+0.317	+.467	+0.787	+12.4
145	+19.249	+0.310	0.934	+0.439	+6.8	+.147	+0.688	+0.312	+.470	+0.780	+12.2
146	+19.444	+0.312	0.914	+0.435	+6.7	+.145	+0.695	+0.305	+.476	+0.773	+11.9
147	+19.622	+0.319	0.903	+0.431	+6.6	+.144	+0.698	+0.302	+.478	+0.766	+11.7
148	+19.805	+0.326	0.891	+0.429	+6.5	+.143	+0.702	+0.298	+.482	+0.762	+11.5
149	+19.997	+0.324	0.884	+0.426	+6.4	+.142	+0.705	+0.295	+.482	+0.756	+11.3
150	+20.180	+0.326	0.876	+0.423	+6.3	+.141	+0.707	+0.293	+.482	+0.751	+11.2
151	+20.366	+0.328	0.866	+0.420	+6.2	+.140	+0.711	+0.289	+.485	+0.746	+11.0
152	+20.560	+0.328	0.856	+0.418	+6.1	+.140	+0.714	+0.286	+.488	+0.742	+10.8
153	+20.757	+0.335	0.844	+0.415	+6.0	+.139	+0.718	+0.282	+.492	+0.737	+10.7
154	+20.956	+0.335	0.838	+0.410	+5.9	+.137	+0.720	+0.280	+.489	+0.728	+10.4
155	+21.135	+0.333	0.831	+0.407	+5.8	+.136	+0.722	+0.278	+.490	+0.723	+10.3
156	+21.320	+0.333	0.824	+0.403	+5.7	+.134	+0.725	+0.275	+.488	+0.715	+10.1
157	+21.497	+0.335	0.813	+0.401	+5.6	+.134	+0.728	+0.272	+.493	+0.712	+9.9
158	+21.672	+0.333	0.807	+0.396	+5.5	+.132	+0.730	+0.270	+.490	+0.703	+9.7
159	+21.838	+0.333	0.800	+0.395	+5.4	+.132	+0.733	+0.267	+.494	+0.702	+9.6
160	+22.032	+0.333	0.793	+0.393	+5.4	+.131	+0.735	+0.265	+.495	+0.698	+9.5
161	+22.222	+0.333	0.781	+0.391	+5.3	+.130	+0.739	+0.261	+.500	+0.694	+9.4
162	+22.403	+0.335	0.777	+0.387	+5.2	+.129	+0.741	+0.259	+.499	+0.688	+9.2
163	+22.592	+0.333	0.770	+0.385	+5.1	+.129	+0.743	+0.257	+.500	+0.684	+9.1
164	+22.796	+0.333	0.755	+0.381	+5.0	+.127	+0.748	+0.252	+.505	+0.677	+8.9
165	+22.982	+0.333	0.750	+0.377	+4.9	+.126	+0.750	+0.250	+.504	+0.671	+8.8
166	+23.181	+0.333	0.737	+0.375	+4.8	+.125	+0.754	+0.246	+.508	+0.665	+8.6

TEST NAME : MDSS-C14

Pt. No.	Str.X (%)	Str.Y (%)	SigV (ksc)	TauH (ksc)	Eu (ksc)	TauH / SigVc	DelU / SigVc	SigV / SigVc	TauH / SigV	TauH / Cu	Eu / Cu
167	+23.365	+0.333	0.733	+0.371	+4.8	+.124	+0.755	+0.245	+.506	+0.659	+8.5
168	+23.546	+0.335	0.728	+0.367	+4.7	+.123	+0.757	+0.243	+.504	+0.652	+8.3
169	+23.723	+0.333	0.717	+0.364	+4.6	+.122	+0.761	+0.239	+.508	+0.647	+8.2
170	+23.899	+0.335	0.711	+0.361	+4.5	+.121	+0.762	+0.238	+.508	+0.642	+8.1
171	+24.085	+0.333	0.708	+0.358	+4.5	+.120	+0.763	+0.237	+.506	+0.636	+7.9
172	+24.262	+0.335	0.698	+0.356	+4.4	+.119	+0.767	+0.233	+.510	+0.632	+7.8
173	+24.447	+0.335	0.692	+0.354	+4.3	+.118	+0.769	+0.231	+.512	+0.629	+7.7
174	+24.643	+0.333	0.685	+0.350	+4.3	+.117	+0.771	+0.229	+.512	+0.622	+7.6
175	+24.830	+0.333	0.680	+0.347	+4.2	+.116	+0.773	+0.227	+.511	+0.617	+7.5
176	+25.029	+0.333	0.668	+0.345	+4.1	+.115	+0.777	+0.223	+.516	+0.612	+7.3
177	+25.212	+0.333	0.662	+0.340	+4.0	+.114	+0.779	+0.221	+.514	+0.604	+7.2
178	+25.395	+0.330	0.654	+0.338	+4.0	+.113	+0.782	+0.218	+.517	+0.600	+7.1
179	+25.597	+0.333	0.646	+0.336	+3.9	+.112	+0.784	+0.216	+.520	+0.597	+7.0
180	+25.808	+0.333	0.640	+0.332	+3.9	+.111	+0.786	+0.214	+.519	+0.590	+6.9
181	+25.988	+0.330	0.637	+0.328	+3.8	+.110	+0.787	+0.213	+.515	+0.583	+6.7
182	+26.171	+0.333	0.628	+0.327	+3.7	+.109	+0.790	+0.210	+.520	+0.580	+6.7
183	+26.352	+0.335	0.623	+0.324	+3.7	+.108	+0.792	+0.208	+.520	+0.576	+6.6
184	+26.538	+0.333	0.619	+0.320	+3.6	+.107	+0.793	+0.207	+.517	+0.569	+6.4
185	+26.700	+0.330	0.616	+0.317	+3.6	+.106	+0.794	+0.206	+.516	+0.564	+6.3
186	+26.886	+0.333	0.607	+0.317	+3.5	+.106	+0.797	+0.203	+.522	+0.563	+6.3
187	+27.062	+0.333	0.598	+0.313	+3.5	+.105	+0.800	+0.200	+.524	+0.557	+6.2
188	+27.252	+0.333	0.592	+0.311	+3.4	+.104	+0.802	+0.198	+.526	+0.553	+6.1
189	+27.441	+0.333	0.587	+0.308	+3.4	+.103	+0.804	+0.196	+.525	+0.548	+6.0
190	+27.651	+0.333	0.578	+0.305	+3.3	+.102	+0.807	+0.193	+.527	+0.542	+5.9
191	+27.822	+0.333	0.577	+0.301	+3.2	+.101	+0.807	+0.193	+.522	+0.535	+5.8
192	+28.004	+0.333	0.569	+0.298	+3.2	+.100	+0.810	+0.190	+.524	+0.530	+5.7
193	+28.183	+0.333	0.562	+0.296	+3.2	+.099	+0.812	+0.188	+.526	+0.526	+5.6

****

ANISOTROPICALLY CONSOLIDATED MDSS TEST

MIT GEOTECHNICAL LAB

****

FILE NAME: DSSC15.PRH

REDUCTION DATA

UNITS: (kg,cm,mVOLTS,VOLTS)

1. TEST NAME : DSS-C15
2. DATE : 03-18-1988
3. OCR : 1
4. VER. CONSOLIDATION STRESS (KSC) : +2.996
5. HOR. CONSOLIDATION STRESS (KSC) : +0.600
6. PRE-SHEAR SAMPLE HEIGHT (cm) : +1.9371
7. VERTICAL STRESS LOAD CELL:
   ZERO: .72
   CF: 13.70491
8. HORIZONTAL SHEAR LOAD CELL:
   ZERO: -1.53
   CF: 6.70298
9. HORIZONTAL DISP. TRANSDUCER, X:
   ZERO: .5639
   CF: -1.81917
10. HORIZONTAL DISP. TRANSDUCER, Y:
    ZERO: -3.324
    CF: -.261
11. VERTICAL DISP. TRANSDUCER, Z1:
    ZERO: -.13785
    CF: .28883
12. VERTICAL DISP. TRANSDUCER, Z2:
    ZERO: .6484
    CF: .29569
13. CONSTANT HEIGHT TRANSDUCER, Z:
    ZERO: .04842
    CF: .3014
14. TEST ANGLE THETA (degrees): 120

TOTAL X DISP. DURING CONSOLIDATION (cm): -.13432

Pt. No.	Str.X (%)	Str.Y (%)	X.Coor. (cm)	SigV (ksc)	TauH (ksc)	Eu (ksc)	TauH / SigVc	DelU / SigVc	SigV / SigVc	TauH / SigV	TauH / Cu	Eu / Cu
1	+0.000	+0.000	-0.134	2.996	-0.295	+9999.0	-.098	+0.000	+1.000	-.098	+0.000	+9999.0
2	-0.003	-0.002	-0.134	2.999	-0.294	-122.6	-.098	-0.001	+1.001	-.098	+0.002	-166.0
3	-0.003	+0.000	-0.134	2.998	-0.291	-397.9	-.097	-0.000	+1.000	-.097	+0.006	-538.6
4	-0.003	-0.002	-0.134	2.997	-0.273	-1927.1	-.091	-0.000	+1.000	-.091	+0.029	-2608.7
5	-0.003	+0.000	-0.134	2.995	-0.260	-3089.3	-.087	+0.000	+1.000	-.087	+0.047	-4182.0
6	-0.003	+0.002	-0.134	2.991	-0.241	-4771.4	-.081	+0.002	+0.998	-.081	+0.073	-6459.1
7	+0.003	+0.010	-0.134	2.986	-0.219	+6761.0	-.073	+0.003	+0.997	-.073	+0.103	+9152.3
8	+0.013	+0.012	-0.134	2.979	-0.195	+2225.1	-.065	+0.006	+0.994	-.066	+0.135	+3012.1
9	+0.030	+0.022	-0.134	2.969	-0.163	+1304.9	-.054	+0.009	+0.991	-.055	+0.178	+1766.5
10	+0.049	+0.027	-0.133	2.961	-0.132	+999.7	-.044	+0.012	+0.988	-.045	+0.220	+1353.3
11	+0.067	+0.036	-0.133	2.940	-0.107	+836.4	-.036	+0.019	+0.981	-.037	+0.254	+1132.2
12	+0.084	+0.039	-0.133	2.925	-0.086	+744.9	-.029	+0.024	+0.976	-.029	+0.283	+1008.4
13	+0.094	+0.043	-0.132	2.904	-0.074	+702.2	-.025	+0.031	+0.969	-.026	+0.299	+950.6
14	+0.106	+0.048	-0.132	2.884	-0.063	+657.2	-.021	+0.038	+0.962	-.022	+0.315	+889.7
15	+0.118	+0.053	-0.132	2.869	-0.051	+620.3	-.017	+0.043	+0.957	-.018	+0.330	+839.7
16	+0.128	+0.056	-0.132	2.856	-0.038	+602.7	-.013	+0.047	+0.953	-.013	+0.348	+815.9
17	+0.140	+0.060	-0.132	2.845	-0.023	+583.5	-.008	+0.051	+0.949	-.008	+0.368	+789.9
18	+0.160	+0.065	-0.131	2.834	-0.004	+545.2	-.001	+0.054	+0.946	-.002	+0.393	+738.1
19	+0.173	+0.070	-0.131	2.821	+0.008	+524.8	+.003	+0.058	+0.942	+.003	+0.411	+710.5
20	+0.189	+0.072	-0.131	2.812	+0.017	+496.8	+.006	+0.062	+0.938	+.006	+0.423	+672.6

TEST NAME : DSS-C15

Pt. No.	Str.X (%)	Str.Y (%)	X.Coor. (cm)	SigV (ksc)	TauH (ksc)	Eu (ksc)	TauH ---- SigVc	DelU ---- SigVc	SigV ---- SigVc	TauH ---- SigV	TauH ---- Cu	Eu -- Cu
21	+0.200	+0.080	-0.130	2.801	+0.027	+483.0	+.009	+0.065	+0.935	+.010	+0.437	+653.9
22	+0.207	+0.085	-0.130	2.783	+0.027	+467.3	+.009	+0.071	+0.929	+.010	+0.437	+632.6
23	+0.212	+0.089	-0.130	2.772	+0.030	+459.1	+.010	+0.075	+0.925	+.011	+0.439	+621.5
24	+0.219	+0.092	-0.130	2.760	+0.034	+451.6	+.011	+0.079	+0.921	+.012	+0.446	+611.3
25	+0.234	+0.094	-0.130	2.753	+0.054	+446.9	+.018	+0.081	+0.919	+.019	+0.472	+605.0
26	+0.261	+0.099	-0.129	2.747	+0.079	+429.6	+.026	+0.083	+0.917	+.029	+0.506	+581.5
27	+0.296	+0.109	-0.129	2.738	+0.109	+408.6	+.036	+0.086	+0.914	+.040	+0.546	+553.1
28	+0.335	+0.116	-0.128	2.719	+0.133	+383.1	+.044	+0.093	+0.907	+.049	+0.579	+518.7
29	+0.375	+0.126	-0.127	2.687	+0.153	+357.8	+.051	+0.103	+0.897	+.057	+0.606	+484.3
30	+0.423	+0.142	-0.126	2.653	+0.175	+333.7	+.058	+0.115	+0.885	+.066	+0.636	+451.7
31	+0.473	+0.157	-0.125	2.612	+0.196	+311.5	+.065	+0.128	+0.872	+.075	+0.665	+421.7
32	+0.532	+0.171	-0.124	2.573	+0.217	+288.8	+.072	+0.141	+0.859	+.084	+0.693	+391.0
33	+0.593	+0.191	-0.123	2.538	+0.237	+269.3	+.079	+0.153	+0.847	+.093	+0.720	+364.6
34	+0.657	+0.213	-0.122	2.501	+0.253	+250.3	+.084	+0.165	+0.835	+.101	+0.742	+338.8
35	+0.717	+0.232	-0.120	2.466	+0.264	+233.9	+.088	+0.177	+0.823	+.107	+0.757	+316.6
36	+0.784	+0.261	-0.119	2.435	+0.281	+220.2	+.094	+0.187	+0.813	+.115	+0.779	+298.1
37	+0.860	+0.287	-0.118	2.404	+0.294	+205.3	+.098	+0.198	+0.802	+.122	+0.797	+278.0
38	+0.936	+0.316	-0.116	2.376	+0.306	+192.8	+.102	+0.207	+0.793	+.129	+0.814	+261.0
39	+1.014	+0.348	-0.115	2.346	+0.316	+181.0	+.106	+0.217	+0.783	+.135	+0.828	+245.0
40	+1.098	+0.382	-0.113	2.309	+0.326	+169.8	+.109	+0.229	+0.771	+.141	+0.841	+229.9
41	+1.177	+0.415	-0.112	2.278	+0.335	+160.6	+.112	+0.240	+0.760	+.147	+0.852	+217.3
42	+1.256	+0.456	-0.110	2.249	+0.342	+152.3	+.114	+0.249	+0.751	+.152	+0.863	+206.2
43	+1.335	+0.488	-0.108	2.223	+0.349	+144.7	+.116	+0.258	+0.742	+.157	+0.872	+195.9
44	+1.419	+0.527	-0.107	2.199	+0.356	+137.6	+.119	+0.266	+0.734	+.162	+0.881	+186.2
45	+1.502	+0.565	-0.105	2.173	+0.362	+131.3	+.121	+0.275	+0.725	+.167	+0.890	+177.8
46	+1.586	+0.606	-0.104	2.148	+0.368	+125.4	+.123	+0.283	+0.717	+.171	+0.898	+169.8
47	+1.675	+0.647	-0.102	2.123	+0.373	+119.7	+.125	+0.291	+0.709	+.176	+0.905	+162.0
48	+1.754	+0.691	-0.100	2.101	+0.377	+114.9	+.126	+0.299	+0.701	+.179	+0.909	+155.5
49	+1.840	+0.729	-0.099	2.080	+0.382	+110.3	+.127	+0.306	+0.694	+.183	+0.916	+149.3
50	+1.928	+0.775	-0.097	2.055	+0.385	+105.8	+.128	+0.314	+0.686	+.187	+0.921	+143.3
51	+2.012	+0.819	-0.095	2.036	+0.389	+102.0	+.130	+0.320	+0.680	+.191	+0.926	+138.1
52	+2.094	+0.862	-0.094	2.018	+0.392	+98.4	+.131	+0.327	+0.673	+.194	+0.930	+133.2
53	+2.178	+0.908	-0.092	2.000	+0.398	+95.4	+.133	+0.332	+0.668	+.199	+0.938	+129.2
54	+2.273	+0.959	-0.090	1.979	+0.400	+91.7	+.133	+0.339	+0.661	+.202	+0.941	+124.2
55	+2.360	+1.022	-0.089	1.956	+0.401	+88.5	+.134	+0.347	+0.653	+.205	+0.942	+119.8
56	+2.451	+1.070	-0.087	1.943	+0.406	+85.8	+.136	+0.352	+0.648	+.209	+0.949	+116.2
57	+2.542	+1.121	-0.085	1.925	+0.408	+83.0	+.136	+0.358	+0.642	+.212	+0.952	+112.3
58	+2.631	+1.172	-0.083	1.905	+0.411	+80.5	+.137	+0.364	+0.636	+.216	+0.956	+108.9
59	+2.722	+1.220	-0.082	1.888	+0.413	+78.0	+.138	+0.370	+0.630	+.218	+0.958	+105.6
60	+2.812	+1.273	-0.080	1.876	+0.415	+75.7	+.138	+0.374	+0.626	+.221	+0.961	+102.5
61	+2.898	+1.321	-0.078	1.864	+0.416	+73.6	+.139	+0.378	+0.622	+.223	+0.962	+99.6
62	+2.990	+1.374	-0.076	1.845	+0.417	+71.5	+.139	+0.384	+0.616	+.226	+0.964	+96.8
63	+3.080	+1.427	-0.075	1.827	+0.420	+69.6	+.140	+0.390	+0.610	+.230	+0.968	+94.3
64	+3.168	+1.483	-0.073	1.813	+0.422	+67.9	+.141	+0.395	+0.605	+.233	+0.971	+92.0
65	+3.261	+1.541	-0.071	1.812	+0.424	+66.2	+.142	+0.395	+0.605	+.234	+0.974	+89.6
66	+3.355	+1.594	-0.069	1.790	+0.427	+64.5	+.142	+0.403	+0.597	+.238	+0.977	+87.3
67	+3.450	+1.652	-0.067	1.772	+0.428	+62.9	+.143	+0.409	+0.591	+.241	+0.979	+85.1
68	+3.539	+1.705	-0.066	1.755	+0.429	+61.4	+.143	+0.414	+0.586	+.245	+0.980	+83.1

TEST NAME : DSS-C15

Pt. No.	Str.X (%)	Str.Y (%)	X.Coor. (cm)	SigV (ksc)	TauH (ksc)	Eu (ksc)	TauH ---- SigVc	DelU ---- SigVc	SigV ---- SigVc	TauH ---- SigV	TauH ---- Cu	Eu -- Cu
69	+3.633	+1.763	-0.064	1.744	+0.431	+60.0	+.144	+0.418	+0.582	+.247	+0.983	+81.2
70	+3.727	+1.821	-0.062	1.731	+0.433	+58.6	+.145	+0.422	+0.578	+.250	+0.986	+79.4
71	+3.823	+1.882	-0.060	1.718	+0.434	+57.2	+.145	+0.427	+0.573	+.253	+0.987	+77.5
72	+3.914	+1.937	-0.058	1.706	+0.435	+55.9	+.145	+0.431	+0.569	+.255	+0.988	+75.7
73	+4.009	+1.998	-0.057	1.696	+0.437	+54.8	+.146	+0.434	+0.566	+.258	+0.991	+74.2
74	+4.105	+2.058	-0.055	1.687	+0.437	+53.5	+.146	+0.437	+0.563	+.259	+0.991	+72.4
75	+4.199	+2.118	-0.053	1.673	+0.438	+52.4	+.146	+0.442	+0.558	+.262	+0.992	+70.9
76	+4.292	+2.179	-0.051	1.662	+0.440	+51.4	+.147	+0.445	+0.555	+.265	+0.995	+69.5
77	+4.389	+2.244	-0.049	1.654	+0.440	+50.2	+.147	+0.448	+0.552	+.266	+0.995	+68.0
78	+4.485	+2.302	-0.047	1.640	+0.440	+49.2	+.147	+0.453	+0.547	+.268	+0.995	+66.6
79	+4.575	+2.362	-0.046	1.631	+0.440	+48.2	+.147	+0.456	+0.544	+.270	+0.995	+65.3
80	+4.670	+2.427	-0.044	1.621	+0.440	+47.2	+.147	+0.459	+0.541	+.271	+0.995	+63.9
81	+4.759	+2.488	-0.042	1.612	+0.440	+46.3	+.147	+0.462	+0.538	+.273	+0.995	+62.7
82	+4.851	+2.545	-0.040	1.605	+0.440	+45.5	+.147	+0.464	+0.536	+.274	+0.995	+61.6
83	+4.946	+2.603	-0.039	1.596	+0.442	+44.7	+.148	+0.467	+0.533	+.277	+0.998	+60.5
84	+5.037	+2.662	-0.037	1.586	+0.443	+43.9	+.148	+0.471	+0.529	+.279	+0.999	+59.5
85	+5.135	+2.727	-0.035	1.577	+0.444	+43.2	+.148	+0.474	+0.526	+.281	+1.000	+58.4
86	+5.230	+2.785	-0.033	1.566	+0.442	+42.3	+.147	+0.477	+0.523	+.282	+0.997	+57.2
87	+5.318	+2.855	-0.031	1.557	+0.441	+41.5	+.147	+0.481	+0.519	+.283	+0.996	+56.2
88	+5.406	+2.916	-0.030	1.550	+0.441	+40.8	+.147	+0.483	+0.517	+.284	+0.996	+55.3
89	+5.503	+2.979	-0.028	1.542	+0.442	+40.2	+.148	+0.485	+0.515	+.287	+0.998	+54.4
90	+5.595	+3.051	-0.026	1.536	+0.442	+39.5	+.148	+0.487	+0.513	+.288	+0.998	+53.5
91	+5.692	+3.116	-0.024	1.527	+0.442	+38.8	+.147	+0.490	+0.510	+.289	+0.998	+52.6
92	+5.789	+3.182	-0.022	1.520	+0.443	+38.2	+.148	+0.493	+0.507	+.291	+0.999	+51.7
93	+5.888	+3.256	-0.020	1.515	+0.443	+37.6	+.148	+0.494	+0.506	+.292	+0.999	+50.9
94	+5.982	+3.330	-0.018	1.505	+0.441	+36.9	+.147	+0.498	+0.502	+.293	+0.996	+49.9
95	+6.074	+3.403	-0.017	1.497	+0.440	+36.3	+.147	+0.501	+0.499	+.294	+0.994	+49.1
96	+6.170	+3.471	-0.015	1.489	+0.438	+35.7	+.146	+0.503	+0.497	+.294	+0.993	+48.3
97	+6.261	+3.546	-0.013	1.481	+0.438	+35.1	+.146	+0.506	+0.494	+.296	+0.992	+47.5
98	+6.357	+3.623	-0.011	1.472	+0.438	+34.6	+.146	+0.509	+0.491	+.298	+0.993	+46.8
99	+6.458	+3.705	-0.009	1.464	+0.437	+34.0	+.146	+0.511	+0.489	+.298	+0.991	+46.0
100	+6.561	+3.780	-0.007	1.458	+0.435	+33.4	+.145	+0.513	+0.487	+.299	+0.989	+45.2
101	+6.664	+3.870	-0.005	1.452	+0.434	+32.8	+.145	+0.516	+0.484	+.299	+0.987	+44.4
102	+6.758	+3.954	-0.003	1.443	+0.430	+32.2	+.144	+0.518	+0.482	+.298	+0.982	+43.6
103	+6.854	+4.036	-0.002	1.435	+0.430	+31.7	+.144	+0.521	+0.479	+.300	+0.982	+43.0
104	+6.957	+4.120	+0.000	1.427	+0.429	+31.2	+.143	+0.524	+0.476	+.301	+0.980	+42.3
105	+7.059	+4.213	+0.002	1.419	+0.428	+30.7	+.143	+0.526	+0.474	+.302	+0.979	+41.6
106	+7.160	+4.300	+0.004	1.414	+0.427	+30.2	+.142	+0.528	+0.472	+.302	+0.977	+40.9
107	+7.261	+4.389	+0.006	1.405	+0.426	+29.8	+.142	+0.531	+0.469	+.303	+0.976	+40.3
108	+7.357	+4.476	+0.008	1.400	+0.422	+29.2	+.141	+0.533	+0.467	+.302	+0.971	+39.6
109	+7.460	+4.565	+0.010	1.393	+0.421	+28.8	+.140	+0.535	+0.465	+.302	+0.969	+39.0
110	+7.559	+4.667	+0.012	1.388	+0.418	+28.3	+.140	+0.537	+0.463	+.302	+0.966	+38.3
111	+7.660	+4.771	+0.014	1.379	+0.414	+27.8	+.138	+0.540	+0.460	+.301	+0.960	+37.6
112	+7.761	+4.879	+0.016	1.369	+0.410	+27.3	+.137	+0.543	+0.457	+.300	+0.955	+36.9
113	+7.857	+4.981	+0.018	1.365	+0.407	+26.8	+.136	+0.544	+0.456	+.298	+0.950	+36.3
114	+7.952	+5.073	+0.020	1.357	+0.405	+26.4	+.135	+0.547	+0.453	+.299	+0.948	+35.8
115	+8.053	+5.169	+0.022	1.350	+0.405	+26.1	+.135	+0.550	+0.450	+.300	+0.947	+35.3
116	+8.159	+5.268	+0.024	1.343	+0.405	+25.7	+.135	+0.552	+0.448	+.301	+0.948	+34.8

TEST NAME : DSS-C15

Pt. No.	Str.X (%)	Str.Y (%)	X.Coor. (cm)	SigV (ksc)	TauH (ksc)	Eu (ksc)	TauH / SigVc	DelU / SigVc	SigV / SigVc	TauH / SigV	TauH / Cu	Eu / Cu
117	+8.263	+5.367	+0.026	1.335	+0.404	+25.4	+.135	+0.554	+0.446	+.303	+0.947	+34.4
118	+8.366	+5.461	+0.028	1.326	+0.403	+25.0	+.134	+0.558	+0.442	+.304	+0.945	+33.9
119	+8.465	+5.550	+0.030	1.319	+0.401	+24.6	+.134	+0.560	+0.440	+.304	+0.942	+33.4
120	+8.571	+5.647	+0.032	1.315	+0.400	+24.3	+.134	+0.561	+0.439	+.304	+0.941	+32.9
121	+8.666	+5.743	+0.034	1.307	+0.397	+24.0	+.132	+0.564	+0.436	+.304	+0.937	+32.4
122	+8.762	+5.836	+0.035	1.301	+0.395	+23.6	+.132	+0.566	+0.434	+.303	+0.934	+32.0
123	+8.859	+5.925	+0.037	1.295	+0.392	+23.3	+.131	+0.568	+0.432	+.303	+0.930	+31.5
124	+8.960	+6.023	+0.039	1.286	+0.394	+23.1	+.131	+0.571	+0.429	+.306	+0.933	+31.2
125	+9.060	+6.125	+0.041	1.278	+0.391	+22.7	+.131	+0.574	+0.426	+.306	+0.929	+30.8
126	+9.161	+6.225	+0.043	1.272	+0.390	+22.4	+.130	+0.576	+0.424	+.306	+0.927	+30.4
127	+9.268	+6.326	+0.045	1.267	+0.389	+22.2	+.130	+0.577	+0.423	+.307	+0.926	+30.0
128	+9.364	+6.429	+0.047	1.256	+0.384	+21.3	+.128	+0.581	+0.419	+.306	+0.920	+29.5
129	+9.467	+6.532	+0.049	1.248	+0.383	+21.5	+.128	+0.584	+0.416	+.307	+0.918	+29.1
130	+9.581	+6.646	+0.051	1.242	+0.381	+21.2	+.127	+0.586	+0.414	+.307	+0.915	+28.7
131	+9.689	+6.766	+0.053	1.230	+0.376	+20.8	+.126	+0.589	+0.411	+.306	+0.909	+28.1
132	+9.787	+6.884	+0.055	1.217	+0.369	+20.4	+.123	+0.594	+0.406	+.303	+0.899	+27.6
133	+9.888	+7.009	+0.057	1.203	+0.363	+20.0	+.121	+0.599	+0.401	+.302	+0.891	+27.0
134	+9.992	+7.151	+0.059	1.189	+0.356	+19.5	+.119	+0.603	+0.397	+.299	+0.881	+26.5
135	+10.100	+7.319	+0.061	1.172	+0.345	+19.0	+.115	+0.609	+0.391	+.294	+0.867	+25.7
136	+10.230	+7.551	+0.064	1.146	+0.329	+18.3	+.110	+0.618	+0.382	+.287	+0.845	+24.8
137	+10.369	+7.901	+0.067	1.101	+0.296	+17.1	+.099	+0.632	+0.368	+.269	+0.800	+23.1
138	+10.489	+8.242	+0.069	1.062	+0.272	+16.2	+.091	+0.646	+0.354	+.256	+0.768	+22.0
139	+10.612	+8.635	+0.071	1.015	+0.250	+15.4	+.083	+0.661	+0.339	+.246	+0.738	+20.9
140	+10.753	+9.160	+0.074	0.955	+0.220	+14.4	+.074	+0.681	+0.319	+.231	+0.698	+19.5
141	+11.157	+11.570	+0.082	0.809	+0.084	+10.2	+.028	+0.730	+0.270	+.104	+0.514	+13.8
142	+13.685	+9.811	+0.131	0.385	-0.059	+5.2	-.020	+0.871	+0.129	-.153	+0.320	+7.0
143	+13.745	+9.807	+0.132	0.369	-0.050	+5.3	-.017	+0.877	+0.123	-.136	+0.332	+7.2
144	+13.804	+9.790	+0.133	0.423	-0.041	+5.5	-.014	+0.859	+0.141	-.097	+0.344	+7.5

****

ANISOTROPICALLY CONSOLIDATED MDSS TEST
MIT GEOTECHNICAL LAB

****

FILE NAME: DSSC16.PRN

REDUCTION DATA
UNITS: (kg,cm,mVOLTS,VOLTS)

1. TEST NAME : DSS-C16
2. DATE : 03-24-1988
3. OCR : 1
4. VER. CONSOLIDATION STRESS (KSC) : +2.997
5. HOR. CONSOLIDATION STRESS (KSC) : +0.600
6. PRE-SHEAR SAMPLE HEIGHT (cm) : +1.9913
7. VERTICAL STRESS LOAD CELL:
   ZERO: .72
   CF: 13.70491
8. HORIZONTAL SHEAR LOAD CELL:
   ZERO: -1.56
   CF: 6.70298
9. HORIZONTAL DISP. TRANSDUCER, X:
   ZERO: 1.0264
   CF: -1.81917
10. HORIZONTAL DISP. TRANSDUCER, Y:
    ZERO: 1.2053
    CF: -.261
11. VERTICAL DISP. TRANSDUCER, Z1:
    ZERO: -.1891
    CF: .28883
12. VERTICAL DISP. TRANSDUCER, Z2:
    ZERO: .7767
    CF: .29569
13. CONSTANT HEIGHT TRANSDUCER, Z:
    ZERO: .17249
    CF: .3014
14. TEST ANGLE THETA (degrees): 150

TOTAL X DISP. DURING CONSOLIDATION (cm): -.28125

Pt. No.	Str.X (%)	Str.Y (%)	X.Coor. (cm)	SigV (ksc)	TauH (ksc)	Eu (ksc)	TauH SigVc	DelU SigVc	SigV SigVc	TauH SigV	TauH Cu	Eu Cu
1	+0.000	+0.000	-0.281	2.997	-0.510	+9999.0	-.170	+0.000	+1.000	-.170	+0.000	+9488.7
2	+0.000	+0.010	-0.281	3.001	-0.493	+9999.0	-.164	-0.001	+1.001	-.164	+0.016	+9488.7
3	+0.002	+0.008	-0.281	3.007	-0.455	+9934.9	-.152	-0.003	+1.003	-.151	+0.051	+9427.9
4	+0.002	+0.017	-0.281	3.018	-0.414	+9999.0	-.138	-0.007	+1.007	-.137	+0.091	+9488.7
5	+0.025	+0.029	-0.281	3.022	-0.349	+1961.9	-.116	-0.008	+1.008	-.115	+0.152	+1861.8
6	+0.070	+0.041	-0.280	3.011	-0.277	+991.4	-.092	-0.005	+1.005	-.092	+0.221	+940.8
7	+0.123	+0.052	-0.279	2.982	-0.208	+735.2	-.070	+0.005	+0.995	-.070	+0.286	+697.7
8	+0.183	+0.059	-0.278	2.951	-0.148	+591.6	-.049	+0.015	+0.985	-.050	+0.343	+561.4
9	+0.241	+0.069	-0.276	2.902	-0.095	+516.6	-.032	+0.032	+0.968	-.033	+0.393	+490.2
10	+0.287	+0.081	-0.276	2.847	-0.065	+465.2	-.022	+0.050	+0.950	-.023	+0.422	+441.4
11	+0.319	+0.085	-0.275	2.802	-0.049	+432.9	-.016	+0.065	+0.935	-.017	+0.437	+410.8
12	+0.354	+0.090	-0.274	2.767	-0.025	+410.6	-.008	+0.077	+0.923	-.009	+0.460	+389.6
13	+0.390	+0.095	-0.273	2.742	-0.006	+387.7	-.002	+0.085	+0.915	-.002	+0.478	+367.9
14	+0.419	+0.102	-0.273	2.714	+0.007	+369.5	+.002	+0.094	+0.906	+.003	+0.490	+350.6
15	+0.441	+0.106	-0.272	2.695	+0.012	+355.4	+.004	+0.101	+0.899	+.005	+0.495	+337.2
16	+0.467	+0.111	-0.272	2.677	+0.033	+348.4	+.011	+0.107	+0.893	+.012	+0.515	+330.6
17	+0.531	+0.116	-0.271	2.656	+0.077	+331.5	+.026	+0.114	+0.886	+.029	+0.556	+314.6
18	+0.619	+0.130	-0.269	2.620	+0.119	+304.7	+.040	+0.126	+0.874	+.046	+0.597	+289.2
19	+0.732	+0.146	-0.267	2.562	+0.159	+273.8	+.053	+0.145	+0.855	+.062	+0.634	+259.9
20	+0.847	+0.168	-0.264	2.499	+0.191	+248.3	+.064	+0.166	+0.834	+.077	+0.665	+235.6

TEST NAME : DSS-C16

Pt. No.	Str.X (%)	Str.Y (%)	X.Coor. (cm)	SigV (ksc)	TauH (ksc)	Eu (ksc)	TauH ---- SigVc	DelU ---- SigVc	SigV ---- SigVc	TauH ---- SigV	TauH ---- Cu	Eu -- Cu
21	+0.971	+0.189	-0.262	2.431	+0.219	+225.0	+.073	+0.189	+0.811	+.090	+0.691	+213.5
22	+1.099	+0.208	-0.259	2.368	+0.246	+206.2	+.082	+0.210	+0.790	+.104	+0.717	+195.6
23	+1.232	+0.236	-0.257	2.311	+0.269	+189.6	+.090	+0.229	+0.771	+.116	+0.739	+179.9
24	+1.366	+0.262	-0.254	2.258	+0.288	+175.2	+.096	+0.247	+0.753	+.128	+0.757	+166.2
25	+1.507	+0.292	-0.251	2.211	+0.307	+162.7	+.103	+0.262	+0.738	+.139	+0.775	+154.4
26	+1.648	+0.325	-0.248	2.164	+0.323	+151.6	+.108	+0.278	+0.722	+.149	+0.790	+143.9
27	+1.808	+0.353	-0.245	2.123	+0.340	+140.9	+.113	+0.292	+0.708	+.160	+0.806	+133.7
28	+1.961	+0.389	-0.242	2.082	+0.353	+132.0	+.118	+0.305	+0.695	+.170	+0.819	+125.2
29	+2.118	+0.424	-0.239	2.039	+0.365	+123.8	+.122	+0.319	+0.681	+.179	+0.830	+117.5
30	+2.291	+0.459	-0.236	2.001	+0.379	+116.4	+.127	+0.332	+0.668	+.190	+0.843	+110.4
31	+2.460	+0.501	-0.232	1.969	+0.389	+109.5	+.130	+0.343	+0.657	+.197	+0.852	+103.9
32	+2.631	+0.539	-0.229	1.932	+0.398	+103.5	+.133	+0.355	+0.645	+.206	+0.861	+98.2
33	+2.806	+0.581	-0.225	1.894	+0.408	+98.1	+.136	+0.368	+0.632	+.216	+0.871	+93.1
34	+2.971	+0.624	-0.222	1.858	+0.415	+93.4	+.139	+0.380	+0.620	+.223	+0.878	+88.6
35	+3.147	+0.668	-0.219	1.830	+0.424	+89.0	+.142	+0.389	+0.611	+.232	+0.886	+84.5
36	+3.324	+0.710	-0.215	1.807	+0.432	+85.0	+.144	+0.397	+0.603	+.239	+0.894	+80.7
37	+3.497	+0.757	-0.212	1.781	+0.438	+81.3	+.146	+0.406	+0.594	+.246	+0.899	+77.1
38	+3.673	+0.800	-0.208	1.753	+0.445	+77.9	+.148	+0.415	+0.585	+.254	+0.906	+74.0
39	+3.861	+0.849	-0.204	1.731	+0.452	+74.7	+.151	+0.422	+0.578	+.261	+0.913	+70.9
40	+4.044	+0.901	-0.201	1.703	+0.458	+71.8	+.153	+0.432	+0.568	+.269	+0.918	+68.1
41	+4.224	+0.953	-0.197	1.686	+0.460	+68.9	+.154	+0.437	+0.563	+.273	+0.920	+65.4
42	+4.402	+0.995	-0.194	1.664	+0.465	+66.4	+.155	+0.445	+0.555	+.279	+0.924	+63.0
43	+4.593	+1.044	-0.190	1.647	+0.468	+63.8	+.156	+0.450	+0.550	+.284	+0.927	+60.6
44	+4.775	+1.094	-0.186	1.625	+0.469	+61.5	+.157	+0.458	+0.542	+.289	+0.929	+58.4
45	+4.958	+1.143	-0.183	1.609	+0.473	+59.5	+.158	+0.463	+0.537	+.294	+0.933	+56.4
46	+5.140	+1.188	-0.179	1.591	+0.477	+57.6	+.159	+0.469	+0.531	+.300	+0.936	+54.6
47	+5.318	+1.225	-0.175	1.576	+0.481	+55.9	+.160	+0.474	+0.526	+.305	+0.940	+53.0
48	+5.492	+1.251	-0.172	1.556	+0.482	+54.2	+.161	+0.481	+0.519	+.310	+0.941	+51.4
49	+5.671	+1.289	-0.168	1.545	+0.485	+52.6	+.162	+0.485	+0.515	+.314	+0.944	+49.9
50	+5.846	+1.345	-0.165	1.529	+0.488	+51.2	+.163	+0.490	+0.510	+.319	+0.946	+48.6
51	+6.030	+1.390	-0.161	1.521	+0.491	+49.8	+.164	+0.493	+0.507	+.323	+0.949	+47.2
52	+6.208	+1.434	-0.158	1.505	+0.493	+48.4	+.164	+0.498	+0.502	+.327	+0.951	+46.0
53	+6.382	+1.479	-0.154	1.495	+0.495	+47.2	+.165	+0.501	+0.499	+.331	+0.954	+44.8
54	+6.570	+1.526	-0.150	1.487	+0.498	+46.0	+.166	+0.504	+0.496	+.335	+0.956	+43.6
55	+6.746	+1.573	-0.147	1.469	+0.498	+44.8	+.166	+0.510	+0.490	+.339	+0.956	+42.5
56	+6.921	+1.618	-0.143	1.460	+0.499	+43.7	+.167	+0.513	+0.487	+.342	+0.957	+41.5
57	+7.106	+1.665	-0.140	1.453	+0.501	+42.6	+.167	+0.515	+0.485	+.345	+0.959	+40.5
58	+7.294	+1.716	-0.136	1.440	+0.503	+41.6	+.168	+0.520	+0.480	+.349	+0.960	+39.5
59	+7.476	+1.759	-0.132	1.427	+0.503	+40.6	+.168	+0.524	+0.476	+.353	+0.961	+38.6
60	+7.661	+1.806	-0.129	1.420	+0.506	+39.8	+.169	+0.526	+0.474	+.356	+0.963	+37.7
61	+7.842	+1.853	-0.125	1.405	+0.507	+38.9	+.169	+0.531	+0.469	+.361	+0.965	+36.9
62	+8.027	+1.907	-0.121	1.403	+0.509	+38.1	+.170	+0.532	+0.468	+.363	+0.967	+36.1
63	+8.204	+1.951	-0.118	1.395	+0.510	+37.3	+.170	+0.535	+0.465	+.366	+0.968	+35.4
64	+8.382	+1.994	-0.114	1.385	+0.512	+36.6	+.171	+0.538	+0.462	+.370	+0.969	+34.7
65	+8.559	+2.034	-0.111	1.380	+0.513	+35.8	+.171	+0.539	+0.461	+.372	+0.971	+34.0
66	+8.739	+2.085	-0.107	1.375	+0.514	+35.2	+.172	+0.541	+0.459	+.374	+0.972	+33.4
67	+8.926	+2.139	-0.104	1.365	+0.517	+34.5	+.172	+0.544	+0.456	+.378	+0.974	+32.7
68	+9.109	+2.186	-0.100	1.355	+0.517	+33.8	+.173	+0.548	+0.452	+.382	+0.974	+32.1

TEST NAME : DSS-C16

Pt. No.	Str.X (%)	Str.Y (%)	X.Coor. (cm)	SigV (ksc)	TauH (ksc)	Eu (ksc)	TauH / SigVc	DelU / SigVc	SigV / SigVc	TauH / SigV	TauH / Cu	Eu / Cu
69	+9.293	+2.231	-0.096	1.349	+0.517	+33.2	+.173	+0.550	+0.450	+.384	+0.975	+31.5
70	+9.481	+2.278	-0.092	1.345	+0.520	+32.6	+.174	+0.551	+0.449	+.387	+0.977	+30.9
71	+9.663	+2.325	-0.089	1.338	+0.522	+32.0	+.174	+0.554	+0.446	+.390	+0.979	+30.4
72	+9.855	+2.370	-0.085	1.332	+0.525	+31.5	+.175	+0.555	+0.445	+.394	+0.982	+29.9
73	+10.030	+2.405	-0.082	1.323	+0.524	+30.9	+.175	+0.559	+0.441	+.396	+0.981	+29.3
74	+10.214	+2.452	-0.078	1.318	+0.526	+30.4	+.175	+0.560	+0.440	+.399	+0.982	+28.9
75	+10.394	+2.499	-0.074	1.318	+0.526	+29.9	+.175	+0.560	+0.440	+.399	+0.982	+28.4
76	+10.580	+2.544	-0.071	1.314	+0.525	+29.3	+.175	+0.562	+0.438	+.399	+0.981	+27.8
77	+10.762	+2.588	-0.067	1.306	+0.526	+28.9	+.175	+0.564	+0.436	+.403	+0.982	+27.4
78	+10.945	+2.635	-0.063	1.301	+0.525	+28.4	+.175	+0.566	+0.434	+.404	+0.982	+26.9
79	+11.136	+2.689	-0.060	1.297	+0.526	+27.9	+.176	+0.567	+0.433	+.406	+0.983	+26.5
80	+11.321	+2.737	-0.056	1.293	+0.529	+27.5	+.177	+0.568	+0.432	+.409	+0.986	+26.1
81	+11.508	+2.781	-0.052	1.287	+0.528	+27.1	+.176	+0.571	+0.429	+.411	+0.985	+25.7
82	+11.698	+2.830	-0.048	1.282	+0.529	+26.6	+.177	+0.572	+0.428	+.413	+0.986	+25.3
83	+11.878	+2.868	-0.045	1.274	+0.528	+26.2	+.176	+0.575	+0.425	+.415	+0.985	+24.9
84	+12.055	+2.922	-0.041	1.266	+0.529	+25.8	+.176	+0.577	+0.423	+.417	+0.985	+24.5
85	+12.241	+2.967	-0.037	1.264	+0.529	+25.5	+.177	+0.578	+0.422	+.419	+0.986	+24.2
86	+12.433	+3.011	-0.034	1.268	+0.531	+25.1	+.177	+0.577	+0.423	+.419	+0.987	+23.8
87	+12.625	+3.057	-0.030	1.272	+0.530	+24.7	+.177	+0.576	+0.424	+.417	+0.986	+23.4
88	+12.803	+3.098	-0.026	1.281	+0.530	+24.4	+.177	+0.572	+0.428	+.414	+0.987	+23.1
89	+12.996	+3.148	-0.022	1.312	+0.531	+24.0	+.177	+0.562	+0.438	+.405	+0.988	+22.8
90	+13.184	+3.193	-0.019	1.337	+0.536	+23.8	+.179	+0.554	+0.446	+.401	+0.992	+22.6
91	+13.371	+3.233	-0.015	1.332	+0.536	+23.5	+.179	+0.556	+0.444	+.402	+0.992	+22.3
92	+13.554	+3.281	-0.011	1.308	+0.536	+23.1	+.179	+0.563	+0.437	+.410	+0.992	+22.0
93	+13.734	+3.326	-0.008	1.243	+0.535	+22.8	+.178	+0.585	+0.415	+.430	+0.991	+21.7
94	+13.925	+3.376	-0.004	1.223	+0.534	+22.5	+.178	+0.592	+0.408	+.437	+0.991	+21.3
95	+14.110	+3.427	-0.000	1.223	+0.535	+22.2	+.178	+0.592	+0.408	+.437	+0.991	+21.1
96	+14.291	+3.477	+0.003	1.231	+0.535	+21.9	+.179	+0.589	+0.411	+.435	+0.991	+20.8
97	+14.473	+3.521	+0.007	1.254	+0.538	+21.7	+.179	+0.581	+0.419	+.429	+0.994	+20.6
98	+14.655	+3.571	+0.011	1.302	+0.540	+21.5	+.180	+0.566	+0.434	+.415	+0.996	+20.4
99	+14.836	+3.609	+0.014	1.305	+0.544	+21.3	+.182	+0.565	+0.435	+.417	+1.000	+20.2
100	+15.021	+3.655	+0.018	1.294	+0.544	+21.0	+.181	+0.568	+0.432	+.420	+0.999	+20.0
101	+15.196	+3.700	+0.021	1.265	+0.541	+20.7	+.181	+0.578	+0.422	+.428	+0.997	+19.7
102	+15.392	+3.746	+0.025	1.210	+0.542	+20.5	+.181	+0.596	+0.404	+.448	+0.998	+19.4
103	+15.600	+3.805	+0.029	1.210	+0.539	+20.2	+.180	+0.596	+0.404	+.445	+0.995	+19.1
104	+15.793	+3.850	+0.033	1.203	+0.539	+19.9	+.180	+0.599	+0.401	+.448	+0.995	+18.9
105	+15.953	+3.893	+0.036	1.201	+0.539	+19.7	+.180	+0.599	+0.401	+.448	+0.995	+18.7
106	+16.142	+3.935	+0.040	1.199	+0.540	+19.5	+.180	+0.600	+0.400	+.451	+0.996	+18.5
107	+16.340	+3.980	+0.044	1.196	+0.542	+19.3	+.181	+0.601	+0.399	+.453	+0.998	+18.3
108	+16.518	+4.034	+0.048	1.197	+0.542	+19.1	+.181	+0.601	+0.399	+.453	+0.998	+18.1
109	+16.710	+4.088	+0.051	1.192	+0.542	+18.9	+.181	+0.602	+0.398	+.454	+0.997	+17.9
110	+16.895	+4.139	+0.055	1.191	+0.542	+18.7	+.181	+0.603	+0.397	+.456	+0.998	+17.7
111	+17.077	+4.184	+0.059	1.185	+0.543	+18.5	+.181	+0.605	+0.395	+.458	+0.998	+17.5
112	+17.270	+4.215	+0.063	1.181	+0.543	+18.3	+.181	+0.606	+0.394	+.460	+0.999	+17.4
113	+17.470	+4.276	+0.067	1.184	+0.544	+18.1	+.181	+0.605	+0.395	+.459	+0.999	+17.2
114	+17.668	+4.327	+0.071	1.180	+0.543	+17.9	+.181	+0.606	+0.394	+.460	+0.999	+17.0
115	+17.847	+4.367	+0.074	1.180	+0.542	+17.7	+.181	+0.606	+0.394	+.459	+0.998	+16.8
116	+18.035	+4.417	+0.078	1.177	+0.540	+17.5	+.180	+0.607	+0.393	+.459	+0.996	+16.6

TEST NAME : DSS-C16

Pt. No.	Str.X (%)	Str.Y (%)	X.Coor. (cm)	SigV (ksc)	TauH (ksc)	Eu (ksc)	TauH ---- SigVc	DelU ---- SigVc	SigV ---- SigVc	TauH ---- SigV	TauH ---- Cu	Eu -- Cu
117	+18.229	+4.464	+0.082	1.167	+0.541	+17.3	+.181	+0.610	+0.390	+.463	+0.997	+16.4
118	+18.419	+4.512	+0.086	1.160	+0.539	+17.1	+.180	+0.613	+0.387	+.465	+0.995	+16.2
119	+18.610	+4.579	+0.089	1.153	+0.538	+16.9	+.179	+0.615	+0.385	+.466	+0.994	+16.0
120	+18.800	+4.631	+0.093	1.152	+0.537	+16.7	+.179	+0.616	+0.384	+.467	+0.994	+15.9
121	+18.987	+4.680	+0.097	1.153	+0.535	+16.5	+.178	+0.615	+0.385	+.464	+0.991	+15.7
122	+19.175	+4.743	+0.101	1.158	+0.532	+16.3	+.178	+0.614	+0.386	+.460	+0.989	+15.5
123	+19.359	+4.786	+0.104	1.160	+0.527	+16.1	+.176	+0.613	+0.387	+.454	+0.983	+15.2
124	+19.554	+4.842	+0.108	1.170	+0.526	+15.9	+.175	+0.610	+0.390	+.449	+0.983	+15.1
125	+19.741	+4.901	+0.112	1.190	+0.523	+15.7	+.174	+0.603	+0.397	+.439	+0.980	+14.9
126	+19.929	+4.964	+0.116	1.186	+0.518	+15.5	+.173	+0.604	+0.396	+.437	+0.975	+14.7
127	+20.124	+5.014	+0.119	1.162	+0.516	+15.3	+.172	+0.612	+0.388	+.444	+0.973	+14.5
128	+20.314	+5.065	+0.123	1.087	+0.511	+15.1	+.170	+0.637	+0.363	+.470	+0.968	+14.3
129	+20.514	+5.136	+0.127	1.063	+0.503	+14.8	+.168	+0.645	+0.355	+.473	+0.961	+14.0
130	+20.715	+5.206	+0.131	1.052	+0.501	+14.6	+.167	+0.649	+0.351	+.476	+0.959	+13.9
131	+20.888	+5.274	+0.135	1.045	+0.494	+14.4	+.165	+0.651	+0.349	+.473	+0.953	+13.7
132	+21.078	+5.339	+0.138	1.036	+0.490	+14.2	+.163	+0.654	+0.346	+.473	+0.948	+13.5
133	+21.283	+5.409	+0.143	1.030	+0.488	+14.1	+.163	+0.656	+0.344	+.474	+0.947	+13.3
134	+21.475	+5.477	+0.146	1.019	+0.482	+13.9	+.161	+0.660	+0.340	+.473	+0.941	+13.1
135	+21.659	+5.535	+0.150	1.009	+0.479	+13.7	+.160	+0.663	+0.337	+.475	+0.938	+13.0
136	+21.845	+5.599	+0.154	0.998	+0.476	+13.5	+.159	+0.667	+0.333	+.477	+0.935	+12.8
137	+22.034	+5.667	+0.158	0.988	+0.473	+13.4	+.158	+0.670	+0.330	+.478	+0.932	+12.7
138	+22.225	+5.734	+0.161	0.979	+0.469	+13.2	+.157	+0.673	+0.327	+.480	+0.929	+12.5
139	+22.412	+5.799	+0.165	0.969	+0.465	+13.0	+.155	+0.677	+0.323	+.480	+0.925	+12.4
140	+22.599	+5.862	+0.169	0.960	+0.459	+12.9	+.153	+0.680	+0.320	+.479	+0.919	+12.2
141	+22.794	+5.928	+0.173	0.951	+0.456	+12.7	+.152	+0.683	+0.317	+.479	+0.916	+12.1
142	+22.986	+5.996	+0.176	0.940	+0.454	+12.6	+.151	+0.686	+0.314	+.482	+0.914	+11.9
143	+23.187	+6.069	+0.180	0.933	+0.449	+12.4	+.150	+0.689	+0.311	+.481	+0.910	+11.8
144	+23.376	+6.136	+0.184	0.919	+0.444	+12.2	+.148	+0.693	+0.307	+.483	+0.905	+11.6
145	+23.575	+6.208	+0.188	0.913	+0.440	+12.1	+.147	+0.695	+0.305	+.482	+0.901	+11.5
146	+23.769	+6.287	+0.192	0.904	+0.435	+11.9	+.145	+0.698	+0.302	+.482	+0.897	+11.3
147	+23.962	+6.356	+0.196	0.895	+0.433	+11.8	+.145	+0.701	+0.299	+.484	+0.895	+11.2
148	+24.153	+6.434	+0.200	0.885	+0.429	+11.7	+.143	+0.705	+0.295	+.485	+0.891	+11.1
149	+24.348	+6.511	+0.204	0.875	+0.424	+11.5	+.142	+0.708	+0.292	+.485	+0.886	+10.9
150	+24.554	+6.599	+0.208	0.866	+0.421	+11.4	+.140	+0.711	+0.289	+.486	+0.883	+10.8
151	+24.749	+6.681	+0.212	0.860	+0.416	+11.2	+.139	+0.713	+0.287	+.483	+0.878	+10.6
152	+24.950	+6.760	+0.216	0.852	+0.413	+11.1	+.138	+0.716	+0.284	+.484	+0.875	+10.5
153	+25.140	+6.842	+0.219	0.842	+0.411	+11.0	+.137	+0.719	+0.281	+.487	+0.873	+10.4
154	+25.331	+6.917	+0.223	0.833	+0.408	+10.9	+.136	+0.722	+0.278	+.490	+0.871	+10.3
155	+25.516	+6.990	+0.227	0.826	+0.406	+10.8	+.135	+0.724	+0.276	+.491	+0.868	+10.2
156	+25.705	+7.075	+0.231	0.819	+0.403	+10.6	+.134	+0.727	+0.273	+.492	+0.866	+10.1
157	+25.904	+7.156	+0.235	0.811	+0.399	+10.5	+.133	+0.729	+0.271	+.492	+0.862	+10.0
158	+26.095	+7.220	+0.238	0.803	+0.397	+10.4	+.133	+0.732	+0.268	+.495	+0.860	+9.9
159	+26.287	+7.308	+0.242	0.795	+0.394	+10.3	+.131	+0.735	+0.265	+.495	+0.857	+9.8
160	+26.496	+7.392	+0.246	0.788	+0.391	+10.2	+.131	+0.737	+0.263	+.496	+0.855	+9.7
161	+26.697	+7.473	+0.250	0.784	+0.388	+10.1	+.129	+0.739	+0.261	+.495	+0.852	+9.6
162	+26.889	+7.574	+0.254	0.779	+0.387	+10.0	+.129	+0.740	+0.260	+.496	+0.851	+9.5
163	+27.079	+7.667	+0.258	0.768	+0.383	+9.9	+.128	+0.744	+0.256	+.499	+0.847	+9.4
164	+27.271	+7.752	+0.262	0.764	+0.381	+9.8	+.127	+0.745	+0.255	+.499	+0.845	+9.3

TEST NAME : DSS-C16

Pt. No.	Str.X (%)	Str.Y (%)	X.Coor. (cm)	SigV (ksc)	TauH (ksc)	Eu (ksc)	TauH ---- SigVc	DelU ---- SigVc	SigV ---- SigVc	TauH ---- SigV	TauH ---- Cu	Eu -- Cu
165	+27.448	+7.850	+0.265	0.757	+0.377	+9.7	+.126	+0.748	+0.252	+.498	+0.841	+9.2
166	+27.639	+7.936	+0.269	0.752	+0.375	+9.6	+.125	+0.749	+0.251	+.499	+0.840	+9.1
167	+27.843	+8.029	+0.273	0.749	+0.371	+9.5	+.124	+0.750	+0.250	+.495	+0.835	+9.0
168	+28.037	+8.123	+0.277	0.748	+0.369	+9.4	+.123	+0.750	+0.250	+.493	+0.834	+8.9
169	+28.239	+8.217	+0.281	0.750	+0.366	+9.3	+.122	+0.750	+0.250	+.489	+0.831	+8.8
170	+28.441	+8.310	+0.285	0.760	+0.364	+9.2	+.122	+0.747	+0.253	+.479	+0.829	+8.7
171	+28.626	+8.414	+0.289	0.781	+0.362	+9.1	+.121	+0.740	+0.260	+.463	+0.827	+8.7
172	+28.822	+8.515	+0.293	0.778	+0.359	+9.0	+.120	+0.740	+0.260	+.461	+0.824	+8.6
173	+29.032	+8.620	+0.297	0.758	+0.356	+8.9	+.119	+0.747	+0.253	+.469	+0.821	+8.5
174	+29.238	+8.739	+0.301	0.706	+0.348	+8.8	+.116	+0.764	+0.236	+.493	+0.814	+8.3
175	+29.434	+8.852	+0.305	0.689	+0.339	+8.6	+.113	+0.770	+0.230	+.492	+0.805	+8.2
176	+29.633	+8.978	+0.309	0.683	+0.334	+8.5	+.111	+0.772	+0.228	+.489	+0.800	+8.1
177	+29.823	+9.094	+0.313	0.681	+0.329	+8.4	+.110	+0.773	+0.227	+.484	+0.796	+8.0
178	+30.020	+9.218	+0.317	0.678	+0.325	+8.3	+.108	+0.774	+0.226	+.479	+0.792	+7.9
179	+30.220	+9.350	+0.321	0.672	+0.321	+8.2	+.107	+0.776	+0.224	+.478	+0.788	+7.8
180	+30.426	+9.492	+0.325	0.665	+0.317	+8.1	+.106	+0.778	+0.222	+.476	+0.784	+7.7
181	+30.626	+9.636	+0.329	0.660	+0.311	+8.0	+.104	+0.780	+0.220	+.472	+0.779	+7.6
182	+30.822	+9.778	+0.333	0.651	+0.307	+7.9	+.102	+0.783	+0.217	+.471	+0.775	+7.5
183	+31.019	+9.916	+0.336	0.645	+0.302	+7.8	+.101	+0.785	+0.215	+.468	+0.770	+7.4
184	+31.208	+10.048	+0.340	0.637	+0.297	+7.8	+.099	+0.788	+0.212	+.466	+0.765	+7.4
185	+31.402	+10.172	+0.344	0.629	+0.295	+7.7	+.098	+0.790	+0.210	+.469	+0.763	+7.3
186	+31.582	+10.297	+0.348	0.622	+0.291	+7.6	+.097	+0.792	+0.208	+.467	+0.759	+7.2
187	+31.780	+10.419	+0.352	0.618	+0.288	+7.5	+.096	+0.794	+0.206	+.465	+0.756	+7.1
188	+31.966	+10.539	+0.355	0.611	+0.285	+7.5	+.095	+0.796	+0.204	+.467	+0.754	+7.1
189	+32.165	+10.651	+0.359	0.607	+0.284	+7.4	+.095	+0.798	+0.202	+.468	+0.753	+7.0
190	+32.361	+10.771	+0.363	0.602	+0.280	+7.3	+.094	+0.799	+0.201	+.466	+0.750	+6.9
191	+32.555	+10.894	+0.367	0.594	+0.278	+7.3	+.093	+0.802	+0.198	+.468	+0.747	+6.9
192	+32.759	+11.006	+0.371	0.587	+0.274	+7.2	+.091	+0.804	+0.196	+.466	+0.743	+6.8
193	+32.957	+11.108	+0.375	0.581	+0.271	+7.1	+.090	+0.806	+0.194	+.465	+0.740	+6.7
194	+33.156	+11.230	+0.379	0.576	+0.267	+7.0	+.089	+0.808	+0.192	+.464	+0.737	+6.7
195	+33.346	+11.371	+0.383	0.570	+0.265	+7.0	+.088	+0.810	+0.190	+.465	+0.735	+6.6
196	+33.554	+11.491	+0.387	0.565	+0.263	+6.9	+.088	+0.811	+0.189	+.465	+0.733	+6.6
197	+33.763	+11.625	+0.391	0.560	+0.259	+6.8	+.087	+0.813	+0.187	+.463	+0.730	+6.5
198	+33.961	+11.766	+0.395	0.553	+0.256	+6.8	+.086	+0.815	+0.185	+.463	+0.727	+6.4

****

ANISOTROPICALLY CONSOLIDATED MDSS TEST

MIT GEOTECHNICAL LAB

****

FILE NAME: DSSC17.PRN

REDUCTION DATA

UNITS: (kg,cm,mVOLTS,VOLTS)

1. TEST NAME : DSS-C17
2. DATE : 05-11-1988
3. OCR : 1
4. VER. CONSOLIDATION STRESS (KSC) : +3.000
5. HOR. CONSOLIDATION STRESS (KSC) : +0.600
6. PRE-SHEAR SAMPLE HEIGHT (cm) : +1.9066
7. VERTICAL STRESS LOAD CELL:
   ZERO: .7
   CF: 13.70491
8. HORIZONTAL SHEAR LOAD CELL:
   ZERO: -1.75
   CF: 6.70298
9. HORIZONTAL DISP. TRANSDUCER, X:
   ZERO: .953
   CF: -1.81917
10. HORIZONTAL DISP. TRANSDUCER, Y:
    ZERO: -3.846
    CF: -.261
11. VERTICAL DISP. TRANSDUCER, Z1:
    ZERO: .7549
    CF: .28883
12. VERTICAL DISP. TRANSDUCER, Z2:
    ZERO: 1.0223
    CF: .29569
13. CONSTANT HEIGHT TRANSDUCER, Z:
    ZERO: .10516
    CF: .3014
14. TEST ANGLE THETA (degrees): 60

TOTAL X DISP. DURING CONSOLIDATION (cm): .15011

Pt. No.	Str.X (%)	Str.Y (%)	X.Coor. (cm)	SigV (ksc)	TauH (ksc)	Eu (ksc)	TauH ---- SigVc	DelU ---- SigVc	SigV ---- SigVc	TauH ---- SigV	TauH ---- Cu	Eu -- Cu
1	+0.000	+0.000	+0.150	3.000	+0.294	+9999.0	+.098	+0.000	+1.000	+.098	+0.000	+9999.0
2	-0.007	-0.002	+0.150	3.000	+0.294	-15.3	+.098	-0.000	+1.000	+.098	+0.001	-47.2
3	-0.007	-0.002	+0.150	3.001	+0.300	-271.2	+.100	-0.000	+1.000	+.100	+0.019	-836.5
4	-0.003	+0.000	+0.150	3.000	+0.318	-2138.2	+.106	-0.000	+1.000	+.106	+0.075	-6594.7
5	+0.010	-0.002	+0.150	2.998	+0.335	+1204.1	+.112	+0.001	+0.999	+.112	+0.127	+3713.8
6	+0.017	+0.002	+0.150	2.995	+0.349	+963.2	+.116	+0.002	+0.998	+.116	+0.169	+2970.8
7	+0.024	+0.002	+0.151	2.992	+0.360	+834.2	+.120	+0.003	+0.997	+.120	+0.205	+2572.8
8	+0.046	+0.005	+0.151	2.998	+0.389	+619.8	+.130	+0.001	+0.999	+.130	+0.294	+1911.5
9	+0.067	+0.005	+0.151	2.995	+0.425	+591.1	+.142	+0.002	+0.998	+.142	+0.405	+1823.1
10	+0.096	+0.020	+0.152	3.001	+0.458	+514.8	+.153	-0.000	+1.000	+.153	+0.507	+1587.8
11	+0.128	+0.022	+0.153	3.001	+0.490	+459.0	+.163	-0.000	+1.000	+.163	+0.605	+1415.7
12	+0.166	+0.034	+0.153	2.995	+0.520	+409.5	+.173	+0.002	+0.998	+.174	+0.698	+1262.9
13	+0.214	+0.044	+0.154	2.981	+0.549	+357.7	+.183	+0.006	+0.994	+.184	+0.786	+1103.2
14	+0.270	+0.056	+0.155	2.954	+0.570	+306.2	+.190	+0.015	+0.985	+.193	+0.851	+944.3
15	+0.333	+0.074	+0.156	2.908	+0.587	+264.1	+.196	+0.031	+0.969	+.202	+0.906	+814.6
16	+0.405	+0.098	+0.158	2.837	+0.601	+227.4	+.200	+0.054	+0.946	+.212	+0.948	+701.4
17	+0.491	+0.132	+0.159	2.746	+0.610	+193.2	+.203	+0.085	+0.915	+.222	+0.975	+595.9
18	+0.583	+0.169	+0.161	2.674	+0.616	+165.8	+.205	+0.109	+0.891	+.230	+0.994	+511.3
19	+0.674	+0.213	+0.163	2.621	+0.618	+144.4	+.206	+0.126	+0.874	+.236	+1.000	+445.2
20	+0.768	+0.263	+0.165	2.583	+0.616	+125.8	+.205	+0.139	+0.861	+.238	+0.993	+388.1

TEST NAME : DSS-C17

Pt. No.	Str.X (%)	Str.Y (%)	X.Coor. (cm)	SigV (ksc)	TauH (ksc)	Eu (ksc)	TauH / SigVc	DelU / SigVc	SigV / SigVc	TauH / SigV	TauH / Cu	Eu / Cu
21	+0.864	+0.309	+0.167	2.544	+0.617	+112.2	+.206	+0.152	+0.848	+.242	+0.996	+346.1
22	+0.959	+0.358	+0.168	2.506	+0.614	+100.2	+.205	+0.165	+0.835	+.245	+0.989	+309.2
23	+1.057	+0.415	+0.170	2.471	+0.613	+90.6	+.204	+0.176	+0.824	+.248	+0.984	+279.4
24	+1.160	+0.466	+0.172	2.430	+0.612	+82.4	+.204	+0.190	+0.810	+.252	+0.982	+254.0
25	+1.262	+0.525	+0.174	2.402	+0.609	+75.0	+.203	+0.199	+0.801	+.254	+0.973	+231.3
26	+1.368	+0.591	+0.176	2.357	+0.606	+68.6	+.202	+0.214	+0.786	+.257	+0.965	+211.5
27	+1.471	+0.650	+0.178	2.335	+0.603	+63.1	+.201	+0.222	+0.778	+.258	+0.954	+194.5
28	+1.572	+0.719	+0.180	2.414	+0.601	+58.6	+.200	+0.195	+0.805	+.249	+0.947	+180.8
29	+1.676	+0.788	+0.182	2.339	+0.598	+54.4	+.199	+0.220	+0.780	+.256	+0.937	+167.8
30	+1.780	+0.854	+0.184	2.225	+0.593	+50.5	+.198	+0.258	+0.742	+.267	+0.924	+155.8
31	+1.886	+0.928	+0.186	2.177	+0.586	+46.5	+.195	+0.274	+0.726	+.269	+0.902	+143.4
32	+1.991	+1.006	+0.188	2.152	+0.581	+43.3	+.194	+0.283	+0.717	+.270	+0.887	+133.6
33	+2.092	+1.082	+0.190	2.129	+0.576	+40.5	+.192	+0.290	+0.710	+.271	+0.871	+124.9
34	+2.201	+1.158	+0.192	2.096	+0.573	+38.1	+.191	+0.301	+0.699	+.273	+0.862	+117.5
35	+2.350	+1.271	+0.195	2.063	+0.566	+34.7	+.189	+0.312	+0.688	+.274	+0.839	+107.2
36	+2.452	+1.350	+0.197	2.068	+0.561	+32.7	+.187	+0.311	+0.689	+.271	+0.823	+100.7
37	+2.562	+1.433	+0.199	2.065	+0.557	+30.8	+.186	+0.312	+0.688	+.270	+0.811	+95.0
38	+2.615	+1.475	+0.200	2.089	+0.555	+30.0	+.185	+0.304	+0.696	+.266	+0.806	+92.5
39	+2.714	+1.561	+0.202	2.072	+0.550	+28.3	+.183	+0.309	+0.691	+.266	+0.791	+87.4
40	+2.822	+1.652	+0.204	2.009	+0.546	+26.8	+.182	+0.330	+0.670	+.272	+0.777	+82.6
41	+2.934	+1.747	+0.206	1.937	+0.540	+25.2	+.180	+0.354	+0.646	+.279	+0.759	+77.6
42	+3.048	+1.850	+0.208	1.880	+0.535	+23.7	+.178	+0.373	+0.627	+.284	+0.744	+73.2
43	+3.167	+1.970	+0.210	1.851	+0.527	+22.0	+.176	+0.383	+0.617	+.285	+0.718	+68.0
44	+3.282	+2.083	+0.213	1.827	+0.518	+20.5	+.173	+0.391	+0.609	+.284	+0.692	+63.3
45	+3.402	+2.206	+0.215	1.801	+0.509	+19.0	+.170	+0.400	+0.600	+.283	+0.663	+58.5
46	+3.518	+2.326	+0.217	1.772	+0.499	+17.5	+.166	+0.409	+0.591	+.282	+0.633	+54.0
47	+3.631	+2.459	+0.219	1.742	+0.489	+16.2	+.163	+0.419	+0.581	+.281	+0.604	+49.9
48	+3.775	+2.672	+0.222	1.712	+0.463	+13.4	+.154	+0.429	+0.571	+.270	+0.521	+41.4
49	+3.875	+2.800	+0.224	1.675	+0.461	+13.0	+.154	+0.442	+0.558	+.275	+0.517	+40.0
50	+3.989	+2.951	+0.226	1.641	+0.451	+11.9	+.150	+0.453	+0.547	+.275	+0.486	+36.6
51	+4.108	+3.116	+0.228	1.606	+0.437	+10.5	+.146	+0.465	+0.535	+.272	+0.442	+32.2
52	+4.234	+3.301	+0.231	1.567	+0.421	+9.0	+.140	+0.478	+0.522	+.269	+0.393	+27.8
53	+4.359	+3.492	+0.233	1.522	+0.405	+7.6	+.135	+0.493	+0.507	+.266	+0.342	+23.6
54	+4.496	+3.722	+0.236	1.470	+0.386	+6.2	+.129	+0.510	+0.490	+.263	+0.286	+19.1
55	+4.652	+4.090	+0.239	1.413	+0.359	+4.2	+.120	+0.529	+0.471	+.254	+0.200	+12.9